SHOUT
SHARE
IT

MBL

Volume 198
Number 1

THE BIOLOGICAL BULLETIN

FEBRUARY 2000

Published by the Marine Biological Laboratory

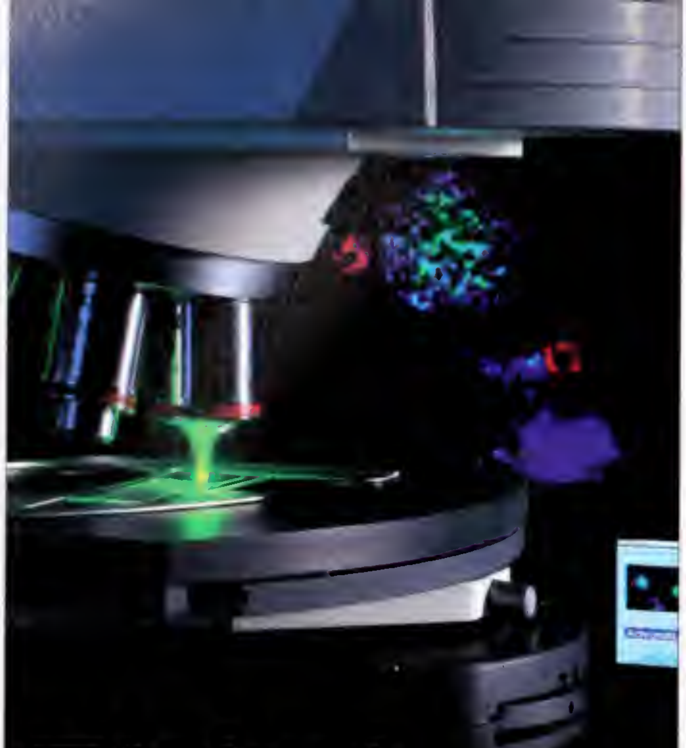

Digital Imaging Platform

Meet the challenges of the digital age with **Axioplan 2 imaging.** Not just a new microscope but a flexible system designed for the future – the digital imaging platform.

Combine **AxioVision** software, with its built-in microscope control, and the new **AxioCam** ultra high resolution digital camera, and you have pure synergy – microscopy and more. Make yours the future-proof choice for high resolution image capture, image processing, archiving – even tele-microscopy. The digital age is with us. Are you?

Carl Zeiss, Inc.
Microscopy & Imaging Systems
One Zeiss Drive
Thornwood, NY 10594

800.223.2243, ext. 7858
micro@zeiss.com
www.zeiss.com/micro

ZEISS

MARINE BIOLOGICAL LABORATORY
COURSE OFFERINGS
JULY – OCTOBER, 2000

Methods in Computational Neuroscience
(July 30 – August 26, 2000)
Directors: William Bialek and Rob de Ruyter van Steveninck, NEC Research Institute

Workshop on Molecular Evolution
(July 30 – August 11, 2000)
Director: Michael Cummings, Marine Biological Laboratory

Molecular Biology of Aging
sponsored by the Ellison Medical Foundation
(August 1 – August 18, 2000)
Directors: Leonard Guarente, Massachusetts Institute of Technology; and Douglas Wallace, Emory University

Molecular Mycology: Current Approaches to Fungal Pathogenesis
(August 7 – August 25, 2000)
Directors: Aaron Mitchell, Columbia University; P.T. Magee, University of Minnesota; and John Edwards, Harbor-UCLA Medical Center

Fundamental Issues in Vision Research
sponsored by the National Eye Institute
(August 13 – August 25, 2000)
Director: David Papermaster, University of Connecticut Health Center

Neural Development & Genetics of Zebrafish
(August 13 – August 26, 2000)
Directors: John Dowling, Harvard University; and Nancy Hopkins, Massachusetts Institute of Technology

Neurobiology & Development of the Leech
(August 13 – September 1, 2000)
Directors: Ronald Calabrese, Emory University; Christie Sahley, Purdue University; and Martin Shankland, University of Texas, Austin

Medical Informatics
sponsored by the National Library of Medicine
(October 1 – October 7, 2000)
Director: James Cimino, Columbia University

Optical Microscopy and Imaging in the Biomedical Sciences
(October 11 – October 19, 2000)
Director: Colin Izzard, State University of New York, Albany

For more information, contact:
Carol Hamel, Admissions Coordinator
508-289-7401 / email: admissions@mbl.edu
OR
Visit our website: courses.mbl.edu

The MBL is an EEO/Affirmative Action Institution

THE
BIOLOGICAL BULLETIN
FEBRUARY 2000

FEB 25 2000

Editor	Michael J. Greenberg	The Whitney Laboratory, University of Florida
Associate Editors	Louis E. Burnett	Grice Marine Laboratory, College of Charleston
	R. Andrew Cameron	California Institute of Technology
	Charles D. Derby	Georgia State University
	Michael LaBarbera	University of Chicago
Section Editor	Shinya Inoué, *Imaging and Microscopy*	Marine Biological Laboratory
Online Editors	James A. Blake, *Keys to Marine Invertebrates of the Woods Hole Region*	ENSR Marine & Coastal Center, Woods Hole
	William D. Cohen, *Marine Models Electronic Record and Compendia*	Hunter College, City University of New York
Editorial Board	Peter B. Armstrong	University of California, Davis
	Ernest S. Chang	Bodega Marine Lab., University of California, Davis
	Thomas H. Dietz	Louisiana State University
	Richard B. Emlet	Oregon Institute of Marine Biology, Univ. of Oregon
	David Epel	Hopkins Marine Station, Stanford University
	Gregory Hinkle	Cereon Genomics, Cambridge, Massachusetts
	Makoto Kobayashi	Hiroshima University of Economics, Japan
	Donal T. Manahan	University of Southern California
	Margaret McFall-Ngai	Kewalo Marine Laboratory, University of Hawaii
	Mark W. Miller	Institute of Neurobiology, University of Puerto Rico
	Tatsuo Motokawa	Tokyo Institute of Technology, Japan
	Yoshitaka Nagahama	National Institute for Basic Biology, Japan
	Sherry D. Painter	Marine Biomed. Inst., Univ. of Texas Medical Branch
	J. Herbert Waite	University of California, Santa Barbara
	Richard K. Zimmer	University of California, Los Angeles
Editorial Office	Pamela Clapp Hinkle	Managing Editor
	Victoria R. Gibson	Staff Editor
	Carol Schachinger	Editorial Associate
	Patricia Burns	Subscription & Advertising Secretary

Published by
MARINE BIOLOGICAL LABORATORY
WOODS HOLE, MASSACHUSETTS

Cover

Several species of sea cucumbers in the order Aspidochirotida respond to irritation by a predator in an unusual—but effective—way. The aboral (or anal) end is turned toward the irritant, the sea cucumber contracts, and a number of tubules detach from the left respiratory tree and are expelled, first through a tear in the cloaca, and then through the anus. These so-called Cuvierian tubules become sticky in the seawater and entangle the predator, immobilizing it. The sea cucumber then crawls away to safety and, at its leisure, repairs the tear in the cloaca and regenerates the lost tubules.

In this issue (pp. 34–49), the complex processes of wound healing and Cuvierian tubule regeneration and growth are described by Didier VandenSpiegel and his colleagues Michel Jangoux and Patrick Flammang. Their observations have been carried out on *Holothuria forskali* from the Bay of Morlaix in Brittany.

The cover photo illustrates a set of Cuvierian tubules from *H. forskali* that are regenerating after a strong stimulus has produced a massive expulsion. Notice that some tubules are completely regrown, while others are at various stages of regeneration (see legend to Fig. 1 on p. 37). The measured response of this specialized response system and the phased process of regeneration lead the authors to conclude that these sea cucumbers have the advantage of "an almost inexhaustible line of defense maintained at limited energy cost."

CONTENTS

Volume 198, No. 1: February 2000

IMAGING AND MICROSCOPY

Zochowski, Michal, Matt Wachowiak, Chun X. Falk, Lawrence B. Cohen, Ying-wan Lam, Srdjan Antic, and Dejan Zecevic
Concepts in Imaging and Microscopy: Imaging membrane potential with voltage-sensitive dyes 1

RESEARCH NOTES

Lambert, Charles C.
Germ-cell warfare in ascidians: sperm from one species can interfere with the fertilization of a second species 22
Tsutsui, Hidekazu, and Yoshitaka Oka
Light-sensitive voltage responses in the neurons of the cerebral ganglion of *Ciona savignyi* (Chordata: Ascidiacea) 26
Bavestrello, Giorgio, Attilio Arillo, Barbara Calcinai, Riccardo Cattaneo-Vietti, Carlo Cerrano, Elda Gaino, Antonella Penna, and Michele Sarà
Parasitic diatoms inside Antarctic sponges 29

PHYSIOLOGY

VandenSpiegel, Didier, Michel Jangoux, and Patrick Flammang
Maintaining the line of defense: regeneration of Cuvierian tubules in the sea cucumber *Holothuria forskali* (Echinodermata, Holothuroidea) 34
Sikes, C. S., A. P. Wheeler, A. Wierzbicki, A. S. Mount, and R. M. Dillaman
Nucleation and growth of calcite on native *versus* pyrolyzed oyster shell folia 50

DEVELOPMENT AND REPRODUCTION

Hadfield, Michael G., Ella A. Meleshkevitch, and Dmitri Y. Boudko
The apical sensory organ of a gastropod veliger is a receptor for settlement cues 67
Ereskovsky, Alexander V.
Reproduction cycles and strategies of the cold-water sponges *Halisarca dujardini* (Demospongiae, Halisarcida), *Myxilla incrustans* and *Iophon piceus* (Demospongiae, Poecilosclerida) from the White Sea. 77

ECOLOGY AND EVOLUTION

Leddy, Holly A., and Amy S. Johnson
Walking *versus* breathing: mechanical differentiation of sea urchin podia corresponds to functional specialization 88
Voight, Janet R., and Anthony Grehan
Egg brooding by deep-sea octopuses in the North Pacific Ocean. 94
Pivkin, Michael V.
Filamentous fungi associated with holothurians from the Sea of Japan, off the Primorye Coast of Russia. . 101

CELL BIOLOGY

Fitt, William K.
Cellular growth of host and symbiont in a cnidarian-zooxanthellar symbiosis 110

SYSTEMATICS

Scheltema, Amélie H., and Christoffer Schander
Discrimination and phylogeny of solenogaster species through the morphology of hard parts (Mollusca, Aplacophora, Neomeniomorpha) 121

STATISTICS

Dewdney, A. K.
A dynamical model of communities and a new species-abundance distribution. 152

THE BIOLOGICAL BULLETIN

THE BIOLOGICAL BULLETIN is published six times a year by the Marine Biological Laboratory, 7 MBL Street, Woods Hole, Massachusetts 02543.

Subscriptions and similar matter should be addressed to Subscription Manager, THE BIOLOGICAL BULLETIN, Marine Biological Laboratory, 7 MBL Street, Woods Hole, Massachusetts 02543. Subscription per year (six issues, two volumes): $225 for libraries; $95 for individuals. Subscription per volume (three issues): $112.50 for libraries; $47.50 for individuals. Back and single issues (subject to availability): $40 for libraries; $20 for individuals.

Communications relative to manuscripts should be sent to Michael J. Greenberg, Editor-in-Chief, or Pamela Clapp Hinkle, Managing Editor, at the Marine Biological Laboratory, 7 MBL Street, Woods Hole, Massachusetts 02543. Telephone: (508) 289-7428. FAX: 508-289-7922. E-mail: pclapp@mbl.edu.

http://www.mbl.edu/BiologicalBulletin/

The home page for the electronic companion to THE BIOLOGICAL BULLETIN—*the Marine Models Electronic Record*—and other BIOLOGICAL BULLETIN publications is available on the World Wide Web at the address shown above.

THE BIOLOGICAL BULLETIN is indexed in bibliographic services including *Index Medicus* and MEDLINE, *Chemical Abstracts, Current Contents, Elsevier BIOBASE/Current Awareness in Biological Sciences,* and *Geo Abstracts.*

Printed on acid free paper,
effective with Volume 180, Issue 1, 1991.

POSTMASTER: Send address changes to THE BIOLOGICAL BULLETIN, Marine Biological Laboratory,
7 MBL Street, Woods Hole, MA 02543.

Copyright © 2000, by the Marine Biological Laboratory

Periodicals postage paid at Woods Hole, MA, and additional mailing offices.
ISSN 0006-3185

INSTRUCTIONS TO AUTHORS

The Biological Bulletin accepts outstanding original research reports of general interest to biologists throughout the world. Papers are usually of intermediate length (10–40 manuscript pages). A limited number of solicited review papers may be accepted after formal review. A paper will usually appear within four months after its acceptance.

Very short, especially topical papers (less than 9 manuscript pages including tables, figures, and bibliography) will be published in a separate section entitled "Research Notes." A Research Note in *The Biological Bulletin* follows the format of similar notes in *Nature.* It should open with a summary paragraph of 150 to 200 words comprising the introduction and the conclusions. The rest of the text should continue on without subheadings, and there should be no more than 30 references. References should be referred to in the text by number, and listed in the Literature Cited section in the order that they appear in the text. Unlike references in *Nature,* references in the Research Notes section should conform in punctuation and arrangement to the style of recent issues of *The Biological Bulletin.* Materials and Methods should be incorporated into appropriate figure legends. See the article by Lohmann *et al.* (October 1990, Vol. **179:** 214–218) for sample style. A Research Note will usually appear within two months after its acceptance.

The Editorial Board requests that regular manuscripts conform to the requirements set below; those manuscripts that do not conform will be returned to authors for correction before review.

1. ***Manuscripts.*** Manuscripts, including figures, should be submitted in quadruplicate, with the originals clearly marked. (Xerox copies of photographs are not acceptable for review purposes.) The submission letter accompanying the manuscript should include a telephone number, a FAX number, and (if possible) an E-mail address for the corresponding author. The original manuscript must be typed in no smaller than 12 pitch or 10 point, using double spacing (*including* figure legends, footnotes, bibliography, etc.) on one side of 16- or 20-lb. bond paper, 8 by 11 inches. Please, no right justification. Manuscripts should be proofread carefully and errors corrected legibly in black ink. Pages should be numbered consecutively. Margins on all sides should be at least 1 inch (2.5 cm). Manuscripts should conform to the *Council of Biology Editors Style Manual,* 5th Edition (Council of Biology Editors, 1983) and to American spelling. Unusual abbreviations should be kept to a minimum and should be spelled out on first reference as well as defined in a footnote on the title page. Manuscripts should be divided into the following components: Title page, Abstract (of no more than 200 words), Introduction, Materials and Methods, Results, Discussion, Acknowledgments, Literature Cited, Tables, and Figure Legends. In addition, authors should supply a list of words and phrases under which the article should be indexed.

2. ***Title page.*** The title page consists of a condensed title or running head of no more than 35 letters and spaces, the manuscript title, authors' names and appropriate addresses, and footnotes listing present addresses, acknowledgments or contribution numbers, and explanation of unusual abbreviations.

3. ***Figures.*** The dimensions of the printed page, 7 by 9 inches, should be kept in mind in preparing figures for publication. We recommend that figures be about 1 times the linear dimensions of the final printing desired, and that the ratio of the largest to the smallest letter or number and of the thickest to the thinnest line not exceed 1:1.5. Explanatory matter generally should be included in legends, although axes should always be identified on the illustration itself. Figures should be prepared for reproduction as either line cuts or halftones. Figures to be reproduced as line cuts should be unmounted glossy photographic reproductions or drawn in black ink on white paper, good-quality tracing cloth or plastic, or blue-lined coordinate paper. Those to be reproduced as halftones should be mounted on board, with both designating numbers or letters and scale bars affixed directly to the figures. All figures should be numbered in consecutive order, with no distinction between text and plate figures and cited, in order, in the text. The author's name and an arrow indicating orientation should appear on the reverse side of all figures.

Color: The Biological Bulletin will publish color figures and plates, but must bill authors for the actual additional cost of printing in color. The process is expensive, so authors with more than one color image should—consistent with editorial concerns, especially citation of figures in order—combine them into a single plate to reduce the expense. On request, when supplied with a copy of a color illustration, the editorial staff will provide a pre-publication estimate of the printing cost.

4. ***Tables, footnotes, figure legends, etc.*** Authors should follow the style in a recent issue of *The Biological Bulletin* in preparing table headings, figure legends, and the like. Because of the high cost of setting tabular material in type, authors are asked to limit such material as much as possible. Tables, with their headings and footnotes, should be typed on separate sheets, numbered with consecutive Roman numerals, and placed after the Literature Cited. Figure legends should contain enough information to make the figure intelligible separate from the text. Legends should be typed double spaced, with consecutive Arabic numbers, on a separate sheet at the end of the paper. Footnotes should be limited to authors' current addresses, acknowledgments or contribution numbers, and explanation of unusual abbreviations. All such footnotes should appear on the title page. Footnotes are not normally permitted in the body of the text.

5. ***Literature cited.*** In the text, literature should be cited by the Harvard system, with papers by more than two authors cited as Jones *et al.*, 1980. Personal communications and material in preparation or in press should be cited in the text only, with author's initials and institutions, unless the material has been formally accepted and a volume number can be supplied. The list of references following the text should be headed Literature Cited, and must be typed double spaced on separate pages, conforming in punctuation and arrangement to the style of recent issues of *The Biological Bulletin*. Citations should include complete titles and inclusive pagination. Journal abbreviations should normally follow those of the U. S. A. Standards Institute (USASI), as adopted by BIOLOGICAL ABSTRACTS and CHEMICAL ABSTRACTS, with the minor differences set out below. The most generally useful list of biological journal titles is that published each year by BIOLOGICAL ABSTRACTS (BIOSIS List of Serials; the most recent issue). Foreign authors, and others who are accustomed to using THE WORLD LIST OF SCIENTIFIC PERIODICALS, may find a booklet published by the Biological Council of the U.K. (obtainable from the Institute of Biology, 41 Queen's Gate, London, S.W.7, England, U.K.) useful, since it sets out the WORLD LIST abbreviations for most biological journals with notes of the USASI abbreviations where these differ. CHEMICAL ABSTRACTS publishes quarterly supplements of additional abbreviations. The following points of reference style for THE BIOLOGICAL BULLETIN differ from USASI (or modified WORLD LIST) usage:

A. Journal abbreviations, and book titles, all underlined (for *italics*)

B. All components of abbreviations with initial capitals (not as European usage in WORLD LIST *e.g., J. Cell. Comp. Physiol.* NOT *J. cell. comp. Physiol.*)

C. *All* abbreviated components must be followed by a period, whole word components *must not* (*i.e., J. Cancer Res.*)

D. Space between all components (*e.g., J. Cell. Comp. Physiol.*, not *J.Cell.Comp.Physiol.*)

E. Unusual words in journal titles should be spelled out in full, rather than employing new abbreviations invented by the author. For example, use *Rit Vísindafjélags Islendinga* without abbreviation.

F. All single word journal titles in full (*e.g., Veliger, Ecology, Brain*).

G. The order of abbreviated components should be the same as the word order of the complete title (*i.e., Proc.* and *Trans.* placed where they appear, not transposed as in some BIOLOGICAL ABSTRACTS listings).

H. A few well-known international journals in their preferred forms rather than WORLD LIST or USASI usage (*e.g., Nature, Science, Evolution* NOT *Nature, Lond., Science, N.Y.: Evolution, Lancaster, Pa.*)

6. ***Reprints, page proofs, and charges.*** Authors of articles in black and white (no color figures) receive their first 50 reprints (without covers) free of charge. Color reprints and additional black-and-white reprints may be purchased; authors will receive order forms. Reprints normally will be delivered about 2 to 3 months after the issue date. Authors (or delegates for foreign authors) will receive page proofs of articles shortly before publication. They will be charged the current cost of printers' time for corrections to these (other than corrections of printers' or editors' errors). Other than these charges for authors' alterations, *The Biological Bulletin* does not have page charges.

Reference: *Biol. Bull.* **198:** 1–21. (February 2000)

Concepts in Imaging and Microscopy

Imaging Membrane Potential With Voltage-Sensitive Dyes

MICHAL ZOCHOWSKI,[1,*] MATT WACHOWIAK,[1] CHUN X. FALK,[2] LAWRENCE B. COHEN,[1,2]
YING-WAN LAM,[1] SRDJAN ANTIC,[1] AND DEJAN ZECEVIC[1]

[1] *Department of Cellular and Molecular Physiology, Yale University School of Medicine New Haven, Connecticut 06520; and* [2] *RedShirtImaging, LLC, Fairfield, Connecticut 06432*

Abstract. Membrane potential can be measured optically using a variety of molecular probes. These measurements can be useful in studying function at the level of an individual cell, for determining how groups of neurons generate a behavior, and for studying the correlated behavior of populations of neurons. Examples of the three kinds of measurements are presented. The signals obtained from these measurements are generally small. Methodological considerations necessary to optimize the resulting signal-to-noise ratio are discussed.

Introduction

An optical measurement of membrane potential using a molecular probe can be beneficial in a variety of circumstances. One advantage is the ability to measure from many locations simultaneously. This is especially important in the study of nervous systems in which many parts of an individual cell, or many cells, or many regions of the nervous system are active at the same time. In addition, optical recording offers the possibility of recording from processes that are too small or fragile for electrode recording.

Several optical properties of membrane-bound dyes are sensitive to membrane potential, including fluorescence, absorption, dichroism, birefringence, fluorescence resonance energy transfer, nonlinear second harmonic generation, and resonance Raman absorption. However, because the vast majority of applications have involved fluorescence or absorption, these will be emphasized in this review. All of the optical signals described here are "fast" signals (Cohen and Salzberg, 1978) that are presumed to arise from membrane-bound dye; they follow changes in membrane potential with time courses that are rapid compared to the rise time of an action potential.

Studies of the molecular mechanisms that result in potential-dependent optical properties have produced evidence supporting three mechanisms (for different dyes): dipole rotation, electrochromism, and a potential-sensitive monomer-dimer equilibrium. Dye mechanisms are discussed in Waggoner and Grinvald (1977), Loew *et al.* (1985), and Fromherz *et al.* (1991).

We begin with examples of results obtained from measurements addressing three quite different neurobiological problems. In all three instances the camera was a photodiode array with only 464 pixels (NeuroPlex; RedShirtImaging, LLC, Fairfield, CT). Despite this low spatial resolution, the camera resolution was not limiting in any of the examples. On the positive side, this camera has an outstanding dynamic range; with an incident intensity of more than 10^{10} photons per frame, it measures signals that are a fractional change ($\Delta I/I$) of one part in 10^5. In addition, it has a frame rate of 1.6 kHz (fast enough to measure most neurobiologically important signals). On the other hand, recently introduced CCD cameras not only have similar frame rates but also have lower dark noise. Thus, in one of the three measurements, we think that improved signal-to-noise ratios could be obtained with a cooled CCD camera. The optical signals in the example measurements are not large—they represent fractional changes in light intensity ($\Delta I/I$) of from 10^{-4} to 3×10^{-2}. Nonetheless, they can be measured with an acceptable signal-to-noise ratio after attention to details of the measurement that are described in the second part of the paper.

Figure 1 illustrates three qualitatively different areas of neurobiology in which imaging membrane potential has been useful. First (left panel), to know how a neuron integrates its synaptic input into its action potential output, one must be able to measure membrane potential wherever synaptic input occurs and at the places where spikes are initiated. Second (middle panel), to understand how a nervous system generates a behavior, the action potential activity of many (all) of the participating neurons must be

---

Received 22 June 1999; accepted 19 October 1999.

[*] To whom correspondence should be addressed. E-mail: mrz@fred.med.yale.edu

This is the fourth in a series of articles entitled "Concepts in Imaging and Microscopy." This series is supported by the Optical Imaging Association (OPIA) and was introduced with an editorial in the April 1998 issue of this journal (Biol. Bull. 194: 99). Other articles in the series are listed on *The Biological Bulletin*'s website at http://www.mbl.edu/html/BB/home.BB.html.

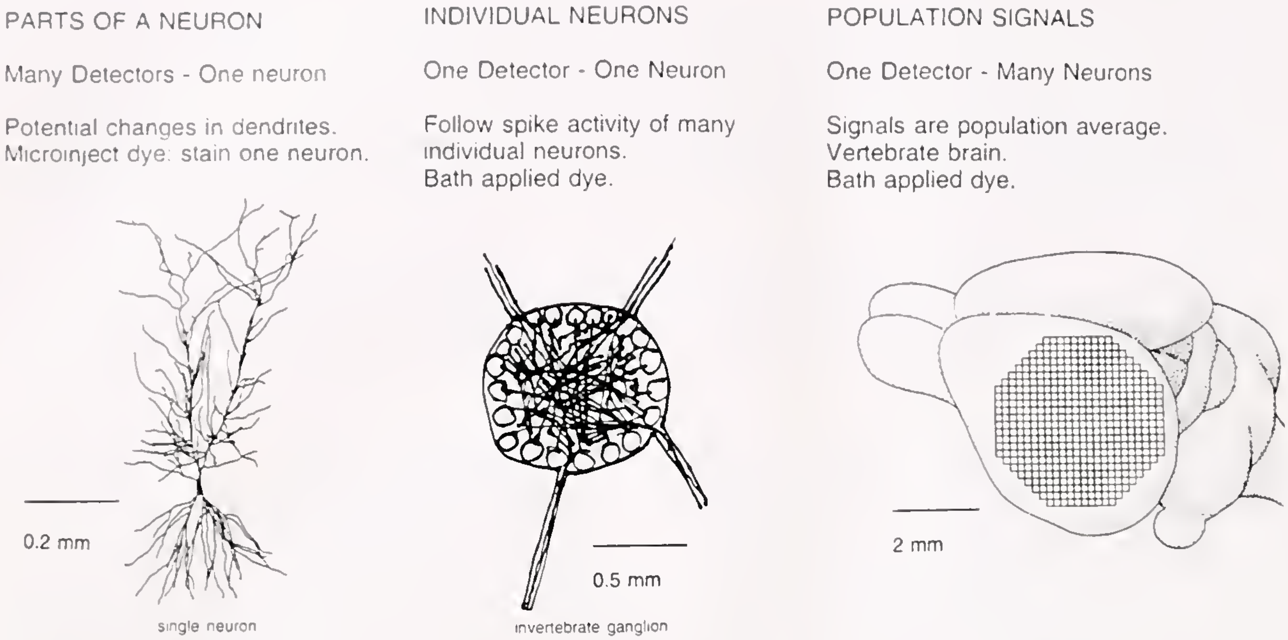
PARTS OF A NEURON
Many Detectors - One neuron
Potential changes in dendrites.
Microinject dye: stain one neuron.
INDIVIDUAL NEURONS
One Detector - One Neuron
Follow spike activity of many individual neurons.
Bath applied dye.
POPULATION SIGNALS
One Detector - Many Neurons
Signals are population average.
Vertebrate brain.
Bath applied dye.
0.2 mm
single neuron
0.5 mm
invertebrate ganglion
2 mm

Figure 1. Schematic of the three kinds of measurements described as examples. (Left) An individual cortical hippocampal CA1 pyramidal cell. Each pixel of the 464-element photodiode array receives light from a small part of the dendrite, axon, or cell body of the neuron. An optical measurement of membrane potential provides information about how the neuron converts its synaptic input into its spike output. (Middle) A slice through an invertebrate ganglion with its cell bodies in a cortex around the outside and neuropil in the middle. Here each detector receives light from one or a small number of cell bodies. A voltage-sensitive dye measurement of spike activity while the ganglion is generating a behavior provides information about how the behavior is generated. (Right) A vertebrate brain with the superimposed 464-element photodiode array (used in all three examples). Each pixel of the array receives light from thousands of cells and processes. The signal is the population average of the change in membrane potential in those cells and processes. The image of the hippocampal neuron was taken from Mainen *et al.* (1996).

measured simultaneously. Third (right panel), responses to sensory stimuli and generation of motor output in the vertebrate brain are often accompanied by synchronous activation of many neurons in widespread brain areas; voltage-sensitive dye recordings allow simultaneous measurement of population signals from many areas. In these three instances, optical recordings have provided kinds of information about the function of the nervous system that were previously unobtainable.

In the second half of the article, we describe the experimental details that are important in obtaining the signal-to-noise ratios achieved in the experiments described in the first section. We discuss signal type, dyes, light sources, photodetectors, and optics.

Three Examples

1. Processes of an individual neuron (Fig. 1, left panel)

Understanding the biophysical properties of single neurons and how they process information is fundamental to understanding how the brain works. With the development of new measuring techniques that allow more direct investigation of individual nerve cells, it became widely recognized, especially during the last 20 years, that dendritic membranes of many vertebrate CNS neurons contain active conductances such as voltage-activated Na^+, Ca^{2+}, and K^+ channels (*e.g.*, Stuart and Sakmann, 1994; Spruston *et al.*, 1995; Magee and Johnston, 1995; Magee *et al.*, 1995). An important consequence of active dendrites is that regional electrical properties of branching neuronal processes will be extraordinarily complex, dynamic, and, in the general case, impossible to predict in the absence of detailed measurements.

To obtain such a measurement one would, ideally, like to monitor, at multiple sites, subthreshold events as they travel from the sites of origin on neuronal processes and summate at particular locations to influence the initiation of action potentials. This goal has not been achieved in any neuron, vertebrate or invertebrate, due to the technical limitations of measurements that employ electrodes. Better spatial resolution necessitates a turn from direct electrical recording to indirect, optical measurements using voltage-sensitive dyes. Recently, the sensitivity of intracellular voltage-sensitive dye techniques for monitoring neuronal processes *in situ* has

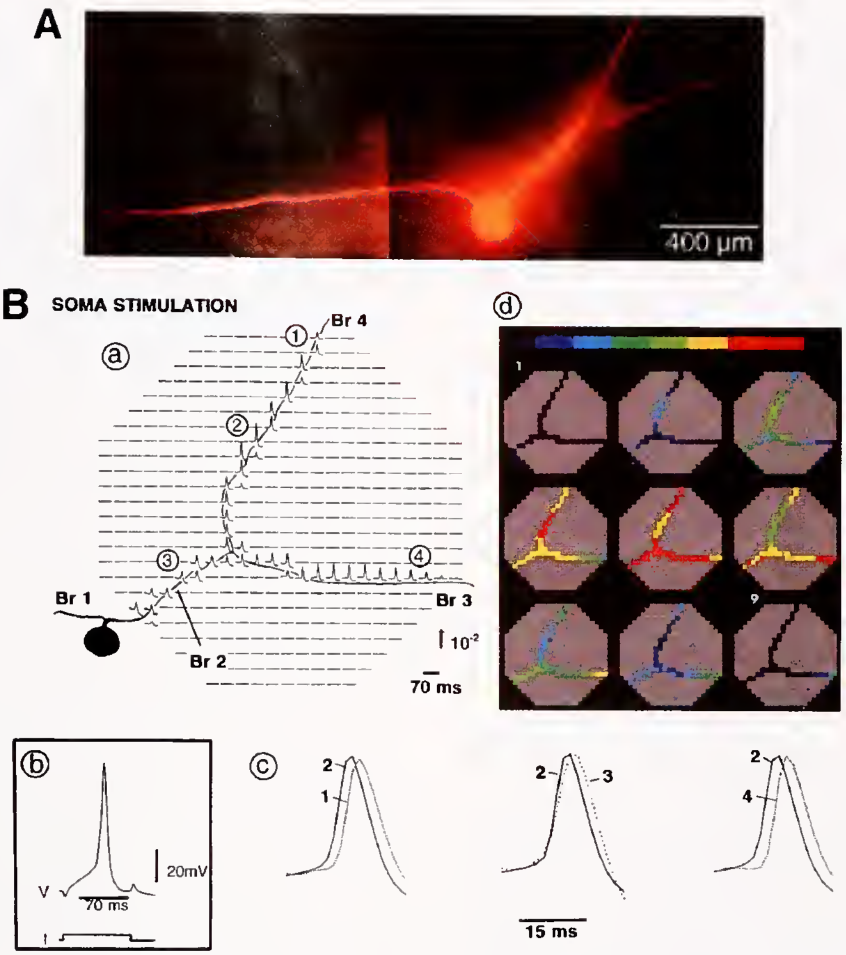

Figure 2. (A) Giant metacerebral neuron from the left cerebral ganglion 12 h after injection with the fluorescent voltage-sensitive dye JPW1114. The cell body and main processes are clearly visible in the unfixed preparation. Excitation wavelength: 540 ± 30 nm; dichroic mirror: 570 nm, long-pass barrier filter: 610 nm. (B) (Ba) Voltage-sensitive dye recording of action potential signals from elements of the photodiode array positioned over the image of axonal arborizations of a metacerebral cell in the left cerebral ganglion. Axonal branches are marked Br 1–4. Spikes were evoked by transmembrane current steps, as shown in (Bb), delivered through the recording microelectrode in the soma. Each optical trace in (Ba) represents 70 ms of recording centered around the peak of the spike as indicated by the time bar in (Bb). Each diode received light from a 50 × 50 μm area in the object plane. (Bc) Recordings from four locations indicated in panel (Ba), scaled to the same height, are compared to determine the site of the origin of the action potential and the direction of propagation. (Bd) Color-coded representation of the data shown in (Ba) indicating the size and location of the primary spike-trigger zone and the pattern of spike propagation. Consecutive frames represent data points that are 1.6 ms apart. The color scale is relative, with the peak of the action potential for each detector shown in red (modified from Zecevic, 1996).

been improved by a factor of roughly 150, allowing direct recording of subthreshold and action potential signals from the neurites of invertebrate neurons (Antic and Zecevic, 1995; Zecevic, 1996). The improvement in the signal-to-noise ratio is based on previous experience from other laboratories (Davila *et al.*, 1974; Grinvald *et al.*, 1987) and on (1) finding an intracellular dye that provides a relatively large fractional change in fluorescence and (2) improvements in the apparatus to increase the incident light intensity, to lower the noise, and to filter more efficiently. Encouraging results have also been obtained in initial studies on vertebrate CNS neurons in brain slices (see below).

An invertebrate neuron. A typical result of a multi-site voltage-sensitive dye recording is shown in Figure 2. The fluorescent image of a metacerebral *Helix* neuron following injection with the fluorescent voltage-sensitive dye JPW1114 is shown in Figure 2A. The image of the cell was projected onto the array of photodiodes as indicated in

Figure 2Ba. This panel represents multi-site recording of action-potential signals from axonal branches Br2, Br3, and Br4, evoked by a transmembrane current step (Fig. 2Bb). Optical signals associated with action potentials, expressed as fractional changes in fluorescent light intensity ($\Delta F/F$), were between 3×10^{-3} and 3×10^{-2} in recordings from the processes. With these measurements it is straightforward to determine the direction and velocity of action-potential propagation in neuronal processes. In Figure 2Bc, recordings from different locations, scaled to the same height, are compared to determine the site of origin of the action potential. The earliest action potential, in response to soma stimulation, was generated near location 2, in the axonal branch Br4, situated in the cerebral-buccal connective outside the ganglion. The spike propagated orthodromically from the site of initiation toward the periphery in branch Br4 and antidromically toward the soma and into the branch Br3 in the external lip nerve. The direction of propagation is clear from the color-coded representation of the data (Fig. 2Bd). This figure shows the potential changes in the branching structure at nine different times separated by 1.6 ms. Red corresponds to the peak of the action potential. The panels show the position of the action-potential trigger zone at location 2 and orthodromic and antidromic spread of the nerve impulse from the site of initiation. The earliest spike was evoked about 1 mm from the soma. The spike-initiation segment in the axon is roughly 300 μm in length and remote from the soma. It appears that under normal conditions, slow depolarizing voltage pulses applied to the soma are electrotonically spread into the processes with little attenuation. These depolarizing pulses initiate action potentials in the processes at remote sites that are more excitable than neighboring segments.

Light scattering in the ganglion limits the maximum useful spatial resolution in this kind of measurement. Thus the 24 × 24 pixel resolution of NeuroPlex appears to be adequate in this circumstance.

On the basis of similar measurements, we recently determined that the *Helix* neuron in Figure 2 has multiple trigger zones that can be independently activated. The precise pattern of action-potential initiation and propagation within the whole branching structure of a neuron can be analyzed by multi-site recording. The information about the spatial and temporal dynamics of neuronal signals can be used to constrain the choice of channel densities and geometrical factors in biophysical models that are used to describe functional properties of neurons.

A vertebrate neuron. It is of considerable interest to apply the same technique to dendrites of vertebrate CNS neurons in brain slices. Apart from our preliminary experiments (Kogan *et al.*, 1995), there is no previous experience in this field. Experiments were carried out on pyramidal neurons in slices from the neocortex of 14- to 18-day-old rats. The fluorescent image of the cell was projected onto the octagonal photodiode array. In the example shown in Figure 3A, the neuron was stimulated, by depolarizing the cell body, to produce a burst of two action potentials. Each trace in Figure 3B represents the output of one photodiode for 44 ms. Optical signals associated with action potentials, expressed as fractional changes in fluorescent light intensity ($\Delta F/F$), were between 10^{-2} and 3×10^{-2} in recordings from the processes. In Figure 3C, the electrical recordings from the soma (smooth line) were compared with the optical signals filtered to eliminate high-frequency noise (dashed line). The time courses of electrical and optical recordings agree well. In panel D, recordings from different locations, scaled to the same height, are compared on an expanded time scale. Each trace is a spatial average from two adjacent detectors. Both spikes in the burst originated near the soma and propagated centrifugally along the apical and basolateral dendrites (action potential back-propagation; Stuart and Sakmann, 1994).

These initial experiments demonstrate several important methodological results. First, it is possible to deposit the dye into the cell without staining the surrounding tissue (keeping background fluorescence low). Second, the pharmacological effects of the dye were completely reversible if the staining pipette was withdrawn, and the cell was allowed to recover for 1–2 h. Third, the level of photodynamic damage already allows meaningful measurements and could be reduced further. Finally, the sensitivity of the dye was comparable to that achieved in the experiments on invertebrate neurons (Zecevic, 1996). In these preliminary experiments, the dye spread for roughly 500 μm into dendritic processes within 2 h. One way to improve the staining is to attach the dye electrode to the distal region on a dendrite as done previously with calcium-sensitive dyes (*e.g.*, Markram and Sakmann, 1994; Schiller *et al.*, 1995). This approach will shorten the time needed for diffusion.

The light intensity at the photodetector in the measurements from the distal process of these neurons is low; the dark noise of the 464-element photodiode array was the limiting noise. In this circumstance a better signal-to-noise ratio should be obtained with a cooled CCD camera (see below). For neurons on the surface of the slice, where light scattering is less of a factor, the additional spatial resolution of the CCD camera might also be useful.

2. *Action potentials from individual neurons (Fig. 1, middle panel)*

Aplysia *abdominal ganglion.* Nervous systems are made up of large numbers of neurons, and many of these are active during the generation of behaviors. The original motivation for developing optical methods was the hope that they could be used to record all of the action-potential activity of all the neurons in simpler invertebrate ganglia during behaviors (Davila *et al.*, 1973). Techniques that use

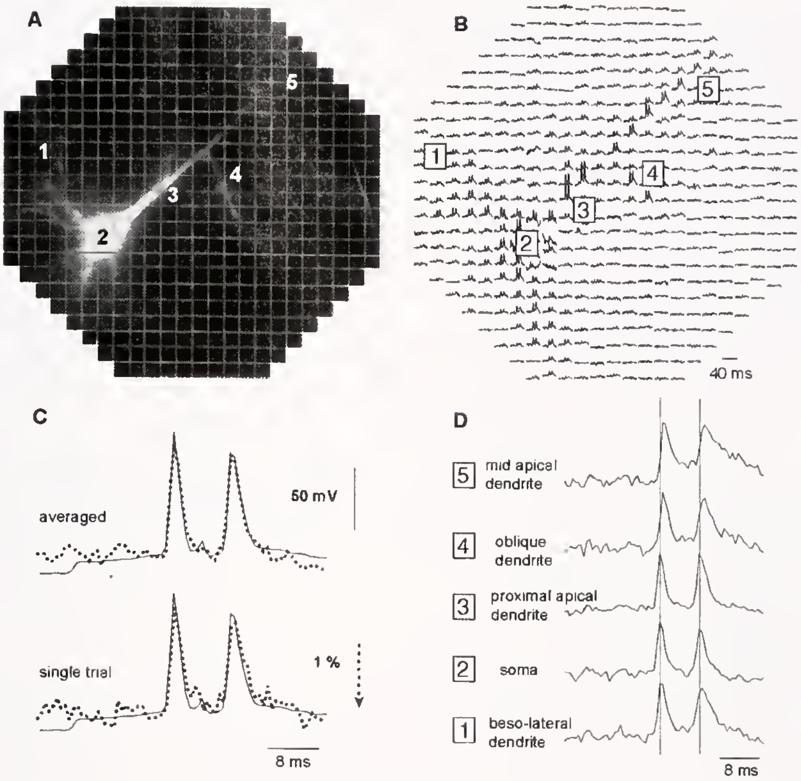

Figure 3. (A) Outline of the 464-element photodiode array superimposed over the fluorescent image of a pyramidal neuron. (B) Single-trial recording of action-potential-related optical signals. Each trace represents the output of one diode. Traces are arranged according to the disposition of the detectors in the array. Each trace represents 44 ms of recording. Each diode received light from a 14 × 14 μm area in the object plane. Spikes were evoked by a somatic current pulse. (C) Comparison of electrical and optical recordings. Upper panel: spatial average of optical signals from eight individual diodes from the somatic region (dotted line) are superimposed on the electrical recording from the soma (solid line). Lower panel: same electrical signal compared with a single-trial optical recording. (D) Action potentials from individual detectors at different locations along the basal, oblique, and apical dendrites. Traces from different locations are scaled to the same height. The increasing delay between the signal from the somatic region and most proximal dendritic segments reflects the propagation velocity (0.22 m/s). At a distance of 230 μm from the soma, the half-width increased from 1.7 to 2.3 ms for the first spike and from 2.2 to 4.6 ms for the second spike in the burst. (Modified from Antic, Major, and Zecevic, 1999.)

microelectrodes are limited in that they can observe single-cell activity in only as many cells as one can simultaneously place electrodes (typically four or fewer neurons). Information about the activity of many cells is essential for understanding the roles of the individual neurons in generating behavior and for understanding how nervous systems are organized.

In the first attempt to use voltage-sensitive dyes in ganglia (Salzberg *et al.*, 1973), we were fortunate to be able to monitor activity in a *single* neuron because the photodynamic damage was severe and the signal-to-noise ratio small. Now, however, with better dyes and methods, the spike activity of hundreds of individual neurons can be recorded simultaneously (Zecevic *et al.*, 1989; Nakashima *et al.*, 1992). In the experiments described below, we measured the spike activity of up to 50% of the approximately 1000 cells in the *Aplysia* abdominal ganglion. Opisthobranch molluscs are favored for this kind of measurement because their central nervous systems have relatively few, relatively large neurons, and almost all of the cell bodies are fully invaded by the action potential. In addition, opisthobranch ganglia are organized with cell bodies on the outside and neuropil in the center. These characteristics are important because the dyes we used stained only the outer, cell body, layer, and the signal-to-noise ratio for action-potential recording would be reduced if the cell bodies did not have a full-sized action potential.

The 464-element silicon photodiode array was placed in the image plane formed by a microscope objective of 25 × 0.4 NA. A single-pole high-pass and a four-pole low-pass Bessel filter in the amplifiers limited the frequency response to 1.5–200 Hz. We used the isolated siphon preparation developed by Kupfermann *et al.* (1971). Considerable effort was made to find conditions that maximized the dye staining while causing minimal pharmacologic effects on the gill-withdrawal behavior. Intact ganglia were incubated in a 0.15 mg/ml solution of the oxonol dye RH155 (Fig. 9), or its diethyl analog, using a protocol developed by Nakashima *et al.* (1992). A light mechanical stimulation (1–2 g) was delivered to the siphon.

The signal-to-noise ratio in the measurements from individual cell bodies is optimal when the light from one cell body falls on one photodetector. With more photodetectors, the light from an individual cell is divided onto more than one detector (with a concomitant reduction in signal-to-noise ratio); with fewer photodetectors than cells, the light from more than one neuron falls on one detector, with a reduction in signal-to-noise ratio for the individual neurons. Thus an array of only 464 detectors is approximately optimal for a ganglion of 1000 neurons.

Because the image of a ganglion is formed on a rectilinear diode array, there is no simple correspondence between images of cells and photodetectors. The light from larger cell bodies falls on several detectors, and its activity is recorded as simultaneous events on neighboring detectors. In addition, because these preparations are multilayered, most detectors receive light from several cells. Thus, a sorting step is required to determine the activity in neurons from the spike signals on individual photodiodes. In the top right of Figure 4, the raw data from seven photodiodes from an array are shown. The activity of four neurons (shown in the raster diagram at the bottom) can account for the spike signals in the top section. Two problems are illustrated in this figure. Both arise from the signal-to-noise ratio. First, there may be an additional spike on detector 116 just before the stimulus (at the arrow), but the signal-to-noise ratio is not large enough to be certain. Second, following the stimulus, there is a great deal of activity, which will obscure small signals. Both problems suggest that the optical recordings are not complete; attempts to determine the completeness suggested that we were detecting the activity of about 50% of the neurons in the *Aplysia* abdominal ganglion (Wu *et al.*, 1994b). The fractional change in transmitted light ($\Delta I/I$) in these signals ranges from about 10^{-4} to 1.5×10^{-3}; the noise is substantially smaller.

The result of a complete analysis is shown in the raster diagram of Figure 5. The 0.5-s mechanical stimulus started at the time indicated by the line labeled "stim." The activity of 135 neurons was detected optically. Similar results have been obtained by Nakashima *et al.* (1992). Because this recording is only 50% complete, the actual number of activated neurons during the gill-withdrawal reflex was estimated to be about 300.

We were surprised at the large number of neurons that were activated by the light touch. Furthermore, a substantial number of the remaining neurons were likely to either be inhibited by the stimulus or receive a large subthreshold excitatory input. It is almost as if the *Aplysia* nervous system is designed so that every cell in the abdominal ganglion cares about this (and perhaps every) sensory stimulus. In addition, more than 1000 neurons in other ganglia are activated by this touch (Tsau *et al.*, 1994). Clearly, information about this very mild and localized stimulus is propagated widely in the *Aplysia* nervous system. These results impose a more pessimistic view of the present understanding of the neuronal basis of apparently simple behaviors in relatively simple nervous systems. Elsewhere we present arguments suggesting that the abdominal ganglion may function as a distributed system (Wu *et al.*, 1994a, b; Tsau *et al.*, 1994).

Guinea pig ganglion. Recently, similar measurements have been made from a vertebrate system, the ganglia of the submucous plexus of the guinea pig small intestine (Obaid *et al.*, 1999). It will be interesting to see if this vertebrate preparation also functions in a distributed manner.

3. Population signals (Fig. 1, right panel)

Turtle olfactory bulb. In the above experiments on *Aplysia* ganglia, each photodetector received light from one or a small number of neurons. In contrast, in measurements from a vertebrate brain (Fig. 1, right panel), each detector received light from a volume of the brain that includes thousands of neurons and processes. The resulting signal is a population average of the change in membrane potential of all of these cells. Populations signals have been recorded from many preparations (*e.g.*, Grinvald *et al.*, 1982a; Orbach and Cohen, 1983; Sakai *et al.*, 1985; Kauer, 1988; Cinelli and Salzberg, 1992; Albowitz and Kuhnt, 1993); the results from turtle are described because of our familiarity with them.

Odor stimuli induce stereotyped local field-potential responses consisting of sinusoidal oscillations of 10 to 80 Hz riding on top of a slow "DC" signal. Since their first discovery in the hedgehog (Adrian, 1942), odor-induced oscillations have been seen in phylogenetically distant species including locust (Laurent and Naraghi, 1994), turtle (Beuerman, 1975), and monkey (Hughes and Mazurowski, 1962). We measured the voltage-sensitive dye signal that accompanies these oscillations in the box turtle; our measurements allowed a more detailed visualization of the spatiotemporal characteristics of the oscillations.

The turtles were anesthetized by placing them in ice for 2 h, then a craniotomy was performed over the olfactory bulb. The dura and arachnoid mater were carefully removed to facilitate staining. The exposed olfactory bulb was stained by covering it with dye solution (RH414, 0.02–0.2 mg/ml) for 60 min; excess dye was washed away with turtle saline. The odor output from the olfactometer was more-or-less square and had a latency of about 100 ms from the onset

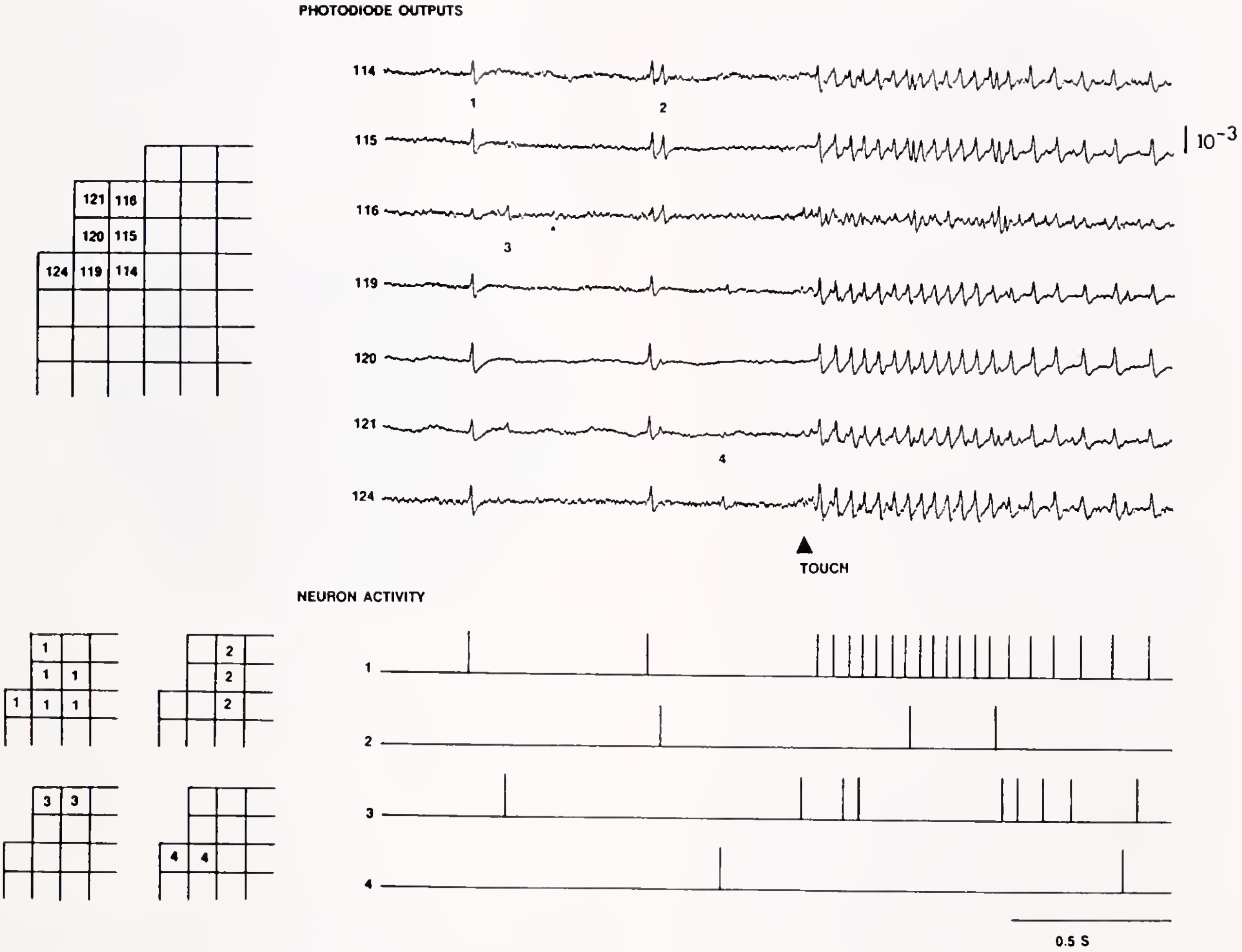

Figure 4. Optical recordings from a portion of a photodiode array from an *Aplysia* abdominal ganglion. The drawing to the left represents the relative position of the detectors whose activity is displayed. In the top right, the original data from seven detectors are illustrated. The numbers to the right of each trace identify the detector from which the trace was taken. The bottom section shows the raster diagram illustrating the results of our sorting of these data into the spike activity of four neurons. At the number 1 in the top section there are synchronously occurring spike signals on all seven detectors. A synchronous event of this kind occurs more than 20 times; we presume that each event represents an action potential in one relatively large neuron. The activity of this cell is represented by the vertical lines on trace 1 of the bottom section. The activity of a second cell is indicated by small signals at the number 4 on 119 and its neighbor, 124. The activity of this cell is represented by the vertical lines on trace 4 of the bottom section. The activity of neurons 2 and 3 was similarly identified. (Modified from Zecevic *et al.*, 1989.)

of the command pulse to the solenoid controlling odor delivery.

We optimized the optics for measurements of epifluorescence at low magnification. In this circumstance the intensity reaching the objective image plane is proportional to the fourth power of the numerical aperture (NA) of the objective (Inoué, 1986). Because conventional microscope optics have small numerical apertures at low magnifications, we assembled a microscope (macroscope) based on a 25-mm focal length, 0.95 f, C-mount, camera lens (used with the C-mount end facing the preparation) (Salama, 1988; Ratzlaff and Grinvald, 1991; Kleinfeld and Delaney, 1996). With a magnification of 4×, the intensity reaching the photodetector was 100 times larger with this lens than with a conventional 4×, 0.16 NA microscope lens. Additional details of the apparatus are given in Wu and Cohen (1993), Wu *et al.* (1998), and Lam *et al.* (2000).

With this 4× magnification each detector will receive light from an area of the object plane that is 170 × 170 μm^2. Because of light scattering by the preparation (see Fig. 12), it would not be possible to achieve better spatial resolution even if the camera had more pixels.

In Figure 6, the recordings from seven selected diodes in a single trial are shown. The location of these diodes is indicated on the image by the numbered squares on the left. In rostral locations (detectors 1 and 2), we found a single oscillation with a relatively high frequency. On a diode from a middle location (detector 4) there was a relatively brief, short-latency oscillation, and on a diode from the caudal bulb (detector 7), the oscillation was of a lower frequency and a long latency. In areas between two regions, the recorded oscillations were combinations of two signals: rostral/middle in detector 3 and middle/caudal in detectors 5 and 6. We named the three oscillations *rostral, middle,* and *caudal.* The fractional change in fluorescence ($\Delta F/F$) in these three signals ranged from about 2×10^{-4} to 10^{-3}; the noise was substantially smaller. In addition, a DC signal, which appears as a single peak after high-pass filtering in Figure 6, was observed over most of the ipsilateral olfactory bulb. Figure 7A shows the time course of an unfiltered recording. Following the start of the odor command pulse, the optical signal rose to a plateau and then continued for several seconds. After a short delay, the rostral oscillations appeared on the DC response. The rostral oscillation had a long latency and a high frequency. The middle oscillation had a short latency and a frequency that was similar to the rostral oscillation. The caudal oscillation had a lower frequency and the longest latency. In addition to differences in frequency and latency, the three oscillations also had different shapes—the rostral and caudal oscillations had relatively sharp peaks, whereas the middle oscillation was more sinusoidal.

Figure 7 shows the time courses of the signals from four detectors from this trial together with multiple-frame images indicating the position and propagation during one cycle of each oscillation. The rostral, middle, and caudal oscillations are clearer after the DC signal was reduced with a high-pass filter (Fig. 7B, C, D). In these multi-frame images, the red color and the area enclosed by the black line indicate the areas in which the signals are larger than 80% and 20% of the maximum signal respectively. The DC signal covered most of the olfactory bulb. The rostral signal (D) propagated in the caudal direction, the middle signal (B) did not appear to propagate, and the caudal signal (C) propagated in a lateral-caudal direction. Prechtl *et al.* (1997) also found that propagation was a characteristic of many oscillations in the turtle visual cortex.

Oscillations are not restricted to the olfactory system. Despite their ubiquity, the roles and functions of oscillation are not well understood. Nevertheless, their ubiquity and the large number of neurons that they involve make it reason-

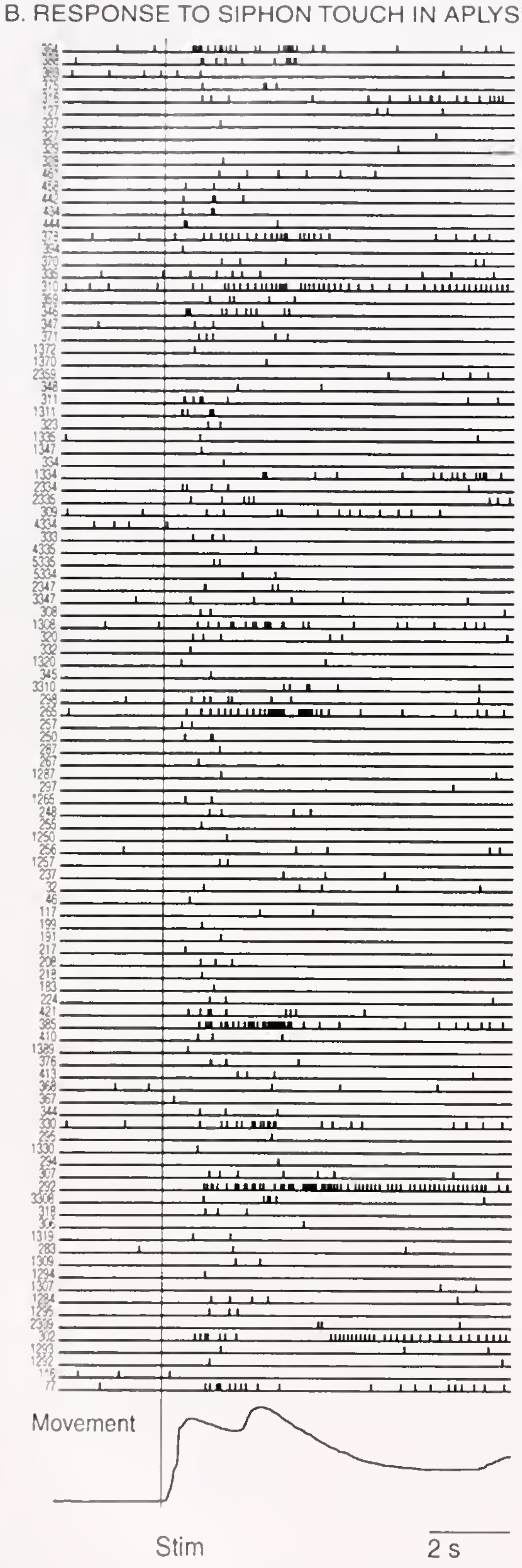

Figure 5. Raster diagram of the action-potential activity recorded optically from an *Aplysia* abdominal ganglion during a gill-withdrawal reflex. The 0.5-s touch to the siphon began at the time of the line labeled STIM. In this recording, activity in 135 neurons was measured. We think this recording is incomplete and that the actual number of active neurons was between 250 and 300. Most neurons are activated by the touch, but one, #4334 (about 1/3 down from the top), was inhibited. This inhibition was seen in repeated trials in this preparation. (Modified from Wu *et al.*, 1994b.)

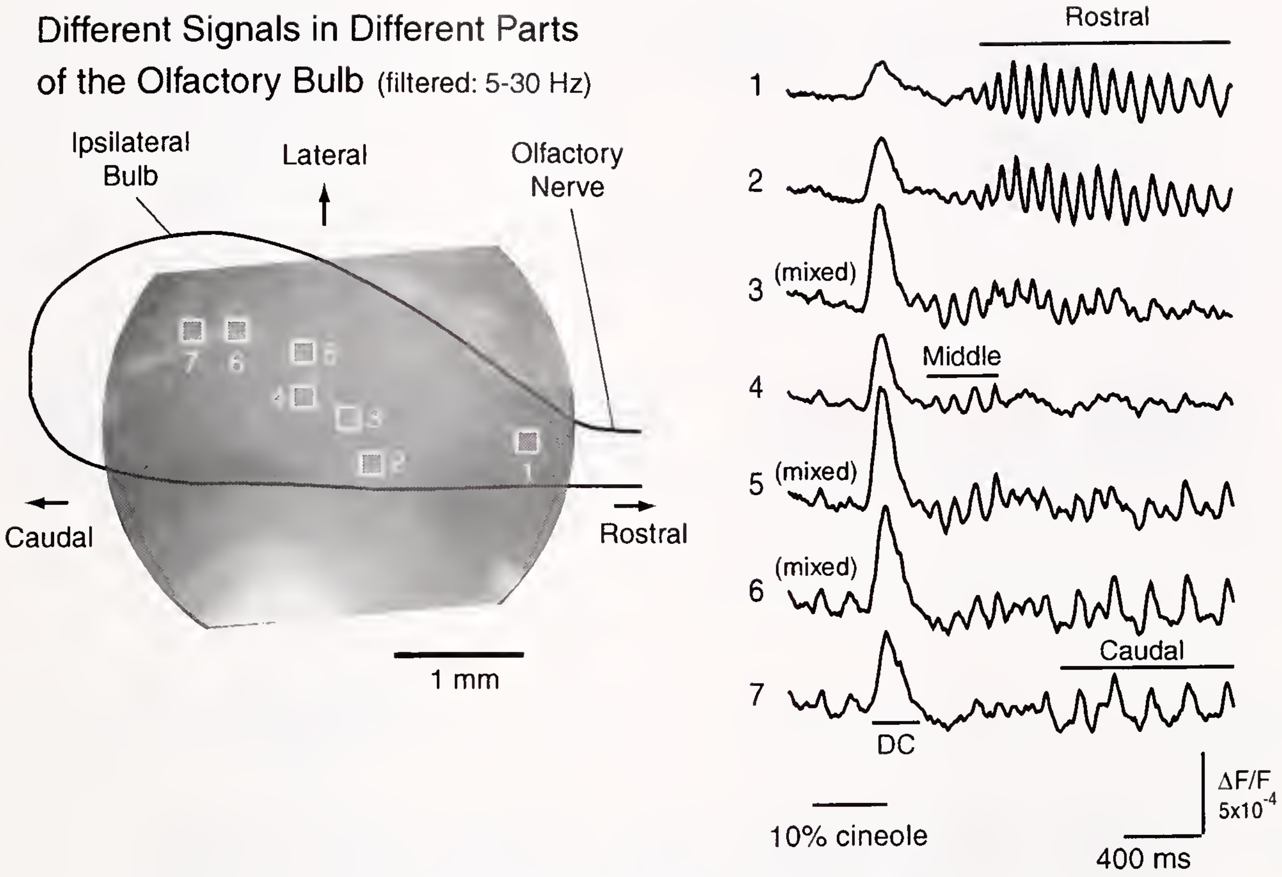

Figure 6. Simultaneous optical recordings from seven areas of an olfactory bulb. An image of the olfactory bulb is shown on the left. Signals from seven selected pixels are shown on the right. The positions of these pixels are labeled with squares and numbers on the image of the bulb. All seven signals have a filtered version of the DC signal at the time indicated by the bar labeled DC. The oscillation in the rostral region has a high frequency and relatively long latency and duration (detectors 1 and 2). The oscillation from the middle region has a high frequency and short latency and duration (detector 4). The oscillation from the caudal region has a lower frequency and the longest latency (detector 7). The signal from detectors between these regions (3, 5, and 6) appears to contain a mixture of two components. The horizontal line labeled "10% cineole" indicates the time of the command pulse to the odor solenoid. The data are filtered by a high-pass digital RC (5 Hz) and low-pass Gaussian (30 Hz) filters. (Modified from Lam *et al.*, 2000.)

able to speculate that oscillations may be important in perception. Our data show that the odor-induced oscillations in the olfactory bulb are substantially more complicated than had been anticipated and that multiple functional population domains are processing olfactory input in parallel.

In vivo *mammalian brain.* Population signals are more difficult to measure from *in vivo* mammalian preparations than from the turtle because the noise from the heartbeat and respiration is greater and because staining is more difficult. Two methods for reducing the movement artifacts from the heartbeat are, together, quite effective. First, a subtraction procedure is used in which two recordings are made but only one of the trials has a stimulus (Orbach *et al.*, 1985). Both recordings are triggered from the upstroke of the electrocardiogram, so they should have similar heartbeat noise. When the trial without the stimulus is subtracted from the trial with the stimulus, the heartbeat artifact is reduced. Second, an airtight chamber is fixed onto the skull surrounding the craniotomy (Blasdel and Salama, 1986). When this chamber is filled with silicon oil and closed, the movements due to heartbeat and respiration are substantially reduced. In combination, these methods reduce the noise from movement artifacts enough that it is no longer the main source of noise in the measurements.

Methods

The three examples given above involve fractional intensity changes that ranged from 10^{-4} to 3×10^{-2}. To measure these signals, the noise in the measurements had to be an even smaller fraction of the resting intensity. In the sections that

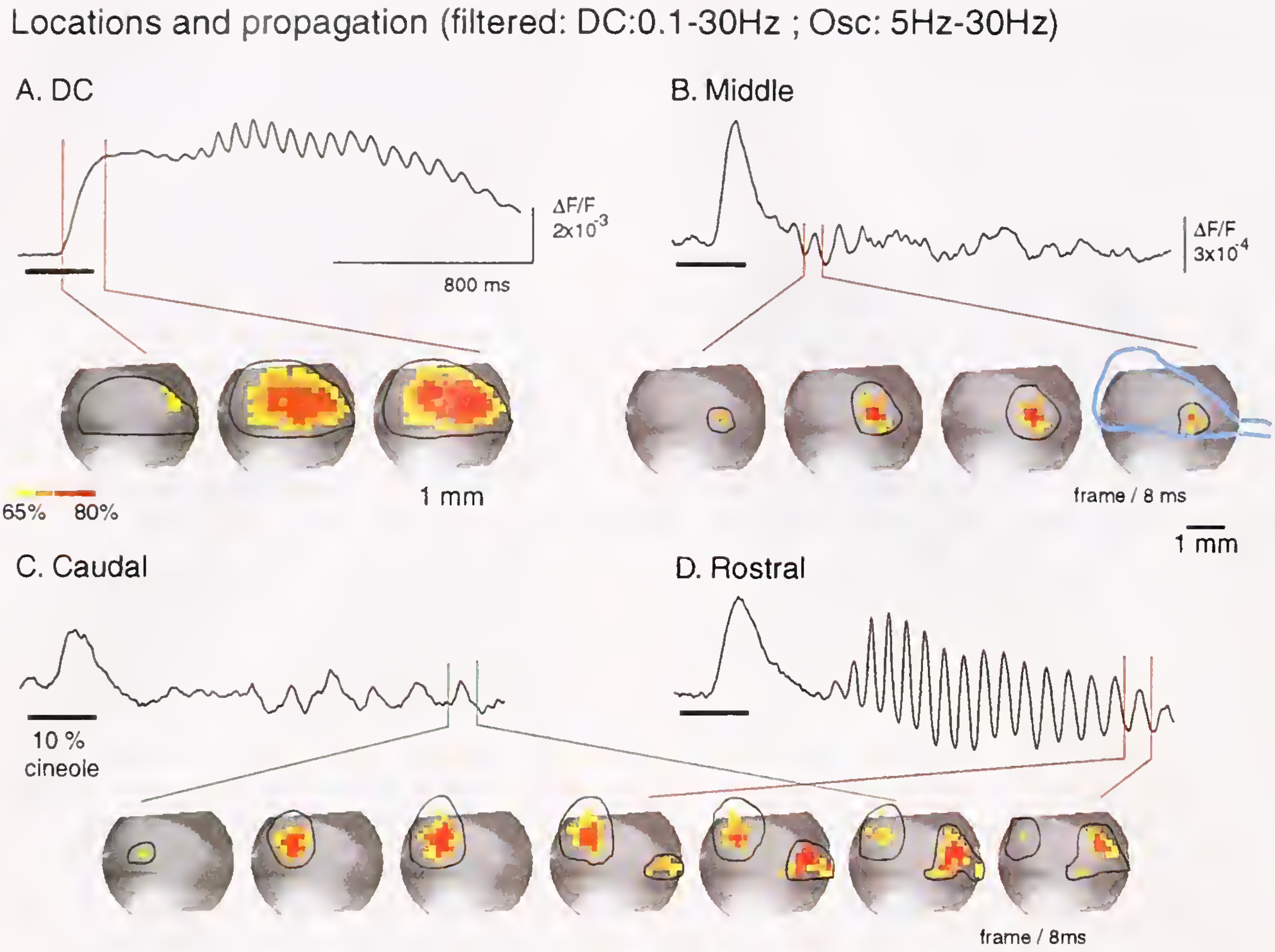

Figure 7. The locations and propagation of the four components from the trial shown in Figure 6. Multiframe pseudo-color displays of the signals are overlaid on the image of the olfactory bulb. The red color and the black contour lines label the areas where the signals are larger than 80% and 20% of the peak. The DC component in this animal covers almost the entire bulb. The other three panels show the position and propagation of one cycle (indicated by the red and green lines) of the three different oscillations. The black horizontal bars indicate the time of the odor command-pulse. The data are filtered by a high-pass digital RC (5 Hz) and low-pass Gaussian (30 Hz) filters. (Modified from Lam *et al.*, 2000.)

follow, some of the considerations necessary to achieve such a low noise are outlined. Two topics that were discussed in earlier reviews will not be covered here: first, evidence showing that these optical signals are fast and potential-dependent; second, evidence that pharmacological effects and photodynamic damage resulting from the voltage-sensitive dyes are manageable (see, *e.g.*, Cohen and Salzberg, 1978; Waggoner, 1979; Salzberg, 1983; Sakai *et al.*, 1985; Cohen and Lesher, 1986; Grinvald *et al.*, 1988; Momose-Sato *et al.*, 1995).

Signal Type

Sometimes it is possible to decide in advance which kind of optical signal will give the best signal-to-noise ratio, but in other situations an experimental comparison is necessary. The choice of signal type often depends on the optical characteristics of the preparation. Birefringence signals are relatively large in preparations that, like axons, are cylindrical and have a radial optic axis. However, in preparations with spherical symmetry (*e.g.*, cell soma), the birefringence signals in adjacent quadrants cancel (Boyle and Cohen, 1980).

Thick preparations (*e.g.*, mammalian cortex) also dictate the choice of signal. In this circumstance transmitted light measurements are not easy (a subcortical implantation of a light guide would be necessary), and the small size of the absorption signals that are detected in reflected light (Ross *et al.*, 1977; Orbach and Cohen, 1983) means that fluorescence is optimal (Orbach *et al.*, 1985).

Another factor that affects the choice of absorption or fluorescence is that the signal-to-noise ratio in fluorescence is more strongly degraded by dye bound to extraneous

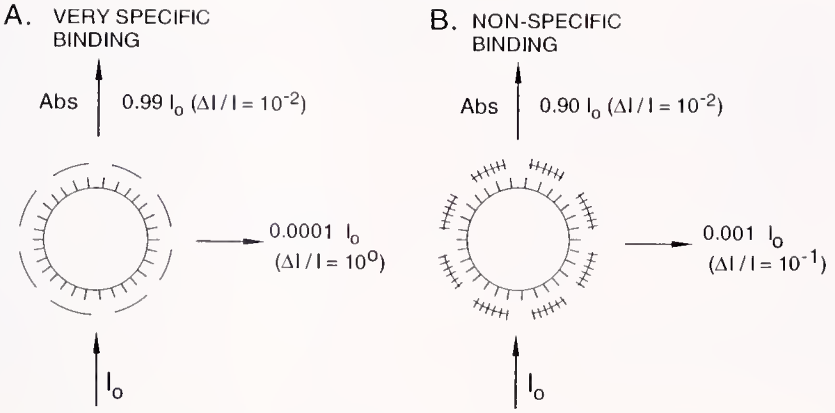

Figure 8. (A) The light transmission and fluorescence intensity when only a neuron binds dye and (B) when both the neuron and extraneous material binds dye. In (A), assuming that one dye molecule is bound for every 2.5 phospholipid molecules, 0.99 of the incident light is transmitted. If a change in membrane potential causes the dye to disappear, the fractional change in transmission is 1%, but in fluorescence it is 100%. In (B), nine times as much dye is bound to extraneous material. Now the transmitted intensity is reduced to 0.9, but the fractional change is still 1%. The fluorescence intensity is increased 10-fold, and therefore the fractional change is reduced by the same factor. Thus, extraneously bound dye degrades fluorescence fractional changes and signal-to-noise ratios more rapidly. (Redrawn from Cohen and Lesher, 1986.)

material. Figure 8 illustrates a spherical cell surrounded by extraneous material. In Figure 8A, dye is bound only to the cell; in 8B, there is 10 times as much dye bound to extraneous material. To calculate the transmitted intensity in Figures 8A and B, we assume that there is one dye molecule for every 2.5 phospholipid molecules and a large extinction coefficient (10^5). The amount of light absorbed by the cell is still only 0.01 of the incident light I_o and thus the transmitted light is 0.99 I_o. Thus, even if this dye completely disappeared due to a change in potential, the fractional change in transmission, $\Delta I/I_o$, would be only 1% (10^{-2}). The amount of light reaching the photodetector in fluorescence is much lower, say 0.0001 I_o, but even so, disappearance of dye would result in a 100% decrease in fluorescence, a fractional change of 10^0. Thus, in situations in which dye is bound only to the cell membrane and only one cell is in the light path, the fractional change in fluorescence is much larger than the fractional change in transmission.

However, the relative advantage of fluorescence is reduced if dye binds to extraneous material. When 10 times as much dye is bound to the extraneous material as was bound to the cell membrane (Fig. 8B), the transmitted intensity is reduced to about 0.9 I_o, but the fractional change in transmission is nearly unaffected. In contrast, the resting fluorescence is now higher by a factor of 10, and the fractional fluorescence change is reduced by the same factor. It does not matter whether the extraneous material is connective tissue, glial membrane, or neighboring neuronal membranes.

In Figure 8B, the fractional change in fluorescence was still larger than in transmission. However, in fluorescence, the light intensity was about 10^3 smaller, which reduces the signal-to-noise ratio. Partly because of the signal degradation due to extraneous dye, fluorescence signals have most often been used in monitoring activity from tissue-cultured neurons. Both fluorescence and absorption signals have been used in measurements from ganglia and brain slices. Fluorescence has always been used in measurements from intact brains.

Dyes

Several voltage-sensitive dyes have been used to monitor changes in membrane potential in a variety of preparations. Figure 9 illustrates four different chromophores: for each, about 100 analogs were synthesized in an attempt to optimize the signal-to-noise ratio that can be obtained in a variety of preparations. This screening was made possible by the efforts of three laboratories: Jeff Wang, Ravender Gupta, and Alan Waggoner, then at Amherst College; Rina Hildesheim and Amiram Grinvald at the Weizmann Institute; and Joe Wuskell and Leslie Loew at the University of Connecticut Health Center.

For each of the four chromophores, 10 or 20 dyes gave roughly the same signal size on squid axons (Gupta *et al.*, 1981). Unfortunately, they often gave very different responses on other preparations, so that several dyes had to be tested. Often, dyes that worked well in squid did poorly in other preparations because they failed to penetrate through connective tissue or along intercellular spaces to the membrane of interest. Others dyes appeared to have a relatively low affinity for neuronal *versus* non-neuronal tissue. Finally, in some cases, the dye penetrated well and the stain-

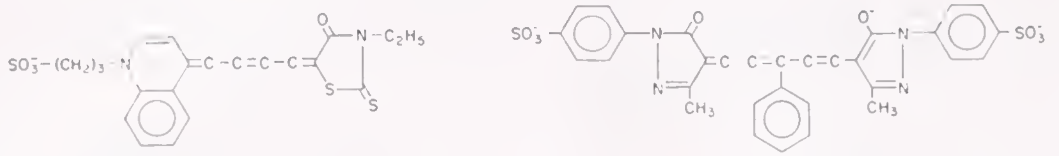

XVII, Merocyanine, Absorption, Birefringence

RH155, Oxonol, Absorption

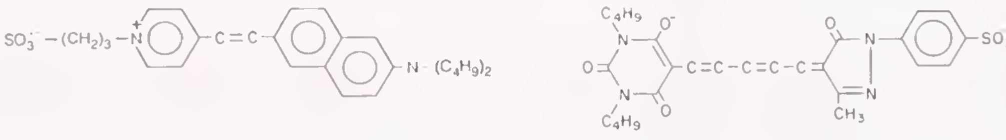

Di-4-ANEPPS, Styryl, Fluorescence

XXV, Oxonol, Fluorescence, Absorption

Figure 9. Examples of four different chromophores that have been used to monitor membrane potential. The merocyanine dye, XVII (WW375), and the oxonol dye, RH155, are commercially available as NK2495 and NK3041 from Nippon Kankoh-Shikiso Kenkyusho Co. Ltd., Okayama, Japan. The oxonol, XXV (WW781) and styryl, di-4-ANEPPS, are available commercially as dye R-1114 and D-1199 from Molecular Probes, Junction City, Oregon.

ing appeared to be specific, but nonetheless the signals were small.

The voltage-sensitive dye signals discussed in this article are presented as the fractional intensity change ($\Delta I/I$). These signals give information about the time course of the potential change but no direct information about its magnitude. In some instances, indirect information about the magnitude of the voltage change can be obtained (*e.g.*, Orbach *et al.*, 1985; Delaney *et al.*, 1994; Antic and Zecevic, 1995). Another approach is the use of ratiometric measurements at two independent wavelengths (Gross *et al.*, 1994). However, to determine the amplitude of the voltage change from a ratio measurement, one must know the fraction of the fluorescence that results from dye not bound to active membrane, a requirement that is only approximately met in special circumstances (*e.g.*, tissue culture).

Measuring Technology

Noise.

1. Shot noise. The accuracy with which light can be measured is limited by the shot noise arising from the statistical nature of photon emission and detection. The number of photons emitted per unit time fluctuates, and if an ideal light source (tungsten filament at 3300°F) emits an average of 10^{16} photons/ms, the root-mean-square (RMS) deviation in the number emitted is the square root of this number, or 10^8 photons/ms. The signal-to-noise ratio is directly proportional to the square root of the number of measured photons and inversely proportional to the square root of the bandwidth of the photodetection system (Braddick, 1960; Malmstadt *et al.*, 1974). The basis for the square-root dependence on intensity is illustrated in Figure 10: in 10A, the result of using a random number table to distribute 20 photons into 20 time windows is shown; in 10B, the same procedure was used to distribute 200 photons into the same 20 bins. Relative to the average light level, there is more noise in the top trace (20 photons) than in the bottom trace (200 photons). The measured signal-to-noise ratios are listed on the right side of Figure 10, and we show that the improvement from A to B is similar to that expected from the square-root relationship. This square-root relationship is indicated by the dotted line in Figure 11, which plots the light intensity divided by the noise in the measurement *versus* the light intensity. In a shot-noise–limited measurement, the signal-to-noise ratio can only be improved by (a) increasing the illumination intensity, (b) increasing the light-gathering efficiency of the measuring system, or (c) reducing the bandwidth.

Because only a small fraction of the 10^{16} photons/ms emitted by a tungsten filament is measured, a signal-to-noise ratio of 10^8 (see above) cannot be achieved. A partial listing of the light losses follows. A 0.9-NA lamp collector lens would collect 0.1 of the light emitted by the source. Only 0.2 of that light is in the visible wavelength; the remainder is infrared (heat). Limiting the incident wavelengths to those that have the signal means that only 0.1 of the visible light is used. Thus, the light reaching the preparation might typically be reduced to 10^{13} photons/ms. If the

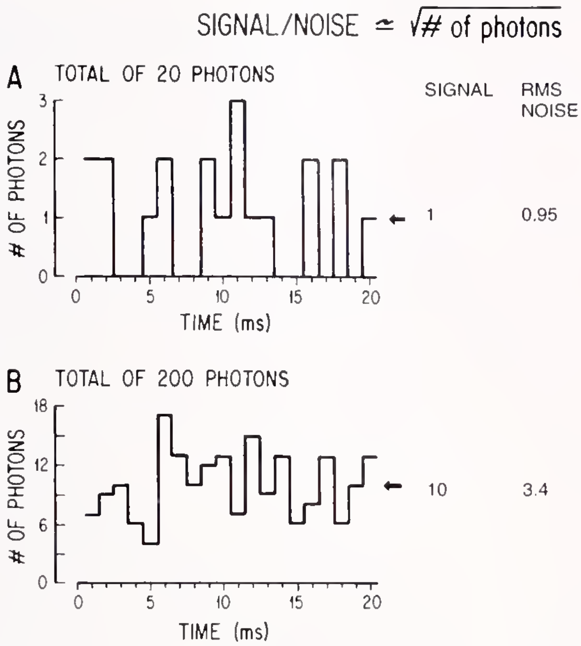

	SIGNAL	RMS NOISE	SIGNAL /NOISE	RATIO OF S/N	PREDICTED S/N RATIO
A	1	0.95	1.05		
				2.8	3.2
B	10	3.4	2.94		

Figure 10. Plots of the results of using a table of random numbers to distribute 20 photons (top, A) or 200 photons (bottom, B) into 20 time bins. The result illustrates that when more photons are measured, the signal-to-noise ratio is improved. On the right, the signal-to-noise ratio is measured for the two results. The ratio of the two signal-to-noise ratios was 0.43, which is close to the value predicted by the relationship that the signal-to-noise ratio is proportional to the square root of the measured intensity. (Redrawn from Wu and Cohen, 1993.)

light-collecting system that forms the image is efficient (*e.g.*, in an absorption measurement), about 10^{13} photons/ms reach the image plane. (In a fluorescence measurement much less light is measured because (a) only a fraction of the incident photons are absorbed by the fluorophores, (b) only a fraction of the absorbed photons appear as emitted photons, and (c) only a fraction of the emitted photons are collected by the objective.) If the camera has a quantum efficiency of 1.0, then, in absorption, a total of 10^{13} photoelectrons/ms are measured. With a camera of 1000 pixels, there are 10^{10} photoelectrons/ms/pixel. The shot noise is 10^5 photoelectrons/ms/pixel; thus the best that can be expected is a relative noise 10^{-5} of the resting light (a signal-to-noise ratio of 100 db). The extra light losses in a fluorescence measurement further reduce the maximum obtainable signal-to-noise ratio.

One way to compare the performance of camera systems and to understand their deviations from optimal (shot-noise–limited) is to determine the light intensity divided by the noise in the measurement and plot that value against the number of photons reaching the photodetector. The dotted line in Figure 11 is such a plot for the ideal case. At high light intensities this ratio is large, and thus small changes in intensity can be detected. For example, at 10^{10} photons/ms, a fractional intensity change of 0.1% can be measured with a signal-to-noise ratio of 100. On the other hand, at low intensities, the ratio of intensity divided by noise is small, and only large signals can be detected. For example, at 10^4 photons/ms, the same fractional change of 0.1% can be measured with a signal-to-noise ratio of 1 only after averaging 100 trials.

In addition, Figure 11 compares the performance of two camera systems, a photodiode array (solid lines) and a cooled CCD camera (dashed lines), with the shot-noise ideal. The photodiode array approaches the shot-noise limitation over the range of intensities from 3×10^6 to 10^{10} photons/ms. This is the range of intensities obtained in absorption measurements and fluorescence measurements on *in vitro* slices and intact brains. On the other hand, the cooled CCD camera approaches the shot-noise limit over the range of intensities from 5×10^3 to 5×10^6 photons/ms. This is the range of intensities obtained from fluorescence experiments on individual cells and neurons. In the discussion that follows we indicate the aspects of the measurements and the characteristics of the two camera systems that cause them to deviate from the shot-noise ideal. The camera sys-

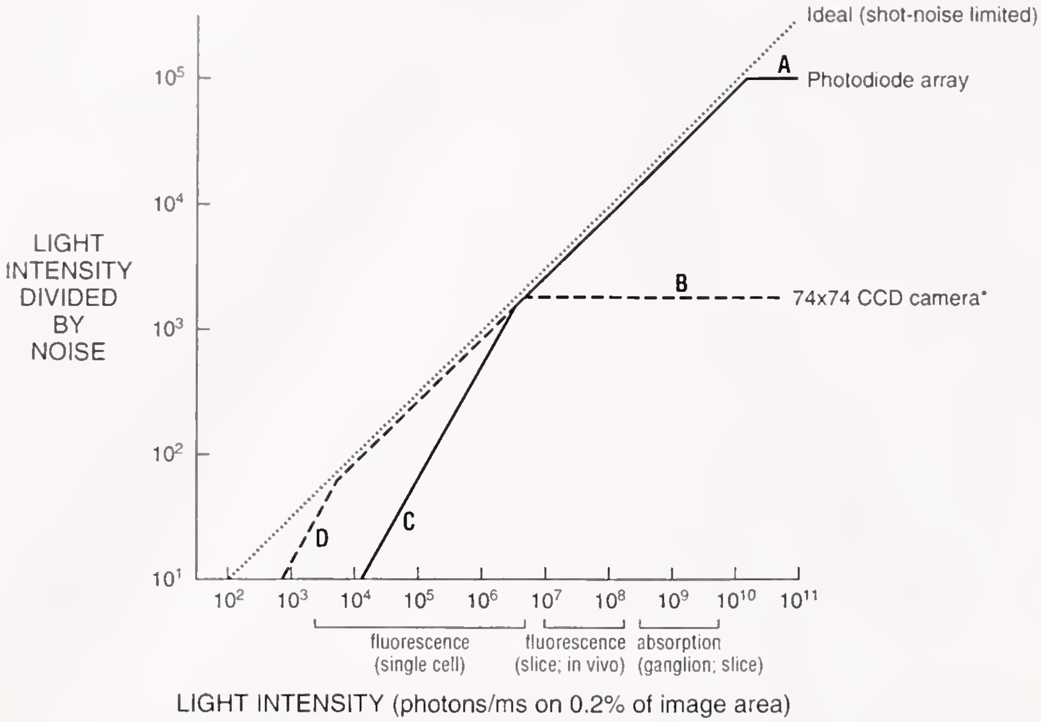

* Cooled, back illuminated, 2kHz frame rate, well size $2{\bullet}10^5$ photoelectrons (10 pixels=0.2% of image area)

Figure 11. The ratio of light intensity divided by the noise in the measurement as a function of light intensity in photons per millisecond for each 0.2% of the object plane. The theoretical optimum signal-to-noise ratio (dotted line) is the shot-noise limit. Two camera systems are shown, a photodiode array with 464 pixels (solid lines) and a cooled, back-illuminated CCD camera with a 2-kHz frame rate and a 74 × 74 pixel resolution (dashed lines). The photodiode array provides an optimal signal-to-noise ratio at higher intensities, whereas the CCD camera is better at lower intensities. The approximate light intensity per detector in fluorescence measurements from a single neuron, fluorescence measurements from a slice or *in vivo* preparation, and in absorption measurements from a ganglion or a slice is indicated along the x axis. The signal-to-noise ratio for the photodiode array falls away from the ideal at high intensities (A) because of extraneous noise and at low intensities (C) because of dark noise. The lower dark noise of the cooled CCD allows it to function at the shot-noise limit at lower intensities until read noise dominates (D). The CCD camera saturates at intensities above 5×10^6 photons/ms/0.2% of the object plane.

tems illustrated in Figure 11 have relatively good dark noise and saturation characteristics; other cameras would be dark-noise–limited at higher light intensities and would saturate at lower intensities.

2. Extraneous noise. A second type of noise, termed extraneous, or technical, noise, is more apparent at high light intensities at which the sensitivity of the measurement is high because the fractional shot noise and dark noise are low. One source of extraneous noise is fluctuations in the output of the light source (see below). Two other sources are vibrations and movement of the preparation. A number of precautions for reducing vibrational noise have been described (Salzberg *et al.*, 1977; London *et al.*, 1987). The pneumatic isolation mounts on many vibration isolation tables reduce vertical vibrations more efficiently than they reduce horizontal movements. We now use air-filled tubes made of soft rubber (Newport Corp, Irvine, CA). Nevertheless it has been difficult to reduce vibrational noise to less than 10^{-5} of the total light. With this amount of vibrational noise, increases in measured intensity beyond 10^{10} photons/ms would not improve the signal-to-noise ratio. Because of vibrational noise, the performance of the photodiode array system is shown reaching a ceiling in Figure 11 (segment A, solid line).
3. Dark noise. Dark noise degrades the signal-to-noise ratio at low light levels. Because the CCD camera is cooled, its dark noise is substantially lower than that of the photodiode array system. The excess dark noise in photodiode array explains why segment C in Figure 11 is substantially to the right of segment D.

Light sources. Three kinds of sources have been used. Tungsten filament lamps are a stable source, but their intensity is relatively low, particularly at wavelengths less than 450 nm. Arc lamps are somewhat less stable but can provide more intense illumination. Until recently, measurements made with laser illumination have been substantially noisier.

1. Tungsten filament lamps. It is not difficult to provide a power supply stable enough that the output of the bulb fluctuates by less than 1 part in 10^5. In absorption measurements, where the fractional changes in intensity are relatively small, only tungsten filament sources have been used. In contrast, fluorescence measurements often have larger fractional changes that will better tolerate light sources with systematic noise, and the measured intensities are lower, making improvements in signal-to-noise ratio from brighter sources attractive.
2. Arc lamps. Opti-Quip, Inc., provides 150-W and 250-W xenon power supplies, lamp housings, and arc lamps with noise in the range of 1 part in 10^4. At 520 ± 45 nm, the 150-W bulb yielded 2–3 times more light than a tungsten filament bulb, and the 250-W bulb was 2–3 times brighter than the 150-W bulb. The extra intensity is especially useful for fluorescence measurements from single neurons. If the dark noise is dominant, then the signal-to-noise ratio improves linearly with intensity; if the shot noise is dominant, the ratio improves as the square root of intensity (Fig. 11).
3. Lasers. It has been possible to take advantage of one characteristic of laser sources. In preparations with minimal light scattering, the laser output can be focused onto a small spot, allowing measurement of membrane potential from small processes in tissue-cultured neurons (Bullen *et al.*, 1997). However, there may be excess noise due to laser speckle (Dainty, 1984).

Optics.

1. Numerical aperture. The need to maximize the number of measured photons has also been a dominant factor in the choice of optical components. In epifluorescence, both the excitation light and the emitted light pass through the objective, and the intensity reaching the photodetector is proportional to the fourth power of the numerical aperture (Inoue, 1986).
2. Objective efficiency. Direct comparison of the intensity reaching the image plane has shown that the light-collecting efficiency of an objective is not completely determined by the stated magnification and NA. Lenses of the same specification can differ by a factor of 5. We presume that these differences depend on the number of lenses, the coatings, and absorbances of glasses and cements. We recommend empirical tests of several lenses for efficiency.

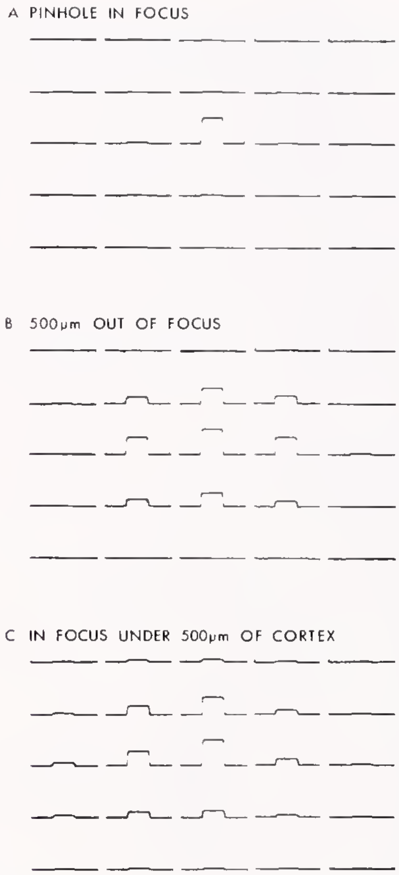

Figure 12. Effects of focus and scattering on the distribution of light from a point source onto the array. (A) A 40-μm pinhole in aluminum foil covered with saline was illuminated with light at 750 nm. The pinhole was in focus. More than 90% of the light fell on one detector. (B) The stage was moved downward by 500 μm. Light from the out-of-focus pinhole was now seen on several detectors. (C) The pinhole was in focus but covered by a 500-μm slice of salamander cortex. Again the light from the pinhole was spread over several detectors. A 10 × 0.4 NA objective was used. Kohler illumination was used before the pinhole was placed in the object plane. The recording gains were adjusted so that the largest signal in each of the three trials would be approximately the same size in the figure. (Redrawn from Orbach and Cohen, 1983.)

3. Depth of focus. Salzberg *et al.* (1977) determined the effective depth of focus for a 0.4-NA objective lens by recording an optical signal from a neuron when it was in focus and then moving the neuron out of focus by various distances. The neuron had to be moved 300 μm out of focus to reduce the size of the signal by 50%. (This result is obtained only when the diameter of the neuron image and the diameter of the detector are similar.) With 0.5-NA optics, a 50% reduction was obtained at 100 μm out of focus (Kleinfeld and Delaney, 1996).
4. Light scattering and out-of-focus light. Light scattering can limit the spatial resolution of an optical measurement. London *et al.* (1987) measured the

scattering of 705-nm light in *Navanax* buccal ganglia. Inserting a ganglion in the light path caused light from a 30-μm spot to spread so that the diameter of the circle of light that included intensities greater than 50% of the total was roughly 50 μm. The spread was greater, to about 100 μm, with light of 510 nm. Figure 12 illustrates the results of similar experiments on the olfactory bulb of the salamander. When no tissue is present, essentially all of the light (750 nm) from a small spot falls on one detector (top of figure); when a 500-μm-thick slice of olfactory bulb is present, the light from the small spot is spread to about 200 μm (bottom of figure). Scattering appears to be greater with mammalian cortex than with olfactory bulb. Thus, light scattering blurs signals in adult vertebrate preparations.

A second source of blurring is signal from regions that are out of focus. For example, if the active region is a cylinder (a column) perpendicular to the plane of focus, and the objective is focused at the middle of the cylinder, then the light from the in-focus plane has the correct diameter at the image plane. However, the light from the regions above and below is out of focus, and its diameter is too large. The middle section of Figure 12 illustrates the effect of moving the small spot of light 500 μm out of focus: the light is spread to about 200 μm. Thus, in preparations with considerable scattering or with out-of-focus signals, the spatial resolution may be limited by the preparation and not by the number of pixels in the imaging device.

Comparison of voltage-sensitive dye and local field potential measurements of population signals. The results in Figure 12 suggest that the spatial resolution of a population signal in a vertebrate brain is limited to about 200 μm by light scattering and out-of-focus signals. This spatial resolution is substantially better than that obtained by recording local field potentials from the surface of the brain. Because the current sources driving these potentials can be below the surface, the spatial patterns are smoothed by the volume-conductor properties of the cortical tissue. Freeman (1978)

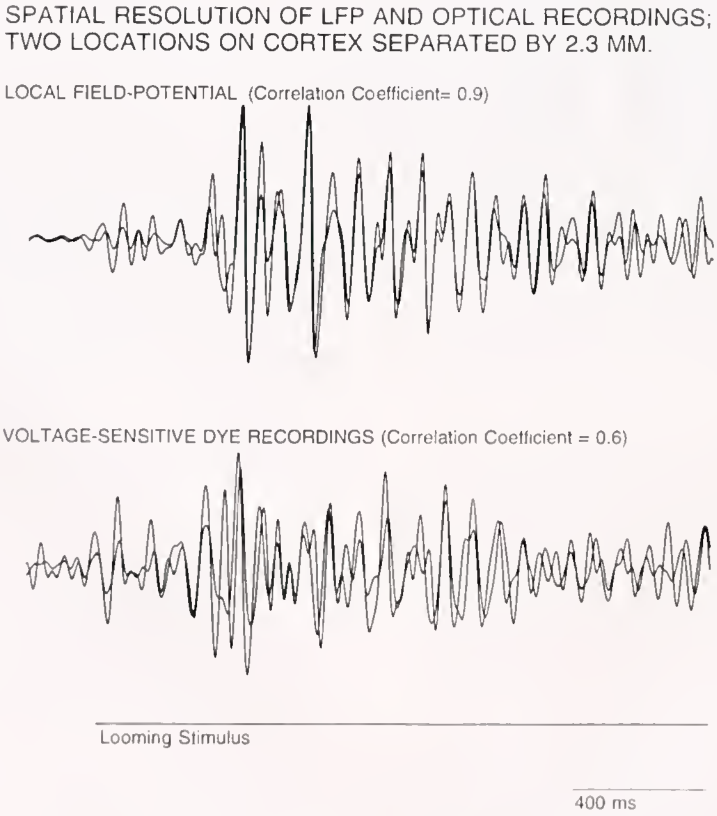

Figure 13. Comparison of simultaneous optical and local-field-potential recordings from two positions on turtle visual cortex that were separated by 2.3 mm. The top pair of superimposed traces are the local-field-potential recordings from the two sites. The bottom pair of traces are the voltage-sensitive-dye recordings from the two sites. There is much less overlap in the optical recordings. Thus, the voltage-sensitive dye recordings have better spatial resolution. Both sets of recordings were band-pass filtered (10–30 Hz). (J. Prechtl, L. B. Cohen, and D. Kleinfeld, unpubl. data.)

reported that spatial Fourier transforms from local field potential measurements had a sharp cutoff at about 1 cycle/mm, suggesting a resolution on the order of 1 mm. Similarly, in the frequency range below 30 Hz, Bullock and McClune (1989) reported a correlation of about 0.9 between two local field potential electrodes spaced 2–3 mm apart on the surface of the brain.

We compared the spatial resolution of the two kinds of measurements by examining simultaneous pairs of recordings from two positions on turtle visual cortex that were separated by 2.3 mm. The top pair of superimposed traces in Figure 13 are the local field potentials. The recordings from the two sites show considerable overlap; the correlation coefficient was 0.9. The bottom pair of traces are the voltage-sensitive dye recordings. These show less overlap—their correlation coefficient was 0.6. Thus, the spatial differences are less blurred with the optical recordings than with the electrode recordings.

We estimated the relative spatial resolution of the two methods by determining the distance on the cortex at which the correlation coefficients would be equal for a pair of voltage-sensitive dye recordings and a pair of local field potential recordings. In six trials from two preparations the correlation coefficients were equal when the two optical measurements were a distance apart that was 0.21 ± 0.05 (SEM) of the distance of the two electrodes. Thus, the optical measurement has a linear spatial resolution about 5 times better than the electrode measurement and a two-dimensional resolution about 25 times better.

Confocal and two-photon microscopes. The confocal microscope (Petran and Hadravsky, 1966) substantially reduces both the scattered and out-of-focus light that contributes to the image. A recent modification using two-photon excitation of the fluorophore further reduces out-of-focus fluorescence and photobleaching (Denk *et al.*, 1995). The spatial resolution of images from intact vertebrate preparations is much better with these types of microscope than with ordinary microscopy. These microscopes have been successfully used to monitor changes in calcium concentration inside small processes of neurons (Eilers *et al.*, 1995; Yuste and Denk, 1995). However, at present the sensitivity of these microscopes is relatively poor and they are relatively slow; there are no reports of their use to measure the small signals obtained with voltage-sensitive dyes of the type discussed in this article. On the other hand, slower voltage-sensitive dye signals have been measured confocally (Loew, 1993).

Random-access fluorescence microscopy. Bullen *et al.* (1997) have used acousto-optic deflectors to construct a random-scanning microscope and were able to measure signals from parts of cultured hippocampal neurons. To reduce the effects of fluctuations in the laser output, the fluorescence signals were divided by the output of a photodetector sampling the incident light. Relatively large signal-to-noise ratios were obtained using voltage-sensitive dyes. This method has the advantage that only a small proportion of the preparation is illuminated, thereby reducing photodynamic damage from the very bright laser light source. However, this method will probably be restricted to preparations such as cultured neurons, in which there is relatively little light scattering.

Photodetectors. Because the signal-to-noise ratio in a shot-noise–limited measurement is proportional to the square root of the number of photons converted into photoelectrons (see above), quantum efficiency is important. Silicon photodiodes have quantum efficiencies approaching the ideal (1.0) at wavelengths at which most dyes absorb or emit light (500–900 nm). In contrast, only specially chosen vacuum photocathode devices (phototubes, photomultipliers, or image intensifiers) have a quantum efficiency as high as 0.15. Thus, in shot-noise–limited situations, a silicon diode has a signal-to-noise ratio that is at least 2.5 times larger. Photographic film has an even smaller quantum efficiency (0.01; Shaw, 1979), and thus has not been used for the kinds of measurements discussed in this paper.

Imaging devices. Many factors must be considered in choosing an imaging system. Perhaps the most important are the requirements for spatial and temporal resolution. Because the signal-to-noise ratio in a shot-noise–limited measurement is proportional to the number of measured photons, increases in either temporal or spatial resolution reduce the signal-to-noise ratio. Our discussion considers systems that have frame rates near 1 kHz. In most of these systems, the camera has been placed in the objective image plane of a microscope. However, Tank and Ahmed (1985) suggested a scheme by which a hexagonal close-packed array of optical fibers is positioned in the image plane, and individual photodiodes are connected to the other end of the optical fibers. NeuroPlex, a 464-pixel photodiode array camera (RedShirtImaging, LLC, Fairfield, CT) is based on this scheme.

Silicon diode arrays.

1. Parallel readout arrays. Diode arrays with from 124 to 1020 elements are now used in several laboratories (*e.g.*, Iijima *et al.*, 1989; Zecevic *et al.*, 1989; Nakashima *et al.*, 1992; Hirota *et al.*, 1995). In addition, Hammamatsu has constructed a system with 2500 elements. These arrays are designed for parallel readout; each detector is followed by its own amplifier, whose output can be digitized at frame rates of 1 kHz. Although the need to provide a separate amplifier for each diode element limits the number of pixels in parallel read-out systems, it contributes to the very large (10^5) dynamic range that these systems can achieve. Amplifiers have been discussed by Wu and Cohen (1993). Two parallel readout array systems are commercially available: Argus-50 (256 pix-

Table 1

Characteristics of fast CCD camera systems (as reported by the manufacturer)

Camera system	Frame rate (HZ) full frame	Well size (×1000 e)	Read noise (electrons)	Back illum.	Bits a-to-d	Pixels
BrainVision[1]	1600				12	92 × 64
Dalsa CA-D1-0128[2]	756				12	128 × 128
LSR, NeuroCAM UltraPix[3]	500	300	5 @ 100 Hz	yes	12	80 × 80
RedShirtImaging NeuroCCD[4]	2700	200	35 @ 1000 Hz	yes	14	74 × 74
TILL Photonics, IMAGO[5]	140	35	14 @ 140 Hz	no	12	160 × 120

A blank space indicates that the data were not available. The World Wide Web sites listed below were accessed on 15 November 1999.

[1] www.brainVision.co.jp

[2] www.dalsa.com

[3] www.lsr.co.uk/cameras/ultragraph.htm

[4] www.redshirtimaging.com

[5] www.till-photonics.com

els), manufactured by Hammamatsu Photonics K.K. (www.hpk.co.jp), and NeuroPlex (464 pixels), by RedShirtImaging, LLC (www.redshirtimaging.com).

2. Serial readout arrays. Use of a serial readout greatly reduces the number of amplifiers. In addition, it is simple to cool CCD (charge-coupled device) chips to reduce the dark noise. However, because of saturation, presently available CCD cameras are not optimal for the higher intensities available in some neurobiological experiments (Fig. 11). The high-intensity limit of the CCD camera is set by the light intensity that fills the electron wells on the CCD chip. This accounts for the bending over of the CCD camera performance at segment B in Figure 11. A dynamic range of even 10^3 is not easily achieved with a CCD camera. A CCD camera will not be optimal for measurements of absorption or for fluorescence measurements on *in vitro* slices and intact brains in measurements where all of the membranes are stained (Fig. 11). The light intensity would have to be reduced, with a consequent decrease in signal-to-noise ratio. On the other hand, CCD cameras are close to ideal for measurements from individual neurons stained with internally injected dyes. Table 1 compares several CCD cameras with frame rates near 1 kHz.
3. Vacuum photocathode cameras. Although the lower quantum efficiencies of vacuum photocathodes are a disadvantage, these devices may have lower dark noise. One such device, a Radechon (Kazan and Knoll, 1968), has an output proportional to the changes in the input. Vacuum photocathode cameras have been used in relatively low time resolution recordings from mammalian cortex (Blasdel and Salama, 1986) and salamander olfactory bulb (Kauer, 1988; Cinelli *et al.*, 1995) and are used in the Imager 2001, Optical Imaging, Inc. (www.opt-imaging.com).

Future Directions

Improvements in Sensitivity

Because the apparatus for measuring light is already reasonably optimized (see above), large improvements in the sensitivity of the techniques that use voltage-sensitive dyes must come from the development of better dyes or from investigating signals from other optical properties of the dyes. The dyes in Figure 9 and most of those synthesized are of the general class named polyenes (Hamer, 1964), a group that was first used to extend the wavelength response of photographic film. It is possible that improvements in signal size can be obtained with new polyene dyes (see Waggoner and Grinvald, 1977, and Fromherz *et al.*, 1991, for a discussion of maximum possible fractional changes in absorption and fluorescence). On the other hand, the fractional change on squid axons has not increased in recent years (Gupta *et al.*, 1981; L. B. Cohen, A. Grinvald, K. Kamino, and B. M. Salzberg, unpub. data), and most improvements (*e.g.*, Grinvald *et al.*, 1982b; Momose-Sato *et al.*, 1995; Tsau *et al.*, 1996; Antic and Zecevic, 1995) have involved synthesizing analogs that work well on new preparations.

The best of the styryl and oxonol polyene dyes have fluorescence changes of 10%–20%/100 mV when the staining is specific to the membrane whose potential is changing (Grinvald *et al.*, 1982b; Loew *et al.*, 1992; Rohr and Salzberg, 1994). Recently, Gonzalez and Tsien (1995) introduced a new scheme for generating voltage-sensitive signals using two chromophores and energy transfer. Although these fractional changes were also in the range of 10%/100 mV, more recent results are about 30% (J. Gonzalez and R. Tsien, pers. comm.). However, because one of the chromophores must be very hydrophobic and does not penetrate into brain tissue, it has not been possible to measure signals with this pair of dyes in intact tissues (T. Gonzalez and R. Tsien, A. Obaid and B. M. Salzberg; pers. comm.).

Bouevitch *et al.* (1993) and Ben-Oren *et al.* (1996) found that membrane potential changed the generation of nonlinear second harmonics from styryl dyes in cholesterol bilayers and in fly eyes. Large (50%) fractional changes were measured. It is hoped that improvements in the illumination intensity will result in larger signal-to-noise ratios.

Ehrenberg and Berezin (1984) have used resonance Raman to study surface potential; these methods might also be applicable for measuring transmembrane potential.

Improvements in Selectivity

An important new direction is the development of methods for neuron-type–specific staining. Three quite different approaches have been tried. First, the use of retrograde staining has been investigated in the embryonic chick and lamprey spinal cords (Tsau *et al.*, 1996). An identified cell class (motoneurons) was selectively stained. In lamprey experiments, spike signals from individual neurons were sometimes measured (Hickie *et al.*, 1996). Further efforts to optimize this staining procedure are needed. Second is the use of cell-type–specific staining developed for fluorescein by Nirenberg and Cepko (1993). It might be possible to use similar techniques to selectively stain cells with voltage-sensitive or ion-sensitive dyes. Third, Siegel and Isacoff (1997) constructed a genetically encoded combination of a potassium channel and green fluorescent protein. When introduced into a frog oocyte, this molecule had a (relatively slow) voltage-dependent signal with a fractional fluorescence change of 5%. Neuron-type–specific staining would make it possible to determine the role of specific neuron types in generating the input-output function of a brain region.

Optical recordings already provide unique insights into brain activity and organization. Improvements in sensitivity or selectivity would make these methods more powerful.

Acknowledgments

The authors are indebted to their collaborators Vicencio Davila, Amiram Grinvald, Kohtaro Kamino, Les Loew, Bill Ross, Brian Salzberg, Alan Waggoner, Jian-young Wu, and Joe Wuskell for numerous discussions about optical methods. The experiments carried out in our laboratories were supported by NIH grant NS08437 and NSF grant IBN-9812301.

Literature Cited

Adrian, E. D. 1942. Olfactory reactions in the brain of the hedgehog. *J. Physiol.* **100:** 459–473.

Albowitz, B., and U. Kuhnt. 1993. Spread of epileptiform potentials in the neocortical slice: recordings with voltage-sensitive dyes. *Brain Res.* **631:** 329–333.

Antic, S., and D. Zecevic. 1995. Optical signals from neurons with internally applied voltage-sensitive dyes. *J. Neurosci.* **15:** 1392–1405.

Antic, S., G. Major, and D. Zecevic. 1999. Fast optical recording of membrane potential changes from dendrites of pyramidal neurons. *J. Neurophysiol.* **82:** 1615–1621.

Ben-Oren, I., G. Peleg, A. Lewis, B. Minke, and L. Loew. 1996. Infrared nonlinear optical measurements of membrane potential in photoreceptor cells. *Biophys. J.* **71:** 1616–1620.

Beuerman, R. W. 1975. Slow potentials of the turtle olfactory bulb in response to odor stimulation of the nose. *Brain Res.* **97(1):** 61–78.

Blasdel, G. G., and G. Salama. 1986. Voltage-sensitive dyes reveal a modular organization in monkey striate cortex. *Nature* **321:** 579–585.

Bouevitch, O., A. Lewis, I. Pinevsky, J. Wuskell, and L. Loew. 1993. Probing membrane potential with nonlinear optics. *Biophys. J.* **65:** 672–679.

Boyle, M. B., and L. B. Cohen. 1980. Birefringence signals that monitor membrane potential in cell bodies of molluscan neurons. *Fed. Proc.* **39:** 2130.

Braddick, H. J. J. 1960. Photoelectric photometry. *Rep. Prog. Physics* **23:** 154–175.

Bullen, A., S. S. Patel, and P. Saggau. 1997. High-speed, random-access fluorescence microscopy: I. High resolution optical recording with voltage-sensitive dyes and ion indicators. *Biophys. J.* **73:** 477–491.

Bullock, T. H., and M. C. McClune. 1989. Lateral coherence of the electrocorticogram: a new measure of brain synchrony. *Electroencephalogr. Clin. Neurophysiol.* **73:** 479–498.

Cinelli, A. R., and B. M. Salzberg. 1992. Dendritic origin of late events in optical recordings from salamander olfactory bulb. *J. Neurophysiol.* **68:** 786–806.

Cinelli, A. R., S. R. Neff, and J. S. Kauer. 1995. Salamander olfactory bulb neuronal activity observed by video rate, voltage-sensitive dye imaging. I. Characterization of the recording system. *J. Neurophysiol.* **73:** 2017–2032.

Cohen, L. B., and S. Lesher. 1986. Optical monitoring of membrane potential: methods of multisite optical measurement. *Soc. Gen. Physiol. Ser.* **40:** 71–99.

Cohen, L. B., and B. M. Salzberg. 1978. Optical measurement of membrane potential. *Rev. Physiol. Biochem. Pharmacol.* **83:** 35–88.

Dainty, J. C. 1984. *Laser Speckle and Related Phenomena.* Springer-Verlag, New York.

Davila, H. V., B. M. Salzberg, L. B. Cohen, and A. S. Waggoner. 1973. A large change in axon fluorescence that provides a promising method for measuring membrane potential. *Nat. New. Biol.* **241:** 159–160.

Davila, H. V., L. B. Cohen, B. M. Salzberg, and B. B. Shrivastav. 1974. Changes in ANS and TNS fluorescence in giant axons from *Loligo. J. Membr. Biol.* **15:** 29–46.

Delaney, K. R., A. Gelperin, M. S. Fee, J. A. Flores, R. Gervais, D. W. Tank, and D. Kleinfeld. 1994. Waves and stimulus-modulated dynamics in an oscillating olfactory network. *Proc. Nat. Acad. Sci.* **91:** 669–673.

Denk, W., D. W. Piston, and W. Webb. 1995. Two-photon molecular excitation in laser-scanning microscopy. Pp. 445–458 in *Handbook of Biological Confocal Microscopy*, J. W. Pawley ed. Plenum Press, New York.

Ehrenberg, B., and Y. Berezin. 1984. Surface potential on purple membranes and its sidedness studied by resonance Raman dye probe. *Biophys. J.* **45:** 663–670.

Eilers, J., G. Callewaert, C. Armstrong, and A. Konnerth. 1995. Calcium signaling in a narrow somatic submembrane shell during synaptic activity in cerebellar Purkinje neurons. *Proc. Nat. Acad. Sci. US* **92:** 10272–10276.

Freeman, W. J. 1978. Spatial Properties of an EEG Event in the Olfactory Bulb and Cortex. *Electroencephalogr. Clin. Neurophysiol.* **44:** 586–605.

Fromherz, P., K. H. Dambacher, H. Ephardt, A. Lambacher, C. O.

Muller, R., Neigl, H. Schaden, O. Schenk, and T. Vetter. 1991. Fluorescent dyes as probes of voltage transients in neuron membranes: progress report. *Ber. Bunsen-Ges. Phys. Chem.* **95:** 1333–1345.

Gonzalez, J. E., and R. Y. Tsien. 1995. Voltage sensing by fluorescence resonance energy transfer in single cells. *Biophys. J.* **69:** 1272–1280.

Grinvald, A., A. Manker, and M. Segal. 1982a. Visualization of the spread of electrical activity in rat hippocampal slices by voltage-sensitive optical probes. *J. Physiol. (Lond)* **333:** 269–291.

Grinvald, A., R. Hildesheim, I. C. Farber, and L. Anglister. 1982b. Improved fluorescent probes for the measurement of rapid changes in membrane potential. *Biophys. J.* **39:** 301–308.

Grinvald, A., B. M. Salzberg, V. Lev-Ram, and R. Hildesheim. 1987. Optical recording of synaptic potentials from processes of single neurons using intracellular potentiometric dyes. *Biophys. J.* **51:** 643–651.

Grinvald, A., R. D. Frostig, E. Lieke, and R. Hildesheim. 1988. Optical imaging of neuronal activity. *Physiol. Rev.* **68:** 1285–1366.

Gross, E., R. S. Bedlack Jr., and L. M. Loew. 1994. Dual-wavelength ratiometric fluorescence measurements of the membrane dipole potential. *Biophys. J.* **67:** 208–216.

Gupta, R. K., B. M. Salzberg, A. Grinvald, L. B. Cohen, K. Kamino, S. Lesher, M. B. Boyle, A. S. Waggoner, and C. H. Wang. 1981. Improvements in optical methods for measuring rapid changes in membrane potential. *J. Membr. Biol.* **58:** 123–137.

Hamer, F. M. 1964. *The Cyanine Dyes and Related Compounds.* Wiley, New York.

Hickie, C., P. Wenner, M. O'Donovan, Y. Tsau, J. Fang, and L. B. Cohen. 1996. Optical monitoring of activity from individual and identified populations of neurons retrogradely labeled with voltage-sensitive dyes. *Soc. Neurosci. Abstr.* **22:** 321.

Hirota, A., K. Sato, Y. Momose-Sato, T. Sakai, and K. Kamino. 1995. A new simultaneous 1020-site optical recording system for monitoring neural activity using voltage-sensitive dyes. *J. Neurosci. Methods* **56:** 187–194.

Hughes, J. R., and J. A. Mazurowski. 1962. Studies on the supracallosal mesial cortex of unanesthetized, conscious mammals. II Monkey. B. Responses from the olfactory bulb. *Electroencephalogr. Clin. Neurophysiol.* **14:** 635–645.

Iijima, T., M. Ichikawa, and G. Matsumoto. 1989. Optical monitoring of LTP and related phenomena. *Soc. Neurosci. Abstr.* **15:** 398.

Inoué, S. 1986. *Video Microscopy.* Plenum Press, New York. p 128.

Kauer, J. S. 1988. Real-time imaging of evoked activity in local circuits of the salamander olfactory bulb. *Nature* **331:** 166–168.

Kazan, B., and M. Knoll. 1968. *Electronic Image Storage.* Academic Press, New York.

Kleinfeld, D., and K. R. Delaney. 1996. Distributed representation of vibrissa movement in the upper layers of somatosensory cortex revealed with voltage-sensitive dyes. *J. Comp. Neurol.* **375:** 89–108.

Kogan, A., W. N. Ross, D. Zecevic, and N. Lasser-Ross. 1995. Optical recording from cerebellar Purkinje cells using intracellularly injected voltage-sensitive dyes. *Brain Res.* **700:** 235–239.

Kupfermann, I., H. Pinsker, V. Castellucci, and E. R. Kandel. 1971. Central and peripheral control of gill movements in *Aplysia. Science* **174:** 1252–1256.

Lam, Y.-w., Lawrence B. Cohen, Matt Wachowiak, and Michal R. Zochowski. 2000. Odors elicit three different oscillations in the turtle olfactory bulb. *J. Neurosci.* In press.

Laurent, G., and M. Naraghi. 1994. Odorant-induced oscillations in the mushroom bodies of the locust. *J. Neurosci.* **14(5 Pt 2):** 2993–3004.

Loew, L. M. 1993. Confocal microscopy of potentiometric fluorescent dyes. *Methods Cell Biol.* **38:** 195–209.

Loew, L. M., L. B. Cohen, B. M. Salzberg, A. L. Obaid, and F. Bezanilla. 1985. Charge-shift probes of membrane potential. Characterization of aminostyrylpyridinium dyes on the squid giant axon. *Biophys. J.* **47:** 71–77.

Loew, L. M., L. B. Cohen, J. Dix, E. N. Fluhler, V. Montana, G. Salama, and J. Y. Wu. 1992. A napthyl analog of the aminostyryl pyridinium class of potentiometric membrane dyes shows consistent sensitivity in a variety of tissue, cell, and model membrane preparations. *J. Memb. Biol.* **130:** 1–10.

London, J. A., D. Zecevic, and L. B. Cohen. 1987. Simultaneous optical recording of activity from many neurons during feeding in *Navanax. J. Neurosci.* **7:** 649–661.

Magee, J. C., and D. Johnston. 1995. Synaptic activation of voltage-gated channels in the dendrites of hippocampal pyramidal neurons. *Science* **268:** 301–304

Magee, J. C., G. Christofi, H. Miyakawa, B. Christie, N. Lasser-Ross, and D. Johnston. 1995. Subthreshold synaptic activation of voltage-gated calcium channels mediate a localized calcium influx into dendrites of hippocampal pyramidal neurons. *J. Neurophysiol.* **74:** 335–342.

Mainen, Z. F., N. T. Carnevalle, A. M. Zador, B. J. Claiborne, and T. H. Brown. 1996. Electronic architecture of hippocampal CA1 pyramidal neurons based on three-dimensional reconstructions. *J. Neurophysiol.* **76:** 1904–1923.

Malmstadt, H. V., C. G. Enke, S. R. Crouch, and G. Harlick. 1974. *Electronic Measurements for Scientists.* Benjamin, Menlo Park, CA.

Markram, H., and B. Sakmann. 1994. Calcium transients in dendrites of neocortical neurons evoked by single subthreshold excitatory postsynaptic potentials *via* low-voltage-activated calcium channels. *Proc. Nat. Acad. Sci.* **91:** 5207–5211.

Momose-Sato, Y., K. Sato, T. Sakai, A. Hirota, K. Matsutani, and K. Kamino. 1995. Evaluation of optimal voltage-sensitive dyes for optical measurement of embryonic neural activity. *J. Membr. Biol.* **144:** 167–176.

Nakashima, M., S. Yamada, S. Shiono, M. Maeda, and F. Satoh. 1992. 448-detector optical recording system: development and application to *Aplysia* gill-withdrawal reflex. *IEEE Trans. Biomed. Eng.* **39:** 26–36.

Nirenberg, S., and C. Cepko. 1993. Targeted ablation of diverse cell classes in the nervous system *in vivo. J. Neurosci.* **13:** 3238–3251.

Obaid, A. L., T. Koyano, J. Lindstrom, T. Sakai, and B. M. Salzberg. 1999. Spatiotemporal patterns of activity in an intact mammalian network with single-cell resolution: optical studies of nicotinic activity in an enteric plexus. *J. Neurosci.* **19:** 3073–3093.

Orbach, H. S., and L. B. Cohen. 1983. Optical monitoring of activity from many areas of the *in vitro* and *in vivo* salamander olfactory bulb: a new method for studying functional organization in the vertebrate central nervous system. *J. Neurosci.* **3:** 2251–2262.

Orbach, H. S., L. B. Cohen, and A. Grinvald. 1985. Optical mapping of electrical activity in rat somatosensory and visual cortex. *J. Neurosci.* **5:** 1886–1895.

Petran, M., and M. Hadravsky. 1966. Czechoslovakian patent 7720.

Prechtl, J. C., L. B. Cohen, B. Peseran, P. P. Mitra, and D. Kleinfeld. 1997. Visual stimuli induce waves of electrical activity in turtle cortex. *Proc. Nat. Acad. Sci. USA* **94:** 7621–7626.

Ratzlaff, E. H., and A. Grinvald. 1991. A tandem-lens epifluorescence microscope: hundred-fold brightness advantage for wide-field imaging. *J. Neurosci. Meth.* **36:** 127–137.

Rohr, S., and B. M. Salzberg. 1994. Multiple site optical recording of transmembrane voltage in patterned growth heart cell cultures: assessing electrical behavior, with microsecond resolution, on a cellular and subcellular scale. *Biophys. J.* **67:** 1301–1315.

Ross, W. N., and L. F. Reichardt. 1979. Species-specific effects on the optical signals of voltage-sensitive dyes. *J. Membr. Biol.* **48:** 343–356.

Ross, W. N., B. M. Salzberg, L. B. Cohen, A. Grinvald, H. V. Davila, A. S. Waggoner, and C. H. Wang. 1977. Changes in absorption, fluorescence, dichroism, and birefringence in stained giant axons: optical measurement of membrane potential. *J. Membr. Biol.* **33:** 141–183.

Sakai, T., A. Hirota, H. Komuro, S. Fujii, and K. Kamino. 1985. Optical recording of membrane potential responses from early embryonic chick ganglia using voltage-sensitive dyes. *Brain Res.* **349:** 39–51.

Salama, G. 1988. Voltage-sensitive dyes and imaging techniques reveal new patterns of electrical activity in heart and cortex. *Proc. SPIE (Int. Soc. Optical Eng.)* **94:** 75–86.

Salzberg, B. M. 1983. Optical recording of electrical activity in neurons using molecular probes. Pp. 139–187 in *Current Methods in Cellular Neurobiology.* J. L. Barker and J. F. McKelvy, eds. Wiley, New York.

Salzberg, B. M., H. V. Davila, and L. B. Cohen. 1973. Optical recording of impulses in individual neurones of an invertebrate central nervous system. *Nature* **246:** 508–509.

Salzberg, B. M., A. Grinvald, L. B. Cohen, H. V. Davila, and W. N. Ross. 1977. Optical recording of neuronal activity in an invertebrate central nervous system: simultaneous monitoring of several neurons. *J. Neurophysiol.* **40:** 1281–1291.

Schiller, J., F. Helmchen, and B. Sakmann. 1995. Spatial profile of dendritic calcium transients evoked by action potentials in rat neocortical pyramidal neurons. *J. Physiol.* **487:** 583–600.

Shaw, R. 1979. Photographic detectors. *Appl. Optics Optical Eng.* **7:** 121–154.

Siegel, M. S., and E. Y. Isacoff. 1997. A genetically encoded optical probe of membrane voltage. *Neuron* **19:** 735–41.

Spruston, N., Y. Schiller, G. Stuart, and B. Sakmann. 1995. Activity-dependent action potential invasion and calcium influx into hippocampal CA1 dendrites. *Science* **268:** 297–300.

Stuart, G. J., and B. Sakmann. 1994. Active propagation of somatic action potentials into neocortical pyramidal cell dendrites. *Nature* **367:** 69–72.

Tank, D., and Z. Ahmed. 1985. Multiple-site monitoring of activity in cultured neurons. *Biophys. J.* **47:** 476A.

Tsau, Y., J. Y. Wu, H. P. Hopp, L. B. Cohen, D. Schiminovich, and C. X. Falk. 1994. Distributed aspects of the response to siphon touch in *Aplysia:* spread of stimulus information and cross-correlation analysis. *J. Neurosci.* **14:** 4167–4184.

Tsau, Y., P. Wenner, M. J. O'Donovan, L. B. Cohen, L. M. Loew, and J. P. Wuskell. 1996. Dye screening and signal-to-noise ratio for retrogradely transported voltage-sensitive dyes. *J. Neurosci. Meth.* **70:** 121–129.

Waggoner, A. S. 1979. Dye indicators of membrane potential. *Annu. Rev. Biophys. Bioeng.* **8:** 47–68.

Waggoner, A. S., and A. Grinvald. 1977. Mechanisms of rapid optical changes of potential sensitive dyes. *Annu. NY Acad. Sci.* **303:** 217–241.

Wu, J. Y., and L. B. Cohen. 1993. Fast multisite optical measurements of membrane potential. Pp. 389–404 in *Fluorescent and Luminescent Probes for Biological Activity.* W. T. Mason, ed. Academic Press, London.

Wu, J. Y., L. B. Cohen, and C. X. Falk. 1994a. Neuronal activity during different behaviors suggests a distributed neuronal organization in the *Aplysia* abdominal ganglion. *Science* **263:** 820–823.

Wu, J. Y., Y. Tsau, H. P. Hopp, L. B. Cohen, A. C. Tang, and C. X. Falk. 1994b. Consistency in nervous systems: trial-to-trial and animal-to-animal variations in the response to repeated application of a sensory stimulus in *Aplysia. J. Neurosci.* **14:** 1366–1384.

Wu, J. Y., Y. W. Lam, C. X. Falk, L. B. Cohen, J. Fang, L. Loew, J. C. Prechtl, D. Kleinfeld, and Y. Tsau. 1998. Voltage-sensitive dyes for monitoring multi-neuronal activity in the intact CNS. *Histochem. J.* **30:** 169–187.

Yuste, R., and W. Denk. 1995. Dendritic spines as basic functional units of neuronal integration. *Nature* **375:** 682–684.

Zecevic, D. 1996. Multiple spike-initiation zones in single neurons revealed by voltage-sensitive dyes. *Nature* **381:** 322–325.

Zecevic, D., J. Y. Wu, L. B. Cohen, J. A. London, H. P. Hopp, and C. X. Falk. 1989. Hundreds of neurons in the *Aplysia* abdominal ganglion are active during the gill-withdrawal reflex. *J. Neurosci.* **9:** 3681–3689.

Reference: *Biol. Bull.* **198:** 22–25. (February 2000)

Germ-Cell Warfare in Ascidians: Sperm From One Species Can Interfere With the Fertilization of a Second Species

CHARLES C. LAMBERT*

Department of Biological Science, California State University, Fullerton, California 92834-6850

Ascidians (invertebrate chordates) are very abundant in many marine subtidal areas. They often live in dense multispecies clumps; thus, interspecific competition for space may be intense. Although most noncolonial species are broadcast spawners, their eggs can be fertilized only by sperm of the same species (1). Multiple fertilization is lethal and all animals have evolved blocks to polyspermy. Ascidian eggs block polyspermy by enzymatic (2) and electrical mechanisms (3). Sperm bind to N-*acetylglucosamine groups on the vitelline coat (4, 5, 6, 7). Follicle cells surrounding the vitelline coat release* N-*acetylglucosaminidase during egg activation (8), preventing the binding of all sperm but a few (2). I show here that this interaction is not species-specific; sperm from one species can cause glycosidase release from follicle cells of a second species. Furthermore, once glycosidase release has been induced, the subsequent addition of sperm from the egg-producing species fails to fertilize a substantial proportion of these eggs. This leads to the hypothesis that sperm from one species of ascidian can interfere with fertilization of a second species. While* intra*specific sperm competition has been well documented in several taxa (9, 10), this is the first record of sperm competition between species, or* inter*specific sperm competition.*

As previously shown by numerous authors (1), ascidian fertilization is species-specific. Eggs of *Phallusia mammillata, Phallusia julinea, Ascidia* (=*Phallusia*) *nigra,* and *Ascidia sydneiensis* are induced to undergo cleavage only when fertilized with sperm from the same species (Table 1). In *Phallusia mammillata* eggs, the failure to fertilize is the result of sperm from *Ascidia mentula, Ciona intestinalis,* and *Ascidiella aspersa* being unable to penetrate the vitelline coat. Penetration of the egg coverings is also involved in the block to hybridization of *Ascidiella aspersa* (11) and *Ascidia malaca* eggs (12, 13). Hybridization is possible after removal of the vitelline coat from eggs of *Ciona intestinalis, Phallusia mammillata, Ascidiella aspersa, Ascidia malaca,* and *Ascidia mentula* (14), and *Ciona savignyi* (15). In eggs from *A. sydneiensis. A. nigra,* and *Phallusia julinea,* the precise mechanism of the block remains unknown; nevertheless, sperm from these species are unable to fertilize the eggs of other species. However, in all other known cases, failure of hybridization is clearly at the level of the egg coverings, so this is also likely to be true for these species.

While fertilization is species-specific, glycosidase release clearly is not (Table 1). Sperm from several different species of ascidians can all induce glycosidase release; in all cases, heterologous sperm were capable of inducing glycosidase release from each of the four species of eggs used. This nonspecific glycosidase release varied considerably between the different egg and sperm combinations; even sperm from *Herdmania momus* (Order Stolidobranchia) elicited glycosidase release from *Ascidia sydneiensis* (Order Phlebobranchia) eggs. However, sperm from the oyster *Saccostrea cucullata* failed to cause glycosidase release from *A. nigra* eggs (data not shown).

The source of the glycosidase is the follicle cells, because sperm induce glycosidase release in the presence of the drug suramin, which prevents the sperm from penetrating the vitelline coat (8). In addition, homologous sperm added to isolated follicle cells of *Phallusia mammillata* (8) and *Ascidia ceratodes* cause glycosidase release (K. McKinney and C. C. Lambert, unpubl. obs., 1997). The nature of this interaction remains unknown, although phospholipase *c* and tyrosine phosphorylation appear to be involved in the actual

---

Received 5 August 1999; accepted 17 November 1999.

* Current address: 12001 11th Ave. NW, Seattle, WA 98177. E-mail: clambert@fullerton.edu

Table I

Glycosidase release and fertilization of ascidian eggs fertilized with homologous and heterologous sperm

Eggs	Sperm	% Glycosidase release	Fertilization (cleavage)
Phallusia mammillata	*P. mammillata*	100% (Control)	Yes
P. mammillata	*Ascidia mentula*	46.92 ± 16.6 (7)	No
P. mammillata	*Ascidiella aspersa*	66.53 ± 8.7 (18)	No
P. mammillata	*Ciona intestinalis*	63.6 ± 16.1 (6)	No
Ascidia (=Phallusia) nigra	*Ascidia nigra*	100% (Control)	Yes
A. nigra	*A. sydneiensis*	71.5 ± 20.4 (4)	No
A. nigra	*Phallusia julinea*	130.25 ± 37.6 (4)	No
Ascidia sydneiensis	*A. sydneiensis*	100% (Control)	Yes
A. sydneiensis	*A. nigra*	117.2 ± 29.2 (6)	No
A. sydneiensis	*Phallusia julinea*	99 ± 45.5 (4)	No
A. sydneiensis	*Herdmania momus*	112.98 ± 26.6 (4)	No
Phallusia julinea	*P. julinea*	100% (Control)	Yes
P. julinea	*A. sydneiensis*	16.1 ± 9.9 (2)	No
P. julinea	*Ascidia nigra*	26.2 ± 17 (6)	No

Note that although fertilization is strictly species-specific, glycosidase release can be initiated in most species by a variety of heterologous sperm. Glycosidase release is expressed as a percentage of that occurring with homologous fertilization. The indicated values are means ± the standard error of the mean. The numbers in parentheses indicate the number of replicates. Normal fertilization was achieved by using 5 μl of a 1:1000 dilution of dry sperm in each 0.5 ml aliquot of eggs. *N*-acetylglucosaminidase activity was measured using a fluorometric assay as in reference 2.

Phallusia mammillata, Ascidia mentula, Ascidiella aspersa, and *Ciona intestinalis* were collected from floating docks near Brest, France. *Ascidia (=Phallusia) nigra, Ascidia sydneiensis* and *Herdmania momus* were collected from floating docks in Keehi Lagoon and Kewalo Basin, Honolulu, Hawaii, and buoys in Apra Harbor, Guam. *Phallusia julinea* was collected from coral reefs in Apra Harbor, Guam.

release (16). Living sperm have not been observed to bind to isolated follicle cells under the microscope; rather, they bounce into the cells and make them move. If the sperm activates a receptor, it may not have to occupy the receptor continuously in order for the glycosidase release to occur.

Since sperm from non-egg (heterologous) species can induce glycosidase release and since the glycosidase reduces sperm binding, it seemed possible for sperm from one species of ascidian to interfere with the actual fertilization of a second species by its own sperm. Accordingly, eggs of *Ascidia sydneiensis, Ascidia nigra,* and *Phallusia julinea* were each exposed to sperm from the other two species, incubated 5 min for the completion of glycosidase release (17), and then re-inseminated with sperm from the egg-producing (homologous) species. In all cases, cleavage was definitely impaired when compared to the controls, which had received only homologous sperm (Table 2). The highest inhibition (44%) occurred in *Ascidia sydneiensis* eggs using *Ascidia nigra* as the first sperm; interestingly, the lowest (10%) also occurred in *A. sydneiensis* eggs first inseminated with *Phallusia julinea* sperm. The reciprocal of *A. nigra* eggs exposed first to *A. sydneiensis* sperm also yielded strong inhibition of *A. nigra* fertilization (27%). This is significant because *A. nigra* and *A. sydneiensis* co-occur in dense aggregations on floats in Keehi Lagoon in Honolulu, Hawaii, and on harbor buoys in Apra Harbor, Guam. *Phallusia julinea* is not evident in Hawaiian harbors, and in Guam it is never a member of the fouling community but always found in reef crevices at the bottom of the bay. Thus it is not likely that eggs of *A. nigra* or *A. sydneiensis* would contact *P. julinea* sperm to an appreciable degree in nature.

In the laboratory, sperm of *A. sydneiensis* and *A. nigra* can clearly interfere with the fertilization of each other's eggs. Does such an interference occur in nature? Direct evidence is lacking on this point, but in Keehi Lagoon and Kewalo Basin in Honolulu *A. nigra* is much more abundant than *A. sydneiensis.* Sperm of *A. nigra* interfere much more (44%) with the fertilization of *A. sydneiensis* eggs than the reverse (27%). I speculate that at least a portion of this unequal abundance is the result of fertilization interference. Ideally, for this to occur both species would have to spawn at about the same time. Although there is considerable information on the spawning of several ascidian species (18, 19, 20), there are apparently no studies on the spawning of any ascidian in the family Ascidiidae, which includes both of these species. However, ascidian sperm are capable of fertilizing eggs 12 h or more after dilution (21), and sperm attraction to eggs is not species-specific (22); consequently spawning does not have to be synchronous for interspecific sperm competition to occur.

These experiments support the hypothesis that foreign sperm can cause a failure in the ability of eggs to be

Table II

Fertilization interference between ascidian species

Egg	First sperm	Second sperm	% Inhibition of cleavage (*n*)
Ascidia sydneiensis	*Ascidia nigra*	*A. sydneiensis*	44 ± 13.7 (5)
A. sydneiensis	*Phallusia julinea*	*A. sydneiensis*	10 ± 5 (2)
Ascidia nigra	*A. sydneiensis*	*A. nigra*	27.7 ± 3.8 (16)
A. nigra	*Phallusia julinea*	*A. nigra*	33.5 ± 9.6 (2)
Phallusia julinea	*A. sydneiensis*	*P. julinea*	27 ± 6.0 (2)
P. julinea	*A. nigra*	*P. julinea*	20 ± 6.0 (2)

In these experiments 2 ml of eggs were first fertilized with 10 ml of a 1:1000 dilution of heterologous sperm, then 5 min later with 10 ml of a 1:1000 dilution of homologous sperm. When the control cells reached the 2-cell stage they were fixed in 1% formaldehyde and the percentage of 2-cell embryos was counted in at least 100 eggs. The mean percentage inhibition of cleavage relative to the controls is indicated ± the standard error of the mean; (*n*) = number of replicates.

fertilized by their own species' sperm. Inhibition of fertilization success in one species by another could enhance the sperm producer's overall reproductive success relative to its competitors. Since space is a limiting resource in the fouling community, reduction of competition by fertilization interference would definitely enhance the success of the interfering species in occupying space (23). Fertilization in the sea is chancy and less than 100% fertilization is the norm (24). These experiments were carried out with sperm concentrations of the homologous species high enough that over 90% of the eggs were routinely fertilized in the controls. It is very likely that reducing the homologous sperm concentration to one that would produce a more realistic level of control fertilization–perhaps 50%–would yield much higher values of heterologous sperm interference. Indeed, nonhomologous sperm can cause the release of at least as much glycosidase activity as homologous sperm in several cases, yet the greatest inhibition is only 44%. Using a lower concentration of homologous sperm might result in a higher level of inhibition. However, even the modest levels of fertilization interference demonstrated here in these preliminary studies could reduce competition for space. The hypothesis of *inter*specific sperm competition is supported by these experiments. This could be an important factor in the distribution and abundance of many broadcast-spawning organisms, including both plants and animals, because all organisms have blocks to polyspermy, many of which involve sperm-induced enzyme release (25). Although fertilization leading to cleavage is species-specific, until now there have been no studies on the specificity of the polyspermy block. The more well-known form of sperm competition involves animals with internal fertilization in which sperm from several males compete to fertilize eggs of the same species (9, 10). This *intra*specific sperm competition also occurs in certain colonial ascidians with internal fertilization (26). Thus ascidians reveal both intra- and interspecific modes of sperm competition.

Acknowledgments

I am grateful to C. Meyer, G. Paulay, and G. Lambert for collecting ascidians in Guam. I thank A. Toulmond and C. Jouin-Toulmond (Station Biologique, Roscoff, France), M. Hadfield (Univ. of Hawaii Mar. Lab., Honolulu, HI), and G. Paulay (Univ. of Guam Mar. Lab., Mangilao, GU) for facilities where this research was conducted. L. Meijer, H. Goudeau, M. Goudeau, and M. Hadfield loaned essential equipment. G. Lambert has my thanks for providing continued insight, encouragement, and assistance on this research and preparation of the manuscript. Partial funding came from Sea Grant support to G. Paulay.

Literature Cited

1. **Reverberi, G. 1971.** Ascidians. Pp. 507–550 in *Experimental Embryology of Marine and Fresh-water Invertebrates.* G. Reverberi, ed. North-Holland, Amsterdam.
2. **Lambert, C. C. 1989.** Ascidian eggs release glycosidase activity at fertilization that aids in the block against polyspermy. *Development* **105:** 415–420.
3. **Goudeau, H., Y. Depresle, A. Rosa, and M. Goudeau. 1994.** Evidence by a voltage clamp study of an electrically mediated block to polyspermy in the egg of the ascidian *Phallusia mammillata. Dev. Biol.* **166:** 489–501.
4. **Lambert, C. C. 1986.** Fertilization-induced modification of chorion N-acetylglucosamine groups blocks polyspermy in ascidian eggs. *Dev. Biol.* **116:** 168–175.
5. **Godknecht, A. J., and T. G. Honegger. 1995.** Specific inhibition of sperm β-N-acetylglucosaminidase by the synthetic inhibitor N-acetylglucosaminono-1,5-lactone O-(phenylcarbamoyl)oxime inhibits fertilization in the ascidian, *Phallusia mammillata. Dev. Growth Differ.* **37:** 183–189.
6. **Honegger, T. G. 1986.** Fertilization in ascidians: Studies on the egg envelope, sperm and gamete interactions in *Phallusia mammillata. Dev. Biol.* **118:** 118–128.
7. **Hoshi, M., S. Takizawa, and N. Hirohashi. 1994.** Glycosidases, proteases and ascidian fertilization. *Semin. Dev. Biol.* **5:** 201–208.
8. **Lambert, C. C., H. Goudeau, C. Franchet, G. Lambert, and M. Goudeau. 1997.** Ascidian eggs block polyspermy by two independent mechanisms, one at the egg plasma membrane, the other involving the follicle cells. *Mol. Reprod. Dev.* **48:** 137–143.
9. **Parker, G. A. 1984.** Sperm competition and the evolution of animal mating strategies. Pp. 1–60 in *Sperm Competition and the Evolution of Animal Mating Systems,* R. L. Smith, ed. Academic Press, Orlando, FL.
10. **Roldan, E. R. S., M. Gomendio, and A. D. Vitullo. 1992.** The evolution of eutherian spermatozoa and underlying selective forces: female selection and sperm competition. *Biol. Rev.* **67:** 551–593.
11. **Villa, L., and E. Patricolo. 1992.** Ascidian interspecific fertilization. I. Preliminary data on the involvement of the follicle cell layer. *Eur. Arch. Biol.* **103:** 25–30.
12. **Patricolo, E., and L. Villa. 1992.** Ascidian interspecific fertilization. II. A study of the external egg coating in hybrid crosses. *Anim. Biol.* **1:** 9–15.
13. **Patricolo, E., and L. Villa. 1995.** Ascidian interspecific fertilization. III. Ultrastructural investigations of sperm-egg interaction. *Eur. J. Morph.* **33:** 433–442.
14. **Minganti, A. 1959.** Lo sviluppo embrionale ed il comportamento dei cromosomi in ibrid tra cinque specie di Ascidie. *Acta Embryol. Morphol. Exp.* **2:** 269–301.
15. **Byrd, J., and C. C. Lambert. 2000.** Mechanism of the block to hybridization and selfing between the sympatric ascidians *Ciona intestinalis* and *Ciona savignyi. Mol. Reprod. Dev.* **55:** 109–116.
16. **Robert, L. K., L. M. Lucio, C. A. Goode, K. McKinney, and C. C. Lambert. 1999.** Activation of a follicle cell surface phospholipase by a tyrosine kinase dependent pathway is an essential event in ascidian fertilization. *Mol. Reprod. Dev.* **54:** 69–75.
17. **McDougall, A., C. Sardet, and C. C. Lambert. 1995.** Different calcium-dependent pathways control fertilization-triggered glycosidase release and the cortical contraction in ascidian eggs. *Zygote* **3:** 251–258.
18. **Lambert, C. C., and C. L. Brandt. 1967.** The effect of light on the spawning of *Ciona intestinalis. Biol. Bull.* **132:** 222–228.
19. **Lambert, G., C. C. Lambert, and D. P. Abbott. 1981.** *Corella* species in the American Pacific Northwest: distinction of *C. inflata* from *C. willmeriana* based upon morphology, reproduction and genetics. *Can. J. Zool.* **59:** 1493–1504.
20. **West, A. B., and C. C. Lambert. 1976.** Control of spawning in the

tunicate *Styela plicata* by variations in the natural light regime. *J. Exp. Zool.* **195:** 263–270.

21. **Bolton, T. F., and J. N. Havenhand. 1996.** Chemical mediation of sperm activity and longevity in the solitary ascidians *Ciona intestinalis* and *Ascidiella aspersa. Biol. Bull.* **190:** 329–335.
22. **Yoshida, M., K. Inaba, and M. Morisawa. 1993.** Sperm chemotaxis during the process of fertilization in the ascidians *Ciona savignyi* and *Ciona intestinalis. Dev. Biol.* **157:** 497–506.
23. **Branch, G. M. 1984.** Competition between marine organisms: ecological and evolutionary implications. *Oceanogr. Mar. Biol. Annu. Rev.* **22:** 429–593.
24. **Levitan, D. R., and C. Petersen. 1995.** Sperm limitation in the sea. *Trends Ecol. Evol.* **10:** 228–231.
25. **Jaffe, L. A., and M. Gould. 1985.** Polyspermy preventing mechanisms. Pp. 223–250 in *Biology of Fertilization,* Vol 3, C. B. Metz and A. Monroy, eds. Academic Press, Orlando, FL.
26. **Yund, P. O. 1998.** The effect of sperm competition on male gain curves in a colonial marine invertebrate. *Ecology* **79:** 328–339.

Reference *Biol. Bull.* **198:** 26–28. (February 2000)

Light-Sensitive Voltage Responses in the Neurons of the Cerebral Ganglion of *Ciona savignyi* (Chordata: Ascidiacea)

HIDEKAZU TSUTSUI AND YOSHITAKA OKA*

Misaki Marine Biological Station, Graduate School of Science, University of Tokyo, Miura,
Kanagawa 238-0225, Japan

Light-responsive behaviors such as siphon contraction (1), phototropism (2), and gamete release (3, 4) have been described in several ascidian species. The pigmented spots around the siphon openers (5), the epithelial cells of the sperm duct (6, 7), and the cerebral ganglion (8) have been suggested to be the photoreceptor candidates underlying these behaviors. However, these arguments have not yet been settled because no direct electrophysiological recordings of light-induced receptor potentials have been reported. In this study, we focused on the cerebral ganglion and performed intracellular recordings from the neurons in the ventral side of the cerebral ganglion in an isolated in vitro *preparation of the neural complex in* Ciona savignyi. *We found that 24%* (n = *115) of the recorded neurons showed various types of voltage responses to light stimuli. Almost all (27/28) of the recorded voltage responses were "on" responses that included hyperpolarizing and depolarizing responses and could be categorized into five types, except for a complex response recorded in one cell; the remaining one (1/28) was a depolarizing "off" response. This is the first report of electrophysiological recordings of light-sensitive voltage responses from ascidian cerebral ganglion neurons.*

Membrane potentials were recorded with intracellular microelectrodes from 115 neurons in the ventral side of the isolated cerebral ganglion of 47 ascidians (see Fig. 1 legend for detail). The resting membrane potential was − 48 ± 12 mV (mean ± SD, *n* = 52), and 52% (*n* = 115) of the recorded neurons showed spontaneous activity consisting of low-frequency (0.1–0.3 Hz) regular discharges of action potentials (Fig. 1B, D). Seventeen percent of the neurons showed spontaneous irregular or bursting discharges of action potentials. The remaining 30% of the neurons were silent (Fig. 1A, C, E). In addition, 24% (28 cells) of the total 115 recorded neurons, including spontaneously active and silent ones, showed voltage responses of various types to light stimuli (Fig. 1). Most of these light responses (27/28 cells) were "on" responses (Fig. 1A–E), and we observed a transient "off" depolarization with a few spikes in only one neuron (not shown). Twenty-six out of the 27 "on" responses could be categorized into five types as follows (Fig. 1): (A) transient hyperpolarization (13 cells); (B) suppression of spontaneous discharge of action potentials (7 cells); (C) transient depolarization (2 cells); (D) transient high-frequency excitatory synaptic inputs (2 cells); (E) sustained depolarization (2 cells). The remaining "on" response consisted of a complex pattern: transient hyperpolarization followed by sustained depolarization accompanying a number of spikes during the light stimulus. This was similar to a mixture of response types A and E. There seemed to be no significant differences in the resting potentials for the five response types. Even the quickest of the five types of responses, type A, showed a latency longer than 500 ms, and the latency of the other types was 3–5 s. There seemed to be no specific distribution of these types of neurons on the ventral surface of the cerebral ganglion. The ability of a cell to respond with more than one response type when presented different light intensities or wavelengths was not investigated.

Hyperpolarizing receptor potentials of the visual cells in the ocellus of ascidian larvae has been described previously (9). Because our type A and B responses also are hyperpolarizing, it is tempting to interpret them as receptor potentials. However, there is also a significant difference between

---

Received 13 July 1999; accepted 2 November 1999.

* To whom correspondence should be addressed. E-mail: okay@mmbs.s.u-tokyo.ac.jp

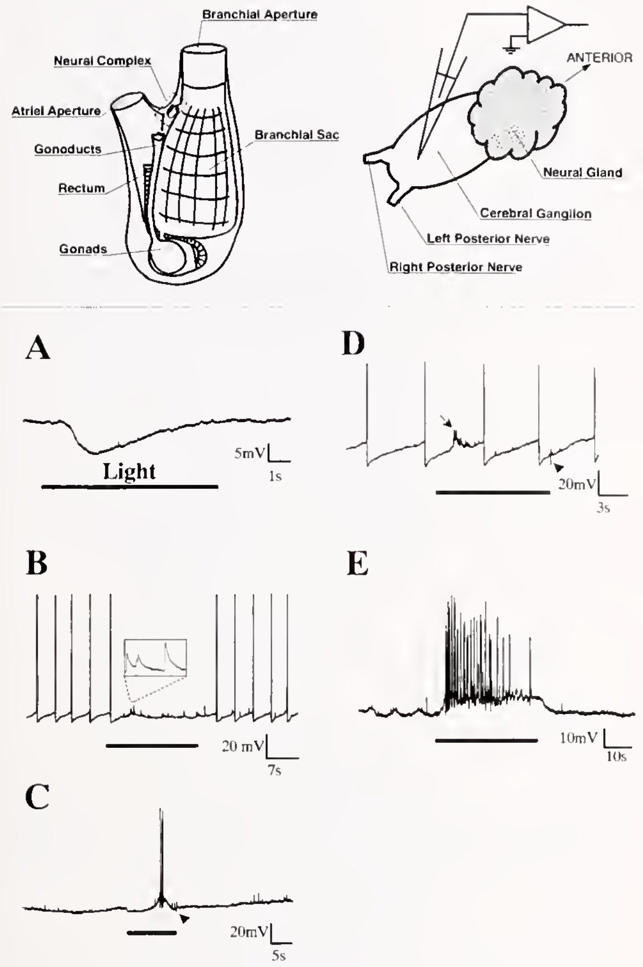

Figure 1. (Top left) Schematic illustration of adult *Ciona savignyi* showing location of major organs. The illustration was modified from Mackie (13). Neural complex is located in the body wall between the two siphons (boxed). (Top right) Ventral view of the isolated neural complex preparation. The neural complex consists of the cerebral ganglion and the neural gland. Recordings were made from neurons of the ventral side of the cerebral ganglion. (Bottom) The 27 "on" voltage responses to light stimuli could be categorized into five types, except for one complex response (see text). The typical response for each type is shown. (A) Transient (<5 s) hyperpolarization (13/27). Longer or continuous light stimulation did not evoke any additional voltage changes after the transient hyperpolarization. (B) Suppression of spontaneous regular discharges (7/27). Small irregular fluctuations of membrane potential indicative of synaptic inputs seemed to increase in frequency during light stimuli. Some of them are enlarged in the inset corresponding to 1 s × 10 mV. (C) Transient depolarization accompanied by a few spikes (2/27). Longer or continuous light stimulation did not evoke any voltage changes after the transient depolarization. (D) Transient high-frequency excitatory synaptic inputs (arrow), which sometimes build up to give rise to an action potential in spontaneously beating neurons. Unlike the type B response, the spontaneous regular discharges were not affected in these cells (2/27). (E) Sustained depolarization during light stimuli, accompanied by a number of spikes with frequency accommodation (2/27). Voltage responses of each neuron against repeated light stimuli were reproducible during the recording period. Arrowheads in C and D indicate stimulus artifacts.

the two; the receptor potential of the larva is fast and sustained, while the type A and type B responses recorded in the present study are slow and transient. We cannot conclude at present which type of response represents the photoreceptor potential, because chemical and electrical synaptic transmissions were not blocked in the present recordings. Actually, the increase in frequency of synaptic inputs in the type D response is a second-order or higher order response that arises from synaptic pathways. However, because all of these responses were recorded from neurons within 'isolated' cerebral ganglion preparations, it is evident that there should be a certain population of photoreceptor cells within the cerebral ganglion of *Ciona savignyi.*

Light-induced gamete release is a well-known behavior of ascidians (3, 4). However, removal of the whole neural complex *in vivo* does not affect this behavior in *Ciona intestinalis* (Tsutsui and Oka, unpubl. data). Similar behavior was reported previously in *Chelyosoma productum* (10). These results may support the existence of an ascidian photoreceptive system or systems other than the cerebral ganglion. It may be an interesting future study to compare the action spectra of the voltage responses of the light-sensitive neurons in the present cerebral ganglion preparation and those of light-induced spawning behavior, such as that measured by Lambert *et al.* (3). Such a comparison would test whether similar photoreceptor processes underlie the control of spawning as well as the voltage responses reported here and would further our understanding of the properties of ascidian photoreceptive systems.

The cerebral ganglion of ascidians has been shown to have many neurons immunoreactive for vertebrate neuropeptides such as GnRH, bombesin, and neurotensin (11,

---

Methods: Ciona savignyi was used for the present electrophysiological study because of the advantageous morphology of its neural complex (composed of closely apposed cerebral ganglion and neural gland). The neural gland of this species is located in the anterior ventral part of the cerebral ganglion (Tsutsui and Oka, unpubl. obs.), and a large ventral surface area of the cerebral ganglion is easily accessible *in vitro* with microelectrodes. The neural complex was dissected out, and muscular tissue and the thin wall of the blood sinus that cover the ventral side of the cerebral ganglion were gently removed. Then, the isolated neural complex preparation was pinned ventral side up in a recording chamber (volume = 400 μl) lined with Sylgard and was perfused with filtered seawater (1 ml/min). The experiments were carried out at room temperature (18–22° C), and the preparation was viable at least for 6 h under these conditions. The neurons on the ventral side of the posterior part of the cerebral ganglion were recorded intracellularly by sharp microelectrodes (pulled from borosilicate glass of o.d. 1.5 mm with inner filaments and filled with 2 *M* KCl; resistance = 40–70 MΩ) under a dissecting microscope. Signals were amplified (by MEZ-8300, Nihon Kohden) and digitized at 3–5 kHz and stored digitally (using Axotape software, Axon Instruments). Light stimuli (3.0×10^4 lux) were delivered to the preparations through an optic fiber from a conventional light source of a 150 W halogen bulb (type 6423, Philips) equipped with a heat-absorbing filter. The light stimulus was controlled manually by a solenoid relay switch. The preparation was kept in the dark (<0.1 lux) for at least 1 min between the light stimuli.

12). Especially, tunicate GnRHs have been biochemically characterized, and the distributions of GnRH neurons have been studied recently (11, 13, 14). The recordings of light-sensitive voltage responses in the present study were made mainly from the posterior ventral part of the cerebral ganglion, the region where substantial numbers of immunoreactive GnRH neurons are distributed in *Ciona intestinalis* (11) and *C. savignyi* (Tsutsui and Oka, unpubl. data). Therefore, the present results show that light-sensitive neurons and GnRH-secreting neurons are located in an overlapping region, and it may be suggested that GnRH release is controlled by light. This possibility is interesting from the viewpoint of the general neuromodulatory functions of GnRH neurons (15, 16). The ascidian cerebral ganglion preparation may, therefore, provide a chance to test this hypothesis.

Acknowledgments

We thank the staff of the Education and Research Center of Bio-resources in Onagawa for their supply of ascidians. We also thank Dr. Arikawa for lending us a luminometer and for a helpful discussion. This study was supported by grant-in-aid for Fundamental Scientific Research from the Ministry of Education, Sports, Science and Culture of Japan to Y. Oka.

Literature Cited

1. **Hecht, S. 1918.** The photic sensitivity of *Ciona intestinalis*. *J. Gen. Physiol.* **1:** 147–166.
2. **Goodbody, I. 1974.** The physiology of ascidians. Pp. 1–49 in *Advances in Marine Biology*, Vol. 11. F. S. Russel, ed. Academic Press, London.
3. **Lambert, C. C., and C. L. Brandt. 1967.** The effect of light on the spawning of *Ciona intestinalis*. *Biol. Bull.* **132:** 222–228.
4. **Numakunai, T., and Z. Hoshino. 1973.** Biology on the ascidian, *Halocynthia roretzi* (Drasche), in Mutsu Bay. I. Differences of spawning time and external features. *Bull. Mar. Biol. Stn. Asamushi.* **14(4):** 191–197.
5. **Dilly, P. N., and J. J. Wolken. 1973.** Studies on the receptors in *Ciona intestinalis*. IV. The ocellus in the adult. *Micron* **4:** 11–29.
6. **Woolacott, R. M. 1974.** Microfilaments and the mechanism of light-triggered sperm release in ascidians. *Dev. Biol* **40:** 186–195.
7. **Woolacott, R. M., and M. R. Porter. 1977.** A synchronized multicellular movement initiated by light and mediated by microfilaments. *Dev. Biol.* **61:** 41–57.
8. **Kajiwara, S., S. Tamotsu, Y. Morita, and T. Numakunai. 1990.** Retinal isomers in the cerebral ganglion of the ascidian, *Halocynthia roretzi*. *Invertebr. Reprod. Dev.* **17:2:** 155–158.
9. **Gorman, A. L. F., J. S. Reynolds, and S. N. Barnes. 1971.** Photoreceptors in primitive chordates: fine structure, hyperpolarizing receptor potentials, and evolution. *Science* **172:** 1052–1054.
10. **Hisaw, F. L. Jr., C. R. Botticelli, and F. L. Hisaw. 1966.** A study of the relation of the neural gland-ganglionic complex to gonadal development in an ascidian, *Chelyosoma productum* Simpson. *Gen. Comp. Endocrinol.* **7:** 1–9.
11. **Tsutsui, H., N. Yamamoto, H. Ito, and Y. Oka. 1998.** GnRH immunoreactive neuronal system in the presumptive ancestral chordate, *Ciona intestinalis* (Ascidian). *Gen. Comp. Endocrinol.* **112:** 426–432.
12. **Fritsch, H. A. E., S. V. Noorden, and A. G. E. Pearse. 1982.** Gastro-intestinal and neurohormonal peptides in the alimentary tract and cerebral complex of *Ciona intestinalis* (Ascidiaceae). *Cell Tissue Res.* **223:** 369–402.
13. **Mackie, G. O. 1995.** 'On the visceral nervous system' of *Ciona*. *J. Mar. Biol. Assoc.* U.K. **75:** 141–151.
14. **Powell, J. F. F., S. M. Reska-Skinner, M. O. Prakash, W. H. Fischer, M. Park, J. E. Rivier, A. G. Craig, G. O. Mackie, and N. M. Sherwood. 1996.** Two new forms of gonadotropin-releasing hormone in a protochordate and the evolutionary implications. *Proc. Natl. Acad. Sci. USA.* **93:** 10461–10464.
15. **Oka, Y., and T. Matsushima. 1993.** Gonadotropin-releasing hormone (GnRH)-immunoreactive terminal nerve cells have intrinsic rhythmicity and project widely in the brain. *J. Neurosci.* **13:** 2161–2176.
16. **Oka, Y. 1997.** The gonadotropin-releasing hormone (GnRH) neuronal system of fish brain as a model system for the study of peptidergic neuromodulation. Pp. 245–276 in *GnRH Neurons: Genes to Behavior*. I. S. Parphar and Y. Sakuma, eds. Brain Shuppan, Tokyo.

Reference: *Biol. Bull.* **198:** 29–33. (February 2000)

Parasitic Diatoms Inside Antarctic Sponges

GIORGIO BAVESTRELLO[1,*], ATTILIO ARILLO[2], BARBARA CALCINAI[2],
RICCARDO CATTANEO-VIETTI[2], CARLO CERRANO[2], ELDA GAINO[3],
ANTONELLA PENNA[4], AND MICHELE SARÀ[2]

[1]*Istituto di Scienze del Mare—Università di Ancona, Via Brecce Bianche, I-60131 Ancona, Italy;* [2]*Dipartimento per lo Studio del Territorio e delle sue Risorse—Università di Genova, Viale Benedetto XV, 5 I-16132 Genova, Italy; and* [3]*Dipartimento di Biologia animale ed Ecologia—Università di Perugia, Via Elce di Sotto I-06123 Perugia, Italy; and* [4]*Istituto di Biochimica—Università di Urbino, I-60118, Italy*

*Antarctic sponges may host large populations of planktonic and benthic diatoms. After settling on the sponge, these diatoms enter its body through pinacocytes (1) and form, there, large mono- or pauci-specific assemblages. Yet the total amount of carbohydrates in the invaded sponge tissue is inversely correlated with that of chlorophyll-*a. *We suggest, therefore, that endobiont diatoms utilize the products of the metabolism of their host as an energy source. This is the first evidence indicating that an endobiotic autotrophic organism may parasitize its animal host. Moreover, this unusual symbiotic behavior could be a successful strategy that allows the diatom to survive in darkness.*

Heterotrophic bacteria, autotrophic cyanobacteria, zoochlorellae, and zooxanthellae are common symbionts in Porifera, where they may actually constitute most of the sponge tissue. Sponges can also harbor fungal populations, the significance of which has been poorly investigated (2). The association of sponges with autotrophic symbionts occurs mainly in tropical (3) and temperate waters (4); it is a fruitful strategy, allowing the sponges to utilize the symbionts as a food source complementary to filter feeding (5, 6).

Diatoms in sponge tissues have rarely been recorded (7), but such associations are widespread in Antarctic waters (1). In fact, most sponges from Terra Nova Bay (Ross Sea, Antarctica) host large populations of both planktonic and benthic diatoms, and these microorganisms are actively taken up by the pinacoderm and thus enter the sponge choanosome (1). This could be an adaptive supplementation of the food supply in the Antarctic ecosystem, because diatoms produce extracellular polysaccharides (8, 9) that sponges might use as energy substrates. On the other hand, the integrity of the diatom shells, the presence of cytoplasm inside the shells, and the formation of large mono- or pauci-specific assemblages inside a single sponge suggest that diatoms are able to complete their entire biological cycle inside the sponge body.

The aim of this study was to investigate the energy source that symbiotic diatoms might provide to Antarctic sponges. To this end, we evaluated the variation in the total carbohydrate content of sponges as a function of the biomass of endobiotic diatoms; biomass was estimated from chlorophyll-*a* concentration.

We examined 39 specimens representing 17 species of sponges (Table 1). The material was collected at Terra Nova Bay (Ross Sea), between 100 and 120 m depth, during the XIII Italian Antarctic Expedition (Austral Summer 1997–1998). The sponges were prepared for ultrastructural study as follows. Immediately after collection, small pieces from each specimen were fixed for 2 h in 2.5% glutaraldehyde in artificial seawater (ASW). The fixed tissues were rinsed, stored in ASW, and then dehydrated in a graded series of ethanol concentrations. Critical point drying was achieved with a CO_2 Pabish CPD 750 apparatus. Samples were examined with a Philips EM 515 scanning electromicroscope, and several species of diatoms were observed (Fig.

Received 29 June 1999; accepted 5 November 1999.

* To whom correspondence should be addressed. E-mail: bavestrello@popcsi.unian.it

Table 1

Chlorophyll-a concentration and carbohydrate content for the sponge specimens analyzed

Specimens	Chlorophyll-*a* (μg/g dwaf)	Total sugars (mg/g dwaf)
Artemisina tubulosa	12.07 ± 0.9	18.30 ± 3.6
Axociella nidificata	27.29 ± 2.5	8.12 ± 0.2
Dendrilla membranosa	29.13 ± 3.6	5.43 ± 0.4
	30.47 ± 2.1	11.40 ± 2.1
	31.65 ± 1.8	7.01 ± 0.6
	21.34 ± 1.9	16.29 ± 2.8
	7.31 ± 1	22.56 ± 1.8
	9.96 ± 0.9	27.06 ± 1.4
	14.43 ± 2.9	9.59 ± 1.1
Ectyodorix ramilobosa	8.47 ± 1.2	19.90 ± 3.1
	20.70 ± 3.1	6.91 ± 1.8
Gellius sp.	17.05 ± 2.4	7.25 ± 2
Gellius sp. 1	37.10 ± 6.9	6.91 ± 1.5
Haliclona dancoi	16.67 ± 2.4	9.92 ± 2.4
	15.05 ± 2.6	21.28 ± 3.2
	15.14 ± 0.9	8.10 ± 1.4
	21.85 ± 1.9	15.92 ± 1.9
Homaxinella balfourensis	14.37 ± 3.1	12.73 ± 2.1
Inflatella belli	5.75 ± 1.6	24.30 ± 3.1
	2.21 ± 0.8	24.41 ± 3.6
Isodictya conulosa	16.48 ± 1.6	12.29 ± 2.2
	13.59 ± 2	9.96 ± 1
Isodictya erinacea	11.86 ± 1.8	15.25 ± 2.8
Microxina benedeni	11.75 ± 3.2	11.21 ± 1.2
Phorbas glaberrima	18.22 ± 2.9	13.13 ± 2.8
	19.04 ± 4	12.73 ± 4.1
Pseudosuberites antarcticus	44.56 ± 3.5	3.32 ± 0.9
Pseudosuberites nudus	27.79 ± 5.6	10.23 ± 1.4
	45.71 ± 5.9	6.23 ± 0.8
	9.13 ± 1.7	17.71 ± 2.5
	11.88 ± 2.1	12.13 ± 1.3
	24.53 ± 4.8	9.23 ± 1.9
	25.65 ± 4.9	5.93 ± 1.4
	19.74 ± 3.6	7.41 ± 2.8
	11.54 ± 2.2	10.48 ± 2.3
Suberites caminatus	32.94 ± 3.8	8.91 ± 1.7
	6.35 ± 2.1	21.08 ± 3.4
	17.25 ± 5.7	7.11 ± 1.5
Tedania charcoti	16.67 ± 3.6	7.11 ± 0.9

Values are the mean of three replicates ± SD; dwaf, dry weight ash free.

1). Among pennate diatoms, *Fragilariopsis curta* (Fig. 1a), *Fragilariopsis* sp. (Fig. 1a, b), *Achnanthes* sp. (Fig. 1c), and *Pseudogomphonema* sp. were the most recurrent species; centric diatoms belonging to the genera *Porosira* (Fig. 1c), *Coscinodiscus*, and *Rhizosolenia* were rarer. For transmission electron microscopy, fragments of selected fixed material were postfixed in 1.0% OsO_4 in ASW at 4°C. After repeated rinsing, these fragments were dehydrated in ethanol and embedded in araldite. Ultrathin sections were cut with a Reichert ultramicrotome equipped with a diamond blade; these sections were gathered on copper grids, stained with uranyl acetate and lead citrate for contrast, and examined with a Philips 300 transmission electron microscope. Micrographs (TEM) of *Fragilariopsis curta* provide evidence that the cytoplasm and thylacoids are intact (Fig. 1d).

The concentrations of chl-*a* in the various sponge specimens were measured and are listed in Table 1. These values differed widely, ranging from 2.2 μg/g in *Inflatella belli*, to 45.7 μg/g in *Pseudosuberites nudus*. High values were found also in *Pseudosuberites antarcticus*, *Gellius* sp. 1., *Suberites caminatus*, and *Dendrilla membranosa*. Strong differences emerged when different specimens of the same species were compared (*e.g.*, from 7.3 to 31.6 μg/g in *D. membranosa;* and from 9.1 to 45.7 μg/g in *P. nudus*). This variation suggests that diatom uptake is fortuitous, depending primarily upon exposure of the sponge surface to diatoms settling upon it, rather than to some species-specific entrapping mechanism.

Carbohydrate in the sponge tissues (Table 1) ranged between 3.3 mg/g in *Pseudosuberites antarcticus* and 27.1 mg/g in *Dendrilla membranosa*. As with the chl-*a* concentration, carbohydrate content varied markedly when different specimens of the same species were compared.

For each specimen, we plotted carbohydrate content as a function of chl-*a* concentration and obtained the inverse correlation that is evident in Figure 2a. When we considered only those specimens belonging to a single species, this same trend was confirmed. In fact, in *Dendrilla membranosa* (Fig. 2b) and *Pseudosuberites nudus* (Fig. 2c), the total sugar content of the sponge tissue decreased as the concentration of chl-*a* increased.

The original aim of this work was to demonstrate that diatoms living inside the sponge tissue might represent a source of food for Antarctic sponges. This hypothesis seemed reasonable because diatoms produce large amounts of polysaccharides (8, 9). But our data show a clear inverse relationship between the amount of chl-*a* and of carbohydrate in sponge tissue. This relationship suggests that, as the population of diatoms within the sponge increases, it consumes more of the carbohydrate or related compounds produced by the sponge. This report, therefore, provides the first indication that diatoms in the field can utilize animal metabolic products as an energy source.

Like those in Antarctic sponges, most heterotrophic diatoms are pennate and occur in benthic habitats, where light is absent or limited and organic substrates are in great supply; such habitats strongly favor heterotrophic growth (10). Furthermore, several diatom species have developed active transport systems that bind to a limited number of organic substrates (glucose, lactate, and glutamate) and that respond to conditions of low light or darkness (11, 12); these diatoms have evolved highly sophisticated and ecologically significant mechanisms for

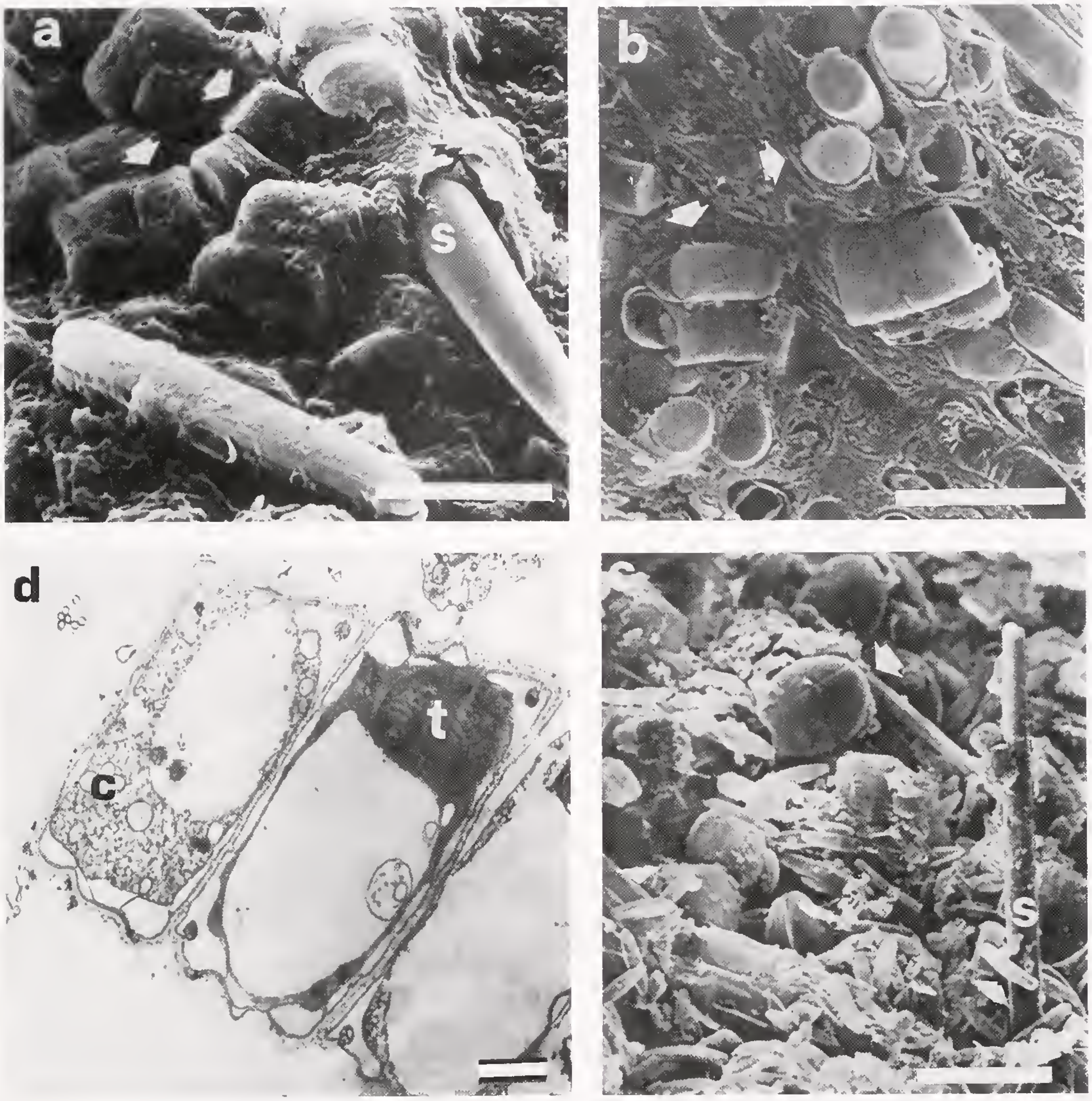

Figure 1. Diatoms living inside Antarctic sponges. (a) Several specimens of *Fragilariopsis curta* (arrows) and a *Fragilariopsis* sp. disposed under the exopinacoderm of *Tedania charcoti* (Scale bar, 50 μm. (b) *Fragilariopsis* sp. (arrows) embedded inside the same sponge (scale bar, 50 μm). (c) Large centric *Porosira* sp. (arrows) and numerous pennate *Achnanthes* sp. (arrow heads) in *Pseudosuberites antarcticus* (scale bar, 100 μm). (d) Transmission electron micrograph of *Fragilariopsis curta* inside the sponge body showing intact cytoplasm (c) and thylocoid (t) (scale bar, 10 μm). s, sponge spicules.

facultative heterotrophy. Mixotrophy, a combination of autotrophy and heterotrophy, is widespread among certain protists and, in particular, among flagellates such as haptophytes (13), dinoflagellates (14, 15, 16, 17), cryptophytes (18), and diatoms (19, 20, 21). Previous documentation of mixotrophy in diatoms was obtained by observations *in vitro*.

The relationship between myxotrophic diatoms and Antarctic sponges can be considered as a sort of symbiosis shifting to parasitism; *i.e.*, the algae can get nourishment, not only by photosynthesis, but also by utilizing organic carbon derived from their host. Although some Antarctic diatoms are considered among the most shade-adapted microalgae (23), the mixotrophy assumed in this report explains the surprising presence of dense diatom populations inside sponges living at 100–120 m depth, where the level of irradiance is very low (24).

Finally, the mechanism that causes a sponge to actively incorporate diatoms is unclear. However, some studies (22) have revealed a tendency of demosponges to incorporate

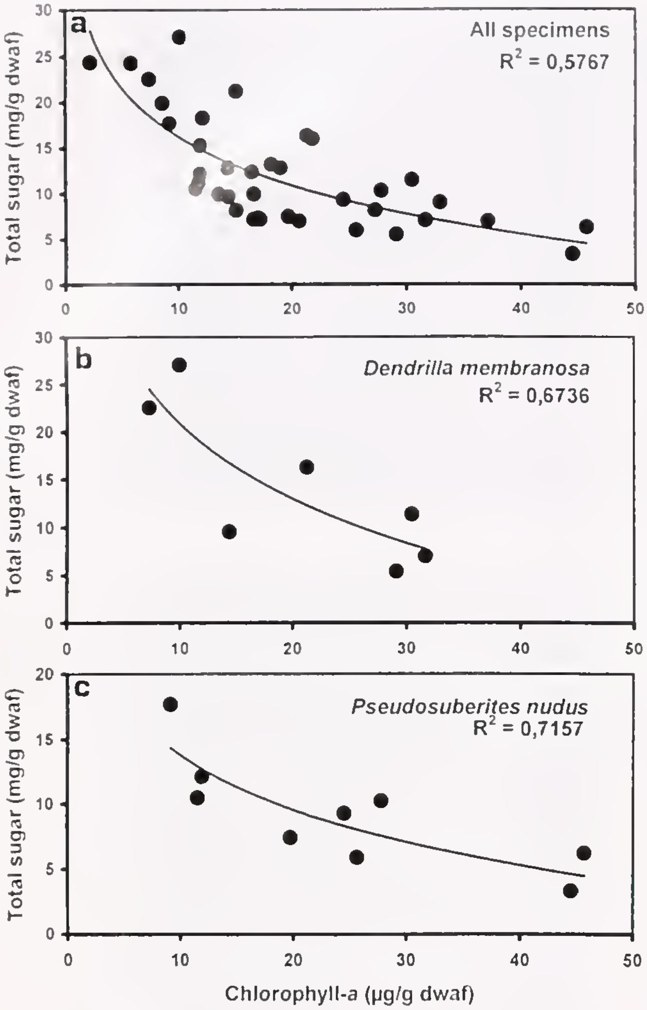

Figure 2. Concentration of chl-*a* as a function of the total amount of carbohydrate. Data from all the sponge specimens tested (a), from different specimens of *Dendrilla membranosa* (b), and from *Pseudosuberites nudus* (c). Each point represents a sponge specimen. The analyses were carried out on three samples of sponge tissue from each specimen. Samples were cylindrical cores of choanosomal tissue, 1 cm in diameter, 2 cm in height. Cores were longitudinally cut, and the two half-portions were tested to evaluate the chl-*a* concentration (as an estimate of diatom population biomass), as well as the total amount of carbohydrate. One subsample was extracted in 90% acetone. The chl-*a* was then assayed by spectrofluorimetry with excitation at 430 nm and emission measured at 668 nm. On the other subsample, the total carbohydrates were assayed: the method was based on the colorimetric reaction of sugars with phenol and sulphuric acid, and D(+) glucose was used as the standard (26).

siliceous particles, and the diatoms, with their siliceous shells, may thus "deceive" the sponge.

In conclusion, our data widen the ecological role of diatoms which, by exploiting the niche provided by sponges—one of the most important Antarctic benthic organisms—illustrate a strong functional link between plankton and benthos (25).

Literature Cited

1. **Gaino, E., G. Bavestrello, R. Cattaneo-Vietti, and M. Sarà. 1994.** Scanning electron microscope evidence for diatom uptake by two Antarctic sponges. *Polar Biol.* **14:** 1–4.
2. **Sarà, M., G. Bavestrello, R. Cattaneo-Vietti, and C. Cerrano. 1998.** Endosymbiosis in sponges: relevance for epigenesis and evolution. *Symbiosis* **25:** 57–70.
3. **Wilkinson, C. R. 1980.** Cyanobacteria symbiotic in marine sponges. Pp. 553–563 in *Endocytobiology. Endosymbiosis and Cell Biology.* W. Schwemmler and H. E. A. Schenk, eds. Walter De Gruyter, New York.
4. **Sarà, M. 1971.** Ultrastructural aspects of the symbiosis between two species of the genus *Aphanocapsa* (Cyanophyceae) and *Ircinia variabilis. Mar. Biol.* **11:** 214–221.
5. **Wilkinson, C. R. 1983.** Net primary productivity in coral reef sponges. *Science* **219:** 410–412.
6. **Arillo, A., G. Bavestrello, B. Burlando, and M. Sarà. 1983.** Metabolic integration between symbiotic cyanobacteria and sponges: a possible mechanism. *Mar. Biol.* **117:** 159–162.
7. **Cox, G., and A. W. D. Larkum. 1983.** A diatom apparently living in symbiosis with a sponge. *Bull. Mar. Sci.* **33:** 943–945.
8. **Myklestad, S., O. Holm-Hansen, K. M. Vårum, and B. Volcani. 1989.** Rate of release of extracellular aminoacids and carbohydrates from the marine diatom *Chaetoceros affinis. J. Plankton Res.* **11:** 763–773.
9. **Myklestad, S. 1995.** Release of extracellular products by phytoplankton with special emphasis on polysaccharides. *Sci. Total Environ.* **165:** 155–164.
10. **Hellebust, J. A., and J. Lewin. 1997.** Heterotrophic nutrition. Pp. 169–197 in *The Biology of Diatoms.* D. Werner, ed. University of California Press, Berkeley.
11. **White, A. W. 1974.** Growth of 2 facultatively heterotrophic marine centric diatoms. *J. Phycol.* **10:** 292–300.
12. **Lewin, J. C., and J. A. Hellebust. 1976.** Heterotrophic nutrition of marine pennate diatom *Nitzschia angularis* var. *affinis. Mar. Biol.* **36:** 313–320.
13. **Tillmann, U. 1998.** Phagotrophy by a plastidic haptophyte, *Prymnesium patelliferum. Aquat. Microb. Ecol.* **14:** 155–160.
14. **Graneli, E., D. M. Anderson, P. Carlsson, and S. Y. Maestrini. 1997.** Light and carbon uptake by *Dinophysis* species in comparison to other photosynthetic and heterotrophic dinoflagellates. *Aquat. Microb. Ecol.* **13:** 177–186.
15. **Legrand, C., E. Graneli, and P. Carlsson. 1998.** Induced phagotrophy in the photosynthetic dinoflagellate *Heterocapsa triquetra. Aquat. Microb. Ecol.* **15:** 65–75.
16. **Skovgaard, A. 1996.** Mixotrophy in *Fragilidium subglobosum* (Dinophyceae): growth and grazing responses as functions of light intensity. *Mar. Ecol. Prog. Ser.* **143:** 247–253.
17. **Tiselius, P., and M. Kuylenstierna. 1996.** Growth and decline of a diatom spring bloom: phytoplankton species composition, formation of marine snow and the role of heterotrophic dinoflagellates. *J. Plankton Res.* **18:** 133–155.
18. **Gervais, F. 1997.** Light dependent growth, dark survival and glucose uptake by cryptophytes isolated from a freshwater chemocline. *J. Phycol.* **33:** 18–25.
19. **Azam, F., and B. E. Volcani. 1974.** Role of silicon in diatom metabolism VI. Active transport of germanic acid in the heterotrophic diatom *Nitzschia alba. Arch. Microbiol.* **101:** 1–8.
20. **Darley, W. M., B. B. Wimpee, and C. T. Ohlman. 1981.** Heterotrophic and photoheterotrophic utilization of lactate by the diatom *Cylindrotheca fusiformis. Br. Phycol. J.* **16:** 423–428.

21. **Tan, C. K., and M. R. Johns. 1996.** Screening of diatoms for heterotrophic eicosapentaenoic acid production. *J. Appl. Phycol.* **8:** 59–64.

22. **Bavestrello, G., A. Arillo, U. Benatti, C. Cerrano, R. Cattaneo-Vietti, L. Cortesogno, L. Gaggero, M. Giovine, M. Tonetti, and M. Sarà. 1995.** Quartz dissolution by the sponge *Chondrosia reniformis* (Porifera, Demospongiae). *Nature* **378:** 374–378.

23. **Palmisano, A. C., J. B. SooHoo, D. C. White, G. A. Smith, G. R. Stanton, and R. H. Burckle. 1985.** Shade-adapted benthic diatoms beneath Antarctic sea ice. *J. Phycol.* **21:** 664–667.

24. **Vanucci, S., and M. Innamorati. 1997.** Available radiation profiles recorded in the Ross Sea. Pp. 281–290 in *Rossmize 1993–95 Data Report I.* F. M. Faranda, L. Guglielmo and P. Povero, eds. Lang Arti Grafiche, Genoa, Italy.

25. **Marcus, N. H., and F. Boero. 1998.** The importance of benthic-pelagic coupling and the forgotten role of the life cycles in coastal aquatic systems. *Limnol. Oceanogr.* **43:** 763–768.

26. **Dubois, M., K. A. Gilles, J. K. Hamilton, P. A. Rebers, and F. Smith. 1956.** Colorimetric method of determination of sugars and related substances. *Anal. Chem.* **28:** 350–356.

Reference: *Biol. Bull.* **198:** 34–49. (February 2000)

Maintaining the Line of Defense: Regeneration of Cuvierian Tubules in the Sea Cucumber *Holothuria forskali* (Echinodermata, Holothuroidea)

DIDIER VANDENSPIEGEL[1,*], MICHEL JANGOUX[1,2], AND PATRICK FLAMMANG[1,†]

[1]*Laboratoire de Biologie marine, Université de Mons-Hainaut, 6 Avenue du Champ de Mars, B-7000 Mons, Belgium; and* [2]*Laboratoire de Biologie marine (CP 160/15), Université Libre de Bruxelles, 50 Avenue F. D. Roosevelt, B-1050 Bruxelles, Belgium*

Abstract. When irritated, individuals of the sea cucumber *Holothuria forskali* expel a few Cuvierian tubules which lengthen, instantly become sticky, and rapidly immobilize most organisms with which they come into contact. After expulsion, the lost tubules are readily regenerated. When only a few tubules have been expelled, there is often a latent period before the regeneration starts. In contrast, when many tubules have been expelled, the regenerative process starts immediately but proceeds in successive waves of 10 to 30 tubules that begin to regenerate at 10-day intervals. However, in all cases, the complete regeneration of a given tubule takes about 5 weeks and may be divided into three successive phases: an initial repair phase including the overall 48-h post-autotomy period, a true regenerative phase taking about 4 weeks to complete, and a growth phase of about one more week. Initial regeneration events occur by epimorphosis, cell proliferation being essential to the regenerative process, whereas late events occur mainly by morphallaxis, with migration of the newly differentiated cells. The mesothelium is the tissue layer in which cell proliferation is the most precocious and the most important, involving both peritoneocytes and undifferentiated cells (which seem to be dedifferentiated peritoneocytes). As regeneration proceeds, the percentage of undifferentiated cells regularly decreases in parallel with the differentiation of granular (adhesive-secreting) cells and myocytes. The myocytes then separate off from the mesothelium and migrate within the connective tissue layer. Three types of pseudopodial cells follow one another in the tubule connective tissue during regeneration. Type 1 cells have all the characteristics of echinoderm phagocytes and may have a fibroclastic function, cleaning the connective tissue compartment before new collagen synthesis starts. Type 2 cells are rather undifferentiated and divide actively. The presence of type 3 cells is closely associated with the appearance of collagen fibers, and it is suggested that they have a fibroblastic function. In the inner epithelium, cells also divide actively, but only those in which spherules have not yet differentiated in the basal intraconnective processes. It appears, therefore, that in the three tissue layers of the tubules, regeneration proceeds by cell dedifferentiation, then proliferation, and finally by differentiation. Cuvierian tubules thus constitute a very efficient defensive mechanism: their large number, sparing use, and particular regeneration dynamics make them an almost inexhaustible line of defense maintained at limited energy cost.

Introduction

Several species of holothuroids (sea cucumbers), all belonging to the order Aspidochirotida, possess a very specialized defensive system: the so-called Cuvierian tubules (Flammang, 1996). This system consists of several hundred tubules whose proximal ends attach to the basal part of the left respiratory tree and whose distal, blind ends float freely in the coelomic cavity. When irritated, the animal curves its aboral end toward the irritating object and undergoes a general contraction. The anus opens, the wall of the cloaca tears, and the free ends of the Cuvierian tubules, together with coelomic fluid, are expelled through the tear and the

---

Received 1 June 1999; accepted 22 November 1999.

[*] Present address: Royal Museum for Central Africa, Invertebrate Section, B-3080 Tervuren, Belgium.

[†] To whom correspondence should be addressed. E-mail: Patrick.Flammang@umh.ac.be

anus. The emitted tubules lengthen, instantly become sticky, and rapidly immobilize most organisms with which they come into contact (VandenSpiegel and Jangoux, 1987). Finally, the expelled tubules autotomize at their attachment point on the left respiratory tree and are left behind as the holothuroid crawls away (Müller *et al.*, 1970; VandenSpiegel and Jangoux, 1987). As only a portion of the tubules are emitted at one time, the total number may suffice for several responses. After expulsion, the lost tubules are readily regenerated (Hyman, 1955).

The fine structure of the Cuvierian tubules in the species *Holothuria forskali* has been described by VandenSpiegel and Jangoux (1987). Quiescent Cuvierian tubules consist of an outer mesothelium, an inner epithelium, and between them, a thick connective tissue layer that includes muscle fibers. The mesothelium is a pseudostratified epithelium made up of two cell layers, namely an apical layer of ciliated peritoneocytes and a basal layer of granular cells filled with densely packed lipoproteic granules. Together, these layers form conspicuous transverse folds that penetrate the underlying connective tissue. Circular and longitudinal myocytes occur under the tips of the mesothelial folds. These cells divide the connective tissue into a thin outer layer (where collagen fibers are directed perpendicularly to the tubule long axis) and a thick inner layer (where collagen fibers are arranged in helixes parallel to the tubular long axis). Nerve processes are associated with the longitudinal muscles; they also occur between the spirally arranged collagen fibers. The tubule lumen is narrow with a highly convoluted limiting epithelium. Epithelial cells are not ciliated; they have basal processes containing enlarged spherules whose contents include mucosubstances and proteins.

The histological organization of Cuvierian tubules, which is quite different from that of the left respiratory tree that bears them, appears to be functionally important for their correct operation (VandenSpiegel and Jangoux, 1987). However, as pointed out by Smiley (1994), the histogenesis of these intriguing organs is virtually unknown. Similarly, nothing is known about the renewal of the Cuvierian tubule stock after expulsion and, consequently, on the way holothuroids maintain their line of defense. We have thus investigated the process of Cuvierian tubule regeneration in the holothuroid *Holothuria forskali.* Our aims were (i) to study the dynamics of the regenerative process and to describe macroscopically the different regeneration stages; (ii) to detail the installation of the different tissue layers, using electron microscopy; and (iii) to determine, through immunohistochemistry and autoradiography, the origin of the cells involved in tubule regeneration.

Materials and Methods

Individuals of *Holothuria forskali* (Delle Chiaje, 1823) were collected at a depth of 20 to 30 m by scuba diving in the bay of Morlaix (Brittany, France). They were transported to the Marine Biology Laboratory of the University of Mons-Hainaut, where they were kept in a marine aquarium with closed circulation (13°C, 33‰ salinity).

Induction of tubule expulsion and sampling of regenerating tubules

The expulsion of Cuvierian tubules was induced mechanically by pinching the dorsal integument of the holothuroids with forceps. Two sets of regenerating animals were investigated: the first set comprised 15 individuals that had been stimulated only once and had expelled about 15 tubules (gentle stimulation); the second set consisted of 25 individuals that had been stimulated repeatedly to induce the expulsion of about 300 tubules (strong stimulation). After tubule expulsion, all the animals were returned to the aquarium and dissected at various times to provide samples for observation macroscopically and with transmission electron microscopy (TEM). Tubules in the process of regeneration were dissected from each set of cucumbers every day for 6 days, and then weekly for 8 weeks. Before dissection, the animals were anesthetized for 1 h in 0.2% propylene phenoxytol (Nipa laboratories, UK; see Hill and Reinschmidt, 1976) in seawater. For the immunohistochemical and autoradiographical studies of Cuvierian tubule regeneration, 10 of the strongly stimulated sea cucumbers were put aside in a separate aquarium for 1 month.

Light and transmission electron microscopy

Regenerating tubules were fixed for 3 h at 4°C in 3% glutaraldehyde in cacodylate buffer (0.1 *M*, pH 7.8; adjusted to 1030 mOsm with sodium chloride), then rinsed in cacodylate buffer and post-fixed for 1 h in 1% osmium tetroxide in the same buffer. After a final wash in buffer, the podia were dehydrated in graded ethanol and embedded in Spurr. Semithin sections (1 μm in thickness) were cut on a Reichert Om U2 ultramicrotome equipped with a glass knife and then stained according to the method of Humphrey and Pittman (1974). Ultrathin sections (40–70 nm) were cut with a Leica UCT ultramicrotome equipped with a diamond knife, stained with uranyl acetate and lead citrate, and observed with a Zeiss EM 10 transmission electron microscope.

Immunohistochemistry

The BrdU/anti-BrdU method was used to study DNA synthesis in the regenerating tubules. After one month of regeneration, five of the strongly stimulated holothuroids were injected intracoelomically with 2 ml of a 2% solution of BrdU (5-bromo-2-deoxyuridine; Aldrich Chemie) in filtered seawater (0.45 μm; Millipore). One hour after injection, the individuals were dissected and their regenerating tubules fixed for 6 h in Allen-Bouin's fluid (Gabe, 1968). They were then rinsed thoroughly in running tap water, dehydrated in graded ethanol, embedded in Paraplast, and sectioned (5 μm). BrdU-containing DNA in the nuclei of proliferating cells was detected by the immunogold-silver staining (IGSS) method (Hacker *et al.*, 1985; adapted for echinoderm tissues in VandenSpiegel *et al.*, 1991). The sections were treated with trypsin (0.1% trypsin in 0.01 *M* sodium barbital, 0.15 *M* NaCl, pH 8.0) for 50 min at 37°C, followed by acid hydrolysis in 3 *M* HCl at 60°C for 30 min. This treatment denatures the DNA and unmasks hidden epitopes. After rinsing in distilled water, the sections were preincubated for 20 min in 5% normal goat serum in 0.01 *M* sodium barbital, 0.15 *M* NaCl, pH 7.4 (veronal buffer-NGS), then incubated overnight at 4°C with mouse anti-BrdU monoclonal antibodies (DAKO A/S) diluted 1:30 in veronal buffer-NGS. After several washes in phosphate-buffered saline (PBS), the sections were incubated for 1 h at room temperature in goat anti-mouse immunoglobulins conjugated to 5 nm gold particles (Auroprobe LM; Amersham) diluted 1:40 in PBS-NGS. Gold particles bound to the immunocomplexes were visualized by a silver precipitation reaction, using a commercial kit (Intense SE TMII; Amersham). The reaction was stopped with distilled water and the sections were counterstained with hemalun and eosin.

Autoradiography

Cell proliferation was also monitored using autoradiography. Tritiated thymidine (150 μCi of a 1 mCi/ml aqueous solution of 5'-^{3}HT; Amersham) was mixed with 1 ml of filtered seawater and injected, through the holothuroid integument, into the coelomic cavity. This injection was performed on five strongly stimulated individuals that had started regenerating Cuvierian tubules one month earlier. One hour after injection, the holothuroids were dissected, and the regenerating tubules were fixed and embedded as for TEM (see above). Semithin sections (1-μm thick) were collected on glass slides and stored in distilled water. All subsequent manipulations took place in a darkroom. The slides were dipped in photographic emulsion (Nuclear research emulsion L5; Ilford) diluted 1:1 in distilled water at 45°C. After air-drying, the coated slides were stored in light-proof boxes at 4°C for 10 days. Exposed slides were developed for 4 min at room temperature in Kodak D19 diluted 1:2 in distilled water, transferred to a stop-bath (2% acetic acid) for 30 s, followed by fixation (10% Acidofix) for 5 min. After rinsing in running tap water, the autoradiographed sections were stained with toluidine blue.

Counting and identification of proliferating cells

Labeled nuclei were counted in sections of regenerating tubules that were processed either by immunohistochemistry or by autoradiography. For each regeneration stage, a labeling index (LI) was determined in the three main tissue layers of the tubules (*i.e.*, the mesothelium, the connective tissue layer, and the inner epithelium). This index represents the percentage of labeled nuclei (LN) compared to the total number of counted nuclei (TN); it is calculated according to the formula: LI = (LN/TN) × 100. For each stage, four counts, each comprising a maximum of 100 nuclei, were done on sections coming from four different regenerating tubules from a single holothuroid.

To identify proliferating cells we used the procedure of Laurent *et al.* (1988), which relies on the fact that tissues labeled with ^{3}HT and embedded in Spurr resin can be observed by both light and electron microscopy. For each regeneration stage, we used three to four ultrathin sections directly followed by one semithin section. The former were observed in TEM, whereas the latter was processed for autoradiography (see above). In most cases, the shape of the labeled cells, as it appeared on the semithin section, was characteristic enough to allow their localization on the ultrathin section. It was therefore possible to identify the cell types involved in DNA synthesis.

Results

Macroscopic observations

Regeneration of the Cuvierian tubules in *Holothuria forskali* was observed after two types of stimulations: gentle stimulations inducing the expulsion of about 15 tubules and strong stimulations inducing the expulsion of about 300 tubules. After a gentle stimulation, tubule expulsion is not always followed by immediate regeneration of new tubules; rather, a latent period of up to 20 days was observed. In addition, the beginning of the regeneration could not be detected without sacrificing the animal. Therefore, a regeneration that followed a gentle stimulation was difficult to study. However, data collected from the staggered dissections have allowed us to estimate that the duration of the regeneration is at least 4 weeks, and that all of the autotomized tubules regenerate synchronously. After a strong stimulation, on the other hand, regeneration starts immediately, although only for a limited number of tubules. Indeed, the regeneration proceeds by groups of 10 to 30 tubules; the beginning of the regeneration in one group being separated from that of the following one by 5 to 10 days. Therefore, about one month after the induction of a massive tubule autotomy, holothuroids have tubules at several stages of regeneration (Fig. 1).

The observation of Cuvierian tubule regeneration after a strong stimulation has allowed us to describe five successive stages in the expulsion-autotomy-regeneration cycle (Fig. 2):

Stage I corresponds to the healing of the damaged tissues followed by the appearance, 2 to 6 days after autotomy, of

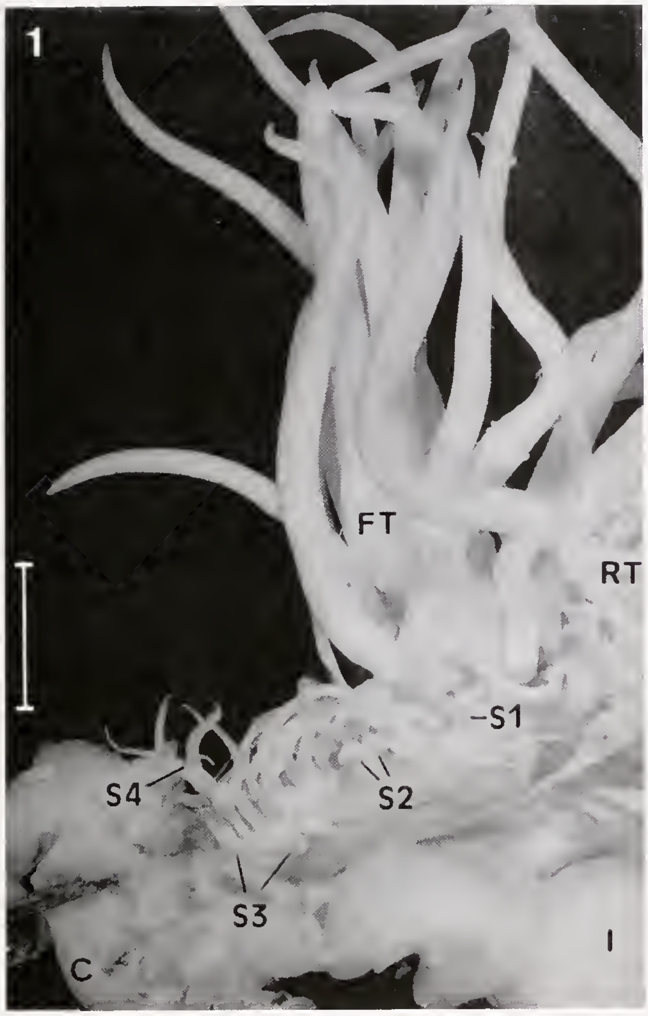

Figure 1. General aspect of regenerating Cuvierian tubules in *Holothuria forskali* 3 weeks after a massive tubule expulsion, showing tubules at different stages of regeneration (bar = 0.5 cm). C, cloaca; FT, fully developed tubule; I, intestine; RT, left respiratory tree; S1–S4, stages 1–4.

a thickening of the wall of the basal part of the left respiratory tree, at the place where the expelled tubules were attached (S1; Figs. 1 and 2).

Stage 2 corresponds to the formation, 8 to 10 days after autotomy, of a translucent spherical structure measuring from 0.1 to 0.4 mm in diameter (S2; Figs. 1 and 2).

Stage 3 corresponds to the development, 10 to 14 days after autotomy, of a translucent club-shaped structure ranging from 1 to 3 mm in length for a maximum diameter of 0.3 mm (S3; Figs. 1 and 2).

Stage 4 corresponds to the transformation of the regenerating structure, 14 to 21 days after autotomy, into a small pale-pink tubule measuring from 4 to 12 mm in length (S4; Figs. 1 and 2). From this stage on, the shape of the regenerating tubule remains constant, only the length and diameter of the tubule increase.

Stage 5 corresponds to the differentiation, 21 to 28 days after autotomy, of a functional tubule that possesses a short basal peduncle and measures from 14 to 22 mm long for a diameter of about 0.65 mm (S5; Fig. 2). Although they are only half the size of a fully developed tubule, regenerating tubules at stage 5 are able to lengthen and become sticky. They reach their full size 28 to 35 days after autotomy.

Ultrastructure of regenerating tubules

Immediately after their expulsion and lengthening, Cuvierian tubules are autotomized at the narrow peduncle that attaches them to the left respiratory tree. The resulting wound is relatively limited and is rapidly closed by migration of mesothelial cells on the coelom side and epithelial cells on the side of the respiratory tree lumen. At the same time, the connective tissue is invaded by very active phagocytes that remove cell debris from the tissue. These large cells have many cytoplasmic inclusions, such as phagosomes, secondary lysosomes, and residual bodies.

Stage 1. Regeneration *sensu stricto* takes place right after wound healing and starts with the formation of a small mesothelial bud that appears as a local thickening of the wall of the basal part of the left respiratory tree. This bud consists of a mass of cells forming a pseudostratified mesothelium in which an outer layer of ciliated adluminal cells (peritoneocytes) covers a few layers of undifferentiated cells (Fig. 3). Peritoneocytes are tack-shaped cells whose apical part lines the coelomic cavity. They are bound to-

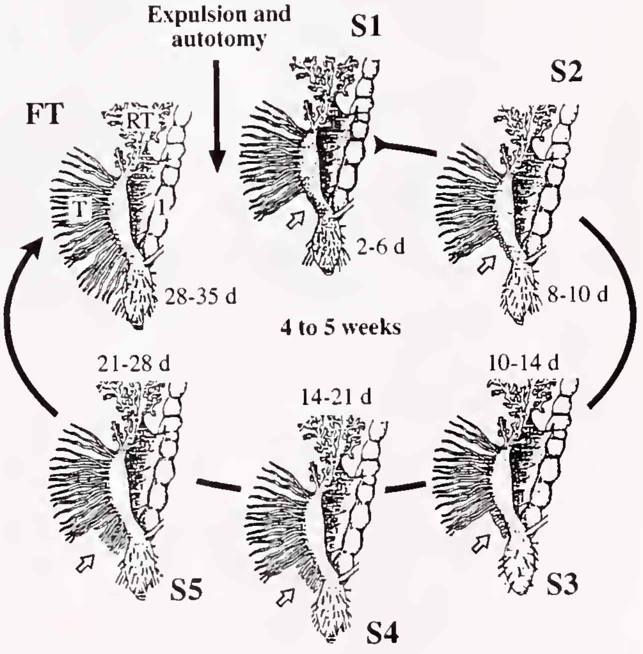

Figure 2. Chronology of the regeneration stages of Cuvierian tubules in *Holothuria forskali*. Open arrows point to the regenerating tubules. FT, fully-developed tubules; I, intestine; RT, left respiratory tree; T, Cuvierian tubules; S1–S5, stages 1–5.

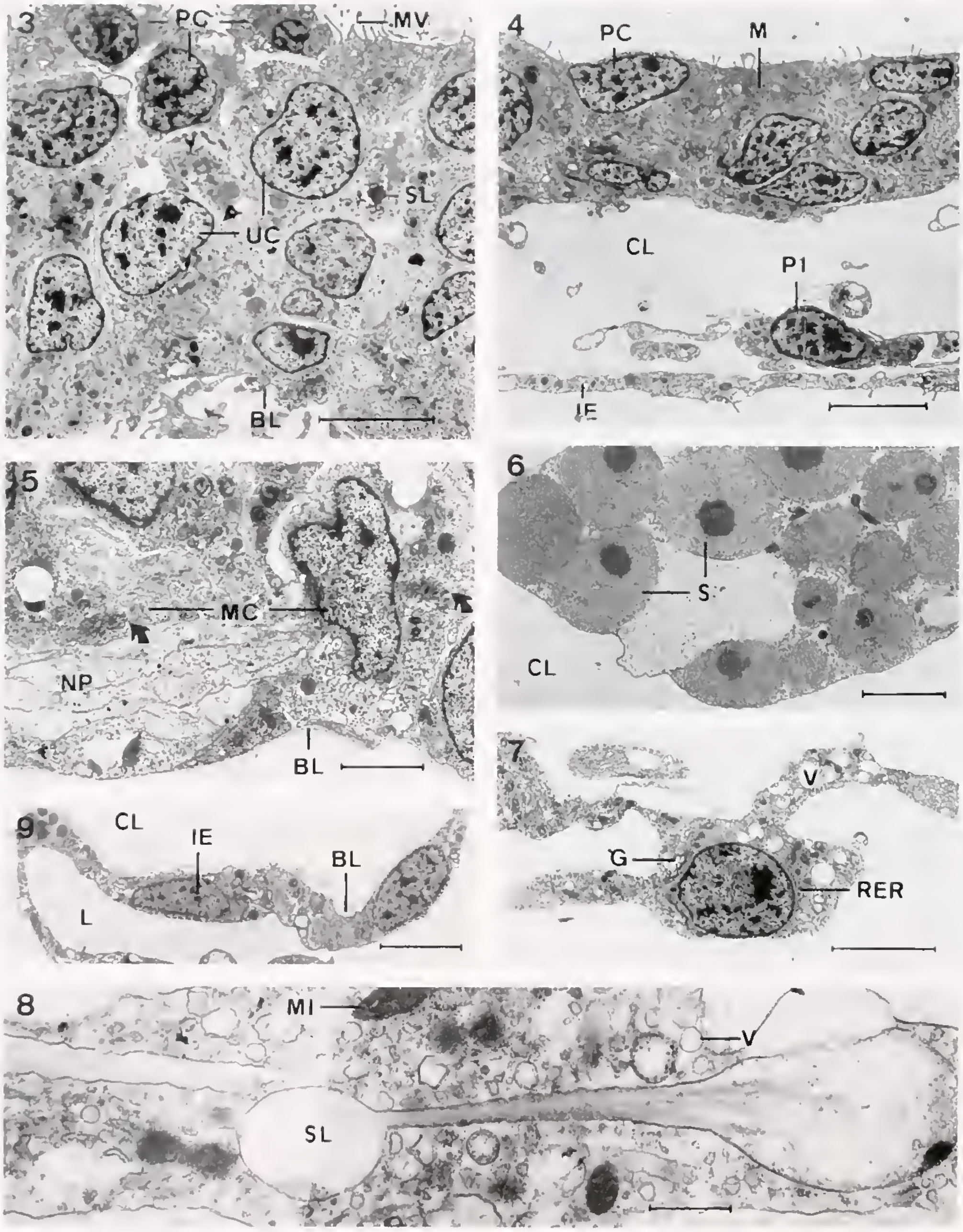

Figures 3–9. *Holothuria forskali.* Ultrastructure of stage 1 and 2 regenerating Cuvierian tubules. BL, basal lamina; CL, connective tissue layer; G, Golgi apparatus; IE, internal epithelium; L, lumen; M, mesothelium; MC, myocyte; MI, mitochondrion; MV, microvillus; NP, nerve plexus; P1, type 1 pseudopodial cell; PC, peritoneocyte; RER, rough endoplasmic reticulum; S, spherule; SL, secondary lysosome; UC, undifferentiated cell; V, vesicle. **Figure 3.** Mesothelium at stage 1 (bar = 5 μm). **Figure 4.** Longitudinal section through the wall of a stage 2 regenerating tubule (bar = 5 μm). **Figure 5.** Detailed view of the basal part of the mesothelium showing the myocytes and the nerve plexus (bar = 2 μm). Arrows indicate bundles of myofilaments. **Figure 6.** Intraconnective spherulocyte (stage 2; bar = 2 μm). **Figure 7.** Intraconnective type 1 pseudopodial cell (stage 2; bar = 4 μm). **Figure 8.** Detailed view of the cytoplasm of a type 1 pseudopodial cell (stage 2; bar = 0.5 μm). **Figure 9.** Longitudinal section through the inner epithelium (stage 2; bar = 4 μm).

gether by an apical zonula adhaerens. Each peritoneocyte bears a single cilium (about 10 μm long) and a few scattered microvilli (Fig. 3). The apical part of the cell houses the nucleus, a juxtanuclear Golgi complex, a well-developed rough endoplasmic reticulum (RER), numerous free ribosomes, some lipid granules, and many mitochondria. Large secondary lysosomes (1 to 1.5 μm in diameter) also occur in the apical cytoplasm. The basal part of the cell, which is thin and elongated, traverses the undifferentiated cell layers before contacting the basal lamina through a hemidesmosome-like structure. Undifferentiated cells are cube-shaped and have a high nuclear-cytoplasmic ratio (Fig. 3). However, although reduced, the perinuclear cytoplasm encloses a well-developed Golgi apparatus and RER, many mitochondria and free ribosomes, lipid granules, and numerous secondary lysosomes (Fig. 3). Undifferentiated cells are connected to the basal lamina through hemidesmosome-like structures, but they are neither bound together nor bound to the peritoneocytes.

Stage 2. At the end of this stage, the regenerating structure already has the three tissue layers characteristic of a non-regenerating Cuvierian tubule, *i.e.*, a mesothelium, a connective tissue layer, and an inner epithelium (Figs. 4, 10).

The general organization of the mesothelium is similar to the one observed in stage 1 except that some myocytes occur among the undifferentiated cells (Figs. 5, 10). Myocytes are cube-shaped. They have a large nucleus and enclose one bundle of myofilaments in their cytoplasm (Fig. 5), which also contains a well-developed RER and numerous mitochondria. No junction connecting the myocytes to the other mesothelial cells was observed. However, each myocyte is anchored to the basal lamina by a hemidesmosome-like structure. A discrete nerve plexus is associated with the mesothelium of stage 2 regenerating tubules. It consists of nerve processes, preferentially located close to the myocytes (Figs. 5, 10).

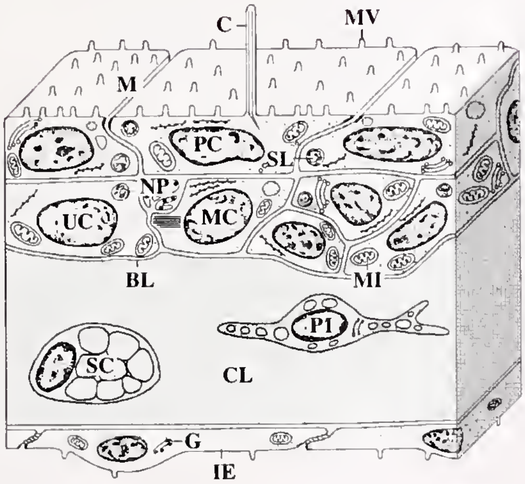

Figure 10. *Holothuria forskali.* Reconstruction of a longitudinal section through the wall of a stage 2 regenerating Cuvierian tubule (not to scale). BL, basal lamina; C, cilium; CL, connective tissue layer; IE, internal epithelium; G, Golgi apparatus; M, mesothelium; MC, myocyte; MI, mitochondrion; MV, microvillus; NP, nerve plexus; P1, type 1 pseudopodial cell; PC, peritoneocyte; SC, spherulocyte, SL, secondary lysosome; UC, undifferentiated cell.

Encompassed between the basal lamina of the mesothelium and that of the inner epithelium, the thin connective tissue layer (about 7.5 μm in thickness) is poor in collagen fibers, but contains many mesenchymatous cells, both spherulocytes and type 1 pseudopodial cells (Figs. 6, 7, 10). Spherulocytes are ovoid to spherical cells, 5 to 10 μm in diameter. Their cytoplasm is packed with spherules that average 3 μm in diameter and enclose an electron-lucent material (Fig. 6). Type 1 pseudopodial cells possess a central, nucleus-containing cell body from which two to three thin cell processes radiate (Figs. 4, 7). Their cytoplasm encloses one or two juxtanuclear Golgi stacks, a well-developed RER, a few lysosomal bodies, many mitochondria, and numerous clear vesicles of various sizes. In some micrographs, large secondary lysosomes enclosing partly decomposed collagen fibrils were observed (Fig. 8).

The inner epithelium delimits a quite large lumen. It consists of only one cell type that strongly resembles the epithelial cells of the respiratory tree at the level where Cuvierian tubules are inserted. These cells are non-ciliated cells that bear a few apical microvilli (Figs. 4, 9, 10). They are connected together through junctional complexes consisting of an apical zonula adherens and a subapical septate desmosome, but they do not attach to the basal lamina. Epithelial cells are flat (2.4 μm in the nucleus-containing thickest part). Their cytoplasm contains a Golgi apparatus, a few scattered mitochondria, and some lipid granules.

Stage 3. The mesothelium is pseudostratified and still comprises peritoneocytes, undifferentiated cells, and myocytes (Figs. 11, 12, 16). Peritoneocytes and undifferentiated cells are similar to those observed in stages 1 and 2. In contrast, myocytes have clearly increased in number and can be divided into two sets according to the orientation of their bundle of myofilaments, either circular or longitudinal. Circular myocytes are always located beneath longitudinal myocytes. They possess a basal cytoplasmic process that penetrates the underlying connective tissue layer and encloses the bundle of myofilaments (Figs. 12, 13). The nerve plexus is more developed than in the previous stage and still preferentially associated with the myocytes (Figs. 12, 16).

The connective tissue layer has increased in thickness (to about 30 μm) and, at this stage, makes up three-quarters of the total thickness of the regenerating tubule wall. As in the previous stage, the connective tissue layer is poor in collagen fibers and contains numerous mesenchymatous cells. Spherulocytes, however, are no longer present; only pseudopodial cells remain. These cells are of two types: type 1 cells, identical to those observed at the previous stage, and type 2 cells; the latter being, by far, the more abundant. Type 2 pseudopodial cells have a particular distribution; they are mainly located just below the basal lamina of the mesothelium (Figs. 13, 16). They have a teardrop shape, the tapered part forming a single process that always faces the basal lamina. These cell processes were sometimes ob-

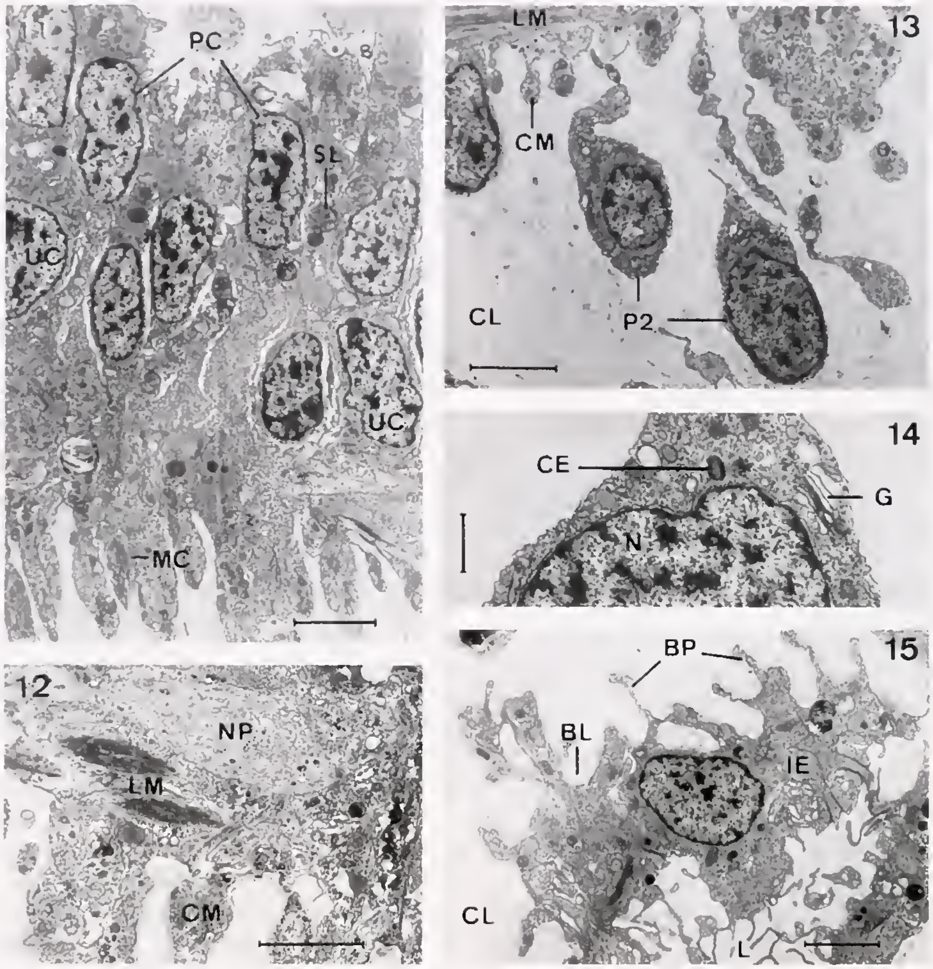

Figures 11–15. *Holothuria forskali.* Ultrastructure of stage 3 regenerating Cuvierian tubules. BL, basal lamina; BP, epithelial cell basal process; CE, centriole; CL, connective tissue layer; CM, circular myocyte; IE, internal epithelium; G, Golgi apparatus; L, lumen; LM, longitudinal myocyte; MC, myocyte; N, nucleus; NP, nerve plexus; P2, type 2 pseudopodial cell; PC, peritoneocyte; SL, secondary lysosome; UC, undifferentiated cell. **Figure 11.** Longitudinal section through the mesothelium (bar = 3 μm). **Figure 12.** Detailed view of the myocytes (bar = 3 μm). **Figure 13.** Intraconnective type 2 pseudopodial cells (bar = 3 μm). **Figure 14.** Detailed view of a type 2 pseudopodial cell (bar = 0.5 μm). **Figure 15.** Transverse section through the inner epithelium (bar = 3 μm).

served contacting the intraconnective basal processes of the circular myocytes (Fig. 13). Type 2 pseudopodial cells have a high nuclear-cytoplasmic ratio. Their reduced perinuclear cytoplasm encloses a Golgi apparatus as well as a pair of centrioles (Fig. 14).

The inner epithelium is only slightly different from that seen in stage 2. The epithelial cells have a more irregular shape and develop two to three basal processes penetrating the underlying connective tissue layer (Figs. 15, 16). These processes are lined by the basal lamina but, as previously, there is no attachment structure between the epithelial cells and this basal lamina.

Stage 4. At this stage of regeneration, the mesothelium develops transversal folds that penetrate the connective tissue layer (Figs. 17, 20). Three cell types may be recognized in the mesothelium: peritoneocytes, granular cells, and myocytes. The undifferentiated cells are no longer present. Peritoneocytes form the coelomic lining and always cover the granular cells. They are tack-shaped with a flattened apical part and a thin elongated basal part. They are now attached to each other through junctional complexes consisting of an apical zonula adherens and a subapical septate desmosome, and to the basal lamina through hemidesmosome-like structures. The nucleus is located in the apical part of the cell where the cytoplasm contains a Golgi apparatus and a few mitochondria (Fig. 17). Granular cells are very flattened and form a subapical cell layer that is accordion-pleated perpendicularly to the long axis of the tubule, each pleat penetrating the underlying connective tissue. The cytoplasm of these cells contains many electron-dense gran-

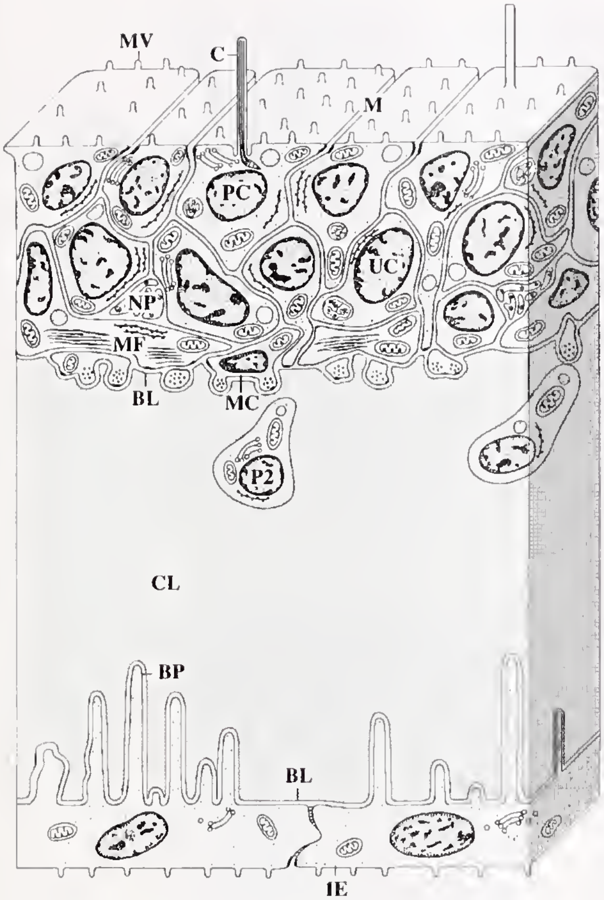

Figure 16. *Holothuria forskali.* Reconstruction of a longitudinal section through the wall of a stage 3 regenerating Cuvierian tubule (not to scale). BL, basal lamina; BP, epithelial cell basal process; C, cilium; CL, connective tissue layer; IE, internal epithelium; M, mesothelium; MC, myocyte; MF, bundle of myofilaments; MV, microvillus; NP, nerve plexus; P2, type 2 pseudopodial cell; PC, peritoneocyte; UC, undifferentiated cell.

ules that range from 0.1 to 0.3 μm in diameter and often occur in the vicinity of a large Golgi apparatus and of a well-developed RER (Fig. 17). Many of the cisternae of the RER are distended and filled with an amorphous material. The nucleus is egg-shaped and usually located in the lowermost part of the cell (*i.e.*, at the base of the pleats). No cellular junctions were observed between the granular cells or between the granular cells and peritoneocytes. However, the granular cells attach to the basal lamina through a hemidesmosome-like structure. Myocytes are located either in the most basal part of the mesothelium (*i.e.*, at the base of the folds), or here and there within the connective tissue layer, where they form an intraconnective muscle layer (Figs. 17, 20). The circular myocytes are always basal to the longitudinal ones. A single basal lamina lines both types of myocytes as well as the rest of the mesothelium. A well-developed nerve plexus is present and is mostly associated with the longitudinal myocytes, whether they are intramesothelial or within the connective tissue (Figs. 17, 20).

The thick connective tissue layer is, from place to place, divided into an outer area and an inner area by the presence of the intraconnective muscle layer. The outer area is thin (about 12 μm thick) and encloses very few collagen fibers and cells. The inner area, on the other hand, is much thicker (about 120 μm thick); it contains many collagen fibers, which show no tridimensional organization, and numerous pseudopodial cells (Fig. 20). Most of the latter are type 3 cells, although a few type 2 cells may still be observed. Type 3 pseudopodial cells possess a central nucleus-containing cell body from which one to three cell processes radiate (Fig. 18). Their characteristic feature is an extensive RER with some very distended cisternae filled with an electron-lucent amorphous material (Fig. 18). Their cytoplasm also contains numerous mitochondria and a well-developed Golgi apparatus. On some micrographs, the Golgi stacks show cisternae ending with spheroidal distentions that enclose a fuzzy material of low electron density (Fig. 19).

The inner epithelium is similar to the one described in stage 3 (Fig. 20).

Stage 5. At this stage, the ultrastructure of the regenerating tubule is very similar to that of a non-regenerating quiescent Cuvierian tubule (or fully developed tubule); the tubules in these two stages differ mostly in their size.

The mesothelium consists of peritoneocytes that cover elongated granular cells. Together they form the conspicuous transversal folds that are characteristic of the nonregenerating tubule mesothelium (Figs. 21, 25). The muscle layer is now completely separated from the mesothelium and is located in the outer part of the connective layer, just under the tips of the mesothelial folds (Figs. 21, 25). This layer comprises outer longitudinal and inner circular myocytes, and it divides the connective tissue layer into a thin outer area and a thick inner area. Numerous nerve processes are associated with the longitudinal myocytes (Figs. 21, 25). An additional cell type, vacuolar cells, has appeared at this stage (Figs. 21, 25). These cells, which are not numerous, are directly connected neither to the mesothelium nor to the muscle layer, but are scattered within the connective tissue outer area, occurring singly or in small clusters of two or three cells. Vacuolar cells are limited by a basal lamina. Their cytoplasm is packed with vacuoles about 0.6 μm in diameter that enclose an electron-lucent heterogeneous material (Fig. 21).

The connective tissue layer still contains numerous type 3 pseudopodial cells that are widely distributed from the mesothelium to the inner epithelium (Figs. 22–25). In its inner area, it encloses densely packed collagen fibers that start to be organized in helixes parallel to the long axis of the tubule. Intermingled with the collagen fibers are slender neurosecretory-like cell processes whose cytoplasm is filled

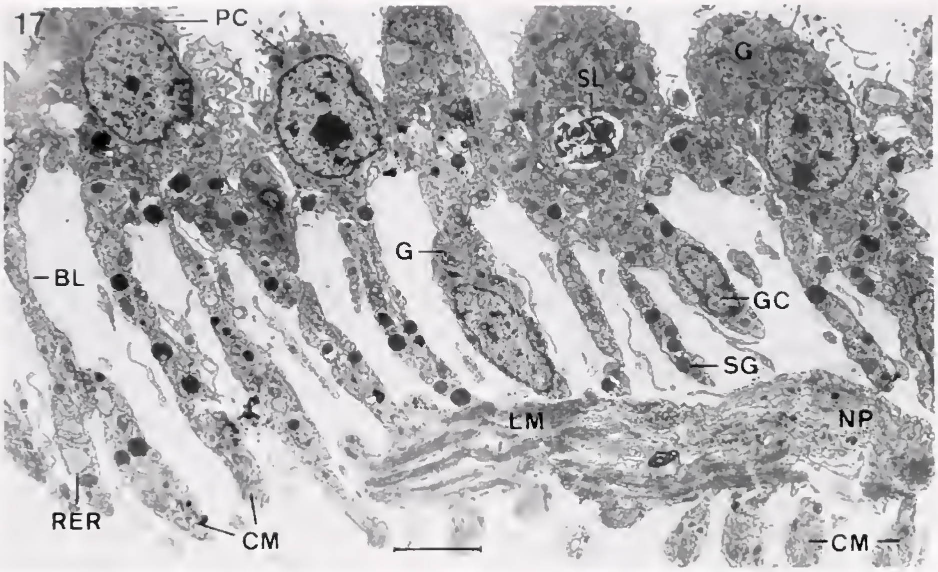

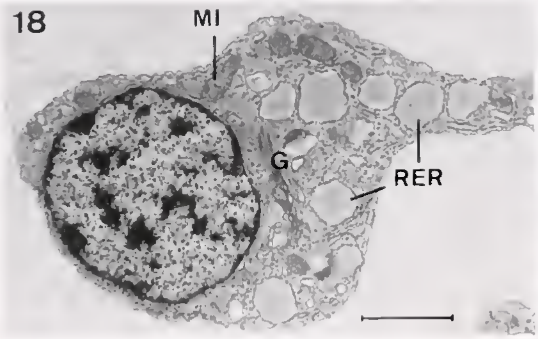

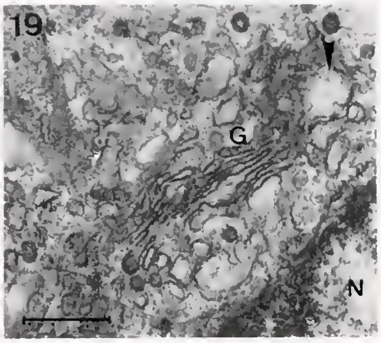

Figures 17–19. *Holothuria forskali.* Ultrastructure of stage 4 regenerating Cuvierian tubules. BL, basal lamina; CM, circular myocyte; G, Golgi apparatus; GC, granular cell; LM, longitudinal myocyte; MI, mitochondrion; N, nucleus; NP, nerve plexus; PC, peritoneocyte; RER, rough endoplasmic reticulum; SG, secretory granule; SL, secondary lysosome. **Figure 17.** Longitudinal section through the mesothelium (bar = 2 μm). **Figure 18.** Intraconnective type 3 pseudopodial cell (bar = 1 μm). **Figure 19.** Detailed view of the cytoplasm of a type 3 pseudopodial cell (the arrowhead indicates a spheroidal distention of a proximal Golgi cisterna; bar = 0.2 μm).

with electron-dense, membrane-bound granules (about 0.2 μm in diameter; Fig. 22). These processes are limited by a basal lamina.

Due to the considerable development of the connective tissue layer, the tubule lumen is narrow with a highly convoluted limiting epithelium. Each epithelial cell possesses one or two intraconnective, basal processes that enclose a few large spherules with a heterogeneous content (Figs. 23–25).

Study of cell proliferation

The distribution and abundance of proliferating cells at each regeneration stage were investigated by immunohistochemistry after BrdU incorporation, and by autoradiography after ^{3}HT incorporation. The intensity and pattern of cellular labeling were identical with both methods. The results show that, in the four first stages of regeneration, labeled nuclei are uniformly distributed in the three tissue layers of the regenerating tubule; *i.e.*, the mesothelium, the connective tissue layer, and the inner epithelium (Figs. 26–29). There is no evidence of a well-defined cell proliferation site. Labeling indices indicated that, in the three tissue layers, DNA-synthesizing cells are most abundant at the beginning of the regenerative process, their number then decreasing regularly in the successive regeneration stages (Fig. 26). In the connective tissue layer, however, the labeling index stays maximum until stage 3 and then regularly decreases (Fig. 26). At stage 5, very few labeled cells are observed in the three tissue layers, although the regenerating tubule measures only half of its final size. Labeled cells were never observed in a non-regenerating Cuvierian tubule.

Proliferating cells were identified by observation of consecutive semithin and ultrathin sections, the former being treated by autoradiography after ^{3}HT incorporation. In the

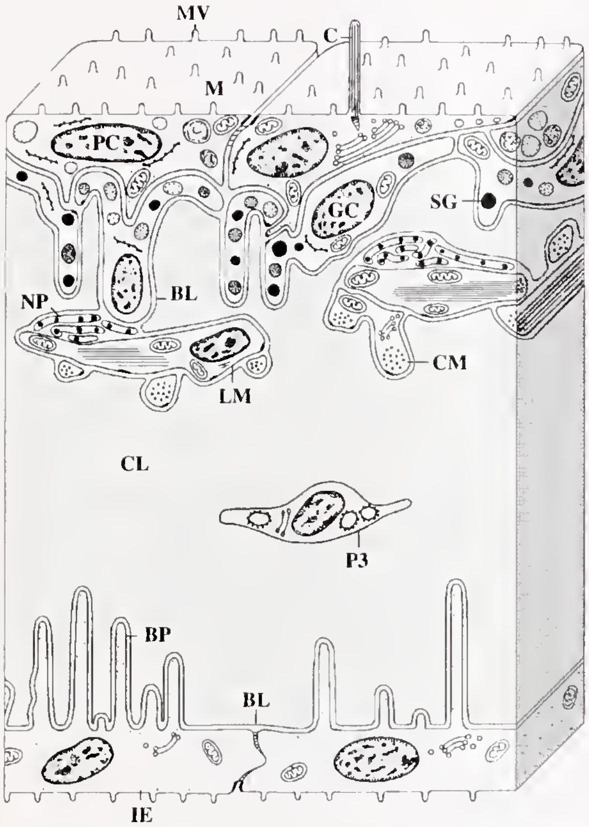

Figure 20. *Holothuria forskali.* Reconstruction of a longitudinal section through the wall of a stage 4 regenerating Cuvierian tubule (not to scale). BL, basal lamina; BP, epithelial cell basal process; C, cilium; CL, connective tissue layer; CM, circular myocyte; IE, internal epithelium; GC, granular cell; LM, longitudinal myocyte; M, mesothelium; MV, microvillus; NP, nerve plexus; P3, type 3 pseudopodial cell; PC, peritoneocyte; SG, secretory granule.

mesothelium, proliferating cells are present from regeneration stage 1 to stage 4. In all these stages, labeled nuclei were always observed in undifferentiated cells and peritoneocytes (Figs. 30, 31). No labeling was detected in myocytes and granular cells, whatever the regeneration stage considered. Labeled cells were observed in the connective tissue layer until the regenerating tubule becomes a small functional tubule (*i.e.*, end of stage 5). These cells were always pseudopodial cells (Figs. 30, 31) and never spherulocytes. Among the three types of pseudopodial cells, labeled nuclei were observed principally, but not exclusively, in type 2 cells (Figs. 29–31). As for the inner epithelium, the labeling was always detected in epithelial cells that had not yet developed piles of spherules in their intraconnective basal processes.

Discussion

Echinoderms in general, and holothuroids in particular, exhibit a remarkable ability to regenerate a missing part of the body (Hyman, 1955). Regeneration in echinoderms generally occurs after evisceration, autotomy, or fission (Emson and Wilkie, 1980). In sea cucumbers, the best studied regenerative model is the intestine regeneration after evisceration (Dawbin, 1949; Mosher, 1956; Bai, 1971; Tracey, 1972; Garcia-Arraras *et al.*, 1998). In this model, formation of the new gut may be subdivided into three successive phases: initial repair, true regeneration, and growth. The same phases were observed in the replacement process of autotomized Cuvierian tubules in *Holothuria forskali.*

Phases of Cuvierian tubule regeneration

The repair phase, which includes the overall 48-h post-autotomy period, comprises wound closure and histolysis of the damaged tissues. During this phase, no clotting of coelomocytes was observed, contrary to what usually occurs during repair of injured tissues in echinoderms (Smith, 1981). This lack of coelomocyte plugging may reflect the rapid closure of the relatively limited wound by the contraction of the circular muscles of the tubule peduncle. Wound closure is followed by re-epithelialization on both the coelomic and luminal sides of the basal part of the left respiratory tree. Phagocytosis of the damaged tissues then takes place within the connective tissue layer. This is the role of the many large and active phagocytic cells observed during this phase. Such cells have been described at wound sites in the five echinoderm classes (Gibson and Burke, 1983; Mladenov *et al.*, 1989; Candia Carnevali *et al.*, 1993; Dubois and Ghyoot, 1995). These cells are generally considered to be derived from coelomic amoebocytes that migrate to the wound site (Smith, 1971a; Dubois and Ghyoot, 1995).

The regenerative process *sensu stricto* starts right after wound healing and takes 3 to 4 weeks to complete. Five stages of regeneration may be recognized. Stage 1 can be defined by the appearance of a thickening of the mesothelium at the site where autotomy took place. This thickening will be the starting point of the new tubule formation. Stage 2 corresponds to the initial appearance of a lumen within the regenerating tubule. The tubule wall therefore acquires its characteristic trilayered structure, which consists of an outer mesothelium, a connective tissue layer, and an inner epithelium. Stage 3 involves a tissue layer proportioning in which the connective tissue layer grows to become the thickest of the three tissue layers, as in non-regenerating Cuvierian tubules. Stage 4 is characterized by the acquisition of the typical tubule shape. Finally, stage 5 is reached when the regenerating tubule becomes functional.

Regeneration is followed by a growth phase. Indeed, the functional tubule formed at the end of the last regeneration stage is only half the size of a non-regenerating Cuvierian tubule. It thus continues to grow for about one more week until it reaches its final size.

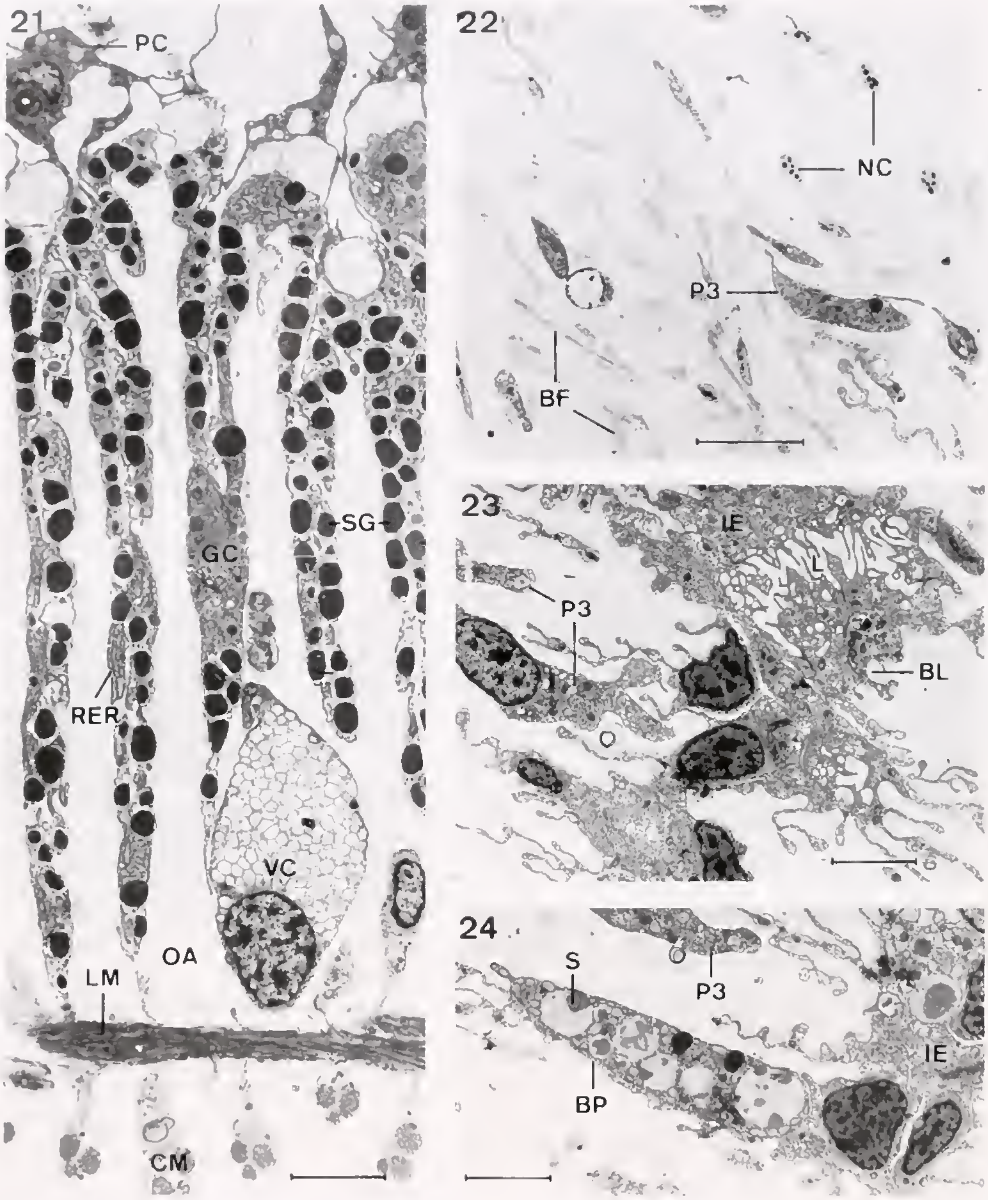

Figures 21–24. *Holothuria forskali.* Ultrastructure of stage 5 regenerating Cuvierian tubules. BF, bundle of collagen; BL, basal lamina; BP, epithelial cell basal process; CM, circular myocyte; IE, internal epithelium; GC, granular cell; L, lumen; LM, longitudinal myocyte; NC, neurosecretory-like cell; OA, outer area of the connective tissue layer; P3, type 3 pseudopodial cell; PC, peritoneocyte; RER, rough endoplasmic reticulum; S, spherule; SG, secretory granule; VC, vacuolar cell. **Figure 21.** Longitudinal section through the mesothelium and the muscle layer (bar = 3 μm). **Figure 22.** Longitudinal section through the inner area of the connective tissue layer (bar = 4 μm). **Figure 23.** Longitudinal section through the inner epithelium (bar = 3 μm). **Figure 24.** Detailed view of an intraconnective basal process of a cell of the inner epithelium (bar = 3 μm).

Cell cycle activity and origin of tissue layers

The use of BrdU and ^{3}HT incorporation has provided further details concerning the role of cell proliferation in Cuvierian tubule regeneration and also, indirectly, concerning the possible contributions of migration and differentiation during regeneration.

In *H. forskali*, our results showed that cell proliferation occurs within each of the three constitutive tissue layers of the regenerating tubule and during the whole regenerative phase, although it was observed only in the mesothelium at stage 1 and only in the connective tissue layer at stage 5. Conversely, no labeled nucleus was observed after stage 5

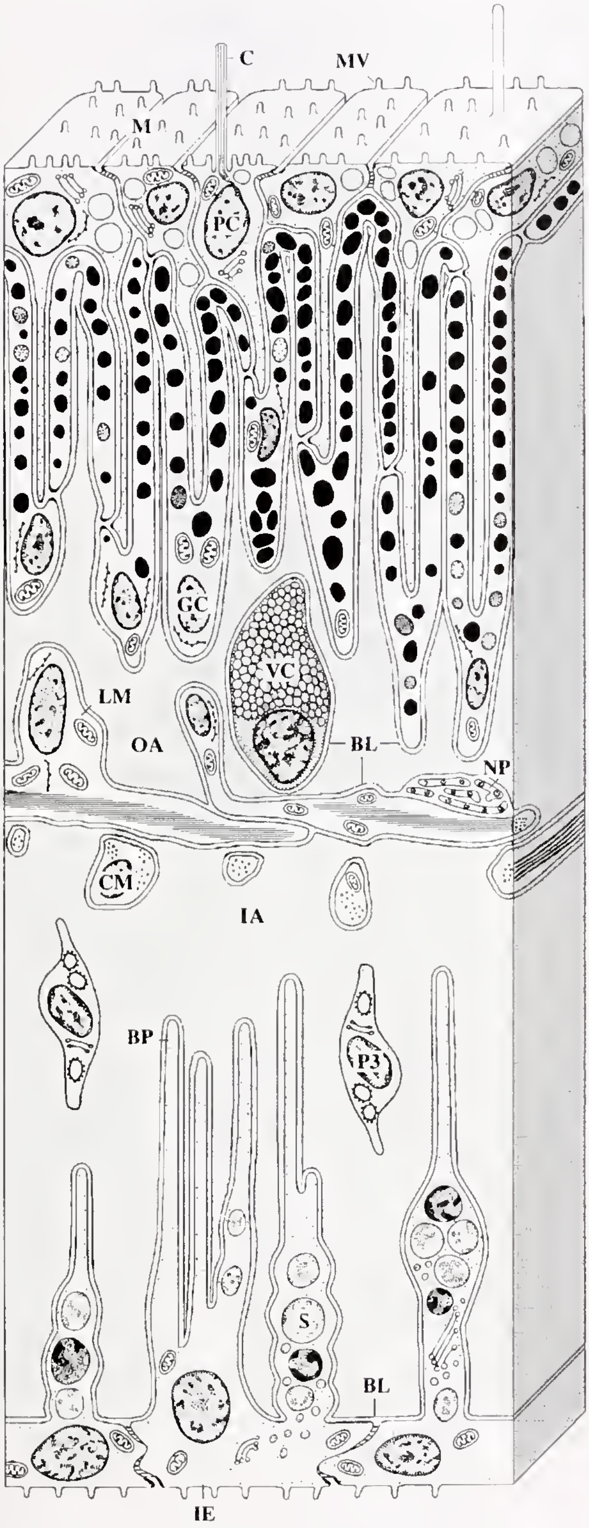

Figure 25. *Holothuria forskali.* Reconstruction of a longitudinal section through the wall of a stage 5 regenerating Cuvierian tubule (not to scale). BL, basal lamina; BP, epithelial cell basal process; C, cilium; CM, circular myocyte; IA, inner area of the connective tissue layer; IE, internal epithelium; GC, granular cell; LM, longitudinal myocyte; M, mesothelium; MV, microvillus; NP, nerve plexus; OA, outer area of the connective tissue layer; P3, type 3 pseudopodial cell; PC, peritoneocyte; S, spherule; VC, vacuolar cell.

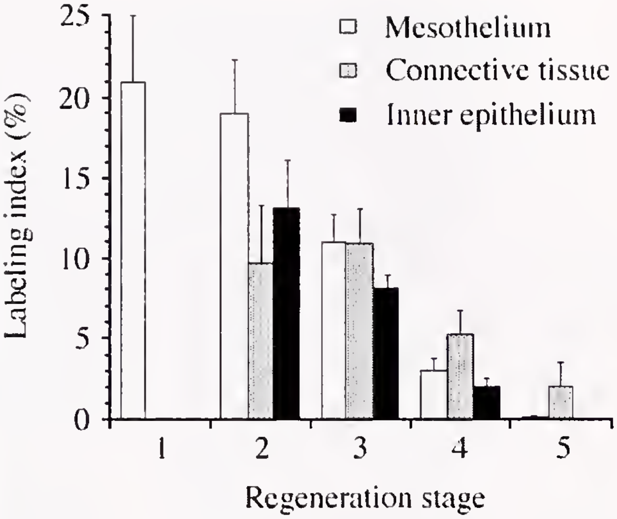

Figure 26. Labeling indices (mean ± SD, $n = 4$) for proliferating cells in the different tissue layers at each stage of Cuvierian tubule regeneration (BrdU/anti-BrdU method).

(*i.e.*, when the regenerating tubule becomes functional), indicating that the growth phase proceeds only by an increase of cell volume, without cell division. Moreover, the absence of DNA-synthesizing cells in non-regenerating Cuvierian tubules indicates that there is no cellular "turnover" and that the cell populations which constitute the tubule tissues must be considered as static (Messier and Leblond, 1960).

During regeneration, the mesothelium is the tissue layer in which cell proliferation is the most precocious and the most important, involving both undifferentiated cells and peritoneocytes. At stage 1, there is an accumulation of actively proliferating undifferentiated cells that form the mesothelial thickening characteristic of this stage. As regeneration proceeds, the percentage of labeled nuclei in the mesothelium regularly decreases in parallel with the differentiation of granular cells on the one hand and myocytes on the other hand. Nucleus labeling was never observed in these two cell types, which therefore do not divide. We were not able to determine the origin of undifferentiated cells, but they probably originate from peritoneocytes. These cells would thus contribute significantly to the regenerative process through dedifferentiation, proliferation, and redifferentiation into other cell types (in this case, granular cells and myocytes). Their relative totipotence in echinoderms is manifested by their ability to proliferate actively during regeneration (Candia Carnevali *et al.*, 1997; present study) and to transdifferentiate into free coelomocytes or myocytes (Vanden Bossche and Jangoux, 1976; Dolmatov *et al.*, 1996; respectively).

In their description of the ultrastructure of non-regenerating Cuvierian tubules, VandenSpiegel and Jangoux (1987) suggested that the intraconnective myocytes were derived

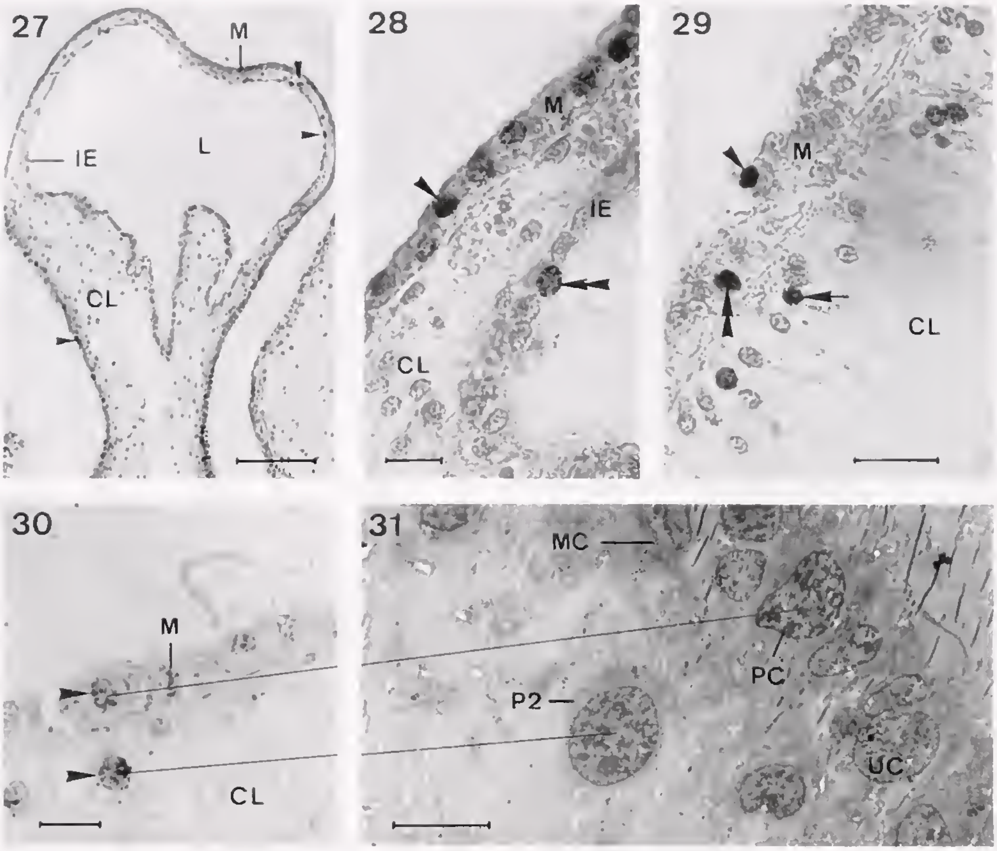

Figures 27–31. *Holothuria forskali.* Detection of proliferating cells in the regenerating Cuvierian tubules. CL, connective tissue layer; IE, internal epithelium; L, lumen; M, mesothelium; MC, myocyte; P2, type 2 pseudopodial cell; PC, peritoneocyte; UC, undifferentiated cell. **Figure 27.** Longitudinal section through a stage 2 regenerating tubule (BrdU/anti-BrdU method) showing labeled nuclei in the three tissue layers (arrowheads; bar = 50 μm). **Figure 28.** Detailed view of the wall of a stage 2 regenerating tubule (BrdU/anti-BrdU method) showing labeled nuclei in the mesothelium (single arrowhead) and in the inner epithelium (double arrowhead) (bar = 5 μm). **Figure 29.** Section through the wall of a stage 3 regenerating tubule (BrdU/anti-BrdU method) showing labeled nuclei in the mesothelium (peritoneocyte, single arrowhead; and undifferentiated cell, double arrowhead) and in the connective tissue layer (type 2 pseudopodial cell, arrow) (bar = 8 μm). **Figures 30 and 31.** Consecutive semithin and ultrathin sections through a stage 3 regenerating tubule. ^{3}HT incorporation in the tubule tissues was revealed by autoradiography on the semithin section (arrowheads, Fig. 29; bar = 5 μm) and the DNA-synthesizing cells were unambiguously identified by observation of the ultrathin section in TEM (Fig. 30; bar = 4 μm).

from the mesothelium. However, they had no direct evidence to corroborate their hypothesis. Our study of regenerating tubules clearly indicates the mesothelial origin of the myocytes which, during the regenerative process, first differentiate as myoepithelial cells and then migrate in the connective tissue layer. This is consistent with the hypothesis of Rieger and Lombardi (1987) on the mesothelial origin of nonepithelial myocytes in echinoderms. This speculative hypothesis was criticized by Cavey and Wood (1990), but has since been strengthened by the work of Stauber (1993) on echinoid lantern muscles, that of Dolmatov *et al.* (1996) on holothuroid longitudinal muscle bands, and now by ours on holothuroid Cuvierian tubule muscles.

The nerve plexus appears early in regeneration and consists only of nerve processes; no cell body was observed. This plexus is first basimesothelial and then migrates in the connective tissue layer with the myocytes. This explains why, in non-regenerating tubules, the nerve plexus is never observed within the mesothelium. Vacuolar cells were originally described as egg-shaped structures and interpreted as sections through a spiral nerve (VandenSpiegel and Jangoux, 1987). However, our reexamination of these structures in the regenerating tubules suggests that they are clusters of vacuolar cells. Because these cells first appear close to the mesothelium and are surrounded by a basal lamina, their origin is probably in the mesothelium. Like myocytes and granular cells, they presumably differentiate from undifferentiated cells. These cells have also been observed in the Cuvierian tubules of other holothuroid species (VandenSpiegel and Jangoux, 1988), but their function remains enigmatic.

In the connective tissue layer, spherulocytes and pseudopodial cells co-occur at the beginning of the regeneration. However, although the pseudopodial cells appear to proliferate actively, spherulocytes show no sign of DNA synthesis and disappear early in the regenerative process. Nevertheless, they presumably play an important role in the early stages of Cuvierian tubule restoration. Indeed, most studies of wound repair in holothuroids have revealed the importance of spherulocytes (Cowden, 1968; Menton and Eisen, 1973). The function generally ascribed to these cells is the formation and maintenance of the ground substance of the extracellular matrix (Fontaine and Lambert, 1977; Byrne, 1986; Jans *et al.*, 1996). In addition, spherulocytes have been put forward as producers of antibacterial compounds and chemotactic agents for other mesenchymatous cells (see Smith, 1981, for review). The latter could account for the recruitment of type 1 pseudopodial cells at the beginning of Cuvierian tubule regeneration.

Three types of pseudopodial cells follow one another in the tubule connective tissue during regeneration. Type 1 cells have all the characteristics of echinoderm phagocytes (*e.g.*, see Dubois and Ghyoot, 1995). The collagen-containing secondary lysosomes observed in some of these cells suggest they may have a fibroclastic function, cleaning up the connective tissue compartment before new collagen synthesis starts. Type 2 cells are characterized by a more rounded shape, a high nuclear:cytoplasmic ratio, and a conspicuous juxtanuclear centriole—all features suggesting that these cells are rather undifferentiated (Fontaine and Lambert, 1977; Smith, 1981). This notion is further supported by the active division of these cells. Type 3 cells possess distended RER cisternae and Golgi stacks ending in spheroidal distentions. RER with distended cisternae has been described both in proven and presumptive echinoderm fibroblasts (Dubois and Ghyoot, 1995; Heinzeller and Welsch, 1994; respectively). Golgi with spheroidal distentions, on the other hand, are a diagnostic feature of vertebrate fibroblasts (Weinstock and Leblond, 1974). We have not observed all the stages of Golgi distentions, including the final collagen granule. Nevertheless, the ultrastructural characteristics of type 3 pseudopodial cells, together with their presence in the regenerating connective tissue close to the time when the collagen fibers appear, strongly support a fibroblastic function for these cells. According to the sequence of appearance of the three types of pseudopodial cells, type 2 cells are probably dedifferentiated type 1 cells that then actively proliferate before differentiating into type 3 cells. Phagocytic cells, undifferentiated mesenchymatous cells, and fibroblasts would thus share lineage relationships, as is the case in echinoids (Dubois and Ghyoot, 1995). Once the regenerating tubule has reached its definitive size, the collagen synthesis presumably stops, as evidenced by the lack of mesenchymatous cells in non-regenerating Cuvierian tubules (VandenSpiegel and Jangoux, 1987). The origin of the tridimensional organization of the collagen in parallel helixes is not clear, but it could be the result of the particular association observed at regeneration stage 3 between type 2 pseudopodial cells and the mesothelium.

In the inner epithelium, cells also divide actively, but only when they have not yet differentiated spherules in their basal intraconnective processes ("undifferentiated epithelial cells"). It appears, therefore, that in the three tissue layers of the Cuvierian tubules, regeneration proceeds by dedifferentiation, then proliferation, and finally differentiation.

Cuvierian tubule regeneration: morphallaxis vs. *epimorphosis*

Regeneration has been described classically as proceeding by one or the other of two mechanisms: (i) morphallaxis, in which cells differentiate or migrate from existing populations, and (ii) epimorphosis, in which mitosis occurs and new cells are produced that either directly replace those lost or form a blastema that goes on to differentiate and replace lost tissue (Bonasoro *et al.*, 1998). In echinoderms, the relative importance of morphallaxis and epimorphosis seems to be variable. Regeneration of longitudinal muscle bands in holothuroids proceeds without cell proliferation and represents a case of cellular morphallaxis (Dolmatov *et al.*, 1996). Similarly, regeneration of the intestine after fission in the apodid holothuroid *Leptosynapta* is an entirely morphallactic mechanism; in this case, the remaining portion of the intestine is remodeled to form a functionally complete organ (Smith, 1971a, b; Gibson and Burke, 1983). Conversely, regeneration of the arm in the crinoid *Antedon mediterranea* is an epimorphic process in which a regenerative blastema is formed (Candia Carnevali *et al.*, 1993, 1995, 1997). Most regenerative processes in echinoderms, however, appear to involve a combination of morphallactic and epimorphic mechanisms. This is the case for the intestine regeneration after evisceration in aspidochirote and dendrochirote holothuroids (Dolmatov, 1992; Garcia Arraras *et al.*, 1998), as well as for the arm regeneration in asteroids (Mladenov *et al.*, 1989; Moss *et al.*, 1998).

Regeneration of the Cuvierian tubules in *H. forskali* also appears to involve both epimorphosis and morphallaxis. Initial regeneration events occur by epimorphosis, cell proliferation being essential to the regenerative process. The mesothelial thickening appearing at stage 1 could be compared to a blastema, that is, an accumulation of undifferentiated cells capable of proliferation and differentiation. However, it is not a true blastema, giving rise to all the tissue layers in the new tubule; rather it is a transitory blastema-like structure that contributes only to the regeneration of the mesothelium, forming mesothelial cells (peritoneocytes and granular cells) and mesothelium-derived cells (myocytes and vacuolar cells). This structure does not contribute to the regeneration of the other two tubule layers—*i.e.*, the connective tissue layer and the inner epithelium—that each enclose their own population of dividing cells. As regeneration proceeds, the percentage of dividing cells decreases, and in the late stages, tubule histogenesis occurs mainly by morphallaxis, with newly differentiated cells migrating from the mesothelium into the connective tissue layer.

The dynamics of Cuvierian tubule regeneration and its implication for the defense mechanism

In holothuroid species that contain Cuvierian tubules, the structures are generally present in large numbers. For example, individuals of *H. forskali* may have between 200 and 600 tubules, depending on their size (VandenSpiegel and Jangoux, 1987). When gently stimulated they expel only a few tubules, but if the stimulation is stronger, tubules can be discharged several times in succession (Bakus, 1968; present study). However, in both cases, only a fraction of the total tubule number will be used. Such a behavior allows a sparing use of the defensive organ (VandenSpiegel and Jangoux, 1987). After expulsion and autotomy, Cuvierian tubules are readily regenerated. In *H. forskali*, our study showed that the complete regeneration of the autotomized tubules, namely the formation of functional, fully developed tubules, takes about 5 weeks. This period starts with the actual beginning of the regenerative process and not with the expulsion and autotomy of the tubules. Indeed, after a gentle stimulation, when only a few (about 15) tubules have been expelled, there is often a latent period that may last up to 3 weeks before the regeneration starts. In contrast, after a strong stimulation, when many (up to 300) tubules have been expelled, the regenerative process starts immediately, but proceeds by successive waves of 10 to 30 tubules that begin to regenerate at 10-day intervals. This pattern of regeneration is advantageous for the sea cucumber because it allows a staggered spending of the energy necessary for regeneration. Holothuroid Cuvierian tubules thus constitute a very efficient defensive mechanism. Indeed, in addition to their remarkable structural organization, which accounts for their adhesive and mechanical properties (VandenSpiegel and Jangoux, 1987), their large number, sparing use, and particular regeneration dynamics also make them an almost inexhaustible line of defense maintained at limited energy cost.

Acknowledgments

We thank Professor P. Lassere for providing facilities at the Observatoire Océanologique de Roscoff (Brittany, France) and P. Postiau for technical assistance. P. Flammang is Research Associate of the National Fund for Scientific Research (NFSR, Belgium). This research was supported by a NFSR grant to M. Jangoux (no. 2.4512.95, Crédit aux Chercheurs). Contribution of the Centre Interuniversitaire de Biologie Marine (CIBIM).

Literature Cited

Bai, M. M. 1971. Regeneration in the holothurian, *Holothuria scabra* Jager. *Indian J. Exp. Biol.* **9:** 467–471.

Bakus, G. J. 1968. Defensive mechanisms and ecology of some tropical holothurians. *Mar. Biol.* **2:** 23–32.

Bonasoro, F., M. D. Candia Carnevali, C. Moss, and M. C. Thorndyke. 1998. Epimorphic *versus* morphalactic mechanisms in arm regeneration of crinoids and asteroids: pattern of cell proliferation and cell lineage. Pp. 13–18 in *Echinoderms: San Francisco*, R. Mooi and M. Telford, eds. Balkema, Rotterdam.

Byrne, M. 1986. The ultrastructure of the morula cells of *Eupentacta quinquesemita* (Echinodermata, Holothuroidea) and their role in the maintenance of the extracellular matrix. *J. Morphol.* **188:** 179–189.

Candia Carnevali, M. D., E. Lucca, and F. Bonasoro. 1993. Mechanisms of arm regeneration in the feather star *Antedon mediterranea:* healing of wound and early stages of development. *J. Exp. Zool.* **267:** 299–317.

Candia Carnevali, M. D., F. Bonasoro, E. Lucca, and M. C. Thorndyke. 1995. Pattern of cell proliferation in the early stages of arm regeneration in the feather star *Antedon mediterranea. J. Exp. Zool.* **272:** 464–474

Candia Carnevali, M. D., F. Bonasoro, and A. Biale. 1997. Pattern of bromodeoxyuridine incorporation in the advanced stages of arm regeneration in the feather star *Antedon mediterranea. Cell Tissue Res.* **289:** 363–374.

Cavey, M. J., and R. L. Wood. 1990. Organization of the adluminal and retractor cells in the coelomic lining from the tube foot of a phanerozonian starfish, *Luidia foliolata. Can. J. Zool.* **69:** 911–923.

Cowden, R. R. 1968. Cytological and histochemical observations on the connective tissue cells and cutaneous wound healing in the sea cucumber *Stichopus badionotus. J. Invertebr. Pathol.* **10:** 151–159.

Dawbin, W. H. 1949. Auto-evisceration and regeneration of viscera in holothurian *Stichopus mollis* (Hutton). *Trans. R. Soc. N.Z.* **77:** 497–523.

Dolmatov, I. Y. 1992. Regeneration of aquapharyngial complex in the holothurian *Eupentacta fraudatrix* (Holothuroidea, Dendrochirota). *Monogr. Dev. Biol.* **23:** 40–50.

Dolmatov, I. Y., M. G. Eliseikina, A. A. Bulgakov, T. T. Ginanova, N. E. Lamash, and V. P. Korchagin. 1996. Muscle regeneration in the holothurian *Stichopus japonicus. Roux's Arch. Dev. Biol.* **205:** 486–493.

Dubois, P., and M. Ghyoot. 1995. Integumentary resorption and collagen synthesis during regression of headless pedicellariae in *Sphaerechinus granularis* (Echinodermata, Echinoidea). *Cell Tissue Res.* **282:** 297–309.

Emson, R. H., and I. C. Wilkie. 1980. Fission and autotomy in echinoderms. *Oceanogr. Mar. Biol. Annu. Rev.* **18:** 155–250.

Flammang, P. 1996. Adhesion in echinoderms. Pp. 1–60 in *Echinoderm Studies*, Vol. 5, M. Jangoux and J. M. Lawrence, eds. Balkema, Rotterdam.

Fontaine, A. R., and P. Lambert. 1977. The fine structure of leucocytes of the holothurian *Cucumaria miniata. Can. J. Zool.* **55:** 1530–1544.

Gabe, M. 1968. *Techniques histologiques.* Masson, Paris.

Garcia-Arraras, J. E., L. Estrada-Rodgers, R. Santiago, I. I. Torres, L. Diaz-Miranda, and I. Torres-Avillan. 1998. Cellular mechanisms of intestine regeneration in the sea cucumber, *Holothuria glaberrima* Selenka (Holothuroidea: Echinodermata). *J. Exp. Zool.* **281:** 288–304.

Gibson, A. W., and R. D. Burke. 1983. Gut regeneration by morphallaxis in the sea cucumber *Leptosynapta clarki* (Heding, 1928). *Can. J. Zool.* **61:** 2720–2732.

Hacker, G., D. Springall, S. VanNoorden, A. Bishop, L. Grimelius, and J. Polak. 1985. The immunogold-silver staining method—a powerful tool in histopathology. *Virchows Arch. B* **406:** 449–461.

Heinzeller, T., and U. Welsch. 1994. Crinoidea. Pp. 9–148 in *Microscopic Anatomy of Invertebrates, Vol. 14: Echinodermata,* F. W. Harrison and F.-S. Chia, eds. Wiley-Liss, New York.

Hill, R. B., and D. Reinschmidt. 1976. Relative importance of the antioxidant and anesthetic properties of propylene phenoxetol in its action as a "preservatie" for living holothurians. *J. Invertebr. Pathol.* **28:** 131–135.

Humphrey, C. D., and F. E. Pittman. 1974. A simple methylene blue-azur II-basic fushin stain for epoxy-embedded tissue secretion. *Stain Technol.* **49:** 9–14.

Hyman, L. H. 1955. *The Invertebrate, Vol. 4 Echinodermata.* McGraw-Hill, New York.

Jans, D., P. Dubois, and M. Jangoux. 1996. Defensive mechanisms of holothuroids (Echinodermata): formation, role, and fate of intracoelomic brown bodies in the sea cucumber *Holothuria tubulosa. Cell Tissue Res.* **283:** 99–106.

Laurent, G., G. Toubeau, J. A. Heuson-Stiennon, P. Tulkens, and P. Maldague. 1988. Kidney tissue repair after nephrotoxic injury: biochemical and morphological characterization. *Crit. Rev. Toxicol.* **19:** 147–183.

Menton, D. N., and A. Z. Eisen. 1973. Cutaneous wound healing in the sea cucumber, *Thyone briareus. J. Morphol.* **141:** 185–204.

Messier, B., and C. P. Leblond. 1960. Cell proliferation and migration as revealed by autoradiography after injection of thymidine-^{3}H into male rats and mice. *Am. J. Anat.* **106:** 247–265.

Mladenov, P. V., B. Bisgrove, S. Asotra, and R. D. Burke. 1989. Mechanisms of arm tip regeneration in the sea star, *Leptasterias hexactis. Roux's Arch. Dev. Biol.* **198:** 19–28.

Mosher, C. 1956. Observations on evisceration and visceral regeneration in the sea-cucumber, *Actinopyga agassizi* Selenka. *Zoologica (N.Y.)* **41:** 17–26.

Moss, C., A. J. Hunter, and M. C. Thorndyke. 1998. Patterns of bromodeoxyuridine incorporation and neuropeptide immunoreactivity during arm regeneration in the starfish *Asterias rubens. Phil. Trans. R. Soc. Lond.* **353:** 421–436.

Müller, M. E. G., R. K. Zahn, and K. Schmid. 1970. Morphologie und Funktion der Cuvierian Organe von *Holothuria forskali* Delle Chiaje (Echinodermata: Holothuroidea: Aspidochirota: Holothuriidae). *Z. Wiss. Zool.* **181:** 219–231.

Rieger, R. M., and J. Lombardi. 1987. Ultrastructure of the coelomic lining in echinoderm podia: significance for concepts in the evolution of muscle and peritoneal cells. *Zoomorphology* **107:** 191–208.

Smiley, S. 1994. Holothuroidea. Pp. 401–471 in *Microscopic Anatomy of Invertebrates, Vol. 14: Echinodermata,* F. W. Harrison and F.-S. Chia, eds. Wiley-Liss, New York.

Smith, G. N. 1971a. Regeneration in the sea cucumber *Letosynapta.* I. The process of regeneration. *J. Exp. Zool.* **177:** 319–330.

Smith, G. N. 1971b. Regeneration in the sea cucumber *Letosynapta.* II. The regenerative capacity. *J. Exp. Zool.* **177:** 331–342.

Smith, V. J. 1981. The echinoderms. Pp. 514–562 in *Invertebrate Blood Cells,* N. A. Ratcliffe and A. F. Rowley, eds. Academic Press, New York.

Stauber, M. 1993. The lantern of Aristotle: organization of its coelom and origin of its muscles (Echinodermata, Echinoidea). *Zoomorphology* **113:** 137–151.

Tracey, D. J. 1972. Evisceration and regeneration in *Thyone okeni* (Bell, 1884). *Proc. Linn. Soc. N. S. W.* **97:** 72–81.

Vanden Bossche, M., and M. Jangoux. 1976. Epithelial origin of starfish coelomocytes. *Nature* **261:** 227–228.

VandenSpiegel, D., and M. Jangoux. 1987. Cuvierian tubules of the holothuroid *Holothuria forskali* (Echinodermata): a morphofunctional study. *Mar. Biol.* **96:** 263–275.

VandenSpiegel, D., and M. Jangoux. 1988. Les tubes de Cuvier d'*Holothuria mammata* Grube, 1840 (Holothuroidea, Echinodermata). *Ann. Soc. R. Zool. Belg.* **118:** 191–198.

VandenSpiegel, D., D. Nonclercq, and G. Toubeau. 1991. Immunocytochemical detection of bromodeoxyuridine in proliferating cells of regenerating Cuvierian tubules of *Holothuria forskali.* Pp 81–85 in *Echinoderm Research 1991,* L. Scalera-Liaci and C. Canicatti, eds. Balkema, Rotterdam.

Weinstock, M., and C. P. Leblond. 1974. Synthesis, migration, and release of precursor collagen by odotonblasts as visualized by autoradiography after [^{3}H]proline administration. *J. Cell Biol.* **60:** 92–127.

Reference: *Biol. Bull.* **198**: 50–66. (February 2000)

Nucleation and Growth of Calcite on Native *Versus* Pyrolyzed Oyster Shell Folia

C. S. SIKES[1,*], A. P. WHEELER[2], A. WIERZBICKI[3], A. S. MOUNT[2], AND R. M. DILLAMAN[4]

[1]*The Mineralization Center, Department of Biological Sciences;* [2]*Department of Biological Sciences, Clemson University, Clemson, South Carolina 29634-1903;* [3]*Department of Chemistry, University of South Alabama, Mobile, Alabama 36688; and* [4]*Department of Biological Sciences, University of North Carolina at Wilmington, Wilmington, North Carolina 28403-3297*

Abstract. The thin sheets of calcite, termed folia, that make up much of the shell of an oyster are covered by a layer of discrete globules that has been proposed to consist of agglomerations of protein and mineral. Foliar fragments, treated at 475°C for 36 h to remove organic matter, were imaged by atomic force microscopy (AFM) as crystals grew on the foliar surfaces in artificial seawater at calcite supersaturations up to 52-fold. Crystals were also viewed later by scanning electron microscopy. After pyrolysis, the foliar globules persisted only as fragile remnants that were quickly washed away during AFM imaging, revealing an underlying morphology on the foliar laths of a tightly packed continuum of nanometer-scale protrusions. At intermediate supersaturations, crystal formation was seen immediately almost everywhere on these surfaces, each crystal having the same distinctive shape and orientation, even at the outset with crystals as small as a few nanometers. In contrast, nucleation did not occur readily on non-pyrolyzed foliar surfaces, and the crystals that did grow, although slowly at intermediate supersaturations, had irregular shapes. Possible crystallographic features of foliar laths are considered on the basis of the morphology of ectopic crystals and the atomic patterns of various surfaces. A model for foliar lath formation is presented that includes cycles of pulsed secretion of shell protein, removal of the protein from the mineralizing solution upon binding to mineral, and mineral growth at relatively high supersaturation over a time frame of about 1 h for each turn of the cycle.

Introduction

The mineral of most molluscan shells is $CaCO_3$ that routinely contains less than a few percents and often less than 1% by weight of the shell as organic material, mostly protein. One objective of shell research is to understand how the shell is put together, particularly the relationships between the mineral and the organic components. The intrinsic appeal of exquisite biominerals like shells has been advanced in recent years by an appreciation of the material properties of the structures (Heuer *et al.*, 1992; Sarikaya *et al.*, 1995; Mann, 1996; Stupp and Braun, 1997; Weiner and Addadi, 1997). A variety of studies have shown that biological composites like shell have particularly favorable properties, including increased durability and resistance to fracture. Such properties are considered to result from the interplay of the organic and inorganic components, even though the organic content is quite low by composite-materials standards.

In the case of the oyster shell, which is composed of calcite and is representative of many kinds of molluscan shell, the mineral even within a few millimeters of the forming edge is formed into layers of thin sheets, termed folia (Tsujii *et al.*, 1958; Carriker and Palmer, 1979; Carriker *et al.*, 1980). The foliar layers form the bulk of the shell. Each foliar sheet is subdivided into units termed laths, with each sheet just one lath unit of up to only a few hundred nanometers in thickness (or height). An entire foliar sheet may be quite large depending in part on the dimensions of the shell, and is composed of many laths laying side by side. Each lath may be typically about 2 μm wide and perhaps up to 10 μm long (Watabe *et al.*, 1958; Watabe and Wilbur, 1961; Watabe, 1965).

We have suggested that the organic component of folia

Received 20 January 1999; accepted 16 November 1999.

* To whom correspondence should be addressed. E-mail: ssikes@usamail.usouthal.edu

consists of foliar globules, which themselves appear to be composites of protein and mineral. The foliar globules are packed closely together and overlay each foliar lath (Sikes *et al.*, 1998). A typical foliar globule is formed into an ellipsoid of about 10 to 40 nm in height, 50 nm in width, and 100 nm in length. Evidence from chemical, enzymatic, immunologic analyses and from both atomic force microscopy (AFM) and scanning electron microscopy (SEM) suggested that the globules are proteinaceous. On the other hand, it also appeared that the foliar globules are mineralized, as evidenced by their dimensions, the measured content of protein in foliar layers, and their invariant appearance when viewed by AFM both dry and in fluids. However, when subjected to conditions of supersaturation with respect to calcite in artificial seawater, including periods of spontaneous nucleation and crystal growth in the bathing fluid, the foliar globules generally did not support crystal growth as viewed continuously by AFM.

The purpose of this investigation was to further probe the identity of the foliar globules through pyrolysis followed by AFM and SEM comparisons of the pyrolyzed and non-pyrolyzed foliar surfaces. Pyrolysis was selected for this purpose because the foliar globules were resistant to treatment with HOCl and NaOH, presumably due to the shielding effect of the mineral component (Sikes *et al.*, 1998). The foliar globules were pyrolyzed by subjecting them to 475°C for 36 h, conditions that are reported to remove all of the organic matter without affecting the mineral (Paine, 1964; Price *et al.*, 1976; Dean, 1992).

Crystal nucleation and growth on pyrolyzed and control surfaces were monitored at supersaturations (Ω) over the range of $\Omega = 10.7$ to 52.5. The extent and morphology of crystal formation were revealed, including the influence of Ω on morphology.

The results showed that the pyrolyzed surface was much more active in promoting crystallization at all levels of Ω. The foliar globules of the control surface did not support crystal formation at the lower values of Ω. At higher Ω, crystals did emerge from foliar globules. These crystals had irregular morphology and appeared to form on the basal (0 0 1) plane of calcite. Conversely, the morphology of ectopic crystals was completely different on pyrolyzed and non-pyrolized (control) surfaces. Morphological and AFM analysis at the atomic level of ectopic crystals on pyrolyzed surfaces suggested that the foliar globules were associated with (1 −1 0) planes and that the *c* axis of calcite was parallel to the long axis of the foliar laths. This indicated that elongation, the principal axis of growth of foliar layers, may occur along the *c* axis, other prominent examples of which include the stacking of nacreous tablets of shells and elongation of echinoderm spicules (Weiner and Addadi, 1997).

The foliar globules did not appear to be nucleation sites for the next foliar layer, at least not at low to moderate levels of supersaturation. Rather, they behaved like composites of protein and (presumably) amorphous $CaCO_3$ that limit thickening of foliar laths and probably contribute to flexibility and durability of the shell. Possible locations for continued mineral growth of the shell include putative, dispersed mineral interconnections along the foliar surfaces, as well as exposed mineral at the leading edges of foliar laths.

A cyclic model of foliar lath formation is proposed on the basis of measured rates of shell enlargement *in vivo*, rates of calcite growth at different levels of Ω *in vitro*, and measured interactions of soluble, oyster-shell protein with calcite *in vitro*. The model includes pulsed secretion for a minute or so of matrix proteins, largely in gelling form, followed by removal of the protein from the mineralizing fluid upon binding to exposed mineral. This interaction of matrix and mineral would limit and shape the underlying mineral lath. Mineral deposition of the next layer would then ensue at relatively high Ω over a time frame of about 1 h. These events would be repeated, with a new foliar layer formed at each turn of the cycle.

Materials and Methods

Oyster shell folia

Freshly shucked shells of the Eastern oyster, *Crassostrea virginica*, were gently fractured by compression with a Carver press at a loading of about 200 psi. Large fractured fragments of shell were then held manually to maintain their orientation, and white, pearlescent foliated chips were picked out by hand while being viewed with a binocular dissecting microscope so that the external (facing the sea) and internal surfaces (facing the mantle) were known. Control chips were then glued, usually with the inner surface up, onto a 12-mm glass disc on a partially air-dried (5 min) 10-μl droplet of commercial polyurethane (Minwax) diluted 3:1 with dichloromethane to promote rapid drying and thin distribution of the polyurethane on the glass. The amount of polyurethane was minimized such that there was enough to provide stable adhesion of the chip to the glass disc during extended viewing in fluids, but without an excess that might wick up onto the upper surface of the chip. The glass disc itself had previously been glued with cyanoacrylate (which was not compatible with viewing in fluids) to an SEM stub for use with an AFM scanner that had been custom-fitted with an SEM stub holder.

There were no clear differences in appearance between inner and outer surfaces of control chips. Only inner surfaces were studied in control treatments. Following AFM viewing, the same chips then were viewed by SEM.

The chips ranged from 1 to 3 mm in linear dimensions and typically weighed less than 1 mg and not more than 3 mg. This made them big enough to manipulate but small enough that they easily fit in the fluid cell of the AFM (volume of about 150 μl) and did not rapidly deplete soluble lattice ions during the flow-through conditions of crystal growth.

Pyrolysis

About 10 foliar chips were placed in a 30-ml glass vial for each treatment in a muffle oven (Blue M Electric Co.) at 475° ± 10 C for 36 h. Following pyrolysis, some vials were capped and the chips stored in air. Other vials were fitted with gas-tight caps and the vials purged with dry nitrogen. The purpose of this treatment was to control for the possible reaction of CO_2 in humid air with the pyrolyzed surface. In yet other cases, some of the pyrolyzed chips were rinsed three times in the vials with 10 ml of $CaCO_3$-saturated water with magnetic stirring for 10 min, followed by decanting of the fluid after each rinse. After the last rinse, the chips were manually blotted onto filter paper, then placed back in the vial, and stored in dry nitrogen. The rinsing fluid was prepared as the supernatant of a slurry of 1 g of reagent-grade calcite in 100 ml of water, stirred for at least 24 h. The purpose of rinsing was to remove any pyrolytic products that may have remained on the surfaces.

If the chips were simply stored in air after pyrolysis, their surfaces were observed to change at the nanometer level over a period of weeks. Initially, the pyrolyzed surfaces appeared to be relatively featureless and free of the globular morphology, but powdery until rinsed clean during imaging in saturated artificial seawater. After weeks to months, however, some nanoscale crystals would develop on the surfaces, even though the chips were stored "dry" in air. Presumably these were calcite crystals that formed as a result of cycles of relatively drier and more humid conditions in the saturated, hydrated layer on crystal surfaces in humid air. Accordingly, all images reported herein were taken from chips that were stored in nitrogen.

To verify the method and to observe the relative stability of control calcite surfaces, chips of calcite similar in size to the foliar chips were subjected to the pyrolytic treatment, stored in air or in dry nitrogen, and observed by AFM both dry and in fluids. The calcite chips were obtained by gently striking a large calcite rhombohedron (~4 cm in length; Watkins Mineral Corp., Wichita Falls, Texas) with a razor edge, producing small rhombohedral fragments. All surfaces of these rhombohedrons were observed by AFM to be the (1 0 4) cleavage surfaces and remained so after pyrolysis, which is understandable in that calcite is stable up to ~825 C (Boynton, 1980; Dean, 1992), above which calcite decomposes to calcium oxide. Crystallographic details and AFM images of calcite (1 0 4) surfaces are presented in following sections about crystal formation on foliar laths.

There was some surface roughening at the nanometer level of the pyrolyzed surfaces of the control, calcite rhombohedrons, which again might result from heating the saturated, hydrated layer. When placed in calcite-saturated fluid, these surfaces smoothed out in a matter of minutes, forming irregularly bordered steps along (1 0 4). When placed in calcite-supersaturated fluid, accretion along the (1 0 4) steps was easily seen, and no surfaces other than (1 0 4) calcite were observed.

The day prior to viewing by AFM, single foliar chips were removed manually from the vial and glued onto glass discs attached to stubs as described above. The chips were then stored overnight in a plastic box so that the polyurethane adhesive became firm. The box was not completely gas-tight, but it was purged with dry nitrogen, shut, and sealed along the edges with Parafilm. Including this treatment, and the interval of up to an hour while the chip was being aligned and positioned under the AFM probe, the chips were only minimally exposed to the atmosphere.

Atomic force microscopy and the crystal growth assay

Constant-force, contact-mode AFM (Digital Instruments) was used, including a flow-through AFM crystal growth assay, as previously described (Sikes *et al.*, 1998). The artificial seawater of the crystal growth experiments consisted of 0.5 M NaCl, 0.01 M KCl, 0.01 M $CaCl_2$, with $NaHCO_3$ varied over the range of 2 to 10 mM. The solutions were prepared at 200 ml in a 250-ml, water-jacketed, glass beaker (Fisher Scientific). Reactions were thermostated at 25° ± 0.1°C by use of a recirculating bath (Neslab, model RTE-210). Fluids were pumped through the fluid cell of the microscope at 75 μl min^{-1} by use of a peristaltic pump (Cole-Parmer, Masterflex) with Silastic tubing.

The pH of the fluids was adjusted to 8.32 ± 0.02 and monitored continuously by pH meter and strip chart. In most experiments, the solutions were completely metastable during the course of crystal growth (*i.e.*, supersaturated but not spontaneously nucleating) such that the pH held steady throughout, both in the inflow and outflow of the fluid cell. This showed that the conditions of crystal growth were essentially held constant, at least in the bulk phase, even when crystals were growing on the surfaces of the folia. This constancy was achieved by keeping the foliar surface area low relative to the volume of the fluid cell and the rate of flow through it. In some cases at higher levels of dissolved inorganic carbon (DIC), crystals of calcite would spontaneously nucleate in the bulk fluid after a few minutes (at 10 mM DIC) or about 20 min (at 7 mM DIC). In these situations, the pH would drift downwards as carbonate ions were removed from solution.

At least three chips were imaged at each supersaturation, including several separate surfaces per chip, except for the treatments at 8 and 10 mM DIC. Under these conditions, crystallization was so rapid and widespread that the suspended crystals interfered with the laser signal of the AFM. In addition, crystals rapidly overgrew each other on the foliar surfaces, obscuring the morphology. In the experiments at lower supersaturations, images were collected at intervals during the period of crystal growth, ranging from several dozen to as many as 200 images per experiment, with a total of approximately 2000 images examined.

Surfaces that exhibited homogeneous foliar morphology were purposefully selected for study. Chips from fractured oyster shell often exhibited surfaces that were more prismatic, chalky, and amorphous, or had mixed morphologies. When these were encountered, the AFM probe was either moved to another location or, if necessary, the chip was discarded.

Scanning electron microscopy

Foliar chips were dehydrated by vacuum at 1 mTorr for 15 min, then coated with a layer of approximately 35 nm of gold in a Hummer X sputter coater (Anatech, Ltd.). Specimens were viewed with a JEOL 848 scanning electron microscope operated at 35 kV.

Calcite models and morphology of ectopic crystals

Computer models of calcite morphology and atomic patterns of lattice planes were made using Cerius^2 molecular modeling software (version 4.0, Molecular Simulations, Inc., San Diego, CA). Plane angles of ectopic crystals and foliar surfaces were measured by means of cross-sectional analysis of AFM images (raw data, before flattening) using AFM imaging software (version 4.1, Digital Instruments, Santa Barbara, CA). Measurements of vertical angles greater than 55° may be subject to a kind of AFM tip artifact, which registers such angles as being approximately 55°. Although this may have been encountered in some cases in the present studies, it certainly was not always the case, with angles significantly greater than 55° frequently encountered. Details of calibration of AFM scanners for measurements of length, width, height, and atomic spacings, as well as procedures to guard against other possible AFM artifacts are given in Sikes *et al.* (1998).

Calculation of supersaturations

Supersaturations (Ω, Table 1) were obtained for calcite at the various levels of DIC for the artificial seawater by use of Mineql+ (version 3.0, Environmental Research Software, Hallowell, ME). The calculation involved dividing the solubility constant for the synthetic seawater (log Ksp = −7.27) into the product of the concentrations of free, ionic calcium ($\sim 10^{-2}$ *M*) and carbonate (level of DIC multiplied by an ionization fraction for CO_3^{2-}, both corrected for ion pairing).

Table 1

Calculated supersaturations (Ω)[a] *of artificial seawater*[b] *with respect to calcite, as determined by use of Mineql+*

Calcium (m*M*)	Free ionic Ca^{2+} (m*M*)[c]	DIC (m*M*)	Free ionic CO_3^{2-} (*M*)[d]	Ω
10	9.91	2	$5.85e^{-5}$	10.7
10	9.82	3	$8.78e^{-5}$	16.3
10	9.78	5	$1.46e^{-4}$	26.9
10	9.70	7	$2.05e^{-4}$	37.2
10	9.66	8	$2.34e^{-4}$	42.7
10	9.57	10	$2.93e^{-4}$	52.5

[a] Calculated as: (free ionic calcium) (free ionic carbonate)/solubility product; representative value for log $K_{sp} = -7.27$ (also based on concentrations of free ions, varies only slightly depending on the ionic composition for each experimental treatment).

[b] 0.5 *M* NaCl, 0.01 *M* KCl, pH 8.30, 25°C, closed to the atmosphere.

[c] Takes ion pairing into account, which increases with increasing DIC.

[d] Takes into account the ionization fraction for carbonate at pH 8.30 as well as ion pairing, particularly as sodium carbonate, in the artificial seawater.

Results

Figure 1 is an atomic force (AF) micrograph of a control chip of fractured oyster shell showing the overall foliar morphology of several sheets of calcite composed of laths lying side by side. A detailed view of a surface of this chip, showing the foliar globules, is shown in the AF micrograph of Figure 2.

The untreated foliar globules in general did not support crystal growth under conditions of $\Omega = 10.7$ or $\Omega = 16.3$ for periods up to 5 h of fluid flow, although crystals did grow in these experiments at edges and scattered sites, where mineral presumably was exposed on the fractured surfaces. The same foliar surface of Figure 2 is seen in Figure 3 after 60 min at $\Omega = 26.9$. Under these conditions, the foliar globules enlarged, and some began to exhibit crystalline morphology, but most retained an amorphous globular morphology (Fig. 4). In general, it was difficult to obtain atomic patterns from the surfaces of the globules as they emerged; however, a hexagonal pattern that was typical of the uppermost surfaces of the emerging globules is shown in Figure 5.

A representative AF micrograph of a foliar chip that was pyrolyzed is shown in Figure 6. Several foliar sheets are evident; again, each is composed of individual laths laying side by side. At this magnification, the control and pyrolyzed chips had similar appearances.

However, as shown in Figure 7 (an unwashed surface, stored in nitrogen, imaged dry), after pyrolysis, the foliar globules were reduced to fragile remnants. These quickly washed away upon viewing in fluid, as seen in Figure 8 (similar surface, stored in nitrogen, but imaged in artificial seawater, saturated with calcite). Although the globules were removed by pyrolysis, after washing the surface was not featureless, but was covered with very small mineral protrusions. When subjected to $\Omega = 10.7$, these protrusions clearly began to grow such that by 5 h, a uniform pattern of obliquely inclined crystal elements was evident (Figs. 9–11). When $\Omega = 16.3$, the crystal elements emerged much more rapidly; by 60 min, they had merged and overgrown

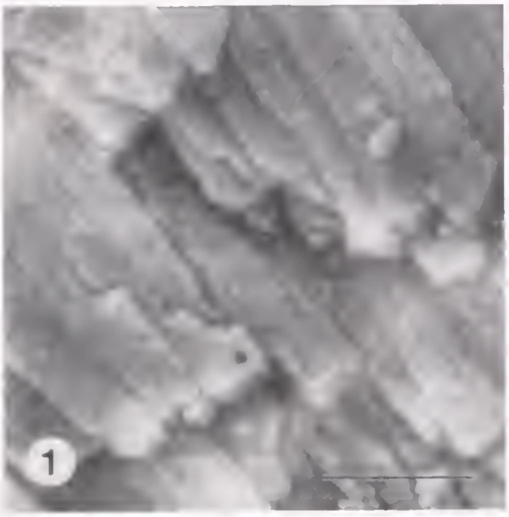

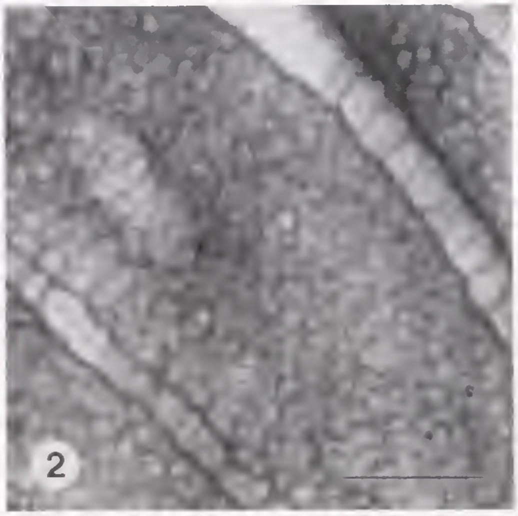

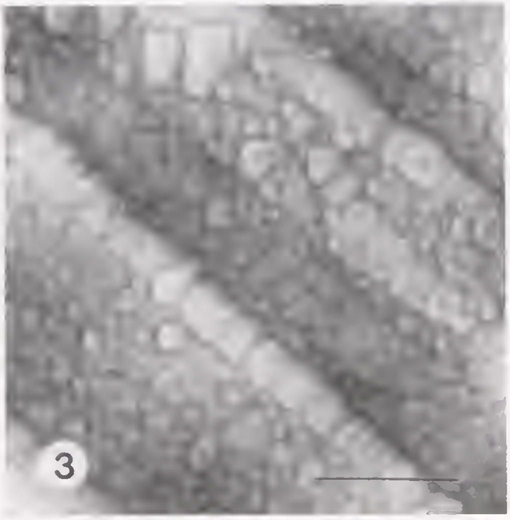

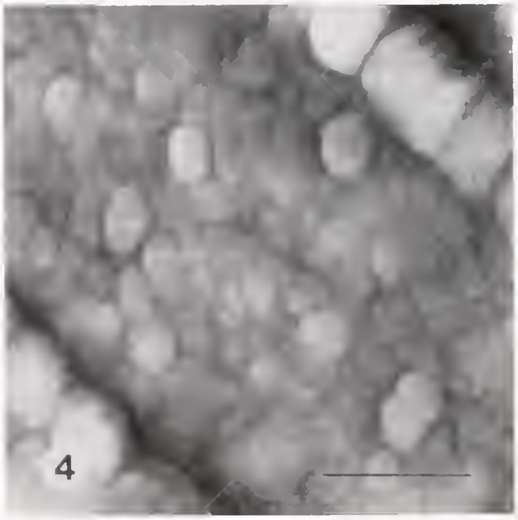

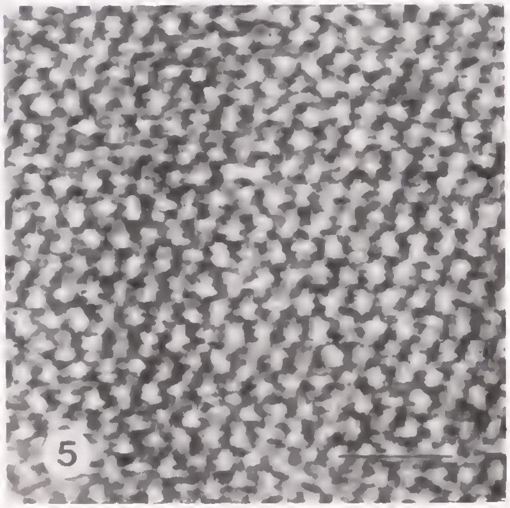

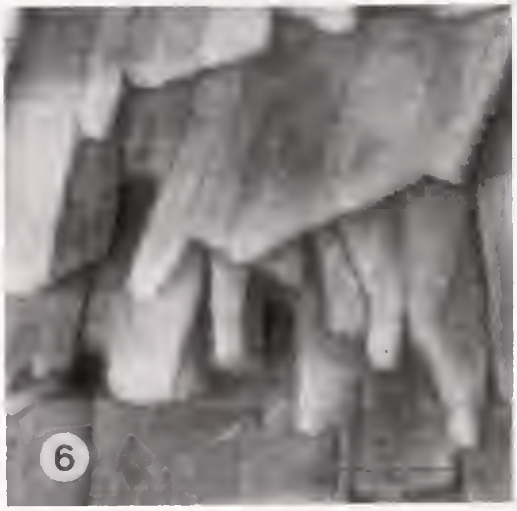

each other, obscuring the original morphology and surface structure (Figs. 12–14).

At $\Omega = 26.9$, crystal growth on pyrolyzed foliar surfaces was essentially instantaneous. Each ectopic crystal had a singular, uniform morphology and orientation along the foliar laths (Figs. 15, 16). For example, as seen in Figure 16, each of the crystals had a shallower surface, that ramped upwards from right to left at an angle of about 45°. The

Figures 1-6. Atomic force micrographs of foliar chips from fractured oyster shell, viewed in artificial seawater.

Figure 1. An untreated, control foliar chip. Total range of elevation within the imaged area = 500 nm; lath heights range from 100 to 260 nm. Scale bar = 2.5 μm.

Figure 2. A foliar surface of the chip of Figure 1. Foliar globular heights range from 10 to 40 nm. The globules are often arranged in linear arrays as shown here, aligned with the long axis of the laths. Scale bar = 0.5 μm.

Figure 3. The foliar surface of Figure 2, viewed in artificial seawater after flow-through crystal growth for 60 min at 10 mM calcium, 5 mM inorganic carbon, pH = 8.3 (Ω = 26.9; see the text). The foliar globules had emerged somewhat and some began to assume crystalline forms: globular heights range from 15 to 50 nm. Scale bar = 0.5 μm.

Figure 4. The foliar surface of Figure 3, same treatment as in Figure 3, showing details of the emerging foliar globules. Scale bar = 0.25 μm.

Figure 5. The atomic pattern of one of the globular surfaces of Figure 4, imaged by contact-mode AFM in artificial seawater, saturated with respect to calcite. Notice the hexagonal pattern of the atoms, consistent with the theoretical spacing of the (0 0 1) surface of calcite (see the text). Scale bar = 2 nm.

Figure 6. A pyrolyzed foliar chip from fractured oyster shell. Total range of elevation within the imaged area = 400 nm. Lath heights range from 120 to 200 nm. Scale bar = 2.5 μm.

other two surfaces of each crystal emerged from the foliar surface diagonally (from upper left to lower right, and from lower left to upper right) at angles of about 70°, as also seen in the SEM of Figure 17. The smallest such crystals that were seen were about 20 nm in length or width and 3 nm in height. This particular experiment was replicated six times, with the same results and morphology of ectopic crystals each time.

Computer models for the purposes of illustrating the possible orientations of ectopic calcite crystals and the angles of their surfaces relative to the substrate are shown in Figures 18 and 19. The atomic relationships of the crystal lattice are shown in Figure 20.

Generally the upper corner was rapidly completed even in the smallest of the crystals that were grown at Ω = 26.9 (Figs. 15–17), and there were no flat regions to probe. However, in a few cases, it was possible to obtain an atomic pattern from the top surface of a forming corner of such an ectopic crystal (Fig. 21). For comparison, the atomic pattern of the sides of the crystals (Fig. 22) was not difficult to obtain, particularly when the laths were presented at an angle relative to the AFM probe so that the sides of the crystals were close to perpendicular relative to the probe. Computer models that we interpret to correspond to the top surface (Fig. 23) and side surfaces (Fig. 24) are also presented.

Correlations between the computer models and the experimental observations. The model in Figure 19 illustrates the general features of the calcite rhombohedron of six sides and eight corners, shown here truncated with small planar surfaces and with the *c* axis vertical, in the plane of the page. The sides (cleavage planes) are the same crystallographically in terms of the spacings of atoms of calcium and molecules of carbonate; they are referred to as the (1 0 4) family of planes. An atomic pattern of a (1 0 4) surface as observed by AFM is shown in Figure 22, and the corresponding computer model of the protruding oxygen atoms of the (1 0 4) surface is shown in Figure 24.

The corners of the calcite rhombohedron, however, are not all the same. In the model of Figure 19, the top and bottom corners are crystallographically equivalent to each other, here truncated with basal (0 0 1) planes, which are perpendicular to the *c* axis (atomic patterns as in computer model of Fig. 20). A crystal that nucleates from a horizontal (0 0 1) plane would form a three-sided pyramid with the *c* axis perpendicular to the nucleating surface. The upper corner would be perfectly centered at the point where the three planes meet. Each plane would occur at an angle of 22.31° with the nucleating surface, as shown in the model of Figure 18b.

On the other hand, the other six corners of the calcite rhombohedron are also crystallographically equivalent to each other and are formed at points where three cleavage planes meet that are not so symmetrically arranged. If one of these corners is turned uppermost so that the *c* axis is horizontal and (0 0 1) vertical, the horizontal planes would be among the family of planes of which (1 −1 0) is a member (atomic patterns as in the model of Fig. 23). A crystal that nucleates from the (1 −1 0) family of planes would form a three-sided pyramid having two sides that form angles of 69.43° with the nucleating surface, with the third side forming a shallower angle of 44.37°, as shown in the model of Figure 18a, and as observed experimentally in the AFM and SEM images of Figures 15–17.

Discussion

Crystallographic aspects

The foliar globules were reduced by pyrolysis to fragile remnants that were firm enough to be imaged by AFM when dry but were rapidly washed away when imaged in calcite-saturated, artificial seawater. This suggested that the globules lost an organic component on pyrolysis but retained a mineral component that either dissolved, broke apart, or both upon treatment with the fluid. These results are consistent with prior evidence from chemical, enzymatic, im-

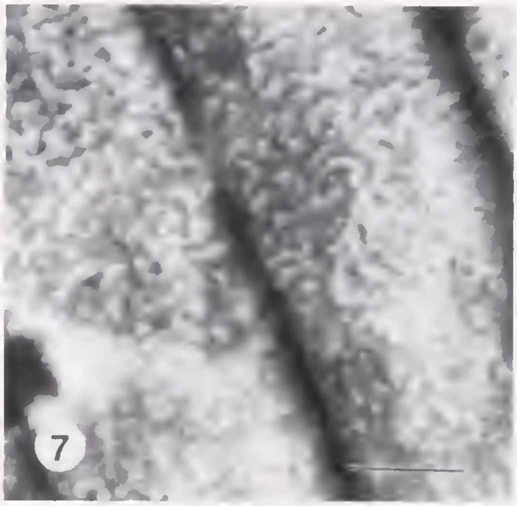
7

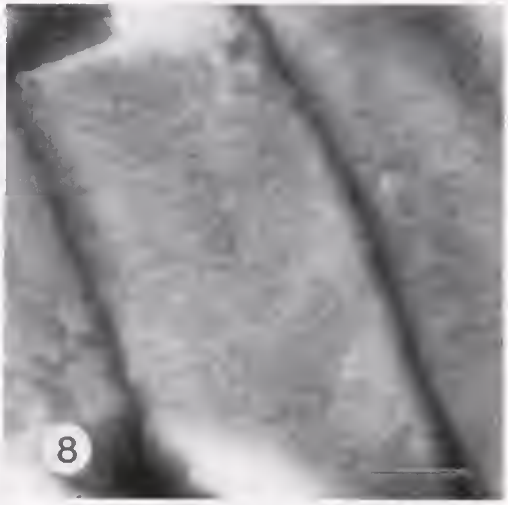
8

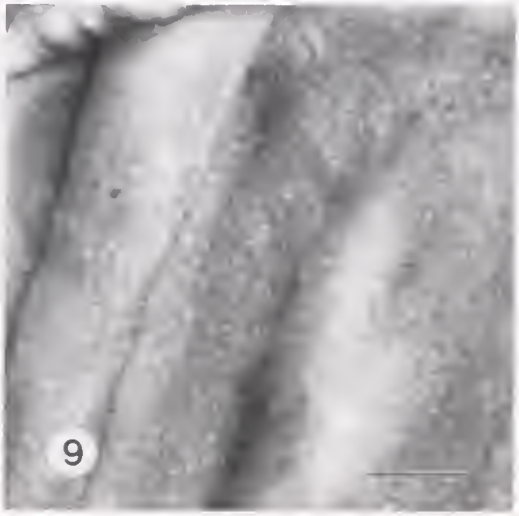
9

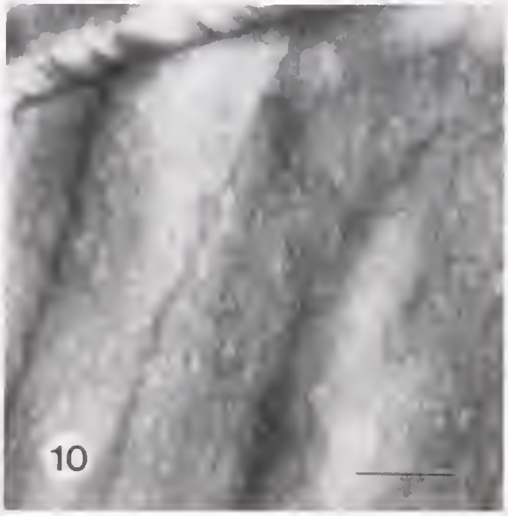
10

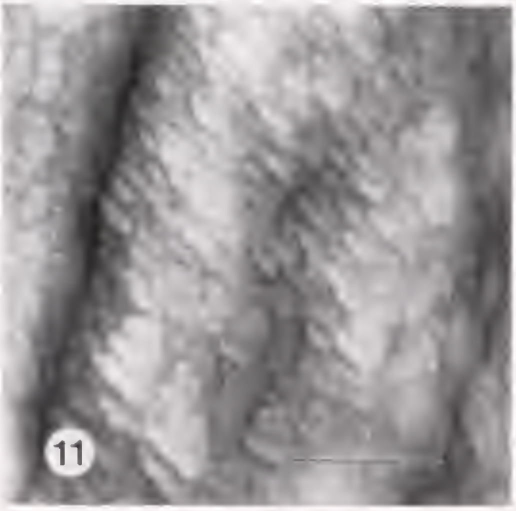
11

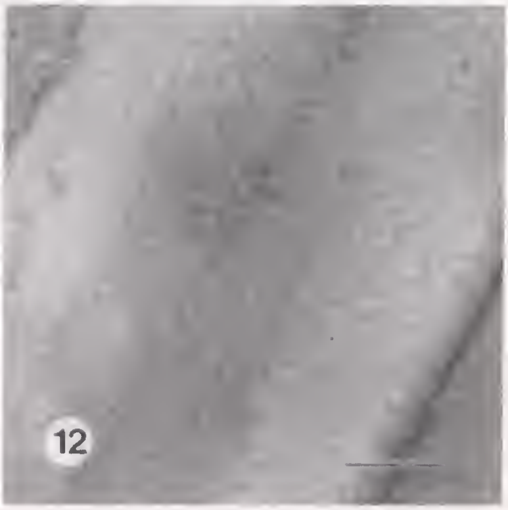
12

munologic, and morphological approaches that had indicated that the foliar globules appeared to be agglomerations of protein molecules and mineral, presumably amorphous calcium carbonate plus other minor constituents (Sikes *et al.*, 1998).

The foliar globules had no crystallographic surface fea-

Figures 7–12. Atomic force micrographs of pyrolyzed foliar chips from fractured oyster shell.

Figure 7. Chip viewed dry. The chip had not been rinsed after pyrolysis. It was stored in nitrogen in a gas-tight vial. Heights of foliar remnants ranged from 8 to 24 nm. Scale bar = 0.5 μm.

Figure 8. Chip viewed in artificial seawater, saturated with respect to calcite. Foliar globular remnants had mostly dissolved or washed away, revealing a fine crystalline texture of crystal elements with heights of about 2 nm that emerge obliquely from the foliar surface. Scale bar = 0.5 μm.

Figure 9. Chip viewed in artificial seawater after flow-through crystal growth for 10 min at 10 m*M* calcium, 2 m*M* inorganic carbon, pH = 8.3 (Ω = 10.7; see text). The crystal elements of the foliar surface began to become more visible. The lateral emergence of crystal blocks from the edges of laths can be seen at the upper left of the image. Scale bar = 0.5 μm.

Figure 10. The same pyrolyzed foliar surface as in Figure 9, viewed under the same conditions after 5 h of crystal growth. The crystal elements of the foliar surface had clearly enlarged; height of the emerging crystal ranged from 2 to 8 nm. Again, the lateral emergence of crystal blocks from the edges of laths can be seen at the upper left of the image. Scale bar = 0.5μm.

Figure 11. The same pyrolyzed foliar surface as in Figure 10, viewed under the same conditions after 5 h of crystal growth. Details of the emerging crystal elements can be seen, including the oblique angle at which they emerge from the foliar surface. Scale bar = 0.25 μm.

Figure 12. A chip viewed in artificial seawater, saturated with respect to calcite. Some of the texture of the crystal elements of the foliar surface can be seen. Scale bar = 0.5 μm.

tures such as planes or angular aspects, and no atomic patterns were obtained from them by AFM. The term *amorphous* is used here to emphasize this lack of crystalline features; it is not necessarily meant to ascribe an exact equivalence between the mineral of the foliar globules and amorphous $CaCO_3$ that might be formed inorganically at high Ω, although such an equivalence is certainly possible. The probable occurrence of amorphous $CaCO_3$ within carbonate biominerals has long been inferred (Lowenstam and Weiner, 1989; Simkiss and Wilbur, 1989; Simkiss, 1994) and has received increased attention as both a common and abundant component of such structures (Aizenberg *et al.*, 1996; Beniash *et al.*, 1997; Weiner and Addadi, 1997).

Another possible indication of the amorphous nature of the mineral component was that the foliar globules did not nucleate calcite crystals from solutions at low supersaturations. When supersaturations were purposefully raised to force crystallization, crystals slowly emerged from the globules. Upon enlargement of the crystals such that flat upper surfaces and sides could be probed, these crystals were observed to have (0 0 1) top surfaces and (1 0 4) sides, and eventually formed a symmetrical pyramid at the upper corner. Such crystals evidently emerged from the basal plane of calcite in the form depicted by Figure 18b, and ultimately fused to form aggregates.

These crystals are not thought to indicate the crystal structure of the underlying calcite lath. Rather, nucleation from the basal plane is known to be promoted by polyanionic proteins from biominerals (Addadi and Weiner, 1985; Addadi *et al.*, 1987), which are one component of the globules, or this may simply be a favored mode of growth from an organic/amorphous $CaCO_3$ composite.

The pyrolyzed foliar surfaces consisted of tightly packed arrangements of mineral protrusions, each of a width of about 10 nm, that emerged obliquely from the plane of foliation (Figs. 8–10). The mineral protrusions, like the original foliar globules, exhibited no identifiable, crystallographic features or atomic patterns. Although pyrolysis certainly destroyed most of the organic component, it is possible that some of the binding groups, such as carboxylates and phosphates of the polyanionic proteins, were actually imbedded as part of the crystal lattice (Mann *et al.*, 1990; Wierzbicki *et al.*, 1994; Sikes and Wierzbicki, 1995, 1996), and thus may remain there even when the rest of the protein is gone. Conceivably, this could disrupt the atomic patterns that might otherwise be revealed by AFM.

Even at the lowest supersaturation (Ω = 10.7) of the study, crystals slowly emerged from the pyrolyzed foliar surfaces over a period of 5 h. The general morphology of the underlying, nanoscale crystal elements of the folia was maintained during this interval at this level of Ω. Although no obvious crystallographic features were seen, the crystal elements did appear to emerge with identical orientation at an approximate angle of 45° to the pyrolyzed foliar surface (Fig. 11).

As the supersaturation was increased to Ω = 26.9, however, clearly observable crystallization was almost instantaneous (Figs. 15–17). The crystals, even the smallest ones with nanometer dimensions on the order of crystal nuclei, all had the same morphology and orientation along the foliar laths. In some cases, the uppermost plane, parallel to the plane of foliation, was resolvable at the atomic level by AFM as the (1 −1 0) surface of calcite (Fig. 21). The crystal morphology, including measurements of angles of the sides of the crystals (one side at ~45°, the other two sides of the pyramids at ~70°) relative to the surface, was consistent with calcite nucleating from one of the (1 −1 0) family of planes, with one of the six "nonbasal" corners uppermost, as depicted in Figure 18a. In this morphology, the *c* axis was parallel to the plane of foliation, aligned with the long axis of foliation. Similarly, the foliar globules are frequently so aligned, forming linear arrays along the long axis of foliation (Figs. 2, 3).

Evidently, pyrolysis had removed the foliar globules and

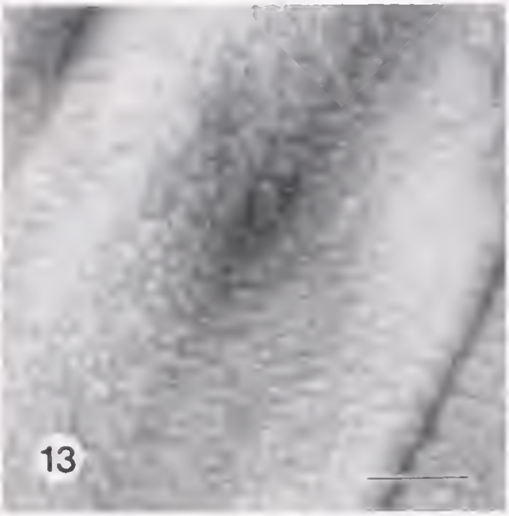
13

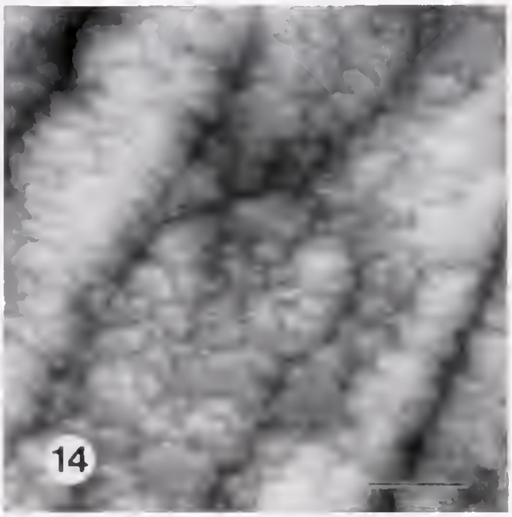
14

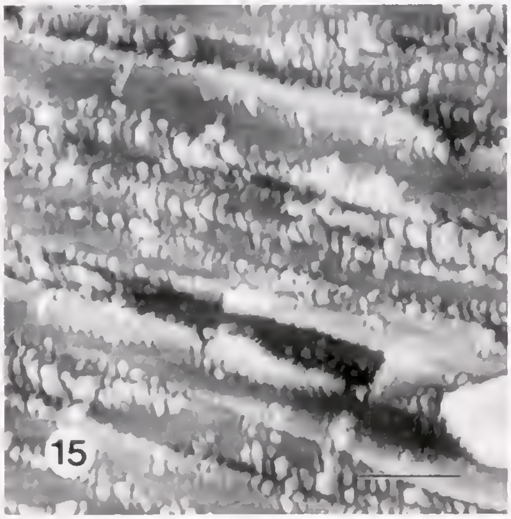
15

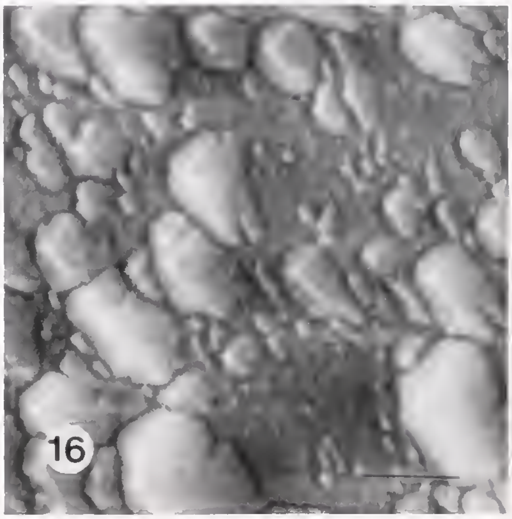
16

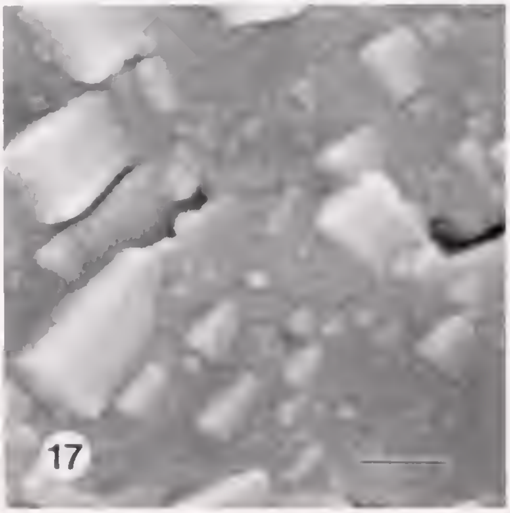
17

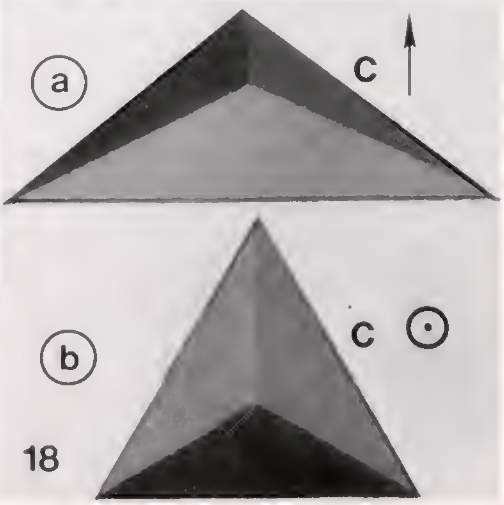

18

exposed (1 −1 0) surfaces that served as nucleation sites for the ectopic crystals. The soluble proteins from oyster shell, as well as other polyanionic adsorbates, are thought to have high affinity for the (1 −1 0) surface of calcite (Berman *et al.*, 1988; Didymus *et al.*, 1993; Albeck *et al.*, 1996), with binding parallel to the *c* axis being one preferred orientation (Wierzbicki *et al.*, 1994). Therefore, it seems consistent that the foliar globules, to the extent that at some point they have

Figure 13. Atomic force (AF) micrograph of the same pyrolyzed surface as in Figure 12, viewed in artificial seawater after flow-through crystal growth for 6 min at 10 m*M* calcium, 3 m*M* inorganic carbon, pH = 8.3 (Ω = 16.3; see the text). The crystal elements of the foliar surface had enlarged. Scale bar = 0.5 μm.

Figure 14. AF micrograph of the same pyrolyzed surface as in Figure 13, viewed under the same conditions, after 30 min of crystal growth. The crystal elements of the foliar surface had continued to grow, merging into larger forms, overgrowing each other and obscuring the original morphology. Scale bar = 0.5 μm.

Figure 15. AF micrograph of a pyrolyzed foliar chip from fractured oyster shell, viewed in artificial seawater after flow-through crystal growth for 7 min at 10 m*M* calcium, 5 m*M* inorganic carbon, pH = 8.3 (Ω = 26.9; see the text). Large numbers of ectopic crystals of characteristic and uniform morphology and orientation had formed almost instantly on the surface. Height of the ectopic crystals ranged from a few nanometers to 250 nm after 7 min. Scale bar = 2.5 μm.

Figure 16. AF micrograph of the same pyrolyzed surface as in Figure 15, viewed under the same conditions after 10 min of crystal growth. The ectopic crystals had nucleated from the foliar surface as asymmetric, three-sided pyramidal forms, each with identical morphology and orientation. The crystals were essentially everywhere on the surface, with the smallest ones a few nanometers in height, and the largest ones in the imaged area about 200 nm in height. Scale bar = 0.5 μm.

Figure 17. A scanning electron micrograph of a pyrolyzed foliar surface treated the same as in Figure 15, again showing the ectopic crystals that emerged from the foliar surface as asymmetric, three-sided pyramidal forms, confirming the morphology as seen in the AFM images. Scale bar = 0.5 μm.

Figure 18. Computer models of three-sided, pyramidal, ectopic crystals, viewed from above. (a) A crystal that would be nucleated from the (1 −1 0) surface of calcite, with the orientation of the *c* axis shown by the arrow pointing upwards in the plane of the page. The surface of each side would be equivalent and of the (1 0 4) type, but the corner is formed asymmetrically at the point where the three sides meet, such that two sides would emerge from the surface at an angle of 69.43°, with the third side emerging at an angle of 44.37°. This model is consistent with the morphology of the ectopic crystals that were grown on the pyrolyzed foliar surface. (b) A crystal that would be nucleated from the (0 0 1) surface of calcite, with the orientation of the *c* axis shown by the symbol indicating perpendicularity to the page. Each surface would be equivalent to the others, with the corner formed symmetrically at the point where the three sides meet. Each side would emerge from the surface at an angle of 22.31°.

similar polyanionic proteins available for binding to shell calcite, might bind to the (1 −1 0) surface, parallel to the *c* axis.

As suggested by previous workers, it seems reasonable to assume that the ectopic crystals will track the underlying biomineral calcite lattice (Okazaki and Inouyé, 1976; Okazaki *et al.*, 1981; Runnegar, 1984), especially if any organic covering is removed from the biomineral. Following this assumption, the foliar surface would appear to be the (1 −1 0) surface of calcite. In addition, the laths evidently elongate along the *c* axis.

This interpretation is consistent with the X-ray data of Taylor *et al.* (1969), who reported that the plane of foliation was parallel to the *c* axis. These authors noted an inclination of the folia relative to the shell surface and were able to arrange the actual plane of foliation to be parallel to the slide on which the shell was mounted by correcting for an angle of 26° at which the folia emerged to form the surface of the shell. On the other hand, mounting the shell itself as parallel to the slide in effect would rotate the plane of foliation by about 26°, which brings one of the (1 0 4) family of planes as perpendicular to the X-ray beam. This is consistent with the findings of Runnegar (1984), who reported (1 0 4) reflections as indicative of inner surfaces in X-ray work with fragments cut from shell. In addition, Runnegar (1984), following the method of Okazaki and Inoué (1976), also grew ectopic calcite at very high Ω (>1000) on bleached shell surfaces, revealing asymmetrical, three-sided pyramidal crystals, perhaps the same as observed herein.

Other workers (Wada, 1963, 1968; Watabe, 1965, 1981) had observed crystallites on folia that were arranged with the *c* axis vertical to the plane of foliation and therefore thought to be nucleated from the (0 0 1) plane. We have also sometimes seen this on control, foliar chips that have prominent ectopic, polygonal crystals that appeared to be nucleated from the basal plane (not shown). As reported herein, the control foliar surfaces may act as nucleation sites for such basal calcite crystals at relatively high levels of supersaturation.

The cycle of mineralization in vivo

The formation of shells as layers of mineral interspersed with organic sheets implies a cyclic process of organic secretion and inorganic mineral growth (*e.g.*, Degens, 1976; Wheeler and Sikes, 1989). Details central to this process are poorly known but include the *in vivo* levels of Ω and the organic components, as well as the relative timing of secretion of lattice ions and organic matrix. The AFM measurements of growth of calcite on shell fragments, together with measurements of shell growth *in vivo*, may provide a way to estimate the effective Ω *in vivo*, as well as the time frame of lath formation, as explained below.

Starting with the possible levels of lattice ions and organic matrix *in vivo*, measurements of the ionic and organic

19

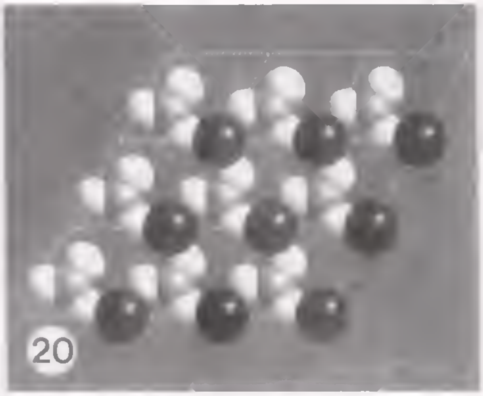
20

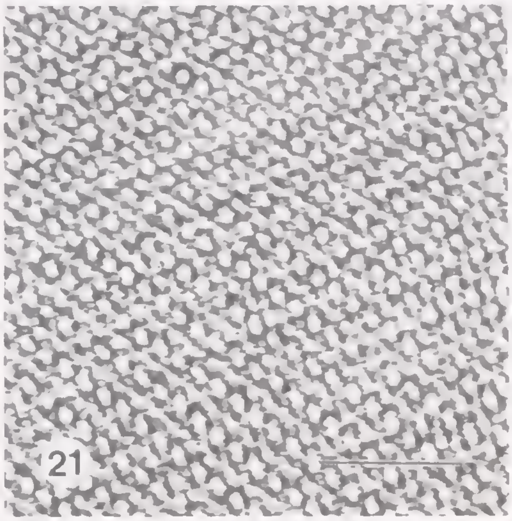
21

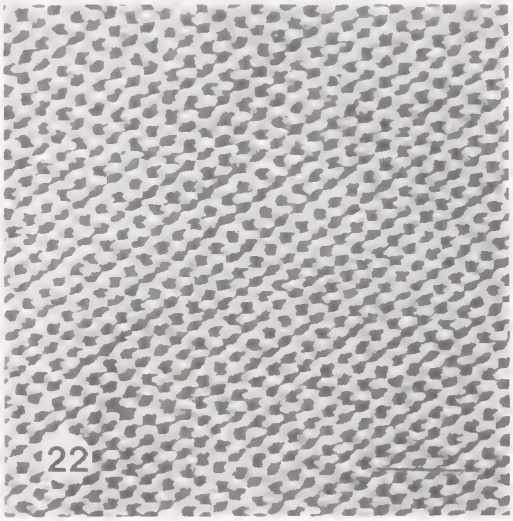
22

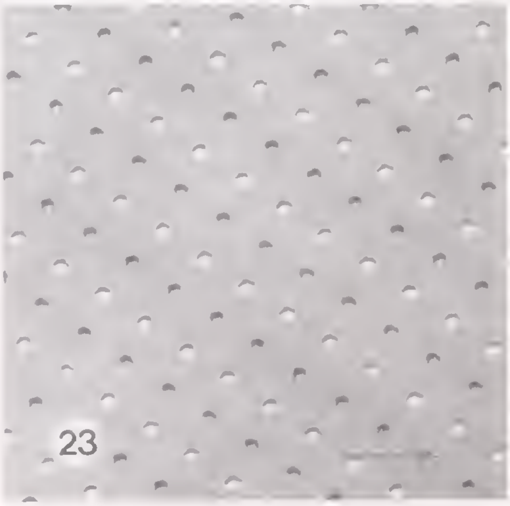
23

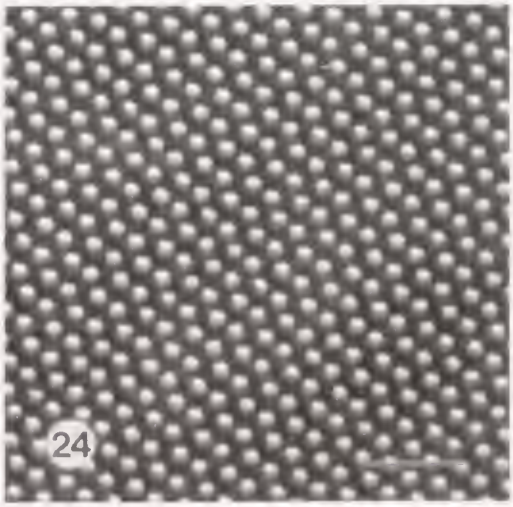
24

composition of extrapallial fluid (EPF, the medium of shell formation), are available by means of exacting microanalysis following attempts to sample the fluid. In the Eastern oyster, the estimate (Crenshaw, 1972) of calcium content was close to that of seawater at nearly 10 m*M*, inorganic carbon was as high as 5 m*M* (with seawater normally at about 2.2 m*M*), but the pH at about 7.4 was notably lower than typical values for seawater (~8.2), which in turn would result in significantly lower levels of carbonate ion. These conditions of the EPF would convert to an Ω of 2.83, which is quite low. Studies of the EPF of other molluscs yielded roughly similar results (Wada and Fujinuki, 1976; Misiogianes and Chasteen, 1979; Nair and Robinson, 1998).

Moreover, other solutes of the EPF such as magnesium,

Figure 19. Computer model of a calcite rhombohedron. The model is depicted with the *c* axis upward, in the plane of the page. Planes are cut through the eight corners. The arrows indicate the bottom and top planes (basal planes), which are (0 0 1) surfaces. The planes through the other corners are the family of (1 −1 0) planes. Each of the sides is a member of the (1 0 4) family of planes.

Figure 20. A computer diagram of the (0 0 1) surface of calcite, showing an upper plane of calcium atoms, and an underlying plane of carbonate groups. Notice how the calcium atoms coordinate with three oxygens of separate underlying carbonate groups. Each calcium atom also would coordinate with three oxygens of separate carbonate groups of a carbonate homoplane (not shown) that would overlay the calcium plane in a similar manner, with successive homoplanes of calcium and carbonate alternating to form the calcite crystal. The *c* axis runs perpendicular to the (0 0 1) plane. The *a* axes are shown as the grid of lines on the diagram. The (1 −1 0) family of planes also run perpendicular to the (0 0 1) plane (or parallel to the *c* axis), emerging perpendicularly from the *a* axes. Scale bar = 0.5 nm.

Figure 21. Atomic force (AF) micrograph of the atomic pattern of one of the uppermost surfaces of the crystals of Figure 16. The spacings of atoms are consistent with the (1 −1 0) surface of calcite. The more clearly resolved rows of atoms (from upper left to lower right) are thought to correspond to protruding oxygens of carbonate groups, with the atoms that tend to blend together in the other rows (also from upper left to lower right) corresponding to calcium atoms that are somewhat recessed into the surface. Scale bar = 3 nm.

Figure 22. AF micrograph of the atomic pattern of one of the sides of the ectopic crystals as in Figure 16, viewed in artificial seawater saturated with respect to calcite. The spacings of atoms are consistent with the (1 0 4) surface of calcite. In this image, each lattice position is thought to correspond to a protruding oxygen atom of the carbonate groups, which are elevated to some extent relative to calcium atoms that occur just below the (1 0 4) surface. Scale bar = 2.0 nm.

Figure 23. A computer diagram of the (1 −1 0) surface of calcite, showing the oxygen atoms (white) of the carbonate groups outermost and the calcium atoms (gray) slightly recessed into the surface. The number of oxygen atoms per unit area of this surface is not nearly as dense as in the (1 0 4) surface, and therefore both the oxygens and the calcium atoms can be seen in AF micrographs of the (1 −1 0) surface. The atoms within one row of oxygens are spaced 4.99 Å apart, with the nearest oxygens in separate rows 8.53 Å apart. This matches within 5% of the atomic spacings of the uppermost, forming surface at the corner of one of the ectopic crystals on a pyrolyzed foliar surface as seen in Figure 21. Note that if only every other row of oxygens of the (1 0 4) surface has the atoms clearly resolved, with the other rows of oxygens having atoms blurred together (again with no calcium atoms observed at all), which can be done by increasing the force of the AFM probe as well as the gain setting, a pattern somewhat similar to the (1 −1 0) pattern can occur. However, the spacings and angles between atoms of the two surfaces still differ, as does the number of atoms per unit area. Scale bar = 1.0 nm.

Figure 24. A computer diagram of the (1 0 4) surface of calcite, showing only the outermost oxygen atoms of carbonate groups, as are seen in AF micrographs of this surface. The calcium atoms are recessed by about 1 Å into the surface and do not show up in AFM's due to the closeness of the surface oxygen atoms. The nearest neighbors of outermost oxygen atoms form rhombohedrons with spacings of 4.24 and 4.99 Å, which matches within 5% of the spacings as seen in Figure 22 of the sides of the ectopic crystals on a pyrolyzed foliar surface. Scale bar = 2.0 nm.

phosphate, small chelants that bind soluble calcium, and organic components like soluble shell proteins are all inhibitory to calcite formation. If these constituents are taken into account, the measurements actually suggest that the EPF is undersaturated with respect to calcium carbonate.

In this regard, Wilbur and Bernhardt (1984) attempted an *in vitro* assay for calcite formation based on prior estimates of the content of EPF. It was necessary to raise calcium to 28.2 mM and inorganic carbon to 7.6 mM at pH = 8.33 (including Mg at 47.2 mM, but no phosphate and no organic compounds) to obtain nucleation after about 20 min at 21°C. These levels of soluble lattice ions correspond to Ω = 72.4. In the absence of Mg, under otherwise similar conditions, we obtained nucleation after about 20 min at Ω = 37.2.

By comparison, seawater itself is considered to be mildly supersaturated with respect to calcite ($\Omega \sim 10$). However, again, the other constituents such as magnesium, phosphate, and organic components act to stabilize seawater so that calcium carbonate does not normally precipitate.

Turning to rates of shell deposition *in vivo*, on the other hand, direct measurements of shell enlargement revealed substantial rates of carbonate deposition that are indicative of notably high supersaturations. For example, in the scallop *Argopecten irradians* and the marine clam *Mercenaria mercenaria*, shell enlargement was measured by radioisotopic approaches to range from about 0.1 to 2.0 μm cm^{-2} h^{-1} (Wilbur and Jodrey, 1952; Wheeler *et al.*, 1975; Wheeler and Wilbur, 1977; Dillaman and Ford, 1982). By dividing by the density of shell, this value was converted to an increase of a single linear dimension such as thickness or elongation of about 35 to 700 nm cm^{-2} h^{-1}.

Regarding the possible levels of Ω *in vivo* as indicated by AFM observations of calcite growth *in vitro*, the measurements of calcite formation on pyrolyzed foliar surfaces under controlled conditions of supersaturation indicated an emergence of foliar crystal elements of about 1 to 2 nm h^{-1} at $\Omega = 10.7$. At $\Omega = 16.3$, the average crystal growth over the surface was about 100 to 150 nm h^{-1}. At $\Omega = 26.9$, on average, the ectopic crystals emerged from pyrolyzed foliar surfaces at 300 to 500 nm h^{-1}. Comparison of these values to the above-referenced measurements of shell thickening suggests that the levels of Ω locally within the EPF must have been in the range of about 16 to 27, and perhaps even somewhat higher, exclusive of the effects of any inhibitory constituents of the EPF that may have been present. If soluble inhibitors of calcite formation were present, the levels of Ω would need to be even higher to drive the observed rates of shell growth.

One issue that affects direct measurement of constituents of the oyster EPF is the ability to obtain fluid for analysis. The mantle lies essentially in contact with the shell and the volume of EPF available for sampling is thus minimal to nonexistent (*e.g.;* see figure 9 of Watabe, 1974; figure 1 of Erben and Watabe, 1974; and figures 2 and 4 of Bevelander and Nakahara, 1980). Consequently, direct analysis of the actual levels of lattice ions and various inhibitors or promoters of crystallization in the fluid of mineralization may be impossible (Wheeler and Sikes, 1989; Wada, 1990)—assuming that there is a fluid as such. Having some bearing on the question of whether fluid is present is Galtsoff's view (1964) that mineralization in the oyster is a kind of solidification within a gel-like layer that is deposited by the mantle on the shell as it grows. He observed rhythmic back-and-forth movements by the mantle on the shell along the direction of foliation. These movements were accompanied by deposition of a highly viscous coating, which subsequently became mineralized (see also Carriker *et al.*, 1980; Carriker, 1996). Crenshaw (1990) and Calvert and Crockett (1997) have further reviewed aspects of biomineral formation within a possibly gel-like precursor.

When extracted by slow dissolution of shell, the shell matrix proteins, most of which are fundamentally similar in amino acid composition, are collected over a continuum of molecular weights (M_w) that ranges into the millions and higher (Wheeler *et al.*, 1988). The higher M_w fractions are gelling materials that are highly interactive with water but not actually water-soluble (Wheeler and Koskan, 1993; Wheeler *et al.*, unpubl. obs.). Some of the lower M_w materials that are released from shell as soluble fractions might also be linked to the gelling matrix when in the shell, but this is not known.

The possible significance of soluble *versus* gelling proteins bears on the question of the effective supersaturation of the mineralizing environment. Even low doses of soluble protein from oyster shell are strongly inhibitory to calcite nucleation (0.1 μg protein ml^{-1} at $\Omega = 42.7$; Wheeler and Sikes, 1989) or growth of calcite seed crystals (0.015 μg protein ml^{-1} cm^{-2} at $\Omega < 5$; Low, 1990; Wheeler *et al.*, 1991). The incorporation of the soluble protein into the crystals under these conditions was measured at 0.4 to 0.5 μg $\mu mole^{-1}$ calcite (Sikes and Wheeler, 1986), which is approximately equal to the amount of the protein that occurs in the folia.

However, if the shell is to grow at the rates that have been measured *in vivo*, which would require levels of Ω that are significantly elevated relative to seawater, it would seem that the shell protein, if present at all during intervals of mineral deposition, would occur in the mineralization fluid in soluble form at levels too low to account for the amount of protein in shell. However, this problem could be overcome if the secretion of shell protein by the mantle were episodic such that intervals of shell growth, during which no inhibitory proteins were present at the site of crystallization, were followed by intervals during which the newly formed mineral layer became covered by proteinaceous material.

In this framework, the measurements of inhibition of calcite formation *in vitro* at low doses of samples of whole EPF (Wilbur and Bernhardt, 1984) may be understood. When 210 μl of EPF from *M. mercenaria* was added to a calcite growth assay, inhibition was observed at roughly the level of 0.1 μg protein ml^{-1} established in other studies (Wheeler and Sikes, 1989). Given the volumes used in the assay, this would suggest that the EPF sample contained about 3 μg of protein, or roughly 15 μg protein ml^{-1} of EPF. This is such a high level that it would totally inhibit shell growth, even at very high Ω, if the protein molecules were present in a soluble form that could interact with the crystal surfaces. On the other hand, if a pulse of protein into the EPF was layered quickly onto a fresh mineral layer of shell and followed by an interval of protein-free EPF of Ω in the range of 16 to 27, the pattern of mineral deposition that is observed in foliar layers could occur. If such intervals of pulsed secretion are on the order of minutes, then samples of EPF, which consist of pooled volumes collected over periods of hours (Wada, 1990), would always contain shell proteins. There is evidence to support these speculations, as follows.

First, the foliar laths have thicknesses in the range 100 to 350 nm. As cited above, the shells of various molluscs have been measured to thicken at rates of 100 to 700 nm h^{-1}, thus formation of individual laths appears to occur at a rate of about 1 or more per h. Each lath is covered by a layer of foliar globules, which are thought to consist of shell protein and amorphous $CaCO_3$. This morphology is consistent with pulsed secretion of the protein, perhaps during an interval of only a few minutes per hour, when the protein is removed from solution by binding to the previously formed mineral. Following that, a period on the order of an hour of protein-free crystal growth would occur. Next, a new organic layer, which appears initially to be a gel (Wheeler *et al.*, unpubl. obs.), is secreted, binds to the lath, and subsequently becomes covered by calcite. Thus, the gelled organic layer also becomes mineralized during this process, apparently in the form of amorphous $CaCO_3$ of the foliar globules.

Conceivably, the next layer of calcite could nucleate from the organic layer, from exposed areas of calcite of the underlying lath, or both. That there are exposed areas of calcite even after the organic layer is bound seems probable because the pyrolyzed foliar chips were firm and did not crumble on handling following removal of the organic materials. This suggested that the mineral was continuous throughout the layers of folia. Direct evidence of continuity of this type has been observed between aragonitic tablets of the nacreous layers of shells (Watabe, 1981; Giles *et al.*, 1995). If there are areas of exposed calcite on the foliar surfaces after the organic layer is bound, these would serve as ready nucleation sites for new laths. Such exposed areas of calcite were not visually evident in the AF micrographs of fractured surfaces of folia, and therefore would necessarily be very small, presumably on the scale of nanometers.

The foliar globules themselves were not particularly effective as nucleation sites, and calcite crystals that were nucleated from them by raising the level of Ω did not appear to have the crystallographic orientation and morphology of the pyrolyzed lath. Hence, each succeeding foliar layer seemed to track the mineral of the underlying layer rather than to derive from the amorphous character of the foliar globules.

Another line of evidence that is consistent with the notion of a cycle of mineralization as presented above involves measurements of interactions of the soluble protein from oyster shell with calcite *in vitro*. When the protein was bound to calcite crystals, the maximum capacity of binding was 0.18 μg cm^2 (Wheeler *et al.*, 1991). Taking a value of 0.5% protein by weight in foliar shell, which agrees well with measurements of protein content of shell extracts, including foliar layers (reviewed in Sikes *et al.*, 1998), and with radioisotopic incorporation of the protein into calcite *in vitro* (Sikes and Wheeler, 1986), there would be 0.5 μg protein per μmole (100 μg) calcite. Using 2.6 as a typical value for the density of shell (Wheeler *et al.*, 1975), there would be 13 mg protein cm^{-3} of shell. If this protein were deployed in layers at 0.18 μg protein cm^{-2}, there would be enough protein to form a stack of 72,222 layers of 1 cm^2 in each cm^3. This corresponds to about 140 nm per layer (including the protein), which is at the low end of the range of thicknesses of a foliar lath.

One problem with these conjectures about binding and coverage involves drawing inferences from *in vitro* studies and applying them to *in vivo* processes. For example, the binding studies were based on measurements of the interaction of the protein with (1 0 4) surfaces of calcite. Moreover, the incorporation studies permitted the protein to interact freely with the growing crystal and likely involved several surfaces. The *in vivo* interaction, on the other hand, appeared mainly to be with the (1 −1 0) surface.

The binding affinity of the protein to the (1 −1 0) surface has been calculated to be higher than to the (1 0 4) surfaces (Wierzbicki *et al.*, 1994; Sikes and Wierzbicki, 1995, 1996). However, the binding capacity and coverage of the surfaces would probably be similar. That is, taking the average oyster shell protein as a globule at 50 kD with a linear dimension of about 5.4 nm (Sikes *et al.*, 1998), each unit of protein would cover about 30 nm^2. The maximum capacity of 0.18 μg of protein per cm^2 of calcite would represent 2.17×10^{12} molecules (50 kD = 8.3×10^{-20} g), or a coverage of 6.5×10^{13} nm^2. Comparing this to 1×10^{14} nm^2 per cm^2 suggests that 0.18 μg of the protein would cover most of 1 cm^2 of calcite regardless of the specific surface. Of course, it is also possible that the protein molecules (and the foliar globules) can form more than a monolayer on the calcite of the laths. This in turn would translate into laths of greater thickness as calculated above, which is often seen in the AFM and SEM images, both herein and in prior studies.

Conclusions

Overall, the evidence can be interpreted to support a hypothesis of pulsed secretion of the shell proteins, depletion of the soluble protein from the EPF upon binding to the mineral of laths, and subsequent intervals of growth of new mineral at relatively high Ω. The pulses of shell proteins might occur in a time frame of minutes, with the interval of mineral growth more on the order of an hour. The hypothesis would include secretion of the proteinaceous material primarily as a gelatinous covering that terminates the growth of the underlying lath and defines its surface as a member of the calcite (1 −1 0) family of planes.

In view of the need to elevate Ω to support the observed rates of folia formation *in vivo*, as well as to overcome the influence of soluble inhibitors in the EPF, it seems necessary for the organism to make significant metabolic investment in mechanisms to generate the mineralizing microenvironment. As indicated in many prior studies and reviews, although perhaps not at the magnitude suggested herein, the necessary supply of lattice ions may be provided by mechanisms such as direct active transport of inorganic carbon or calcium, or a combination of transport processes.

Another factor to consider is the formation of the crystals in thin, unstirred layers that are diffusion-limited. Watabe and coworkers (Watabe *et al.*, 1958; Watabe and Wilbur, 1961) noted that folia formation produced tablet-like morphologies that were similar to $CaCO_3$ crystals grown *in vitro* in unstirred layers, probably initiated in an area of highest Ω with growth toward regions of lower Ω, thus producing directional laths. Although crystallization assays often involve high rates of stirring to eliminate diffusion as a rate-limiting variable, some assays have been run under diffusion-limited conditions with concentration gradients into unstirred layers. It is interesting to note that calcium carbonates so produced frequently do exhibit tabular morphologies that resemble foliar laths to some extent, including crystals grown in the presence of shell protein (Fallini *et al.*, 1996; Weiner and Addadi, 1997). In related observations, Gower (Gower and Tirrell, 1998; Gower, pers. comm.) has noted that at higher concentrations under specific conditions of unstirred supersaturation, low M_w soluble polyaspartates and acidic polypeptides can induce localized droplets of a liquid-like, mineral-precursor phase that converts to calcitic tablets and other $CaCO_3$ structures.

It thus may also be useful to keep in mind that not only can the shell matrix proteins be arranged as the supramolecular assemblage of the gelling material, but also even the soluble molecules of relatively low M_w can agglomerate both in solution and when binding to mineral in the form of ellipsoids of linear dimensions up to about 100 nm (Wierzbicki *et al.*, 1994; Sikes *et al.*, 1998). Such associative behavior of other biomineral proteins such as dentin phosphophoryn, as well as other polyanionic proteins such as casein, has been reviewed by Marsh (1989a, b), who also observed agglomerations of phosphoproteins and mineral salts including amorphous calcium phosphate in nonmineralizing compartments of some molluscs (Marsh and Sass, 1983, 1984, 1985). None of these protein-mineral agglomerations appeared to be very effective as nucleators of crystals of shell or teeth (Marsh, 1986, 1989a, b, 1994).

Similarly, the amelogenins, the principal proteins of the formative stage of tooth enamel, have been shown to form gels composed of agglomerative "nanospheres." These nanospheres have been observed *in vivo* with dimensions of 15 to 20 nm (Fincham *et al.*, 1994, 1995) and *in vitro* with dimensions that range to 100 nm and higher (Wen *et al.*, 1999). The amelogenins are mainly hydrophobic, but they do have anionic C-termini that appear to occur at the surface of the nanospheres and interact there with the calcium hydroxyapatite of enamel. The amelogenin nanospheres are thought to function less in apatite nucleation than in localizing and orienting the developing enamel crystallites prior to their maturation (Fincham *et al.*, 1999).

Examination, by AFM, of the role of such factors and mechanisms in shell formation will require study of calcite growth in the presence and absence of soluble and gelling fractions of oyster shell protein under conditions of static fluids pulsed at different levels of Ω. In addition to further work with fracture surfaces of folia, observations of crystallization on native surfaces of the leading edge where shell formation is initiated will be helpful.

Acknowledgments

This work was supported by grants EHR-9108761 from the National Science Foundation, C-3662 from the Research Corporation, and R/MX 6 from the South Carolina Sea Grant Consortium. We thank JoAn S. Hudson, Director of the EM Facility at Clemson, for her assistance with SEM.

Literature Cited

Addadi, L., and S. Weiner. 1985. Interactions between acidic proteins and crystals: stereochemical requirements in biomineralization. *Proc. Natl. Acad. Sci. USA* **82:** 4110

Addadi, L., J. Moradian, E. Shay, N. G. Maroudas, and S. Weiner. 1987. A chemical model for the cooperation of sulfates and carboxylates in calcite crystal nucleation. Relevance to biomineralization. *Proc. Natl. Acad. Sci. USA* **84:** 2732–2736.

Aizenberg, J., G. Lambert, L. Addadi, and S. Weiner. 1996. Stabilization of amorphous calcium carbonate by specialized macromolecules in biological and synthetic precipitates. *Adv. Mater.* **8:** 222–226.

Albeck, S., S. Weiner, and L. Addadi. 1996. Polysaccharides of intracrystalline glycoproteins modulate calcite crystal growth *in vitro*. *Chem. Eur. J.* **2:** 278–284.

Beniash, E., J. Aizenberg, L. Addadi, and S. Weiner. 1997. Amorphous calcium carbonate transforms into calcite during sea urchin larval spicule growth. *Proc. R. Soc. Lond. B* **264:** 461–465.

Berman, A., L. Addadi, and S. Weiner. 1988. Interactions of sea-urchin skeleton macromolecules with growing calcite crystals—a study of intracrystalline proteins. *Nature* **331:** 546–548.

Bevelander, G., and H. Nakahara. 1980. Compartment and envelope formation in the process of biological mineralization. Pp. 19–27 in *The Mechanisms of Biomineralization in Animals and Plants*, M. Omori and N. Watabe, eds. Tokai University Press, Tokyo.

Boynton, R. S. 1980. *Chemistry and Technology of Lime and Limestone.* J. Wiley, New York.

Calvert, P., and R. Crockett. 1997. Chemical solid free-form fabrication: making shapes without molds. *Chem. Mater.* **9:** 650–663.

Carriker, M. R. 1996. The shell and ligament. Pp. 75–168 in *The Eastern Oyster*, V. S. Kennedy, R. I. E. Newell, and A. F. Eble, eds. Maryland Sea Grant College Publication, College Park.

Carriker, M. R., and R. E. Palmer. 1979. Ultrastructural morphogenesis of prodissoconch and early dissoconch valves of the oyster *Crassostrea virginica*. *Proc. Natl. Shellfish. Assoc.* **69:** 103–128.

Carriker, M. R., R. E. Palmer, and R. S. Prezant. 1980. Functional ultramorphology of the dissoconch valves of the oyster *Crassostrea virginica*. *Proc. Natl. Shellfish. Assoc.* **70:** 139–183.

Crenshaw, M. A. 1972. The inorganic composition of molluscan extrapallial fluid. *Biol. Bull.* **143:** 506–512.

Crenshaw, M. A. 1990. Biomineralization mechanisms. Pp. 1–9 in *Skeletal Biomineralization: Patterns, Processes, and Evolutionary Trends. Volume I*, J. G. Carter, ed. Van Nostrand Reinhold, New York.

Dean, J. A. 1992. *Lange's Handbook of Chemistry.* McGraw-Hill, New York.

Degens, E. T. 1976. *Molecular Mechanisms on Carbonate, Phosphate, and Silica Deposition in the Living Cell.* Springer, Berlin.

Didymus, J. M., P. Oliver, S. Mann, A. L. DeVries, P. V. Hauschka, and P. Westbroek. 1993. Influence of low-molecular weight and macromolecular organic additives on the morphology of calcium carbonate. *J. Chem. Soc. Faraday Trans.* **89:** 2891–2900.

Dillaman, R. M., and S. E. Ford. 1982. Measurement of calcium carbonate deposition in molluscs by controlled etching of radioactively labeled shells. *Mar. Biol.* **66:** 133–143.

Erben, H. K., and N. Watabe. 1974. Crystal formation and growth in bivalve nacre. *Nature* **248:** 128–130.

Falini, G., S. Albeck, S. Weiner, and L. Addadi. 1996. Control of aragonite or calcite polymorphism by mollusk shell macromolecules. *Science* **271:** 67–69.

Fincham, A. G., J. Moradian-Oldak, J. P. Simmer, P. Sarte, E. C. Lau, T. Diekwisch, and H. C. Slavkin. 1994. Self-assembly of a recombinant amelogenin protein generates supramolecular structures. *J. Struct. Biol.* **112:** 103–109.

Fincham, A. G., J. Moradian-Oldak, and H. C. Slavkin. 1995. Evidence for amelogenin "nanospheres" as functional components of secretory-stage enamel matrix. *J. Struct. Biol.* **115:** 50–59.

Fincham, A. G., J. Moradian-Oldak, and J. P. Simmer. 1999. The structural biology of the developing dental enamel matrix. *J. Struct. Biol.* **126:** 270–299.

Galtsoff, P. S. 1964. The American oyster *Crassostrea virginica* Gmelin. *Fish. Bull.* **64:** 1–480.

Giles, R., S. Manne, S. Mann, D. E. Morse, G. D. Stucky, and P. K. Hansma. 1995. Inorganic overgrowth of aragonite on molluscan nacre examined by atomic force microscopy. *Biol. Bull.* **188:** 8–15.

Gower, L. A., and D. A. Tirrell. 1998. Calcium carbonate films and helices grown in solutions of poly(aspartate). *J. Cryst. Growth* **191:** 153–160.

Heuer, A. H., D. J. Fink, V. J. Laraia, J. L. Arias, P. D. Calvert, K. Kendall, G. L. Messing, P. C. Rieke, D. H. Thompson, A. P. Wheeler, A. Veis, and A. I. Caplan. 1992. Innovative materials processing strategies: a biomimetic approach. *Science* **255:** 1098–1105.

Low, K. C. 1990. Adsorption of oyster shell matrix and its peptide analogs onto calcium carbonate: mechanisms of inhibition of crystal growth. Thesis, University of South Alabama, Mobile. 75 pp.

Lowenstam, H. A., and S. Weiner. 1989. *On Biomineralization.* Oxford University Press, New York.

Mann, S., ed. 1996. *Biomimetic Approaches in Materials Science*, VCH Publishers, New York.

Mann, S., J. M. Didymus, N. P. Sanderson, B. R. Heywood, and E. J. A. Samper. 1990. Morphological influence of functionalized and non-functionalized α, Ω-dicarboxylates on calcite crystallization. *J. Chem. Soc. Faraday Trans.* **86:** 1873–1880.

Marsh, M. E. 1986. Biomineralization in the presence of calcium-binding phosphoprotein particles. *J. Exp. Zool.* **239:** 207–220.

Marsh, M. E. 1989a. Self-association of calcium and magnesium complexes of dentin phosphophoryn. *Biochemistry* **28:** 339–345.

Marsh, M. E. 1989b. Binding of calcium and phosphate ions to dentin phosphophoryn. *Biochemistry* **28:** 346–352.

Marsh, M. E. 1994. Polyanions and biomineralization. *Bull. Inst. Oceanogr. (Monaco)* **14(1):** 121–128.

Marsh, M. E., and R. L. Sass. 1983. Calcium-binding phosphoprotein particles in the extrapallial fluid and innermost shell lamella of clams. *J. Exp. Zool.* **226:** 193–203.

Marsh, M. E., and R. L. Sass. 1984. Phosphoprotein particles: calcium and inorganic phosphate binding structures. *Biochemistry* **23:** 1448–1456.

Marsh, M. E., and R. L. Sass. 1985. Distribution and characterization of mineral-binding phosphoprotein particles in bivalvia. *J. Exp. Zool.* **234:** 237–242.

Misogianes, M., and N. D. Chasteen. 1979. A chemical and spectral characterization of the extrapallial fluid of *Mytilus edulis*. *Anal. Biochem.* **100:** 324–334.

Nair, P. S., and W. E. Robinson. 1998. Calcium speciation and exchange between blood and extrapallial fluid of the quahog *Mercenaria mercenaria* (L.). *Biol. Bull.* **195:** 43–51.

Okazaki, K., and S. Inoué. 1976. Crystal property of the larval sea urchin spicule. *Dev. Growth Differ.* **18:** 413–434.

Okazaki, K., R. M. Dillaman, and K. M. Wilbur. 1981. Crystalline axes of the spine and test of the sea urchin *Strongylocentrotus purpuratus*: determination by crystal etching and decoration. *Biol. Bull.* **161:** 402–415.

Paine, R. T. 1964. Ash and calorie determinations of sponge and opisthobranch tissues. *Ecology* **45:** 384–387.

Price, T. J., G. W. Thayer, M. W. LaCroix, and G. P. Montgomery. 1976. The organic content of shells and soft tissues of selected estuarine gastropods and pelecypods. *Proc. Natl. Shellfish. Assoc.* **65:** 26–31.

Runnegar, B. 1984. Crystallography of the foliated calcite shell layers of bivalve molluscs. *Alcheringa* **8:** 273–290.

Sarikaya, M., J. Liu, and I. A. Aksay. 1995. Nacre: properties, crystallography, and formation. Pp. 35–90 in *Biomimetics: Design and Processing of Materials*, M. Sarikaya and I. A. Aksay, eds. American Institute of Physics, New York.

Sikes, C. S., and A. P. Wheeler. 1986. The organic matrix from oyster shell as a regulator of calcification *in vivo*. *Biol. Bull.* **170:** 494–505.

Sikes, C. S., and A. Wierzbicki. 1995. Mechanisms of regulation of crystal growth in selected biological systems. Pp. 183–206 in *Mineral Scale Formation and Inhibition*, Z. Amjad, ed. Plenum Press, New York.

Sikes, C. S., and A. Wierzbicki. 1996. Polyamino acids as antiscalants, dispersants, antifreezes, and absorbent gelling materials. Pp. 249–278 in *Biomimetic Approaches in Materials Science*, S. Mann, ed. VCH Publishers, New York.

Sikes, C. S., A. P. Wheeler, A. Wierzbicki, R. M. Dillaman, and L. De Luca. 1998. Oyster shell protein and atomic force microscopy of oyster shell folia. *Biol. Bull* **194:** 304–316.

Simkiss, K. 1994. Amorphous minerals in biology. *Bull. Inst. Oceanogr. (Monaco)* **14(1):** 49–54.

Simkiss, K., and K. M. Wilbur. 1989. *Biomineralization.* Academic Press, San Diego, CA.

Stupp, S. I., and P. V. Braun. 1997. Molecular manipulation of microstructures: biomaterials, ceramics, and semiconductors. *Science* **277:** 1242–1248.

Taylor, J. D., W. J. Kennedy, and A. Hall. 1969. The shell structure and mineralogy of the bivalvia. Introduction. Nuculacea-Trigonacea. *Bull. Br. Mus. (Nat. Hist.) Zool., Supplement* **3:** 1–125, plates 1–29.

Tsujii, T., G. D. Sharp, and K. M. Wilbur. 1958. Studies on shell formation. VII. The submicroscopic structure of the oyster *Crassostrea virginica*. *J. Biophys. Biochem. Cytol.* **4:** 275–279.

Wada, K. 1963. Studies on the mineralization of the calcified tissue in molluscs. VI. Crystal structure of the calcite grown on the inner surface of calcitostracum. *J. Electron Microsc.* **12:** 224–227.

Wada, K. 1968. Spiral growth of calcitostracum. *Nature* **219:** 62.

Wada, K. 1990. Initiation of mineralization in bivalve molluscs. Pp. 79–92 in *The Mechanisms of Biomineralization in Animals and Plants*, M. Omori and N. Watabe, eds. Tokai University Press, Tokyo.

Wada, K. and T. Fujinuki. 1976. Biomineralization in bivalve molluscs with emphasis on the chemical composition of the extrapallial fluid. Pp. 175–190 in *The Mechanisms of Mineralization in the Invertebrates and Plants*, N. Watabe and K. M. Wilbur, eds. University of South Carolina Press, Columbia.

Watabe, N. 1965. Studies on shell formation. XI. Crystal-matrix relationships in the inner layers of mollusk shells. *J. Ultrastruct. Res.* **12:** 351–370.

Watabe, N. 1974. Crystal growth of calcium carbonate in biological systems. *J. Cryst. Growth* **24/25:** 116–122.

Watabe, N. 1981. Crystal growth of calcium carbonate in the invertebrates. *Prog. Cryst. Growth Charact.* **4:** 99–147.

Watabe, N., and K. M. Wilbur. 1961. Studies on shell formation. IX. An electron microscope study of crystal layer formation in the oyster. *J. Biophys. Biochem. Cytol.* **9:** 761–771.

Watabe, N., D. G. Sharp, and K. M. Wilbur. 1958. Studies on shell formation. VIII. Electron microscopy of crystal growth of the nacreous layer of the oyster *Crassostrea virginica*. *J. Biophys. Biochem. Cytol.* **4:** 281–284, plates 152–156.

Weiner, S., and L. Addadi. 1997. Design strategies in mineralized biological materials. *J. Mater. Chem.* **7:** 689–702.

Wen, H. B., J. Moradian-Oldak, W. Leung, P. Bringas Jr., and A. G. Fincham. 1999. Microstructures of an amelogenin gel matrix. *J. Struct. Biol.* **126:** 42–51.

Wheeler, A. P., and L. P. Koskan. 1993. Large scale thermally synthesized polyaspartate as a biodegradable substitute in polymer applications. *Mater. Res. Soc. Symp. Proc.* **292:** 277–283.

Wheeler, A. P., and C. S. Sikes. 1989. Matrix-crystal interactions in $CaCO_3$ biomineralization. Pp. 95–133 in *Biomineralization: Chemical and Biochemical Perspectives*, S. Mann, J. Webb, and R. J. P. Williams, eds. VCH Publishers, Weinheim, Germany.

Wheeler, A. P., and K. M. Wilbur. 1977. Shell growth in the scallop

Argopecten irradians (Say). II. Processes of shell growth. *J. Molluscan Stud.* **43:** 155–16

Wheeler, A. P., P. L. Blackwelder, and K. M. Wilbur. 1975. Shell growth in the scallop *Argopecten irradians.* I. Isotope incorporation with reference to diurnal growth. *Biol. Bull.* **148:** 472–482.

Wheeler, A. P., K. W. Rusenko, D. M. Swift, and C. S. Sikes. 1988. Regulation of $CaCO_3$ formation by fractions of oyster shell matrix. *Mar. Biol.* **98:** 71–80.

Wheeler, A. P., K. C. Low, and C. S. Sikes. 1991. $CaCO_3$ crystal-binding properties of peptides and their influence on crystal growth. Pp. 72–84 in *Surface Reactive Peptides and Polymers: Discovery and Commercialization,* Symposium Series 444. C. S. Sikes and A. P. Wheeler, eds. ACS Books, Washington, DC.

Wierzbicki, A., C. S. Sikes, B. Drake, and J. Madura. 1994. Atomic force microscopy and molecular modeling of protein and peptide binding to calcite. *Calcif. Tissue Int.* **54:** 133–141.

Wilbur, K. M., and A. M. Bernhardt. 1984. Effects of amino acids, magnesium, and molluscan extrapallial fluid on crystallization of calcium carbonate: *in vitro* experiments. *Biol. Bull.* **166:** 251–259.

Wilbur, K. M., and L. H. Jodrey. 1952. Studies on shell formation. I. Measurement of the rate of shell formation using Ca^{45}. *Biol. Bull.* **103:** 269–276.

Reference: *Biol. Bull.* **198:** 67–76. (February 2000)

The Apical Sensory Organ of a Gastropod Veliger Is a Receptor for Settlement Cues

MICHAEL G. HADFIELD[1,2]*, ELLA A. MELESHKEVITCH[1], AND DMITRI Y. BOUDKO[1]

[1] *Kewalo Marine Laboratory, University of Hawaii, 41 Ahui Street, Honolulu, Hawaii 96813; and*
[2] *Department of Zoology, University of Hawaii at Manoa, Honolulu, Hawaii 96822*

Abstract. On the basis of anatomy and larval behavior, the apical sensory organ (ASO) of gastropod veliger larvae has been implicated as the site of perception of cues for settlement and metamorphosis. Until now, there have been no experimental data to support this hypothesis. In this study, cells in the ASO of veliger larvae of the tropical nudibranch *Phestilla sibogae* were stained with the styryl vital dye DASPEI and then irradiated with a narrow excitatory light beam on a fluorescence microscope. When its ASO cells were bleached by irradiation for 20 min or longer, an otherwise healthy larva was no longer able to respond to the usual metamorphic cue, a soluble metabolite from a coral prey of the adult nudibranch. The irradiated cells absorbed the dye acridine orange, suggesting that they were dying. When larvae not stained with DASPEI were similarly irradiated, or when stained larvae were irradiated with the light beam focused on other parts of the body, there was no loss of ability to metamorphose. Together these data provide strong support for the hypothesis. Potassium and cesium ions, known to induce metamorphosis in larvae of many marine-invertebrate phyla, continue to induce metamorphosis in larvae that have lost the ability to respond to the coral inducer due to staining and irradiation. These results demonstrate that (1) the ASO-ablated larvae have not lost the ability to metamorphose and (2) the ions do not act only on the metamorphic-signal receptor cells, but at other sites downstream in the metamorphic signal transduction pathway.

Introduction

Abundant data demonstrate that most invertebrate larvae succeed in locating appropriate habitats for settlement, metamorphosis, and growth by responding to site-specific chemical cues associated with conspecific individuals, requisite prey, microbial films, or algal or other benthic substrata (Crisp, 1974, 1984; Pawlik, 1992; Hadfield, 1998). Much current research on the subject of larval settlement focuses on the chemical identity of settlement cues and the signal-transduction mechanisms by which external cues stimulate morphogenetic transformations in the larva (*e.g.*, see papers in *Biofouling* 12(1), 1998). Despite more than 50 years of research on metamorphic induction in marine-invertebrate larvae, experimental definition of the exact location on the larval body where these interactions take place—that is, where the chemoreception that results in site-specific larval settlement occurs—is lacking for most groups. The anterior pole of at least some cnidarian planulae includes a region that must contact stimulatory surfaces for metamorphosis to occur (Müller *et al.*, 1977; Freeman and Ridgway, 1987), and there is good evidence that the antennules of barnacle cyprid larvae are the location of receptors for settlement inducers (summarized by Clare, 1995). However, the site of induction has eluded strong inference for the trochophores and trochophore-derived larvae of large marine-invertebrate clades.

Larvae of many phyla behave prior to settlement in a manner that indicates that they are "testing" or "sampling" substrata. For larvae of groups as diverse as phoronids, polychaetes, and chitons, all of which possess an apical tuft of elongate and somewhat stiff cilia, presettlement behavior typically includes swimming near the substratum with their apical ends downward so that the apical tuft brushes or is pressed against the substratum (Barnes and Gonor, 1973; Nott, 1973; Zimmer, 1991; unpublished personal observations on the serpulid polychaete *Hydroides elegans*). Thus the apical tuft, together with its underlying cells, has long been suspected to be the site of detection of substrate-associated cues for settlement. As others have, we refer to

Received 1 July 1999; accepted 3 November 1999.

* To whom correspondence should be addressed. E-mail: hadfield@hawaii.edu

the apical tuft and its associated cells as the apical sensory organ, henceforth abbreviated ASO.

Larvae of opisthobranch gastropods bear a probable sensory structure, derived developmentally and evolutionarily from the ASO of trochophore larvae (Bonar, 1978). Recent papers by Kempf *et al.* (1997) and Marois and Carew (1997) provide elegant details concerning the cellular composition of the ASOs of opisthobranch larvae. This ASO of opisthobranch larvae consists of a set of cilia-bearing receptor cells, some of which send axons directly into the cerebral commissure of the brain; neurons from other ASO cells innervate the velum. Bonar (1978) noted how well situated the structure is, in veliger larvae of the nudibranch *Phestilla sibogae* Bergh 1905, to detect the water-borne chemical cue that arises from the nudibranch's coral prey and induces metamorphosis. An ASO has been demonstrated in prosobranch larvae as well (Uthe, 1995), where Leise (1996) reported that it can be stained with DASPEI, a styryl fluorescent dye.

The only previous experimental data supporting the hypothesis that the ASO is the site of cell-surface receptors for inducers of metamorphosis in invertebrate larvae were provided by Baxter and Morse (1992) for larvae of the gastropod *Haliotis rufescens*. Their experiments revealed that receptors for lysine, a compound known to modify the effects of a metamorphic inducer for which GABA is a receptor agonist, lie on cilia harvested from the larvae of *H. rufescens;* among these cilia were those from the apical tuft. Larvae of the nudibranch *Onchidoris bilamellata* were reported to detect a water-borne cue from the barnacle prey of the adult nudibranch *via* a pair of lateral propodial "ganglia"; however, the barnacle factor induces only reversible settlement behavior, but not metamorphosis, which is dependent on a surface-bound cue (Arkett *et al.*, 1989).

Because all authors who have described details of ASOs in gastropod larvae have argued for a probable role for this organ in induction of settlement and metamorphosis, it is timely to perform robust experimental tests of the hypothesis. In the research presented here, the vital dye DASPEI, known to vitally stain mitochondria (Haugland, 1996) and thus mitochondria-rich sensory cells (Bereiter-Hahn, 1976; Nurse and Faraway, 1989; Balak *et al.*, 1990; Leise, 1996; Boudko *et al.*, 1999), was employed to vitally stain the ASO in veliger larvae of *Phestilla sibogae*, followed by photoablation of the stained organ by fluorescent excitation. Balak *et al.* (1990) reported that labeling lateral-line hair cells of amphibians with DASPEI and exposing them to epifluorscent illumination at 450–490 nm resulted in cell death due to phototoxic conditions arising from photoexcitation of DASPEI.

We attempted to obtain additional evidence of cell death in the ASO by applying the vital dye acridine orange to treated larvae. Acridine orange, long used as a fluorchrome indicator of cell death, becomes intercalated into uncoiled DNA of dying cells when applied at relatively low (*i.e.*, *ca.* 10^{-6} *M*) concentrations (Delic *et al.*, 1991). Although acridine orange can stain RNA, as well as DNA, the red-orange (~650 nm) emission color of the RNA–acridine-orange complex distinguishes it from DNA–acridine-orange emission, which is green (525 nm) (Haugland, 1996). Although some experimentalists have reported acridine-orange staining to be specific to cells undergoing apoptosis (*e.g.*, Abrams *et al.*, 1993), others report similarity of staining between different forms of induced cell death, at least in later stages (reviewed by Darzynkiewicz and Traganos, 1998).

Among the major tools used to study metamorphosis in marine invertebrates has been a growing list of so-called artificial inducers (reviewed by Crisp, 1974, 1984; Pawlik, 1992; Hadfield, 1998). The most useful of these are the cations potassium and cesium, which induce metamorphosis in larvae from seven phyla in the absence of other stimuli (summarized by Herrmann, 1995; Woollacott and Hadfield, 1996). While noting that the entire larval bodies are bathed in elevated potassium or cesium when larvae are treated with these ions, some authors have proposed that K^+ or Cs^+ act by depolarizing the sensory cells that typically bind the natural inducer and thus initiate spikes in neurons extending from those cells (*e.g.*, Baloun and Morse, 1984; Yool *et al.*, 1986; Leitz and Klingmann, 1990; Herrmann, 1995; Woollacott and Hadfield, 1996; Carpizo-Ituarte and Hadfield, 1998). The possibility that K^+ or Cs^+ acts on the entire nervous system (Todd *et al.*, 1991), directly on target tissues (Yool *et al.*, 1986), or at intermediate sites downstream from primary receptors (Jensen *et al.*, 1990; Pechenik *et al.*, 1995) has also been noted. Experimental evidence delineating the site of potassium activity has been difficult to obtain. In the research reported here, we exposed larvae whose ASOs had been photoablated to elevated potassium levels or to cesium in seawater to determine if the larvae could still be induced to metamorphose by these ions.

Phestilla sibogae is an appropriate model organism for studies of the sensory pathway involved in metamorphic induction, because its developmental biology, with special emphasis on induction and activation of metamorphosis, is so well known (*e.g.*, Hadfield, 1978; Hadfield and Pennington, 1990; Miller and Hadfield, 1990; Pires and Hadfield, 1993). In the research reported here, we provide the first experimental evidence that the ASO is the site of reception of external cues to settlement and metamorphosis in larvae of *P. sibogae*, and, by inference, probably in many other larvae that bear prominent apical tufts of cilia.

Materials and Methods

Larval culture. Populations of the tropical Indo-Pacific nudibranch *Phestilla sibogae* are continuously maintained in the authors' laboratory at the Kewalo Marine Laboratory, Honolulu, Hawaii. Adult animals are kept in shallow trays supplied with constantly flowing, unfiltered seawater and with their coral prey, *Porites compressa* Dana 1846, which is collected from the field biweekly. These animals reproduce continuously, each adult laying one to two egg masses per day, and each egg mass containing 2000 to 4000 fertilized eggs. Larvae develop to normal hatching in 6 to 8 days, varying with ambient temperature (annual range = 23°–27°C). After hatching, larvae are maintained in aerated filtered seawater (FSW) containing the antibiotics streptomycin (500 mg/l) and penicillin (50 mg/l) until they have developed the capacity to undergo metamorphosis (*i.e.*, are competent) when appropriately stimulated, typically about 9 days postfertilization (Miller and Hadfield, 1986). In the experiments described here, larvae were used in experiments when 10 or 11 days old.

Labeling ASO cells with DASPEI. Ten- or eleven-day-old larvae of *P. sibogae* were placed in artificial seawater with pH reduced to 5.6 for 1.5 h during which their larval shells were decalcified, a process that does not otherwise injure the larvae, and then returned to natural seawater (Pennington and Hadfield, 1989; Pires and Hadfield, 1993). Because shell-less larvae cannot retract, they cannot conceal the ASO from the irradiation treatment described below. Cells in the ASO were labeled by bathing up to 200 larvae in 50 ml of 0.5 m*M* DASPEI (absorption maximum 461 nm; Molecular Probes Inc., Eugene, OR) in FSW for 30 min, and then rinsing them in 100 ml of FSW for one hour.

Immobilization of larvae. Labeled larvae were immobilized by embedding them in a thin (2–4 mm) layer of 1% low-melting-point agarose (Type VII, Sigma Chemical Co.) in FSW across the bottom of a 10 × 35 mm plastic petri dish (Falcon). The agarose gels at 25°–28°C, which is within the normal range of sea temperature in Hawaii. Survival of larvae in this treatment was usually 100%. To protect the agarose gel from drying, 2 ml of FSW was layered on top of it in each petri dish.

Irradiation of labeled cells. A Zeiss inverted microscope equipped with a mercury light source and fluorescence filters was used to visualize the larvae, selectively irradiate DASPEI-labeled cells in them, and capture photographic images. A small anterior patch of the larval epithelium that included the labeled ASO cells was located with white light and a 40× objective. This area was then exposed to a narrow light beam (20 ± 2 μm) from a mercury source passed through a Zeiss fluorescein filter cube (excitation range 450–490 nm) for 1, 5, 10, 15, or 20 min. After treatment, the larvae were carefully cut free from the agarose, whereupon they resumed swimming in FSW.

Induction of metamorphosis in treated and untreated larvae. After being freed from the agarose, treated larvae were placed in petri dishes containing 5 ml of FSW that had been exposed to the coral *Porites compressa* for 12 h and filtered prior to use. Seawater conditioned with this coral prey of adult *P. sibogae* typically induces settlement and metamorphosis in 90%–100% of competent larvae in 24 h or less (*e.g.*, Pires *et al.*, 1997). The percentage of larvae that had metamorphosed was determined after 24 h; metamorphosis in *P. sibogae* is dramatic and easy to discern (Hadfield, 1978). Each treatment was replicated three times with 15 larvae per replicate. Controls to determine that larvae were metamorphically competent and that they did not metamorphose spontaneously were used in larger numbers (25–50), because it was not necessary to embed these larvae in agarose to make these determinations. The major methods used in the experiments described above are outlined in Figure 1; obvious non-imbedded controls (see below) are not included.

To test whether larvae could be induced to metamorphose with potassium or cesium after the photoinactivation treatment described above, in a separate experiment, treated larvae were released from agarose, allowed to swim in FSW for an hour or more, and then placed in FSW containing either 20 m*M* added potassium or 20 m*M* cesium. Because the maximal metamorphic response to K^+ typically takes about 48 h (Pechenik *et al.*, 1995), these experiments were run for 2 days, and the number that had metamorphosed was determined at 24 and 48 h. Larvae were exposed to cesium seawater for 20 min, returned to FSW, and examined to determine the percentage that metamorphosed after 24 h. Each of three replicates for each variable contained 15 larvae.

Controls. Untreated sibling larvae from the stock culture were employed to determine that larvae were competent to metamorphose when exposed to the coral-conditioned FSW and that larvae did not metamorphose spontaneously without exposure to coral water or other inducers. Larvae were neither decalcified nor embedded in agarose for these controls. Only batches of larvae that yielded 90%–100% metamorphosis within 24 h of exposure to coral water were used in the experiments. To test that the treatment effects (*i.e.*, DASPEI staining plus irradiation of the stained ASO) were those responsible for observed results: (1) larvae were stained with DASPEI but not exposed to 450–490 nm light; (2) unstained larvae were exposed to irradiation focused on the ASO for 20 min; and (3) stained larvae were exposed to irradiation focused on regions of the larvae body other than the ASO. In all of these controls, the larvae were subjected to the same treatments as the experimental larvae, including having their larval shells decalcified and being embedded in low-melting-point agarose.

Acridine orange staining to detect cell death. Untreated control larvae (also decalcified and embedded in agarose) and larvae that had been stained with DASPEI and exposed to radiation focused on the ASO were placed in a seawater solution of acridine orange (2.7×10^{-6} *M*) for 20 min. After exposure to acridine orange, the larvae were examined and photographed on a Zeiss fluorescence microscope

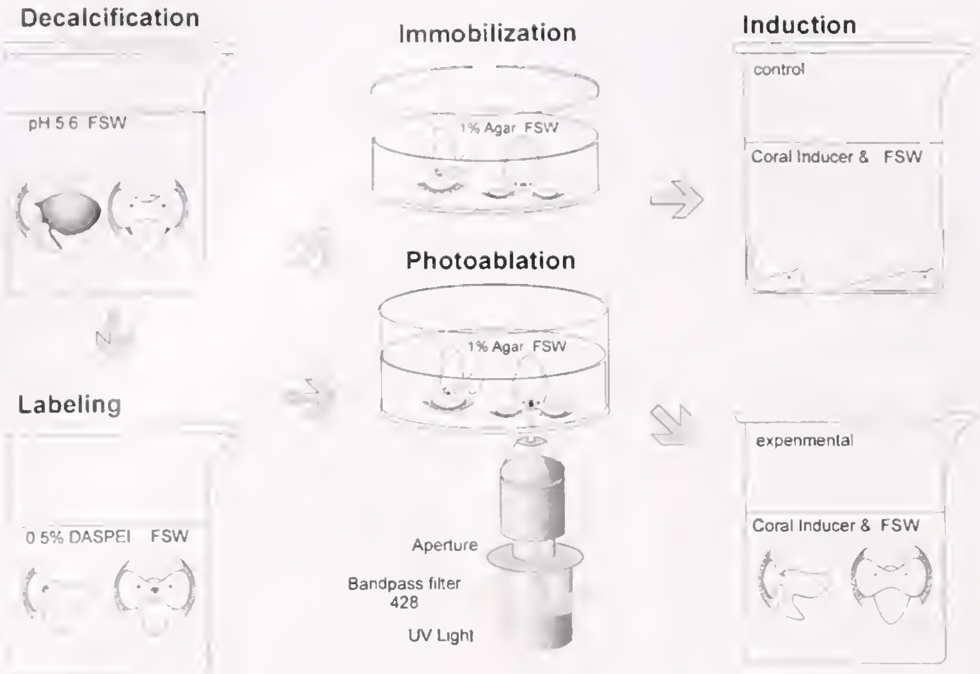

Figure 1. Diagram representing the methods used in photoablation of cells in the apical sensory organ of veliger larvae of *Phestilla sibogae*. Larval shells are decalcified without harm to the larvae, and then the larvae are exposed to DASPEI. Once immobilized in low-melting-point agarose, the larvae are put on the stage of an inverted fluorescence microscope and a 20-μm band of 450–490 nm light is focused on stained cells in the apical sensory organ. The larvae are then freed from agarose and, when swimming, exposed to the metamorphosis-inducing coral extract. Control treatments of unstained larvae are not illustrated.

equipped with filters that include the 436-nm excitation peak for acridine orange. The goal of this experiment was to determine if ASO cells in larvae that had been treated would take up acridine orange while those of untreated larvae would not. Uptake of acridine orange only by treated cells would provide some evidence for cell death, thus photoablation, of those cells.

Data were analyzed with Sigma Plot software, version 5.0 (Jandel Scientific Software Inc.). In instances where there were questions about differences between experimental response variables and controls, the proportional data were subjected to arc-sine transformation and the means compared with 2-sample t tests.

Results

Many but not all larvae that were exposed to DASPEI for 30 min and allowed to wash for one h in FSW displayed specific anterior staining in the ASO (Fig. 2). The locations and numbers (typically 5–6) of stained cells are consistent with their identity as components of the ASO. Unstained larvae displayed no autofluorescence in the ASO. The large prototrochal cells of the vela stained lightly with DASPEI, and various structures in the visceral hump, exposed by decalcification of the larval shell, also absorbed DASPEI, but these regions were easily excluded from the irradiated area. DASPEI was retained by larvae in FSW for periods in excess of one week, even through metamorphosis.

Larvae that had been stained with DASPEI, embedded in low-melting-point agarose, and irradiated with a narrow band of 450–490 nm light focused on the ASO survived well (>90%). When released from agarose and exposed to coral seawater, the typical metamorphic inducer, these larvae metamorphosed in percentages inversely proportional to the duration of irradiation (Fig. 3). The excitatory illumination resulted in photobleaching of the ASO cells; that is, they became colorless. DASPEI-stained cells in non-illuminated parts of the larvae continued to show brilliant fluorescence (Fig. 5A). Very few larvae that had been exposed for as long as 20 min were capable of metamorphosing in response to natural inducer. Excitatory illumination alone did not reduce the ability of larvae to metamorphose in response to coral inducer (Fig. 3, differences in responses in the control labeled P20-CI were not significantly different [$P > .190$] from those in the control labeled CI). DASPEI-stained larvae exposed to the irradiation beam focused on the larval foot instead of on the ASO retained full competence to metamorphose when exposed to the coral inducer (Fig. 4). There were no DASPEI-stained cells in the region

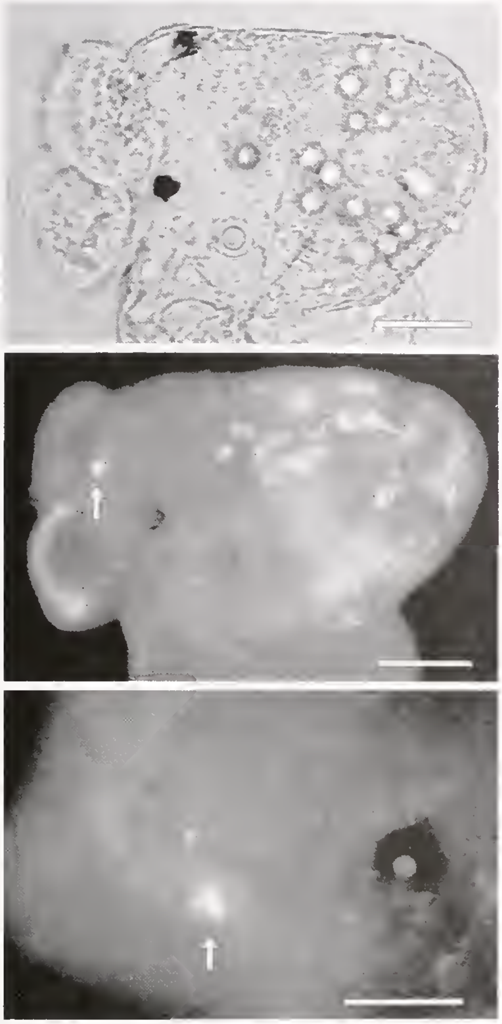

Figure 2. Veliger larvae of *Phestilla sibogae* stained with DASPEI. (top) Bright-field image. (middle) Same specimen photographed with fluorescent light. (bottom) Enlargement of anterior region of the same specimen showing DASPEI staining in 5–6 cells of the apical sensory organ. Scale bars, top and middle = 50 μm, bottom = 25 μm.

irradiated. We conclude that exposure of the stained ASO to intense excitatory irradiation for 20 min resulted in photoablation of the ASO cells, and that subsequent loss of the ability of these larvae to respond to the metamorphic inducer contained in coral seawater is evidence that the irradiated cells were the site of receptors for the inducer. These larvae were otherwise unharmed. They continued to swim normally in FSW, and they had not lost the capacity to metamorphose in response to artificial inducers (see below). The yellow DASPEI fluorescence disappeared from the ASO following excitatory illumination, although it persisted in other regions of the larval body.

When larvae whose ASO cells had been stained with DASPEI and exposed for 20 min to fluorescent irradiation and thus photobleached were placed in a seawater solution of acridine orange, the ASO cells uniquely absorbed the dye and emitted a green fluorescence (Fig. 5). Comparable staining in other cells and organisms has been found specific to induced cell death (Delic *et al.*, 1991; Abrams *et al.*, 1993). ASO cells of untreated larvae did not take up acridine orange. These observations support the conclusion that DASPEI staining followed by fluorescent irradiation of the ASO cells led to their ablation.

When larvae that had undergone the photoablation treatment described above were exposed to seawater containing 20 m*M* cesium ion for 20 min and then transferred to FSW, they underwent normal metamorphosis in large numbers within 24 h (Fig. 6). Similarly treated larvae exposed to seawater containing 20 m*M* excess potassium also metamorphosed in numbers much greater than controls, reaching more than 50% after 48 h (Fig. 6). The latency of the metamorphic response of larvae of *Phestilla sibogae* to potassium ion has been reported previously (Pechenik *et al.*, 1995). Control exposures of treated larvae to coral inducer demonstrated that they were, as in the experiments described above, unresponsive. Low percentages of larvae that metamorphosed after photoablation without inducer (Fig. 6, C-2) or with inducer (Fig. 6, CI in Photoablation bracket) were not significantly different from those in untreated larvae (Fig. 6, CI) (*t* tests, $P \gg 0.05$). We conclude that the site of action of K^+ and Cs^+ in inducing metamorphosis is not on the primary receptor cells, which had been destroyed in the experimental treatment. However, the possibility of multiple sites of metamorphic stimulation by these cations is not eliminated.

Discussion

The data presented here provide compelling evidence that cells in the apical sensory organ bear the receptors for the dissolved molecular inducer of settlement and metamorphosis in larvae of the gastropod *Phestilla sibogae*. Evidence presented by Wodicka and Morse (1991) and Baxter and Morse (1992) demonstrated that receptors for a related receptor pathway are found on cilia harvested from competent larvae of another gastropod, *Haliotis rufescens*. Yool (1985) had earlier demonstrated that these larvae have an apical ciliary structure that is presumably homologous to the ASO of *P. sibogae*. It remains to be demonstrated if the key pathway, that for the settlement/metamorphic inducer (for which GABA is an agonist), is also on the same cilia in larvae of *H. rufescens*. Apical sensory organs have been demonstrated in all opisthobranch larvae that have been examined appropriately (Bonar, 1978; Chia and Koss, 1984; Kempf *et al.*, 1997; Marois and Carew, 1997), as well as in two prosobranch species (Uthe, 1995; Leise, 1996). While it is logical to assume that ASOs in other gastropods have a role in metamorphic induction, experimental evidence for this sensory function has not yet been provided.

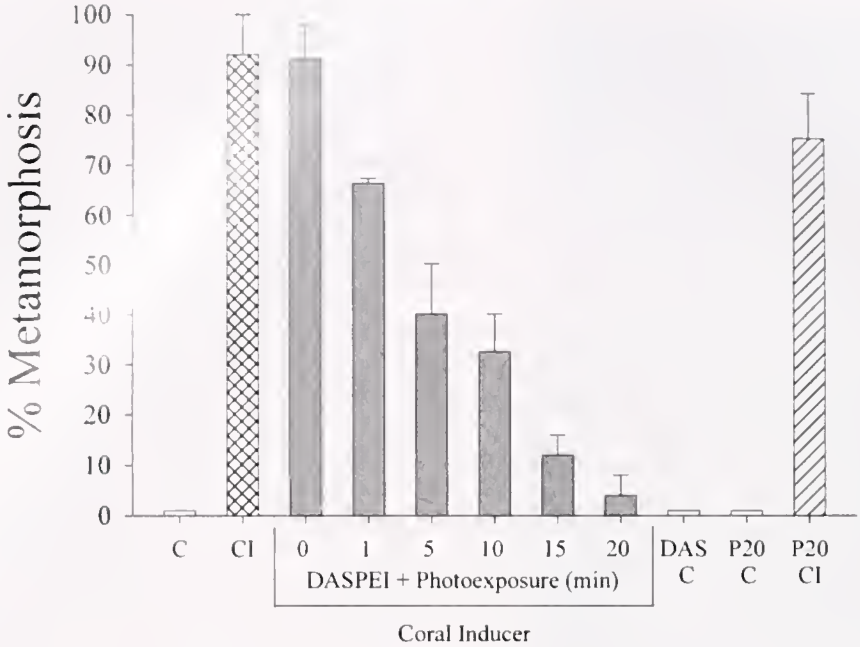

Figure 3. Percent metamorphosis in larvae of *Phestilla sibogae* that have been stained with DASPEI, exposed to fluorescent illumination focused on the stained cells in the apical sensory organ, and exposed to coral metamorphic inducer; bars = mean and SD. Experimental and control larvae embedded in agarose ($n = 3$ replicates, 15 larvae/replicate): DASPEI + Photoexposure, DASPEI-stained larvae exposed to a beam of fluorescent light focused on stained cells of the apical sensory organ for 0–20 min and then placed in coral inducer for 24 h; DAS-C, DASPEI-stained larvae that were not photo-treated nor exposed to coral inducer; P20-C, unstained larvae exposed to fluorescent light for 20 min and not placed in coral inducer; P20-CI, unstained larvae exposed to fluorescent light for 20 min and then placed in coral inducer. CI, untreated larvae exposed to coral inducer for 24 h. Controls with larvae *not* stained nor embedded in agarose ($n = 3$ replicates, 25 larvae/replicate): C, control to determine that the batch of larvae did not show high levels of spontaneous metamorphosis; CI, control to determine that the batch of larvae metamorphosed normally upon exposure to the coral inducer without other treatment. P20-CI was not significantly different from CI (t test, $P > 0.190$).

The homology of key elements of the apical sensory organ of gastropod veligers, and presumably those of other molluscan larvae (Raven, 1966, pp. 143–145), with the apical-tuft/apical-organ complex of the trochophore larvae of polychaetous annelids appears to be sound. The cell lineage for the ASO of larvae of the gastropod *Crepidula fornicata*, described by Conklin (1897), appears to be identical to that for the apical organ of polychaete trochophores; in both larval types, the apical organs arise from descendants of the first-quartet micromeres $1a^1$–$1d^1$ (summarized by Kume and Dan, 1968). Cells bearing apical-tuft cilia appear to arise from the same micromere quartet in polyclad flatworms (Selenka, 1881) and nemerteans (Hörstadius, 1937) that produce pelagic larvae. There thus appears to be great antiquity in the apical sensory organs of larvae of spiralian metazoans, although functional similarities remain to be demonstrated in most cases.

The chemical cues that trigger metamorphosis in larvae of *Phestilla sibogae*, at least some other gastropods, and a number of other invertebrate types are dissolved in seawater (nudibranchs: Thompson, 1958; Hadfield and Scheuer, 1985; Bahamondes-Rojas and Dherbonez, 1990; Lambert and Todd, 1994; prosobranchs: Scheltema, 1961; McGee and Targett, 1989; Boettcher and Targett, 1998; bivalves: Zimmer-Faust and Tamburri, 1994; sipunculans: Rice, 1986; echinoids: Burke, 1984; Pearce and Scheibling, 1990a, 1990b; ascidians: Young and Braithwaite, 1980; barnacles: Rittschof, 1985; crabs: Welch *et al.*, 1997). In contrast, many other larvae detect cues that are absorbed to, or are part of, the chemical structures of more-or-less specific surfaces. Surface-bound cues to settlement for benthic invertebrates include the algal-surface ligands to which larvae of *Haliotis rufescens* respond (Morse and Morse, 1984), barnacle-associated substances that serve as a settlement cue for the barnacle-eating nudibranch *Onchidoris fusca* (Arkett *et al.*, 1989), and bacterial-biofilm substances that stimulate settlement and metamorphosis in competent nectochaete larvae of the polychaete *Hydroides elegans* (Carpizo-Ituarte and Hadfield, 1998) and many other invertebrates. Amazingly few detailed descriptions of larval behavior prior to settlement have been published. However, at least some polychaete trochophores (Nott, 1973; unpub-

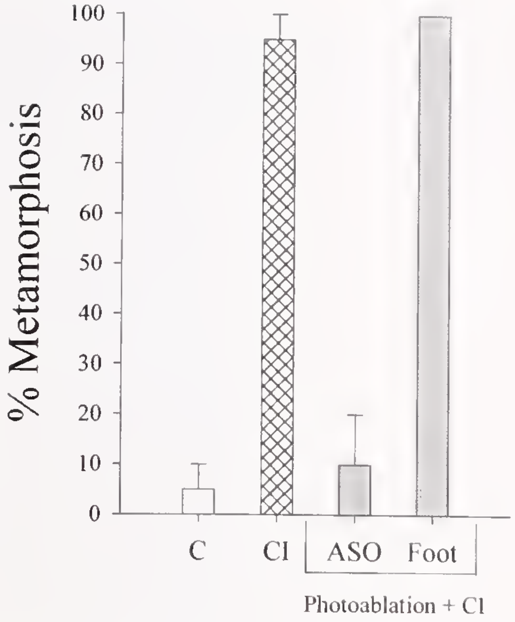

Figure 4. Percent metamorphosis in larvae of *Phestilla sibogae* that were stained with DASPEI, embedded in low-melting-point agarose, exposed for 20 min to fluorescent irradiation aimed either at the apical sensory organ (ASO) or the foot, freed from the agarose, and then placed in coral inducer for 24 h (n = 3 replicates, 15 larvae/replicate); bars = mean and SD. ASO, fluorescent light focused on the ASO; Foot, fluorescent light focused on the foot. Not embedded in agarose were larvae used in C, untreated controls; CI, untreated larvae exposed to coral inducer (n = 3 replicates, 25 larvae/replicate).

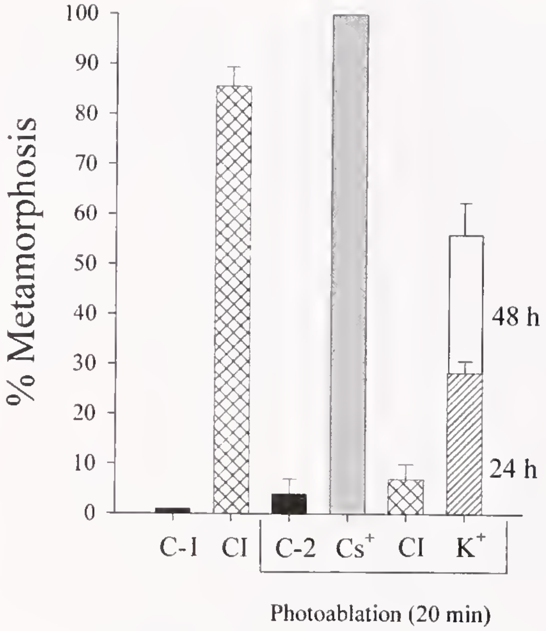

Figure 6. Percent metamorphosis in larvae of *Phestilla sibogae* that had undergone photoablation of apical-sensory-organ (ASO) cells and then exposure to the ionic inducers potassium or cesium; bars = mean and SD. Percent metamorphosis was determined after 24 h in all cases, plus at 48 h for potassium-treated larvae. Experimental treatments (larvae embedded in low-melting-point agarose for light treatment; n = 3 replicates, 15 larvae/replicate) in Photoablation (20 min) bracket, all stained with DASPEI and subjected to 20-min excitatory illumination focused on the ASO: C-2, larvae not placed in coral inducer; CI, larvae exposed to coral inducer; Cs^+, larvae exposed to 20 mM cesium chloride in seawater for 20 min; K^+, larvae continuously exposed to seawater augmented with 20 mM excess potassium chloride. Controls (not embedded in agarose): C-1, untreated larvae not exposed to coral inducer; CI, untreated larvae exposed to coral inducer for 24 h (n = 3 replicates, 25 larvae/replicate). Neither C-2 nor CI with photoablation treatment were significantly different from the untreated-larvae control C-1 (t tests, $P \gg 0.05$).

lished personal observations on larvae of *Hydroides elegans*), larvae of a chiton (Barnes and Gonor, 1973), and veligers of the abalone *Haliotis rufescens* (Wodicka and Morse, 1991) apparently detect absorbed settlement cues by brushing the surfaces of substrata with their apical ciliary tufts during a period before settlement and attachment. We presume that during what has been interpreted as pre-attachment "searching behavior," the larvae apply chemically sensitive cilia to potential settlement sites in a manner that will bring together stimulatory ligands and their specific receptors and initiate neurological signaling for settlement and metamorphosis. Because cilia protrude very little, if at all, from the sensory cells in the apical sensory organ of veligers of *P. sibogae*, they would be of little use in contact chemoreception; additionally, the cilia of these cells are structurally similar to stereocilia—as contrasted with motile cilia—such as those found in other sensory organs (Bonar, 1978). The same is true of the apical sensory cells of veligers of the prosobranch *Littorina littorea* (Uthe, 1995).

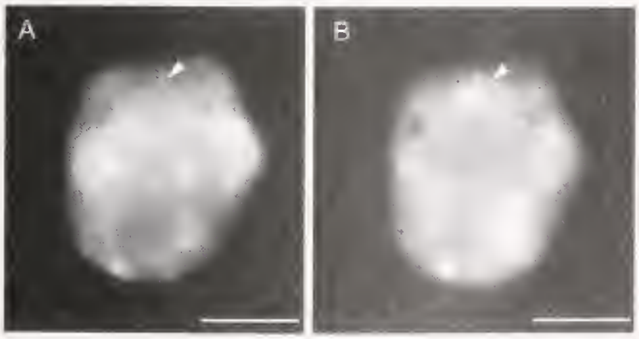

Figure 5. (A) Veliger larva of *Phestilla sibogae* that was stained with DASPEI, embedded in low-melting-point agarose, and subjected to excitatory irradiation focused on the apical sensory organ (ASO) for 20 min. The ASO cells are bleached (compare to Fig. 2B, C), although the DASPEI stain remains in other parts of the larval body. (B) The same larva after 20-min immersion in acridine orange in filtered seawater. The ASO cells emit a pale green fluorescence. Other bright areas, some not visible in both photos, retain DASPEI stain. Scale bars = 100 μm.

Kempf *et al.* (1997) provided detailed ultrastructural and immunocytochemical evidence for the presence of at least three cell types in the apical sensory organs of nudibranch larvae. Three sensory serotonergic neurons are intricately associated with the innervation of the velum, leading the authors to conjecture that these elements of the ASO are mechanosensory and serve as a compensatory system of velar control to "modulate the position of the velar lobes in response to deformations of the pretrochal surface caused by changes in velar orientation." It appears most likely that the cells responsible for chemosensory detection of the metamorphic cue in larvae of *Phestilla sibogae* are the so-called flask-shaped cells (Bonar, 1978; = ampullary cells of Chia and Koss, 1984). These fit in number (five or six in veligers of *P. sibogae* according to Bonar's [1978] ultrastructural study) and location with those that were stained by DASPEI in the current study (Fig. 2), and cells with very similar structure have been shown to be chemosensory in a cephalopod (Lucero *et al.*, 1992).

Acridine orange has long been employed as a vital stain for dying eukaryotic cells (reviewed by Darzynkiewicz and Traganos, 1998). When complexed with DNA, acridine orange fluoresces in the green part of the spectrum (525 nm); as a weak stain for RNA, its emission is reddish (~650 nm) (Haugland, 1996). Although some authors (*e.g.*, Abrams *et al.*, 1993) maintain that acridine orange staining differentiates apoptotic cells (*i.e.*, those dying from "programmed cell death") from necrotic cells, others report the opposite. Darzynkiewicz and Traganos (1998, p. 55) note that both late apoptotic and necrotic cells show green fluorescence at low (*i.e.*, $\sim 10^{-6}$ *M*) concentrations of acridine orange. Experiments conducted by Delic *et al.* (1991, p. 147) demonstrated that acridine orange "intercalates into nuclear DNA following the discharge of lysosomal enzymes *via* a targeted photodynamic reaction triggered by high levels of light intensity." Thus the specific uptake of acridine orange by the larval ASO cells after the photoinactivating treatment employed here appears to support the conclusion that DASPEI staining followed by excitatory irradiation has killed the cells. The applied concentration was in the micromolar range, and cells treated by a presumed photodynamic interaction of UV light with a fluorescent stain brought about the cell death.

The mechanism by which potassium and cesium ions induce metamorphosis in various invertebrate larvae has been a subject of considerable conjecture (*e.g.*, Yool *et al.*, 1986; Todd *et al.*, 1991; Herrmann, 1995; Pechenik *et al.*, 1995; Woollacott and Hadfield, 1996; Carpizo-Ituarte and Hadfield, 1998). A leading hypothesis has centered on the likelihood that elevated external potassium depolarizes excitable sensory cells, presumably those bearing the receptors for external chemical metamorphic inducers, causing these cells to generate electrical spikes that are transmitted through the central nervous system to bring about morphogenesis (*e.g.*, Baloun and Morse, 1984). Cesium, acting as a potent blocker of potassium channels, has been thought to have a similar action (*e.g.*, Carpizo-Ituarte and Hadfield, 1998). However, nearly all those who have carried out such experiments have acknowledged that entire larvae are bathed in the seawater with elevated potassium or cesium ions and that the ions could be acting downstream from the primary chemosensory cells (Todd *et al.*, 1991). We have presented here data consistent with the latter hypothesis, although exactly where downstream awaits clarification. The possibility that K^+ and Cs^+ act on external receptors as well as downstream sites in intact larvae is, of course, not disproven by these experiments. There are undoubtedly numerous synapses in the central nervous system between the ASO and the responding tissues where potassium and cesium could act.

Because it focused on a single gastropod species, the current research provides no support for homology of ASO cells among gastropods or across phyla. However, it does point to profitable future research on this subject. (1) Electron-microscopic study of the ASOs of larvae of *P. sibogae* after the photoablation treatment could reveal exactly which cells were affected, and thus confirm that the flask-shaped cells with nonmotile cilia are the critical receptor cells in metamorphic signaling. (2) If the experiments described here were performed with larvae of other species, across the Mollusca and other spiralian phyla, and similar results obtained, the data would be further evidence for homology. The new data presented here, considered together with experimental data on the molecular attributes of metamorphic-cue receptors in larvae of the abalone (Baxter and Morse, 1987) and the polychaete *Hydroides elegans* (Carpizo-Ituarte and Hadfield, 1998; Holm *et al.*, 1998), provide a framework for investigating the molecular nature of the receptor molecules used by these larvae in settlement-cue perception and the homology of these receptor molecules across phyla. Data on the abalone, *H. elegans*, and *P. sibogae* (Hadfield, unpubl. obs.) strongly suggest that these receptor molecules are *not* members of the G-protein-transduced, 7-transmembrane-domain peptides typical of much chemical perception in animals. Once the specific location of the actual receptor molecules is demonstrated across phyla, and their molecular sequences are known, molecular probes (*e.g.*, *in situ* hybridization) could be employed to provide additional evidence for homology and phylogeny. Similar experimental data obtained from other phyla, especially the noncoelomate spiralians, would greatly expand our understanding of the evolution of the ASO complex and, perhaps, evolutionary relationships among the spiralians.

Acknowledgments

This research was supported by ONR grants N00014-94-1-0524 and N00014-95-1-1015. Many members of our research group at the University of Hawaii's Kewalo Marine Laboratory contributed significantly to maintaining research animals, culturing larvae, and assisting in the research at important moments; we thank them all. We thank Carole Hickman (University of California, Berkeley) for her constructive criticisms and suggestions for improving the manuscript, Richard Strathmann (University of Washington) for assisting the authors in recalling older references on larval settlement behavior, and two anonymous reviewers for suggestions that clarified significant parts of this paper.

Literature Cited

Abrams, J. A., K. White, L. I. Fessler, and H. Steller. 1993. Programmed cell death during *Drosophila* embryogenesis. *Development* **117:** 29–43.

Arkett, S. A., F.-S. Chia, J. I. Goldberg, and R. Koss. 1989. Identified settlement receptor cells in a nudibranch veliger respond to specific cue. *Biol. Bull.* **176:** 155–160.

Bahamondes-Rojas, I., and M. Dherbonez. 1990. Purification partielle de substances glyco-conjuguées capables d'induire la metamorphose des larves competentes d'*Eubranchus doriae* (Trinchese, 1879), mollusque nudibranche. *J. Exp. Mar. Biol. Ecol.* **144:** 17–27.

Balak, K. J., J. T. Corwin, and J. E. Jones. 1990. Regenerated hair cells can originate from supporting cell progeny: evidence from phototoxicity and laser ablation experiments in the lateral line system. *J. Neurosci.* **10:** 2502–2512.

Baloun, A. J., and D. E. Morse. 1984. Ionic control of settlement and metamorphosis in larval *Haliotis rufescens* (Gastropoda). *Biol. Bull.* **167:** 124–138.

Barnes, J. R., and J. J. Gonor. 1973. The larval settling response of the lined chiton *Tonicella lineata*. *Mar. Biol.* **20:** 259–264.

Baxter, G., and D. E. Morse. 1987. G protein and diacylglycerol regulate metamorphosis of planktonic molluscan larvae. *Proc. Natl. Acad. Sci. USA* **84:** 1867–1870.

Baxter, G. T., and D. E. Morse. 1992. Cilia from abalone larvae contain a receptor-dependent G protein transduction system similar to that in mammals. *Biol. Bull.* **183:** 147–154.

Bereiter-Hahn, J. 1976. Dimethylaminostyryl-methyl-pyridinium-iodine (DASPEI) as a fluorescent probe of mitochondria *in situ*. *Biochim. Biophys. Acta* **423:** 1–14.

Boettcher, A. A., and N. M. Targett. 1998. Role of chemical inducers in larval metamorphosis of queen conch, *Strombus gigas* Linnaeus: relationship to other marine invertebrate systems. *Biol. Bull.* **194:** 132–142.

Bonar, D. B. 1978. Ultrastructure of a cephalic sensory organ in larvae of the gastropod *Phestilla sibogae* (Aeolidacea, Nudibranchia). *Tissue Cell* **10:** 153–165.

Boudko, D. Y., M. Switzer-Dunlap, and M. G. Hadfield. 1999. Cellular and subcellular structure of anterior sensory pathways in *Phestilla sibogae* (Gastropoda, Nudibranchia). *J. Comp. Neurol.* **403:** 39–52.

Burke, R. D. 1984. Pheromonal control of metamorphosis in the Pacific sand dollar, *Dendraster excentricus*. *Science* **225:** 442–443.

Carpizo-Ituarte, E. J., and M. G. Hadfield. 1998. Stimulation of metamorphosis in the polychaete *Hydroides elegans* Haswell (Serpulidae). *Biol. Bull.* **194:** 14–24.

Chia, F.-S., and R. Koss. 1984. Fine structure of the cephalic sensory organ in the larva of the nudibranch *Rostanga pulchra* (Mollusca, Opisthobranchia, Nudibranchia). *Zoomorphology* **104:** 131–139.

Clare, A. S. 1995. Chemical signals in barnacles: old problems, new approaches. Pp. 49–67 in *New Frontiers in Barnacle Evolution*, F. R. Schram and J. T. Hoeg, eds. Balkema, Rotterdam.

Conklin, E. G. 1897. The embryology of *Crepidula*. *J. Morphol.* **13:** 1–226.

Crisp, D. J. 1974. Factors influencing the settlement of marine invertebrate larvae. Pp. 177–265 in *Chemoreception in Marine Organisms*, P. T. Grant and A. M. Mackie, eds. Academic Press, New York.

Crisp, D. J. 1984. Overview of research on marine invertebrate larvae, 1940–1980. Pp. 103–126 in *Marine Biodeterioration: an Interdisciplinary Study*, J. D. Costlow and R. C. Tipper, eds. Naval Institute Press, Annapolis, Maryland.

Darzynkiewicz, Z., and F. Traganos. 1998. Measurement of apoptosis. *Adv. Biochem. Eng.-Biotechnol.* **62:** 33–73.

Delic, J., J. Coppey, H. Magdelenat, and M. Coppey-Moisan. 1991. Impossibility of acridine orange intercalation in nuclear DNA of the living cell. *Exp. Cell Res.* **194:** 147–153.

Freeman, G., and E. B. Ridgway. 1987. Endogenous photoproteins, calcium channels and calcium transients during metamorphosis in hydrozoans. *Roux's Arch. Dev. Biol.* **196:** 30–50.

Hadfield, M. G. 1978. Metamorphosis in marine molluscan larvae: an analysis of stimulus and response. Pp. 165–175 in *Settlement and Metamorphosis of Marine Invertebrate Larvae*, F.-S. Chia and M. E. Rice, eds. Elsevier, New York.

Hadfield, M. G. 1998. The D. P. Wilson Lecture: research on settlement and metamorphosis of marine invertebrate larvae: past, present and future. *Biofouling* **12:** 9–29.

Hadfield, M. G., and J. T. Pennington. 1990. The nature of the metamorphic signal and its internal transduction in larvae of the nudibranch *Phestilla sibogae*. *Bull. Mar. Sci.* **46:** 455–464.

Hadfield, M. G., and D. Scheuer. 1985. Evidence for a soluble metamorphic inducer in *Phestilla:* ecological, chemical and biological data. *Bull. Mar. Sci.* **37:** 556–566.

Haugland, R. P. 1996. *Handbook of Fluorescent Probes and Research Chemicals*, 6th edition. Molecular Probes, Eugene, Oregon.

Herrmann, K. 1995. Induction and regulation of metamorphosis in planktonic larvae: *Phoronis müller*i (Tentaculata) as archetype. *Helgol. Meeresunters.* **49:** 255–281.

Holm, E. R., B. T. Nedved, E. Carpizo-Ituarte, and M. G. Hadfield. 1998. Metamorphic-signal transduction in *Hydroides elegans* (Polychaeta: Serpulidae) is not mediated by a G protein. *Biol. Bull.* **195:** 21–29.

Hörstadius, S. 1937. Experiments on determination in the early development of *Cerebratulus lacteus*. *Biol. Bull.* **73:** 317–342.

Jensen, R. A., D. E. Morse, R. L. Petty, and N. Hooker. 1990. Artificial induction of larval metamorphosis by free fatty acids. *Mar. Ecol. Prog. Ser.* **67:** 55–71.

Kempf, S. C., L. R. Page, and A. Pires. 1997. Development of serotonin-like immunoreactivity in the embryos and larvae of nudibranch mollusks with emphasis on the structure and possible function of the apical sensory organ. *J. Comp. Neurol.* **386:** 507–528.

Kume, M., and K. Dan. 1968. *Invertebrate Embryology*. English translation by Jean C. Dan. National Library of Medicine, Public Health Service, U.S. Dept. of Health, Education and Welfare and National Science Foundation, Washington, DC and NOLIT Publishing House, Belgrade.

Lambert, W. J., and C. D. Todd. 1994. Evidence for a water-borne cue inducing metamorphosis in the dorid nudibranch mollusc *Adalaria proxima* (Gastropoda: Nudibranchia). *Mar. Biol.* **120:** 265–271.

Leise, E. M. 1996. The fluorescent dye DASPEI selectively stains the apical ganglion in larval *Ilyanassa obsoleta* (Mollusca, Gastropoda). *Microsc. Res. Tech.* **33:** 496–500.

Leitz, T., and G. Klingmann. 1990. Metamorphosis of *Hydractinia:* studies with activators and inhibitors aiming at protein kinase C and potassium channels. *Roux's Arch. Dev. Biol.* **199:** 107–113.

Lucero, M. T., F. T. Horrigan, and W. F. Gilly. 1992. Electrical responses to chemical stimulation of squid olfactory receptor cells. *J. Exp. Biol.* **162:** 231–249.

Marois, R., and T. J. Carew. 1997. Fine structure of the apical ganglion and its serotonergic cells in the larva of *Aplysia californica*. *Biol. Bull.* **192:** 388–398.

McGee, B. L., and N. M. Targett. 1989. Larval habitat selection in

Crepidula (L.) and its effect on adult distribution patterns. *J. Exp. Mar. Biol. Ecol.* **131:** 195–214.

Miller, S. E., and M. G. Hadfield. 1986. Ontogeny of phototaxis and metamorphic competence in larvae of the nudibranch *Phestilla sibogae* Bergh (Gastropoda: Opisthobranchia). *J. Exp. Mar. Biol. Ecol.* **97:** 95–112.

Miller, S. E., and M. G. Hadfield. 1990. Developmental arrest during larval life and life-span extension in a marine mollusc. *Science* **248:** 356–358.

Morse, A. N. C., and D. E. Morse. 1984. Recruitment and metamorphosis of *Haliotis* larvae induced by molecules uniquely available at the surfaces of crustose red algae. *J. Exp. Mar. Biol. Ecol.* **75:** 191–215.

Müller, W. A., A. Mitze, J. P. Wickhorst, and H. M. Meier-Menge. 1977. Polar morphogenesis in early hydroid development: action of caesium, of neurotransmitters and of an intrinsic head activator on pattern formation. *Roux's Arch. Dev. Biol.* **182:** 311–328.

Nott, J. A. 1973. Settlement of the larvae of *Spirorbis spirorbis. J. Mar. Biol. Assoc. U.K.* **53:** 437–453.

Nurse, C. A., and L. Farraway. 1989. Characterization of Merkel cells and mechanosensory axons of the rat by styryl pyridinium dyes. *Cell Tissue Res.* **155:** 125–128.

Pawlik, J. R. 1992. Chemical ecology of the settlement of benthic marine invertebrates. *Oceanogr. Mar. Biol. Annu. Rev.* **30:** 273–335.

Pearce, C. M., and R. E. Scheibling. 1990a. Induction of metamorphosis of larvae of the green sea urchin, *Strongylocentrotus droebachiensis* by coralline red algae. *Biol. Bull.* **179:** 304–311.

Pearce, C. M., and R. E. Scheibling. 1990b. Induction of settlement and metamorphosis in the sand dollar *Echinarachinius parma:* evidence for an adult-associated factor. *Mar. Biol.* **107:** 363–369.

Pechenik, J. A., M. G. Hadfield, and L. S. Eyster. 1995. Assessing whether larvae of the opisthobranch gastropod *Phestilla sibogae* Bergh become responsive to three chemical cues at the same age. *J. Exp. Mar. Biol. Ecol.* **191:** 1–17.

Pennington, J. T., and M. G. Hadfield. 1989. A simple nontoxic method for decalcification of living invertebrate larvae. *J. Exp. Mar. Biol. Ecol.* **130:** 1–7.

Pires, A., and M. G. Hadfield. 1993. Responses of isolated vela of nudibranch larvae to inducers of metamorphosis. *J. Exp. Zool.* **266:** 234–239.

Pires, A., S. L. Coon, and M. G. Hadfield. 1997. Catecholamines and dihydroxyphenylalanine in metamorphosing larvae of the nudibranch *Phestilla sibogae* Bergh. *J. Comp. Physiol. A* **181:** 187–194.

Raven, C. P. 1966. *Morphogenesis: The Analysis of Molluscan Development*, 2nd ed. Pergamon, Oxford.

Rice, M. E. 1986. Factors influencing larval metamorphosis in *Golfingia misakiana* (Sipuncula). *Bull. Mar. Sci.* **39:** 362–375.

Rittschof, D. 1985. Oyster drills and the frontiers of chemical ecology: unsettling ideas. *Am. Malacol. Bull. Special Ed.* **1:** 111–116.

Scheltema, R. S. 1961. Metamorphosis of the veliger larvae of *Nassarius obsoletus* (Gastropoda) in response to bottom sediment. *Biol. Bull.* **120:** 92–109.

Selenka, E. 1881. *Zoologische Studien. II. Zur Entwicklungsgeschichte der Seeplanarien. Ein Beitrag zur Keimblättlehre und Dezendenz Theorie*, Leipzig, 36 pp.

Thompson, T. E. 1958. The natural history, embryology, larval biology, and post-larval development of *Adalaria proxima* (Alder and Hancock) (Gastropoda Opisthobranchia). *Philos. Trans. R. Soc. Lond.* **242:** 1–58.

Todd, C. D., M. G. Bentley, and J. N. Havenhand. 1991. Larval metamorphosis of the opisthobranch mollusc *Adalaria proxima* (Gastropoda: Nudibranchia): the effects of choline and elevated potassium ion concentration. *J. Mar. Biol. Assoc. U.K.* **71:** 53–72.

Uthe, D. 1995. Fine structure of the cephalic sensory organ in veliger larvae of *Littorina littorea*, (L.) (Mesogastropoda, Littorinidae). *Hydrobiologia* **309:** 45–52.

Welch, J. M., D. Rittschof, T. M. Bullock, and R. B. Forward, Jr. 1997. Effects of chemical cues on settlement behavior of blue crab *Callinectes sapidus* postlarvae. *Mar. Ecol. Prog. Ser.* **154:** 143–153.

Wodicka, L. M., and D. E. Morse. 1991. cDNA sequences reveal mRNAs for two Gα signal transducing proteins from larval cilia. *Biol. Bull.* **180:** 318–327.

Woollacott, R. M., and M. G. Hadfield. 1996. Induction of metamorphosis in larvae of a sponge. *Invertebr. Biol.* **115:** 257–262.

Yool, A. J. 1985. Physiological analysis of the induction of metamorphosis in larvae of *Haliotis rufescens* (Gastropoda: Mollusca). Ph.D. dissertation, University of California, Santa Barbara. 111 pp.

Yool, A. J., S. M. Grau, M. G. Hadfield, R. A. Jensen, D. A. Markell, and D. E. Morse. 1986. Excess potassium induces larval metamorphosis in four marine invertebrate species. *Biol. Bull.* **170:** 255–266.

Young, C. M., and L. F. Braithwaite. 1980. Larval behavior and post-settling morphology in the ascidian, *Chelyosoma productum* Stimpson. *J. Exp. Mar. Biol. Ecol.* **42:** 157–169.

Zimmer, R. L. 1991. Phoronida. Ch. 1. Pp. 1–45 in *Reproduction of Marine Invertebrates, Vol. VI, Echinoderms and Lophophorates.* A. C. Giese, J. S. Pearse, and V. B. Pearse, eds. Boxwood Press, Pacific Grove, California.

Zimmer-Faust, R. K., and M. N. Tamburri. 1994. Chemical identity and ecological implications of a waterborne, larval settlement cue. *Limnol. Oceanogr.* **39:** 1075–1087.

Reference: *Biol. Bull.* **198:** 77–87. (February 2000)

Reproduction Cycles and Strategies of the Cold-Water Sponges *Halisarca dujardini* (Demospongiae, Halisarcida), *Myxilla incrustans* and *Iophon piceus* (Demospongiae, Poecilosclerida) From the White Sea

ALEXANDER V. ERESKOVSKY

Biological Department, St. Petersburg State University, Universitetskaja nab. 7/9, St. Petersburg 199034, Russia

Abstract. The reproductive development of the Demospongiae species *Halisarca dujardini* (Halisarcida), *Myxilla incrustans* and *Iophon piceus* (Poecilosclerida) from Chupa Inlet (Kandalaksha Bay, the White Sea) was studied histologically during 1982–1994 and 1997. These species are all viviparous. *Halisarca dujardini* inhabits shallow waters (1.5–5 m); *M. incrustans* and *I. piceus* are common in a more stable environment at depths between 15 and 25 m. Initiation of sexual reproduction stages is dependent upon water temperature. Reproductive effort is low in *Myxilla incrustans* and *I. piceus* (reproductive elements contribute 7.3% and 12% of maternal tissue volume respectively), but much higher in *H. dujardini* (up to 69% of the parental tissue volume). Reproduction leads to localized destruction of maternal tissue for *M. incrustans* and *I. piceus* and complete disorder of central and basal parts of the choanosoma of *H. dujardini* after each period of reproduction. *Myxilla incrustans* and *I. piceus* reproduce throughout the hydrological summer, but reproduction in *H. dujardini* is restricted to 3 weeks. The average life span of *M. incrustans* and *I. piceus* is more than 4 years, and that of *H. dujardini* is about 7–12 months. The data suggest that *M. incrustans* and *I. piceus* are *K*-strategists, whereas *H. dujardini* is an *r*-strategist.

Introduction

Sponges often dominate benthic communities. For instance, in the southwestern part of the Barents Sea, sponge biomass is about 54% of the total biomass of bottom biocoenoses (Ereskovsky, 1995b). The biocoenoses of *Halichondria panicea* and *H. sitiens* in shallow-water coastal regions of East Murman (Barents Sea) form 71.9% of the total biocoenoses biomass (Propp, 1971). Knowledge of the life history and reproduction cycles of sponges is important for understanding their evolution and role in marine ecosystems. Although some information on reproductive seasons of cold and temperate marine sponges is available (Elvin, 1976; Fell, 1976; Ivanova, 1978; Fell and Jacob, 1979; Chen, 1976; Fell *et al.*, 1979; Fell and Lewandrowsky, 1981; Barthel, 1986, 1988; White and Barthel, 1994), little is known about their reproductive efforts and patterns of anatomical-histological change. These studies have indicated that the examined species are generally *r*-strategists and are responsive to seasonal environmental changes, mainly in water temperature. According to E. R. Pianka (1978), species of sessile macrofauna may be divided into *r*- and *K*-strategists. The first are characterized by high rates of reproduction and growth, high reproductive efforts, and high invasion opportunities in an unstable environment, whereas the second have low reproductive rates, low reproductive efforts, and good adaptation to specialized ecological niches (mainly in stable conditions).

The embryonic development of *Halisarca dujardini* (Halisarcida), the gametogenesis of *Myxilla incrustans* and *Iophon piceus* (Poecilosclerida), and the larval development of *I. piceus* have already been studied (Levi, 1956; Korotkova and Ermolina, 1982; Korotkova and Ereskovsky, 1984; Ereskovsky, 1986; Efremova *et al.*, 1987a, b). This paper describes the reproduction cycles and dependence of different sexual reproduction stages on environmental factors in demosponge species *Halisarca dujardini*, *Myxilla*

Received 9 December 1997; accepted 11 August 1999.
E-mail: eres@sn.pu.ru

incrustans, and *Iophon piceus* from the White Sea (Arctic), with special attention to reproductive efforts (the parental contribution to each phase of reproduction) and maternal tissue state during reproduction.

Materials and Methods

The shallow-water (1.5–5 m) species *Halisarca dujardini* Johnston, 1842 (Ceractinomorpha, Halisarcida) was sampled monthly from December to May and weekly from June to August (1986–1989 and 1991–1994, 1997). *Myxilla incrustans* (Johnston, 1842) and *Iophon piceus* (Vosmaer, 1881) (Demospongiae, Poecilosclerida), found in deeper water (15–25 m), were sampled twice a month from June to September, 1982–1984. Occasional samples of these species were taken in spring and summer from 1985 through 1991 and in 1997. Subtidal sponges were sampled using scuba. For quantitative studies, 90 specimens of *H. dujardini* (sampled from January to August in 1986–1989) and 29 specimens of *I. piceus* and 25 specimens of *M. incrustans* (sampled from June to October in 1983–1984) were investigated. Other specimens of these three species were analyzed for the presence of sexual reproductive elements. To ascertain the minimum lifespan of the three species, in July 1992 a few specimens of each species were marked in their locality. Every year these specimens were monitored for survival.

Immediately after specimens were removed from the water, sponge fragments were fixed in Bouin's and Carnoy's fixatives for light microscopy. Tissue fragments were dehydrated through an ethanol series, placed in celloidin blended with castor oil and then in chloroform, and embedded in paraffin. Sections were cut to a thickness of 6 μm and Meier's hematoxylin, eosin, and Heidenhein ferric hematoxylin. Ten microscopic slides of each specimen were examined.

The number of gametes, embryos, and larvae in parental tissues were calculated using Elvin's equation (Elvin, 1976):

$$N = \delta N(t/D + t)\mathrm{K}. \qquad (1)$$

where N is the number of objects per cubic millimeter of tissue; δN is the average number of objects (gametes, embryos, larvae and spermatic cysts) in the microscope field; t is the thickness of the histological section (here 0.006 mm); D is the diameter of the object; and K is a constant for converting the number of objects in a square millimeter to the number in a cubic millimeter; it is equal to 166.7.

Egg, spermatic cyst, embryo, and unreleased larva volumes were calculated using the equation:

$$V = (1/6)\,D \qquad (2)$$

where V is an object volume and D is its diameter.

The volume of reproductive elements per cubic millimeter of parental tissue was obtained by multiplying N by V. The total sponge volume in breeding season was measured by immersing each specimen into a graduated cylinder filled with water. The volume of water displaced was a measure of the volume of the sponge tissue. Data are presented as mean ± standard error.

A hydrologic thermometer was used to measure water temperature during sampling. Additional information on

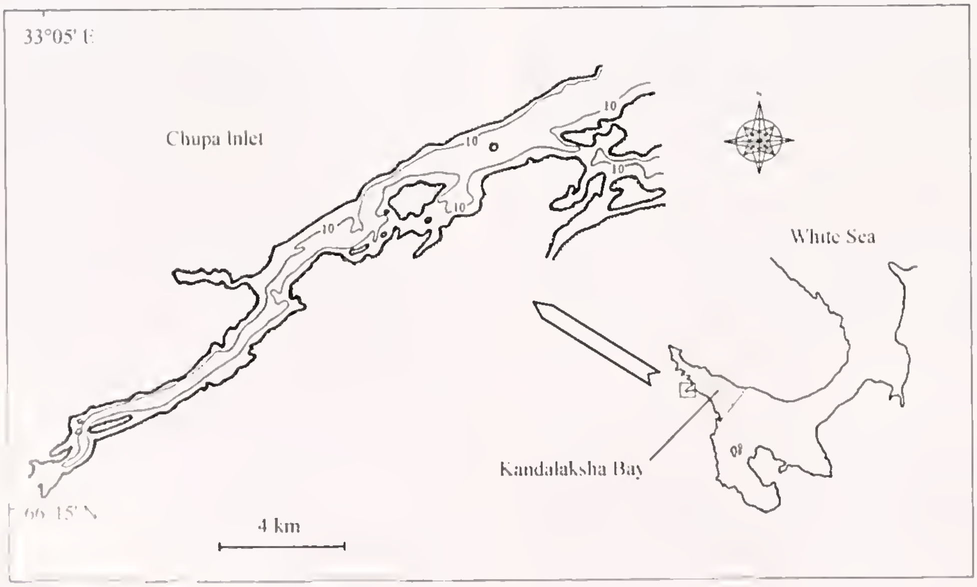

Figure 1. Chupa Inlet, showing the 10-m depth contour; inset illustrates the location of the Inlet in Kandalaksha Bay of the White Sea

seasonal temperature changes at different depths in Chupa Inlet (the White Sea) was obtained from the White Sea Biological Station, Zoological Institute, Russian Academy of Sciences.

Study Area

Seasonal sampling was performed in the Chupa Inlet located in the innermost part of the Kandalaksha Bay, the White Sea (Fig. 1). All oceanologic and climatic data were obtained from Babkov (1982, 1984) and Babkov and Golikov (1984). The region has a long, severe winter and a short, relatively warm summer. From December until mid-May, Chupa Inlet is covered with ice. The average annual water temperature in the Inlet, which has a mean depth of about 20 m, is about 5°C, ranging from −1.5°C in winter to 17°C in summer (Fig. 2a). In autumn and spring the water column is homothermal: the temperature throughout all layers in November does not exceed +2°C and in March ranges from −1.0° to −0.5°C (Babkov, 1982).

Except for the open part of the Kandalaksha Bay, Chupa Inlet is characterized by reduced salinity. The seasonal variation in the 10-m surface layer is between 15‰ and 26‰; fluctuations decrease with depth, and in the bottom layer are not more than 1‰. The minimum surface-layer

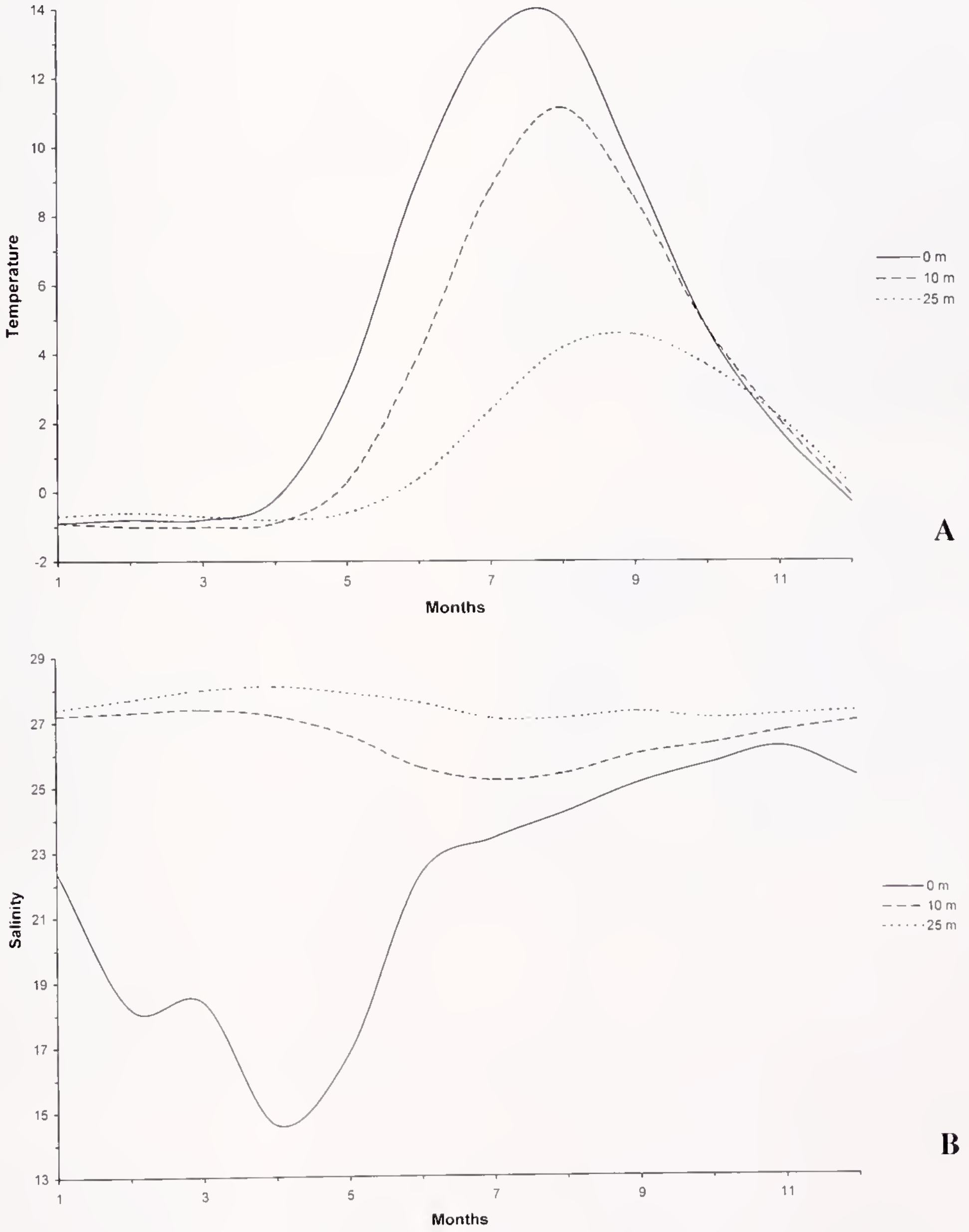

Figure 2. Seasonal changes in temperature (A) and salinity (B) at different depths in Chupa Inlet.

salinity was detected in April, and the maximum in November (Fig. 2b) (Babkov, 1982).

Temperature-salinity-analysis reveals two bodies of water in the region: surface water—boundary depth between 10 and 25 m, yearly temperature average 11°C, salinity not exceeding 27.0‰; and bottom water—water temperature not more than 5°–6°C, salinity exceeding 27‰ (Babkov, 1982; Babkov and Golikov, 1984).

Results

Halisarca dujardini

In the White Sea, *Halisarca dujardini* dwells at depths from 1.5 to 10 m, mainly on the algae *Fucus vesiculosus* and *Laminaria saccharina* and, rarely, on stones. Its body shape is irregular: encrusting, pillowy or clotted in form. Its size varies from 3 to 40 mm in width and from 2 to 6 mm in height. The volume of specimens averages 0.25 to 0.40 cm^3. The body surface is smooth and slimy. Oscules are small, one or several in a specimen. Color varies from milky to greyish-brown.

Halisarca dujardini is a gonochoristic organism. Spermatogenesis occurs at a water temperature of around −0.8°C and lasts for about 4 months. Spermatic cysts containing spermatocytes can be found in the male mesohyl in about the middle of December at a water temperature of about −0.08°C. Male generative cells appear to originate from choanocytes that migrate into the lumen of choanocyte chambers, where spermatogenesis takes place. Choanocyte chambers thereby transform into spermatic cysts with a diameter between 40 and 90 μm. During intensive spermatogenesis (January–March), the mesohyl of the mature male differs greatly from that of an immature individual. It contains neither choanocyte chambers nor channels and pores. At this time the volume of spermatic cysts containing male generative cells amounts to 0.65 ± 0.5 mm^3/mm^3 of tissue (Fig. 3). In March and April, spermatic cysts contain only mature spermatozoa. From mid-December until mid-April, the volume of total reproductive elements (male and female) is nearly equal to the volume of spermatic cysts, differing from it only by the minute volume contributed by early oocytes (Fig. 3). Spermatogenesis and, thereafter, fertilization cease by April or the first week of May.

Early oocytes, 15 to 35 μm in diameter, are first observed during the last third of December, at a water temperature of about −0.6°C. Cytoplasmic growth is recorded until the beginning of June; however, vitellogenesis begins in May, when water temperature is about +2°C. Mature eggs, 110–130 μm in diameter, appear in females at the end of May; their number increases rapidly and their total volume

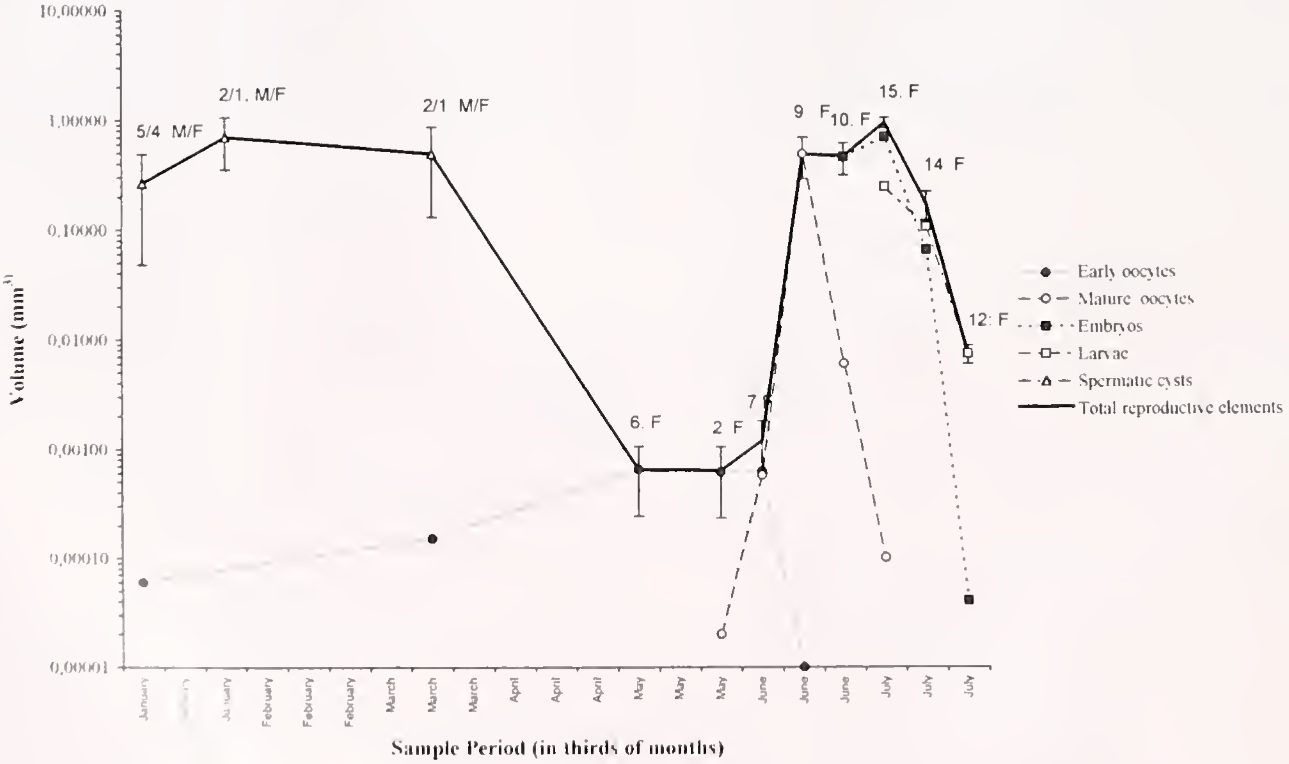

Figure 3. Mean volumes of gametes, embryos, and larvae per cubic millimeter of parental tissue in *Halisarca dujardini* during the reproduction seasons for 1986–1989. Numbers indicate individuals (males/females) analyzed. Vertical bars designate standard errors of the values for total reproductive elements.

reaches 0.49 ± 0.011 mm^3/mm^3 of tissue in mid-June (Fig. 3, 4a).

The development of larvae, namely cleavage and morphogenesis, occurs within a fortnight, from late June until July. During this period water temperature averages about 10°C. The even, asynchronous cleavage results in a coeloblastula, which transforms into a disphaerula larva (Ereskovsky and Gonobobleva, 1999), with a diameter between 120 and 150 μm (Fig. 4b, c). Larvae of *H. dujardini* (disphaerula), consisted of two flagellated sphaeras: external and internal; the internal sphaera was formed by invagination of laternal cells. The disphaerula was completely flagellated—sparsely so on the posterior pole (Ereskovsky and Gonobobleva, 1999). The volume of reproductive elements (cleaving embryos and prelarvae) reaches its maximum from the end of June to the beginning of July and amounts to about 0.69 ± 0.20 $mm^3/1\ mm^3$ of the tissue (*i.e.*, 69.5% of the total sponge volume; Fig. 3). This period is marked by the complete disorder of central and basal parts of the choanosoma, which are now filled with developing larvae (Fig. 4c). Normal tissue organization persists only in the narrow marginal zone of the sponge. Larval emergence occurs rapidly, within about a fortnight, begining before mid-July at a water temperature of about 12°C.

Slow postmetamorphic development of the new generation and postreproduction rehabilitation of parental sponges continues until December. Some parental sponges died and underwent disruption after larval emergence. A general life-history scheme of *H. dujardini* in the White Sea is shown in Figure 5.

Myxilla incrustans *and* Iophon piceus

White Sea populations of two Myxillidae species, *Myxilla incrustans* and *Iophon piceus*, are similar in their main life-history stages. Both species are simultaneous hermaphrodites: oogenesis and spermatogenesis occur at the same time. Gametogenesis and embryogenesis take place only in the choanosoma.

Iophon piceus, in the White Sea, dwells at depths from 3 to 172 m on stony-muddy substrates where the water temperature ranges from −1.15° to 11.5°C and the salinity from 18.6‰ to 29.12‰. The body is irregular—lumpy or flattened and uneven—with a wrinkled and porous surface. The oscules average 0.5 cm in diameter. The body height ranges from 6 to 12 cm and the diameter from 7 to 10 cm. The volume of observed individuals averages 11–16 cm^3. All stages of embryogenesis and gametogenesis in *I. piceus*, including new gonia formation, occur simultaneously (Fig. 6).

Generative cell development in *I. piceus* is usually initiated during February for female elements, and April–May for male elements. Male and female gametogenesis becomes active in mid-May at depths of 15–25 m at an

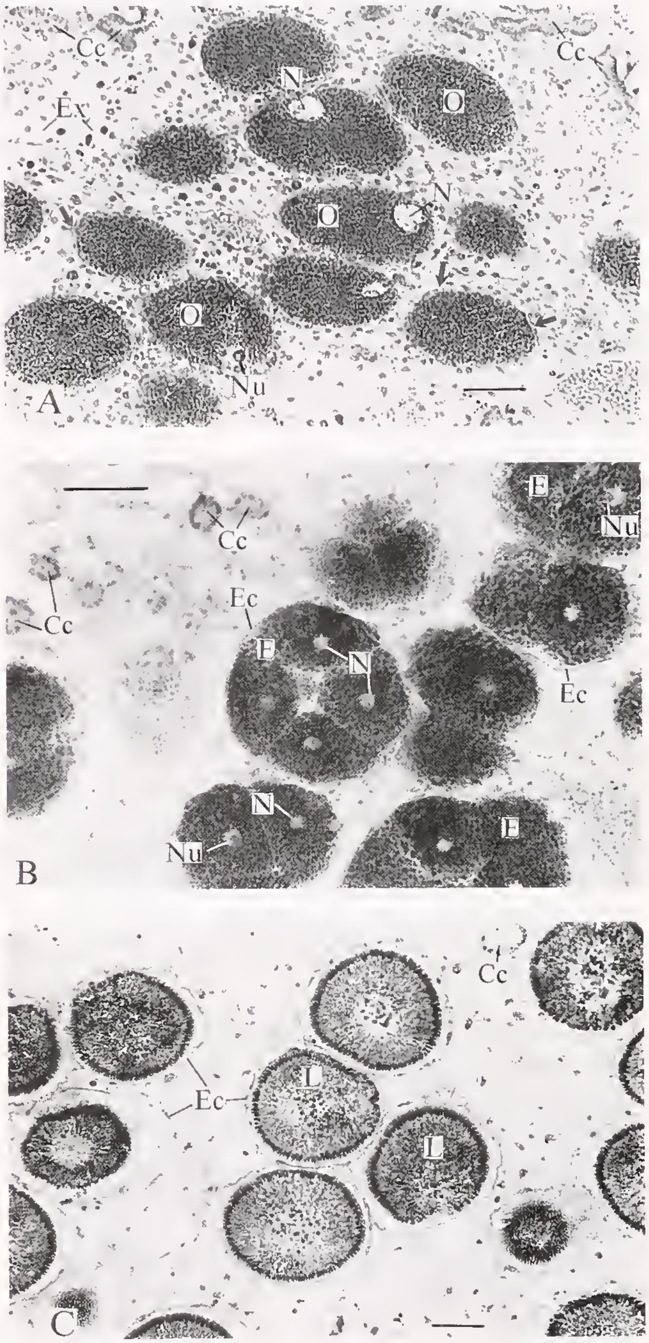

Figure 4. The central part of the choanosoma of *Halisarca dujardini*, showing stages of vitellogenesis, cleaving embryos, and mature larvae. (A) Oocytes (O) in late vitellogenesis, still with prominent nucleus (N) and nucleolus (Nu), are surrounded by cells forming embryonic capsules (arrows). The aquiferous system in this part of the choanosoma is destroyed. There are remnants of exhalant channels (Ex) and choanocyte chambers (Cc) in upper marginal parts of the choanosoma. Scale bar = 50 mm. (B) Cleaving embryos (E) enclosed in embryonic capsules (Ec). As in (A), choanocyte chambers (Cc) remain in upper marginal parts of the choanosoma. Note the nucleus (N) and nucleolus (Nu) of blastomers. Scale bar = 50 μm. (C) Larvae (L) before emission with well-differentiated ciliated cells at their periphery. Scale bar = 50 mm.

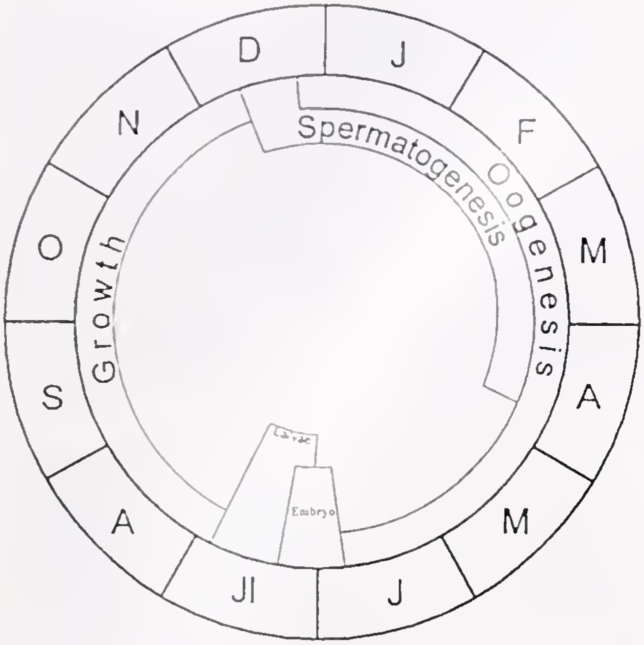

Figure 5. Scheme of the life history of *Halisarca dujardini* at Chupa Inlet, White Sea.

average water temperature of +0.1°C. Egg vitellogenesis and cleavage occur in late June and early July, when water temperature is about +4.2°C. During the last third of June the total volume of reproductive elements in this species amounts to about 0.05 ± 0.021 mm^3/mm^3 of tissue, whereas during the last third of July it amounts to 0.096 ± 0.028 mm^3 (Fig. 7).

The first larvae in *I. piceus* tissues are recorded at the end of July. These are typical parenchymulae common to the order Poecilosclerida. Their oval or oviform body (200 × 260 μm) is evenly covered (except the tailpiece) by flagella that are all of the same length (Ereskovsky, 1986). Larval emergence lasts from the first third of August (when water temperature is about 8°C) to early October, when the larvae constitute the total volume of reproductive elements. In the initial period of this process, the volume of the generative cells and larvae reaches 0.118 ± 0.01 mm^3/mm^3 of tissue (about 12%).

It is notable that only local disintegration of the parental tissues is observed during the period of larval emergence in *I. piceus:* the adjacent choanocyte chambers are destroyed, and some of the choanocytes degenerate. In this case, the ratios of mesohyl cell elements are modified around the region of larvae development (Fig. 6). However, the general anatomical and histological organization of the parental sponge is not changed. Marked specimens of *I. piceus* remained alive (survived) from 1992 to 1995, so their lifespan is more than 4 years. The life-history scheme of White Sea *I. piceus* individuals is represented in Figure 8.

Myxilla incrustans, in the White Sea, inhabits stony-muddy or gravelly-muddy substrates chiefly at depths from 1.5 to 150 m within the temperature range of −0.9° to 14.5°C and the salinity range of 23.3‰ to 28.93‰. The body is irregular, usually lumpy- or pillowy; the surface is uneven, wrinkled, and porous. The average oscule diameter is about 0.8 cm. Specimens are at most 8 cm in height and 7 cm in width. The volume of investigated individuals averaged 7 to 9 cm^3.

Early oocytes are found in *M. incrustans* in late February, and the first spermatic cysts are seen in April-May. Gametogenesis increases in mid-June at a water temperature of about +1.7°C.

During this period, the development of male and female generative cells is continuous (Fig. 9). Vitellogenesis and cleavage persist from mid-July until the beginning of August at a water temperature of about 6°C. At the beginning of this period, the total volume of reproductive elements amounts to 0.019 ± 0.006 mm^3/mm^3 of tissue (Fig. 10). The number of embryos in maternal sponges rapidly increases as the relative amount of fully formed oocytes decreases. By the beginning of August, spermatic cysts are no longer found.

The first larvae are recorded in August. Larvae (typical parenchymulae) are released from September until early October, at water temperatures from 2.5° to 4°C. The volume of all reproductive elements during larval release averages 7.3% (0.73 ± 0.21 mm^3). The general anatomical and histological organization of *M. incrustans* is unchanged after larval release. Marked specimens of *M. incrustans,* like those of *I. piceus,* survived from 1992 to 1995; their lifespan also exceeds 4 years. The life-history scheme of *M. incrustans* in the White Sea is represented in Figure 11.

Rehabilitation processes and vegetative growth occur

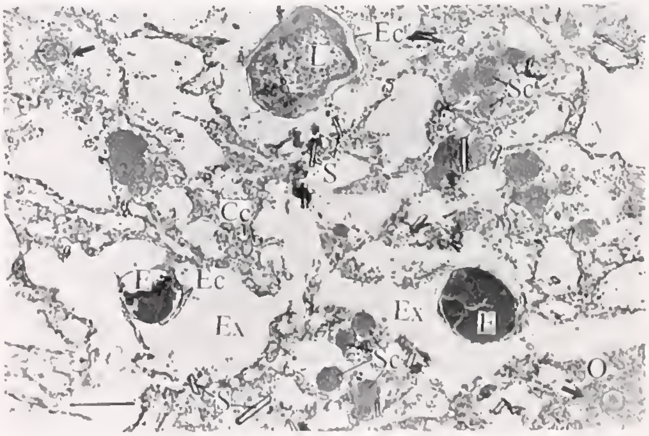

Figure 6. The choanosoma of the simultaneous hermaphrodite *Iophon piceus* during the reproductive period. Vitellogenic oocytes (O) are surrounded by nurse cells (arrows). Cleaving embryos (E) and larvae (L), enclosed in embryonic capsules (Ec) are located close to exhalant channels (Ec). Many spermatic cysts (Sc) can also be seen. Note choanocyte chambers (Cc) and spicules (S). Scale bar = 100 μm.

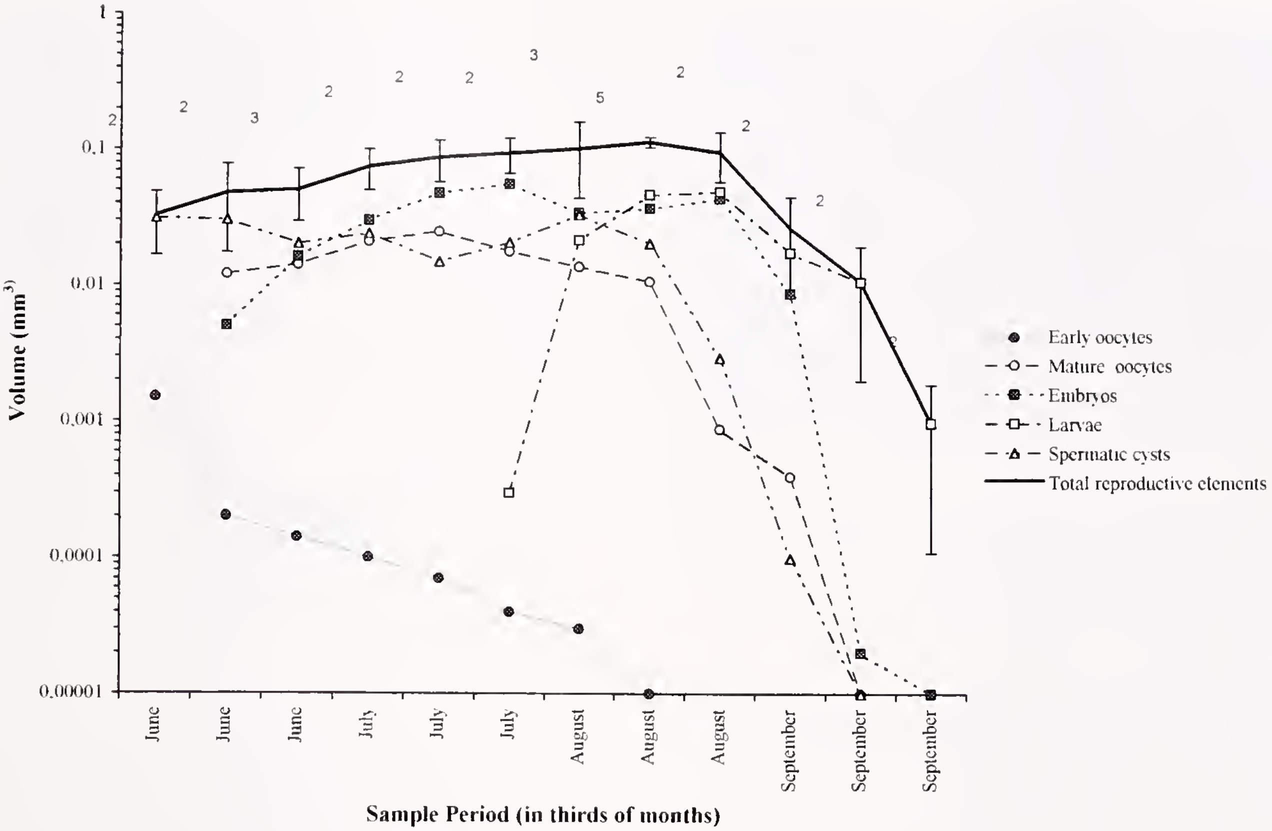

Figure 7. Mean volume of gametes, embryos, and larvae per cubic millimeter of tissue in the hermaphrodite *Iophon piceus* during the reproductive seasons for 1983–1984. For legend, see Figure 4.

during the postreproduction period of both *I. piceus* and *M. incrustans.*

Discussion

As evident from previous investigations (Ereskovsky, 1995b), only eurybiont sponges were able to settle in the White Sea where low salinity and temperature stratification are common. *H. dujardini, I. piceus,* and *M. incrustans* are thus subjected to seasonal fluctuations in temperature, salinity, and nutrition. The influence of these factors is different in the shallow waters populated by *H. dujardini* than in the deeper waters occupied by *I. piceus* and *M. incrustans.* Consequently, these populations have a special set of adaptations, including life and reproduction tactics.

Within its area, *H. dujardini* colonized algae and stones only in littoral-medial vertical zones (0–35 m) having salinities between 16‰ and 35‰ and temperatures from −0.8° to 26.5°C (Ereskovsky, 1993, 1994b, 1995a). It is a widespread subtropical-boreal species, common in the Atlantic Ocean from Mediterranean shallow waters along the Atlantic coast of Europe to the Barents and White Seas, and along the North American coast from Cape Hatteras to the Gulf of Maine (Ereskovsky, 1993, 1994a). *Halisarca dujar-*

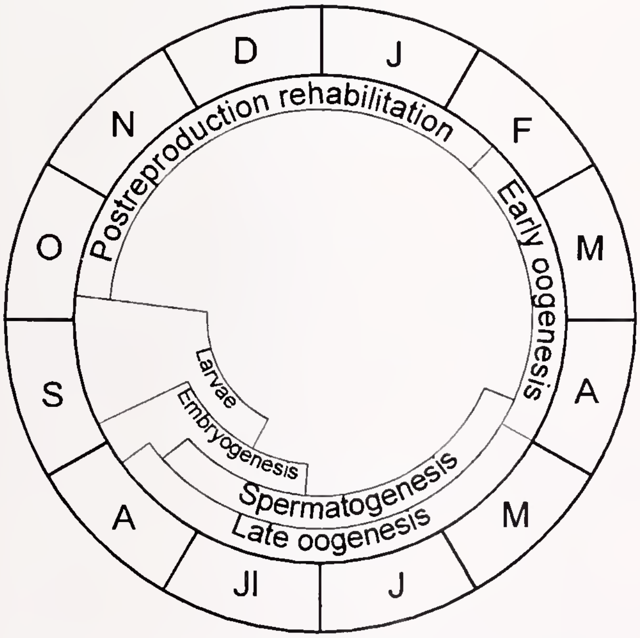

Figure 8. Life-history scheme of *Iophon piceus* in the White Sea.

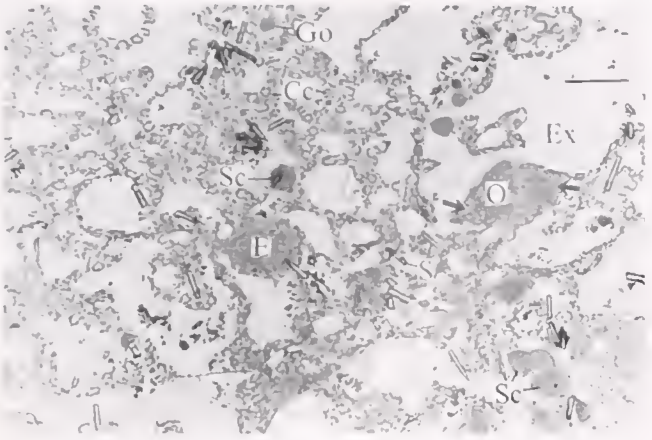

Figure 9. The choanosoma of the simultaneous hermaphrodite *Myxilla incrustans* at the stage of gametogenesis. The growing oocyte (Go) appears to be migrating in mesohyle, a vitellogenic oocyte (O) is surrounded by nurse cells (arrows) and located near the exhalant channel (Ex). Spermatic cysts (Sc) are dispersed in the choanosoma. Note choanocyte chambers (Cc) and spicules (S). Scale bar = 100 μm.

dini inhabits very fluctuating shallow-water environments. This report concerns the northern boundary area of the species—*i.e.*, the circumlittoral zone of the Barents and White Seas where variations in temperature and salinity are acute.

Correlations between different stages of the reproductive cycle and environmental conditions (chiefly temperature) in the White Sea population of *H. dujardini* have been noted here. Gametogenesis starts at an average water temperature of −0.8°C. The connection of spermatogenesis with minimal water temperatures has also been recorded in *H. dujardini* on the Atlantic coast of the United States (Chen, 1976). The onset of vitellogenesis in White Sea sponges correlates with a spring temperature change in May. The disappearance of male spermatic cysts in April suggests that oocytes are fertilized during their cytoplasmic growth. Penetration of the oocyte by sperm during meiotic prophase has been described in the nematode *Brachycoelium*, the annelids *Dinophilus* and *Histriobdella*, and the onychophora *Peripalopsis* (Austin, 1965).

Halisarca dujardini releases larvae during the period of temperature maximum. This is typical for marine hydrobionts in cold waters; the release of their larvae is timed to the momentary summer period of warmest water (Kaufman, 1977; Kasyanov, 1989). Embryogenesis, larval development, and metamorphosis in the White Sea population of *H. dujardini* occupy only about 3 to 4 weeks—from the end of June to the middle of July.

White Sea populations of *M. incrustans* and *I. picea* dwell mostly in more stable and predictable conditions. Eurybathic circumlittoral-highbathyal (1.5–500 m) *M. incrustans* and *I. picea* (Ereskovsky, 1995a) inhabit chiefly stony-muddy substrates. The boreal-arctic species *M. incrustans* is eurychoric: it is found in all Arctic Seas; the southern Pacific boundary of its area is the northern part of

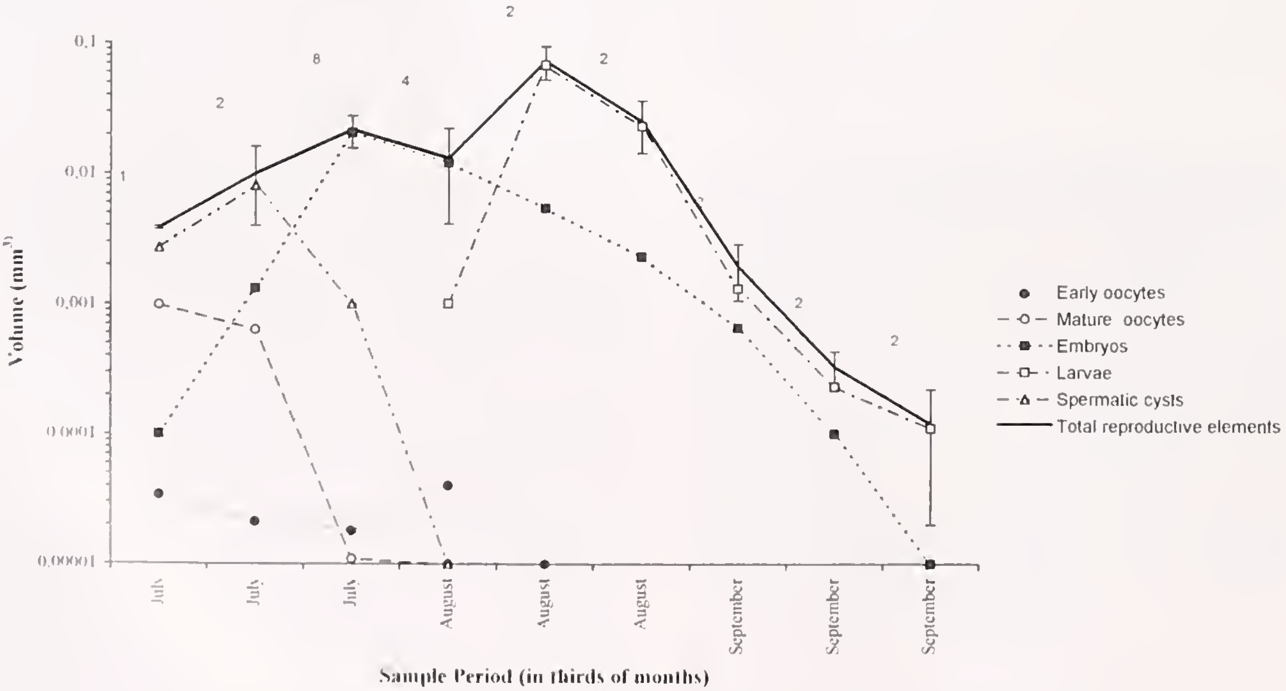

Figure 10. Mean volume of gametes, embryos, and larvae per cubic millimeter of tissue in the hermaphrodite *Myxilla incrustans* during the reproductive seasons for 1983–1984. For legend, see Figure 4.

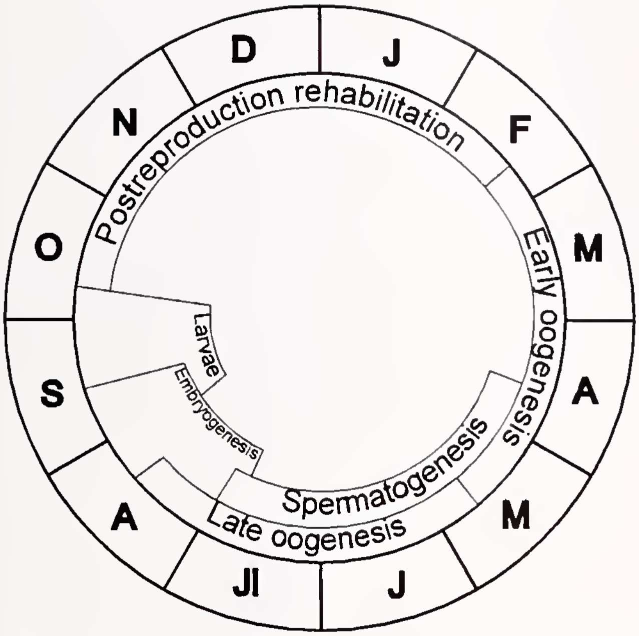

Figure 11. Life-history scheme of *Myxilla incrustans* in the White Sea.

the Sea of Japan and the California bathyal zone; in the Atlantic Ocean it extends south to the western Mediterranean and Cape Cod (Ereskovsky, 1994a).

Thus, *M. incrustans* is apparently a eurythermic (−1.9°–16.2°C) and euryhaline (25‰–35.5‰) species (Ereskovsky, 1994b).

The area of the Pacific highboreal-Arctic species *Iophon piceus* is not so broad. *I piceus* is circumarctic; in the Pacific Ocean it is found near the Northern Kurile Islands, in the Sea of Okhotsk and near Vancouver Island; in the Atlantic Ocean it extends south to Baffin Sea and the Faeroe Islands. Like *M. incrustans,* this species is eurythermic (−1.6°–12.5°C) and euryhaline (25.6‰–35.5‰) (Ereskovsky, 1994b).

It is clear from the reported data that different stages of the sexual cycles in the investigated species correlate well with seasonal environmental changes. Most significantly, the dependence of the main stages of oogenesis (a complicated multi-stage process) upon water temperature should be noted. Thus, deutoplasm growth begins within hydrological spring in all of the populations investigated. Vitellogenesis and egg maturation, as well as embryogenesis, end during hydrological summer—*i.e.,* the warmest season. A similar dependence on temperature has been noted for the developmental stages of some tropical sponge species (Fromont, 1994; Fromont and Bergquist, 1994).

Larval emission in some species is timed to a specific hydrological season in their habitat. On one hand, this relationship is modified by peculiarities of larval development and ecology since organisms are more temperature-sensitive during early ontogenesis than later (Kinne, 1963). On the other hand, the relationship is determined by the species genotype, and larvae are released when the temperature is close to the optimum for the species. But dependence of larval release upon water temperature is further mediated by biogeographical characteristics of the species. For poikilotherms, the temperature of the environment during speciation influences cell and tissue thermoresistance, which is considered to be a species-specific feature (Ushakov, 1989). As a result, temperatures optimal for both life and larval release are closely connected with the conditions that prevailed during the origin of the species and, consequently, with its zoogeographic position (Golikov and Scarlato, 1972; Mileikovsky, 1981). Maximal annual average temperatures most favorable for larval development are recorded within this period (Babkov, 1984).

In this study, special attention was given to the state of maternal tissues in different sexual reproduction stages in each of investigated species. It became evident from previous studies (Ereskovsky and Korotkova, 1997) that sexual and somatic morphogenesis correlate closely in sponge ontogenesis. Thus, somatic tissue state is important for the attainment of different sexual reproductive stages. Sexual and somatic morphogenesis either take place as successive life-cycle stages or occur in parallel, but they vary in correlation with each other due to their equal dependence on internal integrative mechanisms (Simpson and Gilbert, 1974; Fell *et al.,* 1979; Korotkova, 1988).

Owing to the vertical stratification in the Kandalaksha Bay, deep-water *M. incrustans* and *I. piceus* are less exposed to seasonal environmental fluctuations than is the shallow-water *H. dujardini.* It could be suggested then that *M. incrustans* and *I. piceus* are *K*-strategists, whereas *H. dujardini* is an *r*-strategist. Some features of these species may provide additional evidence for such conclusions:

1. Reproductive effort (the contribution by the organism to all parts of reproduction) is low in Myxillidae (about 7.3% of the maternal tissue volume in *M. incrustans* and about 12% in *I. piceus*) but high in *H. dujardini* (69.5% in females and 65% in males).
2. These different levels of reproductive effort result in different degrees of destruction of maternal tissue: only localized destruction in Myxillidae (both *I. piceus* and *M. incrustans*), but widespread destruction in *H. dujardini.*
3. Embryogenesis and larval development last over the hydrological summer in Myxillidae, but only 3 or 4 weeks in *H. dujardini.*
4. The average life span is more than 4 years in *M. incrustans* and *I. piceus* and about 7–12 months in *H. dujardini.*
5. *M. incrustans* and *I. piceus* inhabit a more stable environment than *H. dujardini.*

Similar ecological and reproductive characteristics have been reported for sponges inhabiting different regions. Thus, the volume of reproductive elements in the eurybiont *r*-strategist *Mycale* sp. amounts to 7.5%–20% under stressful conditions in Discovery Bay, Jamaica (Reiswig, 1973). Similar characteristics have been reported for other *r*-strategists such as littoral specimens of *Haliclona permolis* from the Oregon coast of the United States (Elvin, 1976) and the estuarine species *Haliclona loosanoffi* and *Halichondria* sp. (Fell, 1976; Fell and Jacob, 1979; Fell *et al.*, 1979; Fell and Lewandrowsky, 1981; Lewandrowsky and Fell, 1981). Shallow-water *Halichondria panicea* from the Barents (Ivanova, 1978), Baltic (Barthel, 1986, 1988), and White Seas (Ereskovsky, unpubl.) could be classified as a typical opportunist species and an *r*-strategist.

A comprehensive study of marine ecosystems is impossible without data on the reproductive cycles of the species of which they are composed. Knowledge of the peculiarities of both the reproduction strategies of the species and the reproduction tactics of the populations in different regions is thus of great value. The concept of reproduction strategies in sponges is still under development. In analyzing sponge reproduction, it is necessary to consider the maternal tissue state and reproductive effort of the specimens throughout the period of reproduction.

Acknowledgments

I thank Dr. N. V. Maksimovitch and Dr. S. M. Efremova for helpful discussions; Dr. A. A. Golikov for critical view and help with the manuscript; and two anonymous reviewers for critically reading earlier versions of the article. This work was supported by INTAS - 97-857 program.

Literature Cited

Austin, C. R. 1965. *Fertilisation.* Prentice-Hall, Englewood Cliffs, New Jersey.

Babkov, A. I. 1982. Brief hydrological characteristics of the Chupa Inlet of the White Sea. Pp. 3–16 in *Explorations of the Fauna of the Seas* **27.** [In Russian] O. A. Scarlato, ed. Zool. Inst. Acad. Sci. Press, Leningrad.

Babkov, A. I. 1984. About the principles of the hydrological seasons. Pp. 84–88 in *Explorations of the Fauna of the Seas.* **31 (39).** [In Russian] O. A. Scarlato ed. Nauka, Leningrad.

Babkov, A. I., and A. N. Golikov. 1984. *Hydrobiocomplexes of the White Sea.* [In Russian] Zool. Inst. Acad. Sci., Leningrad.

Barthel, D. 1986. On the ecophysiology of the sponge *Halichondria panicea* in Kiel Bight. I. Substrate specificity, growth and reproduction. *Mar. Biol.* **32:** 291–298.

Barthel, D. 1988. On the ecophysiology of the sponge *Halichondria panicea* in Kiel Bight. II. Biomass, production, energy budget and integration in environmental processes. *Mar. Ecol.* **43:** 87–93.

Chen, W. T. 1976. Reproduction and speciation in *Halisarca.* Pp. 113–139 in *Aspects of Sponge Biology,* F. M. Harrison and R. R. Cowden, eds. Academic Press, New York.

Efremova, S. M., A. V. Ereskovsky, and D. B. Tokina. 1987a. Gametogenesis in sponges of the family Myxillidae from the White Sea. 1. Oogenesis in *Myxilla incrustans* and *Iophon piceus* (Demospongiae, Poecilosclerida). *Ontogenez* **18:** 257–262.

Efremova, S. M., A. V. Ereskovsky, and D. B. Tokina. 1987b. Gametogenesis in sponges of the family Myxillidae from the White Sea. 2. Spermatogenesis in *Myxilla incrustans* and *Iophon piceus* (Demospongiae, Poecilosclerida). *Ontogenez* **18:** 263–268.

Elvin, D. W. 1976. Seasonal growth and reproduction of an intertidal sponge *Haliclona permollis* (Bowerbank). *Biol. Bull.* **151:** 108–125.

Ereskovsky, A. V. 1986. Larval formation in *Iophon piceus* (Demospongiae, Poecilosclerida). [In Russian] *Zool. Zh.* **65:** 1614–1621.

Ereskovsky, A. V. 1993. Addition to the fauna of sponges (Porifera) of the White Sea. [In Russian] *Vestn. St.-Petersbg. Univ. Ser. #3.* **2** (10):3–12.

Ereskovsky, A. V. 1994a. Materials to the faunistic study of the White Sea and Barents Sea sponges. 2. Biogeographical and comparative-faunistic analysis. [In Russian] *Vestn. St.-Petersbg. Univ. Ser. #3.* **1** (3):13–26.

Ereskovsky, A. V. 1994b. Materials to the faunistic study of the White Sea and Barents Sea sponges. 3. Dependence of sponge distribution on the temperature and salinity. [In Russian] *Vestn. St.-Petersbg. Univ. Ser. 3.* **3** (17):3–10.

Ereskovsky, A. V. 1995a. Materials to the faunistic study of the White Sea and Barents Sea sponges. 4. Vertical distribution. [In Russian] *Vestn. St.-Petersbg. Univ. Ser. 3.* **1** (3): 3–17.

Ereskovsky, A. V. 1995b. Materials to the faunistic study of the White Sea and Barents Sea sponges 5. Quantitative distribution. *Berliner Geowiss. Abh.* E **16:** 709–714.

Ereskovsky, A. V. 1995c. Materials to the faunistic study of the White Sea and Barents Sea sponges 6. The origin of the White and Barents seas sponge faunas. *Berliner Geowiss. Abh.* E **16:** 715–730.

Ereskovsky, A. V., and E. L. Gonobobleva. 1999. New data on embryonic development of *Halisarca dujardini* Johnston, 1842 (Demospongiae: Halisarcida). *Zoosystema.* In press.

Ereskovsky, A. V., and G. P. Korotkova. 1997. The reasons of sponge sexual morphogenesis peculiarities. Modern problems of Poriferan biology. A. Ereskovsky, H. Keupp, and R. Kohring, eds. *Berliner Geowiss. Abh.* Reihe E. Bd. **20:** 25–33.

Fell, P. E. 1976. The reproduction of *Haliclona loosanoffi* and its apparent relationship to water temperature. *Biol. Bull.* **150:** 200–210.

Fell, P. E., and W. F. Jacob. 1979. Reproduction and development of *Halichondria* sp. in the Mystic Estuary, Connecticut. *Biol. Bull.* **156:** 62–75.

Fell, P. E., and K. B. Lewandrowski. 1981. Population dynamics of the estuarine sponge, *Halichondria* sp., within a New England eelgrass community. *J. Exp. Mar. Biol. Ecol.* **55:** 49–63.

Fell, P. E., K. B. Lewandrowski, and M. Lovice. 1979. Postlarval reproduction and reproductive strategy in *Haliclona loosanoffi* and *Halichondria* sp. Pp. 113–122 in *Biologie des Spongiaires.* C. Levi and N. Boury-Esnault, eds. CNRS, Paris.

Fromont, J. 1994. Reproductive development and timing of tropical sponges (Order Haplosclerida) from the Great Barrier Reef, Australia. *Coral Reefs* **13:** 127–133.

Fromont, J., and P. R. Bergquist. 1994. Reproductive biology of three sponges species of the genus *Xestospongia* (Porifera: Demospongiae: Petrosiida) from the Great Barrier Reef. *Coral Reefs* **13:** 119–126.

Golikov, A. N., and O. A. Scarlato. 1972. Method for indirectly defining optimum temperatures of inhabitancy for marine cold blooded animals. *Mar. Biol.* **20:** 1–5.

Ivanova, L. V. 1978. Morphogenetic processes and seasonal changes of the anatomical and tissue organisation of the Barents Sea sponges *Halichondria panicea* (Pallas). [In Russian] *Arch. Anat. Histol. Embryol.* **10:** 62–71.

Kasyanov, V. L. 1989. *Reproductive Strategy of Marine Bivalve Molluscs and Echinoderms.* [In Russian] Nauka, Leningrad.

Kaufman, Z. S. 1977. *Peculiarities of Sexual Cycles of White Sea Invertebrates.* [In Russian] Nauka, Leningrad.

Kinne, O. 1963. The effects of the temperature and salinity of marine and brackish water animals. I. Temperature. *Oceanogr. Mar. Biol. Annu. Rev.* **1:** 301–340.

Korotkova, G. P. 1988. The integrative mechanisms and morphogenesis (to the problem of evolution of ontogenesis). [In Russian] *Zh. Obshch. Biol.* **69:** 464–475.

Korotkova, G. P., and A. V. Ereskovsky. 1984. Peculiarities of the egg cleavage of White Sea Sponge *Halisarca dujardini* Johnston. [In Russian] *Vestn. Leningr. Univ. Biol.* **21:** 36–42.

Korotkova, G. P., and N. O. Ermolina. 1982. Period of development of the larvae *Halisarca dujardini* (Demospongia). [In Russian] *Zool. Zh.* **61** (10): 1472–1479.

Lévi, C. 1956. Étude de Halisarca de Roscoff. Embriologie et systematique des demosponges. *Arch. Zool. Exp. Gen.* **93:** 1–181.

Lewandrowski, K. B., and P. E. Fell. 1981. Sequential reproduction by different types of specimens of the estuarine sponge, *Halichondria* sp. with an emphasis on reproduction of postlarval specimens. *Int. J. Invertebr. Reprod.* **3:** 227–236.

Mileikovsky, S. A. 1981. *Reproductive Ecology of Marine Benthos.* [In Russian] Nauka, Moscow.

Pianka, E. R. 1978. *Evolutionary Ecology.* Harper and Row, New York.

Propp, M. V. 1971. *The Ecology of the Coastal Associations of the Murman Seaboard of the Barents Sea.* [In Russian] Nauka, Leningrad.

Reiswig, H. M. 1973. Population dynamics of three Jamaican Demospongiae. *Bull. Mar. Sci.* **23:** 191–226.

Simpson, T. L., and J. J. Gilbert. 1974. Gemmulation, gemmule hatching and sexual reproduction in fresh-water sponges. I. The life cycle of *Spongilla lacustris* and *Tubella pennsylvanica. Trans. Am. Microsc. Soc.* **92:** 422–433.

Ushakov, B. P. 1989. *Cell Physiology and the Problem of Species in Poikilotherms.* [In Russian] Nauka, Leningrad.

White, U., and D. Barthel. 1994. Reproductive cycle and oogenesis of *Halichondria panicea* (Pallas) in Kiel Bight. Pp. 297–305 in *Sponges in Time and Space.* R. van Soest, T. van Kempen, and J. Braekman, eds. Balkema, Rotterdam.

Reference: *Biol. Bull.* **198:** 88–93. (February 2000)

Walking *Versus* Breathing: Mechanical Differentiation of Sea Urchin Podia Corresponds to Functional Specialization

HOLLY A. LEDDY[1],* AND AMY S. JOHNSON

Biology Department, Bowdoin College, Brunswick, Maine 04011

Abstract. The podia of sea urchins function in locomotion, adhesion, feeding, and respiration; but different podia on a single urchin are often specialized to one or more of these tasks. We examined the morphology and material properties of podia of the green sea urchin, *Strongylocentrotus droebachiensis,* to determine whether, despite apparent similarities, they achieve functional specialization along the oral-aboral axis through the differentiation of distinct mechanical properties. We found that oral podia, which are used primarily for locomotion and adhesion, are stronger and thicker than aboral podia, which are used primarily for capturing drift material and as a respiratory surface. The functional role of ambital podia is more ambiguous; however, they are longer and are extended at a lower strain rate than other podial types. They are also stronger and stiffer than aboral podia. In addition, all podia become stronger and stiffer when extended at faster strain rates, in some cases by nearly an order of magnitude for an order of magnitude change in strain rate. This strain-rate dependence implies that resistance to rapid loading such as that imposed by waves is high compared to resistance to slower, self-imposed loads. Thus, the serially arranged podia of *S. droebachiensis* are functionally specialized along an oral-aboral axis by differences in their morphology and mechanical properties.

Introduction

The surface of the green sea urchin, *Strongylocentrotus droebachiensis,* like that of all urchins, is covered with five double rows of podia, and these structures are essentially hollow tubes with terminal suckers. The wall of each podium consists of three main layers: an outer epithelium, a middle connective tissue layer, and an inner muscular layer (Florey and Cahill, 1977). Internally, the podium is connected to an ampulla, a sac-like structure that antagonizes podial movement. Contraction of the ampulla forces coelomic fluid into the podium, and thus extends it. Conversely, contraction of the longitudinal muscles shortens the podium and forces coelomic fluid back into the ampulla. All of the podia on *S. droebachiensis* share these characteristics, and all of them are similarly shaped. They exemplify the typical echinoid locomotory podia.

However, podia perform a variety of functions besides locomotion, including adhesion, feeding, shading, sensing, and respiration, and many podia are specialized for one of these functions. Podia in a particular position along the oral-aboral axis tend to perform a particular function and often exhibit morphological features that enhance performance of that function. For example, *Arbacia punctulata* has morphologically differentiated podia, reflecting the separation of respiratory, sensory, and locomotory functions. The aboral podia lack suckers and their larger surface area and thinner walls enhance respiration, the ambital podia are long with minimal suckers to allow sensation in the region around the urchin, and the oral podia are suckered to facilitate locomotion (Fenner, 1973).

Although the podia of *S. droebachiensis* lack these gross morphological differences, there may still be a division of labor between the primarily locomotory oral podia and the primarily respiratory aboral podia. We hypothesize that the podia of this species achieve functional specialization through the differentiation of distinct mechanical properties. The goal of this study was to test our hypothesis that the differences in function of oral, aboral, and ambital podia are

---

Received 21 October 1998; accepted 18 November 1999.

[1] Present Address: Zoology Department, Duke University, Durham, NC 27708.

* Author to whom correspondence should be addressed. E-mail: hal2@acpub.duke.edu

correlated with differences in their mechanical characteristics and morphology.

Materials and Methods

Sea urchins, *Stronglyocentrotus droebachiensis,* were collected subtidally near Monhegan Island, Maine. The animals, ranging in diameter from 45.4 mm to 59.7 mm, were maintained in a recirculating seawater aquarium kept at 10°C and fed *Laminaria* sp. every 2 weeks.

Natural extension

Urchins in a glass aquarium were videotaped, and the natural extension rate and initial length of podia were measured from the digitized video images. The length of a podium was measured from the base to the sucker as it was extending, and just as the podium straightened. Extension rate was quantified as the increase in length (in millimeters) per second, and strain rate was quantified as true strain (the natural logarithm of the ratio of final length to initial length) divided by the time to extend.

Mechanical extension

Podia from three locations on the animal were tested separately: aboral podia are those on the upper surface of the urchin; ambital podia are those occupying a narrow circumferential band at the widest diameter of the urchin; and oral podia are those on the lower surface of the urchin. Urchins were placed in an isotonic solution, 7.5% $MgCl_2 \cdot 6H_20$, at 10°C, for 15 min prior to mechanical tests of their podia and were kept in this solution during the tests (Dales, 1970). The $MgCl_2$ solution prevented muscle contraction, so passive material properties could be tested.

All mechanical tests were performed with an Instron material testing device (Model 4301) that loaded materials at specified rates and simultaneously measured force and extension. Force and extension signals were digitized (12-bit) at 1000 Hz and recorded in a computer. The error in the force measurements was $<\pm 0.001$ N. The error in the extension measurements was $<\pm 0.01$ mm. Tests were conducted as follows. An urchin was strapped in place, and a small, spring-loaded clip was attached to the distal end of a podium. The podium was then pulled perpendicular to the surface of the urchin (in the direction of normal extension) at a constant extension rate until it broke.

Fifteen podia—5 aboral, 5 ambital, and 5 oral—were tested on each urchin at a given extension rate. Each of five urchins were tested at three extension rates: 0.167 mm/s (minimum natural extension rate), 0.708 mm/s (halfway between the mean and the minimum natural extension rates), and 1.25 mm/s (mean natural extension rate). Another set of podia from one urchin was also tested at 3.45 mm/s (maximum natural extension rate).

In comparing lengths of different podial types and calculating strain and strain rate, initial length of the podium (measured between the body wall and the end of the clip) was defined as the point at which force started to increase (above 0.001 N) during the breaking tests, thus indicating that the podium has just started to stretch (Fig. 1a). Nominal stress on a podium was calculated by dividing the force applied by the mean tissue cross-sectional area of podia of that type from that urchin. Nominal strength is the nominal stress at which a material breaks. True strain was calculated by taking the natural logarithm of the length divided by the initial length. Stiffness is the slope of a stress-strain curve and was taken from the upper, linear portion of the J-shaped stress-strain curves (Fig. 1b). Strain rate was calculated by dividing the final strain by the time required to get from initial length to breaking.

Tissue cross-sectional area

Relaxed podia from urchins soaked in 7.5% $MgCl_2 \cdot 6H_20$ were cut off at the base. Although this technique depressurized the podia, it allowed us to compare the three types in as similar a state as possible. The exterior and lumenal diameters of the podia were measured halfway between the base and the sucker with an ocular micrometer (±0.01 mm) on a light microscope. These diameters were used to calculate the total and lumenal cross-sectional areas, and the tissue cross-sectional area was found by subtracting the lumenal cross-sectional area from the total cross-sectional area. Five podia of each type were measured on each urchin.

Results

Structure and natural extension

All oral, ambital, and aboral podia had the same gross morphology (suckered tube) and similar diameters (Table 1). The ambital podia, however, were 67% longer than the aboral and oral podia, and the oral podia had thicker walls and a much greater cross-sectional area of tissue than either the aboral or ambital podia (Table 1). Urchins extended their oral, ambital, and aboral podia at the same rate. Nonetheless, because the ambital podia had the greatest initial length, they also had the lowest strain rate (Table 1).

Mechanical extension tests

All the material properties of all podia were positively dependent on strain-rate (Fig. 2, linear regression analysis, all $P < 0.05$, all d.f. = 86). For the three podial types, the slopes of breaking force, nominal strength, and breaking strain with respect to strain rate were not significantly different (ANCOVA, Table 2). For breaking force and nominal strength, the r^2 of the regressions ranged between 0.44 and 0.58; and for breaking strain, the r^2 of the regres-

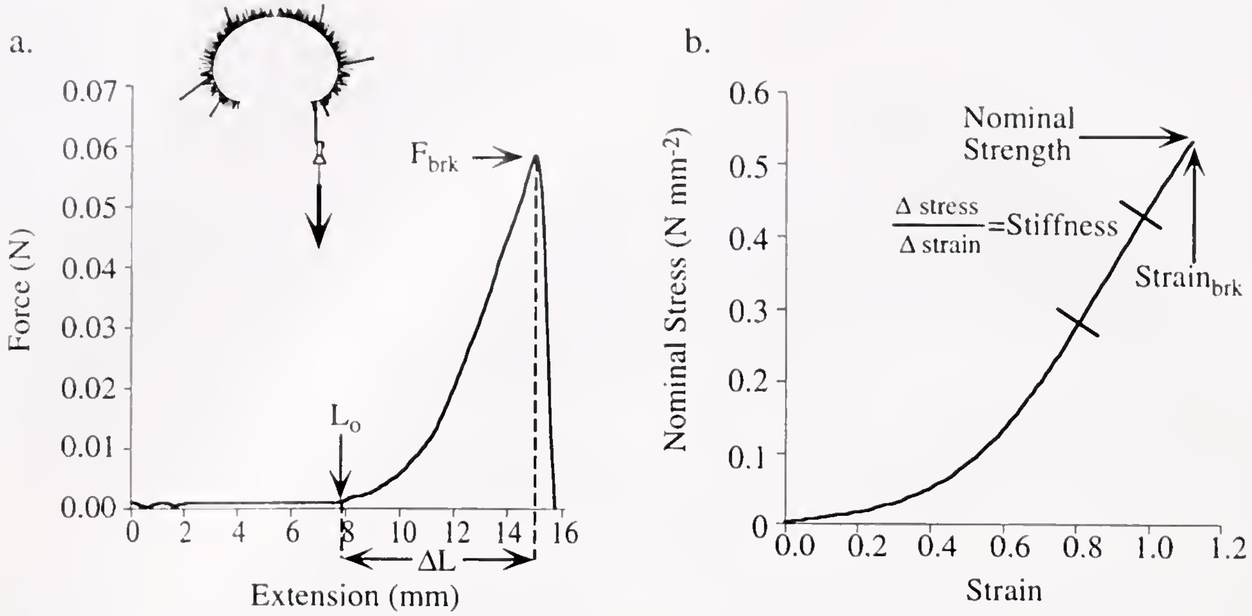

Figure 1. Force-extension (a) and stress-strain (b) curves of an oral podium. L_O, the initial length, is the length at which the podium starts resisting extension; F_{brk} is the force at which the podium breaks, and ΔL is the change in length from L_O to the breaking force. Nominal stress is force divided by cross-sectional area, and strain is the natural logarithm of the length divided by the initial length. Stiffness is the slope of the linear portion of this curve. Nominal strength is the stress at which the podium broke, and Strain_{brk} is the strain at which the podium broke. Inset shows an urchin in the testing setup with one of its oral podia being extended.

sions ranged between 0.09 and 0.13. Thus, although nearly half of the variation in breaking force and nominal strength is explained by variation in strain rate, little of the variation in breaking strain (9%–13%) is explained by variation in strain rate. *A posteriori* comparisons of elevations using Tukey's *Q* (Table 2) revealed that oral podia exhibited higher breaking forces, nominal strengths, and breaking strains than aboral podia; *i.e.*, the oral podia were stronger and stretchier. The ambital podia also exhibited lower breaking forces and breaking strains than did the oral podia, but they were equally strong.

In contrast to the analysis of other material properties, the ANCOVA for nominal stiffness revealed significant differences between slopes (Table 2). In an ANCOVA, when the slopes of the lines are unequal, comparisons of elevations cannot be generalized across all variations in the independent variable (in this case strain rate). Specifically, *a posteriori* comparisons of slopes using Tukey's *Q* revealed that oral podia exhibited less positive strain-rate dependence than did ambital podia. For those comparisons showing no significant difference between slopes, we found that ambital podia were significantly stiffer than aboral podia at all strain

Table 1

Podial morphology and extension rates

	Aboral	Ambital	Oral	ANOVA
				d.f. = 2, 96
Initial length (mm)	7.59 (0.3) a	11.64 (0.5) b	6.26 (0.3) a	$P = 0.0001$
Exterior diameter (mm)	0.67 (0.01)	0.72 (0.01)	0.70 (0.02)	$P = 0.07$
Wall thickness (mm)	0.06 (0.01) a	0.07 (0.01) a	0.11 (0.01) b	$P = 0.0001$
Cross-sect. tissue area (mm^2)	0.12 (0.007) a	0.13 (0.008) a	0.18 (0.009) b	$P = 0.0001$
				d.f. = 2, 89
Extension rate (mm s^{-1})	1.23 (0.16) a	1.30 (0.17) a	1.23 (0.13) a	$P = 0.9$
Strain rate (s^{-1})	0.34 (0.05) a	0.14 (0.03) b	0.45 (0.07) a	$P = 0.0006$

Means (SE) and results of ANOVAs comparing them. Means with different letters are significantly different ($P < 0.05$) by the Fisher PLSD *a posteriori* test.

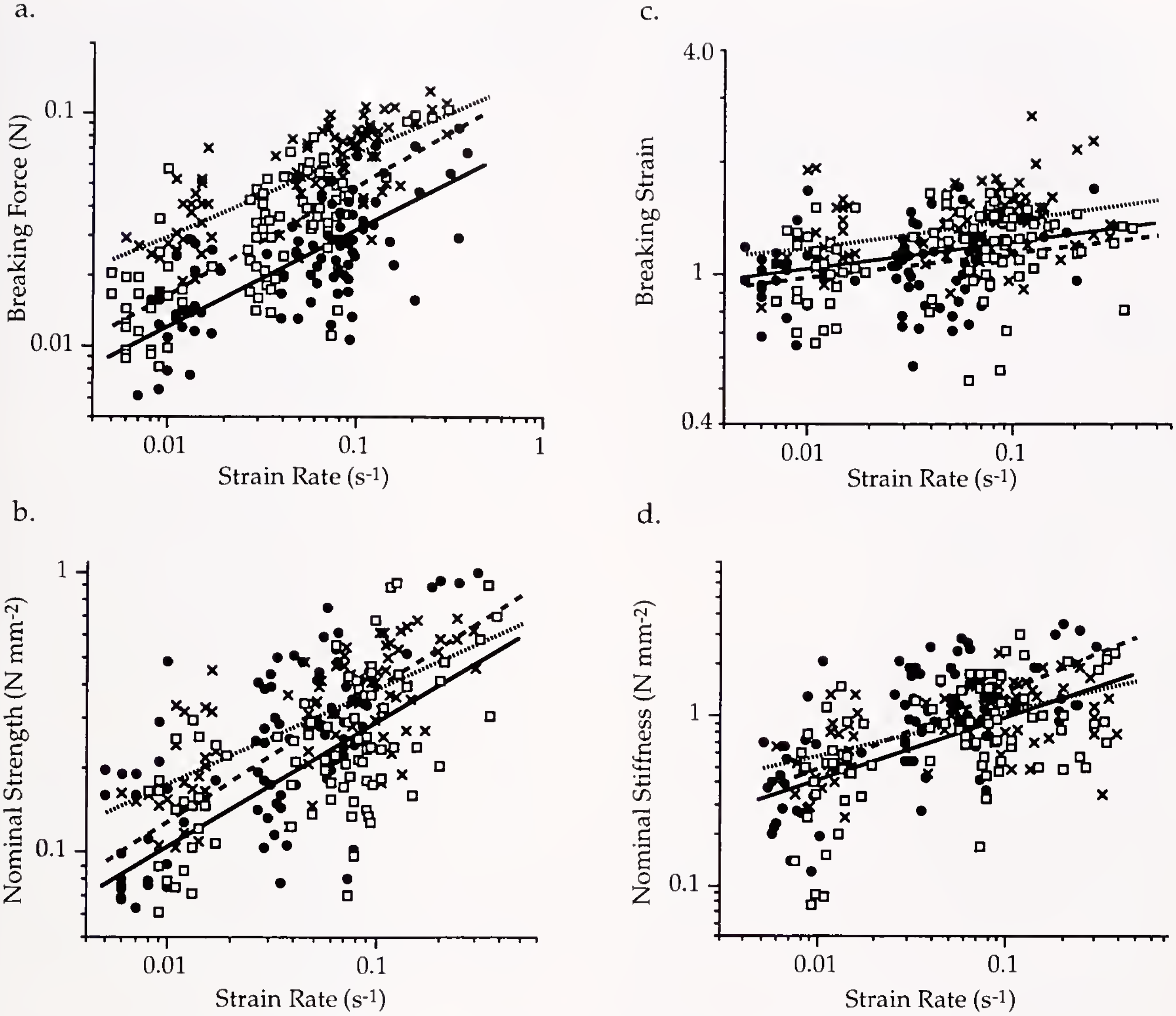

Figure 2. Breaking force (a), nominal strength (b), breaking strain (c), and nominal stiffness (d) are plotted on a log-log scale against strain rate for oral (crosses, dotted line), ambital (filled circles, dashed line), and aboral (open squares, solid line) podia. Lines are least-squares linear regressions. Line slopes and elevations were compared by ANCOVA (Table 2).

rates, and aboral podia were significantly stiffer than oral podia at all strain rates; r^2 values for these regressions ranged from 0.30 to 0.43.

Discussion

Some of the morphological differences found among the podia of other urchins (*e.g.*, presence *versus* absence of suckers) are absent in *Strongylocentrotus droebachiensis*, possibly because the aboral podia, in addition to acting as a respiratory surface, perform other functions that require suckers. For example, drift algae captured by aboral podia may be the primary food source for some urchins (De Ridder and Lawrence, 1982). Furthermore, urchins like *S. droebachiensis*, that live in high-flow environments, may require suckered aboral podia to secure themselves in cracks and to right themselves (Fenner, 1973). Thus, aboral podia, though performing a different set of tasks from oral podia, would still require the same gross morphology.

Although all podia in *S. droebachiensis* do possess suckers, they still exhibit mechanical and morphological differentiation consistent with their location and functional specialization for locomotion or respiration. The greater strength and thicker walls of the oral podia presumably enhance one of their primary functions, which is to resist hydrodynamically generated forces on the urchin (Denny and Gaylord, 1996). Similarly, the thin walls of the aboral

Table 2

Comparison of strain-rate dependent material properties

Material property	Comparison of elevations
(1) Breaking force (N)	Oral > ambital > aboral
(2) Nominal strength (N mm^{-2})	(Oral = ambital) > aboral
(3) Breaking strain	Oral > (ambital = aboral)
(4) Nominal stiffness (N mm^{-2})	Ambital > aboral
	Aboral > oral

Comparisons of elevations for data shown in Figure 2. For material properties (1–3), slopes were not statistically different from each other (ANCOVA, $P > 0.05$, d.f. = 2, 259), so all comparisons of elevations were possible. For nominal stiffness (4), *a posteriori* statistical analysis by Tukey's Q revealed that slopes for ambital and oral podia were significantly different ($P < 0.05$, d.f. = 3, 259), and so that comparison was omitted; all other slopes were statistically similar (Tukey's Q, $P > 0.05$, d.f. = 3, 259). Overall ANCOVA for elevations was always significant (all $P < 0.05$, all d.f. = 2, 261). Symbols indicate results of *a posteriori* statistical analyses by Tukey's Q ($P < 0.05$, d.f. = 3, 259), where "=" means "not significantly different" and ">" means "significantly greater than."

podia, as well as their greater exposure to flow, are well-suited to facilitating gas exchange (Fenner, 1973). The intermediate position of ambital podia combined with their greater length and thinner walls may allow them to function in both oral and aboral capacities; however, a distinct functional role for ambital podia has not yet been determined.

These podial differences arise from differences in both morphology and material properties. Because the oral and ambital podia have equal tissue strength, the greater breaking force of oral podia results solely from a greater cross-sectional area. In contrast, the low breaking force of aboral podia relative to ambital podia is a result of their lower tissue strength, because the cross-sectional areas of these two podial types do not differ from each other. Such differences in tissue strength may be due to fine-scale variation in morphology (*e.g.*, collagen fiber orientation) or tissue composition (*e.g.*, proportion of muscle relative to connective tissue).

All the material properties, especially strength and stiffness, varied positively with strain-rate over the range of natural extension rates observed. In some cases, there was nearly an order of magnitude increase in stiffness or strength for an order of magnitude increase in strain rate. The consequence of this strain-rate dependence to the performance of a given podium is that slow extensions require less energy than do rapid extensions. For a given strain rate, ambital podia require more energy to extend, but because they are extended at lower strain rates, it is unclear whether there are energetic differences in the urchin's own use of different types of podia.

If the strain-rate dependence we quantified extends to the range of strain rates applied by waves, then this mechanical difference would facilitate slower, self-imposed loads but would resist faster, hydrodynamically generated loads. Similarly, Koehl (1977) found that the body wall of sea anemones exhibited greater resistance to rapid loads, such as those imposed by waves, than to slower loads, such as self-imposed forces that function to expand their body.

In a broader context, mechanical differentiation is found in many other structures constructed of serially arranged building blocks in both invertebrates and vertebrates. For example, crinoids reorient passively in flow through variation in the stiffness of the collagen in the joints of their stalk (Wilkie *et al.*, 1993). Also, intervertebral joints in both dolphin (Long *et al.*, 1997) and blue marlin (Long, 1992) exhibit regional mechanical specialization that enhances swimming performance. These diverse structures rely primarily on mechanical differentiation to enhance their performance.

From arthropod segments and appendages to mammalian vertebrae and teeth, this regional specialization of repeating units has arisen many times. Division of labor by regional specialization can increase efficiency by not sacrificing performance to maintain multiple conflicting functions, and serially homologous structures provide a model system in which to examine the evolutionary conflicts between functional design and developmental constraints (Wilson and Hoyle, 1978).

Mechanical specialization can arise from differences in morphology or from differences in material properties of tissues. For example, mechanical specialization of intervertebral joints may result from differences in the morphology of the surrounding vertebrae and from differences in the material properties of the intervertebral disk (Long, 1992). Even when morphological differences have not been detected, mechanical differentiation can play an integral role in enhancing or differentiating performance.

Acknowledgments

This work would not have been possible without the ideas, insight, and comments of O. Ellers and C. K. Johnson. Thanks to E. Archie, Z. Cardon, P. Dickinson, and M. Pratt for their insightful comments on the thesis version of this work and to C. Fuller for urchins. Thanks also to three anonymous reviewers for many helpful comments. This work was supported by a SURDNA Undergraduate Research Foundation Fellowship to H.A.L.

Literature Cited

Dales, R. P. 1970. *Practical Invertebrate Zoology.* University of Washington Press, Seattle.

Denny, M., and B. Gaylord. 1996. Why the urchin lost its spines: hydrodynamic forces and survivorship in three echinoids. *J. Exp. Biol.* **199**(3): 717–729.

De Ridder, C., and J. M. Lawrence. 1982. Food and feeding mechanisms: Echinoidea. Pp. 57–115 in *Echinoderm Nutrition,* M. Jangoux and J. M. Lawrence, eds. A. A. Balkema, Rotterdam.

Fenner, D. H. 1973. The respiratory adaptations of the podia and ampullae of echinoids (Echinodermata). *Biol. Bull.* **145:** 323–339.

Florey, E. A., and M. A. Cahill. 1977. Ultrastructure of sea urchin tube feet. *Cell Tissue Res.* **177:** 195–214.

Koehl, M. A. R. 1977. Mechanical diversity of connective tissue of the body wall of sea anemones. *J. Exp. Biol.* **69:** 107–125.

Long, J. H. Jr. 1992. Stiffness and damping forces in the intervertebral joints of blue marlin (*Makaira nigricans*). *J. Exp. Biol.* **162:** 131–155.

Long, J. H. Jr., D. A. Pabst, W. R. Shepherd, and W. A. McLellan. 1997. Locomotor design of dolphin vertebral columns: bending mechanics and morphology of *Delphinus delphis*. *J. Exp. Biol.* **200:** 65–81.

Wilkie, I. C., R. H. Emson, and C. M. Young. 1993. Smart collagen in sea lilies. *Nature* **366:** 519–520.

Wilson, J. A. and G. Hoyle. 1978. Serially homologous neurons as concomitants of functional specialization. *Nature* **274:** 377–378.

Reference: *Biol. Bull.* 198: 94–100. (February 2000)

Egg Brooding by Deep-Sea Octopuses in the North Pacific Ocean

JANET R. VOIGHT[1,*] AND ANTHONY J. GREHAN[2]

[1] *Department of Zoology, Field Museum of Natural History, Roosevelt Rd. at Lake Shore Dr., Chicago, Illinois 60605; and* [2] *Martin Ryan Marine Science Institute, National University of Ireland, Galway, Ireland*

Abstract. Videotapes made from the submersible *Alvin* on Baby Bare, a 2600-m-deep North Pacific basalt outcrop, and at two other deep-sea localities document that octopuses of the genera *Graneledone* and *Benthoctopus* attach their eggs to hard substrate and apparently brood them through development. The behavior of brooding females was generally similar to that of shallow-water octopuses, but the genera showed apparent differences. In addition to the high density of brooding females observed at Baby Bare, which may relate to the increased availability of exposed hard substrates for egg attachment and of prey, females are suggested to increasingly associate with hard substrates as they mature. The biology of Baby Bare may seem unduly unique because the outcrop is isolated on a sedimented plain and is among the few exposures of hard substrate other than hydrothermal vents that have been explored by submersible. On the sediment-covered ocean floor, the availability of hard substrate may strongly affect the distribution of brooding octopuses. The size and shape of boreholes in 19 of over 400 thyasirid clam shells collected from Baby Bare support the hypothesis that octopuses had preyed upon the clams.

Introduction

Videotapes filmed from submersibles have documented the behavior of deep-sea squids (Moiseev, 1991; Vecchione and Roper, 1991; Roper and Vecchione, 1997) and cirrate octopods (Vecchione and Young, 1997; Villanueva *et al.*, 1997). However, such reports have provided virtually no new information on the benthic octopuses that form the Octopodidae, despite the occurrence of nine recognized genera at depths greater than 1000 m (Voss, 1988a; González *et al.*, 1998). Laboratory studies do not compensate for the near-absence of *in situ* observations of deep-sea octopuses. *Bathypolypus arcticus* is the only species reported from below 1000 m that has survived trawling to be successfully maintained in the laboratory (O'Dor and Macalaster, 1983; Wood *et al.*, 1998). This species, however, is unusual among deep-sea octopuses (Voss, 1988a) in occurring at depths as shallow as 75 m at high latitudes (Wood *et al.*, 1998).

Trawl-collected octopodid specimens generally provide sparse information on behaviors such as maternal care or on the type of prey taken. Because we have had to rely almost exclusively on specimens collected in trawls, our knowledge of these fundamental aspects of deep-sea octopus biology is minimal. The rare discovery of isolated octopodid eggs in a trawl haul has required that generic identification be inferred from developing embryos (O'Shea and Kubodera, 1996), despite our scant knowledge of embryonic development in deep-sea octopodids. Although deep-sea octopuses are presumably predators, as are other cephalopods, the prey taken by hatchlings and adults remains generally unknown (but for exceptions see O'Dor and Macalaster, 1983; Nixon, 1987).

This paper reports submersible observations that document egg attachment and brooding by members of two octopodid genera, *Graneledone* and *Benthoctopus*, at depths greater than 2000 m in the North Pacific Ocean. Documentation of maternal egg care among deep-sea octopuses confirms the presence of this basic behavior in diverse members of the Octopodidae. The very high densities of brooding females discovered on the base and sides of Baby Bare, an 80-m-high basalt outcrop, suggest that substrate suitable for egg attachment may be extremely limiting. We also provide

---

Received 17 May 1999; accepted 25 October 1999

* To whom correspondence should be addressed. E-mail: Jvoight@fmnh.org

evidence to suggest that small octopuses drill the shells of clams on which they feed.

Materials and Methods

In situ *observations*

Videotapes made by the Deep Submergence Vehicle *Alvin* during dives in the North Pacific Ocean at Baby Bare outcrop (47° 42.64'N, 127° 47.15'W; 2640 m) in Cascadia Basin in August 1995, October 1997, and July 1998 form the bulk of the observations reported here. Additional data derive from an ROV *Jason* dive at Baby Bare in 1999, from Alvin dive videotapes taken in July 1994 (R. A. Lutz, pers. comm.) at Middle Valley (48° 27'N, 128° 42'W; 2400–2430 m), a sedimented hydrothermal vent described by Juniper *et al.* (1992), and from two still photographs shot from *Alvin* near the Oregon Subduction Zone in 1984 (J. C. Moore, pers. comm.).

Becker and Wheat (1995) and Mottl *et al.* (1995, 1998) describe the geology of Baby Bare. The extinct volcano is estimated to rise 300 m from a buried ridge crest, but extends only 70 m above the heavily sedimented, 2592-m-deep seafloor. Baby Bare is one of the few volcanic edifices that penetrate the nearly continuous layer of sediment that fills the northern Cascadia Basin between Juan de Fuca Ridge and the continent (Davis *et al.*, 1992a). Basalt exposures on steep, sediment-free slopes of Baby Bare occupy much less than 0.1 km^2 in total area (Mottl *et al.*, 1998). The Baby Bare fauna differs strikingly from that of the surrounding abyssal plain (Grehan *et al.*, 1995; Mottl *et al.*, 1998). Its abundant sponges and echinoderms are typical of the hard-substrate, filter-feeder–dominated seamount fauna, the composition and density of which may reflect the influence of the outcrop on local currents (*e.g.*, Tyler and Zibrowius, 1992; Genin *et al.*, 1992; Rogers, 1994). The fish fauna includes zoarcids, skates, and macrourids. In addition, at Baby Bare, thyasirid clams form locally dense aggregations near springs with water temperatures up to 25°C (Grehan *et al.*, 1995; Mottl *et al.*, 1998). Temperatures were recorded with the *Alvin* and *SUAVE* (SUbmersible System Used to Assess Vented Emissions) heat probes (Massoth *et al.*, 1995).

Octopuses were tentatively identified as members of the genus *Graneledone* if the videotape showed them to have many dorsal skin warts that are especially prominent over the eyes and arm suckers arranged in a single row. Individuals with skin warts in which the arm suckers formed a zig-zag row were also assigned to this genus. Octopuses with smooth skin and two sucker rows (in which the suckers were conspicuously smaller relative to the size of the octopus than in individuals referred to *Graneledone*) were assigned to the genus *Benthoctopus*. Internal examination of 10 specimens collected from Baby Bare, Middle Valley, and Axial Volcano (46°N 130°W, 1459 m) that were identified on videotapes as members of *Graneledone* allowed this generic determination to be tested. These *Alvin*-collected specimens were compared to other North Pacific octopus specimens in the collections of the Field Museum of Natural History, the California Academy of Sciences, and the University of Miami Marine Laboratory, including seven paratypes of *G. pacifica* Voss and Pearcy, 1990.

The specimens lack an ink sac and crop, have irregular radulae and small posterior salivary glands, and the dorsal skin of their mantles and heads bears cartilaginous tubercles that are diagnostic of the genus *Graneledone* (Voss, 1988b). The zig-zag arrangement of arm suckers on some videotaped octopuses was attributed to the presence of more suckers that could be arranged in a strictly single row on arms of that length (Voight, 1993). The species determination is complicated by the possible synonymy of *Graneledone boreopacifica* Nesis, 1982, and *G. pacifica* Voss and Pearcy, 1990. Comparisons of the skin texture and sucker and gill counts of these specimens with seven paratypes of *G. pacifica* and extended study of Northeast Pacific specimens of the genus suggest that more than one species exists, probably segregated by depth (Voight, 1998). Because the 1350-m depth of the type locality of *G. boreopacifica* Nesis, 1982, contrasts sharply with the 2706-m depth of the type locality of *G. pacifica* Voss and Pearcy, 1990, the specimens from Baby Bare and Middle Valley are tentatively assigned to Voss and Pearcy's species, and the one from Axial to Nesis' species. The reproductive condition of four submersible-collected female specimens, including the female tentatively assigned to *G. boreopacifica*, is also reported.

Because no specimens that were identified from the videotapes as members of the genus *Benthoctopus* were collected, their identification remains unconfirmed. Although they might pertain to the genus *Bathypolypus*, the smooth dorsal mantle and the distinctly reversed countershaded coloration of these octopuses suggest otherwise. The apparent absence of octopodid genera other than *Graneledone* and *Benthoctopus* from the deep Northeast Pacific Ocean (Voss, 1988a; Voss and Pearcy, 1990) and the fact that the videotaped octopodids consistently show characters shared with those of specimens of *Benthoctopus* trawled from depths of over 2500 m off the Oregon margin (Voight, unpubl. data) strongly support this generic assignment.

Clam shell collections

Biological collections made at Baby Bare during the three cruises included sediment scoops containing thyasirid clams and clam shells. The hypothesis that octopuses preyed on the clams (Mottl *et al.*, 1998) was tested by comparing boreholes made by shallow-water octopuses (Nixon *et al.*, 1980; Nixon and Maconnachie, 1988) to those discovered in clam shells from Baby Bare. Features characteristic of octopus boreholes are the round or ovoid shape, the beveled cross-section with an external orifice larger than the internal orifice that penetrates the inner shell surface, and the location in or close to the myostracum (Nixon and Maconnachie, 1988). To test whether boring predators preferentially preyed on clams of a given size, the length of each valve collected in 1997 was measured, and median lengths of intact and bored valves were compared. The proportion of bored clam shells was calculated for each year's collection and compared across collections.

Results

In situ *observations*

DSV *Alvin* videotapes made both at Baby Bare and at Middle Valley show unusually high densities of octopuses, as Mottl *et al.* (1998) and Juniper *et al.* (1992) noted. Although octopuses are rarely seen during most submersible dives, 28 octopuses were videotaped during 11 dives at Baby Bare in 1995. One 3-min length of videotape from a 1997 dive shows 9 different octopuses, and 10 octopuses were videotaped by *Jason* in one pass from the outcrop's base to its summit. Observers at Middle Valley report that three or four octopuses could be seen at one time from the submersible, although rarely are such densities recorded on the videotape.

Both at Baby Bare and Middle Valley, octopuses of the genus *Graneledone* were seen moving across open, sedimented areas and sitting with the proximal half of their arms in contact with rocks. All six octopuses collected from open sedimented areas at Middle Valley were fully mature males with several spermatophores. The two nonbrooding female specimens were collected from hard substrate. The female specimen from Middle Valley was collected from beneath an Ocean Drilling Program (ODP) reentry cone that had been installed at Hole 858G in Dead Dog vent field in 1991 (see Davis *et al.*, 1992b: fig. 1). The female from Axial Volcano was collected from among basalt exposures on the caldera wall. Neither octopus was videotaped prior to collection.

Octopuses of *Graneledone* that were videotaped while positioned with their oral, sucker-carrying surface against rocks, or against rock crevices were, when viewed with sufficient detail, found to be brooding eggs attached to almost vertical rock faces or to rock overhangs (Fig. 1). Eggs were frequently only glimpsed above the female's dorsal web sector before they were covered by her web and arms. The eggs were attached to basalt, the only available hard substrate at Baby Bare. At Middle Valley, a brooding female *Graneledone* had attached her eggs to hydrothermally altered and lithified sediment (R. A. Zierenberg, pers. comm.) which also supported anemones, sponges, and ophiuroids, although these were absent from the immediate area of the eggs. A female *Graneledone* was photographed at the Oregon Subduction Zone on a large rock outcrop, roughly 1 km from the nearest cold seep (J. C. Moore, pers. comm.); although eggs can be seen near her upper web, the rock cannot be identified. Videotape from Mama Bare, another small basalt outcrop, also shows octopuses brooding eggs, although on the single dive there, fewer octopuses were seen than at Baby Bare.

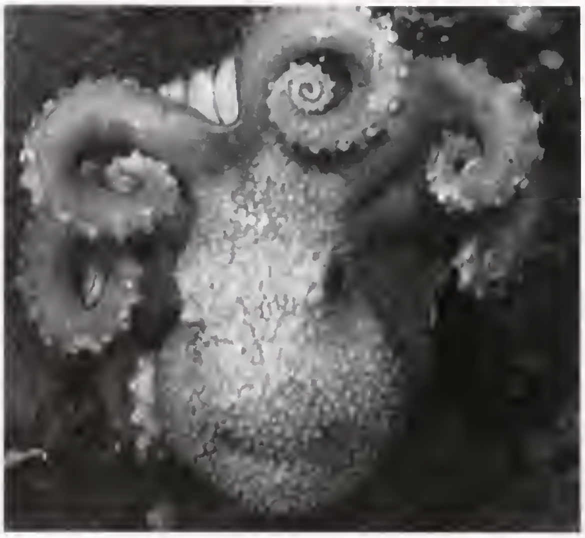

Figure 1. Still from a videotape of a female of *Graneledone pacifica* brooding eggs on a rock exposure at Baby Bare outcrop, *Alvin* Dive 2974, August 1995. Note the heavily textured dorsal mantle, prominent supraocular cirri, and comparatively few arm suckers. Eggs are seen suspended from the rock just above and to the left of the female's web.

A single rock outcrop was visited in both 1998 and 1999. A female of *Graneledone* was present at the outcrop in both years. In 1999, her appearance was consistent with impending senescence: her posture indicated a deterioration of muscle tone, with her arms limply coiled; her skin was mottled and appeared to be flaccid. Unfortunately her clutch could not be examined.

Two eggs collected with the brooding female of *Graneledone* in 1995 (egg length = 25 mm; width = 12.25 mm) contained partially developed embryos. The embryos measured 9.5 mm in mantle length, with 7-mm-long arms that carried up to 30 suckers each. The similarity of these embryos to those reported and illustrated by O'Shea and Kubodera (1996) supports their assignment of the eggs and embryos to *Graneledone*. Embryonic structures were not yet visible in the seven eggs collected with the brooding female in 1998 (size range: 22.0 mm long by 11.2 mm wide to 24.8 by 12.2 mm).

Water temperatures near the brooding sites were recorded during two dives in 1995. The ambient temperature measured with the *SUAVE* probe was 1.83°C (G. J. Massoth, pers. comm.). At the base of a 1.5 m high basalt outcrop on which an octopus brooded eggs, the *Alvin* heat probe recorded a temperature of 3.0°C; within the crevice where the eggs were attached, the temperature was 1.83°C. Tempera-

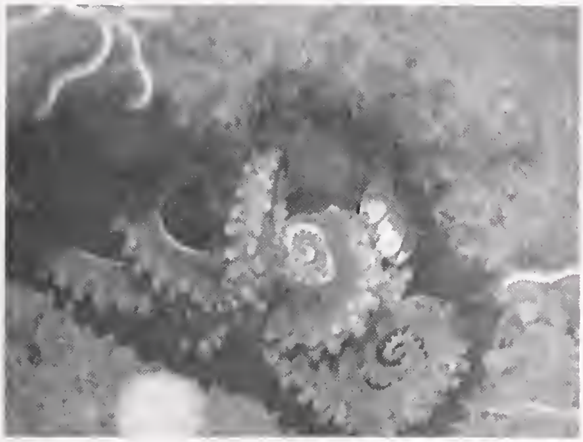

Figure 2. Still from a videotape of a female of *Benthoctopus* brooding eggs inside a rock overhang, *Alvin* dive 2974, August 13, 1995. Note the double rows of arm suckers, the dark ventral web surface, and the much brighter dorsal mantle surface. The oral surface of the animal is positioned away from the egg mass and the tear-shaped eggs are suspended from the roof of the rock crevice.

ture probes inserted into the sediment recorded temperatures as high as 4.5°C, but the water temperature just above the sediments was 1.84°C, only slightly elevated over ambient (G. J. Massoth, pers. comm.).

Brooding individuals of *Benthoctopus* were seen much less often than were those of *Graneledone*. Most members of *Benthoctopus* were observed partially hidden under ledges or in narrow crevices (Fig. 2), on one occasion within 5 m of a congener. Once in both 1995 and 1997, females of both genera brooded eggs in opposite ends of the same cleft in the rock face at Baby Bare. The sequence in which the females moved into the cleft could not be estimated because females of *Benthoctopus* were so deep in the recess of the rock that the developmental stage of their eggs could not be determined for comparison to those of *Graneledone*. Their proximity (within an arm's length) allowed the animals to be compared in size: females of *Benthoctopus* seen brooding at these depths of from 2400 to 2600 m were generally one-half to one-third the size of those of *Graneledone*. This differences in size and in how females were positioned—those of *Benthoctopus* were most often under rock overhangs or inside crevices while those of *Graneledone* were most often positioned against rocks—are likely to have strongly biased the observations toward members of *Graneledone* (*e.g.*, 16 of 20 observations of octopuses in which the genus could be identified in 1995).

Videotapes show that in both genera the eggs are individually attached to the rock by short stalks that rapidly broaden to merge with the large chorion balloon of the egg. This outer egg membrane (chorion) is transparent, allowing the developing embryos to be seen. The developmental stages observed ranged from apparently undeveloped eggs to embryos in the second inversion (terminology of Boletzky, 1987). In clutches guarded by members of *Graneledone*, each egg stalk could be seen to be attached to the rock by dark green cement similar to that reported for *Bathypolypus arcticus* (O'Dor and Macalaster, 1983). Regardless of the egg's stage of development, the color of the cement appeared to be the same. The number of eggs in any given clutch could not be determined.

Differences between the genera, in addition to the morphological characters used to distinguish them, were apparent. Octopuses of *Graneledone* behaved sluggishly, often showing virtually no response to the approach of the submersible. In contrast, individuals of *Benthoctopus* often jetted into the water column, sometimes toward the approaching submersible. While brooding eggs, octopuses of *Graneledone* positioned themselves with their dorsal surface away from the eggs and their oral surface nearest them. In contrast, octopuses of *Benthoctopus* positioned themselves with their oral, sucker-carrying surface facing away from their eggs and their mantle tip pointed toward them. Although observations are few, the eggs brooded by octopuses of *Graneledone* appeared to be more sausage-shaped and the eggs of *Benthoctopus* more teardrop-shaped.

The reproductive organs of all female specimens of *Graneledone* that were collected from hard substrate by submersible were enlarged, and the ovarian eggs of each showed some degree of enlargement (Table 1). The female brooding early-stage eggs collected from Baby Bare in 1998 had the smallest ovarian eggs. The oviducal glands of brooding females were smaller than those of nonbrooding females collected from hard substrate. No prey were apparent in the digestive systems of either brooding female, although the large mass of amber-colored oil in the proximal intestine of the female collected from Baby Bare in 1995 suggested a partially digested egg.

Clam shell collections

Small boreholes were discovered in between 3.8% and 5.1% of the thyasirid clam shells (tentatively identified as *Axinus* sp., near *A. grandis*, E. Southward, pers. comm.) collected (Table 2). Round or slightly oval boreholes were located most often on or near the umbo of the valves. Bored and intact valves do not appear to significantly differ in size (bored: median = 21.75 mm; intact median = 18.75 mm), nor are bored shells biased in handedness (right $n = 8$; left $n = 6$). The outer diameters of the boreholes range from 0.75 to 2 mm, and their inner diameters from 0.4 to 1.5 mm.

Discussion

In situ *observations*

The deep-sea octopus *Graneledone pacifica* and at least one species of *Benthoctopus* attach their eggs to hard substrate and apparently brood them during development. The high densities of brooding octopuses at depths below 2600 m at Baby Bare outcrop and Middle Valley hydrothermal vent field suggest

Table 1

Reported from preserved female specimens collected from hard substrates are mantle lengths in mm, the number and size of ovarian eggs and oviducal gland size and color

Specimen locality & Catalog number	Mantle length (mm)	Ovarian eggs Size (mm)** & appearance	Oviducal gland Size (mm)*: color
Non-Brooding Females			
MV-ODP cone 1994, #FMNH 278063	6.9	15 × 3.8 (*n* = 1), 8.5 × 2.5 (*n* = 65); Most weakly striated	12 × 7.3; Light orange
Axial 1998, #FMNH 282751	136.7	17.5 × 6 (*n* = 72); Filling, striated	14.4 × 9.3; Deep purple
Brooding Females			
Baby Bare 1995	99.3	21.5 × 9 (*n* = 3), 10 × 2.5 (*n* = 63); Flattened	7.4 × 6.2; Light orange
Baby Bare 1998, #FMNH 282750	80.9	8.25 × 2.5 (*n* = 90); Rounded, full	11 × 7.2; Light orange

* Length, measured parallel to the oviduct, by diameter, both in millimeters.

** Length by width, both in millimeters.

that the availability of hard substrate and of potential prey strongly affect octopus distribution in the heavily sedimented deep sea. Boletzky (1994) theorized that maternal care is shared among the Octopodidae, although whether attaching eggs to hard substrates is a synapomorphy of the benthic octopuses remains unknown. A very few shallow-water octopodid species reportedly carry their developing eggs in their web instead of attaching them to substrate (Hochberg *et al.*, 1992), as some bathypelagic octopods are known to do (Young, 1972, 1995). Whether egg attachment is a synapomorphy of the Octopodidae that has undergone reversal in a few species or is a character that has evolved multiple times cannot be assessed because relationships within the family are poorly resolved (Voight, 1997).

The high density of octopuses at Baby Bare and Middle Valley had been linked to the availability of chemosynthetic clams as prey (Juniper *et al.*, 1992; Mottl *et al.*, 1998). The benefits that accrue to hatchling and maturing octopuses from the proximity of potential prey are clear, although mature and brooding individuals of most shallow-water species that have been studied generally reduce their prey intake (Wells and Wells, 1977). Because exposed hard substrate appears to be required for egg attachment, and the floor of the Cascadia Basin is covered by a thick layer of sediment (Davis *et al.*, 1992a; Mottl *et al.*, 1998), the availability in these areas of hard substrate may also attract octopuses.

Table 2

The total number of valves of thyasirid clams collected and examined each year and the number and frequency of bored valves

Year	Total (*n*) dead valves collected	Bored valves	
		n	%
1995	51	2	3.9
1997	272	14	5.1
1998	79	3	3.8
Total	402	19	4.7

The frequency of boreholes does not significantly differ among the collections: $G = 3.68$, df $= 5$, $P > 0.05$.

Individual females may occupy brooding sites for years, as the limited data available indicate that cephalopod eggs develop extremely slowly. Egg size and ambient temperature appear to be the primary determinants of development rates (Boletzky, 1994; B. A. Seibel, pers. comm.). If these factors interact in the same way at temperatures typical of the deep sea—that is, if no compensating mechanism accelerates development at low temperatures—the 25-mm-long eggs of *Graneledone* are calculated to require almost 4 years to develop at ambient temperatures of near 2°C (B. A. Seibel, pers. comm.). Although warm (25°C) springs exist on Baby Bare (Mottl *et al.*, 1998), octopus eggs are brooded in rock crevices on the outcrop's flanks where the temperature is essentially unchanged from ambient. Although eggs attached to the warm basalt could gain heat by conduction, significant heat would probably be lost by radiation as the heat passed through the stalk.

Evidence of limiting substrate has been reported in another deep-water octopodid. The 11- by 6-mm eggs of *Bathypolypus arcticus* develop in about 400 days at temperatures of 5° to 11°C (Wood *et al.*, 1998). Eleven females of this species, and more than 100 eggs, were found enfolded in a single plastic sheet trawled from near Sweden (O'Dor and Macalaster, 1983). We did not observe congeneric females sharing a single substrate at Baby Bare, but females of different genera were seen within an arm's length of each other under the same ledge.

The distribution of maturing females in relation to substrate type appears to shift toward hard substrate. Both of the nonbrooding females collected from hard substrates had enlarged oviducal glands and large ovarian eggs (Table 1), evidence of reproductive maturation (Mangold-Wirz, 1963), but only 1 of the 14 trawl-collected female specimens in the type series (Voss and Pearcy, 1990) shows comparable enlargement of the female reproductive system. The small oviducal glands of brooding females compared to those of females that apparently have not yet spawned (Table 1) may be due to postspawning resorption. The small ovarian eggs in an "obviously exhausted" female of *Graneledone boreopacifica* (Nesis, 1989) may reflect this pattern. The contrast between the reproductive maturity of females collected from hard substrate and the immaturity of those trawled from soft substrate is startling and suggests that maturing females shift habitat preference to increasingly associate with hard substrate, perhaps to secure a brooding site. If increased prey availability were solely responsible for their advanced reproductive maturity, reproductively mature females would occur at a wide range of sizes rather than being among the largest specimens known in the species.

If hard substrate suitable for egg attachment is limiting in the deep sea, high densities of brooding octopuses should be found at sites other than Baby Bare. Despite decades of study given to seamounts, such groups of octopuses have been unreported. The nature of the research that has been conducted at Baby Bare may make its fauna appear unduly unique. Baby Bare is one of the few non-hydrothermal vent structures in the deep sea that has been examined at depth with submersibles. The trawls, rock dredges, epibenthic sleds, and baited traps and hooks that have been most frequently used to sample seamounts (Wilson and Kaufmann, 1987) have focused on seamount summits rather than their bases. Even submersible explorations have most often focused on seamount summits. For example, the Canadian submersible *Pisces IV* documented the biota of Cobb Seamount at 180 m and above (Parker and Tunnicliffe, 1994), depths that are inaccessible to octopuses living at 2600 m. The bases of other seamounts surrounded by heavily sedimented seafloor must be observed to determine whether Baby Bare is unique in having high densities of brooding octopuses.

Clam shell collections

The similarity of the boreholes on thyasirid clam shells collected at Baby Bare to those drilled by shallow-water octopuses in bivalve shells (Nixon *et al.*, 1980; Nixon and Maconnachie, 1988) support the hypothesis that octopuses prey on the clams by drilling their shells. Two caveats reduce the confidence with which octopuses can be identified as predators of the clams. First, borehole morphology and size vary with prey species rather than octopus size (Nixon and Maconnachie, 1988). Second, because Baby Bare lies beneath the depth at which calcium and aragonite passively dissolve, the boreholes may have been enlarged and their edges obscured by shell dissolution. The edges of the boreholes were poorly defined when viewed with scanning electron microscopy (Voight, unpubl. data). Because, however, the boreholes are generally similar to those made by octopuses and no other deep-sea predators known to bore shells were collected during any cruise to Baby Bare, octopuses are concluded to have bored the clam shells. Whether members of one, the other, or both genera bored the clams cannot be assessed. The octopus (an individual of *Benthoctopus*) reported to have grasped clam shells in three of its arms (Mottl *et al.*, 1998) was not observed to prey on them. The presence of crushed gastropod shells in the gut of the specimen of *Graneledone* from Axial Volcano (Voight, unpubl. data) suggests that these octopuses would not drill the thin shells of these clams.

The comparatively small size (28.5 mm or less) and thin shells of the Baby Bare clams indicate that they were bored by small octopuses. Shallow-water octopuses are known to prey on bivalves either by drilling the shell and injecting toxins through the borehole or by grasping the opposing valves with their suckers and forcing them open, usually without damaging the shells (McQuaid, 1994). Small octopuses are more likely to drill small bivalves than are large octopuses; large octopuses are more likely to force the valves apart, leaving little evidence of predation on the shells (McQuaid, 1994). In addition, greater predation pressure may be exerted by small or young octopuses, which may reach very high densities when clutches hatch, than by fully mature and possibly senescent adults. Nixon's (1987) review suggests that deep-sea octopuses opportunistically take small prey, although no evidence had previously suggested that abyssal octopuses prey on clams.

Further opportunities to directly observe the biology of abyssal octopuses may resolve questions raised by this research, including whether egg-brooding sites used by deep-sea octopuses are typically extremely localized, what is the duration of development of these large eggs, and do deep-sea octopuses drill hard-shelled prey such as clams.

Acknowledgments

M. Mottl, chief scientist of the 1995 cruise (supported by NSF grant OCE-93-14632), collected the brooding female with her eggs and shared videotapes. Co-chief Scientists of the 1997 cruise, K. Becker and H. P. Johnson, and J. Cowen, Chief Scientist in 1998 and 1999, graciously made opportunities available to expand earlier observations and make additional collections. R. A. Lutz provided videotape and octopus specimens from Middle Valley. C. J. Moore provided photographs of the Oregon specimens. Assistance of the *Alvin* and *Jason* groups and the crews of the R/V *Atlantis* and *Thomas G. Thompson* was essential in making observations on which this report is based. We thank R. A. Zierenberg, B. A. Seibel, G. J. Massoth, B. Loetel, R. Collin, N. Becker, F. E. Anderson, and two anonymous reviewers for their help. JRV's participation in the 1997 and 1998 cruises was supported by grants from the West Coast and Polar Regions Undersea Research Center at the University of Alaska Fairbanks and NOAA's National Undersea Research Program; her 1999 cruise participation was supported by Marshall Field Fund of the Department of

Zoology, The Field Museum. AJG's participation in the 1995 cruise was funded by a European collaboration grant awarded to Kim Juniper from the Association of Universities and Colleges of Canada.

Literature Cited

Becker, N. C., and C. G. Wheat. 1995. A geological and geophysical investigation of Baby Bare, a site of active hydrothermal venting on the Eastern Flank of Juan de Fuca Ridge. *EOS Amer. Geophys. Union Abst.* **76:** F419.

Boletzky, S. v. 1987. Embryonic phase. Pp. 5–31 in *Cephalopod Life Cycles*, Vol II P. R. Boyle, ed. Academic Press, London.

Boletzky, S. v. 1994. Embryonic development of cephalopods at low temperatures. *Antarct. Sci.* **6:** 139–142.

Davis, E. E., D. S. Chapman, M. J. Mottl, W. J. Bentkowski, K. Dadey, C. Forster, R. Harris, S. Nagihara, K. Rohr, G. Wheat, and M. Whiticar. 1992a. FlankFlux: an experiment to study the nature of hydrothermal circulation in young oceanic crust. *Can. J. Earth. Sci.* **29:** 925–952.

Davis, E. E., K. Becker, T. Pettigrew, B. Carson, and R. MacDonald. 1992b. CORK: A hydrologic seal and downhole observatory for deep-ocean boreholes. *Proc. Ocean Drilling Prog. Init. Rep.* **139:** 43–53.

Genin, A., C. K. Paull, and W. P. Dillion. 1992. Anomalous abundances of deep-sea fauna on a rocky bottom exposed to strong currents. *Deep-Sea Res.* **39:** 293–302.

Gonzalez, A. F., A. Guerra, S. Pascual, and P. Briand. 1998. *Vulcanoctopus hydrothermalis* gen. et sp. nov. (Mollusca, Cephalopoda): an octopod from a deep-sea hydrothermal vent site. *Cah. Biol. Mar.* **39:** 169–184.

Grehan, A. J., C. Moyer, and S. K. Juniper. 1995. The enhanced biological production on Baby Bare, a basalt escarpment on the Flank of Juan de Fuca Ridge (NE Pacific). *EOS. Amer. Geophys. Union Abst.* **76:** F419.

Hochberg, F. G., M. Nixon, and R. B. Toll. 1992. Order Octopoda. Pp. 213–279 in *"Larval" and Juvenile Cephalopods: A Manual For Their Identification*. M. J. Sweeney, C. F. E. Roper, K. M. Mangold, M. R. Clarke, and S. v. Boletzky, eds. *Smith. Contrib. Zool.* **513.**

Juniper, S. K., V. Tunnicliffe, and E. C. Southward. 1992. Hydrothermal vents in turbidite sediments on a Northeast Pacific spreading centre: organisms and substratum at an ocean drilling site. *Can. J. Zool.* **70:** 1792–1809.

Mangold-Wirz, K. 1963. Biologie des Céphalopodes benthiques et nectoniques de la Mer Catalane. *Vie Milieu Supp.* **13:** 1–285.

Massoth, G. J., E. T. Baker, R. A. Feely, D. A. Butterfield, R. E. Embley, J. E. Lupton, R. E. Thomson, and G. A. Cannon. 1995. Observations of manganese and ison at the CoAxial seafloor eruption site, Juan de Fuca Ridge. *Geophys. Res. Lett.* **22:** 151–154.

McQuaid, C. D. 1994. Feeding behaviour and selection of bivalve prey by *Octopus vulgaris* Cuvier. *J. Exp. Mar. Biol. Ecol.* **177:** 187–202.

Moiseev, S. I. 1991. Observation of the vertical distribution and behavior of nektonic squids using manned submersibles. *Bull. Mar. Sci.* **49:** 446–456.

Mottl, M., G. Wheat, D. Kadko, F. Sansone, G. Massoth, A. Grehan, C. Moyer, E. Davis, B. Baker, R. Feely, M. Lilley, J. Gendron, G. Lebon, E. Olson, S. Walker, and N. Becker. 1995. Warm springs discovered on 3.4 Ma Crust, Baby Bare outcrop, Eastern Flank of Juan de Fuca Ridge. FlankFlux 1995. *EOS, Amer. Geophys. Union Abst.* **76:** F419.

Mottl, M., G. Wheat, E. Baker, N. Becker, E. Davis, R. Feely, A. Grehan, D. Kadko, M. Lilley, G. Massoth, C. Moyer, and F. Sansone. 1998. Warm springs discovered on 3.5 Ma oceanic crust, eastern flank of the Juan de Fuca Ridge. *Geology* **26:** 51–54

Nesis, K. N. 1982. *Brief Diagnoses of the Cephalopod Mollusks of the World Ocean.* Light and Food Industry Publishing House, Moscow. 360 pp. [In Russian]

Nesis, K. N. 1989. Teuthofauna of the Okhotsk Sea, distribution and biology of non-coastal species. *Zool. Zh.* **68:** 19–29

Nixon, M. 1987. Cephalopod diets. Pp 201–220 in *Cephalopod Life Cycles II*. P. R. Boyle, ed. Academic Press, London.

Nixon, M., and E. Maconnachie. 1988. Drilling by *Octopus vulgaris* (Mollusca: Cephalopoda) in the Mediterranean. *J. Zool. (Lond.)* **216:** 687–716.

Nixon, M., E. Maconnachie, and P. G. T. Howell. 1980. The effects on shells of drilling by *Octopus*. *J. Zool. (Lond.)* **191:** 75–88.

O'Dor, R. K., and E. G. Macalaster. 1983. *Bathypolypus arcticus*. Pp. 401–410 in *Cephalopod Life Cycles I*, P. R. Boyle, ed. Academic Press, London.

O'Shea, S., and T. Kubodera. 1996. Eggs and larvae of *Graneledone* sp. (Mollusca, Octopoda) from New Zealand. *Bull. Natl. Sci. Mus. (Tokyo) Series A* **22:** 153–164.

Parker, T., and V. Tunnicliffe. 1994. Dispersal strategies of the biota on an oceanic seamount: implications for ecology and biogeography. *Biol. Bull.* **187:** 336–345.

Rogers, A. D. 1994. The biology of seamounts. *Adv. Mar. Biol.* **30:** 305–350.

Roper, C. F. E., and M. Vecchione. 1997. *In situ* observations test hypotheses of functional morphology in *Mastigoteuthis* (Cephalopoda, Oegopsida). *Vie Milieu* **47:** 87–93.

Tyler, P. A., and H. Zibrowius. 1992. Submersible observations of the invertebrate fauna on the continental slope southwest of Ireland (NE Atlantic Ocean). *Oceanol. Acta* **15:** 211–226.

Vecchione, M., and C. F. E. Roper. 1991. Cephalopods observed from submersibles in the Western North Atlantic. *Bull. Mar. Sci.* **49:** 433–445.

Vecchione, M., and R. E. Young. 1997. Aspects of the functional morphology of cirrate octopods: locomotion and feeding. *Vie Milieu* **47:** 101–110.

Villanueva, L., M. Segonzac, and A. Guerra. 1997. Locomotion modes of deep-sea cirrate octopods (Cephalopoda) based on observations from video recordings on the Mid-Atlantic Ridge. *Mar. Biol.* **129:** 113–122.

Voight, J. R. 1993. The arrangement of suckers on octopodid arms as a continuous character. *Malacologia* **35:** 351–359.

Voight, J. R. 1997. Cladistic analysis of the octopods based on anatomical characters. *J. Molluscan Stud.* **63:** 311–325.

Voight, J. R. 1998. Biological investigations of the genus *Graneledone* from abyssal and bathyal depths of the North Pacific Ocean. P. 344 in *Abstracts: World Congress of Malacology*. Washington, DC., R. Bieler and P. M. Mikkelson, eds. Unitas Malacologica.

Voss, G. L. 1988a. The biogeography of the deep-sea Octopoda. *Malacologia* **29:** 295–307.

Voss, G. L. 1988b. Evolution and phylogenetic relationships of deep-sea octopods (Cirrata and Incirrata). Pp. 253–276 in *The Mollusca, Vol 12. Paleontology and Neontology of Cephalopods*, M. R. Clarke and E. R. Trueman, eds. Academic Press, San Diego.

Voss, G. L., and W. Pearcy. 1990. Deep-water octopods (Mollusca; Cephalopoda) of the Northeastern Pacific. *Proc. Calif. Acad. Sci.* **47:** 47–94.

Wells, M. J., and J. Wells. 1977. Cephalopoda: Octopoda. Pp. 291–336 in *Reproduction of Marine Invertebrates Vol. IV. Molluscs: Gastropods and Cephalopods*. A. C. Giese and J. S. Pearse, eds. Academic Press, New York.

Wilson, R. R. Jr., and R. S. Kaufmann. 1987. Seamount biota and biogeography. Pp. 355–377 in *Seamounts, Islands and Atolls*, B. H. Keating, P. Fryer, R. Batiza, and G. W. Beohlert, eds. AGU Geophys. Monog. 43, American Geophysical Union, Washington, DC.

Wood, J. B., E. Kenchington, and R. K. O'Dor. 1998. Reproduction and embryonic development time of *Bathypolypus arcticus*, a deep-sea octopod (Cephalopoda: Octopoda). *Malacologia* **39:** 11–19.

Young, R. E. 1972. Brooding in a bathypelagic octopus. *Pac. Sci.* **26:** 400–404.

Young, R. E. 1995. Aspects of the natural history of pelagic cephalopods of the Hawaiian Mesopelagic-Boundary region. *Pac. Sci.* **49:** 143–155.

Reference: *Biol. Bull.* **198:** 101–109. (February 2000)

Filamentous Fungi Associated With Holothurians From the Sea of Japan, Off the Primorye Coast of Russia

MICHAEL V. PIVKIN

Pacific Institute of Bioorganic Chemistry, Far East Branch of the Russian Academy of Sciences, 690022, Vladivostok, Russia

Abstract. Holothurians (*Holothurioidea, Echinodermata*) are known to contain triterpene glycosides, which show antifungal activity. Nevertheless, fungi can be isolated from all organs of holothurians. During 1995–1996, mycelial fungi from several Far-Eastern holothurians—*Apostichopus japonicus, Eupentacta fraudatrix, Cucumaria japonica*—were collected from the Sea of Japan near the coast of Primorye (Russia) and studied. Twenty-seven species of marine fungi, mostly facultative ones belonging to the mitosporic fungi, were isolated from the holothurians and identified. Fungi isolated from the holothurian surface were more diverse and abundant than those from internal organs and coelomic fluids. Of the holothurians studied, *Cucumaria japonica* was poorest in abundance and diversity of fungi. The fungi *Cladosporium brevicompactum* and *C. sphaerospermum* were common in the holothurian coelom. Because of their high proteolytic activity, these fungi may be pathogenic to holothurians. The detritovorus holothurian *A. japonicus* was shown to modify the fungal assemblages within the marine bottom sediments.

Introduction

Interest [1]in the interactions between echinoderms and other species of marine organisms has intensified in the past few years. In addition to the trophic interrelationships of echinoderms within marine communities (Levin and Voronova, 1979) and diseases caused by bacteria, protists, and other parasites (Jangoux, 1987; Skadsheim *et al.*, 1995), benign, symbiotic interactions between echinoderms and bacteria have received much attention (Bauer and Agertr, 1994; McKenzie and Kelly, 1994; Newton and McKenzie, 1995; Kelly and McKenzie, 1995; Kelly *et al.*, 1995; Thorsen, 1995). However, there is very little information about the fungi of echinoderms. Mortensen (1909) described a peculiar disease in the Antarctic cidaroid echinoids, genera *Rhynochocydaris* and *Ctenocidaris*, which was caused by the fungus-like organism *Echinophyces mirabilis*. More recently, fungi were found to damage the spines of the sea urchins *Diadema antillarum* (Mortensen, 1940) and *Strongylocentrotus franciscanus* (Johnson and Charman, 1970). There is some evidence that fungi are present in the intestine of a sea cucumber, *Apostichopus japonicus*, from the Sea of Japan, but no data are available on their abundance or taxonomy (Levin, 1982).

Despite the lack of data, the presence of fungi in holothurians is of potential importance. Holothurians are known to contain triterpene glycosides, which show fungitoxic, hemotoxic, and cytotoxic activities (Stonik and Elyakov, 1988). The diverse biological activities of the triterpene glycosides depend upon their specific binding to Δ^{-5} sterols (Kalinovskaya *et al.*, 1983; Kalinin *et al.*, 1994, 1996). Such sterols are common in most fungi, but holothurian fungi must be assumed to contain some other sterols that will not bind to holothurian glycosides. In addition, fungi adapted to the effects of triterpene glycosides might produce secondary metabolites having a similar type of action. Thus, the isolation, in pure culture, of fungal strains from holothurians, and a definition of their species diversity would give us an insight into the biochemical mechanisms by which the fungi adapt to triterpene glycosides.

This study had three aims. The first was to establish that fungi are found in and on holothurians—a surprising phenomenon since holothurians are well known as producers of fungitoxic glycosides. The second aim was to prepare a list

Received 21 April 1998; accepted 10 September 1999.
E-mail: Elyakov@stl.ru

of fungi isolated from the holothurians collected along the coast of the Primorye territory in the Sea of Japan. Such a list is basic to any mycological research. In mycology, the substrate from which a fungus was isolated, as well as its area of distribution, are characteristics used in identification, as are the morphological features and genetic distinctions of any species. The final goal was to be able to speculate rationally about the role of holothurian fungi in the environment.

Materials and Methods

Sampling

We studied the fungi from three species of Far-Eastern holothurians: *Apostichopus japonicus*, *Eupentacta fraudatrix*, and *Cucumaria japonica*. In 1995–1996, 10 animals of each species were collected at each of three sites along the Russian coast of the Sea of Japan: (1) the Gulf of Opritchnik, near Cape Skalistyi (44°26′3″N, 135°59′5″E; depth 12–14 m); (2) the Primorye coast (45°51′1″N, 136°37′3″E; depth 111 m); (3) in Trinity Bay of Peter the Great Bay (42°34′6″N, 130°57′58″E; depth 1.5–15 m). Specimens were placed in sterile polyethylene bags and either processed immediately or stored in a refrigerator at 0°–3°C for not more than 48 h.

Two additional types of material were collected at site 3. Feces from *A. japonicus* were obtained by placing five animals in sterile polyethylene cages suspended in the sea at the site for 6 h, then collecting the fecal material in sterile polyethylene bags. Bottom sediments from the habitat of this species were also collected in sterile bags.

Isolation of fungi

Fungi were plated and cultured from five types of material: from three holothurian tissues—surface muscle, intestine, and coelomic fluid—and from feces and bottom sediment.

Holothurian specimens were washed five times in sterile seawater, and 0.5-cm^3 samples of surface muscle and internal organs were dissected. Pieces of these tissues were placed on HA medium (Table 1) in sterile petri dishes. Coelomic fluid was extracted with a sterile syringe and inoculated into HA medium. Fungi from bottom sediments, fecal material, and stomach contents were isolated by dilution plating (Steele, 1967). Colonies from all of these cultures were then reseeded into tubes of Tubaki's medium (Table 1).

Fungal identification and diversity calculation

The fungi were re-subcultured and identified to species using slide cultures as well as morphological characteristics of the colony. Use of slide cultures allows microscopic examination of intact fungal reproductive structures. In this method, melted MA medium (Table 1) is placed on a sterile microscope slide at sufficiently high temperature, and in sufficient amount, to cover half the length of the slide surface and three quarters of its width with a thin, flat layer of agar. When the agar solidified, the fungus was inoculated on the surface by streaking spores in two parallel rows extending the length of the agar layer. The slide cultures were incubated at 22°C in a humid chamber and allowed to grow until reproductive structures appeared (3–7 days). Each fungal isolate was identified using common keys (Thom and Raper, 1945; Raper and Thom, 1949; Ellis, 1971; Gams, 1971; De Hoog, 1972; Samson, 1974; Shmotina and Golovleva, 1974; Tulloch, 1976; Kohlmeyer and Kohlmeyer, 1979; Ramirez, 1982; Bilay and Koval, 1988; Egorova, 1988), and the following media: Czapek's (Ramirez, 1982), MPCA, Tubaki's and MA (Table 1). The equitability and diversity of fungal species from each holothurian species were calculated using the Shannon-Weiner diversity index (Magurran, 1988).

Table 1

Media used in the culture of holothurian fungi

Abbreviation	Medium
HA	*Agar with holothurian broth:* 100 g of a holothurian sample boiled for 30 min in a liter of seawater, filtered, brought up to a liter of distilled water; pH adjusted to 6.8 with NaOH, 20 g of agar added; sterilized at 121°C for 20 min; half a million units of penicillin and 0.5 g of streptomycin added after sterilization.
MPCA	*Potatoes-carrot agar with seawater and yeast extract:* 20 g of potatoes and 20 g of carrot boiled for 30 min in a liter of seawater, crushed, brought up to a liter of distilled water; 0.5 g of yeast extract and 20 g of agar added; pH adjusted to 7.5 with NaOH; sterilized at 121°C for 20 min.
GM	*Gelatinous medium:* 2 g of gelatin in 100 ml of seawater; pH adjusted to 6.8 with NaOH; sterilized at 121°C for 20 min (Bilay, 1982).
MA	*Malt seawater agar:* 5% malt extract agar made up with seawater; pH adjusted to 7.5 with NaOH; sterilized at 112°C for 30 min (Hyde *et al.*, 1987).
	Tubaki's medium with natural seawater: 30 g of glucose, 1 g of peptone, 0.5 g of yeast extract, 1 g of K_2HPO_4, 0.5 g of $MgSO_4 \cdot 7H_2O$, 0.01 g of $FeSO_4 \cdot 7H_2O$, 1 liter of seawater; pH adjusted to 7.5 with NaOH; 15 g of agar added; sterilized at 112°C for 30 min (Tubaki, 1969).

Proteolytic activity of holothurian fungi

Production of extracellular proteases was determined by growing three cultures of each isolate at 22°C on GM media (Table 1) in tubes of 18 mm diameter (Bilay, 1982). Liquefying zones were measured in 7 and 14 days.

Resistance of fungi to glycosides

Resistance of fungi to the action of glycosides extracted from the holothurian *Eupentacta fraudatrix* was detected by the agar diffusion method. The following fungi were tested: *Cladosporium sphaerospermum* from coelomic fluid of *E. fraudatrix, Aspergillus eburneocremeus* from the surface of the holothurian, *Cladosporium cladosporioides* from bottom sediments, *Aspergillus flavipes* from the alga *Fucus evanescens,* and *Candida albicans* KMM 245. Solutions of the glycoside fraction at concentrations of 0.625, 1.25, 2.5, 5, 10, 20, and 40 mg/ml were used in the tests. A total fraction of glycoside, common to these animals (Kalinin *et al.,* 1994) was kindly provided by Dr. Avilov of the Pacific Institute of Bioorganic Chemistry.

Statistical analysis

The statistical significance of the proteolytic activity of the holothurian fungi and their resistance to holothurian glycosides was analyzed by the Fisher exact probability test (Sokal and Rolf, 1981). The results of the investigation of fungal species diversity were evaluated statistically using Student's *t* test (Magurran, 1988).

Results

Species diversity of fungi from holothurians

Twenty-seven species of marine fungi were isolated from various organs and tissues of holothurians and identified (Table 2). Most of these isolates were mitosporic fungi, predominantly *Hyphomycetes* (24 spp.) and *Coelomycetes* (3 spp.). The obligate marine fungi (definition according to Kohlmeyer and Kohlmeyer, 1979) included three species: *Botryophialophora* sp. (*Hyphomycetes*), *Phialophorophoma* sp., and *Coniothirium obiones* (*Coelomycetes*). The facultative marine fungi of holothurians were represented by 24 species of "terrestrial" fungi. All of these species belong to 13 genera of the class *Hyphomycetes.*

Among the holothurians investigated, the mycota of *Eupentacta fraudatrix* were the most diverse. *Cladosporium oxysporum* and *Metarchizium anisopliae* were the fungi that occurred most frequently on the surface of these animals. *Cladosporium sphaerospermum* was the dominant species inside of *E. fraudatrix* and on the surface of *Apostichopus japonicus* and *Cucumaria japonica. Cladosporium brevicompactum* dominated inside of *A. japonicus* and *C. japonica* (Table 2).

Three species of fungi, *Pacilomyces puntonii, C. sphaerospermum,* and *Beauveria alba,* occurred on the gonads of *A. japonicus* and *E. fraudatrix.*

Proteolytic activity of some fungal strains from holothurians

The proteolytic activities of some holothurian fungal strains are listed in Table 3. Of the eight fungal species taken from the surface of the holothurian *Eupentacta fraudatrix,* only one, *Penicillium commune,* had no proteolytic activity. However, the congeneric species *P. herquei* had the highest rate of gelatinous medium liquefaction when compared to other fungal species found on the surface (although the rates for *Acremonium striatisporum* and *Alternaria alternata* were also relatively high). Fungi of the species *Cladosporium sphaerospermum* and *C. brevicompactum* isolated from internal organs of these three holothurians demonstrated higher gelatinolytic activity than the same fungal species isolated from the surface. Indeed, the activity demonstrated by *C. brevicompactum* taken from the internal organs of *Cucumaria japonica* was the highest measured in these experiments.

Resistance of fungi to glycosides of the holothurian Eupentacta fraudatrix

The inhibition of fungal growth by different concentrations of a glycoside fraction taken from *E. fraudatrix* is plotted in Figure 1. These glycosides inhibited *Candida albicans* and fungal strains from bottom sediments and from *Fucus evanescens* (curves Cal, Ccl, Afl) at the lowest concentration (0.625 mg/ml); but the growth of the fungus *Aspergillus eburneocremeus,* isolated from the surface of this holothurian, was stopped only at glycoside concentrations 5 mg/ml or higher (curve Aeb). *Cladosporium sphaerospermum,* isolated from internal organs (curve Csp), was resistant to these holothurian glycosides at 40 mg/ml, a concentration many times higher than it could be in this holothurian (Kalinin *et al.,* 1994, 1996). That fungi from various marine habitats differ in their resistance to the glycosides of *E. fraudatrix* is illustrated in Figure 2. The fungi from this holothurian (top dishes) are more resistant to its glycosides than are fungi from bottom sediments and from *Fucus evanescens* (bottom dishes).

Fungi in the intestine, feces, and habitat of the holothurian Apostichopus japonicus

The abundance and species composition of fungal propagules (conidia, spores, and pieces of mycelia) in the intestine of *A. japonicus,* in its feces, and in the marine sediments it inhabits are set out in Table 4. The abundance of fungi in the bottom sediments was ten times higher than in the intestine of this sea cucumber. However, the abundance of fungi in feces was twice that in samples of bottom sediment taken from the habitat of these holothurians. The species composition of fungi is also different in the sediment, in-

Table 2

Fungi from holothurians, species diversity and distribution

		Eupentacta fraudatrix			*Apostichopus japonicus*			*Cucumaria japonica*		
Taxon		S	I	C	S	I	C	S	I	C
Cladosporium sphaerospermum Penz.			■	■	●	+	+	●		
C. brevicompactum Pidopl. et Deniak		+			X	●	■	■	■	■
C. atrospermum Pidopl. et Deniak		+	+		+	+	+	●		**3**
C. oxysporum Berk. et M. A. Curtis		X			+					
Alternaria alternata (Fr.) Keissl.		+			X					
Aspergillus versicolor (Vuill.) Tirab.			+		+	+	+			
A. eburneocremeus Sappa		+			+					
Epicoccum st. *Phoma* sp.		+					+			
Ulocladium sp.		+			+		**9**			
Aspergillus flavus Link							+			
Acremonium charticola (Lindau) W. Gams		+								
A. fusidioides (Nicot) W. Gams		+								
A. striatisporum (Onions & G. L. Barron) W. Gams		+								
Beauveria alba (Limber) Saccas		+	■							
Botryophialophora sp.*		+								
Coniothirium obiones Jaap*		+								
Metarchizium anisopliae (Metschn.) Sorokin var. *anisopliae* J. R. Johnst.		X								
Oidiodendron sp.		+								
Paecilomices puntonii (Vuill.) Nann.						●	**2**			
Penicillium commune Thom		+								
P. herquei Bainier et Sartory		+								
P. implicatum Biourge		+								
P. roqueforti Thom		+								
P. skrjabinii Schmotina et Golovleva		+								
Phialophorophoma sp.*		+								
Tilachlidium sp.		+								
Verticillium tenerum Ness		+		**25**						
Total number	**27**	24	4	1	8	5	6	3	1	1
†Shannon-Weiner diversity index		2.95			1.67			0.82		
Equitability		0.93			0.76			0.74		

Letters (S, I, C) indicate the holothurian site from which the fungi were isolated: S, surface; I, internal organs; C, coelomic fluid. Symbols indicate the frequency of fungal species occurrence: +, 0%–10%; X, 10%–20%; ●, 20%–40%; ■, more than 40%. Boldface numbers give summary information about the distribution of the fungi among the holothurians. For example, of the 27 fungal species identified, 25 were found on *Eupentacta fraudatrix*; 2 of the 11 species found on *Apostichopus japonicus* were exclusive to that species, and 9 were also found on *E. fraudatrix*; and 3 species of fungi were found on *Cucumaria japonica*, none exclusively.

* Obligate species of marine fungi.

† Differences in species diversity of fungi on the holothurian species are statistically significant at the 99.8% level.

testine, and feces. The intestine has the fewest species, but all of them occur in the sediment and in the feces.

Discussion

The vast majority of fungi isolated from the holothurians were facultative marine species. Only three species of obligate marine fungi were found in the holothurians, and all of them were isolated from the surface of *Eupentacta fraudatrix* (Table 2). Thus, among the holothurians investigated, the facultative marine fungi are more diverse than the obligate ones, although holothurians are rather substrate-specific. In the sea there are not many substrates suitable for fungi, and just for this reason associations between fungi and other organisms are unusual. We should therefore reconsider the general notion that the role of facultative marine fungi in ecology is of little importance.

The presence of fungi on holothurians is unexpected, because holothurian glycosides are highly fungicidal. The glycosides from *E. fraudatrix* have a higher fungicide activity than those from any other holothurian species studied (Kalinin *et al.*, 1994). We therefore determined the resistance of two fungal species from *E. fraudatrix* and two

Table 3

Proteolytic activity of fungal strains from holothurians

Source	Taxon	Proteolytic activity (cm)*
Eupentacta fraudatrix	*Acremonium striatisporum*	4.0 ± 0.2
Surface	*Penicillium commune*	0
	P. herquei	6.0 ± 0.1
	Alternaria alternata	4.5 ± 0.3
	Phialophorophoma sp.	0.8 ± 0.1
	Verticillium tenerum	1.0 ± 0.2
	Cladosporium sphaerospermum	1.0 ± 0.2
	C. brevicompactum	3.0 ± 0.1
Internal organs	*C. sphaerospermum*	6.0 ± 0.3
Apostichopus japonicus	*C. sphaerospermum*	0.5 ± 0.1
Surface	*C. brevicompactum*	0.8 ± 0.1
Internal organs	*C. sphaerospermum*	5.0 ± 0.3
	C. brevicompactum	6.0 ± 0.3
Cucumaria japonica	*C. sphaerospermum*	1.0 ± 0.2
Surface	*C. brevicompactum*	1.2 ± 0.1
Internal organs	*C. brevicompactum*	8.0 ± 0.3

* Differences in proteolytic activity of fungal strains are statistically significant at the 99% confidence level. $P < 0.001$. Values are expressed as the mean, plus or minus the standard deviation.

fungal species from other marine habitats to a glycoside fraction from *E. fraudatrix. Candida albicans* KMM 245 was used as a control. Fungi from *E. fraudatrix* appeared to

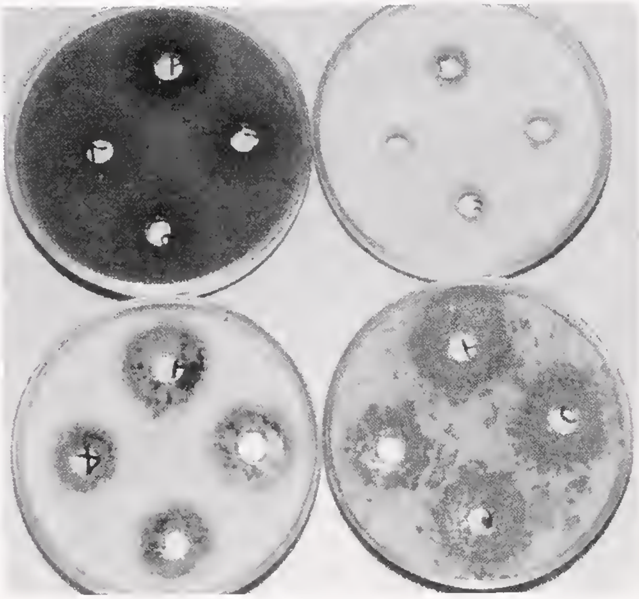

Figure 2. Inhibition of fungal growth by four concentrations of glycoside from the holothurian *Eupentacta fraudatrix.* Glycoside concentrations in each plate are (clockwise from top) 40, 20, 10, and 5 mg/ml. Top left plate: *Cladosporium sphaerospermum* isolated from coelomic fluid of the holothurian (see curve Csp in Fig. 1); Top right: *Aspergillus eburneocremeus* isolated from the surface of the holothurian (curve Aeb in Fig. 1); Bottom left: *Cladosporium cladosporioides* isolated from bottom sediments (curve Ccl in Fig. 1); Bottom right: *Aspergillus flavipes* from the alga *Fucus evanescens* (curve Afl in Fig. 1).

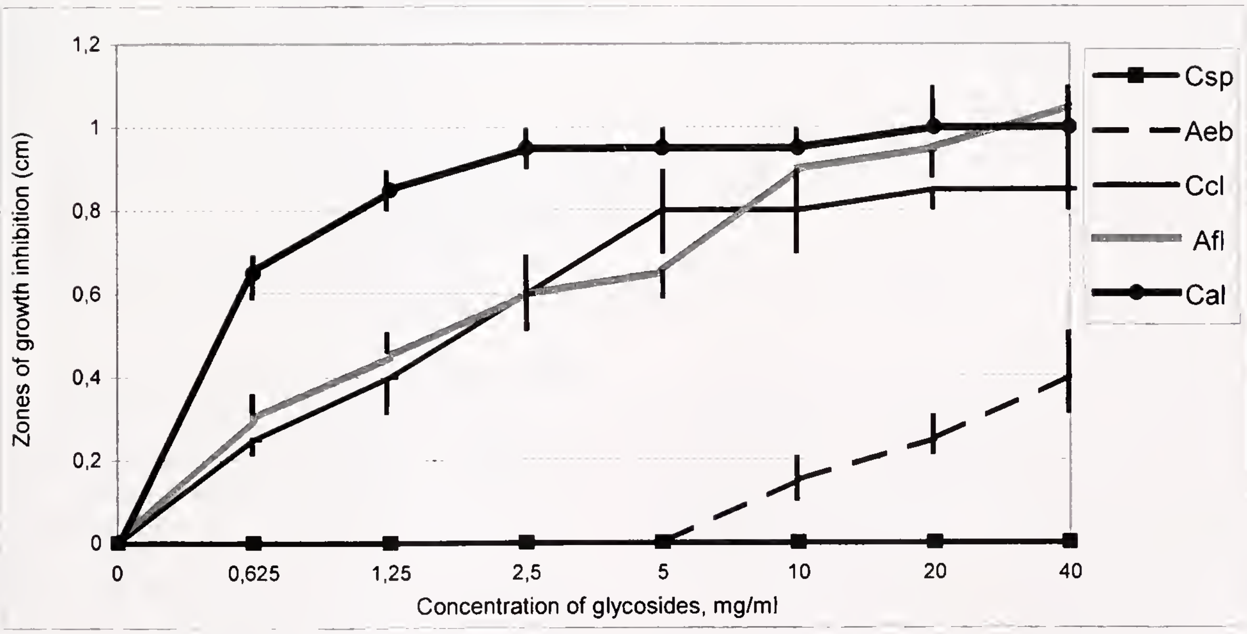

Figure 1. Inhibition of fungal growth by glycosides of the holothurian *Eupentacta fraudatrix.* Curves: Csp, *Cladosporium sphaerospermum* isolated from coelomic fluid of the holothurian. Aeb, *Aspergillus eburneocremeus* isolated from the surface of the holothurian. Ccl, *Cladosporium cladosporioides* isolated from bottom sediments. Afl, *Aspergillus flavipes* isolated from the alga *Fucus evanescens.* Cal, *Candida albicans* KMM 245. Differences in resistance of fungal strains to glycosides are statistically significant at the 99% confidence level. $P < 0.001$.

Table 4

Abundance and fungal species composition of the internal contents and feces of Apostichopus japonicus, *as well as the marine sediments it inhabits*

Fungal taxon	Materials Examined*		
	Bottom sediments (1.3×10^4)	Intestine (0.8×10^3)	Feces (2.6×10^4)
Acremonium fusidioides (Nicot) W. Gams	+	+	+
A. kiliense Grutz			+
A. trachycaulon W. Gams			+
Alternaria alternata (Fr.) Keissl.	+	+	+
Arthrynium sp.	+		+
Aspergillus flavus Link	+		
A. halophilicus C. M. Chr., Paravizas et C. R. Bej.	+		
A. niger Tiegh.	+		
A. sydowi (Bainier et Sartory) Thom et Church	+		
Chaetomium olivaceum Cooke et Ellis	+	+	+
Cladosporium atrospermum Pidopl. et Deniak	+	+	+
C. brevicompactum Pidopl. et Deniak	+	+	+
C. sphaerospermum Penz.	+	+	+
Dendryphiella arenaria Nicot	+	+	+
Oidiodendron truncatum G. L. Barron	+	+	+
Penicillium brevicompactum Dierckx	+		
P. chrysogenum Thom	+		
P. commune Thom	+	+	+
P. herquei Thom	+	+	+
P. thomii Maire	+		
Stilbella aciculosa (Ellis et Everh.) Seifert	+		+
Trichoderma aureoviride Rifai	+	+	+
T. harzianum Rifai	+	+	+
T. viride Rifai	+	+	+
Wallemia sebi (Fr.) Arx	+		
Number of species	23	13	17

* Numbers in parentheses are the number of fungal propagules per gram of material.

have more tolerance for these glycosides than did fungi from other marine substrates (Figs. 1, 2). This suggests that fungicidal glycosides may not limit the ability of certain species of fungi to grow on a holothurian.

More species of fungi inhabit the surface of holothurians than the internal organs and coelomic fluid (Table 2). The mycota of holothurians typically comprises unspecific cosmopolitan species that occur in soils and on various protein-rich substrates (Table 5), whereas the internal fungal assemblages of holothurians are rather specific. Thus, three of seven fungal species isolated from internal organs and coelomic fluid were found in only one holothurian species (Table 2). Four other species were characteristic of the internal mycota of two holothurian species. But none of these fungal species occurred in all three species of these holothurians.

Paecilomyces puntonii and *Beauveria alba* are rare species, found on human skin (De Hoog, 1972; Samson, 1974); they have been isolated from the gonads of *A. japonicus* and *E. fraudatrix,* respectively. The cosmopolitan species *Cladosporium sphaerospermum,* which occurs on various substrates, including ones of animal origin (Ellis, 1971), was also isolated from the gonads of *E. fraudatrix.* Even though the amount of glycosides in gonads can be ten times more than in other organs of these holothurians (Levin, 1982), these species of fungi were found even in such adverse conditions.

The fungal species from *E. fraudatrix* are more diverse than those from any other holothurian species studied; and as indicated above, glycosides from this holothurian have the highest fungicide activity. Triterpene glycosides from *C. japonica* are active against *Candida albicans* and *C. tropicalis* at concentrations higher than 30–50 mg/ml, but they have lower fungicidal activity than other holothurian glycosides (Kalinin *et al.,* 1994). We might expect that the toxicity of secondary holothurian metabolites would influence the species diversity of the fungi associated with these animals; but in fact, the diversity of fungi increases with growing glycoside toxicity.

The investigated holothurians differ in food specialization. *A. japonicus* is an animal that feeds on organic material that has settled to the marine floor. *E. fraudatrix* and *C. japonica* feed on organic particles suspended in the seston. Because the number and diversity of fungi in the bottom sediments are about 100 times higher than those in the water column (Steele, 1967), *A. japonicus* has contact with a much more diverse fungal assemblage than the two other holothurians encounter. Nevertheless, this condition does not provide the greater diversity of fungi associated with *A. japonicus.*

Depth of habitat might also affect fungal diversity. The most deep-sea species, *Cucumaria japonica,* has the fewest fungal species. *A. japonicus* is common at depths down to 100 m and has more diverse mycota than *C. japonica.* The greatest diversity and equitability of fungal species are characteristic of *E. fraudatrix,* which has an optimal depth of 1.5 m but can occur down to 40 m. Therefore, fungal diversity appears to decrease with the depth of the holothurian habitat.

The regions of isolation of these holothurians are also important. In our experience, the species composition of fungi isolated from *C. japonica* collected from areas around the Kuril Islands in 1998 was different from that isolated from *C. japonica* collected in Primorye waters. Fungi that

Table 5

Fungi isolated from holothurians: distribution, habitats, substrates

Taxon	Substrates and distribution	References
Acremonium charticola	Cellulose substrates, human skin (-*Cephalosporium ballagii*), widespread, unknown in the sea.	Gams, 1971
A. fusidioides	Soil, widespread, unknown in the sea.	Gams, 1971
A. striatisporum	Soil, widespread, unknown in the sea.	Gams, 1971
Alternaria alternata	On various marine substrates, widespread.	Johnson and Sparrow, 1961; Jones, 1962, 1963, 1968, 1972
Aspergillus eburneocremeus	Soil, Southeastern Asia, North and South America.	Artemtchuk, 1981; Steele, 1967; Bilay and Koval, 1988
A. flavus	Soil, humans, and animals, seawater, bottom sediments, and coastal sands, widespread.	Thom and Raper, 1945; Bilay and Koval, 1988; Steele, 1967
A. versicolor	Soil, (-*A. versicolor* var. *glauca*) pathogenic for man and animals, bottom sediments, seawater, widespread.	Bilay and Koval, 1988; Blochwitz, 1934; Thom and Raper, 1945; Steele, 1967
Beauveria alba	Insects, human skin, widespread, unknown in the sea.	De Hoog, 1972
Botryophialophora sp.	Allied to *Botryophialophora marina* that inhabits wood, test panels, and coastal sands in the Atlantic and Pacific Oceans.	Linder, 1944; Steele, 1967; Wilson, 1951
Cladosporium atrospermum	Soil, cosmopolitan on various substrates, widespread, unknown in the sea.	Ellis, 1971
C. brevicompactum	Soil, cosmopolitan on various substrates, widespread, unknown in the sea.	Ellis, 1971
C. oxysporum	Soil, cosmopolitan on various cellulose substrates, widespread, unknown in the sea.	Ellis, 1971
C. sphaerospermum	Soil species, cosmopolitan on various substrates including ones of animal origin, widespread, unknown in the sea.	Ellis, 1971
Coniothirium obiones	Saprotrophic species, Atlantic and Indian Oceans.	Kohlmeyer and Kohlmeyer, 1979
Metarchizium anisopliae var. *anisopliae*	Insects, widespread, unknown in the sea.	Latch, 1965; Tulloch, 1976
Oidiodendron sp.	Soil, plants, and others.	Ellis, 1971
Penicillium commune	Soil, contaminants from cheese and other foodstuffs, bottom sediments, seawater, widespread.	Ramirez, 1982; Raper and Thom, 1949; Steele, 1967
P. herquei	Soil, widespread, but not abundant, unknown in the sea.	Raper and Thom, 1949
P. implicatum	Soil, widespread, but not abundant, unknown in the sea.	Raper and Thom, 1949
P. roqueforti	Soil, contaminants from cheese and other foodstuffs, widespread, unknown in the sea.	Ramirez, 1982; Raper and Thom, 1949
P. skrjabinii	Soil, Far East, vicinities of Blagoveshchensk, unknown in the sea.	Shmotina and Golovleva, 1974
Pacilomices puntonii	Human skin, widespread, but not abundant, unknown in the sea.	Samson, 1974
Phialophorophoma sp.	Allied to *Phialophorophoma litoralis* that is found on cellulose substrates, and on the dead alga *Avicennia marina* var. *resinifera*, the Atlantic and Pacific Oceans	Kohlmeyer and Kohlmeyer, 1979
Tilachlidium sp.	Soil, plants, and others.	Ellis, 1971
Ulocladium sp.	Soil, plants, and others, unknown in the sea.	Ellis, 1971
Verticillium tenerum	Soil, widespread, unknown in the sea.	Gams, 1971

were prevalent in isolates from Primorye holothurians were very rare in the cucumbers from the Kuril Islands, where they occurred only in the southern collection sites.

Proteolytic activity is frequently suggested as a factor in fungal pathogenicity (St. Leger *et al.*, 1988; Monod *et al.*, 1995). The body of any holothurian contains 1.9%–9.0% of protein, mainly collagen, and the content of protein exceeds that of all other components of the holothurian body, excluding water (Levin, 1982). Therefore, the ability of fungi to damage holothurian tissues can be estimated from their proteolytic activity, thus precluding the need to inoculate the animals. In particular, the gelatinolytic activity of holothurian fungi, determined simply by measuring the liquefaction of gelatinous medium (denatured collagen), allows us to estimate their pathogenicity. The strains of *Cladosporium sphaerospermum* and *C. brevicompactum* isolated from the internal organs of these holothurians are twice as active in liquefying gelatin as are isolates from their surfaces (Table 3). Note that the fungi of these species often occur in internal organs and coelomic fluid of holothurians; in several cases, the animals contained a monoculture of these fungi species. Recall, furthermore, that *C. sphaerospermum* is resistant to glycosides of *E. fraudatrix* (Fig. 1). These facts indicate that *C. sphaerospermum* and *C. brevicompactum* may be pathogenic for holothurians.

However, the terms "pathogen" for these fungi and "host" for these holothurians must be used with care, because they imply a parasitic relationship between organisms—in this case between a macroorganism and a pathogenic microorganism. To confirm the pathogenicity of a microorganism, the classical method of Koch should be used, and this includes three steps: (1) a search for symptoms of a disease; (2) isolation of potential pathogens into pure culture; (3) artificial inoculation of this organism. In the end, a microorganism can be recognized as pathogenic if all the symptoms of a recognizable disease produced by infection completely coincide with those that appear after artificial inoculation. Such an analysis was not possible in the present study. Therefore, an analysis of gelatinolytic activity was taken as indirect evidence for the ability of a fungus to damage holothurian tissues, and on that basis, fungi isolated from coelomic fluid and internal organs were considered to be *potentially pathogenic*.

Similarly, the term "symbiont" can not be used, because no symbiosis between fungi and holothurians has yet been proven. Since, in our current state of knowledge, the relationship between fungi and holothurians cannot be described as either parasitic or symbiotic, we should consider fungi isolated from a holothurian surface to be *epiphytic*.

We may also ask whether holothurians affect the mycota of bottom sediments; in particular, can they modify the abundance and species composition of these fungi? As mentioned above, *A. japonicus* feeds on marine deposits (Levin, 1982), which include propagules of fungi. A comparison of fungi from bottom sediments and from holothurian feces revealed that *A. japonicus*, armed with the triterpene glycosides, increased the abundance of dematiaceous species of *Hyphomycetes* and eliminated some species of *Moniliaceae* from the bottom sediments (Table 3). Dematiaceous *Hyphomycetes* of the genera *Alternaria*, *Arthrynium*, and *Dendryphiella* passed through the alimentary tract of *A. japonicus* practically without loss of their viability; and the number of fungi of the genus *Cladosporium* even increased under these conditions. But not all dematiaceous *Hyphomycetes* are unaffected by transit through a holothurian. For example, *Wallemia sebi* was isolated from bottom sediments, but occurred in neither the intestine nor the feces of the sea cucumber. *Hyphomycetes* of the family *Moniliaceae* were affected more selectively: *e.g.*, fungi of the genera *Acremonium* and *Trichoderma* were resistant to passage through the sea cucumbers, whereas fungi of the genus *Aspergillus* were not found in feces of these animals. Of all the fungi of the genus *Penicillium* found in bottom sediments, only *P. herquei* and *P. commune* did not lose viability in the intestine of these sea cucumbers.

Fungi from holothurians have never been investigated before. This pioneer report describes the species compositions of fungi from holothurians and their possible ecological role.

Acknowledgments

I acknowledge, with gratitude and affection, the generous help I have received from Prof. M. Jangoux in obtaining information on diseases of Echinodermata. I am most grateful to Miss N. Shepetova for helpful discussions and for translating this article into English. Dr. Kalinin supplied much constructive criticism for which I am grateful. My special thanks to Dr. Yu. Jakovlev for collecting some of the animals and to Dr. S. Avilov for providing glycoside samples. This work was financially supported in part by grant #99-04-49363 of the Russian Foundation for Basic Research and by a grant of the Governor of Primorye.

Literature Cited

Artemichuk, N. J. 1981. *Mycoflora from Sea of USSR.* Nauka. Moscow. (in Russian).

Bauer, J. C., and C. J. Agertr. 1994. Isolation of potentially pathogenic flora from tropical sea urchins in selected West Atlantic and East Pacific sites. *Bull. Mar. Sci.* **55:** 142–150.

Bilay, V. I., ed. 1982. *Methods of Experimental Mycology.* Naukova Dumka. Kiev (in Russian).

Bilay, V. I., and E. Z. Koval. 1988. *Aspergillii.* Naukova. Dumka. Kiev. (in Russian).

Blochwitz, A. 1934. Die Gattung Aspergillus. III Neue Spezies. Varianten und Mutanten der Konidienfarbe. Synonyme und interessante Standorte. *Ann. Mycol.* **32:** 82–89.

De Hoog, G. S. 1972. The genera *Beauveria, Isaria, Tritirachium* and *Acrodontium* gen. nov. *Stud. Mycol.* **1,** Sept. 40 p.

Egorova, L. N. 1988. *Soil Fungi of the Far East.* Nauka, Leningrad. (in Russian).

Ellis, M. B. 1971. *Dematiaceos Hyphomycetes.* Commonwealth Mycological Institute, Kew, England.

Gams, W. 1971. *Cephalosporium-artige Schimmelpilze (Hyphomycetes).* VEB Gustav Fischer Verlag, Jena, Germany.

Hyde, K. D., C. A. Farrant, and E. B. G. Jones. 1987. Isolation and culture of marine fungi. *Bot. Mar.* **30:** 291–303.

Jangoux, M. 1987. Diseases of Echinodermata. I. Agents microorganisms and protistans. *Dis. Aquat. Org.* **2:** 147–162.

Johnson, P. T., and F. A. Charman. 1970. Infection with diatoms and other microorganisms in sea urchin spines (*Strongylocentrotus franciscanus*). *J. Invertebr. Pathol.* **17:** 94–106.

Johnson, T. W., Jr., and F. K. Sparrow, Jr. 1961. *Fungi in Oceans and Estuaries.* Weinheim, New York.

Jones, E. B. G. 1962. Marine fungi. *Trans. Br. Mycol. Soc.* **45:** 93–114.

Jones, E. B. G. 1963. Marine fungi II. Ascomycetes and Deuteromycetes from submerged wood and drift *Spartina. Trans. Br. Mycol. Soc.* **46:** 135–144.

Jones, E. B. G. 1968. The distribution of marine fungi on wood submerged in the sea. Pp. 460–485 in *Biodeterioration of Materials.* A. H. Walters and J. F. Elphick, eds. Elsevier, Amsterdam.

Jones, E. B. G. 1972. The decay of timber in aquatic environments. *Br. Wood Pres. Assoc., Annu. Conv.* 1–18.

Kalinin, V. I., V. S. Levin, and V. A. Stonik. 1994. *The Chemical Morphology: Triterpene Glycosides of Sea Cucumbers (Holothurioidea, Echinodermata).* Dalnauka, Vladivostok. (in Russian).

Kalinin, V. I., M. M. Anisimov, N. G. Prokofieva, S. A. Avilov, Sh. Sh. Afiatullov, and V. A. Stonik. 1996. Biological activities and biological role of triterpene glycosides from holothuroides (Echinodermata). Pp. 139–181 in *Echinoderm Studies.* Vol. 5. M. Jangoux and J. M. Lawrence, eds. Balkema, Rotterdam.

Kalinovskaya, N. I., T. A. Kuznetsova, A. M. Popov, A. S. Antonov, and G. B. Elyakov. 1983. Steroid metabolites of the Far-Eastern Holothurian *Stichopus japonicus* Selenka. *Comp. Biochem. Physiol. B* **76(1):** 167–171.

Kelly, M. S., and J. D. McKenzie. 1995. A survey of the occurrence and morphology of subcuticular bacteria in shelf echinoderms from the north-east Atlantic Ocean. *Mar. Biol.* **123:** 741–756.

Kelly, M. S., M. F. Barker, J. D. McKenzie, and J. Powell. 1995. The incidence and morphology of subcuticular bacteria in the echinoderm fauna of New Zealand. *Biol. Bull.* **189:** 91–105.

Kohlmeyer, J., and E. Kohlmeyer. 1979. *Marine Mycology.* Academic Press. New York.

Latch, G. C. M. 1965. Metar(r)hirizium anisopliae (Metsch.) Sorok. strains in New Zealand and their possible use for controlling pasture inhabiting insects. *N. Z. J. of Agric. Res.* **8:** 384–396.

Levin, V. S. 1982. *Japanese Sea Cucumber.* Dalnauka, Vladivostok (in Russian).

Levin, V. S., and E. I. Voronova. 1979. Assimilation of bacterial food by Japanese sea cucumber. Pp. 121–123 in *Material IV All Union Colloquium on Echinoderm.* Tbilisi, Rep. of Georgia (in Russian).

Linder, D. H. 1994. I. Classification of the marine fungi. Pp. 401–433 in Farlowia, **1**, E. S. Barghorn and D. H. Linder. *Marine Fungi: Their Taxonomy and Biology.*

Magurran, A. E. 1988. *Ecological Diversity and Its Measurement.* Croom Helm, London.

McKenzie, J. D., and M. S. Kelly. 1994. Comparative study of subcuticular bacteria in brittlestars (Echinodermata: Ophiuroidea). *Mar. Biol.* **120:** 65–80.

Monod, M., A. Fatih, K. Jaton-Ogay, S. Paris, and J. P. Latge. 1995. The secreted proteases of pathogenic species of *Aspergillus* and their possible role in virulence. Pp. 1081–1086 in *Can. J. Bot., Fifth Int. Mycol. Congress. Sect E–H.* Aug. 14–21, 1994. Vancouver.

Mortensen, T. 1909. Die Echinoiden. *Dtsch. Subpol. Exp. 1901–1903.* **11** (3): 1–113.

Mortensen, T. 1940. *A Monograf of the Echinoidea. Part III. 1 Aulodonta.* C. A. Reitzel. Copenhagen.

Newton, L. C., and J. D. McKenzie. 1995. Echinoderms and oil pollution: a potential stress assay using bacterial symbionts. *Mar. Pollut. Bull.* **31:** 453–456.

Ramirez, C. 1982. *Manual and Atlas of the Penicillia.* Elsevier Biomedical Press. Amsterdam.

Raper, K. B., and C. Thom. 1949. *A Manual of the Penicillia.* Williams & Wilkins, Baltimore.

Samson, R. A. 1974. Paecilomyces and some allied Hyphomycetes. *Stud. Mycol.* **6:** Centroalbureau voor Schimmelcultures, Baarn, The Netherlands.

Shmotina, G. E., and L. A. Golovleva. 1974. A new species of *Penicillium* isolated from soil in the Amur region. *Mikol. i Fitopatol.* **8:** 530–532 (in Russian).

Skadsheim, A., H. Christie, and H. P. Leinaas. 1995. Population reductions of *Strongylocentrotus droebachiensis* (Echinodermata) in Norway and the distribution of its endoparasite *Echinomermella matsi* (Nematoda). *Mar. Ecol. Prog. Ser.* **119:** 199–209.

Sokal, R. R., and R. J. Rolf. 1981. *Biometry.* 2nd ed. W. H. Freeman, New York.

St. Leger, R. J., P. K. Durrands, A. K. Charnley, and R. M. Cooper. 1988. Role of extracellular chymoelastase in the virulence of *Metharhizium anisopliae* for *Manduca sexta. J. Invertebr. Pathol.* **52:** 285–293.

Steele, W. S. 1967. Fungus populations in marine waters and coastal sands of the Hawaiian, Line, and Phoenix Islands. *Pac. Sci.* **21:** 317–331.

Stonik, V. A., and G. B. Elyakov. 1988. Structure and biologic activities of sponge and sea cucumber toxins. Pp. 107–120 in *Handbook of Natural Toxins and Venoms.* A. Tu, ed. Marcel Dekker, New York.

Thom, C., and C. B. Raper. 1945. *A Manual of the Aspergilli.* Williams and Wilkins, Baltimore.

Thorsen, M. S. 1995. Oxygen gradients and microbiota in the gut of the irregular sea urchin *Echinocardium cordatum* (Spatangoida: Echinodermata). P. 77 in *Echinoderm Research. Proceedings of the Fourth European Echinoderm Colloquium,* 10–13 April, London.

Tubaki, K. 1969. Studies on the Japanese marine fungi. Lignicolous group. III. *Annu. Rep. Inst. Ferment. Osaka* **4:** 12–41.

Tulloch, M. 1976. The genus *Metarhizium. Trans. Br. Mycol. Soc.* **66:** 407–411.

Wilson, I. M. 1951. Notes on some marine fungi. *Trans. Br. Mycol. Soc.* **34:** 540–543.

Reference: *Biol. Bull.* **198:** 110–120. (February 2000)

Cellular Growth of Host and Symbiont in a Cnidarian-Zooxanthellar Symbiosis

W. K. FITT

Institute of Ecology, University of Georgia, Athens, Georgia 30602

Abstract. The hydroid *Myrionema ambionense*, a fast-growing cnidarian (doubling time = 8 days) found in shallow water on tropical back-reefs, lives in symbiosis with symbiotic dinoflagellates of the genus *Symbiodinium* (hereafter also referred to as zooxanthellae). The symbionts live in vacuoles near the base of host digestive cells, whereas unhealthy looking zooxanthellae are generally located closer to the apical end of the host cell. Cytokinesis of zooxanthellae occurred at night, with a peak in number of symbionts with division furrows (mitotic index, MI = 12%–20%) observed at dawn. The MI of zooxanthellae decreased to near zero by the middle of the afternoon and remained there until the middle of the next night. Densities of live zooxanthellae living inside of host digestive cells peaked following cytokinesis, whereas densities of unhealthy looking symbionts were highest just before the division peak. Mitosis of host digestive cells was highest in the evening, also preceding the peak in zooxanthellar MI. This is the first study relating phased host cell division to diel zooxanthellar division in marine cnidarians.

Food vacuoles were prevalent inside of digestive cells of field-collected hydroids within a few hours after sunset and throughout the night, coinciding with digestion of captured demersal plankton. Laboratory experiments showed that food vacuoles appeared in digestive cell cytoplasm within 2 h of feeding with nauplii of *Artemia*. The number and size of food vacuoles per digestive cell and the percentage of digestive cells with food vacuoles all decreased 5–7 h following feeding in laboratory experiments, and by mid-day in field-collected hydroids.

Light and external food supply were important in maintaining phased division of the symbionts, with a lag in response time to both parameters of 11–36 h. Altering light and feeding during the night did not influence the level of the peak MI the next morning, though in one experiment the absence of light slowed final separation of daughter cells at the end of cytokinesis. In another experiment, hydroids starved for 3–7 d and "pulse-fed" *Artemia* nauplii for 1 h at the beginning of the dark period showed continued low symbiont division (<5%) after 11 h, whether maintained in constant light or darkness, implying that most algal division is set more than 24 h prior to actual cytokinesis. Transferred to a 14:10 h light:dark cycle for another 24 h (36 h after feeding), the same hydroids exhibited a "normal" peak MI (*ca.* 15%) at dawn, but zooxanthellae from hydroids kept in constant darkness still showed a low MI. These results show that mitosis of symbiotic dinoflagellates requires three factors: external food; a minimum period of time following feeding (11–36 h), presumably for digestion; and a period of light following feeding, presumably to provide carbon skeletons necessary for completing cytokinesis.

Introduction

Although the ecological significance of cnidarian-zooxanthellar symbioses has been recognized for over 70 years (Yonge and Nichols, 1931), efforts to understand how these associations remain together have been sporadic. Most algal symbioses are characterized by relatively constant densities of symbionts (Reimer, 1971; Muscatine and Pool, 1979; McAuley, 1994), giving rise to theories that symbiotic algae are "regulated" by their hosts. The three proposed modes of maintaining densities of symbionts are (1) expulsion or exocytosis of extra symbionts, (2) digestion of extra symbionts, and (3) control of growth of endosymbionts by superimposition of an external control, or by limiting nutrient supply (Muscatine and Pool, 1979). The first two methods assume that "extra" algae are produced by algal division, and that the host has some mechanism of detecting and responding to increased densities of symbionts, somehow

Received 17 June 1999; accepted 4 November 1999.

E-mail: fitt@sparrow.ecology.uga.edu.

culling supernumerary algae down to the steady-state density. The third method relies on integration of host and symbiont division cycles. Both expulsion and synchronized division are present in most cnidarian-algal symbioses that have been investigated (refs. below), but little evidence exists for digestion of extra symbiotic algae.

The approach taken in this study is patterned after the productive research conducted on hydra-zoochlorellae symbioses. Green algae in the genus *Chlorella* live symbiotically in vacuoles at the base of host digestive cells in some types of *Hydra*, and this symbiosis has been widely used as a model system. In *Hydra*, algal volume per digestive cell is positively correlated with size of the host cell, suggesting that available space is a factor in determining the symbiont population size (Douglas and Smith, 1984). Zoochlorellae divide synchronously within the host cell following host feeding (McAuley, 1982, 1985, 1986); mitosis of digestive cells and their symbiotic algae increases about 12 h after feeding (McAuley, 1982). However, the number of zoochlorellae within dividing host cells increases before the host cells complete cytokinesis (McAuley, 1982, 1986), suggesting that in normal culture conditions zoochlorellae often divide before the host cells do. A similar phenomenon occurs when hydra regenerate (McAuley, 1986). To grow and survive in hydra, zoochlorellae require light as well as food, and their numbers are reduced in animals kept in the dark (Pardy, 1974a, b).

There are few analogous studies on control of cellular proliferation of symbiotic dinoflagellates in marine cnidarian host cells. However, many studies have documented the dissociation of these symbioses; these have largely focused on recent coral "bleaching events," which involve the loss of algal symbionts or their pigments (see references in Jokiel and Coles, 1990). Research in this area indicates that each partner in the symbiosis has its own physiological requirements and tolerances, and that even subtle changes in factors influencing the physiology of either partner may radically alter the steady-state of the symbiosis (*i.e.*, Porter *et al.*, 1989; Iglesias-Prieto *et al.*, 1992; Gates *et al.*, 1992; Fitt *et al.*, 1993, 1995).

Symbiotic dinoflagellates typically show peaks of dividing cells at dawn or at the beginning of the light period. For instance, cultured zooxanthellae maintained on a 14:10 light:dark cycle show division peaks at the beginning of the light period; the peaks are followed by the production of motile cells (Fitt and Trench, 1983). Zooxanthellae living in host gastrodermal cells (Muscastine *et al.*, 1998) exhibit phased division inside of the jellyfish *Mastigias* sp. (Wilkerson *et al.*, 1983), the hydroid *Myrionema amboinense* (Michael and Fitt, 1984; Fitt and Cook, 1990; McAuley and Cook, 1994), the sea anemone *Aiptasia pallida* (Cook *et al.*, 1988), and five species of Indo-Pacific reef corals (Smith and Hoegh-Guldberg, 1987; Hoegh-Guldberg, 1994). In contrast, asynchronous division of symbionts was reported from nine species of reef corals from Discovery Bay, Jamaica (Wilkerson *et al.*, 1988). Studies investigating synchrony of zooxanthellar mitosis with host cell division are generally lacking; limited data from the Caribbean staghorn coral *Acropora cervicornis* indicate night-time peaks in host cell division (Gladfelter, 1983).

The basis for the diel division patterns seen in zooxanthellar symbioses is not clear. It has been suggested that diel cycling of intracellular pH, driven by photosynthetic utilization of intracellular carbon dioxide, may be responsible by providing pulses of diffusible ammonia/ammonium (Fitt *et al.*, 1995). Pulses of nitrogen have long been thought responsible for phased division of phytoplankton in nature (*i.e.*, Doyle and Poore, 1974), and additions of high concentrations of dissolved nitrogen to seawater damped out the diel rhythm of zooxanthellar division in *Pocillopora damicornis* (Hoegh-Guldberg, 1994). That nutrients, either dissolved or from external food, are involved in the division of host cells and zooxanthellae is neither surprising nor as interesting as the temporal relationships between host feeding, availability of nutrients to symbionts, and mitosis of host cells and their intracellular zooxanthellae.

The tropical shallow-water marine hydroid *Myrionema ambionense* shares several characteristics with the green hydra symbiosis, making it a good model system for cellular studies of marine dinoflagellate symbioses: it has relatively rapid growth, it can be maintained in the laboratory, and the dynamics of host and symbiont cell relationships can be analyzed with cell maceration techniques. This study relates natural diel patterns of zooxanthellar division inside of hydroid host cells to diurnal feeding of the host, host cell division, and exposure to natural light:dark cycles.

Materials and Methods

Collection and maintenance of animals

Colonies of the hydroid *Myrionema ambionense* were collected from shallow-water (< 2 m) habitats adjacent to the Discovery Bay Marine Laboratory in Jamaica and used immediately in experiments. In some experiments animals were maintained in glass petri dishes in the laboratory in unfiltered seawater (SW) obtained from the laboratory seawater system at ambient air and water temperature (26°–28°C) and light (*ca.* 80 μE m^{-2}s^{-1}).

Determination of mitotic index (MI), symbiont densities, and vacuoles

Unless indicated otherwise, all experiments involved macerating (David, 1973) 5–10 polyps from each of six colonies of hydroids, each polyp including < 2 mm of stolon. Zooxanthellae from 100 digestive cells were observed and the number of symbionts in each cell was counted. Unhealthy looking zooxanthellae in host cells were counted from the same 100 digestive cells. The unhealthy looking dinoflagellaes were distinguished from their live counterparts by their lack of circular symmetry and relatively uneven and darker coloration (see Fig. 1C). The percentage of zooxanthellae dividing (mitotic index = MI) was determined from microscopic counts of cells with division furrows (doublets). The mean percentage of dividing zooxanthellae from each colony of hydroids was calculated from a minimum total of 1000 zooxanthellae. To determine the time of peak division of zooxanthellae in *Myrionema amboinense*, hydroids from each of the six colonies were collected from the field every 3 h for 24 h, macerated within 15 min of collection, and the MI determined.

The volume of the host cells was determined from their depth and surface area as described in Douglas and Smith (1984). Macerated cells are flattened and not cylindrical; they are variable in length and width but usually have a relatively straight basal edge and rounded apex. The distance between the points at which the upper and lower surfaces of the cell just go out of focus was found to be 9–12 μm, as determined from the scale on the focusing knob of the microscope, so the depth of digestive cells in macerations was taken as 10 μm. Surface areas were determined from length and width (average of widths at top and bottom of cell), measured for rectangular hydranth cells, and diameter for circular tentacle cells. Host cell division was determined by staining mitotic figures of digestive cells in macerated preparations with 4′,6-diamidino-2-phenylindole (DAPI) (Falkowski and Owens, 1982; McAuley, 1982). Number and estimated volume of intracellular vacuoles were also determined from the same 100 digestive cells described above. Only relatively large (>2 μm in diameter) vacuoles were monitored. The number and volume of the vacuoles was compared to the volume of the host cell in one experiment to estimate the relative portion of the cell taken up by vacuoles.

Hydroid growth rate

Five days before the beginning of the growth experiment, colonies of *Myrionema ambionense*, with 2 to 15 polyps, were collected and placed on microscope slides in glass petri dishes. Only colonies that had attached to the slides were subsequently used in experiments. Slides with attached hydroids were placed in SW in glass petri dishes in the laboratory or among natural colonies of hydroids in the field. Animals maintained in the laboratory were fed nauplii of *Artemia*, and the water was changed daily. The polyps were counted and the lengths of the stolons were measured for all experimental animals at the start of the experiment and after 7 days.

Factors influencing mitotic index

The relationship of light and feeding to division of symbiotic dinoflagellates was investigated in two experiments. In the first experiment hydroids were collected from the field in the dark just after dusk or preceding dawn. Half of the hydroids collected at each time were kept in constant dark, the other half in constant light (*ca.* 80 μE m^{-2}s^{-1}). The mitotic index of the zooxanthellae was determined from macerated hydroids, as described above, every 1–2 h for about 16 h after collection.

In the second experiment hydroids were unfed for 3–7 days and then fed *Artemia* nauplii for 1 h at the beginning of the dark period; they were then removed from the food source. Half the animals were subsequently maintained in constant light, the other half in the dark. At dawn (*i.e.*, 11 h following feeding) the MI of the symbionts was determined. Hydroids maintained in the dark were divided into two groups again, and held another 24 h in either a 14:10 h light:dark cycle or in constant dark. The MI was determined again at the next dawn, about 36 h after feeding.

Results

Distribution of zooxanthellae

Zooanthellate digestive cells of *Myrionema ambionense* have two general shapes: columnar from the hypostome (= cup) region of the hydranth (also called digestive cells here, Fig. 1) and circular from the tentacle portion of the hydranth (Fig. 2). The circular form is donut-shaped with a hole where the coelenteron extends up each tentacle (Fig. 2). Intermediate morphologies are found at the base of the tentacles (*i.e.*, Fig. 2c). Healthy looking zooxanthellae were located near the base of host hypostome cells, adjacent to the mesoglea (Fig. 1A–D), and usually at the periphery of tentacle cells, depending on the angle of observation (Fig. 2). Recently fed hydroids maintained in the laboratory also had zooxanthellae at the base of their digestive cells but contained many more vacuoles (Fig. 1B) than seen in unfed hydroids (Fig. 1A). Unhealthy looking zooxanthellae were usually located near the apical end of the cell, between the host nucleus and the coelenteron (Fig. 1C).

Most of the digestive cells in the hypostome of the hydroid contained one, two, or three zooxanthellae; only about a quarter harbored more than three symbionts (Figs. 1, 3). Gastrodermal cells in tentacles appear to develop from digestive cells in the hypostome that migrate from a presumed central division zone. Their bases and cell volume expand as they encircle the inside of the hollow tentacle (Fig. 2C), giving rise to their characteristic circular and semicircular shapes (Fig. 2). In contrast to digestive cells in the hypostome, tentacle cells usually held more than 10 zooxanthellae, with more than 75% of the tentacle cells containing between 10 and 40 zooxanthellae (Fig. 3). The

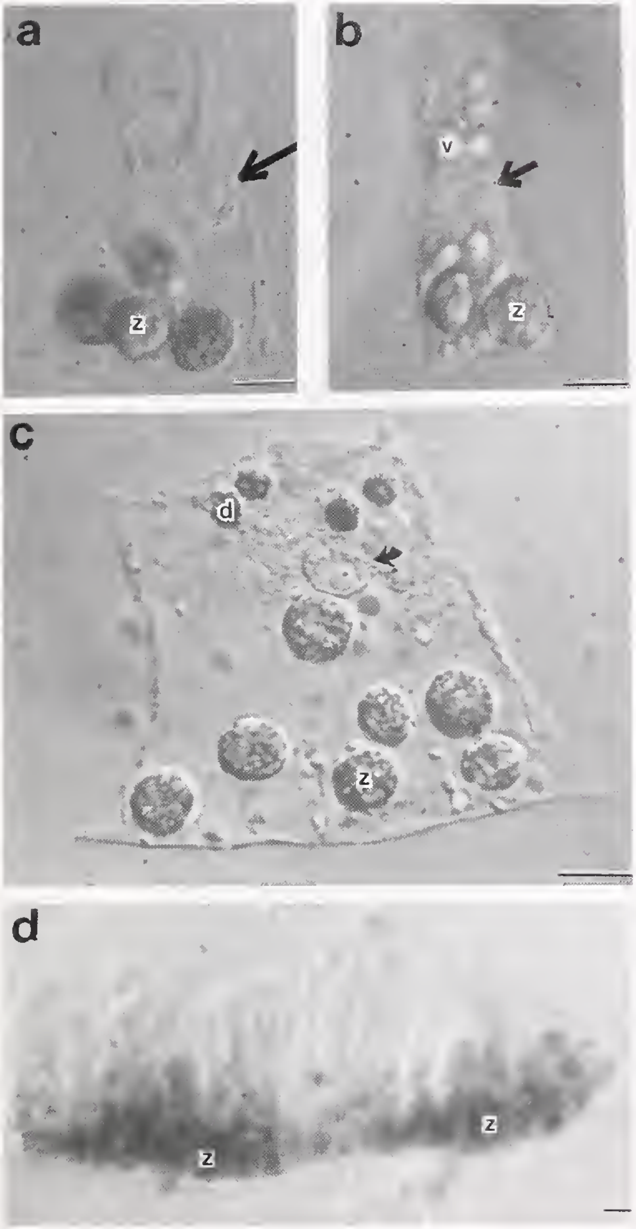

Figure 1. Gastrodermal cells from the hypostome of the hydroid of *Myrionema amboinense*. (a) Columnar digestive cell from hydroids collected in the afternoon containing four healthy looking zooxanthellae (z) and few vacuoles (v). (b) Columnar digestive cell from hydroids collected at night containing two zooxanthellae and numerous vacuoles. (c) Healthy looking zooxanthellae at basal end of this digestive cell contrast with four degenerate or unhealthy looking zooxanthellae (d) at the distal end of the digestive cell. (d) Row of columnar digestive cells from partially macerated polyp showing zooxanthellae at the base, away from the phagocytic distal end of their host cell. Arrows show centrally located host nucleus with prominent nucleolus. Bars = 10 μm.

highest number of symbionts in a single digestive cell was 69, observed in a tentacle cell.

Estimates of the relative volume of digestive cells in relation to their population of symbionts suggest that zooxanthellae may be limited by available space or physiological parameters associated with the size of the host cell. Larger host cells contained more zooxanthellae than smaller host cells, and the number of zooxanthellae residing inside of a digestive cell was directly correlated with the relative volume of the cell (Fig. 4). The average number of zooxanthellae in each hydroid polyp, including 1–2 mm of stalk, was 2.4 ± 0.2 (mean ± SD) × 10^5 ($n = 15$ different colonies).

Growth

Growth of a colony of *Myrionema* was surprisingly constant. When maintained in the laboratory for 1 week, hydroids grew an average of 4.3 ± 0.8 mm stolon length/d ($n = 15$) for each piece of stolon. There was no correlation between growth rate and initial size of the colony (range 1–15 polyps). Both laboratory-maintained and field-monitored colonies roughly doubled their number of polyps over an 8-day period (Fig. 5), regardless of colony size.

Diel patterns of host and symbiont division

Zooxanthellate division (MI = 16.6 ± 1.5%, $n = 6$) from field-collected hydroids peaked at dawn, declining to near zero in the early afternoon and evening (Fig. 6C). Thirty-four percent of the host cells containing zooxanthellae held at least one dividing algal cell over the diel period. The mean density of zooxanthellae per hydranth cell was 2.67. The density of zooxanthellae per hypostome digestive cell was highest in the mid-afternoon following the division peak (*ca.* 2.9 ± 0.1 zooxanthellae per host cell, $n = 6$), and lowest about 3 h after sunset (*ca.* 2.4 ± 0.4 zooxanthellae per host cell, $n = 6$) (Fig. 6C). This implies an average growth rate of about 0.5 zooxanthellae per digestive cell per day. The same value is obtained by multiplying the maximum number of zooxanthellae per host cell (2.9) by the MI (16.6%), again resulting in an increase of about 0.5 zooxanthellae per host cell per day. In other words, both methods show that the number of zooxanthellae in each hydranth digestive cell doubles about every 6 days.

The number of unhealthy looking zooxanthellae also exhibited a diel cycle (Fig. 6B). The number of unhealthy looking zooxanthellae per hydranth digestive cell showed a broad peak at about midnight (four highest data points = 1.04 ± 0.14 unhealthy looking zooxanthellae/cell), and reached a broad low during the day (four lowest data points = 0.72 ± 0.05 dead zooxanthellae/cell). To balance the average growth rate of colonies (doubling time = 8 days) with the average growth rate in number of zooxanthellae (doubling time = 6 days), an average digestive cell would have to lose about 1 zooxanthella every 8 days (0.14 zooxanthellae per day). This rate of loss of zooxanthellae is about half that calculated from the difference in average

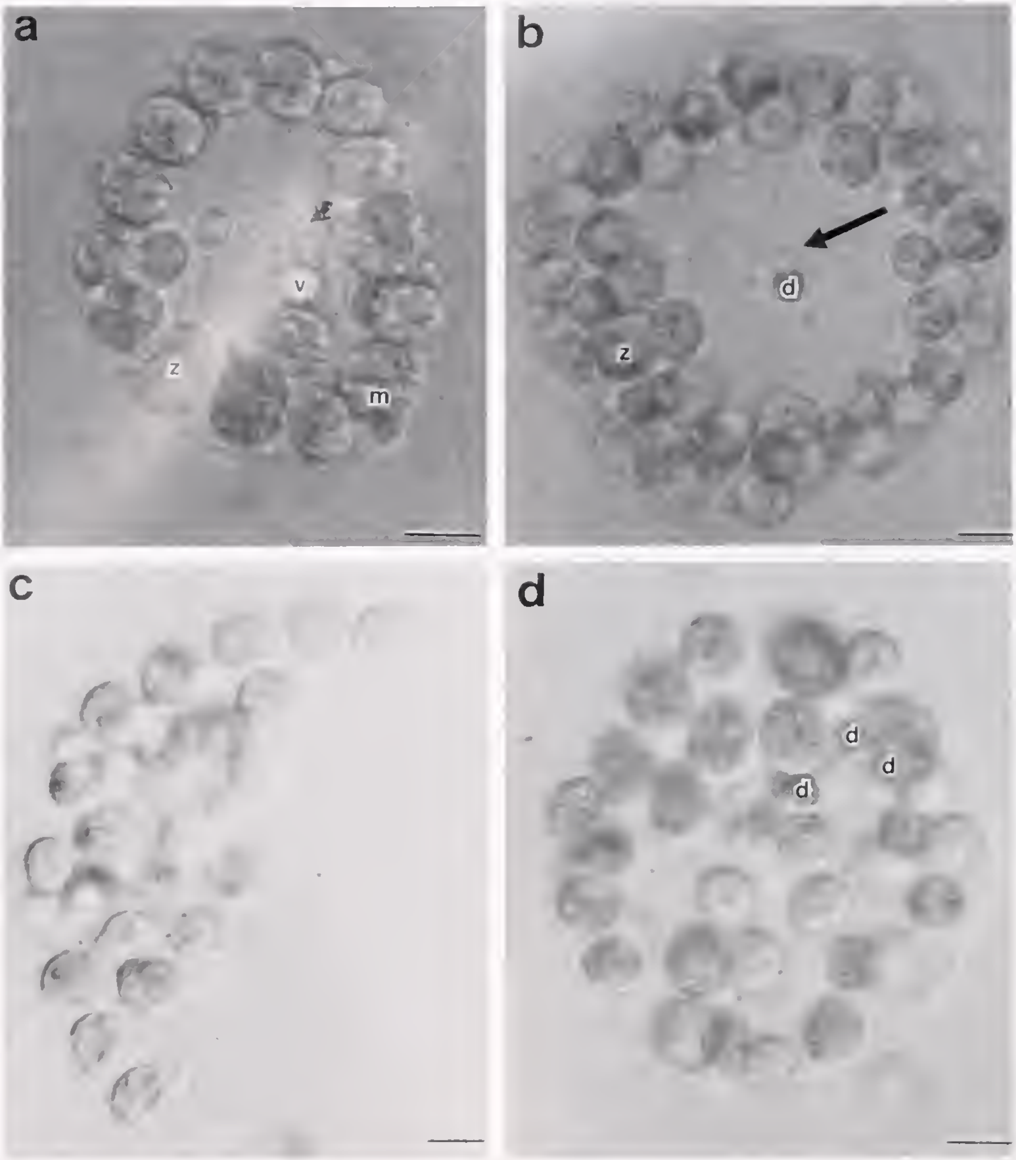

Figure 2. Gastrodermal cells from the tentacles of the hydroid *Myrionema amboinense*. (a, b) Circular disc-shaped digestive cells showing zooxanthellae (z) in the basal portion of the cell which would normally lie adjacent to the mesoglea in the tentacle, host nucleus (arrows) near the center, and lumen (extension of coelenteron) of hollow tentacle immediately below arrow. (c) Half-moon-shaped digestive cell, wrapping around the base of a tentacle. (d) Disc-shaped digestive cell showing degenerate or unhealthy looking zooxanthellae (d) near the center and at one side where the two ends of the base of the cell presumably have met. m = zooxanthella with division furrow indicating cytokinesis at the end of mitosis; v = vacuoles. Arrows show centrally located host nucleus with prominent nucleolus. Bars = 10 μm.

density of dead or moribund-looking zooxanthellae (0.32 zooxanthellae per day) observed over a 24-h period.

Though it was difficult to see final cytokinesis (telophase) of host digestive cells, nuclear staining with DAPI showed that mitosis in these cells (pro-, meta-, and anaphase) occurred predominantly in the evening (peak MI = 2.4 ± 1.3%, $n = 6$ colonies), compared to other times during the day (MI < 1%) (Fig. 6A). These data suggest that cytokinesis (cell separation) occurs first in the early evening, corresponding with the observed decrease in zooxanthellar density per host cell (see above).

Evidence for diel host feeding

Hydroids collected at night and macerated immediately after collection inevitably contained ingested prey items,

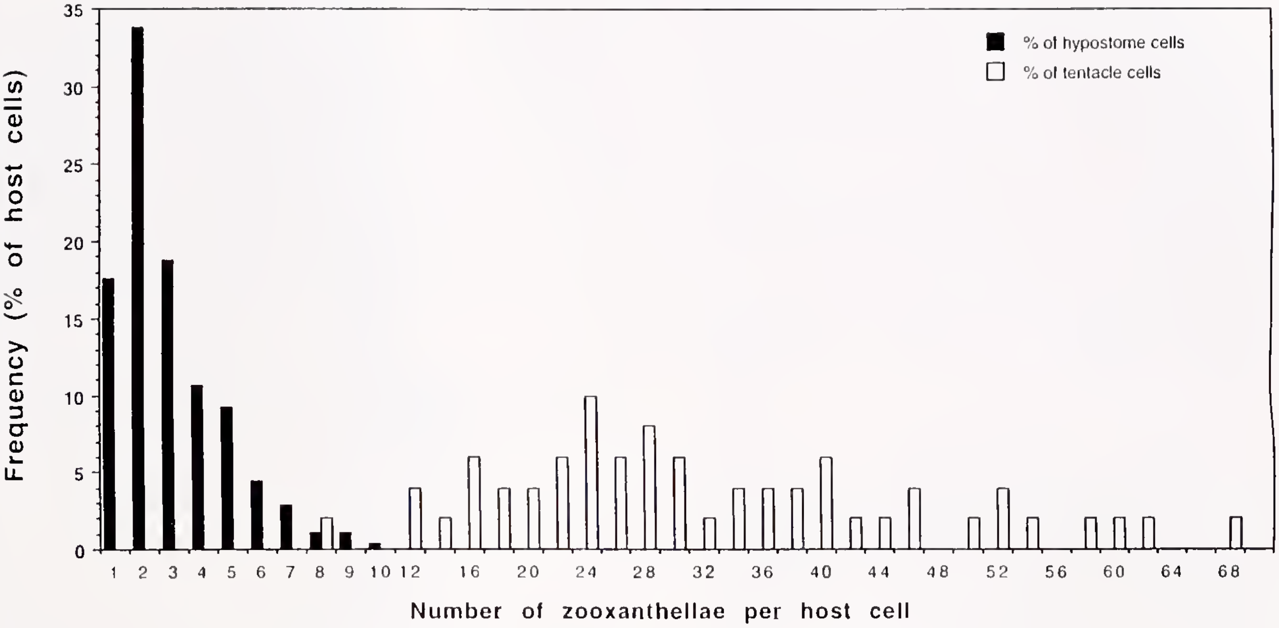

Figure 3. Frequency distribution of host gastrodermal cells of the hydroid *Myrionema ambionense* in relation to density of symbiotic dinoflagellates residing within. Solid bars indicate percent of columnar hypostome cells; clear bars show percent of circular tentacle cells.

such as arthropod exoskeletons, setae, and unidentified debris, that were not present in hydroids collected during the day. In addition, the presence of vacuoles within digestive cells showed a prominent diel cycle, with a rapid rise immediately after dusk in the percentage of digestive cells containing vacuoles and the number of vacuoles per digestive cell (Fig. 6A). Maximum values for these parameters extended from the middle of the night to the morning, then slowly decreased during the morning hours to afternoon lows. This pattern suggested that the vacuoles are actually food vacuoles associated with nighttime feeding by the hydroids. To test this hypothesis, starved animals (3–7 days) were fed brine shrimp nauplii for 1 h in the laboratory, then examined for vacuole formation hourly for the next 13 h. Within 2 h of feeding the percentage of host cells with vacuoles, the number of vacuoles per host cell, and the relative volume of the host cell filled with vacuoles in-

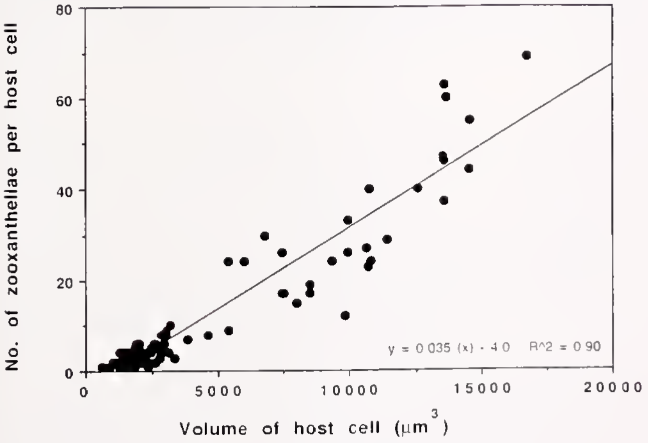

Figure 4. Relationship between number of symbiotic dinoflagellates and the volumn of the host (*Myrionema ambionense*) gastrodermal cells they live in.

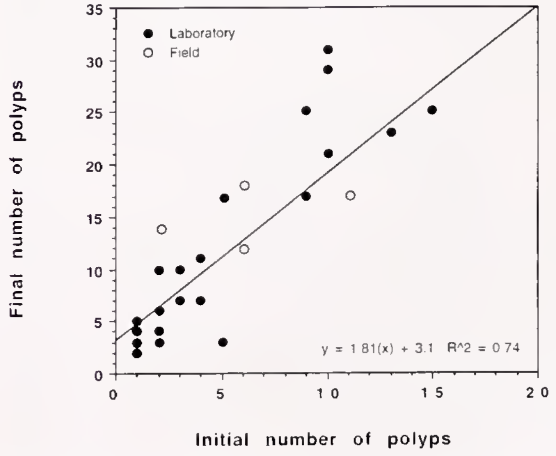

Figure 5. Growth after seven days of different-sized colonies of *Myrionema ambionense* in relation to initial colony size (1–15 polyps). Colonies were attached to glass slides and monitored both in the laboratory and the field.

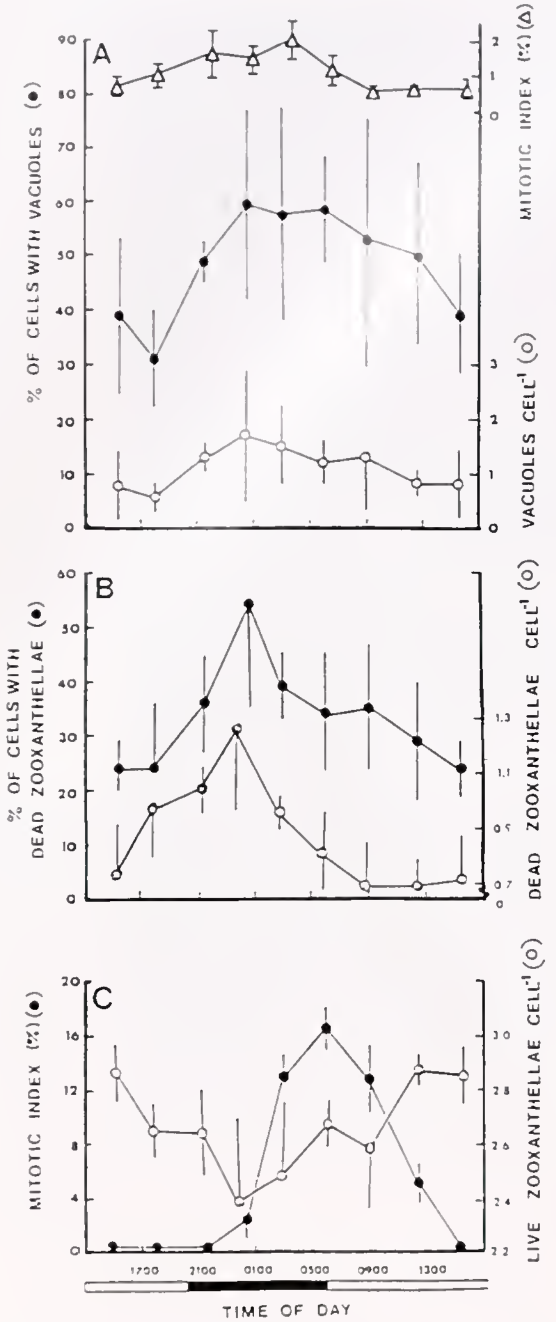

Figure 6. Distribution of symbiotic dinoflagellates (zooxanthellae) and food vacuoles within individual host cells of *Myrionema ambionense* in relation to time of day collected from the field. (A) Percent of hypostome digestive cells containing vacuoles and number of vacuoles per digestive cell and host cell mitotic index. (B) Percent of hypostome digestive cells containing degenerate or unhealthy looking zooxanthellae and number per digestive cell. (C) Percent of zooxanthellae with division furrows (mitotic index) and number of healthy looking zooxanthellae per hydranth digestive cell. Data presented as mean ± SD, *n* = 6. Dark bar on x axis denotes night; open bar indicates daytime.

creased rapidly (Fig. 7). These parameters returned to prefeeding levels about 6–8 h after feeding.

Environmental factors and relationship to diel patterns

The influence of photoperiod and feeding on zooxanthellate division was determined in two experiments. In the first experiment (Fig. 8A), hydroids collected at dusk and maintained without food in either constant light or dark showed the same level and timing of MI as seen in hydroids in the field (Fig. 6). Thus it appears that altering food and the light and dark periods less than 12 h before the expected peak in MI does not influence the division patterns of the zooxanthellae.

Hydroids that were collected from the field at the *end* of the dark period (when MI of symbionts was highest) and maintained in constant light or in constant dark showed

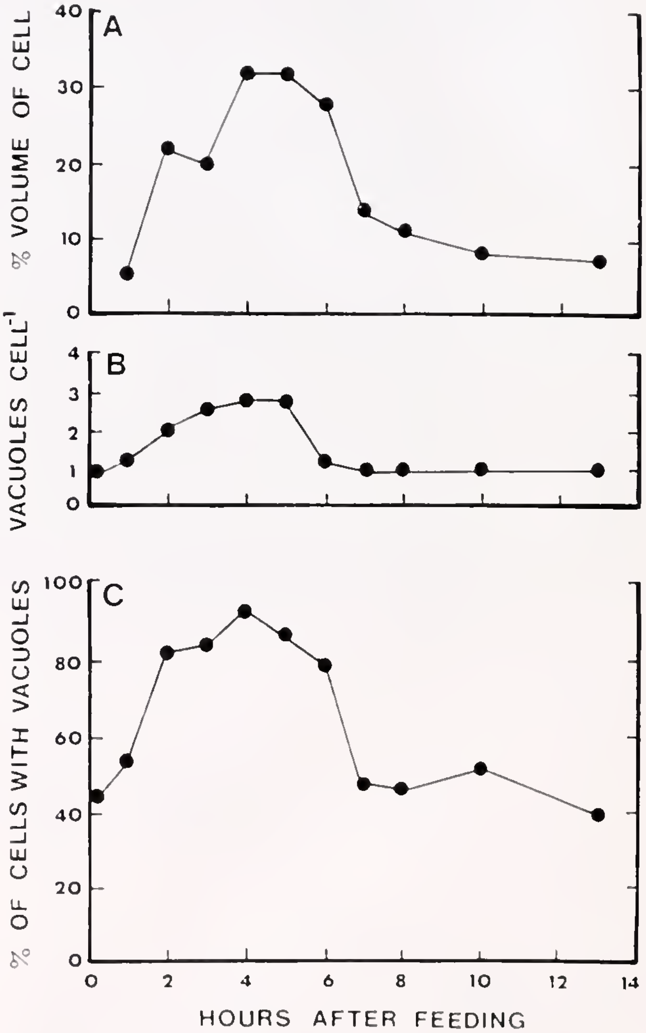

Figure 7. Relationship between vacuole appearance in digestive cells of *Myrionema ambionense* following a 1-h pulse-feeding with nauplii of brine shrimp (time 0). (A) Volume (area) of host cells occupied by vacuoles. (B) Average number of vacuoles per cell. (C) Percentage of digestive cells containing vacuoles. Each data point is the mean of 100 digestive cells from the hypostome.

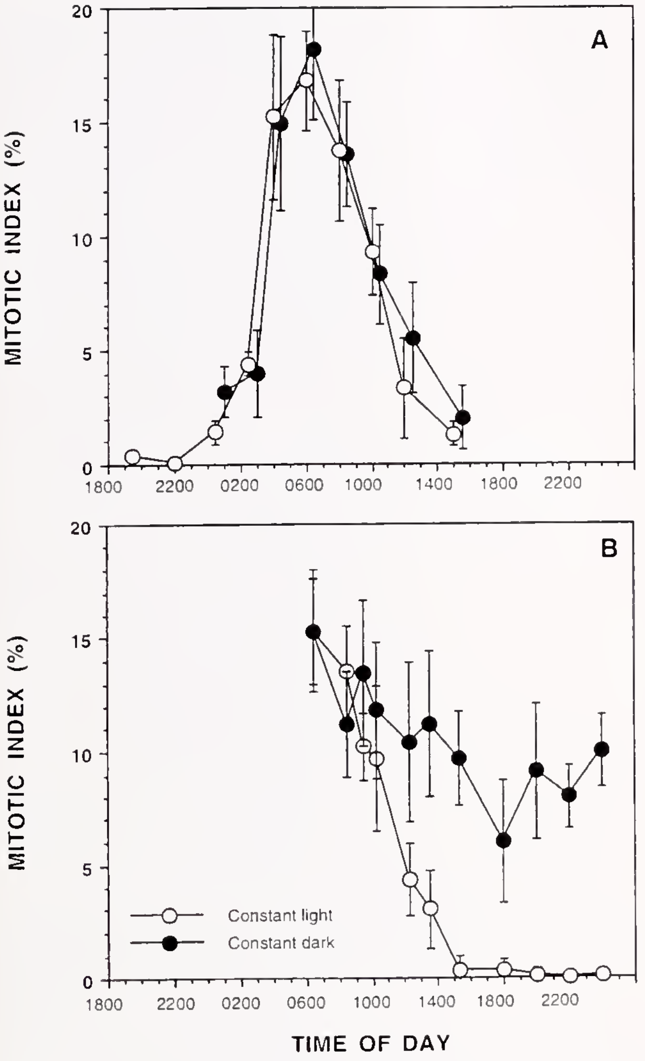

Figure 8. Relationship between mitotic index of symbiotic dinoflagellates residing in digestive cells of *Myrionema amboinense* when hydroids were either (A) collected at dusk (1900) and maintained in either constant light (open symbols) or constant dark (closed symbols) or (B) collected at the end of the night and maintained similarly in either constant light or dark.

slightly different results (Fig. 8B). Zooxanthellae from hydroids maintained in the light showed no changes in the division patterns seen in the field. In contrast, the hydroids maintained in constant darkness showed a slower decline in zooxanthellar cytokinesis during the afternoon period (Fig. 8B), suggesting that light was critical for the final stages of symbiont cytokinesis in this experiment.

In the second experiment, starved hydroids (3–7 days) were pulse-fed for an hour at the beginning of the dark period in the laboratory, then either maintained in constant light or left in the dark (Fig. 9). About 12 h after the pulse-feeding, those hydroids kept under constant light during the night had a higher MI (4.2% ± 1.4% SD, $n = 6$) than those hydroids kept in the dark (1.6% ± 0.9% SD, $n = 6$). The hydroids maintained in the dark for 12 h were then divided into two groups. The group that remained in the dark for an additional 24 h continued to show low algal MI (2.1%), while those moved into a 14:10 h light:dark cycle for 24 h showed a normal level of dividing cells (*ca.* 14.2%) 36 h after feeding. These results show that normal mitosis of symbiotic dinoflagellates in this hydroid requires three factors: external food; a minimum period of time following feeding (11–36 h), presumably for digestion to occur; and a period of light following feeding, presumably to provide carbon skeletons necessary for completing cytokinesis.

Discussion

This study shows that division of zooxanthellae and host cell is synchronized in the marine hydroid *Myrionema amboinense*, and that host feeding and light play an important role in the phased division patterns observed. Most, if not all, zooxanthellae symbioses appear to exhibit phased sym-

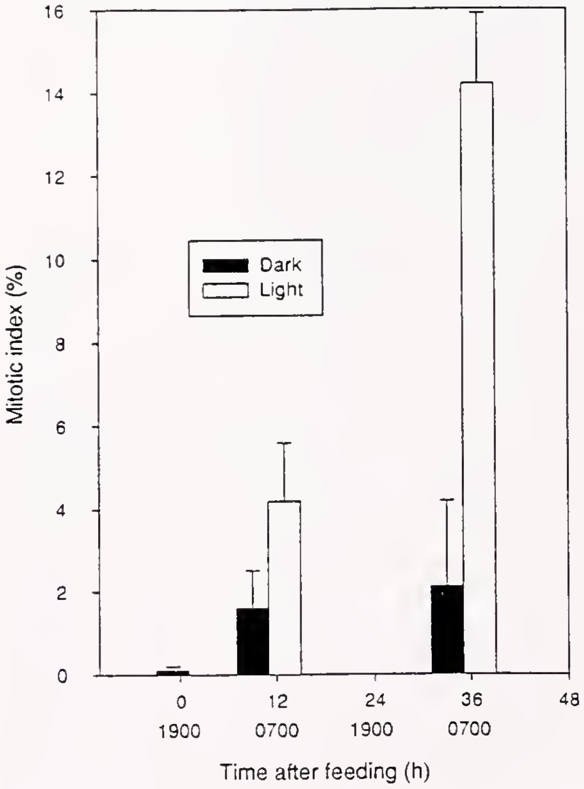

Figure 9. Relationship between feeding, light, and darkness on division (mitotic index) of symbiotic dinoflagellates residing in the hydroid *Myrionema amboinense*. Unfed (3–7 days) hydroids were fed for 1 h at time 0 (1900) and maintained for the next 11 h (12 h after feeding) in either constant dark (filled bars) or light (open bars). Animals kept in the light were then discarded, and those from the dark were maintained an additional 24 h (36 h after feeding) in either constant dark or on a normal 14:10 h light:dark cycle.

biont division *in situ*, with peaks in doublet cells seen around dawn (Michael and Fitt, 1984; Smith and Hoegh-Guldberg, 1987; Fitt and Cook, 1990; Cook and Fitt, 1990; Hoegh-Guldberg and Smith, 1989; McAuley and Cook, 1994; Hoegh-Guldberg, 1994). Symbiotic dinoflagellates in hosts removed from the reef or placed in seawater containing high concentrations of dissolved inorganic nitrogen (DIN) lose their division synchrony. For instance, additions of DIN damped out natural diel patterns of zooxanthellar division in the coral *Pocillopora damicornis* in Hawaii (Hoegh-Guldberg, 1994), and maintenance of the zooxanthellate jellyfish *Mastigias* sp. in the laboratory altered the MI of its symbionts (Muscatine *et al.*, 1986). Perhaps these observations explain asynchronous division of symbionts in nine species of reef corals removed from the reef in Jamaica and maintained in the laboratory in seawater containing high concentrations of DIN (D'Elia *et al.*, 1981; Wilkerson *et al.*, 1988).

This is the first study relating host cell division to zooxanthellar division in marine cnidarians. Research on symbiotic *Hydra* showed peaks in host cell mitosis and division of their *Chlorella* symbionts (cytokinesis) 10–12 h following feeding, such that brief increases in algal density observed before completion of host cell cytokinesis returned the number of symbionts per host cell to a steady-state level (Muscatine and Neckelmann, 1981; McAuley, 1982, 1986). Data from *Myrionema ambionense* suggest that dividing host cells completed cytokinesis *before* their symbiotic dinoflagellates finished dividing, such that *decreases* in symbiont densities were observed in the late afternoon and evening. Early morning cytokinesis of zooxanthellae returned densities of symbionts to their afternoon peak levels. Phased division of endothelial and calicoblastic epithelial coral cells in *Acropora cervicornis* also occurred during the middle of the night, and MI was less than 2% (Gladfelter, 1983). The peak percentage of cells containing mitotic figures in *Myrionema ambionense* was also low compared to the proportion of zooxanthellae dividing daily, due to the likelihood that during the cell cycle mitosis lasts much less than the 3-h sample interval, suggesting that many such events were missed between sample times. For instance, mitosis in well-fed *Hydra* lasted only about 1.5 h (David and Campbell, 1972).

Feeding and light are two factors linked to phased mitosis of zooxanthellae and host digestive cells in *Myrionema ambionense*. Digestive cells in *Hydra* also exhibit a diel periodicity in the mitotic index, with a midnight peak following a daily feeding regime at 1000 h each morning (see references in McAuley, 1994). Similarly, normal feeding of tropical marine cnidarians in nature appears to occur on a diel cycle set by the availability of demersal plankton food (Johannes and Tepley, 1974; Porter, 1974; Alldredge and King, 1977) or alternate sources of nitrogen (see Fitt *et al.*, 1995). Demersal plankton are thought to be most abundant on the reef at dusk and dawn (Glynn, 1973), though densities throughout the night are at least an order of magnitude greater than daytime densities. The data presented in the present study suggest that *Myrionema ambionense* feeds on demersal plankton at night, as evidenced by increased numbers of vacuoles in digestive cells following dusk in field populations of hydroids, and by laboratory feeding experiments (Fig. 7). Feeding on zooplankton provides nitrogen needed for cell growth, and night-time feeding would provide regular diel pulses of nitrogen. Nitrogen pulses are known to influence the timing and amount of algal division (Doyle and Poore, 1974). For instance, some diatoms maintained in the laboratory on a light-dark cycle, or in constant light, exhibited peaks of cell division following a pulse of nitrogen, whereas additions of the same daily total of nitrogen in equal increments throughout the day eliminated the periodicity within 24 h (Quarmby *et al.*, 1982; Yoder *et al.*, 1982). In giant clams, diffusible ammonia/ammonium in seawater is available at night, due to changes in pH within the host, driven by symbiont photosynthesis (Fitt *et al.*, 1995). A similar mechanism of delivering pulses of nitrogen to symbiotic reef corals and other cnidarians may control phased mitosis of their symbiotic dinoflagellates. Indirect support for this hypothesis includes the interesting observation that continuous addition of high concentrations of dissolved nitrogen to the coral *Pocillopora damicornis* caused a damping of diel peaks in MI of their zooxanthellae (Hoegh-Guldberg, 1994).

Light is also required for mitosis of symbiotic dinoflagellates, most likely to provide carbon skeletons needed both for the assimilation of DIN as well as for the respiratory metabolism associated with completion of cytokinesis, as evidenced by damping of the division patterns of zooxanthellae when the normal light:dark period is disturbed (Figs. 8b, 9). The intriguing delay in algal mitosis following feeding of starved hosts (Fig. 9) involves light, and is also seen in green hydra, where peaks in algal MI follow those of the host cells by 12 to 24 h (McAuley, 1985). The results for both symbioses suggest that although host cell mitosis follows host feeding by 12 to 24 h, the algal symbiont cell cycle is set 12 to 24 h later (24–36 h following feeding, depending on the synchronization of light and feeding cycles). These results also suggest that the close regulatory relationship between host and symbiont division may be easily disrupted. For instance, the *Chlorella* symbionts in green hydra will overgrow and actually burst their host digestive cell when unfed hydra are placed in a complex mixture of inorganic nutrients in the light (Muscatine and Necklemann, 1981).

Virtually all zooxanthellate cnidarians appear to expel some of their symbiotic dinoflagellates from their coelenteron on a daily basis (*e.g.*, Reimer, 1971; Hoegh-Guldberg *et al.*, 1987), whereas mass expulsion of zooxanthellae has been attributed to severe osmotic or thermal stress

(Goreau, 1964; Jokiel and Coles, 1977, 1990; Jaap, 1979; Glynn, 1983). The released zooxanthellae may be of normal morphology, with dividing and motile cells, or they may appear unhealthy, as described here. Most researchers feel that expulsion from the host is a way to partially balance increases of symbionts from algal division (Reimer, 1971; Hoegh-Guldberg *et al.*, 1987), and in cases where live zooxanthellae are released, a dispersal mechanism for infecting new hosts (Trench, 1979; Muller-Parker, 1984). Many sea anemones (Steele, 1977) and all of the giant clams (Trench *et al.*, 1981) release motile forms of zooxanthellae daily. Hoegh-Guldberg *et al.*, (1987) monitored a fire coral, a reef-building coral, and two soft corals and found that expulsion increased and most often peaked during the first part of the dark period (night). Smith and Muscatine (1986, pers. comm.) found the same pattern in extrusion of algal pellets from the sea anemone *Aiptasia pulchella*, though Stimson and Kinzie (1991) found peaks in release of zooxanthellae from the coral *Pocillopora damicornis* during the day. Unhealthy looking zooxanthellae seen in digestive cells of *Myrionema* are also most prevalent in the middle of the night. Although actual release by the host *in situ* has not been observed, hydroids maintained in the laboratory in petri dishes inevitably had small pellets made up of unhealthy looking zooxanthellae around them in the morning; presumably these were released by the polyps during the previous night. The density of unhealthy looking symbionts in *Myrionema* was negatively correlated with the density of healthy looking symbionts, such that the appearance of new zooxanthellae helped to balance diel loss from the release of unhealthy looking symbionts and from dilution due to host growth.

The results of this study also relate the high MI of symbiotic dinoflagellates to the rapid growth rates seen in *Myrionema ambionense* in the field (Fig. 5). Fire corals of the genus *Millepora* also grow fast and exhibit high rates of symbiont growth (Wilkerson *et al.*, 1988). These observations suggest that many of the "new" algae originating during mitosis (doubling time = 6 days) are in "new" digestive cells of *Myrionema ambionense* during normal growth of the animal (doubling time = 8 days) and are at least partially responsible for the high growth rates of the host. The role of host feeding and starvation in *Myrionema ambionense*, and the effects of additions of dissolved inorganic nutrients on zooxanthellar division patterns, as well as the role of light in the natural habitat, are investigated further in companion papers (Fitt and Cook, unpubl.). The ease of experimental manipulation, the availability of replicate polyps that can be collected with little or no damage to the reef, and the ability to clearly visualize zooxanthellae in host cells make this zooxanthellar symbiosis potentially amenable to answering some of the outstanding questions in marine symbioses.

Acknowledgments

This project was supported in part by University Research Expeditions of the University of California, National Science Foundation (OCE 9203327 and 9906976), Office of Naval Research (N00014-92-J-1734), and the University of Georgia Research Foundation. I thank the many people who helped in the field work, especially Drs. Robert Trench and Sylvia Chang. Dr. Clay Cook made useful comments on earlier drafts of the manuscript. Contribution #621 from the Discovery Bay Marine Laboratory and #017 from the Key Largo Marine Research Laboratory.

Literature Cited

Alldredge, A. L., and J. M. King. 1977. Distribution, abundance and substrate preferences of demersal reef zooplankton at Lizard Island lagoon, Great Barrier Reef. *Mar. Biol.* **41:** 317–333.

Cook, C. B., and W. K. Fitt. 1990. Some effects of dissolved inorganic nutrients on the growth of zooxanthellae in the hydroid *Myrionema amboinense*. Pp. 285–288 in *Endocytobiology IV*, P. Nardon, ed. INRA, Paris.

Cook, C. B., F. D'Elia, and G. Muller-Parker. 1988. Host feeding and nutrient sufficiency for zooxanthellae in the sea anemone *Aiptasia pallida*. *Mar. Biol.* **98:** 253–262.

David, C. N. 1973. A quantitative method for maceration of hydra tissue. *Wilhelm Roux Arch. Entwicklungsmech. Org.* **171:** 259–268.

David, C. N., and R. D. Campbell. 1972. Cell cycle kinetics and development of *Hydra attenuata*. I. Epithelial cells. *J. Cell Sci.* **11:** 557–568.

D'Elia, C. F., K. L. Webb, and J. W. Porter. 1981. Nitrate-rich groundwater inputs to Discovery Bay, Jamaica: a significant source of N to local reefs? *Bull. Mar. Sci.* **31:** 903–910.

Douglas, A. E., and D. C. Smith. 1984. The green hydra symbiosis. VIII. Mechanisms in symbiont regulation. *Proc. R. Soc. Lond.* **221:** 291–319.

Doyle, R. W., and R. V. Poore. 1974. Nutrient competition and division synchrony in phytoplankton. *J. Exp. Mar. Biol. Ecol.* **14:** 201–210.

Falkowski, P. G., and T. G. Owens. 1982. A technique for estimating phytoplankton division rates by using a DNA-binding fluorescent dye. *Limnol. Oceanogr.* **27:** 776–782.

Fitt, W. K., and C. B. Cook. 1990. Some effects of host feeding on growth of zooxanthellae in the marine hydroid *Myrionema ambionense* in the laboratory and in nature. Pp. 281–284 in *Endocytobiology* IV, P. Narclon, ed. INRA, Paris.

Fitt, W. K., and R. K. Trench. 1983. The relation of diel patterns of cell division to diel patterns of motility in the symbiotic dinoflagellate *Symbiodinium microadriaticum* Freudenthal in culture. *New Phytol.* **94:** 421–432.

Fitt, W. K., H. J. Spero, J. Halas, M. W. White, and J. W. Porter. 1993. Recovery of the coral *Montastrea annularis* in the Florida Keys after the 1987 Caribbean "bleaching event." *Coral Reefs* **12:** 57–64.

Fitt, W. K., T. A. V. Rees, and D. Yellowlees. 1995. Relationship between pH and the availability of dissolved inorganic nitrogen in the zooxanthellae-giant clam symbiosis. *Limnol. Oceanogr.* **40:** 976–982.

Gates, R. D., G. Baghdasarian, and L. Muscatine. 1992. Temperature stress causes host cell detachment in symbiotic cnidarians: implications for coral bleaching. *Biol. Bull.* **182:** 324–332.

Gladfelter, E. H. 1983. Spatial and temporal patterns of mitosis in the cells of the axial polyp of the reef coral *Acropora cervicornis*. *Biol. Bull.* **165:** 811–815.

Glynn, P. W. 1973. Ecology of a Caribbean coral reef. The *Porites* reef flat biotype Pt. II Plankton community with evidence for depletion. *Mar. Biol.* **22:** 1–22.

Glynn, P. W. 1983. Extensive "bleaching" and death of reef corals on the Pacific coast of Panama. *Environ. Conserv.* **10:** 149–154

Goreau, T. F. 1964. Mass expulsion of zooxanthellae from Jamaican reef communities after Hurricane Flora. *Science* **145:** 383–386.

Hoegh-Guldberg, O. 1994. Population dynamics of symbiotic zooxanthellae in the coral *Pocillopora damicornis* exposed to elevated ammonium concentrations. *Pac. Sci.* **48:** 263–272.

Hoegh-Guldberg, O., and G. J. Smith. 1989. Influence of the population density of zooxanthellae and supply of ammonium on the biomass and metabolic characteristics of the reef corals *Seriatopora hystrix* and *Stylophora pistillata*. *Mar. Ecol.* **57:** 173–186.

Hoegh-Guldberg, O., L. R. McCloskey, and L. Muscatine. 1987. Expulsion of zooxanthellae by symbiotic cnidarians from the Red Sea. *Coral Reefs* **5:** 201–204.

Iglesias-Prieto, R., J. L. Matta, W. A. Robins, and R. K. Trench. 1992. Photosynthetic response to elevated temperature in the symbiotic dinoflagellate *Symbiodinium microadriaticum* in culture. *Proc. Natl. Acad. Sci. USA* **89:** 10302–10305.

Jaap, W. C. 1979. Observations on zooxanthellae expulsion at Middle Sambo Reef, Florida Keys. *Bull. Mar. Sci.* **29:** 414–422.

Johannes, R. E., and L. Tepley. 1974. Examination of feeding of the reef coral *Porites lobata in situ* using time-lapse photography. *Proc. 2nd Int. Coral Reef Symp.* **2:** 369–374.

Jokiel, P. L., and S. L. Coles. 1977. Effects of temperature on the mortality and growth of Hawaiian reef corals. *Mar. Biol.* **43:** 201–208.

Jokiel, P. L., and S. L. Coles. 1990. Response of Hawaiian and other Indo-Pacific reef corals to elevated temperature. *Coral Reefs* **8:** 155–162.

McAuley, P. J. 1982. Temporal relationships of host cell and algal mitosis in the green hydra symbiosis. *J. Cell Sci.* **58:** 423–431.

McAuley, P. J. 1985. The cell cycle of symbiotic *Chlorella*. I. The relationship between host feeding and algal cell growth and division. *J. Cell Sci.* **77:** 225–239.

McAuley, P. J. 1986. The cell cycle of symbiotic *Chlorella*. III. Numbers of algae in green hydra digestive cells are regulated at digestive cell division. *J. Cell Sci.* **85:** 623–671.

McAuley, P. J. 1994. Interactions between hosts and symbionts in algal invertebrate intracellular symbioses. *Bot. J. Scotl.* **47:** 97–112.

McAuley, P. J., and C. B. Cook. 1994. Effects of host feeding and dissolved ammonium on cell division and nitrogen status of zooxanthellae in the hydroid *Myrionema amboinense*. *Mar. Biol.* **121:** 343–348.

Michael, W. C., and W. K. Fitt. 1984. Effects of a water-soluble fraction of a crude oil on the coral reef hydroid *Myrionema hargitti:* feeding, growth and algal symbionts. *Mar. Biol.* **84:** 143–154.

Muller-Parker, G. 1984. Dispersal of zooxanthellae on coral reefs by predators on cnidarians. *Biol. Bull.* **167:** 159–167.

Muscatine, L., and N. Neckelmann. 1981. Regulation of numbers of algae in the *Hydra-Chlorella* symbiosis. *Ber. Dtsch. Bot. Ges.* **94:** 571–582.

Muscatine, L., and R. R. Pool. 1979. Regulation of numbers of intracellular algae. *Proc. R. Soc. Lond.* **204:** 131–139.

Muscatine, L., F. P. Wilkerson, and L. R. McCloskey. 1986. Regulation of population density of symbiotic algae in a tropical marine jellyfish (*Mastigias* sp.). *Mar. Ecol.* **32:** 279–290.

Muscatine, L., C. Ferrier-Pages, A. Blackburn, R. D. Gates, G. Baghdasarian, and D. Allemand. 1998. Cell-specific density of symbiotic dinoflagellates in tropical anthozoans. *Coral Reefs* **17:** 329–337.

Pardy, R. L. 1974a. Some factors affecting the growth and distribution of the algal endosymbionts of *Hydra viridis*. *Biol. Bull.* **147:** 105–118.

Pardy, R. L. 1974b. Regulation of the endosymbiotic algae in *Hydra* by digestive cells and tissue growth. *Am. Zool.* **14:** 583–588.

Porter, J. W. 1974. Zooplankton feeding by the Caribbean reef-building coral *Montastrea annularis*. *Proc. 2nd Int. Coral Reef Symp.* **1:** 111–125.

Porter, J. W., W. K. Fitt, H. J. Spero, C. S. Rogers, and M. W. White. 1989. Bleaching in reef corals: physiological and stable isotopic responses. *Proc. Natl. Acad. of Sci. USA* **86:** 9342–9346.

Quarmby, L. M., D. H. Turpin, and P. J. Harrison. 1982. Physiological responses of two marine diatoms to pulsed additions of ammonium. *J. Exp. Mar. Biol. Ecol.* **63:** 173–181.

Reimer, A. A. 1971. Observations on the relationships between several species of tropical Zoanthids (Zoanthidae, Coelenterata) and their zooxanthellae. *J. Exp. Mar. Biol. Ecol.* **7:** 207–214.

Smith, G. J., and O. Hoegh-Guldberg. 1987. Variation in the growth rates of zooxanthellae with coral host colony size and ontogenetic stage is not controlled by changes in the duration of cytokinesis. *EOS* **68:** 724.

Smith, G. J., and L. Muscatine. 1986. Carbon budgets and regulation of the population density of symbiotic algae. *Endocyt. Cell Res.* **3:** 213–238.

Steele, R. D. 1977. The significance of zooxanthellae-containing pellets extruded by sea anemones. *Bull. Mar. Sci.* **27:** 591–594.

Stimson, J., and R. A. Kinzie. 1991. The temporal pattern and rate of release of zooxanthellae from the reef coral *Pocillopora damicornis* (Linnaeus) under nitrogen-enrichment and control conditions. *J. Exp. Mar. Biol. Ecol.* **153:** 63–74.

Trench, R. K. 1979. The cell biology of plant-animal symbiosis. *Annu. Rev. Plant Physiol.* **30:** 485–531.

Trench, R. K., D. S. Wethey, and J. W. Porter. 1981. Observations on the symbiosis with zooxanthellae among the Tridacnidae (Mollusca, Bivalvia). *Biol. Bull.* **161:** 180–198.

Wilkerson, F. P., G. Muller-Parker, and L. Muscatine. 1983. Temporal patterns of cell division in natural populations of endosymbiotic algae. *Limnol. Oceanogr.* **28:** 1009–1014.

Wilkerson, F. P., D. Kobyashi, and L. Muscatine. 1988. Mitotic index and size of symbiotic algae in Caribbean reef corals. *Coral Reefs* **7:** 29–36.

Yoder, J. A., J. Martin, and A. Nill. 1982. Cell division periodicity and the nitrate environment of a marine diatom. *Limnol. Oceanogr.* **27:** 352–357.

Yonge, C. M., and A. G. Nichols. 1931. Studies on the physiology of corals. IV. The structure, distribution, and physiology of the zooxanthellae. *Sci. Rep. Great Barrier Reef Exped.* **1:** 135–176.

Reference: *Biol. Bull.* **198:** 121–151. (February 2000)

Discrimination and Phylogeny of Solenogaster Species Through the Morphology of Hard Parts (Mollusca, Aplacophora, Neomeniomorpha)

AMÉLIE H. SCHELTEMA* AND CHRISTOFFER SCHANDER

Woods Hole Oceanographic Institution, Woods Hole, Massachusetts 02543

Abstract. Ten species in five genera and three families from continental shelf and deep-sea collections of neomenioid Aplacophora (Mollusca) are described, emphasizing external anatomy and hard parts—body shape, radula, epidermal spicules, and copulatory spicules—as well as the reproductive system. One genus and seven species are new: *Plawenia* n.g., *Plawenia sphaera, P. argentinensis, Dorymenia tortilis, Eleutheromenia bassensis, E. minus, Kruppomenia levis,* and *K. delta.* Also included are redescriptions of three published species, emphasizing hard parts for comparisons with the new species and genus: *Dorymenia sarsii* (Koren & Danielssen), *Simrothiella margaritacea* (Koren & Danielssen), and *Plawenia schizoradulata* (Salvini-Plawen). A cladistic analysis of species described here demonstrates the usefulness of hard parts for phylogeny. Specimens came from collections made in the southwest Pacific and the southwest and northeast Atlantic.

Introduction

Aplacophora are vermiform, spicule-covered molluscs that are most numerous and have the greatest diversity of species at depths greater than 200 m in the sea. But their internal anatomy seems to be primitive for the Mollusca, and the vermiform shape derived, a combination thought to be the result of progenesis (Scheltema, 1993, 1996). Aplacophora comprise two taxa, the Neomeniomorpha (=Solenogastres) and the Chaetodermomorpha (=Caudofoveata). Most neomenioids creep by means of a narrow foot on mud bottoms or on hydroids and octocorals upon which they feed; they are hermaphrodites. Chaetoderms are burrowers, feeding upon foraminifera or organic detritus; they are dioecious.

Of the two Aplacophora taxa, we believe the neomenioids are the less derived (Scheltema, 1993, 1996; Scheltema *et al.*, 1994; Ivanov, 1996), and are thus particularly important in considerations of the phylogeny of molluscs. However, the opposite view—that they are more derived—has been expressed (Salvini-Plawen, 1985; Salvini-Plawen and Steiner, 1996).

There are at present fewer than 250 described neomenioid species. However, every deep-sea and continental shelf sample taken with modern equipment, and processed by elutriating the collected sediment through fine screens (<0.4 mm mesh size), will contain at least a few, and sometimes more than a dozen, neomenioid species. Moreover, in regions never before sampled, many or most of these species will be new. By our present estimates, which are based both on the number of undescribed species already collected and on the vast areas of the deep-sea benthic fauna that have yet to be sampled, there are probably some 1000 species worldwide.

Although the works of Salvini-Plawen have raised important evolutionary issues (especially 1972, 1985; also, Salvini-Plawen and Steiner, 1996), aplacophorans have not received broad attention, owing in large part to the difficulty of obtaining living specimens (but see Salvini-Plawen, 1968; Morse, 1979; Morse and Norenberg, 1992; Scheltema and Jebb, 1994). Also, we suggest that the inadequate taxonomic characterization, particularly of neomenioids, has prevented most biologists from becoming seriously involved with them. Authors of most monographs of neomenioids have concentrated on internal anatomy as understood from histology (*e.g.*, Nierstrasz, 1902; Heath, 1911, 1918; Odhner, 1921; Salvini-Plawen, 1978). An important consequence of histological preparation is that hard structures are

---

Received 28 May 1998; accepted 27 October 1999.

* To whom correspondence should be addressed. E-mail: ascheltema@whoi.edu

dissolved or destroyed, and have thus been poorly illustrated. Moreover, careful drawings and photographs of entire organisms have seldom been published (but see Scheltema and Kuzirian, 1991). A few isolated epidermal spicules may have been drawn, but at too small a scale for comparisons with other species. Radulae have not been isolated for illustration: the radular teeth have either been drawn as part of a histological section or reconstructed from sectioned material. Copulatory spicules, which dissolve during histological preparation, have practically never been illustrated at all, yet they are often the most important structures for species determination (*e.g., Eleutheromenia* species; see below). The absence of hard-part and external morphology from neomenioid descriptions reduces the value of the characterization—like describing the soft anatomy of a gastropod, but not its shell or isolated radula. As deep-sea ecologists collect more neomenioids, they are thus unable to identify them from the literature.

This paper therefore focuses on external anatomy and on the morphology of isolated hard parts. Descriptions of genera and species are arranged as follows: *Diagnoses* of genera are arranged in the following order: appearance, spicule type, cuticle, epidermis, radula, and particulars of anatomy from anterior to posterior. Species *Descriptions* are divided into Appearance, Cuticle and epidermis, Epidermal spicules, Radula, Copulatory spicules, Notes on anatomy, and Reproductive system. Following both diagnoses and descriptions are *Remarks* on particulars for species discrimination, problems of classification, and notable anatomical features or puzzles. We expect that specialists and nonspecialists alike will be able to use these descriptions to identify similar species at least to genus.

A second aim of this paper was to perform a preliminary phylogenetic analysis based on both the hard-part morphologies and the soft anatomy briefly described here (particularly the reproductive system). We hope that, as new deep-sea collections become available, this paper will serve as a useful model for describing neomenioid species and for investigating their phylogenetic relationships.

General Anatomy of Neomeniomorpha

Recent accounts of aplacophoran anatomy are given in Salvini-Plawen (1985) and Scheltema *et al.* (1994). A generalized illustration of a neomenioid may be found in Figure 1.

The first characteristics one notices in a neomenioid are the size and shape of the body, and the attitude of the myriad, usually shining aragonite spicules covering the animal—that is, the outer *appearance* (Fig. 11C, E). Body shape varies from almost spherical (Fig. 19D) to greatly elongate (Fig. 6A), and the length of mature individuals varies from 1 or 2 mm to 10 cm or more (Fig. 11C, F). A neomenioid may be spiny, smooth, or rough (Figs. 6, 11).

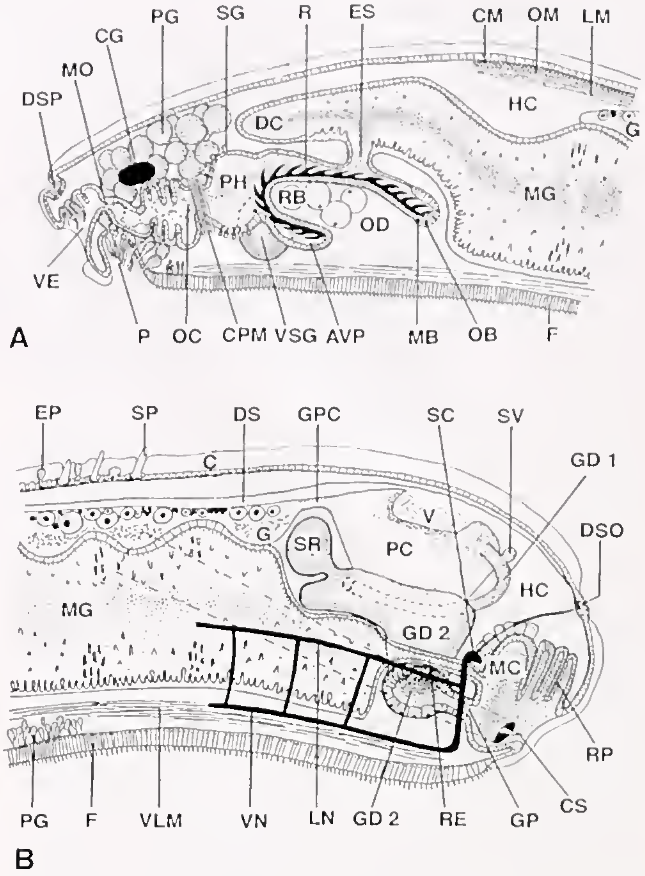

Figure 1. Anatomy of generalized Neomeniomorpha. (A) Anterior. (B) Posterior. AVP anteroventral radular pocket, C cuticle, CG cerebral ganglion, CM circular bodywall muscles, CPM circumpharyngeal muscle, CS copulatory spicule, DC dorsal cecum, DS dorsal sinus/aorta, DSO dorsoterminal sense organ, DSP dorsofrontal sensory pit, EP epidermal papilla, ES esophagus, F foot, G gonad, GD1 upper gametoduct, GD2 lower gametoduct, GP gametopore, GPC gonopericardial duct, HC haemocoel, LM longitudinal bodywall muscles, LN lateral nerve cord, MB membranoblast, MC mantle cavity, MG midgut, MO mouth opening, OB odontoblast, OC oral cavity, OD odontophore, OM oblique bodywall muscles, P pedal pit, PC pericardial cavity, PG pedal gland cell, cells greatly enlarged and numerous anteriorly, PH pharynx, R radula, RB radula bolster, RE rectum, RP respiratory papilla, SC suprarectal commissure, SG salivary gland cell, SP epidermal spicule, SR seminal receptacle, SV seminal vesicle, V ventricle, VE vestibule, VLM ventral longitudinal muscle, VN ventral nerve cord, VSG ventral salivary gland. (Modified from Scheltema *et al.*, 1994.)

The shape of retracted mouth and mantle-cavity openings may be diagnostic (Fig. 15C, H).

The *cuticle* and *epidermis* can be either thick or thin relative to the size of the species. A thick cuticle can occur with a thin epidermis, or a thin cuticle with a thick epidermis, or they may be the same thickness. Gland cells of the epidermis, termed *papillae*, may have long stalks or be unstalked (Fig. 1B, EP); their function has not been determined.

The *epidermal spicules* can be (1) *skeletal* (= tangential)—the spicules lie within the cuticle, at right angles to each other, in one or more layers, spiraling from ventroanterior to dorsoposterior and from dorsoanterior to ventroposterior (Fig. 20A); (2) *upright* (=radial)—arranged in a single layer, more or less erect, usually with the distal ends extending beyond the cuticle (Fig. 19); and (3) *adpressed*, with a single layer of overlapping spicules lying flat against the body wall cuticle (*e.g., Tegulaherpia;* see Scheltema, 1999a, fig. 3A). Species may exhibit one arrangement, a combination of (1) and (2) (Fig. 12A, D), or a combination of (2) and (3) (*e.g., Acanthomenia;* see Scheltema, 1999b, fig. 2). Spicules may be rounded and hollow with a wall surrounding a single space, or solid and flat or rounded, and encompass a variety of shapes and sizes; several types may occur within a single species. The spicules beside the pedal groove are somewhat arcuate, or at least convexly curved on one side, and are arranged in a single longitudinal row on each side of the pedal groove; they often bear a "handle," or *root* (Fig. 8B spicule 5, and Fig. 20G). Most neomenioids have a few to numerous specialized spicules at the entrance to the mantle cavity; these are presumably used in copulation (Fig. 4K, L).

The *radula* of neomenioids may have two teeth per row (*distichous*) (Figs. 11B, 21A), one tooth per row (*monostichous*) (*e.g., Acanthomenia,* see Scheltema, 1999b, fig. 3A, B), or many teeth per row (*polystichous*) (Fig. 2E, F). The terms "biserial" and "monoserial" are ambiguous, having been applied to both a divided radular membrane and a radula with two teeth per row (Scheltema, 1981); these terms are not used here. Distichous radulae are of two types: they are formed of (1) *bars* entirely attached to the radular membrane and bearing denticles or serrations (Figs. 12F, G, 19E, G), or (2) denticulate *hooks* mostly free of the radular membrane (Fig. 11D). A radula is lacking in 20% of known species. Both distichous and polystichous radulae lack a central, median tooth like the rachidians in gastropod radulae, the only exception being in some species of Proneomeniidae (*e.g.,* García-Alvarez *et al.,* 1998). In distichous radulae, the largest denticles are lateral (Figs. 7H, J, 17A, 21F); during growth, denticles are added either medially or by the bifurcation of a pre-existing denticle (Fig. 7H). In many species, the radula passes into, and is enclosed by, an anteroventral radular pocket, or pair of pockets (Figs. 1 AVP; 6B, 19F).

One or more *copulatory spicules* are found in many species of neomenioids (Fig. 14). They are largely or entirely calcitic (Figs. 4A, 9) and secreted in deep, usually paired pockets of the mantle cavity; they are thus of epidermal origin. Accessory spicules may be present (Figs. 20C, 22B, D). The exact function of copulatory spicules has never been determined. They are deciduous or become resorbed in some species, and some may be one-third the total length of an individual.

Notes on anatomy are given here for various species, according to their importance to that species for discrimination or for defining membership in higher ranks. The *tetraneural nervous system,* not described here, is morphologically quite constant among neomenioids. Examples may be found in Salvini-Plawen (1985) and Scheltema *et al.* (1994).

Salivary glands are associated with the radula or, if the radula is absent, with some part of the pharynx (Fig. 1, VSG, SG). In this work, the types of ventral salivary glands were determined according to Welsch and Storch (1973), rather than according to Salvini-Plawen (1978). The glands are usually ventrally paired, simple, multicellular, tubular glands that are elongate or saclike (Figs. 5A, 6B). They are sometimes acinar, or occur in groups of single goblet gland cells, or are compound.

The *midgut* dominates the midregion of the body and is extensive in elongate species. It is *sacculate* (*i.e.,* with lateral pouches) in those species where the midgut wall is interrupted by serially repeated, lateroventral muscles (see Scheltema *et al.,* 1994, fig. 13C). A dorsal cecum may extend anteriorly above the pharynx (Fig. 1A, DC; Scheltema *et al.,* fig. 8C).

The *mantle cavity* contains one or two gametopores, the anus, openings of the copulatory spicule sacs, and usually respiratory folds or papillae. There is usually a dorsoterminal sense organ on the outer dorsal wall of the mantle cavity.

For most species herein, the *reproductive system* is described. As in the chaetoderms, it is unique among molluscs, because the gonads, with only a single exception, empty through paired *gonopericardial ducts* directly into the pericardial cavity (Fig. 1B, GPC); in other molluscs, the gonads empty through gonoducts that bypass the pericardium. The gametes thus pass through the pericardium before entering the (usually) U-shaped, paired, upper and lower gametoducts (=pericardioducts and spawning ducts or shell glands; Stachowitsch, 1992) (Fig. 1B, GD1, GD2). The lower gametoducts, in turn, empty into the small posterior or posteroventral mantle cavity through paired gametopores; or the lower gametoducts unite before opening through a single gametopore. Usually, one or more paired seminal receptacles are found near the union of the upper and lower gametoducts (Figs. 1B, SR; 5A, 5). Seminal vesicles are uncommon; where they do occur, they are found in conjunction with either the gonopericardial ducts or the upper gametoducts (Fig. 6C). Internal fertilization is inferred from the presence of seminal receptacles, from introsperm morphology (Buckland-Nicks and Scheltema, 1995), and from observation of living *Epimenia* (Scheltema and Jebb, 1994).

Materials and Methods

Species were selected from the following collections of Aplacophora: West European Basin (INCAL, 15 July to 11 August, 1976, Centre National de Tri d'Océanographie Biologique [CENTOB]; and RV *Chain* Cruise 106, 15 August to 6 September, 1972, Woods Hole Oceanographic Institution); off Gibraltar (BALGIM, 25 May to 22 June, 1984, CENTOB); Bass Strait (Bass Strait Survey 1979–1984, Museum of Victoria, Australia); and Argentine Basin (RV *Atlantis II* Cruise 60, 10.iii–30.iii.1971).

Taxonomy. Holotypes were drawn under a dissecting microscope equipped with an ocular drawing tube and then photographed. Measurements were made on drawings, either with a map wheel or with dividers. The *length* of a specimen in lateral view is measured along the axial midline; two diameters, the dorsoventral *height* and lateral *width*, are measured in lateral and either dorsal or ventral view, respectively.

Epidermal spicules were dislodged with a needle, either into glycerine in a depression slide or into distilled water on a flat slide; in the latter case, they were then air dried and covered with a coverslip and mountant. These isolated spicules were then illustrated with the aid of an ocular drawing tube. Solid spicules were examined under cross-polarized light, which is broken up into birefringent color bands by the aragonite crystals of the spicules; selected isochromes were drawn and their thickness determined.

Radulae and copulatory spicules were isolated and prepared as follows. The anterior and posterior ends of an individual were cut off and placed in a depression slide with a drop of commercial hypochlorite solution (household bleach), which dissolves the tissue. The radula or copulatory spicules were then teased away from the remaining cuticle and epidermal spicules. The preparations were washed several times by carefully adding and drawing off distilled water with a pipette, and a drop of glycerine was then added. When radular teeth were to be examined with an oil immersion lens, either a temporary or permanent slide was made. In the first case, the radula was transferred into glycerine on a flat slide, and a coverslip was added. To make a permanent slide, the radula was washed in distilled water, then pipetted into a drop of a water-miscible mountant (CMCP-10) on a slide and a coverslip added. After drawings had been made of copulatory spicules in glycerine on a depression slide, permanent slides were prepared. The spicules were washed with distilled water and transferred to a slide with the aid of a micropipetter, which can pick up and release individual spicules. After air-drying, a mountant and coverslip were added. Measurements of radulae, epidermal spicules, and copulatory spicules were made with an ocular micrometer.

Histologic sections were cut at 7 μm (paraffin embedded) or at 1.5 or 3.0 μm (Epon embedded). The former were stained with hematoxylin and Gray's double contrast or with Mallory-Heidenhain trichrome; the Epon sections were stained with azure II and methylene blue. All drawings of sections have the following conventions: (1) *double lines, no stippling, cell walls not indicated:* gonopericardial ducts, seminal receptacles, copulatory spicule sacs; (2) *single line:* dorsal sinus, pericardium, heart; (3) *double lines, stippling only:* seminal vesicles; (4) *double lines, cell walls, no stippling:* upper gametoducts, rectum, mantle cavity; (5) *double lines, stippling, cell walls:* lower gametoducts.

Holotypes, paratypes, and voucher specimens are deposited in, or were borrowed from, the following museums: MNHNP, Muséum National d'Histoire Naturelle, Paris; MV, Museum of Victoria, Melbourne; UIB.Z.M, University of Bergen Zoological Museum, Norway; USNM, National Museum of Natural History, Washington, DC.

Phylogeny. The data matrix for a cladistic analysis was created with MacClade version 3.04 (Maddison and Maddison, 1992). The exhaustive search option in PAUP version 4.0b1 (Swofford, 1998) was used to reconstruct the phylogeny, and MacClade was used for subsequent analysis and interpretation of trees. Decay values (Bremer, 1988, 1994) were calculated with AutoDecay version 4.0 (Eriksson, 1998), and bootstrap and jacknife values were calculated with PAUP version 4.0b1 with 1000 replicates.

Systematic Account

NEOMENIOMORPHA Pelseneer, 1906

Ventroplicida Boettger, 1956; Solenogastres Gegenbaur, 1878 [*partim*], Salvini-Plawen, 1967. *Non* Neomeniamorpha Salvini-Plawen, 1978.

Diagnosis: Aplacophoran molluscs with a narrow footfold in a ventral, longitudinal pedal groove and without a cuticular oral shield or mantle cavity ctenidia; midgut as a combined stomach and digestive gland; monoecius.

Remarks: The telltale ventral groove in a spicule-covered, cylindrical organism immediately identifies it as a neomenioid mollusc.

PRONEOMENIIDAE Simroth, 1893

Type genus. Proneomenia Hubrecht, 1880.

With two genera, *Proneomenia* Hubrecht and *Dorymenia* Heath.

Dorymenia Heath, 1911

Type species. Dorymenia acuta Heath, 1911, by monotypy [Bull. Zool. Nom. 38:185].

Known distribution. Reported from the northeast, southeast, and southwest Pacific Ocean, northeast and northwest Atlantic Ocean, Mediterranean Sea, off East Indies, and Antarctica; 21 species are described from 50 to 3200 m depth.

Diagnosis. Body elongate, slender, smooth, to 10 cm long, with or without posterior fingerlike projection; skeletal spicules hollow, in several layers; upright spicules, if present, solid, paddle-shaped, small; cuticle thick; epidermis thin, with long, stalked epidermal papillae extending through the cuticle; radula polystichous, largest teeth in each row lateral, tooth rows on each side of median line mirror images, some species with a median tooth; anteroventral radular pocket single (Fig. 6B); ventral salivary glands tubular, long, ducts paired or single; midgut sacculate; with one or more dorsoterminal sense organs; paired seminal receptacles single; gametopore single; with paired copulatory spicules; gill folds greatly reduced; mantle cavity with one or more deep anterior pockets.

Remarks. Proneomenia and *Dorymenia* may be synonyms. The sole criterion for separating the two genera is the presence (*Dorymenia*) or absence (*Proneomenia*) of copulatory spicules (see, *e.g.*, Salvini-Plawen, 1978). Dissolution of copulatory spicules is evident in some individuals of both *D. sarsii* and *D. tortilis*, but it is not known whether empty copulatory spicule sacs are retained. However, Hubrecht's (1881) description of the type species *Proneomenia sluiteri* includes illustrations of paired, ventral mantle cavity pockets that appear to be empty copulatory spicule sacs.

Dorymenia sarsii (Koren & Danielssen, 1877)
(Figs. 2C, E, 3A, B, 4E, G, H, J, L)

Neomenia sarsii Koren and Danielssen, 1877; *Proneomenia sarsii* (Kor. & Dan.), Hansen, 1889; *Simrothiella sarsii* (Kor. & Dan.), Pilsbry, 1898; *sarsi* of authors.

Lectotype (Odhner, 1921 [as "prototype"]). UIB.Z.M 2074 (alcohol specimen, anterior and posterior ends missing, removed before Odhner's [1921] investigations; spicule slide): Length >40 mm, height 1.5 and 1.2 mm at anterior end and midbody, respectively. Kristianiafjord [Oslo Fjord], 190–225 m, coll. G. O. Sars.

Voucher specimens. UIB.Z.M 19850: Length ~32 mm, height 2.0 and 1.5 mm at anterior end and midbody, respectively. Herløfjord, 150 m (alcohol specimen, posterior end dissected; spicule slide). UIB.Z.M 53025: Length 46 mm, height 1.9 and 1.4 mm at anterior end and midbody, respectively. Osefjord, 60°30′30″N, 6°55′40″E, 206 m (alcohol specimen, anterior and posterior ends dissected; spicule, radula, and copulatory spicule slides).

Material examined. Lectotype and three lots from the Bergen Museum (UIB.Z.M 53024, 53025, 19850).

Description.

Appearance: With characters of the genus; with posterior fingerlike projection (Fig. 2C). Lengths of examined specimens to 46 mm, height at midbody to 1.5 mm (53 mm by 2.3 mm, Odhner [1921]; 70 mm by 3 mm, Koren & Danielssen [1877; trans. 1879]); anterior height to 2.0 mm; posterior projection to 2.0 mm long, height to 0.5 mm.

Cuticle and epidermis: Cuticle 40 to 50 μm thick, epidermis thinner.

Epidermal spicules: Skeletal spicules to 330 μm long, 19 μm wide, curve shallow, solid distal tips to 25 μm long, wall thickness to 6 μm, proximal end straight, to 45 μm long; spicules < 110 μm in length few (Fig. 3A, B). Upright paddle-shaped spicules sparse, to 103 μm long, 11 μm wide, curved, distal end rounded, bases narrow to wide (Fig. 3B, spicules 1, 2). Spicules from beside pedal groove solid, of two types: (1) flat, thin spicules, one margin straight, the other convex, with narrow root, to 120 μm long, 13 μm wide, <3 μm thick (spicule 4); (2) curved spicules lateral to type 1 round in cross-section with narrow base, to 135 μm long, 9 μm wide (spicule 3).

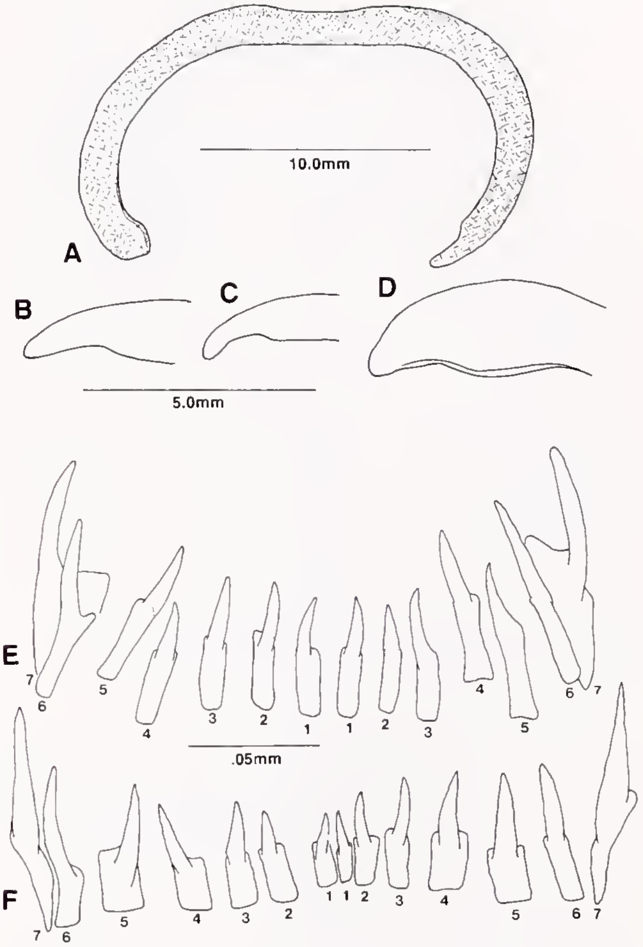

Figure 2. *Dorymenia* species. (A) *Dorymenia tortilis* n. sp. holotype, anterior to left. (B–D) Narrow posterior extension of: (B) *D. tortilis;* (C) *D. sarsii* (Koren & Danielssen); and (D) *cf. D. peroneopsis* Heath. (E) Radula tooth row of *D. sarsii* (voucher UIB.Z.M 53025), and (F) radula tooth row of *D. tortilis* paratype 1; mirror-image teeth numbered on each side of median line.

Radula (one examined, numbers in parentheses from Odhner [1921]): With 14 (16) teeth per row, rows about 28 (>30), with median furrow, length of teeth from 48 μm at median furrow to 93 μm at lateral margin, tooth bases narrow, 10 μm or less (Fig. 2E).

Copulatory spicules (2 individuals examined): Spicules undergoing dissolution in one individual, but accessory copulatory spicules and mantle cavity edge spicules intact; copulatory spicules (Fig. 4E, G) with a short, flaccid hyaline region below a solid, calcium carbonate distal end 500 μm

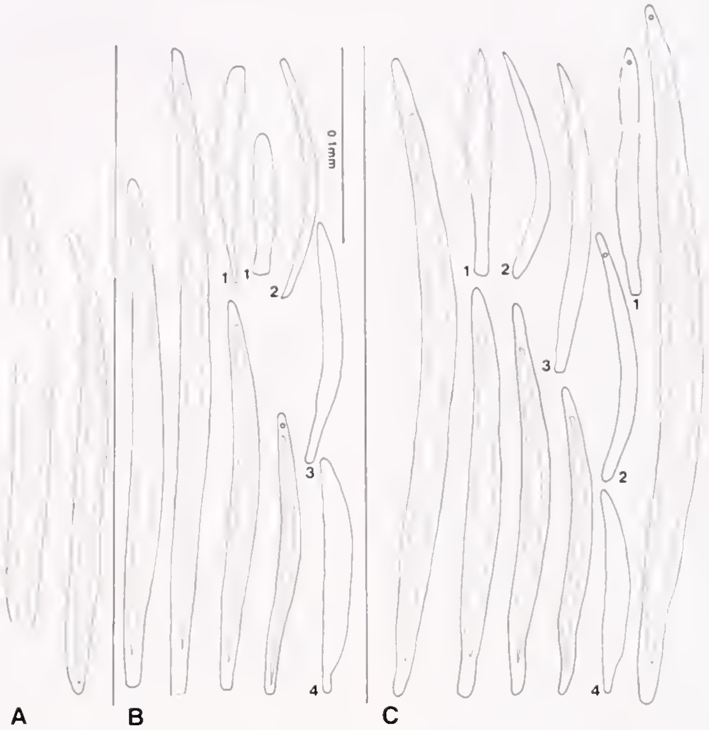

Figure 3. Epidermal spicules of *Dorymenia* species. (A) *Dorymenia sarsii* (Koren & Danielssen) from holotype. (B) *D. sarsii* from voucher UIB.Z.M 19850 and, with small circle at distal end, voucher UIB.Z.M 53025. (C) *Dorymenia tortilis* n. sp., spicules with a small circle at distal end from holotype, all others from paratype 1. Skeletal spicules without numbers; 1 upright paddle-shaped spicules en face; 2 upright paddle-shaped spicules from side; 3 curved rods lateral to 4, overarching pedal groove, and 4 flat spicules from single row beside pedal groove.

long by 90 μm wide; bent, pointed tip 70 μm long, 20 μm at its widest; calcitic portion medially grooved; accessory copulatory spicules to 315 μm long by 28 μm wide, rounded at both ends, triradiate in cross-section (Fig. 4J); epidermal spicules at opening of mantle cavity truncated distally at an angle, to 95 μm long, 8 μm wide (Fig. 18L); in second individual no copulatory spicules present, accessory copulatory spicules undergoing dissolution (Fig. 4H), and mantle cavity edge spicules not found.

Reproductive system: Not re-examined here.

Remarks. The spelling of this species is sometimes found in the literature as *sarsi*, an unnecessary emendation of *sarsii* (for Sarsius: Bull. Zool. Nom. 38:185–186). The exceptional dimensions given by Koren and Danielssen (1877, 1879)), greater than reported or seen since for this species, may be a twofold measuring error; the greatest height of the lectotype is 1.5 mm, reported as 3 mm by Koren and Danielssen. The authors also reversed anterior and posterior ends in their verbal description of body shape. That the lectotype was properly chosen by Odhner (1921) seems to be in no doubt, as it was collected by Sars and is from the type locality.

Dorymenia sarsii appears to be a continental shelf species from Scandinavian waters. The attribution of *Dorymenia* sp. in Scheltema *et al.* (1994) to *D. sarsii* is not correct (Salvini-Plawen, 1997), and does not extend the geographic distribution of *D. sarsii* to the Iberian shelf region.

Dorymenia tortilis sp. n.

(Figs. 2A, B, F, 3C, 4A–D, F, K, 5, 6A–E)

Dorymenia sp., Scheltema *et al.*, 1994 [not *D. sarsii*, Salvini-Plawen, 1997, p. 48], figs. 5c, 7b, 10c, 11c, 13a, b, d–f, 18c, 22e, 23f, 24e, g.

Holotype. MNHNP (alcohol specimen, spicule slide): Length 36.1 mm, height 1.7 mm at anterior end and midbody. NW of Gibraltar, 36°50.4′N, 9°14.9′W, 681 m, BALGIM [CENTOB] CP-03.

Illustrated paratypes 1, 2. MNHNP (no. 1, dissected alcohol specimen; radula, spicule slides); (no. 2, dissected alcohol specimen; spicule, copulatory spicule slides). Type locality.

Material examined. Eight individuals from type locality.

Description.

Appearance: With the characters of the genus; with a posterior fingerlike projection (Figs. 2A, B, 6D); holotype largest individual examined.

Cuticle and epidermis: Cuticle thick, 116 μm; epidermis thin, 12 to 14 μm, with oval to quadrate papillae borne on long, slender stalks.

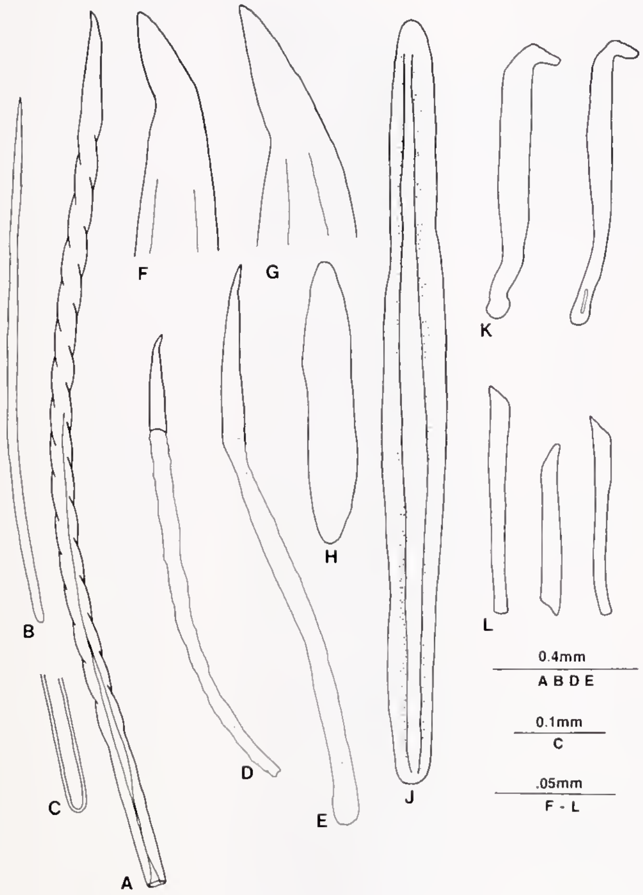

Figure 4. *Dorymenia tortilis* n. sp. and *D. sarsii* (Koren & Danielssen), copulatory spicules. (A) Fully formed spicule of *D. tortilis* (paratype 2) with short, solid distal end and long, twisted, hyaline, proximal end stiffened by crystals of calcium carbonate. (B) Isolated hollow, stiff hyaline rod that will form inner core of a fully developed spicule (paratype 2). (C) Enlarged proximal end of (B). (D, E) Flaccid copulatory spicules undergoing dissolution, with proximal hyaline matrix lacking core and calcium carbonate crystals: (D) *D. tortilis* (paratype 1); (E) *D. sarsii* (voucher UtB.Z.M. 53025). (F, G) Solid distal ends, enlarged, of (A) (*D. tortilis*) and (E) (*D. sarsii*), respectively. (H, J) Triradiate accessory copulatory spicules of *D. sarsii;* (J) fully formed from same individual as (E); and (H) spicule undergoing dissolution from an individual without copulatory spicules (voucher UIB.Z.M 19850). (K, L) Spicules from opening of mantle cavity: (K) *D. tortilis* (paratype 1); (L) *D. sarsii* (voucher UtBZ.M 53025).

Epidermal spicules: Skeletal spicules to 325 μm long, 18 μm wide, curve pronounced, solid tip to 24 μm long, wall thickness to 5 μm, proximal end straight, length to 45 μm; short hollow spicules <110 μm numerous (Fig. 3C). Upright paddle-shaped spicules deeply curved, distally pointed, to 117 μm long, 13 μm wide, base broad (Fig. 3C, spicules 1, 2). Spicules from beside pedal groove solid, of two types: (1) flat spicules, one margin convex, the other concave, to 128 μm long, 13 μm wide, <3 μm thick, with root (spicule 4); (2) lateral to type 1, curved spicules round in cross-section, base narrow to broad, to 153 μm long, 9 μm wide (spicule 3).

Radula (2 examined) with 14 teeth per row, number of rows about 44, length of medial teeth 28 μm, lateral teeth 85 μm, tooth bases broad, 10 to 15 μm (Fig. 2F).

Copulatory spicules (2 examined): Spicules in one individual undergoing dissolution (Fig. 4D), the other with intact spicules (Fig. 4A, F); intact spicule 2.4 mm long by 60 μm wide, with solid, calcium carbonate distal end and long, stiffened, hyaline region twisted around a stiff, hollow, hyaline rod forming a core (Fig. 4A); twisted region stiffened by densely scattered crystals of calcium carbonate aligned with the turns and at angle to each other, spicule less twisted proximally; solid distal end broadly grooved on opposite sides, 270 μm long, 55 μm greatest width in intact spicule, with a bent, pointed tip 38 μm long, 18 μm wide. An isolated, presumably developing solid end not attached to a proximal hyaline portion, tip 50 μm long, 20 μm wide, and an isolated, hollow hyaline core 1.5 mm long, 21 μm wide, also present in individual with intact spicules (Fig. 4B, C).

Notes on anatomy: Anteroventral radular pocket extending posteriorly beneath radular sac (Fig. 6B), with distal teeth undergoing dissolution (Fig. 6E). Paired salivary glands with united ducts opening into base of pharynx beneath radular sac (Fig. 6D). Radular sac divided proximally (Fig. 6B). Dorsoterminal sense organ single, with a large dorsal blood vessel.

Reproductive system: In common with other *Dorymenia* species, paired seminal receptacles single, and anterior pockets of mantle cavity deep (Fig. 5A, B, G; see also Salvini-Plawen, 1978). Dorsal, distal ends of upper gametoducts with three pockets appearing to function as seminal vesicles (Fig. 5A, C, D, 6C). In common with *D. sarsii* (Hansen, 1889), a large, distal, ventral lobe present on each lower gametoduct just before paired gametoducts unite (Fig. 5E, F). Gametoduct opening into the mantle cavity single (Fig. 19G). Distal ends of copulatory spicules borne on papillae.

Remarks. Dorymenia tortilis differs from *D. sarsii* in its (1) broader radular tooth bases, (2) more numerous tooth rows, (3) greater curvature of the skeletal spicules, (4) more numerous short epidermal spicules, (5) greater length and curvature of the paddle-shaped spicules, (6) shape of spicules beside the pedal groove, (7) shorter solid distal ends of the copulatory spicules, (8) spicules at the entrance to the mantle cavity hooked and larger, and (9) absence of accessory copulatory spicules.

Only one other north Atlantic species, *D. peroneopsis* Heath, has a fingerlike terminal extension of the body (Heath, 1918). The type material is unknown, but two recently collected individuals from the North American Basin probably belong to this species. They differ from both eastern Atlantic species in larger size, broader anterior and posterior ends (Fig. 2D), lack of paddle-shaped upright spicules, and presence of paired, fanlike arrays of either

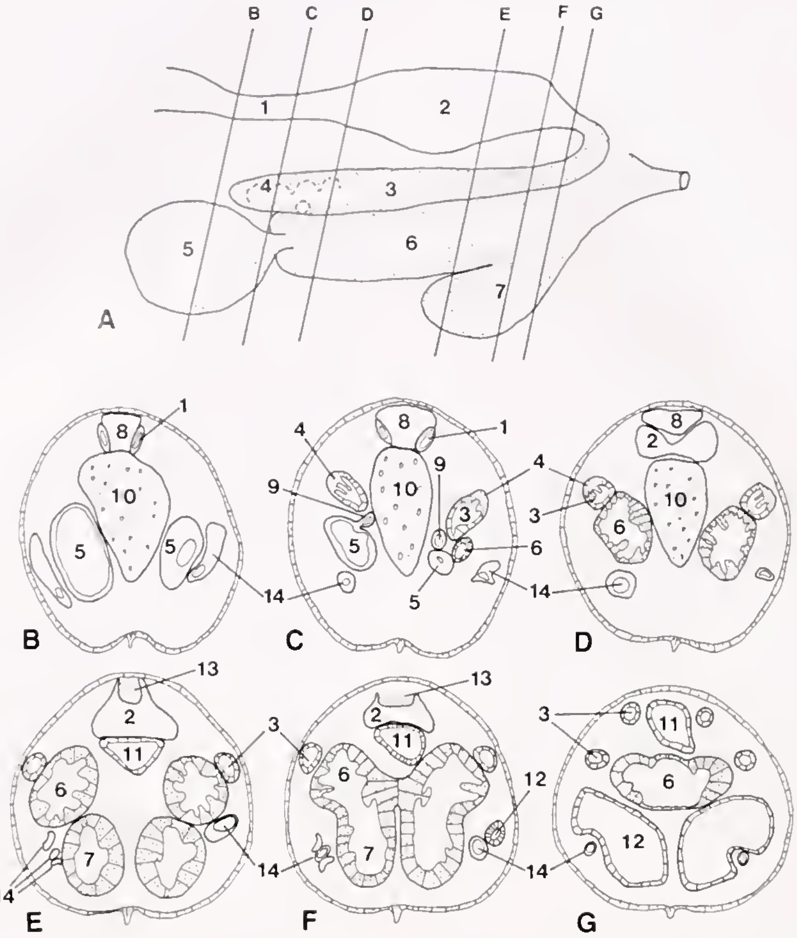

Figure 5. *Dorymenia tortilis* n. sp., reproductive system. (A) Reconstruction from histologic sections, anterior to left. (B–G) Cross-sections indicated in (A) semischematic (see text for description). 1 gonopericardial duct, 2 pericardium, 3 upper gametoduct, 4 region of upper gametoduct serving as seminal vesicle, 5 seminal receptacle, 6 lower gametoduct, 7 ventral lobe of lower gametoduct, 8 dorsal sinus, 9 duct of seminal receptacle, 10 midgut, 11 rectum, 12 mantle cavity pocket, 13 heart, 14 copulatory spicule sac.

copulatory spicules or accessory spicules seen within the open mantle cavity.

PRUVOTINIDAE Heath, 1911

Pruvotiniidae Heath, 1911. Pararrhopaliidae Salvini-Plawen, 1972.

Type genus. Pruvotina Cockerell, 1903.

Remarks. The taxon is poorly defined. Taxa with a combination of hollow upright barbed epidermal spicules, curved hollow skeletal and upright spicules, and a distichous radula with denticulate hooks include *Pruvotina, Pararrhopalia* Simroth, 1893, *Eleutheromenia* Salvini-Plawen, 1967, *Labidoherpia* Salvini-Plawen, 1978, and *Gephyroherpia* Salvini-Plawen, 1978; they were divided into two subfamilies on the basis of salivary gland morphology (Salvini-Plawen, 1978). *Lophomenia* Heath, 1911, *Halomenia* Heath, 1911, *Metamenia* Thiele, 1913, *Hypomenia* van Lummel, 1930, and *Forcepimenia* Salvini-Plawen, 1969, included in two other pruvotinid subfamilies (Salvini-Plawen, 1978), lack barbed spicules.

Eleutheromenia Salvini-Plawen, 1967

Paramenia Pruvot, 1890 [*non* Brauer & Bergenstamm, 1889] [*partim*]; *Pruvotina* Cockerell, 1903 [*partim*]; *Perimenia* Nierstrasz, 1908.

Type species. Paramenia sierra Pruvot, 1890, by monotypy.

Known distribution. Bass Strait and off southeast Australia; western Mediterranean; at depths of 50 to 400 m.

Diagnosis. Small, spiny, stout, with hollow, barbed, upright spicules; with or without dorsal carina; cuticle and epidermis thin, without stalked papillae; radula with distichous hooks; multicellular dorsal salivary glands not opening through a papilla; ventral salivary glands saclike with tubular ducts; midgut not sacculate or indistinctly so; with an elongate pericardial cavity forming an anterior glandular sac ("sac ovigère" of Pruvot [1891]); pericardial glands present; seminal receptacles as saclike extensions of

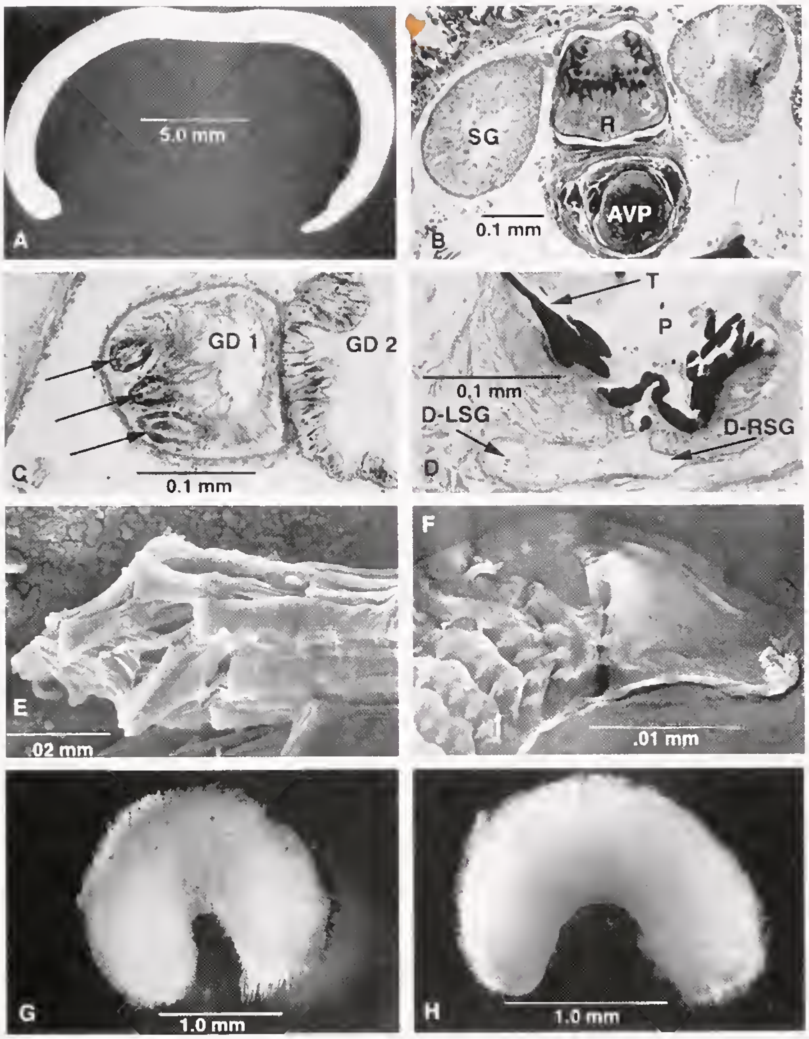

Figure 6. (A–E) *Dorymenia tortilis* n. sp.: (A) Holotype. (B) Cross-section showing single anteroventral radular pocket (AVP), ventral salivary gland (SG), and radula within radular sac (R). (C) Seminal vesicles (arrows) in pockets of upper gametoduct. GD1; GD2, lower gametoduct. (D) Joined ducts of left (D-LSG) and right (D-RSG) ventral salivary glands just before emptying into pharynx (P) beneath radular sac; tooth, T. (E) Anterior end of polystichous radula from anteroventral radular pocket undergoing dissolution. (F, H) *Kruppomenia levis* n. sp.: (F) First-formed triangular tooth retained within anteroventral radular pocket. (H) Holotype. (G) *Kruppomenia delta* n. sp., holotype. In (A, G, and H), anterior is to left and dorsal above.

lower gametoducts; with copulatory spicules; mantle cavity with numerous long respiratory papillae; dorsoterminal sense organ present.

Remarks. When new collections of *E. sierra* from the type locality (Mediterranean) become available, the relationship between *E. sierra* and the two new species described here can be reevaluated.

Eleutheromenia bassensis sp. n.

(Figs. 7E–H, 8A, 9A–D, 11F)

Holotype. MV F83480 (alcohol specimen, spicule slide): Length 2.3 mm, height 0.6 mm, width of anterior end 0.7 mm. Bass Strait, Australia, 38°56.0′S, 145°16.6′E, 70 m (RV *Tangaroa* Stn BSS-S 55 [epibenthic sled], 12.xi.1981).

Illustrated paratypes. MV F83481 (dissected alcohol specimen; slides of epidermal and copulatory spicules); MV F83482 (dissected alcohol specimen; copulatory spicule slide). Type locality.

Material examined. 52 individuals, Bass Strait Survey November 1981, RV *Tangaroa* (number in parentheses; BSS-S, epibenthic sled samples; BSS-G, Smith-MacIntyre grab samples): BSS-S 155, 38°56.0′S, 145°16.6′E, 70 m (25); BSS-G 155, 38°55.5′S, 145°17.0′E, 70 m (1); BSS-S 156, 39°45.9′S, 145°33.5′E, 74 m (1); BSS-S 157, 40°10.9′S, 145°44.3′E, 75 m (1); BSS-S 162, 40°09.4′S, 147°32.6′E, 51 m (7); BSS-G 181, 38°39.8′S, 144°18.2′E, 79 m (2); BSS-S 195, 39°38.2′S, 143°07.2′E, 127 m (2);

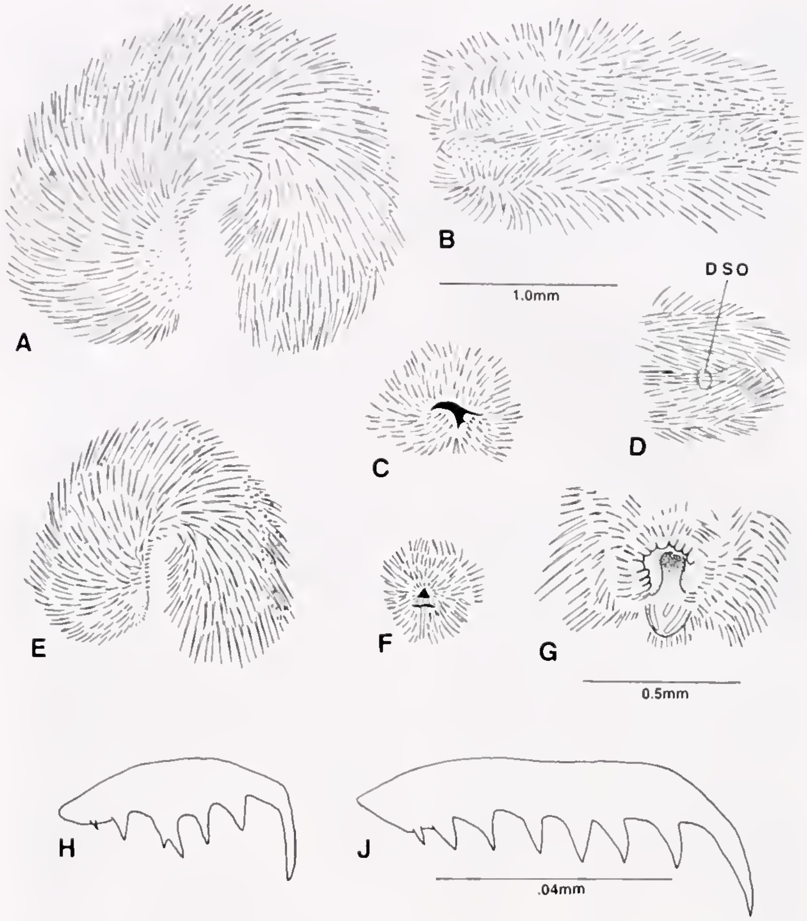

Figure 7. *Eleutheromenia mimus* n. sp. (A–D, J) and *E. bassensis* n. sp. (E–H). (A, E) Holotypes, anterior to left; barbed spicules indicated by small checks. (B) Dorsal view of (A) showing longitudinal rows of barbs. (C) Anterior view of (A). (D) Posterodorsal view of (A), dorsoterminal sense organ (DSO) obvious. (F) Anterior view of individual from type locality showing triangular appearance of contracted mouth opening and horizontal slit of contracted pedal pit. (G) Posterodorsal view of (E) at twice the magnification, open mantle cavity showing copulatory spicules; because the mantle cavity is open, the posterior spicules in (E) are fanned out, unlike those in (A) with mantle cavity opening contracted. (H, J) Single radular teeth from 6th row from formative end of radular sac, lateral denticles on right: (H) *E. bassensis* with 5 denticles, shows incipient 6th denticle forming on the middle denticle (paratype MV F83481); (J) *E. mimus* (paratype MV F83475).

BSS-G 195, 39°38.2′S, 143°07.2′E, 127 m (1); BSS-S 201, 39°08.3′S, 144°43.9′E, 66 m (2); BSS-S 202, 39°00.2′S, 144°33.9′E, 74 m (8); BSS-S 205, 39°13.6′S, 143°55.6′E, 85 m (2).

Description.

Appearance: Very spiny, to 3 mm in length (Figs. 7E, 11F); anterior width to 0.7 mm, height 0.6 mm or less; rounded anteriorly, somewhat truncated posteriorly; retracted mouth opening triangular; pedal pit a lateral slit (Fig. 7F); pedal groove covered by numerous long epidermal spicules; mantle cavity opening subterminal, spicules in brushes on each side, copulatory spicules often protruded (Fig. 7G), dorsoterminal sense organ often externally visible.

Cuticle and epidermis: Cuticle < 25 μm thick, epidermis about 10 μm thick.

Epidermal spicules: Both skeletal and upright spicules numerous, narrow, evenly curved, tapered at both ends, often slightly recurved at base (Fig. 8A); upright spicules to 400 μm long and 9 μm wide, with solid tips usually to 55 μm, a few to >60 μm (Fig. 8A spicules 3); skeletal spicules less than 200 μm long and to 8 μm wide, hidden externally under thickly set, upright spicules; barbed spicules numerous, upright, in longitudinal bands on each side of middorsal crest of crossed upright spicules, to 145 μm long and 9 μm wide, shortest anteriorly, sharply recurved twice at base (spicule 2); upright spicules from anterior end near mouth serrate (spicules 1); spicules along pedal groove to

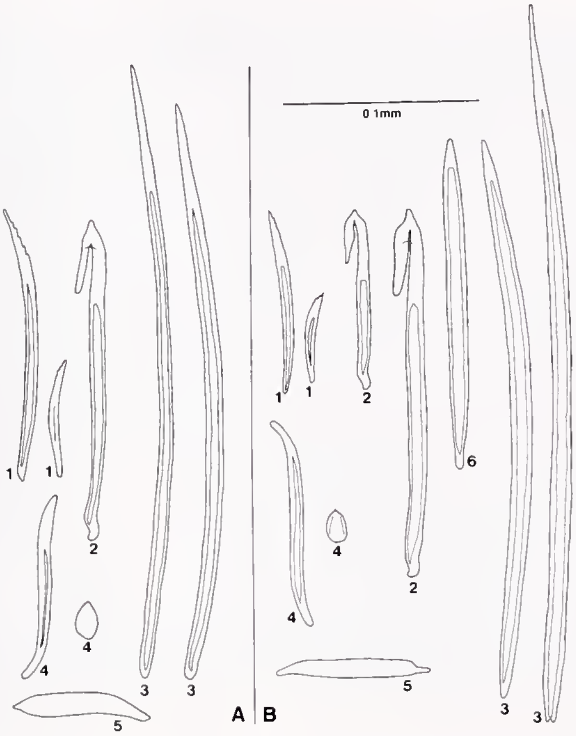

Figure 8. Epidermal spicules of *Eleutheromenia bassensis* n. sp. (A) and *E. mimus* n. sp. (B). 1 serrated spicules from above mouth, 2 barbed spicules and 3 long upright spicules from mid-dorsal region, 4 S-shaped and pointed ovate spicules from edge of mantle cavity, 5 spicules from beside pedal groove, 6 skeletal spicule. In (A), spicules from paratype (MV F83481) except upright spicule on right from another specimen from type locality. In (B), spicules from paratype (MV F83476) except upright spicule on right from another specimen from type locality.

100 μm in length, with a short, narrow base (spicule 5); spicules from opening of mantle cavity S-shaped and pointed ovals (spicules 4).

Radula (2 specimens examined): With 21 to 22 rows, teeth 40 to 45 μm by 10 μm, with 4 to 6 denticles (Fig. 7H).

Copulatory spicules (7 specimens examined): copulatory spicules paired, 2 per sac; one long, rodlike, distally tapered and curved, to 750 μm long by 25 μm wide; the other nearly as long, the distal half flared into a hood with a thickened distal ridge, width 104 μm (Fig. 9A–D).

Notes on anatomy: Large dorsal sinus present, extending far anteriorly. Midgut cecum paired anteriorly, becoming single at level of radula. Mantle cavity surrounded by subepithelial goblet cells.

Reproductive system. As in *E. mimus*.

Remarks. Morphological differences between *E. bassensis*, *E. mimus*, and *E. sierra* are discussed under Remarks for *E. mimus*.

Eleutheromenia mimus sp. n.

(Figs. 7A–D, J, 8B, 9E–G, 10, 11D, E)

Eleutheromenia sp., Scheltema *et al.*, 1994, figs. 3a, c, 7a, 16c, 20a (identification in caption in error), e, 24d.

Holotype. MV F83474 (alcohol specimen, spicule slide): Length 3.1 mm, height 0.8–0.9 mm, width 1.0 mm. Bass

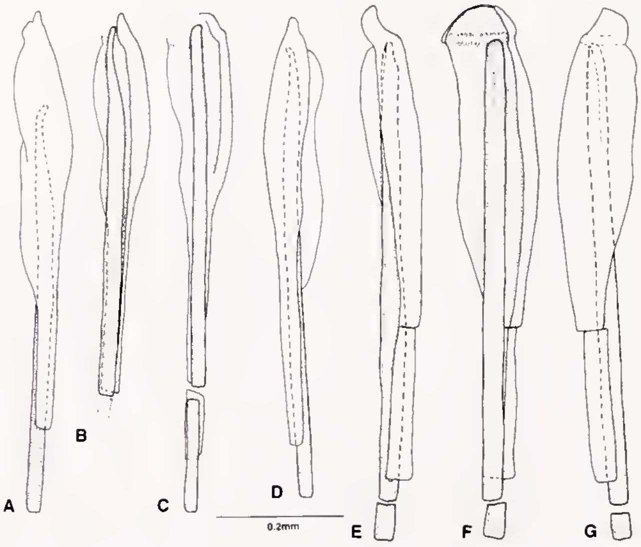

Figure 9. Copulatory spicules of *Eleutheromenia bassensis* (A–D) and *E. mimus* (E–G). The longer, rod-shaped spicule is narrow, tapered, and curved in *E. bassensis;* it is scarcely curved or tapered in *E. mimus* but has a medial groove distally. The hoodlike spicule bears a ridge distally; it is curved above the ridge, more so in *E. mimus* than in *E. bassensis.* The two spicules can move relative to each other; *cf.* spicules (A) and (B). [(A, D) Paratype MV F83481; (B, C) paratype MV F83482; (E–G) paratype MV F83477.]

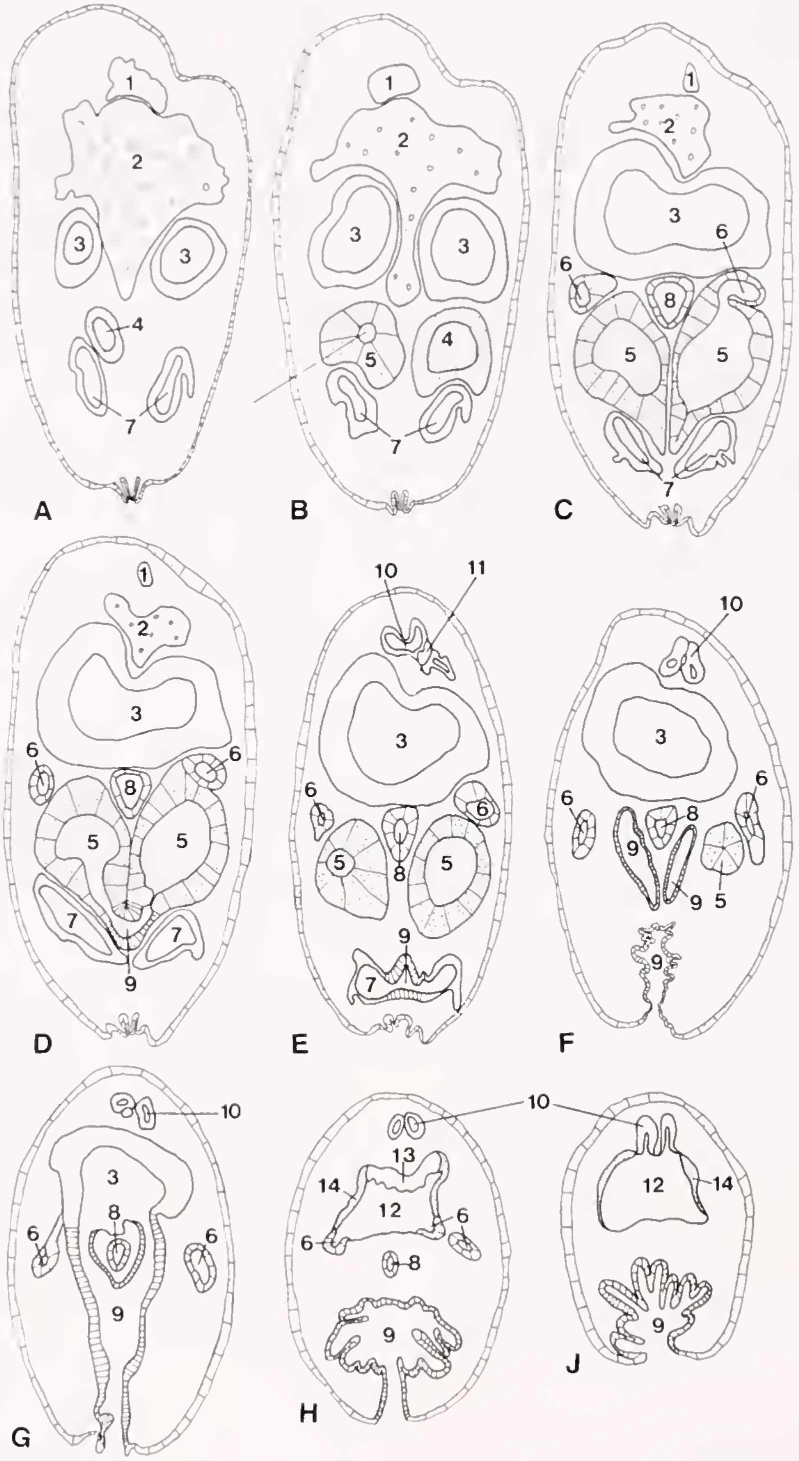
1
2
3
3
4
7
A
1
2
3
3
5
4
7
B
1
2
3
6
6
8
5
5
7
C
1
2
3
6
6
8
5
5
7
7
9
D
10
11
3
6
6
5
8
5
9
7
E
10
3
6
6
8
9
9
5
9
F
10
3
8
6
6
9
G
10
13
14
12
6
6
8
9
H
12
14
9
J

Figure 10. *Eleutheromenia mimus* n. sp., reproductive system, semischematic histologic sections from anterior (A) to posterior (J) (see text for description; reconstruction not attempted owing to obliqueness of sections). 1 gonad, 2 midgut, 3 glandular sac of pericardial cavity, 4 seminal receptacle, 5 lower gametoduct, 6 upper gametoduct, 7 copulatory spicule sac, 8 rectum, 9 mantle cavity, 10 gonopericardial duct, 11 dorsal aorta, 12 pericardium, 13 heart, 14 pericardial glands. Line in B, opening of seminal receptacle into lower gametoduct.

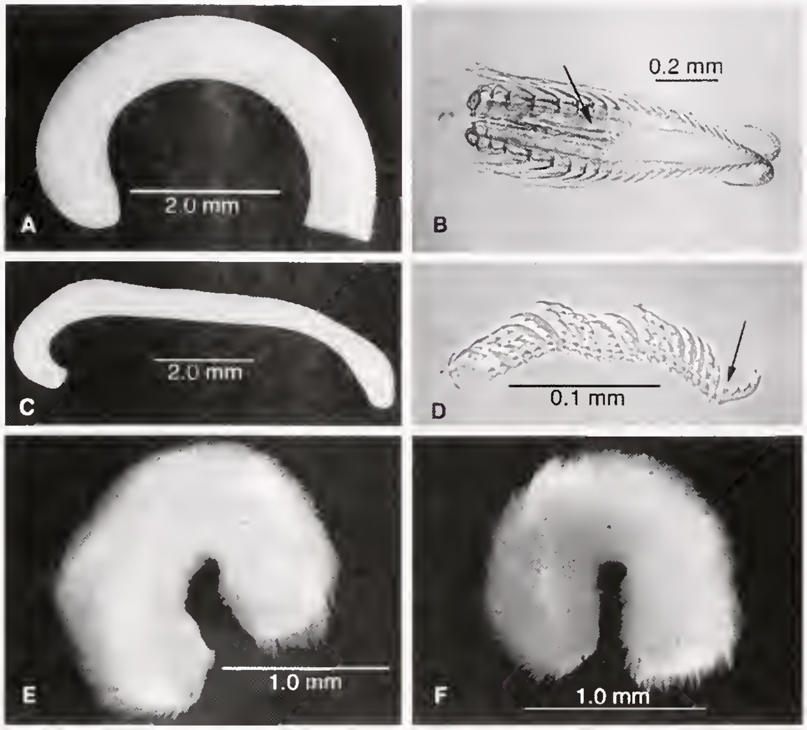

Figure 11. (A–C) *Simrothiella* (=*Solenopus*) *margaritacea* (Koren & Danielssen): (A) *Solenopus margaritaceus* Koren & Danielssen, lectotype. (B) dorsal view of entire radula, short section from radula sac indicated by arrow, greatest length of radula from within anteroventral radular pocket, anterior to left. (C) Voucher 1 (USNM). (D, E) *Eleutheromenia mimus* n. sp.: (D) Radula, one longitudinal row of the distichous radula; arrow, oldest tooth with bifurcating denticle. (E) Holotype. (F) *E. bassensis* n. sp., holotype. In (A, C, E, and F), anterior is to left, dorsal above.

Strait, Australia, 38°52.6′S, 148°25.2′E, 140 m (RV *Tangaroa* Stn BSS-S 170 [epibenthic sled], 15.xi.1981).

Illustrated paratypes. MV F83475 (dissected alcohol specimen, epidermal and copulatory spicule slides); MV F83476 (dissected alcohol specimen, epidermal spicule slide, radula slide); MV F83477 (dissected alcohol specimen, copulatory spicule slide). Type locality.

Material examined. 33 individuals (number in parentheses; all samples from epibenthic sled): Bass Strait Survey, November 1981, RV *Tangaroa* stations BSS-S 169, 38°57.8′S, 148°26.5′E, 120 m (3) and BSS-S 170, 38°52.5′S, 148°25.2′E, 140 m (20); RV *Franklin* July 1986, Slope station 40, 38°17.7′S, 149°11.3′E, 400 m (10).

Description.

Appearance: Similar to *E. bassensis* (Figs. 7A–D, 11E); to 4.4 mm long, height and width to 0.9 mm except width to 1.2 mm at anterior end.

Cuticle and epidermis: Cuticle to 23 μm thick, epidermis thinner, to 16 μm thick.

Epidermal spicules: Types and shapes as in *E. bassensis* (Fig. 8B); upright spicules to nearly 600 μm long and 13 μm wide, solid tips to 55 μm (spicules 3); many skeletal spicules $<$ 200 μm long and to 11 μm in width (spicule 6); barbed spicules to 185 μm by 9 μm, shortest anteriorly (spicules 2); spicules from beside pedal groove usually $<$100 μm by 14 μm (spicule 5); spicules from opening of mantle cavity S-shaped and pointed ovals (spicules 4).

Radula (2 examined): Number of tooth rows 23, teeth 65 μm by 10 μm, denticle number 5 to 9 (Fig. 7J, 11D).

Copulatory spicules (5 specimens examined): Paired, 2 spicules per copulatory spicule sac, rod-shaped spicule to 830 μm by 32 μm, grooved distally, scarcely tapered, not curved distally; hoodlike spicule $>$120 μm wide, with heavy distal ridge and portion of hood distal to ridge deeply curved (Fig. 9E–G).

Notes on anatomy: A pedal commissure sac of unknown function present (see Scheltema *et al.,* 1994, fig. 2c).

Reproductive system: With a large, thick-walled, glandular anterior sac of the pericardial cavity beginning as paired lobes on either side of midgut, becoming a single sac further posteriorly (Fig. 10A–F); cells large, vacuolated, with small, deeply staining granules; sac connecting with mantle cavity through a long, tubelike, dorsoanterior extension of mantle cavity, just anterior to beginning of heart and pericardium proper (Fig. 10F, G); tubelike mantle cavity extension passing around rectum. Gonads emptying into pericardium through unusually long, paired gonopericardial ducts that open into posterior, rather than anterior, part of pericardium (Fig. 10E–J). Pericardium proper short relative to anterior glandular sac. Posterior end of pericardial cavity with pericardial glands (Fig. 10H, J). Seminal receptacles as saclike anterior extensions of the lower gametoducts, without distinct ducts, but separated from gametoducts by a short, tubelike constriction (Fig. 10B, line). Lower gametoducts paired until uniting just as they reach mantle cavity anterior to the tubelike mantle cavity extension that connects with glandular pericardial sac (Fig. 10D). Upper gametoducts arising as usual from ventroposterior end of pericardium and leading forward, joining lower gametoducts just posterior to union of seminal receptacles with lower gametoducts (Fig. 10C–H).

Remarks. E. minus differs from *E. bassensis* in its (1) larger size, (2) longer and wider epidermal spicules, (3) longer radular teeth, (4) more denticles per tooth, and (5) copulatory spicule morphology. The morphology of the copulatory spicules differentiates the two species unequivocally. The rod-shaped spicule in *E. bassensis* is curved distally and is narrower and more tapered than in *E. minus*, whereas the hoodlike spicule in *E. minus* bears a heavier ridge and is more deeply curved distally than in *E. bassensis*. It is likely that *E. bassensis* also has a pedal commissure sac, but this structure was seen only in 1.5-μm sections of *E. minus*. Depth ranges of the two species differ but overlap: *E. bassensis* has been collected from 70 to 127 m, and *E. minus* from 120 to 400 m. They did not occur together in samples, however. Both species differ from *E. sierra* in size and epidermal spicule morphology and lack the distinct dorsal carina of *E. sierra*. Seminal receptacles were considered to be lacking in *E. sierra* (Pruvot, 1891).

The function of the large, glandular pericardial sac at the anterior end of the pericardium is not clear. The sac is only indirectly connected with the gonads through the long gonopericardial ducts that enter the pericardial cavity at its posterior end. Other species of Pruvotinidae are known to have brood chambers, but these are extensions of the mantle cavity, not the pericardium (Salvini-Plawen, 1978).

SIMROTHIELLIDAE Salvini-Plawen, 1978

Type genus. Simrothiella Pilsbry, 1898.

Diagnosis. Neomenioids with body shapes from stout to elongate; epidermal spicules solid or hollow, with or without skeletal spicules; radula distichous with many rows, denticles on a barlike base entirely attached to radular membrane; with paired anteroventral radular pockets either long and spiraled, or short, retaining initial teeth in some taxa.

Remarks. The taxon is currently constituted primarily on the basis of radula morphology (*Simrothiella* Pilsbry, 1898, *Cyclomenia* Nierstrasz, 1902, *Kruppomenia* Nierstrasz, 1903, *Uncimenia* Nierstrasz, 1903 [lacking a radula], *Biserramenia* Salvini-Plawen, 1967, *Birasoherpia* Salvini-Plawen, 1978, *Sialoherpia* Salvini-Plawen, 1978, *Helicoradomenia* Scheltema & Kuzirian, 1991, and *Plawenia* n.g., herein). From the diagnosis above, monophyly of the taxon can be seen to be doubtful and is not reflected in the results of the cladistic analysis below.

Kruppomenia Nierstrasz, 1905

Type species. Kruppomenia minima Nierstrasz, 1905, by monotypy.

Simrothiella Pilsbry, 1898 (*partim*), Salvini-Plawen, 1972.

Known distribution. Norwegian fjords, West European Basin, and the Mediterranean from 100 m or less to >4000 m.

Diagnosis. Stout, small; epidermal spicules hollow, both skeletal and upright; epidermis and cuticle thick; radula ribbon broad with many distichous tooth rows, teeth as extremely narrow bars bearing numerous tiny denticles; anteroventral radular pocket retaining first-formed, triangular tooth; ventral salivary glands short, tubular, paired; with paired saclike seminal receptacles; copulatory spicules 2 or more per copulatory spicule sac; respiratory mantle-cavity folds present; a dorsoterminal sense organ present.

Remarks. This genus is represented by several undescribed species in the West European Basin and adjacent waters. A second species, besides the type, has previously been described (*K. borealis* Odhner, 1921). Copulatory spicules tend to be numerous and elaborate in this genus and serve to distinguish species.

Kruppomenia levis sp. n.

(Figs. 6F, H, 12A–C, F, G, 13A, 14A–D)

Holotype. MNHNP (alcohol specimen, spicule slide): Length 3.3 mm, heights 0.7, 0.9, and 0.9 mm anteriorly, at midbody, and posteriorly, respectively; widths 0.7, 1.1, and 0.9 mm. Bay of Biscay 47°29.8′N, 9°39.2′W, 4327 m (INCAL [CENTOB] OS-08, 11.viii.1976).

Paratypes. No. 1, MNHNP (dissected alcohol specimen, epidermal and copulatory spicule slides), Bay of Biscay 47°34.8′N, 9°33.3′W, 4228 m (BIOGAS VI [CENTOB] DS-76, 23.x.74); no. 2, MNHNP (dissected alcohol specimen, copulatory spicule slide), West European Basin 47°29.8′N, 9°33.4′W, 4268 m (INCAL [CENTOB] DS-16, 9.viii.1976); no. 3, MNHNP (dissected alcohol specimen, epidermal spicule slides), type locality.

Material examined. 22 individuals; see Table 1, with two additional stations: BIOGAS VI (CENTOB) DS-76 (4) and BIOGAS VI DS-77, 4240 m, 47°31.8′N, 9°34.6′W, 24.x.74 (4).

Description.

Appearance: Small, stout, length to 3.9 mm, height to 1.3 mm, height and width greatest at midbody, rounded at both ends (Figs. 6H, 12A); appearance somewhat spiny when epidermal spicules intact, but usually appearing smooth (*levis*) to rough owing to broken state of upright spicules and sediment held between spicules; skeletal spicules form-

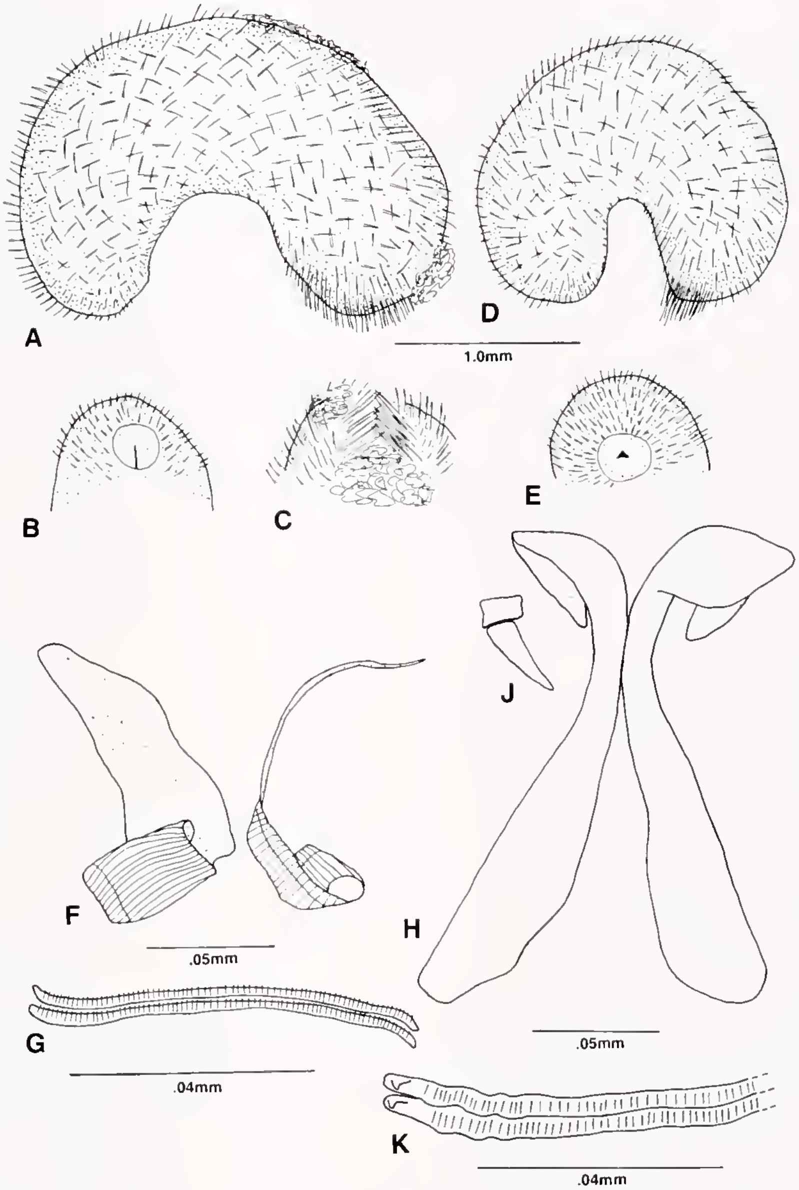

Figure 12. *Kruppomenia levis* n. sp. (A–C, F, G) and *K. delta* n. sp. (D, E, H–K). (A) Holotype of *K. levis*, anterior to left, many upright spicules masked by adhering sediment and with distal ends broken off. (B, C) Ventral views of mouth and spicules covering mantle cavity, respectively, of (A). (F) *K. levis*, entire radula of paratype 1, distal end above, tooth rows indicated sketchily; stippling indicates radular membrane viewed from below. (G) Two adjacent teeth from (F), lateral to left, denticles indicated sketchily: note lateral bend, which appears as longitudinal line in (F). (D, E) *K. delta*, holotype, as in (A, B). (H) *K. delta*, entire radula, paratype 2, distal end above, oblique view, tooth rows not sketched. (J, K) *K. delta*, paratype 3: (J) Two first-formed teeth, scale as in (K) (*cf.* Fig. 24E). (K) Two adjacent teeth, lateral to left, medial portion not illustrated.

ing an open meshwork; contracted mouth opening a vertical slit in flat, circular area without spicules (Fig. 12B); with raised ridge on each side of pedal groove; terminal spicules long and brushlike, meeting at angle above mantle cavity opening (Fig. 12C); cuticle easily torn.

Cuticle and epidermis: Cuticle thick, up to 38 μm; epidermis from thin to thick, 13 μm anteriorly to 38 μm posteriorly, with large, juxtaposed papillae.

Epidermal spicules: Asymmetric, fragile, hollow (Fig. 13A), walls about 2 μm, removable from cuticle only with difficulty; skeletal and upright spicules could not be differentiated, probably similar; many spicules long, to 290 μm anteriorly and 365 μm posteriorly; most distinctive spicules (Fig. 13A, spicules 1, 2, 4, 6, 9) curved from distal end to an abrupt bend 25 to 80 μm above base, widest at bend, to 18 μm, solid tips short, most 11 μm long but to 23 μm, often

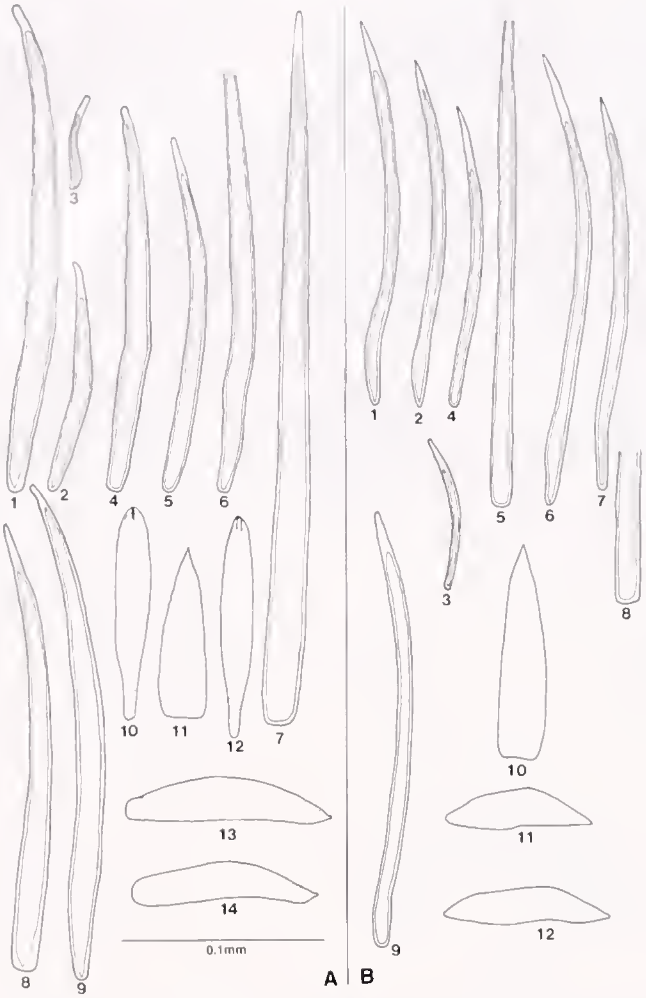

Figure 13. Epidermal spicules of *Kruppomenia levis* n. sp. (A) and *K. delta* (B). Spicules A1–5, 10, 11, 13 from paratype 1; A6–9, 12, 14 from paratype 3; spicules B1–6, 11 from paratype 1; spicules B7–10, 12 from paratype 3. Spicules A1–3, 8, 9 and B1–4, 9 from anterior end, spicule A3 and B3 from near mouth, spicules A4–7 and B5–8 from posterior end, spicules A10–14 and B10–12 from beside pedal groove, A10–12 and B10 probably from area next to mantle cavity opening.

constricted and bent beyond hollow space that fills most of spicule from tip to base; other spicules evenly curved from tip to base (spicule 8), or recurved proximal to bend (spicule 6); spicules from beside pedal groove 1–2 μm thick, base truncated, with distal nipple, to 106 μm long and 23 μm wide, thickest along outside curve and at base (spicules 13, 14); triangular and paddle-shaped, solid, thin (1–2 μm) spicules present posteriorly, to 100 μm and 115 μm long, respectively, probably from beside pedal groove near mantle cavity opening (spicules 10–12).

Radula (3 examined): About 185 μm long, with about 88 rows of narrow, distichous bars bearing numerous tiny (2 μm) denticles and a lateral thickening seen only in histologic sections; teeth bending about one-quarter of the distance from lateral margin, making an axial ridge along length of radula (Fig. 12F, G); most recent teeth 2 μm wide and to 74 μm from lateral to medial margin; first-formed tooth triangular (Fig. 6F); radular apparatus with large bolsters, anteroventral radular pocket broad, paired; proximal end of radular sac divided.

Copulatory spicules (3 individuals examined): 4 per pocket (Fig. 14A–D, spicules 1–4): spicule 1 hollow, elongate, length to >575 μm, distally pointed, basally tapered, curved, twisted around long axis and appearing either proximally broad and distally narrow or proximally narrow and distally broad (*cf.* spicules 1, Fig. 30A, B), distal points of paired number 1 spicules held in close proximity *in situ;* spicules 2 and 3 hollow, distally hooked, narrow, widest just below hook, greatest lengths >412 μm and 273 μm, respectively; spicule 4 shortest, proximally broad and partially wrapped around spicule 1, recurved twice and axially twisted, to 260 μm long; a fifth, very short (46 μm) hook in

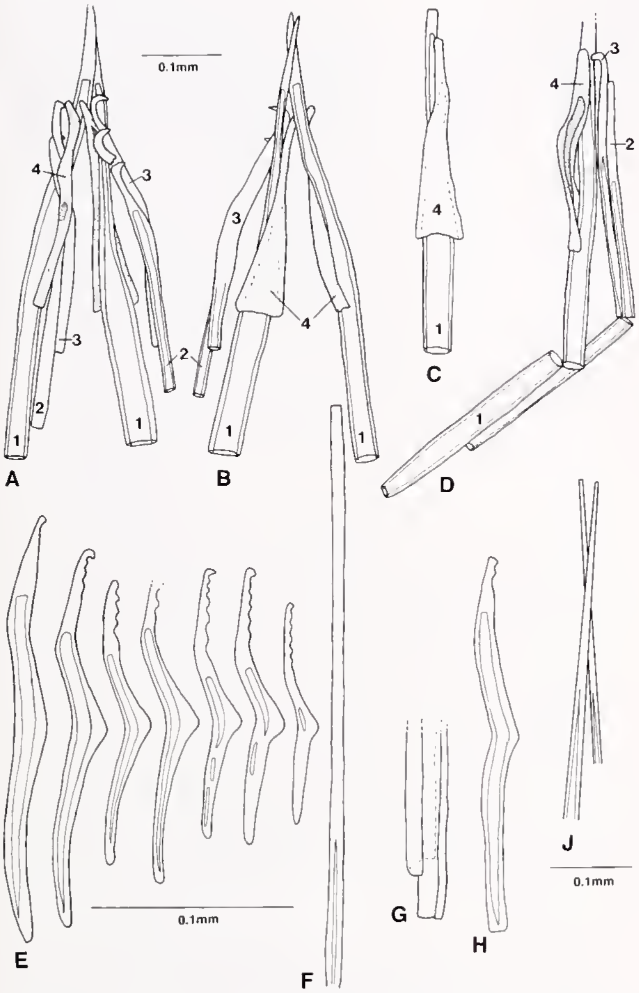

Figure 14. Copulatory spicules of *Kruppomenia levis* n. sp. (A–D) and *K. delta* n. sp. (E–J). (A, B) From paratype 2, ventral and dorsal views, respectively, proximal ends of spicules 1 and 2 broken off, spicules 2 and 3 not shown in (B). (C, D) From paratype 1, distal ends of spicules 1, 2, and 4 broken off; view of spicules C1 and C4 at 90° angle from view (D). (E) Accessory copulatory spicules, teased apart, from paratype 1. (F, G) One of paired main copulatory spicules from paratype 1, distal and proximal ends, respectively, showing two spicules wrapped around each other proximally and a single spicule distally. (H) One of seven accessory copulatory spicules from paratype 3. (J) Distally crossed pair of main copulatory spicules from paratype 3, drawn at same scale as (A–D); *cf.* spicule (F) at larger scale.

one of paired groups (Fig. 14A) may be new spicule in formation.

Notes on anatomy: Pedal pit large, not obvious externally in contracted state. Anterior pharynx a long, narrow tube; midgut not sacculate, with single dorsal cecum. Dorsoterminal sense organ present, not obvious. Mantle cavity with about 46 elongate, slender respiratory papillae.

Reproductive system (not illustrated): Paired seminal vesicles present at posterior ends of gonopericardial ducts. Paired, elongate seminal receptacles empty through long ducts into the unpaired lower gametoduct, which empties dorsally into mantle cavity. Pericardial cavity extending as a narrow, inverted U, both laterally and posteriorly, far over the mantle cavity. Paired upper gametoducts leave the lateral, posterior ends of the pericardial cavity as narrow tubes; anteriorly their relationship to seminal receptacles and lower gametoduct was unclear in examined specimen.

Remarks. Some individuals of *Kruppomenia levis* have numerous epidermal spicules with constricted tips (Fig. 13A, spicules 4, 9), whereas in others they are scarce. For differences between *K. levis* and *K. delta*, see remarks under *K. delta.*

Kruppomenia delta sp. n.
(Figs. 6G, 12D, E, H–K, 13B, 14E–J)

Holotype. MNHNP (alcohol specimen, spicule slide): Length 2.7 mm, heights 0.6, 0.9, and 0.7 mm anteriorly, at midbody, and posteriorly, respectively, widths 0.9, 0.9, and 0.8 mm. Bay of Biscay 47°27.3′N, 9°36.2′W, 4307 m (INCAL [CENTOB] OS-06, 9.viii.1976).

Illustrated paratypes. No. 1, MNHNP (dissected alcohol specimen, epidermal spicule slide); no. 2, MNHNP (dissected alcohol specimen, epidermal spicule slide); type locality. No. 3, MNHNP (dissected alcohol specimen, copulatory spicule slide); Bay of Biscay 47°29.8′N, 9°39.2′W, 4327 m (INCAL [CENTOB] OS-08, 11.viii.1976).

Material examined. 10 individuals; see Table 1.

Description.

Appearance: Small, stout, similar to *Kruppomenia levis*, but smaller; largest individual 2.8 mm, greatest height 0.9 mm, greatest width 0.9 mm; rounded at both ends (Figs. 6G, 12D); appearance somewhat spiny when epidermal spicules intact, but upright spicules often broken, with sediment lodged between them; skeletal spicules forming loose meshwork, cuticle easily torn; contracted mouth triangular in flat, circular area (Fig. 12E); with raised ridge on each side of pedal groove; terminal spicules just above mantle cavity opening long and brushlike, forming tuft (Fig. 12D); otherwise, posterior spicules shorter than in *K. levis.*

Cuticle and epidermis: Not examined.

Epidermal spicules: Asymmetric, fragile, hollow (Fig. 13B), walls about 2 μm; removable from cuticle with difficulty; longest spicules > 225 μm; greatest width to 14 μm (Fig. 13B, spicule 8), but most commonly 7 μm; greatest distance from bend to base 56 μm, most <50 μm (spicules 2, 6, 7, 9); solid tips slender, curved, sometimes with slight distal bend, from 9 to 45 μm long, many > 20 μm (spicules 1, 4, 6); some spicules evenly curved from base to tip, or straight (spicules 4, 5); spicules from beside pedal groove with tapered base, outer margin flattened, to 101 μm long by 20 μm wide (spicules 11, 12), paddle-shaped spicules not observed, but posterior triangular, solid spicules large (spicule 10), to >135 μm long.

Radula (3 examined): Length to 230 μm long, similar to that in *K. levis* but larger (Fig. 12H), teeth to about 78 μm

Table 1

Material examined. Kruppomenia levis, K. delta, *and* Plawenia sphaera *(INCAL [CENTOB])*

Sample	Depth (m)	Lat N	Long W	Date	*K. levis*	*K. delta*	*P. sphaera*
DS-01	2091	57°59.7′	10°39.8′	15.vii.76			16*
DS-02	2081	57°58.8′	10°48.5′	16.vii.76			26
CP-01	2068	57°57.7′	10°55.0′	16.vii.76			3
CP-02	2091	57°58.4′	10°42.8′	16.vii.76			1
DS-05	2503	56°28.1′	11°11.7′	18.vii.76			1
DS-14	4254	47°32.6′	9°35.7′	7.viii.76	1		
DS-15	4211	47°33.4′	9°39.1′	8.viii.76		1	
DS-16	4268	47°29.8′	9°33.4′	9.viii.76	3	1	
OS-06	4316	47°27.3′	9°36.2′	9.viii.76		6*	
OS-07	4249	47°31.8′	9°34.3′	10.viii.76	7		
OS-08	4327	47°29.8′	9°39.2′	11.viii.76	3*	2	

* Type locality.

by 4 μm with a lateral denticle larger than remaining little denticles (Fig. 12K); first-formed tooth triangular (Fig. 12J).

Copulatory spicules (3 individuals examined): Paired, two per sac, one spicule elongate, hollow, to 845 μm long, slender (about 22 μm wide), distal tip straight, solid tip to 255 μm long above hollow space (Fig. 14F, J); second spicule proximal, not seen in its entirety, wrapped part way around elongate spicule (Fig. 14G); distal ends of elongate spicules in close proximity *in situ* (Fig. 14J). With paired groups of seven accessory copulatory spicules (Fig. 14E, H) held tightly together in order of length, from >200 μm (range 205–211 μm) to about 100 μm (range 90–110 μm); spicules hollow, but smaller ones nearly solid; both ends curved, meeting medially at bulge with sharp bend, with none to several little bumps at one end below slight hook, fewest bumps on largest spicules; relationship to elongate copulatory spicules not determined.

Notes on anatomy: Neither pedal pit nor dorsoterminal sense organ obvious externally.

Reproductive system: Not examined.

Remarks. Copulatory spicules unequivocally differentiate *K. delta* and *K. levis* (Fig. 14). Further differences are: epidermal spicules of *K. delta* are (1) more slender and more deeply curved, (2) the largest spicules are shorter, (3) the solid tips are longer and without a constriction, and (4) the distance from the base to the bend is less. (5) Spicules from beside the pedal groove in *K. delta* are basally tapered and the outside margin bent; in *K. levis*, the base is truncated and the outside margin smoothly curved. (6) Terminal spicules, if still present after processing through sieves, are long and brushlike over entire posterior end in *K. levis*, but form a tuft over the mantle cavity opening in *K. delta*. (7) The radula of *K. delta* is larger than in *K. levis*, and the teeth bear a lateral denticle distinctly larger than the comblike denticles. Both species differ from *K. minima* and *K. borealis* by their occurrence at abyssal depths greater than 4000 m, and by body shape from *K. minima*. Unfortunately the types for *K. borealis* (Zoological Museum, University of Oslo, D 25654 and D 28676) are small, poorly dissected specimens without spicules.

Plawenia gen. nov.

Type species. Simrothiella schizoradulata Salvini-Plawen, 1978.

Known distribution. West European Basin and Bay of Biscay; Argentine Basin; off South Shetland Islands; off Peru; off San Diego, California (undescribed species); Japan Trench (undescribed species); and off La Réunion Island, Indian Ocean (undescribed species); from 2000 to nearly 6000 m.

Diagnosis. Body rotund, small, spiny; with thickset, hollow, upright epidermal spicules, skeletal spicules lacking; cuticle and epidermis thick; radular teeth with a strong, lateral buttress beneath large, lateral denticles; long, spiral anteroventral radular pockets retaining initial, triangular teeth; with two pairs of pharyngeal salivary glands, the dorsalmost acinar; seminal receptacles paired, bilobed; lower gametoducts first uniting and then becoming bilobed before emptying into mantle cavity through a papilla; copulatory spicules single, paired; a dorsoterminal sense organ present.

Description.

The following applies to all three species herein described: Epidermal spicules long, thin-walled (2 μm or less), gently curved or straight above an often bent and recurved base (Fig. 16); hollow internal space running from close to base nearly to tip in most spicules; proximal ends flat in widest spicules, flat to rounded in narrower spicules.

Paired anteroventral radular pockets remarkable, with numerous contained rows of teeth spiraled into flat, platelike structures positioned perpendicular to dorsoventral axis of the body; left pocket spiraled counterclockwise, right one clockwise in ventral view (Fig. 19E, F). Teeth with distinctive parts (Fig. 17C, D): (1) a bar thickened laterally into a thick buttress; (2) a serrated or scalloped distal margin of the denticle-bearing membrane; (3) a pair of large, lateral denticles flanking two smaller ones above the buttress; and (4) a medial and distal hemispherical extension of the bar. Original, triangular tooth retained in anteroventral radular pocket (Fig. 17H–K).

Copulatory spicules long, with four distinct sections: (1) a terminal, thickened, conical, curved tip (Fig. 18A–C, F, H); (2) a long, distal, thin-walled, twisted hemispherical channel (Fig. 18F, H) followed by (3) a short, narrow, solid, twisted and furrowed section (Fig. 18E, G, H); and (4) a broad, hollow basal portion (Fig. 18D, E, G). Paired bundles of curved, hollow, thick-walled, accessory copulatory spicules bearing distal protuberances (Fig. 18J, K) present amongst thickly set epidermal spicules adjacent to mantle-cavity opening.

Remarks. No entire, fully developed copulatory spicule was recovered from 10 dissected *Plawenia* individuals. In two small individuals (1.5 mm in *P. sphaera*, 1.4 mm in *P. argentinensis*) the spicules were composed only of distal sections 1 and 2 from just above the solid, yet-to-be-formed midsection (Fig. 18F). In five of six larger individuals, the distal sections of the spicules were missing and the spicules broken, either through the solid midsection (Fig. 18D, G), or somewhat above it (Fig. 18E). In one individual of intermediate size, the basal section was beginning to form while the tip was retained (Fig. 18H). Such a constancy between body size and absence of the distal section perhaps indicates that the distal end is deciduous rather than missing as an artifact of dissection.

The biogeographic questions raised by the distributions of the three *Plawenia* species herein described are provocative. *P. schizoradulata* lives at 4758 m on the Pacific side of the great eastward-bending parabolic arc that stretches from the southern tip of South America through the Scotia Ridge to the islands lying northeast of the Antarctic Peninsula; the benthos is therefore part of the Pacific fauna. The species is also represented by a single individual from the Atacama Trench off Peru at 5821 m (Salvini-Plawen, 1978; specimen not examined by authors). The Scotia Ridge effectively cuts off the deep stenobathyal bottom fauna of the Pacific from the Atlantic. That *P. argentinensis* from the Atlantic Argentine Basin at >4000 m depth shows morphological differences from *P. schizoradulata* is therefore not surprising; what is puzzling is the close similarity between *P. schizoradulata* and *P. sphaera* from only 2091 m in the West European Basin in the northeast Atlantic.

Plawenia schizoradulata (Salvini-Plawen, 1978)

(Figs. 15A–C, 16 spicules 1, 4–7, 17A, B, H, 18C, 19A, B)

Simrothiella schizoradulata Salvini-Plawen, 1978.

Lectotype (herein designated). USNM 749767 (alcohol specimen, spicule slide): Length 2.6 mm, midbody height and width 1.6 and 1.4 mm, respectively (specimen compressed). Drake Passage off South Shetland Islands, 61°45′S, 61°14′W, 4758 m (USARP 4-127, 1.viii.62).

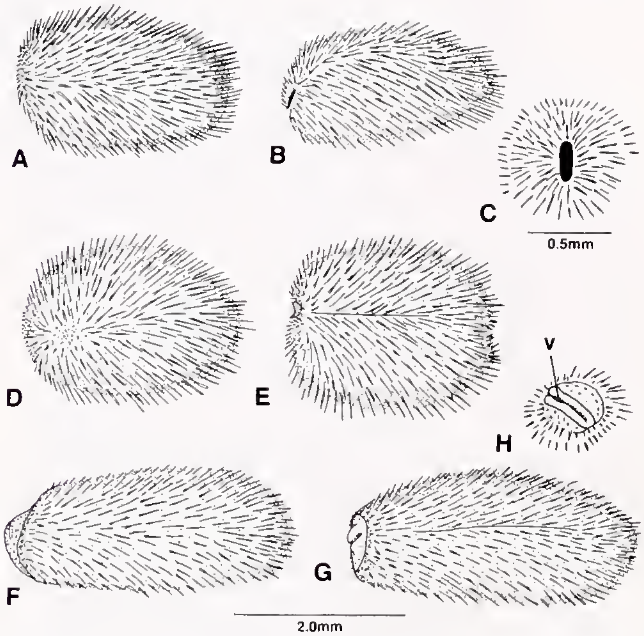

Figure 15. (A–C) *Simrothiella schizoradulata* Salvini-Plawen, lectotype (=*Plawenia schizoradulata*) (A, B) and paralectotype (C). (D, E) *Plawenia sphaera* n. sp., holotype. (F–H) *P. argentinensis* n. sp., holotype. (A, D, F) Lateral views, anterior to left. (B, E, G) Ventral view, (B) Oblique and somewhat compressed. (C, H) Contracted mouth opening, v opening to vestibule.

Paralectotypes. USNM 880322 (dissected alcohol specimen, spicule, radula slides): Length 1.1 mm, width and height 0.6 and 0.8 mm, respectively (specimen compressed), type locality. USNM 880323 (alcohol specimen): Length 1.3 mm, width and height both 0.9 mm, type locality.

Description.

Appearance: Small, rotund, length to 3.5 mm, diameter to 1.6 mm, posterior body narrower than anterior end; contracted mouth long, oval, on a broad, circular, flattened anteroventral area; pedal groove nearly hidden by spicules (Figs. 15A–C, 19A).

Cuticle and epidermis: Cuticle thick, 70–80 μm, epidermis thinner, 25 μm (Salvini-Plawen, 1978).

Epidermal spicules of lectotype and paralectotype: Almost all broken (Fig. 16, spicules 4–7; measurements, Table 2); many bent about one-quarter distance or less from base (spicules 6, 7); widest just above bend, base narrowest just below bend, then widening proximally; spicules beside pedal groove pointed distally, base rounded, without root (spicule 1).

Radula (one examined, small 1.1-mm paralectotype): Rows about 25 between proximal end of radular sac and pharynx, and 35–40 within anteroventral radular pockets; pockets with 2.5 whorls (3.5 whorls, Salvini-Plawen [1978], probably from a larger individual) (Fig. 19B; measurements, Table 2); morphology of distal extension of denticle-bearing

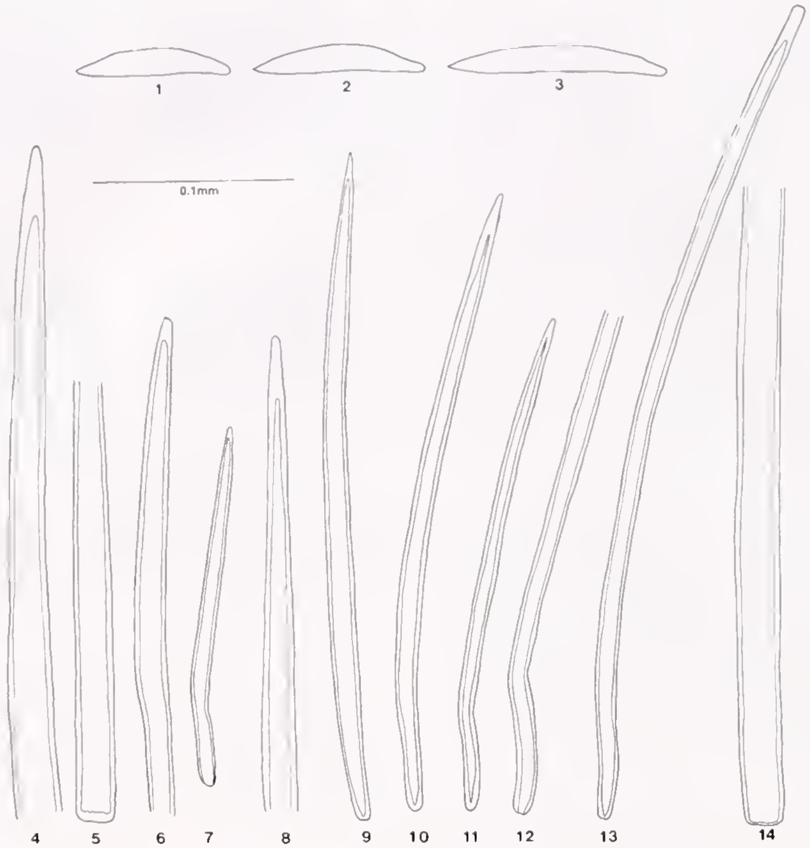

Figure 16. Epidermal spicules of *Plawenia* species. 1, 4–7, *Simrothiella schizoradulata* Salvini-Plawen (=*Plawenia schizoradulata*): spicules 4–6, lectotype; 1, 7, paralectotype. *Plawenia sphaera* n. sp.: spicules 2, 8–11, paratype 1. *P. argentinensis* n. sp.: spicules 3, 12–14, paratype USNM 880319. Spicules 1–3 from beside pedal groove; all other spicules incomplete except 7, 9–11, 13.

membrane not determined (Fig. 17A, B); number of denticles on lateral buttress 4.

Copulatory spicules (one examined): Distal tip dissected from small paralectotype, broadly conical, curved, and furrowed, 20 μm wide at distance of 45 μm proximal to tip (Fig. 18); remainder of spicule either not recovered or not yet formed; accessory copulatory spicules, if present, overlooked.

Notes on anatomy: The internal anatomy of *P. schizoradulata* has been published (Salvini-Plawen, 1978).

Reproductive system: See Salvini-Plawen (1978).

Remarks: For differences from other species, see Remarks under *P. sphaera* and *P. argentinensis* and Table 2.

Plawenia sphaera sp. n.

(Figs. 15D, E, 16 spicules 2, 8–11, 17C, D, J,
18B, G, H, K, 19D–G)

Scheltema *et al.*, 1994, fig. 18e.

Holotype. MNHNP (alcohol specimen, spicule slide): Length 2.4 mm, greatest height and width 1.7 and 1.9 mm, respectively. West European Basin, 57°59.7′N, 10°39.8′W, 2091 m (INCAL [CENTOB] DS-01, 15.vii.1976).

Illustrated paratypes. No. 1, MNHNP (epidermal, copulatory spicule slides; radula slide) and no. 2, MNHNP (epidermal, copulatory spicule slides): type locality. No. 3, MNHNP (epidermal, copulatory spicule slides; radula slide) and no. 4, MNHNP (dissected alcohol specimen, copulatory spicule slide), West European Basin, 57°58.8′N, 10°48.5′W, 2081 m (INCAL [CENTOB] DS-02, 16.vii.76).

Material examined. 68 individuals. See Table 1, also the following: Bay of Biscay, RV *Sarsia* (National Institute of Oceanography, Plymouth, UK): stn 44, 43°40.8′N, 3°35.2′W, 1739 m, 16.vii.67 (20 individuals), and stn 50, 43°46.7′N, 3°38′W, 2379 m, 18.vii.67 (1 individual).

Description.

Appearance: Small, rotund, similar in external appearance to *P. schizoradulata* but smaller; greatest length, height, and width, 2.9, 1.8, and 1.9 mm, respectively (Figs. 15D, 19D); with slight taper posteriorly; with a cleft in long posterior spicules indicating position of dorsoterminal sense organ (Fig. 15E).

Cuticle and epidermis: Cuticle thick, 45 to 50 μm, epidermis thin, 11 to 12 μm.

Epidermal spicules: Long, slender to broad, thin-walled (Fig. 16, spicules 8–11), shape as in *P. schizoradulata* but

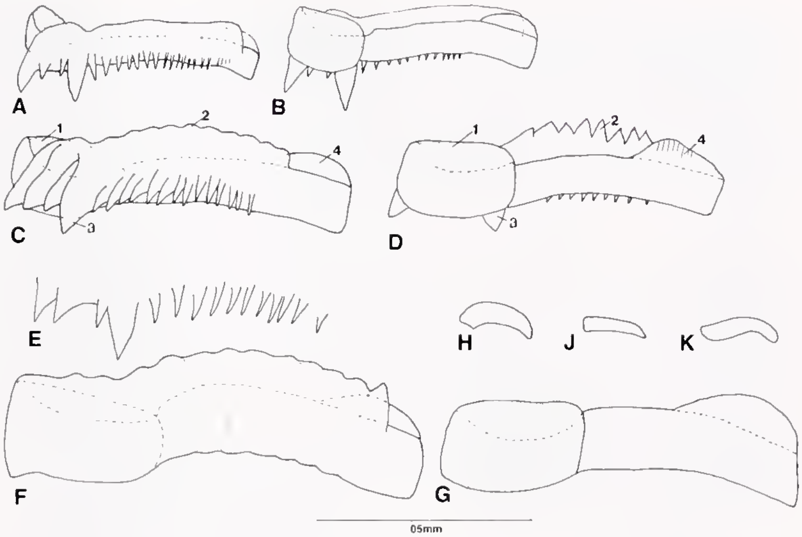

Figure 17. Radular teeth of *Plawenia* species, medial edge to right, distal edge above. (A, B, H) *Simrothiella schizoradulata* Salvini-Plawen, paralectotype (=*Plawenia schizoradulata*). (C, D, J) *Plawenia sphaera* n. sp. (paratypes 1, 3); in (C), distal edge of denticle-bearing membrane (2) serrated as in (D), but serrations covered by adjacent tooth. (E–G, K) *P. argentinensis* n. sp., paratype USNM 880319 (G, K) and USNM 880320 (F). (A, C, E, F) View from above. (B, D, G) View from beneath radular membrane; buttress with stippling. (E) 3rd tooth from proximal end of radular sac, denticles present, lost by 4th tooth as in (F). (H–K) Initial tooth retained at distal end of anteroventral radular pocket. 1 lateral buttress, 2 distal extension of denticle-bearing membrane, 3 large, lateral denticle above buttress, 4 medial and distal hemispherical extension of bar.

largest spicules longer (Table 2); spicules beside pedal groove with a sharp, distal point and proximally narrowed to a slight stem (spicule 2).

Radulae (7 examined, 4 by light microscopy, 3 by SEM, in individuals ranging in length from 1.5 to 2.7 mm; Figs. 17C, D, J; 19E–G; measurements, Table 2): Number of denticles on lateral buttress 4. Tooth structures locking both adjacent and opposed teeth closely to each other, with tips of denticles proximally overlying serrated, distal membrane of next adjacent tooth (Figs. 17D, 2; 19G), and hemispherical medial margin of bar finely denticulate (Fig. 17D, 4), holding opposed teeth in zipperlike arrangement (Fig. 19E).

Copulatory spicules (examined from 6 individuals 1.5 to 2.5 mm long, Fig. 18B, G, H, K; Table 2): Paired, single spicules, proximal two-thirds of spicule hollow, with wall thickened in two longitudinal bands; distal tip narrow, curved, bluntly pointed; accessory copulatory spicules S-shaped with up to 7 distal protuberances, with hollow extending from base up to 4th protuberance; number of accessory spicules per bundle not determined.

Remarks. Histologic descriptions of *P. schizoradulata* (Salvini-Plawen, 1978) are also descriptive of *P. sphaera*, with the additional observation that the more dorsal of the paired pharyngeal glands are acinar. The differences between *P. sphaera* and *P. schizoradulata* are as follows: In *P. sphaera* (1) small individuals are more nearly spherical than small *P. schizoradulata*, with length:height ratios of 1.0 and 1.4, respectively, in individuals less than 1.6 mm long; (2) many epidermal spicules are longer and broader than most of those in *P. schizoradulata;* (3) the distal tips of the copulatory spicules are narrower and more pointed; (4) there are fewer denticles per tooth; (5) there are more rows of teeth; (6) the initial radular teeth are shorter; and (7) the cuticle and epidermis are about one-half the thickness of those in *P. schizoradulata*. Finally, although the differences enumerated here and in Table 2 may seem minor, *P. schizoradulata* belongs to the abyssal Pacific fauna and *P. sphaera* to the upper slope fauna of the northeastern Atlantic. That they could be the same species is not likely given their morphological and biogeographic differences.

Plawenia argentinensis sp. n.

(Figs. 15F–H, 16 spicules 3, 12–14, 17E–G, K, 18A, D–F, J, 19C)

Holotype. USNM 880318 (alcohol specimen, spicule slide): Length 3.4 mm, midbody height and width 1.4 and 1.5 mm, respectively. Argentine Basin, 38°16.9′S, 51°56.1′W, 4382 m (RV *Atlantis II* Cruise 60, Stn 242, 13.iii.1971).

Illustrated paratypes. USNM 880319 and USNM 880320 (both as dissected alcohol specimens, epidermal and copulatory spicule slides, and radula slide); USNM 880321 (dissected alcohol specimen, copulatory spicule slide); type locality.

Material examined. 23 individuals from type locality.

Description.

Appearance: Largest, most elongate and least spiny *Pla-*

wenia species herein described, length to 5.0 mm, height to 1.8 mm, width to 1.6 mm (Figs. 15F, G, 19C); tapered anteriorly, mouth usually protruded with pair of lateral protuberances, contracted vestibule opening often distinct above mouth (Fig. 15H); line of pedal groove distinct.

Cuticle and epidermis: Not examined.

Epidermal spicules: Similar to other two species, but longer and broader (Fig. 16, spicules 12–14; Table 2); spicules from beside pedal groove elongate, distally pointed, without or with slight root (spicule 3).

Radula (2 examined): Teeth without distinct denticles except for the three most recently formed (Fig. 17E, F; measurements, Table 2), otherwise denticles appearing only as rows of slight protuberances; distal margin of denticle-bearing membrane scalloped except medially angular (Fig. 17F).

Copulatory spicules (3 examined): As in *P. sphaera*, but longer and wider, and solid tip longer (Fig. 18A, D–F; Table 2); accessory copulatory spicules about 19 per bundle, short, narrow, curved but not S-shaped, nearly solid or with hollow in central portion of spicule only, protuberances 1 to 3 (Fig. 18J; Table 2).

Remarks. P. argentinensis differs more from the other two *Plawenia* species than they do from each other in (1) size and shape of body, (2) erectness and size of epidermal spicules, (3) morphology of radula, (4) size of copulatory spicules, and (5) size and morphology of accessory copulatory spicules.

Simrothiella Pilsbry, 1898

Type species. Solenopus margaritaceus Koren & Danielssen, 1877, by subsequent designation [1981 Bull. Zool. Nom. 38, Op. 1185].

Known distribution. Between about 70 and 2000 m depth off Ireland and in Norwegian fjords.

Diagnosis. Elongate, smooth; epidermal spicules skeletal, hollow, uprights either not obvious or lacking; cuticle thick, epidermis thin with stalked papillae (Odhner, 1921); radula large, with long anteroventral pockets parallel to long axis of body, spiral restricted to proximal end. Monotypic, but with a second undescribed species from the West European Basin.

Remarks. The type species is described here on the basis

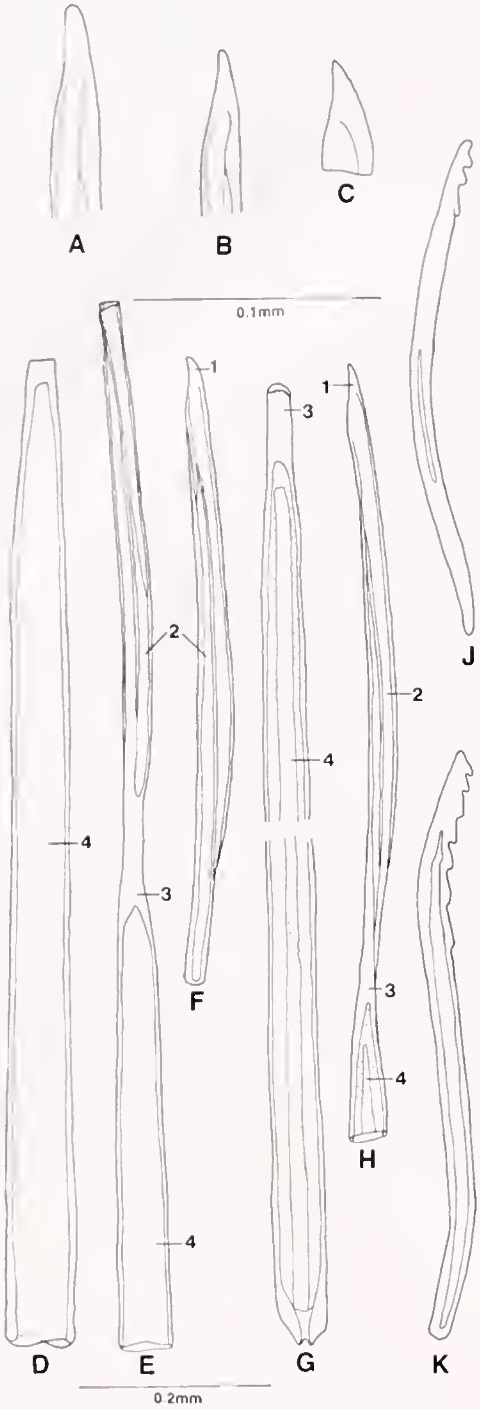

Figure 18. Copulatory spicules of *Plawenia* species; see text for description of sections 1–4. (A, D–F, J) *Plawenia argentinensis* n. sp. (B, G, H, K) *P. sphaera* n. sp. (C) *Simrothiella schizoradulata* Salvini-Plawen, paralectotype (= *Plawenia schizoradulata*). Spicules (A–C) distal tip (section 1): (A) enlargement of tip in (F), turned slightly. (B) Enlargement of tip in (H). (D) completely formed basal portion (section 4): entire distal portion above solid midsection (section 3) missing from 5.0-mm individual (paratype USNM 880320). (E) Incompletely formed basal portion (section 4), narrow, solid midsection (section 3), and proximal part of twisted, hemispherical channel (section 2), distal portion of section 2 and solid tip (section 1) missing from 3.8-mm individual (paratype USNM 880319). (F) Complete distal portion (sections 1, 2) of 1.4-mm individual, solid midsection and basal portion yet to be formed (paratype USNM 880321). (G) Completely formed basal portion (section 4) with thickened areas of spicule wall shown by stippling; solid midsection (section 3) showing furrow (stippling); entire distal portion (sections 1, 2) missing from 2.4-mm individual (paratype 3) (spicule broken during preparation; upper part rotated 90° from lower part). (H) Entire distal portion and midsection (sections 1–3) with basal portion (section 4) just beginning to form, in 2.2-mm individual (paratype 2). (J, K) Accessory copulatory spicules (paratype USNM 880320, paratype 4, respectively). Upper scale refers to spicules (A–C, J, K); lower scale, to spicules (D–H).

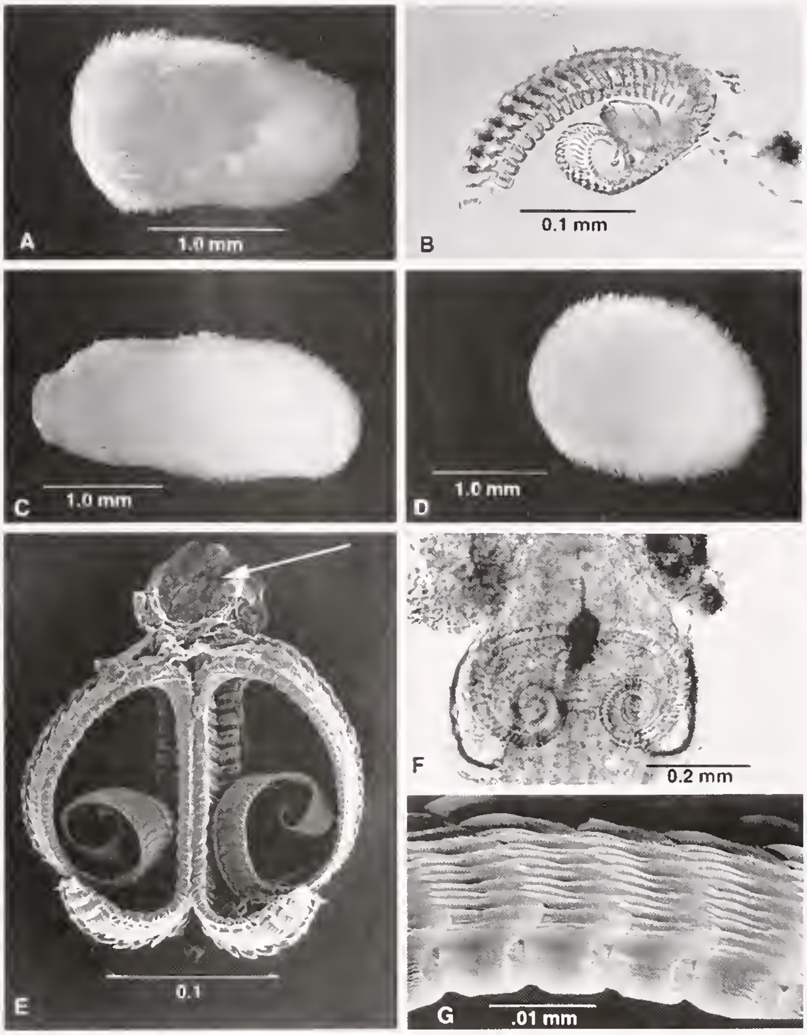

Figure 19. Three species of *Plawenia* n. g. (A, B) *Simrothiella schizoradulata* Salvini-Plawen (=*Plawenia schizoradulata*). (A) Lectotype. (B) Distichous radula, distal spiral with several turns, paralectotype. (C) *Plawenia argentinensis* n. sp., holotype. (D–G) *Plawenia sphaera* n. sp.: (D) Holotype. (E) Entire radula, pharyngeal cuticle indicated by line. (F) Ventral view of radula *in situ* within buccal mass. (G) Interlocking teeth of distichous bars. In (A, C, and D) anterior is to left and dorsal above.

of external morphology and, for the first time, on hard parts isolated from specimens recently collected in the West European Basin and from a museum specimen collected near the type locality. The internal anatomy was described by Odhner (1921).

Simrothiella margaritacea (Koren & Danielssen, 1877)
(Figs. 11A–C, 20–22)

Lectotype. UIB.Z.M 2075. Two incomplete specimens are labeled as G.O. Sars material from the type locality, Kvitingsog [Norway], 75–115 m (as Hvidingsöerne, Stavanger, 40–60 fm [=72–108 m] in Koren & Danielssen (1877 [trans. 1879]) and appear to be syntypes; Odhner (1921) called these specimens "prototype." Chosen here as lectotype is the more complete specimen with the anterior end intact; the second specimen is a paralectotype, UIB.Z.M 66806. Other G.O. Sars specimens from 75–95 m off Kopervik near the type locality are not considered syntypes (UIB.Z.M. 2078).

Illustrated voucher specimen. UIB.Z.M 66807: Length 9.5 mm, heights at anterior, midbody, just anterior to the posterior bulge, and posterior, 0.8, 1.0, 0.8, and 0.8 mm, respectively. Kopervik near type locality, 75–95 m.

Illustrated voucher specimens. USNM 894261 (entire alcohol specimen), length 9.5 mm, heights of anterior, midbody, anterior to posterior bulge, and posterior, 0.6, 0.8, 0.5, and 0.7 mm, respectively; USNM 894262 (dissected alcohol specimen, copulatory spicule slide); USNM 894263 (dissected alcohol specimen, radula slide); USNM 894264 (dissected alcohol specimen, radula slide, copulatory spicule slide); USNM 894265 (dissected alcohol specimen, radula

Table 2

Comparison of three species of Plawenia

	P. schizoradulata	*P. sphaera*	*P. argentinensis*
Body dimensions			
Maximum length	3.5 mm[1]	2.9 mm	5.0 mm
Maximum height	1.6 mm[1]	1.8 mm	1.8 mm
Length:height (range)	1.4–2.2	1.0–2.2	1.8–3.1
Length:height (mean)	1.7	1.6	2.3
Epidermal spicules			
Maximum length, midbody	>458 μm	>528 μm	>725 μm
Maximum length, posterior	—	>700 μm	>766 μm
Maximum width	21 μm	20 μm	23 μm
Length of solid tip, most spicules	≤18 μm	≤18 μm	≤22 μm
Pedal groove, max. l × w × thickness	90 × 13 × 2–3 μm	86 × 14 × 4 μm	108 × 15 × 3.5 μm
Radula[2]			
Number of rows	~65	95–145	146
Number of whorls	3.5[1]	2.5–3.5	2.8
Tooth bar	60 × 10 μm	74 × 10 μm	86 × 13 μm
Number of denticles above bar	19	11–15	11–13[3]
Buttress	19 × 13 μm	27 × 17 μm	35 × 20 μm
Number of denticles above buttress	4	4	4[3]
Length initial tooth	18 μm	14 μm	18 μm
Copulatory spicules			
Length of base	n.d.	890 μm	1,000 μm
Maximum width of base	n.d.	60 μm	80 μm
Length solid midsection	n.d.	180 μm	180 μm
Length distal section	n.d.	520 μm	678 μm
Maximum width distal section	n.d.	30 μm	35 μm
Total length[4]	n.d.	1,590 μm	1,858 μm
Length conical tip above channel	n.d.	36 μm	50 μm
Maximum width conical tip	20 μm	17 μm	20 μm
Max. l. accessory copulatory spic.	n.d	234 μm	196 μm
No. protuberances accessory cop. spic.	n.d.	7	3

[1] Salvini-Plawen (1978).

[2] Radula measurements in *P. schizoradulata* from small paralectotype 1.1 mm long.

[3] Present only in first three most recently formed teeth.

[4] Estimated total length before presumed loss of deciduous distal section.

slide, copulatory and epidermal spicule slides); USNM 894266 (dissected alcohol specimen); West European Basin, 50°58.7′N, 13°01.6′W, 2173 m (RV *Chain* 106, Stn 316,18.viii.72).

Material examined. 38 individuals: type material (2); UIB.Z.M. 2078(6), Kopervik, 75–95 m; UIB.Z.M 15852, 62°01′N, 0°08′E, ~1400 m (*Armauer Hansen* Stn 3, 10–11.v.1914)(4); RV *Chain* 106 Stn 316, 2173 m (26).

Description.

Appearance: Slender, length to 12.0 mm, rounded posteriorly and somewhat pointed subterminally at anterior end (Figs. 20A, B, 11A, C); greatest diameter anterior, to 1.1 mm in height, narrowing to 0.8 mm or less just before the posterior end which swells to 0.9 mm; greatly contracted individuals with constant diameter (*cf.* Figs. 11C, 20A); immature individuals without posterior swelling; contracted mouth a vertical slit, pedal pit small; contracted mantle cavity opening an anterior-posterior slit commencing on a ventral bulge (Fig. 20A); dorsoterminal sense organ present, not obvious; skeletal spicules obvious as an open meshwork, upright spicules not obvious.

Cuticle and epidermis: Not examined.

Skeletal spicules: Hollow, heavy-walled, to 280 μm long by 18 μm wide, walls 5 μm thick (Fig. 20D); lectotype spicules eroded, >144 by 16 μm, walls 5 μm (Fig. 20J);

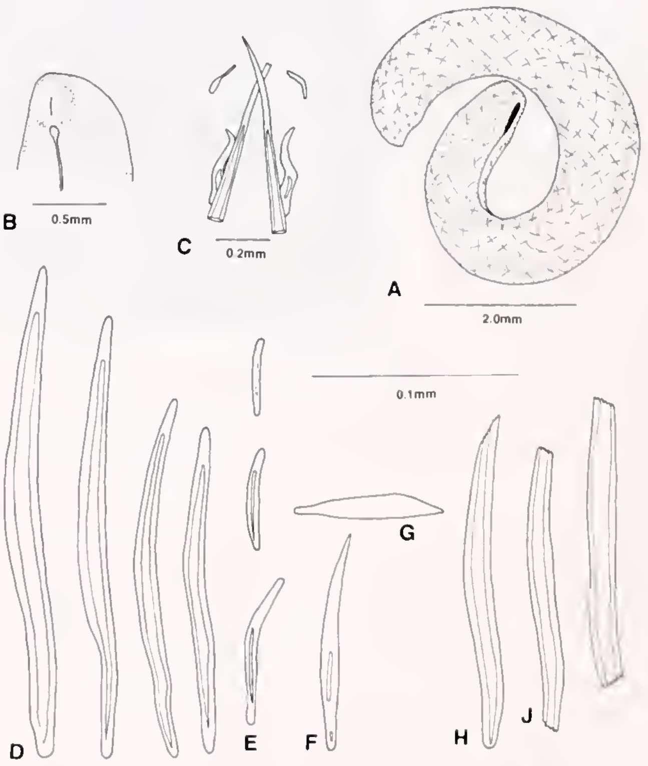

Figure 20. *Simrothiella margaritacea* (Koren & Danielssen). (A) Individual from Kopervik near type locality (voucher specimen before dissection, UIB.Z.M 66807). (B) Pointed anterior end of (A), anteroventral view. (C) Copulatory spicules *in situ* drawn as tissue dissolved in bleach (voucher USNM 894264, West European Basin). (D–G) Epidermal spicules from midbody (voucher USNM 894265, West European Basin): (D) Four skeletal spicules. (E) Upright spicules (vertical row). (F, G) From beside pedal groove, (F) lateral to (G). (H) Spicule from voucher UIB.Z.M 66807, tip eroded. (J) Two spicules, eroded, from lectotype.

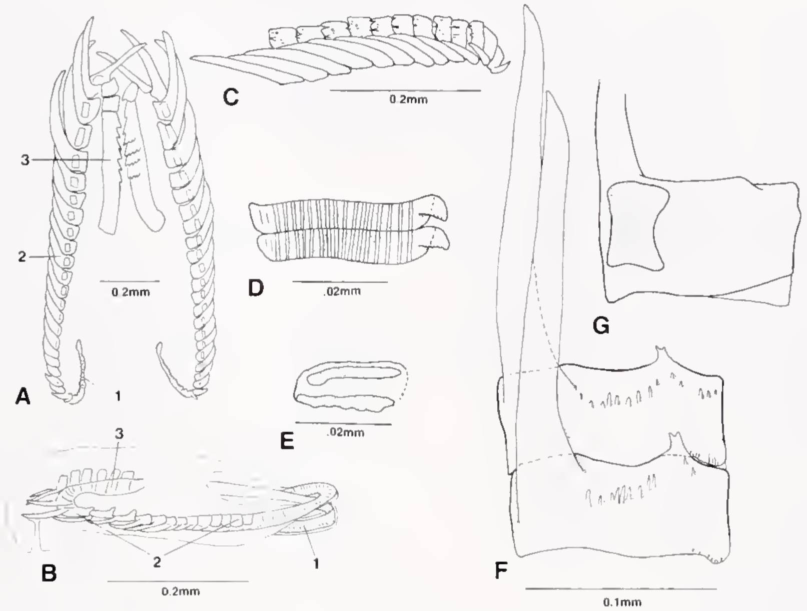

Figure 21. Radula of *Simrothiella margaritacea* (Koren & Danielssen) drawn from three individuals from West European Basin, vouchers USNM 894263 (A, G), USNM 894264 (B–D, F), and USNM 894266 (E); anterior is toward the top in all figures except (B) and (C). (A) Entire radula seen from above; sections 1 and 2 from anteroventral pocket, section 3 from radular sac (*cf.* Fig. 11C). (B) The same in lateral view, anterior to left, showing relation of teeth to buccal mass tissue; drawn during tissue dissolution in bleach. (C) First 12 proximal teeth of section 2 in lateral view, anterior to left. (D) Two teeth from region 1, comblike denticles schematic, medial edge to left; buttress, but not lateral denticles, forming on right (lateral) edge as a downturned hook. (E) First two teeth of anteroventral radular pocket, presumably the original teeth, with denticles not yet formed. (F) Two adjacent teeth ventral and just posterior to pharynx from near the anterior end of the anteroventral radular pocket, viewed from above. (G) Bar portion of tooth similar to those in (G) viewed from beneath radular membrane, showing buttress.

Kopervik voucher, spicules eroded, 170 by 16 μm, walls 5 μm (Fig. 20H); spicules evenly curved and widest above proximal straight or recurved basal section; base up to 67 μm long, solid distal tips to 27 μm long, proximal end rounded; skeletal spicules somewhat shorter anteriorly and posteriorly, to 225 μm; upright spicules small, to 95 μm long by 7 μm wide, curved or bent, hollow space narrow, distal end solid and rounded (Fig. 20E); spicules along pedal groove solid, flat, thin (2 μm), with proximal narrow root, distally pointed, length to 74 μm, greatest width to 14 μm (Fig. 20G); spicules just lateral to these shaped much like skeletal spicules in outline but nearly solid, sharply pointed distally, and shorter, to 106 μm long by 7 μm wide, proximal straight portion to 14 μm long (Fig. 20F).

Radula (6 examined: 1 from Kopervik voucher; 5 from *Chain* 106 Stn 316): Up to nearly 2 mm long, turning 180° so that short radular sac and long anteroventral radular pocket parallel each other and long axis of body, with 3 discrete sections (Figs. 11B, 21A, B): section 1, proximal anteroventral radular pocket as 0.2-mm loops, one lying over the other, initial teeth nondenticulate bars 20 by 3 μm (Fig. 21E); next teeth comblike bars about 45 by 9 μm at center of section 1, denticle number 14–18 (Fig. 21D); section 2, main part of anteroventral radular pocket and longest section of radula, about 1 mm long, proximal teeth with bar 50 by 15 μm bearing 17 comblike denticles and a lateral denticle 27 μm long, laterally buttressed (Fig. 21C); teeth of section 2 gradually enlarging anteriorly, largest tooth with bar 130 by 90 μm, lateral denticle to 280 μm long, heavily buttressed, other denticles of bar scattered, small, and varying in pattern and number among individuals (Fig. 21F, G); section 3, radular sac 0.5 to 0.6 mm long with 7–9 developing teeth, long lateral denticles ill-defined, with proximal stretch of membrane 0.2 mm long without defined teeth (Figs. 11B, 21A); at ventral bend of radula from the sac into the pharynx, lateral teeth obvious, pointing anteriorly (Figs. 11B, 21A).

Copulatory spicules (5 examined): Paired, 2 per sac (Fig. 22C); one spicule long, curved, hollow, to 1.2 mm long, 93 μm wide in curved view (Fig. 22G), narrower in view where spicule appears straight (Fig. 22C); solid distal ends pointed and approximated *in situ* (Fig. 20C), with thick core surrounded by added thin layer of calcium carbonate, perhaps as "wings" (Fig. 22E); second spicule shorter, hollow, to 370 μm long, S-shaped, base partially wrapped around long spicule, from 90 μm in widest view to 30 μm in

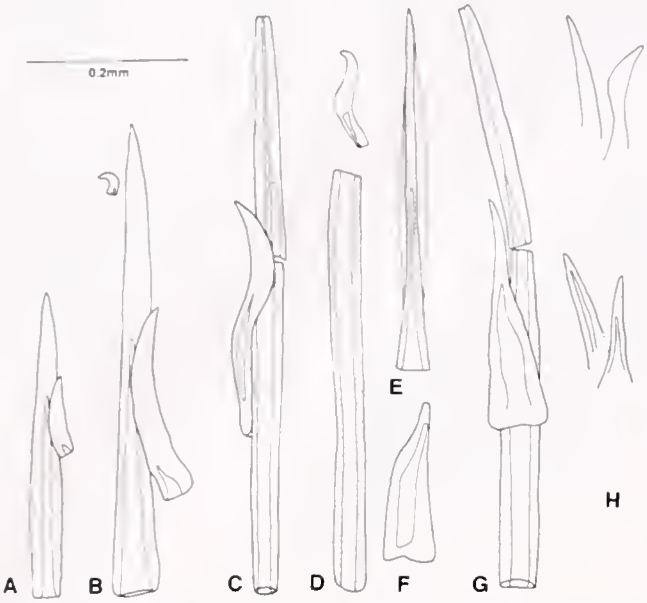

Figure 22. Copulatory spicules of *Simrothiella margaritacea* (Koren & Danielssen) (see also Fig. 20C). (A, B) growth stages, (A) from 8.3 mm individual (voucher USNM 894263), (B) from individual <7 mm (voucher USNM 864262) with accessory spicule above. (C–G) Paired spicules from voucher 5 (voucher USNM 864265), specimen length not known: (C and G) two views of one of pair, proximal end broken off; (D–F) second of pair, (D) proximal to and broken off from distal portion (E) of long spicule, wall and solid distal portion with stippling, accessory spicule above. (H) Above and below, paired, mostly (decalcified spicules of voucher specimen from Kopervik near type locality (UIB.Z.M 66807); solid lines indicate part still calcified, dotted lines indicate remaining uncalcified thin membrane. Decalcification due to dissolution during preservation.

narrowest, axially twisted such that solid distal end widest in narrowest view of base and narrowest in widest view of base (Fig. 22C, G); single, short accessory spicules paired, to 152 μm, base straight, slightly hollowed proximally, distally solid, deeply curved into distal hook (Fig. 22B, D); growth stages of copulatory spicules (Fig. 22A, B, D, E) imperfectly correlated with size of individual.

Reproductive system: See Odhner (1921).

Remarks. The recently collected material from the West European Basin was identified as *Simrothiella margaritacea* by comparing the following: (1) epidermal spicule width and wall width with the lectotype and Kopervik voucher spicules (Fig. 20D, H, J); (2) width and shape of the anterior end of the body with the lectotype (Fig. 11A); (3) shape and size of the anterior and posterior ends of the body with the Kopervik voucher; (4) radula with the radula of the Kopervik voucher; and (5) size and shape of copulatory spicules with those from the Kopervik voucher (Fig. 22H).

Elements of copulatory spicules of *S. margaritacea* are much like those in *Kruppomenia levis* (*cf.* Fig. 14A). The comblike denticles of early teeth are similar to those in *Kruppomenia* and *Plawenia* radulae, but the original tooth in *S. margaritacea* is a nondenticulate bar, not a triangle.

The radular teeth have not achieved full size when they are first released from the radular sac into the pharynx (Figs. 11B, 21A). Additional growth must therefore take place at the distal end of the anteroventral pocket.

Results of Cladistic Analysis

A single species in each of the 5 genera described here, plus a species with a monostichous radula, *Lyratoherpia incali* Scheltema (1999b), were the subjects of a cladistic analysis. Twenty-six characters from an original set of 42 were selected for the analysis. The 16 excluded characters were uninformative in the present data set and included such autapomorphies as polystichous and monostichous radulae (*Dorymenia* and *Lyratoherpia*, respectively). Of the selected characters, 6 are associated with the radula, 5 with spicules, 11 with soft-part anatomy, and 4 with body shape. The characters and their states are listed in Appendix 1. All characters were treated as unordered and were equally weighted. Since the homology of a number of characters is unknown or disputable, we chose to use presence-absence coding. This type of coding is simple and intuitive, and it has the added advantage that exact homologies between character states need not be known (Pleijel, 1995).

The resulting phylogenetic trees were rooted by outgroup analysis (*e.g.*, Nixon and Carpenter, 1993), with *Helicoradomenia juani* Scheltema & Kuzirian as the outgroup, since it possesses characters that are considered to be less derived. Among these characters are the radula, which is similar to the radula of the Middle Cambrian *Wiwaxia* (see Schander and Scheltema, in press), and spicules that are solid, a condition known through ontogeny to be plesiomorphic to hollow spicules (Scheltema and Jebb, 1994).

The cladistic analysis resulted in one shortest tree, 46 steps long (Fig. 23). The overall consistency and retention indices (CI, RI) are 0.5652 and 0.5349, respectively. One clade has a decay index of 4, and the others of 1. The character transformations are found in Appendix 2.

Discussion

The external and hard-part morphologies of the 10 species and 5 genera of neomenioid aplacophorans described here provide a basis for aplacophoran taxonomy (*i.e.*, discrimination of taxa), as well as for phylogeny (*i.e.*, the evolutionary relationships among taxa).

Taxonomy

We conclude that histologic preparations by themselves will not provide morphological evidence adequate for discriminating with certainty among closely related species. For example, the two species of *Eleutheromenia* are indistinguishable from their soft anatomy, yet hard parts, particularly the copulatory spicules (Fig. 9), do distinguish them,

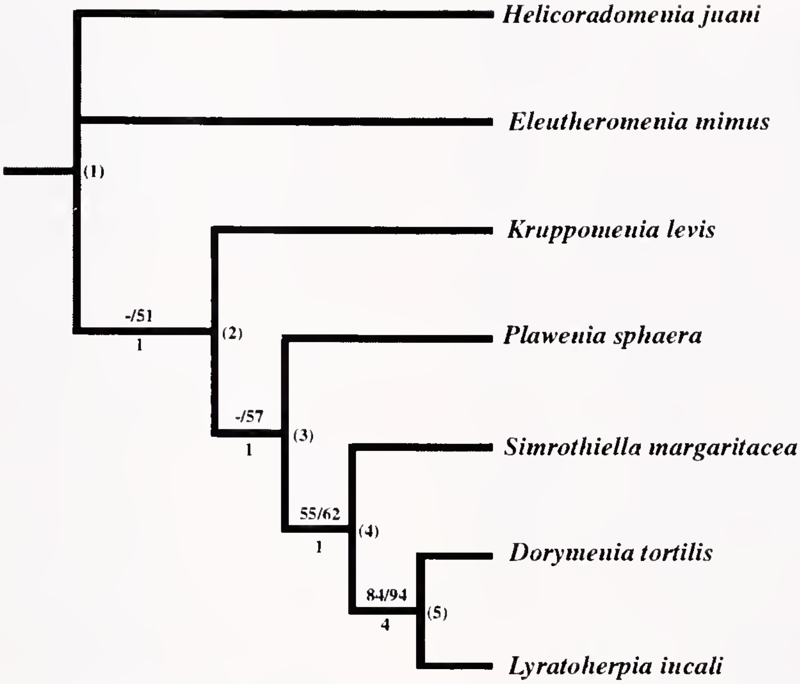

Figure 23. The single shortest tree, 46 steps long, obtained from an exhaustive search of the data matrix in Appendix 1; CI 0.5652, RI 0.5349. Numerals within parentheses are references to the nodes indicated in Appendix 2. Numerals above branches are bootstrap/jacknife values, and numerals below are decay values.

and the differences in size of their epidermal spicules and radular teeth are species related, and not due simply to variation within a species. Only measurements of the largest epidermal spicules were useful for species recognition. Analysis of a large number of spicules from a single individual would be meaningless in this regard, for it would hide the truly distinctive character—the size of the largest epidermal spicules produced in each species.

The two closely related *Kruppomenia* species are distinguished here on hard parts alone, that is, the differences in radula and copulatory spicule morphology (Figs. 12F–K, 14). Even though the differences in epidermal spicules are subtle, one can, with practice, quickly discern the differing lengths between the base and proximal bend (Fig. 13). Although *K. levis* and *K. delta* co-occur in some epibenthic sled samples (Table 1), they should not necessarily be considered sympatric; sled trawls, particularly those taken at abyssal depths, often traverse a mile or so of ocean floor and probably collect organisms from several populations.

Dorymenia sarsii and *D. tortilis* can be differentiated by the spicules at the opening of the mantle cavity (Fig. 4K, L), as well as by the differences listed under Remarks for *D. tortilis*. Finally, species of *Plawenia* are differentiated by a combination of hard-part and external morphologies (Table 2).

Higher taxa can also be determined from hard parts and body shape. Thus, although members of both genera are elongate and smooth, *Dorymenia* and *Simrothiella* species have very different radulae (Figs. 2E, F, 21). *Plawenia* species are immediately recognizable by their nearly spherical bodies with long, hollow spicules that are upright, but not skeletal (Fig. 15, 19A, C, D). *Kruppomenia* species are brought together by their distinctive, long, broad, ribbonlike radula bearing narrow, serrated teeth, as well as by their short, blunt bodies (Fig. 12). *Eleutheromenia* species belong to a taxon with hollow, barbed spicules and a radula with distichous hooks.

Soft internal anatomy will always be important for phylogeny and often for the determination of higher ranks. What is emphasized here is that identification of species should not depend on histology, and higher taxa should reflect external and hard-part morphologies.

Phylogeny

Because the bootstrap values were relatively low, and few genera and species were included, we refrain from defining clade names (de Queiroz and Gauthier, 1990; Schander and Thollesson, 1995; Cantino *et al.,* 1997). Although the figured tree (Fig. 23) cannot define clades, the usefulness of characters from hard parts in phylogenetic analyses is clear from the average consistency indexes: for radula characters, 0.58; for soft-part anatomy, 0.59; for spicule characters, 0.47; and for external appearance, 1.

In a reanalysis of 22 published phylogenetic studies of Gastropoda, three types of characters were compared: shell, soft anatomy, and "other," which included the radula (Schander and Sundberg, 1997). The results showed that all three character groups had about the same consistency and retention indices, and the conclusion was that all three types of characters are necessary for proper assessment of evolutionary relationships. We likewise find that all types of characters should be used for aplacophorans.

Although the small data set included here is too incomplete to shed light on evolutionary relationships among all neomenioids, it serves as an example of usefulness of hard parts in cladistic analysis. In particular, there is no support for a clade Simrothiellidae (*cf.* Salvini-Plawen, 1978). The indices do give strong support for the clade *Lyratoherpia* + *Dorymenia,* but in the present analysis this clade is based mostly on absences (Appendix 2, node 4 → node 5), several arising from derivations of the radular apparatus (Scheltema, Kerth, and Kuzirian, unpubl.). Thus, these two taxa share a condition of being derived, and the cladogram should not be interpreted as indicating monophyly. Future phylogenetic analyses utilizing many more taxa are certain to suggest a different relationship.

Acknowledgments

Specimens were generously provided to us by the Centre National de Tri d'Océanographie through M. Segonzac; by Howard L. Sanders and J. Frederick Grassle from cruises of the Woods Hole Oceanographic Institution under several grants from the National Science Foundation; and from the Museum of Victoria, Australia. The loan of type specimens from the following Museums is gratefully acknowledged: University of Bergen Zoological Museum; Zoological Museum, University of Oslo; and the U.S. National Museum of Natural History. We wish to thank Thomas Dahlgren, the Tuesday afternoon invertebrate discussion group, and two anonymous reviewers for helpful comments that led us to revise the discussion substantially and to add a preliminary phylogenetic analysis of the neomenioid aplacophorans described here. The following figures, with changes herein, first appeared in the *Microscopic Anatomy of Invertebrates,* Vol. 5: *Mollusca* I, pp. 13–54, Wiley-Liss, Inc.: 1A, 4A, 5A, 6C, 9D, and 19E. This work was completed with support from a National Science Foundation PEET grant (Partnerships for Enhancing Expertise in Taxonomy) DEB-9521930 to AHS and from the Radman Ernst Colliander Foundation, Helge Ax:son-Johnson Foundation, Göteborgs Kungliga Vetenskaps- och Vitterhetssamhälle, and Adelbertska Foundation to CS.

Contribution no. 9746 from the Woods Hole Oceanographic Institution.

Literature Cited

Bremer, K. 1988. The limits of amino acid sequence data in angiosperm phylogenetic reconstruction. *Evolution* **42:** 795–803.

Bremer, K. 1994. Branch support and tree stability. *Cladistics* **10:** 295–304

Buckland-Nicks, J., and A. H. Scheltema. 1995. Was internal fertilization an innovation of early Bilateria? Evidence from sperm structure of a mollusc. *Proc. R. Soc. Lond. Ser. B* **261:** 11–18.

Cantino, P. D., R. G. Olmstead, and S. J Wagstaff. 1997. A comparison of phylogenetic nomenclature: a botanical case study. *Syst. Biol.* **46**(2): 313–331.

de Queiroz, K., and J. Gauthier. 1990. Phylogeny as a central principle in taxonomy: phylogenetic definitions of taxon names. *Syst. Zool.* **39:** 307–322.

Eriksson, T. 1998. *AutoDecay. Version 4.0.* Hypercard stack distributed by the author. http://www.bergianska.se/personal/TorstenE/AutoDecay/AD4.stack.sea.hqx

García-Alvarez, O., V. Urgorri, and L. v. Salvini-Plawen. 1998. *Dorymenia troncosoi* sp. nov. (Mollusca Solenogastres: Proneomeniidae), a new species from the South Shetland Islands (Antarctica). *Polar Biol.* **20:** 382–387.

Hansen, G. A. 1889. Neomenia, Proneomenia, und Chätoderma. *Bergens Mus. Aarsber. 1888* No. 6, 12 pp.

Heath, H. 1911. The Solenogastres. Reports on the scientific results of the expedition to the tropical Pacific . . . by the "Albatross" . . . . *Mem. Mus. Comp. Zool.* **45**(1): 1–179.

Heath, H. 1918. Solenogastres from the Eastern Coast of North America. *Mem. Mus. Comp. Zool.* **45**(2): 185–263.

Hubrecht, A. A. W. 1881. *Proneomenia sluiteri* gen. et sp. n., with remarks upon the anatomy and histology of the Amphineura. *Niederl. Arch. Zool. 1881,* Suppl. 9, 75 pp.

Ivanov, D. L. 1996. Origin of Aculifera and problems of monophyly of higher taxa in molluscs. Pp. 59–65 in *Origin and Evolutionary Radiation of the Mollusca,* J. D. Taylor, ed. Oxford University Press, Oxford.

Koren, J., and D. C. Danielssen. 1877. Beskrivelse over nye arter, henhorende til slaegten *Solenopus,* samt nogle oplysninger om dens organisation. *Arch. Math. Naturvid.* [Christiana] **2:** 120–128.

Koren, J., and D. C. Danielssen. 1879. Descriptions of new species belonging to the genus *Solenopus,* with some observations on their organization. *Ann. Mag. Nat. Hist. Ser. 5* **3:** 321–328.

Maddison, W. P., and D. R. Maddison. 1992. *MacClade: Analysis of Phylogeny and Character Evolution.* Version 3.0. Sinauer Associates, Sunderland, MA

Morse, M. P. 1979. *Meiomenia swedmarki* gen. et sp. n., a new interstitial solenogaster from Washington, USA. *Zool. Scr.* **8:** 249–253.

Morse, M. P., and J. L. Norenburg. 1992. Observation and descriptions of *Meiomenia arenicola* Salvini-Plawen 1985 (Mollusca: Aplacophora), an interstitial Solenogaster from Fort Pierce, Florida. *Proc. Biol. Soc. Wash.* **105:** 674–682.

Nierstrasz, H. F. 1902. *The Solenogastres of the Siboga-Expedition. Siboga-Exp.* Vol. 47. E. J. Brill, Leyden. 46 pp.

Nierstrasz, H. F. 1905. *Kruppomenia minima* und die Radula der Solenogastren. *Zool. Jahrb., Abt. Anat. Ont.* **21:** 655–702.

Nixon, K. C., and J. M. Carpenter. 1993. On outgroups. *Cladistics* **9:** 413–426.

Odhner, N. H. 1921. Norwegian Solenogastres. *Bergens Mus. Arb. 1918–1919, Natur. raekke* No. 3: 1–86.

Pleijel, F. 1995. On character coding for phylogeny reconstruction. *Cladistics* **11:** 309–315.

Pruvol, G. 1891. Sur l'organisation de quelques néoméniens des côtes de France. *Arch. Zool. Expér. Gén. Ser. 2* **9:** 699–805.

Salvini-Plawen, L. v. 1968. Über einige Beobachtungen an Solenogastres (Mollusca, Aculifera). *Sarsia* **31:** 131–142.

Salvini-Plawen, L. v. 1972. Zur Morphologie und Phylogenie der Mollusken: Die Beziehungen der Caudofoveata und der Solenogastres als Aculifera, als Mollusca und als Spiralia. *Z. Wiss. Zool.* **184:** 205–394.

Salvini-Plawen, L. v. 1978. Antarktische und subantarktische Solenogastres (eine Monographie: 1898–1974). *Zoologica* **44:** 1–315.

Salvini-Plawen, L. v. 1985. Early evolution and the primitive groups. Pp. 59–150 in *The Mollusca Vol. 10 Evolution,* E. R. Trueman and M. R. Clarke, eds. Academic Press, Orlando.

Salvini-Plawen, L. v. 1997. Fragmented knowledge on West-European and Iberian Caudofoveata and Solenogastres. *Iberus* **15:** 35–50.

Salvini-Plawen, L. v., and G. Steiner. 1996. Synapomorphies and plesiomorphies in higher classification of Mollusca. Pp. 29–51 in *Origin and Evolutionary Radiation of the Mollusca,* J. D. Taylor, ed. Oxford University Press, Oxford.

Schander, C., and A. H. Scheltema. In press. An alternative interpretation of the affinities of the Lower and Middle Cambrian fossil *Wiwaxia corrugata* (Matthew, 1899) from studies of the Aplacophora. *Am. Malacol. Bull.*

Schander, C., and P. Sundberg. 1997. Useful characters in gastropod phylogeny—soft information or hard facts? Chapter IV, Pp. 1–6, in C. Schander, *Taxonomy and phylogeny of the Pyramidellidae (Mollusca, Gastropoda, Heterobranchia).* Ph.D. thesis, Göteborg University, Sweden.

Schander, C., and M. Thollesson. 1995. Phylogenetic taxonomy—some comments. *Zool. Scr.* **24:** 263–268.

Scheltema, A. H. 1981. Comparative morphology of the radulae and alimentary tracts in the Aplacophora. *Malacologia* **20:** 361–383.

Scheltema, A. H. 1988. Ancestors and descendents: relationships of the Aplacophora and Polyplacophora. *Am. Malacol. Bull.* **6:** 57–68.

Scheltema, A. H. 1993. Aplacophora as progenetic aculiferans and the coelomate origin of mollusks as the sister taxon of Sipuncula. *Biol. Bull.* **184:** 57–78.

Scheltema, A. H. 1996. Phylogenetic position of Sipuncula, Mollusca and the progenetic Aplacophora. Pp. 53–58 in *Origin and Evolutionary Radiation of the Mollusca,* J. D. Taylor, ed. Oxford University Press, Oxford.

Scheltema, A. H. 1999a. Two solenogaster molluscs, *Ocheyoherpia trachia* n. sp. from Macquarie Island and *Tegulaherpia tasmanica* Salvini-Plawen from Bass Strait (Aplacophora, Neomeniomorpha). *Rec. Aust. Mus.* **51:** 23–31.

Scheltema, A. H. 1999b. New eastern Atlantic neomenioid aplacophoran molluscs. *Ophelia* **51**(1): 1–28.

Scheltema, A. H., and M. Jebb. 1994. Natural history of a solenogaster mollusc from Papua New Guinea, *Epimenia australis* (Thiele) (Aplacophora, Neomeniomorpha). *J. Nat. Hist.* **28:** 1297–1318.

Scheltema, A. H., and A. M. Kuzirian. 1991. *Helicoradomenia juani* gen. et sp. nov., a Pacific hydrothermal vent Aplacophora (Mollusca: Neomeniomorpha). *Veliger* **34:** 195–203.

Scheltema, A. H., M. Tscherkassky, and A. M. Kuzirian. 1994. Aplacophora. Pp. 13–54 in *Microscopic Anatomy of Invertebrates Vol 5: Mollusca,* F. W. Harrison and A. J. Kohn, eds. Wiley-Liss, New York.

Stachowitsch, M. 1992. *The Invertebrates: An Illustrated Glossary.* Wiley-Liss, New York. 676 pp.

Swofford, D. L. 1998. *Phylogenetic Analysis Using Parsimony.* Version 4.0b1. Sinauer Associates, Sunderland, MA.

Welsch, U., and V. Storch. 1973. *Comparative Animal Cytology and Histology.* Seattle, University of Washington Press.

Appendix 1

Data matrix and list of characters: 0 absent, 1 present

	11111111112222222
Taxon/node	12345678901234567890123456
Dorymenia tortilis	00000101?01011110010101101
Eleutheromenia mimus	10000?01?10101011110010010
Helicoradomenia juani	11000010010100101110010110
Kruppomenia levis	11111010110101010010110010
Plawenia sphaera	11101010110100011001001110
Simrothiella margaritacea	11111010001011011001?01101
Lyratoherpia incali	00000100?01010100101100110

1. Distichous radula: with 2 teeth per row (Figs. 11B, D, 12F, H, 19B, E, F, 21)
2. Bar base: radula on a bar entirely attached to radular ribbon (Figs. 6F, 12G, K, 19G, 21)
3. Original tooth: retained in anteroventral radular pocket (Figs. 6F, 12J, 21E)
4. Serrate teeth: denticles as fine serrations (Figs. 6F, 12F, G, H, K, 21D)
5. Tooth buttress: thickened radula base beneath lateral denticles (Figs. 17, 21G)
6. Unipartite membrane: radular membrane not divided (Scheltema, 1988)
7. Paired anteroventral pocket (Fig. 19F, 21A)
8. Single anteroventral pocket (Fig. 6B)
9. Original tooth triangular (Fig. 6F)
10. Stout body shape (Figs. 6G, H, 11E, F, 19A, C, D)
11. Elongate body shape (Figs. 6A, 11C)
12. Rounded body ends (Figs. 7A, E, 12A, D, 15)
13. Pointed or lobate body ends (Figs. 2A–D, 11C)
14. Skeletal spicules: spicules within cuticle, at right angles to each other (Figs. 2A, 12A, D, 20A)
15. Solid spicules (Fig. 3 spicules 1–3)
16. Hollow spicules (Figs. 3 [except spicules 1–4], 8, 13, 16, 20D–J)
17. Accessory copulatory spicules (Figs. 18J, K, 20C, 22B and D small spicules)
18. Copulatory spicule hood: main spicule with a second spicule wrapped around it (Fig. 9)
19. Single seminal receptacle (Figs. 5A, 10A, B)
20. Multiple seminal receptacles (Scheltema *et al.*, 1994, fig. 24h, i)
21. Seminal vesicle (Fig. 6C)
22. Respiratory papillae (Scheltema *et al.*, 1994, fig. 11d)
23. Respiratory folds (Scheltema *et al.*, 1994, fig. 11c)
24. Midgut sacculations (Scheltema *et al.*, 1994, fig. 13c)
25. Single-cell epidermal glands (Scheltema *et al.*, 1994, fig. 5d–g)
26. Multiple cell epidermal glands (Scheltema *et al.*, 1994, fig. 5a, c)

Appendix 2

List of character transformations

Branch	Character	Change	Branch	Character	Change
node 1 → node 2	3 (Original tooth)	0 → 1	node 5 → *Dorymenia*	8 (Single anteroventral pocket)	0 → 1
	5 (Tooth buttress)	0 → 1		19 (Single seminal receptacle)	0 → 1
	9 (Triangular original tooth)	0 → 1		20 (Multiple seminal receptacles)	1 → 0
	18 (Copulatory spicule hood)	1 → 0	node 5 → *Lyratoherpia*	14 (Skeletal spicules)	1 → 0
	21 (Seminal vesicle)	0 → 1		16 (Hollow spicules)	1 → 0
node 2 → node 3	19 (Single seminal receptacle)	1 → 0		18 (Copulatory spicule hood)	0 → 1
	20 (Multiple seminal receptacles)	0 → 1		23 (Respiratory folds)	1 → 0
	22 (Respiratory papillae)	1 → 0		25 (Single-cell epidermal glands)	0 → 1
	23 (Respiratory folds)	0 → 1		26 (Multiple-cell epidermal glands)	1 → 0
	24 (Midgut sacculations)	0 → 1	node 4 → *Simrothiella*	4 (Serrate teeth)	0 → 1
node 3 → node 4	9 (Triangular original tooth)	1 → 0	node 3 → *Plawenia*	14 (Skeletal spicules)	1 → 0
	10 (Stout body shape index < 5)	1 → 0		21 (Seminal vesicle)	1 → 0
	11 (Elongate body shape index ≥ 5)	0 → 1	node 2 → *Kruppomenia*	4 (Serrate teeth)	0 → 1
	12 (Rounded body ends)	1 → 0		17 (Accessory copulatory spicules)	1 → 0
	13 (Pointed or lobate body ends)	0 → 1	node 1 → *Eleutheromenia*	2 (Bar base)	1 → 0
	25 (Single-cell epidermal glands)	1 → 0		7 (Paired anteroventral pocket)	1 → 0
	26 (Multiple-cell epidermal glands)	0 → 1		8 (Single anteroventral pocket)	0 → 1
node 4 → node 5	1 (Distichous radula)	1 → 0	node 1 → *Helicoradomenia*	14 (Skeletal spicules)	1 → 0
	2 (Bar base)	1 → 0		15 (Solid spicules)	0 → 1
	3 (Original tooth)	1 → 0		16 (Hollow spicules)	1 → 0
	5 (Tooth buttress)	1 → 0		24 (Midgut sacculations)	0 → 1
	6 (Unipartite membrane)	0 → 1			
	7 (Paired anteroventral pocket)	1 → 0			
	15 (Solid spicules)	0 → 1			
	17 (Accessory copulatory spicules)	1 → 0			

Reference: Biol. Bull. 198: 152–165. (February 2000)

A Dynamical Model of Communities and a New Species-Abundance Distribution

A. K. DEWDNEY

Dept. of Zoology (and Dept. of Computer Science), The University of Western Ontario,
London, Ontario, Canada N6A 5B7

Abstract. It is known to many field biologists that biosurveys of natural communities tend to produce a J-shaped curve when the numbers of species are plotted against abundances. In other words, when the number of species of abundance k is plotted against k (running from 1 to some large number), the resulting distribution peaks at the lowest abundance, then forms a concave ramp as it approaches zero at the far end of the abundance axis. Does this distribution represent a single formula operating behind the scenes, or does it represent several formulas, appropriate for different types of community? Or does it represent no particular formula at all?

The research reported here has three components: (1) The analysis of a new dynamical system that simulates multispecies communities (producing J-curves in the process) and the derivation of the "logistic-J" distribution, as the underlying community equilibrium curve; (2) the summary of a general theory of sampling as a bridge between natural communities and samples of them; (3) the evaluation of extant proposals for species-abundance distributions by application of a general theory of sampling or by cross-comparison *via* 100 biosurveys randomly selected from the literature.

Introduction

A glance at the species/abundance distribution for almost any community of organisms surveyed in the literature reveals a distinct tendency for the community-as-sampled to have more species at lower abundances than at higher ones. In fact the number of species per abundance tends to be highest at the lowest abundance and thereafter to taper somewhat in the manner of the empirical distribution shown in Figure 1. In biological folklore (if not in the literature), this curve is known as the "J-curve," owing to its resemblance to a backwards letter J.

To speak of "*the* J-curve," however, begs a very large question. Is there a single theoretical distribution that underlies virtually all natural communities? Although it seems almost too much to ask, this may well be the case.

Prior distributions

In spite of the fact that the J-curve is a commonplace observation (Williams, 1964), one of the most popular theoretical distributions, namely the lognormal distribution (Preston, 1948), shows little resemblance to it. As shown in Figure 2 (upper), the lognormal distribution is essentially a normal distribution that has been compressed at the low end and drawn out at the high end, both operations effected by a single logarithmic transformation.

Conspicuously absent from the lognormal distribution is the sharp peak at the low abundance end. To save it from such a discrepancy, its proposer has postulated a "veil line" (See Fig. 2), a vertical line of truncation that has the desired effect, more or less. Preston argued that samples of a natural community do not follow the same distribution as the community itself: all the species below a certain abundance (the veil line) simply fail to show up in samples.

This claim is fundamentally wrong (Dewdney, 1998). Indeed, species that fail to show up in a sample are veiled by a very different line, as shown in Figure 2 (lower). In this figure we use an unrealistic species/abundance distribution to illustrate the difference between the "veil line" and the "veil curve." Far from being a vertical, straight line, the true veil curve is a sloping, sigmoidal one. The species above or to the left of the veil curve will tend to be absent from the sample. As proved in the recently developed general mathematical theory of sampling (Dewdney, 1998), the removal

Received 30 December 1997; accepted 10 November 1999.
E-mail: akd@csd.uwo.ca

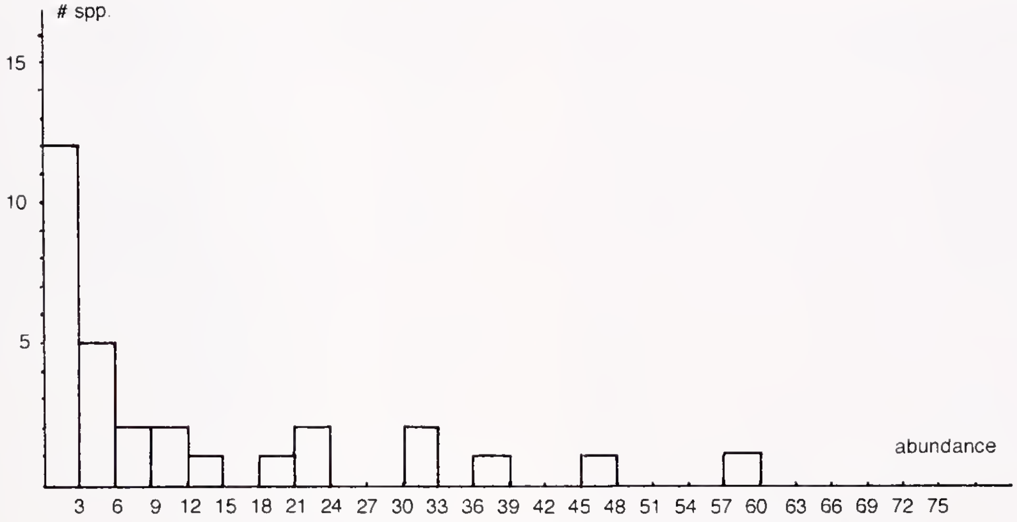

Figure 1. A typical species-abundance distribution (McCabe and Weber, 1994).

of these species cannot change the shape or formula of the distribution, only its parameter values. It follows that when we apply the veil curve to the lognormal distribution, we must get a new, complete lognormal distribution, not a truncated one.

The metastudy reported in this paper compares two theoretical proposals for the distribution of species abundance in natural settings. But it does not even consider the lognormal distribution: if the lognormal were present in nature, the first abundance categories would have to be smaller than succeeding ones. Not one case of this has turned up in the 50 randomly selected biosurveys used in the metastudy. This observation, coupled with the new sampling theory, means that the lognormal distribution, as a descriptor of abundances in natural settings, is effectively dead.

A closely related distribution, the negative binomial (Pielou, 1975), also uses the veil line concept and suffers from the same unrealistic shape when unveiled, so to speak. This distribution is therefore also not considered in the metastudy and for the same reasons. It is no longer usable as

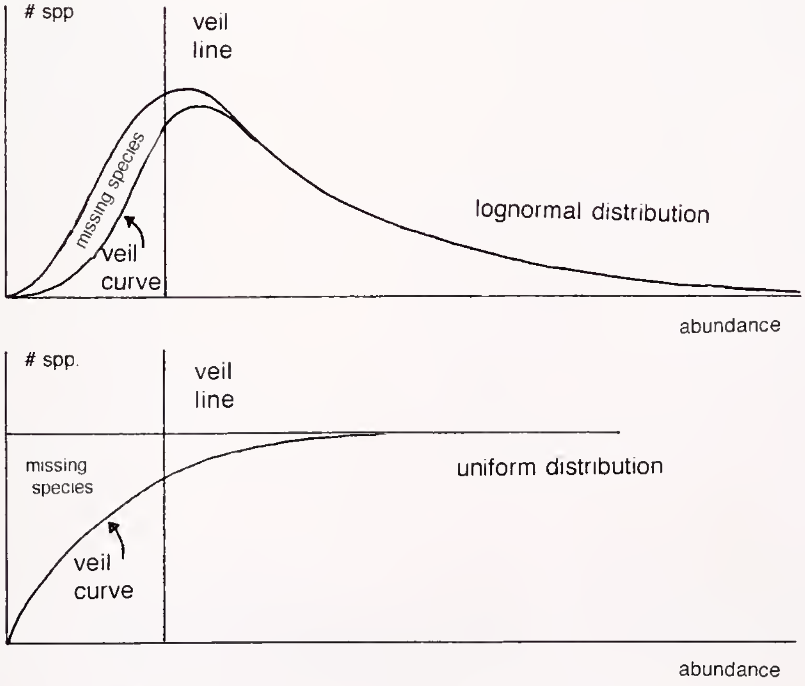
# spp
veil line
missing species
veil curve
lognormal distribution
abundance
# spp.
veil line
missing species
veil curve
uniform distribution
abundance

Figure 2. Veil line and veil curve for the lognormal distribution.

a descriptor of natural abundances. One may suspect that a general theory of sampling was not developed until now because of the confusion created by the mistaken concept of the veil line.

The other leading contender for species/abundance distribution of choice has been the log-series distribution developed by C. B. Williams and R. A. Fisher (Fisher *et al.*, 1943). As shown in Figure 3 below, it has the right general shape, being most sharply peaked at the low abundance end and tapering in concave fashion to zero.

Williams originally believed that the curve ought to be hyperbolic (Williams, 1964). Such a curve has the general form of $1/k$, where k represents abundance. But Fisher pointed out that the area under the hyperbolic function was infinite, hardly desirable in a statistical distribution! He suggested altering the hyperbolic function by inserting a convergent series that forced the area under the curve to converge to a finite value. (There is no biological reason for this alteration.) The probability density function (pdf) is therefore

$$x^k/k,$$

where k is an abundance and x^k is the convergent series, x being a parameter that is strictly less than 1 (but usually close to it). When used in the field, the distribution contains an additional factor α that reflects the number of individual organisms in the sample. But α is not a parameter, and the log-series is known as a one-parameter distribution. It has been noted (May, 1975) that the log-series distribution has points of superiority over the lognormal.

Theory: a new individual-based dynamical model

Independently of concerns about the state of theoretical abundance distributions, the author had constructed an individual-based (Judson, 1994) dynamical system (Dewdney, 1997) that was originally intended as an exploratory tool for probing the abundance distributions of heavily predaceous communities such as stream benthic protists (Dewdney, 1996). In this model, an arbitrary number of species, each with an arbitrary population size, preyed on one another in the following manner: Within each iteration, two individuals (not species) are chosen at random. One individual ingests the other, reproducing in consequence. It is called the multispecies logistic system, or MSL system, for short. The adjective "logistic" was chosen because the total biomass (number of individuals) remained fixed as a simple consequence of the basic trophic act. Thus very abundant species were less likely to ingest other species as they approached the logistic limit.

The MSL system was embedded in a computer program, written in Turbo Pascal and running on a 486 computer. One hundred iterated pair selections (births and deaths) make up one "cycle" (a programming convenience). After each cycle, the program displays a histogram of species *versus* abundances. It permits the user to select any number of

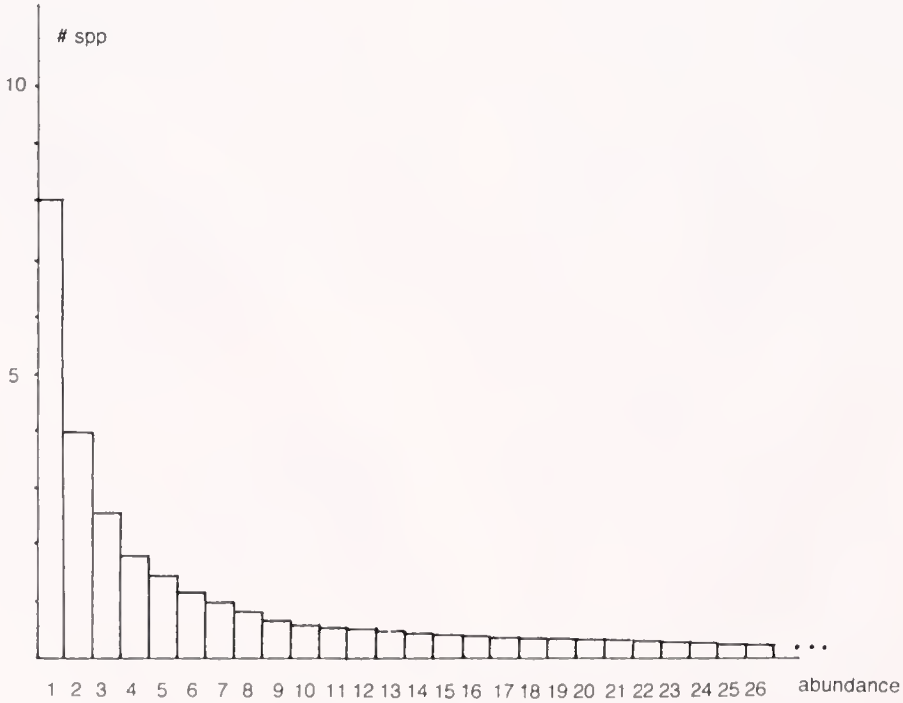

Figure 3. The log-series distribution.

species, as well as initial abundances for each. The program comes equipped with an "extinction switch," essential to the program's usefulness. With the extinction switch "on," any species having abundance 1 will, when eaten, disappear from the simulation. With the extinction switch "off," species with abundance 1 will not be eaten, although they can (and do) end up preying on other species, with a possibility of subsequent further increase.

With 200 species, each with initial abundance of 20, a 486 computer takes about 10 minutes to drive the MSL system to equilibrium (extinction switch off). Initially, the species appear as a sharp spike at 20, then spread out into a binomial distribution with 20 as mean. However, the species continue to drift in abundance until the shape of the distribution changes radically. A peak forms at the low end, and a long tail appears on the right.

Surprisingly, the process stops when the distribution curve reaches what can only be described as a "J-shape," retaining roughly that shape for as long as the computer is run. The higher the initial average abundance, the shorter the initial spike. At very high abundances, there are only occasional, small spikes at the lowest abundance.

The appearance of a J-curve invariably surprises those who would predict that a binomial (or normal) distribution must result or that, contrariwise, all but a few of the species will migrate to the low end. In the next section we show how a large metastudy of extant biosurveys has already begun to indicate that distributions produced by the MSL system cannot be distinguished statistically from typical biosurvey species abundance distributions.

The MSL program is capable of calculating the average of the distributions it produces at each cycle. Figure 4 shows such an averaged distribution. The height of each bar in the histogram represents the average number of species that occupied the corresponding abundance category from the onset of equilibrium. Because the behavior of the MSL at the high abundance end has special interest, the frequencies have been inverted in Figure 4, appearing above the bars as a separate plot of isolated points. These will be examined presently.

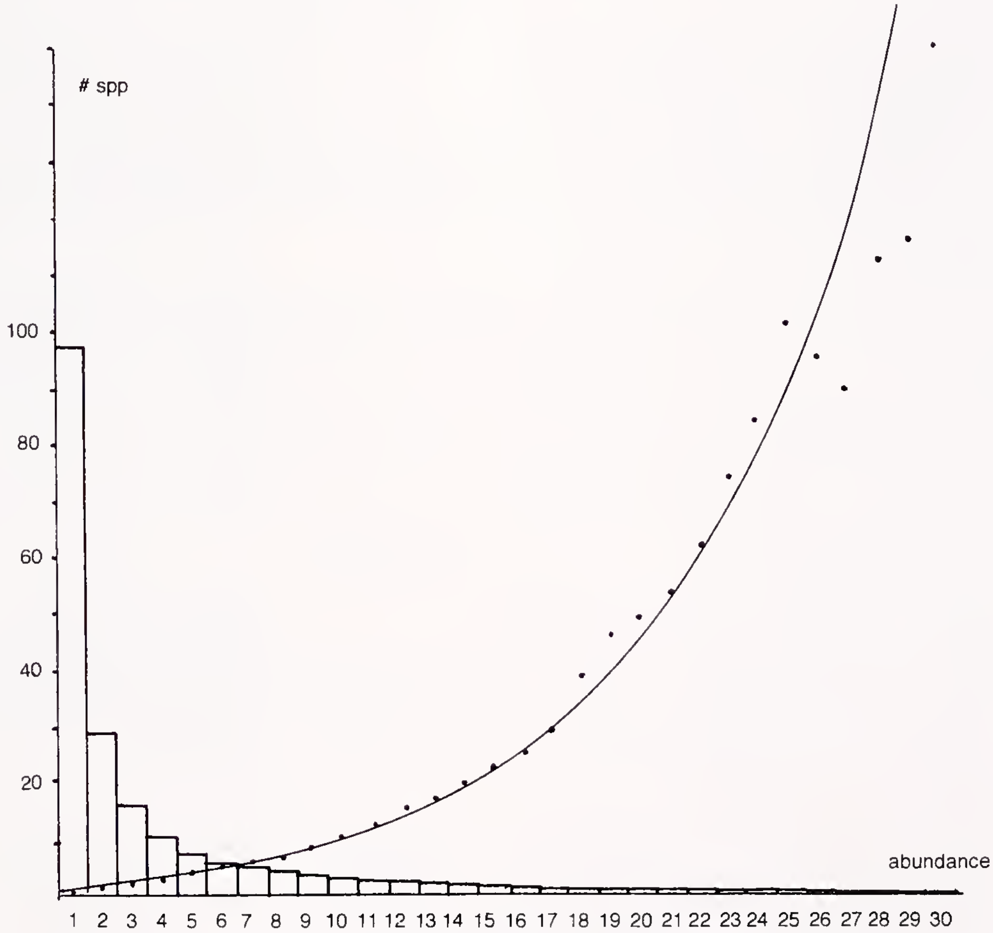

Figure 4. An average distribution produced by the multispecies logistic system, and a plot of inverted average frequencies.

Most natural communities of interest do not have the low average abundance used in the computer run for Figure 4. Instead of in the tens, average abundances may easily run into the thousands or even millions. In other words, the overall shape of the distribution shown in Figure 4 would be more typical of a sample than of a community. As mentioned earlier, when the MSL system is run with such high abundances, there is little or no peak at the low abundance end. The distribution resembles instead the idealized pattern shown in Figure 6, as explained later. Nevertheless, when the extinction switch is turned on during such an equilibrium state, species occasionally visit the low end, either to escape again or to become extinct. The time between successive extinctions grows at a modestly exponential rate.

Far from being unrealistic, this is precisely what we expect in natural communities. For example, the island biogeography theory of R. H. MacArthur and E. O. Wilson (1967) recognizes that isolated communities naturally lose a certain percentage of species every year. They estimate that when the island of Krakatoa achieved equilibrium between immigrants and extinction losses in its bird community at roughly 27 species, the turnover rate was about 1.13% of species annually.

Anticipating the discussion at the end of this article, we may imagine for the moment that the MSL describes birds as well as microorganisms. A community of 27 species of "birds" with an average of 200 individuals per species typically loses about 9 species during 1000 cycles of operation. Each cycle involves 100 reproductive events. If half the total bird population (*i.e.*, females), namely 2700 individuals, reproduce in one year, then 27 cycles corresponds to the passage of one year. Thus 1000 cycles corresponds to 37 years and a loss of 33.3% of its species over the period. This corresponds to a rate of at least 0.9% of the species every year. This figure is certainly close enough to the MacArthur and Wilson (1967) figure to make the only claim that is necessary in this context: the rate of species loss in the MSL system appears to be of the right order of magnitude. To explore equilibrium conditions, the MSL system can be run with the extinction switch "off."

Variations of the underlying MSL dynamical system make little difference to the outcome. These have included (1) changing the food web so that predation follows a cyclic order, (2) redefining the food web to include four compartments: plants, herbivores, carnivores, and saprobes, (3) running separate communities in which randomly selected individuals may migrate from one "patch" to another. In all cases the same J-curve apparently re-emerges. This robust character of the J-curve seems to indicate a phenomenon more fundamental than predation or other trophic behavior at work. In fact, the essential feature of the MSL is that each species vibrates stochastically, in effect. In other words, each species in the system performs a constrained random walk in the sense that (a) at each abundance each species has an equal probability of decrease as increase, and (b) the total abundance of all species remains constant. Typically, species may be said to be in a *stochastic orbit* about the mean abundance, with a majority having less than the mean abundance at any time.

Assuming only this fundamental property and assuming for the moment an infinite number of species, it is easy to prove that, at equilibrium,

$$k \cdot f(k) = (k + 1) \cdot f(k + 1).$$

In other words, at equilibrium the probability of a species of abundance k increasing equals the probability of a species of abundance $k + 1$ decreasing. This equation has essentially only one solution, namely $f(k) = 1/k$.

The foregoing analysis paves the way for the finite case. Since the number N of individuals in the MSL system remains constant during a run, no species can ever have abundance greater than $N - R + 1$. At equilibrium, in the ideal sense of this analysis, there must be a number Δ at (and beyond) which $f(k) = 0$. The number Δ may well be less than the absolute limit just cited. We assume (but cannot prove directly) that the function f is driven to zero in the following manner,

$$p(k) \cdot k \cdot f(k) = p(k + 1) \cdot (k + 1) \cdot f(k + 1)$$

Here we have postulated what dynamicists call a "forcing function," which acts to drive the values of f to zero at the limiting k-value of Δ. This equation can also be solved readily.

$$f(k) = 1/(k \cdot p(k))$$

If $f(\Delta) = 0$ then there is an obvious singularity at $k = \Delta$. The simplest function capable of such behavior is

$$p(k) = (\Delta - k)^{-1}$$

and the function f can therefore be rewritten,

$$f(k) = (\Delta - k)/k$$

or, equivalently,

$$f(k) = (1 - \delta k)/k,$$

where $\delta = 1/\Delta$. Anticipating the addition of a normalizing constant presently, we can multiply f by any constant we like in the process of developing a convenient mathematical expression for the density function.

The logistic-J distribution

The *logistic-J distribution* (discrete version) has the following pdf:

$$f(k) = c(1/k - \delta); \quad k = 1 \ to \ \Delta,$$

where the abundance k runs from 1 to a maximum Δ called the *outer limit* and δ is the inverse of Δ. The latter parameter is not a hard limit, but an average maximum, as will be made clear later. This particular pdf has one parameter, Δ, the constant c being simply a function of Δ. When the MSL system reaches equilibrium, one finds a species with abundance greater than Δ about half the time.

In a more general setting, where the distribution is to apply equally to real communities and samples of them, it is useful to have the logistic-J distribution in continuous form:

$$f(x) = c(1/x - \delta),\ \varepsilon \leq x \leq \Delta,$$

$$= o,\ \text{elsewhere}$$

In this form an additional parameter, ε, appears. Called the *inner limit*, it represents the average lower limit of abundances in a community or as reflected in a sample of that community. For example, abundances in a sample may be given as density data wherein the lowest abundance might be 0.25. Or sample abundances may start at 5, say. Superficially, the use of epsilon resembles a veil line, but it has nothing to do with sampling. Instead, it represents the average minimum abundance in the community of organisms *per se*.

The constant c is simply shorthand for the standard normalizing constant for pdfs. In this case,

$$c = (\ln(\Delta/\varepsilon) - 1)^{-1}$$

The pdf f is defined to be zero outside of the interval (ε, Δ). As a mathematical convenience, we adopt the notation $L(\varepsilon, \delta)$ for the logistic-J distribution with parameters ε and δ.

In the case of the frequencies generated by the MSL system, as shown in Figure 3, the appropriate logistic-J distribution f has been calculated. To demonstrate that the distribution of frequencies produced by the MSL system does indeed appear to follow the logistic-J distribution, we have inverted the theoretical values, plotting them as a smooth curve, for comparison with the (inverted) model-generated values. It will be seen that the agreement is as close as can be expected, bearing in mind that the smallest statistical fluctuations at the high abundance end will, when inverted, produce relatively large fluctuations in the (point) plot shown in the figure. The overall trend is clear. The inverted theoretical curve approximates the inverted MSL points about as well as can be expected. The distribution produced by the MSL appears to be logistic-J.

The parameters ε and δ define a logistic-J distribution completely. A useful visualization of the significance of these parameters is presented in Figure 5, which shows a standard hyperbola ($f(x) = 1/x$) in relation to axes rendered in thick lines. Two other axis systems, rendered in lighter lines, are superimposed on the figure. In the first axis system the hyperbola has the formula $1/x$, and in the other axis systems it has logistic-J formulas, to be explained presently. The logistic-J distribution corresponds to a section of the standard hyperbola, the origin of the section being determined by the parameters ε and δ.

According to the sampling theory derived by the author

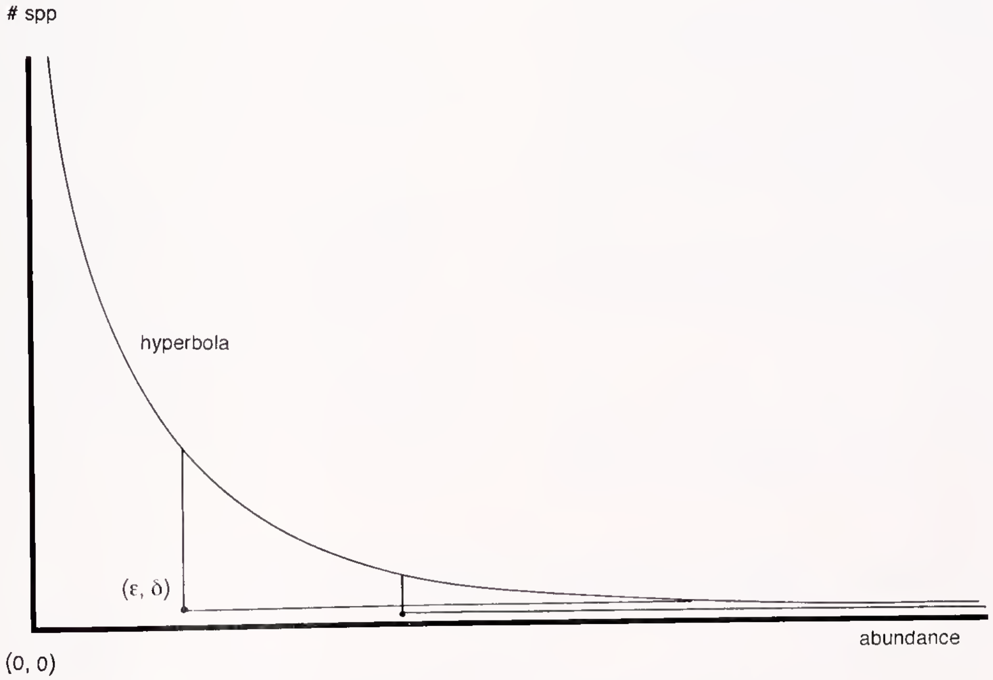

Figure 5. Logistic-J probability density functions based on the standard hyperbola.

(Dewdney, 1998), it is possible to draw a direct relationship between a sample distribution and the distribution prevailing in the community from which the sample was drawn. The theory applies to all candidate distributions, including the logistic-J, where it has a particularly simple form. Suppose a field biologist samples a community of organisms with intensity r, that is, observes/collects $100r\%$ of the individuals in each species (to within the usual statistical fluctuations). If the distributions are logistic-J and the biologist finds the sample abundances following $L(\varepsilon, \delta)$, then the community abundances follow the distribution $L(\varepsilon/r, r\delta)$. Thus if $r = 0.05$ and the biologist finds $L(0.3, 0.004)$, then he or she may reasonably estimate the community sample as following the distribution $L(6.0, 0.0002)$ (in which the outer limit is therefore 5000).

The sample distribution may be thought of as the left-hand hyperbolic section in Figure 5, while the community distribution may be thought of as the one on the right. In this context, however, continuous figures are a little misleading. Since the community distribution is actually discrete and the abundances are normally much larger than those in a corresponding sample, we may represent the distribution of abundances in a community somewhat in the manner of the idealized diagram in Figure 6, in which individual species appear as small squares separated by spaces that increase in a modestly exponential manner from left to right. The very modest peak in the right-hand logistic-J distribution of Figure 5 would correspond to the relatively small space between the first two species in Figure 6.

The actual spacings shown above derive from the logistic-J distribution and are based on the hypothesis that communities actually follow the logistic-J distribution. As such, the actual distribution would hardly appear so nicely arranged. Clumps and gaps would abound, just as they do in the MSL system when it is operated with parameters that correspond to communities rather than samples of communities. However, even if they follow some other kind of distribution, it must be a J-curve (according to Dewdney, 1998) and the actual distribution would not be noticeably different from a perturbed version of the one shown in Figure 6.

The biosurvey metastudy

For the past few years the author has been gathering abundance surveys from the literature. Called "biosurveys" here, they cover four kingdoms of life (there being apparently few biosurveys of Bacteria or Archaea, if any). They were taken in polar, boreal, temperate, and tropical biomes of every type: terrestrial, freshwater, and marine. The intention is to include, ultimately, 100 "randomly selected" biosurveys in the study. Biosurveys selected for the study have three criteria to fulfill: They must (a) include at least 30 species, (b) not exclude uncommon or low abundance species, (c) not use numbers that are anecdotal or order-of-magnitude figures. So far, out of about 70 biosurveys selected at random, 50 have passed these criteria (and these criteria alone), to be included in the study.

Ideally, a "random selection" of biosurveys would require (a) a list of all the biosurveys ever taken and (b) a random number generator to select items from the list. Unfortunately, no such grand list exists. However, in the context of the metastudy reported here, "random" only needs to mean "not prejudicing the outcome." In other words, it makes no difference how biosurveys are selected from the literature, provided that nothing in the selection process tends to turn up surveys that favor the logistic-J distribution in some way. It is impossible, in any case, even by visual examination of abundance data in a typical biosurvey, to decide whether it would fit one distribution better than another. Even so, the research assistants who did most of the selecting were instructed to scan through *Biological Abstracts* and other databases and to note every biosurvey encountered. If the journal happened to be in our library, the assistant then went to the article in question and, if the total number of species was 30 or more, made a copy of the paper. The author then applied the remaining criteria, rejecting papers that failed to meet conditions (b) or (c), as stated in the previous paragraph, but *accepting all others without prejudice.*

Occasionally, in this process, the author would note that one kingdom of life or another was under-represented. The assistants were occasionally instructed to find more biosurveys on fungi, protists, plants, or what have you. Besides the papers selected by assistants, the metastudy includes a biosurvey by the author (#1) and two papers by biological colleagues (#19, 20) who had heard of the study and volunteered their findings without knowing exactly what I expected to find.

At the present point, halfway through the study, the emphasis has been very much on the animal kingdom:

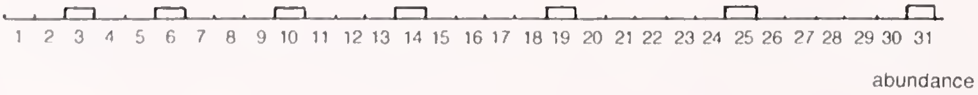

Figure 6. Idealized distribution of species in a large community.

Fungi/Lichens	6
Protista	3
Plantae	5
Animalia	36

The Animalia set includes 10 fish surveys, 7 of birds, 1 of herptiles, 10 of insects, 2 of crustaceans, 1 of molluscs, 4 of "invertebrates," and 1 of "macrofauna." The Plantae set has 3 herbaceous plant surveys, 1 of trees and 1 of mosses. In various combinations, the surveys were conducted in 27 temperate, 16 tropical/subtropical, and 7 boreal/polar locations. General habitat types included 27 terrestrial, 11 freshwater, and 12 marine.

For each biosurvey selected for the study, a species-abundance histogram was created, as outlined in the foregoing section. Some biosurveys gave raw counts for a specific community of organisms, others gave density data. In all cases, the continuous version of the logistic distribution was used, illustrating its great flexibility. The log-series was also applied to both kinds of survey data, according to the method outlined in Magurran (1988). Its normal range had to be extended (in a mathematically defensible way) to handle density and percentage data, however. This extension did not detract from its ability to fit natural communities.

The chi-square test (Hays and Winkler, 1971) is normally used in goodness-of-fit applications to produce a statistic that describes how closely the theoretical distribution fits empirical data. In this study, however, the test was used in comparative mode, a legitimate practice that involved a direct comparison of chi-square scores to determine which theoretical distribution best fit the 50 biosurveys overall.

Figure 7 shows a portion of two consecutive lines from a chi-square table. When the statistic has been computed for both the logistic-J and the log-series distributions in relation to a specific biosurvey, it might well be that one statistic had 5 degrees of freedom and the other had 6.

In the present context, the degrees of freedom to apply in a given instance of the chi-square test is determined by the number of abundance categories into which the data has been divided minus the number of independent parameters in the distribution. Since the log-series distribution has just one parameter, whereas the logistic-J has two, the log-series distribution was typically tested at one higher degree of freedom, an advantage that exactly compensates for the reduced descriptive power that accompanies fewer parameters.

Suppose for example, that a particular biosurvey matches the logistic-J and the log-series with exactly the same chi-square value, say 5.321. The *P* value along the top of the table is simply the cutoff probability beyond which the fit would be rejected in normal applications. For example, a chi-square value of 5.321 at 5 degrees of freedom is less than 6.62568, and this means that the fit must be "accepted" at the 0.75 level.

In fact, as normally used, the chi-square test, like all goodness of fit tests, works best as a rejector of fits. If the chi-square statistic were greater than 6.62568, then it could be rejected at the 0.75 level, meaning that one could reject the fit and be 75% positive that no mistake was made in the rejection. However, the test is not symmetrical in relation to "acceptance" and rejection. If accepted, we can say only that the fit was not rejected. Acceptance amounts to nothing like a proof that the accepted theoretical distribution is the actual underlying source of variation. Nor could it. There is an infinity of distribution functions that could be cooked up, all of them quite different from each other, all of them fitting the empirical data equally well.

Although we will not be using the chi-square test in rejection/acceptance mode, the foregoing introduction serves to introduce the *P* values that are crucial to the metastudy reported here.

Returning to the example where both the logistic-J and log-series happen, by coincidence, to have exactly the same chi-square score of 5.321, we can work out the corresponding *P* values by a simple process called linear interpolation. The *P* value gives us a direct comparison between the two scores. Thus at 5 degrees of freedom the chi-square value of 5.321 corresponds to a *P* value of 0.607, while at 6 degrees of freedom, the chi-square value of 5.321 corresponds to a *P* value of 0.497. In this case then, the log-series chi-square score (0.497) would be superior to the logistic-J score (0.607).

This example not only illustrates how more degrees of freedom translates, other things being equal, into a lower *P* value, but how the *P* values themselves make it possible to translate between chi-square scores at different degrees of freedom. Since the mapping between chi-square scores and their corresponding *P* values is 1-1, it is reversible. In other

p value: **df**	0.50	0.75	0.90	0.95
⋮				
5	4.35146	6.62568	9.23635	11.0705 . . .
6	5.34812	7.84080	10.6446	12.5916 . . .
⋮				

Figure 7. Two lines from a chi-square table.

words, we can start with a chi-square score at one degree of freedom, map that score into a corresponding P value, then turn around and map the P value into a chi-square score at some other degree of freedom, it being guaranteed (by the definition of the P value) that the scores will be comparable. The chi-square distribution with 10 degrees of freedom was selected as the "currency" of choice, 10 being an intermediate value over all the degrees of freedom that actually occurred in the metastudy. Each chi-square score, whether for the log-series or for the logistic-J distribution, was normalized in this fashion into the corresponding chi-square score at 10 degrees of freedom.

Appendix Table 1 displays the raw chi-square score and the corresponding normalized scores (at 10 degrees of freedom) for both the logistic-J and the log-series distributions, as applied to each biosurvey used so far in the metastudy. All chi-square scores were calculated by a program written in Turbo Pascal by the author and run for both sets of data. The right-hand column of the table displays the difference between the normalized scores.

The average normalized score for the logistic-J distribution over all 50 biosurveys was 10.653, while the average score for the log-series distribution was 12.949. The latter score is significantly higher, as revealed by a paired sample interval estimate (Wonnacott and Wonnacott, 1982). In this technique the paired differences are subjected to a means test specialized for paired data such as we treat in Figure 8. A confidence interval based on these data yields an average difference in normalized scores of 2.296 ± 1.547, which may be interpreted as follows: the probability that the two means differ by less than $2.296 - 1.547 = 0.749$ is 5%. Indeed, a better interval at 99% confidence of 2.296 ± 2.063 can also be constructed. Here, with probability of only 1%, the two means differ by no less than $2.296 - 2.063 = 0.233$. The difference, though small, is apparently real: With 99% probability, the mean chi-square score for the logistic-J distribution is definitely lower than the mean chi-square score for the log-series distribution on the same data. The logistic-J distribution outperforms the log-series distribution in this sense.

Not only are the test score means apparently different, but the average score of the logistic-J distribution also appears to be optimal or near-optimal, and in two ways.

The mean of the chi-square distribution with n degrees of freedom is exactly n, and the variance is $2n$ (Hays and Winkler, 1971). Thus the chi-square distribution at 10 degrees of freedom has a mean of 10.0. The average normalized chi-square score for the logistic-J distribution, 10.653, is obviously not far from optimal, whereas the average normalized chi-square score for the log-series distribution, 12.949, is further away.

Under the null hypothesis, a distribution that was the actual source of variation in the biosurvey data would tend to have a score of around 10. On the other hand, the rather high variance, 20.0 in this case, serves as a warning not to take the closeness too seriously. Even if the logistic-J had achieved an average normalized score of 10.0, it could easily have been as much as one standard deviation (4.47) away from the optimal score, and in either direction.

The median of the chi-square distribution for a given number of degrees of freedom is the score that corresponds to a P value of 0.500. Under the null hypothesis for the chi-square distribution with 10 degrees of freedom, we would expect half the scores to be less than 9.342. As it happens, some 23 of the normalized logistic-J scores have this property, whereas only 17 of the normalized log-series scores are less than 9.342.

Taken together with the near-certain superiority of the logistic-J distribution over the log-series, this evidence may be interpreted as reasonably strong support for the hypothesis that abundances in natural communities follow the logistic-J distribution.

A final result is worth reporting. The version of the logistic-J distribution that appears in this study used an estimate for the parameter Δ based on the mean and lowest category frequency of the empirical distribution. The resulting value of Δ may therefore be interpreted as a prediction of the maximum abundance for every biosurvey in the study. Since the predicted maximum abundance is only an average value, we would expect that if the predictions were accurate in this sense, the average value of the maximum abundances in the biosurveys would be fairly close to the average predicted values.

To test this hypothesis, the ratio (percentage) of actual maximum abundance to that predicted by the logistic-J distribution was calculated for each biosurvey and the results plotted as percentages, as in Figure 8.

As it turns out, the average percentage ratio of maximum abundances is 99.1%. This means that the 50 predicted (average) maximum abundances behaved as would be expected if the communities in question followed the logistic-J distribution. Although highly accurate, this result must

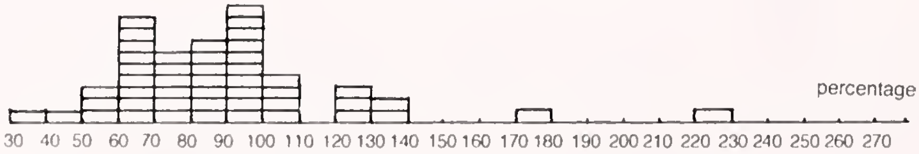

Figure 8. The distribution of maximum abundances *vs.* outer limits.

again be interpreted with some caution, as the statistic is apt to suffer from a high variance. Nevertheless, this result also supports the hypothesis, and from a quite different direction.

Summary

There are two hypotheses implicit in the foregoing. The first hypothesis is that all natural communities follow the logistic-J distribution. The second hypothesis hinges on what level of interpretation is applied to the MSL system itself.

The first hypothesis has little meaning until the word "community" is defined. We define a *place* as any connected volume within the biosphere, a *time* as the period between two clock/calendar readings, and the *supercommunity* connected with this place and time as the set of all living organisms within the space over the time in question. A "community," as we shall use the word, will be a subset of the supercommunity. Although somewhat too abstract to be very useful, we may restrict the meaning somewhat by allowing as "subsets" only taxonomically related organisms or those related by similar size or by being found in the same habitat type or, in general, any sense of the word habitually used in the field. Although the MSL system models only supercommunities, a compartmentalized version of the model reveals the same distribution obtaining within compartments (*e.g.*, herbivores).

The first hypothesis, that all natural communities follow the logistic-J distribution, has been supported by three separate outcomes of the metastudy:

First, the logistic-J distribution significantly outperforms the log-series distribution as a descriptor of abundances in communities. As already seen, the lognormal distribution, when truncated properly, has no resemblance at all to empirical data. With the two most commonly used distributions thus eliminated, there remains no serious alternative to the logistic-J distribution;

Second, the logistic-J has a normalized chi-square score that exceeds the median about half the time. Not only does it outperform the log-series distribution in this respect, but its closeness to the expected number of such scores, namely 25, might be interpreted as another hint of optimality.

Third, the scores of the logistic-J distribution on the biosurveys considered as a whole reproduce the chi-square distribution itself. This can happen only if the null hypothesis is always (or almost always) true of the biosurveys in the study. The possibility remains that another theoretical distribution is the proper one, but it will so closely resemble the logistic-J as to be perpetually indistinguishable from it, given the results of the metastudy so far.

Fourth, the average outer limit predicted by the logistic-J distribution matches the average maximum abundance of the biosurveys themselves. This would also be true if all the biosurveys had the logistic-J as their underlying distribution.

The second hypothesis, concerning the mechanism underlying the logistic-J distribution, necessarily involves reflection on the MSL system itself. But the MSL model has three levels of interpretation that are mutually compatible, but successively more general. As originally intended, it was to reflect the high levels of predation to be found in stream benthic micro-environments (Dewdney, 1997).

At the next level of interpretation, individuals are not ingesting each other, but merely trading biomass for reproductive enabling. This view covers not only predation, but competition for sunlight (as when one plant shades out another, taking biomass that would, in effect, have been accumulated by the shaded plant), and saprobic activity of fungi and bacteria. Obviously, this view stretches the MSL system considerably but, as we have already seen, the basic model system is "detail hungry." When altered to employ fractional trophism or when modified to operate on the basis of definite food webs, it still produces J-curves.

At the third level of interpretation, even the trophic activity is irrelevant. All that matters is that a given organism is as likely to reproduce as it is to die before reproducing. Although this may not be true over short periods of time for actual species, a certain long-term birth/death equiprobability surely prevails for every species that has survived to the present day. In other words, regardless of the individuals involved, a species has been as likely to increase, in the long run, as it was to decrease. The ratio, after all, is the number of successful reproductions divided by the number of deaths.

The notions of *a priori* probabilities of death or reproduction are not very useful, unfortunately. There is no way to measure them and no way to predict the outcome even if they turned out to be equal. In direct contradiction to what any theorist (including the author) might have guessed, the seeming stability implied by equal probabilities of decline or abundance is an illusion. Instead of a normal (or even a lognormal) distribution, a J-curve invariably results. This would be just as true of any natural system obeying such an hypothesis as it is of the MSL system. Taken literally, the behavior of the MSL system would predict that most populations will appear to be regulated (Turchin, 1995), at least somewhat, by density over the short run, while appearing increasingly stochastic in the long run.

We shall adopt a hypothesis that is nearly equivalent to this. At any time (seasonal and cyclic effects aside) and in any community, it is unpredictable whether the next change in the population of a given species will be an increase or a decrease. Indeed, we hypothesize that all species in all communities are continually undergoing what may be called "stochastic vibration." In the MSL system, species continually orbit the mean population size. At any time, most have smaller populations, some have larger populations, and a few have much larger ones. In a purely random manner, some very abundant species decline, ultimately to very small numbers, while others increase dramatically and for no apparent reason. Such an increase in a real community (that followed such a regimen) would usually have many causes that chanced to work together, or sometimes a single cause that happened to dominate all other factors.

Such unpredictability does not amount to a claim of nondeterminism. Perhaps a reasonable analogy will be found in the stock market. Although thousands of investment decisions, each of them deterministic for the individuals concerned, will play a role in the price of a stock over the period of a week, no one can predict the eventual effect of those decisions on the price. No one, after all, knows all the investors and their buying patterns. It is reasonably well understood that stock prices are "random" in this sense (Malkiel, 1985).

Although it would be very difficult to test, the stochastic vibration hypothesis has one important philosophical implication. It amounts to a confession of ignorance about the normal causes of change in abundance of populations, the contributing factors being in most cases beyond observation or calculation. It does not, however, signal a state of despair. It merely injects a note of realism into any project that would ascribe changes in abundance to single factors.

Consider an individual plant, for example. Upon germination and up to reproductive maturity, it may be killed by too much sun or too little, by excess cold or heat, by foraging animals, by fungal or other pathogenic attack, by parasites, by trampling, by overshadowing, by root competition, by excess dryness or humidity, by flooding, by environmental toxins, and so on. Most of these events are completely unpredictable, especially those driven by the weather—which, being chaotic, cannot be predicted with any certainty beyond a day or two. Over a season, some of the plants in a local community will succumb to one of these factors and die.

To reproduce, a plant must first produce seeds. But the flower may not develop properly, the pollinating insect may not visit the plant, the pollinator may not be carrying the right pollen (in the case of cross-pollinating plants), and so on. When ovaries are fertilized, the game gets even rougher. That most plants produce rather large numbers of seed testifies to the fact that most seeds either do not germinate or die after germination. They may land on bad soil, be eaten by animal scavengers, be attacked by fungus, become desicated, and so on.

The logistic-J distribution, including its underlying dynamical system and the stochastic behavior of its species, is here proposed as the major organizing factor present in all natural communities of living things. As such, it would have rather important implications in a number of fields, not least biodiversity assessment and the theory of evolution. Two brief remarks may serve for the time being.

There are many different definitions of biodiversity, no two alike (Magurran, 1988). If it is ultimately concluded that most communities of living organisms follow the logistic-J distribution, then a new and uniform approach to the problem of biodiversity assessment can be developed. One may calculate the "biodiversity" of a community of organisms, not as a single number (a hopeless project [Gaston, 1995]) but as a triplet, (R, ε, Δ). These numbers would be estimates of those parameters for the community as a whole, derived *via* samples that are subjected to the transformations outlined in Dewdney (1998). And the abundances in such communities can be largely reconstructed from these numbers, although our theory says nothing about which species would have which abundances.

In the theory of evolution, it might be asked whether the stochastic vibrations hypothesized here for species might also prevail at the generic and higher taxonomic levels. Williams (1964) observed that the J-curve also emerges if one plots genera against species, not in a community this time, but in standard taxonomic lists. For example, if one counts the number of bird genera that have 1 species, 2 species, and so on, a J-curve emerges. This can be done within families or orders. It may be that genera "vibrate" in the sense that, through evolutionary time, they lose and gain species more or less at random (*i.e.*, unpredictably and with no overall discernible pattern).

Finally, the J-curve, whether one regards it as being logistic-J or not, tells us that within any community of organisms, especially somewhat isolated or patchy ones, there will be many species with relatively small populations—far more than is commonly realized, even by many field biologists. Such populations will be more readily subject to mutational change, since new genes have a much better chance of spreading through them. From this viewpoint, the low abundance end of the J-curve may be identified not only as the grave of evolution, but its cradle, as well.

Acknowledgments

The author thanks the following colleagues for valuable discussions and encouragement: Laszlo Orloci and Dianne Fahselt of the UWO Plant Sciences Dept., Gary Umphrey of the UWO Zoology Dept., Bert Finnamore of the Alberta Museum, and David Shorthouse of Laurentian University. The author thanks research assistants Dianne Bowman, Monika Havelka, Kellie White, and Dave Muzia for their help, as well as the referees who, one hopes, will feel their work worthwhile. Finally, who can properly thank the thousands of field biologists who annually census the Earth's biota, providing the only secure foundation for meaningful theories of abundance?

The research reported in this paper is described in a monograph, draft copies of which can be obtained by contacting the

author. The monograph contains a field manual for the logistic-J distribution which may be requested separately.

Literature Cited

Dewdney, A. K. 1996. *Micro-ecology in a Small Stream.* Monograph, Environmental Science Program, The University of Western Ontario, London, Canada.

Dewdney, A. K. 1997. A dynamical model of abundances in natural communities. *COENOSES* **12(2–3):** 67–76.

Dewdney, A. K. 1998. A general theory of the sampling process with applications to the "veil line." *Theor. Popul. Biol.* **54:** 294–302.

Fisher, R. A., S. A. Corbet, and C. B. Williams. 1943. The relation between the number of species and the number of individuals in a random sample of an animal population. *J. Anim. Ecol.* **12:** 42–58.

Gaston, K. J. 1995. Pp. 1–18 in *Population Dynamics: New Approaches and Synthesis.* N. Cappuccino and P. W. Price, eds. Academic Press, San Diego.

Hays, W. L., and R. L. Winkler. 1971. *Statistics: Probability, Inference, and Decision.* Holt, Rinehart and Winston, New York.

Judson, O. P. 1994. The rise of the individual-based model in ecology. *Trends Ecol. Evol.* **9(1):** 9–14.

MacArthur, R. H., and E. O. Wilson. 1967. *The Theory of Island Biogeography.* Princeton University Press, Princeton, NJ.

Magurran, A. E. 1988. *Ecological Diversity and Its Measurement.* Princeton University Press, Princeton, NJ.

Malkiel, B. G. 1985. *A Random Walk Down Wall Street.* W. W. Norton, New York.

May, R. M. 1975. Patterns of species abundance and diversity. Pp. 81–120 in *Ecology and Evolution of Communities.* M. L. Colby and J. M. Diamond, eds. Harvard University Press, Cambridge, MA.

McCabe, T. L., and C. N. Weber. 1994. The robber flies (Diptera: Asilidae) of the Albany Pinebush. *Gt. Lakes Entomol.* **27(3):** 157–159.

Pielou, E. C. 1975. *Ecological Diversity.* John Wiley, New York.

Preston, E. F. 1948. The commonness, and rarity, of species. *Ecology* **29:** 254–283.

Turchin, P. 1995. Pp. 19–39 in *Population Dynamics: New Approaches and Synthesis.* N. Cappuccino and P. W. Price, eds. Academic Press, San Diego.

Williams, C. B. 1964. *Patterns in the Balance of Nature.* Academic Press, London.

Wonnacott, R. J., and T. T. Wonnacott. 1982. *Statistics: Discovering its Power.* John Wiley, New York.

Appendix

Table 1

Chi square scores and corresponding normalized scores for the logistic-J and log-series distributions on 50 biosurveys

Ref	logistic c2	@ 10 df	log-ser.c2	@ 10 df	difference
1	18.659 @ 18	10.330	26.079 @ 17	17.054	+6.724
2	14.345 @ 8	17.054	18.347 @ 8	20.483	+3.429
3	3.064 @ 3	10.625	2.802 @ 4	8.331	−2.294
4	2.785 @ 5	6.904	7.286 @ 5	13.420	+6.516
5	9.804 @ 12	7.967	15.455 @ 12	12.664	+4.697
6	7.371 @ 4	15.391	5.181 @ 6	9.113	−6.278
7	1.031 @ 3	6.201	4.643 @ 4	11.369	+5.168
8	0.532 @ 3	4.662	3.450 @ 5	7.946	+3.284
9	0.762 @ 4	4.070	3.521 @ 7	5.851	+1.781
10	6.036 @ 6	10.227	4.778 @ 6	8.560	−1.667
11	0.142 @ 3	2.742	4.632 @ 4	9.739	+6.997
12	0.439 @ 5	2.236	2.808 @ 7	4.828	+2.592
13	5.809 @ 9	6.637	11.368 @ 9	12.523	+5.886
14	42.206 @ 27	11.523	46.972 @ 28	14.818	+3.295
15	5.410 @ 3	14.635	3.941 @ 4	10.265	−4.370
16	5.004 @ 3	13.970	4.637 @ 4	11.369	−2.601
17	5.667 @ 8	7.725	2.452 @ 9	2.971	−4.754
18	2.068 @ 3	6.445	5.471 @ 5	10.920	+4.475
19	6.195 @ 5	11.946	10.365 @ 7	14.085	+2.139
20	3.139 @ 4	8.946	12.796 @ 6	18.481	+9.535
21	12.525 @ 13	9.509	17.087 @ 15	11.600	+2.091
22	10.012 @ 9	11.099	10.986 @ 10	10.984	−0.115
23	3.493 @ 8	4.865	7.120 @ 9	8.040	+3.175
24	5.289 @ 6	9.259	5.541 @ 8	7.279	−1.980
25	24.986 @ 17	16.173	18.421 @ 19	9.406	−6.767
26	2.934 @ 5	7.144	11.826 @ 6	17.379	+10.235
27	8.839 @ 9	9.868	30.380 @ 11	29.588	+19.720
28	20.169 @ 18	11.471	33.425 @ 18	22.846	+11.375
29	3.271 @ 6	6.463	3.827 @ 7	6.176	−0.287
30	49.519 @ 41	12.536	57.258 @ 38	23.037	+10.501
31	6.134 @ 5	11.856	4.291 @ 5	9.248	−2.608
32	36.117 @ 20	21.157	36.607 @ 22	19.787	−1.370
33	3.167 @ 4	8.998	3.642 @ 5	8.237	−0.761
34	9.882 @ 9	10.958	13.366 @ 10	13.351	+2.393
35	7.551 @ 3	17.843	7.886 @ 4	16.126	−1.717
36	2.269 @ 3	9.123	2.174 @ 4	7.196	−1.927
37	11.366 @ 5	18.394	13.106 @ 6	18.742	+0.348
38	8.647 @ 4	17.147	13.759 @ 5	20.847	+3.700
39	16.479 @ 10	16.497	15.413 @ 11	14.199	−2.298
40	27.078 @ 15	20.048	59.643 @ 15	19.613	−0.435
41	9.360 @ 12	6.612	13.325 @ 14	9.331	+2.719
42	4.217 @ 6	7.789	8.166 @ 8	10.253	+2.464
43	1.291 @ 4	5.364	1.025 @ 5	3.663	−1.701
44	8.023 @ 4	16.312	8.820 @ 6	13.741	−2.571
45	0.561 @ 4	3.469	3.223 @ 6	6.388	+2.919
46	0.631 @ 3	5.002	1.619 @ 5	4.878	−0.124
47	4.659 @ 4	11.394	55.147 @ 8	29.588	+18.194
48	26.590 @ 10	23.605	75.212 @ 16	29.588	+5.983
49	13.625 @ 11	12.472	12.555 @ 11	11.458	1.014
50	4.800 @ 5	9.970	6.979 @ 7	10.099	+0.129
Total		532.633		648.058	
Average		10.653		12.961	

The papers used in the metastudy are listed in the order that they appear in this table and are numbered accordingly.

1. **Dewdney, A. K. 1996.** *Ecology in a Small Stream.* Monograph, Environmental Science Program, UWO, London, Ontario, Canada.

2. **Griffiths, R. W., S. Thornley, and T. A. Edsall. 1991.** Limnological aspects of the St. Clair River. *Hydrobiologia* **219:** 97–123.

3. **Griffiths, R. W. 1991.** Environmental quality assessment of the St. Clair River as reflected by the distribution of benthic macroinvertebrates in 1985. *Hydrobiologia* **219:** 143–164.

4. **Hill, J. K., K. C. Hamer, L. A. Lace, and W. M. T. Banham. 1995.** Effects of selective logging on tropical forest butterflies on Buru, Indonesia. *J. Appl. Ecol.* **32:** 754–760.

5. **Hutto, R. L. 1995.** Composition of bird communities following stand-replacement fires in northern Rocky Mountains (U.S.A.) conifer forests. *Conserv. Biol.* **9(5):** 1041–1058.

6. **Al-Safadi, M. M. 1991.** Freshwater macrofauna of stagnant waters in Yemen Arab Republic. *Hydrobiologia* **210:** 203–208.

7. **Novak, R. O., and W. F. Whittingham. 1968.** Soil and litter microfungi of a Maple-Elm-Ash floodplain community. *Mycologia* **60:** 776–787.

8. **McCabe, T. L., and C. N. Weber. 1994.** The robber flies (Diptera Asilidae) of the Albany Pinebush. *Gt. Lakes Entomol.* **27(3):** 157–159.

9. **Harper, F. P., and F. Harper. 1982.** Mayfly communities in a Laurentian watershed (Insecta: Ephemeroptera). *Can. J. Zool.* **60:** 2828–2840.

10. **Gutierrez, D., and R. Menendez. 1995.** Distribution and abundance of butterflies in a mountain area in the northern Iberian peninsula. *Ecography* **18:** 209–216.

11. **Barlocher, F., and B. Kendrick. 1974.** Dynamics of the fungal population on leaves in a stream. *J. Ecol.* **62:** 761–791.

12. **White, D. H., J. S. Hatfield, P. W. Sykes, Jr., and J. T. Seginak. 1996.** Habitat associations of birds in the Georgia Piedmont during winter. *J. Field Ornithol.* **67(1):** 159–166.

13. **Thiollay, J.-M. 1996.** The role of traditional agroforests in the conservation of rainforest bird diversity in Sumatra. *Conserv. Biol.* **9(2):** 335–353.

14. **Varga, S. 1965.** *Vascular Plant Inventory of the Backus Tract.* The Long Point Region Conservation Authority, Simcoe, Ontario, Canada.

15. **Short, T. M., J. A. Black, and W. J. Birge. 1991.** Ecology of a saline stream community responses to spatial gradients of environmental conditions. *Hydrobiologia* **226:** 167.

16. **Colwell, M. A., and S. L. Dodd. 1995.** Waterbird communities and habitat relationships in coastal pastures of northern California. *Conserv. Biol.* **9(4):** 827–834.

17. **Aoki, T., and S. Tokumasu. 1995.** Dominance and diversity of the fungal communities on fir needles. *Mycol. Res. J.* **99(12):** 1439–1449.

18. **Vuori, K.-M., and I. Joensuu. 1996.** Impact of forest drainage on the macroinvertebrates of a small boreal headwater stream: do buffer zones protect lotic biodiversity? *Biol. Conserv.* **77:** 87–95.

19. & 20. **Maycock, P. F., and D. Fahselt. 1992.** Vegetation of stressed calcareous screes and slopes in Sverdrup Pass, Ellesmere Island, Canada. *Can. J. Bot.* **70:** 2359–2377.

21. **Caley, M. J. 1995.** Community dynamics of tropical reef fishes: local patterns between latitudes. *Mar. Ecol. Prog. Ser.* **129:** 7–18.

22. **Lowry, J. K. 1975.** Soft bottom macrobenthic community of Arthur Harbor, Antarctica. Paper 1 in *Biology of the Antarctic Seas V,* D. L. Pawson, ed. *Antarctic Research Series* **23(1):** 1–18.

23. **Haila, Y., O. Jarvinen, and R. A. Vaisanen. 1980.** Habitat distribution and species associations of land bird populations on the Aland Islands, SW Finland. *Ann. Zool. Fenn.* **17:** 87–106.

24 **Stein, D. L., B. N. Tissot, M. A. Hixon, and W. Barss. 1992.** Fish-habitat associations on a deep reef at the edge of the Oregon continental shelf. *Fish. Bull. (Wash. DC)* **90:** 540–551.

25. **Winemiller, K. O., and M. A. Leslie. 1992.** Fish assemblages across a complex, tropical freshwater/marine ecotone. *Environ. Biol. Fishes* **34:** 29–50.

26. **Catling, P. M., and L. P. Lefkovitch. 1989.** Associations of vascular epiphytes in a Guatemalan cloud forest. *Biotropica* **21(1):** 35–40.

27. **Janzen, D. H. 1973.** Sweep samples of tropical foliage insects description of study sites, with data on species abundances and size distributions. *Ecology* **54(3):** 659–666.

28. **Lackey, J. B. 1938.** A study of some ecologic factors affecting the distribution of protozoa. *Ecol. Monogr.* **8(4):** 503–527.

29. **Wilson, E. O. 1987.** The arboreal ant fauna of Peruvian Amazon forest: a first assessment. *Biotropica* **19(3):** 245–251.

30. **Williams, C. B. 1964.** (See general Literature Cited.)

31. **Jennings, S., A. S. Brierly, and J. W. Walker. 1994.** The inshore fish assemblies of the Galapagos Archipelago. *Biol. Conserv.* **70:** 49–57.

32. **Bongers, F., J. Popma, J. Meave del Castillo, and J. Carabias. 1988.** Structure and floristic composition of the lowland rain forest of Los Tuxtlas, Mexico. *Vegetatio* **74:** 55–80.

33. **Busby, W. H., and J. R. Parmelee. 1996.** Historical changes in a herpetofaunal assemblage in the Flint Hills of Kansas. *Am. Midl. Nat.* **135:** 81–91.

34. **Bohning-Gaese, K., and H.-G. Bauer. 1996.** Changes in species abundance, distribution, and diversity in a central European bird community. *Conserv. Biol.* **10:** 175–187.

35. **Walters, K. 1991.** Influences of abundance, behavior, species composition, and ontogenetic stage on active emergence of meiobenthic copepods in subtropical habitats. *Mar. Biol.* **108:** 207–215.

36. **Salvado, H., and M. del Pilar Gracia. 1991.** Response of ciliate populations to changing environmental conditions along a freshwater reservoir. *Arch. Hydrobiol.* **123(2):** 239–255.

37. **Niemela, J., Y. Haila, and E. Halme. 1988.** Carabid beetles on isolated islands and on the adjacent Aland mainland variation in colonization success. *Ann. Zool. Fenn.* **25:** 133–143.

38. **Yoklavich, M. M., G. M. Cailliet, J. P. Barry, D. A. Ambrose, and B. S. Antrim. 1991.** Temporal and spatial patterns in abundance and density of fish assemblages in Elkhorn Slough, California. *Estuaries* **14:** 465–480.

39. **Sukumar, R., H. S. Dattaraja, H. S. Suresh, J. Radhakrishnan, R. Vasudeva, S. Nirmala, and N. V. Joshi. 1992.** Long-term monitoring of vegetation in a tropical deciduous forest in Mudumalai, southern India. *Curr. Sci.* **62:** 608–616.

40. **Terborgh, J., S. K. Robinson, T. A. Parker, III, C. Munn, and N. Pierpont. 1990.** Structure and organization of an Amazonian bird community. *Ecol. Monogr.* **60:** 213–238.

41. **Cowx, I. G., W. O. Young, and J. M. Hellawell. 1984.** The influence of drought on the fish and invertebrate populations of an upland stream in Wales. *Freshwater Biol.* **14:** 165–177.

42. **Samways, M. J. 1990.** Species temporal variability: epigaeic ant assemblages and management for abundance and scarcity. *Oecologia* **84:** 482–490.

43. **Kemp, W. P. 1992.** Temporal variation in rangeland grasshopper (Orthoptera Acrididae) communities in the steppe region of Montana, USA. *Can. Entomol.* **124:** 437–450.

44. **Brunner, I., F. Brunner, and G. A. Laursen. 1992.** Characterization and comparison of macrofungal communities in an *Alnus tenuifolia* and an *Alnus crispa* forest in Alaska. *Can. J. Bot.* **70:** 1247–1258.

45. **Spanier, E., S. Pisanty, M. Tom, and G. Almog-Shtayer. 1989.** The fish assemblage on a coralligenous shallow shelf off the Mediterranean coast of northern Israel. *J. Fish Biol.* **35:** 641–649.

46. **Hornbach, D. J., A. C. Miller, and B. S. Payne. 1992.** Species composition of the mussel assemblages in the upper Mississippi River. *Malacol. Rev.* **25:** 119–128.

47. **Holmquist, J. G., G. V. N. Powell, and S. M. Sogard. 1989.** Decapod and stomatopod assemblages on a system of seagrass-covered mud banks in Florida Bay. *Mar. Biol.* **100:** 473–483.

48. **Tzeng, W.-N., and Y.-T. Wang. 1992.** Structure, composition and seasonal dynamics of the larval and juvenile fish community in the mangrove estuary of Tanshui River, Taiwan. *Mar. Biol.* **113:** 481–490.

49. **Butler, L. 1992.** The community of macrolepidopterous larvae at Cooper's Rock State Forest, West Virginia: a baseline study. *Can. Entomol.* **124:** 1149–1156.

50. **Merrett, N. R., R. L. Haedrich, J. D. M. Gordon, and M. Stehmann. 1991.** Deep demersal fish assemblage structure in the Porcupine Seabight (eastern North Atlantic): results of single warp trawling at lower slope to abyssal soundings. *J. Mar. Biol. Assoc. UK* **71:** 359–373.

Instructions for Submitting Digital Art

The Biological Bulletin will accept figures submitted in electronic form; however, digital art must conform to the following guidelines. Contact the editorial office for further information.

Format. Acceptable graphic formats are TIFF and EPS. Color submissions must be in EPS format, saved in CMKY mode.

Software. Preferred software is Adobe Illustrator or Adobe Photoshop for the Mac and Adobe Photoshop for Windows. Specific instructions for artwork created with varoius software programs are available on the Web at the Digital Art Information Site maintained by Cadmus Professional Communications at
http://cjs.cadmus.com/da/home.html

Resolution. The minimum requirements for resolution are 1200 DPI for line art and 300 for halftones.

Size. All digital artwork must be submitted at its acutal printed size so that no scaling is necessary.

Multipanel figures. Figures consisting of individual parts (*e.g.*, panels A, B, C) must be assembled into final format and submitted as one file.

Hard copy. Files must be accompanied by hard copy for use in case the electronic version is unusable.

Disk identification. Disks must be clearly labeled with the following information: author name and manuscript number; format (PC or Macintosh); name and version of software used.

Authors who create digital images are wholly responsible for the quality of their material, including color and halftone accuracy. *The Bulletin* will use authors' digital art as submitted, and will not alter the digital files in any way.

Volume 198 Number 2

THE BIOLOGICAL BULLETIN

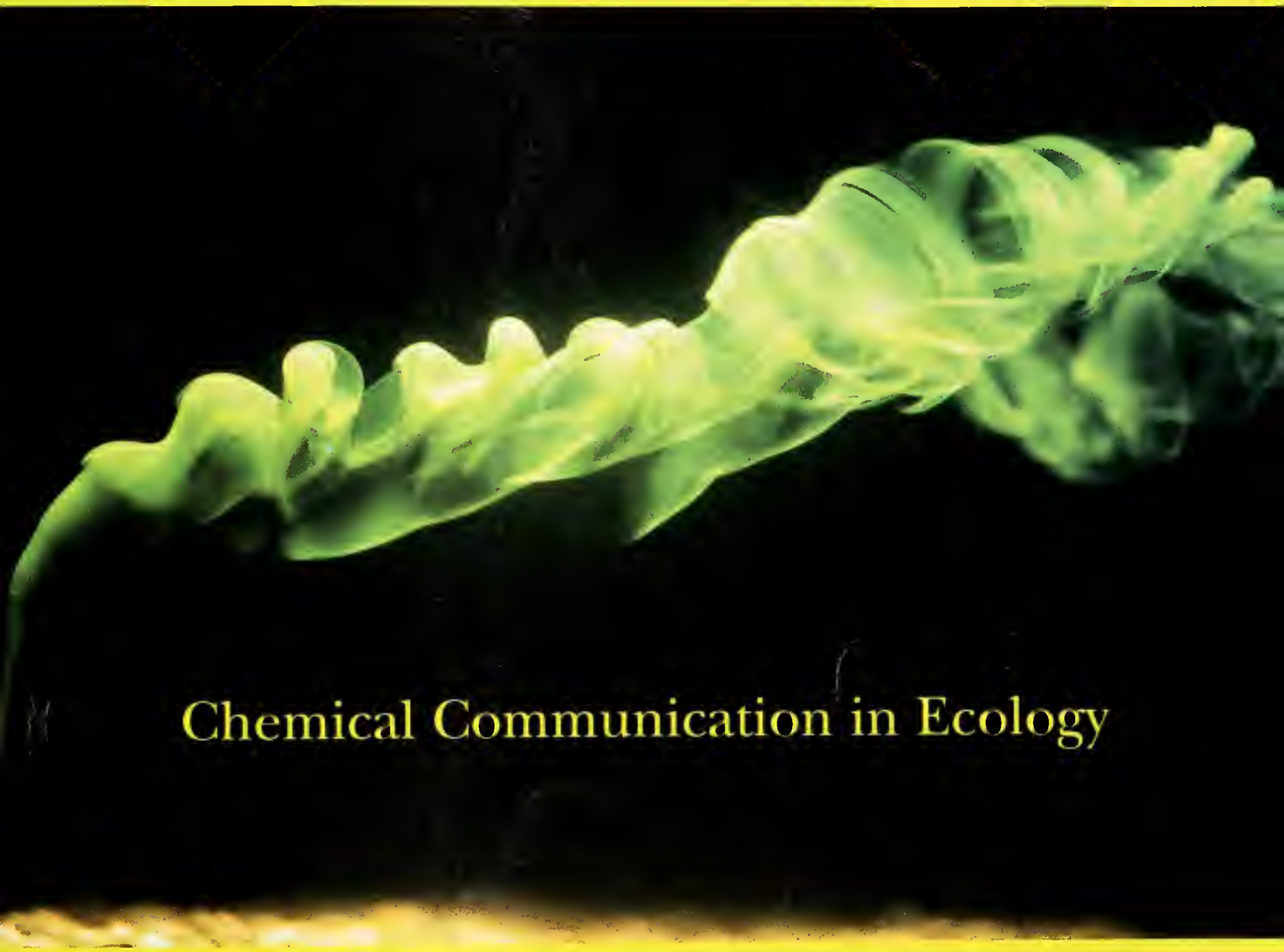

Chemical Communication in Ecology

APRIL 2000

Published by the Marine Biological Laboratory

Digital Imaging Platform

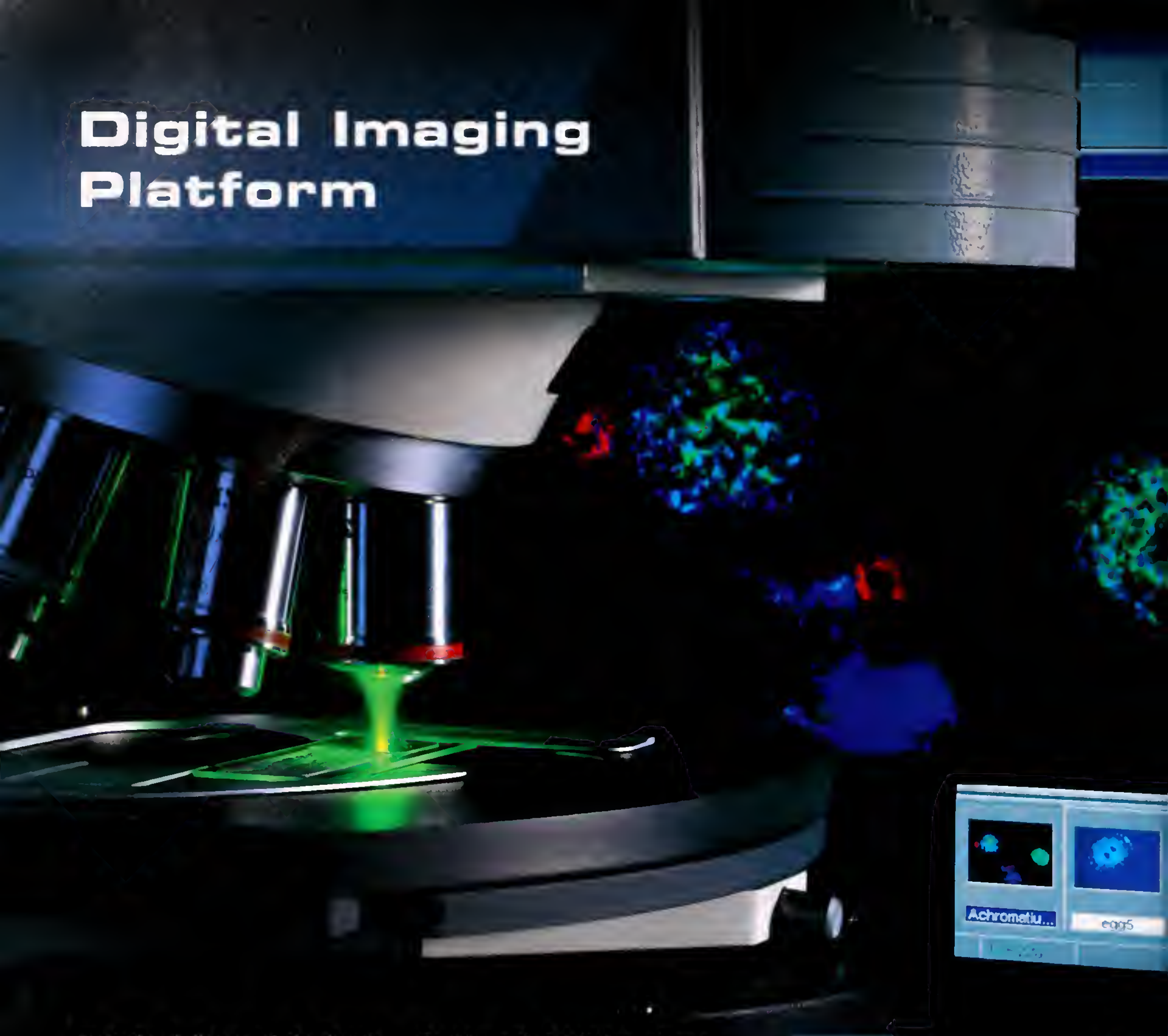

Meet the challenges of the digital age with **Axioplan 2 Imaging.** Not just a new microscope but a flexible system designed for the future – the digital imaging platform. A system that is set up and controlled by computer, with images captured and stored by computer, that communicates with other computers – truly digital from start to finish.

Combine with **AxioVision** software, with its built-in microscope control, and the new **AxioCam** ultra-high resolution digital camera and you have pure synergy – microscopy and more. Make yours the future-proof choice for high resolution image capture, image processing, archiving – even tele-microscopy. The digital age is with us. Are you?

AxioCam
ZEISS

Carl Zeiss, Inc.
Microscopy & Imaging Systems
One Zeiss Drive
Thornwood, NY 10594

800.233.2343, ext. 7858
micro@zeiss.com
www.zeiss.com/micro

ZEISS

THE
BIOLOGICAL BULLETIN
APRIL 2000

APR 24 2000

Editor	Michael J. Greenberg	The Whitney Laboratory, University of Florida
Associate Editors	Louis E. Burnett	Grice Marine Biological Laboratory, College of Charleston
	R. Andrew Cameron	California Institute of Technology
	Charles D. Derby	Georgia State University
	Michael LaBarbera	University of Chicago
Section Editor	Shinya Inoué, *Imaging and Microscopy*	Marine Biological Laboratory
Online Editors	James A. Blake, *Keys to Marine Invertebrates of the Woods Hole Region*	ENSR Marine & Coastal Center, Woods Hole
	William D. Cohen, *Marine Models Electronic Record and Compendia*	Hunter College, City University of New York
Editorial Board	Peter B. Armstrong	University of California, Davis
	Ernest S. Chang	Bodega Marine Lab., University of California, Davis
	Thomas H. Dietz	Louisiana State University
	Richard B. Emlet	Oregon Institute of Marine Biology, Univ. of Oregon
	David Epel	Hopkins Marine Station, Stanford University
	Gregory Hinkle	Cereon Genomics, Cambridge, Massachusetts
	Makoto Kobayashi	Hiroshima University of Economics, Japan
	Esther M. Leise	University of North Carolina Greensboro
	Donal T. Manahan	University of Southern California
	Margaret McFall-Ngai	Kewalo Marine Laboratory, University of Hawaii
	Mark W. Miller	Institute of Neurobiology, University of Puerto Rico
	Tatsuo Motokawa	Tokyo Institute of Technology, Japan
	Yoshitaka Nagahama	National Institute for Basic Biology, Japan
	Sherry D. Painter	Marine Biomed. Inst., Univ. of Texas Medical Branch
	J. Herbert Waite	University of California, Santa Barbara
	Richard K. Zimmer	University of California, Los Angeles
Editorial Office	Pamela Clapp Hinkle	Managing Editor
	Victoria R. Gibson	Staff Editor
	Carol Schachinger	Editorial Associate
	Patricia Burns	Subscription & Advertising Secretary

Published by
Marine Biological Laboratory
Woods Hole, Massachusetts

Cover

The photograph on the cover captures the odor plume that emanates from the excurrent siphon of a hard clam, *Mercenaria mercenaria* (credit: R.K. Zimmer and M.J. Weissburg). The plume contains a diversity of metabolites, and these act as chemical signals that trigger the search responses of predators. But a successful predation depends upon the shape of the plume, and thus upon the hydrodynamic properties of the water flow above and around the excurrent siphon of the clam. The plume was visualized by injecting fluorescein dye into the excurrent flow, right at the excurrent siphon, and the photograph was shot under slit illumination.

The cover highlights a set of review articles that arise from a symposium entitled *Chemical Communication in Ecology* (pp. 167–253). The symposium—held in San Diego late in 1998, and sponsored by the Western Society of Naturalists—was meant to promote recent ideas and findings about chemical communication and animal navigation and to provide ecologists and evolutionary biologists with a fresh perspective on the critical roles of chemical signaling processes in the natural environment.

Technical and conceptual advances have begun to widen the field of chemical communication systems, providing new opportunities for study. New instruments and analytical techniques are being used to identify the chemical structures of signal molecules, and to measure their synthesis, physical transport, and changing distribution over scales of time and space that are relevant to the processing of chemosensory information. Moreover, the effects of these chemical signals on target organisms can now be rigorously determined, in molecular detail and under environmentally realistic conditions. As a result, chemical communication is known to govern an increasing number of biotic interactions among plants, animals, and microbes, and the mechanisms underlying that regulation are coming to be known. Unfortunately, the ecological and evolutionary implications of chemical communication have rarely been considered. The review articles in this issue are among the first attempts at such a synthesis.

THE BIOLOGICAL BULLETIN

THE BIOLOGICAL BULLETIN is published six times a year by the Marine Biological Laboratory, 7 MBL Street, Woods Hole, Massachusetts 02543.

Subscriptions and similar matter should be addressed to Subscription Manager, THE BIOLOGICAL BULLETIN, Marine Biological Laboratory, 7 MBL Street, Woods Hole, Massachusetts 02543. Subscription per year (six issues, two volumes): $225 for libraries; $95 for individuals. Subscription per volume (three issues): $112.50 for libraries; $47.50 for individuals. Back and single issues (subject to availability): $40 for libraries; $20 for individuals.

Communications relative to manuscripts should be sent to Michael J. Greenberg, Editor-in-Chief, or Pamela Clapp Hinkle, Managing Editor, at the Marine Biological Laboratory, 7 MBL Street, Woods Hole, Massachusetts 02543. Telephone: (508) 289-7428. FAX: 508-289-7922. E-mail: pclapp@mbl.edu.

http://www.mbl.edu/BiologicalBulletin/

The home page for the electronic companion to THE BIOLOGICAL BULLETIN—*the Marine Models Electronic Record*—and other BIOLOGICAL BULLETIN publications is available on the World Wide Web at the address shown above.

THE BIOLOGICAL BULLETIN is indexed in bibliographic services including *Index Medicus* and MEDLINE, *Chemical Abstracts, Current Contents, Elsevier BIOBASE/Current Awareness in Biological Sciences,* and *Geo Abstracts.*

Printed on acid free paper,
effective with Volume 180, Issue 1, 1991.

POSTMASTER: Send address changes to THE BIOLOGICAL BULLETIN, Marine Biological Laboratory,
7 MBL Street, Woods Hole, MA 02543.

Copyright © 2000, by the Marine Biological Laboratory

Periodicals postage paid at Woods Hole, MA, and additional mailing offices.
ISSN 0006-3185

INSTRUCTIONS TO AUTHORS

The Biological Bulletin accepts outstanding original research reports of general interest to biologists throughout the world. Papers are usually of intermediate length (10–40 manuscript pages). A limited number of solicited review papers may be accepted after formal review. A paper will usually appear within four months after its acceptance.

Very short, especially topical papers (less than 9 manuscript pages including tables, figures, and bibliography) will be published in a separate section entitled "Research Notes." A Research Note in *The Biological Bulletin* follows the format of similar notes in *Nature.* It should open with a summary paragraph of 150 to 200 words comprising the introduction and the conclusions. The rest of the text should continue on without subheadings, and there should be no more than 30 references. References should be referred to in the text by number, and listed in the Literature Cited section in the order that they appear in the text. Unlike references in *Nature,* references in the Research Notes section should conform in punctuation and arrangement to the style of recent issues of *The Biological Bulletin.* Materials and Methods should be incorporated into appropriate figure legends. See the article by Lohmann *et al.* (October 1990, Vol. **179:** 214–218) for sample style. A Research Note will usually appear within two months after its acceptance.

The Editorial Board requests that regular manuscripts conform to the requirements set below; those manuscripts that do not conform will be returned to authors for correction before review.

1. ***Manuscripts.*** Manuscripts, including figures, should be submitted in quadruplicate, with the originals clearly marked. (Xerox copies of photographs are not acceptable for review purposes.) The submission letter accompanying the manuscript should include a telephone number, a FAX number, and (if possible) an E-mail address for the corresponding author. The original manuscript must be typed in no smaller than 12 pitch or 10 point, using double spacing (*including* figure legends, footnotes, bibliography, etc.) on one side of 16- or 20-lb. bond paper, 8 by 11 inches. Please, no right justification. Manuscripts should be proofread carefully and errors corrected legibly in black ink. Pages should be numbered consecutively. Margins on all sides should be at least 1 inch (2.5 cm). Manuscripts should conform to the *Council of Biology Editors Style Manual,* 5th Edition (Council of Biology Editors, 1983) and to American spelling. Unusual abbreviations should be kept to a minimum and should be spelled out on first reference as well as defined in a footnote on the title page. Manuscripts should be divided into the following components: Title page, Abstract (of no more than 200 words), Introduction, Materials and Methods, Results, Discussion, Acknowledgments, Literature Cited, Tables, and Figure Legends. In addition, authors should supply a list of words and phrases under which the article should be indexed.

2. ***Title page.*** The title page consists of a condensed title or running head of no more than 35 letters and spaces, the manuscript title, authors' names and appropriate addresses, and footnotes listing present addresses, acknowledgments or contribution numbers, and explanation of unusual abbreviations.

3. ***Figures.*** The dimensions of the printed page, 7 by 9 inches, should be kept in mind in preparing figures for publication. We recommend that figures be about 1 times the linear dimensions of the final printing desired, and that the ratio of the largest to the smallest letter or number and of the thickest to the thinnest line not exceed 1:1.5. Explanatory matter generally should be included in legends, although axes should always be identified on the illustration itself. Figures should be prepared for reproduction as either line cuts or halftones. Figures to be reproduced as line cuts should be unmounted glossy photographic reproductions or drawn in black ink on white paper, good-quality tracing cloth or plastic, or blue-lined coordinate paper. Those to be reproduced as halftones should be mounted on board, with both designating numbers or letters and scale bars affixed directly to the figures. All figures should be numbered in consecutive order, with no distinction between text and plate figures and cited, in order, in the text. The author's name and an arrow indicating orientation should appear on the reverse side of all figures.

Color: The Biological Bulletin will publish color figures and plates, but must bill authors for the actual additional cost of printing in color. The process is expensive, so authors with more than one color image should—consistent with editorial concerns, especially citation of figures in order—combine them into a single plate to reduce the expense. On request, when supplied with a copy of a color illustration, the editorial staff will provide a pre-publication estimate of the printing cost.

4. ***Tables, footnotes, figure legends, etc.*** Authors should follow the style in a recent issue of *The Biological Bulletin* in preparing table headings, figure legends, and the like. Because of the high cost of setting tabular material in type, authors are asked to limit such material as much as possible. Tables, with their headings and footnotes, should be typed on separate sheets, numbered with consecutive Roman numerals, and placed after the Literature Cited. Figure legends should contain enough information to make the figure intelligible separate from the text. Legends should be typed double spaced, with consecutive Arabic numbers, on a separate sheet at the end of the paper. Footnotes should be limited to authors' current addresses, acknowledgments or contribution numbers, and explanation of unusual abbreviations. All such footnotes should appear on the title page. Footnotes are not normally permitted in the body of the text.

5. ***Literature cited.*** In the text, literature should be cited by the Harvard system, with papers by more than two authors cited as Jones *et al.*, 1980. Personal communications and material in preparation or in press should be cited in the text only, with author's initials and institutions, unless the material has been formally accepted and a volume number can be supplied. The list of references following the text should be headed Literature Cited, and must be typed double spaced on separate pages, conforming in punctuation and arrangement to the style of recent issues of *The Biological Bulletin*. Citations should include complete titles and inclusive pagination. Journal abbreviations should normally follow those of the U. S. A. Standards Institute (USASI), as adopted by Biological Abstracts and Chemical Abstracts, with the minor differences set out below. The most generally useful list of biological journal titles is that published each year by Biological Abstracts (biosis List of Serials; the most recent issue). Foreign authors, and others who are accustomed to using The World List of Scientific Periodicals, may find a booklet published by the Biological Council of the U.K. (obtainable from the Institute of Biology, 41 Queen's Gate, London, S.W.7, England, U.K.) useful, since it sets out the World List abbreviations for most biological journals with notes of the USASI abbreviations where these differ. Chemical Abstracts publishes quarterly supplements of additional abbreviations. The following points of reference style for The Biological Bulletin differ from USASI (or modified World List) usage:

A. Journal abbreviations, and book titles, all underlined (for *italics*)

B. All components of abbreviations with initial capitals (not as European usage in World List *e.g., J. Cell. Comp. Physiol.* NOT *J. cell. comp. Physiol.*)

C. *All* abbreviated components must be followed by a period, whole word components *must not* (*i.e., J. Cancer Res.*)

D. Space between all components (*e.g., J. Cell. Comp. Physiol.*, not *J.Cell.Comp.Physiol.*)

E. Unusual words in journal titles should be spelled out in full, rather than employing new abbreviations invented by the author. For example, use *Rit Vísindafjélags Islendinga* without abbreviation.

F. All single word journal titles in full (*e.g., Veliger, Ecology, Brain*).

G. The order of abbreviated components should be the same as the word order of the complete title (*i.e., Proc.* and *Trans.* placed where they appear, not transposed as in some Biological Abstracts listings).

H. A few well-known international journals in their preferred forms rather than World List or USASI usage (*e.g., Nature, Science, Evolution* NOT *Nature, Lond., Science, N.Y.; Evolution, Lancaster, Pa.*)

6. ***Reprints, page proofs, and charges.*** Authors may purchase reprints in lots of 100. Forms for placing reprint orders are sent with page proofs. Reprints normally will be delivered about 2 to 3 months after the issue date. Authors (or delegates for foreign authors) will receive page proofs of articles shortly before publication. They will be charged the current cost of printers' time for corrections to these (other than corrections of printers' or editors' errors). Other than these charges for authors' alterations, *The Biological Bulletin* does not have page charges.

Reference: *Biol. Bull.* **198:** 167. (April 2000)

Importance of Chemical Communication in Ecology

RICHARD K. ZIMMER

Department of Biology, University of California, Los Angeles, California 90095-1606

Chemical communication—the unsung ecological process—is finally coming into its own. Sensory perception of chemical signals strongly influences, for example, predation, courtship and mating, kinship recognition, and habitat colonization. The critical importance of knowing the mechanisms by which environmental chemical stimuli influence ecological and evolutionary processes is widely recognized. Yet, with few notable exceptions, such mechanisms are only now being identified.

The study of chemical communication systems presents an exciting challenge. New instrumentation, analytical techniques, and conceptual approaches are being used to identify the structures and concentrations of signal molecules, and to measure their distributions over those time and space scales relevant to the processing of chemosensory information. Recent technological advances provide outstanding opportunities for new discoveries, allowing quantification of chemical production and physical transport of, and biological responses to, a given environmental signal molecule. By rigorously determining the effects of chemical signals on organisms under environmentally realistic conditions, these findings can be integrated within a larger evolutionary and ecological framework.

Such research is also of great importance in evaluating environmental impacts and developing policies. National and international management plans and research agendas designed to mitigate human impacts and preserve biological diversity have included little or no consideration of environmental chemical signals. But because chemical communication is pervasive in virtually every natural biological system, chemical signaling processes should be considered in determining the impacts of perturbations (human or otherwise) to that system.

The purpose of the symposium from which the papers that follow are derived was to promote recent findings and new ideas on chemical communication and animal navigation. Its function was to provide ecologists and evolutionary biologists with a fresh perspective on the critical role of chemical signaling processes in helping to structure populations and communities. Although most presentations drew on marine examples, the symposium emphasized the general significance of temporal and spatial scales (*e.g.*, organism size, locomotory speed), properties of fluid environments, and in some cases, the chemistry of signal molecules. Examples of chemical communication were described for organisms living in air or water, and illustrations were drawn from a diversity of organisms: microbes, copepods, crabs, moths, birds, and other animals. By exploring a wide range of systems, the symposium also provided an examination of the constraints on chemical communication imposed by different physicochemical environments and biological designs.

Whereas chemical communication is known to govern many biotic interactions among plants, animals, and microbes, in particular, there has been very little synthesis of such effects as they relate to ecology and evolution, in general. The next six papers are some of the first such syntheses. These studies highlight what is known, as well as speculating on probable but as yet unestablished chemical communications. The intent is to whet the appetites of ecologist and evolutionist alike with the myriad flavors of chemical stimuli that engender biological responses in nature.

Reference: *Biol. Bull.* **198:** 168–187. (April 2000)

Chemical Signaling Processes in the Marine Environment

RICHARD K. ZIMMER[1] AND CHERYL ANN BUTMAN[2]

[1]*Department of Biology, University of California, Los Angeles, California 90095-1606; and* [2]*Applied Ocean Physics and Engineering Department, Mail Stop 12, Woods Hole Oceanographic Institution, Woods Hole, Massachusetts 02543*

Abstract. Understanding the mechanisms by which environmental chemical signals, chemical defenses, and other chemical agents mediate various life-history processes can lead to important insights about the forces driving the ecology and evolution of marine systems. For chemical signals released into the environment, establishing the principles that mediate chemical production and transport is critical for interpreting biological responses to these stimuli within appropriate natural, historical contexts. Recent technological advancements provide outstanding opportunities for new discoveries, thus allowing quantification of interactions between hydrodynamic, chemical, and biological factors at numerous spatial and temporal scales. Past work on chemically mediated processes involving organisms and their environment have emphasized habitat colonization by larvae and trophic relationships. Future research priorities should include these topics as well as courtship and mating, fertilization, competition, symbiosis, and microbial chemical ecology. There are now vast new opportunities for determining how organisms respond to chemical signals and employ chemical defenses under environmentally realistic conditions. Integrating these findings within a larger ecological and evolutionary framework should lead to improved understanding of natural physicochemical phenomena that constrain biological responses at the individual, population, and community levels of organization.

Introduction

> *"Better Things for Better Living Through Chemistry"*—
> Former DuPont corporate slogan

The foundation of biological sciences is evolution, which stresses phylogenetic relationships. Therefore, questions relating to speciation, biogeography, and biodiversity are particularly compelling. Improved understanding of how chemical signals and other chemical agents interact with the environment can lead to important insights about the natural selective forces driving ecology and evolution. If, for example, organisms release waterborne compounds into the environment, investigations must focus on the principles of chemical production and transport. The structures, concentrations, and fluxes of bioactive molecules must be identified, and the rates of advection and diffusion (molecular and turbulent) must be measured to establish chemical distributions over time and in space. Knowledge of these factors makes it possible to analyze the constraints imposed by natural physicochemical phenomena on biological responses at individual, population, and community levels (Fig. 1).

Chemical mediation of ecological interactions

Chemistry indeed mediates a variety of critical ecological interactions. Considerable information is now available on the many types of biological responses to environmental chemical stimuli. Sensory perception of chemical signals, for example, strongly influences predation (Zimmer-Faust, 1989; Leonard *et al.*, 1999), courtship and mating (Gleeson *et al.*, 1984; Hardege *et al.*, 1996), aggregation and school formation (Hamner *et al.*, 1983; Ratchford and Eggleston, 1998), and habitat selection (Morse, 1991; Pawlik, 1992). Additionally, prey organisms (both animals and plants) of-

Received 21 September 1999; accepted 13 December 1999.

This paper was originally presented at a symposium titled *Chemical Communication and Ecology*. The symposium, which was held in San Diego, California, on 30 December 1998, was invited by the Western Society of Naturalists as part of its annual meetings.

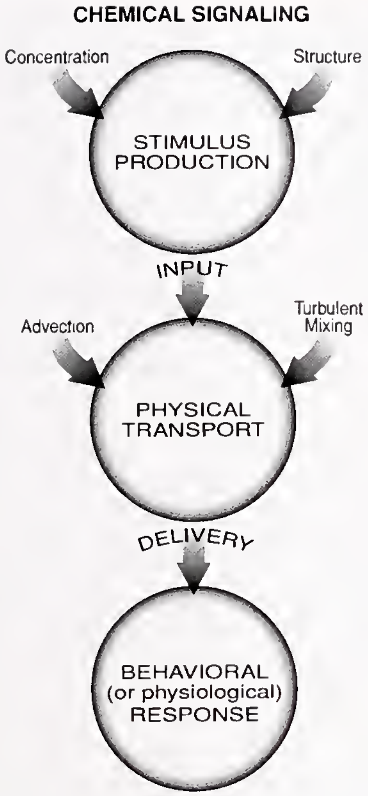

Figure 1. Diagram of the factors that determine the production, transport, and perception of waterborne chemical signals by a macroscopic organism.

ten produce chemical defenses that render their tissues unpalatable to primary or secondary consumers (Bakus *et al.*, 1986; Paul, 1992; Hay, 1996). Although chemicals are widely recognized as having critical importance ecologically, largely unexplored are the mechanisms by which such stimuli contribute to processes that structure communities. Marine natural products chemistry and chemical ecology are in their infancy and have emphasized studies of secondary metabolites acting as toxins and antifeedants. Still, outstanding examples are emerging in which either chemical signals or secondary metabolites are known to regulate the behavioral or physiological responses of individuals at lower trophic levels (Simenstad *et al.*, 1978; Hay, 1992; Steinberg *et al.*, 1995). These regulatory effects are then transferred to consumers at higher trophic levels with profound impacts on the distributions and abundances of organisms.

The physical and chemical properties of habitats can determine the nature and success of ecological interactions. In terrestrial environments, for example, compounds with high vapor pressures (low molecular weights, hydrophobic) facilitate chemical transport in air. Because the requirement for gaseous volatility imposes strong constraints on molecular designs, the isolation and identification of signal molecules by gas chromatography and mass spectrometry is often straightforward. By comparison, much less is understood about chemically mediated interactions in aquatic habitats. Aqueous solubility (imparted mainly by electronic charge or hydrophilicity), rather than gaseous volatility, may constrain the types of substances principally acting as waterborne chemical agents. Even insoluble compounds can provide effective chemical signals when suspended and transported by fluid flow in the water column. The identities of cues mediating habitat selection (including settlement by and metamorphosis of larvae), predator avoidance, mating, and social interactions in aquatic environments have thus far proven elusive except in a few isolated cases (*e.g.*, Howe and Sheikh, 1975; Sleeper *et al.*, 1980; Hardege *et al.*, 1996).

Feeding attraction and deterrence: examples of chemically mediated ecological processes

Nevertheless, an impressive body of knowledge has now accumulated concerning feeding stimulants and attractants released from animal flesh. These compounds are believed to be primarily amino acids, although there also may be effects of quaternary ammonium bases, nucleotides and nucleosides, and organic acids (Carr, 1988; Carr *et al.*, 1996). The sensory basis for animal perception of amino acids, including complex mixtures, has been studied extensively for 70 years, especially in crustaceans and fishes (Luther, 1930; Case, 1964; Ellingsen and Døving, 1986; Valentincic *et al.*, 1994; Derby *et al.*, 1996). With a single exception, however, the hypotheses that amino acids and other small metabolites are attractants and stimulants have not been tested under field conditions simulating the natural fluxes of these materials from intact live or injured prey or from carrion. The exception was a series of field experiments in which mud snails (*Ilyanassa obsoleta*) were significantly attracted to injured prey and carrion, but not to intact prey (Zimmer *et al.*, 1999). Synthetic mixtures of amino acids, simulating fluids leaking from injured prey, were also highly attractive. When field trials were performed to assess the relative effects of amino acid composition, concentration, mean volume flow rate (of chemical input), and flux (concentration × flow rate), only flux was directly correlated with the number of mud snails attracted. The foraging behavior of mud snails is thus more tightly coupled to the release and physical transport of chemical stimuli than to the molecular properties of specific amino acids.

Feeding deterrents, including terpenes, acetogenins, alkaloids, halogenated hydrocarbons, and polyphenols, are commonly found in marine microbes, plants, and sedentary animals (Hay and Fenical, 1988; Paul, 1992; Pawlik, 1993). These substances are mostly hydrophobic and sequestered within tissues rather than released into the environment.

Because, in many cases, their identities are known—or can be determined following bioassay-guided separation—feeding deterrents have served as valuable probes for investigating the ecological impacts of chemically mediated interactions (*e.g.*, Vervoort *et al.*, 1998; Nagle *et al.*, 1998). Direct tests at environmentally realistic doses have been performed in field habitats. Some deterrent compounds inhibit feeding (McClintock and Janssen, 1990; Pennings *et al.*, 1994), kill or suppress the growth of competitors (Jackson, 1977; Thacker *et al.*, 1998) and microbial pathogens (King, 1986; Gil-Turner *et al.*, 1989), and diminish substrate colonization by plant and animal propagules (Woodin *et al.*, 1993; Lindquist and Hay, 1996). Many members of marine communities benefit from feeding deterrents. Bivalve molluscs feeding on toxic dinoflagellates accumulate poisons in certain body tissues. If sea otters, fishes, and birds forage on the toxin-laden portions of these bivalves, they may become sick or die. Otters are also known, however, to feed selectively on the least-toxic tissues and are chemically deterred from eating the toxins. Moreover, otters appear to have been historically absent from areas where dinoflagellate blooms were common (Kvitek *et al.*, 1991). Nonetheless, poisons produced by blooms of both dinoflagellates and cyanobacteria potentially alter the structure and production of communities through their effects on predators (Paerl, 1988; Noga *et al.*, 1996; Nagle and Paul, 1998).

The Importance of Chemical Signaling Processes in Marine Ecology

Organism recognition of chemical stimuli

There is ample evidence that chemical composition, concentration, flux, and hydrodynamic transport all have profound effects on chemically mediated ecological interactions. For example, small peptides with arginine or lysine at their carboxy termini induce ovigerous mud crabs (*Rhithropanopeus harrisii*) to release and disperse brooded embryos and induce oyster (*Crassostrea virginica*) larvae to settle near conspecific adults (Forward *et al.*, 1987; Browne *et al.*, 1998). Moreover, in contrast to the more typical sigmoid-shaped dose/response curve, chemical induction in these marine organisms occurs only within a very narrow range in concentration, spanning less than one order of magnitude.

Animals can distinguish the quality of chemical stimuli by recognizing either novel compounds or unique blends of common substances in mixtures (Carr, 1988). Based on the qualitative chemical properties of food, animals express markedly different feeding preferences in natural habitats. For instance, oyster drills (*Urosalpinx cinerea*) differentiate between barnacle, mussel, and oyster prey. The stimuli that evoke foraging by oyster drills are low molecular weight peptides, presumably with novel structures (Rittschof *et al.*, 1984). In contrast, Caribbean spiny lobsters (*Panulirus argus*) can be trained in the laboratory to discriminate between different mixtures of identical compounds (including amino acids, organic acids, amine bases, and nucleotides). When presented at the same concentration and flux, each mixture is recognized as having its own unique composition that characterizes the tissues of either crab, oyster, shrimp, or fish (Derby *et al.*, 1989; Fine-Levy *et al.*, 1989).

Role of hydrodynamics

Turbulent odor plumes operate at macroscopic scales and are common features of the marine environment (Fig. 2). They form olfactory seascapes through which animals must navigate in order to locate resources and avoid potential hazards (Nevitt *et al.*, 1995). Turbulent odor plumes can be described by stable, mean concentration profiles averaged over relatively long time scales that animals may use for orientation, *i.e.*, *via* chemotaxis (movement in response to a gradient in chemical concentration) (Ingram and Hessler, 1983; Sainte-Marie and Hargrave, 1987). However, an organism's neural or behavioral response time in an odor-mediated search is much faster than the time necessary to generate mean concentration profiles (Gomez *et al.*, 1994; Zimmer-Faust *et al.*, 1995; Gomez and Atema, 1996). Field measurements made at shorter, biologically relevant time scales indicate that turbulent plumes are not characterized by well-defined gradients, but contain discrete odor filaments (eddies) separated by clean water (Zimmer-Faust *et al.*, 1988; Atema *et al.*, 1991; Finelli *et al.*, 1999). Under these conditions, organisms larger than a few millimeters are unlikely to use chemotaxis in navigating towards a distant odor source because their sensory systems sample faster than the averaging time scale to perceive a stable gradient (Fig. 3).

Still, large animals like blue crabs (*Callinectes sapidus*) employ their chemical senses while searching for valuable resources (Pearson and Olla, 1977). Crab success in locating live intact clams (*Mercenaria mercenaria*) was highly dependent on the hydrodynamic transport of metabolite attractants by both advection (bulk flow) and turbulent mixing. In fact, perception of chemical stimuli caused crabs to move upstream, but flow provided the signpost directing crab navigation. Predatory success was highest at a free-stream flow speed of 1 cm/s (smooth-turbulent bottom boundary layer, $u_* = 0.1$ cm/s), but rapidly decayed in the absence of flow (because there was no polarization for chemical stimulus to direct locomotion) and at flow speeds ≥ 4 cm/s (transitional to rough-turbulent bottom boundary layer, $u_* \geq 0.3$ cm/s; Weissburg and Zimmer-Faust, 1993, 1994) (Fig. 4). These results indicate that mechanisms governing the transport of chemical signals can have profound influences not only on sensory and behavioral mechanisms, but also on predation which, in turn, can mediate community structure. Blue crab chemosensory systems appear

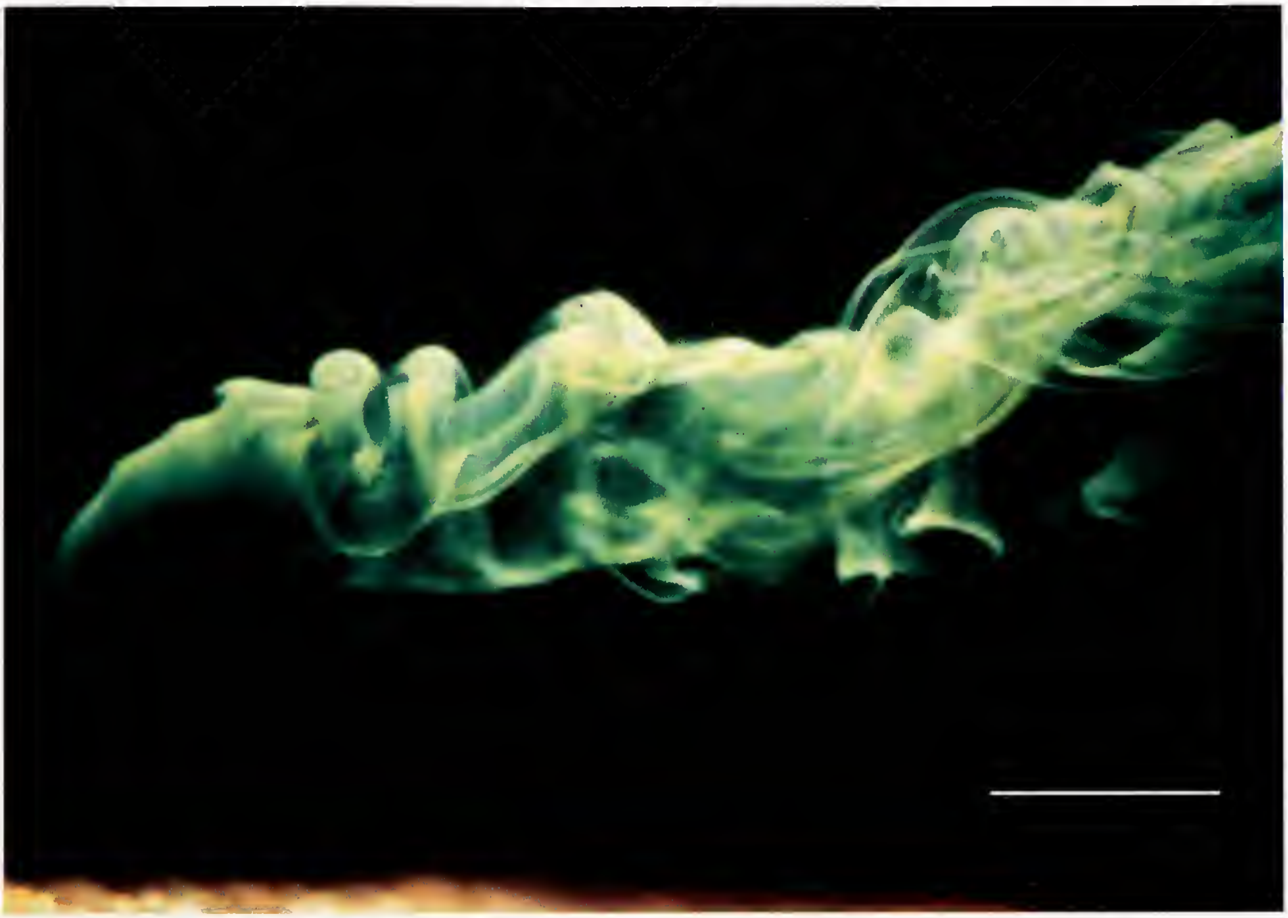

Figure 2. Odor plume produced by the release of metabolites from the excurrent siphon of a hard clam, *Mercenaria mercenaria*. Flow was visualized by releasing fluorescein dye through the excurrent siphon and photographed using slit illumination. The metabolites act as chemical signals triggering search responses by predators, but the likelihood of predatory success depends on the physical dynamics of water flow. Scale bar = 2 cm.

geared primarily to extracting information from hydrodynamically smooth flows. Thus, estuarine habitats with either no or high flows conceivably could provide prey with refuges from crab predation.

Chemicals are transported from regions of high to low concentration *via* molecular and turbulent diffusion. Whereas these processes operate at small (molecular) and large (turbulence) scales, at intermediate spatial scales, undiluted chemical patches can be transported in organized fluid tracks. In such flows, rotating parcels of fluid—vortices—are shed periodically in the lee of a flow disturbance, such as the organism emitting the signal (Doall *et al.*, 1998; Weissburg *et al.*, 1998; Yen, 2000). This alternating pattern of vortex shedding creates "streets" of odor packets of a characteristic size and frequency (Fig. 5). Vortex streets develop in the lee of relatively large objects (*e.g.*, 1 cm in diameter) in relatively slow flows (*e.g.*, 0.1–1 cm/s) or of small objects (*e.g.*, 100 μm in diameter) in fast flows (*e.g.*, 10–100 cm/s). Chemical signals transported in vortex streets create coherent chemical trails—"information highways"—that can be used by animals searching for mates, food, and other resources. In the water column, for example, copepods may locate mates by navigating along streets containing pheromone vortices shed downstream of conspecifics (Weissburg, 2000; Yen, 2000). Likewise, odor vortices generated from decaying animal matter may guide lysianassid amphipods and other scavengers to ephemeral prey in relatively slow-flow regions, such as protected bays and estuaries, the deep-sea, and polar regions (Busdosh *et al.*, 1982; Kaufmann, 1992; Tamburri and Barry, 1999).

Provided below are examples of how chemical signals dictate trophic and defense relationships for a wide variety of marine organisms. The examples are grouped as a function of spatial dimension to emphasize that chemical signaling phenomena are now known to operate at scales from less than millimeters to greater than kilometers. That is, the sea contains a vast array of chemical information—dissolved, in suspension, attached to substrates and associated

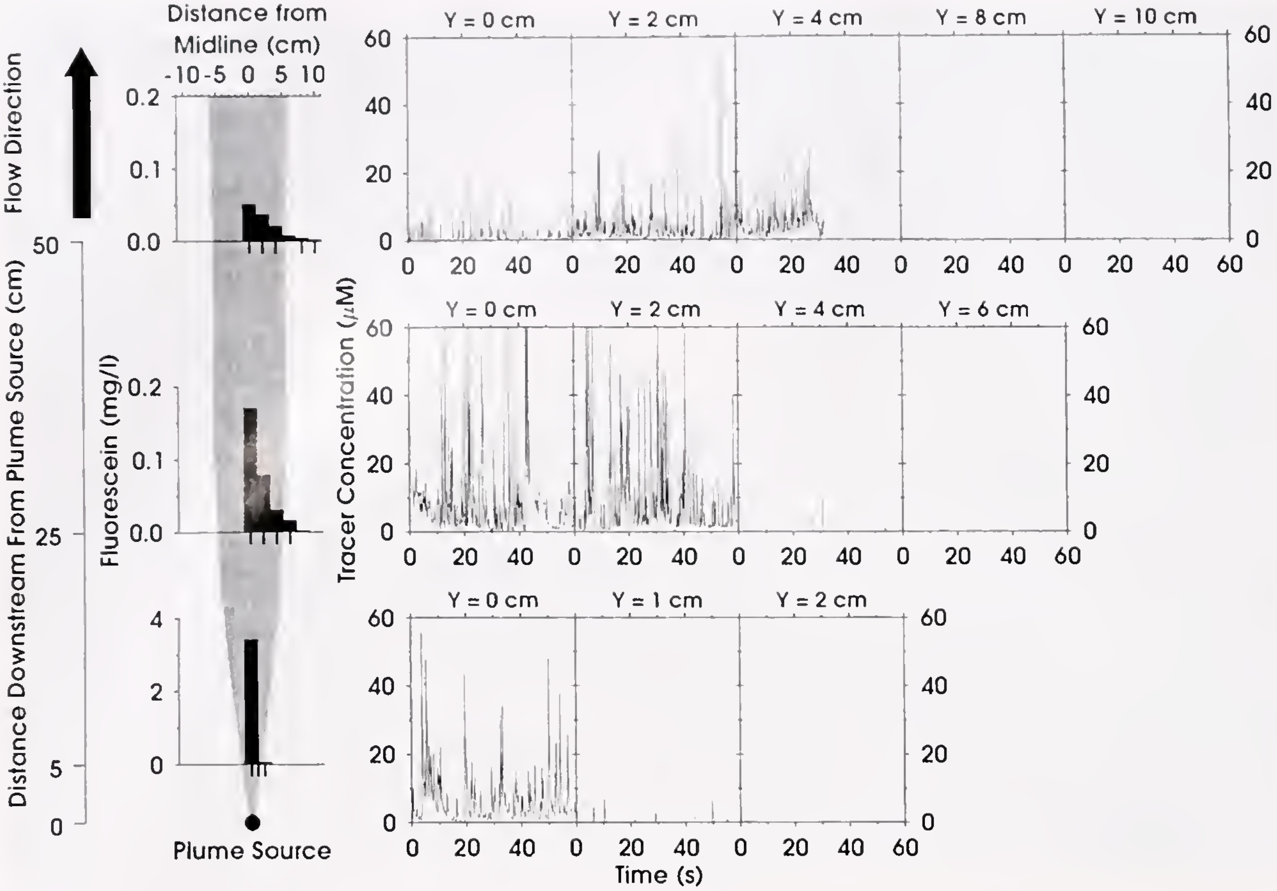

Figure 3. Representative concentration distributions downstream from a point source in a estuarine tidal creek (from Zimmer-Faust *et al.*, 1995). Histograms show fluorescein concentrations (mg/l) in samples collected over 1-min intervals at 5 cm (bottom row), 25 cm (middle row), and 50 cm (top row) downstream from the source and at 0, 2, 4, 6, 8, and 10 cm from the midline of the plume. Note that the scale differs between fluorescein concentrations at downstream locations. The visible region of the fluorescein plume at each position is denoted by shading. Panels to the right of the histograms represent 60-s records of instantaneous fluctuations in dopamine (tracer) concentration, measured at 10 Hz with a carbon fiber microelectrode (150 µm diam), at locations where the fluorescein was sampled. The left-most panel in each row is the sample from the midline of the plume, and successive panels are samples from 2, 4, 8, and 10 cm from the midline (see tick marks on histogram axes for sampling sites). Highly concentrated bursts of dopamine were common in all samples taken within the visible portion of the plume.

with organisms—that is critically involved in various aspects of the biology and ecology of the fauna, flora, and microbes.

Use of chemical signals at small scales

The production of dissolved organic matter (DOM) in certain microenvironments can locally elevate concentrations of compounds relative to surrounding habitats, creating stable chemical gradients (Azam and Ammerman, 1984; Alldredge and Cohen, 1987). At spatial scales smaller than the tiniest turbulent eddies (roughly less than 1 mm), turbulent mixing is relatively unimportant and chemical transport is dominated by molecular diffusion and advection (Fig. 6). Under these circumstances, flagellated bacteria swim in a straight line ("smooth run"), then stop and turn ("tumble") before swimming again (Berg, 1983). The chemosensory responses of microorganisms to concentration gradients can trigger changes in tumbling frequency that interrupt swimming more or less often and alter the time-averaged swimming paths.

The net result of these changes in swimming behavior is a biased random walk where cells migrate either towards or away from regions of elevated concentrations (Armitage, 1992; Manson, 1992). Positive chemotaxis, or chemical attraction, occurs when the tumbling frequency of a cell decreases in response to contact with a region of relatively high concentration, irrespective of a change in swimming speed (Berg and Brown, 1972; Adler, 1975). The process is

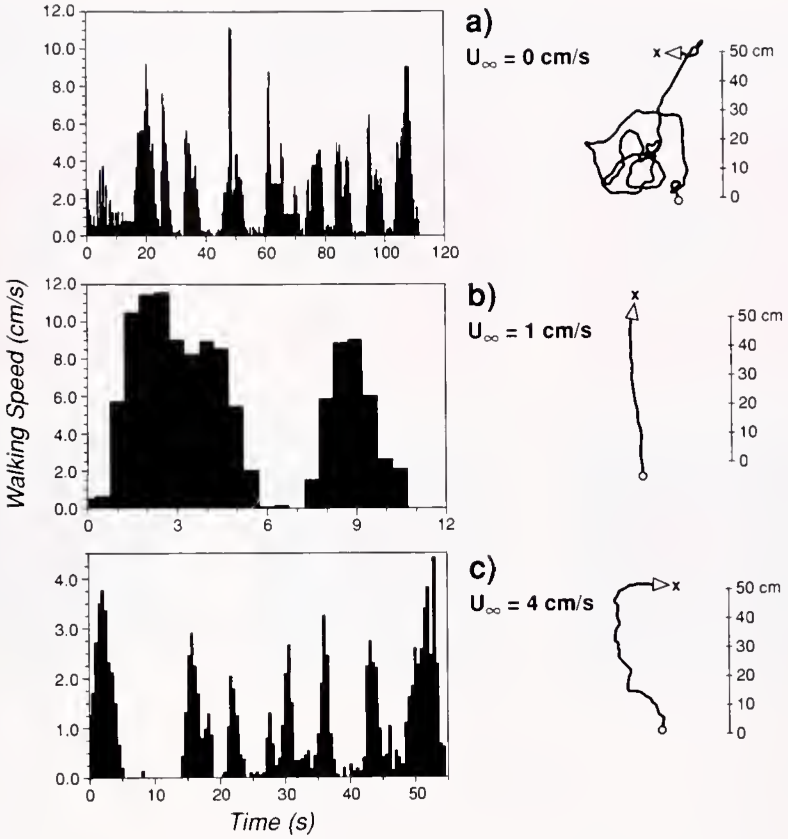

Figure 4. Using computer-assisted video motion analysis, traces to the right are paths walked by blue crabs as they searched for clams in a 10-m-long raceway flume at flow speeds of 0, 1, and 4 cm/s (top to bottom). Each 'O' marks the location where a search began, and each 'X' indicates the ultimate site of clam capture. Graphs to the left are histograms of walking speed *versus* time plotted for each path displayed to the right. The most efficient paths were those walked by crabs in 1 cm/s flow. In each case, intermittent walking and stopping characterized a search. The "stop interval" was defined as the time when crabs reset their attack angle (*i.e.*, turned) before moving on.

called chemotaxis even though cells do not navigate strictly with respect to a chemical concentration gradient. In the turbulent mixed layer of the ocean, positive chemotaxis increases the exposure between cells and nutrient patches (Bowen *et al.*, 1993). When these nutrients are taken up and used in metabolism, prolonged exposure leads to higher

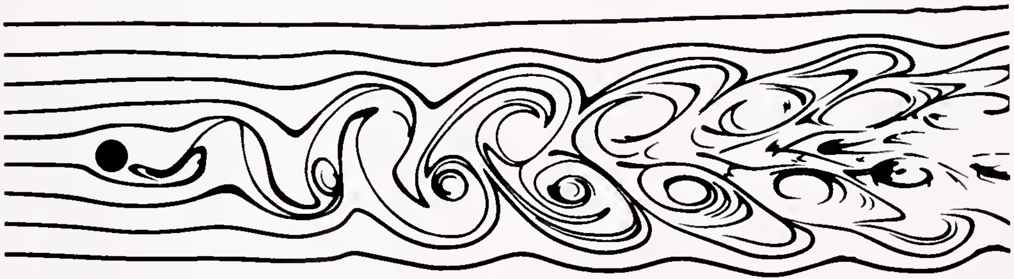

Figure 5. Artist's interpretation of a von Kármán vortex street in the wake of a circular cylinder, from a photograph by Peter Bradshaw (Van Dyke, 1982). Reynolds number (Re) of about 300 (where Re = LU/ν; L = characteristic length scale, U = characteristic velocity scale and ν = kinematic viscosity of the fluid) is at the upper limit for stability of the vortex street, as indicated by the breaking up of the vortices at the downstream edge of the drawing. At lower Re a pair of vortices forms in the lee of the cylinder but is not shed into the flow, and at higher Re the vortices break up completely into a disorganized turbulent wake.

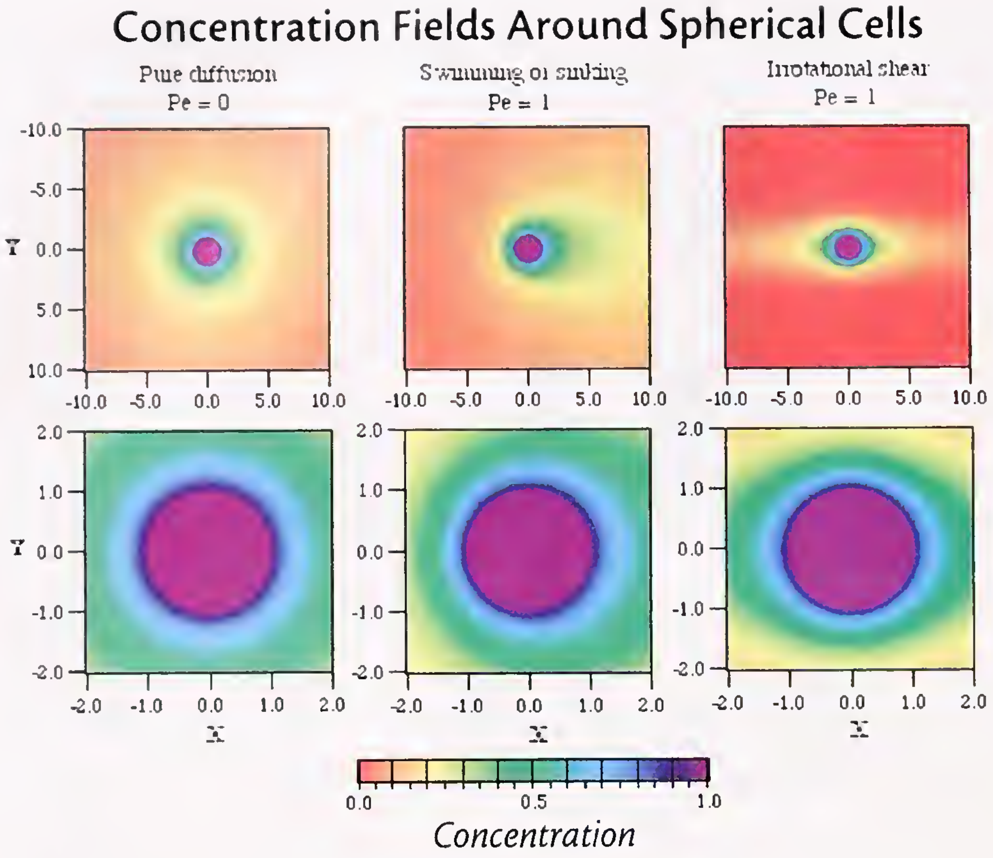

Figure 6. Concentration distributions of a hypothetical chemical signal molecule uniformly released from the surfaces of microscopic point sources (purple circles) in three different flow regimes: stagnant water (pure diffusion, no advective transport); uniform flow (*i.e.*, cell swimming or sinking in stagnant water; the cell is moving from right to left so flow is from left to right); and laminar shear flow (uniaxial extensional flow), where the third dimension can be visualized by rotation about the x-axis. The Peclet number (Pe) is a measure of advective transport relative to molecular diffusion (where $Pe = LU/D_m$; L = characteristic length scale, U = characteristic velocity scale, and D_m = coefficient of molecular diffusion). The upper panel illustrates the concentration field at distances up to 10 cell radii from the center of the cell. The lower panel is a "blow-up" of the concentration field near the cell surface, up to a distance of two radii from the center of the cell. In the absence of fluid motion a diffusive boundary layer extends to about nine cell radii from the cell surface. Uniform and shear flows distort the boundary layer and steepen the concentration gradient in certain regions. Because transport *via* diffusion is dominant in the thinnest regions of the boundary layer, cells in uniform or shear flow will experience enhanced rates of chemical signal release compared to nonmotile cells in stagnant water. This illustration was provided as a courtesy by L. Karp-Boss, and methods used in calculating concentration distributions appeared in Karp-Boss *et al.* (1996).

rates of cell division and population growth. Because microbial communities are critical to global biogeochemical cycling, mechanisms pertaining to chemotaxis and nutrient uptake have considerable significance.

Chemical signals are known to regulate the trophic relationships of corals. All species of reef-building corals have mutualistic symbioses with unicellular algae, called zooxanthellae, which live within the coral cells and are abundant in tissues exposed to sunlight (Muscatine, 1990). Although reef corals are uniquely versatile in their ability to procure nutrients and energy, they principally depend on the translocation of carbon from their algal symbionts to meet their energy demands (Falkowski *et al.*, 1984). The release of translocated materials from the algae is controlled by chemical communication with the coral host. Specifically, the chemical signal that induces carbon release is a mixture of free amino acids unique to the tissues of corals and other cnidarian species (Gates *et al.*, 1995, 1999).

Use of chemical signals at large scales

In the open ocean, chemical signaling helps structure both animal and plant communities. Dinoflagellates and other phytoplankton cells, for instance, create dense blooms at convergent zones where high nutrient levels occur in surface waters. These cells have extremely high concentrations of dimethylsulfoniopropionate (DMSP) that equalize osmotic pressure between the cytoplasm and external ocean environment, thus maintaining a constant cell volume (Vairavamurthy *et al.*, 1985; Dacey *et al.*, 1987; Matrai and Keller, 1994). When phytoplankton cells burst open during zooplankton grazing, DMSP is released into the seawater and is enzymatically degraded to dimethylsulfide (DMS) and acrylic acid (Dacey and Wakeham, 1986) (Fig. 7). The acrylic acid in seawater may act as a chemical deterrent against protozoan grazers (Wolfe *et al.*, 1997; Wolfe, 2000). In contrast, DMSP serves as a chemoattractant to biodegradatory bacteria (Zimmer-Faust *et al.*, 1996), and atmospheric DMS guides seabirds over kilometers to rich zooplankton feeding grounds (Nevitt *et al.*, 1995; Nevitt, 2000).

Chemistry is important in the evolution of marine communities. Species distributions and animal abundances in kelp forests, for example, are strongly influenced by invertebrate grazing on bottom-attached algae (*e.g.*, Dean *et al.*, 1984; Harrold and Reed, 1985). In the North Pacific Ocean, sea otter predation on invertebrates substantially reduces the intensity of herbivory on kelps (Estes and Palmisano, 1974). In contrast, temperate Australasia has no known predator of comparable influence and the intensity of herbivory on kelps is significantly higher than in the North Pacific. From experimental results it appears that chronically high rates of herbivory in Australasia have selected for high concentrations of kelp chemical defenses and increased tolerances of these substances by herbivores (Estes and Steinberg, 1988; Steinberg *et al.*, 1995). Top-level consumers may thus strongly influence the ecology and evolution of kelp-herbivore interactions, mediated through the production of plant chemical defenses.

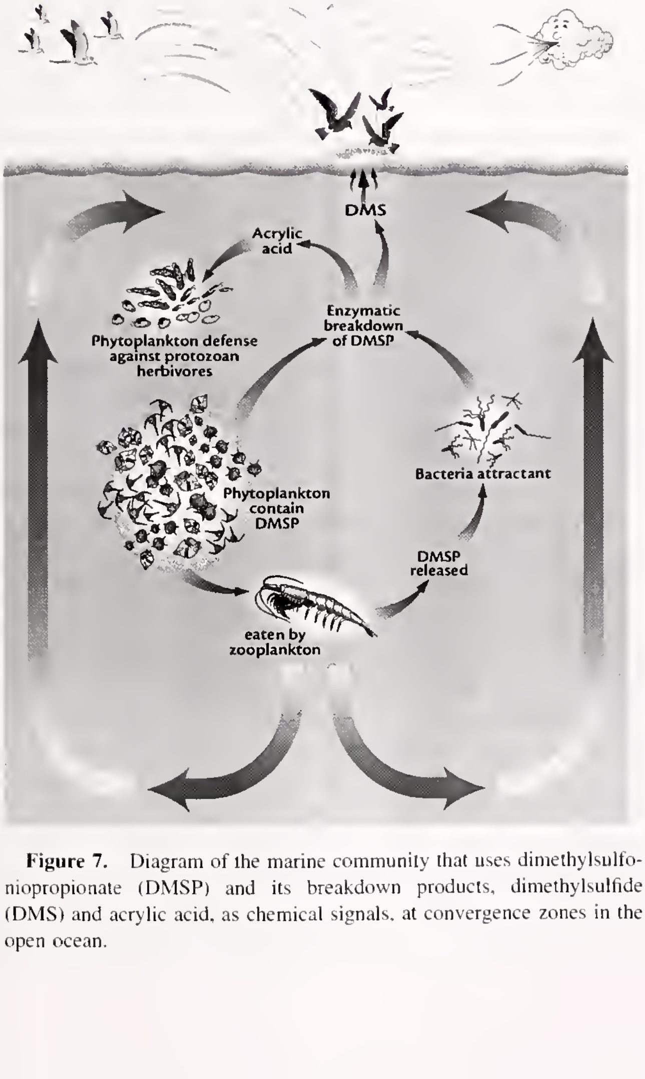
DMS
Acrylic acid
Enzymatic breakdown of DMSP
Phytoplankton defense against protozoan herbivores
Bacteria attractant
Phytoplankton contain DMSP
DMSP released
eaten by zooplankton

Figure 7. Diagram of the marine community that uses dimethylsulfoniopropionate (DMSP) and its breakdown products, dimethylsulfide (DMS) and acrylic acid, as chemical signals, at convergence zones in the open ocean.

Current State of the Field

Identification of ecologically relevant molecules

Significant progress in identifying ecologically relevant molecules is being made for marine systems, particularly on secondary metabolites acting as chemical defenses. The structures of more than 2000 secondary metabolites have been fully characterized (Hay, 1996, pers. comm.). Most of these substances can be extracted from animals, plants, and microbes by organic solvents (such as methanol or dichloromethane). The compounds are separated by reversed-phase or hydrophobic-interaction HPLC and gas chromatography before structures are identified by means of mass spectrometry, NMR, and other spectroscopic methods. Because secondary metabolites are available in partially or fully purified forms, they provide outstanding tools for quantitative studies. They are now being used to investigate the synthesis, inducibility, and seasonal and geographical variability in chemical defenses (Paul and van Alstyne, 1992; Steinberg, 1995; Cronin and Hay, 1996; McClintock, 1997; Targett and Arnold, 1998). Also under study are mechanisms of detoxification and patterns of associations (mutualism, commensalism, and parasitism), including coevolution, between chemically defended and nondefended species (Gil-Turner *et al.*, 1989; Vrolijk and Targett, 1992; Targett *et al.*, 1995; Stachowicz and Hay, 1996). These results will undoubtedly expand understanding of the direct consequences of chemically mediated interactions to provide more predictive insights about population regulation and community structure.

Purifications of ecologically relevant molecules other than secondary metabolites are often more challenging, and thus advances are occurring more slowly. Considerable effort has been expended in identifying environmental signal molecules that induce marine larvae to settle and metamorphose (Morse, 1990; Pawlik, 1992; Rodriquez *et al.*, 1993). This research has met limited success because many of these morphogens are (1) unstable, (2) tightly complexed (adsorbed or bound) with other molecules, or (3) present in only trace amounts. Neurotransmitters, such as gamma-aminobutyric acid (GABA) and dihydroxyphenylalanine (DOPA), have been suggested to mimic the function of natural signal molecules (Morse *et al.*, 1979; Morse, 1985;

Bonar *et al.*, 1990; Boettcher and Targett, 1998), but the peripheral or central neural site (or sites) of action by these mimetics is still unclear. Progress to date on at least partial purification of metamorphic inducers is encouraging (Hadfield and Pennington, 1990; Morse and Morse, 1991; Zimmer-Faust and Tamburri, 1994; Krug and Manzi, 1999), and will be particularly compelling when such research is coupled with physiological studies able to isolate the chemoreceptors. Recently, however, promising advances have been made towards isolating these chemoreceptor proteins from the cilia of abalone larvae (Wodicka and Morse, 1991; Baxter and Morse, 1992).

Remarkably few attempts have been made to characterize the structures of pheromones other than sperm attractants. Courtship and mating pheromones can be difficult to identify because breeding seasons are short and materials hard to obtain. Specific courtship behavioral acts are often troublesome to discriminate from other activities, thus making bioassay of active material impossible in some cases. Still, outstanding progress has been made towards elucidating the structures of mating pheromones in brown algae (Maier and Muller, 1986; Boland, 1995), polychaete worms (Zeeck *et al.*, 1994; Hardege *et al.*, 1996), and fishes (Dulka *et al.*, 1987; Sorensen, 1992). Whereas terpenes and other hydrocarbons appear to be the principal pheromones in worms and brown algae, steroid hormones and their metabolites produced by ovulating female fish are potent attractants to mature males in some species.

Gamete recognition factors embedded in cell membranes have been identified for a variety of marine organisms. These substances play a critical role in establishing barriers to cross-fertilization between individuals, thus leading to genetic isolation and speciation in the sea (Knowlton, 1993; Palumbi, 1994). In sea urchins, for example, glycoproteins located in the egg vitelline envelope are recognized by the sperm acrosome protein, bindin. Bindin has lectin-like properties enabling it to bind egg glycoproteins (Foltz and Lannarz, 1994; Hofmann and Glabe, 1994). In abalone sperm, lysin—a rapidly evolving protein—recognizes species-specific glycoproteins of the egg vitelline envelope (Lee and Vacquier, 1992). Similarly, in rotifers, surface glycoproteins on the female body surface bind to unique receptor proteins on the male corona and confer species specificity in mating (Snell *et al.*, 1995). Thus, fertilization in marine organisms is often controlled by chemical communication operating at the surface membranes of sperm and eggs.

Proteins, peptides, organic nitrogen bases, carbohydrates, fatty and humic acids, and other types of chemicals are all putative agents mediating ecological processes in the ocean (Gurin and Carr, 1974; Pawlik and Faulkner, 1986; Rittschof, 1990; Forward *et al.*, 1997; Krug and Manzi, 1999). Such wide diversity in the structures has, perhaps, slowed progress towards isolating and identifying specific chemical markers because different analytical approaches have been required on almost a case-by-case basis. Natural waterborne cues in trace amounts below chemical analytical detection limits often have strong biological effects. Purifications can thus require significant efforts in concentrating (and desalting) these substances while avoiding contaminant introductions.

One strategy used by organisms for producing chemical signals is to synthesize a novel substrate for each cue needed, as with anthopleurine, an alarm pheromone in the sea anemone (Howe and Sheikh, 1975). Another effective method is to employ a polymeric system with different repeating units. Peptides, a well-known class of polymer, are logical signal molecules within organisms and aquatic environments for several reasons. First, because of the charged nature of the terminal primary amine and carboxylic acid groups at neutral pH, peptides are water-soluble and not volatile. Second, the machinery (enzymes), templates (DNA, through mRNA), and structural units (amino acids) for producing peptides are already in every living organism (Lehninger *et al.*, 1993). Third, using the 20 coded amino acids available in eukaryotic systems, a vast variety of information can be presented in a short amino acid sequence; with as few as five amino acids, there are $20^5 =$ 3.2 million possible unmodified peptides. Finally, intracellular and extracellular proteases can degrade peptides to their constituent amino acids, thus terminating signal initiation (but not necessarily propagation; Hughes, 1978; Decho *et al.*, 1998).

In fact, peptides are emerging as important chemical cues in marine environments (Rittschof, 1990). Recent work with sand dollar, abalone, and oyster larval settlement (Burke, 1984; Morse and Morse, 1984; Zimmer-Faust and Tamburri, 1994) indicate that the inducing agents are small peptides from conspecifics or plants associated with juvenile habitats (Table 1). Nitrogen fixation and heterocyst formation in cyanobacteria is inhibited by peptides (Yoon and Golden, 1998), whereas abdominal pumping (for larval release and dispersal) in mud crab is stimulated by small peptide cues (Forward *et al.*, 1987). Remarkably, these peptide signals in oysters, mud crabs, and cyanobacteria are all structurally related to the carboxy-terminal sequence of mammalian C5a anaphylatoxin, a potent white blood cell chemoattractant. The receptors responsible for transmitting peptide signals in marine organisms have yet to be isolated and characterized. Nevertheless, quantitative structure-activity relationships (QSARs) have been modeled to relate the physicochemical properties of signal molecules to their biological functions (Browne *et al.*, 1998). Similarities between the anaphylatoxins and the oyster/mud crab/cyanobacteria peptides suggest that there may be homology among their respective receptors. Sequence analysis of the receptor protein for C5a indicates that it belongs to the rhodopsin superfamily (Boulay *et al.*, 1991; Gerard and Gerard, 1991). Members of the rhodopsin receptor family

Table 1

Examples of natural peptide signal molecules or their synthetic analogs

Environment	Compound*	Organism	Biological effect	Study
Marine	gly-gly-arg	Oyster	Settlement of larvae	Browne *et al.*, 1998
	gly-ile-arg	Mud crab	Release of larvae	Forward *et al.*, 1987
	arg-gly-ser-gly-arg	Cyanobacteria	Inhibition of heterocyst formation	Yoon and Golden, 1998
Terrestrial	tyr-gly-leu-ala-arg	Guinea pig	Contraction of ileum muscle	Konig, 1993
	met-glu-leu-gly-arg	Human	White blood cell chemotaxis	Ember *et al.*, 1992

* Abbreviations for amino acids are standard three-letter codes: ala, alanine; arg, arginine; gly, glycine; glu, glutamic acid; ile, isoleucine; leu, leucine; met, methionine; ser, serine; tyr, tryosine

bind a variety of molecular species, ranging from catecholamines and lipids to modestly sized proteins. By analogy, the receptors mediating responses in oyster larvae, mud crabs, and cyanobacteria may also belong to the rhodopsin class. There might even be an evolutionary link between the more primitive receptors functioning in external chemical communication among marine organisms and the internal receptors for mammalian neuroreactive and immunoreactive agents (Haldane, 1954; Carr, 1988).

Interactive effects of chemical and hydrodynamic factors

The process of larval settlement in benthic invertebrates is one of the best-studied systems thus far in terms of the interactive effects among chemical signals, hydrodynamics and animal behavior. Even so, only a few species have been studied and largely in controlled laboratory flow regimes. For half a century or more, the pervasive perception that small planktonic organisms are passively transported by flow fostered the notion that active larval behaviors can be important only at the time of settlement and in response only to surface-adsorbed chemical cues (Thorson, 1966; Crisp, 1974; Scheltema, 1974; Butman, 1987). Interdisciplinary research over the last decade has revealed, however, that larvae respond to waterborne as well as adsorbed chemical cues (Hadfield and Scheuer, 1985; Zimmer-Faust and Tamburri, 1994; Krug and Manzi, 1999). In addition, larvae can be passively transported by or actively respond to the flow regime (Mullineaux and Butman, 1991; Pawlik *et al.*, 1991; Mullineaux and Garland, 1993; Pawlik and Butman, 1993) (Fig. 8). Some of the most tractable study systems involve gregarious species because the settlement cue is associated with the adults.

Larvae of the gregarious reef-building "honeycomb worm," *Phragmatopoma lapidosa californica*, are induced to settle only by cement secreted by adults during tube building (Jensen and Morse, 1984). The cue involved may be a free fatty acid (Pawlik, 1986; Pawlik and Faulkner, 1986) or a DOPA moiety in a proteinaceous molecule (Jensen and Morse, 1988; Jensen *et al.*, 1990). The exact identity of the cue remains unresolved and is irrelevant to the research described here. In flume experiments in which larvae were given a choice of sand coated with cement ("tube sand") and "control sand" (non-inductive) over a range of flow speeds, larval supply to the bed was highest in intermediate flows (Pawlik and Butman, 1993). Still, metamorphosis was largely confined to the tube-sand treatment (Fig. 9). Direct observations indicated that larvae actively avoided settling in the slowest flows and were physically prevented from settling in the fastest flows. Thus, larval supply was determined by the flow; however, active behavioral responses of the larvae to a chemical cue (tube cement) ultimately determined their irreversible commitment to remain at the touchdown site.

In contrast to the honeycomb worm, gregarious oyster (*Crassostrea virginica*) larvae respond to waterborne chemical cues associated with adults (Zimmer-Faust and Tamburri, 1994). The dissolved cue changes the swimming behavior of suspended larvae, bringing them closer to the bed (Turner *et al.*, 1994; Tamburri *et al.*, 1996) and thus significantly increasing the rates at which they are swept by turbulent eddies into contact with the bottom. For oysters, settlement may be a two-step, two-scale process in which, first, larvae in the water column are induced to swim toward the bed in regions of adult habitat and, second, larvae are induced to attach if they land on appropriate substratum. The first induction probably occurs over scales of centimeters to meters (Browne and Zimmer, unpubl. data) and the second over scales of millimeters to centimeters, ultimately creating large oyster reefs several kilometers long.

Importance of understanding sensory systems

The sensory capabilities of an organism are important because there are vital links between stimulus production/transmission and behavior, and between individual behavior and larger scale dynamics in the abundance and spatial/temporal distributions of organisms (Renninger *et al.*, 1995; Wood *et al.*, 1995; Zimmer *et al.*, 1999). The nervous system represents an important filter for translating environmental features into sensory stimuli, and then into a behavioral task (Carr and Derby, 1986; Trapido-Rosenthal

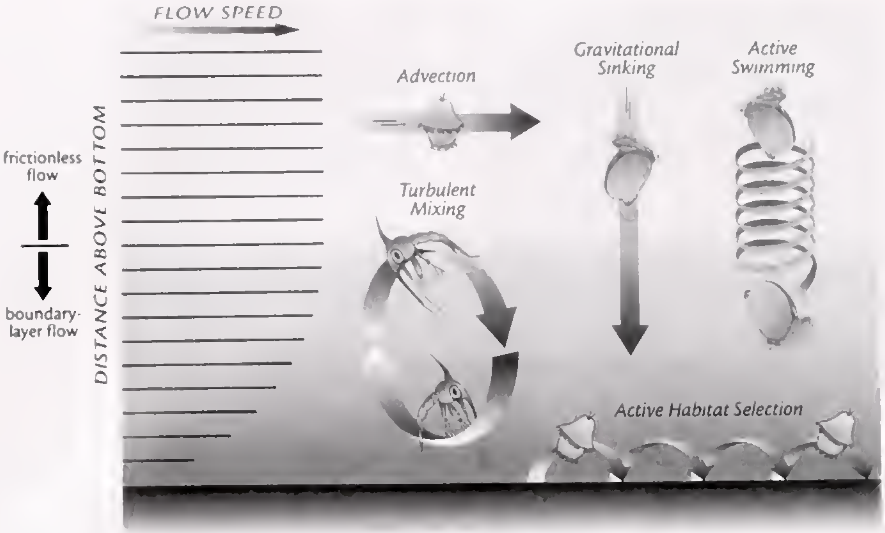

Figure 8. Diagram of the factors affecting larval transport and settlement within near-bottom waters. Larvae may be passively transported in the horizontal direction by advection, and in the vertical direction by gravity and turbulent mixing. Active movements of the larvae in response to dissolved chemical cues and other factors (*e.g.*, light, gravity, pressure) can transport them vertically within the water column. Active swimming along the seafloor and testing of the substrate for adsorbed chemical cues and other factors (*e.g.*, sediment characteristics, microbial populations, cracks and crevices in hard substrates) at each touchdown site may ultimately determine settlement locations.

et al., 1987; Zimmer-Faust *et al.*, 1988; Sorensen *et al.*, 1998). Investigations on sensory physiology, particularly in conjunction with behavioral and population studies, can fill a need in establishing linkages between stimulus space, behavior, and demographic consequences of decisions made by individual organisms.

Recent research into sensory biology has delved into how the properties of complex chemical stimuli are coded by the nervous systems to modulate the motility patterns of organisms (Derby *et al.*, 1989; Lynn *et al.*, 1994). Concomitant with these developments were increasing efforts to understand the linkages between the natural physical and chemical environments and the properties of animal perceptual systems (Finelli *et al.*, 1999; Moore *et al.*, 1999). Taken together, these two lines of inquiry provide information on how biologically relevant natural stimuli are translated into specific strategies for navigation, orientation, and guidance during the search for resources. Recent studies have documented the properties of chemosensory cells (and occasionally other neural elements) in effective coding of chemical signal parameters that may specify the identity, direction, and distance to stimulus sources (Borroni and Atema, 1988; Gomez *et al.*, 1994; Gomez and Atema, 1996). Such efforts mostly have been applied to the physiological and behavioral strategies of large animals, particularly crustaceans and fishes. Research on planktonic organisms is much less mature, but recent investigations on the sensory ecology of zooplankton suggest interest in this topic as well (Strickler *et al.*, 1997; Bundy *et al.*, 1998; Paffenhoefer, 1998; Davis *et al.*, 1999).

Technology and Conceptual Approaches

Current limitations

Advances in understanding marine chemical ecology and communication have been constrained by limitations in technology and conceptual approaches. In particular, exhaustive studies have been performed on the relationship between chemoreception and behavioral responses of some macroscopic, but few microscopic, organisms. Because the magnitude of turbulence typically covaries with flow speed, surface roughness, and animal size, and because turbulent mixing dilutes waterborne chemical stimuli and creates patchiness in chemical distributions, new innovative studies are required to help identify the controlling variables. To reduce the effects of turbulence, devices such as y-tubes and choice mazes have been constructed either to straighten the flow artificially or to create unrealistically low flow speeds or turbulence (*e.g.*, Vadas *et al.*, 1994; Grove and Woodin, 1996; Ratchford and Eggleston, 1998). Although these devices increase investigator control over chemical stimulus environments, they frequently create artificial patterns of contact between the experimental subject and signal molecules. The rate at which a sensor naturally encounters a chemical stimulus depends on the amount of material released per unit time and the hydrodynamic forces governing

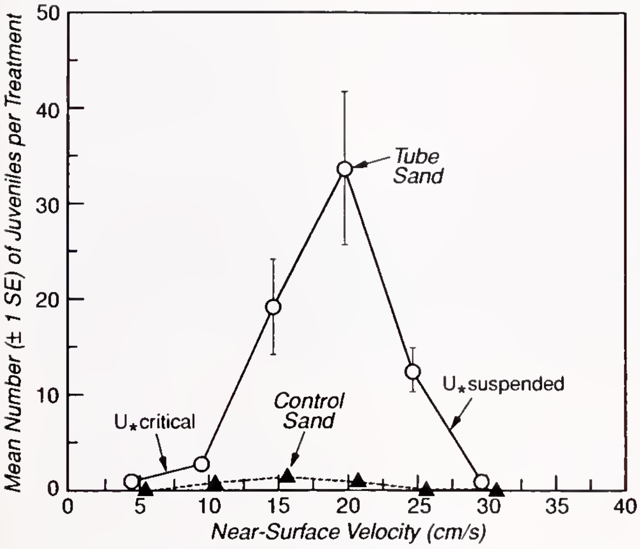

Figure 9. Settlement (*i.e.*, metamorphosed juveniles) of *Phragmatopoma lapidosa californica* larvae in an inductive "tube sand" (open circles) and a "control sand" (closed triangles) treatment over a range of laboratory flume flows (see text) (from Pawlik and Butman, 1993). The magnitude and variation in larval supply as a function of flow speed were similar between the two sediment treatments (data not shown), but larvae metamorphosed almost exclusively in response to the adsorbed chemical cue associated with the tube-sand treatment. Observations of the movement of "larval mimics"—plastic spheres with sinking rates similar to the downward swim speeds of the larvae—in each flow are indicated on the tube-sand plot. The boundary shear velocity (u_*) for initiation of particle motion ($u_{*\text{critical}}$) was between 0.26 and 0.47 cm/s (near-surface velocities of 5 and 10 cm/s, respectively), and the u_* for which particles made brief excursions into the water column ($u_{*\text{suspended}}$) was greater than 1.03 cm/s (near-surface velocity of 25 cm/s). Observations of larvae indicated that they actively avoided settling in the slowest flows and were physically prevented from settlement in the fastest flows.

chemical transport (Koehl, 1996). These encounter rates determine the behavioral responses of animals to chemical signals and indirectly control a variety of ecological interactions that structure communities. To avoid serious artifacts that could render results equivocal, it is imperative that laboratory and field studies reproduce stimulus environments that are naturally experienced by animals, plants, and microbes.

Technology for studying chemical/flow interactions

Usually, relevant flow parameters have not been quantified in either laboratory or field experiments on chemosensory-mediated behavior (*e.g.*, Moore and Lepper, 1997; Swenson and McClintock, 1998; Zhou and Rebach, 1999). Measurements of the mean flow speed reveal only the bulk, advective transport of dissolved chemicals. Considerably more information is needed about the flow in order to describe the distribution of waterborne cues in a turbulent environment. Research on chemically mediated processes requires measurements that characterize the rates at which chemical stimuli are mixed, dispersed, and diluted. Prior studies have been valuable for establishing the potential or scope for response. However, natural field or laboratory flow regimes generally were not sufficiently characterized at the temporal and spatial scales relevant to sensory systems. Thus, it is difficult or impossible to use results from most of these studies to predict ecological interactions in the field.

Instruments and techniques for creating and characterizing specific field flow environments and for tracking chemicals and particles in flow have significantly improved over the last decade. Large flumes, wave tanks, and Couette flow cells (discussed below), for example, can be designed to produce realistic one-dimensional, unidirectional, turbulent; oscillatory; or laminar-shear flows, respectively (van Wazer *et al.*, 1963; Nowell *et al.*, 1989; Miller *et al.*, 1992). Technologies for measuring flow velocities include laser Doppler and acoustic Doppler velocimetry, and digital particle image velocimetry (Nezru and Rodi, 1986; Agrawal and Belting, 1988; Prasad and Sreenivasan, 1990). Chemical concentration distributions now can be determined with a variety of waterborne chemical tracers, such as rhodamine WT or fluorescein dye release combined with laser-induced fluorescence imaging (O'Riordan *et al.*, 1993); sulfur hexafluoride release coupled with gas chromatographic determinations (Wanninkhof *et al.*, 1991); and electrochemical release combined with microsensor measurements (Moore *et al.*, 1989). Many of these instruments and techniques can be used in both laboratory and field settings.

Flumes to simulate the bottom boundary-layer environment

The availability to biologists of increasingly sophisticated flumes and other flow tanks has, perhaps, outpaced the availability of hydrodynamicists interested in collaborating on interdisciplinary experiments. Or, biologists have not sought their advice. At any rate, there appears to be considerable confusion as to the correct flume size and operating conditions for a given research problem. Because the fundamental characteristics of the flow transporting a chemical signal can be a critical determinant of how and when the signal is detected or utilized by an organism, laboratory flow regimes must be scaled to represent (*i.e.*, be "dynamically similar" to) the field flows of interest. Moreover, most ocean flows relevant to chemical transport are turbulent, but most small flumes can achieve laminar (nonturbulent) flow, at best.

There is an excellent, quantitative discussion of flume design for simulating benthic flow environments in Nowell and Jumars (1987), and more qualitative treatments appear in Vogel and LaBarbara (1978), Muschenheim *et al.* (1986) and Vogel (1994). We briefly summarize those recommendations of Nowell and Jumars (1987) that are most relevant for experiments involving organism detection of chemical signals in a turbulent flow field. This discussion is largely conceptual; actual flume dimensions, channel configurations, and flow forcing mechanisms would depend on the intended purpose of a given flume.

The near-bed flow regime can be adequately simulated in a flume because the frictional drag of the bottom on the flow determines the general nature of this fluid-dynamic regime. In the region directly above the bottom, called the "boundary layer," there is a vertical gradient in velocity until an asymptote is reached, where the bed no longer influences the flow. Because only a relatively thin layer of fluid is affected by the boundary, the structure of the flow within tens of centimeters of the bed will be similar between a flume and the field as long as certain scaling laws have been satisfied. The small, simple flumes that are easily constructed (Vogel and LaBarbera, 1978; Vogel, 1994) generally cannot be used for research problems for which it is important to simulate the structure of the flow and chemical-concentration fields within the bottom boundary layer. These flumes are useful, for example, in studying the forces on an individual or small group of benthic organisms placed in the flow (*e.g.*, Koehl, 1977; Denny *et al.*, 1985; Okamura, 1985). Such flumes are inappropriate, however, for studies of animal navigation in a turbulent odor plume because the flow regime at the "working section" (where measurements are made or experiments conducted, see Fig. 10) typically is not dynamically similar to the field, well characterized, or reproducible.

Flume flow regimes that simulate field flow should be steady, fully developed (boundary layer has grown to the water surface), uniform (no variation in the cross-stream or along-channel direction), and one-dimensional (mean velocity varies only in the vertical direction). Large flumes—channel dimensions typically of 5–10-m long, 50–70-cm wide, and 10–20-cm deep—with appropriate flow-driving mechanisms are required for flow-field studies in order to deliver to the working section a well-characterized and reproducible flow that mimics the field flow regime of interest. The channel dimensions are driven by the following fluid-dynamic considerations (refer to Fig. 10). (1) Entrance conditions—The channel entrance should be configured to help the flow "forget" where it has been (*e.g.*, recirculating in narrower pipes or around channel bends). (2) Exit conditions—The channel terminus should be designed so the flow does not "anticipate" its exit (*i.e.*, avoiding sudden increases or decreases in water depth that would affect the upstream flow). (3) Channel length—A sufficiently long channel is required so that the boundary layer can grow to the water surface before reaching the working section. (4) Channel width-to-depth ratio—An adequate ratio of channel width to depth is needed so that secondary (cross-stream) circulations resulting from the side-wall boundary layers are confined to a relatively small region next to the walls. In addition, a sufficient water depth is required so that the boundary layer is a reasonable representation of nature and to minimize free-surface effects (*e.g.*, organisms on the bottom affecting flow at the surface and *vice versa*).

Violating any one of these requirements may result, at best, in boundary layers that are not described by the classical theory and measurement of open-channel flows (Henderson, 1966; Schlichting, 1979; Nezu and Rodi, 1986), and thus, can be characterized only by exhaustive measurements under each hydrodynamic condition. Such fluid motions also may mix and transport chemicals in ways that are uncharacteristic of field flows and cannot be easily extrapolated to natural habitats. In contrast, a modest set of measurements is required to characterize fluid motion in well-designed flumes, where highly predictable "well-behaved" hydrodynamic regimes are described in a vast literature of empirical observations and theory on open-channel flow. Such flows can mimic nature—for example, estuarine tidal currents or unidirectional currents in the deep sea.

Other flow tanks

Whereas flumes can be used to conduct chemical signaling experiments under turbulent, unidirectional flow conditions, more specialized flow tanks are required to study effects under other hydrodynamic conditions. Two fluid-transport cases that are particularly germane to an understanding of chemical signaling processes in the marine environment are oscillatory and laminar-shear flows.

Waves are a pervasive feature of the ocean. Chemical transport under waves would differ substantially from that in steady flows, with shorter advective transport distances and greater mixing in waves (Grant and Madsen, 1986; Denny, 1988). Oscillatory flows in the upper water column are generated by free-surface waves that can intensify and break as the water shoals. In contrast, oscillatory flows in the water column are generated by internal waves that can occur in a wide range of water depths. In the laboratory, wave tanks and U-tubes are used to simulate the fundamental characteristics of oscillatory flows. A wave tank produces free-surface waves and consists of a long rectangular channel with a wave generator at one end and a beach at the other (Denny, 1988). A U-tube is a vertically oriented U-shaped water tunnel in which the flow is forced back and forth through the horizontal working section by pistons located at one end (Turner and Miller, 1991a, b). Although the resulting flows are nearly sinusoidal, U-tubes are better able to generate the relatively fast oscillatory flows characteristic of waves that cannot always be reasonably mimicked in wave tanks.

In laminar-shear flows, there is a velocity gradient and adjacent layers of fluid slide past each other without mixing. These nonturbulent flows occur at length scales smaller than

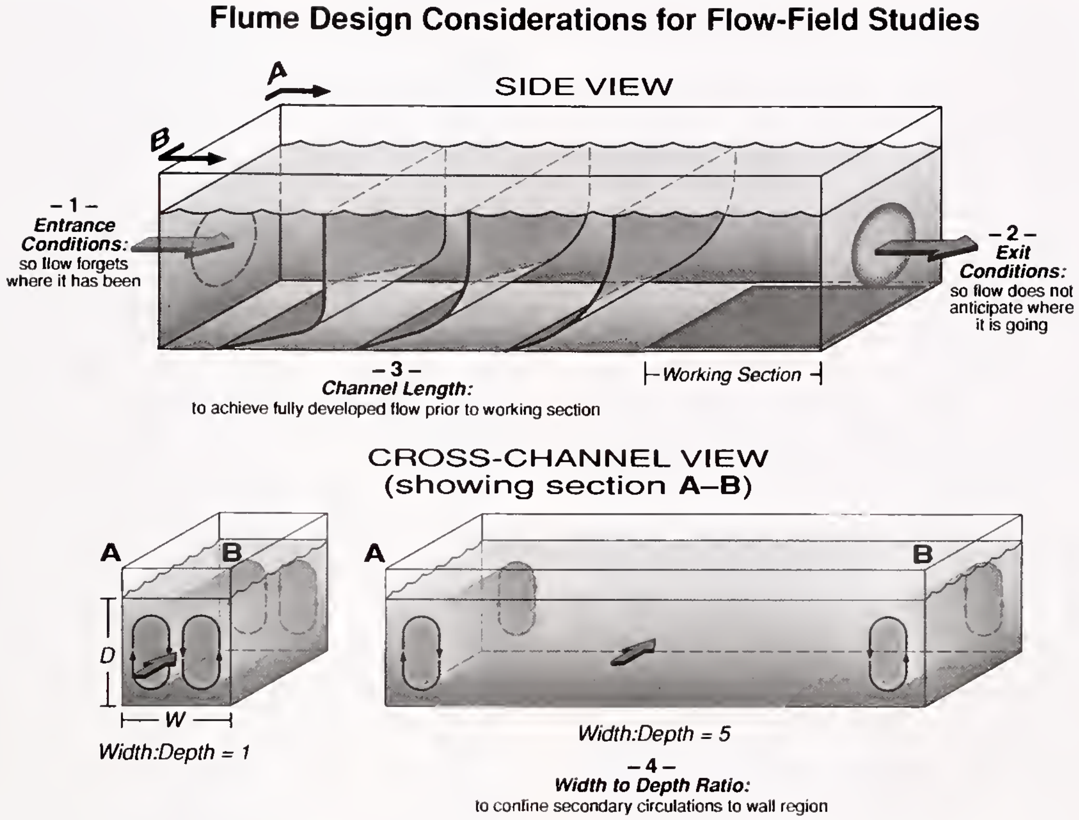
Flume Design Considerations for Flow-Field Studies
SIDE VIEW
A
B
– 1 – Entrance Conditions: so flow forgets where it has been
– 2 – Exit Conditions: so flow does not anticipate where it is going
– 3 – Channel Length: to achieve fully developed flow prior to working section
Working Section
CROSS-CHANNEL VIEW (showing section A–B)
A
B
D
W
Width:Depth = 1
A
B
Width:Depth = 5
– 4 – Width to Depth Ratio: to confine secondary circulations to wall region

Figure 10. The four design considerations—entrance conditions, exit conditions, channel length, and channel width to depth ratio—in constructing a flume for flow-field studies on chemical signaling processes (taken largely from text in Nowell and Jumars, 1987). The side view of the channel (top) is not drawn to scale; a channel length 50–100 times the water depth is generally required for fully developed flow. The specific channel length depends on the range of flow speeds and types (laminar, turbulent) of flow required for the experiments (*e.g.*, see Table 1 in Nowell and Jumars, 1987). Specific entrance and exit conditions to achieve the desired goals depend on the flow-driving mechanism (pump, conveyor belt of paddles, etc.) and the channel configuration (racetrack, return pipe under flume with head tank, etc.). Growth of the boundary layer is shown in the channel region upstream of the working section. If the boundary layer is fully developed prior to the working section, the flow is then one-dimensional (varying only in the vertical) and uniform (not changing in the stream-wise direction) along the working section. The cross-channel view (bottom) shows hypothetical secondary flows (large eddies) generated by the flume side walls. The proportion of the channel width affected by these eddies depends on the ratio of channel width to depth. A minimum ratio of about 5 (shown on right) is generally considered sufficient to confine the eddies to a relatively narrow region next to the walls (Nakagawa *et al.*, 1983; Nowell and Jumars, 1987; Trowbridge *et al.*, 1989). In contrast, a width-to-depth ratio of unity (shown at left) may result in eddies that cover a large portion of the cross-stream area. The nature and strength of secondary circulations can vary with flume design, however, so empirical studies are required to document these flows.

the lower limit of turbulence (of the order of 1 mm for strong turbulence; Shimeta *et al.*, 1995). They also occur, at least intermittently, in the "viscous sublayer"—the small region directly adjacent to a surface in a boundary-layer flow. Because of the small scales over which they occur, chemical transport in laminar-shear flows is relevant only for very tiny organisms, such as small zooplankton, protozoans, phytoplankton, and bacteria. A Couette flow cell—one cylinder nested inside another, with a water-filled gap in between—can be used to create one-dimensional laminar-shear flow. The cylinders must be counter-rotated to avoid instabilities associated with spinning just the inner or outer cylinder (Drazin and Reid, 1981).

Summary and Conclusions: Exciting Future Opportunities and Challenges

Substantial discoveries of chemical interactions between organisms and their environments are now becoming possible because of new conceptual and technological innovations. Recent instrumentation development allows access to even remote field sites. Studies on chemical attractants evoking predation and mechanisms by which scavengers find organic food falls are under way from the coastal ocean to the deep sea. Research on chemical agents as factors regulating habitat selection and colonization is also being vigorously pursued. It is critical for investigators to continue probing the identities of chemicals having these important functions. However, the scope of work must expand significantly beyond secondary metabolites as chemical defenses to include substances that serve other ecological roles. Structures and concentrations of particulate- and organism-bound compounds must be addressed, but in relation to the more elusive waterborne chemical agents. Past investigations have tended to emphasize chemical identities while largely ignoring crucial vehicles of chemical transport. Animal chemical sensors respond quickly when patches of signal molecules are contacted. Because these sensors can detect intermittent (or pulsed) chemical stimuli at 4–5 hertz (Gomez and Atema, 1996), mean concentrations and time-averaged distributions of bioactive compounds might not be indicative of the information available to animals searching for valuable resources. Hence, transport mechanisms relating to such microscale patchiness must be elucidated. Once behavioral and ecological interactions between organisms are better understood, they could be modeled as functions of chemical production and transport dynamics.

Purifications of ecologically relevant molecules other than secondary metabolites will be challenging. Success has been limited in the past because many of these substances are unstable, bind tightly with other molecules, occur in highly complex mixtures, or are found in trace amounts. Nevertheless, recent developments in chemical analytical methods show exciting promise for future research. A wide array of particulate resins is now available to help remove and concentrate bioactive molecules from seawater. Furthermore, fluorescent-labeled antibodies and lectins have been used for partial characterization of the carbohydrate and protein structures of the mating pheromones of rotifers and copepods, respectively, as well as for identification of sites of pheromone reception (Snell *et al.*, 1995; Lonsdsale *et al.*, 1996). Moreover, molecular biological techniques (cDNA encoding a precursor protein and mRNA pheromone transcripts) have been used with mass spectrometry and microsequencing to determine the complete peptide structure of the mating pheromone in sea hares (*Aplysia californica*) (Painter *et al.*, 1998). Finally, mathematical modeling procedures have been developed for predicting the complete structures of novel molecules without the need for fully purified compounds (Browne *et al.*, 1998), and for identifying the taxonomic classes of phytoplankton by using mixtures of chemical markers (MacKey *et al.*, 1996). Creative approaches combining traditional chemistry with new technological methods, such as those described above, seem especially valuable for describing ecologically important factors that structure communities.

Because chemical interactions are vital to all life processes, future research can encompass an almost infinite array of subjects. Therefore, it seems prudent to emphasize those interactions having the greatest ecological significance. A strong foundation of knowledge has now accumulated on the chemical mediation of habitat colonization by larvae and of trophic relationships. Because predation and larval supply are major factors regulating populations and structuring communities, these are particularly cogent lines of inquiry. Chemical effects on essential processes, such as mating, fertilization, competition, and symbiosis, also warrant future studies. Similarly, the chemical ecology of marine microbes is a crucial topic for continuing investigation. Microbes synthesize toxins as secondary metabolites, and they release signal molecules into the environment. These poisons can kill consumers; but when borrowed by eukaryotic hosts, they can subdue prey, deter predators, and chemically defend host embryos. Extracellular secretions are known to regulate the phenotypic expression of bacteria and significantly affect biofilm formation and host infection. When bacterial densities in biofilms or symbiotic interactions become too high, for example, cells release *N*-acylhomoserine lactones to the environment (Pearson *et al.*, 1991; Fuqua *et al.*, 1996; Milton *et al.*, 1997). These substances function as quorum-sensing molecules and lead to the production of antibiotics by bacteria in self-regulating microbial populations. In recent years, microbial pathogens have had large impacts on a variety of organisms including corals, fishes, motile invertebrates, and seaweeds (Hughes, 1994; Alstatt *et al.*, 1996; Burkholder, 1998). An understanding of the chemistry mediating host-pathogen interactions would be an especially welcome addition to population and community ecology.

The consequences of chemically mediated interactions will be an exciting challenge to understand fully. Substantial insight can be gained from the considerable information already available at the individual level. Optimality, signal-detection, and game theories will be helpful in exploring evolutionary relationships between organisms that produce chemical signals and those that receive them with knowledge of the costs and benefits of interactions to reproductive fitness. The collective responses of individuals can be used to predict the dynamics of populations. By way of illustration, rates at which planktonic larvae colonize benthic habitats have been modeled from relationships between larval population densities, swimming (or sinking) speeds, and hydrodynamic forces (Eckman *et al.*, 1994). The effects of chemical cues on swimming and settlement can be easily added to these models. There is a critical need for blending research on chemistry and physics to understand ecological processes—such as larval delivery to adult habitats—that significantly impact populations and communities, and to integrate these studies on chemical mediation within a broader environmental and evolutionary context.

Chemical interactions do not operate in isolation. Discovering their full biological impacts will present an exacting challenge and require interdisciplinary studies on multiple scales of time and space.

Acknowledgments

We thank T. W. Snell, M. J. Weissburg, and G. A. Nevitt for their valuable insights on gamete recognition factors, linkages between sensory physiology and behavior, and the role of dimethylsulfide as an environmental signal molecule, respectively. J. Doucette was responsible for putting our thoughts into illustrations, for which we are especially grateful. Preparation of this manuscript was supported by awards from the National Science Foundation (OCE 97-29972, OCE 97-29980, and OCE 97-51050); the National Sea Grant College Program (R/CZ-152) through the National Marine Biotechnology Initiative; the National Geographic Society; the Council on Research at UCLA; the Pew Fellowship on Conservation and the Environment (NEA 97-04); and the Stanley W. Watson Senior Scientist Chair at WHOI. The students and instructors of the Marine Chemosensory Ecology course at Friday Harbor Laboratories (Summer, 1999), sponsored by the Office of Naval Research (N00014-99-1-0482), contributed to the ideas described in this paper. Contribution number 10,032 of the Woods Hole Oceanographic Institution.

Literature Cited

Adler, J. 1975. Chemotaxis in bacteria. *Annu. Rev. Biochem.* **44:** 341–356.

Agrawal, Y. C., and C. J. Belting. 1988. Laser velocimetry for benthic sediment transport. *Deep-Sea Res.* **35:** 1047–1067.

Alldredge, A. L., and Y. Cohen. 1987. Can microscale chemical patches persist in the sea? Microelectrode study of marine snow. *Science* **235:** 689–691.

Alstatt, J. M., R. F. Ambrose, J. M. Engle, P. L. Haaker, K. D. Lafferty, and P. T. Raimondi. 1996. Recent declines of black abalone *Haliotis cracherodii* on the mainland coast of central California. *Mar. Ecol. Prog. Ser.* **142:** 185–192.

Armitage, J. P. 1992. Behavioral responses in bacteria. *Annu. Rev. Physiol.* **54:** 683–714.

Atema, J., P. A. Moore, L. P. Madin, and G. A. Gerhardt. 1991. Subnose-1: electrochemical tracking of odor plumes at 900 M beneath the ocean surface. *Mar. Ecol. Prog. Ser.* **74:** 303–306.

Azam, F., and J. W. Ammerman. 1984. Cycling of organic matter by bacterioplankton in pelagic ecosystems: microenvironmental considerations. Pp. 345–360 in *Flows of Energy*, M. J. R. Fisher, ed. Academic Press, New York.

Bakus, G. J., N. M. Targett, and B. Schulte. 1986. Chemical ecology of marine organisms: an overview. *J. Chem. Ecol.* **12:** 951–987.

Baxter, G. T., and D. E. Morse. 1992. Cilia from abalone larvae contain a receptor-dependent G protein transduction system similar to that in mammals. *Biol. Bull.* **183:** 147–154.

Berg, H. C. 1983. *Random Walks in Biology.* Princeton University Press, Princeton.

Berg, H. C., and D. A. Brown. 1972. Chemotaxis in *Escherichia coli. Nature* **239:** 500–504.

Boettcher, A. A., and N. M. Targett. 1998. Role of chemical inducers in larval metamorphosis of queen conch, *Strombus gigas* Linnaeus: relationship to other marine invertebrate systems. *Biol. Bull.* **194:** 132–142.

Boland, W. 1995. The chemistry of gamete attraction: chemical structures, biosynthesis, and (a)biotic degradation of algal pheromones. *Proc. Natl. Acad. Sci. USA* **92:** 37–43.

Bonar, D. B., S. L. Coon, M. Walch, R. M. Weiner, and W. Fitt. 1990. Control of oyster settlement and metamorphosis by endogenous and exogenous chemical cues. *Bull. Mar. Sci.* **46:** 484–498.

Borroni, P. F., and J. Atema. 1988. Adaptation in chemoreceptor cells. I: Self-adapting backgrounds determine thresholds and cause parallel shifts of dose-response functions. *J. Comp. Physiol. A* **164:** 67–74.

Boulay, F., L. Mery, M. Tardif, L. Brouchon, and P. Vignais. 1991. Expression cloning of a receptor for the C5a anaphylatoxin on differentiated HL-60 cells. *Biochemistry* **30:** 2993–2999.

Bowen, J. D., K. D. Stolzenbach, and S. W. Chisholm. 1993. Simulating bacterial clustering around phytoplankton cells in a turbulent ocean. *Limnol. Oceanogr.* **38:** 36–51.

Browne, K. A., M. N. Tamburri, and R. K. Zimmer-Faust. 1998. Modelling quantitative structure-activity relationships between animal behaviour and environmental signal molecules. *J. Exp. Biol.* **201:** 245–258.

Bundy, M. H., T. F. Gross, H. A. Vanderploeg, and J. R. Strickler. 1998. Perception of inert particles by calanoid copepods: behavioral observations and a numerical model. *J. Plankton Res.* **20:** 2129–2152.

Burke, R. D. 1984. Pheromonal control of metamorphosis in the Pacific sand dollar, *Dendraster excentricus. Science* **225:** 442–443.

Burkholder, J. M. 1998. Implications of harmful microalgae and heterotrophic dinoflagellates in management of sustainable marine fisheries. *Ecol. Appl.* **8:** S37–S62.

Busdosh, M., G. A. Robilliard, K. Tarbox, and C. L. Beehler. 1982. Chemoreception in an Arctic amphipod crustacean: a field study. *J. Exp. Mar. Biol. Ecol.* **62:** 261–269.

Butman, C. A. 1987. Larval settlement of soft-sediment invertebrates: the spatial scales of patterns explained by active habitat selection and the emerging role of hydrodynamical processes. *Oceanogr. Mar. Biol. Annu. Rev.* **25:** 113–165.

Carr, W. E. S. 1988. The molecular nature of chemical stimuli in the aquatic environment. Pp. 3–27 in *The Sensory Biology of Aquatic Animals*, J. Atema, R. R. Fay, A. N. Popper, and W. N. Tavolga, eds. Springer-Verlag, New York.

Carr, W. E. S., and C. D. Derby. 1986. Chemically stimulated feeding behavior in marine animals: implications of chemical mixtures and involvement of mixture interactions. *J. Chem. Ecol.* **12:** 989–1011.

Carr, W. E. S., J. C. Netherton III, R. A. Gleeson, and C. D. Derby. 1996. Stimulants of feeding behavior in fish: analyses of tissues of diverse marine organisms. *Biol. Bull.* **190:** 149–160.

Case, J. 1964. Properties of the dactyl chemoreceptors of *Cancer antennarius* Stimpson and *C. productus* Randall. *Biol. Bull.* **127:** 428–446.

Crisp, D. J. 1974. Factors influencing the settlement of marine invertebrate larvae. Pp. 177–263 in *Chemoreception in Marine Organisms*, P. T. Grant and A. M. Mackie, eds. Academic Press, New York.

Cronin, G., and M. E. Hay. 1996. Induction of seaweed chemical defenses by amphipod grazing. *Ecology* **77:** 2287–2301.

Dacey, J. W. H., and S. G. Wakeham. 1986. Oceanic dimethylsulfide: production during zooplankton grazing on phytoplankton. *Science* **233:** 1314–1316.

Dacey, J. W. H., G. M. King, and S. G. Wakeham. 1987. Factors controlling emission of dimethylsulfide from salt marshes. *Nature* **330:** 643–645.

Davis, A. D., T. M. Weatherby, D. K. Hartline, and P. H. Lenz. 1999.

Myelin-like sheaths in copepod axons. *Nature* **398:** 571.

Dean, T. A., S. C. Schroeter, and J. Dixon. 1984. Grazing by red and white sea urchins and its effect on the recruitment and survival of kelp. *Mar. Biol.* **78:** 301–313.

Decho, A. W., K. A. Browne, and R. K. Zimmer-Faust. 1998. Chemical cues: why basic peptides are signal molecules in marine environments. *Limnol. Oceanogr.* **43:** 1410–1417.

Denny, M. W. 1988. *Biology and the Mechanics of the Wave-Swept Environment.* Princeton University Press, Princeton.

Denny, M. W., T. L. Daniel, and M. A. R. Koehl. 1985. Mechanical limits to size in wave-swept organisms. *Ecol. Monogr.* **55:** 69–102.

Derby, C. D., M. N. -Giardot, P. C. Daniel. and J. B. Fine-Levy. 1989. Odor discrimination of mixtures: behavioral, electrophysiological and theoretical studies using the spiny lobster. Pp. 65–82 in *Perception of Complex Smells and Taste,* D. G. Laing, W. S. Cain, R. L. McBride, and B. W. Ache, eds. Academic Press, New York.

Derby, C. D., M. Hudson, B. A. Livermore, and W. H. Lynn. 1996. Generalization among related complex odorant mixtures and their components: analysis of olfactory perception in the spiny lobster. *Physiol. Behav.* **60:** 87–95.

Doall, M. H., S. P. Colin, J. R. Strickler, and J. Yen. 1998. Locating a mate in 3D: the case of *Temora longicornis. Philos. Trans. R. Soc. Lond. B* **353:** 681–689.

Drazin, P., and W. Reid. 1981. *Hydrodynamic Stability.* Cambridge University Press, Cambridge.

Dulka, J. G., N. E. Stacey, P. W. Sorensen, and G. J. van der Kraak. 1987. Sex steroid pheromone synchronizes male-female spawning readiness in the goldfish. *Nature* **325:** 251–253.

Eckman, J. E., F. E. Werner, and T. F. Gross. 1994. Modeling some aspects of behavior on larval settlement in a turbulent boundary layer. *Deep-Sea Res. II* **41:** 185–208.

Ellingsen, O. F., and K. B. Døving. 1986. Chemical fractionation of shrimp extracts inducing bottom food search behavior in cod (*Gadus morhua*). *J. Chem. Ecol.* **12:** 155–168.

Ember, J. A., S. D. Sanderson, S. M. Taylor, M. Kawahara, and T. E. Hugli. 1992. Biologic activity of synthetic analogs of C5a anaphylatoxin. *J. Immunol.* **148:** 3165–3173.

Estes, J. A., and J. F. Palmisano. 1974. Sea otters: their role in structuring nearshore communities. *Science* **185:** 1058–1060.

Estes, J. A., and P. D. Steinberg. 1988. Predation, herbivory, and kelp evolution. *Paleobiology* **14:** 19–36.

Falkowski, P. G., Z. Dubinsky, L. Muscatine, and J. W. Porter. 1984. Light and the bioenergetics of a symbiotic coral. *BioScience* **34:** 705–709.

Fine-Levy, J. B., P. C. Daniel, M.-N. Girardot, and C. D. Derby. 1989. Behavioral resolution of quality of odorant mixtures by spiny lobsters: differential aversive conditioning of olfactory responses. *Chem. Senses* **14:** 503–524.

Finelli, C. M., N. D. Pentcheff, R. K. Zimmer-Faust, and D. S. Wethey. 1999. Odor transport in turbulent flows: constraints on animal navigation. *Limnol. Oceanogr.* **44:** 1056–1071.

Foltz, K. R., and W. J. Lennarz. 1994. The molecular basis of sea urchin gamete interactions at the egg plasma membrane. *Dev. Biol.* **5:** 233–242.

Forward, R. B., Jr., D. Rittschof, and M. C. De Vries. 1987. Peptide pheromones synchronize crustacean egg hatching and larval release. *Chem. Senses* **12:** 491–498.

Forward, R. B., Jr., R. A. Tankersley, D. Blondel, and D. Rittschof. 1997. Metamorphosis of the blue crab *Callinectes sapidus:* effects of humic acids and ammonium. *Mar. Ecol. Prog. Ser.* **157:** 277–286.

Fuqua, W. C., S. C. Winans, and E. P. Greenberg. 1996. Census and consensus in bacterial ecosystems: the luxR-luxI family of quorum-sensing transcriptional regulators. *Annu. Rev. Microbiol.* **50:** 727–751.

Gates, R. D., O. Hoegh-Guldberg, M. J. McFall-Ngai, K. Y. Bil, and L. Muscatine. 1995. Free amino acids exhibit anthozoan "host factor" activity: They induce the release of photosynthate from symbiotic dinoflagellates *in vitro. Proc. Natl. Acad. Sci. USA* **92:** 7430–7434.

Gates, R. D., K. Y. Bil, and L. Muscatine. 1999. The influence of anthozoan "host factor" on the physiology of a symbiotic dinoflagellate. *J. Exp. Mar. Biol. Ecol.* **232:** 241–259.

Gerard, N. P., and C. Gerard. 1991. The chemotactic receptor for human C5a anaphylatoxin. *Nature* **349:** 614–617.

Gil-Turner, M. S., M. E. Hay, and W. Fenical. 1989. Symbiotic marine bacteria chemically defend crustacean embryos from a pathogenic fungus. *Science* **246:** 116–118.

Gleeson, R. A., M. A. Adams, and A. B. Smith, III. 1984. Characterization of a sex pheromone in the blue crab, *Callinectes sapidus:* crusteedysone studies. *J. Chem. Ecol.* **10:** 913–921.

Gomez, G., and J. Atema. 1996. Temporal resolution in olfaction: stimulus integration time of lobster chemoreceptor cells. *J. Exp. Biol.* **199:** 1171–1179.

Gomez, G., R. Voigt, and J. Atema. 1994. Frequency filter properties of lobster chemoreceptors cells determined with high-resolution stimulus measurement. *J. Comp. Physiol. A* **174:** 803–811.

Grant, W. D., and O. S. Madsen. 1986. The continental shelf bottom boundary layer. *Annu. Rev. Fluid Mech.* **18:** 265–305.

Grove, M. W., and S. A. Woodin. 1996. Conspecific recognition and host choice in a pea crab, *Pinnixa chaetopterana* (Brachyura: Pinnotheridae). *Biol. Bull.* **190:** 359–366.

Gurin, S., and W. E. S. Carr. 1974. Chemoreception in *Nassarius obsoletus:* the role of specific stimulatory proteins. *Science* **174:** 293–295.

Hadfield, M. G., and J. T. Pennington. 1990. Nature of the metamorphic signal and its internal transduction in larvae of the nudibranch *Phestilla sibogae. Bull. Mar. Sci.* **46:** 455–464.

Hadfield, M. G., and D. Scheuer. 1985. Evidence for a soluble metamorphic inducer in *Phestilla:* ecological, chemical and biological data. *Bull. Mar. Sci.* **37:** 556–566.

Haldane, J. B. S. 1954. La signalisation animale. *Annee Biol.* **58:** 89–98.

Hamner, W. M., P. P. Hamner, S. W. Strand, and R. W. Gilmore. 1983. Behavior of Antarctic krill, *Euphausia superba:* chemoreception, feeding, schooling and molting. *Science* **220:** 433–435.

Hardege, J. D., M. G. Bentley, M. Beckmann, and C. Mueller. 1996. Sex pheromones in marine polychaetes: volatile organic substances (VOS) isolated from *Arenicola marina. Mar. Ecol. Prog. Ser.* **139:** 157–166.

Harrold, C., and D. C. Reed. 1985. Food availability, sea urchin grazing and kelp forest community structure. *Ecology* **66:** 1160–1169.

Hay, M. E. 1992. Seaweed chemical defenses: their roles in the evolution of feeding specialization and in mediating complex interactions. Pp. 93–118 in *Ecological Roles for Marine Secondary Metabolites,* V. J. Paul, ed. Explorations in Chemical Ecology Series, Comstock Publishing Associates, Ithaca, NY.

Hay, M. E. 1996. Marine chemical ecology: What's known and what's next. *J. Exp. Mar. Biol. Ecol.* **200:** 103–134.

Hay, M. E., and W. Fenical. 1988. Marine plant-herbivore interactions: the ecology of chemical defense. *Annu. Rev. Ecol. Syst.* **19:** 111–145.

Henderson, F. M. 1966. *Open Channel Flow.* Macmillan, New York.

Hofmann, A., and C. G. Glabe. 1994. Bindin, a multifunctional sperm ligand and the evolution of new species. *Semin. Dev. Biol.* **5:** 233–242.

Howe, N. R., and Y. M. Sheikh. 1975. Anthopleurine: a sea anemone alarm pheromone. *Science* **189:** 386–388.

Hughes, J. 1978. Opioid peptides. Pp. 283–293 in *Neuronal Information Transfer,* A. Karlin, V. M. Tennyson, and H. J. Vogel, eds. Academic Press, New York.

Hughes, T. P. 1994. Catastrophes, phase shifts, and large-scale degradation of a Caribbean coral reef. *Science* **265:** 1547–1551.

Ingram, C. L., and R. R. Hessler. 1983. Distribution and behavior of scavenging amphipods from the central North Pacific. *Deep-Sea Res.* **30:** 683–706.

Jackson, J. B. C. 1977. Competition on marine hard substrata: the adaptive significance of solitary and colonial strategies. *Am. Nat.* **111:** 743–767.

Jensen, R. A., and D. E. Morse. 1984. Intraspecific facilitation of larval recruitment: gregarious settlement of the polychaete *Phragmatopoma californica* (Fewkes). *J. Exp. Mar. Biol. Ecol.* **83:** 107–126.

Jensen, R. A., and D. E. Morse. 1988. The bioadhesive of *Phragmatopoma californica* tubes: a silk-like cement containing L-DOPA. *J. Comp. Physiol. B* **158:** 317–324.

Jensen, R. A., D. E. Morse, R. L. Petty, and N. Hooker. 1990. Artificial induction of larval metamorphosis by free fatty acids. *Mar. Ecol. Prog. Ser.* **67:** 55–71.

Karp-Boss, L., E. Karp-Boss, and P. A. Jumars. 1996. Nutrient fluxes to phytoplankton osmotrophs in the presence of fluid motion. *Oceanogr. Mar. Biol. Annu. Rev.* **34:** 71–107.

Kaufmann, R. S. 1992. The behavior, physiology and ecology of scavenging lysianassoid amphipods, with comparisons between shallow- and deep-water species. Ph.D. dissertation, University of California, San Diego.

King, G. M. 1986. Inhibition of microbial activity in marine sediments by a bromophenol from a hemichordate. *Nature* **323:** 257–259.

Knowlton, N. 1993. Sibling species in the sea. *Annu. Rev. Ecol. Syst.* **24:** 189–216.

Koehl, M. A. R. 1977. Effects of sea anemones on the flow forces they encounter. *J. Exp. Biol.* **69:** 87–105.

Koehl, M. A. R. 1996. Small scale fluid dynamics of olfactory antennae. *Mar. Freshw. Behav. Physiol.* **27:** 127–141.

Konig, W. 1993. *Peptide and Protein Hormones: Structure, Regulation, Activity: A Reference Manual.* VCH Press, New York.

Krug, P. J., and A. E. Manzi. 1999. Waterborne and surface-associated carbohydrates as settlement cues for larvae of the specialist marine herbivore *Alderia modesta. Biol. Bull.* **197:** 94–103.

Kvitek, R. G., A. R. DeGrange, and M. K. Beitler. 1991. Paralytic shellfish poisoning toxins mediate feeding behavior of sea otters. *Limnol. Oceanogr.* **36:** 393–404.

Lee, Y. H., and V. D. Vacquier. 1992. The divergence of species-specific abalone sperm lysins is promoted by positive Darwinian selection. *Biol. Bull.* **182:** 97–104.

Lehninger, A. L., D. L. Nelson, and M. M. Cox. 1993. *Principles of Biochemistry,* 2nd ed. Worth Publishers, New York.

Leonard, G. H., M. D. Bertness, and P. O. Yund. 1999. Crab predation, waterborne cues, and inducible defenses in the blue mussel, *Mytilus edulis. Ecology* **80:** 1–14.

Lindquist, N., and M. E. Hay. 1996. Palatability and chemical defense of marine invertebrate larvae. *Ecol. Monogr.* **66:** 431–450.

Lonsdale, D. J., and T. W. Snell. 1996. Lectin binding to surface glycoproteins on *Coullana* spp. (Copepoda: Harpacticoida) can inhibit mate guarding. *Mar. Freshw. Behav. Physiol.* **27:** 153–162.

Luther, W. 1930. Versuche über die Chemorezeption der Brachuren. *Z. Vgl. Physiol.* **12:** 177–205.

Lynn, W. H., E. A. Meyer, C. E. Peppiatt, and C. D. Derby. 1994. Perception of odor mixtures by the spiny lobster, *Panulirus argus. Chem. Senses* **19:** 331–347.

MacKey, M. D., D. J. MacKey, H. W. Higgins, and S. W. Wright. 1996. CHEMTAX—a program for estimating class abundances from chemical markers: application to HPLC measurements of phytoplankton. *Mar. Ecol. Prog. Ser.* **144:** 265–283.

Maier, I., and D. G. Müller. 1986. Sex pheromones in algae. *Biol. Bull.* **170:** 145–175.

Manson, M. D. 1992. Bacterial motility and chemotaxis. *Adv. Microb. Physiol.* **33:** 3699–3704.

Matrai, P., and M. D. Keller. 1994. Total organic sulfur and dimethylsulfoniopropionate in marine phytoplankton: intracellular variations. *Mar. Biol.* **119:** 61–68.

McClintock, J. B. 1997. A review of the chemical ecology of Antarctic marine invertebrates. *Am. Zool.* **37:** 329–342.

McClintock, J. B., and J. Janssen. 1990. Pteropod abduction as a chemical defense in a pelagic Antarctic amphipod. *Nature* **346:** 462–464.

Miller, D. C., M. J. Bock, and E. J. Turner. 1992. Deposit and suspension feeding in oscillatory flows and sediment fluxes. *J. Mar. Res.* **50:** 489–520.

Milton, D. L., A. Hardman, M. Camara, S. R. Chhabra, B. W. Bycroft, G. S. A. B. Stewart, and P. Williams. 1997. Quorum sensing in *Vibrio anguillarum:* characterization of vanI/vanR locus and identification of the autoinducer *N*-(3-oxodecanoyl)-L-homoserine lactone. *J. Bacteriol.* **179:** 3004–3012.

Moore, P. A., and D. M. E. Lepper. 1997. Role of chemical signals in the orientation behavior of the sea star *Asterias forbesi. Biol. Bull.* **192:** 410–417.

Moore, P. A., G. A. Gerhardt, and J. Atema. 1989. High resolution spatio-temporal analysis of aquatic chemical signals using microelectrochemical electrodes. *Chem. Senses* **14:** 823–840.

Moore, P. A., D. M. Fields, and J. Yen. 1999. Physical constraints of chemoreception in foraging copepods. *Limnol. Oceanogr.* **44:** 166–177.

Morse, A. N. C. 1991. How do planktonic larvae know where to settle? *Am. Sci.* **79:** 154–167.

Morse, A. N. C., and D. E. Morse. 1984. Recruitment and metamorphosis of *Haliotis* larvae induced by molecules uniquely available at the surfaces of crustose red algae. *J. Exp. Mar. Biol. Ecol.* **75:** 191–215.

Morse, D. E. 1985. Neurotransmitter-mimetic inducers of larval settlement and metamorphosis. *Bull. Mar. Sci.* **37:** 697–706.

Morse, D. E. 1990. Recent progress in larval settlement: closing the gap between molecular biology and ecology. *Bull. Mar. Sci.* **46:** 465–483.

Morse, D. E., and A. N. C. Morse. 1991. Enzymatic characterization of the morphogen recognized by *Agaricia humilis* (Scleractinian coral) larvae. *Biol. Bull.* **181:** 104–122.

Morse, D. E., N. Hooker, H. Duncan, and L. Jensen. 1979. γ-Aminobutyric acid, a neurotransmitter, induces planktonic abalone larvae to settle and metamorphose. *Science* **204:** 407–410.

Mullineaux, L. S., and C. A. Butman. 1991. Initial contact, exploration, and attachment of barnacle cyprids settling in flow. *Mar. Biol.* **110:** 93–103.

Mullineaux, L. S., and E. D. Garland. 1993. Larval recruitment in response to manipulated field flows. *Mar. Biol.* **116:** 667–683.

Muscatine, L. 1990. The role of symbiotic algae in carbon and energy flux in coral reefs. Pp. 75–87 in *Coral Reefs: Ecosystems of the World,* Vol. 25, Z. Dubinsky, ed. Elsevier, Amsterdam.

Muschenheim, D. K., J. Grant, and E. L. Mills. 1986. Flumes for benthic ecologists: theory, construction and practice. *Mar. Ecol. Prog. Ser.* **28:** 185–196.

Nagle, D. G., and V. J. Paul. 1998. Chemical defense of a marine cyanobacterial bloom. *J. Exp. Mar. Biol. Ecol.* **225:** 29–38.

Nagle, D. G., F. T. Camacho, and V. J. Paul. 1998. Dietary preferences of the opisthobranch mollusc *Stylocheilus longicauda* for secondary metabolites produced by the tropical cyanobacterium *Lyngbya majuscula. Mar. Biol.* **132:** 267–273.

Nakagawa, H., I. Nezu, and A. Tominaga. 1983. Secondary currents in straight channel flow and the relation to its aspect ratio. Pp. 3.8–3.18 in *Fourth Symposium on Turbulent Shear Flows,* Karlsruhe, Germany.

Nevitt, G. A. 2000. Olfactory foraging by Antarctic Procellariiform seabirds: life at high Reynolds numbers. *Biol. Bull.* **198:** 245–253.

Nevitt, G. A., R. R. Veit, and P. M. Karieva. 1995. Dimethyl sulfide as a foraging cue for Antarctic Procellariiform seabirds. *Nature* **376:** 680–682.

Nezu, I., and W. Rodi. 1986. Open channel flow measurements with a laser Doppler anemometer. *J. Hydraulic Eng.* **112:** 335–355.

Noga, E. J., L. Khoo, J. R. Stevens, Z. Fan, and J. M. Burkholder. 1996. Novel toxic dinoflagellates cause epidemic diseases in estuarine fish. *Mar. Pollut. Bull.* **32:** 219–224.

Nowell, A. R. M., and P. A. Jumars. 1987. Flumes: theoretical and experimental considerations for simulation of benthic environments. *Oceanogr. Mar. Biol. Annu. Rev.* **25:** 91–112.

Nowell, A. R. M., P. A. Jumars, R. F. Self, and J. B. Southard. 1989. The effects of sediment transport and deposition on infauna: results in a specially designed flume. Pp. 247–268 in *Ecology of Marine Deposit Feeders*, G. Lopez, J. Levinton, and G. Taghon, eds. Lecture Notes on Coastal and Estuarine Studies 31, Springer-Verlag, New York.

Okamura, B. 1985. The effects of ambient flow velocity, colony size, and upstream colonies on the feeding success of Bryozoa. II. *Conopeum reticulum* (Linnaeus), an encrusting species. *J. Exp. Mar. Biol. Ecol.* **89:** 69–80.

O'Riordan, C. A., S. G. Monismith, and J. R. Koseff. 1993. A study of concentration boundary-layer formation over a bed of model bivalves. *Limnol. Oceanogr.* **38:** 1712–1729.

Paerl, H. W. 1988. Nuisance phytoplankton blooms in coastal, estuarine, and inland waters. *Limnol. Oceanogr.* **33:** 823–847.

Paffenhoefer, G.-A. 1998. On the relation of structure, perception and activity in marine planktonic copepods. *J. Mar. Systems* **15:** 457–473.

Painter, S. D., B. Clough, R. W. Garden, J. V. Sweedler, and G. T. Nagle. 1998. Characterization of *Aplysia* attractin, the first waterborne peptide pheromone in invertebrates. *Biol. Bull.* **194:** 120–131.

Palumbi, S. R. 1994. Genetic divergence, reproductive isolation, and marine speciation. *Annu. Rev. Ecol. Syst.* **24:** 189–216.

Paul, V. J., ed. 1992. *Ecological Roles for Marine Secondary Metabolites.* Explorations in Chemical Ecology Series, Comstock Publications Associates, Ithaca, NY.

Paul, V. J., and K. L. van Alstyne. 1992. Activation of chemical defenses in the tropical green algae, *Halimeda* spp. *J. Exp. Mar. Biol. Ecol.* **160:** 191–203.

Pawlik, J. R. 1986. Chemical induction of larval settlement and metamorphosis in the reef-building tube worm *Phragmatopoma californica* (Polychaeta: Sabellariidae). *Mar. Biol.* **91:** 59–68.

Pawlik, J. R. 1992. Chemical ecology of the settlement of benthic marine invertebrates. *Oceanogr. Mar. Biol. Annu. Rev.* **30:** 273–335.

Pawlik, J. R. 1993. Marine invertebrate chemical defenses. *Chem. Rev.* **93:** 1911–1922.

Pawlik, J. R., and C. A. Butman. 1993. Settlement of a marine tube worm as a function of current velocity: interacting effects of hydrodynamics and behavior. *Limnol. Oceanogr.* **38:** 1730–1740.

Pawlik, J. R., and D. J. Faulkner. 1986. Specific free fatty acids induce larval settlement and metamorphosis of the reef-building tube worm *Phragmatopoma californica* (Fewkes). *J. Exp. Mar. Biol. Ecol.* **102:** 301–310.

Pawlik, J. R., C. A. Butman, and V. R. Starczak. 1991. Hydrodynamic facilitation of gregarious settlement of a reef-building tube worm. *Science* **251:** 421–424.

Pearson, J. P., K. M. Gray, L. Passador, K. D. Tucker, A. Eberhard, B. H. Iglewski, and E. P. Greenberg. 1991. Structure of the autoinducer required for expression of *Pseudomonas aeruginosis* virulence genes. *Proc. Natl. Acad. Sci. USA* **91:** 197–201.

Pearson, W. H., and B. L. Olla. 1977. Chemoreception in the blue crab, *Callinectes sapidus. Biol. Bull.* **153:** 346–354.

Pennings, S. C., S. R. Pablo, V. J. Paul, and J. E. Duffy. 1994. Effects of sponge metabolites in different diets on feeding by three groups of consumers. *J. Exp. Mar. Biol. Ecol.* **180:** 137–149.

Prasad, R. R., and K. R. Sreenivasan. 1990. Quantitative three-dimensional imaging in the structure of passive scalar fields in fully turbulent flows. *J. Fluid Mech.* **216:** 1–34.

Ratchford, S. G., and D. B. Eggleston. 1998. Size- and scale-dependent chemical attraction contribute to an ontogenetic shift in sociality. *Anim. Behav.* **56:** 1027–1034.

Renninger, G. H., L. Kass, R. A. Gleeson, C. L. Van Dover, B.-A. Battelle, R. N. Jinks, E. D. Herzog, and S. C. Chamberlain. 1995. Sulfide as a chemical stimulus for deep-sea hydrothermal vent shrimp. *Biol. Bull.* **189:** 69–76.

Rittschof, D. 1990. Peptide-mediated behaviors in marine organisms: evidence for a common theme. *J. Chem. Ecol.* **16:** 261–272.

Rittschof, D., R. Shepherd, and L. G. Williams. 1984. Concentration and preliminary characterization of a chemical attractant of the oyster drill, *Urosalpinx cinerea. J. Chem. Ecol.* **10:** 63–79.

Rodriquez, S., F. Patricio-Ojeda, and N. Inestrosa. 1993. Settlement of benthic marine invertebrates. *Mar. Ecol. Prog. Ser.* **97:** 193–207.

Sainte-Marie, B., and B. T. Hargrave. 1987. Estimation of scavenger abundance and distance of attraction to bait. *Mar. Biol.* **94:** 431–443.

Scheltema, R. S. 1974. Biological interactions determining larval settlement of marine invertebrates. *Thalassia Jugosl.* **10:** 263–269.

Schlichting, H. 1979. *Boundary-Layer Theory,* 7th ed. McGraw-Hill, New York.

Shimeta, J., P. A. Jumars, and E. J. Lessard. 1995. Influences of turbulence on suspension feeding by planktonic protozoa: experiments in laminar shear fields. *Limnol. Oceanogr.* **40:** 845–859.

Simenstad, C. A., J. A. Estes, and K. W. Kenyon. 1978. Aleuts, sea otters, and alternative stable-state communities. *Science* **200:** 403–411.

Sleeper, H. L., V. J. Paul, and W. Fenical. 1980. Alarm pheromones from the marine opisthobranch, *Navanax inermis. J. Chem. Ecol.* **6:** 57–70.

Snell, T. W., R. Rico-Martinez, L. N. Kelly, and T. E. Battle. 1995. Identification of a sex pheromone from a rotifer. *Mar. Biol.* **123:** 347–353.

Sorensen, P. W. 1992. Hormonally derived sex pheromones in goldfish: a model for understanding the evolution of sex pheromone systems in fish. *Biol. Bull.* **183:** 173–177.

Sorensen, P. W., T. A. Christensen, and N. E. Stacey. 1998. Discrimination of pheromonal cues in fish: emerging parallels with insects. *Curr. Opin. Neurobiol.* **8:** 458–467.

Stachowicz, J. J., and M. E. Hay. 1996. Facultative mutualism between an herbivorous crab and a coralline alga: advantages of eating noxious seaweeds. *Oecologia* **105:** 377–387.

Steinberg, P. D. 1995. Seasonal variation in the relationship between growth rate and phlorotannin production in the kelp *Ecklonia radiata. Oecologia* **102:** 169–173.

Steinberg, P. D., J. A. Estes, and F. C. Winter. 1995. Evolutionary consequences of food chain length in kelp forest communities. *Proc. Natl. Acad. Sci. USA* **92:** 8145–8148.

Strickler, J. R., K. D. Squires, H. Yamazaki, and A. H. Abib. 1997. Combining analog turbulence with digital turbulence. *Sci. Mar.* **61:** 197–204.

Swenson, D. P., and J. B. McClintock. 1998. A quantitative assessment of chemically mediated rheotaxis in the asteroid, *Coscinasterias tenuispina. Mar. Freshw. Behav. Physiol.* **31:** 63–80.

Tamburri, M. N., and J. P. Barry. 1999. Adaptations for scavenging by three diverse bathyl species, *Eptatretus stouti, Neptunea amianta* and *Orchomene obstusus. Deep-Sea Res.* **46:** 2079–2093.

Tamburri, M. N., C. M. Finelli, D. S. Wethey, and R. K. Zimmer-Faust. 1996. Chemical induction of larval settlement behavior in flow. *Biol. Bull.* **191:** 367–373.

Targett, N. M., and T. M. Arnold. 1998. Predicting the effects of brown algal phlorotannins on marine herbivores in tropical and temperate oceans. *J. Phycol.* **34:** 195–205.

Targett, N. M., A. A. Boettcher, T. E. Targett, and N. H. Vrolijk. 1995. Tropical marine herbivore assimilation of phenolic-rich plants. *Oecologia* **103:** 170–179.

Thacker, R. W., M. A. Becerro, W. A. Lumbang, and V. J. Paul. 1998. Allelopathic interactions between sponges on a tropical reef. *Ecology* **79:** 1740–1750.

Thorson, G. 1966. Some factors influencing the recruitment and establishment of marine benthic communities. *Neth. J. Sea Res.* **3:** 267–293.

Trapido-Rosenthal, H. G., W. E. S. Carr, and R. A. Gleeson. 1987. Biochemistry of an olfactory purinergic system: dephosphorylation of excitatory nucleotides and uptake of adenosine. *J. Neurochem.* **49:** 1174–1182.

Trowbridge, J. H., W. R. Geyer, C. A. Butman, and R. J. Chapman. 1989. *The 17-Meter Flume at the Coastal Research Laboratory. Part II: Flow Characteristics.* Woods Hole Oceanographic Institution, Technical Report WHOI-89-11. 37 pp.

Turner, E. J., and D. C. Miller. 1991a. Behavior of a passive suspension-feeder (*Spiochaetopterus oculatus* (Webster)) under oscillatory flow. *J. Exp. Mar. Biol. Ecol.* **149:** 123–137.

Turner, E. J., and D. C. Miller. 1991b. Behavior and growth of *Mercenaria mercenaria* during simulated storm events. *Mar. Biol.* **111:** 55–64.

Turner, E. J., R. K. Zimmer-Faust, M. A. Palmer, M. Luckenbach, and N. D. Pentcheff. 1994. Settlement of oyster (*Crassostrea virginica*) larvae: effects of water flow and a water-soluble chemical cue. *Limnol. Oceanogr.* **39:** 1579–1593.

Vadas, R. L., M. T. Burrows, and R. N. Hughes. 1994. Foraging strategies of dogwhelks, *Nucella lapillus* (L.): interacting effects of age, diet and chemical cues to the threat of predation. *Oecologia* **100:** 439–450.

Vairavamurthy, A., M. O. Andreae, and R. L. Iversen. 1985. Biosynthesis of dimethyl propiothetic by *Hymenomonas carterae* in relation to sulfur source and salinity variations. *Limnol. Oceanogr.* **30:** 59–70.

Valentincic, T., S. Weigert, and J. Caprio. 1994. Learned olfactory discrimination versus innate taste responses to amino acids in channel catfish (*Ictalurus punctatus*). *Physiol. Behav.* **55:** 865–873.

Van Dyke, M. 1982. *An Album of Fluid Motion.* Parabolic Press, Stanford, CA.

Van Wazer, J. R., J. W. Lyons, K. Y. Kim, and R. E. Colwell. 1963. *Viscosity and Flow Measurement.* Interscience, New York.

Vervoort, H. C., J. R. Pawlik, and W. Fenical. 1998. Chemical defense of the Caribbean ascidian *Didemnum conchyliatum. Mar. Ecol. Prog. Ser.* **164:** 221–228.

Vogel, S. 1994. *Life in Moving Fluids: The Physical Biology of Flow,* 2nd ed. Princeton University Press, Princeton.

Vogel, S., and M. LaBarbera. 1978. Simple flow tanks for research and teaching. *BioScience* **28:** 638–643.

Vrolijk, N. H., and N. M. Targett. 1992. Biotransformation enzymes in *Cyphoma gibbosum* (Gastropoda: Ovulidae): implications for detoxification of gorgonian allelochemicals. *Mar. Ecol. Prog. Ser.* **88:** 237–246.

Wanninkhof, R., J. R. Ledwell, and A. J. Watson. 1991. Analysis of sulfur hexafluoride in seawater. *J. Geophys. Res. Oceans* **96:** 8733–8740.

Weissburg, M. J. 2000. The fluid dynamical context of chemosensory behavior. *Biol. Bull.* **198:** 188–202.

Weissburg, M. J., and R. K. Zimmer-Faust. 1993. Life and death in moving fluids: hydrodynamic effects on chemosensory-mediated predation. *Ecology* **74:** 1428–1443.

Weissburg, M. J., and R. K. Zimmer-Faust. 1994. Odor plumes and how blue crabs use them in finding prey. *J. Exp. Biol.* **197:** 349–375.

Weissburg, M. J., M. H. Doall, and J. Yen. 1998. Following the invisible trail: mechanisms of chemosensory mate tracking by the copepod *Temora longicornis. Philos. Trans. R. Soc. Lond. B* **353:** 701–712.

Wodicka, L. M., and D. E. Morse. 1991. cDNA sequences reveal mRNAs for two Gα signal transducing proteins from larval cilia. *Biol. Bull.* **180:** 318–327.

Wolfe, G. V. 2000. The chemical defense ecology of marine unicellular plankton: constraints, mechanisms, and impacts. *Biol. Bull.* **198:** 225–244.

Wolfe, G. V., M. Steinke, and G. O. Kirst. 1997. Grazing-activated chemical defense in a unicellular marine alga. *Nature* **387:** 894–897.

Wood, D. E., R. A. Gleeson, and C. D. Derby. 1995. Modulation of behavior by biogenic amines and peptides in the blue crab, *Callinectes sapidus. J. Comp. Physiol. A* **177:** 321–333.

Woodin, S. A., R. L. Marinelli, and D. E. Lincoln. 1993. Allelochemical inhibition of recruitment in a secondary assemblage. *J. Chem. Ecol.* **19:** 517–530.

Yen, J. 2000. Life in transition: balancing inertial and viscous forces by planktonic copepods. *Biol. Bull.* **198:** 213–224.

Yoon, H.-S., and J. W. Golden. 1998. Heterocyst pattern formation controlled by a diffusable peptide. *Science* **283:** 935–938.

Zeeck, E., J. D. Hardege, A. Willig, N. Ikekawa, and Y. Fujimoto. 1994. Sex pheromones in marine polychaetes: steroids from ripe *Nereis succina. Steroids* **59:** 341–344.

Zhou, T., and S. Rebach. 1999. Chemosensory orientation of the rock crab *Cancer irroratus. J. Chem. Ecol.* **25:** 315–330.

Zimmer, R. K., J. E. Commins, and K. A. Browne. 1999. Regulatory effects of environmental chemical signals on search behavior and foraging success. *Ecology* **80:** 1432–1446.

Zimmer-Faust, R. K. 1989. The relationship between chemoreception and foraging behavior in crustaceans. *Limnol. Oceanogr.* **34:** 1367–1374.

Zimmer-Faust, R. K., and M. N. Tamburri. 1994. Chemical identity and ecological implications of a waterborne, larval settlement cue. *Limnol. Oceanogr.* **39:** 1075–1087.

Zimmer-Faust, R. K., R. A. Gleeson, and W. E. S. Carr. 1988a. The behavioral response of spiny lobsters to ATP: evidence for mediation by P_2-like chemosensory receptors. *Biol. Bull.* **175:** 167–174.

Zimmer-Faust, R. K., J. M. Stanfill, and S. B. Collard, III. 1988b. A fast, multi-channel fluorometer for investigating aquatic chemoreception and odor trails. *Limnol. Oceanogr.* **33:** 1586–1595.

Zimmer-Faust, R. K., C. M. Finelli, N. D. Pentcheff, and D. S. Wethey. 1995. Odor plumes and animal navigation in turbulent water flow: a field study. *Biol. Bull.* **188:** 111–116.

Zimmer-Faust, R. K., M. P. de Souza, and D. C. Yoch. 1996. Bacterial chemotaxis and its potential role in marine dimethylsulfide production and biogeochemical sulfur cycling. *Limnol. Oceanogr.* **41:** 1330–1334.

Reference: *Biol. Bull.* **198:** 188–202. (April 2000)

The Fluid Dynamical Context of Chemosensory Behavior

MARC J. WEISSBURG

School of Biology, Georgia Institute of Technology, Atlanta, Georgia 30332-0230

Abstract. The fluid mechanical environment provides the context in which denizens of aquatic realms, as well as terrestrial creatures, use chemoperception to search for objects. Our ability to understand the nature of olfactory-guided navigation rests on our proficiency at characterizing the fluid dynamic setting and at relating properties of flow to behavioral and sensory mechanisms. This work reviews some fluid dynamical concepts that are particularly useful in describing aspects of flow relevant to chemosensory navigation, and it considers studies of orientation in animals in light of these principles. Comparisons across broadly different fluid environments suggest that particular sensory and behavioral mechanisms may be tailored to specific flow regimes and stimulus environments. This is clearly evident when examining animals that operate in high *vs.* low Reynolds number flows. In other cases, animals may converge on common solutions in given flow regimes in spite of differences in taxonomic class or size. Potential parallels may include behavior of aquatic *vs.* terrestrial arthropods, and animals without fixed reference points in flows dominated by molecular *vs.* turbulent diffusion. In an effort to add further fluid dynamical underpinnings to navigational strategies, I suggest how simple nondimensional categorization of behavior in relation to flow may aid in identifying the forces underlying common elements, even across animals of seemingly disparate size and scale.

Introduction

Aquatic animals rely on chemosensory abilities for nearly every task necessary for their survival, although we, as terrestrial animals, may have difficulty appreciating the information that they are able to obtain. Nonetheless, habitat choice (Pawlik, 1992; Zimmer-Faust and Tamburri, 1994; Ratchford and Eggleston, 1998), prey perception (Koehl and Strickler, 1981; Weissburg and Zimmer-Faust, 1993, 1994), predator avoidance (Kats and Dill, 1998), and mating (Gleeson, 1982; Kelley *et al.*, 1998; Yen *et al.*, 1998) have all been shown to be strongly associated with chemical cues in a variety of organisms. Even a brief survey of chemical communication systems suggests that over ecological and evolutionary time spans, chemical signaling processes affect individual organisms from the microscopic to the macroscopic, as well as their populations and communities (Zimmer and Butman, 2000).

In the last decade, great strides have been made in understanding the role of chemosensory cues in the marine and freshwater communities. The initial focus on identifying the sources and molecular nature of chemical cues, and their behavioral effects, has given way to efforts to understand the spatial and temporal properties of chemical signals. This shift occurred in response to the realization that the properties of fluids and fluid motion play a pivotal role in structuring chemical signals available to aquatic organisms. Various studies suggest that the fluid dynamical regime sets boundary conditions on behavioral abilities through its effects on the information contained in the odor signal (Moore and Atema, 1991; Weissburg and Zimmer-Faust, 1993, 1994; Weissburg *et al.*, 1998). The clear conclusion from these investigations is that the hydrodynamic context of chemosensory behavior is an important component of the animal's chemical environment.

The purpose of this contribution is to give a broad overview of the effects of hydrodynamic forces on the nature of waterborne chemical signals; such an overview is necessarily rooted in an appreciation of fluid dynamic regimes. At this nascent stage of our investigations, a relatively simple

Received 9 April 1999; accepted 17 November 1999.

E-mail: marc.weissburg@biology.gatech.edu

This paper was originally presented at a symposium titled *Chemical Communication and Ecology*. The symposium, which was held in San Diego, California, on 30 December 1998, was invited by the Western Society of Naturalists as part of its annual meetings.

approach can serve to outline the essential elements critical for studies that can firmly link chemosensory navigation to the fluid regime. This information is currently embodied in a number of fields of inquiry, and collecting it into a single place may help to define a set of approaches and tools to aid others in investigating orientation to chemical cues. Secondly, in reviewing studies on navigation, general patterns emerged that link certain sensory strategies to particular fluid environments. These connections are explored. In this regard, a particular problem is how to compare animals of widely differing size and scale. Proceeding from the discussion of fluid properties and animal strategies, I offer a basic model that uses nondimensional parameters to establish the dynamic similarity between animals in different flow environments. In much the same way as simple fluid dynamical quantities allow comparison of flow that is size and scale independent, developing methods for the non-dimensionalization of navigation may be a way for comparing abilities and locomotory performance in seemingly disparate creatures.

Scope

I take as a model the problem of an animal finding a relatively discrete object, such as a food item or mate. This process is at an intermediate scale between processes that affect the microdistribution of odor signals around and through olfactory appendages (Koehl, 1996), and the large-scale mixing that determines the signals that wide-ranging animals use to find a source (Dittman and Quinn, 1996). The focus is on aquatic creatures, for two reasons. First, at biological scales of interest, fluid dynamics in air is somewhat intransigent; it has been difficult to quantitatively describe odor source dynamics in sufficient detail. Secondly, working in aquatic habitats affords an unparalleled opportunity to examine a large range of fluid dynamic environments. Orientation to olfactory signals has been shown to take place in viscous and turbulent flows that conservatively span a range of Reynolds numbers (see below) of at least 4 orders of magnitude (Weissburg, 1997). Considering orientation in diffusive environments or creeping flows experienced by microorganisms extends the lower boundary of the Re range by 100- to 1000-fold. At this stage of investigation, I believe it is comparisons across a large range of fluid mechanical states that will provide us the most insights into the coupling between navigational performance, sensory strategies, and odor properties. Although the experimental focus is predominantly in the aquatic realm, the results also may be relevant to terrestrial organisms. Analysis of flow rates, length scales, and fluid properties between air and water, and the organisms therein, suggests that they are dynamically similar environments with respect to odor signals entrained in flows. Similar behaviors expressed by various aquatic and terrestrial creatures points toward convergent solutions to common problems of orientation and navigation in seemingly disparate odor landscapes.

Mechanisms of Transport in Fluids

Broadly speaking, the movement of substances dissolved in fluids results from either one of two processes; diffusion, which represents the random molecular motion of substances, and transport by the moving fluid.

Diffusion

When fluid motion has a minor impact on the distribution of odorants, the chemical signal environment is accurately modeled by a well-known family of diffusion equations, as covered for instance, in Dusenbery (1992). The dynamics of a signal in this environment cause a rapid spread of the odorant front, which is symmetric from the point of origin, creating an exponentially decaying continuous gradient in the intensity of the chemical signal. The rapid initial spread of the odor cloud is followed by a slow decline through time that results in an increasingly shallower spatial gradient (*e.g.*, Dusenbery, 1992). Since organisms have a defined threshold concentration for the induction of chemically mediated search, this results in a signal that reaches a maximum radius of detectability when the edge of the odor front is at the organism's perceptual limit. Thereafter, continued diffusion dilutes the odor concentration such that the active space that can be perceived by an individual diminishes, and the edge of detectability shrinks.

Transport in flow

When fluid motion cannot be ignored, the dynamics of odorant transport become considerably more complex. The concentration of odorants will reflect advection of the odorant by the mean (or bulk) flow, and diffusion due to turbulence. The general theory of turbulence is quite extensive and beyond the scope of this presentation, but it is essential to appreciate a few points. First, although turbulence is ubiquitous, it is not always an important aspect of fluid flow, and a number of flow environments in which chemosensory orientation takes place are largely free from this type of fluid motion. Second, turbulence is intrinsically a chaotic process in which local vectors and velocities of fluid motion vary unpredictably. Conceptually, flow streamlines in laminar flows remain parallel to each other, and therefore largely aligned with the direction of mean transport. In contrast, turbulent flows contain regions where local flows are oriented in any direction with respect to the bulk flow. Lastly, although turbulence may be quantified, only the intrinsic tendencies of turbulent fluid motion may be described by time-averaged descriptions of its intensity, spatial or temporal distributions, etc. Thus, unlike other flow scenarios, it is impossible to predict the instantaneous odor concentration at a given point when turbulent motion is present. This simple fact has set serious constraints on our understanding of the properties of these signals and the animal strategies that are designed to operate in these environments.

In the ocean, turbulence arises from a variety of sources that operate on scales larger than that relevant for organisms tracking their predators, prey, or mates (Svendsen, 1997). These eddies tend to approximate the scale of the flow, and they correspond to a length on the order of the water depth or boundary layer thickness (see below, Sanford, 1997). However, the energy contained at large scales is transferred to successively smaller scales by a process known as the Kolmogorov cascade (Tennekes and Lumely, 1972). If we imagine that turbulent fluid motion is in the form of coherent eddy structures (those where flows are rotational), this process can be envisioned as the breakup of larger eddies into a series of ever smaller structures. This process reaches its lower limit when viscous interactions between fluid molecules dissipate the energy contained in fluid motion. This limit, the smallest eddy size containing turbulent energy, is the Kolmogorov length scale and is predictable from a variety of fluid mechanical quantities. Most importantly, increases in turbulence extend the energy cascade to smaller and smaller spatial scales before viscosity takes hold. In the open ocean, this lower limit is typically between 0.2 and 3 mm (Denman and Gargett, 1995; Jiménez, 1997; Sanford, 1997). An important consequence of the energy cascade is that regardless of the source of turbulence, at length scales in the millimeter range, the statistical properties ought to be independent of the mechanism and relate only to turbulence intensity (Jiménez, 1997).

Another important source of turbulence occurs where a fluid flows over a solid object. The fluid in contact with a solid interface is at rest and represents a momentum sink. Viscosity acts to dissipate momentum in the fluid so that turbulent structures appear, resulting in a cascade as described above (Schlichting, 1987). Even when fluid motion is initially laminar, this process will eventually result in boundary layer flows assuming a turbulent character. These flows are of great importance to many aquatic organisms that forage, escape, and seek dwellings on the sea floor.

Useful Hydrodynamic Properties

While the character of a flow is difficult to describe exactly, a number of useful parameters exist that allow a rough description of the nature of the fluid environment. These consist of a handful of dimensionless parameters that index the importance of various fluid properties or transport mechanisms. The most basic measure, which remains the starting point for discussions of fluid flow, is the Reynolds number:

$$\mathrm{Re} = \frac{lU}{v} \tag{1}$$

where l is a length factor, U is fluid velocity, and v is kinematic viscosity. The Reynolds number represents the ratio of inertial to viscous interactions in the fluid, or alternatively, a ratio of the time scales of inertial transport *via* eddies to dissipation of momentum *via* molecular interactions in the fluid. When $\mathrm{Re} \ll 1$, viscosity dominates, and the character of the flow is orderly and predictable. Particles move along streamlines that remain parallel to each other, a characteristic referred to as laminar flow. This is the regime most conducive to the modeling of chemical signal structure, since the relative unimportance of inertial forces largely restricts spreading of molecules to molecular diffusion. As Re increases ($\gg 1$), inertia becomes the dominant force and the flow becomes increasingly chaotic. Local fluid velocity exhibits substantial fluctuations and is thought of as consisting of a variable flow component superimposed onto a mean flow. Turbulence intensity (u') then corresponds to the root mean square of velocity fluctuations. Unfortunately, no set point clearly demarcates the transition between laminar and turbulent flow regimes, and so Re is only a rough approximation that is best confirmed by measurement or visualization. The importance of turbulence for chemical signal transmission cannot be overstated. Even at moderate turbulence levels, such as those characterizing open-ocean environments (Gargett, 1997; Sanford, 1997), the rate of dispersion of chemical signals is by orders of magnitude greater that that sustainable by diffusive mechanisms.

Flows over solid objects are characterized by a distinct velocity gradient dictated by the no-slip condition at the object surface (Fig. 1). Fluid velocity is zero at the interface and increases logarithmically with height above the surface. This region of growth is termed the boundary layer and is taken to extend to the point where fluid velocity is 99% of the nominal (free-stream) value. The boundary layer grows as it moves over an object, and for a flat plate, the rate of increase is proportional to the square root of the distance from the upstream edge of the plate (Schlichting, 1987; Denny, 1988). At any given location, the thickness is inversely proportional to $U^{1/2}$. The dependence of boundary layer thickness on both distance and U presents difficulties for experiments conducted in flow channels, since the boundary layer thickness changes rapidly during its initial development. Flumes used to examine orientation behavior must present walking or crawling animals with boundary layers that do not change substantially during locomotion to the source (*e.g.*, Weissburg and Zimmer-Faust, 1993, 1994).

As for any flow, boundary layers may be laminar or turbulent, and the transitional Re can be evaluated in any number of ways. Over a smooth flat plate, Re must exceed 3.5×10^5 to 10^6, which corresponds to a water current of 0.34 to 1 m s^{-1}, for turbulence to result (Denny, 1993). In

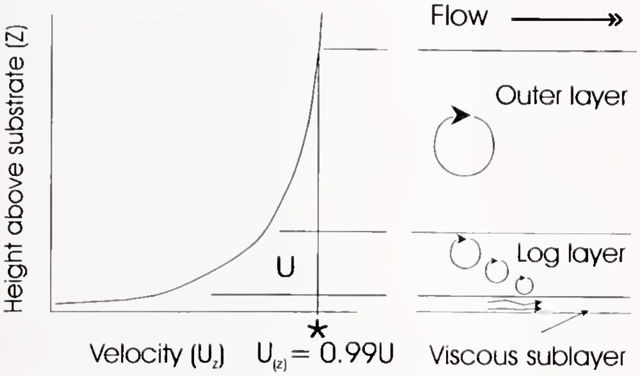

Figure 1. Dependency of flow velocity U(z) on height above the substrate (z) and structure within a turbulent benthic boundary layer. The boundary layer is defined as extending to the height where U(z) reaches 99% of the free-stream velocity, marked on the *x*-axis. The flow profile of a turbulent boundary layer profile is qualitatively depicted on the right, which shows the generation of large eddies in the outer layer, momentum transfer and the Kolmogorov cascade in the log layer (which accounts for approximately 30% of the total boundary layer), and laminar flow in the viscous sublayer. Note that whereas this example shows the boundary layer developing over a substrate, a turbulent boundary layer can develop over any surface immersed in flow.

this instance, the length factor, l, is the distance from the leading edge, and the resulting quantity is often referred to as the local Re. A more precise relationship given by Pedley (1997) specifies that the Re must exceed 244 when l is the boundary layer thickness. It is evident from these relationships that many, if not most, boundary layer flows of biological interest will be turbulent, particularly when chemical signals are entrained in flows over a substrate. Also, note that the intensity of turbulence is not constant in these types of flows; u' is maximal in the region of the boundary layer where the relationship between velocity and the log of the height above the substrate is linear (the log-layer). In open channel (*e.g.*, flume) flows, u' seems to reach a peak where $Z/H \approx 0.05$, where H is the flow depth (Nezu and Rodi, 1986) and Z is height above the substrate. It is therefore likely that many animals will have sensors in locations within the boundary layer where turbulence is rather vigorous.

Like politics, boundary layers are local phenomena. The practical choice of length and velocity scales is contingent on the precise relationship between the object of interest and the flow in its immediate vicinity. Whereas the benthic boundary layer is the signal environment for a foraging crustacean, a parasitic copepod investigating the olfactory cues on a moving blue crab is more strongly affected by the boundary layer around its target than by the flow over the substrate. Multiple boundary layers exist simultaneously, and the choice of inappropriate parameters will result in a poor characterization of the relevant flow properties.

The character of boundary layer flows is often related to the roughness Reynolds number,

$$\mathrm{Re}^* = \frac{u^*\mathrm{D}}{v} \qquad (2)$$

where u^*, is the shear velocity and D is the hydraulic roughness length, which for nonrippled substrates corresponds simply to the diameter of the grains forming the bed (*e.g.*, Weissburg and Zimmer-Faust, 1993). The shear velocity is the scalar of momentum flux in a boundary layer, or roughly, the velocity at which momentum is transferred. It thus is an index of the extent to which turbulent (shear) stresses are transmitted through the boundary layer. A number of authors provide rules of thumb or empirical relationships for estimating these quantities (*e.g.*, Denny, 1988). Observations suggest that the outer regions of a boundary layer begin to feel the effects of turbulence when $3.5 < \mathrm{Re}^* < 6$, and the turbulence extends all the way to the bottom when $75 > \mathrm{Re}^* > 100$ (Schlichting, 1987).

As previously discussed for the open ocean, turbulent fluid motion in a boundary layer is involved in a cascade that transfers fluid mechanical energy to smaller and smaller spatial scales. Again the largest eddies approximate the scale of the flow, and the lower (Kolmogorov) limit, η, is related to turbulence intensity (Tennekes and Lumley, 1972):

$$\eta = \left[\frac{\mathrm{kZ}v^3}{u^{*3}}\right]^{1/4} \qquad (3)$$

where k is the empirically derived von Karman's constant equal to about 0.4. However, molecular diffusive forces continue to redistribute chemical signals (and other scalar quantities such as heat), so that the length scale of the smallest scale fluctuations of these quantities ultimately is determined by the molecular diffusivity $\mathrm{D_m}$:

$$\eta_s = \left[\frac{\eta v}{\mathrm{D_m}}\right]^{-1/2} \qquad (4)$$

where η_s, the Batchelor microscale, is smallest size for chemical fluctuations (Mann and Lazier, 1991). In open-ocean conditions, this limit is estimated to be on the order of 10^{-2}–10^{-4} m (Sanford, 1997), while it has been empirically measured to be 10^{-4} m or smaller in benthic boundary layer flows at moderate shear velocities (Moore *et al.*, 1992).

Although Re can provide some estimate of the importance of inertial *vs.* diffusive transport, its utility largely stems from its relationship to turbulence. In an attempt to further clarify the role of flow *vs.* diffusion in biological situations, a number of workers (*e.g.*, Moore *et al.*, 1999) have used the Peclet number:

$$\mathrm{Pe} = \frac{\mathrm{lU}}{\mathrm{D_m}} \qquad (5)$$

This quantity is a more direct index of the importance of advective transport relative to molecular diffusion. Since the time scale of diffusion is proportional to l^2/D_m, and the time scale of advection to l/U, the Peclet number also is accurately viewed as an index of diffusive to advective time scales. As Pe increases, diffusive processes are relatively less important in governing the rate of delivery of a chemical species to an organism or its sensor. Pe is far greater than unity in most contexts, such as a lobster moving through a turbulent odor plume. The distance (l) over which chemical cues must be transported is large, and advection is the predominant mechanism. In contrast, molecular diffusion assumes an important role in the movement of materials around microorganisms or individual sensilla. In these cases the length scales are small, and fluid velocity is often low since the structure may lie within a boundary layer.

A parameter that has so far received far less attention by workers investigating odor signal transmission is the Strouhal number. This parameter relates to the frequency with which eddies are generated by an object in flow. For a cylindrical object, such as a bivalve siphon that projects with its long axis into the flow, vortices are shed alternately from the top and bottom with a predictable frequency,

$$\mathrm{St} = \frac{fD}{U} \tag{6}$$

where D is the diameter, and f is the frequency of vortex shedding. Interestingly, St is roughly constant when $100 > \mathrm{Re} > 10^5$, meaning that for an object of a given diameter, there will be a linear increase in shedding frequency with velocity (White, 1991). Over most of this range, the regularly alternating pattern of shedding, known as a vortex street, is present. A vortex street may exist at an Re of up to 10^7, although it becomes increasingly chaotic (Lugt, 1995). Such vorticies can presumably entrain odorants and impose a dominant frequency on signals transmitted in their wake, although there has been little experimental work on this aspect of fluid flow.

Biologically Relevant Signals

Signals in the diffusive realm

Chemical signals in which diffusion is the predominant transport agent include gradients followed by bacteria and other small organisms. These types of situations are particularly amenable to modeling, given the ease with which diffusional gradients may be represented analytically with a small number of physical constants. Key observations are that locating a source in these environments is affected by properties such as animal size, shape, motility, and gradient strength (Dusenbery, 1997, 1998a, b). The mechanism most frequently identified is indirect orientation (kinesis *sensu* Dusenbery, 1992), in which travel in the direction of increasing stimulus strength results in a decreased probability of changing direction (Berg, 1975). In general, a gradient may be sampled using either spatial or temporal comparisons. Larger animals are at an advantage, since they can spread receptors over a greater distance and move more rapidly, thus increasing the ability to sample gradients in either the temporal or spatial domain. Additionally, for the smallest unicells, Brownian motion will set constraints on sampling by rotating the cell and changing the orientation of receptors on its surface. As a result, although spatial sampling is generally superior, temporal sampling is favored in weak gradients and low stimulus concentrations that require longer stimulus integration times (Dusenbery, 1998a). Although there are few systematic comparisons, temporal sampling is the commonly observed strategy, perhaps because it extends the range of gradients that contain useful information. Since it is possible to solve for the critical gradient decay lengths that determine the effectiveness of each type of sampling mechanism, it may be possible to arrive at general conclusions about the environments and organisms in which each type of mechanism should be found.

Organisms that respond to chemical cues in diffusive environments are not only bacteria, but also ciliates (Verity, 1988), flagellates (Crenshaw, 1996), and spermatazoa of both plant and animals (Ward *et al.*, 1985). One common thread among these representatives of diverse phyla is that they often move along a helical trajectory. Helical motion occurs when a body rotates around its central axis and translates through space simultaneously. Crenshaw, in a series of papers (reviewed in Crenshaw, 1996), has refined the mathematical and observational tools necessary to quantitatively analyze this type of behavior. He finds that by suitable adjustments in the rotational velocity, animals or cells can align the axis of their helical path along a chemical gradient, providing another mechanism for orienting to chemical gradients that is successful over a wide range of kinematic parameters (Crenshaw, 1993). This mode of orientation is suitable for an organism that has a single chemoreceptor on its surface, or a population of receptors distributed equally across its body, and that depends on temporal comparisons of stimulus intensity obtained as it moves through the gradient. This mode of orientation is thus a special class of klinotaxis (temporal sampling), designated as helical klinotaxis by Crenshaw (1996), and represents a direct guidance mechanism. To date, this strategy has been identified only in cells or organisms propelled by flagellar or ciliary motion in very low Re environments. In these situations, where flows are reversible, propulsion is achieved only by asymmetric motions of the cilia or flagella, and this may create movement that is naturally helical.

Diffusive transport is also common for larger creatures tracking both food (Hamner and Hamner, 1977) and mates (Weissburg *et al.*, 1998; Yen *et al.*, 1998). Males of the copepod species *Temora longicornis* can track females over trail lengths as long as 10 cm, or about 100 body lengths

(Doall *et al.*, 1998; Weissburg *et al.*, 1998; Yen *et al.*, 1998). Calculated on the basis of the average size (1–2 mm) and swimming velocity (3–6 mm/s) of these copepods, the Re of these flows is about 0.3–0.6. Here, the slow diffusive transport of chemical signals compared to the relatively rapid diffusion of momentum creates (see Yen, 2000) a chemical signal that more properly resembles a coherent trail hanging in three-dimensional space. There is no flow information present, and behavioral analysis strongly suggests that spatial comparisons facilitate detection of the diffusing trail edges, whereas temporal comparisons mediate up-gradient progress (Weissburg *et al.*, 1998). It is important to note that, in this case, diffusion acts not as an agent of transmission but in precisely the opposite manner; slow diffusion restricts the spread of chemical signals, thus favoring the existence of a defined chemical trail. The edges of the trail move only a few hundred micrometers during the trail's useful life, and the difference in concentration along the length of the trail is estimated to be only 100-fold. Early reports (Katona, 1973) argued for diffusion as a transport mechanism bringing the pheromomal cue to the expectant male, but the time scales over which this operates are clearly too long to account for observed behavior (Yen *et al.*, 1998).

Orientation in these low Re situations appears to be a fundamentally different set of mechanisms than those postulated for orientation in turbulent flows (see below), particularly because there is little flow information to aid the animal in determining the up-gradient direction. Flow information may be restricted to situations in which animals shed more intense fluid disturbances, as when some planktors transiently achieve velocities of several hundred body lengths per second (Yen and Strickler, 1996), and reach a fluid regime that is transitional between laminar and turbulent flow. Vortices are shed during this transition that also appear to be used in mate tracking in the copepod *Acartia hudsonica* (Doall *et al.*, 1999). Perhaps animals detect chemical signals in these structures as well, and use these flavored eddies to locate their mates by relying on both flow and chemical signals. Some animals that seem to rely on chemical trails do so in conjunction with other cues that supplement the information obtained from perception of odor. The swimming patterns of a number of copepods and other plankton such as shrimp and bivalve larvae suggest that the perception of a chemical cue invokes downward movement (Hamner and Hamner, 1977; Tamburri *et al.*, 1992; Tsuda and Miller, 1998). For animals that track sinking or downward-swimming objects, use of gravity is a quite reliable strategy for resolving ambiguity about the direction in which the trail was made. Odor becomes a stimulus that releases geotactic orientation behavior, which frees the animal from having to perform complex processing to extract gradient information from the chemical signal itself.

For animals that operate in these low Re environments, diffusive transport preserves trail coherence. Ambient fluid motion and turbulent mixing may dissipate or break a trail, resulting in a signal that cannot easily be tracked, particularly through the use of odor alone. As suggested above, one compensatory strategy is to use supplemental cues that are correlated with general direction towards the source. Another is to perform olfactory guided behaviors in environments where dissipative forces are minimal. Some species of copepods appear to aggregate where the rate of energy dissipation is low (*e.g.*, Mackas *et al.*, 1993; Incze *et al.*, 1996), perhaps because stable zones in the ocean are the most permissive of navigation along diffusive trails and extend the spatial and temporal limits over which these trails can guide animal movement. It is unknown whether animals in the field commonly follow trails over distances as long as those observed in the laboratory.

Signals in turbulent flows

Given the magnitude of fluid motion (centimeters per second to meters per second) and length scales (centimeters to meters) in which creatures such as insects, decapod crustaceans, fish, echinoderms, and gastropods operate, many will track objects in regimes where turbulence is a prevailing aspect of the flow. Studies of moths over several decades have led to an acute appreciation of the consequences of this fact and forced us to revise many of our ideas on chemosensory tracking. The most critical change in thinking has been an abandonment of diffusion models of odor plume structure as a way to examine stimulus concentration.

The earliest formulation of time-averaged plume structure applied to insect navigation was derived by Sutton (1953); it solves for the concentration C from a source emitting continuously at a rate J, for a point at a downstream distance r and angle θ from the midline of the plume:

$$C_{(r,\theta)} = \frac{J}{4\pi r D_e} \exp\left[-(1 - \cos\theta)\frac{rU}{2D_e}\right] \qquad (7)$$

Here, D_e is a constant of eddy diffusivity, a measure of dispersion by turbulence that is analogous to the molecular diffusivity and which must be empirically determined depending on the flow scenario. The odor concentration is Gaussian across the axis of the plume, but it decays with l/r in the downstream direction. Other formulations are specific to particular types of flows, such as the equation derived by Pasquill and Smith (1983) for boundary layers. An advantage of this model is that it uses u^*, an easily derived quantity.

Whereas the equations give the time-averaged structure of the plume (Fig. 2), the animal itself uses chemosensors that operate at fine spatial and rapid temporal scales and perceives the plume as a series of filaments of intense odorant concentration interspersed with periods when the

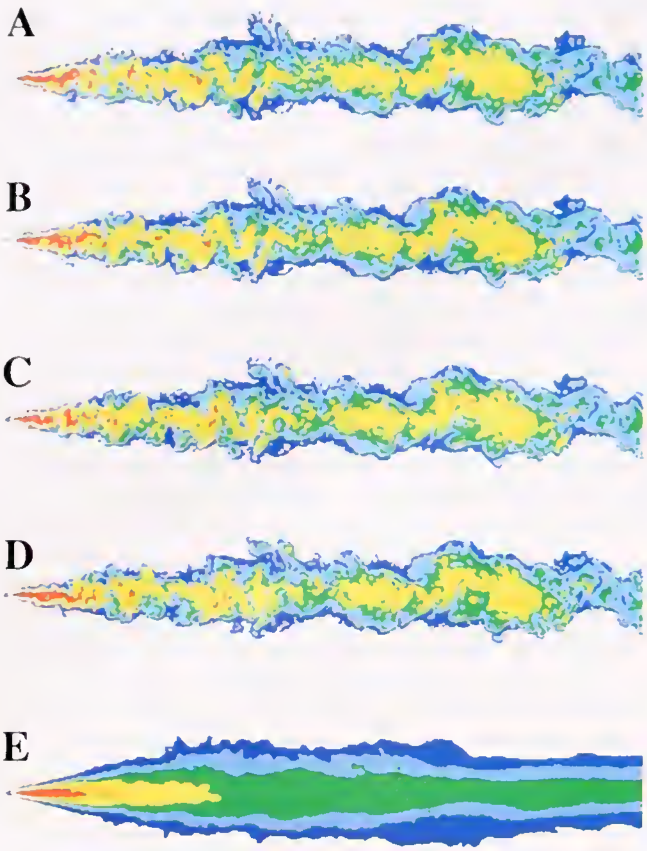

Figure 2. Instantaneous *vs.* time-averaged views of odor jets. This picture is a series of laser-induced fluorescence (LIF) images of dye concentration of an odor plume in flow (concentration expressed as color: red is highest, blue is lowest concentration). A–D represent a series of images on a rapid time scale (4 ns frame, 30 ms between successive frames), and show the fine-scale structure of the plume. Note how coherent eddy structures persist and move downstream. E is an average of about 1000 images, and is equivalent to modeling the time-averaged structure of the plume using equation 7. The jet is approximately 1 m long and 15 cm wide, with an initial source concentration of rhodamine 6G equal to 200μg/l.

concentration is low or undetectable. Given the nature of turbulence, there is appreciable variation in the intensity and duration of each odor filament, and the information represented by turbulent diffusion models does not depict the signals received by the animal. It has been known for some time (reviewed by Murlis *et al.*, 1992; Vickers, 2000) that insects do not respond to mean concentrations predicted by these models. A recent report concerning aquatic plumes suggests that a tracker averaging a finite series of instantaneous measurements of odor concentration cannot estimate the time-averaged Gaussian plume structure (Finelli *et al.*, 1999) during navigation. Extracting information from each contact with a discrete odor pulse is the only alternative.

The filamentous structure of odor plumes has been reasonably well characterized in marine realms, at least under certain conditions. Investigators using flow visualization techniques, as well as chemical microprobes that measure at fine spatial and temporal scales, have verified that aquatic odor plumes consist of rapidly fluctuating signals (Moore and Atema, 1991; Moore *et al.*, 1994; Finelli *et al.*, 1999). Patchy odor distributions are a general rule for conditions under which animal tracking has been observed in the laboratory. At turbulence levels characteristic of natural habitats ($u^* \approx 0.1$–1), odor pulses generally are brief (<1 s) with long periods of odor absence. Consistent with studies in terrestrial habitats (Murlis *et al.*, 1992), intermittence reflects two processes with different spatial and temporal scales. The largest scale eddies cause the plume to meander across stream, imparting large periodicity to the fluctuations of odor intensity at a single point. This process continues until the plume is dispersed to about the same size as the large flow structures. Concomittantly, the plume remains relatively coherent on a small scale until its width exceeds the Kolmogorov size. Thereafter, it becomes torn apart and filamentous due to the action of turbulence at these scales.

Aquatic animals tracking waterborne odor plumes display movement patterns that are consistent with the general mechanisms proposed for insects (Vickers, 2000). When tracking odor plumes, various animals use zig-zag trajectories, including decapod crustaceans (Moore *et al.*, 1991; Weissburg and Zimmer-Faust, 1993), salmon and sharks (Johnsen, 1987), and deep water macrourid fish (Tamburri and Barry, 1999). These behaviors are either the result of an internally generated pattern of counterturns released by odor contact, as has been postulated for salmon and sharks (Johnsen, 1987), or are the result of movements to opposite edges of the plume, coupled with a subsequent turn into the main axis that is mediated directly by the stimulus itself (Weissburg and Zimmer-Faust, 1993, 1994). In lobsters, evidence gleaned from simultaneous recording of stimulus patterns and animal movements strongly suggests that differences in odor concentration across the body axis turn the animal towards the stronger stimulus and back into the plume (Atema, 1996). Blue crabs seem to track along the edges of odor plumes quite well in the field, lending further support to this perceptual mechanism. This tropotactic discrimination of boundaries is the same strategy as that postulated for tracking copepods, and depends on reasonably discrete plume edges that permit the detection of stimulus asymmetry. As the plume widens, zigzagging is expected to be more pronounced, and observations of blue crab behavior in turbulent flows show this to be the case (Weissburg and Zimmer-Faust, 1993, 1994). Again, the parallels between animals in high *vs.* low Re flows are striking; male copepods also increase their tacks across the trail when females lay down more diffuse signals (Weissburg *et al.*, 1998).

One of the consistent elements in the tracking of aquatic chemical trails is the reliance on flow as an orienting stimulus released by the detection of odor. Blue crabs (Weissburg and Zimmer-Faust, 1993, 1994), sharks (Hodgson and Mathewson, 1971), and a number of species of fish (Johnsen, 1987), flatworms (Bell and Tobin, 1982), and gastropods (Brown and Rittschof, 1984) all show odor-conditioned response to flow or have difficulty locating odor sources in quiescent environments. Odor-conditioned rheotaxis may be the aquatic analog of amenotactic responses displayed by insects.

One of the major difficulties in studying orientation in turbulent flows is that the odor and flow information available to the animal is impossible to either compute or model with the required degree of complexity. One approach is a throwback to the early days when investigators applied Suttonian diffusion models to plume dynamics. Thus, Baird and his colleagues (Jumper and Baird, 1991; Baird *et al.*, 1996) have applied turbulent diffusion approximations to compute the spread of pheromones from midwater fish. Using empirically determined coefficients of turbulent diffusion, they model the concentration gradient of an odor cloud as it changes through time. Turbulent diffusion constants are analogous to molecular diffusion constants but are 10^5 to 10^6 times greater, since transport occurs by turbulent flow instead of random molecular motion. These types of models have the advantage of calculating odor gradients using measured physical constants, and they capitalize on the fact that midwater habitats are unbounded and thus amenable to modeling using a simple diffusion approximation. These models have produced useful conclusions about the time and space scales over which these clouds remain detectable, but one potential problem is that they do not consider the fine-scale structure that may be so critical in orientation. However, animals in these situations might indeed track gradients by having stimulus integration times that exceed the relevant scales of the fine structure imbedded in the odor cloud. Only recently have we had sampling capabilities at spatial scales (centimeters to meters) that would allow us to answer the question of whether a swimming fish is more likely to perceive such structures as gradients or as a series of discrete patches. If the former, then studies of bacterial chemotaxis become more relevant because they have identified a number of key parameters that affect orientation efficiency. Animal size, movement speed, and tendency to be randomly reoriented during search should prove to be as critical for orientation in gradients produced by turbulent diffusion as they are for those produced by molecular diffusion.

Behavioral Implications of Fluid Flow Regimes

High vs. low Re environments

Although the important elements of the various flow scenarios cannot be easily summarized, a crude but accurate perception is that low Re viscous environments are characterized by slowly changing signals, low flow, and continuous gradients. In contrast, high Re regimes produce a signal structure that is chaotic, intermittent, and occurs against a bulk flow that is perceptible to navigating animals.

A consequence of these dramatic differences is that animals inhabiting various fluid milieus may have arrived at different orientation strategies. Animals in turbulent environments are likely to rely on flow to provide a general direction towards the source, since extracting this information from the odor signal itself appears challenging. Animals in these environments also utilize flow to narrow their search windows in the absence of odor, and cast across steam when they initially search for, or lose contact with, the plume (Weissburg and Zimmer-Faust, 1993, 1994).

A copepod searches for its mate in a viscous realm, where the Re is roughly 10^3 to 10^4 less than that of a typical decapod, and consequently relies on mechanisms other than those used by their larger brethren. Without flow, copepods search in three dimensions to locate the odor boundaries, and direction towards the source comes only from temporal comparisons of odor intensity (Doall *et al.*, 1998; Weissburg *et al.*, 1998; Yen *et al.*, 1998). Interestingly, animals in both types of environments seem to use similar methods of edge detection, suggesting that for both diffusive trails and turbulent plumes, the borders of a signal source retain sufficient integrity and gradient steepness to be perceptible by spatial sampling.

A second fundamental difference between animals in diffusive *vs.* turbulent regimes may be the integration time over which they acquire chemosensory information. For animals in turbulent flows, the transient nature of the stimulus forces the sensory system to rely on rapid integration of brief odor pulses. Lobster olfactory neurons can encode some stimulus features in about 200 ms (Gomez and Atema, 1996), which is clearly an adaptation to a filamentous plume structure. Although the time constants of other aquatic organisms are not known, a reasonable expectation is that animals that follow gradients may have slower integration times.

One of the greatest challenges in research on chemosensory orientation in high Re environments is to understand how animals extract information from the evanescent signals that characterize turbulent flows. Although tropotaxis seems a robust mechanism for edge detection, the strategy mediating movement to the source is less well known. In principle, odor pulses in aquatic odor plumes may contain information that can be used to extract directional information (Atema, 1996), and investigators have proposed that some animals may use this information during tracking (reviewed in Weissburg, 1997). However, this type of strategy seems considerably more complex than a simple mechanism whereby the mere detection of odor presence triggers a response to an orienting stimulus (flow, gravity, light) that points to the source.

The above arguments suggest that further studies of chemosensory navigation should consider the potential interactions between chemical cues and other stimuli. For animals that perceive current, perhaps navigation in response to the detection of individual, rapid odor transients is restricted to a range of narrow conditions comprising relatively swift unidirectional flows. Sadly, there is little information on perceptual limits in response to flow. Ebina and Wiese (1984) suggest that crayfish align to current velocities as low as 0.1 cm/s, but comparative data are lacking. The consequences of oscillatory flows, or complicated flow patterns that occur in the presence of underwater structural heterogeneity, are also unknown. Do animals in these situations extract information from properties of odor pulses, or do they have other strategies? Lastly, studying animals with a fixed frame of reference may bias our perspective. In their three-dimensional world, fish or other midwater animals may not have access to other orienting stimuli unless the odor is predictably aligned to the vertical axis. Current direction would generally not be perceptible to the fish from its own Lagrangian perspective, except in certain unusual cases. Westerberg (1984) presents an interesting hypothesis describing the use of shear gradients at strong density discontinuities to detect flow direction. It is unknown whether such animals have a means of detecting flow, extract information from properties of odor pulses, or follow gradients. If the last alternative is true, then turbulent diffusion models capture the necessary signal properties. Of course, gradient-following mechanisms set serious limits on orientation, since the integrated signal (which will be weaker than the peak intensities in a pulse) must be perceptible, and intensity differences must be detectable through space or time.

Nondimensional parameterization of behavior

Now that we have a number of animal models for orientation in flows, it becomes possible to take a comparative approach. Simply put, is the behavior of a blue crab (or lobster) functionally the same as that of a moth? The directness of the question disguises the complexity of the answer, since the resolution requires us to compare animals of different sizes, movement velocities, and taxonomic affiliations that live in differing fluid regimes.

One of the strengths of hydrodynamic theory is that the character of the flow can be compared across habitats and in different fluids by using Re, Pe, etc. However, this is only a partial solution, and a more definitive answer requires us to compare the behavior of animals with respect to the properties of the flow, rather than simply comparing the flows themselves. In effect, we must arrive at nondimensional quantities for behavior in relation to fluid flow. Proceeding from the idea that a few simple quantities may help identify such a comparative framework, I present two such nondimensional parameters that incorporate hydrodynamic and behavioral properties. Clearly, this is a first attempt, and its real utility may be to suggest approaches of greater rigor that incorporate more realistic assumptions and quantities.

Consider an animal in flow that has a fixed frame of reference as it moves in an odor plume (Fig. 3). The animal moves at a constant velocity v, and samples its environment with a fixed frequency f. Its navigational strategy encompasses two critical tasks: it must move in the direction of increasing stimulus intensity, and it must stay within the borders of the plume.

The results of our previous studies of insects and crustaceans suggest that the key parameter mediating up-gradient progress is the rate of contact with discrete odor filaments. These studies also emphasize the importance of rapid sampling, since individual measurements collected over a longer time period result in dilution by mixing odor-containing filaments with clean fluid. This may render average concentrations below the limits of detectability. Animals can, however, gain information about the properties of the plume at a given location by collecting a number of rapid samples and then averaging these measurements. Successive averaging of odor pulse properties (intensity, slope, length, etc.) could then be used to judge progress towards the source. In essence, this is the method used by various investigators to reconstruct the time-averaged properties of a plume along its length and breadth, using a sensor that collects a number of rapid samples at a series of discrete locations.

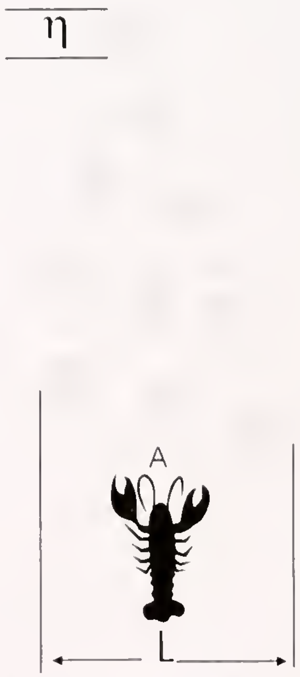

Figure 3. Illustration of the parameters used to calculate the temporal and spatial integration factors (TIF and SIF respectively). A lobster with an antenullar span A and sampling frequency f, is moving at velocity v in an odor plume with a Kolmogorov size η. The overall width of the plume is given by the characteristic eddy size L.

The mechanism described above depends on the animal's sampling rate relative to the scale of variation in the odor plume. Assume that the Kolmogorov limit represents the length scale of the fine structure of the plume. Then, it becomes possible to define the temporal integration factor (TIF), a nondimensional estimate of the sampling ability of the animal, as:

$$\frac{\eta}{vf^{-1}} \tag{8}$$

When this number exceeds 1, the animal is either sufficiently slow or samples with sufficient rapidity to detect many odor filaments at each point in the plume that it moves through. In other words, as TIF increases, the animal increases its ability to reconstruct the time-averaged view of the odor through an average of a number of instantaneous samples. A TIF $\ll$ 1 corresponds to extremely intermittent sensing of the plume.

A similar number may be defined for integrating across space, and I assume that the ability of an animal to determine its position transverse to the plume axis corresponds to the spatial integration factor (SIF). The SIF represents the width of the animal's sensor span (its ambit, A) relative to the width of the plume, which as a first approximation is on the order of the length scale of the dominant eddy size L. Thus, the SIF is:

$$A/L \tag{9}$$

When SIF is large, the animal samples broadly across the plume and has a high probability of detecting an edge beneficial for tropotactic orientation. When SIF is small, the animal is less able to determine its position from information obtained at a single location, and is therefore more likely to move across stream during navigation.

I calculated TIF and SIF for aquatic and terrestrial arthropods, using published values. Crabs and lobsters move at velocities of 1–10 cm/s (Moore *et al.*, 1991; Weissburg and Zimmer-Faust, 1994), and various species of moths fly through odor plumes at speeds of 30–100 cm/s (*e.g.*, Baker and Haynes, 1987; Mafra-Neto and Cardè, 1998). The Kolmogorov scale ranges from about 0.1 to 1 mm for aquatic benthic habitats, evaluated at a height of 6 cm above the bed (the approximate location of the antennules), using either published values (Sanford, 1997) or calculations based on measurements in laboratory flumes or field sites (Weissburg and Zimmer-Faust, 1993; Finelli *et al.*, 1999). Kolmogorov scales in terrestrial habitats range from 1 to 10 mm (Murlis *et al.*, 1992). Length scales, L, in crustacean habitats are expected to be on the order of 10 to 100 cm, based on typical flow depths in environments favored by blue crabs, and in terrestrial realms range between 1 and 10 m (Murlis *et al.*, 1992). Ambit sizes may be either the maximum body diameter, as for animals that use chemosensors across the body surface, or the spread of olfactory appendages such as antennae. I used values ranging from 1 to 10 cm for crustaceans, and 1 to 10 mm for insects. Sampling rates for aquatic and terrestrial arthropods are assumed to be 4 and 10 Hz, respectively, based on an analysis of physiological properties of their chemosensory systems (Christensen *et al.*, 1995; Atema, 1996).

The TIF values for aquatic animals range from 0.4 to 0.004, and for moths calculations give values between 0.3 and 0.001. SIF values are about 1 to 100 and 10^{-2} to 10^{-4} for aquatic and terrestrial arthropods respectively. Both the smaller ambit and the larger length scales conspire to produce the very low SIF scores in moths as opposed to crustaceans. We may be underestimating L in marine habitats given the narrow range of natural flows that have been examined, and these SIF scores may decrease with further investigations.

The computations indicate that animals in both realms sample on a similar scale relative to the fine structure of the plume, although aquatic creatures have a larger ability to compare across the spatial domain. This latter observation may explain why crabs and lobsters seem to rely on tropotactic comparisons, whereas moths have no similar mechanism. In neither case do the TIF scores suggest much of an ability to acquire a time-averaged view of the plume on the basis of a series of rapid samples. This is in accordance with the bulk of current behavioral observations that animals use odor perception simply to release orientation to flow or wind direction. For both terrestrial and aquatic organisms, sampling rates must increase at least threefold for their abilities to match the pulse length scales in even the most benign conditions, and increases of 100- to 1000-fold are required to permit extensive sampling in most habitats. It may be impossible for chemosensory transduction to operate at sufficiently high frequencies to be generally useful as a means to acquire this type of time-averaged information, given that response latencies of olfactory cells range from 50 to 500 ms (Restrepo *et al.*, 1995). Decreases in locomotory velocity also may be untenable in light of the magnitude of the necessary reduction, particularly for flying animals that must maintain sufficient speed to remain airborne. Substrate-bound animals face no such constraints beyond the need to find distant objects within a limited time, but this still may prevent them from moving slowly enough to achieve the necessary sampling rates. Consequently, the pressures imposed by the scales of plume variation may have forced the evolution of sensory strategies that do not rely on the ability to time average. Interestingly, the TIF scores suggest dynamic similarity of navigational strategies, and moths and aquatic creatures may have converged on similar sampling capabilities relative to the fine-scale structure of their respective odor environments.

Moths and crabs occupy different quadrants of a 2 × 2 matrix of TIF *vs.* SIF scores (Table 1). I am unable to

Table 1

Temporal and spatial integration factor scores versus *organismal and behavioral properties*

	Temporal Integration Factor (TIF)	
Spatial Integration Factor (SIF)	Low	High
Low	Low sampling rate and low spatial integration. Probable strategy: odor-conditioned taxis. Representative animal: moths.	High sampling rate and low spatial integration. Probable strategy: chemotaxis. Representative animal: gastropods?
High	Low sampling rate and high spatial integration. Probable strategy: odor-conditioned taxis and tropotaxis. Representative animal: lobsters, blue crabs.	High sampling rate and high spatial integration. Probable strategy: chemotaxis and tropotaxis. Representative animal: sea stars?

The table defines the four possible combinations of TIF and SIF that represent the different states of animal sampling with respect to their fluid dynamic environment, and describes, for each, the relative abilities to sample in spatial and temporal domains, the probable strategies that will result in effective orientation, and the types of organisms that might be expected to display these abilities. In these cases, chemotaxis refers to the use of temporal comparisons of gradient strength, and tropotaxis corresponds to spatial sampling.

uncover examples of animals that sample at a fine scale (high TIF), although in principle, such conditions are possible. In aquatic realms, slow-moving animals with sensors deep within the boundary layer may represent such cases, and they may operate in a milieu accurately modeled with time-averaged Gaussian formulations. Echinoderms are relatively large, but not fleet of foot, suggesting high scores for both SIF and TIF. Although sampling frequency for these animals is unknown, even very low values still allow sufficient resolution at the boundary layer conditions relevant to crustaceans; with a 10 mm/s movement speed (*e.g.*, Moore and Lepper, 1997) and a sensor height of 1 cm, a 1 Hz sampling frequency gives a TIF of 10. Gastropods are a likely candidate for possessing high TIF but low SIF, given their sluggish crawling speed and small size. On the basis of the foregoing analysis, we might expect an echinoderm to employ a combination of temporal and spatial sampling strategies, but spatial comparisons are unlikely to be of use to a gastropod.

The foregoing analysis does not imply that fine temporal sampling is impossible in air. In fact, it may be even more likely in air under appropriate conditions, since kinematic viscosity in air is 8–14 times greater than in seawater over a temperature range of 0°–30°C. Thus, under equal flow velocities and turbulence conditions, and for animals of equal size and movement velocity, the Kolmogorov size limit is about 4.75–7 times larger (eq. 3) in air than in water. Put another way, an insect could move seven times more quickly, or sample seven times more slowly, and have the same temporal sampling ability as an oceanic creature under similar flows. Indeed, the low TIF in insects is primarily a function of their exceedingly high flight speeds, suggesting that crawling or walking terrestrial arthropods potentially could act in a way similar to that of denizens of the aquatic benthos.

Unresolved Issues

Our understanding of the mechanics of navigation, particularly in turbulent flows, is still in its infancy. Although a model incorporating rapid responses to odor filaments, tropotactic edge detection, and reliance on flow captures the essence of the orientation strategy, substantial gaps remain. Of immediate concern is identifying the range of critical stimulus parameter values that results in effective orientation. If up-current progress is largely mediated by the presence of detectable odor pulses, as it appears to be in moths (Vickers, 2000), then deleterious effects of turbulence may simply be due to increased intermittence that makes sustained progress less likely. During pheromonal tracking, the upstream surge of a moth in response to odor decays rapidly, and the moth begins to move cross-steam between successive stimulations. Rare encounters with odor pulses result in large cross-stream tracks that may take the insect out of contact with the plume, and that result in indirect trajectories to the source. Increased turbulence also causes more indirect trajectories in blue crabs (Weissburg and Zimmer-Faust, 1994), and this movement pattern seems to be correlated with greater signal variation and intermittence (although the expanded width of the odor plume and the inaccuracy of edge detection mechanisms may also be partially responsible). However, many foraging animals appear to respond to both the variance and the mean values of encounters with prey (Stephens and Krebs, 1986), and these two parameters interact to affect behavior. One possibility is that as the concentration of the odor pulse is increased, tracking occurs at more intermittent conditions as well. Such a scenario would hold if the propensity to engage in cross-stream casting in the absence of odor decreases with concentration, and it would be interesting to explore the potential interactions between intermittence and peak odor intensity during chemosensory tracking.

It is also clear that at this stage we have examined only a narrow range of stimulus conditions, and have rarely characterized the flow using standard fluid mechanical descriptors. One newly emerging issue is how the interaction between the release properties of the signal source and the ambient flow affects the resulting signal. Using laser-induced fluorescence to map odor concentrations at a fine scale, initial studies (Roberts, Webster, and Weissburg, unpub. obs.) suggest that the difference between jet and current velocities strongly determines the character of the signal (Fig. 4). When the jet velocity is matched to that of the ambient flow, plumes appear highly filamentous, and coherent structures retain their integrity far downstream of the source. As jet velocity is increased, the plumes become mixed more thoroughly, and the fine-scale features tend to vanish within a cloud of increasing homogeneity. These effects are most probably due to changes in shear-induced mixing at the border between the jet and the ambient fluid. As the velocity differential increases, the shear between the jet and the fluid is more pronounced, and results in greater mixing between the odor-laden jet and the clean water surrounding it. Previous studies have tended to use jets with high exit velocities relative to the ambient fluid (Weissburg, 1997; but see Finelli *et al.*, 1999), which nicely mimic certain types of odor sources (*e.g.*, actively pumping bivalves), but not others (*e.g.*, passively leaking objects). Before coming to firm conclusions about the nature of olfactory orientation, prudence dictates further exploration of the behavior of animals under different odor release conditions and geometries.

A real challenge for future investigators will be to verify that the plume morphology observed in flume flows adequately reflects plume structure in the field. The savvy student of chemosensory navigation in turbulent flows needs to be aware that laboratory characterizations have sometimes been compromised by inadequate flume designs. Acceptable principles of flume geometry and flow manipulation have been articulated, most recently by Nowell and Jumars (1987), and are summarized in Zimmer and Butman (2000). Unfortunately their recommendations have not always been incorporated into studies of animal navigation or chemical signal properties. Even when appropriate flow channels have been utilized, work in open-channel flumes incorporates strong assumptions regarding the properties of bottom boundary layers (*e.g.*, fully developed equilibrium flow) that may or may not be realized in the field. Studies in natural habitats are rare, and they have sometimes validated, at least qualitatively, the more extensive laboratory studies. However, in at least one case, boundary layers observed in nature are not consistent with laboratory studies in fully developed equilibrium flows (Hart *et al.*, 1996), suggesting that chemical signals entrained in natural habitats may not always be easily understood from currently available data.

One problem that is difficult to circumvent is that most open-channel flumes are rarely big enough to permit the large-scale meandering of the plume that is possible in less bounded natural habitats. The largest eddy size sustained in flume flows is on the order of the water depth (one reason why flumes must be much wider than deep—see Nowell and Jumars, 1987), which may or may not approximate the largest eddies in the field. These meanders induce a low-frequency component to the odor fluctuations, and hence could be of considerable importance to animals attempting to track plumes. These low-frequency components have not been well investigated in either the laboratory or the field. In addition to constraints imposed by flume geometry, the long temporal sampling necessary to capture these long-period components has not been performed, and obtaining the long-term records necessary to characterize larger scale plume movements should have high priority in future studies of plume dynamics.

Although flow fulfills a critical function for some animals in terms of specifying a general direction towards the source, investigators have suggested that it may be used for other purposes during orientation. It may, for instance, help steer an animal back into a plume (Weissburg, 1997). Alternatively, a coherent eddy containing odor may be a special cue due to the coincidence of information on both flow and odor. That animals may utilize this mechanism is suggested by the observations of Doall (discussed above) regarding mate-following in *Acartia hudsonica*, whereas Atema (1996) has speculated that larger animals may use such cues in a similar fashion.

If the co-occurrence of flow and odor is indeed part of the strategic repertoire of chemoperception, than its utility surely depends on the flow characteristics. In low Re, the two signals will be correlated for only as long as a vortex shed by an animal remains in motion. In *Temora longicornis*, vortices in the wake of a vigorously moving animal retain fluid motion for no more than 0.5 s (van Duren *et al.*, 1998). Thus, the receiver must be close to the source to have any likelihood of encountering the signal during the brief time that it contains both flow and odor information.

In high Re flows, the constraints on detecting coincident signals are quite different. Because of the energy (Kolmogorov) cascade, the fluid movements that create a given odor-containing eddy may subsequently transfer their energy to smaller length scales, leaving an odor signature that no longer reflects the fluid mechanical disturbances involved in its creation. Whether or not the superimposed patterns of velocity and odor concentration contain information is contingent on the strength of the correlation between velocity and odor fluctuations through both space and time. The integrity of chemical structures moving downstream in flow suggests that these two measures may be only loosely associated, but careful, simultaneous measurements of odor and velocity fluctuations are needed before a final conclusion is reached.

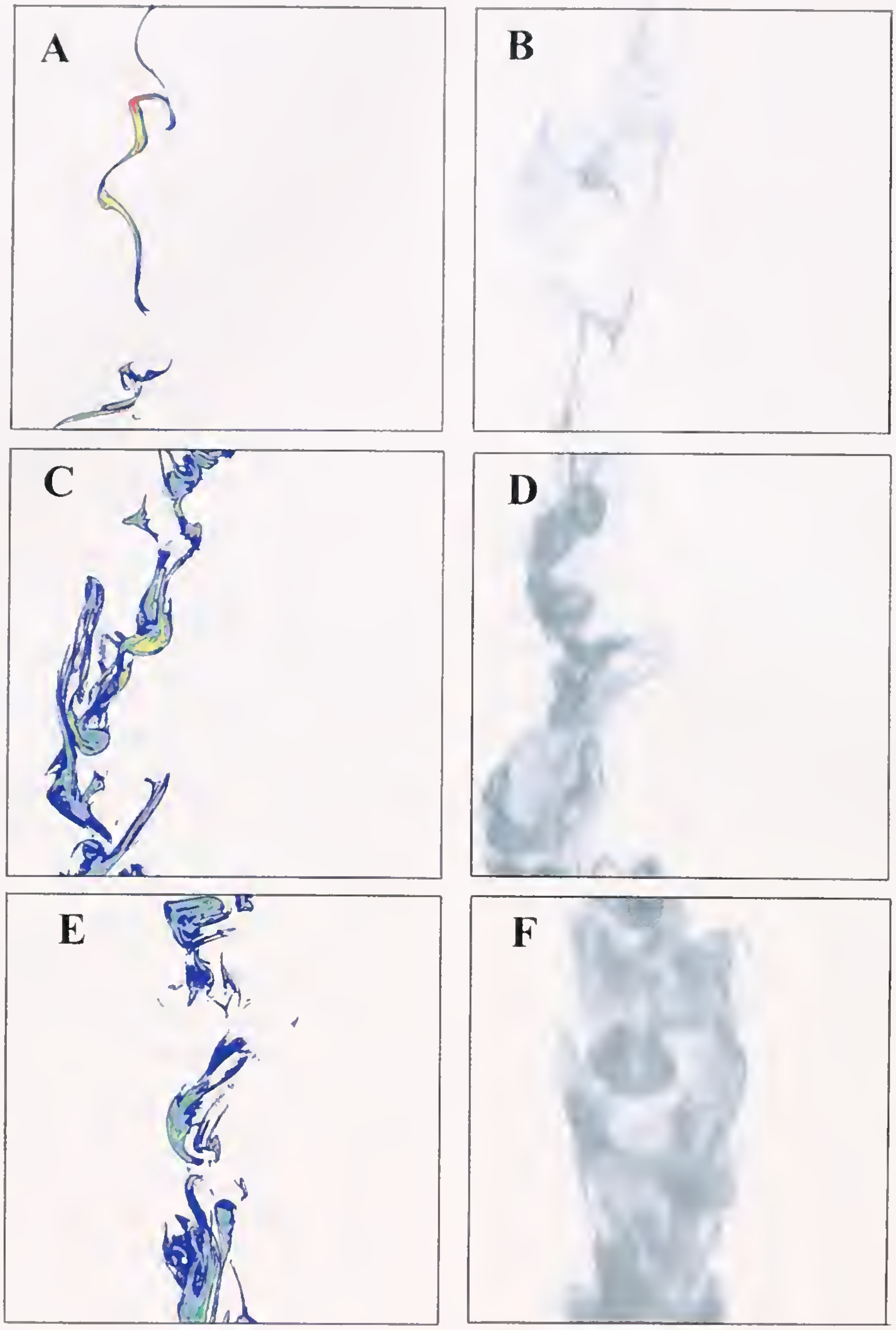

Figure 4. Paired laser-induced fluorescence (LIF) and dye visualization of an odor jet at different exit velocities. The left panels show LIF images, and the right panels show dye visualizations. All pictures were taken with a flow velocity of 5 cm/s, and the jet nozzle (2 mm i.d.) located 8 cm above the bottom, and pictures were taken at a distance of 60 cm downstream from the source using a concentration of rhodamine 6G equal to 200 μg/l. Each pair of images represents the same flow conditions, although at different times, and the images were chosen to provide representative views of the odor at each flow regime. Images were false colored so that concentration increases from blue (lowest) to red (highest). (A–B) exit velocity 5 cm/s; (C–D) exit velocity 20 cm/s; (E–F) exit velocity 40 cm/s. When the release rate is isokinetic to the flow, the resulting odor signal is coherent, filamentous, and with local regions of high intensity. As jet velocity increases, the odor source becomes mixed more thoroughly and concentrations are lower, in spite of the increase in the amount of dye released. The field is approximately 15 × 15 cm.

Concluding Remarks

Sensory systems are adaptations to their signal environment, and behavioral responses to chemical signals must be considered in the context of the fluid mechanical structures that determine the spatial and temporal properties of odor cues. Across a broad span of different taxonomic groups, organisms in particular fluid regimes characterized by Re, Kolmogorov scales, and other basic fluid mechanical properties converge upon common strategies of locomotion and orientation.

Our studies of chemosensory orientation have reached a stage where comparisons across taxa, if properly phrased, present an exciting opportunity to attain a more precise understanding of sensory and behavioral mechanisms. To advance further, we must continue our trend of placing the animal firmly in its fluid mechanical environment and probing more finely the properties of fluid flow and signal structure that have significant impacts on locomotory performance. The framework for our investigations should be to draw appropriate linkages between animals that operate in similar or dissimilar environments. Do copepods and ants have functionally similar abilities? Has the seeming dynamic similarity between crabs and moths really resulted in equivalent strategies? Is it possible to gain insights into the orientation of midwater creatures through studies of bacterial chemotaxis? Our abilities to develop creative approaches to these questions will, in large measure, determine our progress in understanding the sensory ecology of chemoperception.

Acknowledgments

Thanks to Dick Zimmer for organizing the cross-disciplinary symposium stressing the comparative philosophy. Conversations with David Dusenbery, David Fields, Terry Snell, Mario Tamburri, and Jeannette Yen were essential in broadening my approach, while my fluid dynamical colleagues Phil Roberts and Don Webster were always ready with a life-preserver, and provided access to unpublished data and LIF images. Funding from the Office of Naval Research (N00014-98-1-0076) has allowed me to continue to explore the fluid flow and its relation to animal navigation.

Literature Cited

Atema, J. 1996. Eddy chemotaxis and odor landscapes: exploration of nature with animal sensors. *Biol. Bull.* **191:** 129–138.

Baird, R. C., H. Johari, and G. Y. Jumper. 1996. Numerical simulation of environmental modulation of chemical signal structure and odor dispersal in the open ocean. *Chem. Senses* **21:** 121–134.

Baker, T. C., and K. F. Haynes. 1987. Manoeuvres used by flying male oriental fruit moths to relocate a sex pheromone plume in an experimentally shifted wind field. *Physiol. Entomol.* **12:** 263–279.

Bell, W. J., and T. R. Tobin. 1982. Chemo-orientation. *Biol. Rev.* **57:** 219–260.

Berg, H. C. 1975. Chemotaxis in bacteria. *Annu. Rev. Biophys. Bioeng.* **4:** 119–136.

Brown, B., and D. Rittschof. 1984. Effects of flow and concentration of attractant on newly hatched oyster drills *Urosalpinx cinerea* (Say). *Mar. Behav. Physiol.* **11:** 75–93.

Christensen, T. A., T. Heinbockel, and J. G. Hildebrand. 1995. Olfactory information processing in the brain: encoding chemical and temporal features of odors. *J. Neurobiol.* **30:** 82–91.

Crenshaw, H. 1993. Orientation by helical motion III. Microrganisms can orient to stimuli by changing the direction of their rotational velocity. *Bull. Math Biol.* **55:** 231–255.

Crenshaw, H. 1996. A new look at microrganisms: rotating and translating. *Am. Zool.* **36:** 608–618.

Denman, K. L., and A. E. Gargett. 1995. Biological-physical interactions in the upper ocean: the role of vertical and small scale mixing processes. *Annu. Rev. Fluid Mech.* **27:** 225–255.

Denny, M. W. 1988. *Biology and Mechanics of the Wave-swept Environment.* Princeton University Press, Princeton, NJ.

Denny, M. W. 1993. *Air and Water: The Biology and Physics of Life's Media.* Princeton University Press, Princeton, NJ.

Dittman, A. H., and T. P. Quinn. 1996. Homing in Pacific salmon: mechanisms and ecological basis. *J. Exp. Biol.* **199:** 83–91.

Doall, M. H., S. P. Colin, J. R. Strickler, and J. Yen. 1998. Locating a mate in 3D: the case of *Temora longicornis. Philos. Trans. R. Soc. Lond. B* **353:** 681–689.

Doall, M. H., J. R. Strickler, and J. Yen. 1999. The spatial-temporal scales of interactions between copepods: implications for sensory systems and encounter rates. Abstr. American Society of Limnology and Oceanography Aquatic Sciences Meeting, Santa Fe, New Mexico, February 1–5.

Dusenbery, D. B. 1992. *Sensory Ecology.* W. H. Freeman, New York.

Dusenbery, D. B. 1997. Minimum size-limit for useful locomotion by free-swimming microbes. *Proc. Natl. Acad. Sci. USA* **94:** 10949–10954.

Dusenbery, D. B. 1998a. Spatial sensing of stimulus gradients can be superior to temporal sensing for free-swimming bacteria. *Biophys. J.* **74:** 2272–2277.

Dusenbery, D. B. 1998b. Fitness landscapes for effects of shape on chemotaxis and other behaviors in bacteria. *J. Bacteriol.* **180:** 5978–5983.

Ebina, Y., and K. Wiese. 1984. A comparison of neuronal and behavioural thresholds in the displacement sensitive pathway of the crayfish *Procambarus. J. Exp. Biol.* **107:** 45–55.

Finelli, C. M., N. D. Pentcheff, R. K. Zimmer-Faust, and D. S. Wethey. 1999. Odor transport in turbulent flows: constraints on animal navigation. *Limnol. Oceanogr.* **44:** 1056–1071.

Gargett, A. E. 1997. "Theories" and techniques for observing turbulence in the oceanic euphotic zone. *Sci. Mar.* **61 (Suppl. 1):** 25–45.

Gleeson, R. A. 1982. Morphological and behavioral identification of the sensory structures mediating pheromone reception in the blue crab, *Callinectes sapidus. Biol. Bull.* **163:** 162–171.

Gomez, G., and J. Atema. 1996. Temporal resolution in olfaction I: Stimulus integration time of lobster chemoreceptor cells. *J. Exp. Biol.* **199:** 1771–1779.

Hamner, P., and W. M. Hamner. 1977. Chemosensory tracking of scent trails by the planktonic shrimp *Acetes sibogae australis. Science* **195:** 886–888.

Hart, D. D., B. D. Clark, and A. Jasentuliyana. 1996. Fine-scale field measurement of benthic flow environments inhabited by stream invertebrates. *Limnol. Oceanogr.* **41:** 297–308.

Hodgson, E. S., and R. F. Mathewson. 1971. Chemosensory orientation of sharks. *Ann. NY Acad. Sci.* **188:** 174–182.

Incze, L. S., P. Aas, and T. Ainaire. 1996. Distributions of copepod nauplii and turbulence on the southern flank of Georges Bank: implications for feeding by larval cod (*Gadus morhua*). *Deep-Sea Res.* 1855–1873.

Jiménez, J. 1997. Oceanic turbulence at millimeter scales. *Sci. Mar.* **61 (Suppl. 1):** 47–56.

Johnsen, P. B. 1987. New directions in fish orientation studies. Pp. 85–101 in *Signposts in the Sea*, W. F. Herrnkind and A. B. Thistle, eds. University of Florida Press, Tallahassee, FL.

Jumper, G. Y. Jr., and R. C. Baird. 1991. Location by olfaction: a model and application to the mating problem in the deep-sea hatchetfish *Argyropelecus hemigymus*. *Am. Nat.* **138:** 1431–1458.

Katona, S. K. 1973. Evidence for sex pheromones in planktonic copepods. *Limnol. Oceangr.* **18:** 574–583.

Kats, L. B., and L. M. Dill. 1998. The scent of death: chemosensory assessment of predation risk by prey animals. *Ecoscience* **5:** 361–394.

Kelly, L. S., T. W. Snell, and D. J. Lonsdale. 1998. Chemical communication during mating of the harpactacoid *Tigriopus japonicus*. *Philos. Trans. R. Soc. Lond. B* **353:** 737–744.

Koehl, M. A. R. 1996. Small scale fluid dynamics of olfactory antennae. *Mar. Freshw. Behav. Physiol.* **27:** 127–141.

Koehl, M. A. R., and J. R. Strickler. 1981. Copepod feeding currents: food capture at low Reynolds number. *Limnol. Oceangr.* **26:** 1062–1073.

Lugt, H. J. 1995. *Vortex Flow in Nature and Technology*. Krieger, Malabar, FL.

Mackas, D. L., H. Sefton, C. B. Miller, and A. Raich. 1993. Vertical habitat partitioning by large calanoid copepods in the oceanic subarctic Pacific during spring. *Prog. Oceangr.* **32:** 259–294.

Mafra-Neto, A., and R. T. Cardé. 1998. Rate of realized interception on pheromone pulses in different wind speeds modulates almond moth orientation. *J. Comp. Physiol. A* **182:** 563–572.

Mann, K. H., and J. R. N. Lazier. 1991. *Dynamics of Marine Ecosystems: Biological-physical Interactions in the Oceans*. Blackwell Scientific, Cambridge, MA.

Moore, P. A., and J. Atema. 1991. Spatial information in the three-dimensional fine structure of an aquatic odor plume. *Biol. Bull.* **181:** 408–418.

Moore, P. A., and D. M. E. Lepper. 1997. Role of chemical signals in the orientation behavior of the sea star *Asterias forbesi*. *Biol. Bull.* **192:** 410–417.

Moore, P. A., N. Scholz, and J. Atema. 1991. Chemical orientation of lobsters, *Homarus americanus*, in turbulent odor plumes. *J. Chem. Ecol.* **17:** 1293–1307.

Moore, P. A., R. K. Zimmer-Faust, S. L. BeMent, M. J. Weissburg, J. M. Parrish, and G. A. Gerhardt. 1992. Measurement of microscale patchiness in a turbulent aquatic odor plume using a semiconductor-based microprobe. *Biol. Bull.* **183:** 138–142.

Moore, P. A., M. J. Weissburg, J. M. Parrish, R. K. Zimmer-Faust, and G. A. Gerhardt. 1994. Spatial distribution of odors in simulated benthic boundary layer flows. *J. Chem. Ecol.* **20:** 255–279.

Moore, P. A., D. M. Fields, and J. Yen. 1999. Physical constraints of chemoreception in foraging copeopds. *Limnol. Oceangr.* **44:** 166–177.

Murlis, J., J. S. Elkinton, and R. T. Cardé. 1992. Odor plumes and how insects use them. *Annu. Rev. Entomol.* **37:** 505–532.

Nezu, I., and W. Rodi. 1986. Open-channel flow measurements with a laser Doppler anemometer. *J. Hydraulic Engineering* **112:** 335–355.

Nowell, A. R. M., and P. A. Jumars. 1987. Flumes: theoretical and experimental considerations for simulation of benthic environments. *Oceanogr. Mar. Biol. Annu. Rev.* **25:** 91–112.

Pasquill, F., and F. B. Smith. 1983. *Atmospheric Diffusion*, 3rd ed. Wiley, New York.

Pawlik, J. R. 1992. Chemical ecology of the settlement of benthic marine invertebrates. *Oceanogr. Mar. Biol. Annu. Rev.* **30:** 272–335.

Pedley, T. J. 1997. Introduction to fluid dynamics. *Sci. Mar.* **61 (Soppl. 1):** 7–24

Ratchford, S. G., and D. B. Eggleston. 1998. Size- and scale-dependent chemical attraction contribute to an ontogenic shift in sociality. *Anim. Behav.* **56:** 1027–1034.

Restrepo, D., J. H. Teeter, and D. Schild. 1995. Second messenger signaling in olfactory transduction. *J. Neurobiol.* **30:** 37–48.

Sanford, L. P. 1997. Turbulent mixing in experimental ecosystem studies. *Mar. Ecol. Prog. Ser.* **161:** 265–293.

Schlichting, H. 1987. *Boundary Layer Theory*, 2nd ed. McGraw-Hill, New York.

Stephens, D. W., and J. Krebs. 1986. *Foraging Theory*. Princeton University Press, Princeton, NJ.

Sutton, O. G. 1953. *Micrometeorology*. McGraw-Hill, New York.

Svendsen, H. 1997. Physical oceanography and marine ecosystems: some illustrative examples. *Sci. Mar.* **61 (Suppl. 1):** 93–108.

Tamburri, M. N., and J. P. Barry. 1999. Adaptations for scavenging by three diverse bathyal species, *Eptatretus stouti*, *Neptunea amianta* and *Orchomene obtusus*. *Deep-Sea Res.* **46:** 2079–2093.

Tamburri, M. N., R. K. Zimmer-Faust, and M. L. Tamplin. 1992. Natural sources and properties of chemical inducers mediating settlement of oyster larvae: a re-examination. *Biol. Bull.* **183:** 327–338.

Tennekes, H., and J. L. Lumley. 1972. *A First Course in Turbulence*. MIT Press, Cambridge, MA.

Tsuda, A., and C. B. Miller. 1998. Mate finding in *Calanus marshallae* (Frost). *Philos. Trans. R. Soc. Lond. B* **353:** 713–720.

van Duren, L. A., E. J. Stamhuis, and J. J. Videler. 1998. Reading the copepod personal ads: increasing encounter probability with hydrodynamic signals. *Philos. Trans. R. Soc. Lond. B* **353:** 691–700.

Verity, P. G. 1988. Chemosensory behavior in marine planktonic ciliates. *Bull. Mar. Sci.* **43:** 772–782.

Vickers, N. J. 2000. Mechanisms of animal navigation in odor plumes. *Biol. Bull.* **198:** 203–212.

Ward, G. E., C. J. Brokaw, D. L. Garbers, and V. D. Vacquier. 1985. Chemotaxis of *Arbacia punctulata* spermatozoa to resact, a peptide from the egg jelly layer. *J. Cell. Biol.* **101:** 2324–2329.

Weissburg, M. 1997. Chemo- and mechanosensory orientation by crustaceans in laminar and turbulent flows: from odor trails to vortex streets. Pp. 215–246 in *Orientation and Communication in Arthropods*, M. Lehrer, ed. Birkhauser Verlag, Basel, Switzerland.

Weissburg, M. J., and R. K. Zimmer-Faust. 1993. Life and death in moving fluids: hydrodynamic effects on chemosensory-mediated predation. *Ecology* **74:** 1428–1443.

Weissburg, M. J., and R. K. Zimmer-Faust. 1994. Odor plumes and how blue crabs use them to find prey. *J. Exp. Biol.* **197:** 349–375.

Weissburg, M. J., M. H. Doall, and J. Yen. 1998. Following the invisible trail: kinematic analysis of mate tracking in the copepod *Temora longicornis*. *Philos. Trans. R. Soc. Lond. B* **353:** 701–712.

Westerberg, H. 1984. The orientation of fish and the vertical stratification at fine- and micro-structure scales. Pp. 179–203 in *Mechanisms of Migration in Fishes*. NATO Advanced Research Institute on mechanisms of migration in fishes. Plenum, New York.

White, F. M. 1991. *Viscous Fluid Flow*. 2nd ed. McGraw-Hill, New York.

Yen, J. 2000. Life in transition: balancing inertial and viscous forces by planktonic copepods. *Biol. Bull.* **198:** 213–224.

Yen, J., and J. R. Strickler. 1996. Advertisement and concealment in the plankton: what makes a copepod hydrodynamically conspicuous. *Invertebr. Biol.* **115:** 191–205.

Yen, J., M. J. Weissburg, and M. H. Doall. 1998. The fluid physics of signal perception by mate tracking copepods. *Philos. Trans. R. Soc. Lond. B* **353:** 787–804.

Zimmer, R. K., and C. A. Butman. 2000. Chemical signaling processes in the marine environment. *Biol. Bull.* **198:** 168–187.

Zimmer-Faust, R. K., and M. Tamburri. 1994. Chemical identity and ecological implications of a waterborne, larval settlement cue. *Limnol. Oceanogr.* **39:** 1075–1087.

Reference: *Biol. Bull.* **198:** 203–212. (April 2000)

Mechanisms of Animal Navigation in Odor Plumes

NEIL J. VICKERS

Department of Biology, University of Utah, Salt Lake City, Utah 84112

Abstract. Chemical signals mediate many of life's processes. For organisms that use these signals to orient and navigate in their environment, where and when these cues are encountered is crucial in determining behavioral responses. In air and water, fluid mechanics impinge directly upon the distribution of odorous molecules in time and space. Animals frequently employ behavioral mechanisms that allow them to take advantage of both chemical and fluid dynamic information in order to move toward the source. In turbulent plumes, where odor is patchily distributed, animals are exposed to a highly intermittent signal. The most detailed studies that have attempted to measure fluid dynamic conditions, odor plume structure, and resultant orientation behavior have involved moths, crabs, and lobsters. The behavioral mechanisms employed by these organisms are different but generally integrate some form of chemically modulated orientation (chemotaxis) with a visual or mechanical assessment of flow conditions in order to steer up-current or upwind (rheo- or anemo-taxis, respectively). Across-stream turns are another conspicuous feature of odor-modulated tracks of a variety of organisms in different fluid conditions. In some cases, turning is initiated by detection of the lateral edges of a well-defined plume (crabs), whereas in other animals turning appears to be steered according to an internally generated program modulated by odor contacts (moth counterturning). Other organisms such as birds and fish may use similar mechanisms, but the experimental data for these organisms is not yet as convincing. The behavioral strategies employed by a variety of animals result in orientation responses that are appropriate for the dispersed, intermittent plumes dictated by the fluid-mechanical conditions in the environments that these different macroscopic organisms inhabit.

Introduction

By and large, life exists in one of two fluid environments, air or water. These media offer a vast array of different conditions, even the most severe of which have been successfully colonized by life. Although the range of conditions that support life appears to be extremely broad, the fact that air and water are fluids means that, in principle, they are governed by the same physical laws (Denny, 1993). Thus the physical behavior of fluids is important to organisms that orient with respect to chemical signals, because fluid dynamics impinge directly upon the distribution of odorant molecules in time and space. Furthermore, the fluid environment also impinges directly upon the locomotory activity of organisms. Hence, fluid conditions dictate both the dispersal of odor molecules in the environment and the ability of organisms to orient to the signal being transported. The physical nature of air and water with particular reference to biological systems has been excellently reviewed in considerable detail elsewhere (Denny, 1993; Vogel, 1994; Weissburg, 1997, 2000), so the brief discourse here will serve as the framework for the more substantive treatment that will be given to the mechanisms employed by animals to navigate and orient with respect to chemical signals. The focus will be on macroscopic animals, although examples of smaller life-forms will be used where appropriate.

The ability to sense and respond to the chemicals present in the environment exists in virtually all living creatures from unicellular bacteria to complex, multicellular organisms. The scale of these organisms covers many orders of magnitude, from the smallest single cell to the largest creatures that exist today. Biological as well as physical limitations must, therefore, have shaped the types of chemical signals that a particular organism can detect and respond to effectively.

Received 6 July 1999; accepted 24 November 1999.

E-mail: vickers@biology.utah.edu

This paper was originally presented at a symposium titled *Chemical Communication and Ecology*. The symposium, which was held in San Diego, California, on 30 December 1998, was invited by the Western Society of Naturalists as part of its annual meetings.

What is an Odor Plume, or How do Fluid Physics Affect the Distribution of Odor Molecules in Time and Space?

When molecules escape a solid substrate they become subject to physical forces in the fluid. What features of fluids are important in determining how molecules are dispersed once those molecules become fluid-borne? In a fluid that is not moving, molecules that escape the substrate form a concentration gradient that is highest closest to the source and lowest at points farthest away. Obviously, the molecular weight of a molecule has a significant impact on the time taken for a concentration gradient to be established throughout a given volume of fluid. Where molecular diffusion is the main force driving the distribution of molecules, the only signal available to an animal is the chemical itself and its spatiotemporal gradient.

For organisms of our scale it seems hard to envisage situations in which fluids are completely static and molecular diffusion is the predominant force responsible for distributing molecules. However, many organisms exist at scales where molecular diffusion is the salient force behind the distribution of chemical signals. Take a bacterium, for example, that exists within a small volume of fluid. Diffusion will distribute molecules emitted by a source, allowing a concentration gradient to form and orientation with respect to that gradient to occur. Nevertheless, for most macroscopic organisms, fluid movement has a major effect upon the dispersion of chemical signals. If we imagine a simple situation in which a fluid is flowing smoothly over a source of chemical molecules, the fluid is actually static at the point of contact with the substrate. The diffusive sublayer is the region closest to the substrate, where fluid motion comes to rest. This sublayer is one of several that together constitute what is known as the boundary layer (Denny, 1993; Vogel, 1994; Weissburg, 1997, 2000). Across the boundary layer there is a velocity gradient until the fluid reaches 99% of the mean flow velocity (Weissburg, 1997, 2000). Boundary layers have important implications that affect both the distribution and detection of chemical signals, and they are, therefore, of particular importance to animals that use chemical cues to orient. For molecules that pass through the boundary layer, molecular diffusion continues but, depending upon the conditions (such as flow speed of the fluid), the movement of the fluid now plays the major role in distributing molecules in time and space. In smooth, steady-flow environments, the interaction between molecules and flow forms a plume that has relatively distinct boundaries, with a strong gradient across the transverse axis and a weaker longitudinal gradient.

Laminar flow conditions, like molecular diffusion, are relatively uncommon. Anyone who has been fascinated by the patterns of smoke or steam issuing from a chimney and being transported downwind will immediately appreciate the fact that fluid flow is rarely stable. Instead, swirling and eddies within the moving air seem to play a major role in distributing smoke particles. The chaotic movements of the fluid are known as turbulence and are caused by fluctuations in velocity. Turbulence may be caused by, among other things, the flow of fluids around stationary objects (that may or may not be acting as sources of chemical emission) that induce the formation of eddies and vortices in their wake. Various mathematical terms can be used to describe the nature of the fluid environment (*e.g.*, the Reynolds number). A complete description of these terms and their implications for fluid flow can be found in extensive reviews elsewhere (Denny, 1993; Vogel, 1994; Belanger and Willis, 1996; Weissburg, 1997, 2000).

Importantly, particles being transported in turbulent eddies have a tendency to move down a concentration gradient, but turbulent diffusion is a property of how the fluid moves and not of the particles themselves. Therefore, in a plume created by turbulent diffusion, unlike one produced by simple molecular diffusion, the molecular weight of a molecule does not impact its distribution. Consequently, molecules that are released from the substrate at a certain ratio should retain their relative concentrations in situations where turbulent flow dominates. Hence, odor blends could comprise molecules of widely varying molecular weight. This certainly may be the case for odors that are passively released into the environment (those from plants, for example, may be a mixture of compounds of low and high molecular weights). However, odor mixtures that are actively produced and emitted (such as the female-produced pheromonal mixtures of different moth species) are not highly divergent, probably because the biosynthetic pathways responsible for manufacturing the molecules have been well conserved over evolutionary time.

Another attribute of turbulent flow conditions is that the mean direction and speed of fluid flow may be relatively constant, but the instantaneous flow pattern at any point in the plume might be difficult to predict—local flow fields may even be heading in the direction opposite to mean flow. The physical conditions that result in the turbulent dispersal of molecules therefore have several important effects that impinge upon the use of chemical signals by animals for navigation:

1. Particles are distributed intermittently. Small-scale eddies can result in fine-scale intermittency, whereas larger scale intermittency is caused by shifts in the direction of flow and results in plume meandering. The odor patches themselves may contain information that can be used to orient and locate the odor source.
2. Fluid flow properties and their effects upon the distribution of odorous molecules in time and space are potential sources of information for navigation.
3. Once dispatched from a source, odors comprising

more than one molecule are present as a blend and retain their ratios relative to one another, even though there may be disparities in the molecular weights of the constituent molecules.

To produce changes in the behavior of an organism, odorants must be detected by some type of chemosensory structure. Physical constraints similar to those that affect the release of molecules into a fluid are equally important in their detection. Most significantly, because detectors are housed in solid structures around which the moving fluid is displaced, the detector has a boundary layer associated with it that odorous molecules must traverse before their capture by the chemosensory apparatus (Vogel, 1983; Loudon *et al.*, 1994; Koehl, 1996). Boundary layers around olfactory appendages can be affected by the speed with which the organism is moving relative to the fluid or by movements of the appendages themselves through the fluid (*e.g.*, antennule flicking in lobsters, Moore *et al.*, 1991a). Thus, the external morphology of a chemosensory appendage and its position relative to the animal's body (which will experience a different boundary layer) may play an important role in determining the efficiency of the olfactory structure in capturing chemical cues.

Information Available in Odor Plumes

From the brief discussion above it should be clear that several sources of information about the position of an odor source origin relative to the organism in question can potentially be extracted from the odor plume. Of course, this assumes that arrival at or movement away from the odor source is the behavioral objective of the organism in question. Two potential sources of information that pertain to the location of an odor source are discussed:

1. Presence or absence of the odor and any gradients associated therewith

The presence or absence of odor is obviously a crucial feature of any odor plume, and how animals respond to odor or odor loss has helped us understand the mechanisms animals use to navigate. In the absence of flow or visual stimuli associated with the origin of odor emission, the chemical signal itself is the only source of information that can be extracted. In such cases, the ability to detect the chemical gradient can be used to locomote toward or away from the odor source. Mechanisms known to be used for orienting with respect to chemical gradients include chemotaxis or chemokinesis and rely upon the ability to sample the milieu either spatially (comparing inputs to more than one chemosensory structure at the same time and responding to balance inputs—more correctly known as tropotaxis) or temporally (sampling at one location, moving, then sampling again—more correctly known as klinotaxis). Taxes refer to the ability to direct motion relative to the source of stimulation, *e.g.*, up or down a chemical gradient; kineses are generally reserved for situations in which some measure of locomotory output increases or decreases, but the resulting motion is random with respect to the stimulus source (see Bell and Tobin, 1982, for review of these terms). This latter discussion serves to emphasize that understanding both the locomotory activity of an organism and the strategy for sampling the odor environment are important in accurately describing the behavioral mechanisms utilized.

In turbulent odor plumes the fluid dynamic conditions play a major role in creating the spatiotemporal distribution of odor molecules. Several studies have measured odor plume structure either in water or air to determine odor parameters that have the potential to be extracted and used by animals that navigate in odor plumes (Murlis, 1986, 1997; Murlis *et al.*, 1992; Moore and Atema, 1991; Zimmer-Faust *et al.*, 1995; Finelli *et al.*, 1999). In a laboratory flume, dopamine-sensitive carbon fiber microelectrodes have been used to measure fine-scale odor plume structure (Moore *et al.*, 1989; Moore and Atema, 1991). Other studies have utilized the same electrochemical techniques in combination with fluorometric measurements (the fluorescein dye used also provides a useful visible marker) to characterize odor plume structure under known hydrodynamic conditions in a simple aquatic environment such as an estuarine tidal creek (Zimmer-Faust *et al.*, 1995; Finelli *et al.*, 1999). Measurements at fast temporal time scales show that the odor plume is highly intermittent, with bursts of high odor concentration interspersed with low or zero concentration. In addition, the peaks and onset slopes of odor transients vary systematically along both transverse and longitudinal axes of odor plumes (Moore and Atema, 1991; Zimmer-Faust *et al.*, 1995; Finelli *et al.*, 1999). The lateral edges of these aquatic plumes were represented by a sharp decline in the presence of both the electrochemical tracer and the fluorescein dye over a short distance. This transverse gradient was much greater than any concentration gradient along the longitudinal axis of the plume (Zimmer-Faust *et al.*, 1995). As distance from the source increased, odor plumes tended to spread horizontally and vertically, and mean peak height and slope of odor fluctuations decreased (Moore and Atema, 1991; Zimmer-Faust *et al.*, 1995; Finelli *et al.*, 1999). Nevertheless, much larger fluctuations in concentration than might be predicted from time-averaged plume models were detected far downstream (Moore and Atema, 1991; Zimmer-Faust *et al.*, 1995). Organisms that orient in such plumes may use intermittency or cues derived from the shape of odor pulses to steer in the direction of the odor source (see below; Weissburg, 1997). The fluid dynamic properties of air and terrestrial recording sites result in greater odor-plume intermittency compared to aquatic sites such as an estuarine creek. Indeed, airborne plumes created by an ion source and measured in the field are highly intermittent (Murlis, 1986, 1997; Murlis *et al.*, 1992), so much so that even in the plume the signal has been estimated to be absent for 60% to 90% of the time (Murlis, 1997).

2. Odor presence or absence coupled with fluid flow information (mechanical or visual)

The presence of flow (either smooth or turbulent) provides an additional source of information that can be integrated with the detection of chemical signals. Because the direction of mean fluid motion is downstream of an odor source, any odor that is detected must have come from upstream. By resolving direction of fluid movement, an organism can determine what direction to take towards a distant and frequently unseen source of odor. The mechanism for the detection of flow depends, to a large degree, upon the life history of the organism in question. For animals that dwell on a fixed substrate, flow can be detected by mechanical means—*i.e.*, pressure differences detected by mechanoreceptors located on the animal's body, head, or other appendages. The direction of flow can be gauged by the deflection of mechanosensors with reference to the substrate. Detection of flow in this manner can be compromised by locomotory activity that will also stimulate mechanoreceptors. For this type of flow detection to operate efficiently, the organism must be able to distinguish movement of the flow due to the flow itself from activity in mechanoreceptive cells resulting from locomotion. In other substrate-bound organisms, flow direction can be estimated by differential cooling: a dog's nose and your own finger, wetted and held in the air, are instruments for detecting wind direction. Animals that orient to odor sources while flying or swimming are faced with a somewhat more complex task. Even though mechanical detectors can be stimulated by the activities of flying or swimming, the need to discriminate between movement of the fluid due to flow and movement of the fluid due to self-propulsion through it means that mechanoreception may not be a particularly reliable source of information for determining flow direction. Vision is far more reliable because locomotion can be referenced to fixed points in the environment such as the ground pattern or riverbed. In fact, experiments with flying moths and other insects have shown the extraordinary degree to which these creatures rely upon visual feedback in making their way upwind in an odor plume (Kennedy, 1939; David, 1986; Colvin *et al.*, 1989).

Biological Limitations

In addition to the constraints imposed by the physics of the fluid medium in which an organism exists, many biological constraints must be included in any understanding of how animals navigate and orient with respect to odor plumes. These biological restrictions can be broken into several categories that can be generally applied to all organisms, no matter what their size and scale:

Transduction

The first limitation concerns the speed with which chemical signals can be transduced by a chemosensory system. The ability to quickly process information arriving at the periphery is essential because it affects the entire response of the organism. For example, how frequently can the milieu be sampled and how well can sequentially arriving pulses be resolved (*i.e.*, how close can two pulses be without being perceived as a single pulse)? These sampling parameters may be particularly important for most macroscopic organisms whose olfactory environment includes turbulent plumes and intermittency as normal features. The threshold of response may also be an important constraint in responding to chemical signals. A certain number of molecules of the same type may have to arrive simultaneously (or within the integration period of the sensor) to produce a response in the sensory apparatus. Even the simplest systems are limited by the speed with which odorant molecules are cleared from their receptors (Denny, 1993). Molecules that occupy a binding site effectively prevent a receptor from responding to future encounters with odor. Thus rates of sensory adaptation and disadaptation certainly influence the ability of an organism to respond to repeated chemical stimuli. In animals with even simple nervous systems these peripheral processes may have higher order corollaries such as habituation and learning that can affect the behavioral performance.

Processing

The second important biological limitation is how quickly information is processed by the organism. Processing may or may not involve communication with other cells. For example, transduction of chemical signals by a unicellular bacterium in a chemical gradient may not be followed immediately by a response, because other biochemical pathways have to be activated before the cell changes direction or rate of locomotion. Similarly, in organisms with a multicellular nervous system, the existence of chemical connections between neurons imposes an inevitable delay between transduction events at the periphery and the resulting behavioral response. This delay affects the rapidity with which an organism can respond to the chemical environment.

Behavior

Behavioral limitations include constraints imposed by the organism itself. There are obvious gross restrictions which include, for example, only being able to walk or run instead of fly. In addition, there are finer locomotory limitations. In other words, a bacterium can move only so many body lengths or make directional changes only so many times every second; each species of moth has a maximum sustainable flight speed, etc. Of course, there will be variation among individuals, but each organism has an upper limit. These behavioral effects are not independent of delays caused by the transduction and processing events mentioned above but are inclusive of them; together they can be considered as a behavioral latency. Taken together, these biological constraints influence the speed with which organisms perceive and react to changes in the chemical environment. Our own ability to notice such changes is constrained by our ability to resolve differences in the behavioral output of organisms. Marked changes can be readily observed, but more subtle variations in behavior may reflect important fine-tuning of locomotory activity that might easily be overlooked with observational techniques that do not sample the behavior at a sufficiently fast frequency.

Mechanisms of Navigation in Odor Plumes

One cannot help but notice that dissimilar organisms tend to have similar paths in solving odor-orientation problems (Fig. 1). Crabs and lobsters pursue somewhat meandering upstream paths when stimulated by appropriate odors (Fig. 1A, B). A male moth orienting to a calling female or a synthetic sex-pheromone source (Fig. 1C), a procellariiform bird homing in on a potential source of food, and a salmon orienting to its native stream all must move against the mean direction of fluid flow, and all make turns during their upstream progress (the latter two examples are illustrated in fig. 1 from Arbas *et al.*, 1993). This observation is based upon the similarity of the tracks that the animals follow through space as they navigate toward an odor source, although we must bear in mind the important distinction between those creatures that fly or swim freely through their fluid surroundings (moth, fish, bird) and those that orient while in contact with the substrate (crab, lobster). Even for animals in similar situations, we cannot assume that the behavioral mechanisms that underlie the production of their tracks are the same, even though this assumption is a tempting one. Instead each organism must be viewed within the context of the particular conditions under which the behavior occurs naturally, because these are likely to represent the pressures that have shaped the behavioral and transduction/processing mechanisms over evolutionary time-scales.

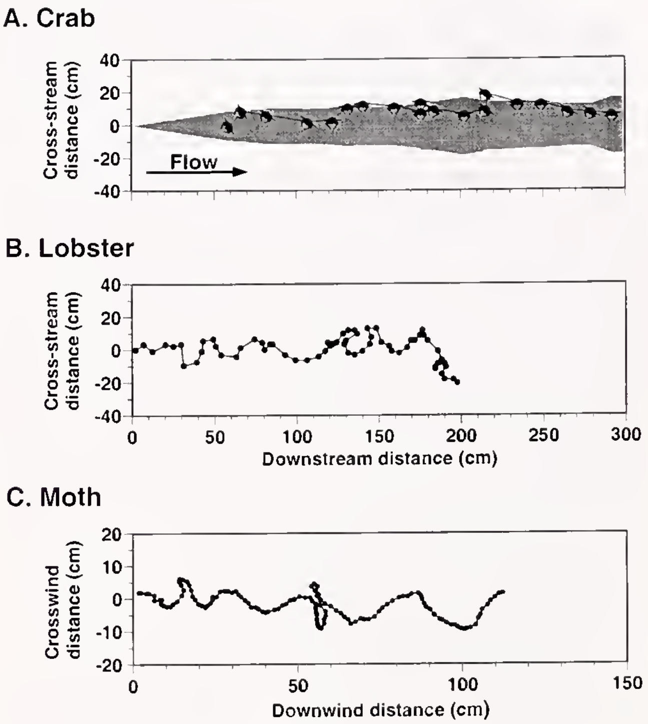

Figure 1. Different organisms frequently have similar paths through space during odor-mediated orientation. However, the similarity in trajectories does not necessarily mean that each animal is employing the same orientation mechanism. (A) A crab, *Callinectes sapidus*, orienting toward an odor source created by a clam in a tidal creek. Flow velocity is 10 cm/s, and the crab's position is marked at 1-s intervals (from Zimmer-Faust *et al.*, 1995, with permission). The boundaries of the plume as visualized by fluorescein dye are indicated by the shaded area. The crab is thought to use a combination of rheotactic and chemotactic orientation mechanisms. (B) The lobster, *Homarus americanus*, orienting to an odor source of homogenized mussel in an experimental flume. Flow velocity was approximately 1 cm/s, and the lobster's position is marked at 1-s intervals (from Moore *et al.*, 1991b, with permission). The results of this study suggested that lobsters used a chemotropotactic orientation mechanism. (C) Flight track of a male moth, *Heliothis virescens*, responding to a point-source of female sex-pheromone. The wind speed was 60 cm/s. Note that the position of the moth is marked every 1/30th s, as compared to the crab and lobster tracks. Male moths have been shown to use a visually guided mechanism to compensate for wind-induced drift and steer upwind (optomotor anemotaxis). The reversals from one side of the wind line to the other that occur along the track are the result of a second program of internally generated turns known as counterturning. Both anemotactic and counterturning mechanisms are modulated by contact with odor. In all three situations, the direction of fluid flow is from left to right (as indicated in A). Note that the scales for A and B are the same, whereas C is enlarged. In A and B, the odor source was located at the graph origin ($X = 0$, $Y = 0$), whereas in C the pheromone source was located about 30 cm further upwind, to the left, of the graph origin.

Nevertheless, in each of the examples above it seems possible that the fluid environment provides either visual or mechanical stimuli that might be integrated with odor information to provide some measure of the direction of flow. The upwind flight of male moths under the olfactory influence of female-emitted pheromone has been particularly well-studied and extensively reviewed recently (Baker and Vickers, 1997; Cardé and Mafra-Neto, 1997; Kaissling, 1997; Willis and Arbas, 1997; Vickers, 1999). Thus an extensive review of olfactory-mediated flight in moths seems unnecessary here. Only relatively specific comments will be made, while integrating the moth system with those of other animals that orient with respect to turbulent, intermittent odor plumes to point out common features of the navigational mechanisms.

Integrating flow and odor detection

As was mentioned earlier, the most reliable method for animals that actively fly or swim to detect direction of fluid flow is to reference movement relative to stationary objects in the environment. This has long been known to occur in insects, as Kennedy (1939) first demonstrated with mosquitoes flying in a plume constituted of his own exhaled breath. Much subsequent work on flying male moths orienting in a pheromone plume has shown that these animals are extremely sensitive to movements of the ground pattern (for example, see Baker and Vickers, 1994). Essentially, the fluid movement causes a discrepancy between the animal's direction of movement (heading or course) in the fluid and static objects in the environment. Resolution of the resultant drift is hypothesized to enable moths to steer more or less into the wind and also to ascertain whether they are making progress against the wind or are "losing ground," *i.e.*, being carried downwind (Baker and Vickers, 1997; Cardé and Mafra-Neto, 1997; Kaissling, 1997; Willis and Arbas, 1997; Vickers, 1999).

The evidence for such visually steered mechanisms in other animals is not yet as convincing, largely because the data derive from observational rather than manipulative, experimental studies. Observations of the flight trajectories and behavior of procellariiform birds over the open sea has shown that they approach sources of odor produced by slicks from downwind, presumably using their extremely well-developed olfactory systems (Nevitt, 1999). Perhaps some sort of visual feedback is utilized to determine wind direction. However, it is not clear how pelagic birds integrate visual cues with olfactory signals, given that the entire ocean is heaving and swelling and otherwise certainly not stationary. The possibility exists that these birds exploit some other mechanism to determine wind direction. The slick odor sources used in such experiments must be essentially invisible to an approaching bird unless other individuals have already arrived at the site, thereby providing visual cues themselves. Thus, the birds that first arrive are presumably the ones most capable of locating the odor source through olfactory signals alone or through olfaction integrated with visual/mechanical cues, and future studies should focus on those species. In other field studies, petrels and shearwaters were observed to approach food sources, nesting colonies, and individual nesting sites under cover of darkness and always from downwind (Grubb, 1972, 1974, 1979). Under such conditions, darkness may preclude the use of visual feedback for the purposes of determining wind-induced drift, again raising the possibility that other mechanisms are employed.

In many species of fish, odor-modulated navigation also appears to occur with the animal moving up-current. However, in only one species has experimental evidence been accumulated that indicates that up-current movement in the presence of odor relies upon visual feedback from objects in the environment (Emanuel and Dodson, 1979). Sharks are also able to locate sources of odor, perhaps by using a combination of rheotactic (an oriented response with respect to the direction of water flow) and chemotactic mechanisms (Hodgson and Mathewson, 1971).

Turning behaviors

Another common feature of the tracks of animals that fly, swim, or walk to odor sources is that up-current progress rarely occurs in directly straight lines (Fig. 1). Most animals observed thus far tend to switch back and forth across the direction of fluid flow. In flying moths, this phenomenon has been well-studied and the mechanism underlying it debated (Baker and Vickers, 1997; Cardé and Mafra-Neto, 1997; Willis and Arbas, 1997; Witzgall, 1997). A number of experiments, which have been summarized in greater detail (Baker and Vickers, 1997; Cardé and Mafra-Neto, 1997; Vickers, 1999), suggest that the species-specific turning rates are driven by an internal "clock" that results in regular reversals from one side of the wind line to the other as the moth makes net progress toward the source. The mechanism, known as counterturning, is integrated with the visually steered compensation for wind-induced drift; together these mechanisms produce the upwind zigzagging flight tracks typical of many insects flying to an odor source (Fig. 1C). Other animals such as birds (Arbas *et al.*, 1993) perform similar maneuvers during upwind flight in response to odor, but again, the actual mechanisms underlying the behavior have not been examined under rigorous experimental conditions. Likewise, fish such as salmon were observed to zigzag as they returned to their home streams (Johnsen and Hasler, 1980).

Substrate-dwelling animals that inhabit aquatic environments have been the focus of many studies upon odor-mediated behavior. Fluid dynamics are somewhat easier to measure and manipulate in the aquatic realm, and so these studies are particularly enlightening as to the relationship between fluids, odors, and the potential mechanisms employed by animals to locate odor sources. Both crabs and lobsters have been the subjects of intensive investigation (Weissburg and Zimmer-Faust, 1993, 1994; Zimmer-Faust *et al.*, 1995; Moore *et al.*, 1991b). For the blue crab, *Callinectes sapidus*, flow is an important cue in determining successful orientation to an odor source. No-flow or high-flow conditions resulted in poor orientation responses, whereas a slow flow speed resulted in high levels of source location (Weissburg and Zimmer-Faust, 1993). These experiments suggested that males made orientation responses with respect to the direction of flow (rheotaxis). In addition, these crabs also used chemotaxis, as evidenced by their turning behavior upon crossing the relatively sharp lateral edges of the plume. The turning behavior of *C. sapidus* is therefore distinct from that of flying moths, which respond to an internal turning clock rather than to the detection of a lateral chemical gradient. The lobster *Homarus americanus* also responded to odor plumes but appeared to rely more upon the information contained within and between odor pulses for orientation than upon the direction of flow itself (Moore *et al.*, 1991b). Thus, these animals may use simultaneous bilateral comparisons to remain or turn into the plume and sequential comparisons of odor intensity to advance toward the source (Weissburg, 1997).

Recording odor plume dynamics and behavior simultaneously

In general, the study of fluid dynamics in air is somewhat less tractable than in water. One of the ways that our knowledge of orientation mechanisms and odor plume dynamics has been advanced in recent years is by utilizing techniques that can detect odors or odor representatives. Murlis and co-workers used ion generators and detectors to measure odor plume dynamics in terrestrial habitats (Murlis, 1986, 1997; Murlis *et al.*, 1992). These studies have been particularly instructive in establishing the types of odor stimuli that might be encountered by flying insects, for example.

The actual olfactory appendages of insects have also been successfully used to determine odor plume structure and dynamics. The moth antenna is easily detached and can be readily hooked up to electrodes. Electrical activity measured across the antenna is thought to represent the compound activity of the olfactory receptor cells housed in cuticular projections that often cover the antennal surface by the thousand. The resulting electroantennogram (EAG) has been useful in visualizing pheromone plume structure. Baker and Haynes (1989) used EAGs to measure plume structure in the field and pushed an EAG preparation along a wind tunnel toward a pheromone source to simulate the odor plume that a flying male encounters (Baker and Vickers, 1994). An EAG preparation transported by an intact flying male gave an impression of the frequency and magnitude of olfactory stimulation that a male moth encounters as he flies upwind in a pheromone plume emitted by a single, point-source (Vickers and Baker, 1994a). Lobsters transporting an electrochemical microelectrode and "back pack" gave a similar impression of their olfactory world at the olfactory receptor level (Basil and Atema, 1994). These studies are important because they have allowed us to visualize not only the dynamics of the odor plume but also the kinds of information that are being detected by the actual peripheral olfactory sensors and transmitted to the brain for further processing. Moreover, studies of this type should reveal to what extent odor plume dynamics are altered by locomotory activity or movement of sensory appendages, an important consideration given that most of the measurements of plume structure to date have used stationary detectors.

Orientating in "restricted" sensory environments

Experiments that alter the sensory world of an animal can be informative as to the mechanisms that those animals use. For example, moths forced to fly through a visually depauperate "blank" tube were unable to remain oriented with respect to a pheromone plume compared to situations in which the visual environment was enriched (Vickers and Baker, 1994b). Baker and Keunen (1982) stopped the wind for flying oriental fruit moths, leaving a stationary plume, suspended in the air. Deprived of the wind-induced drift that is thought to be necessary for steering upwind, some males were still able to locate the odor source, suggesting that other mechanisms can be invoked under certain conditions.

Some animals, however, exist in environments that afford only limited sensory feedback. Such situations might pose navigational problems for these creatures. How, for example, might fish or whales orient with respect to chemical signals in mid-ocean where stationary visual reference points are unavailable because everything drifts in the same current? How do deep-sea dwellers orient where visual cues are unavailable due to the lack of illumination? How do pelagic sea birds reference wind direction with respect to the rolling ocean, moving beneath them? What do insects in dark forests or cave-dwelling animals do when chemical signals beckon, but visual references are unavailable to tell them the direction of flow? Presumably, chemical signals still have a role to play in all these situations. Atema (1995) has suggested that some animals might be able to use "eddy chemotaxis" to orient with respect to chemical cues. In this case, the actual mechanical deformations in the fluid that are associated with the chemical signal are important in guiding locomotory activity. It is certain that mechanical deformation and vortices associated with other organisms can play a significant role in altering the behavior of other organisms. Recently, Yen and co-workers (Doall *et al.*, 1998; Weissburg *et al.*, 1998; Yen *et al.*, 1998) demonstrated that male copepods have the remarkable ability to quite literally track down conspecific females by following their wake structures and possibly the chemical signals contained therein. These tiny planktonic creatures also engaged in "casting" behavior when the mechanical/chemical trail went cold. There are other senses too, that may conceivably be integrated with chemoreceptive input to provide a sense of direction toward an odor source. For example, electric fish are able to "see" their environment: maybe they can use this sense to resolve deformations of the fluid world that they inhabit and couple this information with chemical input to orient toward an odor source. The lateral line of fish may provide mechanical cues associated with fluid conditions. Perhaps animals can "visualize" fluid flow by means of sonar or thermal sensory systems, particularly in the aquatic realm. In short, any sensory modality that can provide an indication of some attribute of the fluid environment is likely to have been exploited in one way or another. At present our search image is somewhat biased by those sensory modalities that we are most attuned to, namely vision and sound, but animals never cease to amaze us by either the extraordinary heights to which some of their senses are adapted or the existence of "sixth" senses that we simply do not possess.

Changing strategies as a result of moving in and out of odor—or how to span odor gaps?

Intermittency is a feature of any odor plume that is generated in a turbulent fluid environment (Murlis, 1986, 1997; Murlis *et al.*, 1992; Moore and Atema, 1991; Zimmer-Faust *et al.*, 1995; Finelli *et al.*, 1999). By moving in and out of turbulent plumes, organisms are likely to increase intermittency, producing even greater fluctuations in the chemical signal. From an animal's perspective, an important issue revolves around the decision of when to alter behavior in response to odor onset and loss (or perceived loss). Failure to act appropriately may reduce the chances of a timely arrival at a source of odor. On the other hand, some gaps can probably be ignored because they do not represent relevant changes in the stimulus and responding to them would reduce search efficiency. Thus animals must be able to determine how quickly to respond to gaps in odor and what kinds of changes in stimulus parameters (*e.g.*, frequency or concentration) or shifts in flow environment must elicit a response and what kinds can be ignored. The effects of the pulsatile structure of odor plumes upon moth flight behavior have been investigated. Vickers and Baker (1992) determined that male *H. virescens* required the generation of a certain number of pulses per second in order to sustain upwind flight. At a production frequency of fewer than four filaments per second, males were unable to locate the odor source. Subsequent studies revealed that males are actually capable of responding to encounters with individual filaments of odor and, after intercepting an odor filament, they make brief upwind surges towards the source (Vickers and Baker, 1994a, 1996). Other experiments using males of a distantly related moth species, *Cadra cautella*, revealed that this species also responds to encounters with single strands of pheromone (Mafra-Neto and Cardé, 1994, 1996). In both species, the frequency of filament generation has a significant effect upon the directness of upwind flight: the faster the frequency, the straighter the flight. Measurements on *H. virescens* revealed that both the anemotactic component of upwind flight and the counterturning were affected by the number of odor pulses available (Vickers and Baker, 1996; Vickers, 1999). Thus both mechanisms are directly modulated by odor encounters. These findings have been reviewed extensively recently (Baker and Vickers, 1997; Cardé and Mafra-Neto, 1997; Vickers, 1999).

Relatively little is known about how other organisms respond to odor gaps, or even about how long a time between odor stimuli is necessary to trigger the adoption of a new strategy. A simple strategy to handle gaps in odor stimulation is to arrest upstream movement and wait for olfactory stimulation to resume. This would seem to be particularly advantageous when the flow is relatively steady (producing plumes that do not meander too much), the organism is a substrate dweller, and the target emitting the signal is relatively sessile. Thus, a blue crab tracking the plume emitted by a sedentary mussel is a good example (Zimmer-Faust *et al.*, 1995). Moths do not switch to a new mechanism but adjust both anemotactic and counterturning programs to result in tracks that move side-to-side perpendicular to the direction of mean flow. This behavior, known as casting, is viewed as a way for the animal to resume contact with the odor plume. Casting in *H. virescens* involves increased vertical as well as lateral excursions, thereby facilitating a three-dimensional search of space (Vickers and Baker, 1996). Under certain circumstances, the animals will eventually drift back downwind; videorecordings of oriental fruit moth tracks in the field have shown that, on occasion, these insects will actually pursue a downwind course, perhaps in a effort to regain the odor plume (Baker and Haynes, 1997). Once contact is re-established, the insect may resume upwind flight, trying again to locate the source.

Future Directions

Clearly, there are relatively few systems in which the relationship between fluid dynamics, odor plumes, and animal orientation have even begun to be worked out. One can only hope that future endeavors will include organisms of varying scale that inhabit all types of fluid environment. On the basis of the various mechanisms animals employ to locate odor sources, I suggest that the following areas should prove fruitful for future research.

The olfactory environment

Much of our understanding has come from studies in which discrete odor sources have been used as the source of stimulation in relatively simple fluid environments (laboratory flumes and wind tunnels, tidal creeks and open fields). The actual environments organisms inhabit are considerably more complex in olfactory content and fluid dynamic properties. For example, the trajectories and structure of pheromone plumes created in a forest are different from those in an open field (Elkinton *et al.*, 1987; Willis *et al.*, 1994).

How are an animal's orientation responses modulated in more complex fluid mechanical situations? Are novel mechanisms employed? Understanding how the cues available in such landscapes are sorted, discriminated, and processed will provide insight into the behavioral mechanisms that animals use in their habitat.

Behavioral capabilities in natural arenas

We still know very little about the behavioral capabilities of animals. How far away from an odor source, for example, will a male moth orient, and how do the behavioral mechanisms change as the male approaches the source? Recent field experiments have shown that males generate faster airspeeds and counterturn less frequently farther away from a pheromone source (9–11 m) (Vickers and Baker, 1997). For practical reasons, laboratory studies in wind tunnels or flumes examine the behavior at 1–2 m from the source. How do the fluid dynamics affect the distribution and shape of odor pulses at greater spatial and temporal scales? What are the spatial, temporal, and fluid dynamical limits of behavioral responsiveness? These questions remain largely unanswered.

Odor plume dynamics

Locomotion. It is clear that the locomotor tactics of animals can change the perceived structure of an odor plume. Stationary measures of odor plumes have been and will continue to be instructive. However, an animal must move in order to locate an odor source. To what extent are stationary measurements of odor plume structure affected by introducing movement? Do two moths experience the same kinds of odor pulse fluctuations if one is 1 m away from an odor source and the other is 20 m away, flying twice as fast, and turning less often?

Neurobiology. What features of odor plume structure are detected and represented by peripheral and central nervous systems? Some studies have used neurobiological preparations such as EAGs (Baker and Haynes, 1989; Vickers and Baker, 1994a) or receptor neuron recordings (Baker *et al.*, 1988; Van der Pers and Minks, 1993) to track peripheral events associated directly with actual, behaviorally relevant odor fluctuations instead of with odor tracers or ions. Further experiments that combine neurobiological measurements of actual odor with detection of electrochemical or ion tracers (*e.g.*, Murlis *et al.*, 1990) could be extremely informative in determining those features of filamentous odor plumes that are extracted by the nervous system.

These suggestions are, of course, not exhaustive, but they do seem attainable in the foreseeable future. In conclusion, the importance of fluid dynamics in distributing odors in time and space has clearly been demonstrated in the few systems that have been thoroughly studied. A growing number of observational and experimental reports have strengthened the notion that animals are efficient at locating sources of odor in their habitats. Their orientation responses are appropriate for the types of odor plume that they typically encounter. Our current understanding of a limited number of model systems in relatively simple settings provides a solid foundation for future endeavors to understand the vital role that chemical signals play in mediating many of life's interactions.

Acknowledgments

Thanks are due to Dick Zimmer for the invitation to participate in the symposium at the Western Society of Naturalists meeting in December 1998 and for his great enthusiasm and positive criticism of an earlier version of this manuscript.

Literature Cited

Arbas, E. A., M. A. Willis, and R. Kanzaki. 1993. Organization of goal-oriented locomotion: pheromone-modulated flight behavior of moths. Pp. 159–198 in *Biological Neural Networks in Invertebrate Neuroethology and Robotics*, R. D. Beer, R. E. Ritzmann, and T. McKenna, eds. Academic Press, San Diego, CA.

Atema, J. 1995. Eddy chemotaxis and odor landscapes: exploration of nature with animal sensors. *Biol. Bull.* **191:** 129–138.

Baker, T. C., and K. F. Haynes. 1989. Field and laboratory electroantennographic measurements of pheromone plume structure correlated with oriental fruit moth behavior. *Physiol. Entomol.* **14:** 1–12.

Baker, T. C., and K. F. Haynes. 1996. Pheromone-mediated optomotor anemotaxis and altitude control exhibited by male oriental fruit moths in the field. *Physiol. Entomol.* **21:** 20–32.

Baker, T. C., and L. P. S. Kuenen. 1982. Pheromone source location by flying moths: a supplementary non-anemotactic mechanism. *Science* **216:** 424–427.

Baker, T. C., and N. J. Vickers. 1994. Behavioral reaction times of male moths to pheromone filaments and visual stimuli. Pp. 838–841 in *Olfaction and Taste XI*, K. Kurihara, N. Suzuki, and H. Ogawa, eds. Springer-Verlag, Tokyo, Japan.

Baker, T. C., and N. J. Vickers. 1997. Pheromone-mediated flight in moths. Pp. 248–264 in *Pheromone Research: New Directions*, R. T. Cardé and A. K. Minks, eds. Chapman and Hall, New York.

Baker, T. C., B. S. Hansson, C. Löfstedt, and J. Löfqvist. 1988. Adaptation of antennal neurons is associated with cessation of pheromone-mediated upwind flight. *Proc. Natl. Acad. Sci. U.S.A.* **85:** 9826–9830.

Basil, J., and J. Atema. 1994. Lobster orientation in turbulent odor plumes: simultaneous measurement of tracking behavior and temporal odor patterns. *Biol. Bull.* **187:** 272–273.

Belanger, J. H., and M. A. Willis. 1996. Adaptive control of odor-guided locomotion: behavioral flexibility as an antidote to environmental unpredictability. *Adapt. Behav.* **4:** 217–253.

Bell, W. J., and T. R. Tobin. 1982. Chemo-orientation. *Biol. Rev.* **57:** 219–260.

Colvin, J., J. Brady, and G. Gibson. 1989. Visually-guided, upwind turning behaviour of free-flying tsetse flies in odour-laden wind: a wind-tunnel study. *Physiol. Entomol.* **14:** 31–39.

Cardé, R. T., and A. Mafra-Neto. 1997. Mechanisms of flight of male moths to pheromone. Pp. 275–290 in *Pheromone Research: New Directions*, R. T. Cardé and A. K. Minks, eds. Chapman and Hall, New York.

David, C. T. 1986. Mechanisms of directional flight in wind. Pp. 49–57 in *Mechanisms in Insect Olfaction*, T. L. Payne, C. E. J. Kennedy, and M. C. Birch, eds. Clarendon Press, Oxford, United Kingdom.

Denny, M. W. 1993. *Air and Water: the Biology and Physics of Life's Media.* Princeton University Press, Princeton, NJ.

Doall, M. H., S. P. Colin, J. R. Strickler, and J. Yen. 1998. Locating a mate in 3D: the case of *Temora longicornis. Philos. Trans. R. Soc. Lond. B* **353:** 681–689.

Elkinton, J. S., C. Schal, T. Ono, and R. T. Cardé. 1987. Pheromone puff trajectory and upwind flight of male gypsy moths in a forest. *Physiol. Entomol.* **12:** 399–406.

Emanuel, M. E., and J. J. Dodson. 1979. Modification of the rheotropic behavior of the male rainbow trout (*Salmo gairdneri*) by ovarian fluid. *J. Fish. Res. Board Can.* **36:** 63–68.

Finelli, C. M., N. D. Pentcheff, R. K. Zimmer-Faust, and D. S. Wethey. 1999. Odor transport in turbulent flows: constraints on animal navigation. *Limnol. Oceanogr.* **44:** 1056–1071.

Grubb, T. C. 1972. Smell and foraging in shearwaters and petrels. *Nature* **237:** 404–405.

Grubb, T. C. 1974. Olfactory navigation to the nesting burrow in Leach's petrel (*Oceanodroma leucorrhoa*). *Anim. Behav.* **22:** 192–202.

Grubb, T. C. 1979. Olfactory guidance of Leach's storm petrel to the breeding island. *Wilson Bull.* **91:** 141–143.

Hodgson, E. S., and R. F. Mathewson. 1971. Chemosensory orientation in sharks. *Ann. NY Acad. Sci.* **188:** 174–182.

Johnsen, P. B., and A. D. Hasler. 1980. The use of chemical cues in the upstream migration of coho slamon, *Oncorhyncus kisutch* Walbaum. *J. Fish Biol.* **17:** 67–73.

Kaissling, K.-E. 1997. Pheromone-controlled anemotaxis in moths. Pp. 343–374 in *Orientation and Communication in Arthropods*, M. Lehrer, ed. Birkhauser Verlag, Basel, Switzerland.

Kennedy, J. S. 1939. The visual responses of flying mosquitoes. *Proc. Zool. Soc. London A* **109:** 221–242.

Koehl, M. A. R. 1996. Small scale fluid dynamics of olfactory antennae. *Mar. Freshw. Behav. Physiol.* **27:** 127–141.

Loudon, C., B. A. Best, and M. A. R. Koehl. 1994. When does motion relative to neighboring surfaces alter the flow through arrays of hairs? *J. Exp. Biol.* **193:** 233–254

Mafra-Neto, A., and R. T. Cardé. 1994. Fine-scale structure of pheromone plumes modulates upwind orientation of flying moths. *Nature* **369:** 142–144.

Mafra-Neto, A., and R. T. Cardé. 1996. Dissection of the pheromone-modulated flight of moths using single-pulse response as a template. *Experientia* **52:** 373–379.

Moore, P. A., and J. Atema. 1991. Spatial information in the three-dimensional fine structure of an aquatic odor plume. *Biol. Bull.* **181:** 408–418.

Moore, P. A., G. A. Gerhardt, and J. Atema. 1989. High resolution spatio-temporal analysis of aquatic chemical signals using microelectrochemical electrodes. *Chem. Senses* **14:** 829–840.

Moore, P. A., J. Atema, and G. A. Gerhardt. 1991a. Fluid dynamics and microscale chemical movement in the chemosensory appendages of the lobster *Homarus americanus. Chem. Senses* **16:** 663–674.

Moore, P. A., N. Scholz, and J. Atema. 1991b. Chemical orientation of lobsters, *Homarus americanus*, in turbulent odor plumes. *J. Chem. Ecol.* **17:** 1293–1307.

Murlis, J. 1986. The structure of odour plumes. Pp. 27–38 in *Mechanisms in Insect Olfaction*, T. L. Payne, C. E. J. Kennedy, and M. C. Birch, eds. Clarendon Press, Oxford, United Kingdom.

Murlis, J. 1997. Odor plumes and the signals they provide. Pp. 221–231 in *Pheromone Research: New Directions*, R. T. Cardé and A. K. Minks, eds. Chapman and Hall, New York.

Murlis, J., M. A. Willis, and R. T. Cardé. 1990. Odour signals: patterns in time and space. Pp. 6–17 in *Proceedings of the Tenth International Symposium on Olfaction and Taste*, K. B. Doving, ed. Graphic Communication Systems, Oslo, Norway.

Murlis, J., J. S. Elkinton, and R. T. Cardé. 1992. Odor plumes and how insects use them. *Annu. Rev. Entomol.* **37:** 505–532.

Nevitt, G. 1999. Foraging by seabirds on an olfactory landscape. *Am. Sci.* **87:** 46–53.

Van der Pers, J. N. C., and A. K. Minks. 1993. Pheromone monitoring in the field using single sensillum recording. *Entomol. Exp. Appl.* **68:** 237–245.

Vickers, N. J. 1999. The effects of chemical and physical features of pheromone plumes upon the behavioral responses of moths. Pp. 63–76 in *Advances in Chemical Signals in Vertebrates*, R. E. Johnston, D. Müller-Schwarze, and P. W. Sorenson, eds. Kluwer Academic/Plenum Publishers, New York.

Vickers, N. J., and T. C. Baker. 1992. Male *Heliothis virescens* sustain upwind flight in response to experimentally pulsed filaments of their sex-pheromone. *J. Insect Behav.* **5:** 669–687.

Vickers, N. J., and T. C. Baker. 1994a. Reiterative responses to single strands of odor promote sustained upwind flight and odor source location by moths. *Proc. Natl. Acad. Sci. U.S.A.* **91:** 5756–5760.

Vickers, N. J., and T. C. Baker. 1994b. Visual feedback in the control of pheromone-mediated flight of *Heliothis virescens* males (Lepidoptera: Noctuidae). *J. Insect Behav.* **7:** 605–632.

Vickers, N. J., and T. C. Baker. 1996. Latencies of behavioral response to interception of filaments of sex pheromone and clean air influence flight track shape in *Heliothis virescens* (F.) males. *J. Comp. Physiol. A* **178:** 831–847.

Vickers, N. J., and T. C. Baker. 1997. Flight of *Heliothis virescens* males in the field in response to sex pheromone. *Physiol. Entomol.* **22:** 277–285.

Vogel, S. 1983. How much air passes through a silk moth's antenna? *J. Insect Physiol.* **29:** 597–602.

Vogel, S. 1994. *Life in Moving Fluids.* 2nd ed. Princeton University Press, Princeton, NJ.

Weissburg, M. J. 1997. Chemo- and mechanosensory orientation by crustaceans in laminar and turbulent flows: from odor trails to vortex streets. Pp. 214–246 in *Orientation and Communication in Arthropods*, M. Lehrer, ed. Birkhauser Verlag, Basel, Switzerland.

Weissburg, M. J. 2000. The fluid dynamical context of chemosensory behavior. *Biol. Bull.* **198:** 188–202.

Weissburg, M. J., and R. K. Zimmer-Faust. 1993. Life and death in moving fluids: hydrodynamic effects on chemosensory-mediated predation. *Ecology* **74:** 1428–1443.

Weissburg, M. J., and R. K. Zimmer-Faust. 1994. Odor plumes and how blue crabs use them in finding prey. *J. Exp. Biol.* **197:** 349–375.

Weissburg, M. J., M. H. Doall, and J. Yen. 1998. Following the invisible trail: kinematic analysis of mate-tracking in the copepod *Temora longicornis. Philos. Trans. R. Soc. Lond.* **353:** 701–712.

Willis, M. A., and E. A. Arbas. 1997. Active behavior and reflexive responses: another perspective on odor-modulated locomotion. Pp. 304–319 in *Pheromone Research: New Directions*, R. T. Cardé and A. K. Minks, eds. Chapman and Hall, New York.

Willis, M. A., C. T. David, J. Murlis, and R. T. Cardé. 1994. Effects of pheromone plume structure and visual stimuli on the pheromone-modulated upwind flight of male gypsy moths (*Lymantria dispar*) in a forest (Lepidoptera: Lymantriidae). *J. Insect. Behav.* **7:** 385–409.

Witzgall, P. 1997. Modulation of pheromone-mediated flight in male moths. Pp. 265–274 in *Pheromone Research: New Directions*, R. T. Cardé and A. K. Minks, eds. Chapman and Hall, New York.

Yen, J., M. J. Weissburg, and M. H. Doall. 1998. The fluid physics of signal perception by mate-tracking copepods. *Philos. Trans. R. Soc. Lond.* **353:** 787–804.

Zimmer-Faust, R. K., C. M. Finelli, N. D. Pentcheff, and D. S. Wethey. 1995. Odor plumes and animal navigation in turbulent water flow: a field study. *Biol. Bull.* **188:** 111–116.

Reference: *Biol. Bull.* **198:** 213–224. (April 2000)

Life in Transition: Balancing Inertial and Viscous Forces by Planktonic Copepods

JEANNETTE YEN

*Marine Sciences Research Center, State University of New York at Stony Brook,
Stony Brook, New York 11794-5000*

Abstract. Copepods (1–10 mm aquatic crustaceans moving at 1–1000 mm s^{-1}) live at Reynolds numbers that vary over 5 orders of magnitude, from 10^{-2} to 10^3. Hence, they live at the interface between laminar and turbulent regimes and are subject to the physical constraints imposed by both viscous and inertial realms. At large scales, the inertially driven system enforces the dominance of physically derived fluid motion; plankton, advected by currents, adjust their life histories to the changing oceanic environment. At Kolmogorov scales, a careful interplay of evenly matched forces of biology and physics occurs. Copepods conform or deform the local physical environment for their survival, using morphological and behavioral adaptations to shift the balance in their favor. Examples of these balances and transitions are observed when copepods engage in their various survival tasks of feeding, predator avoidance, mating, and signaling. Quantitative analyses of their behavior give measures of such physical properties of their fluid medium as energy dissipation rates, molecular diffusion rates, eddy size, and eddy packaging. Understanding the micromechanics of small-scale biological-physical-chemical interactions gives insight into factors influencing large-scale dynamics of copepod distribution, patchiness, and encounter probabilities in the sea.

Introduction

Flow patterns created by solid objects moving through a fluid are influenced by viscous and inertial forces. To evaluate the relative importance of viscous and inertial momentum fluxes in this solid-fluid interaction, the Reynolds number can be estimated:

$$\mathrm{Re} = \mathrm{UL}/v \qquad \text{(Table 1, Eq. 1)}$$

where U is the relative flow speed between object and fluid, L is the diameter of the object moving against the flow, and v is the kinematic viscosity (Table 1, Eq. 4).

For pelagic copepods, L varies from 10 μm for the width of a food-particle-capturing seta to 1–3 cm for the span of the antennules. These copepods exhibit movement speeds encompassing a range from less than 1 mm s^{-1} for flow past setae to as much as 1 m s^{-1} for escape speeds. Hence, the range of Re realms experienced by copepods spans 5 orders of magnitude, from Re = $[10^{-2}]$ to $[10^3]$. This is considered a transition zone in flow, where routine swimming and feeding take place at low Re regimes and laminar fields, whereas escapes and captures occur at high Re realms in quasi-turbulent fields. Naganuma (1996) suggests that the "flourishing dominance of the calanoids is based on the advantage of living on the border of different worlds," the viscous and inertial. The author gives examples of activities executed by the copepod in both regimes, but does not discuss mechanisms by which the copepods derive an advantage from these physical forces. In this article, I consider how planktonic copepods make this transition to enhance the detection of chemical and fluid-mechanical signals.

Signaling in a Laminar and Quasi-Turbulent Regime

Every time a copepod moves through water, it causes a fluid deformation. If the flow is above the threshold for a mechanosensory response or contains a chemical whose concentration is above the threshold for a chemosensory response, the feature is a signal, conveying information about the propagator. Such information as size, shape, scent, speed, distance, and direction of movement are important

---

Received 7 July 1999; accepted 8 February 2000.

E-mail: jyen@notes.cc.sunysb.edu

This paper was originally presented at a symposium titled *Chemical Communication and Ecology*. The symposium, which was held in San Diego, California, on 30 December 1998, was invited by the Western Society of Naturalists as part of its annual meetings.

Table 1

Equations to describe some biological-physical-chemical interactions of plankton

Eq No.	Equation	Definition of terms	Source
(1)	$\mathrm{Re} = UL/v$	Re = Reynolds number = ratio of inertial to viscous momentum flux U = relative velocity L = length of object facing flow v = kinematic viscosity	(Tennekes & Lumley, 1972)
(2)	$\mathrm{Pe} = UL/D$	Pe = Peclet number = ratio of advection to diffusion U = relative velocity L = length D = molecular diffusivity coefficient	(Andrews, 1983)
(3)	$t_D = r_D^2/4D$	t_D = characteristic diffusion time D = molecular diffusivity coefficient r_D = characteristic diffusion length	(Dusenbery, 1992)
(4)	$v = 10^{-2}\ \mathrm{cm}^2\ \mathrm{s}^{-1}$	v = kinematic viscosity	(Vogel, 1994)
(5)	$D = 10^{-5}\ \mathrm{cm}^2\ \mathrm{s}^{-1}$	D = molecular diffusion coefficient for a small chemical molecule	(Jackson, 1980)
(6)	$T = (\delta^2/\varepsilon)^{1/3}$	T = eddy turnover time δ = length scale ε = energy dissipation rate	(Jiménez, 1997)

criteria for distinguishing between prey, predator, mate, host, or small-scale turbulent features. In response, the receiver will approach, retreat, orient, or continue as it was with respect to the location of the signal. One way to study signal structure is to categorize the signals by the movements that generated them.

Sinking

When a copepod sinks, no appendages are moving. Streamlines hug the body, and water beyond the body form is barely disturbed. Prey that are sinking akinetically remain undetected by mechanoreceptive predators (Kerfoot, 1978). Metabolic energy is conserved in this recovery period. While a copepod or prey item is sinking, there is little self-generated noise to interfere with the perception of the fluid-mechanical signal, so that the hydrodynamic perceptive field is at its largest. The chemical signal must be transmitted to the receptor by the slow process of diffusion.

Generating a feeding current

Movement of cephalic appendages of copepods generates feeding currents, and analyses of the feeding current reveal that it is a low Re laminar field, in which flow is orderly and streamline trajectories are predictable (Koehl and Strickler, 1981; Strickler, 1982). Each streamline projects to a specific location in three-dimensional space, and the copepod flow field serves as a map of the near-field fluid volume where each receptor receives input from signal sources at relatively defined locations. Andrews (1983) modeled the effect of the flow on the structure of the odor phycosphere, which is exuded by an algal food particle, entrained in the sheared field of the copepod feeding current. His study predicted that the shear would stretch and deform the odor field. Within the feeding current, the Peclet number > 1 (Table 1, Eq. 2; Andrews, 1983). This Peclet value indicates that sheared diffusion is the dominant force distorting the distribution of odor, whereas Fickian diffusion has little time to act to change the structure of the odorant. The deformation separates the leading edge of the active space of the algal odor field from the alga. When the edge intersects the antennulary receptor, the activated receptor gives the copepod early warning of the approach of the algal cell, allowing the copepod time to re-orient to the incoming food particle. This particle sensing and capture behavior was confirmed using high-speed cinematography (Koehl and Strickler, 1981), and the deformation of the odor field was measured using electrochemical techniques (Moore *et al.*, 1999).

In the analysis of the flow field of a freely swimming copepod, Strickler (1982) defines the field as doubly sheared: speed falls off with horizontal distance from the body axis and with distance upward from the mouthparts. Hence, receptors along the antennules and mouthparts are subject to different flow regimes. Those receptors concentrated on the mouthparts (Friedman and Strickler, 1975) receive input from a cone-like volume extending out from the copepod along the central axis of the flow field. The direction of this axis, which determines whether the flow passes over or passes by the antennulary sensors en route to the mouth, can vary for different species of copepods (Strickler, 1982; Tiselius and Jonsson, 1990; Yen *et al.*, 1991; Bundy and Paffenhöfer, 1996) and can change when recognized signals elicit motor responses. Koehl and Strickler (1981) noted changes in flow orientation, which can be accompanied by changes in appendage and body orientation, in response to the odor in the alga-containing streamline of flow. Gill and Poulet (1988) note changes in the beat frequency of flow-generating appendages in response to amino acid mixtures. At the mouthparts, flow can be fast, due to proximity to flow-generating appendages. Particles make contact with receptors nearly simultaneously with activation by the odor fields, suggesting that responses will be mediated by contact chemoreception as well as by remote detection of odors.

The paired antennules are the appendages that extend the farthest horizontally from the body. Since flow speed decreases with horizontal distance from the body axis, the antennulary receptors experience a gradient in the flow. From analyses of the morphology of the sensory array, it appears that the distribution of receptors is suited to the hydrodynamic flow structure. Sensors form a linear array of putative chemical and fluid-mechanical sensors along the copepod antennules (Strickler and Bal, 1973; Chacon-Barrientos, 1980; Dourdeville, 1981; Fleminger, 1985; Yen and Nicoll, 1990; Weatherby *et al.*, 1994; Bundy and Paffenhöfer, 1996; Boxshall *et al.*, 1997; Paffenhöfer, 1998; Boxshall and Huys, 1998). Mechanoreceptors, often found evenly distributed along the antennule to a dense tuft at the distal tip, experience a gradient in flow from high speed near the proximal end to low speeds at the distal end where the tip is exposed to flow most similar to the ambient regime. The presumed use of sensors at the distal tip is for predator detection and the use of proximal sensors is for prey detection (Lenz and Yen, 1993). The results of Doall (1995) show a match between the spatial distribution of mechanosensory setae along the antennules and the three-dimensional structure of the prey-attack volume. Feathered and long setae expose large surface areas to flow and therefore should be better able to detect low speeds, whereas short stiff hairs protected in the boundary layer are gauged for high flow speeds. Having different lengths embedded in the flow allows the boundary layer to act as a flow-attenuating filter (see Weissburg, 2000, for definition of boundary layers). This is similar to the difference between superficial neuromasts and mechanosensors buried within the lateral line canal of fish (Coombs and Janssen, 1990). Furthermore, the different spacings between sensors, from the greatest distance between distal tips (which can be more than one centimeter) to the smallest separation between individual setae (on the order of micrometers) enable copepods to detect shear at the centimeter-micrometer spatial scale. According to Markl (1978), "the variability in these cuticular structures much more than differences in response characteristics of the sensory cells themselves are responsible for the large variability of mechanoreceptive function of the arthropod hairs." Since small changes in size and speed cause large changes in hydrodynamic structure at low Re—especially within the range experienced by copepods—it is essential that copepods be capable of detecting these differences with their mechanoreceptors. Such changes correspond to signals of prey, predators, mates, hosts, or small-scale turbulence, and it is important to respond correctly to these signals.

The proximal region of the antennules is located adjacent to the flow-generating appendages, suggesting that the flow across the antennules is fast in this area. Here, we often find the highest density of chemoreceptors along the antennule (Huys and Boxshall 1998). Such high flow speeds could facilitate the detection of chemical signals by thinning boundary layers, thus shortening the time needed for the signal molecule to diffuse to the receptor (Table 1, Eq. 3). Male copepods of the species *Temora longicornis* may thin the boundary layer surrounding their receptors since they increase their swimming speed upon detecting the female odor, accelerating as they follow the mating trails. Preliminary physiological evidence indicates that copepod antennules are capable of detecting odorants such as amino acids (Yen *et al.*, 1998). In several species, differences in the structure of the female and male antennulary setation (Griffiths and Frost, 1976; Fleminger, 1985; Hallberg *et al.*, 1992; Boxshall *et al.*, 1997; Boxshall and Huys, 1998) suggest that males rely more on chemosensory cues than do females. In *Euchaeta* (Boxshall *et al.*, 1997), the male, when molting into the final reproductive stage, acquires a second set of aesthetascs in exchange for its mechanoreceptive prey detection setae in the proximal region. The simultaneous loss of feeding mouthparts indicates the importance of these new sensors for mate detection. In some members of the Eucalanidae, doubled aesthetascs are present along almost the entire length of the male antennules; in other calanoid families, such aesthetascs, when present, are restricted to the proximal part of the antennule (Boxshall and Huys, 1998). Since the diffusion time through the boundary layer (Table 1, Eq. 3) is a rate-limiting step in odor perception, placement of the mate detection chemoreceptive setae within the proximal high flow zone maximizes the efficiency of odor detection. Under these physical constraints, efficient mate detection is probably one of the strongest selection pressures requiring this morphology. However, although the morphology strongly suggests an adaptive response to a surrounding flow gradient, the role of the antennule in detecting chemical signals specifically carried by the feeding currents of freely swimming copepods has not yet been experimentally demonstrated.

The forces of biology and physics are evenly matched at the scale of copepods. Given the importance of the feeding current as a sensory field, it is advantageous for the copepod to maintain this fluid structure. Analyses of the strength of the biologically generated flow in the feeding current and that of the physically derived flow of small-scale turbulence suggest the hypothesis that a careful interplay of evenly matched forces of biology and physics occurs at the scale of copepods. Under most circumstances, biological forces dominate, since turbulent length scales rarely extend to the scale of copepods (η is greater than 1 mm for near-surface breaking waves, and ranges to 10 cm in a stratified water column (Sanford, 1997)). In the most energetic regions of the water column, the Kolmogorov flow speeds can be equivalent to the feeding-current speeds (Fields and Yen, 1997). However, these flow speeds are the average of the fluctuating component of turbulence. There will be the rogue wave of small-scale turbulence that disrupts the sensory field of a copepod. However, shear is strongly intermittent (Karp-Boss *et al.*, 1996). The energy from small-scale turbulence is at the dissipative range of fluid motion, whereas energy for feeding currents is continuously fueled by metabolic resources of the copepod. The feeding current may actually contribute energy at the lower end of the physical energy cascade. Yamazaki and Squires (1996) found that copepod swimming speeds are larger than velocity fluctuations in the seasonal thermocline and conclude that organism motion can be independent of local turbulent fields. Hence, a feeding current may momentarily be eroded by small-scale turbulence, but the biologically generated feature can be rebuilt.

At the scale of a copepod, biologically derived fluid motion is equal to and can be "stronger" than or dominant over physically derived fluid motion in its ability to deform the local fluid environment to generate a feeding current. In the face of the intruding external turbulent regime, the familiar territory of its sensory field is maintained. Within their sensory field, copepods can enhance their capability for signal detection by the coordination of flow direction and the location of sensory receptors. Water-borne signals are entrained from a complex realm of small-scale turbulence into the simpler grid-like structure of the copepod feeding current. Hydrodynamic noise is reduced within the low Re flow, further enhancing signal detection. By creating the laminar orderly structure of the feeding current, a copepod can assess the fine-scale distribution of chemicals entrained from the somewhat chaotic structure of small-scale turbulence. Information from a three-dimensional space is collapsed onto a two-dimensional external sensory array—the paired antennules—or onto the point sensor of the mouth. The copepod uses the fluid environment to accomplish much information processing externally, leaving the few hundred sensors and several hundred brain cells with a limited number of responses. The laminar flow of the feeding current simplifies the local environment and reduces the complexity of three-dimensional information processing, thus enhancing the detection of water-borne signals.

Cruising

In the cruising mode, the copepod moves ahead into the water that it pulls in towards its mouthparts. The antennulary sensors project into flow not yet disturbed by the copepod's movements, thus maximizing the signal-to-noise ratio. With little flow separation behind the plankter, the wake is thinner than the object moving through the water (see fig. 3D in Yen and Strickler, 1996). Not only is there minimal disturbance ahead of the copepod, but the smoothness of the trail indicates there is minimal disturbance within the wake. The Re estimated from these movements of the copepod and fluid is less than 10. Therefore, viscous forces dominate. What is the effect on signal structure and transmission? For the fluid-mechanical signal, viscosity attenuates flow. Within a few seconds, flows of millimeters per second quickly decay below the threshold levels of detection (Yen *et al.*, 1998). For the chemical signal, viscosity limits diffusion to molecular processes, and since molecular diffusion of a small chemical molecule is 1000 times slower than the dissipation of momentum (Table 1, Eqs. 4, 5), chemical signals are preserved. The signals appear as discrete trails and do not become diffuse plumes. The odorant is retained within the confines of the trail, with little mixing outside the trail. Molecular diffusive processes slowly expand the trail so that in 10 s, the signal is less than the threshold of a copepod's sensor (Yen *et al.*, 1998), implying that the copepod must find the trail within 10 s.

The structure of trail-like wakes has important consequences for copepods that use chemoreception to find their mates. The ability of the 1-mm copepod *Temora longicornis* to follow the trails of mates for up to 10 s after the trail was created confirms that, at the scale of this species, molecular diffusion acts to restrict the transport of the chemical so the trail persists until the male copepod finds it (Doall *et al.*, 1998; Weissburg *et al.*, 1998; Yen *et al.*, 1998). The observation that the male follows the trail precisely in three-dimensional space, indicating no change in odor structure, further confirms that eddy diffusion is minimal at these short (<10 s), small (<10 cm) scales. The copepod finds the trail because of the strong across-plume gradient, yet half the time he takes the trail direction away from the female because of a weak along-plume gradient (Doall *et al.*, 1998; Yen *et al.*, 1998). Analysis of the change over time in the location of the edge-detecting male, whose position is hypothesized to represent the location of the diffusing edge of the pheromonal trail, provides an estimate of $D = 2.7 \times 10^{-5}$ cm^2 s^{-1}, very close to the molecular diffusion coefficient of a small chemical molecule (Table 1, Eq. 5; Yen *et al.*, 1998). Observations of a male that lost the trail, at the moment when the female hopped, point to the importance of keeping the trail intact and not disrupting the signal. Because turbulence is known to elicit escapes and hops (Hwang *et al.*, 1994), it is important for copepods to reside in areas of low turbulence when mating signals are needed. When a male copepod loses the trail, he exhibits an isotropic search pattern. The minimal flow is not used for orientational guidance, as is essential to larger organisms in high Re flow (crabs, lobsters: Weissburg and Zimmer-Faust, 1993; Weissburg, 2000). The search is confined within a Kolmogorov-sized volume, suggestive of a strategy adapted to life at the Kolmogorov scale, where water motion is limited by viscosity. Observations that copepods reside in layers of high Richardson's number (Gallager *et al.*, 1997) or low epsilon (ε; Incze, 1996) also provide evidence of the importance of water stability to preserve these communication signals for successful mating and subsequent recruitment into the population.

Further analysis of the trails of *Temora* can give an indication of the type of eddy field wherein mate-tracking behavior can occur. The characteristic eddy turnover time T at size δ can be estimated as a function of the energy dissipation rate ε (Eq. 6, Table 1; Jiménez, 1997). In mating interactions of a copepod, the trail length could represent the eddy size, and the trail lifetime could represent the eddy turnover time. For *T. longicornis,* female trails are found within 10 s and can be tracked for 3.4 cm (Doall *et al.*, 1998; Weissburg *et al.*, 1998). If δ = 3.4 cm and T = 10 s, then the upper limit of ε would be 1.16×10^{-2} cm^2 s^{-3}, a fairly energetic regime. These copepods come from Long Island Sound, a coastal semi-enclosed environment where turbulent mixing can be strong. Jiménez (1997) lists energy dissipation rates for coastal environments ranging from 10^{-3} to 100 cm^2 s^{-3}. If this relationship in Equation 6, Table 1, is used to estimate ε from copepod behavior, it predicts that copepods with faster swimming speeds along the trail could live in areas of lower stability, whereas copepod trails that persist longer would indicate that the copepods are living in quiescent layers.

Vincent and Meneguzzi (1991) describe small-scale turbulence not as chaotic, but as having "organized structures", in which viscosity acts to correlate flow (Yamazaki, 1993). Coherent, correlated, and persistent physical features remain identifiable within the fluid motion of turbulent flows. One coherent small-scale turbulent structure is the vortex tube (Vincent and Meneguzzi, 1991). Yamazaki (1993) considers whether these structures help or hinder plankton interactions. Comparative analyses show many similarities in the structure of vortex tubes and copepod mating trails (see Table 2). The spatial aspect ratio and the temporal persistence of copepod trails and vortex tubes are remarkably similar (Table 2). Shear defines the boundaries of both features, yet the velocity gradients have slight differences. The shear intensity along a mating trail decreases downstream from the signal source, the swimming female copepod. Near the copepod, the shear gradient of the feeding/locomotory current is nonlinear, with an e-folding of 2.5 mm (falls by a factor exp (-1); Yen *et al.*, 1991), in contrast to the linear shear defining the edges of vortex tubes (Lazier and Mann, 1989). To ensure that the male has no trouble distinguishing his mate's trail from common vortex tubes, the female adds her pheromonal chemicals.

Mating trails represent Kolmogorov scales. I propose the hypothesis that copepod behavior can be used as a measure of the Kolmogorov temporal and spatial scales (Table 2).

Table 2

Comparison of the properties of the biologically created copepod mating trail and those for the physically derived small-scale turbulent feature, a vortex tube

Mating trail	Kolmogorov scale
Isotropic (no directional flow)	Isotropic
Length = 5–10 cm	Millimeter to centimeter scale
Exploratory reach	Eddy size
10–50 mm long: 1–5 mm wide	10 : 1 aspect ratio
5–10 s	10 s persistence
Chemical pheromone:	
$D = 10^{-5}$ cm^2 s^{-1}	None*
Higher velocity gradient	Linear shear*

* Distinct.

The following observations, made on a few species of copepods in isolated experiments, led me to suggest this approach for the use of the copepod as a biosensor of the distribution of momentum and mass at Kolmogorov scales.

1. The volume searched and the isotropic search pattern inscribe a Kolmogorov eddy. The similarity in size and the lack of directional flow suggest that the male's behavior may be used as a measure of the Kolmogorov spatial scale.
2. The temporal change in the location of the odor-trail-edge-detecting copepod gave a diffusion coefficient similar to that for the molecular diffusion of a small chemical molecule. Here, the male's behavior provides a measure of the temporal scale.
3. The energy dissipation rate, estimated from eddy turnover time and eddy size for the mating trails, provides one estimate—based on copepod behavior—of the intensity of the local small-scale turbulence that closely matches known measurements of physical mixing in the copepod's local environment.
4. The similarity in (a) the response time of a copepod to the diffusing chemical trail and (b) the lifetime of a vortex tube suggests that copepods have evolved to create and respond to signals at the same time and length scales as small-scale turbulence.

These observations for the copepod species *Temora longicornis* (Doall *et al.*, 1998; Weissburg *et al.*, 1998; Yen *et al.*, 1998) suggest that it has adapted to the limitations imposed by the physical environment. This copepod constructs communication signals and enacts behavior within the constraints of transitional Re realms. Analysis of similar behavior of other copepods may provide us with representations of the temporal and spatial measures of Kolmogorov scales of fluid physical motion.

Escaping

As mentioned in the introduction, routine swimming and feeding take place in low Re regimes and laminar fields, whereas escapes and captures occur at high Re realms in quasi-turbulent fields. During escapes, vortices and toroids are shed (Yen and Strickler, 1996). To achieve the power needed to move at escape speeds that can reach up to $1\ \text{m s}^{-1}$ (Fields, 1996), the copepod executes a series of jumps that rely on its larger swimming legs rather than on the small cephalic appendages that are used for generating the feeding current or for travel *via* laminar cruising. During the recovery stroke of swimming legs in a jump, the oar-like rami are feathered so they form a median longitudinal keel (Boxshall, 1985). During the escape, the antennules are folded against the body sides with legs flattened against the urosome and the caudal rami folded shut like a closed fan (Fig. 1). Analyses of high-speed jumps show that jets are formed when the swimming legs collapse against the urosome during escape maneuvers (Strickler *et al.*, 1995; Liu, 1996). Examination of the copepod skeletal system reveals the design features for maximum efficiency in the jump (Boxshall, 1985). The prosome-urosome joint in copepods has a transverse pivot line with extensive arthrodial membrane (thinner than the cuticle) dorsally and ventrally that permits considerable dorsoventral, but little lateral, flexion. The evolution of the prosome with its complex ventral wall lacking articulation between somites appears to have been closely linked to the perfection of the jumping mode of locomotion. Manton (1977) stated that "the whole skeletal system concerned with the copepod's jump is of such strength as to prevent unwanted flexure which might detract from the force of the jump." Contraction of the dorsal longitudinal musculature, which fans out laterally in the urosome to a broad dorsal-to-lateral insertion inside the anal somite (Boxshall, 1985), may act to close the fan-like caudal rami into a narrow tail, telescoping somites within the preceding one.

Not only is the skeletal system designed for maximum efficiency, but the resultant body form further allows copepods to attain and maintain maximum observed escape speeds of $1\ \text{m s}^{-1}$ (Fields and Yen, 1997) to enter into the inertial realm of $Re = 1000$. When executing an escape, the copepod adopts a profound change in morphology—from an expanded form to a smooth streamlined shape (Fig. 1). In the expanded non-escape posture, the horizontal caudal fan may be important in controlling the pitch, or attitude, of the copepods and also may act as a stabilizer in reducing roll about the longitudinal axis (Strickler, 1975). In the streamlined form, the copepod may spiral around its central long axis (pers. obs.). In this escape posture, streamlining changes the pressure field behind the copepod where the fluid gradually decelerates in the rear, little or no separation occurs, and the object is literally pushed forward by the wedgelike closure of the fluid behind it (Vogel, 1994). The gain from adopting a streamlined morphology, effective at high Re, implies that, indeed, copepods do operate within an

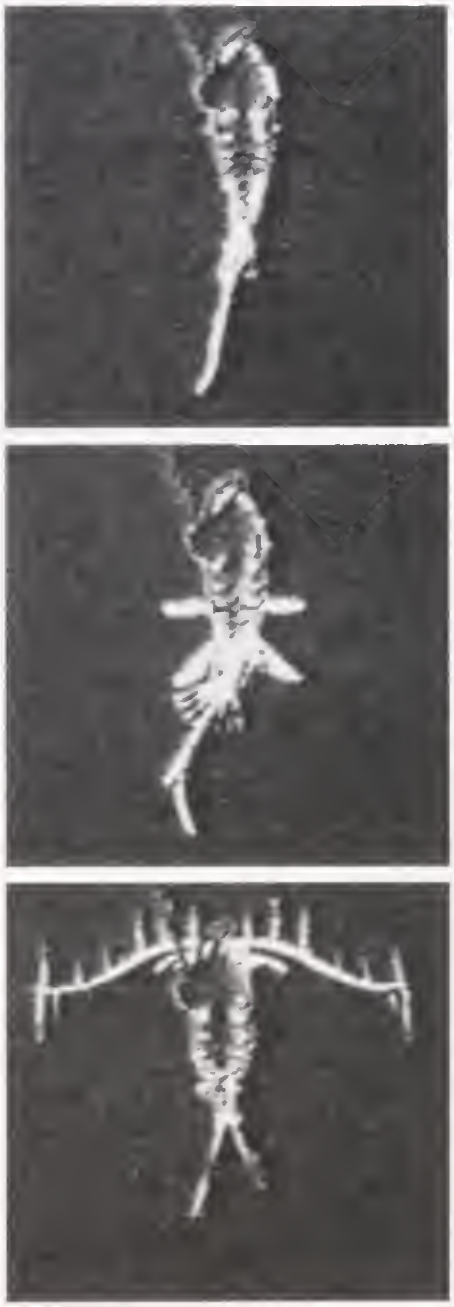

Figure 1. Escape postures of *Euchaeta rimana* adult female (prosome length 2.4 mm). (Top) Streamlined body form during escape glide of copepod moving at Reynolds numbers greater than 500, showing antennules parallel to body, swimming legs folded close to body, and caudal rami collapsed into a narrow tail. (Middle) Body form during power thrust of the escape, showing antennules folded parallel to body and exopods of the swimming legs extended and caudal rami flared. (Bottom) Body form when swimming and hovering prior to escape, with antennules positioned at right angles to body. The panels were placed in this spatial order to depict how the body form changes in the direction of an upward escape.

inertial realm. The necessity for an effective escape from predators has driven the evolution of the streamlined form of copepods.

When a large copepod escapes, toroidal vortices are found in its wake as larger appendages translate larger parcels of water (Fig. 2). A toroidal shape can be viewed as a vortex ring due to the vorticity produced by viscosity between the jet and the ambient fluid (Weihs, 1977). A toroidal vortex gets larger by entrainment of surrounding fluid and slower by loss of its original impulse (Shariff and Leonard, 1992; as cited by Vogel, 1994). Analyses of the change in volume and distance traveled by the toroidal vortex allow an estimate of the relative importance of diffusive to advective forces within this copepod wake. Here, 250 ms after the copepod has released the torus, the torus continued to grow by 20% over the past 50 ms (see Fig. 3; Table 3). The water continues to coast 0.4 s after the source has left the scene, further evidence of entrance into an inertial realm. In fact, it takes another 2 s before the Peclet number approaches 1 and advection is balanced by diffusion (from Table 1, Eq. 2, $Pe = 1$ when $U = 1\ \mu m\ s^{-1}$; from Table 3, Eq. 3, $t = 2.55$ s for $U = 1\ \mu m\ s^{-1}$). Since these wakes were visualized within a strong density gradient, they may be smaller and slower than natural wakes formed in an ambient density gradient (see Gries *et al.*, 1999) and may inaccurately estimate the time needed to reach a balance between advection and diffusion. During this time, odor placed within the torus is dispersed by advection. A signal of mixed modality is created when the concentrated odor of excreted metabolites is encased in the jet-like wake shed by an escaping copepod. The concentration of odorant in the wake will be more dilute than that in the laminar trail because viscous forces do not restrict the advective disruption of odors *within* the wake of a swimming copepod. This rapid odorant dilution may be more difficult to follow if a chemosensory predator chases the copepod prey. The energetic hydromechanical signal also may frighten predators because of the apparent large size and strength, a form of aposematism. It also may act as a decoy, since the source is distant from the signal. When in proximity to the source, the hydromechanical signal has directional information that guides the male copepod when he executes the final capture of his mate at the end of the pheromonal trail (Yen *et al.*, 1998).

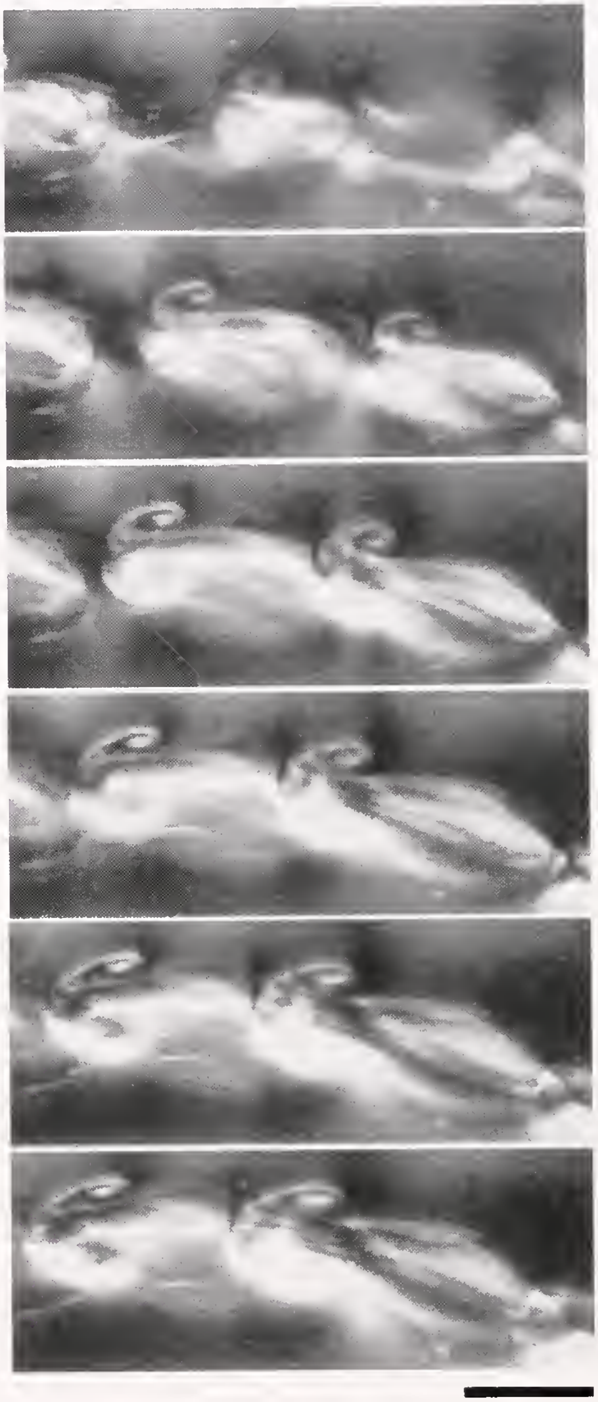

Figure 2. Dynamic analysis of figure 3A in Yen and Strickler (1996) showing the sequence of toroid structures separated by 67 ms. Note the lack of change in the location of the initiation point of the toroid, the advective movement of the head of the hydrodynamic feature, the vortices formed as the water moves, the growth of the toroid over 333 ms, and the fine-scale patchiness in color intensity (which can correspond to chemical concentration: for methods, see Strickler *et al.*, 1995). Scale bar = 4 mm.

The odorant distribution within the torus also is not the same as expected from diffusion. According to Okubo (1984), "an essential difference between the mechanisms of molecular and turbulent diffusion exists, where the flux of a property by molecular diffusion takes place always from the higher concentration to the lower concentration and is proportional to the concentration gradient. Turbulent flux, however, need not always be in the direction of down-gradient of the mean concentration nor can it always be described as diffusion." Close examination of the Schlieren image, where the brightness of the signal can be representative of the concentration gradient (Strickler *et al.*, 1995), shows

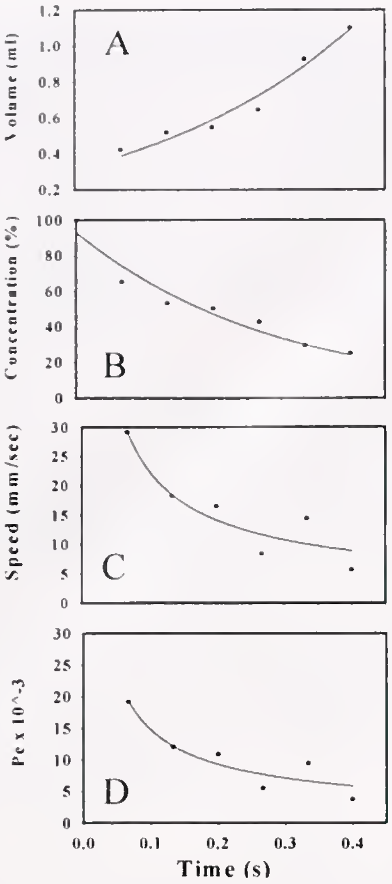

Figure 3. Dynamics of toroid growth in the wake of an escaping copepod. The rightmost full toroid in Figure 2 is analyzed here. (A) Increase in the volume of the toroid. Volume was determined by estimating the chord length of the toroid and the average width and calculating the volume using the formula for a cylinder. The values were fit with a sigmoid equation (see Table 2). (B) Decrease in concentration of a hypothetical odorant, presuming the initial concentration is 100%. Data were fit with a two-parameter exponential decay curve. (C) Decline in the speed of the toroid as it moves away from the location where it was created by the copepod. Data were fit with a two-parameter exponential decay curve. (D) Decline in Peclet number showing a strong influence of advective forces over a period of seconds. Data were fit with a one-parameter power function. Fitted equations appear in Table 3.

how the biological activity of copepod eddies contributes to the rates of change of tracer microstructures. Figure 2 shows separate vortices created by the intermittent jets of an escaping copepod, expanding in volume, driven by the momentum imparted by the escaping organism. In this type of eddy packaging, odor is not dispersed along a diffusive gradient and can be observed patchily distributed in a spatial pattern characteristic of the advective movement within the vortex. Analysis of the microstructure shows that the signal is dispersed unevenly within the advective feature yet the boundaries still are delineated by the encroachment of viscous fluid. As described by Gries *et al.* (1999), the physical structure of the wake constrains the patchy distribution of nutrients released by the zooplankton. Copepods may follow the patchy odor distribution within a toroid with a less directed routing than when following a laminar trail. Copepods do respond to different structures with different behaviors. For example, when a slowly advancing hovering copepod created a diffuse wake below her, the mate-tracking male was found to cast within the wake in a zigzag fashion. This behavior was very different from the tracking of the exact three-dimensional trail of a male following a cruising female (Doall *et al.*, 1998; Weissburg *et al.*, 1998). The male took a longer time to zigzag within a diffuse trail than to quickly follow the thin trail left by a cruising female copepod (Weissburg *et al.*, 1998). The combined information from the flow signal and patchy odor signal influences the mechanisms that guide the plankter to the source.

Signaling is affected by the balance of viscous and inertial forces. Copepods take advantage of the transition between laminar and incipient turbulent flow to maximize the efficiency of movements. They modify their morphology and speed of movement to conform to the laws of fluid physics. The escaping copepod is much more streamlined than the sinking or slow-swimming copepod with all its sensors deployed. These differences affect the signals generated in the various copepod gaits. The slow swimming of the low-drag, minimal-surface-area oblate spheroid form of the nauplius leaves little trace of its presence or passage. The cruising of the adult copepod leaves a coherent laminar trail with a strong chemical signal but a weak fluid-mechanical signal. The high speed of the streamlined escaping

Table 3

Dynamics of toroid formation by escaping copepods (see legend for Figure 3)

	TOROID 2 (at t = 0.067 s; at t = 0.4 s)	TOROID 3 (at t = 0.067 s; at t = 0.4 s)	Fitted equation	R^2
Copepod speed (cm s^{-1})	38 (initial)	30 (initial)		
Toroid volume (ml)	0.2; 1.2	0.2; 1.2	$V = 35.9/(1+e^{(t-1.49)/0.32})$	0.965 (1)
Concentration (% original)	100; 20	100; 20	$C = 93e^{-3.4t}$	0.948 (2)
Toroid speed (mm s^{-1})	38, 4.1	30; 5.7	$v = 36.58e^{-4.2t}$	0.848 (3)
Peclet number	28,000; 3,075	19,000; 3,750	$Pe = 3180t^{-0.67}$	0.868 (4)

copepod leaves energetic jets that contain strong fluid-mechanical signals retaining chemical signals within the borders.

A consequence of movement through transitional fluid regimes is that the relative strength of the chemical and fluid-mechanical signals changes: the fluid-mechanical signal increases in importance at high Re within the range experienced by copepods. Responding to the input from the shift in sensory modalities and the difference in the dissipation rate of momentum which is 1000 times faster than the diffusion rate of mass (Table 1, Eqs. 4, 5), copepods adjust their behavioral responses to suit this transition in the mixture of fluid-mechanical and chemical signals. Fast responses resulting in predator avoidance or carnivory tend to be elicited by short-lived fluid-mechanical signals, whereas slow responses resulting in grazing, swarming, and mate-tracking tend to be elicited by persistent chemical signals. The careful diversion to the mouth of the alga-carrying odor-laden streamline in the feeding current and the exact mate-tracking elicited by chemical signals as well as the accurate prey-attacks and oriented escapes elicited by fluid-mechanical signals exemplify the precision maintained in the directed response of copepods to water-borne signals. Analysis of the chemical paths followed or the locations of escape from shear may provide additional behavioral indicators of the distribution of mass or momentum.

Ecological Consequences of Small-Scale Biological-Physical-Chemical Interactions

Encounter probabilities

In 1995, Haury and Yamazaki examined the length scale at which the shift occurs between biologically controlled (growth rate, swimming ability, perception distance) and physically controlled (*e.g.*, turbulence, vertical current shear) distributions of zooplankton. They found a dichotomy in the magnitude of the discrepancy between the known perception distances of planktonic organisms and nearest-neighbor distances (NND) between conspecifics measured within patches. "The discrepancy suggests that (i) the signals used to maintain aggregations are not yet identified, and/or (ii) copepods are more sensitive to known signals than we can measure or explain theoretically." Our studies of mating interactions address both of these suggestions. The documentation of chemical mating trails and the sensitivity of copepods to the Kolmogorov-scale distribution of momentum and mass changed the measure of reactive distance, a key parameter in plankton encounter models. We found that mate-tracking copepods can be separated by straight-line reaction distances of up to 3.4 cm where male copepods follow curved trails up to 6.5 cm long with pursuit distances of up to 13.8 cm (pursuit distances can be longer than the trail when the copepod backtracks; Doall *et al.*, 1998). These studies have increased our measure of reaction distances by 10- to 100-fold from the one-to-two-bodylength (<5 mm) reaction distances of copepods to algal or animal prey. Nearest-neighbor distances of commonly found swarm densities (1–5 cm in patches of 10^4 to 10^6 copepods m^{-3}; Haury and Yamazaki, 1995) are now comparable to reactive distances, making sense of the significance of patchiness. Plankton can rely on local thin layers and patches as areas of intense activity and high encounter probabilities in which survival strategies can be completed. By migrating to layers where the persistence of communication signals is maximized or most amplified, copepods can aggregate at the pycnocline to reduce NND and enhance encounter probabilities.

Encounter probability can be improved not only by larger perceptive radii and swarming but also by changes in speed and swimming directionality, and copepods engage in these modifications. Rapid chemo-orientation in response to female trails allows the male copepod to catch up to his mate. In contrast to the three-dimensional isotropic trails of *Temora, Calanus* females leave vertical trails, and the male performs a search dance primarily in the horizontal plane (Tsuda and Miller, 1998). Perpendicular swimming patterns, which improve the efficiency of encounter (Gerritsen, 1980), also have been documented for male and female *Euchaeta* (Yen, 1988). Hence, discoveries in the micromechanics of mate detection have improved our understanding of encounter probabilities within patches and, as a consequence of increased encounter rates between mates, larger scale population dynamics will be enhanced by the improved likelihood of reproductive success.

Spatial sorting

In spatial sorting, the distribution of copepod populations results in an apparent match between the intensity of the physical forces and the intensity of various biological functions (such as making feeding currents or escaping). Comparison of the feeding currents of copepods from energetically different environments (Fields, 1996; Fields and Yen, 1996) shows a correlation between the flow speed and the strength of physical mixing: copepods are found in ocean layers in which Kolmogorov flow speeds are similar to the feeding current flow speed. Spatial sorting may be occurring to minimize the expenditure needed to maintain the feeding current that is a requisite for gathering chemical signals. The sensitivity of copepods to a threshold level of shear appears to be related to the energy level of their environment, higher levels of shear are necessary to elicit escapes from coastal copepods, while lower intensities elicit responses from open-ocean copepods (Fields and Yen, 1997). This suggests that these organisms have adapted their sensory systems or have been sorted spatially to zones where the shear levels are less than their behavioral threshold signal strength, minimizing energy loss to unreasonable responses. The discovery of the persistence of mating trails, necessary for the essential survival tactics of reproduction and the perpetuation of the species, further suggests that, to preserve mating signals, copepods may seek regions where turbulent eddy diffusion is minimal and stability is high. Indeed, Mackas *et al.*, (1993), Mackas and Miller (1990), and Incze (1996) found copepods vertically distributed according to ε. Haury *et al.* (1990) found that after a storm, zooplankton are selectively mixed to a distribution different from their vertical separation under less energetic conditions. To ensure the efficiency of mate-finding, copepods may avoid areas of high turbulence where flow patterns elicit escapes (Hwang *et al.*, 1994); the escape wakes disperse the odor trail, creating an intermittent signal that cannot be followed. The fact that, without mating, no future generations are supported attests to the strength of the evolutionary pressures on copepods to reside in an oceanic zone where the strength of the biological signal and the sensitivity of the organism closely match the physical energy of the fluid environment.

Concluding Remarks

In 1988, Yamazaki and Osborn asked: "How are creatures affected by the mean and fluctuating portions of the circulation? Have they responded to the temporal and spatial distribution of turbulence? Are they adapted to the 'variability of the ocean' rather than the 'mean'?" Analyses of copepod behavior show responses to both scales of fluid motion. The timing of the life history of eel larvae to transit times of the Sargasso Sea gyre (Harden Jones, 1968) and the timing of the vertical migration of estuarine plankters to the direction of tidal excursions (Cronin, 1982; Forward and Rittschof, 1994) show adaptations to the mean flow. In this study, copepod behavior reveals adaptations to the fluctuating component of ocean flow. Avoidance of rogue waves of small-scale turbulence is required for mating success, but living in an ocean layer with similar biological and physical ε is fine for feeding success since the feeding current can be rebuilt. The physically derived fluid motion can enforce the zonation of copepod species to ocean layers in which the environmental turbulence is similar to the strength of the biologically created flow and to copepod sensitivity.

In 1984, Strickler stated that "Viscosity acts as a selective force in the evolution of copepods" and "copepods take advantage of [this]." In 1993, Yamazaki commented, "Zooplankton have evolved behavioral adaptations to flow patterns." Recent results indicate that not only is viscosity an important force but so are inertial forces. Inertial forces distribute the odorant within the wake and convey information about the size and speed of the propagator. Viscous forces act to restrict chemical diffusion within the hydrodynamic borders and attenuate the flow signal within seconds and millimeters. Suitable responses to these variations in the spatial distribution and temporal persistence of chemical and fluid-mechanical signals contribute to the success of copepods in the sea. Perceptive volumes, signals, and response times similar to the length and time scales of small-scale turbulent features suggest that copepods are adapted to the physical constraints of Kolmogorov scales. Within the whorl of a copepod, biological and physical forces are in a fair competition for dominance. At these small scales, copepods can conform or deform the physical environment for their survival, using morphological and behavioral adaptations to shift the balance in their favor.

Acknowledgments

I thank Dr. Richard Zimmer for inviting me to participate in the timely interdisciplinary symposium that he organized at the meeting of the Western Society of Naturalists, December 1998, in San Diego, California. I am grateful to Drs. Richard Zimmer, Marc Weissburg, David Fields, and two anonymous reviewers for their insightful comments. I thank Professor Rudi Strickler for discussing ideas and for working with me to obtain the images, originally in color, for Figure 2. Support for this work comes from the National Science Foundation grant OCE-9314934 and the Office of Naval Research contract N000 1494 10696. This is contribution 1182 of the Marine Sciences Research Center.

Literature Cited

Andrews, J. C. 1983. Deformation of the active space in the low Reynolds number feeding current of calanoid copepods. *Can. J. Fish. Aquat. Sci.* **40:** 1293–1302.

Boxshall, G. A. 1985. The comparative anatomy of two copepods, a predatory calanoid and a particle-feeding mormonilloid. *Phil. Trans. R. Soc. Lond. B* **311:** 303–377.

Boxshall, G. A., and R. Huys. 1998. The ontogeny and phylogeny of copepod antennules. *Phil. Trans. R. Soc. Lond B* **353:** 765–786.

Boxshall, G. A., J. Yen, and J. R. Strickler. 1997. Functional significance of the sexual dimorphism in the array of setation elements along the antennules of *Euchaeta rimana* Bradford. *Bull. Mar. Sci.* **61:** 387–398.

Bundy, M. H., and G-A. Paffenhöfer. 1996. Analysis of flow fields associated with freely swimming calanoid copepods. *Mar. Ecol. Prog. Ser.* **133:** 99–113.

Chacon-Barrientos, Y. 1980. Ultrastructure of sensory units on the first antennae of calanoid copepods. M. S. thesis, University of Ottawa, Ontario. 81 pp.

Coombs, S., and J. Janssen. 1990. Water flow detection by the mechanosensory lateral line. Pp. 89–123 in *Comparative Perception, Vol. II: Complex Signals.* W. C. Stebbins and M. A. Berkley, eds. John Wiley, New York.

Cronin, T. 1982. Estuarine retention of larvae of the crab *Rhithropanopeus harrisii. Estuarine Coastal Shelf Sci.* **15:** 109–131.

Doall, M. H., S. P. Colin, J. R. Strickler, and J. Yen. 1998. Locating a mate in 3D: the case of *Temora longicornis. Phil. Trans. R. Soc. Lond. B* **353:** 681–689.

Doall, M. H., 1995. The components of predation between *Euchaeta rimana,* a predatory calanoid copepod, and smaller copepods. species. M. S. thesis. State University of New York, Stony Brook, NY.

Dourdeville, T. A. 1981. A physical and physiological analysis of near-field displacement reception by the calanoid copepod, *Cen-*

tropages typicus Kroyer. M.S. thesis, State University of New York, Stony Brook, NY.

Dusenbery, D. B. 1992. *Sensory Ecology.* W. H. Freeman, New York.

Fields, D. M. 1996. Interactions of marine copepods with a moving fluid environment. Ph.D. thesis. State University of New York, Stony Brook, NY.

Fields, D. M., and J. Yen. 1996. The escape behavior of *Pleuromamma xiphias* from a quantifiable fluid mechanical disturbance. Pp. 323–339 in *Zooplankton: Sensory Ecology and Physiology, Vol. 1.* P. H. Lenz, D. K. Hartline, J. E. Purcell, and D. L. Macmillan, eds. Gordon Breach Publishers, Amsterdam.

Fields, D. M., and J. Yen. 1997. The escape behavior of marine copepods in response to a quantifiable fluid mechanical disturbance. *J. Plankton Res.* **19:** 1289–1304.

Fleminger, A. 1985. Dimorphism and possible sex change in copepods of the family Calanidae. *Mar. Biol.* **88:** 273–294.

Forward, R. B., and D. Rittschof. 1994. Photoresponses of crab megalopae in offshore and estuarine waters: implications for transport. *J. Exp. Mar. Biol. Ecol.* **182:** 183–192.

Friedman, M. M., and J. R. Strickler. 1975. Chemoreceptors and feeding in calanoid copepods (Arthropoda: Crustacea). *Proc. Natl. Acad. Sci. USA* **72:** 4185–4188.

Gallager, S. M., C. S. Davis, A. W. Epstein, A. Solow, and R. C. Beardsley. 1997. High resolution observations of plankton spatial distributions correlated with hydrography in the Great South Channel, Georges Bank. *Deep-Sea Res. II* **43:** 1627–1663.

Gerritsen, J. 1980. Sex and parthenogenesis in sparse populations. *Am. Nat.* **115:** 718–742.

Gill, C. W., and S. A. Poulet. 1988. Responses of copepods to dissolved free amino acids. *Mar. Ecol. Prog. Ser.* **43:** 269–276.

Gries, T., K. Johnk, D. Fields, and J. R. Strickler. 1999. Size and structure of 'footprints' produced by *Daphnia:* impact of animal size and density gradients. *J. Plankton Res.* **21:** 509–523.

Griffiths, A. M., and B. W. Frost. 1976. Chemical communication in the marine planktonic copepods *Calanus pacificus* and *Pseudocalanus* sp. *Crustaceana* **30:** 1–9.

Hallberg, E., K. U. I. Johansson, and R. Elofsson. 1992. The aesthetasc concept: structural variation of putative olfactory receptor cell complexes in Crustacea. *Microsc. Res. Tech.* **22:** 325–335.

Harden Jones, F. R. 1968. *Fish Migration,* 2nd Ed. Edward Arnold, London.

Haury, L. R., and H. Yamazaki. 1995. The dichotomy of scales in the perception and aggregation behavior of zooplankton. *J. Plankton Res.* **17:** 191–197.

Haury, L. R., H. Yamazaki, and E. C. Itsweire. 1990. Effects of turbulent shear flow on zooplankton distribution. *Deep-Sea Res.* **37:** 447–461.

Hwang, J-S., J. H. Costello, and J. R. Strickler. 1994. Copepod grazing in turbulent flow: elevated foraging behavior and habituation of escape responses. *J. Plankton Res.* **16:** 421–431.

Incze, L. S. 1996. Small-scale biological-physical interactions. *Proc. GOM Ecosys. Dyn.* **97:** 105–116.

Jackson, G. A. 1980. Phytoplankton growth and zooplankton grazing in oligotrophic oceans. *Nature* **284:** 439–441.

Jiménez, J. 1997. Oceanic turbulence at millimeter scales. *Sci. Mar.* **61:** 47–56.

Karp-Boss, L., E. Boss, and P. A. Jumars. 1996. Nutrient fluxes to planktonic osmotrophs in the presence of fluid motion. *Oceanogr. Mar. Biol. Annu. Rev.* **34:** 71–107.

Kerfoot, W. C. 1978. Combat between predatory copepods and their prey: *Cyclops, Epischura,* and *Bosmina. Limnol. Oceanogr.* **23:** 1089–1102.

Knebl, M. A. R., and J. R. Strickler. 1981. Copepod feeding currents: Food capture at low Reynolds number. *Limnol. Oceanogr.* **26:** 1062–1073.

Lazier, J. R. N., and K. H. Mann. 1989. Turbulence and the diffusive layers around small organisms. *Deep-Sea Res.* **36:** 1721–1733.

Liu, J. C. 1996. Effects of morphology on the biomechanics of the high speed escape reaction of copepods: developmental and species differences. M. S. thesis, State University of New York, Stony Brook, NY.

Mackas, D. L., H. Sefton, C. B. Miller, and A. Raich. 1993. Vertical habitat partitioning by large calanoid copepods in the oceanic subarctic Pacific during spring. *Prog. Oceanogr.* **32:** 259–294.

Mackas, D. M., and C. B. Miller, 1990. Vertical distribution of major copepod species in the Subarctic Pacific. *EOS* **7:** 180.

Manton, S. M. 1977. *The Arthropoda, Habits, Functional Morphology and Evolution.* Clarendon Press, Oxford.

Markl, H. 1978. Adaptive radiation of mechanoreception. Pp. 319–344 in *Sensory Ecology Reviews and Perspectives.* M. A. Ali, ed. Plenum, New York.

Moore, P. A., D. M. Fields, and J. Yen. 1999. Physical constraints of chemoreception in foraging copepods. *Limnol. Oceangr.* **44:** 166–177.

Naganuma. T. 1996. Calanoid copepods: linking lower-higher trophic levels by linking lower-higher Reynolds numbers. *Mar. Ecol. Prog. Ser.* **136:** 311–313.

Okubo, A. 1984. Oceanic turbulent diffusion of abiotic and biotic species. Pp. 390-406 in *Mathematical Ecology, Lecture Notes in Biomathematics. Vol. 54.* S. Levin, ed. Springer-Verlag, New York.

Paffenhöfer, G-A. 1998. On the relation of structure, perception and activity in marine planktonic copepods. *J. Mar. Sys.* **15:** 457–473.

Sanford, LP. 1997. Turbulent mixing in experimental ecosystem studies. *Mar. Ecol. Prog. Ser.* **161:** 265–293.

Shariff, K., and A. Leonard, 1992. Vortex rings. *Annu. Rev. Fluid Mech.* **24:** 235–279.

Strickler, J. R. 1975. Swimming of planktonic *Cyclops* species (Copepoda, Crustacea): pattern, movements and their control. Pp. 599–613 in *Swimming and Flying in Nature,* T.Y.-T. Wu, C. J. Brokaw, and C. Brennan, eds. Plenum, New York.

Strickler, J. R. 1982. Calanoid copepods, feeding currents, and the role of gravity. *Science* **218:** 158–160.

Strickler, J. R. 1984. Sticky water: a selective force in copepod evolution. Pp. 187–239 in *Trophic Interactions Within Aquatic Ecosystems,* D. G. Meyers and J. R. Strickler, eds. Westview, Boulder, CO.

Strickler, J. R., and A. L. Bal. 1973. Setae of the first antennae of the copepod *Cyclops scutifer* (Sars): their structure and importance. *Proc. Natl. Acad. Sci. USA* **70:** 2656–2659.

Strickler, J. R., D. Ono, and J. Reimer. 1995. Spatial filtering in microscopy: the use of matched filters to see further in time and space. *Zool. Studies 34 (Suppl. I):* 227–228.

Tennekes, H., and J. L. Lumley. 1972. *A First Course in Turbulence.* MIT Press, Cambridge.

Tiselius, P., and P. R. Jonsson. 1990. Foraging behavior of six calanoid copepods: observations and hydrodynamic analysis. *Mar. Ecol. Prog. Ser.* **66:** 23–33.

Tsuda, A., and C. B. Miller. 1998. Mate finding in *Calanus marshallae* (Frost). *Phil. Trans. Roy. Soc. Lond. B* **353:** 713–720.

Vincent, A., and M. Meneguzzi. 1991. The spatial structure and statistical properties of homogenous turbulence. *J. Fluid Mech.* **225:** 1–20.

Vogel, S. 1994. *Life in Moving Fluids.* Princeton University Press, Princeton, NJ.

Weatherby, T. M., K. K. Wong, and P. H. Lenz. 1994. Fine structure of the distal sensory setae on the first antennae of *Pleuromamma xiphias* (Giesbrecht (Copepoda). *J. Crust. Biol.* **14:** 670–685.

Weihs, D. 1977. Periodic jet propulsion of aquatic creatures. *Fortschr. Zool.* **24:** 171–175.

Weissburg, M. J. 2000. The fluid dynamical context of chemosensory behavior. *Biol. Bull.* **198:** 188–202.

Weissburg, M. J., and R. K. Zimmer-Faust. 1993. Life and death in moving fluids: hydrodynamic effects on chemosensory-mediated predation. *Ecology* **74:** 1428–1443.

Weissburg, M. J., M. H. Doall, and J. Yen. 1998. Following the invisible trail: mechanisms of chemosensory mate tracking by the copepod *Temora. Phil. Trans. R. Soc. Lond. B* **353:** 701–712.

Yamazaki, H. 1993. Lagrangian studies of planktonic organisms: perspectives. *Bull. Mar. Sci.* **53:** 265–278.

Yamazaki, H., and T. R. Osborn. 1988. Review of oceanic turbulence: implications for biodynamics. Pp. 215–234 in *Toward a Theory on Biological-Physical Interactions in the World Ocean.* B. J. Rothschild, ed. Kluwer Academic, Boston.

Yamazaki, H., and K. D. Squires. 1996. Comparison of oceanic turbulence and copepod swimming. *Mar. Ecol. Prog. Ser.* **144:** 299–301.

Yen, J. 1988. Directionality and swimming speeds in predator-prey and male-female interactions of *Euchaeta rimana,* a subtropical marine copepod. *Bull. Mar. Sci.* **43:** 175–193.

Yen, J., and N. T. Nicoll. 1990. Setal array on the first antennae of a carnivorous marine copepod *Euchaeta norvegica. J. Crust. Biol.* **10:** 327–340.

Yen, J., and J. R., Strickler. 1996. Advertisement and concealment in the plankton: What makes a copepod hydrodynamically conspicuous? *Invertebr. Biol.* **115:** 191–205.

Yen, J., B. G. Sanderson, J. R. Strickler, and A. Okubo. 1991. Feeding currents and energy dissipation by *Euchaeta rimana,* a subtropical pelagic copepod. *Limnol. Oceanogr.* **36:** 362–369.

Yen, J., M. J. Weissburg, and M. H. Doall. 1998. The fluid physics of signal perception by a mate-tracking copepod. *Phil. Trans. R. Soc. Lond. B* **353:** 787–804.

Reference: *Biol. Bull.* **198:** 225–244. (April 2000)

The Chemical Defense Ecology of Marine Unicellular Plankton: Constraints, Mechanisms, and Impacts

GORDON V. WOLFE*

Shannon Pt. Marine Center, Western Washington University, 1900 Shannon Pt. Rd., Anacortes, Washington 98221

Abstract. The activities of unicellular microbes dominate the ecology of the marine environment, but the chemical signals that determine behavioral interactions are poorly known. In particular, chemical signals between microbial predators and prey contribute to food selection or avoidance and to defense, factors that probably affect trophic structure and such large-scale features as algal blooms. Using defense as an example, I consider physical constraints on the transmission of chemical information, and strategies and mechanisms that microbes might use to send chemical signals. Chemical signals in a low Re, viscosity-dominated physical environment are transferred by molecular diffusion and laminar advection, and may be perceived at nanomolar levels or lower. Events that occur on small temporal and physical scales in the "near-field" of prey are likely to play a role in cell-cell interactions. On the basis of cost-benefit optimization and the need for rapid activation, I suggest that microbial defense system strategies might be highly dynamic. These strategies include compartmented and activated reactions, utilizing both pulsed release of dissolved signals and contact-activated signals at the cell surface. Bioluminescence and extrusome discharge are two visible manifestations of rapidly activated microbial defenses that may serve as models for other chemical reactions as yet undetected due to the technical problems of measuring transient chemical gradients around single cells. As an example, I detail an algal dimethylsulfoniopropionate (DMSP) cleavage reaction that appears to deter protozoan feeding and explore it as a possible model for a rapidly activated, short-range chemical defense system. Although the exploration of chemical interactions among planktonic microbes is in its infancy, ecological models from macroorganisms provide useful hints of the complexity likely to be found.

Introduction

In contrast to the multicellular organisms whose chemical ecology is adapted to turbulent environments of high or intermediate Reynolds number, planktonic marine microbes that are generally well below 1 mm in size are the focus of this paper. This extremely diverse and ecologically important group includes mostly unicellular prokaryotes (bacteria and archaea) and eukaryotes (protists: algae and protozoa) that range in size from <1 to 200 μm (Fig. 1). This realm is dominated by viscous forces, and chemical information is transmitted by "simple" diffusion and advective laminar flow. But although the behavioral and chemosensory abilities of unicellular microbes have been known for nearly a century (Jennings, 1906; Schaeffer, 1910) and the general physical, chemical, and molecular regulation of microbial signaling and behavior have been recognized for decades (Carlile, 1975; Berg and Purcell, 1977; Levandowsky and Hauser, 1978; Aaronson, 1981; Van Houten *et al.*, 1981), they remain poorly understood. Recent calculations suggest that microbial chemosensory adaptations to diffusive environments may be even more sophisticated than previously thought (Dusenbery, 1998). This realm also remains largely unexplored experimentally due to profound technical difficulties of observation.

In this paper, I review and synthesize physiological information from model cell-biology systems with physical limitations on microbial signaling in aqueous environments, focusing on food selection and chemical defense as an example of the potentially complex chemical ecology of

---

Received 6 April 1999; accepted 16 November 1999.

* Current address: Dept. of Biological Sciences, California State University, Chico, Chico, California 95929-0515. E-mail: gwolfe2@csuchico.edu

This paper was originally presented at a symposium titled *Chemical Communication and Ecology*. The symposium, which was held in San Diego, California, on 30 December 1998, was invited by the Western Society of Naturalists as part of its annal meetings.

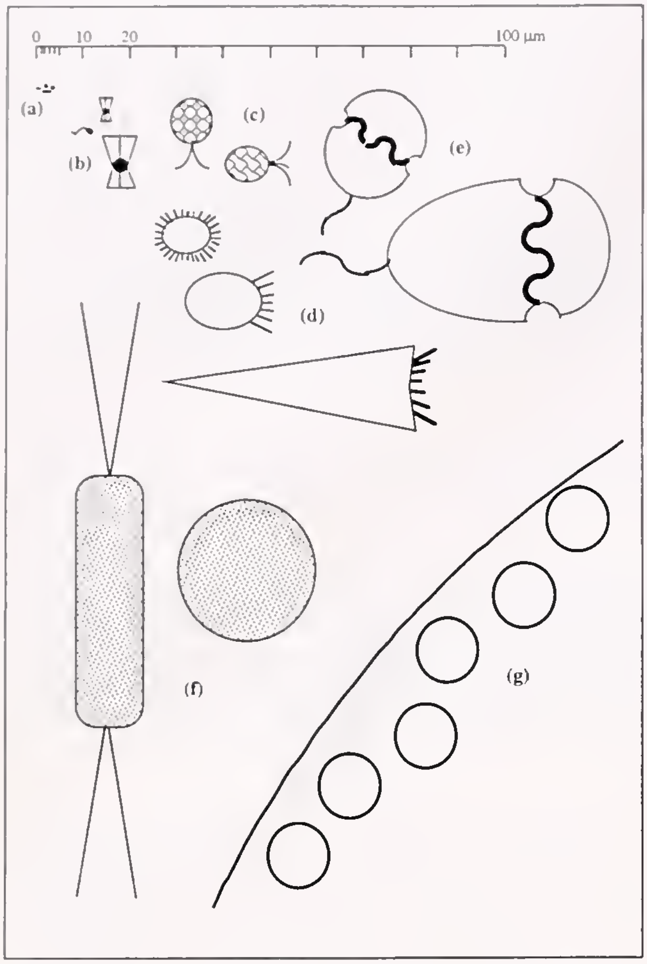

Figure 1. Size range of unicellular marine plankton. The illustration is purely schematic and indicates just a few major groups, most of which include both autotrophic and heterotrophic taxa. Included are bacteria and prochlorophytes (a); nanoflagellates, including heterotrophs (b) and autotrophic haptophytes (c); oligotrichous, hypotrichous, and tintinnid ciliates (d); dinoflagellates (e); and diatoms (f). Also shown for comparison is a millimeter-scale colony of the nanoflagellate *Phaeocystis pouchetii* with cells arranged at the periphery (g); 200 μm is a rough upper size limit for most marine protists, and a lower limit for metazoan grazers. However, many cells have projections of considerable complexity that greatly increase their effective size, such as choanoflagellate feeding baskets (b) or diatom spines (f).

marine plankton. I then explore microbial defense-system strategies and signal mechanisms as limited by physical and physiological potential. These suggest that dynamic events which occur on small temporal and physical scales are likely to be important, although their measurement poses great technical challenges. I detail a reaction hypothesized to affect protozoan feeding selectivity that might serve as a model for rapidly activated, short-range microbial deterrence systems. Finally, I briefly examine trophic and evolutionary implications of planktonic chemical defense, and suggest that ecological models from macroorganisms will provide useful hints about the probable complexity of interactions. The literature holds many fascinating glimpses into the complex world of microbial signaling, spread widely among many disciplines such as fluid physics, chemical ecology, microbiology, immunology, biochemistry, molecular biology, and oceanography. I will be able to touch on many aspects of these topics only briefly, and have tried to provide a recent and somewhat comprehensive list of sources for further information.

Rationale: the microbial biosphere

Microbes dominate evolutionary history: for over half of Earth's existence, the biosphere was entirely microbial (Knoll and Lipps, 1993; Roberts *et al.*, 1996). This reign led to the evolution of vast genetic diversity (Barns and Nierzwicki-Bauer, 1997; Pace, 1997); for example, prokaryotic (bacterial and archaeal) metabolic pathways affect all major biogeochemical cycles and led to the oxidation of the Earth's surface (Falkowski and Raven, 1997; Fenchel *et al.*, 1998).

In the present-day biosphere, microbes are most obviously the exclusive colonizers of extreme environments (Karl, 1995; Gross, 1998), but are surprisingly important to global productivity. The oceans are microbially dominated ecosystems (Sherr and Sherr, 1991), and although marine plankton constitute less than 0.5% of global biomass, they contribute nearly 50% of global net primary production (Field *et al.*, 1998). In most of the ocean, nutrient concentrations are low, and osmotrophs have evolved towards small sizes to optimize nutrient uptake. Therefore, much of marine primary production is dominated by pico- and nonoplankton less than 20 μm in size. These organisms are eaten primarily by protozoan grazers, which are also the major grazers of marine bacteria (Sherr and Sherr, 1994), and are therefore important recyclers of nutrients in the upper oceans (Strom, 2000). They are also critical trophic links between their prey and larger metazoan grazers (Fessenden and Cowles, 1994), forming the base of the marine food web (Pomeroy, 1992).

Microbial signaling

A signal is a directed communication: the transfer of information between two organisms *via* a biogenic stimulus that can be perceived by a sensory system and evoke an adaptive response (Dusenbery, 1992). Signals received at the cell surface are conveyed intracellularly by several major mechanisms, including ion-channel-linked receptors, G protein-linked receptors and enzyme-linked receptors (Van Houten, 1994). Ca^{2+} and cyclic AMP are important molecules in mediating signal transduction and may also act externally to the cell (O'Day, 1990; Louis *et al.*, 1993). For example, mechanosensors in ciliates are driven by Ca^{2+} ion currents (Hennessey, 1989), resulting in excitatory action potential waves that pass over the surface of the cell, causing rapid depolarization and hyperpolarization and leading to synchronized ciliary motion for movement (Febvre-Chavalier *et al.*, 1989).

Protozoa also have cell-surface signal receptors that recognize vertebrate and plant hormones as varied as polypeptides, cytokines, indolacetic acid, and opiates (Csaba, 1996). These vertebrate and plant signal molecules can promote chemotaxis (Köhidai *et al.*, 1994), phagocytosis (Rabinovitch and De Stefano, 1971; Renaud *et al.*, 1995), and other responses (Kovaács *et al.*, 1997). Protozoa also produce hormone molecules (LeRoith *et al.*, 1982) that may interact with cell receptors (Marino and Wood, 1993). The adaptive significance for these signaling molecules in protists is poorly understood, but evolution of such signals and their receptors probably led to cellular hormonal systems in higher organisms (Carr, 1989). Almost nothing is known about such signaling in most environmentally important protists, especially in marine environments.

Receptor sensitivities and reaction times depend on diffusion of signal molecules and binding strengths. The signal-to-noise ratio (S/N) scales as $(tDCR)^{0.5}$ (Dusenbery, 1992), where R is the effective receptor radius, C the signal concentration for a signal with diffusion constant D, and t the integration time. For $S/N \sim 1$, $t \sim 0.1$ s, $R \sim 0.1$ μm and $D \sim 10^{-6}$ cm^2 s^{-1}, C is about 10^{-9} *M*, a value consistent with observations. Receptor sensitivity—the minimal concentration for detectable S/N—scales as $(Rt)^{-2}$. Since small cells cannot increase receptor size, longer integration times may be used to increase sensitivity (Dusenbery, 1992).

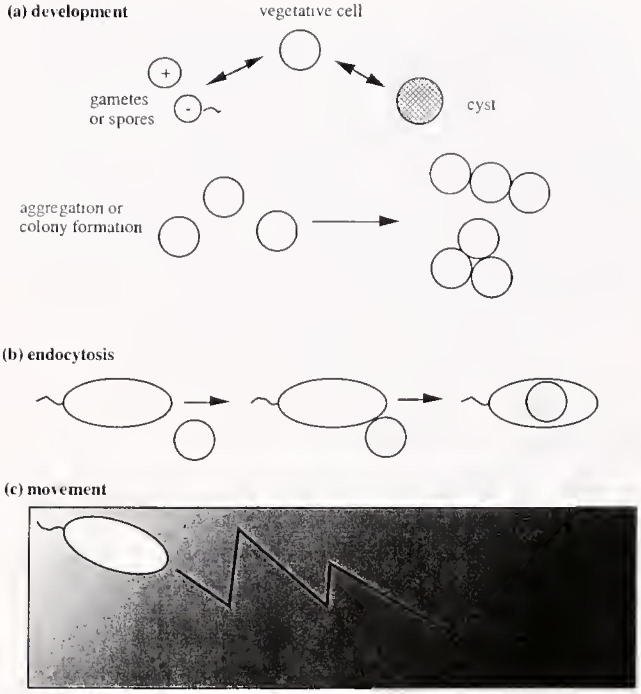

Figure 2. General microbial responses to chemical signals. (a) Developmental (life-cycle) responses include sexual reproduction or encystment; (b) attachment responses include aggregation or colony formation (intraspecific) or endocytosis (intra- or interspecific); (c) movement responses to chemical gradients include changes in swimming speed (taxis) or frequency of turning (kinesis).

Behavioral responses to signals

Signaling between cells in multicellular organisms encompasses such activities as cell movement and adhesion, development, differentiation, and programmed cell death (apoptosis); electrochemical signal propagation and cellular signaling networks; and predator-prey (phagocytotic) interactions. Although typically studied in vertebrate systems, nearly all probably originated in unicellular microbes (Carlile, 1975; Kurjan and Taylor, 1993; Csaba and Müller, 1996) and have been studied in detail for a few protozoan models (*Paramecium, Tetrahymena, Dictyostelium* [Loomis, 1982; Gall, 1986; Devreotes, 1989]).

Although microorganisms lack the specialized physical development of multicellular animals and plants, they have complex and sophisticated sensory and behavioral adaptations to their environment (Jennings, 1906). Microbes respond to stimuli by development, attachment (intraspecific) or endocytosis (interspecific), or movement. Developmental changes (Fig. 2a) are intraspecific and include mating, encystment, and aggregation or colony formation; they often operate by contact-mediated recognition processes (Calleja, 1984). A model system is the cellular slime mold *Dictyostelium*, explored for its insights into the evolution of multicellularity (Loomis, 1982). Endocytosis (Fig. 2b) is usually interspecific, but the close relation between phagocytosis and mating (sex) has long been noted (Margulis and Sagan, 1987). Phagocytosis can be mediated by prey-excreted or prey-surface molecules (Rabinovitch and De Stefano, 1971; Brown *et al.*, 1975; Vogel *et al.*, 1980; Wright and Silverstein, 1986; Kiersnowska *et al.*, 1988). Contact and recognition of prey often seem to be distinct processes, although this is poorly understood (Peck, 1985; Ricci *et al.*, 1996).

Protist movements include swimming, surface gliding (benthic diatoms, desmids), or crawling (ameboid movement due to protoplasmic streaming). Here I focus on swimming, the dominant mode among plankton. The two main marine protozoan groups are flagellates and ciliates (Fenchel, 1987), whose propulsion systems operate by similar mechanisms. Flagellates use one or more flagella (= whip; also termed undulopodia [Margulis *et al.*, 1990] to differentiate them from the structurally different bacterial flagella). Ciliated cells are covered in an array of shorter cilia (= hair); metachronous depolarization waves passing over the ciliate cell cause coordinated ciliary movement for motion (Hennessey, 1989; Clark *et al.*, 1993). Protozoa typically swim at about 200 μm s^{-1} (flagellates) to 1000

μm s^{-1} (ciliates). Given body lengths of less than 200 μm, most microbes thus operate in a viscosity-dominated realm (Re $\ll$ 1) where fluid motions are completely reversible in time (Purcell, 1977). Although swimming speed increases with cell size, power requirements increase more rapidly than propulsive force, limiting speeds for larger cells (Fenchel, 1987, p. 20). Protists are less affected by random thermal (Brownian) movement than are smaller bacteria, and they can orient and position, often swimming in helical motions that may help in orientation (Crenshaw, 1992).

The Chemical Dynamics of Microbial Trophic Interactions

Finding and selecting prey

In most marine waters the plankton constitute an extremely dilute suspension, usually less than 10 ppm by volume. Therefore, a major challenge for predatory microbes is finding prey sufficient to maintain (rapid) growth, and detection of prey at a distance would seem to be an advantage in locating food (Buskey and Stoecker, 1988). Many protists show responses to chemical gradients in space or time. Chemotaxis is stimulus-oriented (directed) movement, whereas chemokinesis is stimulus-induced movement without directional orientation. The latter is much more common; it includes both orthokinesis (change in linear velocity) and klinokinesis (change in rate of turning, Fig 2e) and is based on adaptation mechanisms (Machemer and Teunis, 1996).

There are several major feeding modes. Raptorial feeders (Fenchel, 1987) directly intercept prey following random contact. Collision-based prey capture is determined by the effective prey cross-section, which scales as $S_p = (r_g + r_p)^2$ where r_g and r_p denote the radii of spherical grazer and prey. Grazers encounter prey at a rate of $E = \pi/3\ S_p\ N_p\ (3v_g^2 + v_p^2)/v_g$ where N_p is the prey density and v the speeds (Gerritsen and Strickler, 1977); the frequency of encounters thus increases with relative speed (prey speeds are often small compared to grazers). Filter feeders, the other major feeding mode typified by ciliates and some flagellates, generate feeding currents that bring prey towards grazer cells. Particle capture is determined by particle size, the shear fields produced by feeding currents, and capture structures (Fenchel, 1980; Jonsson, 1986; Monger and Landry, 1991).

However they capture prey, all predators need to obtain high-quality nutrients and nutritional balance while avoiding toxic prey. Although acute responses that result from ingestion of a small number of highly toxic prey (death, reduced growth or reproductive rates) have been noted in some laboratory studies (Sykes and Huntley, 1987; Hansen, 1995), it is not clear how these operate in natural populations. However, subacute effects, which affect feeding behavior by stimulating avoidance or rejection of protected prey, are probably as or more important. There is increasing evidence that prey selection is based on chemical cues determined during prey capture, handling, or ingestion, leading to rejection following prey capture (*e.g.*, Taniguchi and Takeda, 1988; Stoecker *et al.*, 1995), but these cues are little understood at present. Such cues are not necessarily limited to highly toxic cells or compounds (Stoecker *et al.*, 1981; Rassoulzadegan and Fenaux, 1984; DeMott, 1986; Cowles *et al.*, 1988; Sanders, 1988; Van Donk *et al.*, 1997).

Defense problems and strategies

How might a single cell defend itself against predation? Constitutive toxicants are self-hazardous and costly to maintain in the face of shifting predation risk. It is also clear that for unicellular organisms, which have no tissue to sacrifice, repelling or discouraging attack is better than post-ingestion toxicity. Induced defense responses—phenotypic modification in response to predator cues—are widespread among macroorganisms and increasingly recognized as important defense strategies (Karban and Baldwin, 1997; Tollrian and Harvell, 1999). These changes are often slow, requiring gene transcription and growth or development, and typically occur on time scales of hours to days. Although examples of such responses exist among planktonic microbes (ciliates [Kusch, 1993; Kusch, 1995]), the short time scales of microbial encounters suggest more immediate deterrents. Here, I consider several strategies that may have adaptive advantages to microbial chemical defense.

Compartmentation. One general strategy for sequestering self-toxic compounds is compartmentation (Fowden and Lea, 1979). Large organisms may have specialized tissues or organs for safely containing toxicants (Hefetz and Blum, 1978; Rossini *et al.*, 1997). In vascular plants, vacuoles often serve as compartments to concentrate toxins (Wagner, 1978; Wink, 1997). All eukaryotic cells have highly compartmented organelles and many produce highly toxic metabolites (Hall and Strichartz, 1990; Plumley, 1997). So-called harmful algal bloom (HAB) taxa produce paralytic toxicants that inhibit metazoan nerve conduction (Cembella, 1998), such as the saxitoxins (Hall *et al.*, 1990). Although these toxins may function as grazing deterrents (Turner and Tester, 1997; Turner *et al.*, 1998) or allelopathic compounds (Dakshini and Dakshini, 1994; Subba Rao *et al.*, 1995; Windust *et al.*, 1996; Sugg and VanDolah, 1999), evidence is contradictory, and their ecological functions are poorly understood. However, most appear to be produced constitutively and may pose a hazard to the algae that synthesize them. Compartmentation may reduce autotoxicity; saxitoxins in *Gonyaulax* and okadaic acid in *Prorocentrum* localize to chloroplasts (Anderson and Cheng, 1988; Zhou and Fritz, 1994).

Activated reactions. Compartmentation also is used in "activated' reactions," whereby a grazer-initiated signal causes a rapid reaction that produced a feeding deterrent.

Examples of such systems in macroalgae (Paul and van Alstyne, 1992) and vascular plants include some of the best-known plant defense systems, including hydrolysis of glucosinolates (Newman *et al.*, 1992) and cyanogenesis (Jones *et al.*, 1978). These generally appear to be mixing reactions initiated when grazing injury disrupts compartmented enzyme-substrate systems. Such systems are elegant solutions to minimizing self-toxicity and the energetic cost of defense capability. Since microbes typically operate on short time scales, and predator-prey interactions may occur in seconds, rapid defense systems or strategies ought to be favored evolutionarily, but no direct observations of activated chemical systems in unicellular organisms have yet been reported. This is probably due to the technical difficulties of detecting transient and small-scale chemical gradients around single cells. Only recently has a first report even demonstrated the production of a compartmented mixing reaction in a phospholipid bilayer system similar in size to a eukaryotic nanoplankter cell (Chiu *et al.*, 1999).

However, several observable examples of compartmented, rapidly activated microbial defense reactions might serve as conceptual models for the rapid production of chemical signals. One is mechanically stimulated bioluminescence, produced by many marine dinoflagellates (*e.g.*, *Pyrocystis, Pyrodinium, Gonyaulax*, or *Noctiluca* [Johnson *et al.*, 1985; Anderson *et al.*, 1988]). In these organisms, light is emitted when the enzyme luciferase oxidizes a substrate, luciferin, contained in small vesicles called scintillons. Luciferin is normally prevented from reacting by attachment to a luciferin-binding protein; mechanical distortion of the cell plasma membrane generates an electrical action potential that traverses the cell in less than a microsecond (Nicolas *et al.*, 1975), creating an influx of protons that releases luciferin for oxidation. The result is a near-synchronous sequence of scintillon microflashes that collectively appear as a pulse of light. The reaction functions for defense against metazoan grazers, acting as a "burglar alarm" to attract predators of the grazers (Esaias and Curl Jr., 1972; White, 1979; Buskey and Swift, 1985; Mensinger and Case, 1992; Abrahams and Townsend, 1993).

The other example involves exocytosis, the release of chemicals sequestered inside vesicles to the cell exterior, by vesicle fusion with the cell plasma membrane. Extrusomes are organelles common to most ciliates and dinoflagellates (Bouck and Sweeney, 1966; Dodge and Greuet, 1987; Görtz, 1988), and also found in some other taxa, that explosively release toxicysts, trichocysts, or nematocysts from the cell surface. This release is triggered by mechanical distortion of the cell surface or by chemical (polyamino) cues (Plattner *et al.*, 1985) mediated by GTP-binding proteins (Peterson, 1991). Nematocysts and toxicysts are used to secure and immobilize prey (Wesenberg and Antipa, 1970), but the role of trichocysts has long been a puzzle (Mast, 1906; Haacke-Bell *et al.*, 1990). Recent evidence suggests that trichocyst discharge causes swimming reversal in *Paramecium* (Harumoto, 1994) and thus functions for defense, physically driving prey ciliates away from predators (Harumoto and Miyake, 1991; Knoll *et al.*, 1991). A particularly fascinating example is the hypotrich ciliate *Euplotidium itoi*. This species carries symbiotic epibionts termed epixenosomes (Rosati, 1999) that contain extrusomes (Rosati *et al.*, 1993). *Euplotidium* cells lacking epixenosomes are much more susceptible to predation by the ciliate *Litonotus*, suggesting that these organelles function for defense of the host cell (Rosati *et al.*, 1999).

Although extrusomes are visible polymerization reactions, triggered exocytosis may also be a fundamental method of chemical communication among microbes. Exocytotic reactions are a widespread and highly conserved method of cellular communication within multicellular organisms and occur over time scales ranging from minutes to microseconds (Almers, 1990; Burgoyne and Morgan, 1993). They include such diverse phenomena as histamine release by mast cells following inflammation (Gomperts *et al.*, 1994), neutrophil phagocytosis (Suzaki *et al.*, 1997), sperm acrosomal and egg activation reactions during fertilization (Jaffe, 1985; Tilney, 1985), and neurotransmitter release at nerve synapses (von Gersdorff and Matthews, 1994).

Multifunctional systems. Compartmented and activated reactions not only are rapid but may be very efficient energetically, since no protein synthesis is required for initiation. Another strategy to improve efficiency is to use defense molecules for multiple purposes. For example, tetrodotoxin, the nerve-impulse inhibitor produced by the pufferfish *Fugu*, also functions as a mating pheromone (Matsumura, 1995). This compound is concentrated in gametes that otherwise would be especially vulnerable to predation. Ciliate extrusomes probably play multiple roles: *Paramecium* trichocysts aid in both food capture and escape from predation (Wesenberg and Antipa, 1970; Harumoto and Miyake, 1991).

Carr (1988) pointed out that many biochemical intermediates, such as amino acids, nucleic acids, and fatty acids, and their derivatives, are often in the high millimolar range inside cells. However, the background concentrations of these labile molecules in aqueous environments are nanomolar or below. Within this enormous concentration range, many such molecules show chemosensory activity for a variety of organisms. Therefore, active release or conversion of concentrated solute pools may provide easily detectable signals to potential predators, while utilizing precursor molecules that are used for other processes and not costly in the absence of predation. The costs of defense in planktonic microbes have only recently been addressed (Kusch and Kuhlmann, 1994) and warrant further study.

Table 1

Chemical defense signal mechanisms, chemical signals can include both trophic and toxic compounds

	Excreted signal	Contact signal	Post-ingestion signal
Molecules	Small molecules but varied structures: organic and amino acids, sugars, short-chain lipids and derivatives	Glycoproteins, glycolipids, polypeptides	Varied: toxicants or toxins
Signal properties	Aqueous solubility, diffusivity, lability, toxicity	Specificity, toxicity	Toxicity or concentration
Signal location	Aqueous environment	Cell surface	Cell interior
Effect or mode of action	Negative kinesis/taxis: repellent	Release following capture: deterrent	Subsequent inhibition of feeding or toxicity, reduced digestability or growth efficiency
Benefit level	Individual or population, including competitors	Individual	Population of genets

Signal mechanisms

I next consider possible strategies for conveying chemical deterrence signals, in the order they might be perceived by a grazer (Table 1). They include signals excreted to the environment, cell-surface signals, and internal toxins that act following ingestion. Long-range chemical signals may act as repellents, preventing the initiation of feeding by causing the predator to orient away from a potential prey; closer-range signals may act as deterrents, repelling predators that have attempted to feed (Lindstedt, 1971). Signals might be presented continuously or activated in response to some trigger (Fig. 3).

The mechanisms of chemical signaling by microbes, though obscure, must be considered in the context of physical and physiological constraints on signal production and reception. I consider them in the general context of plankton ecology and physiology. This discussion is necessarily conceptual since the technical difficulties of measuring cell-cell chemical interactions *in vivo* are profound; we cannot yet detect the events that may occur in the brief instant when predator and prey meet. How do microbes convey chemical signals? What kinds of infochemicals are used by marine plankton?

Excreted signals. Low-molecular-weight metabolites include photosynthetic sugars, amino acids and derivatives, and also polypeptides and even some small lipids and proteins. Although polar compounds have relatively low membrane permeabilities, Bjørnson (1988) has suggested that small cells with large surface-to-volume ratios may unavoidably "leak" metabolites at potentially high rates. Whether such leakage is passive or active is poorly known; phototrophs in particular may actively excrete compounds to release excess reducing power under high irradiance, although the adaptive purpose is still contentious (Wood and van Valen, 1990). Therefore, as they approach prey, predators swim through gradients of excreted metabolites (Fig. 3a), a zone termed the phycosphere (Sieburth, 1968; Bell and Mitchell, 1972), which may serve to advertise the presence of the prey. Some protozoa can clearly detect excreted prey metabolites (Hauser *et al.*, 1975a; Levandowsky and Hauser, 1978; Van Houten *et al.*, 1981; Bennett *et al.*, 1988; Verity, 1988), and although movement for chemical searches requires constant energy in the non-inertial low Re environment, swimming costs are a trivial fraction of protozoan energy budgets (Fenchel, 1987). Whether protozoan grazers can use gradients to locate individual prey cells is less certain (Jackson, 1987).

It would seem advantageous for prey to also exude signal deterrents to keep grazers at a distance and thus avoid any possibility of damage during handling. However, because the time for molecular diffusion scales as $r^2/6D$ and $D < 10^3$ $\mu m^2\ s^{-1}$, this limits rapid signal transport to "near-field" regions within a few to a hundred micrometers. Beyond, turbulence at the millimeter scale also dissipates microzone gradients, although the impact is still controversial (Mitchell *et al.*, 1985; Alldredge and Cohen, 1987). (Much consideration has focused on detection of these microzones by bacteria, whose physical and physiological constraints and mechanisms may be very different from those of larger protozoa [Bowen *et al.*, 1993; Mitchell *et al.*, 1996; Blackburn *et al.*, 1998]).

Furthermore, the energetics of production of steady-state "far-field" signal gradients is likely to be unfavorable for small cells. Signal concentration decreases as r^{-1} as it diffuses outward, and beyond the near-field region within a few grazer body lengths (*e.g.*, $>200\ \mu m$), even compounds that are highly concentrated inside cells have signal-to-noise ratios too low for detection. This problem is analogous to that of mate location by pheromones, considered by Dusenbery and Snell (1995). Their analysis suggested that for organisms that locate mates (or prey) by random contact, the considerable metabolic cost of signal production is not

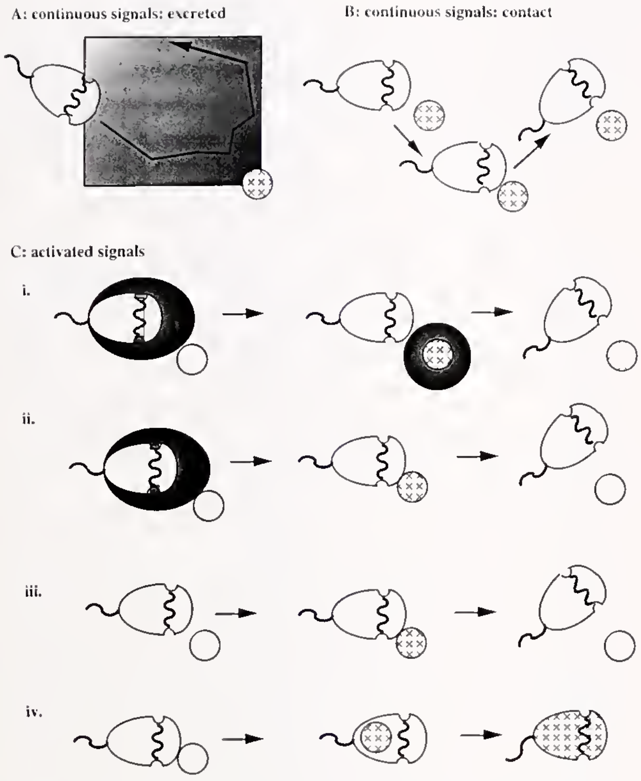
A: continuous signals: excreted
B: continuous signals: contact
C: activated signals
i.
ii.
iii.
iv.

Figure 3. Hypothetical defense mechanisms. The predator is shown as a schematic dinoflagellate with longitudinal and transverse flagella; the prey is a small circle. Prey that contain defense signals or toxins are indicated by cross-hatching. (A, B) Continuous signal mechanisms. (A) Excreted signals may create a gradient around the prey that can be detected and result in avoidance *via* negative chemokinesis (increased frequency of turning down gradient). (B) Cell-surface signals cause release following contact. (C) Activated signals may operate briefly by several mechanisms: (i) In pulse-pulse interaction, the prey is activated by a chemical or physical signal received from the predator and responds by excretion of a signal pulse that acts as a momentary deterrent. (ii) In pulse-contact mechanism, the prey is activated by a pulsed signal eminating from the predator, but the deterrent signal occurs only after predator-prey contact. (iii) In contact-contact interaction, prey activation and signal are caused by predator-prey cell contact. (iv) In a "suicide" mechanism, activation occurs following ingestion. The latter is the only mechanism that must be toxic in order to exert a selective advantage at the prey population level.

worthwhile below a critical body size, which is probably 200 μm in water, the range of most planktonic unicellular prey.

However, unsteady excretion may be a useful way to signal cells in close proximity (Fig. 3c, part i). Diffusive-signal pulse speeds scale as $6Dr^{-1}$, so pulses move at 6000–600 μm s^{-1} within 1–10 μm of a cell for $D \sim 10^{-5}$ cm^2 s^{-1}. Such signal fronts may precede grazer cells for very brief distances and possibly alert a prey cell, but the rapid decrease in concentration with radius makes this unlikely to be effective. Ciliary or flagellar propulsion systems typically operate at 50 Hz or slower; within the 20-ms beat time, receptor integration could detect ~100 n*M* signal pulses, but whether such brief events could be transduced and converted to kinetic responses is unknown. One well-known example of pulsed signaling occurs in the social amoeba *Dictyostelium discoides.* Aggregates of cells relay waves of cAMP to control reproductive development (Nanjundiah, 1973; Devreotes, 1982). The waves vary in concentration from 10–1000 n*M* but occur over much longer (minute) time scales.

Contact signals. Once predator and prey come into immediate proximity, direct contact offers the next of chemical transmission (Fig. 3b, c). Contact-mediated defense systems are well-known in protozoa (Fig. 3c, ii and iii). The "avoidance reaction" in ciliates is caused by massive ciliary hyperpolarization in response to chemical or mechanical cues (Jennings, 1906). Extrusome discharge occurs during predator-prey contact (Wesenberg and Antipa, 1970; Harumoto and Miyake, 1991; Knoll *et al.,* 1991).

More fundamentally, contact-mediated signaling mechanisms are a universal hallmark of cellular communication within multicellular organisms. Such signals are usually extensions of the cell plasma membrane, the carbohydrate-rich glycocalyx, which contains both glycoproteins and proteoglycans secreted into the extracellular space and adsorbed onto the cell surface. Two major classes of compounds appear to mediate most cell-contact interactions: protein-sugars and polypeptides take major roles in self-recognition and as attractants and deterrents (Köhidai and Csaba, 1996). The rich variety of oligosaccharide structures that can be formed with a limited set of oligomers and glycosidic linkages probably contributes to their utility for protein recognition (Sharon and Lis, 1993; Lowe, 1994). Lectins, proteins that bind specific oligosaccharide groups, function universally for "self *vs.* non-self" discrimination and have been hypothesized to be precursors of vertebrate immune systems (Burnet, 1971; Popescu and Misevic, 1997). They are used universally by microbes for intraspecific chemical communication (Doyle, 1994), mediating such intraspecific activities as adhesion or settlement (Kirchman *et al.,* 1982), cell agglutination and colony formation (Waite *et al.,* 1995), and mating interactions (van den Ende, 1985; Delmonte Corrado *et al.,* 1997). Their signaling role in phagocytosis is still poorly understood, but they probably contribute to predator-prey recognition in some systems (Rabinovitch and De Stefano, 1971; Brown *et al.,* 1975; Hellio and Ryter, 1980; Vogel *et al.,* 1980).

Peptide or polypeptide signals are the other major class of surface-active signals; both excreted and cell-surface peptides probably play major roles in signaling. Peptide signals and surface receptors occur widely in protozoa (LeRoith *et al.,* 1982; Freiburg, 1993; Luporini *et al.,* 1995; Ortenzi and Luporini, 1995), and many protozoa have receptors for vertebrate hormones (reviewed above). Peptide cues released to the environment act for self-recognition (Kusch, 1999) or as mating pheromones (Beale, 1990), and they may stimulate chemosensory responses (Leick and Hellung-Larsen, 1985; Köhidai *et al.*, 1994; Kuhlmann *et al.*, 1997) or have mitogenic activity (Vallesi *et al.*, 1995). Little is known about peptide-mediated signaling among marine planktonic protists, but peptides probably function universally as chemocues in the marine environment (Rittschof, 1990; Decho *et al.*, 1998).

Post-ingestion (suicide) signals. The final frontier of chemical defense signaling follows ingestion and involves inhibitory reactions or highly toxic prey molecules. Constitutive toxins, already discussed, may incapacitate grazers (Hansen, 1989; Hansen *et al.*, 1992). Metazoan grazers may regurgitate toxic prey (Huntley *et al.*, 1986), but expelled cells appear to be damaged and suffer lower growth rates.

From an evolutionary viewpoint, suicide signals seem to make little sense for microbes without tissue to sacrifice: selection for such mechanisms is unlikely because the prey organism does not survive to reproduce. However, there may be benefit to a population of genetically identical asexually dividing prey (genets). If the pool of grazers is small relative to prey, then inhibition of grazing by the loss of a small fraction of the prey population may increase the prey gene pool; this perspective is analogous to viewing microbial populations as extended multicellular organisms or superorganisms. The extent to which genetic diversity occurs among clonal plankton is just beginning to be known (Oppen *et al.*, 1996). However, reducing grazing pressure *via* toxic suicide mechanisms may allow competitor prey to avoid grazing pressure and thus decrease the fitness of toxic prey. Rather, deterrence strategies that force a grazer to select another prey would both improve survival of individuals and remove competition.

A Model Mechanism for Planktonic Deterrence

I next present a possible dynamic chemical defense model that may be widespread among marine unicellular algae, involving the cleavage of β-dimethylsulfoniopropionate (DMSP) to dimethyl sulfide (DMS), acrylate, and a proton:

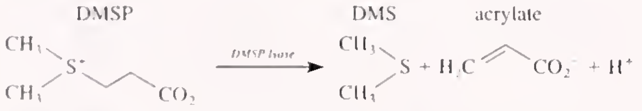

DMSP is produced by many marine algae and is especially prominent in haptophytes and dinoflagellates (Keller *et al.*, 1989b). It is highly nontoxic and is an excellent compatible osmolyte (Dickson and Kirst, 1987). It may also serve for transmethylation reactions (Ishida and Kadota, 1968) or act as a cryoprotectant (Karsten *et al.*, 1996). The enzyme DMSP lyase (DL) has been identified in several algae and appears to be constitutive, but activity is highly variable within algal classes or even between species or strains (Steinke *et al.*, 1996, 1998). The basis for this variability and the functions of this reaction are not yet known. Many details on the chemistry and biology of DMSP, DMS, and related compounds can be found in several symposia proceedings (Saltzman and Cooper, 1989; Kiene *et al.*, 1996).

DMSP cleavage: strain specificity and behavior

The unicellular nanoplanktonic (2–20 μm) haptophyte alga *Emiliania huxleyi* provides a hint of the variability of the DMSP lyase enzyme within a species. Axenic strains were obtained from the Bigelow-Provasoli culture collection (CCMP, Boothbay Harbor, ME) and maintained in serial batch cultures. All strains contained near-equal concentrations of DMSP, but *in vitro* DMSP lyase activity of sonicated cells was high in strains 373 and 379 but low in 370 and 374 (Wolfe and Steinke, 1996; Steinke *et al.*, 1998); different pH and salt enzyme optima were also observed among the strains (Steinke *et al.*, 1998).

In all strains, although DMSP lyase is a constitutive enzyme, cleavage—deduced from DMS production—does not appear to occur in healthy growing cells (Wolfe and Steinke, 1996; Fig. 4a). Rather, stresses such as cell lysis caused immediate activation of the reaction, which was hypothesized to be a result of mixing compartmented substrate and enzyme (Wolfe and Steinke, 1996). Viral lysis of the DL-containing haptophyte *Phaeocystis pouchetii* also initiates DMS production (Malin *et al.*, 1998). However, complete lysis may not be necessary: merely sparging water containing *Phaeocystis* colonies activates DMS production (Wolfe *et al.*, 2000). It also appears that DMSP cleavage can be stimulated in other haptophytes and dinoflagellates by mechanical stress (bubbling or shaking) or by chemical triggers that activate exocytosis, such as polyamino compounds (Wolfe, unpubl. data). Therefore, algae with high *in vitro* DMSP lyase activity may only potentially cleave DMSP *in vivo;* I term this DMSP-cleavage potential, or DCP. When high-DCP prey are grazed, DMS is produced (Fig. 4b), apparently only during or following ingestion (Fig. 4c).

Selective ingestion of low-DCP prey

Although there is considerable variation in specificity of feeding responses by heterotrophic dinoflagellates and ciliates to different strains of *E. huxleyi,* there is a striking correlation of feeding inhibition with prey DCP. Some grazers (*Oxyrrhis marina*) show subtle feeding selectivity: rather than near-total inhibition of ingestion, this taxon ingests and grows successfully on high-DCP strains (Fig. 4b) but ingests them at lower rates (Wolfe *et al.*, 1997) or selects against them in prey mixtures (Fig. 4c, Wolfe *et al.*, 1997). Other grazers (the dinoflagellates *Amphidinium* and *Gymnodinium* spp. and a urotrichous ciliate) are much more sensitive: they readily ingest low-DCP *E. huxleyi* prey

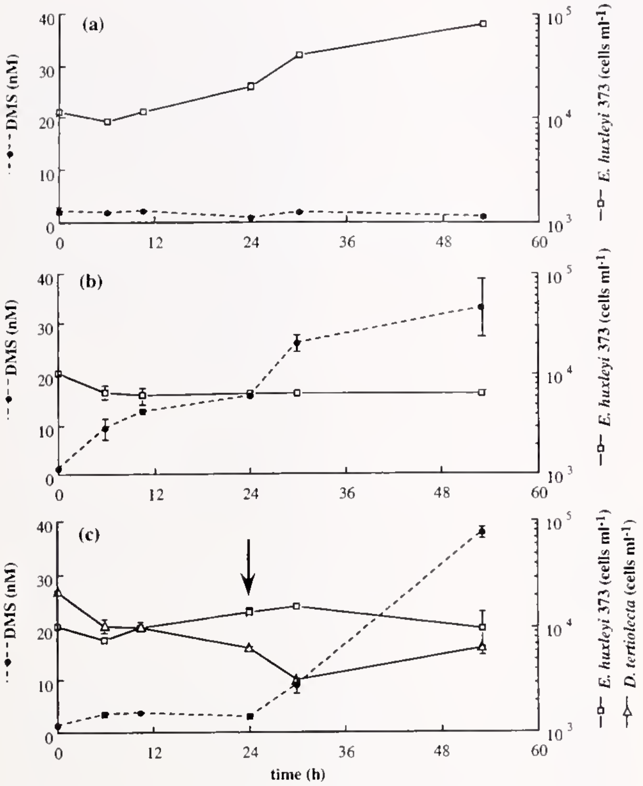

Figure 4. Example of dimethylsulfide (DMS) production during ingestion of *Emiliania huxleyi* with high potential for cleavage of β-dimethylsulfoniopropionate (DMSP) by the dinoflagellate *Oxyrrhis marina*, illustrating DMSP cleavage activated by ingestion of prey. DMS is shown as black circles and dashed lines, while prey cell numbers (on a log scale) are shown by white circles. (a) *E. huxleyi* alone grew exponentially and produced no DMS. (b) Addition of *Oxyrrhis* cropped growth and produced continuous DMS. (c) *Oxyrrhis* fed a food mixture containing the chlorophyte *Dunaliella tertiolecta* (white triangles) and *E. huxleyi*. 373 showed feeding selectivity, feeding on *Dunaliella* exclusively during the first 24 h. Despite the presence of physical and chemical grazing cues present during this period, DMS production did not begin until *Emiliania* cells were ingested (arrow). Data points are means of duplicates, with ranges as error bars.

(strains 370, 374), but ingestion of high DCP strains is low or zero (Fig. 5). These grazer taxa are more representative of surface waters and probably co-occur with *Emiliania*, although the identities of natural grazers are not yet known.

Prey strains are morphologically similar, and gross chemical composition (total C, N, protein, lipid, carbohydrate, mineral, dry weight [S. Strom and Wolfe, unpubl. data]) suggests only minor variations among strains. Although lipid profiles and specific metabolite pools are not known and may vary among strains, prey DMSP and pigment profiles also show little variation, as do cell-surface carbohydrates (Wolfe, unpubl. data). Therefore, although there are likely to be other factors that contribute to feeding selectivity, DCP is the only clear polymorphism that covaries with feeding selectivity and probably plays a role in deterring various protozoan grazers.

Possible deterrence mechanisms

The mechanism for feeding deterrence by DMSP cleavage is still poorly understood. The DMSP cleavage reaction was hypothesized to be compartmented (Wolfe *et al.*, 1997). DMSP and analogs have been found localized in the cytoplasm or vacuoles of other microorganisms (Schlenk *et al.*, 1970) and vascular plants (Hall *et al.*, 1978; Leigh *et al.*, 1981; Matoh *et al.*, 1987), and algal DLs are membrane-bound enzymes (de Souza *et al.*, 1996). However, the locations of DMSP and DLs in algae are unknown.

Observations with *Oxyrrhis* suggested that the DMSP cleavage reaction occurs during or after ingestion, and the DMS produced during grazing can be a sensitive signal of ingestion (Wolfe and Steinke, 1996; Fig. 4b, c). This observation led to the hypothesis that, following their ingestion, prey cells containing compartmented DMSP and DL lyse, causes a mixing reaction. DMS would presumably diffuse rapidly from predators to be detected as the reaction

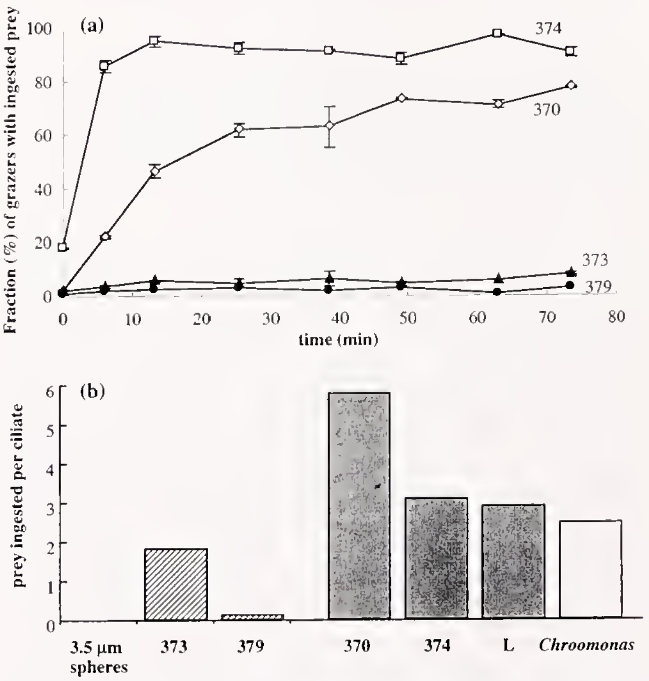

Figure 5. Example of selective ingestion of *Emiliania huxleyi* strains by (a) the dinoflagellate *Amphidinium.*, showing rapid ingestion of low-DCP *Emiliania* strains 370 and 374 but little or no ingestion of equal titers of high-DCP strains 373 and 379. Data points are means of duplicates, with ranges as error bars. (b) Similar behavior by a urotrichous ciliate. High-DCP strains (cross-hatching) were ingested at low rates, similar to plastic spheres, while low-DCP strains (grey) were ingested at high rates, similar to preferred *Chroomonas* prey. Selective ingestion in both examples resulted on grazer growth or survival on low-DCP prey strains, but no growth on high-DCP strains.

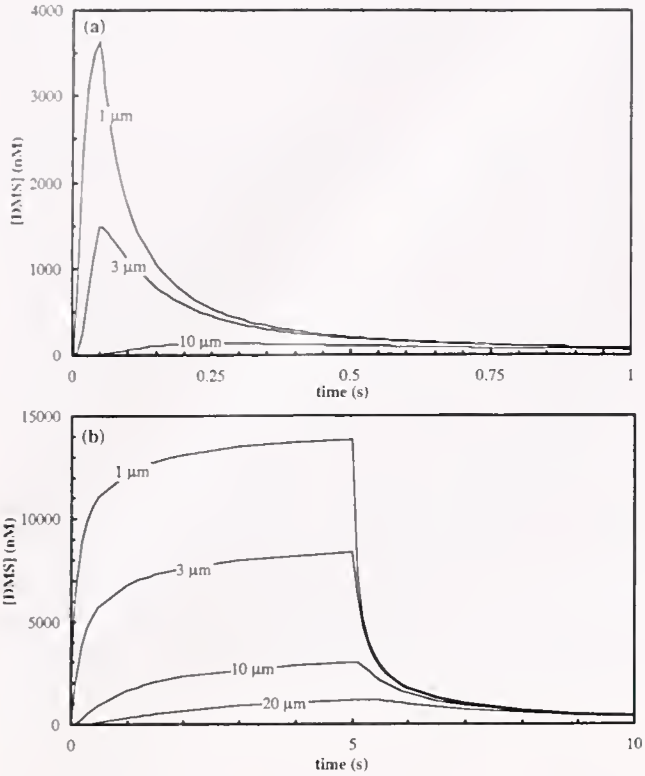

Figure 6. Model of brief β-dimethylsulfoniopropionate (DMSP) cleavage, showing a diffusive pulse of dimethylsulfide (DMS) proceeding outward from a spherical prey cell. (a) DMS concentration in the field near a 5-µm prey cell following short (50-ms) cleavage reaction. Curves are denoted by distance (µm) from the prey cell surface. (b) DMS concentration following a longer (5-s) cleavage reaction.

signal, but acrylic acid would be ionized above pH 4.4 and remain internal. In support of this hypothesis, most *E. huxleyi* DLs have a mildly acidic pH optimum (Steinke *et al.*, 1998) and retain significant activity even at pH 4–6, the probable range during formation of food vacuoles. DCP rates in high-activity strains could cleave 100% of prey DMSP in a few minutes following ingestion, times typical for food vacuole formation, and thus produce concentrated acrylate inside protist food vacuoles at levels (*ca.* 70 m*M*) that have been shown to be toxic or have antimicrobial activity (Sieburth, 1960, 1961; Thijsse, 1964; Bringmann and Kühn, 1980).

Thus, the original DMSP cleavage hypothesis was an activated form of a "suicide" reaction (Fig. 3c, iv), although this mechanism now appears unlikely. Even protozoa that ingest high-DCP prey and promote the reaction show no overt toxicity. Moreover, most grazers simply do not ingest high-DCP strains of prey (Fig. 5), and bulk DMS production is not measured. Clearly, for these grazers, the deterrent signal must occur before ingestion. If the DMSP cleavage reaction were activated by an excreted or contact-mediated grazer cue, could it produce a signal that might be detected by a grazer without producing measurable bulk DMS or acrylate?

Consider a 5-µm diameter *E. huxleyi* cell containing 6.5 fmol of DMSP. This cell has a volume of 65 µm^3. If DMSP is distributed evenly throughout the cell, its concentration is 100 m*M*; any subcellular localization will increase this concentration even higher. High-DCP strains have *in vitro* DL activity approaching 10 fmol DMSP cleavage min^{-1} cell^{-1} (Wolfe and Steinke, 1996; Steinke *et al.*, 1998). For this calculation I assume for simplicity a conservative *in vivo* activity of 4 fmol min^{-1}, or 0.067 fmol s^{-1}; the cell can thus cleave DMSP at a rate of about 1% s^{-1}.

Suppose that a physical or chemical disturbance near the cell—possibly following contact by a predator, or in response to near-field hydrodynamic disturbance—activates the reaction briefly. The DMS generated would rapidly permeate the cell membrane; acrylic acid permeability is highly pH-dependent; ionized acrylate would remain inside, while protonated acrylic acid would permeate the cell membrane and become ionized outside the cell.

The resulting "pulse" of DMS can be calculated by simple diffusion, approximated as a spherically symmetric point source at $r = 0$. I consider two cases for pulses of different lengths. For an instantaneous pulse of duration t_o, the concentration pulse diffusing from the cell is given by $C(r,t) = i\,t_o\,(4\pi Dt)^{-3/2} \exp(-r^2/4Dt)$ (Berg, 1983), where $i = 0.067$ fmol s^{-1} and $D \sim 10^{-6}$ cm^2 s^{-1} (100 µm^2 s^{-1}). The pulse moves outward as a wavefront whose radial velocity diminishes as $6Dr^{-1}$. The peak concentration diminishes as r^{-3}, and the concentration gradient scales as r^{-5} due to rapid dissipation. An example in which $t_o = 50$ ms is shown in Figure 6a. In this time, 0.003 fmol of algal DMSP, or 0.05%, is cleaved. The pulse moves rapidly outward near the cell, reaching 1 µm from the surface in 20 ms, 5 µm in 94 ms, and 10 µm in 260 ms, but taking 4.6 s to reach 50 µm. The peak concentration at 1 µm is 5.7 µ*M*, which decays rapidly to only 0.13 µ*M* at 10 µm.

For longer pulses, $C(r,t) = i\,(4\pi Dt)^{-1} \operatorname{erfc}(r\,[4Dt]^{-1/2})$ (Berg, 1983). Figure 6b shows the concentration field produced by a production pulse 5 s long. In this time, 0.33 fmol of algal DMSP, or 5%, is cleaved. Over the 5 s of steady production, the pulse peak builds up, but although the amount of signal released is 100-fold larger than the prior example, the peak concentration is less than 3-fold greater, reaching 15 µ*M* at 1 µm from the cell surface. However, the integrated pulse is much longer, and the concentration decay is less, so the signal strength at longer distances is much greater: at 10 µm from the cell about 5 s later the peak concentration is nearly 20-fold higher than for the short pulse. When production stops, the concentrations rapidly decay.

These examples, though hypothetical, reveal some interesting strategies for near-field pulsed signals. Since grazer receptor sensitivity is likely to be in the nanomolar range,

Table 2

Phytoplankton that have negative chemical effects on zooplankton predators

Class	Prey genera	Predators	Effects*	References
Cyanophyceae	*Trichodesmium*	Copepods	AT	Hawser *et al.*, 1992
	Cyanobacteria spp.	Copepods, daphnids, cladocerans, rotifers	AV, AT, FI, GR	DeMott and Moxter, 1991; DeMott *et al.*, 1991; Kirk and Gilbert, 1992; Haney *et al.*, 1995
Bacillariophyceae	*Phaeodactylum, Thalassiosira*	Copepods	FI	Shaw *et al.*, 1995
Prymnesiophyceae	*Emiliania*	Dinoflagellates, ciliates	AV	Wolfe and Steinke, 1996; Wolfe *et al.*, 1997; Strom and Wolfe, unpublished data
	Phaeocystis	Ciliates, copepods	AV	Admiraal *et al.*, 1986; Estep *et al.*, 1990; Hansen *et al.*, 1990
	Chrysochromulina	Ciliates, copepods	AT, GR	Carlsson *et al.*, 1990; Nielsen *et al.*, 1990; Turiff *et al.*, 1995
Dinophyceae	*Alexandrium*	Ciliates, copepods	AT, GR, AV	Hansen, 1989; Bagøien *et al.*, 1996; Teegarden and Cembella, 1996
	Gymnodinium	Copepods	AT, GR, AV	Fiedler, 1982; Bagøien *et al.*, 1996
	Dinophysis	Copepods	AV	Carlsson *et al.*, 1995
Chrysophyceae	*Olisthodiscus*	Tintinnids, rotifers	AT, FI, GR	Verity and Stoecker, 1982; Egloff, 1986

* AT = Acute Toxicity, FI = Feeding Inhibition, AV = Avoidance, GR = Growth Reduction.

peaks at micromolar concentrations should be easily detectable. If peak concentration is key and grazers are at contact or near-contact, it makes little sense energetically to emit a pulse of 5 s relative to 0.05 s; only roughly 3% of the additional potential concentration maximum is achieved. But if perception of signals requires longer integration times, or if the grazers to be signaled are at a distance of several prey body lengths, longer pulses may be useful. Such short events are difficult to measure because they have little effect on bulk DMS concentrations. Assuming 10^4 prey cells ml^{-1}, prey DMSP titers would be equivalent to 65 n*M* bulk DMSP. Even if every prey cell were activated and converted 5% of its DMSP, the bulk DMS produced would be only 3.5 n*M*, barely above typical background levels of 1–3 n*M*.

The behavioral responses of dinoflagellate and ciliate grazers to gradients of DMS, DMSP, and acrylate are currently being investigated. Predator swimming behavior in response to gradients of dissolved cues and specific prey strains was filmed and analyzed by computer-aided motion analysis (Sjoblad and Mitchell, 1979; Zimmer-Faust *et al.*, 1996), and preliminary observations suggest that *Amphidinium*'s motions are greatly inhibited by acrylate (R. Zimmer, pers. comm.). However, additions of nanomolar concentrations of DMSP, rather than acrylate or DMS, inhibit feeding (S. Strom, unpubl. data). The signal potential of these compounds is clear, but their sense is not.

Ecological Implications of Plankton Defenses in Food Webs

How might planktonic predator-prey interactions, such as chemical defense effects on feeding selectivity, affect microbial food webs, trophic ecology, and biogeochemical impacts? I briefly examine several aspects.

Selective feeding and trophic structure

Many algae are toxic to, or avoided by, metazoan or protozoan grazers (Table 2). Although early studies focused on prey containing highly potent toxicants, it is likely that other strategies that affect predator feeding selectivity may be more important and widespread. Many marine protozoan grazers are known to selectively ingest or reject particular prey [Table 3, (Stoecker *et al.*, 1986; Taniguchi and Takeda, 1988; Verity, 1991; Stoecker *et al.*, 1995; Strom and Loukos, 1998)], and prey preferences differ among predators (Rapport *et al.*, 1972; Hansen *et al.*, 1996; Buskey, 1997; Strom and Loukos, 1998). Different grazer taxa and functional groups may have different selection capabilities. For example, filter feeders may select prey according to size and hydrodynamic characteristics, whereas raptorial feeders may use chemodetection to avoid contacting and capturing noxious prey. Although the feeding mechanisms of suspension (filter) feeders strongly determine the size spectrum of particles that they can capture, many also appear to discriminate between similarly sized particles with different chemical characteristics (Stoecker, 1988; Verity, 1991).

Different selective feeding mechanisms can have very different consequences for the long-term persistence of prey populations. For example, a grazer that consistently prefers a given prey type can, in the absence of a physical or behavioral refuge, ultimately eliminate that prey type from the environment. On the other hand, selection behavior that varies as prey abundance or community composition changes can stabilize predator-prey dynamics and create a

Table 3

Examples of selective ingestion by planktonic protozoa

Grazer	Ingestion preference*	References
Ciliates		
Eutintinnus pectinis	Prefers *Isochrysis* to *Dunaliello*	Heinbokel, 1978
Favella taraikaensis	Rejects captured *Heterosigma, Rhodomonas*	Taniguchi and Takeda, 1988
Favella sp.	Prefers dinoflagellates to other algae	Stoecker *et al.*, 1981
	Prefers live *vs.* dead cells	Stoecker, 1988
	Prefers inert microspheres to dead cells	
Balanion sp.	Prefers dinoflagellates to other algae	Stoecker *et al.*, 1986
	Prefers dinoflagellates to latex microspheres	
Strombilidium spiralis	Prefers *Isochrysis* to *Cafeteria*	Verity, 1991
Tintinnopsis	Prefers *Paraphysomonas* to *Dunaliella*	Verity, 1991
Flagellates		
Gymnodinium fungiforme	Prefers specific strains of *Dunaliella*	Spero and Morée, 1981
Oxyrrhis marina	Prefers *Dunaliella* to beads	Tarran, 1991
	Avoids high-DCP *E. huxleyi* strains (in mixtures)	Wolfe *et al.*, 1997
Amphidinium sp.	Avoids high-DCP *E. huxleyi* strains	Strom and Wolfe, unpublished data
Protoperidinium sp.	Prefers diatoms	Jacobsen and Anderson, 1986

* DCP = DMSP Cleavage Potential.

refuge for prey populations (Strom and Loukos, 1998). The degree of feeding specialization or generality is poorly known for planktonic protists, as are even the natural co-distributions of predator and prey taxa. Recent evidence on bacterivore grazers suggests that predation can cause major shifts in food abundance and taxa (Hahn and Höfle, 1998; Jürgens *et al.*, 1999). Such "top-down" control probably extends to other members of the microbial food web, but the degree to which chemical cues play a role in such selection is not yet known.

Competition: algal blooms

Bloom-forming algal taxa increasingly are being studied because of their potential to disrupt marine food-chains and cause toxicity to humans (harmful algal blooms, HABs [Hallegraeff, 1995]). Evidence suggests that HABs are increasing in coastal environments as a result of nutrification. Most blooms are seasonal, but in the past decade there have been novel reports of essentially indefinite blooms. Coastal Texas has experienced a "brown tide" of the chrysophyte *Aureococcus* for over five years, while an *E. huxleyi* bloom in the Bering Sea has persisted for two years (Vance *et al.*, 1998); both blooms have had dramatic impacts on regional food webs.

The role of antipredator defenses or toxins in establishing and maintaining such blooms is poorly understood (Turner and Tester, 1997; Turner *et al.*, 1998) but probably contributes to their success (Buskey and Hyatt, 1995; Buskey *et al.*, 1997). A decade ago, Keller *et al.*, (1989a) observed that many bloom-forming algal taxa form considerable DMSP and suggested the likelihood that blooms contribute to global DMS emissions. Many taxa from the Haptophyceae and Dinophyceae, two dominant bloom-forming groups, not only produce concentrated DMSP but seem to have high DL activity (Table 4); several appear to operate as activated systems. *Phaeocystis pouchetii,* a bloom-forming haptophyte closely related to *Emiliania,* has a colonial life stage that forms large (1-mm) colonies concentrated in spherical shells of polysaccharide mucus (van Rijssel *et al.*, 1997) that are critical to its widespread ecological success (Lancelot and Rosseau, 1994). *P. pouchetii* appears to have a

Table 4

β-dimethylsulfoniopropionate (DMSP) and DMSP lyase (DL) activity in bloom-forming marine phytoplankton (blank = not determined)

Class/taxa	Strain	m*M* DMSP	DL[1]	Mode[2]
Prymnesiophyceae				
Chrysochromulina polylepis	ED1/ED2	192–395		
Prymnesium parvum	CCMP 708	179–223	<0.02	LA?
Phaeocystis pouchetii	677-3	260	3.1	EX
Phaeocystis sp.	Labrador sea			LA?
Emiliania huxleyi	Various	75–110	0.01–12.6	LA
Dinophyceae				
Alexandrium tamarense	CCMP 115	282–292	17.0–23.2	LA
A. tamarense	CCMP 118	460	36.5	LA
A. fundyense	CCMP 1719	640	30.5	LA
Amphidinium carterae	AMPHI	2202		
Gonyaulax spinifera	GP60e	145		
Gymnodinium breve	CCMP 718	109	<0.01	

[1] *In vitro* activity: fmol DMS cell^{-1} min^{-1} @ 10–20 m*M* DMSP, 30°C, pH 6.0.

[2] DMSP lyase mode of action: LA = lysis-activated, EX = extracellular.

cell-surface DL (Stefels and van Boekel, 1993) and may pump DMSP across the cell membrane and cleave it externally, where the acrylate produced becomes highly concentrated at the colony surface (Noordkamp *et al.*, 1998). This may help deter mesozooplankton grazers, although grazing on this taxon is highly variable (Weisse *et al.*, 1994). Measurements of *in situ* DL activity and of grazing rates on algal populations (Stefels *et al.*, 1995) will be necessary to assess the deterrent role of this reaction in bloom formation and maintenance.

Populations and evolution

Andrews (1991), in a pioneering attempt to forge unifying themes, has compiled an excellent comparison of ecological concepts between micro- and macroorganisms. However, little has been done to apply models of organismal behavior and ecology from the macroscopic world to understanding interactions among microbes, through concepts such as coevolution of predator and prey (Bernays, 1998; Lima, 1998), functional defense groups or defense guilds (Atsatt and O'Dowd, 1976), and complex multitrophic interactions (De Moraes *et al.*, 1998). And yet, just as multicellular organisms and their sensory systems derived ultimately from microbial ancestors, the organismal interactions of the macroscopic world also probably reflect earlier models developed in microbial populations, modified by changes in physical scaling and developmental complexity.

Just as microbial sensory systems most likely evolved into those of multicellular organisms (Carlile, 1975; Anderson, 1989; Carr, 1989), conserved microbial behaviors and organismal interactions may be the basis of those we know so well from "higher" animals and plants. However, applying macroscopic world ecological concepts to microbes requires caution. Many standard concepts in macroscale ecology simply break down in the microbial realm, and one reason the protists are so poorly studied is that they do not fall neatly into standard biological divisions. For example, metabolic and nutritional modes are astonishingly diverse and fluid; it is estimated that a large fraction of photoautotrophic plankton can simultaneously use heterotrophic nutrition (mixotrophy), either by uptake of dissolved organic solutes or by ingestion of organic particles (Boraas *et al.*, 1988; Stoecker, 1992). This capability blurs delineation of primary and secondary producers, or herbivores and carnivores. Trophic interrelations and levels are fluid and difficult to distinguish (Pomeroy, 1992), and terms like "grazer" and "predator" are used interchangeably. Community-level patterns such as succession, niche occupation, and coevolution are only crudely known, and even the species concept is poorly defined for microbes that divide both sexually and asexually (Manhart and McCourt, 1992; Wood and Leatham, 1992; Colwell *et al.*, 1995) and where horizontal gene transfer appears rapid and rampant (Dahlberg *et al.*, 1998). Even where the concepts have meaning, they are poorly constrained by current data on natural populations. For example, genetic variation is just beginning to be known within phytoplankton classes or species (Costas *et al.*, 1995; Medlin *et al.*, 1996; Larsen and Medlin, 1997; Scholin, 1998), much less within natural populations (Brand, 1989) or blooms (Gallagher, 1998)—and even less is known of marine protozoa (Lim *et al.*, 1996).

Microbial signals as kairomones

Signals emitted to the environment are likely to be intercepted and used by receivers other than those intended; such cues benefit the receiver and are termed kairomones. Well known from plant-insect studies, byproducts of microbial deterrence are just beginning to be discovered. A beautiful example is the peptide "A-factor" excreted by *Amoeba proteus*, which inhibits phagocytosis and is used for self recognition to avoid cannibalism (Kusch, 1999). Exposure to this peptide induces the potential prey ciliate *Euplotes* to produce armored "wings" or "helmets" that make it too large to be ingested by *Amoeba* (Wicklow, 1997). It is likely that a complex of multitrophic chemical interactions, similar to that emerging from better-known terrestrial systems, also occurs in marine plankton.

The DMSP-DMS-acrylate system and close chemical analogs show widespread chemical signal activity and have the potential to act as kairomones at many spatial scales. DMSP is a sensitive chemoattractant for the heterotrophic dinoflagellate *Crypthecodinium cohnii* (Hauser *et al.*, 1975b), which feeds on the surfaces of decaying macroalgae. DMSP is also a close chemical analog of quaternary or tertiary amines known to act as alarm cues in metazoans, including anthopleurine (Howe and Sheikh, 1975) and homarine (McClintock *et al.*, 1994). Such compounds may stimulate cholinergic receptors (Mackie and Grant, 1974), possibly giving them broad activity to vertebrates and invertebrates. Trimethylamine, a volatile nitrogen analog of DMS produced microbially as a decay byproduct, appears to initiate vertical migration in freshwater daphnids (Boriss *et al.*, 1999) as a defense against predatory fish (Nesbitt *et al.*, 1996). Micromolar levels of DMS and acrylate may act as attractants for marine bacteria (Sjoblad and Mitchell, 1979; Zimmer-Faust *et al.*, 1996). Many volatile fatty acids also probably function as signals; they have the useful properties of being soluble in both water and lipid, volatile, and rapidly degraded. Formic acid, a close analog of acrylic acid, is a well-known alarm and defense signal in the formacine ants from which it was first isolated (Löfqvist, 1976). Finally, DMS produced from DMSP sequestered at higher trophic levels may act as a chemoattractant for vertebrates such as procellariiform seabirds (Nevitt *et al.*, 1995; Nevitt, 1998, 2000), helping them to locate food patches.

Conclusions and Research Challenges

I have tried to synthesize information about the physical constraints and physiological adaptations to chemical signaling between microbes in environments characterized by low Reynolds numbers. Several general themes emerge to suggest the importance of short-range or contact mechanisms acting over very short time scales; activated reactions; multifunctional defense systems or components; and the multiple interpretations of chemical signals by many different receivers.

The behavioral, temporal, and spatial scales of unicellular microbes are small, difficult to determine experimentally, and unfamiliar to human experience. Clearly, the technical challenges of measuring "what the cell sees" are vast. We have just begun to measure the microscale structure and perception of fluid flow around millimeter-sized grazers (Moore *et al.*, 1999, and other papers in this volume), much less around protozoans 50- to 100-fold smaller. Even the static microscale distributions of microbial populations are only beginning to be visualized (Müller-Niklas *et al.*, 1996; Krembs *et al.*, 1998); their chemical interactions are a still greater challenge. From a chemical perspective, ecologists need to consider not only the constituents of microbes that may act as deterrents or signals, but also reactions that are activated in response to subtle cues and do not occur in ungrazed prey.

Chemical ecology in environmentally important planktonic microbial populations is in its infancy. This state is not surprising given the recency of information on the basic diversity, structure, and stability of marine microbial populations (Allsopp *et al.*, 1995); moreover, the application of macroecological concepts to microbial ecology has barely begun (Andrews, 1991). Nonetheless, chemically mediated, behavioral microbial interactions are probably important and may result in large-scale changes in trophic structure and function. Synthesis of work at the chemical, genetic, physiological, behavioral, and population levels will also be necessary to understand microbial chemical communication and its impact in the environment, but it is easy to predict that a rich world of microbial chemical communication, both adversarial and mutualistic, awaits researchers who venture into this difficult realm.

Acknowledgments

I thank Dick Zimmer for inviting me to participate in this symposium and for stimulating interdisciplinary discussion of chemical ecology. Michael Steinke and Suzanne Strom conducted many of the DMSP-cleavage and grazing experiments, shared unpublished data, and were key contributors to the ideas presented. Peter Jumars, Dick Zimmer, and an anonymous reviewer provided critical comments and suggested many improvements. This work was supported by grants from NASA (NAGW-3737) and NSF (OCE-97-5051).

Literature Cited

Aaronson, S. 1981. *Chemical Communication at the Microbial Level.* CRC Press, Boca Raton, FL.

Abrahams, M. V., and L. D. Townsend. 1993. Bioluminescence in dinoflagellates: a test of the burglar alarm hypothesis. *Ecology* **74:** 258–260.

Admiraal, W., and L. A. H. Venekamp. 1986. Significance of tintinnid grazing during blooms of *Phaeocystis pouchetii* (Haptophyceae) in Dutch coastal waters. *Neth. J. Sea. Res.* **20:** 61–66.

Alldredge, A., and Y. Cohen. 1987. Can microscale chemical patches persist in the sea? Microelectrode study of marine snow, fecal pellets. *Science* **235:** 689–671.

Allsopp, D., R. R. Colwell, and D. L. Hawksworth, eds. 1995. *Microbial Diversity and Ecosystem Function.* CAB International, Wallingford, UK.

Almers, W. 1990. Exocytosis. *Annu. Rev. Physiol.* **52:** 607–624.

Anderson, D. M., and T. P.-O. Cheng. 1988. Intercellular localization of saxitoxins in the dinoflagellate *Gonyaulax tamarensis. J. Phycol.* **24:** 17–22.

Anderson, D. M., D. M. Nosenchuck, G. T. Reynolds, and A. J. Walton. 1988. Mechanical stimulation of bioluminescence in the dinoflagellate *Gonyaulax polyedra* Stein. *J. Exp. Mar. Biol. Ecol.* **122:** 277–288.

Anderson, P. A. V., ed. 1989. *Evolution of the First Nervous Systems.* Plenum Press, New York.

Andrews, J. H. 1991. *Comparative Ecology of Microorganisms and Macroorganisms.* Springer-Verlag, New York.

Atsatt, P. R., and D. J. O'Dowd. 1976. Plant defense guilds. *Science* **193:** 24–29.

Bagøien, E., A. Miranda, B. Reguera, and J. M. Franco. 1996. Effects of two paralytic shellfish toxin producing dinoflagellates on the pelagic harpacticoid copepod *Euterpina acutifrons. Mar. Biol.* **126:** 361–369.

Barns, S. M., and S. Nierzwicki-Bauer. 1997. Microbial diversity in modern subsurface, ocean, and surface environments. Pp. 35–80 in *Geomicrobiology: Interactions Between Microbes and Minerals,* J. F. Banfield and K. H. Nealson, eds. Mineralogical Society of America, Washington, DC.

Beale, G. 1990. Self and nonself recognition in the ciliate protozoan *Euplotes. Trends Genet.* **6:** 137–139.

Bell, W., and R. Mitchell. 1972. Chemotactic and growth responses of marine bacteria to algal extracellular products. *Biol. Bull.* **143:** 265–277.

Bennett, S. J., R. W. Sanders, and K. G. Porter. 1988. Chemosensory responses of heterotrophic and mixotrophic flagellates to potential food sources. *Bull. Mar. Sci.* **43:** 764–771.

Berg, H. C. 1983. *Random Walks in Biology.* Princeton University Press, Princeton.

Berg, H. C., and E. M. Purcell. 1977. Physics of chemoreception. *Biophys. J.* **20:** 193–219.

Bernays, E. A. 1998. Evolution of feeding behavior in insect herbivores. *Bioscience* **48:** 35–44.

Bjornson, P. K. 1988. Phytoplankton exudation of organic matter: why do healthy cells do it? *Limnol. Oceanogr.* **33:** 151–154

Blackburn, N., T. Fenchel, and J. Mitchell. 1998. Microscale nutrient patches in planktonic habitats shown by chemotactic bacteria. *Science* **282:** 2254–2256.

Boraas, M. E., K. W. Estep, P. W. Johnson, and J. M. Sieburth. 1988. Phagotrophic phototrophs: the ecological significance of mixotrophy. *J Protozool.* **35:** 249–252.

Boriss, H., M. Boersma, and K. H. Wiltshire. 1999. Trimethylamine induces migration of waterfleas. *Nature* **398:** 382.

Bouck, G. B., and B. M. Sweeney. 1966. The fine structure and ontogeny of trichocysts in marine dinoflagellates. *Protoplasma* **61:** 205–223.

Bowen, J. D., K. D. Stolzenbach, and S. W. Chisholm. 1993. Simulating bacterial clustering around phytoplankton cells in a turbulent ocean. *Limnol. Oceanogr.* **38:** 36–52.

Brand, L. E. 1989. Review of genetic variation in marine phytoplankton species and the ecological implications. *Biol. Oceanogr.* **6:** 397–409.

Bringmann, G., and R. Kühn. 1980. Comparision of the toxicity thresholds of water pollutants to bacteria, algae, and protozoa in the cell multiplication inhibition test. *Water Res.* **14:** 231–241.

Brown, R. C., H. Bass, and J. P. Coombs. 1975. Carbohydrate binding proteins involved in phagocytosis by *Acanthamoeba. Nature* **254:** 434–435.

Burgoyne, R. D., and A. Morgan. 1993. Regulated exocytosis. *Biochem. J.* **293:** 305–316.

Burnet, F. M. 1971. "Self-recognition" in colonial marine forms and flowering plants in relation to the evolution of immunity. *Nature* **232:** 230–235.

Buskey, E. J. 1997. Behavioral components of feeding selectivity of the heterotrophic dinoflagellate *Protoperidinium pellucidum. Mar. Ecol. Prog. Ser.* **153:** 77–89.

Buskey, E. J., and C. J. Hyatt. 1995. Effects of the Texas (USA) 'brown tide' alga on planktonic grazers. *Mar. Ecol. Prog. Ser.* **126:** 285–292.

Buskey, E. J., and D. K. Stoecker. 1988. Locomotory patterns of the planktonic ciliate *Favella* sp.: adaptations for remaining within food patches. *Bull. Mar. Sci.* **43:** 783–796.

Buskey, E. J., and E. Swift. 1985. Behavioral responses to oceanic zooplankton to simulated bioluminescence. *Biol. Bull.* **168:** 263–275.

Buskey, E. J., P. A. Montagna, A. F. Amos, and T. E. Whitledge. 1997. Disruption of grazer populations as a contributing factor to the initiation of the Texas brown tide algal bloom. *Limnol. Oceanogr.* **42:** 1215–1222.

Calleja, G. B. 1984. *Microbial Aggregation.* CRC Press, Boca Raton, FL.

Carlile, M. J., ed. 1975. *Primitive Sensory and Communication Systems.* Academic Press, London.

Carlsson, P., E. Granéli, and P. Olsson. 1990. Grazer elimination through poisoning: one of the mechanisms behind *Chrysochromulina polyepis* blooms? Pp. 116–122 in *Toxic Marine Phytoplankton,* E. Granéli, B. Sundström, L. Edler, and D. M. Anderson, eds. Elsevier, New York.

Carlsson, P., E. Granéli, G. Finenko, and S. Y. Maestrini. 1995. Copepod grazing on a phytoplankton community containing the toxic dinoflagellate *Dinophysis acuminata. J. Plankton Res.* **17:** 1925–1938.

Carr, W. E. S. 1988. The molecular nature of chemical stimuli in the aquatic environment. Pp. 3–28 in *Sensary Biology of Aquatic Animals,* J. Atema and R. R. Fay, eds. Springer-Verlag, New York.

Carr, W. E. S. 1989. Chemical signaling systems in lower organisms: a prelude to the evolution of chemical communication in the nervous system. Pp. 81–94 in *Evolution of the First Nervous Systems,* P. A. V. Anderson, ed. Plenum Press, New York.

Cembella, A. D. 1998. Ecophysiology and metabolism of paralytic shellfish toxins in marine microalgae. Pp. 383–403 in *NATO Advanced Workshop on the Physiological Ecology of Harmful Algal Blooms,* D. M. Anderson, A. M. Cembella, and G. Hallegraef, eds. Springer, Berlin.

Chiu, D. T., C. F. Wilson, F. Ryttsen, A. Stromberg, C. Farre, *et al.* 1999. Chemical transformations in individual ultrasmall biomimetic containers. *Science* **283:** 1892–1895.

Clark, K. D., T. M. Hennessey, and D. L. Nelson. 1993. External GTP alters the motility and elicits an oscillating membrane depolarization in *Paramecium tetraurelia. Proc. Natl. Acad. Sci. USA* **90:** 3782–3786.

Colwell, R. R., R. A. Clayton, B. A. Ortiz-Conde, D. Jacobs, and E. Russek-Cohen. 1995. The microbial species concept and biodiversity. Pp. 3–15 in *Microbial Diversity and Ecosystem Function,* D. Allsopp, R. R. Colwell, and D. L. Hawksworth, eds. CAB International, Wallingford, UK.

Costas, E., R. Zardoya, J. Bautista, A. Garrido, C. Rojo, and V. López-Rodas. 1995. Morphospecies *vs.* genospecies in toxic marine dinoflagellates: an analysis of *Gymnodinium catenatum/Gyrodinium impudicum* and *Alexandrium minutum/A. lusitanicum* using antibodies, lectins, and gene sequences. *J. Phycol.* **31:** 801–807.

Cowles, T. J., R. J. Olson, and S. W. Chisholm. 1988. Food selection by copepods: discrimination on the basis of food quality. *Mar. Biol.* **100:** 41–49.

Crenshaw, H. C. 1992. Orientation by helical motion. III. Microorganisms can orient to stimuli by changing the direction of their rotational motion. *Bull. Math. Biol.* **55:** 231–255.

Csaba, G. 1996. Evolutionary significance of the hormone recognition capacity in unicellular organisms. Development of hormone receptors. Pp. 1–28 in *Signaling Mechanisms in Protozoa and Invertebrates,* G. Csaba and W. E. G. Müller, eds. Springer, Berlin.

Csaba, G., and W. E. G. Müller, eds. 1996. *Signaling Mechanisms in Protozoa and Invertebrates.* Springer, Berlin.

Dahlberg, C., M. Bergström and M. Hermansson. 1998. *In situ* detection of high levels of horizontal plasmid transfer in marine bacterial communities. *Appl. Environ. Microbiol.* **64:** 2670–2675.

Dakshini, I., and K. M. M. Dakshini. 1994. Algal allelopathy. *Bot. Rev.* **60:** 182–197.

De Moraes, C. M., W. J. Lewis, P. W. Paré, H. T. Alborn, and J. H. Tumlinson. 1998. Herbivore-infested plants selectively attract parasitoids. *Nature* **393:** 570–573.

de Souza, M. P., Y. P. Chen, and D. C. Yoch. 1996. Dimethylsulfoniopropionate lyase from the macroalga *Ulva curvata:* purification and characterization of the enzyme. *Planta* **199:** 433–438.

Dechn, A. W., K. A. Browne, and R. K. Zimmer-Faust. 1998. Chemical cues: why basic peptides are signal molecules in marine environments. *Limnol. Oceanogr.* **43:** 1410–1417.

Delmonte Corrado, M. U., D. Locatelli, L. Paleari, and G. Bottiroli. 1997. Lectin-binding sites involved in *Paramecium primaurelia* mating pair formation. *J. Eukaryot. Microbiol.* **44:** 603–608.

DeMott, W. R. 1986. The role of taste in food selection by freshwater zooplankton. *Oecologia* **69:** 334–340.

DeMott, W. R., and F. Moxter. 1991. Foraging on cyanobacteria by copepods: responses to chemical defenses and resource abundance. *Ecology* **72:** 1820–1834.

DeMott, W. R., Q.-X. Zhang, and W. W. Carmichael. 1991. Effects of toxic cyanobacteria and purified toxins on the survival and feeding of a copepod and three species of *Daphnia. Limnol. Oceanogr.* **36:** 1346–1357.

Devreotes, P. 1989. *Dictyostelium discoideum:* a model system for cell-cell interactions in development. *Science* **245:** 1054–1058.

Devreotes, P. N. 1982. Chemotaxis. Pp. 117–168 in *The Development of* Dictyostelium discoideum. Academic Press, New York.

Dickson, D. M. J., and G. O. Kirst. 1987. Osmotic adjustment in marine eukaryotic algae: the role of inorganic ions, quaternary ammonium, tertiary sulfonium and carbohydrate solutes. *New Phytol.* **106:** 645–655.

Dodge, J. D., and C. Greuet. 1987. Dinoflagellate ultrastructure and complex organelles. Pp. 92–142 in *The Biology of Dinoflagellates,* F. J. R. Taylor, ed. Blackwell Scientific, Oxford.

Doyle, R. J. 1994. Introduction to lectins and their interactions with microorganisms. Pp. 1–65 in *Lectin-Microorganism Interactions,* R. J. Doyle and M. Slifkin, eds. Marcel Dekker, New York.

Dusenbery, D. B. 1992. *Sensory Ecology.* W. H. Freeman, New York.

Dusenbery, D. B. 1998. Spatial sensing of stimulus gradients can be superior to temporal sensing for free-swimming bacteria. *Biophys. J.* **74:** 2272–2277.

Dusenbery, D. B., and T. W. Snell. 1995. A critical body size for use of pheromones in mate location. *J. Chem. Ecol.* **21:** 427–438.

Egloff, D. A. 1986. Effects of *Olisthodiscus luteus* on the feeding and reproduction of the marine rotifer *Synachaeta cecilia. J. Plankton Res.* **8:** 263–274.

Esaias, W. E., and H. C. Curl, Jr. 1972. Effect of dinoflagellate bioluminescence on copepod ingestion rates. *Limnol. Oceanogr.* **17:** 901–907.

Estep, K. W., J. C. Nejstgaard, H. R. Skjoldal, and F. Rey. 1990. Predation by copepods upon natural populations of *Phaeocystis pouchetii* as a function of the physiological state of the prey. *Mar. Ecol. Prog. Ser.* **67:** 235–249.

Falkowski, P. G., and J. A. Raven. 1997. *Aquatic Photosynthesis.* Blackwell Scientific, Malden, MA.

Febvre-Chavalier, C., A. Bilbaut, J. Febvre, and Q. Bone. 1989. Membrane excitability and motile responses to the protozoa, with particular attention to the heliozoan *Actinocoryne contractilis.* Pp. 237–253 in *Evolution of the First Nervous Systems,* P. A. V. Anderson, ed. Plenum Press, New York.

Fenchel, T. 1980. Relation between particle size selection and clearance in suspension-feeding ciliates. *Limnol. Oceanogr.* **25:** 733–738.

Fenchel, T. 1987. *Ecology of Protozoa: the Biology of Free-living Phagotrophic Protists.* Science Tech, Madison, WI.

Fenchel, T., G. M. King, and T. H. Blackburn. 1998. *Bacterial Biogeochemistry: the Ecophysiology of Mineral Cycling.* Academic Press, San Diego.

Fessenden, L., and T. J. Cowles. 1994. Copepod predation on phagotrophic ciliates in Oregon coastal waters. *Mar. Ecol. Prog. Ser.* **107:** 103–111.

Fiedler, P. C. 1982. Zooplankton avoidance and reduced grazing responses to *Gymnodinium splendens* (Dinophyceae). *Limnol. Oceanogr.* **27:** 961–965.

Field, C. B., M. J. Behrenfeld, J. T. Randerson, and P. Falkowski. 1998. Primary production of the biosphere: integrating terrestrial and oceanic components. *Science* **281:** 237–240.

Fowden, L., and P. J. Lea. 1979. Mechanism of plant avoidance of autotoxicity by secondary metabolites, especially by nonprotein amino acids. Pp. 135–160 in *Herbivores: Their Interaction with Secondary Plant Metabolites,* G. A. Rosenthal and D. H. Janzen, eds. Academic Press, New York.

Freiburg, M. 1993. Identification of cell surface polypeptides of the hypotrich *Euplotes octocarinatus. Archiv Protistenkunde* **143:** 311–318.

Gall, J. G., ed. 1986. *The Molecular Biology of Ciliated Protozoa.* Academic Press, Orlando, FL.

Gallagher, J. C. 1998. Genetic variation in harmful algal bloom species: an evolutionary ecology approach. Pp. 225–242 in *NATO Advanced Workshop on the Physiological Ecology of Harmful Algal Blooms,* D. M. Anderson, A. M. Cembella, and G. Hallegraef, eds. Springer, Berlin.

Gerritsen, J., and J. R. Strickler. 1977. Encounter probabilities and community structure in zooplankton: a mathematical model. *J. Fish. Res. Board Can.* **34:** 73–82.

Gomperts, B. D., I. Hide, J. P. Bennett, A. Pizzey, and P. E. R. Tatham. 1994. The exocytotic reaction of permeabilized mast cells. Pp. 217–231 in *Toxins and Exocytosis,* D. Suput and R. Zorec, eds. New York Academy of Sciences, New York.

Görtz, H.-D., ed. 1988. *Paramecium.* Springer-Verlag, Berlin.

Gross, M. 1998. *Life on the Edge.* Plenum Trade, New York.

Haacke-Bell, B., R. Hohenberger-Bregger, and H. Plattner. 1990. Trichocysts of *Paramecium*: secretory organelles in search of their function. *Eur. J. Protistol.* **25:** 289–305.

Hahn, M. W., and M. G. Höfle. 1998. Grazing pressure by a bacterivorous flagellate reverses the relative abundance of *Comamanas acidovorans* PX54 and *Vibrio* strain CB5 in chemostat cocultures. *Appl. Environ. Microbiol.* **64:** 1910–1918.

Hall, J. L., D. M. R. Harvey, and T. J. Flowers. 1978. Evidence for the cytoplasmic localization of betaine in leaf cells of *Suaeda maritima. Planta* **140:** 59–62.

Hall, S., and G. Strichartz, eds. 1990. *Marine Toxins: Origin, Structure, and Molecular Pharmacology.* American Chemical Society, Washington, DC.

Hall, S., G. Strichartz, E. Moczydlowski, A. Ravindran, and P. B. Reichardt. 1990. The saxitoxins: sources, chemistry, and pharmacology. Pp. 29–65 in *Marine Toxins: Origin, Structure, and Molecular Pharmacology,* S. Hall and G. Strichartz, eds. American Chemical Society, Washington, DC.

Hallegraeff, G. M. 1995. Harmful algal blooms: a global overview. Pp. 1–22 in *Manual on Harmful Marine Microalgae,* G. M. Hallegraeff, D. M. Anderson, A. D. Cembella, and H. O. Enevoldsen, eds. UNESCO, Paris.

Haney, J. F., J. J. Sasner, and M. Ikawa. 1995. Effects of products released by *Aphanizomenon flos-aquae* and purified saxitoxin on the movements of *Daphnia carinata* feeding appendages. *Limnol. Oceanogr.* **40:** 263–272.

Hansen, B., K. S. Tande, and U. C. Berggreen. 1990. On the trophic fate of *Phaeocystis pouchetii* (Hariot): III. Functional responses in grazing demonstrated on juvenile stages of *Calanus finmarchicus* (Copepoda) fed diatoms and *Phaeocystis. J. Plankton Res.* **12:** 1173–1187.

Hansen, F. C., H. J. White, and J. Passarge. 1996. Grazing in the heterotrophic dinoflagellate *Oxyrrhis marina*: size selectivity and preference for calcified *Emiliania huxleyi* cells. *Aquat. Microb. Ecol.* **10:** 307–313.

Hansen, P. J. 1989. The red tide dinoflagellate *Alexandrium tamarense*: effects on behaviour and growth of a tintinnid ciliate. *Mar. Ecol. Prog. Ser.* **53:** 105–116.

Hansen, P. J. 1995. Growth and grazing response of a ciliate feeding on the red tide dinoflagellate *Gyrodinium aureolum* in monoculture and in mixture with a non-toxic alga. *Mar. Ecol. Prog. Ser.* **121:** 65–72.

Hansen, P. J., A. D. Cembella, and O. Moestrup. 1992. The marine dinoflagellate *Alexandrium ostenfeldii*: paralytic shellfish toxin concentration, composition, and toxicity to a tintinnid ciliate. *J. Phycol.* **28:** 597–603.

Harumoto, T. 1994. The role of trichocyst discharge and backward swimming in escaping behavior of *Paramecium* from *Dileptus margaritifer. J. Eukaryot. Microbiol.* **41:** 560–564.

Harumoto, T., and A. Miyake. 1991. Defensive function of trichocysts in *Paramecium. J. Exp. Zool.* **260:** 84–92.

Hauser, D. C. R., M. Levandowsky, and J. M. Glassgold. 1975a. Ultrasensitive chemosensory responses by a protozoan to epinephrine and other neurochemicals. *Science* **190:** 285–286.

Hauser, D. C. R., M. Levandowsky, S. H. Hunter, L. Chunosoff, and J. S. Hollwitz. 1975b. Chemosensory responses by the heterotrophic marine dinoflagellate *Crypthecodinium cohnii. Microb. Ecol.* **1:** 246–254.

Hawser, S. P., J. M. O'Neill, M. R. Roman, and G. A. Codd. 1992. Toxicity of blooms of the cyanobacterium *Trichodesmium* to zooplankton. *J. Appl. Phycol.* **4:** 79–86.

Hefetz, A., and M. S. Blum. 1978. Biosynthesis and accumulation of formic acid in the poison gland of the carpenter ant *Camponotus pennsylvanicus. Science* **201:** 454–455.

Heinbokel, J. F. 1978. Studies on the functional role of tintinnids in the southern California bight. I. Grazing and growth rates in laboratory cultures. *Mar. Biol.* **47:** 177–189.

Hellio, R., and A. Ryter. 1980. Relationships between anionic sites and lectin receptors in the plasma membrane of *Dictyostelium discoideum* and their role during phagocytosis. *J. Cell Sci.* **41:** 89–104.

Hennessey, T. M. 1989. Ion currents of *Paramecium*: effects of mutations and drugs. Pp. 215–234 in *Evolution of the First Nervous Systems*, P. A. V. Anderson, ed. Plenum Press, New York.

Howe, N. R., and Y. M. Sheikh. 1975. Anthopleurine: a sea anemone alarm pheromone. *Science* **189:** 386–388.

Huntley, M., P. Sykes, S. Rohan, and V. Marin. 1986. Chemically-mediated rejection of dinoflagellate prey by the copepods *Calanus pacificus* and *Paracalanus parvus*: mechanism, occurrence and significance. *Mar. Ecol. Prog. Ser.* **28:** 105–120.

Ishida, Y., and H. Kadota. 1968. Participation of dimethyl-β-propiothetin in transmethylation reaction in *Gyrodinium cohnii*. *Bull. Jpn. Soc. Sci. Fish.* **34:** 699–705.

Jackson, G. A. 1987. Simulating chemosensory responses of marine microorganisms. *Limnol. Oceanogr.* **32:** 1253–1266.

Jacobson, D. M., and D. M. Anderson. 1986. Thecate hetrotrophic dinoflagellates: feeding behavior and mechanisms. *J. Phycol.* **22:** 249–258.

Jaffe, L. F. 1985. The role of calcium explosions, waves, and pulses in activating eggs. Pp. 127–165 in *Biology of Fertilization*, C. B. Metz and A. Monroy, eds. Academic Press, Orlando, FL.

Jennings, H. S. 1906. *Behavior of the Lower Organisms.* Columbia University Press, New York.

Johnson, C. H., S. Inoué, A. Flint, and J. W. Hastings. 1985. Compartmentalization of algal bioluminescence: autofluorescence of bioluminescent particles in the dinoflagellate *Gonyaulax* as studied with image-intensified video microscopy and flow cytometry. *J. Cell Biol.* **100:** 1435–1446.

Jones, D. A., R. J. Keymer, and W. M. Ellis. 1978. Cyanogenesis in plants and animal feeding. Pp. 21–34 in *Biochemical Aspects of Plant and Animal Coevolution*, J. B. Harborne, ed. Academic Press, London.

Jonsson, P. R. 1986. Particle size selection, feeding rates and growth dynamics of marine planktonic oligotrichous ciliates (Ciliophora: Oligotrichina). *Mar. Ecol. Prog. Ser.* **33:** 265–277.

Jürgens, K., J. Pernthaler, S. Schalla, and R. Amann. 1999. Morphological and compositional changes in a planktonic bacterial community in response to enhanced protozoan grazing. *Appl. Environ. Microbiol.* **65:** 1241–1250.

Karban, R., and I. T. Baldwin. 1997. *Induced Responses to Herbivory.* University of Chicago Press, Chicago.

Karl, D. M., ed. 1995. *The Microbiology of Deep-Sea Hydrothermal Vents.* CRC Press, Boca Raton, FL.

Karsten, U., K. Kück, C. Vogt, and G. O. Kirst. 1996. Dimethylsulfoniopropionate production in phototrophic organisms and its physiological function as a cryoprotectant. Pp. 143–153 in *Biological and Environmental Chemistry of DMSP and Related Sulfonium Compounds*, R. P. Kiene, P. Visscher, G. Kirst, and M. Keller, eds. Plenum Press, New York.

Keller, M. D., W. K. Bellows, and R. R. L. Guillard. 1989a. Dimethyl sulfide production by marine phytoplankton: an additional impact of unusual blooms. Pp. 101–115 in *Novel Phytoplankton Blooms*, E. M. Cooper, V. M. Bricelj, and E. J. Carpenter, eds. Springer-Verlag, Berlin.

Keller, M. D., W. K. Bellows, and R. R. L. Guillard. 1989b. Dimethyl sulfide production in marine phytoplankton. Pp. 167–183 in *Biogenic Sulfur in the Environment*, E. S. Saltzman and W. J. Cooper, eds. American Chemical Society, Washington, DC.

Kiene, R. P. 1993. Measurement of dimethylsulfide (DMS) and dimethylsulfoniopropionate (DMSP) in seawater and estimation of DMS turnover rates. Pp. 601–610 in *Handbook of Methods in Aquatic Microbial Ecology*, P. F. Kemp, B. F. Sherr, E. B. Sherr, and J. J. Cole, eds. Lewis Publishers, Boca Raton, FL.

Kiene, R. P., P. Visscher, G. Kirst, and M. Keller, eds. 1996. *Biological and Environmental Chemistry of DMSP and Related Sulfonium Compounds*, Plenum Press, New York.

Kiersnowska, M., R. K. Peck, and G. de Haller. 1988. Cell to cell recognition between the ciliate *Pseudomicrothorax dubius* and its food organisms: the role of surface charges. *Protoplasma* **143:** 93–100.

Kirchman, D. L., S. Graham, D. Reish, and R. Mitchell. 1982. Lectins may mediate in the settlement and metamorphosis of *Janua* (*Dexiospira*) *brasiliensis* Grube (Polychaeta: Spirorbidae). *Mar. Biol. Lett.* **3:** 131–142.

Kirk, K. L., and J. J. Gilbert. 1992. Variation in herbivore response to chemical defenses: zooplankton foraging on toxic cyanobacteria. *Ecology* **73:** 2208–2217.

Knoll, A. H., and J. H. Lipps. 1993. Evolutionary history of prokaryotes and protists. Pp. 19–29 in *Fossil Prokaryotes and Protists*, J. H. Lipps, ed. Blackwell Scientific, Boston.

Knoll, G., B. Haacke-Bell, and H. Plattner. 1991. Local trichocyst exocytosis provides an efficient escape mechanism for *Paramecium* cells. *J. Eur. Protistol.* **27:** 381–385.

Köhidai, L., and G. Csaba. 1996. Different and selective chemotactic responses of *Tetrahymena pyriformis* to two families of signal molecules: lectins and peptide hormones. *Acta Microbiol. Immunol. Hung.* **43:** 83–91.

Köhidai, L., P. Kovacs, and G. Csaba. 1994. Chemotactic response of unicellular *Tetrahymena* to a leukocyte attractant peptide and its repellent derivate: evolutionary conclusions. *Cell Biol. Int.* **18:** 119–122.

Kovács, P., W. E. G. Müller, and G. Csaba. 1997. A lectin-like molecule is discharged from mucocysts of *Tetrahymena pyriformis* in the presence of insulin. *J. Eukaryot. Microbiol.* **44:** 487–491.

Krembs, C., A. R. Juhl, R. A. Long, and F. Azam. 1998. Nanoscale patchiness of bacteria in lake water studied with the spatial information preservation method. *Limnol. Oceanogr.* **43:** 307–314.

Kuhlmann, H.-W., C. Brünen-Nieweler, and K. Heckmann. 1997. Pheromones of the ciliate *Euplotes octacarinatus* not only induce conjugation but also function as chemoattractants. *J. Exp. Zool.* **277:** 33–48.

Kurjan, J., and B. L. Taylor, eds. 1993. *Signal Transduction: Prokaryotic and Simple Eukaryotic Systems.* Academic Press, San Diego.

Kusch, J. 1993. Behavioural and morphological changes in ciliates induced by the predator *Amoeba proteus*. *Oecologia* **96:** 354–359.

Kusch, J. 1995. Adaptation of inducible defense in *Euplotes daiadaleos* (Ciliophora) to predation risks by various predators. *Microb. Ecol.* **30:** 79–88.

Kusch, J. 1999. Self-recognition as the original function of an amoeban defense-inducing kairomone. *Ecol.* **80:** 715–720.

Kusch, J., and H.-W. Kuhlmann. 1994. Cost of *Stenostomum*-induced morphological defence in the ciliate *Euplotes octocarinatus*. *Arch. Hydro.* **130:** 257–267.

Lancelot, C., and V. Rosseau. 1994. Ecology of *Phaeocystis*: the key role of colony forms. Pp. 229–245 in *The Haptophyte Algae*, J. C. Green and B. S. C. Leadbeater, eds. Clarendon Press, Oxford.

Larsen, A., and L. K. Medlin. 1997. Inter- and intraspecific genetic variation in twelve *Prymnesium* (Haptophyceae) clones. *J. Phycol.* **33:** 1007–1015.

Leick, V., and P. Hellung-Larsen. 1985. Chemosensory responses in *Tetrahymena*: the involvement of peptides and other signal substances. *J. Protozool.* **32:** 550–553.

Leigh, R. A., N. Ahmad, and R. G. Wyn Jones. 1981. Assessment of glycinebetaine and proline compartmentation by analysis of isolated beet vacuoles. *Planta* **153:** 34–41.

LeRoith, D., A. S. Liotta, J. Roth, J. Shiloach, M. E. Lewis, C. B. Pert, and D. T. Krieger. 1982. Corticotropin and β-endorphin-like materials are native to unicellular organisms. *Proc. Natl. Acad. Sci. USA* **79:** 2086–2090.

Levandowsky, M., and D. C. R. Hauser. 1978. Chemosensory responses of swimming algae and protozoa. *Int. Rev. Cytol.* **53:** 145–210.

Lim, E. L., D. A. Caron, and E. F. Delong. 1996. Development and field application of a quantitative method for examining natural assemblages of protists with oligonucleotide probes. *Appl. Environ. Microbiol.* **62:** 1416–1423.

Lima, S. L. 1998. Nonlethal effects in the ecology of predator-prey interactions. *Bioscience* **48:** 25–34

Lindstedt, K. J. 1971. Chemical control of feeding behavior. *Comp. Biochem. Physiol.* **39A:** 553–581.

Löfqvist, J. 1976. Formic acid and saturated hydrocarbons as alarm pheromones for the ant *Formica rufa. J. Insect Physiol.* **22:** 1331–1346.

Loomis, W. F., ed. 1982. *The Development of* Dictyostelium discoideum. Academic Press, New York.

Louis, J. M., C. L. Saxe III, and A. R. Kimmel. 1993. Two transmembrane signaling mechanisms control expression of the cAMP receptor gene CAR1 during *Dictyostelium* development. *Proc. Natl. Acad. Sci. USA* **90:** 5969–5973.

Lowe, J. B. 1994. Carbohydrate recognition in cell-cell interactions. Pp. 163–205 in *Molecular Glycobiology*, M. Fukuda and O. Hindsgaul, eds. IRL Press, Oxford.

Luporini, P., A. Vallesi, C. Miceli, and R. A. Bradshaw. 1995. Chemical signalling in ciliates. *J. Eukaryot. Microbiol.* **42:** 208–212.

Machemer, H., and P. F. M. Teunis. 1996. Sensory-motor coupling and motor responses. Pp. 379–402 in *Ciliates: Cells as Organisms*, K. Hausmann and P. C. Bradbury, eds. Gustav Fischer, Stuttgart.

Mackie, A. M., and P. T. Grant. 1974. Interspecies and intraspecies chemoreception by marine invertebrates. Pp. 105–141 in *Chemoreception in Marine Organisms*, P. T. Grant and A. M. Mackie, eds. Academic Press, London.

Malin, G., W. H. Wilson, G. Bratbak, P. S. Liss, and N. H. Mann. 1998. Elevated production of dimethylsulfide resulting from viral infection of *Phaeocystis pouchetii. Limnol. Oceanogr.* **43:** 1389–1393.

Manhart, J. R., and R. M. McCourt. 1992. Molecular data and species concepts in the algae. *J. Phycol.* **28:** 730–737.

Margulis, L., and D. Sagan. 1987. Sex: the cannibalistic legacy of primordial androgynes. Pp. 23–38 in *The Evolution of Sex*, J. M. Smith *et al.*, eds. Harper & Row, San Francisco.

Margulis, L., J. O. Corliss, M. Melkonian, and D. J. Chapman, eds. 1990. *Handbook of Protoctista.* Jones and Bartlett, Boston.

Marino, M. J., and D. C. Wood. 1993. β-endorphin modulates a mechanoreceptor channel in the protozoan *Stentor. J. Comp. Physiol. A* **172:** 233–240.

Mast, S. O. 1906. The reactions of *Didinium nasutum* (Stein) with special reference to the feeding habits and the function of trichocysts. *Biol. Bull.* **16:** 91–118.

Matoh, T., J. Watanabe, and E. Takahashi. 1987. Sodium, potassium, chloride, and betaine concentrations in isolated vacuoles from salt-grown *Atriplex gmelini* leaves. *Plant Physiol.* **84:** 173–177.

Matsumura, K. 1995. Tetrodotoxin as a pheromone. *Nature* **378:** 563–564

McClintock, J. B., B. J. Baker, M. T. Hamann, W. Yoshida, M. Slattery, *et al.* 1994. Homarine as a feeding deterrent in common shallow-water Antarctic lamellarian gastropod *Marseniopsis mollis*: a rare example of chemical defense in a marine prosobranch. *J. Chem. Ecol.* **20:** 2539–2549.

Medlin, L. K., G. L. A. Barker, L. Campbell, J. C. Green, P. K. Hayes, *et al.* 1996. Genetic characterisation of *Emiliania huxleyi* (Haptophyta). *J. Mar. Syst.* **9:** 13–31

Mensinger, A. F., and J. F. Case. 1992. Dinoflagellate luminescence increases susceptibility of zooplankton to teleost predation. *Mar. Biol.* **112:** 207–210

Mitchell, J. G., A. Okubo, and J. A. Fuhrman. 1985. Microzones surrounding phytoplankton form the basis for a stratified marine microbial ecosystem. *Nature* **316:** 58–59.

Mitchell, J. G., L. Pearson, and S. Dillon. 1996. Clustering of marine bacteria in seawater enrichments. *Appl. Environ. Microbiol.* **62:** 3716–3721.

Monger, B. C., and M. R. Landry. 1991. Prey-size dependency of grazing by free-living marine flagellates. *Mar. Ecol. Prog. Ser.* **74:** 239–248.

Moore, P. A., D. M. Fields, and J. Yen. 1999. Physical constraints of chemoreception in foraging copepods. *Limnol. Oceanogr.* **44:** 166–177.

Müller-Niklas, G., M. Agis, and G. J. Herndl. 1996. Microscale distribution of bacterioplankton in relation to phytoplankton: results from 100-nl samples. *Limnol. Oceanogr.* **41:** 1577–1582.

Nanjundiah, V. 1973. Chemotaxis, signal relaying and aggregation morphology. *J. Theor. Biol.* **42:** 63–105.

Nesbitt, L. M., H. P. Riessen, and C. W. Ramcharan. 1996. Opposing predation pressures and induced vertical migration responses in *Daphnia. Limnol. Oceanogr.* **41:** 1306–1311.

Nevitt, G. 1998. Foraging by seabirds on an olfactory landscape. *Am. Sci.* **87:** 46–53.

Nevitt, G. A. 2000. Olfactory foraging by Antarctic procellariiform seabirds: life at high Reynolds numbers. *Biol. Bull.* **198:** 245–253.

Nevitt, G. A., R. R. Veit, and P. Kareiva. 1995. Dimethyl sulphide as a foraging cue for Antarctic Procellariiform seabirds. *Nature* **376:** 680–682.

Newman, R. M., Z. Hanscom, and W. C. Kerfoot. 1992. The watercress glucosinolate-myrosinase system: a feeding deterrent to caddisflies, snails and amphipods. *Oecologia* **92:** 1–7.

Nicolas, M.-T., G. Nicolas, C. H. Johnson, J.-M. Bassot, and J. W. Hastings. 1975. Characterization of the bioluminescent organelles in *Gonyaulax polyedra* (dinoflagellates) after fast-freeze fixation and antiluciferase immunogold staining. *J. Cell Biol.* **105:** 723–735.

Nielsen, T. G., T. Kiorboe, and P. K. Bjørnsen. 1990. Effects of a *Chrysochromulina polylepis* subsurface bloom on the planktonic community. *Mar. Ecol. Prog. Ser.* **62:** 21–35.

Noordkamp, D. J. B., M. Schotten, W. W. C. Gieskes, L. J. Forney, J. C. Gottschal, and M. van Rijssel. 1998. High acrylate concentrations in the mucus of *Phaeocystis globosa* colonies. *Aquat. Microb. Ecol.* **16:** 45–52.

O'Day, D. H., ed. 1990. *Calcium as an Intracellular Messenger in Eucaryotic Microbes.* American Society for Microbiology, Washington, DC.

Oppen, M. J. H. v., H. Klerk, J. L. Olsen, and W. T. Stam. 1996. Hidden diversity in marine algae: some examples of genetic variation below the species level. *J. Mar. Biol. Assoc. UK* **76:** 239–242.

Ortenzi, C., and P. Luporini. 1995. Competition among homologous polypeptide hormones of the ciliate *Euplotes raikovi* for binding to each other's cell receptors. *J. Eukaryot. Microbiol.* **42:** 242–248.

Pace, N. R. 1997. A molecular view of microbial diversity and the biosphere. *Science* **276:** 734–740.

Paul, V. J., and K. L. van Alstyne. 1992. Activation of chemical defenses in the tropical green algae *Halimeda* spp. *J. Exp. Mar. Biol. Ecol.* **160:** 191–203.

Peck, R. K. 1985. Feeding behavior of the ciliate *Pseudomicrothorax dubius* is a series of morphologically and physiologically distinct events. *J. Protozool.* **32:** 492–501.

Peterson, J. B. 1991. Small GTP-binding proteins associated with secretory vesicles of *Paramecium. J. Protozool.* **38:** 495–501.

Plattner, H., R. Stürzl, and H. Matt. 1985. Synchronous exocytosis in *Paramecium* cells. IV. Polyamino compounds as potent trigger agents for repeatable trigger-redocking cycles. *Eur. J. Cell Biol.* **36:** 32–37.

Plumley, F. G. 1997. Marine algal toxins: biochemistry, genetics, and molecular biology. *Limnol. Oceanogr.* **42:** 1252–1264.

Pomeroy, L. R. 1992. The microbial food web. *Oceanus* **35:** 28–32.

Popescu, O., and G. N. Misevic. 1997. Self-recognition by proteoglycans. *Nature* **386:** 231–232.

Purcell, E. M. 1977. Life at low Reynolds number. *Am. J. Physics* **45:** 3–11.

Rabinovitch, M., and M. J. De Stefano. 1971. Antibody and plant agglutinins stimulate phagocytosis of erythrocytes by *Acanthamoeba. Nature* **234:** 412–413.

Rapport, D. J., J. Berger, and D. B. W. Reid. 1972. Determination of food preference of *Stentor coeruleus. Biol. Bull.* **142:** 103–109.

Rassoulzadegan, F., and L. Fenaux. 1984. Effect of flavor and size on selection of food by suspension-feeding plutei. *Limnol. Oceanogr.* **29:** 357–361.

Renaud, F. L., I. Colon, J. Lebron, N. Ortiz, F. Rodriguez, and C. Cadilla. 1995. A novel opioid mechanism seems to modulate phagocytosis in *Tetrahymena. J. Eukaryot. Microbiol.* **42:** 205–207.

Ricci, N., A. Morelli, and F. Verni. 1996. The predation of *Litonotus* on *Euplotes*: a two step cell-cell recognition process. *Acta Protozool.* **35:** 201–208.

Rittschof, D. 1990. Peptide-mediated behaviors in marine organisms: evidence for a common theme. *J. Chem. Ecol.* **16:** 261–272.

Roberts, D. M., P. Sharp, G. Alderson, and M. A. Collins, eds. 1996. *Evolution of Microbial Life.* Cambridge University Press, Cambridge.

Rosati, G. 1999. Epixenosomes: symbionts of the hypotrich ciliate *Euplotidium itoi. Symbiosis* **26:** 1–23.

Rosati, G., F. Verni, and P. Lenzi. 1993. "Epixenosomes": peculiar epibionts of the ciliate *Euplotidium itoi.* The formation of the extrusive apparatus and the ejecting mechanism. *Eur. J. Protistol.* **29:** 238–245.

Rosati, G., G. Petroni, S. Quochi, L. Modeo, and F. Verni. 1999. Epixenosomes: peculiar epibionts of the hypotrich ciliate *Euplotidium itoi* defend their host against predators. *J. Eukaryot. Microbiol.* **46:** 278–282.

Rossini, C., A. B. Attygalle, A. González, S. R. Smedley, M. Eisner, J. Meinwald, and T. Eisner. 1997. Defensive production of formic acid (80%) by a carabid beetle (*Galerita lecontei*). *Proc. Natl. Acad. Sci. USA* **94:** 6792–6797.

Saltzman, E. S., and W. J. Cooper, eds. 1989. *Biogenic Sulfur in the Environment.* ACS, Washington, DC.

Sanders, R. W. 1988. Feeding by *Cyclidium* sp. (Ciliophora, Scuticociliatida) on particles of different sizes and surface properties. *Bull. Mar. Sci.* **43:** 446–457.

Schaeffer, A. A. 1910. Selection of food in *Stentor coeruleus. J. Exp. Zool.* **8:** 75–132.

Schlenk, F., J. L. Dainko, and G. Svihla. 1970. The accumulation and intracellular distribution of biological sulfonium compounds in yeast. *Arch. Biochem. Biophys.* **140:** 228–236.

Scholin, C. A. 1998. Morphological, genetic, and biogeographic relationships of the toxic dinoflagellates *Alexandrium tamarense, A. catenella,* and *A. fundyense.* Pp. 12–27 in *NATO Advanced Workshop on the Physiological Ecology of Harmful Algal Blooms,* D. M Anderson, A. M. Cembella, and G. Hallegraef, eds. Springer, Berlin.

Sharon, N., and H. Lis. 1993. Carbohydrates in cell recognition. *Sci. Am.* **268:** 82–89.

Shaw, B. A., P. J. Harrison, and R. J. Anderson. 1995. Feeding deterrence properties of apo-fucoxanthinoids from marine diatoms. II Physiology of production of apo-fucoxanthinoids by the marine diatoms *Phaeodactylum tricornutum* and *Thalassiosira pseudonana,* and their feeding deterrent effects on the copepod *Tigriopus californicus. Mar. Biol.* **124:** 473–481.

Sherr, E. B., and B. F. Sherr. 1991. Planktonic microbes: tiny cells at the base of the ocean's food webs. *Trends Ecol. Evol.* **6:** 50–54.

Sherr, E. B., and B. F. Sherr. 1994. Bacterivory and herbivory: key roles of phagotrophic protists in pelagic food webs. *Microb. Ecol.* **27:** 223–235.

Sieburth, J. M. 1960. Acrylic acid, and "antibiotic" principle in *Phaeocystis* blooms in Antarctic waters. *Science* **132:** 676–677.

Sieburth, J. M. 1961. Antibiotic properties of acrylic acid, a factor in the gastrointestinal antibiosis of polar marine animals. *J. Bacteriol.* **82:** 72–79.

Sieburth, J. M. 1968. The influence of algal antibiosis on the ecology of marine microorganisms. Pp. 63–94 in *Advances in Microbiology of the Sea,* M. R. Droop and E. J. F. Wood, eds. Academic Press, London.

Sjoblad, R. D., and R. Mitchell. 1979. Chemotactic responses of *Vibrio alginolyticus* to algal extracellular products. *Can. J. Microbiol.* **25:** 964–967.

Spero, H. J., and M. D. Morée. 1981. Phagotrophic feeding and its importance to the life cycle of the holozoic dinoflagellate, *Gymnodinium fungiforme. J. Phycol.* **17:** 43–51.

Stefels, J., and W. H. M. van Boekel. 1993. Production of DMS from dissolved DMSP in axenic cultures of the marine phytoplankton species *Phaeocystis* sp. *Mar. Ecol. Prog. Ser.* **97:** 11–18.

Stefels, J., L. Dijkhuizen, and W. W. C. Gieskes. 1995. DMSP-lyase activity in a spring phytoplankton bloom off the Dutch coast, related to *Phaeocystis* sp. abundance. *Mar. Ecol. Prog. Ser.* **123:** 235–243.

Steinke, M., C. Daniel, and G. O. Kirst. 1996. DMSP lyase in marine macro- and microalgae: intraspecific differences in cleavage activity. Pp. 317–324 in *Biological and Environmental Chemistry of DMSP and Related Sulfonium Compounds,* R. P. Kiene, P. Visscher, G. Kirst, and M Keller, eds. Plenum Press, New York.

Steinke, M., G. V. Wolfe, and G. O. Kirst. 1998. Partial characterization of dimethylsulfoniopropionate (DMSP) lyase in 6 strains of *Emiliania huxleyi. Mar. Ecol. Prog. Ser.* **175:** 215–225.

Stoecker, D. K. 1988. Are marine planktonic ciliates suspension-feeders? *J. Protozool.* **35:** 252–255.

Stoecker, D. K. 1992. "Animals" that photosynthesize and "plants" that eat. *Oceanus* **35:** 24–27.

Stoecker, D. K., R. R. L. Guillard, and R. M. Kavee. 1981. Selective predation by *Favella ehrenbergii* (Tinninnia) on and among dinoflagellates. *Biol. Bull.* **160:** 136–145.

Stoecker, D. K., T. L. Cucci, E. M. Hulbert, and C. M. Yentsch. 1986. Selective feeding by *Balanion* sp. (Ciliata: Balanioidae) on the phytoplankton that best support its growth. *J. Exp. Mar. Biol. Ecol.* **95:** 113–130.

Stoecker, D. K., S. M. Gallager, C. J. Langdon, and L. H. Davis. 1995. Particle capture by *Favella* sp. (Ciliata, Tintinnida). *J. Plankton Res.* **17:** 1105–1124.

Strom, S. L. 2000. Bacterivory: interactions between bacteria and their grazers. Pp. 351–386 in *Microbial Ecology of the Oceans,* D. L. Kirchman and R. Mitchell, eds. John Wiley, London.

Strom, S. L., and H. Loukos. 1998. Selective feeding by protozoa: model and experimental behaviors and their consequences for population stability. *J. Plankton Res.* **20:** 831–846.

Subba Rao, D. V., Y. Pan, and S. J. Smith. 1995. Allelopathy between *Rhizosolenia alata* (Brightwell) and the toxigenic *Pseudonitzschia pungens* f. *multiseries* (Hasle). Pp. 691–686 in *Harmful Marine Algal Blooms,* P. Lassus, G. Arzul, E. E. Le Denn, P. Gentien, and C. Marcaillou-LeBaut, eds. Lavoisier, Paris.

Sugg, L. M., and R. M. VanDolah. 1999. No evidence for an allelopathic role of okadaic acid among ciguatera-associated dinoflagellates. *J. Phycol.* **35:** 93–103.

Suzaki, E., H. Kobayashi, Y. Kodama, T. Masujima, and S. Terakawa. 1997. Video-rate dynamics of exocytotic events associated with phagocytosis in neutrophils. *Cell Motil. Cytoskeleton* **38:** 215–228.

Sykes, P. F., and M. E. Huntley. 1987. Acute physiological reactions of *Calanus pacificus* to selected dinoflagellates: direct observations. *Mar. Biol.* **94:** 19–24.

Taniguchi, A., and Y. Takeda. 1988. Feeding rate and behavior of the tintinnid ciliate *Favella taraikaensis* observed with a high speed VTR system. *Mar. Microb. Food Webs* **3:** 21–34.

Tarran, G. A. 1991. Aspects of the grazing behaviour of the marine dinoflagellate *Oxyrrhis marina,* Dujardin. Ph.D. dissertation, University of Southampton, UK.

Teegarden, G. J., and A. D. Cembella. 1996. Grazing of toxic dinoflagellates, *Alexandrium* spp., by adult copepods of coastal Maine: implications for the fate of paralytic shellfish toxins in marine food webs. *J. Exp. Mar. Biol. Ecol.* **196:** 145–176.

Thijsse, G. J. E. 1964. Fatty-acid accumulation by acrylate inhibition of β-oxidation in an alkane-oxidizing *Pseudomonas. Biochim. Biophys. Acta* **84:** 195–197.

Tilney, L. G. 1985. The acrosomal reaction. Pp. 157–213 in *Biology of Fertilization,* C. B. Metz and A. Monroy, eds. Academic Press, Orlando, FL.

Tollrian, R., and C. D. Harvell, eds. 1999. *The Ecology and Evolution of Inducible Defenses.* Princeton University Press, Princeton.

Turiff, N., J. A. Runge, and A. D. Cembella. 1995. Toxin accumulation and feeding behaviour of the planktonic copepod *Calanus finmarchicus* exposed to the red-tide dinoflagellate *Alexandrium excavatum. Mar. Biol.* **123:** 55–64.

Turner, J. T., and P. A. Tester. 1997. Toxic marine phytoplankton, zooplankton grazers, and pelagic food webs. *Limnol. Oceanogr.* **42:** 1203–1214.

Turner, J. T., P. A. Tester, and P. J. Hansen. 1998. Interactions between toxic marine phytoplankton and metazoan and protistan grazers. Pp. 453–474 in *NATO Advanced Workshop on the Physiological Ecology of Harmful Algal Blooms,* D. M. Anderson, A. M. Cembella, and G. Hallegraef, eds. Springer, Berlin.

Vallesi, A., G. Giuli, R. A. Bradshaw, and P. Luporini. 1995. Autocrine mitogenic activity of pheromones produced by the protozoan ciliate *Euplotes raikovi. Nature* **376:** 522–524.

van den Ende, H. 1985. Sexual agglutination in *Chlamydomonas. Adv. Microb. Physiol.* **26:** 89–123.

Van Donk, E., M. Lürling, D. O. Hessen, and G. M. Lokhorst. 1997. Altered cell wall morphology in nutrient-deficient phytoplankton and its impact on grazers. *Limnol. Oceanogr.* **42:** 357–364.

Van Houten, J. 1994. Chemosensory transduction in eukaryotic microorganisms: trends for neuroscience? *Trends Neurosci.* **17:** 62–71.

Van Houten, J., D. C. R. Hauser, and M. Levandowsky. 1981. Chemosensory behavior in protozoa. Pp. 67–124 in *Biochemistry and Physiology of Protozoa,* M. Levandowsky and S. H. Hutner, eds. Academic Press, New York.

van Rijssel, M., C. E. Hamm, and W. W. C. Gieskes. 1997. *Phaeocystis globosa* (Prymnesiophyceae) colonies: hollow structures built with small amounts of polysaccharides. *Eur. J. Phycol.* **32:** 185–192.

Vance, T. C., C. T. Baier, R. D. Brodeur, K. O. Coyle, M. B. Decker, *et al.* 1998. Aquamarine waters recorded for the first time in eastern Bering Sea. *Eos* **79:** 121.

Verity, P. G. 1988. Chemosensory behavior in marine planktonic ciliates. *Bull. Mar. Sci.* **43:** 772–782.

Verity, P. G. 1991. Feeding in planktonic protozoans: evidence for non-random acquisition of prey. *J. Protozool.* **38:** 69–76.

Verity, P. G., and D. Stoecker. 1982. Effects of *Olisthodiscus luteus* on the growth and abundance of tintinnids. *Mar. Biol.* **72:** 79–87.

Vogel, G., L. Thilo, H. Schwarz, and R. Steinhart. 1980. Mechanism of phagocytosis in *Dictyostelium discoideum*: phagocytosis is mediated by different recognition sites as disclosed by mutants with altered phagocytotic properties. *J. Cell Biol.* **86:** 456–465.

von Gersdorff, H., and G. Matthews. 1994. Dynamics of synaptic vesicle fusion and membrane retrieval in synaptic terminals. *Nature* **367:** 735–739.

Wagner, G. J. 1978. Compartmentation in plant cells: the role of the vacuole. Pp. 1–45 in *Cellular and Subcellular Localization in Plant Metabolism,* L. L. Creasy and G. Hrazdina, eds. Plenum Press, New York.

Waite, A. M., R. J. Olson, H. G. Dam, and U. Passow. 1995. Sugar-containing compounds on the cell surfaces of marine diatoms measured using concanavalin A and flow cytometry. *J. Phycol.* **31:** 925–933.

Weisse, T., K. Tande, P. Verity, F. Hansen, and W. Gieskes. 1994. The trophic significance of *Phaeocystis* blooms. *J. Mar. Syst.* **5:** 67–79.

Wesenberg, H., and G. Antipa. 1970. Capture and ingestion of *Paramecium* by *Didinium nasutum. J. Protozool.* **17:** 250–270.

White, H. H. 1979. Effects of dinoflagellate bioluminescence on the ingestion rates of herbivorous zooplankton. *J. Exp. Mar. Biol. Ecol.* **36:** 217–224.

Wicklow, B. J. 1997. Signal-induced defensive phenotypic changes in ciliated protists: morphological and ecological implications for predator and prey. *J. Eukaryot. Microbiol.* **44:** 176–188.

Windust, A. J., J. L. C. Wright, and J. L. McLachlan. 1996. The effects of the diarrhetic shellfish poisoning toxins, okadaic acid and dinosphysistoxin-1, on the growth of microalgae. *Mar. Biol.* **126:** 19–25.

Wink, M. 1997. Compartmentation of secondary metabolites and xenobiotics in plant vacuoles. Pp. 141–169 in *The Plant Vacuole,* R. A. Leigh and D. Sanders, eds. Academic Press, San Diego.

Wolfe, G. V., and M. Steinke. 1996. Grazing-activated production of dimethyl sulfide (DMS) by two clones of *Emiliania huxleyi. Limnol. Oceanogr.* **41:** 1151–1160.

Wolfe, G. V., M. Steinke, and G. O. Kirst. 1997. Grazing-activated chemical defense in a unicellular marine alga. *Nature* **387:** 894–897.

Wolfe, G. V., M. Levasseur, G. Cantin, and S. Michaud. 2000. DMSP and DMS dynamics and microzooplankton grazing in the Labrador Sea: application of the dilution technique. *Deep-Sea Res.* **I.** (In press).

Wood, A. M., and T. Leatham. 1992. The species concept in phytoplankton ecology. *J. Phycol.* **28:** 723–729.

Wood, A. M., and L. M. van Valen. 1990. Paradox lost? On the release of energy-rich compounds by phytoplankton. *Mar. Microb. Food Webs* **4:** 103–116.

Wright, S. D., and S. C. Silverstein. 1986. Overview: the function of receptors in phagocytosis. Pp. 41.4–41.14 in *Cellular Immunology,* L. A. Herzenberg, C. Blackwell, and L. A. Herzenberg, eds. Blackwell Scientific, Oxford.

Zhou, J., and L. Fritz. 1994. Okadaic acid antibody localizes to chloroplasts in the DSP-toxin-producing dinoflagellates *Prorocentrum lima* and *Prorocentrum maculosum. Phycologia* **33:** 455–461.

Zimmer-Faust, R. K., M. P. de Souza, and D. C. Yoch. 1996. Bacterial chemotaxis and its potential role in marine dimethylsulfide production and biogeochemical sulfur cycling. *Limnol. Oceanogr.* **41:** 1330–1334.

Reference: *Biol. Bull.* **198:** 245–253. (April 2000)

Olfactory Foraging by Antarctic Procellariiform Seabirds: Life at High Reynolds Numbers

GABRIELLE A. NEVITT

Section of Neurobiology, Physiology and Behavior, University of California, Davis, California 95616

Abstract. Antarctic procellariiform seabirds forage over vast stretches of open ocean in search of patchily distributed prey resources. These seabirds are unique in that most species have anatomically well-developed olfactory systems and are thought to have an excellent sense of smell. Results from controlled experiments performed at sea near South Georgia Island in the South Atlantic indicate that different species of procellariiforms are sensitive to a variety of scented compounds associated with their primary prey. These include krill-related odors (pyrazines and trimethylamine) as well as odors more closely associated with phytoplankton (dimethyl sulfide, DMS). Data collected in the context of global climatic regulation suggest that at least one of these odors (DMS) tends to be associated with predictable bathymetry, including upwelling zones and seamounts. Such odor features are not ephemeral but can be present for days or weeks. I suggest that procellariiforms foraging over vast distances may be able to recognize these features reflected in the olfactory landscape over the ocean. On the large scale, such features may aid seabirds in navigation or in locating profitable foraging grounds. Once in a profitable foraging area, procellariiforms may use olfactory cues on a small scale to assist them in locating prey patches.

Introduction

How olfactory-guided search strategies operate over distances of hundreds or thousands of kilometers has not been rigorously studied in most organisms that use them, yet these behaviors stand as some of the most remarkable navigational feats of nature. Pacific salmon (*Oncorhynchus* sp.), for example, migrate thousands of kilometers to specific streams. This behavior is thought to be guided largely by smells learned earlier in life (for review, see Hasler and Scholz, 1983; Nevitt and Dittman, 1998). Green sea turtles (*Chelonia mydas*) nesting on Ascension Island in the middle of the Atlantic Ocean are guided there from feeding grounds off the coast of South America, presumably by a redundant set of mechanisms that possibly includes an ability to smell their island birth place (for review, see Lohmann, 1992).

To explain such behaviors, it is commonly assumed that animals are able to recognize and follow odors emanating from a distant source. This logic predicts that a recognizable odor signature emanates from a site, forming a gradient that can be detected thousands of kilometers away. By some adaptive behavioral mechanism such as turning or swimming upstream in response to the odor cue, the animal focuses its directional movement to locate the source of the odor plume. This hypothesis thus suggests that a salmon entering a river system should be able to detect the scent of its homestream waters from many hundreds of kilometers downstream. Similarly, a sea turtle foraging off the coast of Brazil should be able to detect and respond to odors emanating from a remote island thousands of kilometers away. But the physical parameters that dictate these behaviors do not support such scenarios. Odors are transported in a turbulent environment, suggesting that gradients are not easy to follow (see discussion in Dusenbery, 1992). Moreover, concentrations of site-specific odors would be small and probably undetectable from the distances being considered.

My laboratory has been studying this problem in a novel context—olfactory foraging at sea by Antarctic procellariiform seabirds (Order Procellariiforms). These tube-nosed seabirds include the petrels, albatrosses, and shearwaters. Procellariiform seabirds forage over hundreds and even thousands of kilometers in search of patchily distributed food resources, most notably krill, squid, and fish (reviewed in Prince and Morgan, 1987, and Warham, 1990). Members of this order have among the largest olfactory bulbs of any bird, suggesting that olfaction plays a fundamental role in foraging behavior (Bang, 1965, 1966). Experimental trials performed at sea and from land have shown that many

Received 1 July 1999; accepted 24 November 1999.

E-mail: ganevitt@ucdavis.edu

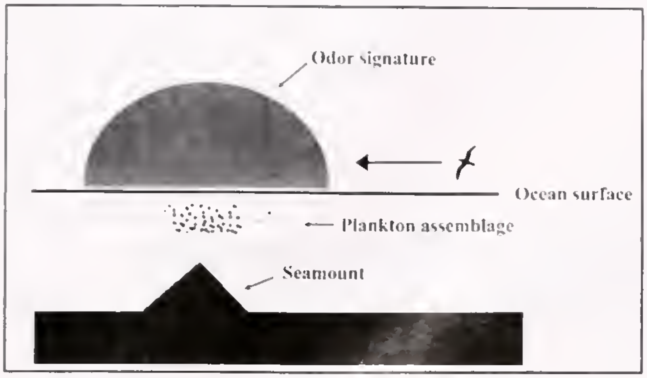

Figure 1. A theoretical olfactory landscape in the atmosphere reflects biological activity over a seamount. This is an area of upwelling where primary productivity tends to be high. A seabird may be alerted to a potentially productive foraging area as it encounters a change in the olfactory landscape. Elements are not drawn to scale.

species are attracted to fishy odors (*e.g.*, cod liver oil, tuna oil, or fish homogenate). Such studies suggest that procellariiforms use their sense of smell to locate food patches (Grubb, 1972; Hutchison and Wenzel, 1980; Lequette *et al.*, 1989; Nevitt *et al.*, 1995).

On a broader scale, we are only beginning to investigate how procellariiforms use naturally occurring scented compounds as foraging and navigation cues (Figs. 1 and 2). I suggest that odors serve at least three distinct functions. First, for species that travel long distances to forage, contours in an odor landscape superimposed upon the ocean's surface may serve as olfactory guideposts that mark the path the seabird follows (see also Waldvogel, 1987). For example, a seabird might gain directional information by traveling along a shelf break or another bathymetric feature that is marked by a consistent olfactory signature in the atmosphere (Fig. 2A). Second, olfactory landscapes may demarcate large-scale areas where prey is likely to be found (Figs. 1 and 2B). Such areas include upwelling zones or seamounts where primary productivity is likely to be high (Fig. 1). Finally, odor cues emitted from prey or directly associated with prey may assist seabirds using area-restricted search to locate prey patches (Fig. 2C). This area-restricted search has been described elsewhere (Nevitt and Veit, 1999) and is likely to involve both visual cues provided by foraging conspecifics and olfactory cues from prey. Although these findings do not support a gradient or bicoordinate odor-map mechanism as proposed for homing pigeons (Papi *et al.*, 1972; Wallraff, 1981), they do fit well with other models that more realistically describe atmospheric transport of directional olfactory cues for birds (see review by Waldvogel, 1987). Our work expands upon this earlier effort by identifying dimethyl sulfide (DMS) as a specific component of the olfactory landscape that procellariiform seabirds can detect.

Foraging at Different Spatial Scales

Procellariiform seabirds breed on oceanic islands and spend most of their lives at sea. During the breeding season, members of this order are tied to the nesting colony and are thus restricted to central place foraging strategies (Stephens and Krebs, 1986). They must regularly return to the colony either to relieve their mates during the incubation stage or to provision their offspring. Their prey resources are patchy and ephemeral, and foraging grounds may be considerable distances from breeding colonies. These seabirds employ highly efficient flight styles (Pennycuick, 1982, 1987), and thus may be constrained less by their own energetic limitations than by time and energetic limitations imposed on them during the breeding season when mates and chicks depend on successful foraging trips.

I speculate that procellariiform seabirds must confront two fundamental problems to forage efficiently. They must first employ large-scale foraging strategies to locate resource-rich areas where the probability of encountering a prey patch is high. Then they must shift to smaller scale foraging behaviors to pinpoint accessible prey patches within these foraging areas. How have different procellariiform species solved these problems?

One approach is to forage along a path where prey might be encountered opportunistically (Fig. 3, top, reviewed by Weimerskirch, 1998). Wandering albatrosses (*Diomedea exulans*) regularly use this first foraging scenario, searching for and exploiting resources continuously upon leaving the colony (Jouventin and Weimerskirch, 1990; Weimerskirch *et al.*, 1993; 1994). Satellite tracks of individual breeding wandering albatrosses have shown that these seabirds routinely forage along thousands of kilometers during incubation periods and when provisioning chicks on the nest

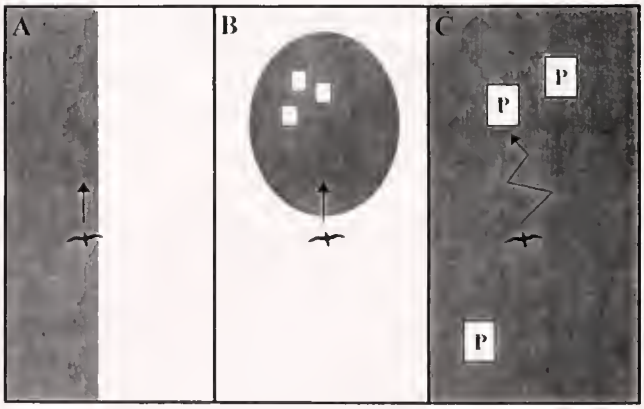

Figure 2. Three ways procellariiform seabirds might use odor features. (A) A large-scale boundary may provide consistent directional information for piloting. (B) A large-scale odor signature may indicate a productive area of the ocean where prey is likely to be found. (C) Once in a productive area, birds may track prey using smell. For each diagram, odor features are indicated in gray. White squares depict prey patches in B and C. Elements of these three models are not drawn to scale.

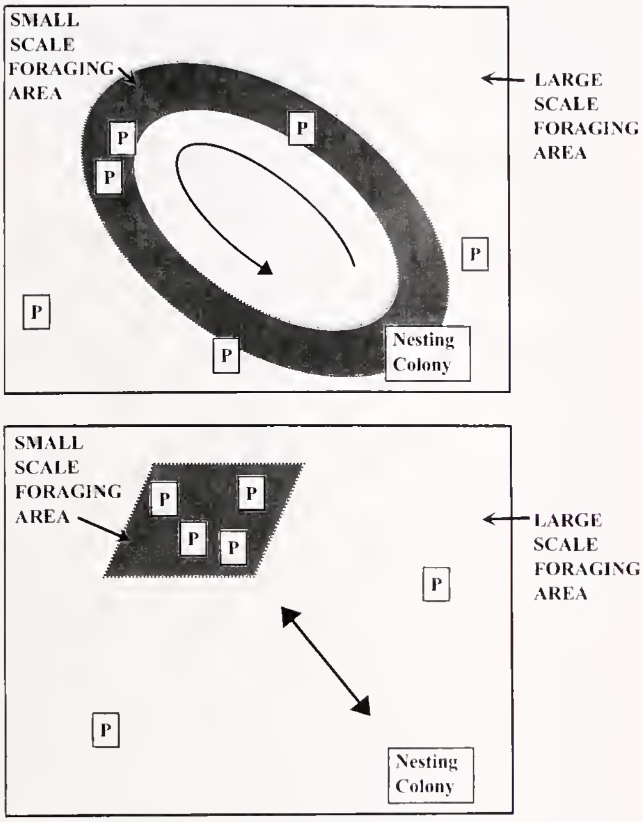
SMALL SCALE FORAGING AREA
LARGE SCALE FORAGING AREA
P
P
P
P
P
P
Nesting Colony
SMALL SCALE FORAGING AREA
LARGE SCALE FORAGING AREA
P
P
P
P
P
P
Nesting Colony

Figure 3. Two strategies used by long-distance foragers. (Top) Opportunistic foraging along a theoretical route (shaded grey) where prey is likely to be encountered. (Bottom) Commuting to distant foraging localities (shaded grey). For both models, white boxes labeled "P" indicate theoretical prey patches. Elements are not drawn to scale.

(Jouventin and Weimerskirch, 1990). Additionally, results from stomach temperature devices deployed in foraging wandering albatrosses indicate that these seabirds feed regularly throughout a foraging trip, swallowing on average one prey item every 100 km (Weimerskirch and Wilson, 1992). Several studies have shown that this species feeds primarily on deep-water squid (*e.g.*, Onychoteuthidae, Cranchiidae, and Histioteuthidae: Weimerskirch *et al.*, 1986; Rodhouse *et al.*, 1987; Ridoux, 1994) that live well beyond the diving capacities of these seabirds (Croxall and Prince, 1994).

How these birds find this prey resource is still not known. It has been suggested that wandering albatrosses may feed at night when squid migrate to the surface (Croxall and Prince, 1994) or on carrion associated with the foraging activity of sperm whales (Ainley *et al.*, 1984). Another interesting but unexplored possibility is that wandering albatrosses exploit this resource by systematically foraging in areas where this food source is likely to be available, such as along established routes where sperm whales forage. Whether these seabirds also use large-scale olfactory features as guideposts (as shown in Fig. 2A) for foraging has not yet been explored, but presents an interesting avenue for future study. On the small scale, we hypothesize that, as seabirds forage along a course, odor cues emitted by prey enhance encounter rates by, in effect, increasing the prey patch size, thereby increasing foraging efficiency (as in Fig. 2C). Through simulations of dispersion profiles of fishy-smelling scented compounds (trimethylamine), Clark and Shah (1992) have shown that odor emissions may extend the detectability of a small (0.5 m) prey patch by kilometers. The olfactory sensitivities of wandering albatrosses to squid-related odors have not been explored, but albatrosses have been seen to recruit to fishy odors (*e.g.*, herring oil, cod liver oil) in experimental trials (Nevitt, unpubl. data), suggesting that they do pay attention to olfactory cues (see also Hutchison and Wenzel, 1980).

The second strategy that foraging procellariiforms use is to commute directly from the colony to feeding grounds, often hundreds or thousands of kilometers away (Fig. 3, bottom; *e.g.*, Weimerskirch, 1998). To find such locations, procellariiforms may rely on spatial memory, experience, olfactory guideposts, and other navigational cues (*e.g.*, celestial or magnetic). It is unlikely that they are able to perceive prey-related odor cues emanating from such extreme distances, but they could use large-scale olfactory features in the environment as indicators that they have arrived in an area where foraging is likely to succeed (Fig. 2B; Nevitt *et al.*, 1995; Nevitt, 1999a). Olfactory cues may operate on a large scale by alerting seabirds to specific areas of the ocean where food is likely to be available, and thus worth the energetic costs of launching a small-scale search. According to this logic, long-distance foragers would use a change in the odor landscape as a feature in the environment that indicates they have arrived at a specific destination (as in Figs. 1B and 2B). It should be noted that these foraging destinations, particularly upwelling zones or fronts, are not constant but may fluctuate to some degree in space. An olfactory feature that mirrors productivity in a vast expanse of open ocean would provide the foraging seabird with direct and instantaneous feedback that it has reached its foraging destination. Such feedback might trigger a behavioral switch to begin an area-restricted search (as in Fig. 2C). This search would be aimed at locating specific prey patches, and as mentioned above, might involve both olfactory and visual modalities (Nevitt and Veit, 1999).

Evidence for this idea comes largely from two sources: atmospheric data showing associations of biogenic scented compounds with prey resources or areas where prey is likely to aggregate (Fig. 4; see discussion below) and satellite telemetry data collected from foraging seabirds such as black-browed albatross (*Thalassarche melanophrys*, Cherel and Weimerskirch, 1995; Weimerskirch, 1998), grey-headed albatross (*Thalassarche chrysostoma*, Prince *et al.*, 1998), light-mantled sooty albatross (*Phoebetria palpebrata*, Weimerskirch and Robertson, 1994), Southern Buller's albatross (*Thalassarche bulleri*, Sagar and Weimerskirch, 1996), waved albatross (*Phoebetria irrorata*,

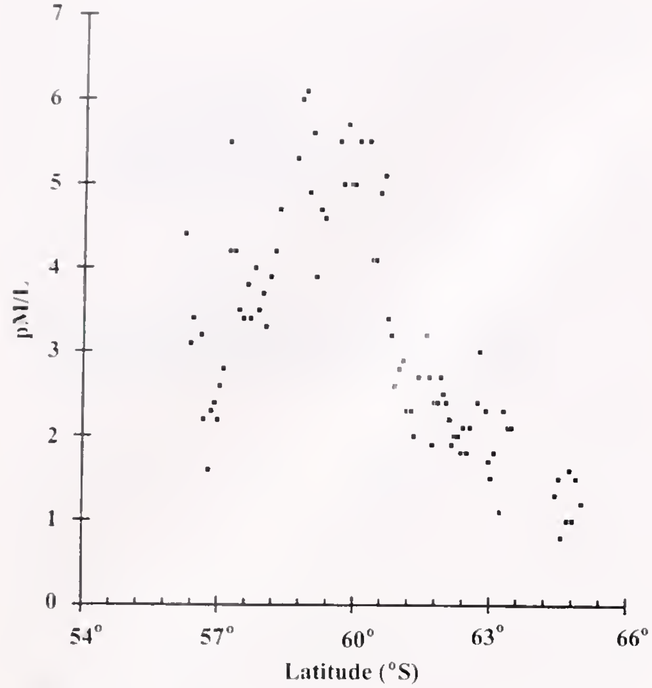

Figure 4. Profile of atmospheric dimethyl sulfide (DMS) measured across the Drake Passage during the RITS cruise, 1993. This profile reflects the polar frontal zone and is an obvious feature in the olfactory landscape. Sampling methods are described elsewhere (Yvon *et al.*, 1996; Bates and Quinn, 1997).

Anderson *et al.*, 1998), and white-chinned petrels (*Procellaria aequinoctialis*, Catard and Weimerskirch, 1998). Black-browed albatrosses, for example, travel thousands of kilometers to forage at distant feeding grounds. These seabirds begin an area-restricted search only upon arrival (Veit and Prince, 1997, also see discussion in Nevitt and Veit, 1999). Optimal foraging models suggest that animals exploiting distant food sources should move rapidly and directly to feeding areas to minimize time spent in transit, and once there, should remain until they have met their energy needs (Charnov, 1976; Stephens and Krebs, 1986). Thus, it may be more efficient in terms of both time and energy to ignore less significant foraging opportunities en route and travel directly to areas of known productivity. Moreover, identifiable odor molecules that are linked to productive areas of ocean are likely to be important cues for a foraging seabird.

Dimethyl Sulfide as a Signal Molecule

Sulfur compounds are abundant in polar waters (Berresheim, 1987; Gibson *et al.*, 1990a, b, 1996; Yang *et al.*, 1992, 1994; Crocker *et al.*, 1995; Turner *et al.*, 1995), and recent experimental evidence suggests that many procellariiforms may use at least one of these compounds—dimethyl sulfide (DMS)—as a foraging cue (Nevitt *et al.*, 1995). Marine DMS is a byproduct of the metabolic decomposition of dimethylsulfoniopropionate (DMSP) in marine phytoplankton (most notably *Phaeocystis pouchetii*). Laboratory studies indicate that this process is dramatically accelerated during grazing by zooplankton (Dacey and Wakeham, 1986; Kellor *et al.*, 1989; Daly and DiTullio, 1996).

DMSP, the biogenic precursor to DMS, is synthesized exclusively by phototrophs (Trossat *et al.*, 1996; Gage *et al.*, 1997; Kocsis *et al.*, 1998). Some marine algae also contain the enzyme DMSP lyase (Nishiguchi and Goff, 1995; de Souza *et al.*, 1996; Stefels and Dijkhuizen, 1996; Steinke *et al.*, 1996, 1998) that cleaves DMSP to form DMS and acrylic acid. In algal blooms dominated by DMSP-containing taxa such as the haptophytes *Emiliania huxleyi* or *Phaeocystis pouchetii*, DMS production is often highest after algal biomass peaks and is associated with bloom decline or senescence (Nguyen *et al.*, 1988; Matrai and Keller, 1993; Gibson *et al.*, 1996; Zimmer-Faust *et al.*, 1996). This pattern is particularly pronounced in polar and subpolar regions where bloom dynamics are highly seasonal, leading to dramatic pulses of DMS production (Crocker *et al.*, 1995) that saturate bacterial DMS consumption (Wolfe *et al.*, in press). This process results in significant DMS release to the atmosphere. Zooplankton grazing also results in DMSP release or DMS production by similar mechanisms. This has been observed for grazers ranging from protozoans (Wolfe *et al.*, 1994; Wolfe and Steinke, 1996) to metazoans such as calanoid copepods (Dacey and Wakeham, 1986; Levasseur *et al.*, 1996; Christaki *et al.*, 1996) or krill (Tokunaga *et al.*, 1977; Daly and DiTullio, 1996). Thus, DMS production is often associated with zooplankton feeding (Leck *et al.*, 1989; Cantin *et al.*, 1996) and may even be used as a measure of grazing rate in some instances (Kwint and Kramer, 1996; Wolfe and Steinke, 1996).

Zooplankton retain algal DMSP and transfer it to higher trophic levels; in fact the breakdown of DMSP to DMS and acrylic acid has been shown to cause odor problems in seafood products (G. Wolfe, California State University, Chico, pers. comm.). In an early study, Sieburth (1959, 1960, and 1961) reported high concentrations of acrylic acid in the gastrointestinal systems of penguins, which depressed their microfloral populations. These seabirds fed on krill containing DMSP from the alga *Phaeocystis*, a dominant taxon in Antarctic waters. Thus, both DMS and acrylic acid are good candidates for chemical signals that operate across temporal and spatial scales, ranging from picoplankton (Bell and Mitchell, 1972; Hauser *et al.*, 1975) to vertebrates.

Because DMS is transferred to the atmosphere, this signal molecule might serve as a guidepost to a seabird trying to locate and exploit zooplankton-rich areas. Mesoscale spatial patterns of DMS production are complex and need to be better quantified, but DMS production has been linked to the presence of krill (Daly and DiTullio, 1996) and to areas where primary productivity is traditionally high (Fig. 4; McTaggart and Burton, 1992). If procellariiform seabirds can detect DMS, then emissions that last for several days present distinct features in the odor landscape that may indicate locations where foraging is likely to be productive (Berresheim, 1987; Nevitt *et al.*, 1995).

Seabirds Can Smell Dimethyl Sulfide

To test seabirds' responses to DMS in the field, experiments from our laboratory have involved presenting seabirds with scented slicks and aerosols. These experiments (Nevitt *et al.*, 1995; Nevitt, 1999b) were conducted at sea near South Georgia Island (54°30′ S, 37°00′ W), a region of the world that supports an extensive assemblage of procellariiform seabirds (Croxall *et al.*, 1984). Seabirds were presented with DMS-scented vegetable oil slicks paired with plain vegetable oil slicks as controls. At some locations, seabirds were presented with slicks scented with cod liver oil, an odor complex known to attract procellariiforms (*e.g.*, Hutchison and Wenzel, 1980). We predicted that if seabirds were attracted to DMS and used it as a foraging cue, then their behavioral response to DMS should mirror their response to cod liver oil.

Results from these slick experiments showed that DMS-scented slicks attracted some species of procellariiforms as much as twice as frequently as control slicks did. The response was also species-specific. Cryptic species including prions (*Pachyptila* sp.), white-chinned petrels (*Procellaria aequinoctialis*), Wilson's storm-petrels (*Oceanites oceanicus*), and black-bellied storm-petrels (*Fregetta tropica*) showed a significant interest in DMS-scented slicks as compared with control slicks, whereas more visible species such as Cape petrels (*Daption capense*) and black-browed, grey-headed, and wandering albatrosses showed no noticeable differences in their responses to the two slicks. Moreover, patterns of recruitment to cod-liver-scented slicks were similar to patterns observed in response to DMS-scented slicks, suggesting that DMS was just as potent as this food-related odor in attracting certain species (see Nevitt, 1999b).

The use of DMS as a foraging cue was tested in a different set of experiments in which we monitored the degree to which individuals zigzagged upwind when presented with scented and unscented aerosols (Nevitt *et al.*, 1995). This behavior had been described previously (Hutchison and Wenzel, 1980), and it presumably directs the seabird to the source of an odor plume—in this case an aerosol delivery system. We predicted that if a seabird were interested in DMS, then it would zigzag more in the presence of a DMS-scented plume than of an unscented aerosol spray, and that this behavior could be measured as a difference in turning rate. Results from experiments supported our previous findings: white-chinned petrels showed a 25% increase in their turning rate when presented with a DMS-scented aerosol. (Note that these seabirds had also displayed a significant attraction to DMS-scented slicks as compared with plain vegetable oil.) Black-browed albatrosses, on the other hand, did not turn any more frequently in response to DMS-scented aerosols than in response to controls, suggesting that these seabirds do not use this specific odor cue to locate prey patches (as in Fig. 2C; note that behaviors represented in Fig. 2A and B were not addressed in this study).

Procellariiforms May Associate with Natural Emissions of Dimethyl Sulfide

To begin to explore whether procellariiforms forage in areas where atmospheric DMS is naturally elevated, we have recently analyzed seabird survey data collected as part of the 1993 Radioactively Important Trace Species (RITS) cruise. The cruise track crossed the Drake Passage to Palmer Station on the Antarctic Peninsula, continued southwest to about 67° S, 140° W, and then headed north to 57° N, 140° W. Sulfur, carbon, and nitrogen gas phase species were measured to quantify their cycling in the surface ocean and to calculate the exchange of these compounds between the ocean and the atmosphere. Methods for sampling atmospheric DMS are described elsewhere (Yvon *et al.*, 1996; Bates and Quinn, 1997).

Seabird observations were performed from 66°S in the Southern Ocean to 30°S in the Pacific Ocean over a period of 11 days. To determine background species compositions, all seabirds within a 100-m box, positioned 100 m off the bow of the ship, were counted using standard methods (Tasker *et al.*, 1984). All observations were conducted in a blind manner, in which the observer was not informed of the local DMS levels. To determine possible correlations between seabird abundance and local concentrations of atmospheric DMS, we examined the percent frequency (per hour) of 24 procellariiform species at low (0–4.0 p*M*/l for atmospheric DMS; 0–1.0 nmol for seawater DMS), medium (4.1–8.0 pM/l; 1.1–2.0 nmol), and high (8.1–12.5 p*M*/l; 2.1–3.0 nmol) concentrations of DMS.

We observed a similar distribution of species at low (Fig. 5A) and medium (Fig. 5B) atmospheric DMS concentrations, but only blue petrels (*Halobaena caerulea*) and prions (*Pachyptila* sp.) were observed when atmospheric DMS levels were highest (Fig. 5C). In addition, blue petrels and prions were most abundant when atmospheric DMS levels were highest (Fig. 6: (A) Kruskal-Wallis test statistic = 16.110, $P < 0.0001$, df = 2 for blue petrels; (B) Kruskal-Wallis test statistic = 12.503, $P = 0.002$, df = 2 for prions. Tests were performed with Dunn-Sidak corrections to avoid Type-I errors). This finding is consistent with results from earlier work indicating enhanced recruitment of prions to DMS in controlled studies (Nevitt *et al.*, 1995; no data are available for blue petrels). As discussed above, DMS production is an indicator of krill grazing (*e.g.*, Daly and DiTullio, 1996), and most prion diets are composed predominantly of crustaceans, including krill, amphipods, and copepods (*e.g.*, Imber, 1981; Prince and Copestake, 1990; Ridoux, 1994; Liddle, 1994; Reid *et al.*, 1997). Similarly,

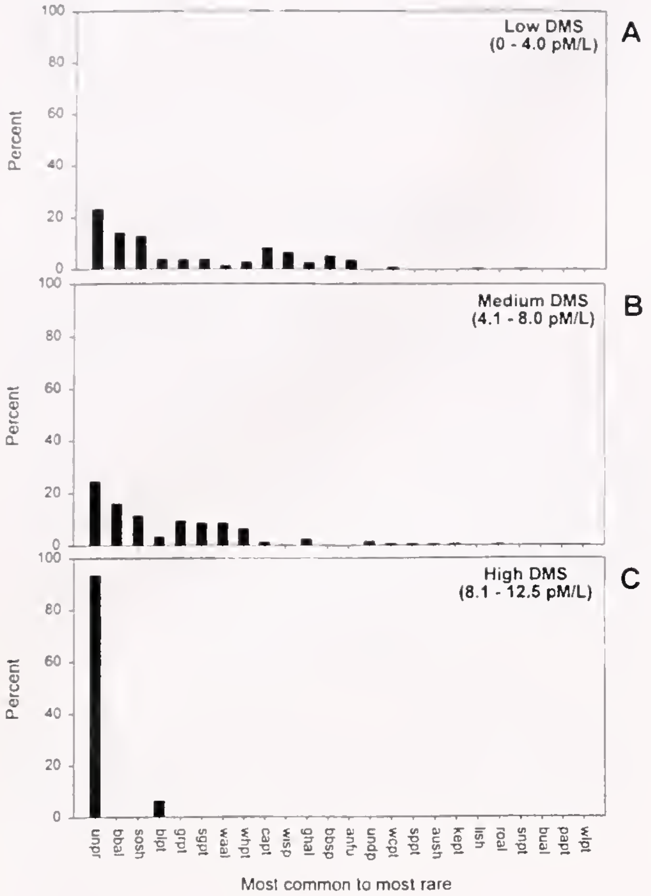

Figure 5. Percent composition of procellariiform seabirds at low (A), medium (B), and high (C) atmospheric concentrations of dimethyl sulfide (DMS). Total number of bird observations was 2860 (low = 620, medium = 682, and high = 1558). Species abbreviations: unpr = unidentified prion (*Pachyptila* sp.); bbal = black-browed albatross (*Thalassarche melanophris*); sosh = sooty shearwater (*Puffinus griseus*); blpt = blue petrel (*Halobaena caerulea*); grpt = grey petrel (*Procellaria cinerea*); sgpt = southern giant petrel (*Macronectes giganteus*); waal = wandering albatross (*Diomedea exulans*); whpt = white-headed petrel (*Pterodroma lessonii*); capt = Cape petrel (*Daption capense*); wisp = Wilson's storm-petrel (*Oceanites oceanicus*); ghal = grey-headed albatross (*Thalassarche chrysostoma*); bbsp = black-bellied storm-petrel (*Fregetta tropica*); anfu = Antarctic fulmar (*Fulmarus glacialoides*); undp = unidentified diving petrel (*Pelecanoides* sp.); wcpt = white-chinned petrel (*Procellaria aequinoctialis*); sppt = soft-plumaged petrel (*Pterodroma mollis*); aush = Audubon's shearwater (*Puffinus lherminieri*); kept = Kerguelen petrel (*Pterodroma brevirostris*); lish = little shearwater (*Puffinus assimilis*); roal = royal albatross (*Diomedea epomophora*); snpt = snow petrel (*Pagodroma nivea*); bual = Buller's albatross (*Thalassarche bulleri*); papt = Parkinson's petrel (*Procellaria parkinsoni*); wlpt = Westland petrel (*Procellaria westlandica*).

crustaceans are the major prey type for blue petrels (Prince, 1980; Steele and Klages, 1986).

This is the first study to show a significant association between a naturally occurring scented compound and a species of foraging procellariiform seabird. The study is preliminary and does not rule out the possibility that other procellariiforms use DMS or other naturally occurring scented compounds as foraging cues—clearly more work needs to be done. But this result is curious because prions use a foraging behavior unique among procellariiforms; whereas most petrels grasp their prey, prions (or "whale birds") can also filter feed, foraging by skimming over the surface of the water. Morphological adaptations for this foraging strategy include a dorsoventrally compressed bill with comb-like lamellae fringing the side of the palate as well as an elastic buccal pouch for holding prey between the rami of the mandibles. Scattered blue petrels frequently associate with prion flocks (Nevitt, pers. obs.) and may cue off the foraging behavior of prions. These seabirds also have serrations on the sides of the upper mandibles, although these lamellae are not developed to the same degree as in prions. Although little information is available about the visual or olfactory acuity of these seabirds, unpublished work examining prion eye structure suggests that they may not be as well adapted for visual foraging as other procellariiforms that have been studied (G. Martin, University of Birmingham, UK, pers. comm.). Whether other adaptations make prions particularly well suited to using olfactory cues to forage needs to be studied in greater detail.

Questions for the Future

Years of effort only begin to scratch the surface of any complex biological problem. But this is an exciting time to be studying the sensory aspects of how seabirds forage,

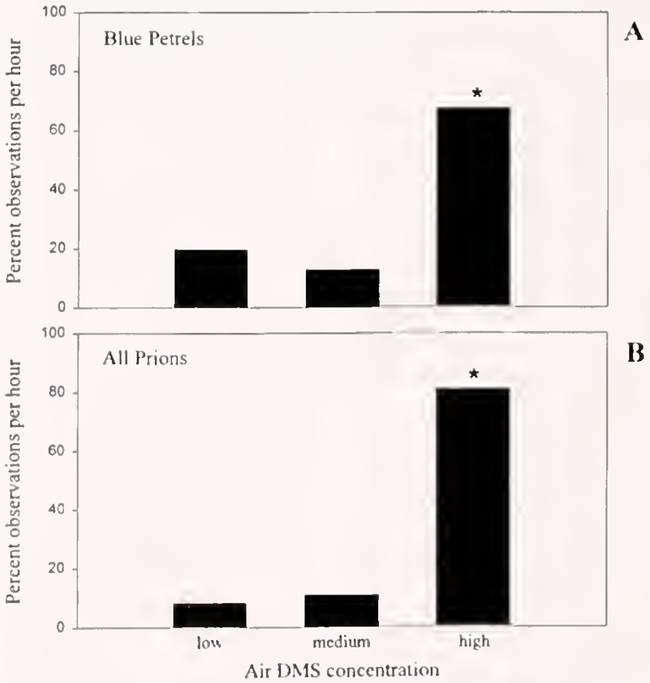

Figure 6. Observations of (A) blue petrels (*Halobaena caerulea*) and (B) prions (*Pachyptila* sp.) at low, medium, and high atmospheric concentrations of dimethyl sulfide (DMS). Significant differences ($P < 0.05$) are indicated (*).

especially since telemetry technology is beginning to allow researchers to address long-standing questions directly from the perspective of a foraging seabird. Since many of these seabirds are large and highly efficient fliers, it is currently possible to instrument them with a variety of devices for monitoring fine-scale behavioral parameters such as turning rate, time spent on the water, and frequency of feeding events (Weimerskirch and Wilson, 1992; Wilson *et al.*, 1995; reviewed by Weimerskirch, 1998). Until recently, most telemetry applications have focused on clarifying basic foraging biology (where do birds go, how frequently do they eat, etc.), rather than on the sensory mechanisms underlying how procellariiforms locate productive feeding areas or prey patches. Potential studies relevant to olfactory foraging include (1) quantifying fine-scale movement patterns while seabirds are en route to foraging areas, (2) identifying whether turning rate changes relative to wind direction once a bird begins an area-restricted search, and (3) identifying how sensory deprivation may influence these and other parameters. As technology improves, it should soon be possible to equip seabirds with sensors that can measure biologically relevant odors in the environment. Such methods will allow researchers to monitor behavioral activity in conjunction with environmental parameters relevant to olfaction.

A second area of study is to examine how different species interact with each other to locate and exploit ephemeral prey resources, and how different sensory adaptations have evolved to shape these interactions. Odors most likely work in conjunction with other cues, particularly visual cues provided by prey as well as by other foraging seabirds or marine mammals. Interspecific behavioral interactions appear to follow consistent trends both at mixed-species feeding aggregations (Harrison *et al.*, 1991) and at experimental olfactory trials performed at sea (Nevitt *et al.*, 1995; Nevitt, 1999a, b). Where procellariiforms forage in mixed-species aggregations, some species dominate these interactions (*e.g.*, giant petrels, which are known to prey upon other petrels) while others (*e.g.*, storm-petrels) tend to avoid them. Different olfactory abilities or adaptations may play a role in defining what foraging strategies different species use in various situations. For example, a heightened sense of smell may give some species a competitive edge in opportunistically locating prey before being displaced by other species (Nevitt, 1999b). This is consistent with our findings that smaller, cryptic species such as prions and storm-petrels responded strongly to DMS-scented slicks whereas larger, more visible species did not. If these storm-petrels, for example, have superior olfactory abilities, they may be able to locate and exploit prey patches before larger species arrive. In addition, since they are cryptic, they may be more difficult for potential competitors to spot. This type of interspecific interaction has also been observed between turkey vultures (*Cathartes aura*) and black vultures (*Coragyps atratus*). Where these species co-occur, turkey vultures are able to find prey more quickly using a well-developed sense of smell. In this case, the smaller black vultures search visually for the larger turkey vultures and then displace them from their find (Buckley, 1997).

Finally, one of the most complex and difficult challenges continues to be identifying and measuring scented compounds associated with natural distributions of prey. Knowing which odors different species can physiologically detect and use as foraging cues will enhance our understanding of species-specific foraging strategies, distribution, and behavior. This information will give us the ability to develop and apply models of olfactory foraging on a broader scale to better understand how odors emitted by prey might extend the range at which a prey patch would be detected by a foraging seabird. Such a framework will be critical in exploring how changes in prey distribution and density might affect the foraging success of procellariiforms.

Acknowledgments

I thank Tim Bates and Beverly Agler for providing technical assistance in the field. Thanks also to the crew and scientific support staff of the R/V *Surveyor*. Lisa Holsinger and Victoria Zvonkina assisted with data entry and analysis. I am grateful to Kate Clark for proofreading and for technical assistance in constructing several figures and to Gordon Wolfe for his invaluable contribution to the DMS discussion. The comments of Peter Hodum, Jason Watters, and Kate Clark improved earlier versions of this paper. Finally, I am indebted to Richard Zimmer for his vision in organizing this symposium and for inviting me to submit this manuscript.

Literature Cited

Ainley, D. G., E. F. O'Connor, and R. J. Boekelheide. 1984. The marine ecology of the birds in the Ross Sea, Antarctica. *Ornithol. Monogr.* **32:** 1–97.

Anderson, D. J., A. J. Schwandt, and H. D. Douglas. 1998. Foraging ranges of Waved Albatrosses in the eastern Tropical Pacific Ocean. Pp. 180–185 in *Albatross Biology and Conservation*, G. Robertson and R. Gales, eds. Surrey Beatty, Sydney, Australia.

Bang, B. G. 1965. Anatomical adaptations for olfaction in the snow petrel. *Nature* **205:** 513–515.

Bang, B. G. 1966. The olfactory apparatus of tube-nosed birds (Procellariiformes). *Acta Anat.* **65:** 391–415.

Bates, T. S., and P. K. Quinn. 1997. Dimethyl sulfide (DMS) in the equatorial Pacific Ocean (1982 to 1996): evidence of a climate feedback? *Geophys. Res. Letters* **24:** 861–864.

Bell, W., and R. Mitchell. 1972. Chemotactic and growth responses of marine bacteria to algal extracellular products. *Biol. Bull.* **143:** 265–277.

Berresheim, H. 1987. Biogenic sulfur emissions from the subantarctic and Antarctic oceans. *J. Geophys. Res.* **92:** 13,245–13,262.

Buckley, N. J. 1997. Experimental tests of the information-center hypothesis with black vultures (*Coragyps atratus*) and turkey vultures (*Cathartes aura*). *Behav. Ecol. Sociobiol.* **41:** 267–279.

Cantin, G., M. Levasseur, M. Gosselin, and S. Michaud. 1996. Role of zooplankton in the mesoscale distribution of surface dimethyl sulfide concentrations in the Gulf of St. Lawrence, Canada. *Mar. Ecol. Prog. Ser.* **141:** 103–117.

Catard, A., and H. Weimerskirch. 1998. Satellite tracking of petrels and albatrosses: from the tropics to Antarctica. *Ostrich* **69:** 152.

Charnov, E. L. 1976. Optimal foraging, the marginal value theorem. *Theor. Popul. Biol.* **9:** 129–136.

Cherel, Y., and H. Weimerskirch. 1995. Seabirds as indicators of marine resources: black-browed albatrosses feeding on ommastrephid squids in Kerguelen waters. *Mar. Ecol. Prog. Ser.* **129:** 295–300.

Christaki, U., S. Belviso, J. R. Dolan, and M. Corn. 1996. Assessment of the role of copepods and ciliates in the release to solution of particulate DMSP. *Mar. Ecol. Prog. Ser.* **141:** 119–127.

Clark, L., and P. S. Shah. 1992. Information content of odor plumes: what do Leach's storm-petrels know? Pp. 421–427 in *Chemical Signals in Vertebrates VI,* R. L. Doty and D. Müller-Schwarze, eds. Plenum Press, New York.

Crocker, K. M., M. E. Ondrusek, R. L. Petty, and R. C. Smith. 1995. Dimethyl sulfide, algal pigments and light in an Antarctic *Phaeocystis* sp. bloom. *Mar. Biol.* **124:** 335–340.

Croxall, J. P., and P. A. Prince. 1994. Dead or alive, night or day: how do albatrosses catch squid? *Antarct. Sci.* **6:** 155–162.

Croxall, J. P., P. A. Prince, I. Hunter, S. J. McInnes, and P. G. Copestake. 1984. The seabirds of the Antarctic Peninsula, islands of the Scotia Sea, and Antarctic continent between 80°W and 20°W: their status and conservation. Pp. 637–666 in *Status and Conservation of the World's Seabirds,* J. P. Croxall, P. G. H. Evans, and R. W. Schreiber, eds. ICBP, Cambridge, United Kingdom.

Dacey, J. W. H., and S. G. Wakeham. 1986. Oceanic dimethyl sulfide: production during zooplankton grazing on phytoplankton. *Science* **233:** 1314–1316.

Daly, K. L., and G. R. DiTullio. 1996. Particulate dimethylsulfoniopropionate removal and dimethyl sulfide production by zooplankton in the Southern Ocean. Pp. 223–238 in *Biological and Environmental Chemistry of DMSP and Related Sulfonium Compounds.* R. P. Kiene, P. T. Visscher, M. D. Kellor, and G. O. Kirst, eds. Plenum Press, New York.

de Souza, M. P., Y. P. Chen, and D. C. Yoch. 1996. Dimethylsulfoniopropionate lyase from the macroalga *Ulva curvata:* purification and characterization of the enzyme. *Planta* **199:** 433–438.

Dusenbery, D. B. 1992. *Sensory Ecology.* W. H. Freeman, New York. 558 pp.

Gage, D. A., D. Rhodes, K. D. Nolte, W. A. Hicks, T. Leustek, A. J. L. Cooper, and A. D. Hanson. 1997. A new route for synthesis of dimethylsulphoniopropionate in marine algae. *Nature* **387:** 891–894.

Gibson, J. A. E., R. C. Garrick, H. R. Burton, and A. R. McTaggart. 1990a. Dimethyl sulfide and the alga *Phaeocystis pouchetii* in Antarctic coastal waters. *Mar. Biol.* **104:** 339–346.

Gibson, J. A. E., R. C. Garrick, H. R. Burton, and A. R. McTaggart. 1990b. Dimethyl sulfide levels in the ocean close to the Antarctic continent. *Geomicrobiol. J.* **6:** 179–184

Gibson, J. A. E., K. M. Swadling, and H. R. Burton. 1996. Acrylate and dimethyl sulfoniopropionate (DMSP) concentrations during an Antarctic phytoplankton bloom. Pp. 213–222 in *Biological and Environmental Chemistry of DMSP and Related Sulfonium Compounds,* R. P. Kiene, P. Visscher, G. Kirstand, and M. Keller, eds. Plenum Press, New York.

Grubb, T. C., Jr. 1972. Smell and foraging in shearwaters and petrels. *Nature* **327:** 404–405.

Harrison, N. M., M. J. Whitehouse, D. Heinemann, P. A. Prince, G. L. Hunt Jr., and R. R. Veit. 1991. Observations of multi-species feeding flocks around South Georgia. *Auk* **108:** 801–810.

Hasler, A. D., and A. T. Scholz. 1983. *Olfactory Imprinting and Homing in Salmon.* Springer-Verlag, New York. 134 pp.

Hauser, D. C. R., M. Levandowsky, S. H. Hunter, L. Chunosoff, and J. S. Hollwitz. 1975. Chemosensory responses by the heterotrophic marine dinoflagellate *Crypthecodinium cohnii. Microb. Ecol.* **1:** 246–254.

Hutchison, L. V., and B. M. Wenzel. 1980. Olfactory guidance in foraging by procellariiforms. *Condor* **82:** 314–319.

Imber, M. J. 1981. Diets of storm petrels *Pelagodroma* and *Garrodia* and of prions *Pachyptila* (Procellariiformes). Pp. 63–88 in *Proceedings of the Symposium on Birds of the Sea and Shore,* J. Cooper, ed. African Seabird Group, Cape Town, South Africa.

Jouventin, P., and H. Weimerskirch. 1990. Satellite tracking of wandering albatrosses. *Nature* **343:** 746–748.

Kellor, M. D., W. K. Bellows, and R. R. Guillard. 1989. Dimethyl sulphide production in marine phytoplankton. Pp. 167–182 in *Biogenic Sulfur in the Environment.* E. S. Saltzman and W. J. Cooper, eds. American Chemical Society, Washington, DC.

Kocsis, M. G., K. D. Nolte, D. Rhodes, T.-L. Shen, D. A. Gage, and A. D. Hanson. 1998. Dimethylsulfoniopropionate biosynthesis in *Spartina alterniflora. Plant Physiol.* **117:** 273–281.

Kwint, R. L. J., and K. M. Kramer. 1996. A new sensitive tracer for the determination of zooplankton grazing activity. *J. Plankton Res.* **18:** 1513–1518.

Leck, C., U. Larsson, L. E. Bagander, S. Johansson, and S. Hajdu. 1989. DMS in the Baltic Sea—annual variability in relation to biological activity. *J. Geophys. Res.* **95:** 3353–3363.

Lequette, B., C. Verheyden, and P. Jouventin. 1989. Olfaction in sub-Antarctic seabirds: its phylogenetic and ecological significance. *Condor* **91:** 732–735.

Levasseur, M., S. Michaud, J. Egge, G. Cantin, J. C. Nejstgaard, R. Sanders, E. Fernandez, P. T. Solberg, B. Heimdal, and M. Gosselin. 1996. Production of DMSP and DMS during a mesocosm study of an *Emiliania huxleyi* bloom: influence of bacteria and *Calanus finmarchicus* grazing. *Mar. Biol.* **126:** 609–618.

Liddle, G. M. 1994. Interannual variation in the breeding biology of the Antarctic prion *Pachyptila desolata* at Bird Island, South Georgia. *J. Zool. Lond.* **234:** 125–139.

Lohmann, K. J. 1992. How sea turtles navigate. *Sci. Am.* **266:** 82–88.

Matrai, P. A., and M. D. Keller. 1993. Dimethyl sulfide in a large-scale coccolithophore bloom in the Gulf of Maine. *Continental Shelf Res.* **13:** 831–843.

McTaggart, A. R., and H. Burton. 1992. Dimethyl sulfide concentrations in the surface waters of the Australasian Antarctic and Subantarctic oceans during an austral summer. *J. Geophys. Res.* **97:** 14,407–14,412.

Nevitt, G. 1999a. Foraging by seabirds on an olfactory landscape. *Am. Sci.* **87:** 46–53.

Nevitt, G. 1999b. Olfactory foraging in Antarctic seabirds: a species-specific attraction to krill odors. *Mar. Ecol. Prog. Ser.* **177:** 235–241.

Nevitt, G., and A. Dittman. 1998. A new model for olfactory imprinting in salmon. *Integr. Biol.* **1:** 215–223.

Nevitt, G. A., and R. R. Veit. 1999. Mechanisms of prey patch detection by foraging seabirds. Pp. 2072–2082 in *Proceedings of the 22nd International Ornithological Congress,* N. J. Adams and R. H. Slotow, eds. BirdLife South Africa, Johannesburg.

Nevitt, G. A., R. R. Veit, and P. M. Kareiva. 1995. Dimethyl sulphide as a foraging cue for Antarctic Procellariiform seabirds. *Nature* **376:** 680–682.

Nguyen, B. C., S. Belviso, N. Mihalopoulos, J. Gostan, and P. Nival. 1988. Dimethyl sulfide production during natural phytoplankton blooms. *Mar. Chem.* **24:** 133–141.

Nishiguchi, M. K., and L. J. Goff. 1995. Isolation, purification, and characterization of DMSP lyase (dimethylpropiothetindethiomethylase (4.4.1.3)) from the red alga *Polysiphonia paniculata. J. Phycol.* **31:** 564–574.

Papi, F., L. Fiore, V. Fiachi, and S. Benvenuti. 1972. Olfaction and homing pigeons. *Monitore Zool. Ital.* **6:** 85–95.

Pennycuick, C. J. 1982. The flight of petrels and albatrosses (Procellariiformes), observed in South Georgia and its vicinity. *Philos. Trans. R. Soc. Lond.* **B300:** 75–106.

Pennycuick, C. J. 1987. Flight of seabirds. Pp. 43–62 in *Seabirds: Feeding Biology and Role in Marine Ecosystems*, J. P. Croxall, ed. Cambridge University Press, Cambridge.

Prince, P. A. 1980. The food and feeding ecology of blue petrel (*Halobaena caerulea*) and dove prion (*Pachyptila desolata*). *J. Zool. Lond.* **190:** 59–76.

Prince, P. A., and P. G. Copestake. 1990. Diet and aspects of Fairy Prions breeding at South Georgia. *Notornis* **37:** 59–69.

Prince, P. A., and R. A. Morgan. 1987. Diet and feeding ecology of Procellariiformes. Pp. 135–171 in *Seabirds: Feeding Ecology and Role in Marine Ecosystems*, J. P. Croxall, ed. Cambridge University Press, Cambridge.

Prince, P. A., J. P. Croxall, P. N. Trathan, and A. G. Wood. 1998. The pelagic distribution of South Georgia albatrosses and their relationships with fisheries. Pp. 137–167 in *Albatross Biology and Conservation*, G. Robertson and R. Gales, eds. Surrey Beatty, Sydney, Australia.

Reid, K., J. P. Croxall, and T. M. Edwards. 1997. Interannual variation in the diet of the Antarctic Prion *Pachyptila desolata* at South Georgia. *Emu* **97:** 126–132.

Ridoux, V. 1994. The diets and dietary segregation of seabirds at the subantarctic Crozet Islands. *Mar. Ornithol.* **22:** 1–192.

Rodhouse, P. G., M. R. Clarke, and A. W. A. Murray. 1987. Cephalopod prey of the Wandering Albatross *Diomedea exulans*. *Mar. Biol.* **91:** 1–10.

Sagar, P. M., and H. Weimerskirch. 1996. Satellite tracking of Southern Buller's Albatrosses from the Snares, New Zealand. *Condor* **98:** 649–652.

Sieburth, J. M. 1959. Antibacterial activity of Antarctic marine phytoplankton. *Limnol. Oceanogr.* **4:** 419–424.

Sieburth, J. M. 1960. Acrylic acid, an "antibiotic" principle in *Phaeocystis* blooms in Antarctic waters. *Science* **132:** 676–677.

Sieburth, J. M. 1961. Gastrointestinal microflora of Antarctic birds. *J. Bacteriol.* **77:** 521–531.

Steele, W. K., and N. T. Klages. 1986. Diet of the blue petrel at sub-Antarctic Marion Island. *S. Afr. J. Zool.* **21:** 252–256.

Stefels, J., and L. Dijkhuizen. 1996. Characteristics of DMSP-lyase in *Phaeocystis* sp. (Prymnesiophyceae). *Mar. Ecol. Prog. Ser.* **131:** 307–313.

Steinke, M., C. Daniel, and G. O. Kirst. 1996. DMSP lyase in marine macro- and microalgae: intraspecific differences in cleavage activity. Pp. 317–324 in *Biological and Environmental Chemistry of DMSP and Related Sulfonium Compounds*, R. P. Kiene, P. Visscher, G. Kirst, and M. Keller, eds. Plenum Press, New York.

Steinke, M., G. V. Wolfe, and G. O. Kirst. 1998. Partial characterization of dimethyl sulfoniopropionate (DMSP) lyase in 6 strains of *Emiliania huxleyi*. *Mar. Ecol. Prog. Ser.* **175:** 215–225.

Stephens, D. W., and Krebs, J. R. 1986. *Foraging Theory*. Princeton University Press, Princeton. 247 pp.

Tasker, M. L., P. H. Jones, T. Dixon, and B. F. Blake. 1984. Counting seabirds at sea from ships: a review of the methods employed and suggestions for a standardized approach. *Auk* **101:** 567–577.

Tokunaga, T., H. Iida, and K. Nakamura. 1977. Formation of dimethyl sulfide in Antarctic krill, *Euphausia superba*. *Bull. Jpn. Soc. Sci. Fish.* **43:** 1209–1217.

Trossat, C., K. D. Nolte, and A. D. Hanson. 1996. Evidence that the pathway of dimethylsulfoniopropionate biosynthesis begins in the cytosol and ends in the chloroplast. *Plant Physiol.* **111:** 965–973.

Turner, S. M., P. D. Nightingale, W. Broadgate, and P. S. Liss. 1995. The distribution of dimethyl sulphide and dimethylsulphoniopropionate in Antarctic waters and sea ice. *Deep Sea Res.* **42:** 1059–1080.

Veit, R. R., and P. A. Prince. 1997. Individual and population level dispersal of Black-browed and Grey-headed Albatrosses in response to Antarctic krill. *Ardea* **85:** 129–134.

Waldvogel, J. A. 1987. Olfactory navigation in homing pigeons: are the current models atmospherically realistic? *Auk* **104:** 369–379.

Wallraff, H. G. 1981. The olfactory component of pigeon navigation: steps of analysis. *J. Comp. Physiol.* **143:** 411–422.

Warham, J. 1990. *The Petrels: Their Ecology and Breeding Systems*. Academic Press, New York. 440 pp.

Weimerskirch, H. 1998. Foraging strategies of southern albatrosses and their relationship with fisheries. Pp. 168–179 in *Albatross Biology and Conservation*, G. Robertson and R. Gales, eds. Surrey Beatty, Sydney, Australia.

Weimerskirch, H., and G. Robertson. 1994. Satellite tracking of light-mantled sooty albatrosses. *Polar Biol.* **14:** 123–126.

Weimerskirch, H., and R. P. Wilson. 1992. When do wandering albatrosses *Diomedea exulans* forage? *Mar. Ecol. Prog. Ser.* **86:** 297–300.

Weimerskirch, H., P. Jouventin, and J. C. Stahl. 1986. Comparative ecology of the six albatross species breeding on the Crozet Islands. *Ibis* **128:** 195–213.

Weimerskirch, H., M. Salamolard, F. Sarrazin, and P. Jouventin. 1993. Foraging strategy of Wandering Albatrosses through the breeding season: a study using satellite telemetry. *Auk* **110:** 325–342.

Weimerskirch, H., C. P. Doncaster, and F. Cuénot-Chaillet. 1994. Pelagic seabirds and the marine environment: foraging patterns of wandering albatrosses in relation to prey availability and distribution. *Proc. R. Soc. Lond. Ser. B* **255:** 91–97.

Wilson, R. P., H. Weimerskirch, and P. Lys. 1995. A device for measuring seabird activity at sea. *J. Avian Biol.* **26:** 172–176.

Wolfe, G. V., and M. Steinke. 1996. Grazing-activated production of dimethyl sulfide (DMS) by two clones of *Emiliania huxleyi*. *Limnol. Oceanogr.* **41: 1151–1160.**

Wolfe, G. V., E. B. Sherr, and B. S. Sherr. 1994. Release and consumption of DMSP from *Emiliania huxleyi* during grazing by *Oxyrrhis marina*. *Mar. Ecol. Prog. Ser.* **111:** 111–119.

Wolfe, G. V., M. Levasseur, G. Cantin, and S. Michaud. In press. Microbial production and consumption of dimethyl sulfide (DMS) in the Labrador Sea. *Aquat. Microb. Ecol.*

Yang, H., A. R. McTaggart, A. T. Davidson, and H. Burton. 1992. Natural productivity of acrylic acid and dimethyl sulphide during a summer bloom of *Phaeocystis pouchetii* in Antarctic coastal water. *Antarct. Res.* **3:** 26–43.

Yang, H., A. R. McTaggart, A. T. Davidson, and H. Burton. 1994. Measurement of acrylic acid and dimethyl sulfide in Antarctic coastal water during a summer bloom of *Phaeocystis pouchetii*. Proc. MIPR Symp. *Polar Biol.* **7:** 43–52.

Yvon, S. A., E. S. Saltzman, D. J. Cooper, T. S. Bates, and A. M. Thompson. 1996. Atmospheric sulfur cycling in the tropical Pacific marine boundary layer (12°S, 135°W): a comparison of field data and model results. 1. Dimethylsulfide. *J. Geophys. Res.* **101:** 6899–6909.

Zimmer-Faust, R. K., M. P. de Souza, and D. C. Yoch. 1996. Bacterial chemotaxis and its potential role in marine dimethylsulfide production and biogeochemical sulfur cycling. *Limnol. Oceanogr.* **41:** 1330–1334.

Reference: *Biol. Bull.* **198:** 254–260. (April 2000)

Endolithic Fungi in Reef-Building Corals (Order: Scleractinia) Are Common, Cosmopolitan, and Potentially Pathogenic

CHRISTOPHER J. BENTIS*, LES KAUFMAN, AND STJEPKO GOLUBIC

Boston University Marine Program (B.U.M.P.), Biological Research Building, Boston University,
5 Cummington Street, Boston, Massachusetts 02215

Reef-building corals appear to exist in dynamic equilibria with four principal partners: interconnected polyps of a colonial coelenterate, endosymbiotic dinoflagellate zooxanthellae residing in the host's endoderm, endolithic algae that penetrate coral skeletons, and endolithic fungi that attack both endolithic algae and the polyps. Although reports of fungal and algal-like endoliths in corals date back almost 150 years (1) and evidence of a fossil history extends as far back as the Upper Devonian (~370 ma) (2), most attention has been paid to the structure (3), function (4, 5), and diversity (6) of the coral-zooxanthellae interactions, ignoring the endolithic members of the consortium. Recently, Le Campion-Alsumard et al. *(1995) (7, 8) described an interrelationship between endolithic algae and fungi within the massive coral* Porites lobata *Dana 1846 (Poritidae), on Moorea island near Tahiti, French Polynesia. Fungi were also found to penetrate the most recently deposited skeletal material and to be associated with pearl-like skeletal deposits formed by polyps of* P. lobata *in response to attack by their heterotrophic, endolithic symbionts. Here we extend these observations to the pocilloporid coral* Pocillopora eydouxi *and to the acroporid corals* Acropora cytherea, Acropora humulis, *and* Montipora cf. studeri, *collected at Johnston Atoll, central Pacific Ocean. Our observations suggest that direct coral-fungal interaction is widespread, not only geographically, but taxonomically as well. Thus, fungal endoliths, acting as opportunistic pathogens, may play a greater role in the ecology of coral reef systems than previously recognized.*

The oligophotic, siphonal green alga *Ostreobium quekettii* is ubiquitous in skeletons of live corals (9, 10). It is also common in other carbonate substrates, including dead shells and limestone, down to a depth of 300 m in clear waters of the Bahamas (11). Two other phototrophic organisms were reported from skeletons of live corals, the filamentous cyanobacterium *Plectonema terebrans* and conchocelis stages of bangiacean rhodophytes (12). Endolithic fungi in coral skeletons are equally common. They penetrate the corallum (euendolithic) and are often intermingled with endolithic algae, frequently parasitizing the latter (7). Fungi attack algal filaments by specialized hyphal branches, or haustoria, and often continue to grow inside algal filaments. Dense populations of algal and fungal endoliths have been associated with black-stained bands in specimens of *P. lobata* (13).

Although skeletons of dead corals are bored by a variety of endolithic microorganisms, there has been no evidence that endoliths can penetrate the layer of tissue that covers living coral surfaces, leading to the conclusion that infestation by a limited number of specialized endoliths occurs early in the life of a coral, and that endolithic algae and fungi continue to grow in parallel with the accretion of the corallum (8). Most filaments of *O. quekettii* and endolithic fungi extend in the direction of the axes of skeletal growth. In *P. lobata*, borings were detected in newly deposited skeletal spines (pali), demonstrating that the endoliths are able to keep up with the rates of skeletal accretion (7, fig. 2). The pearl-like skeletal deposits are always associated with fungal attacks during the residence of polyps in actively growing calicies. The polyps encapsulate the advancing hypha into dense repair aragonite, forming a distinct skeletal structure referred to as a "cone" (7).

The present study has two main objectives: to determine whether the relationship exhibited between *P. lobata* and endolithic fungi as described from the island of Moorea, in

Received 7 July 1999; accepted 29 November 1999.

*To whom correspondence should be addressed. E-mail: cbentis@bu.edu

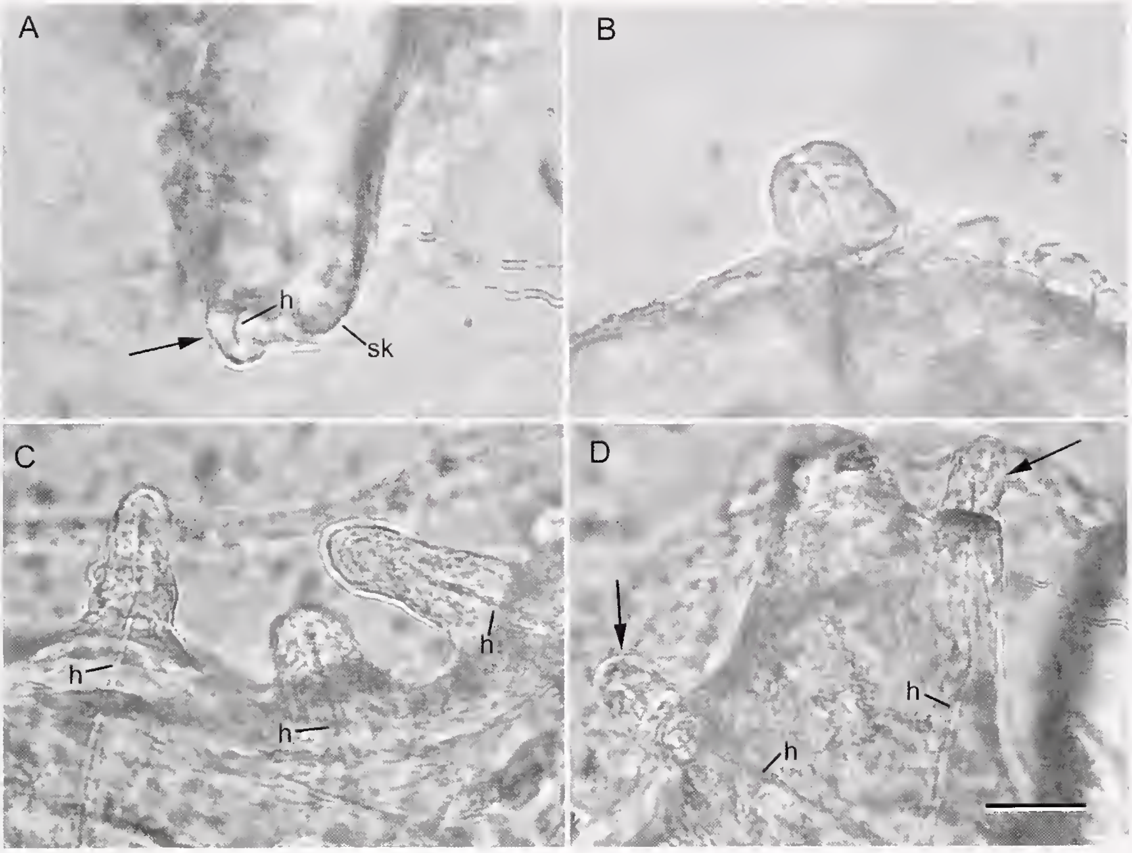

Figure 1. Conical protuberances encapsulating endolithic fungi. (A) *Acropora cytherea*. Cone (arrow) deposited around fungal hypha (h) on skeletal surface (sk) at tip of axial septum. (B) *A. cytherea*. Cone, composed of layers of repair aragonite encasing a fungal hypha on corallite wall. (C) *Pocillopora eydouxi*. Cluster of three cones. Note tracks of fungal hyphae (h) approaching corallum surface, at base of cones. (D) *P. eydouxi*. Side view of skeletal spine (see Fig. 2C) penetrated by endolithic fungal hyphae (h). Hyphae interact with adjacent coral tissue and initiate external deposition of repair aragonite by the coral polyp, resulting in the formation of cones (arrows). Transmitted light photomicrographs; scale bar = 10 μm.

Samples of *A. cytherea* and *P. eydouxi* were collected at Johnston Atoll (16°44′N; 169°32′W) in February and June 1999, respectively. Petrographic thin sections were prepared according to the modified method of Golubic *et al.* (29). Samples were fixed in the field in either 2.5% glutaraldehyde (0.1 *M* cacodylate buffer, pH 8.0), or 2.5% formaldehyde, dehydrated in a graded acetone series, embedded in SPURRS low-viscosity resin (Polysciences, Inc., Warrington, PA) and cured at 70°C for 8 h. Thin sections were observed on an Olympus BX60 light microscope connected to a Sony CCD-IRIS/RGB (Hyper HAD) color video camera. Images were digitized using a personal computer equipped with an Integral Technologies, Inc. "Flashpoint 128" frame capture board, and analyzed with Image-Pro Plus 4.0.1 (Media Cybernetics, Inc.) software.

the eastern Pacific (7), and Mayotte, in the western Indian Ocean (13) exists in other corals, and if so, whether endolithic microboring fungi are able to keep pace with skeletal accretion rates and to interact with corals that exhibit rapid axial growth. The corals selected for study were *Pocillopora eydouxi* and *Acropora cytherea*. At Johnston Atoll, the mean (± SD) annual growth rates of these corals (50.4 mm y^{-1} ± 13.4, $n = 16$; and 93.21mm y^{-1} ± 31.8, $n = 21$) are about 5 and 10 times that of *P. lobata* (13.1 mm y^{-1} ± no data, $n = 12$), respectively (14). Distribution of endoliths and coral-fungal interactions were also investigated on selected specimens of *Montipora* cf. *studeri* and *Acropora humulis*. Ultimately, the purpose of our study was to determine whether endolithic fungi interact with corals on a broader taxonomic scale than previously recognized, and thus pose a potential threat to entire coral reef ecosystems.

Examination of *A. cytherea* and *P. eydouxi* in petrographic thin sections revealed the presence of algal and fungal endoliths, as well as the presence of cone-like protrusions on the surface of the corallum in both species. Conical structures were observed on walls and on septa of both axial and radial corallites in *A. cytherea* (Fig. 1A, B) and on walls, septa, and spines of corallites in *P. eydouxi* (Figs. 1C, D; 2C, D). Fungal-coral interactions (cones) occurred regularly at the growth front of the colony in each of these species (Fig. 1A, D). Cones were not evenly dis-

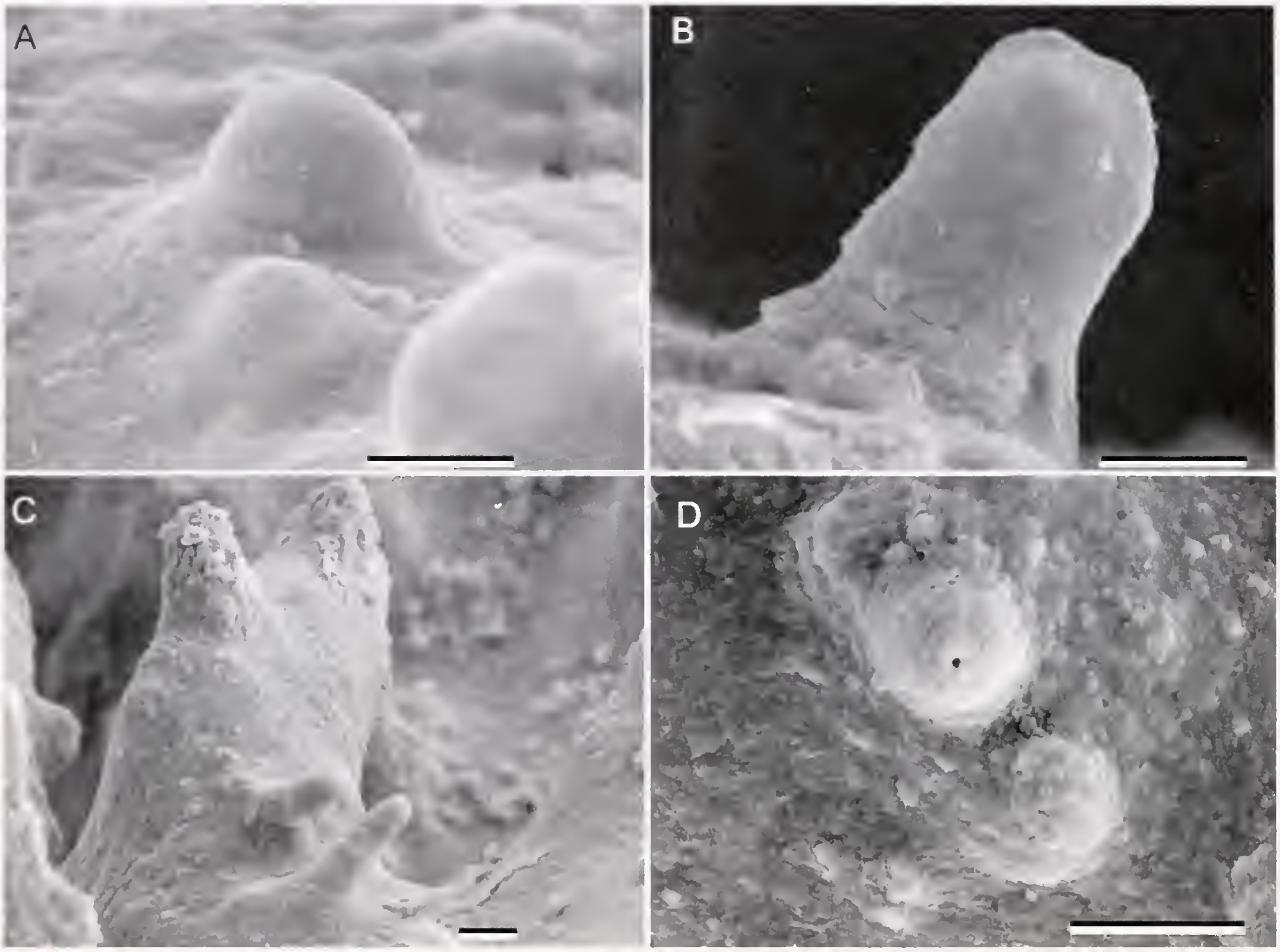

Figure 2. Conical defense structures. (A, B) *Montipora* cf. *studeri*. Cluster of cones and a large solitary cone. Sample was collected in May 1998 at Johnston Atoll, air-dried, and sputter coated with gold-paladium. (C) *Pocillopora eydouxi*. Skeletal spine with two elongated, nonperforated cones protruding from corallum surface near base of spike. Cone-like structures at top of spike were observed regularly and cannot be confirmed as defense structures from this preparation. (D) *P. eydouxi*. Top view of cone on wall of superficial corallite perforated by endolithic fungal hypha. Bore hole clearly visible at apex of cone. Note neighboring nonperforated cone (below right). Specimen treated with 5.25% sodium hypochlorite (Clorox) to remove organic matter, then sputter coated with gold-paladium. Scanning electron micrographs; scale bars = 10 μm.

tributed on the surface of the corallum: they occurred either singly (Figs. 1A, B, D; 2B) or in clusters of several neighboring cones (Figs. 1C; 2A, C, D). Cones observed in this study were similar in both shape and size (Table 1) to those described for *P. lobata* (*cf.* 7). Each cone was penetrated by an axially positioned, unbranched fungal hypha (Fig. 1A-D). As the polyp responded by producing the cone, the hypha continued to penetrate along the axis of the defense structure (Fig. 1). The polyp combated the continued penetration of the hypha by accreting subsequent layers of repair aragonite. In superficial regions of the colonies examined, where live coral tissue had been actively accreting skeletal carbonate immediately prior to collection, nearly every cone remained sealed (Fig. 2C). Only four of the cones observed in superficial corallites were perforated at their vertices (Fig. 2D), marking a possible successful breach of a corallite during the residence of its polyp. At present, the effect of the invading hypha on the penetrated coral tissue is unknown.

Hyphae of the endolithic fungi were observed to run just below the skeletal surface and to branch frequently, with branches directed toward the surface of the corallum (Fig. 3). Diameters of boring tunnels left in the skeleton by endolithic fungi, including those tunnels observed within cones, fell well within the range of those reported from *P. lobata* (Table 1).

In addition to attempting to penetrate occupied corallites, endolithic fungi were observed to attack filaments of the endolithic alga *O. quekettii* (Fig. 4), which was present in all corals under study. Haustorial attachments of fungal hyphae

Table I

Dimensions of microbial endoliths and conical defense structures; all units are in micrometers (μm); values in parentheses represent the standard deviation and are followed by the number of observations (n)

Measurement	*Acropora cytherea*	*Acropora humulis*	*Montipora* cf. *studeri*	*Porites eydouxi*	*Porites lobata**
Cone height	6.71 (±0.31), *n* = 76	11.22 (±4.09), *n* = 16	15.47 (±3.16), *n* = 6	27.01 (±10.81), *n* = 59	10.73 (±3.28), *n* = 26
Cone width	12.73 (±0.48), *n* = 76	18.14 (±4.10), *n* = 16	19.07 (±2.80), *n* = 6	13.88 (±2.69), *n* = 59	10.80 (±2.0), *n* = 55
Max/min cone height	17.82/2.32	21.81/6.60	29.63/7.4	59.98/9.57	20/no data
Max/min cone width	30.08/7.4	20.67/12.35	29.39/12.41	22.38/10.18	20.07/7.0
Fungal diameter	1.43 (±0.53), *n* = 80	1.52 (±0.28), *n* = 61	1.32 (±0.30), *n* = 21	1.20 (±0.20), *n* = 25	1.48 (±0.27), *n* = 49
Max/min fungal diameter	4.12/0.32	2.36/.7	1.68/.39	1.66/.77	2.5/1
Algal diameter	3.86 (±1.0), *n* = 12	10.84 (±2.95), *n* = 10	4.25 (±0.80), *n* = 80	4.59 (±1.08), *n* = 25	5.93 (±1.28), *n* = 37
Max/min algal diameter	5.76/2.67	14.35/4.32	5.91/2.72	7.00/2.83	3.5/10

* Data for *P. lobata* from reference 7.

to algal filaments were also similar to those observed in *Porites lutea* and *P. lobata* (7, 13). However, since we could not determine whether the filaments of *O. quekettii* were alive at the time of fungal attachment, the nature of this relationship (*i.e.*, saprophytic or parasitic) could not be resolved.

In fractured samples of *M.* cf. *studeri*, a macroscopically visible green band was observed extending parallel to the basal plate about 2 cm below the growing coral surface. Examination of scanning electron micrographs of resin-cast preparations revealed that the green band contained both algal and fungal filaments (Fig. 5). Some of the filaments in the lower part of the green band exited the corallum and spanned pore spaces. These filaments, which inhabited internal spaces in the corallum, were calcified (*cf.* 15) (Fig. 6). They should be described as cryptoendolithic rather than euendolithic, the latter referring only to filaments that penetrate through the carbonate of the corallum (*cf.* 16) (Fig. 5). No internal green banding and no cryptoendolithic filaments were detected in the other corals under study. The absence of green banding in skeletons of the faster growing species examined, despite the confirmed presence of endolithic algae, is consistent with the proposed mechanism of band formation, which predicts that green bands form during periods of reduced skeletal accretion rates (8).

The results presented here establish that the relationship between hermatypic corals and endolithic fungi, previously documented for *P. lobata* (7, 13), also occurs in corals with rapid axial growth. In addition, we extend evidence of this phenomenon to a second and third family of important reef-building corals, the Acroporidae and the Pocilloporidae. Lastly, we extend farther the already widespread geographical documentation of this phenomenon from Moorea, French Polynesia (17°30′S: 149°50′W) (7), and Mayotte, Comoros Archipelago (44°27′N: 1°8′W) (13), to our study

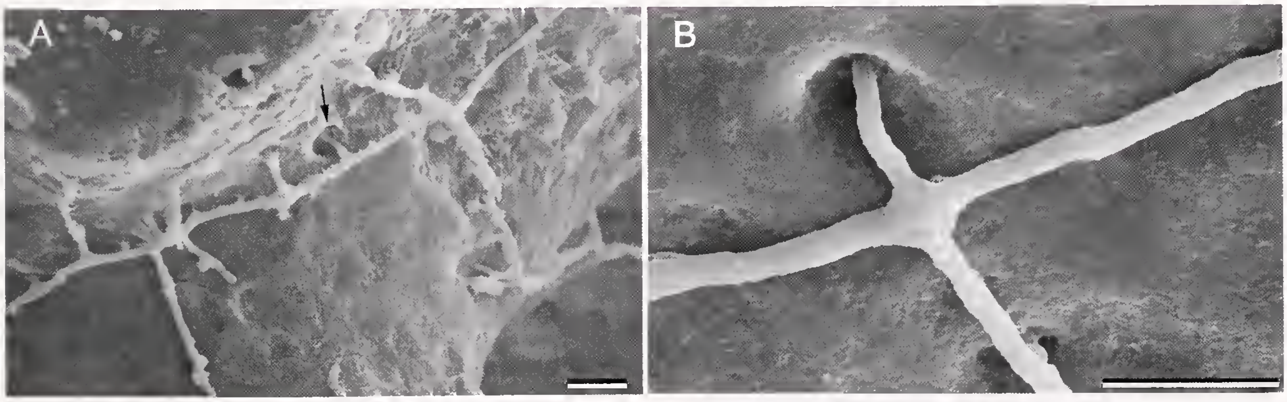

Figure 3. Pattern of euendolithic fungal borings. (A) *Acropora cytherea*. Hypha associated with conical defense structure (arrow). (B) *A. humulis*. Euendolithic fungal hyphae associated with two separate cones on corallum surface. Samples were prepared by resin-embedding and casting, followed by carbonate removal (partial-etching) with 3% HCl (*cf.* 29, 30). Fungal and algal borings are replicated as filaments, and cones appear as hollow structures observed from inside. Scanning electron micrographs; scale bars = 10 μm.

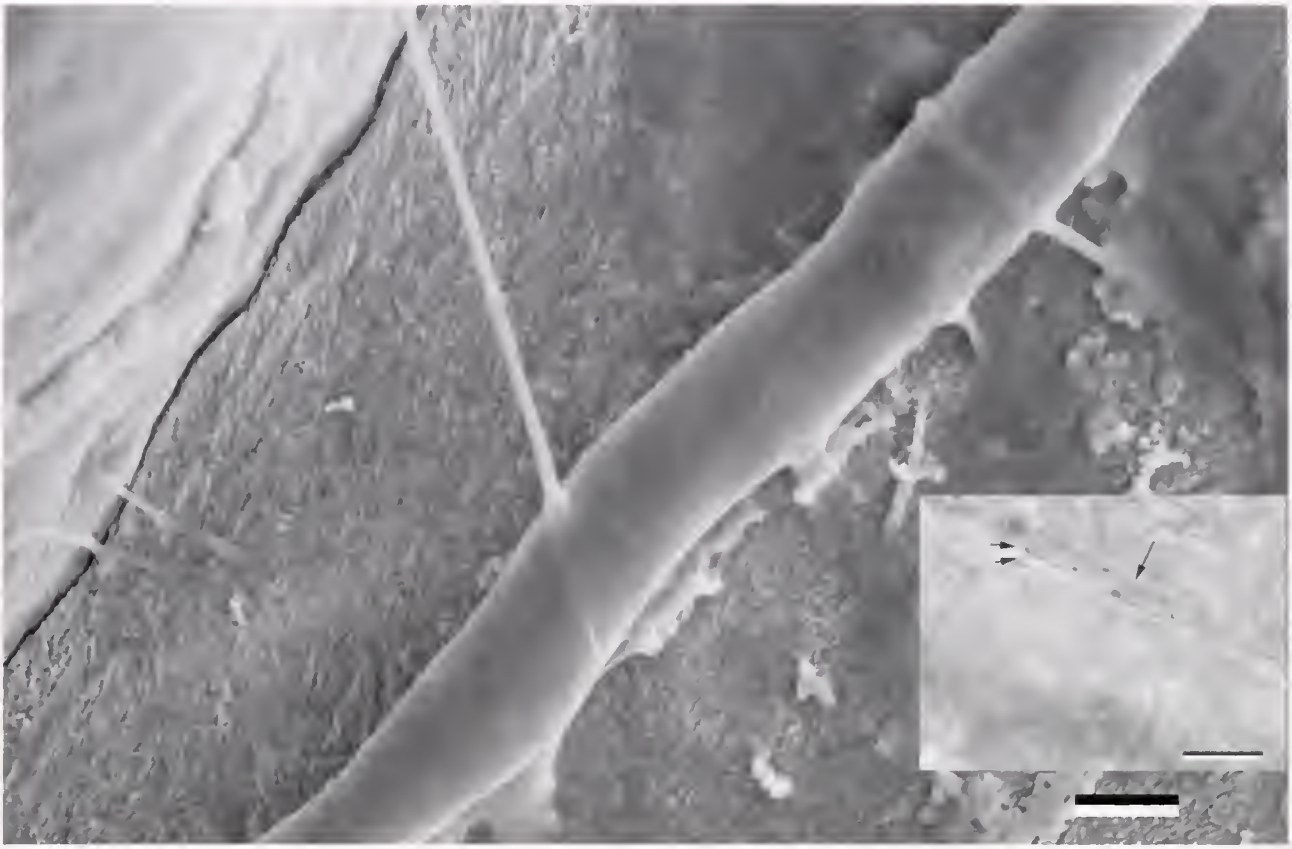

Figure 4. Resin-cast, euendolithic *Ostreobium quekettii* filament attacked by fungal hyphae in corallum of *Acropora humilis*. Note texture of aragonite crystals in background. Scanning electron micrograph; scale bar = 10 μm. (Inset) *A. cytherea:* euendolithic fungal hypha approaching algal filament (single arrow) and fungal haustorium forming ring around it (double arrow). Transmitted light photomicrograph of petrographic thin section; scale bar = 10 μm.

site at Johnston Atoll (16°44′N; 169°32′W), recognized as one of the most isolated coral reef habitats in the world (17).

Similar published observations suggest the possible ubiquity and circumtropical distribution of this phenomenon. For example, Constantz (18, figs 2e, f) depicted structures (which the author referred to as "skeletal granulations") in *Diploria labrynthiformis*, a West Indian faviid coral, that were nearly identical in size and shape to cones described from *P. lobata* (7) and observed in our study. Lukas (10) reported endolithic fungi to be present in 10 out of 12 species of Atlantic and Caribbean corals examined, spanning 8 genera. Scherer (19) recorded conical structures, somewhat larger but similar in shape, in *Colpophyllia* and *Montastrea*, and attributed them to endolithic algae (19). Sato (20) described cone formation by polyps in response to attempted algal penetration into occupied corallites, thus providing an independent account of the same phenomenon. The diameters of penetrating filaments described in both Scherer (19) and Sato (20) are significantly larger than the diameters of the fungal hyphae we observed, and correspond closely to the ranges reported for *O. quekettii*. The response of the polyps, however, is similar in that layers of compact, fine crystalline repair carbonate are deposited at points of attempted endolith penetration.

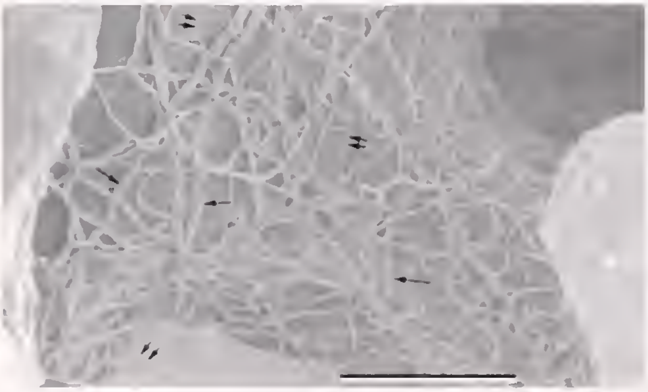

Figure 5. Resin cast microborings of euendolithic *Ostreobium quekettii* filaments (single arrows) and fungal hyphae (double arrows) within the range of the green band in *Montipora* cf. *studeri*. Scanning electron micrograph; scale bar = 100 μm.

The nature of the defense response exhibited by corals in

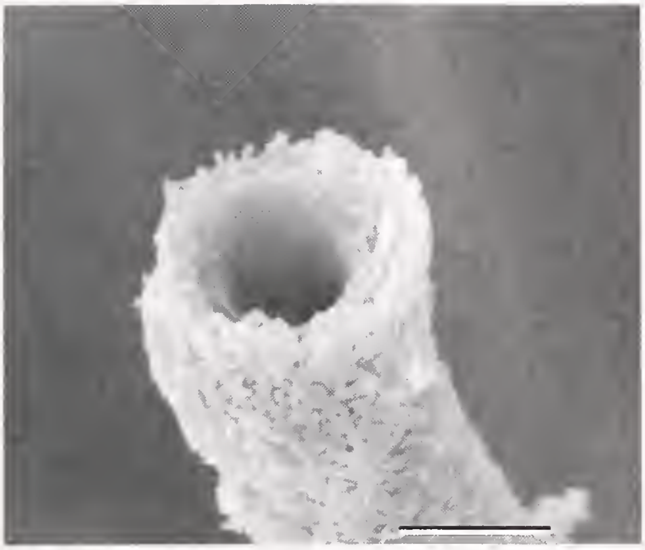

Figure 6. Calcified cryptoendolithic filament in *Montipora* cf. *studeri*. Same preparation as Fig. 2A, B. Scanning electron micrograph; scale bar = 5 μm.

response to chronic interactions with endolithic fungi, and perhaps to less frequent interactions with endolithic algae, suggests a dependence on their ability to rapidly deposit $CaCO_3$ at sites of attempted endolith penetration. Thus, factors that directly or indirectly impair skeletogenesis in corals—such as elevated sea surface temperature (21), coastal eutrophication (22), and increased atmospheric CO_2 (23)—could compromise the ability of corals to defend themselves against endolithic fungal attack. Seasonal fluctuations in environmental variables that affect skeletal growth, such as the intensity of photosynthetically active radiation (PAR) or of UV-B (24), may also affect the relative frequency of coral-fungal interactions. Thus, a coral's inability to deposit sufficient repair aragonite, in conjunction with factors that may increase the frequency of coral-fungal interactions, could increase the regularity with which hyphae are successful in breaching the skeletal surface of actively growing corallites (Fig. 2D). This is likely to be deleterious to the host coral's health.

Intensified defense activity of corals against endolithic fungi may, in turn, compromise a coral's ability to defend itself against other pathogens such as bacteria (25) or to invest energy in other processes, such as tissue regeneration, that maintain the integrity of the colony (26). The ability of corals to recover following bleaching events may also be weakened by their active defense against chronic attack by endolithic fungi (see Figs.1 and 2).

Much attention has been drawn to emerging epizootics as threats to the welfare of coral reefs (27, 28). The conclusions from the present study indicate that reef corals exist in precarious dynamic equilibria involving all four symbiotic partners. Morbidity could, therefore, result from a disturbance in this equilibrium in which either endolithic fungi become successful opportunistic pathogens or the increased frequency of fungal attacks compromises the host sufficiently to succumb to additional pathogens. Thus, a shift in this balance, involving active defense against chronic host-fungal interactions within reef-building corals, may render endolithic fungi a previously unrecognized threat to coral reef ecosystems worldwide.

Acknowledgments

We thank Steven Oliver and Spence Smith for collecting samples, and Dr. Phillip Lobel for his support. We also thank the Boston University Earth Sciences Department, specifically Dr. Joel Sparks, for granting us access to their facilities. Funding was provided by a grant from the U.S. Army Research Office (# DAAG55-98-1-0304) for the Johnston Atoll Ocean and Reef Ecosystem Study.

Literature Cited

1. **Kölliker, A. 1859.** On the frequent occurrence of vegetable parasites in the hard structures of animals. *Roy. Soc., Proc.* **10:** 95–99.
2. **Kobluk, D., and M. Risk. 1974.** Devonian boring algae or fungi associated with micrite tubules. *Can. J. Earth Sci.* **11:** 1606–1610.
3. **Schwarz, J. A., D. A. Krupp, and V. M. Weis. 1999.** Late larval development and the onset of symbiosis in the scleractinian coral Fungia scutaria. *Biol. Bull.* **196:** 70–79.
4. **Muscatine, L., L. Chad, and R. Marian. 1981.** Estimating the daily contribution of carbon from zooxanthellae to animal respiration. *Limnol. Oceanogr.* **26:** 601–611.
5. **Barnes, D., and C. Crossland. 1982.** Variability in the calcification rate of Acropora acuminata measured with radioisotopes. *Coral Reefs* **1:** 53–57.
6. **Rowan, R., and N. Knowlton. 1995.** Intraspecifc diversity and ecological zonation in coral-algal symbioses. *Proc. Natl. Acad. Sci.* **92:** 2850–2853.
7. **Le Campion-Alsumard, T., S. Golubic, and K. Priess. 1995.** Fungi in corals: symbiosis or disease? Interaction between polyps and fungi causes pearl-like skeleton biomineralization. *Mar. Ecol. Prog. Ser.* **117:** 137–147.
8. **Le Campion-Alsumard, T., S. Golubic, and P. Hutchins. 1995.** Microbial endoliths in the skeletons of live and dead corals: Porites lobata (Moorea, French Polynesia). *Mar. Ecol. Prog. Ser.* **117:** 149–157.
9. **Lukas, K. 1969.** An investigation of the filamentous, endolithic algae in shallow water corals from Bermuda. In: Reports on research – the 1968 seminar on organism-sediment interrelationships, R.Ginsburg, and P. Garrett, eds. *Bermuda Biol. Stn. Res. Spec. Publ.* **2:** 145–152.
10. **Lukas, K. 1973.** Taxonomy and ecology of the endolithic microflora of reef corals with a review of the literature on endolithic microphytes. Ph.D. thesis, University of Rhode Island, Kingston.
11. **Kiene, W., G. Radtke, M. Gektidis, S. Golubic, and K. Vogel. 1995.** Factors controlling the distribution of microborers in Bahamian reef environments. *Facies* **32:** 176–188.
12. **Laborel, J. and T. Le Campion-Alsumard. 1979.** Infestation massive du squelette de coraux vivant par des Rhodophycees de type Conchocelis. *C R. Acad. Sci. Ser. III* **288:** 1575–1577.
13. **Priess, K., T. Le Campion-Alsumard, S. Golubic, F. Gadel, and B.**

Thomassin. 1999. Fungi in corals: discoloration and density banding. *Mar. Ecol. Prog. Ser.* (in press).

14. **Jokiel, P. L., and W. A. Tyler III. 1992.** Distribution of stony corals in Johnston Atoll lagoon. *Proc. Seventh Int. Coral Reef Symp. Guam* **2:** 683–692.
15. **Schroeder, J. 1972.** Calcified filaments of an endolithic alga in recent Bermuda reefs. *Neus. Jahrb. Geol. Palaeont. Montash.* **1:** 16–33.
16. **Golubic, S., I. Friedmann, and J. Schneider.** 1981. The lithobiontic ecological niche, with special reference to microorganisms. *J. Sedim. Petrol.* **51:** 475–478.
17. **Maragos, J. E., and P. Jokiel. 1986.** Reef corals of Johnston Atoll: one of the world's most isolated reefs. *Coral Reefs* **4:** 141–150.
18. **Constantz, B. R. 1986.** Coral skeleton construction: a physiochemically dominated process. *Palaios* 1: 152–157.
19. **Scherer, M. 1974.** The influence of two endolithic microorganisms on the diagenesis of recent coral skeletons. *Neues Jahrb. Geol. Palaeontol. Monh.* **9:** 557–566.
20. **Sato, T. 1989.** An abnormal microstructure in the skeletons of recent and fossil scleractinian corals, its cause and diagenesis. *Earth Sci.* **7:** 200–210.
21. **Hoegh-Guldberg, O., and B. Salvat. 1995.** Periodic mass-bleaching and elevated sea level temperatures: bleaching of outer reef slope communities in Moorea, French Polynesia. *Mar. Ecol. Prog. Ser.* **121:** 181–190.
22. **Marubini, F., and P. Davies. 1996.** Nitrate increases zooxanthellae population density and reduces skeletogenesis in corals. *Mar. Biol.* **127:** 319–328.
23. **Kleypas, J. A., R. W. Buddemeier, D. Archer, J. Gattuso, C. Langdon, and B. Opdyke. 1999.** Geochemical consequences of increased atmospheric carbon dioxide on coral reefs. *Science* **284:** 118–120.
24. **Stimson, J. 1996.** Wave-like outward growth of some table- and plate- forming corals, and a hypothetical mechanism. *Bull. Mar. Sci.* **58:** 301–313.
25. **Kushmaro, A., E. Rosenberg, M. Fine, and Y. Loya. 1997.** Bleaching of the coral *Oculina patagonica* by *Vibrio* AK-1. *Mar. Ecol. Prog. Ser.* **147:** 159–165.
26. **Meesters, E., and R. Bak. 1995.** Age related deterioration of a physiological function in the branching coral *Acropora palmata. Mar. Ecol. Prog. Ser.* **121:** 203–209.
27. **Bruckner, A. W., R. J. Bruckner, and E. H. Williams Jr. 1997.** Spread of black-band epizootic through the coral reef system in St. Ann's Bay, Jamaica. *Bull. Mar. Sci.* **61:** 919–928.
28. **Richardson, L., W. Goldberg, K. Kuta, R. Aronson, G. Smith, K. Ritchie, J. Halas, J. Feingold, and S. Miller. 1998.** Florida's mystery coral killer identified. *Nature* **392:** 557–558.
29. **Golubic, S., G. Brent, and T. Le Campion. 1970.** Scanning electron microscopy of endolithic algae and fungi using a multipurpose casting-embedding technique. *Lethaia* **3:** 203–209.
30. **Golubic, S., S. Campbell, and C. Spaeth. 1983.** Kunstharzausgusse fossilier Mikroben-Bohrgange. *Der Prapartor.* **29:** 197–200.

Reference: *Biol. Bull.* **198:** 261–271. (April 2000)

Impact of a Castrating Trematode, *Neophasis* sp., on the Common Whelk, *Buccinum undatum*, in the Northern Gulf of St. Lawrence

FRANÇOISE TÉTREAULT[1], JOHN H. HIMMELMAN[1,*], AND LENA MEASURES[2]

[1]*Département de biologie and GIROQ (Groupe interuniversitaire de recherches océanographiques du Québec), Université Laval, Québec City, Québec, Canada G1K 7P4; and* [2]*Fisheries and Oceans Canada, Institut Maurice-Lamontagne, Mont-Joli, Québec, Canada G5H 3Z4*

Abstract. We observed heavy trematode infections of whelks, *Buccinum undatum*, from the Mingan Islands, eastern Canada, by larval stages of a species of *Neophasis*. Only sexually mature whelks were infected, 23% of mature females and 15% of mature males, and prevalence increased rapidly with whelk size. In most cases the parasite completely occupied the gonad, causing castration. The digestive gland was also infected, although to a lesser degree (0% to 50% occupation), and a marked reduction in the mass of the penis was associated with the infection. A decrease in the proportion of whelks with a highly infected digestive gland between May and August 1994 suggested mortality of infected individuals. Whelks held for 12 to 15 months in the laboratory retained the infection but did not show significant mortalities (possibly because food was abundant and predators absent). The larval stage of *Neophasis* sp. found in whelks was a cercaria; however, the tail easily detached. The putative infective stage (metacercaria) was not observed but may be present in whelks in late winter and early spring. Other trematode parasites observed were adult *Steringophorus furciger* in the stomach and larval *Renicola* sp. in the digestive gland.

Introduction

Parasitic castration is the partial or total inhibition of gametogenesis of a host species due to the activity or physical presence of a parasite (Cheng, 1983). Many larval trematodes castrate their gastropod hosts (Cheng, 1964; Lauckner, 1986), and gigantism and modifications of secondary sexual characteristics may also occur (Rothschild, 1936, 1941; McClelland and Bourns, 1969; Mouritsen and Jensen, 1994; Gorbushin, 1997). Because castrating parasites may decrease the number of breeding individuals within gastropod populations (Kuris, 1973, 1974; Lauckner, 1986), infected populations may show declines or strong fluctuations in abundance (Lie, 1973; Combes, 1982; Lauckner, 1986; Huxham *et al.*, 1993; Lafferty, 1993).

Køie (1969) identified four castrating larval trematodes in a Danish population of the common whelk, *Buccinum undatum* L. 1758: (1) *Zoogonoides viviparus* (Olsson, 1868) Odhner, 1902; (2) *Neophasis anarrhichae* (= *N. lageniformis*) (Nicoll, 1909) Bray, 1987; (3) *Cercaria buccini* (Lebour, 1911); and (4) an unidentified species of *Renicola*, Cohn, 1904. The first three are found in both the gonad and digestive gland and the fourth only in the digestive gland. Infections by *Z. viviparus* and *N. anarrhichae* result in a light grey appearance of the infected organs, whereas *C. buccini* does not affect the color of the infected organs (Lebour, 1911), and *Renicola* sp. forms light yellow bodies in the digestive gland. Other parasites of *B. undatum* identified by Køie (1969) are the turbellarian commensal *Graffilla buccinicola* (Jameson, 1897), found in the digestive gland and stomach, and the trematode *Steringophorus furciger* (Olsson, 1867) Odhner, 1902, present only in the stomach. Hamel (1989) observed larval trematode parasites in the gonad and digestive gland of 15% of adult *B. undatum* in the Mingan Islands, Gulf of St. Lawrence, eastern Canada, and indicated that the characteristics of the infection were similar to those described by Køie (1969) for *Z. viviparus* and *N. anarrhichae*.

In our study we identified one trematode in *B. undatum* as

Received 12 November 1998; accepted 8 December 1999.

* To whom correspondence should be addressed. E-mail: john.himmelman@bio.ulaval.ca

belonging to the genus *Neophasis*, which has life cycles involving one or two intermediate hosts (gastropod, fish) and a teleost final host (Bray and Gibson, 1991). Caudate cercaria develop in the gastropod, become free-living, and encyst as metacercaria in bivalve molluscs and fish that are later preyed upon by the final fish host. In *Neophasis anarrhichae*, *B. undatum* apparently serves as the only obligate intermediate host. Caudate cercariae develop within rediae in the whelks. The cercarial tail is shed within the redia, and the noncaudate cercaria is considered a metacercaria that does not encyst (Koie, 1973). Final hosts are carnivorous teleosts belonging to the genus *Anarhichas*, which acquire the parasite by preying on infected whelks. Encysted metacercariae of an unidentified *Neophasis* have been reported on the mesentery of American plaice, *Hippoglossoides platessoides*, and in the gut of Atlantic cod, *Gadus morhua*, from Canadian waters (Appy and Burt, 1982). Bray and Gibson (1991) indicated that this immature trematode may be *Neophasis burti* Bray and Gibson, 1991.

Buccinum undatum is the most abundant carnivore in the benthic community in the Mingan Islands in the northern Gulf of St. Lawrence (Jalbert *et al.*, 1989; Himmelman, 1991). It is also of commercial importance in the Gulf of St. Lawrence and St. Lawrence Estuary. From 1991 to 1993, 700 metric tons of whelks were harvested annually in Quebec and 30% of this harvest came from the Mingan Islands (Savard, 1994).

Several characteristics of the biology of the common whelk make it especially vulnerable to fishery over-exploitation. First, recolonization of over-exploited sites is likely to be slow because the whelk lacks a pelagic larval stage and adults move only by crawling. Further, stocks are limited by a slow growth rate. In the Mingan Islands, whelks attain a shell length of 75 to 80 mm, the size at sexual maturity, in 6 to 8 y (Martel *et al.*, 1986; Savard, 1994). At present the fishery is not limited by a minimal capture size. In 1993, 25% of whelks collected measured <75 mm (Savard, 1994) and thus had not reproduced. A decrease in the average size of harvested whelks has been recorded in several fishery zones and may indicate over-exploitation. Although such a decrease has not yet been observed in the Mingan Islands, it is likely to happen given the intensity of the fishery.

The objective of our study was to identify parasites of the common whelk, *Buccinum undatum*, in the northern Gulf of St. Lawrence and to evaluate their impact on the whelk. We sampled a large number of whelks during two periods in summer 1994 to determine the prevalence of parasites (proportion of whelks infected) and to quantify their effects on different body organs. In addition, we studied morphological changes in parasites over time in the laboratory. Finally, we exposed American plaice to larval *Neophasis* sp. from *B. undatum* to determine whether larval *Neophasis* would develop and mature to the adult stage and thus permit identification to species.

Materials and Methods

We sampled whelks from the Mingan Islands (50° 35′ N, 63° 35′ W), in the northern Gulf of St. Lawrence (Fig. 1). Using scuba, we collected all whelks (buried and unburied) that measured 10 to 110 mm in shell length and were found within 1 m of either side of two 160-m long transects parallel to the shoreline at Cap du Corbeau on Île du Havre, one at 6 m and the other at 15 m in depth. Whelks were abundant on the sediment bottom in this area. We collected 327 whelks in May 1994 and 313 in August 1994.

All whelks were frozen, and later dissected to identify and determine the prevalence of parasites. After measuring the shell length of each animal, we fragmented the shell with a hammer to remove the soft tissues intact. Then, the gonad, penis, remaining reproductive organs, digestive gland, and other body components were separated and weighed (after draining on paper toweling for 10 min). A dissecting microscope was used to examine each organ for parasites. In examining the gonad and digestive gland, we pressed the tissues between two 7.5 × 7.5 cm glass plates to facilitate the search for parasites, and visually estimated the proportion of the organs occupied by parasites (the larvae were too abundant to be counted). Samples of larvae found in each infected whelk were isolated and preserved in AFA

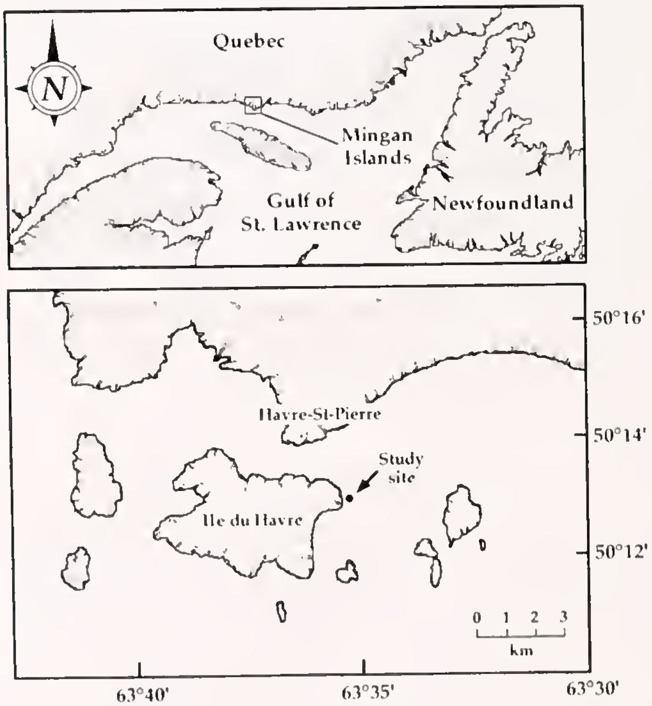

Figure 1. Location of the study site, Cap du Corbeau, in the Mingan Islands in the northern Gulf of St. Lawrence, Canada.

(a solution of alcohol, formalin, and acetic acid; Pritchard and Kruse, 1982) for later identification.

We identified parasites to genus based on the morphology of different stages. Preserved parasites were examined with a microscope, first without staining and then using Scheider's acetocarmine stain (Pritchard and Kruse, 1982). Further, to obtain the adult stages required for species identification of larval parasites from the gonad and digestive gland, we attempted to infect American plaice, *Hippoglossoides platessoides*, which is a host for several trematodes (Bray and Gibson, 1991). Plaice, measuring 15 to 20 cm in total length, were collected in June 1994 by trawling at a depth of 53 m near Matane (48° 53′ N, 67° 19′ W) in the St. Lawrence Estuary. In November 1994, using forceps, we placed pieces of infected gonad, from freshly killed whelks (collected in the Mingan Islands in October 1994), into the stomachs of six plaice. The plaice were first anesthetized by placing them for 1–3.5 min in 2 l of seawater containing 0.3 g of tricaine methanesulfonate (MS-222). Following treatment, the plaice were kept in well-oxygenated water for 24 h to recuperate. The six exposed plaice were maintained at 25‰ to 28‰ salinity and 4.4° to 10.4°C for 10 to 20 d in a 130-l tank at the Maurice-Lamontagne Institute. Four other nonexposed plaice, which served as controls, were maintained under the same conditions in another 130-l tank. After 10 to 20 d, the plaice were killed by cervical dislocation, dissected, and examined for intestinal trematodes.

We also examined changes in parasitic infections over time in 80 whelks measuring 80–110 mm in shell length. These specimens were collected in October 1994 from along the same two transects at Cap du Corbeau, and using the same methods, as in May and August. These whelks were maintained at 25‰ to 28‰ salinity and 4.4° to 10.4°C in two 130-l tanks until January 1996. Using the technique described above, we examined a first sample of 30 whelks in November 1995 and a second sample of 45 whelks in January 1996. Five whelks died during this laboratory study and were frozen for later examination. We recorded the size of cercariae and rediae in whelks collected from the field in May and August 1994, and from the laboratory sampling in November 1995 and January 1996, from images projected through a drawing tube attached to a Leitz diaplan (×40) microscope using a digitizer and computer (using Sigmascan image analysis software, version 3.90; SPSS Inc., Chicago, IL).

To evaluate the influence of sex and sampling period (May and August) on the prevalence of parasites in gonadal and digestive gland tissues, and on the proportion of these organs infected, we applied log-linear models adjusted to three-dimensional contingency tables (Legendre and Legendre, 1984). Only significant models were retained, and the best model describing the data was determined using the partitioning method. For the analysis of prevalence, only sexually mature whelks (>75 mm in shell length; Martel *et al.*, 1986) were used since parasites were absent in immature whelks. Because the proportion of the gonad and digestive gland occupied by parasites varied markedly, different categories were used for the two organs: 0%–90% and 90%–100% classes for the gonad and four 25% classes for the digestive gland. All statistical analyses were performed using the BMDP4F statistical program (Dixon, 1985).

We compared the somatic mass and shell length of the parasitized and nonparasitized whelks with a Mann-Whitney *U* test. To eliminate the confounding effect of parasitism on reproductive organs and the digestive gland, we used eviscerated mass, defined as the total mass minus the mass of the digestive gland, gonad, penis, and remaining reproductive organs. Given the slow growth of whelks, we assumed that there was no impact of sampling period on eviscerated mass and shell length and therefore pooled the May and August samples for the analyses.

Because the number of opercular striae can be used as an estimate of age of *B. undatum* (Santarelli and Gros, 1985), we used these striae to evaluate whether the age of infected and noninfected whelks was different. We compared the number of operculum striae of infected and noninfected whelks using Mann-Whitney *U* tests.

To evaluate the effect of parasites on the penis, we compared penis mass of infected and noninfected whelks, in May and again in August, using Mann-Whitney *U* tests. To determine the effect of the parasite on penis mass, we first determined the regression of penis mass to shell length for noninfected whelks and then calculated the deviation in penis mass of infected whelks compared to this relationship. As the distribution of residuals was normal, a Student's *t* test was used to test the hypothesis that the mean of the residuals was equal to 0 (Zar, 1984); a value different than 0 ($P < 0.05$) would indicate that the parasite affected penis mass.

Results

Identification of parasites in the gonad and digestive gland

Our examination of whelks collected in May and August 1994 in the Mingan Islands revealed that cercariae and rediae of one species of trematode infected both the gonad and the digestive gland. The cercariae possessed an oral sucker at the anterior portion of the body and a ventral sucker in the middle of the body (Fig. 2A). They also possessed a straight, nonfurcate tail and eyespots located anterolateral to the oral sucker. Rediae had only an oral sucker and a small pharynx in the anterior portion of the body (Fig. 2B). The shape of the cercariae varied in different seasons. Cercariae were most elongated in August 1994 (mean length = 395 μm; mean width = 70 μm) and least in January 1996 (mean length = 199 μm; mean width = 98 μm). The tail was easily detached in May but not on the other dates. Rediae were cylindrical and less variable in

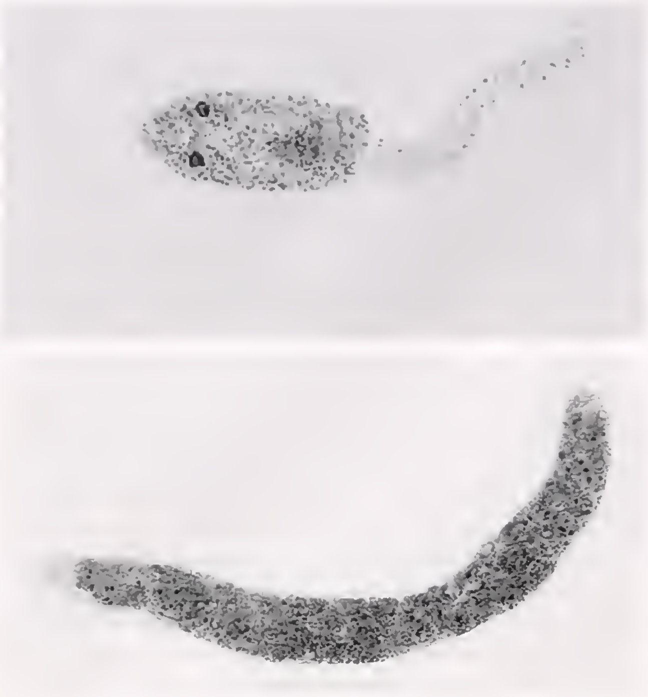

Figure 2. Stages of the trematode *Neophasis* sp. from live tissues of the whelk *Buccinum undatum*. (Top) A cercaria with eyes and a straight, nonfurcate tail. (Bottom) A redia containing several cercariae.

shape over time than cercariae. They were longest in August 1994 (mean length = 2190 μm) and shortest in November 1995 (1325 μm). In May and August 1994 some rediae did not contain cercariae, whereas in November 1995 and January 1996 all contained cercariae.

The presence in the cercarial stage of eyes at the anterior portion of the body and a straight, nonfurcate tail placed this parasite in the genus *Neophasis* (Stafford, 1904). Our identification to genus was confirmed by Dr. R. A. Bray at the British Museum of Natural History London (pers. comm.). We found no adult *Neophasis* in the digestive systems of the American plaice (*Hippoglossoides platessoides*) that we had attempted to infect, and thus we could not identify the species of *Neophasis*.

In noninfected whelks, the gonads were yellow to orange in color, and the digestive gland was brown (Fig. 3A, B). In contrast, the gonad and digestive gland of whelks infected with larval *Neophasis* sp. were light grey (Fig. 3C, D), owing to the color of the cercariae and rediae that replaced the tissues. Larvae of *Neophasis* sp. were also found in other reproductive organs—the albumin gland of females and the seminal vesicle of males.

Prevalence of Neophasis *sp. in whelks in the field*

Larvae of *Neophasis* sp. were present only in sexually mature whelks (Fig. 4). Three of the log linear models (Table 1) testing the effect of sex (S) and sampling date (M) on prevalence (P) were significant ($\alpha = 0.05$); of these, Model B, $\ln E = P + S + M + SM + PS$, best described the data (Table 1). This model indicated that only sex influenced prevalence. Female whelks were more infected ($P = 0.05$) by larval *Neophasis* sp. than were males (22.9% *vs.* 15.4%). In both sexes, prevalence markedly increased with increasing whelk size and exceeded 90% for whelks measuring more than 90 mm in shell length.

The infected whelks were the largest (Figs. 4, 5) and also seemed to be oldest (Fig. 5). Shell length was greater for infected than noninfected whelks (Fig. 5: females: $U = 14.02$, $n = 218$, $P < 0.001$; males: $U = 12.40$, $n = 246$, $P < 0.001$), and the same trend was indicated for eviscerated mass, although it was significant only in males (Fig. 5: females: $U = 1.3$, $n = 218$, $P = 0.25$; males: $U = 6.96$, $n = 246$, $P = 0.01$). Finally, the number of operculum striae tended to be greater for infected than noninfected whelks (Fig. 5; females: $U = 4.98$, $n = 77$, $P = 0.026$; males: $U = 3.69$, $n = 73$, $P = 0.055$).

Effects of Neophasis *sp. on the whelk*

In all cases, the gonad was the organ most infected by larval *Neophasis* sp. (Fig. 6). None of the models testing the influence of sex and sampling date on the proportion of the gonad occupied by parasites were significant. Thus, no differences between females and males or between the two sampling periods were indicated. In 97% of infected whelks, cercariae and rediae occupied more than 90% of the gonad. The one individual with a lower portion of the gonad infected by larval *Neophasis* sp. (20%) was a male collected in August 1994 (Fig. 6).

The proportion of the digestive gland infected with cercariae and rediae was much lower than for the gonad and exceeded 50% in only a few whelks (Fig. 6). Two log linear models (Table 1) testing the effect of sex and sampling date on the proportion of the digestive gland occupied by the parasite were significant ($\alpha = 0.05$), and the partitioning method indicated that Model B, $\ln E = O + S + M + OM + SM$, best described the data (Table 1). This model indicated that only sampling period influenced the proportion of digestive gland occupied by the parasite. The proportion of the digestive gland occupied by larval *Neophasis* sp. in infected whelks dropped between May and August (Fig. 6). For example, 45% of the infected whelks had more than 25% of the digestive gland infected in May compared to 8% in August.

In both May and August, the regression of penis mass to shell length was positive for noninfected males (Fig. 7: May: $n = 122$, $r^2 = 0.26$, $P < 0.001$; August: $n = 93$, $r^2 = 0.29$, $P < 0.001$), but the mean residual penis mass of infected whelks compared to the regressions for noninfected whelks differed from 0 (May: $n = 21$, $t = 18.514$, $P <$

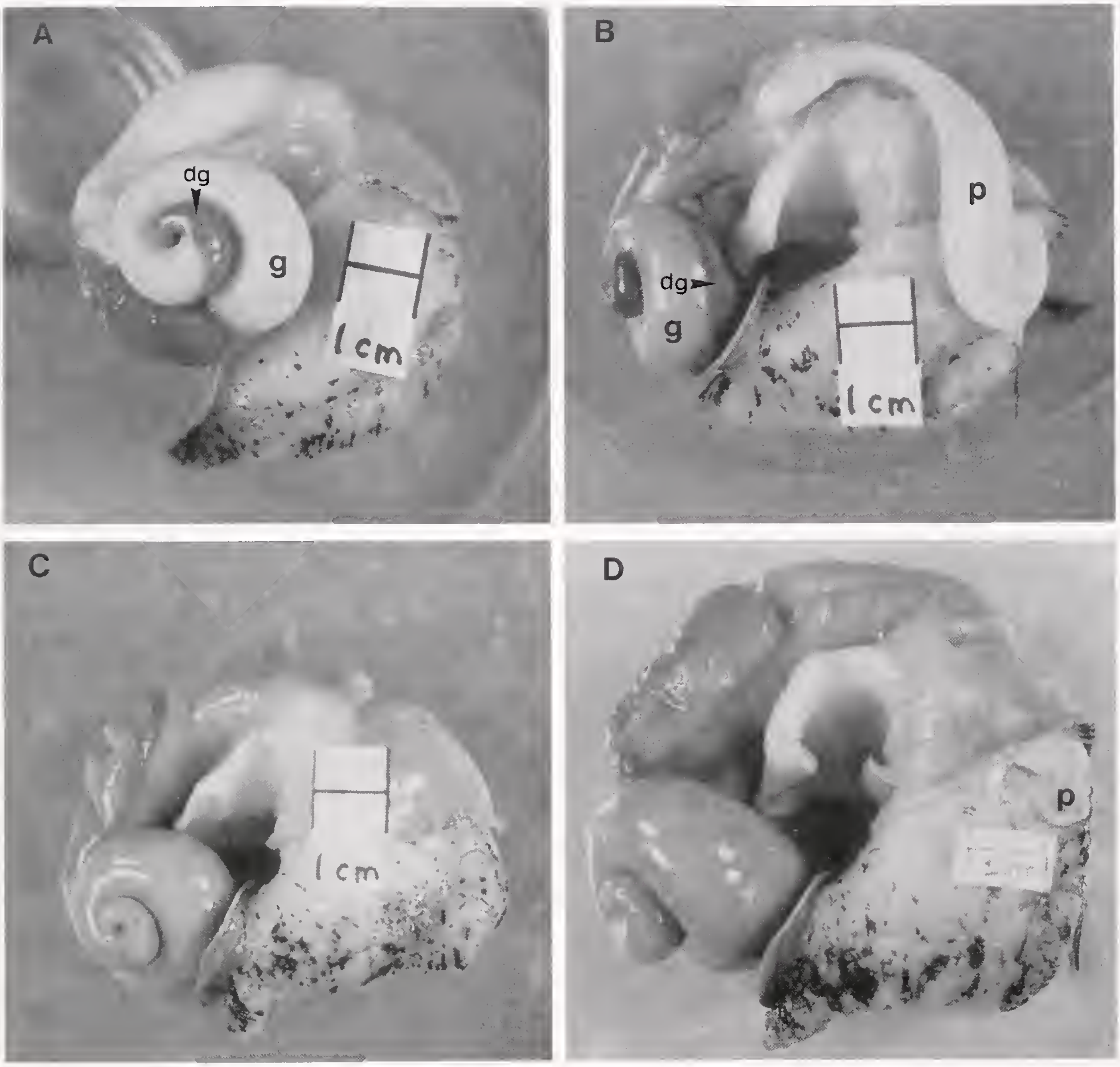

Figure 3. Whelks, *Buccinum undatum*, with the shell removed. The gonad (g) is clearly distinct from the digestive gland (dg) in the uninfected female (A) and male (B) because of different coloration, whereas these organs are less easily distinguished in the infected female (C) and male (D) because of similar coloration (light grey). Note the strong atrophy of the penis (p) of the infected male (D).

0.001; August: $n = 18$, $t = -6.427$, $P < 0.001$). Penis mass was markedly smaller for infected males (Fig. 7).

Neophasis *sp. infections in whelks in the laboratory*

Whelks sampled from the laboratory in November 1995, after 12 months in captivity, had larval *Neophasis* sp. in 20.0% of females (3/15) and 0% of males (0/15). In one of the three infected females, larval *Neophasis* sp. had invaded the gills and mucus gland tissues, a condition never observed in the whelks collected in May and August 1994 from the field. In January 1996, after 15 months in the laboratory, 17.4% of females (4/23) and 4.5% of males (1/22) were infected. The prevalence of *Neophasis* sp. in the laboratory whelks (dissected in November 1995 and January 1996) tended to be greater for females than males, but not significantly so (Fisher exact probability test, $P = 0.056$). For females, the prevalence in the laboratory was similar to that in the field sampling ($G = 0.39$, $n = 261$, $P = 0.53$), but was lower for males (Fisher exact probability test, $P = 0.039$). Five whelks died during captivity, and three of

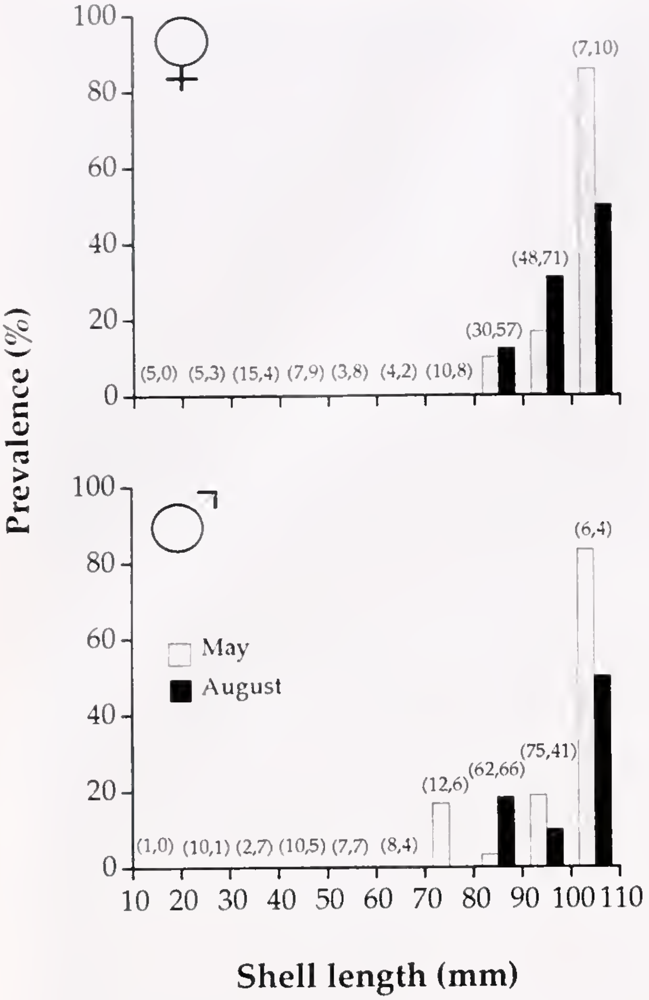

Figure 4. Relation of prevalence (%) of the trematode *Neophasis* sp. in female and male whelks, *Buccinum undatum*, to whelk size for individuals collected in May and August 1994. Numbers in parentheses indicate sample size in May and August, respectively.

these did not contain *Neophasis* sp. or other parasites. The other two were too decomposed to permit adequate examination.

Other parasites

Another trematode, which appeared to also be of the genus *Neophasis*, was observed in the digestive gland of some whelks, but did not affect the appearance of this organ. It probably had little effect on these whelks because the intensity of infection was low, a mean of 1.2 immature trematodes per whelk and a maximum of 3. It was larger (mean body length = 2.36 mm, SE = 0.22) than the cercariae and rediae of the above *Neophasis* species, anterior eyes and a pharynx were visible, and no specimens were observed with a tail. Due to the poor condition of these trematodes, we could not determine if they contained cercariae or if gonads were present. This parasite was found in 5.4% of whelks in May (1 immature female, 1 immature male, 4 adult females, 11 adult males) and 7.9% of whelks in August (9 immature females, 6 immature males, 3 adult females, 5 adult males).

We noted the presence of yellow bodies, 1–2 cm in diameter, in the digestive gland in some whelks (2 females and 3 males in May, 3 females and 1 male in August, and 1 female and 1 male in January 1996). The digestive glands were preserved in 10% formalin. Examination of 5-μm thick sections of digestive glands containing these bodies (stained with hematoxylin-eosin) revealed another trematode within the empty tubules of the digestive gland. It appeared to have the cercarial characteristics of the genus *Renicola*: oral and ventral suckers, a short undivided tail, no stylet or eyes, and the pharynx small or absent. This parasite was previously reported by Koie (1969) for *Buccinum undatum* in Danish waters.

One adult digenetic trematode observed in the stomach of about 12% of the whelks was identified as *Steringophorus furciger*, a parasite previously reported from the stomach of whelks in the Mingan Islands by Hamel (1989) and from the stomach of American plaice in the Gulf of St. Lawrence by Scott (1975) and Scott and Scott (1988).

Discussion

Identification of parasites in the gonad and digestive gland

The adult stage is required for specific identification of *Neophasis*; because we did not succeed in infecting American plaice (*Hippoglossoides platessoides*) with larval

Table 1

Difference between best adjusted models (significant at 5%) relating impact of sex (S) and sampling month (M) to prevalence (P) and proportion of digestive gland occupied (O) by Neophasis *sp.*

Model	Log-likelihood ratio df	 LLR	 Probability value
Prevalence			
(a) lnE = P + S + M + SM + PM + PS	1	0.15	0.70
difference between (a) and (b)	1	0.18	0.67
(b) lnE = P + S + M + SM + PS	2	0.33	0.85
difference between (b) and (c)	1	1.76	0.18
(c) lnE = P + S + M + SM + PM	2	2.09	0.35
Digestive gland			
(a) lnE = O + S + M + OS + OM + SM	2	2.79	0.25
(b) lnE = O + S + M + OM + SM	4	5.33	0.26
difference between (a) and (b)	2	2.54	0.28

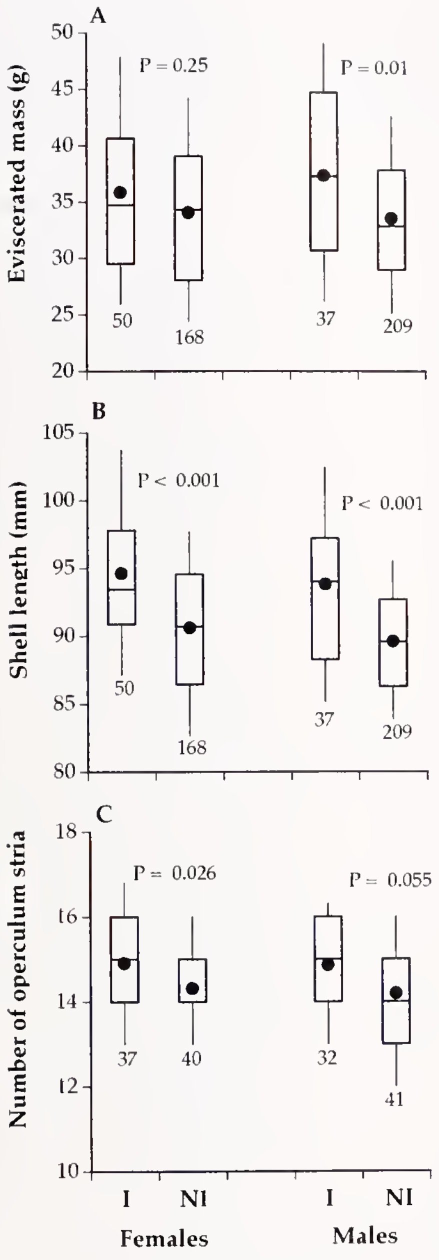

Figure 5. Eviscerated mass (A), shell length (B), and number of operculum striae (C) of female and male whelks, *Buccinum undatum*, infected (I) and noninfected (NI) by *Neophasis* sp., in May and August 1994. The Mann-Whitney *U* test was used to compare the eviscerated mass and shell length of infected and noninfected whelks. Numbers above box plots are probabilities, and numbers below are sample sizes. The top, middle, and lower horizontal lines show the 75th, 50th, and 25th percentiles, respectively. The black circle indicates the mean, and the vertical lines extend from the 10th to the 90th percentiles.

Neophasis sp. from *Buccinum undatum*, we could not determine the species. It is possible that larvae were not infective or that plaice were an unsuitable host. Four species of *Neophasis* Stafford, 1904 [Family: Acanthocolpidae] are described from the North Atlantic: (1) *Neophasis anarrhichae* (Nicoll, 1909) Bray, 1987; (2) *N. burti* Bray and Gibson, 1991; (3) *N. oculatus* (Levinsen, 1881) Miller, 1941; and (4) *N. pusilla* Stafford, 1904 (see Bray and Gibson, 1991, and Gibson, 1996). Bray and Gibson (1991) indicate that *N. burti* may be synonymous with *N. oculatus*, and *N. pusilla* synonymous with *N. anarrhichae*. The species found in whelks in the Mingan Islands may be *N. anarrhichae* since this is the only species thus far described from *B. undatum* (Lebour, 1908, 1911; Køie, 1969; Bray and Gibson, 1991). However, we saw only tailed cercariae, albeit the tails easily detached within redia. Lebour (1910) observed cercariae with and without tails within the same redia (and the tails were easily detached). Køie (1973) rarely found tailed cercaria and considered tailless cercaria as metacercaria that do not encyst but are infective to the final host, as described by Lebour (1910). Possibly, the retention of the tail in cercaria is a function of geographic differences; for example, perhaps in cold Canadian waters the tail is retained longer. *B. undatum* is the only intermediate host, and the final hosts are wolffish of the family Anarhichadidae (*Anarhichas denticulatus*, *A. lupus*, and *A. minor*), which become infected by ingesting parasitized whelks. An abundance of broken whelk shells is usually found at the entrance of dens of *A. lupus* in the Mingan Islands, which suggests that whelks are a major prey (pers. obs.). The final hosts of other species of *Neophasis* are fishes of the families Cottidae, Cyclopteridae, Zoarcidae, and Gadidae (Bray and

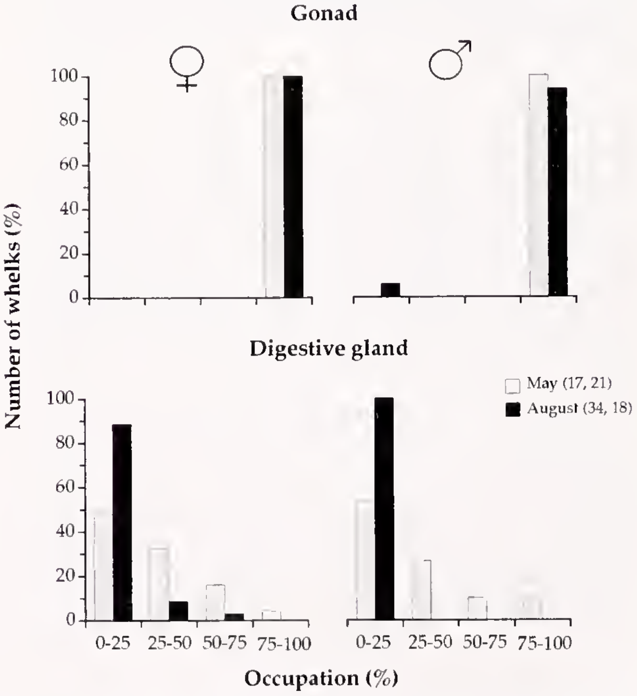

Figure 6. Proportion of the gonad and digestive gland occupied by the trematode *Neophasis* sp. in female and male whelks, *Buccinum undatum*, collected in May and August 1994. Numbers in parentheses indicate the sample size of infected females and males, respectively.

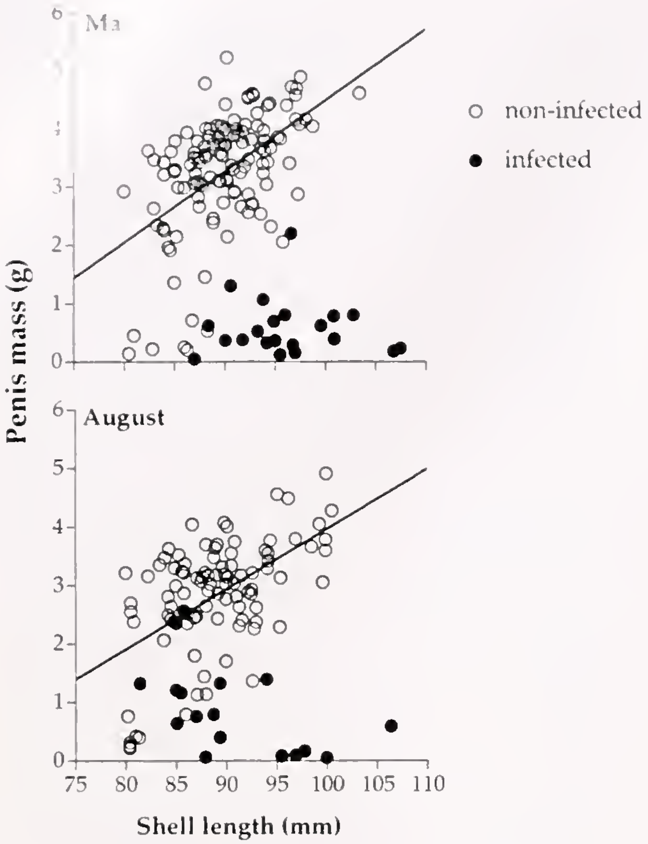

Figure 7. Relation of penis mass to shell length for whelks, *Buccinum undatum*, infected (dark circles) and noninfected (open circles) by the trematode *Neophasis* sp. in samples collected in May and August 1994

Gibson, 1991), and all of the above-mentioned families of fishes are present in the Mingan Islands (Thomas and Himmelman, 1988). Whereas members of the genus *Neophasis* have been reported from American plaice from the North Atlantic (Bray and Gibson, 1991), none have been reported in American plaice or other fishes from the Gulf of St. Lawrence (Scott, 1975). However, *Neophasis* sp. is reported from cod from the southern Gulf of St. Lawrence, although infections were probably accidental (Appy and Burt, 1982). According to Køie (1973), pleuronectiforme fish may acquire *N. anarrhichae*, but the parasites do not mature and infections are lost within a few days.

The persistence of larval *Neophasis* sp. in whelks collected in October 1994 and maintained in the laboratory for 12 to 15 months suggests that the parasite persists in the whelk for long periods. Similarly, Køie (1969) sampled whelks for 12 consecutive months and concluded that the parasite persists in all seasons. Although we did not observe tailless cercariae (metacercariae) during our study, this infective stage may be present in whelks during late winter or early spring.

Prevalence of Neophasis *sp.*

Two hypotheses may explain the increased prevalence of larval *Neophasis* sp. with increasing size for sexually mature whelks (Figs. 4, 5). First, larger whelks may be more frequently infected because they have been exposed to parasites for a longer time. Second, castrating trematodes eliminate energetic demands for reproduction and thereby may increase the growth rate of somatic tissues, a phenomena known as gigantism (*e.g.*, Rothschild, 1936, 1941; McClelland and Bourns, 1969; Mouritsen and Jensen, 1994; Gorbushin, 1997). That the number of opercular striae was greater on infected whelks than on noninfected ones (Fig. 5) suggests that the infected whelks were older, which is consistent with the first hypothesis. If this is true, the hypothesis of gigantism is not necessary to explain the positive relation between size and infection rate. Nevertheless, a comparison of growth rates of infected and noninfected whelks of similar size is needed to provide a more direct test of the gigantism hypothesis.

Gigantism has been reported primarily in short-lived gastropods (Sousa, 1983). Long-lived species, such as *B. undatum*, may devote more energy to tissue repair and may thereby be less likely to display gigantism when parasitized. In whelks in the Mingan Islands, the energy required to repair damage may be high because the redial stages of *Neophasis* digest extracorporally and later absorb host materials through the mouth or tegument (Køie, 1971). Thus, rediae may require more energy from their host than sporocysts that absorb nutrients through the body wall without damaging host tissues (Sousa, 1983; Vernberg and Vernberg, 1974). The effect of parasitic castration on the growth rate of infected individuals may further depend on host population density and parasite species. For instance, Gorbushin (1997) found that the growth rate of *Hydrobia ventrosa* tends to be stunted by the parasitic trematode *Bunocotyle progenetica* when host density is high, but is significantly increased when host density is low. In contrast, under field conditions, trematode species from the families Nocotylidae and Bunocotylidae have no effect on the growth rate of *Hydrobia ulvae* and *H. ventrosa* (Gorbushin, 1997).

We observed a higher prevalence of *Neophasis* sp. in female whelks than in males in May and August 1994 (Fig. 4). Hughes and Answer (1982) found a similar difference between female and male *Littorina littorea* infected by trematodes. Our understanding of prevalence patterns is restricted by the limited knowledge of how *Neophasis* miracidiae infect whelks and of the resistance of whelks to infections. Possible explanations are that females (1) are more exposed to the parasite because their activities differ from those of males (*e.g.*, egg laying; feeding rates possibly vary because of greater reproductive investment, Martel *et al.*, 1986), (2) are less resistant to infections, or (3) retain infections for a longer period. A greater prevalence of *Neophasis* sp. in females than in males was further observed in the sample collected in October 1994, which was maintained in the laboratory.

Effects of Neophasis *sp. on the whelk*

In the Mingan Islands, *Neophasis* sp. is strongly associated with gonadal tissues of sexually mature whelks. In this respect, it is similar to the trematodes infecting the gastropod *Littorina littorea* (Hughes and Answer, 1982). In contrast, in Denmark, *Neophasis anarrhichae* infects the digestive gland of immature whelks as well as the gonad and digestive gland of mature individuals (Køie, 1969). Studies are needed to elucidate why *Neophasis* sp. is absent in the digestive gland of immature whelks in the Mingan Islands.

In both sampling periods, the gonads of infected whelks were almost completely occupied by the parasite (Fig. 6). This strongly suggests rapid proliferation of the parasite once inside the host. In contrast, the digestive gland was much less infected, and percentage occupation decreased markedly from May to August in both sexes (Fig. 6). The decrease could be due to either tissue repair or mortality of infected whelks. Køie (1971) observed high mortalities of whelks infected with *N. anarrhichae*, suggesting that the animals eventually die from infection. This is also suggested by the massive tissue damage caused by *Neophasis* and because scars, which would indicate healing, have not been observed (Køie, 1971, this study). That we observed no mortality of infected whelks kept in the laboratory for 15 months might have been because food was abundant and predators absent. A number of studies demonstrate a negative effect of trematode parasites on gastropods when environmental conditions are unfavorable (Vernberg and Vernberg, 1963, 1967; Sousa and Gleason, 1989), and some castrating trematodes are known to cause death of their hosts (Stunkard, 1964; Lauckner, 1986). Mortality could be due directly to the parasite or indirectly to predation. Potential predators of adult whelks in the Mingan Islands are numerous and include the asteroids *Leptasterias polaris* and *Asterias vulgaris* (see Dutil, 1988); the common eider, *Somateria mollissima* (see Guillemette *et al.*, 1992); and the wolffish, *Anarhichas lupus.*

Both our study and that of Køie (1969) show that an atrophy of the penis is associated with the presence of castrating trematodes in *Buccinum undatum* (Fig. 7). This probably results from the destruction of the gonad, which produces sexual hormones (Caullery, 1950). The high degree of destruction of the reproductive organs by *Neophasis* sp. makes these organs virtually nonfunctional. Neither our study nor that of Køie (1969) provided evidence that the parasite could cause a change of sex.

Other parasites

The genus *Renicola* was identified in the digestive gland of a small proportion of whelks in our study and in that of Køie (1969). The sporocysts (with cercariae) of the genus *Renicola* infect the digestive gland and gonads of gastropods, causing castration and, in massive infections, death (Stunkard, 1964). Gastropods are the first intermediate host, and cercariae leave through the gills to encyst in the gill tissue of bivalves.

Steringophorus furciger is a trematode parasite usually found in the stomach of flatfish (Scott, 1975; Bray and Gibson, 1980; Scott and Scott, 1988). It feeds on the host's food, and the intensity of the infection can exceed 100 parasites per host individual (Polyanski, 1955). Køie (1969) considered its presence in the stomach of whelks accidental and related to the similar use of food resources by whelks and flatfish. It likely has little effect on whelks from the Mingan Islands because of its low intensity (1–4 parasites per host).

Of the four trematodes infecting *Buccinum undatum* in the Mingan Islands, *Neophasis* sp. clearly has the greatest effect on its host. Although the prevalence of *Steringophorus furciger* was similar to that of *Neophasis* sp., it caused little or no tissue damage and did not invade the gonad. Even though *Renicola* sp. clearly damaged the digestive gland of whelks, its effect on the population is probably negligible owing to its low prevalence. In contrast, *Neophasis* sp. likely markedly affects whelk populations in the Mingan Islands, given that it castrates large numbers of mature individuals.

In undisturbed populations, the relationship between host and castrating parasites normally attains an equilibrium over time, as in prey/predator interactions (Curio, 1988). Additional pressures on host populations, such as those likely to be caused by a fishery, potentially destabilize such relationships. Destabilization is a strong possibility for the whelk/*Neophasis* interaction because both the commercial whelk fishery and *Neophasis* infections reduce the numbers of reproducing whelks.

Acknowledgments

We thank C. Berger, S. Blanchet, M. C. Giasson, P. Girard, and M. Vaugeois for their help in field and laboratory work. We are grateful to D. J. Arsenault, S. Morissette, and R. Rochette for valuable discussions and precious help during the preparation of the manuscript. This study was supported by an NSERC operating grant to John H. Himmelman.

Literature Cited

Appy, R. G., and M. D. B. Burt. 1982. Metazoan parasites of cod. *Gadus morhua* L., in Canadian Atlantic waters. *Can. J. Zool.* **60:** 1573–1579.

Bray, R. A., and D. I. Gibson. 1980. The Fellodistomidae (Digenea) of fishes from northeast Atlantic. *Bull. Br. Mus. (Nat. Hist.) Zool.* **37:** 199–293.

Bray, R. A., and D. I. Gibson. 1991. The Acanthocolpidae (Digenea) of fishes from the north-east Atlantic: the status of *Neophasis* Stafford, 1904 (Digenea) and the study of North Atlantic forms. *Syst. Parasitol.* **19:** 95–117.

Caullery, M. 1950. *Le parasitisme et la symbiose.* 2nd ed. G. Doin, Paris. 358 pages.

Cheng, T. C. 1964. *The Biology of Animal Parasites.* W. B. Saunders, London. 727 pages.

Cheng, T. C. 1983. Studies on parasitic castration: aminopeptidase activity levels and protein concentrations in *Ilyanassa obsoleta* (Mollusca) parasitized by larval trematodes. *J. Invertebr. Pathol.* **42:** 42–50.

Combes, C. 1982. Trematodes: antagonism between species and sterilizing effects on snails in biological control. *Parasitology* **84:** 151–175.

Curio, E. 1988. Behavior and parasitism. Pp. 149–160 in *Parasitology in Focus*, H. Mehlhorn, ed. Springer, Berlin.

Dixon, W. J. 1985. *BMDP Statistical Software*. University of California Press, Berkeley. 733 pages.

Dutil, C. 1988. Partage des ressources alimentaires et comportement de prédation des étoiles de mer de la communauté infralittorale du golfe du Saint-Laurent. Master's thesis, Université Laval, Québec. 77 pages.

Gibson, D. I. 1996. Trematoda. Pp. 192–195 in *Guide to the Parasites of Fishes of Canada. Part IV.* L. Margolis and Z. Kabata, eds., *Can. Spec. Publ. Fish. Aquat. Sci.* **124.**

Gorbushin, A. M. 1997. Field evidence of trematode-induced gigantism in *Hydrobia* spp. (Gastropoda: Prosobranchia). *J. Mar. Biol. Assoc. UK* **77:** 785–800.

Guillemette, M., R. C. Ydenberg, and J. H. Himmelman. 1992. The role of energy intake rate in prey and habitat selection of common eiders *Somateria mollissima* in winter: a risk-sensitive interpretation. *J. Anim. Ecol.* **61:** 599–610.

Hamel, J. R. 1989. Régime alimentaire et comportements d'alimentation et de reproduction du gastéropode *Buccinum undatum* (L.) dans le nord du golfe du Saint-Laurent. Master's thesis, Université Laval, Québec. 39 pages.

Himmelman, J. H. 1991. Diving observations of subtidal communities in the northern Gulf of St. Lawrence. *Can. Spec. Publ. Fish. Aquat. Sci.* **113:** 319–332.

Hughes, R. N., and P. Answer. 1982. Growth, spawning and trematode infection of *Littorina littorea* (L.) from an exposed shore in North Wales. *J. Molluscan Stud.* **48:** 321–330.

Huxham, H., D. Raffaelli, and A. Pike. 1993. The influence of *Cryptocotyle lingua* (Digenea: Platyhelminthes) infections on the survival and fecundity of *Littorina littorea* (Gastropoda: Prosobranchia); an ecological approach. *J. Exp. Mar. Biol. Ecol.* **168:** 223–238.

Jalbert, P., J. H. Himmelman, P. Béland, and B. Thomas. 1989. Whelks (*Buccinum undatum*) and other subtidal invertebrate predators in the northern Gulf of St. Lawrence. *Nat. Can.* **116:** 1–15.

Køie, M. 1969. On the endoparasites of *Buccinum undatum* L. with special reference to the trematodes. *Ophelia* **6:** 251–279.

Køie, M. 1971. On the histochemistry and ultrastructure of redia of *Neophasis lageniformis* (Lebour, 1910) (Trematoda, Acanthocolpidae). *Ophelia* **9:** 113–143.

Køie, M. 1973. The host parasite interface and associated structures of the cercaria and adult *Neophasis lageniformis* (Lebour, 1910). *Ophelia* **12:** 205–219.

Kuris, A. M. 1973. Biological control: implications of the analogy between the trophic interactions of insect pest-parasitoid and snail-trematode systems. *Exp. Parasitol.* **33.** 365–379.

Kuris, A. M. 1974. Trophic interactions: similarity of parasitic castrators to parasitoids. *Q. Rev. Biol.* **49:** 129–148.

Lafferty, K. D. 1993. Effects of parasitic castration on growth, reproduction and population dynamics of the marine snail *Cerithidae californica. Mar. Ecol. Prog. Ser.* **96:** 229–237.

Lauckner, G. 1986. Ecological effects of larval trematode infestation on littoral marine invertebrate populations. *Int. J. Parasitol.* **17:** 391–398.

Lebour, M. V. 1908. Fish trematodes on the Northumberland coast. *Northumb. Sea Fish. Rep.* **1907:** 23–67.

Lebour, M. V. 1910. *Acanthopsolus lageniformis*, n. sp., a trematode in the catfish. *Northumb. Sea Fish. Rep.* **1909:** 29–35.

Lebour, M. V. 1911. A review of the British marine cercariae. *Parasitol.* **4:** 416–456.

Legendre, L., and P. Legendre. 1984. *Écologie Numérique*. Vol II, 2nd ed., Masson and Presses l'Université du Québec, Paris. 335 pages.

Lie, K. J. 1973. Larval trematode antagonism: principles and possible application as a control method. *Exp. Parasitol.* **33:** 343–349.

Martel, A., D. H. Larrivée, K. R. Klein, and J. H. Himmelman. 1986. Reproductive cycle and seasonal feeding activity of the neogastropod *Buccinum undatum. Mar. Biol.* **92:** 211–221.

McClelland, G., and T. K. R. Bourns. 1969. Effects of *Trichobilharzia ocellata* on growth, reproduction, and survival of *Lymnae stagnalis. Exp. Parasitol.* **24:** 137–146.

Mouritsen, K. N., and K. T. Jensen. 1994. The enigma of gigantism: effect of larval trematodes on growth, fecundity, egestion and locomotion in *Hydrobia ulvae* (Pennant) (Gastropoda: Prosobranchia). *J. Exp. Mar. Biol. Ecol.* **181:** 53–66.

Polyanski, Y. I. 1955. Studies on the parasitology of the fish in the northern seas of URSS. Parasites of fish of the Barents Sea. *Tr. Zool. Inst.* **19:** 5–170.

Pritchard, M. H., and G. O. W. Kruse. 1982. *The Collection and Preservation of Animal Parasites.* University of Nebraska Press, Lincoln, NE. 141 pages.

Rothschild, M. 1936. Gigantism and variation in *Peringia ulvae* Pennant 1777, caused by infection with larval trematodes. *J. Mar. Biol. Assoc. UK* **30:** 537–546.

Rothschild, M. 1941. The effect of trematode parasites on the growth of *Littorina neritoides* (L.). *J. Mar. Biol. Assoc. UK* **25:** 69–80.

Santarelli, L., and P. Gros. 1985. Détermination de l'âge et de la croissance de *Buccinum undatum* L. (Gastropoda: Prosobranchia) à l'aide des isotopes stables de la coquille et de l'ornementation operculaire. *Oceanol. Acta* **8:** 221–229.

Savard, L. 1994. Rapport sur l'état des invertébrés en 1993: crustacés et mollusques des côtes du Québec et crevette nordique de l'estuaire et du golfe du Saint-Laurent. *Can. Manuscr. Rep. Fish. Aquat. Sci.* **2257:** 82–92.

Scott, J. S. 1975. Incidence of trematode parasites of American plaice (*Hippoglossoides platessoides*) of the Scotian Shelf and Gulf of St. Lawrence in relation to fish length and food. *J. Fish. Res. Board Can.* **32:** 479–483.

Scott, W. B., and M. G. Scott. 1988. Atlantic Fishes of Canada. *Can. Bull. Fish. Aquat. Sci.* **219:** 731 pages.

Sousa, W. P. 1983. Host life history and the effect of parasitic castration on growth: a field study of *Cerithidea californica* Haldeman (Gastropoda: Prosobranchia) and its trematode parasites. *J. Exp. Mar. Biol. Ecol.* **73:** 273–296.

Sousa, W. P., and M. Gleason. 1989. Does parasitic infection compromise host survival under extreme environmental conditions? The case for *Cerithidea californica* (Gastropoda: Prosobranchia). *Oecologia* **80:** 456–464.

Stunkard, H. W. 1964. Studies on the trematode genus *Renicola*: observations on the life-history, specificity, and systematic position. *Biol. Bull.* **126:** 467–489.

Thomas, M. L. H., and J. H. Himmelman. 1988. Influence of predation on shell morphology of *Buccinum undatum* L. on Atlantic coast of Canada. *J. Exp. Mar. Biol. Ecol.* **115:** 221–236.

Vernberg, W. B., and F. J. Vernberg. 1963. Influence of parasitism on the thermal resistance of mud-flat snail, *Nassarius obsoleta* Say. *Exp. Parasitol.* **14:** 330–332.

Vernberg, W. B., and F. J. Vernberg. 1967. Interrelationships between parasites and their host III. Effect of larval trematodes on the thermal metabolic response of their molluscan host. *Exp. Parasitol.* **20:** 225–231.

Vernberg, W. B., and F. J. Vernberg. 1974. Metabolic pattern of a trematode and its host: a study in the evolution of physiological responses. Pp. 161–172 in *Symbiosis in the Sea*, W. B. Vernberg, ed. Belle W. Baruch Library in Marine Science, University of South Carolina, Columbia, SC.

Zar, J. H. 1984. *Biostatistical Analysis*, 2nd ed., Prentice Hall, Englewood Cliffs, NJ. 718 pages.

Reference: *Biol. Bull.* **198:** 272–283 (April 2000)

Vacuolar-type ATPase in the Accessory Boring Organ of *Nucella lamellosa* (Gmelin) (Mollusca: Gastropoda): Role in Shell Penetration

ERIC S. CLELLAND AND A. S. M. SALEUDDIN*

Department of Biology, York University, Toronto, Ontario, Canada M3J 1P3

Abstract. The structure and function of the accessory boring organ (ABO) of muricid gastropods has been described in numerous studies, and the ABO of *Nucella lamellosa* was found to be similar to those of other muricid species. The active cap region of the ABO is composed of tall, mitochondria-rich cells with distinct brush borders at their apicies, surrounding a hemolymph-containing central sinus. Using antibodies specific for vacuolar-type ATPase (V-ATPase), enzyme immunoreactivity was found to be limited to the brush border of the epithelial cells. Electron immunohistochemistry revealed that V-ATPase immunoreactivity resides in the plasma membranes of the microvilli. Immunodot blotting using yeast V-ATPase as a positive control confirmed the specificity of the reactions. SDS-PAGE of membrane suspensions from the ABO revealed protein bands of the requisite molecular weight for V-ATPase subunits. Western blots suggest that antibodies raised against mammalian V-ATPase subunits recognize subunits of the molluscan V-ATPase. The molecular weights of these identified subunits are similar to those in mammals. The V-ATPase-specific inhibitor bafilomycin A_1 inhibited ATPase activity in samples of ABO homogenate by about 10% relative to control, providing further evidence for the presence of V-ATPase. Specific V-ATPase activity was about 67 picomoles of inorganic phosphate per microgram of protein per minute in the homogenate. Collectively this evidence strongly suggests that a vacuolar-type proton transporting ATPase is present in the brush border of the accessory boring organ of *Nucella lamellosa*, and is responsible for acidifying secretions from this gland. Similarities between the ABO, osteoclasts, and the mantle of freshwater bivalves also suggest that the mechanism for decalcification of calcareous substrates is conserved.

Introduction

Nucella lamellosa is a predatory marine snail of the family Muricidae (=Muricacea); it is commonly found in intertidal and subtidal zones along the Pacific Northwest coast of North America, ranging from the Aleutian Islands to Santa Cruz, California (Collins *et al.*, 1996). Muricid gastropods such as whelks and oyster drills feed on a variety of invertebrates such as bivalves, barnacles, small crabs, polychaetes, and occasionally carrion (Fretter and Graham, 1962; Carriker, 1981; West, 1986, 1988). The snails use a chemomechanical process to bore through bivalve shells and other calcareous substrates. This process combines the secretion of acidic solution from the accessory boring organ (ABO), to soften the shell, with the rasping action of the radula, to remove the loosened material. Acidity as low as pH 3.8 (~4 pH units lower than the surrounding seawater) has been measured within bore holes created by drilling muricids (Carriker and Van Zandt, 1967). The ABO of muricids is located in the anterior region of the sole of the foot, and is everted by hydrostatic pressure of the hemolymph in actively drilling animals. The ABO consists of a cap (about 1–2.5 mm diameter) and stalk (about 0.4 mm in length); the cap is composed of a central sinus surrounded by a single layer of tall (200–300 μm), mitochondria-rich epithelial cells. These cells also possess prominent apical brush borders, are separated from the sinus by a thin, often indistinct basement membrane, and communicate with one another *via* gap junctions. The structure of the muricid ABO and the mechanism of shell boring by muricid (and naticid) gastropods have been reviewed by Carriker (1981).

Webb and Saleuddin (1977) postulated that acid ATPase

Received 14 October 1999; accepted 27 December 1999.

* To whom correspondence should be addressed. E-mail: saber@yorku.ca

pumps residing in the apical membranes of the ABO epithelial cells are responsible for acidifying the secretions from the muricid ABO. Vacuolar-type ATPase (V-ATPase) proton pumps are now known to be present in all eukaryotic cells, where they energize endomembranes (Finbow and Harrison, 1997). V-ATPases have also been detected in the plasma membrane of specialized cells in many animal epithelial tissues such as frog skin (Ehrenfeld and Klein, 1997), gills of freshwater fish (Lin *et al.*, 1994) and crustaceans (Onken and Putzenlechner, 1995), and in insect Malpighian tubules (Al-Fifi *et al.*, 1998) and midguts (Schweikel *et al.*, 1989), where they are used to generate transmembrane potentials that power the transport of other ions (*e.g.*, Na^+, K^+, CO_3^-). In osteoclasts (Nordström *et al.*, 1997), kidney collecting-duct cells (Brown *et al.*, 1988), urinary bladders (Lubansky and Arruda, 1985), epididymis (Brown *et al.*, 1997), salivary glands (Just and Walz, 1994), and the mantle of freshwater bivalves (Hudson, 1993; da Costa *et al.*, 1999), V-ATPases serve to acidify the extracellular environment by extruding protons from the cytoplasm of epithelial cells. Comprehensive reviews of V-ATPases are found in Brown and Breton (1996); Finbow and Harrison (1997); Harvey *et al.* (1998); Nelson and Harvey (1999); Wieczorek *et al.* (1999). Cells that possess plasma membrane V-ATPase pumps have common characteristics that closely resemble those of the epithelial cells of the muricid ABO. Furthermore, models describing V-ATPase-driven proton transport in various animal tissues (see Harvey *et al.*, 1998) are similar to the Webb and Saleuddin (1977) model describing proton transport in muricid ABOs; however, V-ATPases were unknown at the time of this earlier publication.

In this study we investigated a muricid ABO to determine whether V-ATPase pumps are present. Taking advantage of the conserved structure of V-ATPase molecules (Nelson and Harvey, 1999) and the cross reactivity (across phyla) of antibodies raised against V-ATPase subunits (Russell *et al.*, 1992), we probed sections of ABO tissue using primary antibodies directed against the A (~70 kDa), B (~60 kDa), and d (~39 kDa) subunits of the V-ATPase enzyme. Immunoblotting studies on extracts of ABOs were also completed. Additionally, the specific V-ATPase inhibitor bafilomycin A_1 (Bowman *et al.*, 1988) was used in assays of ATPase activity in ABO extracts to reveal the contribution of V-ATPase to the overall ATPase activity.

Materials and Methods

Animals

Specimens of *Nucella lamellosa* were obtained from Westwind Sealab Supplies, Victoria, British Columbia, at various times throughout the year. The animals were maintained in 50-l aquaria in artificial seawater (ASW; Instant Ocean from Aquarium Systems, Mentor, Ohio), pH 7.2–8.0; 950–1000 mmol/kg H_2O, at 5°C under a 12L:12D photoperiod. Live blue mussels were provided as the major food source. Under these conditions, the snails appeared to thrive, feeding regularly and depositing egg sacs on the walls of the aquaria.

Experimental animals ranging in length from 2 to 5 cm were chosen at random and narcotized in ASW diluted with an equal volume of 20% $MgSO_4 \cdot 7H_2O$ (Pantin, 1964). The shells were cracked using a bench vise, and the soft body was removed and rinsed clean of shell fragments. In accordance with the procedure of Carriker *et al.* (1963), the animals were cut in two at the base of the visceral hump, separating the viscera from the pedal mass. The pedal mass was pinned in a paraffin-based dissecting dish, with the ventral sole of the foot spread uppermost so as to expose the crypt of the retracted boring organ. Gentle pressure was applied to evert the ABO. The ABO, along with a short portion of the stalk, was excised using iridectomy scissors and fine forceps.

Accessory boring organs for microscopic examination were transferred to the appropriate fixative, while those to be used for biochemical assay, immunoblotting, or gel electrophoresis were transferred to homogenization buffer for immediate processing or were frozen in liquid nitrogen and stored at −80°C until required.

Chemicals and Antibodies

Unless otherwise specified, all chemicals were reagent grade, and were obtained from Sigma-Aldrich Canada Ltd.

Affinity-purified polyclonal antibodies raised against bovine V-ATPase d (39 kDa) and B (~60 kDa) subunits (raised in rabbit) and monoclonal antibodies raised against yeast (*Saccharomyces cerevisiae*) V-ATPase B (~60 kDa) and A (~70 kDa) subunits were donated by Dr. Sergio Grinstein and Dr. Morris Manolson of the University of Toronto. A sample of yeast V-ATPase was also supplied by Dr. Manolson.

Light microscopy

Accessory boring organs were excised from *Nucella* and fixed in Hollande Bouin's fixative for 12–18 h. The tissues were rinsed in distilled water, dehydrated, and embedded in paraffin. Serial sections of 8 μm thickness were deparaffinized, rehydrated, and stained in Mallory-Heidenhain for 5 min (Humason, 1967). Sections were viewed using a Leitz orthoplan microscope, and micrographs were taken using a Wild-Heerbrugg MPS 45/51S system.

Light microscope immunocytochemistry

Accessory boring organs were fixed and embedded as above. Serial sections were mounted on multiwell glass slides coated with 0.5% chrome alum and 0.5% gelatin. Sections to be used with alkaline-phosphatase-conjugated secondary antibodies were treated with 20% acetic acid for 30 min after rehydration; those probed with HRP (horseradish peroxidase)-conjugated secondary antibodies were treated with 0.3% H_2O_2 in methanol for 30 min prior to rehydration in graded ethanol. Secondary antibody conjugates (Sigma) were raised in goat and directed against either rabbit or mouse whole IgG. The antibodies were conjugated to either alkaline phosphatase or HRP. Tissues were rinsed in glass distilled water (ddH_2O), followed by two or three rinses in phosphate buffered saline (PBS). Nonspecific binding was blocked by incubation in PBS containing 5% normal goat serum (NGS) and 0.2% Triton X-100 (incubation buffer) for 1 h. Primary antibodies were applied undiluted from the stock provided (~20 μl was sufficient to cover each section), and sections were incubated for 12–18 h at 4°C. Control sections were maintained in incubation buffer without antibody. Following incubation, the primary antibodies were removed with several changes of incubation buffer over a period of 30 min. The sections were then incubated in secondary antibody conjugate (diluted 1:50 in incubation buffer) for 1 h at 22°C, then rinsed in PBS (three rinses, 5 min each) and finally in ddH_2O. Peroxidase was localized using Sigma Fast DAB Tablets (3,3′-diaminobenzidine tetrahydrochloride/H_2O_2), then sections were dehyrated and mounted as above. Alkaline phosphatase was localized using Sigma Fast BCIP/NBT tablets (5-bromo-4-chloro-3-indolyl-phosphate/nitro blue tetrazolium). The sections were mounted in aqueous media (5% polyvinyl alcohol; 30% glycerol), viewed, and photographed.

Transmission electron microscopy

Accessory boring organs were excised and fixed in a solution of 1% glutaraldehyde-0.1% paraformaldehyde in filtered ASW for 1 h at 22°C, then postfixed for 1 h in 1% aqueous osmium tetroxide at 0°C. Following fixation, the ABOs were rinsed in distilled water, dehydrated in graded ethanol, and embedded in epoxy resin. Thin sections (~80 nm thick) were cut using a diamond knife, floated onto Formvar-coated single-slot grids, and stained with uranyl acetate and lead citrate. Sections were viewed in a Philips EM201 transmission electron microscope.

Electron microscope immunocytochemistry

Accessory boring organs were excised from *Nucella;* rinsed in ASW; and fixed in 2% paraformaldehyde, 0.075 *M* lysine, 0.01 *M* sodium meta-periodate, in 0.037 *M* phosphate buffer, pH 7.4 (PLP fixative; McClean and Nakane, 1974) for 2 h at 22°C. The tissues were thoroughly rinsed in distilled water, dehydrated to 70% ethanol, and embedded in LR-White resin (London Research Laboratories). The resin was polymerized under ultraviolet light for 96 h at 4°C. Thin sections were cut as described, collected on Formvar-coated 200 mesh nickel grids, and allowed to anneal overnight. The grids were first rinsed in distilled water and then in PBS, as for paraffin sections, and incubated in 5% NGS in PBS for 1 h to block nonspecific binding sites. Grids were floated on 25-μl droplets of primary antibody (anti-d subunit), and incubated in a humid chamber for 12 h at 22°C. The grids were rinsed three times in buffer (20 min each rinse) and incubated for 1 h in 10-nm gold-conjugated secondary antibody (BDH). Unbound secondary antibody was rinsed away with three changes (10 min each) of PBS and distilled water. The grids were stained with uranyl acetate and viewed as above.

Tissue preparation

Fresh or frozen ABOs (15 to 20) were homogenized on ice in 3 to 4 times their volume in buffer containing 20 m*M* Tris-HCl; 250 m*M* sucrose; 1 m*M* phenylmethyl sulfonyl fluoride (PMSF); 1 m*M* ethylene glycol bis (β-aminoethyl ether) *N, N, N′, N′*-tetraacetic acid (EGTA); 1 m*M* dithiothreitol (DTT); pH 7.4 (Rautiala *et al.*, 1993) using a motorized Teflon pestle in 1.5 ml polypropylene Eppendorf tubes. The homogenate was centrifuged at 1000 × *g* at 4°C for 15 min. The supernatant was collected, and the pellet was resuspended and recentrifuged. The resultant supernatant was combined with the first and used for ATPase assays without further purification, because more highly purified samples showed an apparent loss of activity.

For polyacrylamide gels and immunoblotting, the 1000 × *g* supernatant was subjected to further purification. It was centrifuged at 15,000 × *g* for 20 min, and the pellet discarded. The supernatant from this step was transferred to polyallomer centrifuge tubes, diluted with homogenization buffer to 500 μl, and centrifuged for 90 min at 100,000 × *g* using a Beckman Optima L-90K ultracentrifuge and SW65 rotor. The resultant supernatant was collected and the membrane pellet resuspended in 20–25 μl double distilled water (ddH_2O). Samples of the 15,000 × *g* and the 100,000 × *g* supernatants, as well as the membrane suspension, were frozen in liquid nitrogen and stored at −80°C until required.

Protein determination

Processed tissues were analyzed for their protein content using a Bio-Rad protein assay kit, which utilizes the method of Bradford (1976). Protein content was determined by comparison to a standard curve produced using bovine serum albumin (BSA).

Gel electrophoresis

SDS-PAGE was carried out using a Bio-Rad Mini-Protean II system. Samples diluted in buffer (50% H_2O; 0.0625% Tris-HCl, pH 6.8; 10% glycerol; 2% SDS; 5% 2-β mercaptoethanol; 0.0013% bromo-phenol blue) 1:4, were loaded onto 4%–15% (w/v) linear gradient SDS-PAGE precast gels (BioRad) or onto 9% (w/v) SDS-PAGE gels *via*

3.3% (w/v) stacking gels (Laemmli, 1970). The gels were run at 100 V for about 1 h, rinsed with ddH_2O, and stained for protein using Coomassie brilliant blue R-250 in fixative (40% methanol, 10% acetic acid). Nonspecific staining was removed in a solution of 40% methanol and 10% acetic acid. Gels were vacuum dried onto blotting paper and photographed.

Immunoblotting

For dot blots, samples of the 15,000 × *g* supernatant (3 μg or 15 μg total protein per sample) or purified yeast V-ATPase (1-μl and 2-μl samples) were pipetted onto methanol-activated PVDF membranes (0.45-μm pore size, Gelman Sciences) and allowed to air dry. The membranes were rinsed in Tris-buffered saline (TBS; 20 m*M* Tris-HCl, 500 m*M* NaCl, pH 7.5). Immunoblotting was carried out essentially according to Sheng and Schuster (1992). Experimental blots and positive control membranes were incubated with polyclonal antibodies (either anti-d or anti-B V-ATPase subunit) diluted 1:1000 in incubation buffer (TBS containing 0.5% BSA and 0.02% NaN_3) for 12 h at 4°C. Negative controls were kept in incubation buffer without primary antibody. The membranes were washed and probed using alkaline-phosphatase-conjugated anti-Ig G antibodies (diluted 1:4000 in incubation buffer) for 1 h at 22°C. After washing out the unbound secondary antibodies, the membranes were rinsed with several changes of ddH_2O, and staining was developed with Sigma Fast BCIP/NBT tablets. The membranes were allowed to air dry, and then photographed.

For Western blotting, 10-μg samples of the 100,000 × *g* resuspended pellet (diluted 1:4 in running buffer) and markers were loaded onto 9% SDS-PAGE gels and electrophoresed as described above. The gels were removed, rinsed in ddH_2O, then placed in transfer buffer (25 m*M* Tris, 192 m*M* glycine, 20% v/v methanol, pH 8.3) and equilibrated for 30 min with gentle agitation. PVDF membranes were wetted in 100% methanol and also allowed to equilibrate in transfer buffer. Blotting was completed using the Bio-Rad Mini Trans-Blot module for the Mini-Protean II system. Transfer was completed overnight at 4°C, after which the membranes were allowed to air dry, allowing the protein to adhere tightly to the PVDF membrane. Membranes were then placed in a solution of 0.3% H_2O_2 for 10 min to block endogenous peroxidase activity, rinsed in ddH_2O and TBS, then nonspecific binding sites were blocked as for the dot blots. Primary antibodies were applied as described for the dot blots and incubated overnight at 4°C. The membranes were washed in incubation buffer, incubated in 1% nonfat milk in TBS, and rinsed in incubation buffer. At this time the membranes were rinsed in TBS (3 times, 10 min each), and a "Histomark" Streptavidin-HRP system kit was employed (Kirkegaard and Perry Laboratories Inc. (KPL), Gaithersberg, Maryland). The membranes were incubated for 30 min at room temperature in 10% v/v NGS provided with the kit. The membranes were then transferred to the biotinylated antibody solution provided (diluted 1:4 in TBS) and incubated a further 30 min. The membranes were rinsed (3 times, 5 min each) in TBS containing 1% NGS, and incubated in streptavidin-peroxidase (diluted 1:4 from that provided) for an additional 30 min. Following this treatment, the membranes were rinsed in several changes of TBS, then in distilled water. Banding patterns were revealed using KPL TrueBlue peroxidase substrate. The membranes were allowed to dry, and were photographed.

ATPase assays

Ten to twenty-five microlitres of the homogenate (~15 μg protein per tube) were placed in 1.5-ml Eppendorf tubes, in 145 μl of assay buffer (2 m*M* $MgCl_2$, 20 m*M* KCl, 0.1 m*M* EGTA, 0.3 mg/ml BSA, 0.5 m*M* sodium azide (NaN_3) [to inhibit mitochondrial ATPase activity], 30 m*M* Tris-HCl, pH 7.5; modified from Al-Fifi *et al.*, 1998). To experimental samples, 5 μl of bafilomycin A_1 (Sigma) stock solution (10 μg diluted in 500 μl dimethylsulfoxide (DMSO)) was added, giving a final concentration of 1 μ*M* for the inhibitor. DMSO alone was added to the controls (Onken and Putzenlechner, 1995). Samples were incubated for 30 min at 22°C to allow the inhibitors to react. To initiate the ATPase reaction, 50 μl of 12 m*M* Mg^{2+}-ATP was added to the sample tubes (3 m*M* final concentration). The samples were reacted for 45 min at 37°C in a water bath, following which 400 μl of a 1:1 mixture of 1% polyoxyethylene 10 lauryl ether in distilled deionized water, and 1% ammonium molybdate in 0.9 *M* H_2SO_4 was added to stop the reaction (procedure modified from Atkinson *et al.*, 1973). The tubes were kept at room temperature for 10 min to allow the yellow color to develop. Absorbancy was then measured at 390 nm. The relative quantity of inorganic phosphate (Pi) was determined by comparison to a standard curve produced using phosphate standards as described by Atkinson *et al.* (1973). The total activity is expressed as the amount of Pi produced per microgram of total protein per minute. The V-ATPase activity was determined to be the difference between the amount of Pi produced by the controls in the absence of bafilomycin and the amount produced by experimental samples with bafilomycin.

Statistical analysis

Student's *t* tests were completed on the experimental ATPase assay data using GraphPad Instat v. 2.0 (GraphPad Software, San Diego, California).

Results

Structure of the Accessory Boring Organ

The structure of the ABO in *Nucella lamellosa* is shown in Figure 1, and is similar to that described for other muricids, in particular to that of *Thais (N.) lapillus* (Webb and Saleuddin, 1977). The cap of the ABO consists of a single layer of epithelial cells (e), surrounding a central sinus (s). The epithelial cells possess a distinct apical brush border (b). The stalk of the ABO invaginates into the foot (f), and also contains a sinus (s). The brush border of the epithelial cells is about 10–15 μm in height, and the cells themselves are tall (200–300 μm) and thin, with irregular basal infoldings abutting the central sinus. There is no distinct demarcation between the epithelial cells and the sinus. Interstitial spaces can be seen between the cells, providing additional surface area to the sinus. Nuclei are identifiable in the basal third of the cells, and other organelles occur distally to them. Strands of muscle and connective tissue can be observed spanning the sinus, loosely connecting the epithelium to the more muscularized stalk. The muscle in the stalk is probably involved in retracting the ABO into its vestibule within the foot.

By contrast, the surrounding foot epithelium (arrowheads) is composed of shorter columnar cells (~40 μm in height) without a brush border. An obvious basement membrane underlies these cells, separating them from the foot tissue below. The foot epithelium is composed mainly of goblet cells, which undoubtedly secrete mucus, serving to lubricate the foot and to seal it tightly to the substrate when the snail is drilling. At the electron microscope level, the apical area of the ABO epithelial cells (Fig. 2) shows the long microvilli (mv) that make up the brush border of the ABO, and the many mitochondria (m) within the cells. Dense granules are also present in the apical region of the cells. Gap junctions (gj) occurring between adjacent epithelial cells are commonly seen in the apical region (Fig. 3). These junctions are thought to facilitate communication between the cells, ensuring rapid and uniform response of the ABO epithelium (Webb and Saleuddin, 1977).

Immunocytochemical localization

Positive immunoreaction for V-ATPase was obtained using anti-d subunit primary antibody, with either alkaline phosphatase or HRP conjugates as secondary antibodies (Figs. 4, 5, 6). Immunoreaction was localized exclusively to the brush border region of the ABO. The surrounding foot epithelium (acting as built-in control for the sections) and other areas of the ABO showed no immunostaining. Sec-

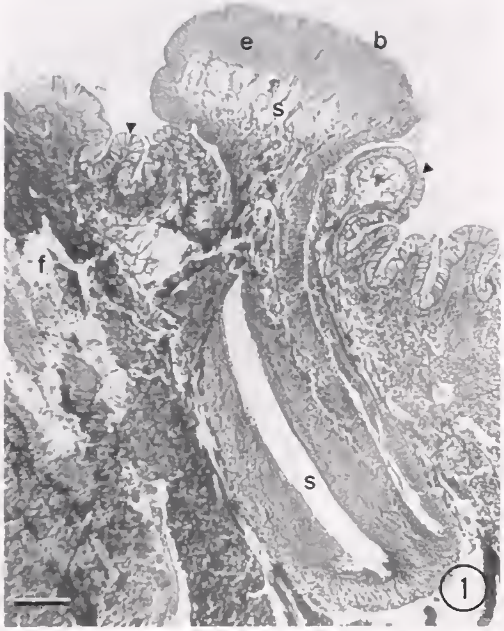

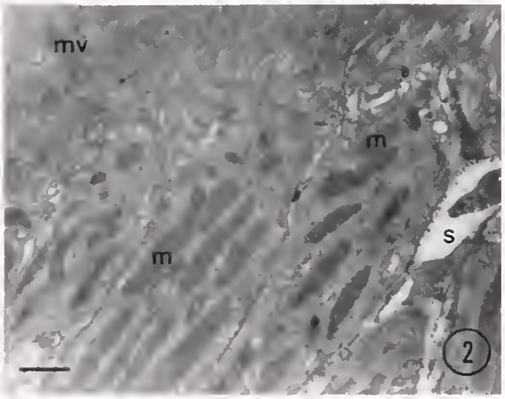

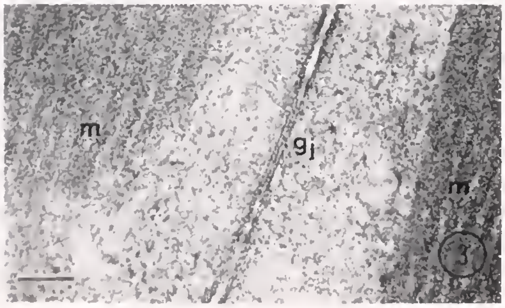

Figures 1–3. The accessory boring organ (ABO) of *Nucella lamellosa*.

Figure 1. Section of an everted ABO stained with Mallory-Heidenhain quick stain. Note the mushroom shape of the organ. The cap is comprised of a single layer of epithelial cells (e) surrounding a central sinus (s), which is continuous with the sinus in the stalk. The stalk invaginates into the foot (f). The epithelial cells of the ABO cap are long (200–300 μm), with a prominent brush border (b). By contrast, the epithelial cells of the surrounding foot tissue (arrow heads) are short (40 μm). Muscle is seen in the left hand side of the stalk, and is presumably used to retract the ABO into its crypt (vestibule) in the foot. Scale bar: 200 μm.

Figure 2. Electron micrograph of the apical region of the ABO cap epithelium. Note the long microvilli (mv) of the brush border, the numerous mitochondria (m), and the interstitial spaces (s) between the cells. Dense granules seen in the cells may contain degradative enzymes. Scale bar: 1.5 μm.

Figure 3. Electron micrograph illustrating the presence of gap junctions (gj) between adjacent cells of the ABO cap. Also note the mitochondria (m). Scale bar: 100 nm.

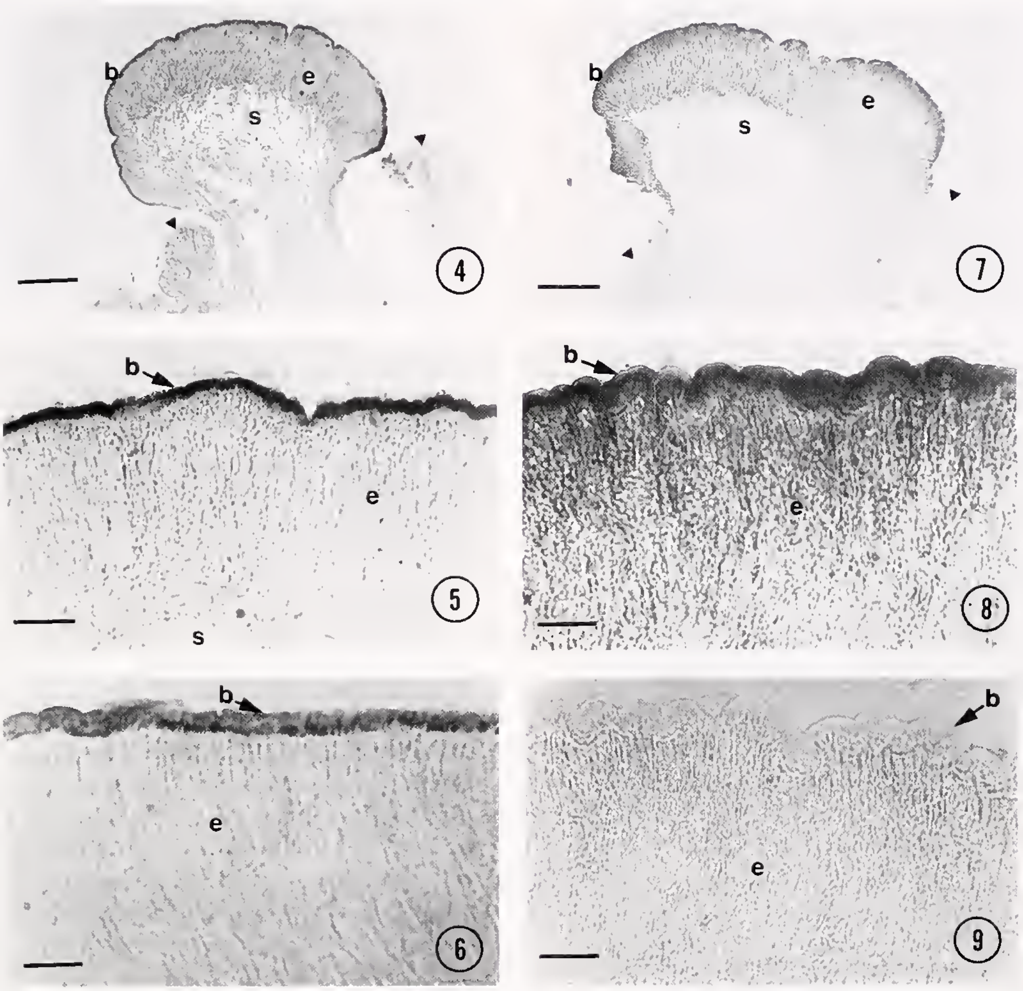

Figures 4–9. Immunohistochemical localization of vacuolar-type ATPase (V-ATPase) in whole accessory boring organ (ABO) of *Nucella lamellosa*.

Figure 4. This section was probed with polyclonal antibody to the V-ATPase d (39-kDa) subunit and alkaline-phosphatase-conjugated secondary antibody. Immunoreactive sites were visualized with BCIP/NBT. Immunostaining is exclusive to the brush border of the ABO (b). Immunostaining is absent in the foot epithelium (arrowheads). e, epithelial cells; s, sinus. Scale bar: 100 μm.

Figure 5. Magnified image of the ABO shown in Figure 4. Note the positive reaction for V-ATPase in the brush border (b). e, epithelium; s, sinus. Scale bar: 75 μm.

Figure 6. This section was probed with the anti-39kDa primary antibody (as above) and HRP-conjugated secondary antibody. Immunoreactive sites were visualized using DAB-H_2O_2. The immunostaining is exclusive to the brush border (b). e, epithelium. Scale bar: 40 μm.

Figure 7. This section was probed with monoclonal antibody to the V-ATPase B (60-kDa) subunit, primary antibody, and alkaline-phosphatase-conjugated secondary antibody. Immunoreactive sites were visualized with BCIP/NBT. Immunostaining is exclusive to the brush border of the ABO (b). Arrowheads, foot epithelium; e, epithelial cells; s, sinus. Scale bar: 100 μm.

Figure 8. Magnified image of the ABO seen in Figure 7. Very intense immunostaining is noted in the brush border (b). e, epithelium. Scale bar: 25 μm.

Figure 9. ABO probed only with alkaline-phosphatase-conjugated secondary antibody and BCIP/NBT. No immunostaining is apparent in the brush border (b). e, epithelium. Scale bar: 25 μm.

tions incubated in anti-B subunit polyclonal antibody showed the same immunostaining pattern. Both the anti-B subunit (Figs. 7 and 8) and anti-A subunit monoclonal antibodies showed positive staining for V-ATPase within the brush border. Control sections incubated without a primary antibody (Fig. 9) exhibited no immunoreaction. Immuno-electron micrographs of a section of an ABO treated with anti-d subunit primary antibody and gold-conjugated secondary antibody showed immunoreactivity (Fig. 10). The reactive sites for the V-ATPase antibody are located in the microvilli of the epithelial cells, as evident by the presence of gold particles in the microvilli. The gold parti-

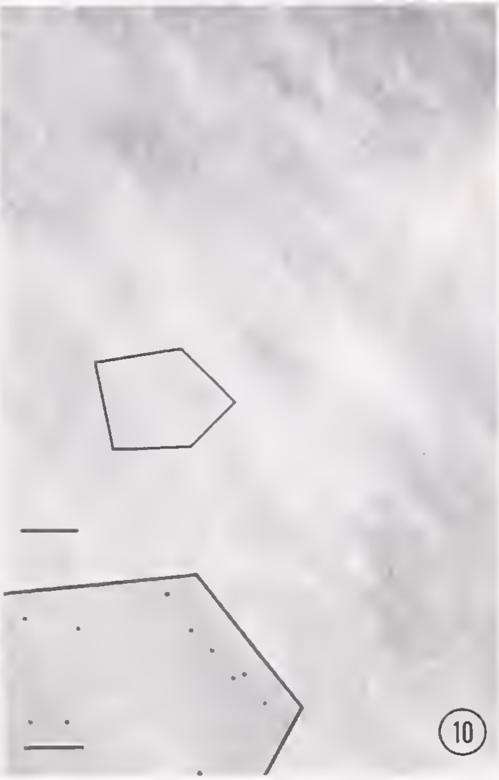

Figure 10. Immuno-electron micrograph of the microvilli (mv) that form the brush border of the accessory boring organ (ABO) of *Nucella lamellosa.* The section was probed with primary antibody to the V-ATPase d (39-kDa) subunit and gold-conjugated secondary antibody. The presence of 10-nm gold particles in the micrograph reveals that the immunoreactive sites for V-ATPases are located in the microvillar membrane. Scale bar: 200 nm. The inset shows the gold particles (outlined in black) that lie close to the plasma membranes of the microvilli. Scale bar: 50 nm.

cles underlie the membranes of the microvilli (inset), since the d subunit closely associates with the transmembrane (V_0) domain in assembled molecules. These results suggest that V-ATPases are present in the plasma membranes of the microvilli of the ABO epithelial cells.

Molecular weight determination

Electropherograms of the 100,000 × *g* membrane resuspension on SDS-polyacrylamide gels (Fig. 11) revealed several peptide bands. Peptides with molecular weights of approximately 70, 60, and 39 kDa (arrowheads) may correspond to subunits A, B, and d, V-ATPase subunits. Other bands corresponding to the remaining V-ATPase subunits (not indicated) are also present. V-ATPase peptides are known to be highly conserved across kingdoms, phyla, genera, and species (Forgac, 1998). Note that in Figure 11, the lower molecular weight standards (17.6 and 7.5 kDa) of the marker lanes run with the dye front (large arrowhead), so that the lower molecular weight peptides are unresolved. The 9% gel was found to be suitable for use in western blotting since markers of 32.6 kDa and higher molecular weights were clearly resolved. The remainder of the bands seen on the gel are presumably peptides of a variety of other membrane molecules (Na^+/K^+-ATPase, ion channel proteins, etc.).

Samples of purified yeast V-ATPase (positive control) and of the 15,000 × *g* gland extract supernatant were applied to PVDF membrane and probed using the polyclonal antibodies and alkaline-phosphatase-conjugated secondary antibodies (Fig. 12). Lane a shows positive immunoreaction to samples of yeast V-ATPase (2-μl samples [top] and 1 μl samples [bottom]) that were probed with the anti-B polyclonal antibody. Lanes b, c, and d were made with samples of the 15,000 × *g* supernatant (15 μg protein [top] and 3 μg protein [bottom]). Lane b and lane c were probed with polyclonal antibodies directed against the B and d V-ATPase subunits respectively. These samples also show positive immunoreactivity. Samples in lane d were incubated without primary antibody and act as negative controls.

Western blots obtained from protein transferred from a 9% SDS-polyacrylamide gel are shown in Figure 13. Markers, indicated on the outside lanes, were also run in the lanes between sections of the membrane incubated in either anti-d (39 kDa) polyclonal antibody (a), anti-B (~60 kDa) polyclonal antibody (b), or without a primary antibody (c). Note that two lanes appear in each section of the blot between the marker lanes. A single nonspecific band occurring slightly below the 70 kDa markers is seen in all the blots. This is probably the result of a protein reacting with the TrueBlue peroxidase substrate. Blot a clearly reveals positive staining with the anti-39-kDa antibody. A single band is observed in each lane somewhat below the 42.8-kDa markers. This band

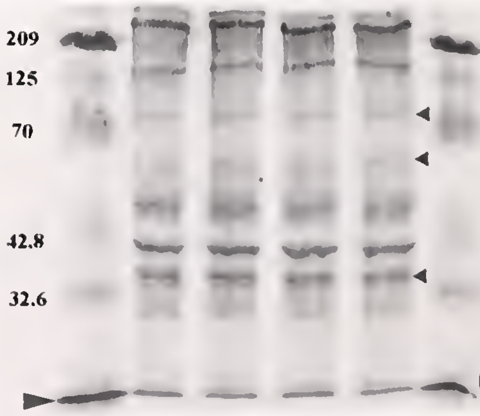

11

Figure 11. Discontinuous SDS-PAGE (9% gel) of ABO membranes. Molecular weight standards are shown in the outside lanes. The 9% gels were found to be suitable for western blotting, since our antibodies are specific for subunits exceeding 32.6 kDa. The center lanes of the gel show the banding pattern observed in the ABO membrane. Peptides corresponding to the molecular weight of A, B, and d V-ATPase subunits are indicated (arrowheads).

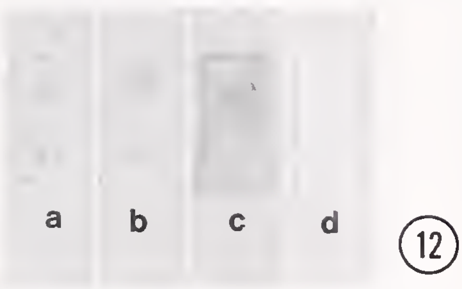

Figure 12. Samples of purified yeast V-ATPase (a: 2 μl, upper; 1 μl lower) and of the 15,000 × *g* supernatant of ABO extract (b, c, d: 15 μg protein, upper; 3 μg protein, lower) were spotted onto PVDF membrane, and probed with primary antibodies and alkaline-phosphatase-conjugated secondary antibodies. Color was developed with BCIP/NBT. a (positive control) and b were probed with the anti-B (~60-kDa) subunit primary antibody, while c was probed with the anti-d (39-kDa) subunit primary antibody. All except d (negative control) show positive staining for V-ATPase.

does not appear in b or c. It appears that the antibody binds to a peptide that has a relative molecular weight corresponding to the subunit against which it was raised. Blot b reveals a positive reaction lying immediately beneath the nonspecific band, at about 60 kDa. It appears that this antibody also recognizes a peptide that corresponds to the subunit against which it was raised. Faint bands occurring in a and b near the 125-kDa marker are possibly due to endogenous peroxidase activity; alternatively, they could reveal peptides with epitopes similar to those recognized by the antibodies. The control blot c shows only the single nonspecific band, indicating that the immunostaining apparent in a and b results from the specific binding of the V-ATPase antibodies to their respective subunits.

ATPase assays

Assays conducted to determine the effect of bafilomycin on the release of Pi reveal that the quantity of Pi detected is significantly lower in samples containing the inhibitor than in the control samples. Three separate homogenates were assayed, and the difference was observed in each case. The results (Table 1) reveal that about 10% of the inorganic phosphate detected in the ATPase assays is liberated by V-ATPase. The remainder of the Pi detected is presumably liberated by other phosphatases present in the homogenates or by the degradation of the Mg^{2+}-ATP substrate during the incubation periods. V-ATPase activity, defined as the average of the mean differences between control and inhibited trials of the three experiments, is 67.0 ± 13.3 (SEM) pmol Pi/(μg protein · min).

Discussion

Muricid snails such as the frilled whelk, *Nucella lamellosa,* normally prey on a variety of invertebrates such as bivalves, gastropods, barnacles, and other small crustaceans that have a protective calcareous external shell. To feed, the snail must usually bore a hole through this shell. Drilling is completed by a chemomechanical process that combines the action of chemical secretions derived from the accessory boring organ (ABO), to soften the shell materials, with the rasping action of the radula on the shell (Carriker, 1981). The secretion is acidic (Carriker and Van Zandt, 1967) and contains degradative enzymes (Webb and Saleuddin, 1977; Carriker and Williams, 1978). Hydrochloric acid is thought to be the inorganic acid secreted by the ABO because the etchings it produces on bivalve shells are similar to those produced by excised ABOs (Carriker *et al.,* 1963; Carriker, 1978, 1981). Webb and Saleuddin (1977) proposed that an acid ATPase pump located on the apical membrane of the ABO is responsible for secreting the acid from the ABO. The presence of V-ATPase pumps in molluscan epithelia has been implied in electrophysiological studies of the outer mantle epithelium in *Unio complanatus* (Hudson, 1993) and in *Anodonta cygnea* (da Costa *et al.,* 1999). Bafilomycin A_1 was seen to collapse the short circuit current across the apical membrane and prevent the extrusion of protons into the mantle cavity. Protons are extruded into this space, where they are buffered by the shell, which is thought to relieve acid loading in the tissues when the clam is closed (Hudson, 1993). Osteoclasts also use V-ATPase pumps located in their ruffled borders (Väänänen *et al.,* 1990) to extrude protons into the extracellular environment. The

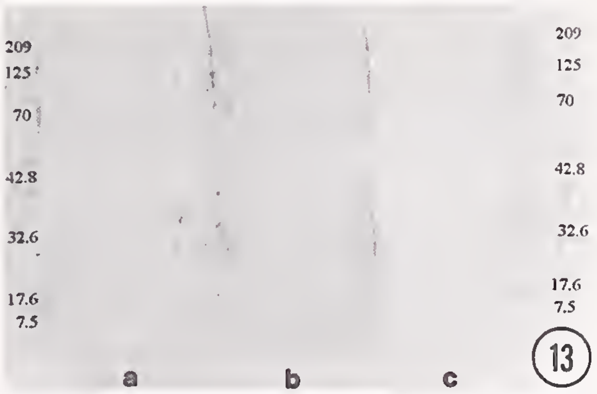

Figure 13. Western blots obtained from membrane preparations. Peptides were transferred onto PVDF membranes from a 9% SDS-PAGE gel. Kaleidoscope markers are shown on each side, and between each blot. The dye front is indicated by the arrowheads. Two lanes appear in each of blots a, b, and c. Blot a was probed with the V-ATPase anti-d (39-kDa) subunit primary antibody and blot b with the anti-B (~60-kDa) subunit primary antibody (polyclonal); c was a negative control. Primary antibodies were detected using a Streptavidin-HRP system, and color was developed using TrueBlue peroxidase substrate. Positive reaction is seen for both V-ATPase subunits, with each antibody binding to its appropriate subunit in the ABO V-ATPase molecule. A single nonspecific band occurring below the 70-kDa marker is seen in a, b, and c. Faint bands seen in and b near the 125-kDa marker are possibly due to endogenous peroxidases or to peptides with epitopes similar to those recognized by the antibodies.

Table 1

ATPase activities in homogenates of accessory boring organ, expressed as nanomoles of inorganic phosphate per microgram of total protein per minute

	Homogenate 1	Homogenate 2	Homogenate 3
Control activity (No inhibitor)	0.4726 ± 0.0026 (5)	1.065 ± 0.0205 (3)	0.6445 ± 0.0060 (4)
Inhibited activity (With bafilomycin)	0.4308 ± 0.0042 (8)	0.993 ± 0.0185 (3)	0.5573 ± 0.0052 (4)
Mean difference (V-ATPase activity)	0.0419***	0.0720*	0.0873**
T	7.20	2.61	11.03
Mean difference/Control mean	0.088 (8.8%)	0.067 (6.7%)	0.136 (13.6%)

The average V-ATPase activity in the three homogenates is 0.067 nmol (67 pmol)/(μg total protein · min) ± 0.0133, or approximately 10% of the average activity in the control assays. Values are mean ± the standard error. The number of experiments is in parentheses. Student's *t* values are indicated (T). Asterisks indicate level of significance: *** $P < 0.0001$; ** $P \leq 0.001$; * $P \leq 0.05$.

osteoclasts anchor to bone, and they extrude protons and chloride ions into bone-resorbing compartments, where the resulting acid dissolves the mineralized component of the bone and activates lysosomal enzymes that break down the bone matrix (Wieczorek *et al.*, 1999). These processes are much like the extrusion of protons from the ABO to dissolve a bivalve shell.

The structure of the ABO in *Nucella lamellosa* was found to conform to that of other muricid gastropods (Carriker *et al.*, 1963; Person *et al.*, 1967; Nylen *et al.*, 1969; Webb and Saleuddin, 1977) and to the analogous regions of the naticid ABO (Bernard and Bagshaw, 1969). The epithelial cells of the ABO have so many mitochondria that they are termed mitochondria-rich (MR) cells. They possess a distinctive brush border that forms a continuum across the ABO surface. These cells communicate *via* gap junctions, and they may respond in unison to chemical or mechanical stimuli. A thin, often indistinct basement membrane separates the MR cells from the underlying hemolymph-filled sinus. This structure presumably allows for efficient transfer of oxygen, nutrients, and metabolites, thus enhancing the aerobic metabolism of the cells (Webb and Saleuddin, 1977), and may also permit elastic stretching of the ABO. Dense granules in the ABO epithelial cells are thought to contain enzymes, such as acid phosphatase, that are secreted from the ABO to dissolve the organic matrix of the substrate being drilled (Webb and Saleuddin, 1977; Carriker and Williams, 1978), thus acting in a fashion similar to lysosomal enzymes secreted by osteoclasts (Wieczorek *et al.*, 1999).

Many of the features described in the epithelial cells of the ABO are common in proton transporting MR cells of other animals, which are known to possess V-ATPases in their plasma membranes (Brown and Breton, 1996). Gap junctions are also known to occur in V-ATPase-containing cells (such as insect follicle cells) in which a coordinated response is required (Harvey *et al.*, 1998). High levels of carbonic anhydrase activity are another feature of these MR cells, and this characteristic is shared by muricid ABOs. The enzyme catalyzes the production of free protons *via* the carbonic acid pathway (Chétail and Fournié, 1969; Webb and Saleuddin, 1977). Elevated cytochrome oxidase, succinic dehydrogenase, and lactate dehydrogenase activities have also been detected in actively drilling muricids (Person *et al.*, 1967), suggesting that the mitochondria are metabolically active during the boring process. Presumably ATP production is linked to increased activity of the V-ATPase proton transporters, which serve to extrude protons from the ABO.

Immunocytochemical staining at the light microscopic level reveals that all four V-ATPase antibodies used in our studies bind to sites within the brush border of the MR cells in the ABO. Immuno-electron microscopy also indicates that the V-ATPase-reactive sites are located in the microvilli of the MR cells. Immunogold particles attached to V-ATPase antibodies are seen to underlie the plasma membrane of the microvilli. This localization occurs because the antibody is directed against the 39-kDa "d" subunit of the enzyme, which closely associates with the transmembrane domain of V-ATPases. These antibodies are known to cross-react with their corresponding subunits in either yeast or bovine samples (pers. comm. from Dr. Morris Manolson, University of Toronto) and in general, V-ATPase antibodies raised against a given species will react with most other V-ATPases (even across kingdoms) because of the homologous nature of their peptide sequences (Russell *et al.*, 1992). Our results are in accord with the localization of V-ATPase in the apical region of MR cells in a variety of animals—for example, in pavement cells in the gills of freshwater fish (Lin *et al.*, 1994; Sullivan *et al.*, 1995); in distal duct cells of the cockroach salivary glands (Just and Walz, 1994); in the midgut, Malpighian tubules, and silk glands of lepidopterans (Schweikel *et al.*, 1989; Pietrantonio and Gill, 1995; Azuma and Ohta, 1998); and in the MR cells of the toad urinary bladder (Brown *et al.*, 1988). V-ATPases have also been localized in the plasma membrane of osteoclasts (Väänänen *et al.*, 1990), for which the name "single celled epithelia" has been coined (Brown and Breton, 1996).

SDS-PAGE and immunoblotting provided additional immunological evidence to support the identity of V-ATPase pumps. Gel electrophoresis revealed that a membrane preparation of ABO homogenate contains peptides with molecular weights that are similar to those of V-ATPase subunits. Additional bands in the gel reflect the impurity of our sample. Furthermore, dot and western immunoblots of samples derived from ABO homogenates stained positive for V-ATPase. The western blots show that polyclonal antibodies raised against mammalian V-ATPase subunits cross-react to the equivalent peptides of V-ATPases found in the ABO. This suggests that the ABO V-ATPase is homologous to other known V-ATPase species.

Finally, identification of V-ATPase was established pharmacologically using the specific V-ATPase inhibitor bafilomycin A_1 (Bowman *et al.*, 1988). ATPase assays were conducted on the 1000 × *g* supernatant of ABO homogenates obtained from 15–20 animals. Three separate pooled ABO homogenates were produced and assayed for ATPase activity. Each 1000 × *g* supernatant provided sufficient protein to assay a minimum of three control and three inhibited trials. About 10% of the phosphate liberated in the control samples was seen to be derived from V-ATPase. V-ATPase activity ranged from 41.90 to 87.25 pmol Pi/(μg protein · min), with an average of ~67 pmol/(μg protein · min). The disparity in the ATPase activities among the three ABO homogenates can be attributed primarily to variation in the amount of V-ATPase actually present in each homogenate (total protein was determined, so inclusion of excess foot tissue, for example, would lower the V-ATPase content) and to variation in the amount of Pi released through dissociation of endogenous ATP or other phosphorylated substrates during tissue processing and assay procedures. The activity of the ABO V-ATPase is comparable to that reported in other animals: Onken and Putzenlechner (1995) reported V-ATPase activities of 20 and 10 pmol Pi/(μg protein · min) in filtrates from the posterior and anterior gills of *Eriocheir sinensis*, respectively, whereas Al-Fifi *et al.* (1998) found a higher activity of 192.3 pmol Pi/(μg protein · min) in a 600 × *g* supernatant obtained from the homogenates of Malpighian tubules in *Locusta*, and Sallman *et al.* (1986) reported V-ATPase activities of 30.8 pmol Pi/(μg protein · min) and 42.4 pmol Pi/(μg protein · min) in homogenates respectively obtained from the cortex and medulla of human kidneys.

The structural, immunological, and biochemical investigations undertaken in this study provide clear evidence that V-ATPase is present in the ABO of *Nucella lamellosa*, and that this V-ATPase shares structural similarity with other V-ATPase species. On the basis of these findings, we can revise the Webb and Saleuddin (1977) model describing the mechanism of proton transport by a muricid ABO. The revised model (Fig. 14) contains V-ATPase proton pumps in the microvilli of the ABO epithelial (MR) cells. The presumed presence of chloride-bicarbonate antiporters in the basolateral membranes, apical chloride channels, and paracellular chloride transport is consistent with current

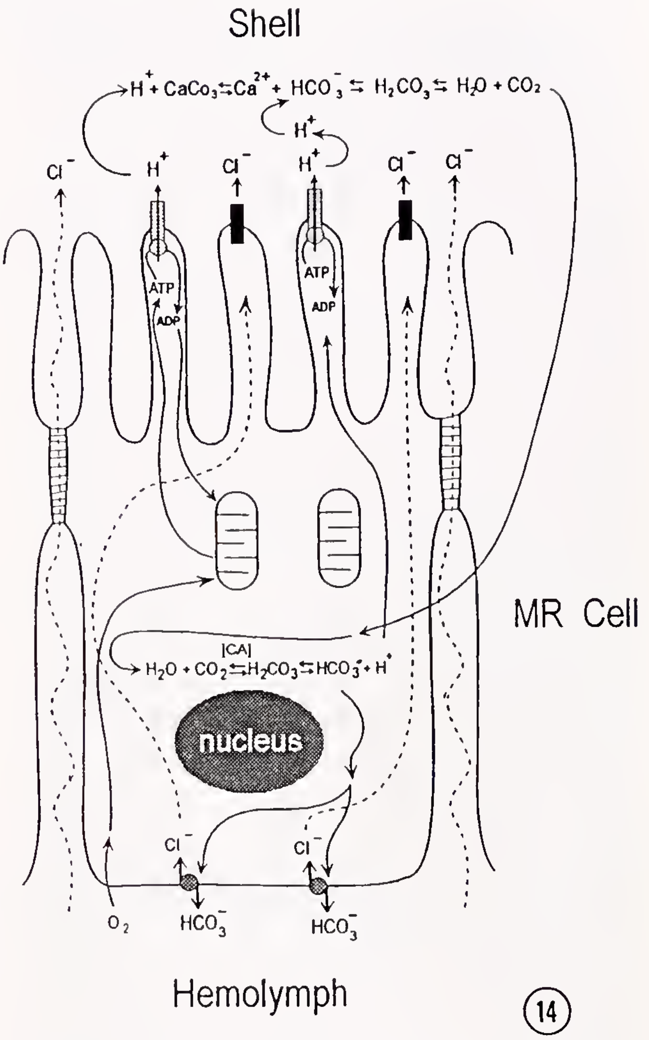
Shell
$H^+ + CaCO_3 \leftrightharpoons Ca^{2+} + HCO_3^- \leftrightharpoons H_2CO_3 \leftrightharpoons H_2O + CO_2$
H+
Cl-
H+
Cl-
H+
Cl-
Cl-
Cl-
ATP
ADP
ATP
ADP
MR Cell
[CA]
$H_2O + CO_2 \leftrightharpoons H_2CO_3 \leftrightharpoons HCO_3^- + H^+$
nucleus
Cl-
Cl-
O2
HCO3-
HCO3-
Hemolymph
14

Figure 14. Revised model of the mechanism of proton transport in the muricid accessory boring organ (ABO). Carbonic anhydrase (CA) catalyzes the production of H^+ and HCO_3^- *via* the carbonic acid pathway. Bicarbonate is removed from the mitochondria-rich (MR) epithelial cell *via* basal HCO_3^-/Cl^- antiporters, while protons are extruded from the cell into the bore hole by V-ATPase pumps located in the microvilli. Mitochondria generate ATP to power the extrusion process, generate metabolic CO_2 for the carbonic acid reaction, and provide a reducing environment to stabilize the V-ATPase molecules. Chloride ions exit the cell *via* apical ion channels, and possibly by paracellular routes. The protons and chloride ions (HCl) act to dissolve the mineralized component ($CaCO_3$) of the shell, while degradative enzymes also present in the secretions of the ABO break down the organic matrix. Carbon dioxide liberated from the dissolving shell may diffuse into the cell to enhance the carbonic acid reaction. The presence of HCO_3^-/Cl^- antiporters and, as speculated here, of chloride ion channels is based on comparable studies of mitochondria-rich cells in other animal epithelia.

models describing MR cells in many animal epithelia such as insect Malpighian tubules (Maddrell and O'Donnell, 1992; Beyenbach, 1995; Pannabecker, 1995; Brown and Breton, 1996; Harvey *et al.*, 1998).

V-ATPases actively pump protons from the cytoplasm and extrude them into the bore hole. Chloride is also extruded from the cells *via* ion channels and perhaps paracellularly between the MR cells. Protons combine with the chloride ions in the extracellular space, forming hydrochloric acid. As mentioned, it has been suggested that HCl is the acid in the secretion from muricid and naticid ABOs (Carriker *et al.*, 1963; Carriker, 1978, 1981), and the revised model is consistent with these studies. Bicarbonate is eliminated from the cells into the hemolymph by anion transporters as shown, and chloride is transferred into the cell as a counter ion. Other ion transporters are probably present, but are excluded from this diagram for clarity. The model accounts for all the structural features of the MR cells (as discussed by Webb and Saleuddin, 1977), but it now identifies the proton pump and can account for the presence of HCl in ABO secretions. Moreover, our revised model places the muricid ABO into the group of animal epithelia that use V-ATPase pumps to acidify extracellular environments.

No attempt was made in this study to identify the degradative enzymes in the secretion of the ABO, but our model is not inconsistent with the presence of lysosomal enzymes (such as indicated by Webb and Saleuddin, 1977). Such enzymes could be used to degrade the organic components of shells (*e.g.*, periostracum and shell matrix protein, chitin in crustaceans, or keratinized structures such as elasmobranch egg capsules), in a manner similar to the degradation of bone matrix by lysosomal enzymes secreted by osteoclasts (Wieczorek *et al.*, 1999). Dense granules observed in the MR cells may in fact contain such enzymes. It is well known that one of the major functions of intracellular V-ATPases is the acidification of endosomes such as lysosomes and peroxisomes, particularly in phagocytic cells, which is necessary for the activation of lysosomal enzymes (Grinstein *et al.*, 1992). V-ATPases in the apical membrane of the ABO could serve the same function, acidifying the secretions from the ABO to activate secreted enzymes. Mucus secreted from the goblet cells of the surrounding foot epithelium or from the MR cells of the ABO could serve to protect the ABO from acidic and enzymatic degradation. The localization of V-ATPase pumps in the epithelium of the muricid ABO, reported here, and their presence in the shell-facing mantle epithelia of freshwater bivalves (Hudson, 1993; da Costa *et al.*, 1999) and in the membranes of osteoclasts (Väänänen *et al.*, 1990) suggests that the mechanism for decalcification of calcareous substrates is conserved.

It is interesting to speculate on the method of regulation of the V-ATPases in the ABO. The mechanism could quite simply be the inactivation of the catalytic domains or their dissociation from the proton-transporting domains when the ABO is flaccid, and the reactivation/reassociation of the V-ATPases in engorged organs. In the engorged state, hemolymph filling the sinus of the ABO would aerate the MR cells, enabling enhanced aerobic metabolism in the mitochondria. In addition to producing ATP as the energy source, this activity could produce a reducing environment in the apical region of the cells, stabilizing the V-ATPase pumps (Merzendorfer *et al.*, 1997). In the flaccid state, blood supply is shut off to the ABO, inhibiting aerobic metabolism and leading to the oxidation and inactivation of the V-ATPases. It is also possible that factors acting as hormones enter the ABO *via* the hemolymph and pass through the thin basement membrane of the MR cells to act on the V-ATPases. Their effects may be direct, or they may act through mediators such as the 35-kDa V-ATPase cytosolic activator peptide in bovine kidneys (Zhang *et al.*, 1992).

Acknowledgments

This study was supported by a grant from NSERC, Canada to ASMS. We thank Dr. Sergio Grinstein and Dr. Morris Manolson of the University of Toronto for their gifts of antibodies, Dr. Michael O'Donnell of McMaster University for his insights into invertebrate V-ATPases, and Drs. Hamid Khan and Spencer Mukai of York University, for their technical assistance. Thanks also to Dr. Barry G. Loughton for editing the manuscript.

Literature Cited

Al-Fili, Z. I. A., S. L. Marshall, D. Hyde, J. H. Anstee, and K. Bowler. 1998. Characterization of ATPases of apical membrane fractions from *Locusta migratoria* Malpighian tubules. *Insect Biochem. Mol. Biol.* **28:** 201–211.

Atkinson, A., A. D. Gatenby, and A. G. Lowe. 1973. The determination of inorganic orthophosphate in biological systems. *Biochim. Biophys. Acta* **320:** 195–204.

Azuma, K., and Y. Ohta. 1998. Changes in H^+-transporting vacuolar-type ATPase in the anterior silk gland of *Bombyx mori* during metamorphosis. *J. Exp. Biol.* **201:** 479–486.

Bernard, F. R., and J. W. Bagshaw. 1969. Histology and fine structure of the accessory boring organ of *Polinices lewisi* (Gastropoda, Prosobranchia). *J. Fish. Res. Board Can.* **26:** 1451–1457.

Beyenbach, K. W. 1995. Mechanism and regulation of electrolyte transport in Malpighian tubules. *J. Insect Physiol.* **41:** 197–207.

Bowman, E. J., A. Siebers, and K. Altendorf. 1988. Bafilomycins: a class of inhibitors of membrane ATPases from microorganisms, animal cells, and plant cells. *Proc. Natl. Acad. Sci. USA* **85:** 7972–7976.

Bradford, M. 1976. A rapid and sensitive method for the quantitation of microgram quantities of protein utilizing the principle of protein-dye binding. *Anal. Biochem.* **72:** 248–254

Brown, D., and S. Breton. 1996. Mitochondria-rich proton-secreting epithelial cells. *J. Exp. Biol.* **199:** 2345–2358.

Brown, D., S. Hirsch, and S. Gluck. 1988. Localization of a proton-pumping ATPase in rat kidney. *J. Clin. Invest.* **82:** 2114–2126.

Brown, D., P. J. S. Smith, and S. Breton. 1997. Role of V-ATPase-rich cells in acidification of the male reproductive tract. *J. Exp. Biol.* **200:** 257–262.

Carriker, M. R. 1978. Ultrastructural analysis of dissolution of the shell of the bivalve *Mytilus edulis* by the accessory boring organ of the gastropod *Urosalpinx cinerea*. *Mar. Biol.* **48:** 105–134.

Carriker, M. R. 1981. Shell penetration and feeding by naticacean and muricacean predatory gastropods: a synthesis. *Malacologia* **20:** 403–422.

Carriker, M. R., and D. Van Zandt. 1967. Gastropod *Urosalpinx:* pH of accessory boring organ while boring. *Science* **158:** 920–922.

Carriker, M. R., and L. G. Williams. 1978. The chemical mechanism of shell dissolution by predatory boring gastropods: a review and an hypothesis. *Malacologia* **17:** 143–156.

Carriker, M. R., D. B. Scott, and G. N. Martin. 1963. Demineralization mechanism of boring gastropods. Pp. 55–89 in *Mechanisms of Hard Tissue Destruction*, R. F. Sognannaes, ed. American Association for the Advancement of Science, Washington, DC.

Chétail, M., and J. Fornié. 1969. Shell-boring mechanism of the gastropod *Purpura (Thais) lapillus:* a physiological demonstration of the role of carbonic anhydrase in the dissolution of $CaCO_3$. *Am. Zool.* **9:** 983–990.

Collins, T. M., K. Frazer, A. R. Palmer, G. J. Vermeij, and M. R. Brown. 1996. Evolutionary history of northern hemisphere *Nucella* (Gastropoda, Muricidae): Molecular, morphological, ecological, and paleontological evidence. *Evolution* **50:** 2287–2304.

da Costa, A. R., P. F. Oliveira, C. Barrias, and H. G. Ferreira. 1999. Identification of a V-type proton pump in the outer mantle epithelium of *Anodonta cygnea*. *Comp. Biochem. Physiol.* **123:** 337–342.

Ehrenfeld, J., and U. Klein. 1997. The key role of the H^+ V-ATPases in acid-base balance and Na^+ transport processes in frog skin. *J. Exp. Biol.* **200:** 247–256.

Finbow, M. E., and M. A. Harrison. 1997. The vacuolar H^+-ATPase: a universal proton pump of eukaryotes. *Biochem. J.* **324:** 697–712.

Forgac, M. 1998. Structure, function and regulation of the vacuolar (H^+)-ATPases. *FEBS Lett.* **440:** 258–263.

Fretter, V., and A. Graham. 1962. Chapter 10: Feeding. Pp. 240–262 in *British Prosobranch Molluscs. Their Functional Anatomy and Ecology*. The Ray Society. London.

Grinstein, S., A. Nanda, G. Lukacs, and O. Rotstein. 1992. V-ATPases in phagocytic cells. *J. Exp. Biol.* **172:** 179–192.

Harvey, W. R., S. H. P. Maddrell, W. H. Telfer, and H. Wieczorek. 1998. H^+ V-ATPases energize animal plasma membranes for secretion and absorption of ions and fluids. *Am. Zool.* **38:** 426–441.

Hudson, R. L. 1993. Bafilomycin-sensitive acid secretion by mantle epithelium of the freshwater clam, *Unio complanatus*. *Am. J. Physiol.* **264:** R946–R951.

Humason, G. L. 1967. *Animal Tissue Techniques*. 2nd ed. W. H. Freeman, San Francisco. Pp. 16, 165.

Just, F., and B. Walz. 1994. Immunocytochemical localization of Na^+/K^+ ATPase and V-H^+-ATPase in the salivary glands of the cockroach, *Periplaneta americana*. *Cell Tissue Res.* **278:** 161–170.

Laemmli, U. K. 1970. Cleavage of structural proteins during the assembly of the head of bacteriophage T4. *Nature* **227:** 680–685.

Lin, H., D. C. Pfeiffer, A. W. Vogl, J. Pan, and D. J. Randall. 1994. Immunolocalization of H^+-ATPase in the gill epithelia of rainbow trout. *J. Exp. Biol.* **195:** 169–183.

Lubansky, H. J., and A. L. Arruda. 1985. Plasma membrane proton-ATPase of a turtle bladder epithelial cell line. *J. Biol. Chem.* **260:** 4035–4040.

Maddrell, S. H. P., and M. J. O'Donnell. 1992. Insect Malpighian tubules: V-ATPase action in ion and fluid transport. *J. Exp. Biol.* **172:** 417–429.

McLean, I. W., and P. K. Nakane. 1974. Periodate-lysine-paraformaldehyde: a new fixative for immunoelectron microscopy. *J. Histochem. Cytochem.* **22:** 1077–1083.

Merzendorfer, H., R. Gräf, M. Huss, W. R. Harvey, and H. Wieczorek. 1997. Regulation of proton-translocating V-ATPases. *J. Exp. Biol.* **200:** 225–235.

Nelson, N., and W. R. Harvey. 1999. Vacuolar and plasma membrane proton-adenosine-triphosphatases. *Physiol. Rev.* **79:** 361–385.

Nordström, T., L. D. Shrode, O. D. Rotstein, R. Romanek, T. Goto, J. N. M. Heersche, M. F. Manolson, G. F. Brisseau, and S. Grinstein. 1997. Chronic extracellular acidosis induces plasmalemmal vacuolar type H^+ ATPase activity in osteoclasts. *J. Biol. Chem.* **272:** 6354–6360.

Nylen, M. U., D. V. Provenza, and M. R. Carriker. 1969. Fine structure of the accessory boring organ of the gastropod *Urosalpinx*. *Am. Zool.* **9:** 935–965.

Onken, H., and M. Putzenlechner. 1995. A V-ATPase drives active, electrogenic and Na^+-independent Cl^- absorption across the gills of *Eriocheir sinensis*. *J. Exp. Biol.* **198:** 767–774.

Pannabecker, T. 1995. Physiology of the Malpighian tubule. *Annu. Rev. Entomol.* **40:** 493–510.

Pantin, C. F. A. 1964. Narcotization. Pp. 5–7 in *Notes On Microscopical Technique for Zoologists*. Cambridge University Press, London.

Person, P., A. Smarsh, S. J. Lipson, and M. R. Carriker. 1967. Enzymes of the accessory boring organ of the muricid gastropod *Urosalpinx cinerea follyensis*. I. Aerobic and related oxidative systems. *Biol. Bull.* **133:** 401–410.

Pietrantonio, P. V., and S. S. Gill. 1995. Immunolocalization of the 17 kDa vacuolar H^+-ATPase subunit c in *Heliothis virescens* midgut and Malpighian tubules with an anti-peptide antibody. *J. Exp. Biol.* **198:** 2609–2618.

Rautiala, T. J., A. M. P. Koskinen, and H. K. Väänänen. 1993. Purification of vacuolar ATPase with bafilomycin C_1 affinity chromatography. *Biochem. Biophys. Res. Commun.* **194:** 50–56.

Russell, V. E. W., U. Klein, M. Reuveni, D. D. Spaeth, M. G. Wolfersberger, and W. R. Harvey. 1992. Antibodies to mammalian and plant V-ATPases cross react with the V-ATPase of insect cation-transporting plasma membranes. *J. Exp. Biol.* **166:** 131–143.

Sallman, A. L., H. J. Lubansky, Z. Talor, and J. A. L. Arruda. 1986. Plasma membrane proton ATPase from human kidney. *Eur. J. Biochem.* **157:** 547–551.

Schweikl, H., U. Klein, M. Schindlbeck, and H. Wieczorek. 1989. A vacuolar-type ATPase, partially purified from potassium transporting plasma membranes of tobacco hornworm midgut. *J. Biol. Chem.* **264:** 11136–11142.

Sheng, S., and S. M. Schuster. 1992. Simple modifications of a protein immunoblotting protocol to reduce nonspecific background. *Biol. Techniques* **13:** 704–708.

Sullivan, G. V., J. N. Fryer, and S. F. Perry. 1995. Immunolocalization of proton pumps $(H^+$-ATPase) in pavement cells of rainbow trout gill. *J. Exp. Biol.* **198:** 2619–2629.

Väänänen, H. K., E.-K. Karhukorpi, K. Sunddquist, B. Wallmark, I. Roininen, T. Hentunen, U. Tuukkanen, and P. Lakkakorpi. 1990. Evidence for the presence of a proton pump of the vaculolar H^+-ATPase type in the ruffled border of osteoclasts. *J. Cell Biol.* **111:** 1305–1311.

Webb, R. S., and A. S. M. Saleuddin. 1977. Role of enzymes in the mechanism of shell penetration by the muricid gastropod, *Thais lapillus* (L.). *Can. J. Zool.* **55:** 1846–1857.

West, L. 1986. Intertidal variation in prey selection by the snail *Nucella (=Thais) emarginata*. *Ecology* **67:** 798–809.

West, L. 1988. Prey selection by the tropical snail *Thais melones:* a study of interindividual variation. *Ecology* **69:** 1839–1854.

Wieczorek, H., D. Brown, S. Grinstein, J. Ehrenfeld, and W. R. Harvey. 1999. Animal plasma membrane energization by proton-motive V-ATPases. *BioEssays* **21:** 637–648.

Zhang, K., Z. Q. Wang, and S. Gluck. 1992. Identification and partial purification of a cytosolic activator of H^+-ATPases from mammalian kidney. *J. Biol. Chem.* **267:** 9701–9705.

Reference: *Biol. Bull.* **198:** 284–298. (April 2000)

Light-Limitation on Predator-Prey Interactions: Consequences for Metabolism and Locomotion of Deep-Sea Cephalopods

BRAD A. SEIBEL[1,*], ERIK V. THUESEN[2], AND JAMES J. CHILDRESS[3]

[1] *Rosenstiel School of Marine and Atmospheric Science, Marine Biology and Fisheries, 4600 Rickenbacker Causeway, Miami, Florida 33149;* [2]*Evergreen State College, Laboratory 1, Olympia, Washington 98505; and* [3]*Oceanic Biology Group, Marine Science Institute, University of California, Santa Barbara, California 93106*

Abstract. The present study attempts to correlate the metabolism and locomotory behavior of 25 species of midwater Cephalopoda from California and Hawaii with the maximal activities of key metabolic enzymes in various locomotory muscle tissues. Citrate synthase (CS) and octopine dehydrogenase (ODH) activities were used as indicators of aerobic and anaerobic metabolic potential respectively. CS activity in mantle muscle is highly correlated with whole-animal rates of oxygen consumption, whereas ODH activity in mantle muscle is significantly correlated with a species' ability to buffer the acidic end-products of anaerobic metabolism. Both CS and ODH activities in mantle muscle declined strongly with a species' habitat depth. For example, CS and ODH activities ranged respectively from 0.04 units g^{-1} and 0.03 units g^{-1} in the deep-living squid *Joubiniteuthis portieri*, to 8.13 units g^{-1} and 420 units g^{-1} in the epipelagic squid *Sthenoteuthis oualaniensis*. The relationships between enzymatic activities and depth are consistent with similar patterns observed for whole-animal oxygen consumption. This pattern is believed to result from a relaxation, among deep-living species, in the need for strong locomotory abilities for visual predator/prey interactions; the relaxation is due to light-limitation in the deep sea. Intraspecific scaling patterns for ODH activities may, for species that migrate ontogenetically to great depths, reflect the counteracting effects of body size and light on predator-prey detection distance. When scaled allometrically, enzymatic activities for the giant squid, *Architeuthis* sp., suggest a fairly active aerobic metabolism but little burst swimming capacity. Interspecific differences in the relative distributions of enzymatic activities in fin, mantle, and arm tissue suggest an increased reliance on fin and arm muscle for locomotion among deep-living species. We suggest that, where high-speed locomotion is not required, more efficient means of locomotion, such as fin swimming or medusoid arm propulsion, are more prevalent.

Introduction

The evolutionary path leading to modern cephalopods is poorly known due to a limited fossil record of soft-bodied cephalopods. There has, however, been much speculation based on the better fossil record of the shelled cephalopods from which modern forms evolved. Packard (1972) noted that most shelled cephalopods went extinct and modern forms, the coleoids, radiated over roughly the same geological time period as did the fishes. He further hypothesized that "competition" (which in his definition consisted of all "negative" biotic interactions, including predation) with these fishes through visually based interactions led to the (convergent) evolution of modern coleoid cephalopods (Packard, 1972). Although the timing of Packard's scenario is now in doubt, the influence of visually mediated "competition" with vertebrate predators on cephalopod evolution is widely accepted (Aronson, 1991). Packard's model provides a useful framework within which to address physiological and behavioral adaptations to the deep sea.

Packard's evolutionary model suggests that cephalopods initially retreated into the deep sea to avoid vertebrate predators encroaching out into oceanic waters. A suite of

Received 8 June 1999; accepted 19 November 1999.

[*] To whom correspondence should be addressed. E-mail: bseibel@rsmas.miami.edu

adaptations for mobility allowed them to compete effectively with fishes in visual predator/prey interactions and facilitated the reinvasion of shallow waters by modern coleoid cephalopods (Packard, 1972).

Among these adaptations was the reduction and internalization of the shell and later, an increase in mantle volume and the development of powerful propulsive mantle muscles (Wells and O'Dor, 1991). As a result, some squids today are among the most powerful swimmers in the oceans (O'Dor and Shadwick, 1989). Squids that occupy the well-lit epipelagic waters have metabolic rates unmatched by any other aquatic poikilotherm. Epipelagic squids, most of which are negatively buoyant, rely somewhat on fins for hovering, maneuvering, and stabilization (Hoar *et al.*, 1994). When attacked, however, they escape using powerful jet propulsion that produces considerable speed and may even thrust the animals out of the water (Cole and Gilbert, 1970). Both fishes and cephalopods move forward by accelerating water backwards. Fish undulate through the water, pushing large volumes back at low speeds with their broad tails. Jetting squids must force the small volumes of water taken into the mantle cavity out through an even smaller funnel opening (O'Dor and Webber, 1986). Squids must accelerate this water to much higher speeds to gain similar momentum. This results in low Froude efficiency (Vogel, 1994). A squid, therefore, takes about twice the energy to go only half as fast as the average fish (O'Dor and Webber, 1986). This constraint is compensated for by high metabolic rates, remarkable circulatory systems, and upregulated biochemical pathways (O'Dor and Webber, 1986).

Those species that have either remained in or reinvaded the deep sea do not interact with fishes or other taxa in extended visually based interactions. Deep-sea fishes and cephalopods do possess well-developed eyes and do use bioluminescent displays to attract prey or confuse predators. However, bioluminescence is a relatively weak, transient light source. Interactions under such light regimes are likely to take place over short distances that do not require strong locomotory abilities (Marshall, 1979; Herring *et al.*, 1994; Fleisher and Case, 1995). Life without extended, visually based "competition" should be accompanied by a reduction in locomotory capacity, and therefore, energy usage or metabolic rate. This is the basis of the visual interactions hypothesis put forward by Childress and colleagues (see Childress, 1995, for review). The visual interactions hypothesis states that reduced metabolic rates among deep-living fishes and crustaceans relative to shallower living species reflects reduced locomotory requirements for visually cued predator/prey interactions in the low levels of ambient light found in the deep sea. In support of this hypothesis, Seibel *et al.* (1997) reported a strong decline in oxygen consumption rate with increasing habitat depth among pelagic cephalopods.

Seibel *et al.* (1997) further observed that the decline in metabolic rates with increasing habitat depth among pelagic cephalopods is more pronounced than that reported for fishes or crustaceans (Childress, 1995). Because fin swimming is inherently more efficient than jet propulsion, some of this reduction in energy usage in deep-living cephalopods could result from the use of fins, instead of jet propulsion, as the primary means of locomotion. Where high speeds are not a priority, dependence on fins for locomotion reduces the cost of transport. Direct observations of the behavior and locomotion of deep-living pelagic animals are limited to occasional sightings from submersibles and remotely operated vehicles (Vecchione and Roper, 1991; Hunt, 1996; Roper and Vecchione, 1997; Villanueva *et al.*, 1997; Vecchione and Young, 1997; Hunt and Seibel, 2000). These observations, while extremely important, can give only qualitative information on the locomotory abilities of these organisms.

One method for quantifying the metabolic and locomotory capacities of animals is to determine the maximum activities of enzymes unique to different catabolic pathways. Enzymatic activities in various locomotory muscle tissues have been shown to correlate well with locomotory behavior in cephalopods (Baldwin and England, 1980; Baldwin, 1982; Seibel *et al.*, 1998; Hunt and Seibel, 2000). The present study measured the enzymatic activities variously in fin, mantle, arm, and heart muscle of pelagic cephalopods to investigate the interplay between metabolism and locomotion, especially as these parameters vary with habitat depth.

Materials and Methods

Collection

Cephalopods were captured on nine cruises aboard the R/V *Point Sur* and R/V *New Horizon* between September 1992 and September 1996. Sampling was primarily in an area 160 km west of Point Conception, California (34°37′N, 122°42′W to 34°30′N, 123°20′W), and off Oahu, Hawaii (21°20′N, 158°20′W to 21°35′N, 158°35′W). Animals were collected in an opening/closing Mother Tucker trawl with a 10-m^2 mouth. The net was equipped with a 30-l thermally protecting cod end that reduced mechanical damage and heat shock to animals during recovery (Childress *et al.*, 1978). Ship speed was kept very low (0.5–1 kn) to decrease turbulence and abrasion in the net and to reduce the number of animals collected in the cod end. Upon reaching the surface, specimens were weighed on a precision, motion-compensated shipboard balance (Childress and Mickel, 1980) and immediately dissected. Tissues were frozen in liquid nitrogen. All animals used in this study were alive on board ship prior to dissection, with the exception of the giant squid, *Architeuthis* sp. (see below). Animals were identified to species with the aid of several sources (Young, 1972; Roper *et al.*, 1984; Sweeney *et al.*, 1992; F. G.

Hochberg, pers. comm.; R. E. Young, pers. comm.; N. A. Voss, pers. comm.). Voucher specimens were preserved for verification of identifications and are deposited at the Museum of Natural History, Santa Barbara, California.

A single specimen of the giant squid, *Architeuthis* sp., was collected dead on 3 June 1999 by the charterboat *Top Dog* (Capt. Phil Slaga and Mate Bo Spieler) in the Gulf Stream off the Florida Keys and brought to the Rosenstiel School of Marine and Atmospheric Science (RSMAS). The specimen was in "fresh" condition but missing the distal one-third of the mantle (fins), the tentacles, and the ends of all arms but R1. The specimen was kept either on ice or in a refrigerated cold room for about 3 days prior to dissection. The mantle length (ML) was approximately 1000 mm (700 mm + est 300 mm). Using the relationship described by O'Dor (1988; $\text{Mass} = 20\ \text{ML}[\text{m}]^3$) for ommastrephid squids including the jumbo squid, *Dosidicus gigas*, we predict a wet weight of approximately 20 kg for the present specimen. The mass–length relationship described by O'Dor (1988) appears consistent with mass–length values reported for *Architeuthis* in the literature (see Ellis, 1998, for a comprehensive list of collected specimens). The specimen of *Architeuthis* sp. (UMML31.312b) is housed in the Marine Invertebrate Museum at RSMAS.

Dissections

Tissue was extracted variously from the left ventral mantle, left fin, left second arm, and left branchial heart. It has been shown that mantle muscle of some cephalopods is divided into distinct layers analogous to vertebrate white and red muscle (Bone *et al.*, 1981; Mommsen *et al.*, 1981). No attempt was made to locate or sample these layers separately. Although the relative abundance of "red" or "white" muscle fiber types in differently sized individuals may be a proximal cause for some of the scaling patterns observed (Preuss *et al.*, 1997), it cannot be an evolutionary driving force for the scaling relationships (Seibel *et al.*, 1998). Some deep-living specimens have a gelatinous tissue covering the musculature. We attempted to remove this tissue from the muscle prior to freezing.

Enzymes

Sections of approximately 0.5 g of fin, mantle or arm, or whole branchial hearts were homogenized in varying dilutions of 0.01 *M* Tris homogenization buffer, pH 7.5, at 10°C in Duall hand-held glass homogenizers kept on ice. Homogenate was centrifuged at 6600 × *g* for 5 min at 5°C. Aliquots of 25–50 μl of sample supernatant were placed in 1-ml quartz cuvettes under nonlimiting substrate conditions to be assayed for enzyme activity. Maximal enzymatic activities (V_{max}) were measured with a Shimadzu UV160U spectrophotometer equipped with a water-jacketed cuvette holder connected to a recirculating water bath. Measurements were carried out at 20°C and atmospheric pressure.

Octopine dehydrogenase (ODH; EC.1.5.1.11) and lactate dehydrogenase (LDH; EC.1.1.1.8) were assayed as indicators of anaerobic metabolic potential according to the methods of Baldwin and England (1980). ODH catalyzes the terminal glycolytic reaction in cephalopods, resulting in the reductive condensation of pyruvate and arginine to form octopine. This reaction maintains redox balance in the cell when oxygen is limiting. Because the rate of this reaction is the sum of ODH and LDH activities, ODH values were obtained by subtracting the rate due to LDH assayed in the absence of arginine. Citrate synthase (CS; EC.4.1.3.7) was used as a correlate of aerobic metabolism. It was assayed according to the methods of Thuesen and Childress (1994). CS is an important regulatory enzyme and functions in the first step of the citric acid cycle (Hochachka *et al.*, 1975). Species' mean enzymatic activities were plotted as a function of minimum depth of occurrence (MDO), defined as the depth below which 90% of the individuals of a given species were captured, and of body mass.

Statistical analysis

All data analyses were performed with Statview ver. 2.0 or SuperANOVA ver. 1.11 statistics programs (Abacus Concepts, Inc., Berkeley, CA). Simple linear regressions, *t* tests and analysis of covariance (ANCOVA) were used. Mean values given are followed by the standard error. Confidence intervals for regression exponents are at the 95% level. *P* values for regression coefficients are from *F* tests. ANCOVA was used to test whether the slopes and elevations of the various relationships were significantly different from zero and from each other. Regression slopes were declared significant when their slopes differed from zero at the 95% confidence level. In some cases nonparametric tests were used (Kendall rank correlation coefficient).

Results

The activities of octopine dehydrogenase (ODH), lactate dehydrogenase (LDH), and citrate synthase (CS) in mantle, fin, arm, and branchial heart muscle tissue for 26 species of pelagic cephalopods are presented in Table 1. Mean ODH activities of mantle muscle are significantly correlated with the buffering capacity of mantle tissue (Seibel *et al.*, 1997; $y = 1.11x + 11.75$; $r^2 = 0.81$; $P = 0.0025$; $n = 8$; Fig. 1). This result supports the use of this enzyme as an indicator of anaerobic metabolic potential. With the exception of mantle muscle for the Bolitaenidae (*Japetella* and *Eledonella*) and branchial heart tissue in all species, LDH activity was generally less than 10% of ODH activity. Mean CS activities are significantly correlated with mean oxygen consumption rates (Seibel *et al.*, 1997; $y = 0.72x - 0.04$; $r^2 = 0.85$;

Table 1

Enzymatic activity expressed as units (μmoles substrate converted to product min^{-1}) g^{-1} wet weight in mantle (m), fin (f), arm (a) and heart (h) tissue of pelagic cephalopods

Species	MDO (m)	tissue	*n*	Wet weight (g) range	Enzymatic activity (mean ± SE)*		
					CS (units g^{-1})	ODH (units g^{-1})	LDH (units g^{-1})
California							
Order Teuthoidea							
Gonatus onyx	100	m	4	1.06-31.08	7.85 ± 1.47	29.82 ± 7.26	1.17 ± 0.15
Brooding specimens		m	2	99.68-138.6	0.88, 1.63	1.61, 12.47	0.03, 0.51
		a	1		1.65	23.34	1.61
Gonatus pyros	100	m	1	6.12	7.72	28.14	1.25
		f	1		1.50	9.71	1.23
		a	1		0.84	5.92	0.75
		h	1		13.82	18.01	10.29
Abraliopsis falco	50	m	5	0.51–8.16	6.27 ± 0.63	40.96 ± 5.46	1.83 ± 0.79
		f	4	0.51–8.16	7.80 ± 0.42	25.69 ± 6.53	1.69 ± 0.19
		a	1	0.51	2.89	10.19	2.43
Pterygioteuthis gemmata	100	m	2	0.13, 0.43	5.47, 9.87	42.76, 77.65	1.66, 3.80
Histioteuthis heteropsis	150	m	11	0.47–33.97	1.68 ± 0.21	11.40 ± 0.80	0.45 ± 0.10
		f	5	1.79–12.68	1.46 ± 0.36	10.34 ± 4.09	0.47 ± 0.18
		a	9	0.47–11.41	0.59 ± 0.15	0.89 ± 0.15	0.18 ± 0.05
		h	3	11.41–33.97	5.73 ± 2.34	2.23 ± 0.09	n.d.
Octopoteuthis deletron	100	m	1	8.19	0.10	0.06	0.07
		f	1		1.03	9.84	0.26
		a	1		0.21	2.97	0.17
Chiroteuthis calyx	300	m	7	5.93–75.86	1.37 ± 0.26	50.69 ± 8.99	0.68 ± 0.09
		f	5	5.93–41.45	5.49 ± 0.59	69.02 ± 10.17	1.33 ± 0.41
		a	5	5.93–89.02	0.11 ± 0.05	1.83 ± 0.81	0.10 ± 0.05
		h	4	5.93–89.02	7.57 ± 2.89	16.19 ± 8.27	5.41 ± 1.41
Galiteuthis phyllura	300	m	3	5.19–106.0	1.31 ± 0.66	50.15 ± 15.77	0.41 ± 0.04
		f	3		2.05 ± 1.33	30.37 ± 8.70	0.98 ± 0.25
		a	3		1.77 ± 0.37	31.48 ± 1.34	0.84 ± 0.19
Cranchia scabra	10	m	1	35.39	1.41	29.39	1.45
		f	1		2.66	27.85	0.92
		a	1		1.06	23.15	1.61
Bathyteuthis berryi	800	m	2	1.7, 24.9	2.51, 0.89	0.27, 1.85	0.06, 0.08
		f	2		0.45, 1.73	0.43, 1.37	0.15, 0.18
		a	2		0.59, 1.58	0.63, 1.78	0.09, 0.43
Order Octopoda							
Japetella heathi	600	m	5	9.75–162.5	0.19 ± 0.03	0.32 ± 0.21	3.06 ± 0.65
		a	3	9.75–91.59	1.68 ± 0.86	22.27 ± 10.40	4.54 ± 1.63
Order Vampyromorpha							
Vampyroteuthis infernalis	600	m	25	0.45–1050	0.21 ± 0.02	3.07 ± 0.48	0.11 ± 0.02
		f	23	4.74–1050	0.52 ± 0.07	5.37 ± 1.22	0.17 ± 0.03
		a	14	0.45–666	0.08 ± 0.01	1.34 ± 0.24	0.02 ± 0.01
Florida							
Order Teuthoidea							
Architeuthis sp.	—	m	1	2×10^5	0.76	7.22	0.51
Hawaii							
Order Sepioidea							
Heteroteuthis hawaiiensis	110	m	1	5.06	4.91	81.17	1.65
		f	1		3.20	47.64	0.86
Order Teuthoidea							
Sthenoteuthis oualaniensis	10	m	1	110.0	8.13	420.9	1.34
		f	1		2.28	133.04	1.75
		a	1		1.96	25.33	2.19
		h	1		26.66	26.69	9.41
Brachioteuthis sp.	10	m	1	1.49	4.74	86.79	1.17
		f	1		8.64	29.79	1.12
		a	1		1.51	10.36	1.02

Table 1 (*Continued*)

Species	MDO (m)	tissue	n	Wet weight (g) range	Enzymatic activity (mean ± SE)* CS (units g^{-1})	ODH (units g^{-1})	LDH (units g^{-1})
Leachia pacifica	50	m	1	0.51	0.50	18.52	1.96
		f	1		3.63	78.08	2.76
		a	1		3.06	30.90	7.86
Abraliopsis pacificus	50	m	2	0.37,1.30	3.58, 6.81	61.33, 113.08	1.33, 1.41
		f	1	1.30	10.25	28.37	0.98
		a	2	0.37,1.30	0.54, 1.48	44.73, 49.87	0.84, 0.76
Histioteuthis hoylei	150	m	3	1.27–5.19	2.86 ± 0.71	0.74 ± 0.13	0.60 ± 0.05
		f	3		5.82 ± 1.59	3.56 ± 1.98	0.14 ± 0.02
		a	3		0.34 ± 0.21	0.09 ± 0.06	0.10 ± 0.02
Mastigoteuthis famelica	375	m	2	4.06,7.32	0.61, 0.85	6.22, 7.45	0.06, 0.26
		f	2		1.26, 2.09	2.66, 3.85	0.08, 0.16
		a	2		0.26, 0.39	1.61, 2.44	0.08, 0.24
		h	1	7.32	7.22	4.96	1.03
Chiroteuthis imperator	300	m	4	14.94–53.36	0.26 ± 0.24	30.90 ± 5.31	0.68 ± 0.09
		f	3	27.65–53.36	5.33 ± 1.03	44.49 ± 10.27	1.33 ± 0.41
		a	3		0.25 ± 0.05	4.16 ± 1.80	0.10 ± 0.05
		h	2		17.98, 22.47	15.64, 31.26	7.70, 7.72
Joubiniteuthis portieri	500	m	2	36.00,48.99	0.01, 0.06	0.04, 0.02	n.d.
		f	2		5.33, 3.84	0.05, 0.05	0.00, 0.06
		a	2		0.02, 0.02	0.01, 0.06	0.02, 0.00
		h	2		0.08, 0.86	0.04, 0.52	0.43, 0.51
Liocranchia valdivia	500	m	6	0.92–21.28	1.64 ± 0.43	28.08 ± 4.37	0.46 ± 0.23
		a	4	1.49–2.47	2.25 ± 0.62	14.00 ± 2.05	0.91 ± 0.28
Sandilops sp.	300	m	2	1.22,6.44	1.22, 1.80	17.03, 17.20	0.06, 0.29
		f	2		0.78, 1.96	6.07, 14.83	0.12, 0.15
		a	1	1.22	2.89	17.69	0.32
Taonius pavo	400	m	1	1.06	3.16	22.87	0.52
Order Octopoda							
Japetella diaphana	700	m	11	8.96–325.7	0.16 ± 0.02	0.39 ± 0.14	2.59 ± 0.30
		a	4		0.44 ± 0.11	17.24 ± 5.62	2.36 ± 0.61
		h	3		2.39 ± 0.97	n.d.	7.50 ± 2.74
Eledonella pygmaea	975	m	4	27.65–300.0	0.25 ± 0.03	1.19 ± 0.42	1.74 ± 0.30
		a	4		0.26 ± 0.07	9.55 ± 2.51	0.78 ± 0.21
		h	3		1.61 ± 0.64	0.06 ± 0.06	2.78 ± 0.06

Measurements were made at 20°C. Minimum depths of adult occurrence (MDO) are also listed.

* CS: citrate synthase; ODH: octopine dehydrogenase; LDH: lactate dehydrogenase; n.d. not detected; units, μmole substrate converted to product per min.

$P = 0.0001$; $n = 21$), which supports the use of CS as an indicator of aerobic metabolic potential (Fig. 2).

The highest CS activities overall were found in branchial heart muscle; mean values ranged from 0.47 units g^{-1} in the deep-living squid *Joubiniteuthis portieri*, to 26.66 units g^{-1} in the epipelagic squid *Sthenoteuthis oualaniensis*. Mean citrate synthase activities of mantle muscle ranged from 0.04 units g^{-1} for *J. portieri* to 8.13 units g^{-1} for *S. oualaniensis*. For comparison, CS activity in mantle muscle of the market squid, *Loligo opalescens*, is 8.0 (Ballantyne *et al.*, 1981). The highest CS activity in fin muscle was found in *Abraliopsis pacificus* (10.25 units g^{-1}). The lowest fin CS activity was found in *Octopoteuthis deletron* (1.03 units g^{-1}).

Mean ODH activity in mantle muscle ranged from 0.03 units g^{-1} for *Joubiniteuthis portieri* to 420.9 units g^{-1} in *Sthenoteuthis oualaniensis*. For comparison, ODH activities in *Illex illecebrosus*, another active ommastrephid squid, ranged from 297 units g^{-1} in outer mantle muscle to 860 units g^{-1} in middle mantle muscle (Mommsen *et al.*, 1981). Mean ODH activity in fin muscle ranged from 0.05 units g^{-1} in *J. portieri* to 133.04 units g^{-1} in *S. oualaniensis*.

Joubiniteuthis portieri is unusual in having extremely low activities of both CS and ODH in mantle muscle. ODH was also virtually absent from fin muscle of this species. Fin CS activity, however, was similar to that found in related squid families. The family Bolitaenidae (*Japetella* and *Eledonella*) differed from others in having higher activities of LDH than of ODH in mantle muscle. However, ODH in arm tissue was much higher than LDH in arm or mantle tissue. Except in the octopods and cranchiid squids, CS activity in

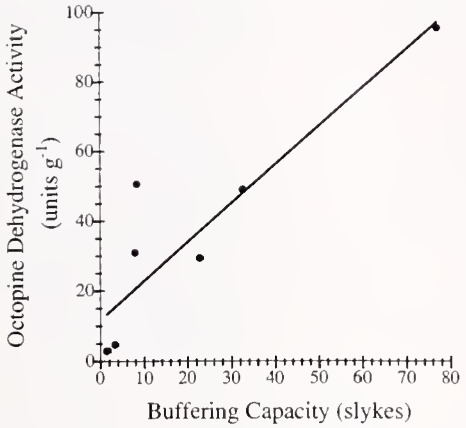

Figure 1. Correlation between octopine dehydrogenase activity (units g^{-1}) and buffering capacity (slykes) of pelagic cephalopods (Seibel *et al.*, 1997). The regression is significant ($y = 1.11x + 11.75$; $r^2 = 0.81$; $P = 0.0025$; $n = 8$).

the arm tissue was generally lower than that found in either mantle or fin tissue.

Depth

There was a strong decline in mean mantle muscle CS activity with increasing minimum depth of occurrence (Fig. 3) in species from both California ($y = 1398.8x^{-1.23\pm0.32}$; $r^2 = 0.68$; $P = 0.01$; $n = 9$) and Hawaii ($y = 227.5x^{-1.06\pm0.57}$; $r^2 = 0.69$; $P = 0.0029$; $n = 10$). There was also a strong decline in mean ODH activity with increasing MDO (Fig. 4) in species from both California ($y = 3.78 \times 10^4x^{-1.54\pm0.41}$; $r^2 = 0.67$; $P = 0.007$; $n = 9$) and Hawaii ($y = 2.88 \times 10^4x^{-1.60\pm1.11}$; $r^2 = 0.58$; $P = 0.01$; $n = 10$). There were not significant relationships between CS or ODH and MDO in fin or arm tissue for either California or Hawaii ($P > 0.05$). Included in these analyses were *Vampyroteuthis infernalis* (Seibel *et al.*, 1998) and *Gonatus onyx* (Hunt and Seibel, 2000). Citrate synthase ($y = 192.87x^{-0.66\pm0.63}$; $r^2 = 0.47$; $P = 0.04$; $n = 9$) and ODH (Kendall rank correlation coefficient; $P = 0.02$) activity in branchial heart tissue also declined significantly with in-

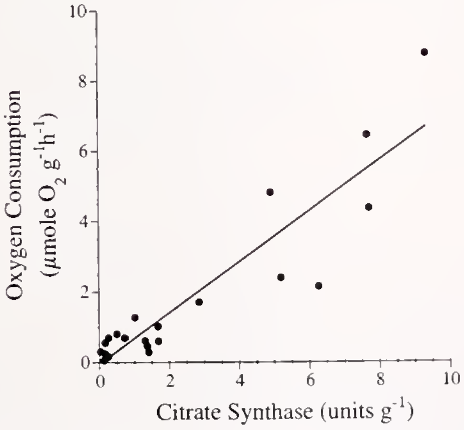

Figure 2. Correlation between mean citrate synthase activity (units g^{-1}) and mean mass-specific oxygen consumption rate (μmole O$_2$ g^{-1}h^{-1}; Seibel *et al.*, 1997) for pelagic cephalopods. The regression is significant ($y = -0.043 + 0.72x$; $r^2 = 0.85$; $P = 0.0001$; $n = 21$).

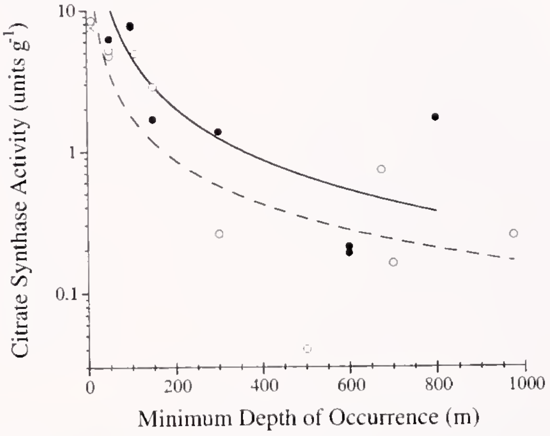

Figure 3. Mean citrate synthase activity in mantle muscle declines significantly with increasing minimum depth of occurrence (m) in Californian (solid circles, solid line; $y = 1398.8x^{-1.23\pm0.32}$; $r^2 = 0.68$; $P = 0.01$; $n = 9$) and Hawaiian (open circles, dashed line; $y = 227.5x^{-1.06\pm0.57}$; $r^2 = 0.69$; $P = 0.0029$; $n = 10$) pelagic cephalopods. For comparison, mantle muscle CS activity for *Loligo opalescens* is also shown (×; 8.0 units g^{-1}; Ballantyne *et al.*, 1981).

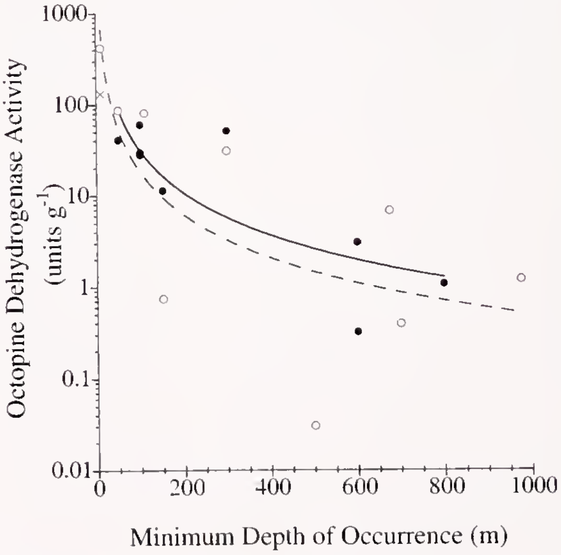

Figure 4. Mean octopine dehydrogenase activity in mantle muscle also declined significantly with increasing MDO (m) in Californian ($y = 3.78 \times 10^4x^{-1.54\pm0.41}$; $r^2 = 0.67$; $P = 0.007$; $n = 9$) and Hawaiian ($y = 2.88 \times 10^4x^{-1.60\pm1.11}$; $r^2 = 0.58$; $P = 0.01$; $n = 10$) pelagic cephalopods. Symbols as in Fig. 3. For comparison, mantle muscle ODH activity for *Loligo opalescens* is also shown (×; 132 units g^{-1}; Ballantyne *et al.*, 1981).

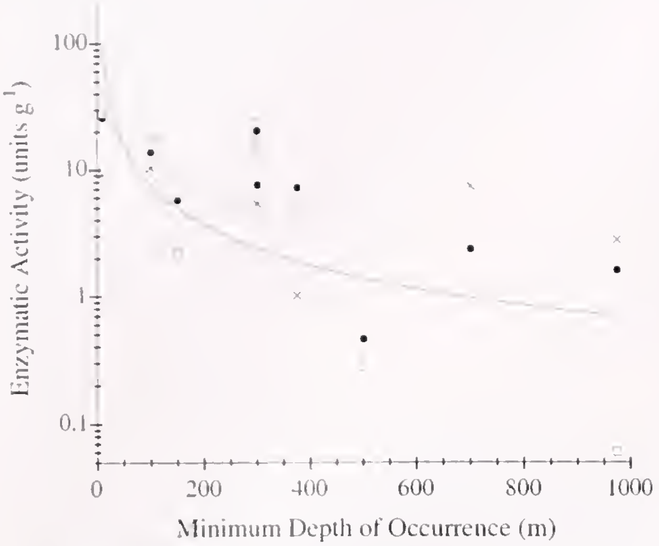

Figure 5. Mean activities of citrate synthase ($y = 192.87x^{-0.66\pm0.63}$; $r^2 = 0.47$; $P = 0.04$; $n = 9$), octopine dehydrogenase ($y = 845x^{-1.10\pm0.50}$; $r^2 = 0.38$; Kendall rank correlation coefficient, $P = 0.02$), and lactate dehydrogenase (×) in branchial heart of pelagic cephalopods as a function of minimum depth of occurrence. Symbols as in Fig. 3.

creasing MDO (Fig. 5). There was no significant relationship between heart LDH activity and MDO. There were no differences between Hawaiian and Californian animals for any parameter measured (ANCOVA; $P > 0.05$).

Excluded from the analyses with depth were species of the family Cranchiidae and *Octopoteuthis deletron*. The use of transparency for crypsis by cranchiid squids relieves them of some of the selective pressure associated with the well-lit epipelagic zone (Seapy and Young, 1986; Seibel *et al.*, 1997; Johnsen and Widder, 1998). In fact, some cranchiid species remain in near-surface waters until adulthood and then migrate suddenly to great depths where spawning occurs (Young, 1975). On the basis of the depths provided in Table 1 (estimated from Roper and Young, 1975), there is no relationship between any enzymatic activities and MDO for cranchiid squids. *O. deletron* is unique in that the fins comprise a larger percentage of the body weight than does mantle muscle (B. A. Seibel, unpubl. data). Therefore, the enzymatic activities of mantle muscle may not provide accurate estimates of metabolism in this species. The correlations between enzymatic activities and buffering capacity (Fig. 1) or MO_2 (Fig. 2) were created using values for *O. deletron* fin muscle rather than mantle muscle. Furthermore, the specimens captured in previous studies were too few to permit accurate assessment of habitat depth for this species. Inclusion of the cranchiids and *O. deletron* does not significantly alter the results of any of the regressions using the depths in Table 1. Also excluded was the giant squid, *Architeuthis* sp. Minimum depth for this species is unknown: the only depth information comes from three juveniles captured at the surface (Roper and Young, 1972; Lu, 1986) and an adult tentacle that apparently broke off at 500 m (Robison, 1989).

Scaling

Citrate synthase activity generally declined with increasing body mass according to the equation $y = aW^b$, where a is a constant, W is wet weight, and b is the scaling coefficient. Scaling relationships for mantle muscle CS activity were significant in several cases (Fig. 6). The scaling relationships for *Histioteuthis heteropsis* ($y = 2.10x^{-0.25\pm0.14}$; $r^2 = 0.55$; $P < 0.01$; $n = 11$), *Chiroteuthis calyx* ($y = 4.20x^{-0.39\pm0.25}$; $r^2 = 0.76$; $P = 0.01$; $n = 7$), and *Japetella diaphana* ($y = 0.40x^{-0.29\pm0.15}$; $r^2 = 0.88$; $P = 0.004$; $n = 11$) were within the normal range found for aerobic metabolic scaling in a variety of animals (Schmidt-Nielsen, 1984). Significant scaling of CS activity in mantle muscle also exists for *Gonatus onyx* (Hunt and Seibel, 2000; Fig. 6) and *Vampyroteuthis infernalis* (Seibel *et al.*, 1998; Fig. 6). When data for the species were combined, there was significant negative scaling of mantle muscle CS activity for the family Cranchiidae as well ($y = 2.18x^{-0.29}$; $r^2 = 0.63$; $P = 0.04$; $n = 14$; Fig. 7). While significant positive scaling of fin muscle CS was previously found in *Vampyroteuthis infernalis* (Seibel *et al.*, 1998), no significant scaling relationships were found for fin muscle CS for any species in the present study.

Glycolytic enzymes of pelagic animals typically scale with a positive slope (Somero and Childress, 1980; Chil-

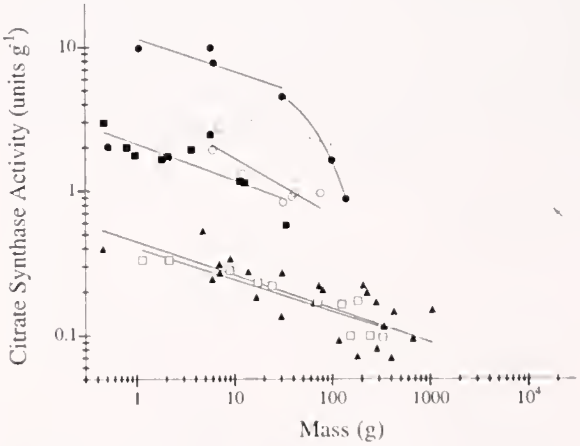

Figure 6. Citrate synthase activities for *Chiroteuthis calyx* (open circles; $y = 4.20x^{-0.39\pm0.25}$; $r^2 = 0.76$; $P = 0.01$; $n = 7$), *Histioteuthis heteropsis* (solid squares; $y = 2.10x^{-0.25\pm0.14}$; $r^2 = 0.55$; $P < 0.01$; $n = 11$), and *Japetella diaphana* (open squares; $y = 0.40x^{-0.29\pm0.15}$; $r^2 = 0.88$; $P = 0.004$; $n = 8$) as a function of body mass (g). Data are also shown for *Vampyroteuthis infernalis* (from Seibel *et al.*, 1998; closed triangles) and *Gonatus onyx* (from Hunt and Seibel, in press; closed circles). The two largest specimens of *G. onyx* were brooding egg masses and were in progressive stages of senescence. *Architeuthis* sp. (×) is shown at its estimated body mass of 20 kg. The dashed line represents an extrapolation to 10 g body mass using a scaling coefficient of −0.25.

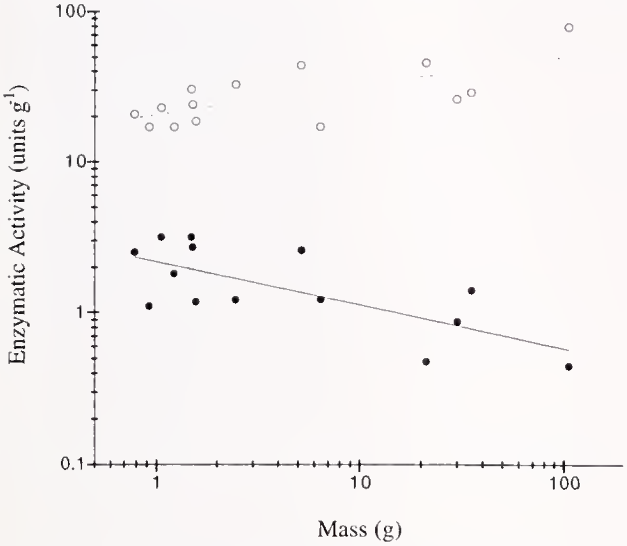

Figure 7. Activities of octopine dehydrogenase (open circles; $y = 20.6x^{0.20}$; $r^2 = 0.75$; $P = 0.002$; $n = 14$) and citrate synthase (closed circles; $y = 2.18x^{-0.29}$; $r^2 = 0.63$; $P = 0.04$; $n = 14$) in mantle muscle of individuals of cranchiid squid species (*Galiteuthis phyllura, Cranchia scabra, Liocranchia valdivia, Sandilops* sp., *Taonius pavo*) as a function of body mass.

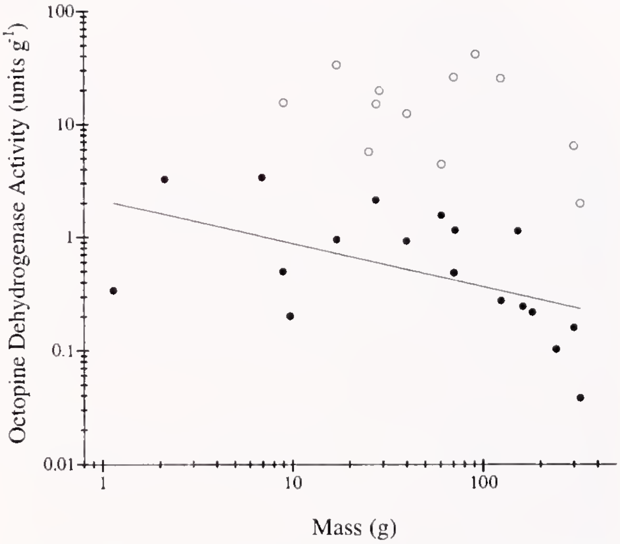

Figure 9. Octopine dehydrogenase activities in mantle (closed circles; $y = 2.12x^{-0.38\pm0.33}$; $r^2 = 0.28$; $P = 0.025$; $n = 18$) and arm (open circles) tissue as a function of body mass (g) for octopods within the family Bolitaenidae (*Japetella diaphana, J. heathi,* and *Eledonella pygmaea*).

dress and Somero, 1990; Seibel *et al.,* 1998). However, ODH activity in many cephalopod species or families in the present study either showed no relationship with body size or scaled negatively (Figs. 8, 9, 10). ODH scaled negatively for both mantle ($y = 5.03x^{-0.39\pm0.14}$; $r^2 = 0.62$; $P = 0.035$; $n = 7$) and fin ($y = 5.16x^{-0.33\pm0.06}$; $r^2 = 0.90$; $P = 0.014$; $n = 5$) muscle of *C. calyx* (Fig. 8). When data were combined, there was significant negative scaling of ODH activity in mantle muscle of bolitaenid species (*Japetella, Eledonella*) as well ($y = 2.12x^{-0.38\pm0.33}$; $r^2 = 0.28$; $P = 0.025$; $n = 18$; Fig. 9). No relationship existed between ODH activity in arm muscle and body mass for any species. ODH in mantle muscle for all cranchiid species combined scaled positively ($y = 20.6x^{0.20}$; $r^2 = 0.75$; $P = 0.002$; $n = 14$; Fig. 7). No significant scaling relationships existed for ODH activity of any histioteuthid species. When combined, however, ODH in fin muscle of *Histioteuthis heteropsis* and *H. hoylei* increased dramatically with increasing body mass ($y = 1.36x^{1.00\pm0.53}$; $r^2 = 0.62$; $P = 0.004$; $n = 8$; Fig. 10).

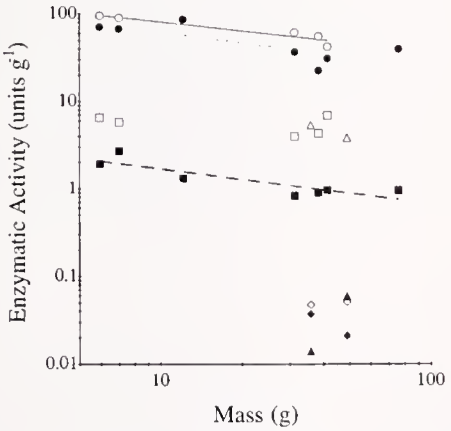

Figure 8. Activities of citrate synthase (squares) in fin (open symbols) and mantle (closed symbols; see Fig. 6) and octopine dehydrogenase (circles) in fin (open symbols; $y = 5.16x^{-0.33\pm0.06}$; $r^2 = 0.90$; $P = 0.014$; $n = 5$) and mantle (closed symbols; $y = 5.03x^{-0.39\pm0.14}$; $r^2 = 0.62$; $P = 0.035$; $n = 7$) of *Chiroteuthis calyx* as a function of body mass (g). For comparison, CS (triangles) and ODH (diamonds) in fin (open symbols) and mantle (closed symbols) for *Joubiniteuthis portieri* are also shown.

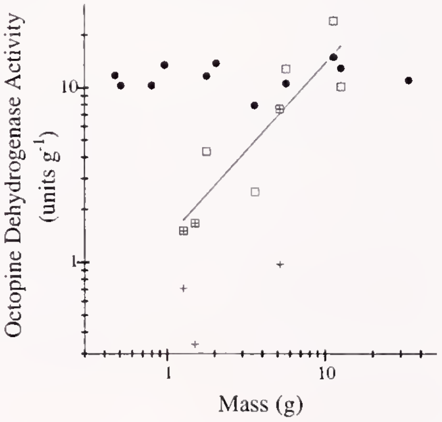

Figure 10. Octopine dehydrogenase activity of mantle muscle in *Histioteuthis heteropsis* (closed circles) and *H. hoylei* (plus signs) as a function of body mass (g). ODH activity in fin muscle (squares; $y = 1.36x^{1.00\pm0.53}$; $r^2 = 0.62$; $P = 0.004$; $n = 8$; Fig. 10) for *H. heteropsis* (open symbols) and *H. hoylei* (with plus signs) are also shown.

Critique of the Methods

Validation of enzyme measurements

In the present study we use V_{max} measurements of CS and ODH as indicators of maximal capacity for flux through aerobic and anaerobic metabolic pathways, respectively. Newsholme and Crabtree (1986) suggest two criteria that must be met in order to validate this approach. First, the enzyme must catalyze a nonequilibrium reaction. Newsholme and Crabtree (1986) suggest that there are a few master regulatory (nonequilibrium) enzymes in each pathway and that other near-equilibrium enzymes are in concentrations vastly exceeding the *in vivo* flux rates. Variation in the concentrations of near-equilibrium enzymes are, therefore, unrelated to environmental or ecological factors. CS is known to be an important regulatory enzyme that feeds carbon into the citric acid cycle (Hochachka *et al.*, 1975; Vetter, 1995). LDH and ODH, on the other hand, operate near equilibrium, and their concentrations are thought to be in excess of that required for forward flux through the glycolytic pathway. However, phylogenetic analysis has demonstrated that variations in LDH concentration do indeed have adaptive significance (Pierce and Crawford, 1997). Furthermore, it was recently demonstrated that the apparent excess concentrations of some near-equilibrium enzymes are closely matched to the requirements for flux through the pathway *in vivo* (Staples and Suarez, 1997). Octopine dehydrogenase is the only enzyme unique to anaerobic metabolism in cephalopods. Other supposed "flux-generating" enzymes in the glycolytic pathway participate in aerobic energy production as well. ODH is the terminal enzyme in energy-producing pathways when energy demand exceeds oxygen supply. Any energy expenditure beyond the capacity of aerobic pathways in the mitochondria must be covered by glycolysis, and pyruvate must be converted to octopine to maintain redox balance in the cytosol. The ODH-catalyzed step may, therefore, be considered rate-limiting.

The second requirement for useful measurement of V_{max} values is the experimental demonstration that they quantitatively indicate the *in vivo* capacity for flux through a pathway. This can be done by comparing the *in vitro* enzyme activity with the measured or calculated flux through the pathway, either directly by measurement of metabolite concentrations or indirectly from oxygen uptake measurements. In the case of anaerobic pathways, correlation with buffering capacity proves useful. In the present study, ODH activity in mantle tissue correlates well with buffering capacity (Fig. 1), whereas CS activity correlates with oxygen consumption (Fig. 2)

Temperature and pressure

Measurements of enzymatic activity in the present study were done under saturating substrate and co-factor concentrations, and are thus estimates of maximal capacity for metabolic flux (V_{max}) through the particular enzyme-catalyzed step in a pathway. V_{max} is a product of enzyme concentration ($[E]$) and catalytic efficiency (k_{cat}). For organisms living at similar environmental temperatures and hydrostatic pressures, k_{cat} values appear to be highly conserved, and V_{max} values are, therefore, essentially estimates of $[E]$. However, poikilotherms with low body temperature typically possess enzymes that are less rigid and thermally stable than those from warm-adapted species. Similarly, species from high-pressure environments also have more rigid enzymes that resist volume changes (Hochachka and Somero, 1984). Rigidity, required for enzyme stability, results in low catalytic efficiency. The deep sea is unique in that its inhabitants are exposed to both low temperature and high hydrostatic pressure. This trade-off results in some deep-living species having pressure-insensitive (rigid) enzymes that are only 60% as efficient (lower k_{cat}) as homologous enzymes from shallow-living species (Somero and Siebenaller, 1979). Although this difference may contribute to our observation of low enzymatic activity among deep-living cephalopod species, it is insufficient to explain the several orders of magnitude difference in enzymatic activity observed here between deep- and shallow-living cephalopod species. Rather, these differences in V_{max} result primarily from differences in $[E]$ (Childress and Somero, 1979).

Destabilization of weak bonds by high temperatures can cause denaturation of proteins and thus inactivation of enzymes. The added rigidity of pressure-insensitive enzymes will increase their thermal stability to some extent. However, denaturation temperatures (*i.e.*, Arrhenius breakpoint temperatures) have been shown to correlate with species' habitat temperatures (Dahlhoff *et al.*, 1991). Midwater temperatures vary from roughly 3°C at 1500 m to 10° to 20°C at the surface, depending on region and season. The measurement temperature chosen here, 20°C, is significantly higher than the habitat temperature of most of the species studied. However, there is generally a large "buffer zone" between habitat temperature and denaturation temperature. Thus, the Arrhenius breakpoint temperature for most enzymes in most organisms is considerably greater than 20°C. Even the antarctic krill, *Euphausia superba*, which never sees temperatures above 2°C, has an optimum temperature of 40°C for citrate synthase (Vetter and Buchholz, 1998). Our own measurements in *Vampyroteuthis infernalis* and *Cirrothauma murrayi* as well as in antarctic pteropod molluscs and deep-sea benthic octopods revealed breakpoint temperatures greater than 35°C for ODH and LDH (Seibel, unpubl. data.). The measurement temperature chosen here is sufficiently high to allow greater detectability of enzymes that are in low concentrations. It is important to keep in mind, however, that *in situ* temperature differences between species will lead to a greater difference in metabolic rate than indicated by the enzymatic activities measured here (Childress and Somero, 1979).

Phylogeny

The analyses presented here generally assume, for statistical purposes, the independence of species as individual data points. Some authors (Harvey and Pagel, 1991; Felsenstein, 1985) have warned, however, that physiological traits of species reflect, to varying degrees, both their historical environments and their phylogenetic affinities. Failure to consider phylogenetic relationships for statistical analyses may overestimate the degrees of freedom for regressions. An "analysis of higher nodes" (Harvey and Pagel, 1991) presents one possible solution to this problem. This analysis partitions the total variation among species into components representing each of the nested levels in a taxonomy (*i.e.*, the variation between species within a genus, genera within a family, families within an order, etc.). Such an analysis on the present data set reveals that the majority of the variation lies between families within an order, and thus families are the appropriate taxon for the most independent comparisons (Seibel, 1998). However, with few exceptions, there is only a single representative from a given family within each region studied (California or Hawaii). Therefore, our degrees of freedom for each regional analysis are not greatly exaggerated. Reanalysis using mean enzymatic activities for each family does not significantly change any of our regressions or conclusions (Seibel, 1998). For midwater cephalopods, phylogenetic trees based on sequences of the cytochrome *c* oxidase I gene have recently become available (Carlini and Graves, 1999). Preliminary analysis of the present data set using phylogenetic independent contrasts (Felsenstein, 1985) based on these phylogenetic trees (Carlini and Graves, 1999) appear to support our findings (Carlini and Seibel, unpubl. data). Childress (1995) argued that low metabolic rates among midwater organisms are probably not a phylogenetic artifact for two reasons. First, there is considerable divergence of closely related groups as a function of habitat depth, and second, there is strong evidence of convergence between distantly related groups (phyla) living at similar depths.

Discussion

Depth

Citrate synthase (CS) activity and octopine dehydrogenase (ODH) activity in mantle muscle decline significantly with increasing minimum depth of occurrence (Figs. 3, 4). This is in agreement with the visual interactions hypothesis, which states that deeper living animals will have lower metabolic rates than their shallower living counterparts as a result of relaxed selection for strong locomotory abilities for predator-prey interactions in the light-limited deep sea (Childress, 1995). This hypothesis is supported by the presence of a decline among visually orienting pelagic animals (fishes, crustaceans, and cephalopods; Childress, 1995; Seibel *et al.*, 1997), and the lack of a decline among nonvisual pelagic organisms, such as medusae and worms (Thuesen and Childress, 1993a, b, 1994). It is further supported by the lack of a decline among benthic organisms that have greater opportunities for refuge and crypsis (Childress *et al.*, 1990; Seibel and Childress, 2000). In shallow benthic environments, visually cued predation pressure selects for chromatophore patterns and other cryptic displays rather than for powerful propulsive muscles that allow escape from predators. Similarly, in the deep sea, the limited visual interaction that occurs between cephalopods and their predators has resulted in cryptic behaviors such as bioluminescence. Although low metabolic rates are certainly advantageous for life in regions of low oxygen or low food availability, regional comparisons have shown that metabolic rates are not specific adaptations to these factors (Childress, 1995; Seibel *et al.*, 1997; Childress and Seibel, 1998; Seibel *et al.*, 1999). The finding that enzymatic activities are similar for cephalopod species from California and Hawaii, regions that differ dramatically in their oxygen and biomass profiles, supports this assertion.

Further evidence of reduced metabolism and locomotory capacity among deep-sea cephalopods was provided by enzymatic activities in branchial heart muscle. We observed a significant decline in both CS and ODH activity in branchial heart tissue of pelagic cephalopods (Fig. 5). This makes sense, given a reduction in overall metabolic and locomotory expenditure in the deep sea. In fishes, however, this reduction is apparently accomplished only by a reduction in heart size (Childress and Somero, 1979). Ratios of CS to ODH are higher in branchial heart muscle than in locomotory muscles of cephalopods, reflecting the typical aerobic poise of heart metabolism (Dreidzic *et al.*, 1990). The relatively high activities of LDH at all depths in branchial heart muscle may be poised to reconvert lactate, produced in low concentration by the large locomotory muscles, to pyruvate as discussed by Storey (1977). LDH in both mantle and heart muscle is similar at all depths. Octopine, the product of arginine and pyruvate, is typically metabolized in the muscle tissue of cephalopods (Pörtner, 1994). This allows the resynthesis of arginine-phosphate, a high-energy buffer equivalent of creatine phosphate in vertebrates, in active muscles. ODH in heart tissue of cephalopods is probably related to increased work during and after burst locomotion.

Locomotion

Oxygen consumption in pelagic cephalopods declines with increasing habitat depth more sharply (higher slope, *b*) than in either fishes or crustaceans (Seibel *et al.*, 1997). The same trend appears to be true for CS ($b = -1.23$) and ODH ($b = -1.54$) activity in cephalopod mantle muscle (Figs. 3, 4) compared to malate dehydrogenase ($b = -0.68$) or LDH ($b = -0.69$) in fish white muscle (Childress and Somero, 1979). Seibel *et al.* (1997) suggested that the relative steepness of these relationships is a result of differences in locomotory efficiency between deep and shallow-living cephalopods. Because fin swimming is inherently more efficient than jet propulsion (Hoar *et al.*, 1994), and because high speeds are not a priority in the deep sea, much of the observed reduction in energy usage among deeper living cephalopod species may result from their use of fins as the primary means of propulsion (Wells, 1994; Seibel *et al.*, 1997).

The decline in mantle muscle CS and ODH activity and the lack of a decline in fin muscle CS and ODH with depth support the contention that there is a relative increase in the use of fins for propulsion among deeper living animals compared to the use of mantle muscle. The lack of a decline in arm muscle CS and ODH suggests either that deeper living species are utilizing arms for medusoid swimming, or that species at all depths utilize arms for activities, such as defense or prey capture, that require similar metabolic potential regardless of habitat depth. Medusoid swimming has been observed previously for cirrate octopods (Vecchione and Roper, 1991; Vecchione and Young, 1997; Villanueva *et al.*, 1997) and some histioteuthid squids (Voss *et al.*, 1998). These possibilities are explored further below.

The patterns of enzymatic activity with habitat depth support the contention that deeper living species generally have lower metabolic rates and increased efficiency of locomotion due, in part, to a greater relative use of fins for both routine and burst swimming. However, the enzymatic activities presented here and elsewhere (Seibel *et al.*, 1998; Hunt and Seibel, 2000) vary considerably within a species as a function of body mass or ontogeny. Consideration of intraspecific scaling relationships reveals a much clearer picture of the relative distribution of enzymes in locomotory tissues of midwater cephalopods.

Scaling and ontogenetic vertical migration

Aerobic metabolic enzymatic activities (CS) in *Histioteuthis heteropsis, Chiroteuthis calyx, Japetella diaphana, Vampyroteuthis infernalis* (Seibel *et al.*, 1998), and *Gonatus onyx* (Hunt and Seibel, 2000) decreased significantly with increasing body mass (Fig. 6). A similar relationship was observed for species within the family Cranchiidae (Fig. 7). Mass-specific aerobic metabolism typically decreases with increasing body mass (Schmidt-Nielsen, 1984). The evolutionary cause of these relationships is not well understood, but is believed to derive from increased opportunities for energy savings in larger animals as a result of reduced costs for such geometrically controlled (*i.e.*, surface:volume) processes as thermoregulation in mammals or ion regulation in fishes (Childress and Somero, 1990).

Childress and Somero (1990) also discussed scaling of glycolytic enzymes in fishes and concluded that the positive scaling coefficients for most locomotory muscles are an adaptation for size-independent acceleration used during predator-prey interactions. Larger animals are required to accelerate proportionally faster than small animals to escape predators or capture prey. This is dependent on the scaling of predator-prey detection distances. The positive scaling of LDH activity observed for *Corphaenoides armatus* (Siebenaller *et al.*, 1982), a permanently deep-living fish, supports this hypothesis, as does the positive scaling of ODH activity in *Vampyroteuthis infernalis* mantle, fin, and arm tissue (Seibel *et al.*, 1998). Because *C. Armatus* and *V. infernalis* live at constant depths (constant light levels) through ontogeny, detection distance is determined primarily by body size.

The absence of significant scaling relationships or the presence of negative scaling relationships for enzymes of anaerobic metabolic pathways among many midwater cephalopods (Figs. 8, 9, 10) may reflect the ontogenetic vertical migrations undertaken by these species whereby successive developmental stages occupy progressively deeper depths (Roper and Young, 1975). Shallow-living juveniles of such species experience greater visibility, but detection distances are small due to their small size. Deep-living adults experience reduced visibility in the poorly lit deep sea, so that detection distances remain small even though the animals are larger. This trade-off may negate the positive scaling of anaerobic metabolism typically observed in pelagic animals.

The negative scaling of ODH activity in *Gonatus onyx* (Hunt and Seibel, 2000) supports this hypothesis. *G. onyx* undergoes an ontogenetic migration to great depths where spawning and egg-brooding take place (Hunt and Seibel, 2000; Seibel *et al.*, 2000; see also Fig. 6). It is further supported by negative scaling of ODH in *Chiroteuthis calyx* (Fig. 8) and in mantle muscle of bolitaenid octopods (Fig. 9), as well as by the lack of scaling relationship for ODH in *Histioteuthis heteropsis* mantle muscle (Fig. 10). All of these species undergo ontogenetic migrations to deep water (Roper and Young, 1975).

ODH in mantle muscle within the family Cranchiidae scales positively (Fig. 7). Although members of this family undergo ontogenetic vertical migrations, their use of transparency for crypsis reduces their predator/prey detection distances regardless of habitat depth (Seibel *et al.*, 1997; Johnsen and Widder, 1998). Detection distance depends only on size for these species.

Chiroteuthid clade

When body size is factored out, enzymatic activity in fin muscle and mantle muscle can be compared. From Figure 8 it can be seen that fin muscle CS and ODH activity is much higher than mantle muscle activity at all body sizes for *Chiroteuthis calyx. C. imperator, Joubiniteuthis portieri*, and *Mastigoteuthis famelica*, all members of the chiroteuthid clade (Young, 1991; Carlini and Graves, 1999), are also apparently strong fin swimmers. In fact, *J. portieri* has virtually no enzymatic activity in mantle muscle, but the CS activities in its fin muscle are similar to those in related midwater squids. In a shipboard aquarium, *Joubiniteuthis portieri* swam vigorously with constant fin motion and only a few mantle contractions beyond those used for respiration (Seibel, pers. obs.). The enzymatic activities of *M. famelica* do not unambiguously support fin swimming. Although CS activity is higher in fin than mantle muscle, the reverse is true of ODH activity. However, this species has been observed from submersibles to be swimming almost exclusively using the fins (Roper and Vecchione, 1997). Furthermore, the regions of the brain associated with fin swimming are extremely well-developed in mastigoteuthid species (Dilly *et al.*, 1977; Young, 1977), and the fins themselves are quite large. The low ODH activity in fin relative to mantle muscle in *M. famelica* may reflect the small size (4–7 g) of these specimens, because jet propulsion may be more efficient than fin swimming at small sizes (O'Dor and Webber, 1986). Scaling relationships are not known for this species.

Histioteuthidae

ODH activity in fin muscle of *Histioteuthis heteropsis* and *H. hoylei*, combined, scales with a large positive slope (Fig. 10). Mantle muscle ODH of *H. heteropsis* is independent of body mass (Fig. 10). The significance of this finding is that fin muscle in deeper living adult *H. heteropsis* has higher ODH activity than mantle muscle, which suggests an ontogenetic gait-transition whereby the use of fins for burst swimming becomes relatively more important through ontogeny. This transition coincides with an ontogenetic descent to deeper, darker water. Jet propulsion may actually be more efficient than fin swimming at small sizes (O'Dor and Webber, 1986). An ontogenetic gait-transition was reported for *Vampyroteuthis infernalis* (Seibel *et al.*, 1998) as well. However, in that case, the transition from jet propulsion to fin swimming occurs as a distinct metamorphosis, rather than gradually through ontogeny.

Despite similar fin muscle ODH activities and metabolic rates (Seibel *et al.*, 1997), *Histioteuthis heteropsis* and *H. hoylei* have drastically different mantle muscle ODH activities. It appears that fin muscle enzymatic activities are always considerably higher than mantle muscle activities in *H. hoylei*. The mantle is also relatively longer in *H. heteropsis* than in *H. hoylei* (Voss *et al.*, 1998). *Histioteuthis hoylei* may rely on fins for swimming at all sizes and depths. Some histioteuthids have been observed swimming with their arms, like medusae and cirrate octopods (Voss *et al.*, 1998; see below). Enzymatic activities do not support this possibility for *H. hoylei*, however.

Bolitaenidae

Enzymatic activity is much higher in arm muscle than in mantle muscle of bolitaenid octopods (*Japetella diaphana, J. heathi, Eledonella pygmaea*; Fig. 9). A similar pattern was observed for the cirrate octopod *Opisthoteuthis californiana* (Seibel *et al.*, 1998). This may reflect the use of arms for medusoid swimming, as has been observed for some cirrate octopods (Roper and Brundage, 1972; Vecchione and Roper, 1991; Vecchione and Young, 1997). However, limited shipboard observations on swimming behavior in *Japetella heathi* did not reveal medusoid swimming. Rather, mantle muscle was predominantly used for jet propulsion. Furthermore, *J. heathi* appeared to expel water through the lateral mantle "inlets" in addition to the funnel. A similar "triple jet" arrangement was described for the epipelagic octopod *Ocythoe tuberculata* (Packard and Wurtz, 1994). At extremely low speeds, jet propulsion is apparently not so costly (Vogel, 1994). A triple jet arrangement allows bolitaenids to process larger amounts of water, resulting in efficient low-speed swimming. The high enzymatic activity in arm tissue may be used in prey capture or defense.

Architeuthidae

The giant squid, *Architeuthis* sp. reaches lengths of over 20 m. Despite its enormous size, no biologist has ever seen one alive in its natural habitat. The elusiveness of this species has spurred considerable myth regarding its predatory abilities (Ellis, 1998). However, many scientists now agree that *Architeuthis* is a sit-and-wait predator with little swimming ability (Bidder, 1970). This belief is based primarily on the observation that *Architeuthis* accumulates ammonium in its muscle tissues, presumably for buoyancy (Voight *et al.*, 1994; see below). The present measurements provide the first estimates of metabolism and locomotory ability for this poorly known genus. The mantle muscle CS activity, according to the relationship in Figure 2, predicts an oxygen consumption rate of 0.50 μmole O_2 $g^{-1}h^{-1}$, which is similar to that of most ammoniacally buoyant squids (Seibel *et al.*, 1997). However, normalizing this value allometrically to 10 g body mass for comparison with other species (assuming a scaling coefficient of -0.25; Fig. 6) gives a value of 3.34 μmole O_2 $g^{-1}h^{-1}$. This value is closer to muscular squids, such as the enoploteuthids and gonatids, than to the ammoniacal squids with which it is commonly compared (Fig. 6; Table 1).

The capacity for burst swimming appears to be quite low. Octopine dehydrogenase activity (7.22 units g^{-1}) is lower than that found here for some ammoniacal species (Table 1). *Architeuthis* is believed to undergo an ontogenetic migration. Juveniles have been found at the surface (Roper and Young, 1972; Lu, 1986), whereas adults are believed to reside in midwater (Robison, 1989). If *Architeuthis* does indeed undergo an ontogenetic descent, then we might assume that juveniles have much greater anaerobic capacity than adults (see Figs. 8, 9; and Hunt and Seibel, 2000).

O'Dor (1988) suggested, on the basis of scaling of migratory ranges in smaller squid, that *Architeuthis* could, if it wanted to, circle the globe in under 80 days. He suggested that the apparently weaker muscle tissue of *Architeuthis* relative to shallow-living squids is not necessarily evidence against strong swimming ability *per se.* He suggested, rather, that burst swimming may be limited and that perhaps *Architeuthis* requires only "cruising muscle" (O'Dor, 1988). This hypothesis is consistent with the relatively high aerobic, but low anaerobic, capacity measured here.

The present specimen was kept on ice or in a refrigerated cold room for at least 3 days prior to dissection. It is not known how long it had been dead at the surface of the ocean before collection or to what extent the enzymes may have degraded. We view the present measurements as conservative estimates.

Buoyancy

Many midwater cephalopods possess some means of achieving neutral buoyancy, whereas most epipelagic squids are negatively buoyant and rely on constant swimming for lift. Some midwater squids accumulate high quantities of ammonium ions that are lighter than seawater and thus provide a buoyant force (Denton and Gilpin-Brown, 1973; Clarke *et al.*, 1979; Voight *et al.*, 1994). The difference in metabolic potential between shallow- and deep-living species may, therefore, be partially accounted for by differing energy requirements for support in the water column as a result of interspecific differences in density.

However, strong locomotion requires a high protein content that precludes neutral buoyancy. Therefore, relaxed requirements for strong locomotory abilities allow the exploitation of buoyancy mechanisms. The need for strong swimming determines the practicality of buoyancy (Childress and Nygaard, 1974; Seibel *et al.*, 1997). Some of the variation in enzymatic activity at a given habitat depth certainly reflects differences in the type of buoyancy mechanism employed or in the relative distribution of buoyancy-related compounds within the body. For example, the cranchiid and chiroteuthid squids have very high mantle muscle ODH activities relative to histioteuthids despite having similar oxygen consumption rates (Seibel *et al.*, 1997). This may be, in part, due to differing distributions of ammonium in the bodies of these groups. The cranchiids store ammonium in a separate coelomic compartment and have none in the mantle tissue. Chiroteuthids store large quantities of ammonium in two enlarged arms (as adults) and have relatively little in mantle muscle. Histioteuthids, on the other hand, store the majority of their ammonium in mantle tissue (Denton and Gilpin-Brown, 1973; Clarke *et al.*, 1979; Voight *et al.*, 1994). Despite these differences, we do not believe that the overall patterns of enzymatic activity with depth or body mass are specifically related to buoyancy.

Light-limitation on predator-prey interactions

The ecological and evolutionary implications of low levels of ambient light in the deep sea have long been recognized (see reviews in Herring *et al.*, 1990). By reducing predator-prey detection distances, low light levels in the deep sea influence behavior (Hunt and Seibel, 2000), vertical distribution (Young *et al.*, 1980), morphology, reproduction (Seibel *et al.*, 2000), and metabolism (Childress, 1995; Seibel *et al.*, 1997). Relaxed selection for strong locomotory abilities in the deep sea allows the adoption of energy-saving buoyancy mechanisms (Childress and Nygaard, 1974). Similarly, we argue here that relaxed requirements for locomotory ability have allowed the evolution of efficient means of locomotion by deep-sea cephalopods. Enzymatic activities from the present study generally appear to correlate well with locomotory behaviors previously hypothesized on the basis of morphology (Bidder, 1970; Clarke, 1988), angular acceleration receptors (Young, 1989), brain structure (Young, 1977), or direct observations from submersibles (Hunt, 1996). In the deep sea, where high speeds are not strongly selected for, use of fins or arms for locomotion reduces the cost of transport. We point out only a general trend toward more efficient means of locomotion in the deep sea: the tremendous variation in swimming behaviors and morphologies among species contributes much of the variation to our data set.

Acknowledgments

We thank the captains and crews of the R/V *New Horizon* and *Pt. Sur* and the charter boat *Top Dog* for assistance in collection of specimens. We thank R. K. Suarez, F. G. Hochberg, N. Voss, and A. L. Alldredge for constructive comments on the manuscript. We thank J. Hunt for informative discussions concerning deep-sea cephalopods, and A. Zimmerman, M. Biondi, and J. Freytag for their assistance at sea. This research was supported by NSF grants OCE-9301374, OCE-9415543, and OCE-9115551 to J.J.C. and, in part, by the Rosenstiel School of Marine and Atmospheric Science Postdoctoral Fellowship and a Western Society of Malacologists Student Grant to B.A.S.

Literature Cited

Aronson, R. B. 1991. Ecology, paleobiology and evolutionary constraint in the octopus. *Bull. Mar. Sci.* **49:** 245–255.

Baldwin, J. 1982. Correlations between enzyme profiles in cephalopod muscle and swimming behavior. *Pac. Sci.* **36:** 349–356.

Baldwin, J., and W. R. England. 1980. A comparison of anaerobic energy metabolism in mantle and tentacle muscle of the blue-ringed octopus, *Hapalochlaena maculosa,* during swimming. *Aust. J. Zool.* **28:** 407–412.

Ballantyne, J. S., P. W. Hochachka, and T. P. Mommsen. 1981. Studies on the metabolism of the migratory squid, *Loligo opalescens*: enzymes of tissues and heart mitochondria. *Mar. Biol. Lett.* **2:** 75–85.

Bidder, A. M. 1970. Some problems of cephalopod locomotion. *Proc. Symp. Mollusca Ernakulam, Cochin* (Mar. Biol. Assoc., India) **III.** 1029–1052.

Bone, Q., A. Pulsford, and A. D. Chubb. 1981. Squid mantle muscle. *J. Mar. Biol. Assoc. UK* **61:** 327–342.

Carlini, D. B., and J. E. Graves. 1999. Phylogenetic analysis of cytochrome *c* oxidase I sequences to determine higher-level relationships within the coleoid cephalopods. *Bull. Mar. Sci.* **64:** 57–76.

Childress, J. J. 1995. Are there physiological and biochemical adaptations of metabolism in deep-sea animals? *Trends Ecol. Evol.* **10:** 30–36.

Childress, J. J., and T. M. Mickel. 1980. A motion compensated ship-board precision balance system. *Deep-Sea Res.* **27A:** 965–970.

Childress, J. J., and M. H. Nygaard. 1974. The chemical composition and relative buoyancy of midwater crustaceans as a function of depth off Southern California. *Mar. Biol.* **27:** 225–238.

Childress, J. J., and B. A. Seibel. 1998. Life at stable low oxygen levels: adaptations of animals to oceanic oxygen minimum layers. *J. Exp. Biol.* **201:** 1223–1232.

Childress, J. J., and G. N. Somero. 1979. Depth related enzymic activities in muscle, brain and heart of deep-living pelagic marine teleosts. *Mar. Biol.* **52:** 273–283.

Childress, J. J., and G. N. Somero. 1990. Metabolic scaling: a new perspective based on scaling of glycolytic enzyme activities. *Am. Zool.* **30:** 161–173.

Childress, J. J., A. T. Barnes, L. B. Quetin, and B. H. Robison. 1978. Thermally protecting cod ends for recovery of living deep-sea animals. *Deep-Sea Res.* **25:** 419–422.

Childress, J. J., D. L. Cowles, J. A. Favuzzi, and T. J. Mickel. 1990. Metabolic rates of benthic deep-sea decapod crustaceans decline with increasing depth primarily due to the decline in temperature. *Deep-Sea Res.* **37:** 929–949.

Clarke, M. R. 1988. Evolution of buoyancy and locomotion in recent cephalopods. *Mollusca* **12:** 203–213.

Clarke, M. R., E. J. Denton, and J. B. Gilpin-Brown. 1979. On the use of ammonium for buoyancy in squids. *J. Mar. Biol. Assoc. UK* **59:** 259–276.

Cole, K. S., and D. L. Gilbert. 1970. Jet propulsion of squid. *Biol. Bull.* **138:** 245–246.

Dahlhoff, E., J. O'Brien, G. N. Somero, and R. D. Vetter. 1991. Temperature effects on mitochondria from hydrothermal vent invertebrates: evidence for adaptation to elevated and variable habitat temperatures. *Physiol. Zool.* **64:** 1490–1508.

Denton, E. J., and J. B. Gilpin-Brown. 1973. Floatation mechanisms in modern and fossil cephalopods. *Adv. Mar. Biol.* **11:** 197–268.

Dilly, P. N., M. Nixon, and J. Z. Young. 1977. *Mastigoteuthis*—the whip-lash squid. *J. Zool. (Lond.)* **181:** 527–559.

Driedzic, W. R., B. D. Sidell, J. M. Stewart, and I. A. Johnston. 1990. Maximal activities of enzymes of energy metabolism in Cephalopod systemic and branchial hearts. *Physiol. Zool.* **63:** 615–629.

Ellis, R. 1998. *The Search for the Giant Squid.* Lyons Press, New York. 322 pp.

Felsenstein, J. 1985. Phylogenies and the comparative method. *Am. Nat.* **126:** 1–25.

Fleisher, K. J., and J. F. Case. 1995. Cephalopod predation facilitated by dinoflagellate luminescence. *Biol. Bull.* **189:** 263–271.

Harvey, P. H., and M. D. Pagel. 1991. *The Comparative Method in Evolutionary Biology.* Oxford University Press, New York. 239 pp.

Herring, P. J., A. K. Campbell, M. Whitfield, and L. Maddock. 1990. *Light and Life in the Sea.* Cambridge University Press. Cambridge. 341 pp.

Herring, P. J., P. N. Dilly, and C. Cope. 1994. The bioluminescent organs of the deep-sea cephalopod *Vampyroteuthis infernalis* (Cephalopoda: Vampyromorpha). *J. Zool. (Lond.)* **223:** 45–55.

Hoar, J. A., E. Sim, D. M. Webber, and R. K. O'Dor. 1994. The role of fins in the competition between squid and fish. Pp. 27–33 in *Mechanisms and Physiology of Animal Swimming.* L. Maddock, Q. Bone, and J. M. V. Rayner, eds. Cambridge University Press, Cambridge.

Hochachka, P. W., and G. N. Somero. 1984. *Biochemical Adaptation.* Princeton University Press. Princeton, NJ. 537 pp.

Hochachka, P. W., K. B. Storey, and J. Baldwin. 1975. Squid muscle citrate synthase: control of carbon entry into the Krebs cycle. *Comp. Biochem. Physiol.* **52B:** 193–199.

Hunt, J. C. 1996. The behavior and ecology of midwater cephalopods from Monterey Bay: submersible and laboratory observations. Ph.D. dissertation, University of California, Los Angeles.

Hunt, J. C., and B. A. Seibel. 2000. Life history of *Gonatus onyx*. I. Ontogenetic changes in habitat, behavior and physiology. *Mar. Biol.* (in press).

Johnsen, S., and E. A. Widder. 1998. Transparency and visibility of gelatinous zooplankton from the Northwestern Atlantic and Gulf of Mexico. *Biol. Bull.* **195:** 337–348.

Lu, C. C. 1986. Smallest of the largest: first record of giant squid larval specimen. *Australian Shell News* **53:** 9.

Marshall, N. B. 1979. *Developments in Deep-Sea Biology.* Blandford Press, Poole, England. 566 pp.

Mommsen, T. P., J. Ballantyne, D. MacDonald, J. Gosline, and P. W. Hochachka. 1981. Analogues of red and white muscle in squid mantle. *Proc. Natl. Acad. Sci. USA* **78:** 3274–3278.

Newsholme, E., and B. Crabtree. 1986. Maximum catalytic activity of some key enzymes in provision of physiologically useful information about metabolic fluxes. *J. Exp. Zool.* **239:** 159–167.

O'Dor, R. K. 1988. The energetic limits on squid distributions. *Malacologia* **29:** 113–119.

O'Dor, R. K., and R. E. Shadwick. 1989. Squid, the olympic cephalopods. *J. Ceph. Biol.* **1:** 33–54.

O'Dor, R. K., and D. M. Webber. 1986. The constraints on cephalopods: why squid aren't fish. *Can. J. Zool.* **64:** 1591–1605.

Packard, A. 1972. Cephalopods and fish: the limits of convergence. *Biol. Rev.* **47:** 241–307.

Packard, A., and M. Wurtz. 1994. An octopus, *Ocythoe,* with a swimbladder and triplejets. *Philos. Trans. R. Soc. Lond. B.* **344:** 261–275.

Pierce, V. A., and D. L. Crawford. 1997. Phylogenetic analysis of glycolytic enzyme expression. *Science* **276:** 256–259.

Pörtner, H. O. 1994. Coordination of metabolism, acid-base regulation and haemocyanin function in cephalopods. Pp. 131–148 in *Physiology of Cephalopod Molluscs: Lifestyle and Performance Adaptotions.* H. O. Pörtner, R. K. O'Dor, and D. L. MacMillan, eds. Gordon and Breach, New York.

Preuss, T., Z. N. Lebaric, and W. F. Gilly. 1997. Post-hatching development of circular mantle muscles in the squid *Loligo opalescens. Biol. Bull.* **192:** 375–387.

Robison, B. H. 1989. Depth of occurrence and partial chemical composition of a giant squid, *Architeuthis,* off Southern California. *Veliger* **32:** 39–42.

Roper, C. F. E., and W. L. Brundage. 1972. Cirrate octopods with associate deep-sea organisms: new biological data based on deep benthic photographs (Cephalopoda). *Smithson. Contrib. Zool.* **121:** 1–46.

Roper, C. F. E., and M. Vecchione. 1997. *In situ* observations test hypotheses of functional morphology in *Mastigoteuthis* (Cephalopoda. Oegopsida). *Vie Milieu* **47:** 87–93

Roper, C. F. E., and R. E. Young. 1972. First records of juvenile giant squid *Architeuthis* (Cephalopoda. Oegopsida). *Proc. Biol. Soc. Wash.* **85:** 205–222.

Roper, C. F. E., and R. E. Young. 1975. Vertical distribution of pelagic cephalopods. *Smithson. Contrib. Zool.* **209:** 1–51

Roper, C. F. E., M. J. Sweeney, and C. E. Nauen. 1984. *FAO Species Catalogue. Vol. 3. Cephalopods of the World. An Annotated and Illustrated Catalogue of Species of Interest to Fisheries. FAO Fisheries Synopsis.* **125,** 277 pp.

Schmidt-Nielsen, K. 1984. *Scaling: Why Is Animal Size So Important?* Cambridge University Press, Cambridge 241 pp.

Seapy, R. R., and R. E. Young. 1986. Concealment in epipelagic pterotracheid heteropods (Gastropoda) and cranchiid squids (Cephalopoda). *J. Zool. (Lond.)* **210A:** 137–147.

Seibel, B. A. 1998. Metabolism and locomotion of cephalopods in relation to habitat depth. Ph.D. dissertation, University of California, Santa Barbara. 260 pp.

Seibel, B. A., and J. J. Childress. 2000. Metabolism of benthic octopods (Cephalopoda) in relation to habitat depth and hypoxia. *Deep-Sea Res.* (in press).

Seibel, B. A., E. V. Thuesen, J. J. Childress, and L. A. Gorodezky. 1997. Decline in pelagic cephalopod metabolism with habitat depth reflects differences in locomotory efficiency. *Biol. Bull.* **192:** 262–278.

Seibel, B. A., E. V. Thuesen, and J. J. Childress. 1998. Flight of the vampire: ontogenetic gait-transition in *Vampyroteuthis infernalis* (Cephalopoda: Vampyromorpha). *J. Exp. Biol.* **201:** 2413–2424.

Seibel, B. A., F. Chausson, F. Lallier, F. Zal, and J. J. Childress. 1999. Vampire blood: respiratory physiology of the vampire squid (Cephalopoda: Vampyrmorpha) in relation to the oxygen minimum layer. *Exp. Biol. Online* **4:** 1–10.

Seibel, B. A., F. G. Hochberg, and D. B. Carlini. 2000. Life history of *Gonatus onyx*: deep-sea spawning and post-spawning egg care. *Mar. Biol.* (in press).

Siebenaller, J. F., G. N. Somero, and R. L. Haedrich. 1982. Biochemical characteristics of macrourid fishes differing in their depths of distribution. *Biol. Bull.* **163:** 240–249.

Somero, G. N., and J. J. Childress. 1980. A violation of the metabolism-size scaling paradigm: activities of glycolytic enzymes in muscle increase in larger-size fish. *Physiol. Zool.* **53:** 322–337.

Somero, G. N., and J. F. Siebenaller. 1979. Inefficient lactate dehydrogenases of deep-sea fishes. *Nature* **282:** 100–102.

Staples, J., and R. K. Suarez. 1997. Honeybee flight muscle phosphoglucose isomerase: matching enzyme capacities to flux requirements at a near-equilibrium reaction. *J. Exp. Biol.* **200:** 1247–1254.

Storey, K. B. 1977. Tissue specific isozymes of octopine dehydrogenase in the cuttlefish, *Sepia officinalis.* The roles of octopine dehydrogenase and lactate dehydrogenase in *Sepia. J. Comp. Physiol.* **115:** 159–169.

Sweeney, M. J., C. F. E. Roper, K. M. Mangold, M. R. Clarke, and S. V. Boletzky, eds. 1992. "Larval" and juvenile cephalopods: a manual for their identification. *Smithson. Contrib. Zool.* **513.**

Thuesen, E. V., and J. J. Childress. 1993a. Enzymatic activities and metabolic rates of pelagic chaetognaths: lack of depth-related declines. *Limnol. Oceanogr.* 38: [illegible] 948

Thuesen, E. V., and J. J. Childress. 1993b. Metabolic rates, enzyme activities, and chemical compositions of some deep-sea pelagic worms, particularly *Nectonemertes mirabilis* (Nemertea; Hoplonemertinea) and *Poeobius meseres* (Annelida: Polychaeta). *Deep-Sea Res. Part I* **40:** 937–951

Thuesen, E. V., and J. J. Childress. 1994. Oxygen consumption rates and metabolic enzyme activities of oceanic California medusae in relation to body size and habitat depth. *Biol. Bull.* **187:** 84–98.

Vecchione, M., and C. F. E. Roper. 1991. Cephalopods observed from submersibles in the Western North Atlantic. *Bull. Mar. Sci.* **49:** 433–445.

Vecchione, M., and R. E. Young. 1997. Aspects of the functional morphology of cirrate octopods: locomotion and feeding. *Vie Milieu* **97:** 101–110.

Vetter, R. A. H. 1995. Ecophysiological studies on citrate synthase: (II) enzyme regulation of selected crustaceans with regard to life-style and the climatic zone. *J. Comp. Physiol. B* **165:** 56–61.

Vetter, R. A. H., and F. Buchholz. 1998. Kinetics of enzymes in cold-stenothermal invertebrates. Pp. 190–211 in *Cold Ocean Physiology.* H. O. Portner, and R. C. Playle, eds. Cambridge University Press, Cambridge.

Villanueva, R., M. Segonzac, and A. Guerra. 1997. Locomotion modes of deep-sea cirrate octopods (Cephalopoda) based on observations from video recordings on the Mid-Atlantic Ridge. *Mar. Biol.* **129:** 113–122.

Vogel, S. 1994. *Life in Moving Fluids: The Physical Biology of Flow.* Princeton University Press, Princeton, NJ.

Voight, J. R., H. O. Poertner, and R. K. O'Dor. 1994. A review of ammonia-mediated buoyancy in squids (Cephalopoda: Teuthoidea). *Mar. Freshw. Behav. Physiol.* **25:** 193–203.

Voss, N. A., K. N. Nesis, and P. G. Rodhouse. 1998. The cephalopod family Histioteuthidae (Oegopsida): systematics, biology, and biogeography. In *Systematics and Biogeography of Cephalopods II.* N. A. Voss, M. Vecchione, R. Toll, and M. J. Sweeney, eds. *Smithson. Contrib. Zool.* **586:** 290–372.

Wells, M. J. 1994. The evolution of a racing snail. Pp. 1–12 in *Physiology of Cephalopod Molluscs: Lifestyle and Performance Adaptations.* H. O. Pörtner, R. K. O'Dor, and D. L. Macmillan, eds. Gordon and Breach, Amsterdam.

Wells, M. J., and R. K. O'Dor. 1991. Jet propulsion and the evolution of the cephalopods. *Bull. Mar. Sci.* **49:** 419–432.

Young, J. Z. 1977. Brain, behavior and evolution of cephalopods. In *The Biology of Cephalopods.* M. Nixon and J. B. Messenger, eds. *Symp. Zool. Soc. Lond.* **38:** 377–434

Young, J. Z. 1989. The angular acceleration receptor system of diverse cephalopods. *Philos. Trans. R. Soc. Lond. B* **325:** 189–237.

Young, R. E. 1972. The systematics and areal distribution of pelagic cephalopods from the seas off southern California. *Smithson. Contrib. Zool.* **97:** 1–159.

Young, R. E. 1975. *Leachia pacifica* (Cephalopoda, Teuthoidea): spawning habitat and function of the brachial photophores. *Pac. Sci.* **29:** 19–25.

Young, R. E. 1991. Chiroteuthid and related paralarvae from Hawaiian waters. *Bull. Mar. Sci.* **49:** 162–185.

Young, R. E., E. M. Kampa, S. D. Maynaurd, F. M. Mencher, and C. F. E. Roper. 1980. Counterillumination and the upper depth limits of midwater animals. *Deep-Sea Res. Part A* **27:** 671–691

Reference: *Biol. Bull.* **198:** 299–305. (April 2000)

Phylogeny of Gastrotricha: a Morphology-Based Framework of Gastrotrich Relationships

RICK HOCHBERG* AND MARIANNE K. LITVAITIS

Department of Zoology and Center for Marine Biology, University of New Hampshire, Durham, New Hampshire

Abstract. Currently, the phylum Gastrotricha is divided into the orders Macrodasyida and Chaetonotida, with the structure of the myoepithelial pharynx being an important distinguishing feature. Macrodasyida currently has six recognized families, and Chaetonotida comprises seven families. However, within-group relationships are poorly understood. To arrive at a better understanding of gastrotrich systematics and phylogeny, we performed the first cladistic analysis of nearly all known gastrotrich genera using 71 morphological characters. Results suggest that the Gastrotricha is a monophyletic group (supported by 82% of bootstrap replications) with its most primitive taxa distributed among the families Dactylopodolidae and Neodasyidae. Monophyly of Macrodasyida and Chaetonotida was supported by 90% and 52% bootstrap replications, respectively. Within the Macrodasyida, the families Dactylopodolidae, Turbanellidae, Macrodasyidae, and Thaumastodermatidae all formed monophyletic clades. The families Planodasyidae and Lepidodasyidae were paraphyletic. Among the Chaetonotida, the marine family Xenotrichulidae was monophyletic, supported by 51% of bootstrap replications. A second clade containing all freshwater families was supported by 62% bootstrap values. However, Chaetonotidae were paraphyletic. Using this analysis as a framework, we now can explore possible patterns of evolution within it, and arrive at a consensus of the gastrotrich ground pattern. Moreover, in future molecular studies of metazoan phylogeny, we will be able to select gastrotrich species that are more appropriate representatives of the phylum.

Introduction

Gastrotrichs figure prominently in metazoan phylogeny because they share a suite of complex morphological characteristics with several other members of the Bilateria, including the Gnathostomulida and the Nematoda. But their microscopic size, their cryptic interstitial habitat, and the lack of fossil record have exacerbated the usual barriers to phylogenetic analysis. As a consequence, gastrotrichs are one of the least understood groups of aquatic invertebrate animals. Furthermore, the relationship of Gastrotricha to other extant metazoans is uncertain; results from recent molecular and morphological studies are in conflict (Winnepenninnckx *et al.*, 1995; Littlewood *et al.*, 1996; and Wallace *et al.*, 1996). The currently accepted classification of the phylum Gastrotricha is based on morphological features (Hummon, 1982; Ruppert, 1988) and has two monophyletic orders, the Macrodasyida and Chaetonotida. Both orders are defined primarily by the structure of the myoepithelial pharynx (Ruppert, 1991), yet several other characteristics are important in the systematic classification of genera (Hummon, 1982; Ruppert, 1988; Ruppert, 1991) (Fig. 1).

Accepted morphological homologies supporting gastrotrich monophyly include the presence of unique, cuticle-covered duo-gland adhesive organs (Tyler and Rieger, 1980), a multilayered epicuticle (Rieger and Rieger, 1977), and cuticle-covered locomotory and sensory cilia (Rieger and Rieger, 1977). Other features often used to categorize gastrotrichs—cross-striated muscles (Travis, 1983), monociliated epidermis (Rieger, 1976), triradiate myoepithelial pharynx (Schmidt-Rhaesa *et al.*, 1998), and bilayered nature of the cuticle (Schmidt-Rhaesa *et al.*, 1998)—are plesiomorphies and, therefore, of limited systematic value. Of particular significance is the presence of a monociliated epidermis; this condition is considered a primitive trait among Metazoa (Rieger, 1976). A monociliated epidermis is found in several gastrotrich taxa (Rieger, 1976), including the Dactylopodolidae and Neodasyidae, arguing further for their basal positions within their respective orders. That the

---

Received 16 July 1999; accepted 16 December 1999.

* To whom correspondence should be addressed. E-mail: rickh@cisunix.unh.edu

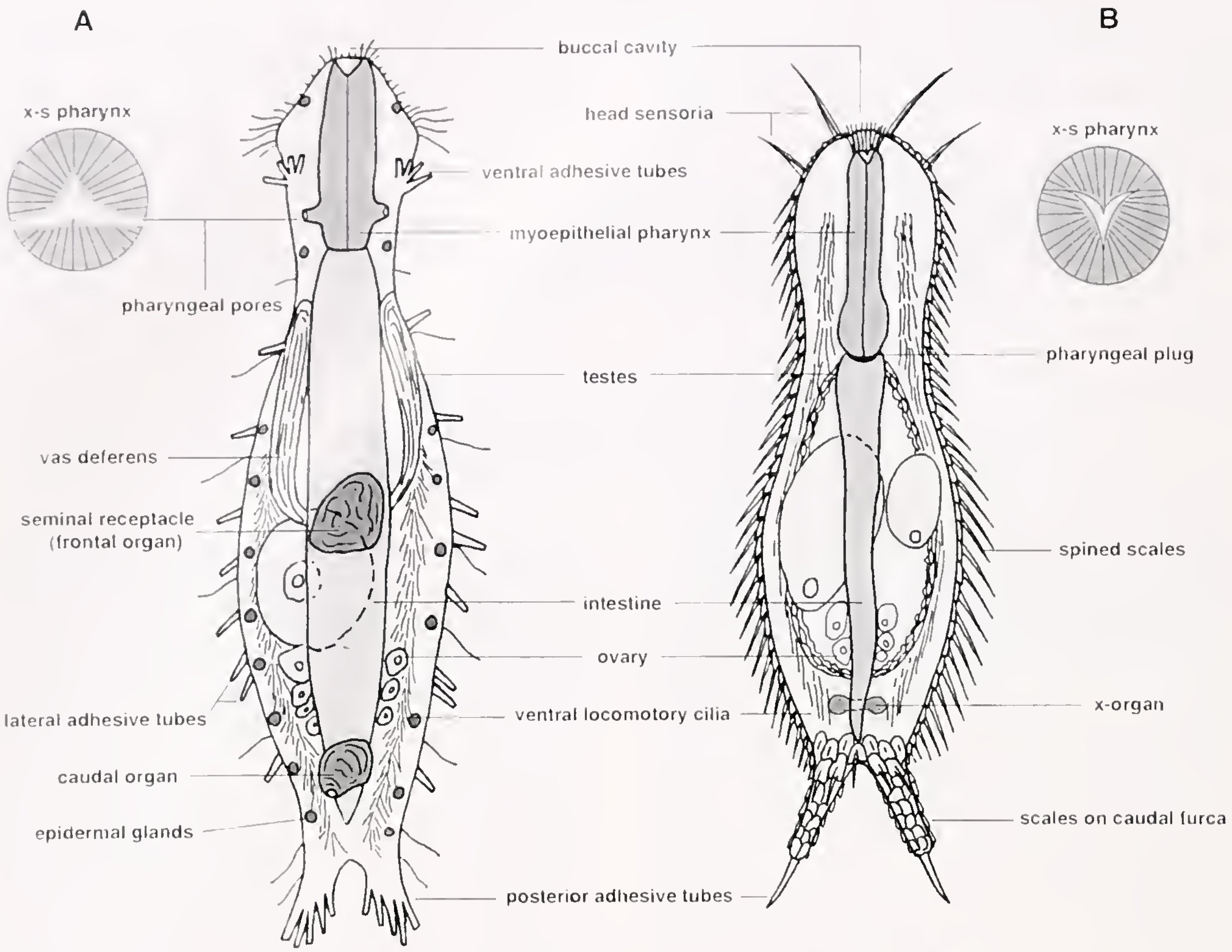
A
B
x-s pharynx
buccal cavity
head sensoria
ventral adhesive tubes
myoepithelial pharynx
pharyngeal pores
x-s pharynx
pharyngeal plug
testes
vas deferens
seminal receptacle
(frontal organ)
spined scales
intestine
ovary
lateral adhesive tubes
ventral locomotory cilia
x-organ
caudal organ
epidermal glands
scales on caudal furca
posterior adhesive tubes

Figure 1. Schematic representation of (A) a macrodasyidan and (B) a chaetonotidan gastrotrich, showing characters separating the two orders. Cross-sections through pharynges show orientation of lumen and, in the macrodasyidan, the pharyngeal pores.

order Chaetonotida may be paraphyletic with respect to the phylum Nematoda, as suggested previously (Ruppert, 1982), is indicated by similarities in cuticular and pharyngeal ultrastructure (upright Y-shaped lumen, pharyngeal-intestinal valve), and pharyngeal innervation. Because of the complete absence of locomotory cilia in Nematoda, in conjunction with several other morphological characters, we agree with Lorenzen (1985) that the Nematoda is, at best, a sister taxon to the Gastrotricha.

Materials and Methods

We have analyzed relationships of nearly all known gastrotrich genera and evaluated them using parsimony analysis (PAUP 4.0*; Swofford, 1999). Eighty-one characters were used in the analysis, all unordered and unweighted (Table 1). For maximum parsimony, default settings included ACCTRAN, and multistate taxa were treated as uncertainties. Bootstrap options included 1000 replicates of 81 characters. Full heuristic searches were performed with starting trees obtained by stepwise random addition (10 replicates with two trees held at each step). Tree bisection-reconnection (TBR) branch swapping was performed with the MULTREES option to save all minimum-length trees. Two genera, *Marinellina* and *Undula*, were excluded from the analysis due to a lack of information. The Gnathostomulida and Nematoda were used as outgroups. The data matrix is available upon request from the first author.

Results

Our analysis resulted in a monophyletic Gastrotricha (82% bootstrap values). Within the phylum, Chaetonotida (supported by 52% of bootstrap replications) and Macrodasyida (90% of bootstrap replications) formed two monophyletic clades (Fig. 2). Although the Macrodasyida is a

Table 1

Characters and character states used in parsimony analysis of Gastrotricha (a = absent, p = present)

Adhesive Tubes

1. Cuticularized adhesive organs (tubes) (0 = a, 1 = p)
2. Lateral adhesive tubes (0 = a, 1 = p)
3. Lateral adhesive organs indistinguishable, present as minute papillae (0 = a, 1 = p)
4. Ventrally placed anterior adhesive tubes (0 = a, 1 = p)
5. Anterior adhesive tubes in arc-like orientation (0 = a, 1 = p)
6. Anterior adhesive tubes on a mobile elevated base (0 = a, 1 = p)
7. Anterior adhesive tubes arranged together—as hands or clumps (0 = a, 1 = p)
8. Posterior adhesive tubes (0 = a, 1 = p)
9. Rounded caudal end bearing numerous adhesive tubes (0 = a, 1 = p)
10. Caudal end with tail-like extension bearing adhesive tubes (0 = a, 1 = p)
11. Caudal end with elongate peduncle bearing adhesive tubes (0 = a, 1 = p)
12. Caudal end is biramous/forked (0 = a, 1 = p)
13. Caudal end with only 2 adhesive tubules (0 = a, 1 = p)
14. Proximal/distal separation of caudal adhesive tubules on elongate peduncle (0 = a, 1 = p)
15. Median caudal cone (0 = a, 1 = p)
16. Caudal furca reduced to bilateral protuberances without adhesive tubes (0 = otherwise, 1 = p)
17. Ventrally placed extraordinary adhesive tubes as Seitenfüsschen (0 = a, 1 = p)
18. Seitenfüsschen as paired "brocha" tubules (0 = a, 1 = p)
19. Seitenfüsschen as single "cirrata" tubules (0 = a, 1 = p)

Alimentary System

20. Condition of buccal capsule (0 = simple opening, 1 = extended/folded/etc.)
21. Wide flaring buccal region (0 = a, 1 = p)
22. Shape of myoepithelial pharyngeal lumen (0 = a, 1 = Y-shape, 2 = upside-down Y-shape)
23. Pharyngeal clefts (0 = a, 1 = p)
24. Myoepithelial pharynx with cilia (0 = a, 1 = p)
25. Microvilli penetrate pharynx exocuticle (0 = a, 1 = p)
26. Pharyngeal foldings/plug (0 = a, 1 = p)
27. Pharyngeal intrusions "teeth" (0 = a, 1 = p)
28. Small pharyngeal pores (0 = a, 1 = p)
29. Ciliated gut epithelium (0 = a, 1 = p)
30. Distinct head enclosing most of the pharynx (0 = a, 1 = p)

Body Wall

31. Y-cells derived from longitudinal muscle block (0 = a, 1 = p)
32. Muscle striation pattern (0 = X-Striated, 1 = Oblique)
33. Y-cell with myofilaments (0 = a, 1 = p)
34. Epidermal glands with band-like contents (0 = a, 1 = p)
35. Circular muscles (0 = p, 1 = a)
36. Circular muscles absent from lateral body regions (0 = p, 1 = a)
37. Dorsal epidermal glands (0 = absent, 1 = present)
38. Body shape (0 = elongate, 1 = ten-pin)

Ciliation

39. Epidermal ciliation (0 = monociliation, 1 = multiciliation, 2 = no ciliation)
40. One pair of short "cirri" (0 = a, 1 = p)
41. Ventral cilia and head sensoria modified as cirri (0 = a, 1 = p)
42. Construction of ventral and head cirri (0 = a, 1 = constructed as a singular unit, 2 = each cilium with own cuticle)
43. *Stylochaeta*-type ciliation (0 = a, 1 = p)
44. Ventral locomotory cilia restricted to head region as a distinct patch (0 = a, 1 = p)
45. Ventral locomotory cilia present in 2 longitudinal rows (0 = a, 1 = p)
46. Longitudinal rows of locomotory cilia abbreviated at mid-body region (0 = otherwise, 1 = p)
47. Cilia covered with cuticle (0 = a, 1 = p)

Cuticle

48. Scales constructed from basal cuticular layer—form solid endocuticular thickenings (0 = a, 1 = p)
49. Cuticular hooks/ancres (triancres, tetrancres, pentancres) (0 = a, 1 = p)
50. Spines sculpted from surface zone of basal cuticular layer (not originating from flat scales) (0 = a, 1 = p)
51. Keeled scales derived from surface-zone of basal cuticular layer (0 = a, 1 = p)
52. Ventrolateral hydrofoil scales derived from surface-zone of basal cuticular layer (0 = a, 1 = p)

Table 1 (*Continued*)

53. Surface zone (of basal layer) spines present in groups (0 = a, 1 = p)
54. Surface-zone (of basal layer) scales (0 = a, 1 = p)
55. Surface-zone (of basal layer) scales lacking stalk and endplate (0 = a, 1 = p)
56. Surface-zone (of basal layer) scales in ventral interciliary field (0 = a, 1 = p)
57. Surface-zone (of basal layer) scales in ventral interciliary field reduced to terminal field (0 = a, 1 = p)
58. Elongate scale-covered furca (0 = a, 1 = p)
59. Head plates (0 = a, 1 = p)

Nervous System/Sense Organs
60. At least one pair of "soft, palp-like organs" on head (0 = a, 1 = p)
61. Club-shaped tentacles on head (0 = a, 1 = p)
62. Posterior nerve cords leaving circumpharyngeal ganglion (0 = multiple, 1 = 2 total)
63. Cephalic chemoreceptors present as piston pits, pestles, cones or palps (0 = a, 1 = p)
64. Single pair of posterior head cones (0 = a, 1 = p)
65. Number of longitudinal tracts of pharyngeal nerves (0 = >3 nerves, 1 = 3 nerves)

Reproductive System
66. Paired ova mature in anterior to posterior direction (0 = a, 1 = p)
67. Sperm ducts join caudal organ (0 = a, 1 = p)
68. Seminal receptacle (frontal organ) (0 = a, 1 = p)
69. Caudal organ (penis) (0 = a, 1 = p)
70. Complex frontal and caudal organs without tissue connection (0 = connection present, 1 = connection absent, 2 = not applicable)
71. Rosette organ (0 = a, 1 = p)
72. Paired testis (0 = otherwise, 1 = p)
73. Reduced left testis—single right testis only (0 = otherwise, 1 = p)
74. Reflexed vas deferens (0 = a, 1 = p)
75. Lumen of caudal and frontal organs continuous (0 = a, 1 = p)
76. Parthenogenesis (0 = a, 1 = p)
77. U-shaped gonad with caudal anastomosis (0 = a, 1 = p)
78. Vas deferentia (0 = elongate, 1 = reduced/absent)
79. Testes present as bilateral packets in post-parthenogenetic phase (0 = testes otherwise, 1 = p, 2 = no testes)
80. X-organ (0 = a, 1 = p)
81. Condition of vas deferentia (0 = a, 1 = separate, paired or unpaired, 2 = paired and fused)

highly heterogeneous group defined primarily by pharyngeal structure (Ruppert, 1991), the presence of groups of adhesive tubules (Hummon, 1982; Ruppert, 1988), and curious reproductive organs (Ruppert and Shaw, 1977; Ruppert, 1978), our analysis confirmed several monophyletic families within the order (Fig. 2). In fact, characters of the latter two organ systems substantiate monophyly of the two ecologically most diverse families, the Turbanellidae and Thaumastodermatidae (Fig. 2). These two families occur in nearly all marine environments at all depths, inhabit a wide array of sand types, and are probably among the most ubiquitous and successful groups of interstitial animals. As noted previously (Ruppert, 1988), the Lepidodasyidae is an unnatural taxon difficult to define on current morphological criteria. Our analysis found a paraphyletic Lepidodasyidae with some genera clustering with other families, although with low bootstrap values (Fig. 2). The monophyletic Dactylopodolidae (95% bootstrap values) is affirmed as the most primitive macrodasyidan family, with retention of several plesiomorphic traits including epidermal monociliation, alimentary canal ciliation, cross-striated muscles, and separate multiple nerve cords in some genera (Fig. 2). Additional research on this family, in particular the relatively unknown *Dendrodasys* and *Dendropodola*, should further elucidate the ground pattern for the Gastrotricha.

Bootstrap values advocating a monophyletic Chaetonotida are relatively strong (52%), and values for the monophyly of the suborder Paucitubulatina are even more robust (93%) (Fig. 2). All chaetonotidans are largely defined by the configuration of the pharyngeal lumen (upright Y-shaped) and the absence of pharyngeal pores. But often, body-shape ("ten-pin") and the absence of anterior or lateral adhesive tubules are the most easily seen diagnostic characters. The monogeneric Multitubulatina, however, contains an anomalous vermiform *Neodasys* that shares traits with both Macrodasyida and Paucitubulatina. However, unlike all other members of the Chaetonotida, *Neodasys* is highly elongate and in possession of some potentially plesiomorphic characteristics: hermaphroditic gonads, complex reproductive organs, monociliated epidermis, smooth cuticle, and numerous adhesive tubules (Ruppert, 1991). Furthermore, the adhesive organ of *Neodasys* lacks a releaser gland (Tyler *et*

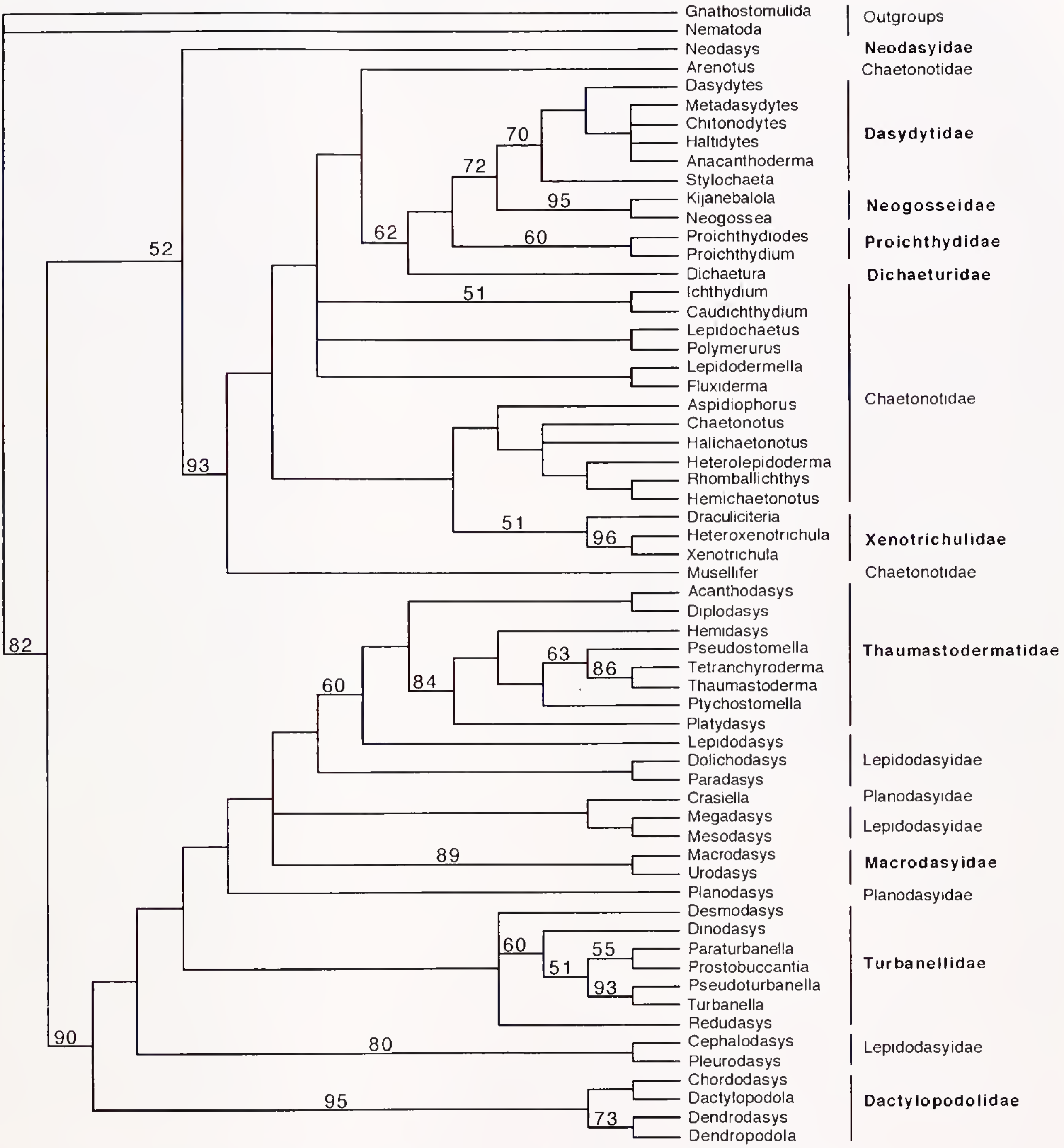
Gnathostomulida
Nematoda
Outgroups
Neodasys
Neodasyidae
Arenotus
Chaetonotidae
Dasydytes
Metadasydytes
Chitonodytes
Haltidytes
Anacanthoderma
Stylochaeta
Dasydytidae
Kijanebalola
Neogossea
Neogosseidae
Proichthydiodes
Proichthydium
Proichthydidae
Dichaetura
Dichaeturidae
Ichthydium
Caudichthydium
Lepidochaetus
Polymerurus
Lepidodermella
Fluxiderma
Aspidiophorus
Chaetonotus
Halichaetonotus
Heterolepidoderma
Rhomballichthys
Hemichaetonotus
Chaetonotidae
Draculiciteria
Heteroxenotrichula
Xenotrichula
Xenotrichulidae
Musellifer
Chaetonotidae
Acanthodasys
Diplodasys
Hemidasys
Pseudostomella
Tetranchyroderma
Thaumastoderma
Ptychostomella
Platydasys
Thaumastodermatidae
Lepidodasys
Dolichodasys
Paradasys
Lepidodasyidae
Crasiella
Planodasyidae
Megadasys
Mesodasys
Lepidodasyidae
Macrodasys
Urodasys
Macrodasyidae
Planodasys
Planodasyidae
Desmodasys
Dinodasys
Paraturbanella
Prostobuccantia
Pseudoturbanella
Turbanella
Redudasys
Turbanellidae
Cephalodasys
Pleurodasys
Lepidodasyidae
Chordodasys
Dactylopodola
Dendrodasys
Dendropodola
Dactylopodolidae
70
72
95
62
60
52
51
93
51
96
82
63
86
60
84
89
60
55
51
93
90
80
95
73

Figure 2. Consensus tree (50% Majority-Rule) of 59 gastrotrich genera. Tree length = 175 steps; CI = 0.503, RC = 0.450. Numbers at nodes represent percentages of 1000 bootstrap replications. Families indicated by bold type are monophyletic.

al., 1980). The presence of only one gland type in the adhesive organ is interpreted as a plesiomorphy when viewed in combination with the retention of other primitive traits (Tyler *et al.*, 1980). Still, the presence of duogland adhesive organs in all Gastrotricha has not been confirmed, and it remains to be seen whether the presence of only a single gland is actually the "primitive" condition or is secondarily derived.

Within the Paucitubulatina, the largest and structurally most diverse family—the Chaetonotidae—appears to be paraphyletic (Fig. 2). This highly speciose taxon (>250 spp.) is extremely heterogeneous with respect to cuticular armature, habitat type, and reproductive anatomy. The family is presumed to have evolved in the freshwater benthos, radiating into the marine environment secondarily (Kisielewski, 1990). Yet, the existence of a very basal marine genus, *Musellifer*, might also argue for a marine origin. Resolution of this vastly diverse taxon will undoubtedly improve with greater attention to its reproductive anatomy (presence of hermaphroditic organs is unknown for many genera; the homology of the X-organ is in question) and the complex microstructure of both scales and spines.

Still, several important monophyletic groupings were confirmed within the Chaetonotida, including the entirely freshwater Dasydytidae, Neogosseidae, and Proichthydidae (Fig. 2). Our analysis thus confirmed a clade of freshwater families with 62% of bootstraps. In addition, the marine family Xenotrichulidae and the subfamily Xenotrichulinae were also monophyletic (Fig. 2).

Discussion

The current analysis goes beyond classification; it is aimed at an elucidation of phylogenetic trends. In particular, trends in nervous-system structure in the Gastrotricha are revealed within the tree topology of the Macrodasyida. Basal genera often have multiple, separate nerve cords (4 in *Dactylopodola*), whereas more derived genera show partial fusion of nerve cords (4 fuse into 2 in *Turbanella*) or presumably complete fusion (2 in Thaumastodermatidae). The functional significance of this transition series is unknown; moreover, the trend is more ambiguous than supposed because other "intermediate" forms like *Cephalodasys maximus* show fusion ("schmelzen") of multiple (12) nerve cords, followed by subsequent bifurcation (Wiedermann, 1995). Other trends are also evident. For example, changes in reproductive biology (from hermaphroditic to parthenogenetic) seem to have occurred in chaetonotidan transitions from marine to freshwater biotopes.

This cladistic analysis also provides evidence that many characters used to define gastrotrichs in morphology-based phylogenies of extant Metazoa often are apomorphic for the phylum and, therefore, inappropriate. For example, Wallace *et al.* (1996) used the characters parthenogenesis, syncytial epidermis, and hypodermic impregnation in their analysis. The first two characters are known only in some chaetonotidans, and the third is unconfirmed except for the family Macrodasyidae and is unknown in basal taxa such as Dactylopodolidae. Backeljau *et al.* (1993) incorrectly used eutely (found only in some chaetonotidans) and radial cleavage (gastrotrichs have aberrant bilateral cleavage) as characters defining gastrotrichs as a whole in their analysis. Finally, Zrzavy *et al.* (1998) used the character pseudocoelomate in their analysis, although all gastrotrichs are acoelomate.

Our cladistic analysis also provides a good test for molecular phylogenetic studies. Several earlier molecular studies have focused on derived taxa (*Chaetonotus* sp., *Lepidodermella squamata*) to resolve phylum-level relationships (Winnepenninckx *et al.*, 1995; Littlewood *et al.*, 1998; Zrzavy *et al.*, 1998; Ruiz-Trillo *et al.*, 1999). Such taxa are particularly easy to culture, but their utility as representative models is questionable. *Lepidodermella squamata* is especially controversial because it inhabits fresh water and is parthenogenetic—characteristics that are uncommon among chaetonotidans and virtually absent in macrodasyidans. The use of such derived forms should be avoided until the systematics of the Chaetonotida is better resolved.

Additionally, molecular systematics place the Gastrotricha in a variety of positions within the metazoan tree: as a sister group to either the Acanthocephala (Carranza *et al.*, 1997), the Gnathostomulida (Littlewood *et al.*, 1998), the Nematomorpha (Carranza *et al.*, 1997), or the Platyhelminthes (Winnepenninckx *et al.*, 1995). Other studies place the Gastrotricha basal to most of the Bilateria (Carranza *et al.*, 1997), or to the Lophotrochozoa (Ruiz-Trillo *et al.*, 1999) or the Spiralia (Littlewood *et al.*, 1998). We, however, contend that the position of the Gastrotricha remains questionable until more primitive gastrotrich species are used, namely *Neodasys* or species of the Dactylopodolidae. These additions to the molecular data set would be a good test of tree strength and confirmation of their branching point from the remaining phyla.

A comprehensive and congruent classification of the phylum Gastrotricha is essential if its origin and phylogenetic significance are to be fully appreciated. The currently accepted classification is in dire need of revision, especially concerning the order Chaetonotida and the family Lepidodasyidae. At the same time, though, previous work on the systematics of the phylum has successfully navigated the treacheries of convergence and parallelism and displayed good phylogenetic congruence (Remane, 1933; Hummon, 1982; Ruppert, 1988). Yet, despite the rather small size of the phylum, the species are highly variable in particular characters (*e.g.*, adhesive tubes, ciliary patterns, cuticular sculpture, reproductive anatomy), and recognition of plesiomorphy is often difficult.

Our study presents an evolutionary hypothesis for all Gastrotricha. Within this morphological framework, we now can address specific questions of relationships within and among individual gastrotrich taxa. For example, characters of the nervous system (*i.e.*, number of nerve cords, fusion, distribution of neurotransmitters) can now be evaluated in light of the presumed primitiveness of the Dactylopodolidae. This framework also allows for a more careful selection of gastrotrich species representing the phylum as a whole in future global molecular studies.

Literature Cited

Backeljiau, T., B. Winnepenninckx, and L. De Bruyn. 1993. Cladistic analysis of metazoan relationships: A reappraisal. *Cladistics* **9:** 167–181.

Carranza, S., J. Baguñá, and M. Riutort. 1997. Are the Platyhelminthes a monophyletic primitive group? An assessment using 18S rDNA sequences. *Mol. Biol. Evol.* **14:** 485–497.

Hummon, W. D. 1982. Gastrotricha. Pp. 857–863 in *Synopsis and Classification of Living Organisms.* Vol. 1, S. P. Parker, ed. McGraw-Hill, New York.

Kisielewski, J. 1990. Origin and phylogenetic significance of freshwater psammic Gastrotricha. *Stygologia* **5(2):** 87–92.

Littlewood, D. T. J., M. J. Telford, K. A. Clough, and K. Rohde. 1998. Gnathostomulida—an enigmatic metazoan phylum from both morphological and molecular perspectives. *Mol. Phylogenet. Evol.* **9(1):** 72–79.

Lorenzen, S. 1985. Phylogenetic aspects of pseudocoelomate evolution. Pp. 210–223 in *The Origins and Relationships of Lower Invertebrates.* S. C. Morris, J. D. George, R. Gibson, and H. M. Platt, eds. Clarendon, Oxford.

Remane, A. 1933. Gastrotricha. Pp. 121–186 in *Handbuch der Zoologie,* II Band, 1 Hälfte. W. Kükenthal and T. Krumbach, eds. Walter de Gruyter, Berlin.

Rieger, R. M. 1976. Monociliated epidermal cells in Gastrotricha: significance for concepts of early metazoan evolution. *Z. Zool. Syst. Evolutionsforsch.* **14:** 198–226.

Rieger, G. E., and R. M. Rieger. 1977. Comparative fine structure study of the gastrotrich cuticle and aspects of cuticle evolution within the aschelminthes. *Z. Zool. Syst. Evolutionsforsch.* **15:** 81–124.

Ruiz-Trillo, I., M. Riutort, D. T. J. Littlewood, E. A. Herniou, and J. Baguñá. 1999. Acoel flatworms: earliest extant bilaterian metazoans, not members of Platyhelmintes. *Science* **283:** 1919–1923.

Ruppert, E. E. 1978. The reproductive system of gastrotrichs. II. Insemination in *Macrodasys:* a unique mode of sperm transfer in Metazoa. *Zoomorphologie* **89:** 207–228.

Ruppert, E. E. 1982. Comparative ultrastructure of the gastrotrich pharynx and the evolution of myoepithelial foreguts in Aschelminthes. *Zoomorphologie* **99:** 181–200.

Ruppert, E. E. 1988. Gastrotricha. Pp. 302–311 in *Introduction to the Study of Meiofauna.* R. P. Higgins and H. Thiel, eds. Smithsonian Institution Press, Washington, DC.

Ruppert, E. E. 1991. Gastrotricha. Pp. 41–109 in *Microscopic Anatomy of Invertebrates. Volume 4: Aschelminthes.* F. Harrison and E. E. Ruppert, eds. Wiley-Liss, New York.

Ruppert, E. E., and K. Shaw. 1977. The reproductive system of gastrotrichs. I. Introduction with morphological data for two new *Dolichodasys* species. *Zool. Scr.* **6:** 185–195.

Schmidt-Rhaesa, A., T. Bartolomaeus, C. Lemburg, U. Ehlers, and J. R. Garey. 1998. The position of the Arthropoda in the phylogenetic system. *J. Morph.* **238:** 263–285.

Swofford, D. L. 1999. PAUP*. Phylogenetic Analysis Using Parsimony (*and Other Methods). Verson 4.1.1b. Sinauer Associates, Sunderland, MA.

Travis, P. B. 1983. Ultrastructural study of body wall organization and Y-cell composition in the Gastrotricha. *Z. Zool. Syst. Evolutionsforsch.* **21:** 52–68.

Tyler, S., and G. E. Rieger. 1980. Adhesive organs of the Gastrotricha. I. Duo-gland organs. *Zoomorphologie* **95:** 1–15.

Tyler, S., L. A. Melanson, and R. Rieger. 1980. Adhesive organs of the Gastrotricha. II. The organs of *Neodasys. Zoomorphologie* **95:** 17–26.

Wallace, R. L., C. Ricci, and G. Melone. 1996. A cladistic analysis of pseudocoelomate (aschelminth) morphology. *Invertebr. Biol.* **115(2):** 104–112.

Wiedermann, A. 1995. Zur Ultrastruktur des Nervensystems bei *Cephalodasys maximus* (Macrodasyida Gastrotricha). *Microfauna Mar.* **10:** 173–233.

Winnepenninckx, B., T. Backelijau, L. Y. Mackey, J. M. Brooks, R. De Wachter, S. Kumar, and J. Garey. 1995. 18S rRNA data indicate that aschelminthes are polyphyletic in origin and consist of at least three distinct clades. *Mol. Biol. Evol.* **12(6):** 1132–1137.

Zrzavy, J., S. Mihulka, P. Kepka, and A. Bezdka. 1998. Phylogeny of the Metazoa based on morphological and 18S ribosomal DNA evidence. *Cladistics* **14:** 249–285.

MetaMorph

THE LEADER IN BIO-IMAGING

16 Years of Excellence in Fluorescence and High Performance Applications

- 6-DIMENSIONAL IMAGING
- GFP
- INTRACELLULAR CALCIUM
- MOTION ANALYSIS & PARTICLE TRACKING
- HIGH SPEED Z-SERIES
- LIVE/DEAD ASSAYS
- FLUORESCENCE IMMUNOCYTOCHEMISTRY
- HIGH SPEED RATIO FLUORESCENCE
- TIME LAPSE

UNIVERSAL IMAGING CORPORATION

www.image1.com 610-344-9410 sales@image1.com

JOIN US AT MBL'S ANALYTICAL AND QUANTITATIVE LIGHT MICROSCOPY COURSE, MAY 4-12, WOODS HOLE, MA

MARINE BIOLOGICAL LABORATORY
OFFICE OF EDUCATION

EDUCATIONAL PROGRAMS

OVERVIEW: Educational programs at the MBL provide opportunities for intensive academic inquiry under the guidance of expert and distinguished faculty. The teaching staff of each MBL course is drawn from a variety of research institutions and frequently outnumbers the student enrollment.

SUMMER COURSES have been a central part of the Laboratory's mission since its founding more than a century ago. The opportunity for exchange with members of the summer research community, as well as for intensive individual research, makes these programs unique in science education.

Summer courses last from six to nine weeks, and consist of formal lectures integrated with laboratory instruction and research. Laboratories emphasize application of the most current techniques. Summer courses are designed for graduate students, postdocs and independent investigators actively engaged in research.

SPECIAL TOPICS COURSES are intensive educational programs, one to five weeks long, providing experience in specialized research techniques, or are lecture and laboratory courses in topics of current interest. Generally, these courses are designed for graduate students, postdoctoral fellows, and other professionals actively engaged in research.

MBL courses are supported by a wide range of donors. The overall MBL educational program has been underwritten by gifts from the Howard Hughes Medical Institute and the Burroughs Wellcome Fund.

For more information about our courses, contact:
Carol Hamel, Admissions Coordinator
508-289-7401 / email: admissions@mbl.edu

Visit our website:
http://courses.mbl.edu

The MBL is an EEO/Affirmative Action Institution

CONTENTS

Volume 198, No. 2: April 2000

CHEMICAL COMMUNICATION IN ECOLOGY

Zimmer, Richard K.
Importance of chemical communication in ecology. . . . 167
Zimmer, Richard K., and Cheryl Ann Butman
Chemical signaling processes in the marine environment 168
Weissburg, Marc J.
The fluid dynamical context of chemosensory behavior 188
Vickers, Neil J.
Mechanisms of animal navigation in odor plumes . . . 203
Yen, Jeannette
Life in transition: balancing inertial and viscous forces by planktonic copepods 213
Wolfe, Gordon V.
The chemical defense ecology of marine unicellular plankton: constraints, mechanisms, and impacts . . . 225
Nevitt, Gabrielle A.
Olfactory foraging by Antarctic procellariiform seabirds: life at high Reynolds numbers 245

RESEARCH NOTE

Bentis, Christopher J., Les Kaufman, and Stjepko Golubic
Endolithic fungi in reef-building corals (Order: Scleractinia) are common, cosmopolitan, and potentially pathogenic 254

PARASITOLOGY

Tétreault, Françoise, John H. Himmelman, and Lena Measures
Impact of a castrating trematode, *Neophasis* sp., on the common whelk, *Buccinum undatum*, in the northern Gulf of St. Lawrence 261

PHYSIOLOGY

Clelland, Eric S., and A.S.M. Saleuddin
Vacuolar-type ATPase in the accessory boring organ of *Nucella lamellosa* (Gmelin) (Mollusca: Gastropoda): role in shell penetration 272

ECOLOGY AND EVOLUTION

Seibel, Brad A., Erik V. Thuesen, and James J. Childress
Light-limitation on predator-prey interactions: consequences for metabolism and locomotion of deep-sea cephalopods 284
Hochberg, Rick, and Marianne K. Litvaitis
Phylogeny of Gastrotricha: a morphology-based framework of gastrotrich relationships 299

Volume 198

Number 3

THE BIOLOGICAL BULLETIN

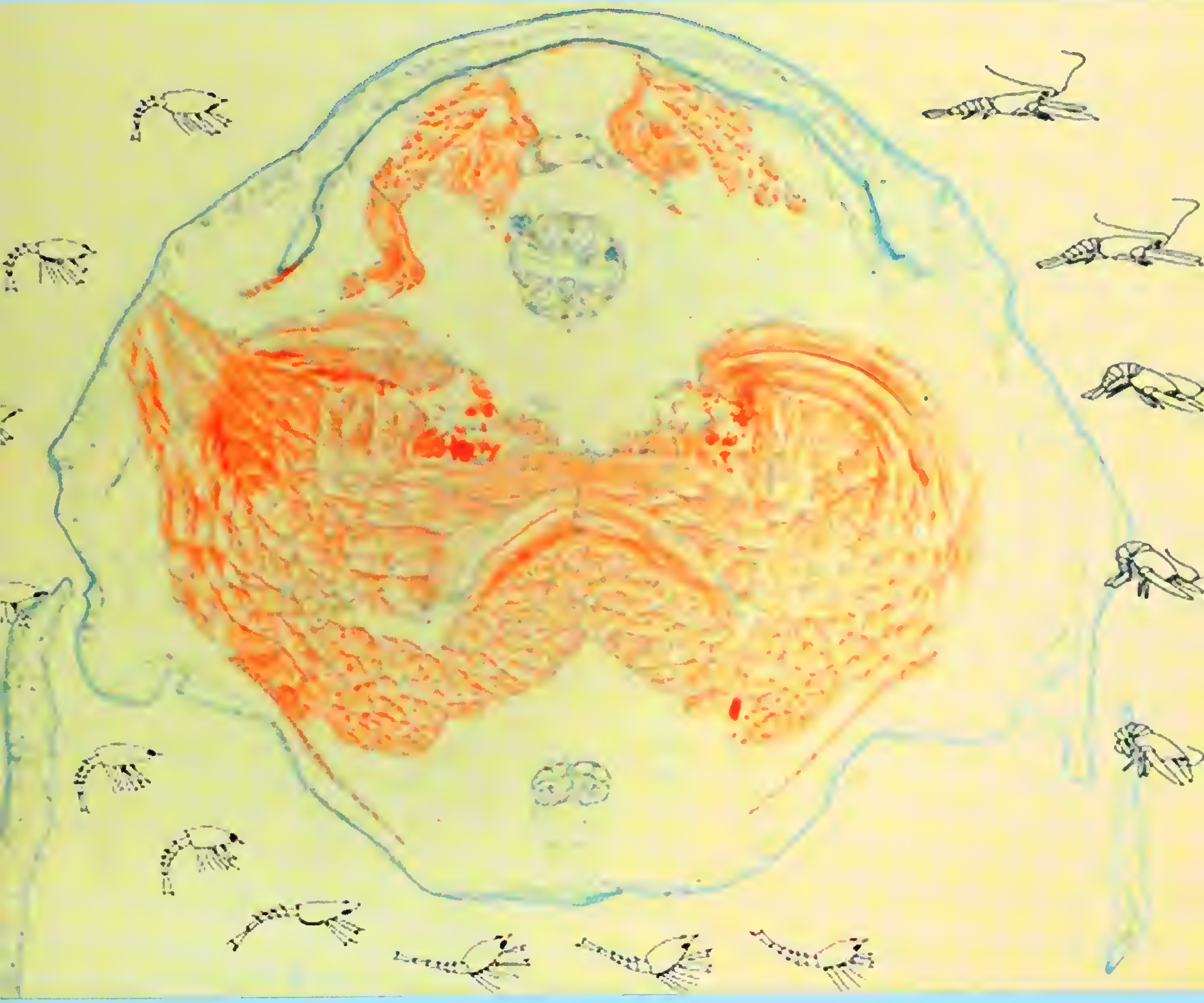

JUNE 2000

Published by the Marine Biological Laboratory

Trouble finding images?

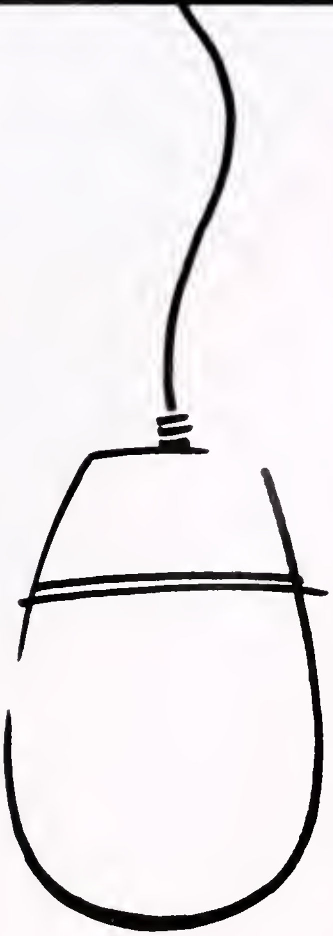

click. click. sorted.

Save time with Phylum, the easy to use software for finding and organising digital images.

Mac & Windows versions.

TWAIN & Adobe Photoshop® plug-in ready for a low cost imaging solution.

Download the free version now!

improvision Phylum™

www.phylumforfree.com

MARINE BIOLOGICAL LABORATORY
OFFICE OF EDUCATION

✧ EDUCATIONAL PROGRAMS ✧

Overview

Educational programs at the MBL provide opportunities for intensive academic inquiry under the guidance of expert and distinguished faculty. The teaching staff of each MBL course is drawn from a variety of research institutions and frequently outnumbers the student enrollment.

Summer Courses

Summer courses have been a central part of the Laboratory's mission since its founding more than a century ago. The opportunity for exchange with members of the summer research community, as well as for intensive individual research, makes these programs unique in science education.

Summer courses last from six to nine weeks, and consist of formal lectures integrated with laboratory instruction and research. Laboratories emphasize application of the most current techniques. Summer courses are designed for graduate students, postdocs and independent investigators actively engaged in research.

Special Topics Courses

Special topics courses are intensive educational programs, one to five weeks long, providing experience in specialized research techniques, or are lecture and laboratory courses in topics of current interest. Generally, these courses are designed for graduate students, postdoctoral fellows, and other professionals actively engaged in research.

MBL courses are supported by a wide range of donors. The overall MBL educational program has been underwritten by gifts from the Howard Hughes Medical Institute and the Burroughs Wellcome Fund.

For more information about our courses, contact:
Carol Hamel, Admissions Coordinator
508-289-7401 / email: admissions@mbl.edu

OR

Visit our website:
http://courses.mbl.edu

The MBL is an EEO/Affirmative Action Institution

THE
BIOLOGICAL BULLETIN
JUNE 2000

Editor	Michael J. Greenberg	The Whitney Laboratory, University of Florida
Associate Editors	Louis E. Burnett	Grice Marine Biological Laboratory, College of Charleston
	R. Andrew Cameron	California Institute of Technology
	Charles D. Derby	Georgia State University
	Michael LaBarbera	University of Chicago
Section Editor	Shinya Inoué, *Imaging and Microscopy*	Marine Biological Laboratory
Online Editors	James A. Blake, *Keys to Marine Invertebrates of the Woods Hole Region*	ENSR Marine & Coastal Center, Woods Hole
	William D. Cohen, *Marine Models Electronic Record and Compendia*	Hunter College, City University of New York
Editorial Board	Peter B. Armstrong	University of California, Davis
	Ernest S. Chang	Bodega Marine Lab., University of California, Davis
	Thomas H. Dietz	Louisiana State University
	Richard B. Emlet	Oregon Institute of Marine Biology, Univ. of Oregon
	David Epel	Hopkins Marine Station, Stanford University
	Gregory Hinkle	Cereon Genomics, Cambridge, Massachusetts
	Makoto Kobayashi	Hiroshima University of Economics, Japan
	Esther M. Leise	University of North Carolina Greensboro
	Donal T. Manahan	University of Southern California
	Margaret McFall-Ngai	Kewalo Marine Laboratory, University of Hawaii
	Mark W. Miller	Institute of Neurobiology, University of Puerto Rico
	Tatsuo Motokawa	Tokyo Institute of Technology, Japan
	Yoshitaka Nagahama	National Institute for Basic Biology, Japan
	Sherry D. Painter	Marine Biomed. Inst., Univ. of Texas Medical Branch
	J. Herbert Waite	University of California, Santa Barbara
	Richard K. Zimmer	University of California, Los Angeles
Editorial Office	Pamela Clapp Hinkle	Managing Editor
	Victoria R. Gibson	Staff Editor
	Carol Schachinger	Editorial Associate
	Patricia Burns	Subscription & Advertising Secretary

Published by
MARINE BIOLOGICAL LABORATORY
WOODS HOLE, MASSACHUSETTS

Cover

Adult lobsters and crayfish escape from predators or threatening conspecifics by "tailflicking"—a rapid and often rhythmic flexing of the abdomen. This behavior and its neuronal basis, particularly the involvement of the medial and lateral giant fibers, are well known. The manner in which escape behavior and its morphological and neurological manifestations change during development has also been studied in juveniles of the American lobster *Homarus americanus*.

In this issue (pp. 307–318), D.J. Jackson and D.L. Macmillan describe and compare the escape behaviors and related morphologies in the larval and juvenile stages of *H. americanus* with those in the immature stages of the direct developing crayfish *Cherax destructor*. They compare these observations with those made on adults, and relate the differences to the different environmental pressures faced by the organisms as they develop.

The image on the cover shows a cross-section through the abdomen of the earliest free-living stage of *C. destructor*. The blue, bilobed structure below the large red muscle mass is the ventral nerve cord, and the four giant fibers—paired axons of the laterals and medials—are visible just under the dorsal surface of this cord. The small drawings superimposed on the cross-section represent the escape movements of a stage 1 larva (series on the left) and an adult (right series) in response to a mechanical stimulation. The top image in both series is at 0 s after stimulation, and there are 20 ms between images (details in Fig. 1, p. 310). Although the larval stages of *H. americanus* have giant medial fibers, as revealed by serial cross-sections of the abdomen (Fig. 6, p. 314), these are not actively involved in escape tailflicking. Furthermore, larval tailflicks are characterized by an initial abdominal extension rather than flexion. This abdominal extension also forms a discrete behavior, termed a starburst response, the adaptive nature of which is discussed in this report.

JUN 28 2000

CONTENTS

VOLUME 198, NO. 3: JUNE 2000

NEUROBIOLOGY AND BEHAVIOR

Jackson, D.J., and D.L. Macmillan
Tailflick escape behavior in larval and juvenile lobsters (*Homarus americanus*) and crayfish (*Cherax destructor*) 307

Pires, Anthony, Roger P. Croll, and Michael G. Hadfield
Catecholamines modulate metamorphosis in the opisthobranch gastropod *Phestilla sibogae* 319

PHYSIOLOGY

Williamson, Jane E., Rocky de Nys, Naresh Kumar, David G. Carson, and Peter D. Steinberg
Induction of metamorphosis in the sea urchin *Holopneustes purpurascens* by a metabolite complex from the algal host *Delisea pulchra* 332

Wendt, Dean E.
Energetics of larval swimming and metamorphosis in four species of *Bugula* (Bryozoa) 346

McNamara, John C., and Márcia R. Ribeiro
The calcium dependence of pigment translocation in freshwater shrimp red ovarian chromatophores 357

DEVELOPMENT AND REPRODUCTION

Lauzon, Robert J., Baruch Rinkevich, C.W. Patton, and Irving L. Weissman
A morphological study of nonrandom senescence in a colonial urochordate 367

Selvakumaraswamy, P., and M. Byrne
Vestigial ophiopluteal structures in the lecithotrophic larvae of *Ophionereis schayeri* (Ophiuroidea) . . . 379

Young, Craig M., and Sophie B. George
Larval development of the tropical deep-sea echinoid *Aspidodiadema jacobyi:* phylogenetic implications 387

ECOLOGY AND EVOLUTION

Park, Joong-Ki, and Diarmaid Ó Foighil
Genetic diversity of oceanic island *Lasaea* (Mollusca: Bivalvia) lineages exceeds that of continental populations in the northwestern Atlantic 396

Sherrard, Kristin M.
Cuttlebone morphology limits habitat depth in eleven species of *Sepia* (Cephalopoda: Sepiidae) . . . 404

* * *

Index for Volume 198 415

THE BIOLOGICAL BULLETIN

THE BIOLOGICAL BULLETIN is published six times a year by the Marine Biological Laboratory, 7 MBL Street, Woods Hole, Massachusetts 02543.

Subscriptions and similar matter should be addressed to Subscription Manager, THE BIOLOGICAL BULLETIN, Marine Biological Laboratory, 7 MBL Street, Woods Hole, Massachusetts 02543. Subscription per year (six issues, two volumes): $225 for libraries; $95 for individuals. Subscription per volume (three issues): $112.50 for libraries; $47.50 for individuals. Back and single issues (subject to availability): $40 for libraries; $20 for individuals.

Communications relative to manuscripts should be sent to Michael J. Greenberg, Editor-in-Chief, or Pamela Clapp Hinkle, Managing Editor, at the Marine Biological Laboratory, 7 MBL Street, Woods Hole, Massachusetts 02543. Telephone: (508) 289-7428. FAX: 508-289-7922. E-mail: pclapp@mbl.edu.

---

http://www.mbl.edu/BiologicalBulletin/

The home page for the electronic companion to THE BIOLOGICAL BULLETIN—*the Marine Models Electronic Record*—and other BIOLOGICAL BULLETIN publications is available on the World Wide Web at the address shown above.

THE BIOLOGICAL BULLETIN is indexed in bibliographic services including *Index Medicus* and MEDLINE, *Chemical Abstracts, Current Contents, Elsevier BIOBASE/Current Awareness in Biological Sciences,* and *Geo Abstracts.*

Printed on acid free paper,
effective with Volume 180, Issue 1, 1991.

POSTMASTER: Send address changes to THE BIOLOGICAL BULLETIN, Marine Biological Laboratory,
7 MBL Street, Woods Hole, MA 02543.

Copyright © 2000, by the Marine Biological Laboratory

Periodicals postage paid at Woods Hole, MA, and additional mailing offices.
ISSN 0006-3185

INSTRUCTIONS TO AUTHORS

The Biological Bulletin accepts outstanding original research reports of general interest to biologists throughout the world. Papers are usually of intermediate length (10–40 manuscript pages). A limited number of solicited review papers may be accepted after formal review. A paper will usually appear within four months after its acceptance.

Very short, especially topical papers (less than 9 manuscript pages including tables, figures, and bibliography) will be published in a separate section entitled "Research Notes." A Research Note in *The Biological Bulletin* follows the format of similar notes in *Nature.* It should open with a summary paragraph of 150 to 200 words comprising the introduction and the conclusions. The rest of the text should continue on without subheadings, and there should be no more than 30 references. References should be referred to in the text by number, and listed in the Literature Cited section in the order that they appear in the text. Unlike references in *Nature,* references in the Research Notes section should conform in punctuation and arrangement to the style of recent issues of *The Biological Bulletin.* Materials and Methods should be incorporated into appropriate figure legends. See the article by Lohmann *et al.* (October 1990, Vol. **179:** 214–218) for sample style. A Research Note will usually appear within two months after its acceptance.

The Editorial Board requests that regular manuscripts conform to the requirements set below; those manuscripts that do not conform will be returned to authors for correction before review.

1. ***Manuscripts.*** Manuscripts, including figures, should be submitted in quadruplicate, with the originals clearly marked. (Xerox copies of photographs are not acceptable for review purposes.) The submission letter accompanying the manuscript should include a telephone number, a FAX number, and (if possible) an E-mail address for the corresponding author. The original manuscript must be typed in no smaller than 12 pitch or 10 point, using double spacing (*including* figure legends, footnotes, bibliography, etc.) on one side of 16- or 20-lb. bond paper, 8 by 11 inches. Please, no right justification. Manuscripts should be proofread carefully and errors corrected legibly in black ink. Pages should be numbered consecutively. Margins on all sides should be at least 1 inch (2.5 cm). Manuscripts should conform to the *Council of Biology Editors Style Manual,* 5th Edition (Council of Biology Editors, 1983) and to American spelling. Unusual abbreviations should be kept to a minimum and should be spelled out on first reference as well as defined in a footnote on the title page. Manuscripts should be divided into the following components: Title page, Abstract (of no more than 200 words), Introduction, Materials and Methods, Results, Discussion, Acknowledgments, Literature Cited, Tables, and Figure Legends. In addition, authors should supply a list of words and phrases under which the article should be indexed.

2. ***Title page.*** The title page consists of a condensed title or running head of no more than 35 letters and spaces, the manuscript title, authors' names and appropriate addresses, and footnotes listing present addresses, acknowledgments or contribution numbers, and explanation of unusual abbreviations.

3. ***Figures.*** The dimensions of the printed page, 7 by 9 inches, should be kept in mind in preparing figures for publication. We recommend that figures be about 1 times the linear dimensions of the final printing desired, and that the ratio of the largest to the smallest letter or number and of the thickest to the thinnest line not exceed 1:1.5. Explanatory matter generally should be included in legends, although axes should always be identified on the illustration itself. Figures should be prepared for reproduction as either line cuts or halftones. Figures to be reproduced as line cuts should be unmounted glossy photographic reproductions or drawn in black ink on white paper, good-quality tracing cloth or plastic, or blue-lined coordinate paper. Those to be reproduced as halftones should be mounted on board, with both designating numbers or letters and scale bars affixed directly to the figures. All figures should be numbered in consecutive order, with no distinction between text and plate figures and cited, in order, in the text. The author's name and an arrow indicating orientation should appear on the reverse side of all figures.

Color: The Biological Bulletin will publish color figures and plates, but must bill authors for the actual additional cost of printing in color. The process is expensive, so authors with more than one color image should—consistent with editorial concerns, especially citation of figures in order—combine them into a single plate to reduce the expense. On request, when supplied with a copy of a color illustration, the editorial staff will provide a pre-publication estimate of the printing cost.

4. ***Tables, footnotes, figure legends, etc.*** Authors should follow the style in a recent issue of *The Biological Bulletin* in preparing table headings, figure legends, and the like. Because of the high cost of setting tabular material in type, authors are asked to limit such material as much as possible. Tables, with their headings and footnotes, should be typed on separate sheets, numbered with consecutive Roman numerals, and placed after the Literature Cited. Figure legends should contain enough information to make the figure intelligible separate from the text. Legends should be typed double spaced, with consecutive Arabic numbers, on a separate sheet at the end of the paper. Footnotes should be limited to authors' current addresses, acknowledgments or contribution numbers, and explanation of unusual abbreviations. All such footnotes should appear on the title page. Footnotes are not normally permitted in the body of the text.

5. ***Literature cited.*** In the text, literature should be cited by the Harvard system, with papers by more than two authors cited as Jones *et al.*, 1980. Personal communications and material in preparation or in press should be cited in the text only, with author's initials and institutions, unless the material has been formally accepted and a volume number can be supplied. The list of references following the text should be headed Literature Cited, and must be typed double spaced on separate pages, conforming in punctuation and arrangement to the style of recent issues of *The Biological Bulletin*. Citations should include complete titles and inclusive pagination. Journal abbreviations should normally follow those of the U. S. A. Standards Institute (USASI), as adopted by Biological Abstracts and Chemical Abstracts, with the minor differences set out below. The most generally useful list of biological journal titles is that published each year by Biological Abstracts (biosis List of Serials; the most recent issue). Foreign authors, and others who are accustomed to using The World List of Scientific Periodicals, may find a booklet published by the Biological Council of the U.K. (obtainable from the Institute of Biology, 41 Queen's Gate, London, S.W.7, England, U.K.) useful, since it sets out the World List abbreviations for most biological journals with notes of the USASI abbreviations where these differ. Chemical Abstracts publishes quarterly supplements of additional abbreviations. The following points of reference style for The Biological Bulletin differ from USASI (or modified World List) usage:

A. Journal abbreviations, and book titles, all underlined (for *italics*)

B. All components of abbreviations with initial capitals (not as European usage in World List *e.g., J. Cell. Comp. Physiol.* NOT *J. cell. comp. Physiol.*)

C. *All* abbreviated components must be followed by a period, whole word components *must not* (*i.e., J. Cancer Res.*)

D. Space between all components (*e.g., J. Cell. Comp. Physiol.*, not *J.Cell.Comp.Physiol.*)

E. Unusual words in journal titles should be spelled out in full, rather than employing new abbreviations invented by the author. For example, use *Rit Vísindafjélags Islendinga* without abbreviation.

F. All single word journal titles in full (*e.g., Veliger, Ecology, Brain*).

G. The order of abbreviated components should be the same as the word order of the complete title (*i.e., Proc.* and *Trans.* placed where they appear, not transposed as in some Biological Abstracts listings).

H. A few well-known international journals in their preferred forms rather than World List or USASI usage (*e.g., Nature, Science, Evolution* NOT *Nature, Lond., Science, N.Y.; Evolution, Lancaster, Pa.*)

6. ***Reprints, page proofs, and charges.*** Authors may purchase reprints in lots of 100. Forms for placing reprint orders are sent with page proofs. Reprints normally will be delivered about 2 to 3 months after the issue date. Authors (or delegates for foreign authors) will receive page proofs of articles shortly before publication. They will be charged the current cost of printers' time for corrections to these (other than corrections of printers' or editors' errors). Other than these charges for authors' alterations, *The Biological Bulletin* does not have page charges.

CONTENTS
for Volume 198

No. 1, February 2000

IMAGING AND MICROSCOPY

Zochowski, Michal, Matt Wachowiak, Chun X. Falk, Lawrence B. Cohen, Ying-wan Lam, Srdjan Antic, and Dejan Zecevic
Concepts in Imaging and Microscopy: Imaging membrane potential with voltage-sensitive dyes 1

RESEARCH NOTES

Lambert, Charles C.
Germ-cell warfare in ascidians: sperm from one species can interfere with the fertilization of a second species 22
Tsutsui, Hidekazu, and Yoshitaka Oka
Light-sensitive voltage responses in the neurons of the cerebral ganglion of *Ciona savignyi* (Chordata: Ascidiacea) 26
Bavestrello, Giorgio, Attilio Arillo, Barbara Calcinai, Riccardo Cattaneo-Vietti, Carlo Cerrano, Elda Gaino, Antonella Penna, and Michele Sarà
Parasitic diatoms inside Antarctic sponges 29

PHYSIOLOGY

VandenSpiegel, Didier, Michel Jangoux, and Patrick Flammang
Maintaining the line of defense: regeneration of Cuvierian tubules in the sea cucumber *Holothuria forskali* (Echinodermata, Holothuroidea) 34
Sikes, C. S., A. P. Wheeler, A. Wierzbicki, A. S. Mount, and R. M. Dillaman
Nucleation and growth of calcite on native *versus* pyrolyzed oyster shell folia 50

DEVELOPMENT AND REPRODUCTION

Hadfield, Michael G., Ella A. Meleshkevitch, and Dmitri Y. Boudko
The apical sensory organ of a gastropod veliger is a receptor for settlement cues 67
Ereskovsky, Alexander V.
Reproduction cycles and strategies of the cold-water sponges *Halisarca dujardini* (Demospongiae, Halisarcida), *Myxilla incrustans* and *Iophon piceus* (Demospongiae, Poecilosclerida) from the White Sea. 77

ECOLOGY AND EVOLUTION

Leddy, Holly A., and Amy S. Johnson
Walking *versus* breathing: mechanical differentiation of sea urchin podia corresponds to functional specialization 88
Voight, Janet R., and Anthony Grehan
Egg brooding by deep-sea octopuses in the North Pacific Ocean. 94
Pivkin, Michael V.
Filamentous fungi associated with holothurians from the Sea of Japan, off the Primorye Coast of Russia. . 101

CELL BIOLOGY

Fitt, William K.
Cellular growth of host and symbiont in a cnidarian-zooxanthellar symbiosis. 110

SYSTEMATICS

Scheltema, Amélie H., and Christoffer Schander
Discrimination and phylogeny of solenogaster species through the morphology of hard parts (Mollusca, Aplacophora, Neomeniomorpha) 121

STATISTICS

Dewdney, A. K.
A dynamical model of communities and a new species-abundance distribution. 152

No. 2, April 2000

CHEMICAL COMMUNICATION IN ECOLOGY

Zimmer, Richard K.
Importance of chemical communication in ecology. . . . 167
Zimmer, Richard K., and Cheryl Ann Butman
Chemical signaling processes in the marine environment 168
Weissburg, Marc J.
The fluid dynamical context of chemosensory behavior 188
Vickers, Neil J.
Mechanisms of animal navigation in odor plumes . . . 203
Yen, Jeannette
Life in transition: balancing inertial and viscous forces by planktonic copepods 213
Wolfe, Gordon V.
The chemical defense ecology of marine unicellular plankton: constraints, mechanisms, and impacts . . . 225
Nevitt, Gabrielle A.
Olfactory foraging by Antarctic procellariiform seabirds: life at high Reynolds numbers 245

RESEARCH NOTE

Bentis, Christopher J., Les Kaufman, and Stjepko Golubic
Endolithic fungi in reef-building corals (Order: Scleractinia) are common, cosmopolitan, and potentially pathogenic 254

PARASITOLOGY

Tétreault, Françoise, John H. Himmelman, and Lena Measures
Impact of a castrating trematode, *Neophasis* sp., on the common whelk, *Buccinum undatum*, in the northern Gulf of St. Lawrence 261

PHYSIOLOGY

Clelland, Eric S., and A.S.M. Saleuddin
Vacuolar-type ATPase in the accessory boring organ of *Nucella lamellosa* (Gmelin) (Mollusca: Gastropoda): role in shell penetration 272

ECOLOGY AND EVOLUTION

Seibel, Brad A., Erik V. Thuesen, and James J. Childress
Light-limitation on predator-prey interactions: consequences for metabolism and locomotion of deep-sea cephalopods 284
Hochberg, Rick, and Marianne K. Litvaitis
Phylogeny of Gastrotricha: a morphology-based framework of gastrotrich relationships 299

No. 3, June 2000

NEUROBIOLOGY AND BEHAVIOR

Jackson, D.J., and D.L. Macmillan
Tailflick escape behavior in larval and juvenile lobsters (*Homarus americanus*) and crayfish (*Cherax destructor*) 307
Pires, Anthony, Roger P. Croll, and Michael G. Hadfield
Catecholamines modulate metamorphosis in the opisthobranch gastropod *Phestilla sibogae* 319

PHYSIOLOGY

Williamson, Jane E., Rocky de Nys, Naresh Kumar, David G. Carson, and Peter D. Steinberg
Induction of metamorphosis in the sea urchin *Holopneustes purpurascens* by a metabolite complex from the algal host *Delisea pulchra* 332
Wendt, Dean E.
Energetics of larval swimming and metamorphosis in four species of *Bugula* (Bryozoa). 346
McNamara, John C., and Márcia R. Ribeiro
The calcium dependence of pigment translocation in freshwater shrimp red ovarian chromatophores 357

DEVELOPMENT AND REPRODUCTION

Lauzon, Robert J., Baruch Rinkevich, C.W. Patton, and Irving L. Weissman
A morphological study of nonrandom senescence in a colonial urochordate 367
Selvakumaraswamy, P., and M. Byrne
Vestigial ophiopluteal structures in the lecithotrophic larvae of *Ophionereis schayeri* (Ophiuroidea) . . . 379
Young, Craig M., and Sophie B. George
Larval development of the tropical deep-sea echinoid *Aspidodiadema jacobyi*: phylogenetic implications 387

ECOLOGY AND EVOLUTION

Park, Joong-Ki, and Diarmaid Ó Foighil
Genetic diversity of oceanic island *Lasaea* (Mollusca: Bivalvia) lineages exceeds that of continental populations in the northwestern Atlantic 396

Sherrard, Kristin M.
Cuttlebone morphology limits habitat depth in eleven species of *Sepia* (Cephalopoda: Sepiidae) . . . 404

* * *

Index for Volume 198 415

Reference: *Biol. Bull.* **198:** 307–318. (June 2000)

Tailflick Escape Behavior in Larval and Juvenile Lobsters (*Homarus americanus*) and Crayfish (*Cherax destructor*)

D. J. JACKSON[1,*] AND D. L. MACMILLAN[2]

[1] *Department of Zoology and Entomology, University of Queensland, St. Lucia, Queensland 4072, Australia; and* [2] *Department of Zoology, University of Melbourne, Parkville, Victoria 3052, Australia*

Abstract. We examined the escape behavior of larvae and postlarvae of the American lobster (*Homarus americanus*) and of adult immature (stage ADI) crayfish (*Cherax destructor*). Responses to standardized water jet stimuli delivered through a pipette were observed and analyzed. Lobster larvae did not respond to stimuli within 60 ms, indicating that they do not have functional giant fibers. The first movement by lobster larvae in response to water jet stimuli was a hyperextension of the abdomen. Larval escape responses also showed very little habituation. Postlarval lobsters and ADI crayfish showed the same range of responses as adult animals. Displacement efficiency of tailflicks exhibited by the different animals and stages was examined and related to the morphology of the animals. A separate behavior from tailflicking by larval lobsters in response to water jet stimuli was also observed. Here, the abdomen was hyperextended and the thoracic appendages were promoted. We termed this behavior a "starburst" response. The features of the tailflicking behavior suggest that it evolved to make the larvae difficult prey to handle for small, slower moving predators, and possibly to allow them to ride the bow waves of faster moving predators.

Introduction

Adult lobsters (*Homarus americanus*) and crayfish (*Cherax destructor*) escape from threats by predators and conspecifics by executing rapid, rhythmic flexions and extensions of the abdomen in a behavior commonly called tailflicking. This behavior has been studied over several decades both because of its intrinsic importance to the behavioral ecology of the animal and because of the insights it can provide into the neuroethology of escape (see recent review by Edwards *et al.*, 1999). Crayfish, mainly *Procambarus clarkii,* have been particularly well studied (last reviewed by Wine and Krasne, 1982), but there are also data on some other species such as the Norway lobster (*Nephrops norvegicus:* Newland and Neil, 1990), the hermit crab (*Pagurus pollicarus:* Umbach and Lang, 1981), the American lobster (*H. americanus:* Davis and Davis, 1973; Govind and Lang, 1976; Lang *et al.*, 1977) and the Australian crayfish (*C. destructor:* Cooke, 1985; Cooke and Macmillan, 1985; Davey and Macmillan, 1991).

Because of this extended series of investigations, we know a great deal about tailflicking behavior and its neuronal basis. Three types of escape tailflick have been described: the medial giant (MG) tailflick, the lateral giant (LG) tailflick, and the nongiant (NonG) tailflick. The names refer to the involvement or otherwise of the giant axon, or fiber, systems that run the length of the ventral nerve cord in many malacostracan crustaceans. The medial giant fibers (MGFs) are activated by threatening stimuli to the head and anterior end of the animal. The action potentials generated travel posteriorly, synapsing as they go with sets of neurons that promote the legs and flex all the abdominal segments. The consequence is an MG tailflick in which the body is streamlined and propelled linearly backwards. The lateral giant fibers (LGFs) are excited only by mechanical stimuli to the tail and posterior end of the animal. Action potentials in the LGFs travel anteriorly but do not cause contractions in the last two abdominal segments (*i.e.,* the first two segments through which they pass). Because only the ante-

Received 15 November 1999; accepted 2 February 2000.

*To whom correspondence should be addressed. E-mail: djackson@zoology.uq.edu.au

Abbreviations: ADI, adult immature; LG, lateral giant; LGF, lateral giant fibers; MG, medial giant; MGF, medial giant fibers; NonG, nongiant.

rior abdominal segments contract during an LG tailflick, the animal pitches forwards and upwards so that its trajectory carries it appropriately away from the vicinity of the threat (Mittenthal and Wine, 1973). The giant fibers appear to fire only once during any given escape episode, producing either a single tailflick or the first in a series of tailflicks in which subsequent tailflicks do not involve the giant fibers (Shrameck, 1970; Wine and Krasne, 1972; Cooke, 1985). Tailflicks occurring in the absence of giant fiber activity are called nongiant tailflicks. Because of the large diameter and concomitant fast conduction velocity of the giant axons, there is no time for sensory feedback during tailflicks they trigger. Giant mediated tailflicks are therefore stereotyped, open-loop behaviors. Nongiant tailflicks occur with a number of sensory feedback loops operating, so they can vary in form. They can, for example, somersault an animal back to an upright position following an LG tailflick, move an animal in a curved path away from a threat, or otherwise adjust the orientation of the animal in three-dimensional space. Tailflicking escape behavior habituates rapidly to repeated stimuli, so that adult animals typically fail to produce a response to the fifth stimulus in a sequence of stimuli spaced minutes apart (Krasne and Woodsmall, 1969).

Distinguishing between the three types of tailflick while observing freely behaving animals is not necessarily easy. It is not yet clear how often giant fiber tailflicks are produced during extended periods of intermittent tailflicking such as occur during antagonistic encounters between conspecific males. LG flips are sometimes distinguishable when the characteristic LG body position occurs in the first tailflick in a series of flips. MG and NonG tailflicks are not distinguishable on body position alone. If the exact time at which a tailflick was initiated by the threatening stimulus is known, as in a contrived experimental situation, it is possible to distinguish between giant and nongiant tailflicks on the basis of the latency to the onset of movement. If movement occurs within about 20 ms of the stimulus, the tailflick must necessarily have been generated by giant fiber activation. Nongiant tailflicks appear only after about 60 ms, and usually after considerably longer (150 ms) intervals (Wine and Krasne, 1972).

The general features of escape tailflicking discussed above come from studies of adult animals. But behaviors that have evolved to increase the fitness of adults may not be appropriate for juveniles or larvae, which may face different predators and operate in environments in which the physically and biologically significant features may be spatially and temporally different. Lang *et al.* (1977), for example, found that the threshold for triggering an escape response in juvenile American lobsters slowly increased as the animals grew and as they developed larger claws with which to defend themselves. Accompanying this change was an increasing tendency to move into a defense posture when threatened. Fricke (1984, 1986) described neurophysiological changes accompanying these behavioral ones. Morphological changes during development are a particularly important consideration in an animal like *H. americanus* in which the first three stages are larval and pelagic. Not only are the body proportions different than in later stages, but they swim in an entirely different manner, using the exopodites of the walking legs rather than the pleopods of the abdomen as small juveniles do (Herrick, 1909). These exopodites are lost on the molt from the larval stage III to the first postlarval stage IV. In contrast, *C. destructor* undergoes direct development. It has no larval stages, and the young have the same body shape as the adult, albeit with different body proportions. In both species, the larvae and juveniles are small, have different body proportions and locomotory patterns and potentially different predators, so one would expect the evolution of different escape behavior patterns from those exhibited by the adult.

There is an extensive literature on the large-scale movements of planktonic animals associated with their vertical migration, aggregation, dispersal, and settlement, but recent studies have highlighted the importance of small-scale behavioral responses to their fitness and survival (Keough and Downes, 1982; Haury and Yamazaki, 1995; Lenz *et al.*, 1996). Here we report on the escape swimming and tailflicking behavior of the three larval and first postlarval stages of the lobster, *H. americanus,* and of the posthatching stage of the Australian crayfish, *C. destructor,* which is similar in size to the larval stages of *H. americanus.* The investigation was designed particularly to permit observations on the behavior of larval and juvenile animals to be compared with the larger literature on adult behavior to identify differences likely to reflect the different evolutionary selection pressures.

Materials and Methods

Animals

Larvae of the American lobster, *Homarus americanus,* were obtained from the lobster rearing facility at the New England Aquarium, Boston, Massachusetts; held in fresh aerated seawater at 8°C at the Marine Biological Laboratory, Woods Hole, Massachusetts; and fed *Artemia* twice a day. Holding aquaria were cleaned every second day. Work on the Australian crayfish, *Cherax destructor,* was conducted at the Zoology Department, University of Melbourne, Australia. Adult animals were obtained from a local supplier, held in large aquaria maintained at 15°–17°C, and fed dry prawnfood pellets weekly. Gravid females were isolated in 5-l buckets and the first motile and independent stage, ADI (adult immature following the nomenclature of Sandeman and Sandeman [1991]), was collected for experimentation.

Experimental cells and water jet

The behavior of the animals was filmed in individual acrylic plastic cells 40 mm wide × 40 mm long × 20 mm deep for larval and stage IV *H. americanus*, and 60 mm wide × 60 mm long × 15 mm deep for ADI *C. destructor*. Transparent walls allowed the video camera to be mounted looking vertically down or horizontally across the cell. For latency and habituation experiments, the animals were stimulated with a water jet delivered through a Pasteur pipette drawn to a fine tip (Schmitz, 1992). The pipette was connected to an elevated water reservoir by a silicon tube with a solenoid valve in the line. The duration of the jet (40 ms) was adjusted by controlling the solenoid with an electronic stimulator. The possibility of visual stimulation was reduced by using a fine clear pipette. Animals did not respond to its slow approach or proximity in the absence of a water jet. The amplitude of the water jet was controlled by adjusting the height of the water reservoir above the test cell. Three heights were used, which we termed low (50-cm elevation), intermediate (100-cm elevation), and high (200-cm elevation). These three heights produced water jets with velocities of 0.78 ± 0.037 mm/ms, 1.11 ± 0.007 mm/ms, and 1.48 ± 0.038 mm/ms (mean ± one standard deviation) respectively. The velocity, shape, and other characteristics of the water jet were characterized and calibrated by placing rhodamine dye in the reservoir and filming 10 jets.

Video filming

Videotapes were recorded with a Sony Hi8 video camera and played back on a high-resolution video recorder with single frame advance (Panasonic AG 6730). The camera had a set frame speed of 50/s (*i.e.*, a 20-ms sample rate) and an adjustable shutter speed that could range from 1/1000 s to 1/50 s (allowing each frame to be exposed for 1 to 20 ms). Slow shutter speeds (1/50 s) were used for determining the frame in which rapid movement first occurred because a blurred image was produced. Faster shutter speeds (1/1000 s) were used when sharp images were required or when it was important to determine how much movement had occurred between frames; for example, when viewing the dye front in water jet calibrations. White graph paper with 1-mm ruled squares was placed behind or beneath the cell during filming so that the animal's trajectory and speed of movement could be measured directly from the video image on a flat-screen monitor. Only tailflicks that took place in the plane perpendicular to the video camera were analyzed, and were easily identified. The behavioral recordings were played back frame by frame, and individual frames were selected for measurement, drawing, or other analyses. To measure the distance traveled by a tailflick, tracings of the animal's body were taken from the flat screen monitor relative to a selected point on the gridline background. The eye was chosen as a reference point on the animal for calculation of the linear distance traveled. However, the limitation of this method when calculating the distance traveled by LG tailflicks must be recognized, as the rotational component of this tailflick is not taken into account.

A light-emitting diode (LED) was placed in the field of view and connected to the delayed pulse output of the stimulator. By delaying the LED flash for a short interval after the signal that opened the solenoid valve, and placing rhodamine dye in the stream during calibration trials, we were able to synchronize the LED flash with the emergence of the clear stimulus stream from the end of the pipette during experiments. The only requirement for the accuracy of this method was that the distance between the tip of the pipette and the animal be constant at the moment the stimulus was triggered. This was standardized with the animal relative to the gridline background and checked on the video record; samples in which this condition was violated were discarded. Accuracy became less of a problem as we became experienced at manipulating the animals and the pipette.

Histology

Animals were fixed in Bouin's fixative, embedded in wax, sectioned at 7 μm, and stained with Mallory's triple stain for viewing on a light microscope equipped for microphotography.

Morphological measurements

Abdominal measurements were taken by pinning fixed animals out on an agar plate, and measuring dimensions through a graticule in a 10× eyepiece mounted on a dissecting microscope. Abdominal lengths were taken from the tip of the telson (including the setae for stages III and IV *H. americanus* and ADI *C. destructor*) to the anterior edge of the first abdominal segment.

Results

Time interval between stimulus and movement and form of the movements

Images of body position over time during tailflick responses by larvae and stage IV postlarvae of *Homarus americanus* showed that larval responses to our water jet stimulus differed in many ways from those of stage IV juveniles (Fig. 1). First, and most noticeably, the latency between the stimulus and the first tailflick movement was different. Latency data were compared by one-way ANOVA, followed by a Student-Newman-Keuls test for multiple contrasts. The earliest sign of movement in response to the water jet was never seen before 60 ms in the three larval stages, and was usually much later and very variable (mean 139 ± 116 ms) (Table 1). There was no

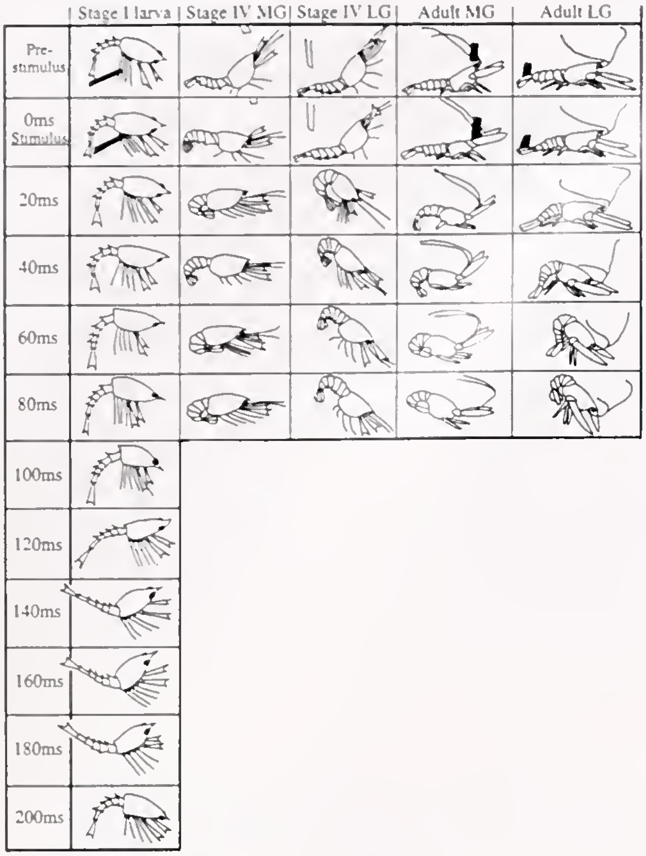

Figure 1. Comparisons of latency to response and initial escape movements by *Homarus americanus* at three stages of development: stage I larva, stage IV postlarva, and adult. The larval escape response is the same irrespective of stimulus direction and larval stage, so a representative stage I response is shown. Although stage IV animals are able to respond to anterior and posterior stimulation with medial giant fiber (MG) and lateral giant fiber (LG) tailflicks as shown here, most responses observed during this study were of nongiant fiber origin. None of the three larval stages displayed tailflicks that could be attributed to giant fiber activity. The blocked stimulus used on the stage I larva and the adult animals represents a mounted pin and a metal rod respectively. The clear stimulus used on the stage IV postlarva represents a water jet stimulus. Note the comparative speed with which stage IV animals are able to complete MG and LG flicks compared to the adult. This is due to the relatively shorter distance the giant fiber action potential travels in smaller animals.

difference in escape latency among the three larval stages ($P > 0.3$). Because of this absence of responses faster than 20 ms, we concluded that the three larval stages of *H. americanus* do not possess functional giant fiber tailflicks. In contrast, stage IV juveniles exhibited two classes of escape flip that started within 20 ms. The speed of these responses is comparable with the values for giant fiber tailflicks in the literature (see Wine and Krasne, 1972) and with our own brief measurements of adult *H. americanus* (data not shown). Furthermore, the MGF and LGF tailflick body movements were clearly distinguishable when the stimulus was applied to the anterior and posterior ends of the animal respectively (Fig. 1), and they were characteristic of the trajectories produced by MG and LG tailflicks (Wine, 1984). From these results we concluded that stage IV *H. americanus* has functional giant fiber tailflicks. Giant fiber flicks by stage IV *H. americanus* had tailflick latencies significantly faster ($P < 0.0001$) than those of the larval stages. Stage IV juveniles did not, however, usually respond to the water jet stimulus with a giant-fiber-mediated tailflick, and another class of responses with longer latencies indicated that they could also produce NonG tailflicks (Table 1). On average, these NonG tailflicks had a latency significantly longer than the mean latency of each of the larval stages ($P < 0.0001$).

Another striking difference between the responses of the larval stages and stage IV animals was that the first movement seen following the long response time was invariably an extension of the abdomen rather than a flexion (Fig. 1). We termed this movement a hyperextension because the abdomen was curved back dorsally, apparently as far as the segmental joints would allow. In all three larval stages, abdominal hyperextension prior to a tailflick was far greater than any degree of extension achieved by stage IV postlarvae. Furthermore, once maximum hyperextension had been reached, this position was held for an average of 127 ± 7 ms before flexion, and therefore displacement, began. If a larva made a second flick, that also was usually preceded by a hyperextension. If there were subsequent tailflicks, abdominal extension resembled that of postlarvae and did not involve a hyperextension. All three larval stages showed this behavior.

ADI *Cherax destructor* produced tailflicks in which movement was well under way in less than 20 ms. As in stage IV *H. americanus*, these tailflicks were concluded to be of giant fiber origin due to their short latency and characteristic trajectories. ADI *C. destructor* also produced

Table 1

Escape latencies to water jet stimulus by Homarus americanus *and* Cherax destructor

Species	Stage	Class of tailflick	n	Mean latency in ms (mean ± SD)
H. americanus	I	Nongiant	346	145 ± 101
H. americanus	II	Nongiant	282	135 ± 132
H. americanus	III	Nongiant	341	137 ± 115
H. americanus	IV	Giant	13	≤20
H. americanus	IV	Nongiant	278	195 ± 147
C. destructor	ADI	Giant	592	≤20
C. destructor	ADI	Nongiant	70	51 ± 14

Flicks that commenced within 20 ms were attributed to giant fiber activation, and an estimate of standard deviation of their latency was not possible due to the constraints of the camera. Flicks of a longer latency were attributed to nongiant fiber activation. n is the total number of responses observed for each class of tailflick by 6 animals of each species and stage.

NonG tailflicks with latencies of 60 ms or more. On average, ADI NonG tailflicks had latencies significantly shorter than *H. americanus* larvae and stage IV NonG tailflicks ($P < 0.001$). The latency and types of responses exhibited by ADI animals in response to water jet or mechanical stimuli were similar to those of adult animals (Fig. 2). Giant fiber tailflicks were also elicited far more regularly than in stage IV *H. americanus:* 89.4% of *C. destructor* tailflicks were due to giant fiber activation, but only 5.4% of *H. americanus* tailflicks were of a latency short enough to be attributed to giant fiber activity.

Table 2

Summary table of distance travelled on the first flick by Homarus americanus *stages I, II, III, and IV and* Cherax destructor *ADI*

Species	Stage	Class of flick	*n*	Distance travelled in ms (mean ± SD)
H. americanus	I	Nongiant	14	2.45 ± 1.00
H. americanus	II	Nongiant	17	2.60 ± 1.44
H. americanus	III	Nongiant	17	5.55 ± 1.77
H. americanus	IV	Medial giant	13	15.04 ± 3.64
H. americanus	IV	Lateral giant	3	6.37 ± 7.70
C. destructor	ADI	Medial giant	10	16.03 ± 2.32
C. destructor	ADI	Lateral giant	10	5.88 ± 2.14

n is the number of tailflicks measured.

Trajectories and distances traveled following the different types of tailflicks

Unlike the MG and LG tailflicks of stage IV *H. americanus* and ADI *C. destructor,* the direction of an incoming stimulus or the location of first contact with the body did not appear to determine the trajectory of the path followed by the larvae of *H. americanus* during tailflick sequences; tailflicks appeared to be made in random directions. Statistical tests on the distance-traveled data were made by one-way ANOVA, followed by Student-Newman-Keuls tests for multiple comparisons. The first tailflick by stage I and II larvae moved them a very short distance (Table 2). Stage III larvae traveled significantly farther than stages I and II ($P < 0.05$), and MG-mediated tailflicks in stage IV animals were significantly greater than stage III tailflicks ($P = 0.001$). These MG flips were also directional, as described in the preceding section. LG flicks did not carry stage IV animals very far on the first flick because the rotational component pitches the animal upward and forward away from the posterior threat. The results for the first tailflick by ADI *C. destructor* were comparable with those of stage IV *H. americanus* (Table 2).

We also examined the distance traveled during the first and second tailflicks in sequences of multiple tailflicks. All larval stages of *H. americanus* traveled farther on the second tailflick, whereas stage IV postlarvae traveled farther following the first (MG) tailflick (Fig. 3). Due to the rotational component of an LG flick, stage IV *H. americanus* and ADI *C. destructor* traveled farther on the second NonG flip. None of the recorded MG flips by *C. destructor* were followed by subsequent tailflicks (Fig. 3). On average, ADI *C. destructor* were able to travel 6.5 times farther than stage I *H. americanus* on the first MG flick (Table 2). Stage IV *H. americanus* MG and LG flicks did not differ significantly from ADI *C. destructor* MG or LG flicks respectively in terms of distance traveled.

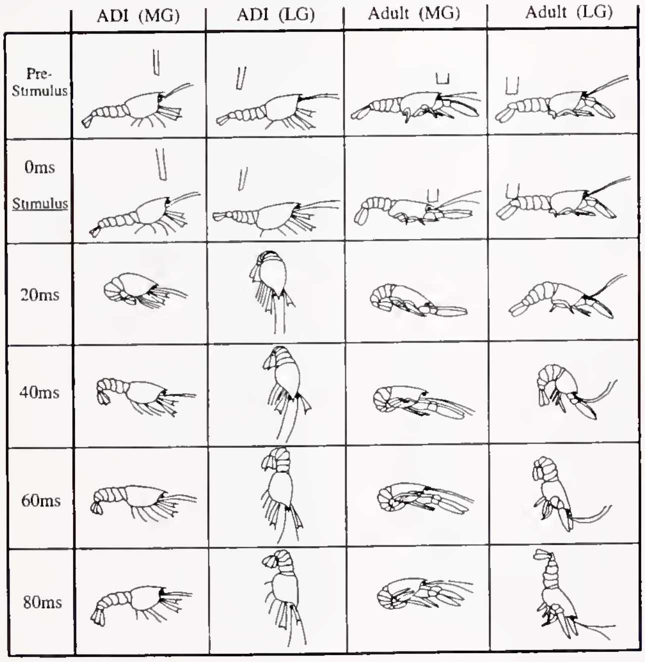

Figure 2. Comparisons of latency to response and initial escape movements by *Cherax destructor* at two stages of development: ADI and adult. ADI animals respond to anterior and posterior stimulation with essentially the same form of response shown to be due to medial giant fiber (MG) and lateral giant fiber (LG) activity in adult animals. Posterior and anterior stimulation were applied with a water jet to an ADI animal, and with a metal rod to an adult. Note the comparative speed with which ADI animals are able to complete MG and LG flicks compared to the adult. This is due to the shorter distance the giant fiber action potential travels in smaller animals.

Morphology of the tailfan and abdomen

We looked for reasons for the significant difference between the distance traveled by stage III larvae compared to stages I and II. The addition of setae and uropods at stage III (Fig. 4) would seem to allow stage III animals to generate more thrust during a tailflick, and the increase in abdominal size (and therefore muscle mass) would presumably allow these animals to generate the force required to drive the proportionally larger tailfan. Stage IV postlarvae have larger tailfans than stage III larvae (Fig. 4); the paddle-like

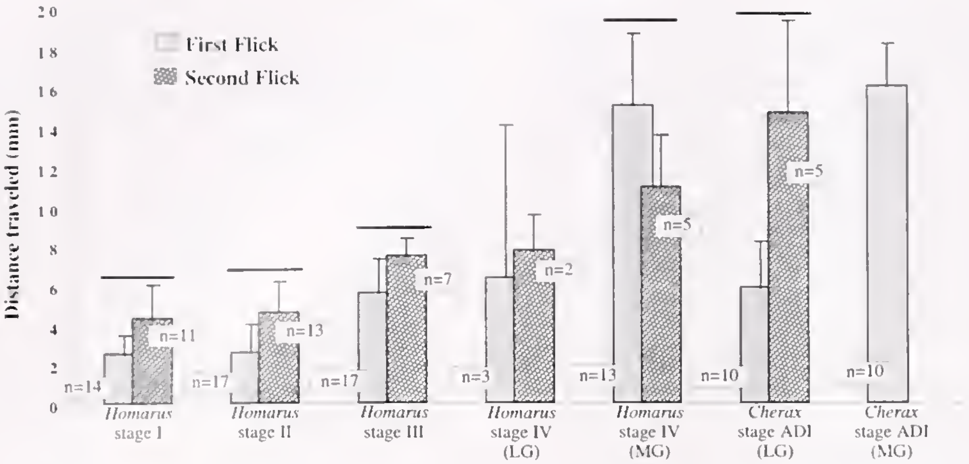

Figure 3. Distance traveled on the first two consecutive tailflicks following stimulation by *Homarus americanus* (stages I to IV) and *Cherax destructor* (ADI). Larvae and stage IV of *H. americanus* were stimulated with a mounted needle; *C. destructor* was stimulated with a water jet. Medial giant (MG) and Lateral giant (LG) flips were elicited in stage IV *H. americanus* and *C. destructor* by stimulating anteriorly and posteriorly respectively. Distances that differ significantly ($P < 0.05$) between the first and second flip are topped by a horizontal bar. Error bars are standard deviations of the mean. Data were tested for differences between the first and second flick within each stage by a two-tailed *t* test.

exopodites that are used by the larval stages to remain in the water column presumably increase drag during tailflicking.

A one-way ANOVA followed by a Student-Newman-Keuls test for multiple comparisons was used to test for differences between abdominal lengths; abdominal length is presumably a gross reflection of the muscle mass available for flexion. Interestingly, the abdominal length of stage I larvae of *H. americanus* does not differ significantly from that of ADI *C. destructor* ($P = 0.064$), although the latter are able to travel 6.5 times farther on the first tailflick (Fig. 3). In larvae of Stages II, III, and IV, the abdomens are significantly longer than in stage I ($P < 0.0001$; Table 3, Fig. 5).

Histology of the giant fibers

Transverse sections of the ventral nerve cord of the mid-abdomen of *H. americanus* larvae showed clear evi-

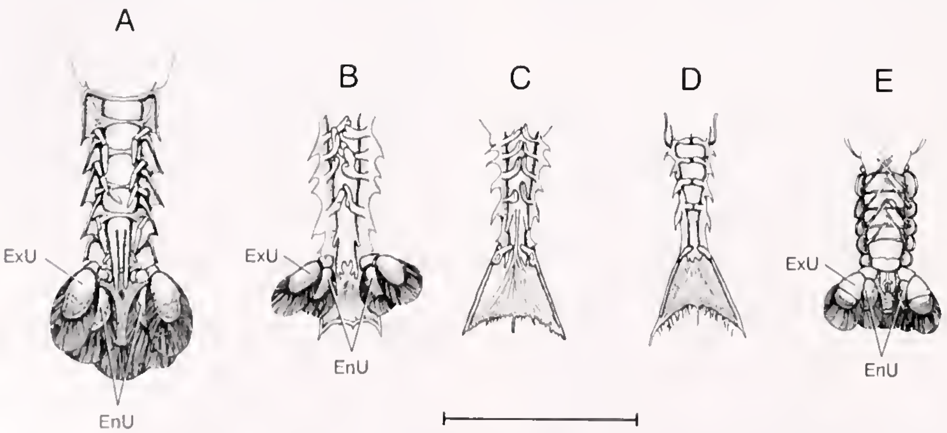

Figure 4. Ventral abdominal view of *Homarus americanus* stages IV, III, II, and I (A–D respectively) and *Cherax destructor* ADI (E). Note the increase in size that accompanies each successive molt in *H. americanus*, and that it is in stage III larvae that the endopodite (EnU) and exopodite (ExU) of the uropod first appear. These appendages make tailflicks more efficient and propel the animal a significantly greater distance than stage I or II larvae. Note the difference in size between *H. americanus* stage IV abdomens and *C. destructor* abdomens. *C. destructor* are able to travel the same distance as stage IV postlarvae, and over 6 times farther than stage I *H. americanus*. The setae of the pleopods in stage IV *H. americanus* and *C. destructor* have been omitted for clarity of presentation. Scale bar = 5 mm.

Table 3

Tailfan and abdominal dimensions for Homarus americanus *and* Cherax destructor

Species	Stage	*n*	Tailfan width in mm (mean ± SD)	Abdomen length in mm (mean ± SD)
H. americanus	I	13	2.24 ± 0.13	4.16 ± 0.28
H. americanus	II	13	2.36 ± 0.07	4.89 ± 0.21
H. americanus	III	5	2.48 ± 0.33	6.80 ± 0.80
H. americanus	IV	7	3.85 ± 0.35	6.81 ± 0.40
C. destructor	ADI	9	2.83 ± 0.19	4.36 ± 0.13

Tailfan widths for *H. americanus* stages III and IV and *C. destructor* ADI include uropods and setae, and abdominal lengths were taken from the tip of the telson (including the setae for stages III and IV *H. americanus* and ADI *C. destructor*) to the anterior edge of the first abdominal segment.

dence of the MG fiber in all three stages. No large-diameter axon was detected in the lateral region where the LG fiber is found in the adult (Fig. 6A); more than ten thousand sections were examined, from 6 stage I animals, 5 stage II animals, 6 stage III animals, and 3 stage IV animals. Unfortunately, the sections of stage IV *H. americanus* were not of a high enough quality to draw any conclusions. Both MG and LG fibers were clearly present in most of the sections taken from the same region in ADI *C. destructor* (Fig. 6B).

Habituation of tailflick responses

To investigate the habituation of the tailflick escape response in larval and postlarval *H. americanus* and juvenile *C. destructor*, we presented animals with a water jet stimulus at 1-min intervals and counted the number of tailflicks in response to each stimulus. Fricke (1984) also successfully employed a water jet stimulus to measure the rate of habituation in another species of crayfish, *Procambarus clarkii.* Although many other researchers use tactile stimuli to elicit tailflicks in crayfish (Krasne and Woodsmall, 1969; Wine and Krasne, 1969; Wine *et al.*, 1975), Wine and Krasne (1972) emphasize that the suddenness of onset of a stimulus is most important. We found that all animals continued to tailflick for 60 min in response to stimuli of the strengths used in these experiments. Because stimulus intensity can affect the rate of habituation, we examined the effect of water jets of three velocities. Groups of six replicate animals from each developmental stage were presented with one of three stimulus amplitudes at 1-min intervals for 20 min. Three animals from each group were stimulated a further 40 times. Animals were not reused in any experiments. Using repeated measures ANOVA over 20 stimuli, we found no difference between stages I to IV in the number of tailflicks executed over time (Table 4). However, there was a significant interaction between stimulus intensity and stimulus number, such that stronger stimuli initially evoked more tailflicks (Table 3 and Fig. 7). We fitted logarithmic curves to the data obtained for the three amplitudes of stimulation (Fig. 7) and found evidence for a slight initial habituation over time that eventually reaches a plateau so that animals continue to respond with multiple tailflicks even after 60 stimuli. Although stage IV animals did not differ from the three larval stages in the number of responses over time, the variability between the number of responses and stimulus number (as measured by the r^2 value) decreases with developmental stage (Fig. 8A–D). The trend towards habituation is also more obvious.

Unlike *H. americanus*, ADI *C. destructor* did not show

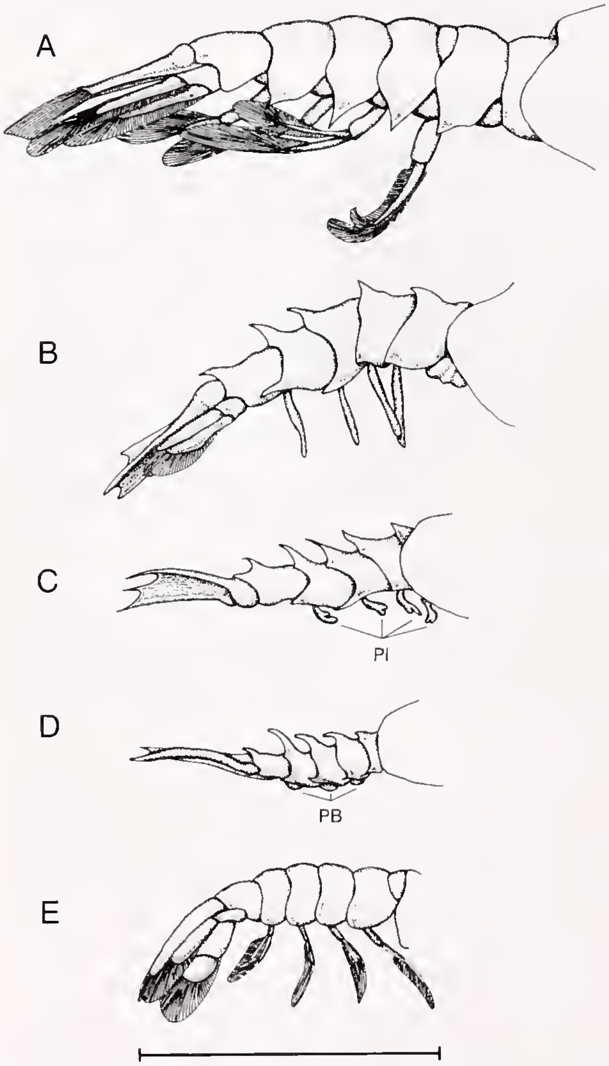

Figure 5. Lateral abdominal view of *Homarus americanus* stages IV, III, II, and I (A–D respectively) and *Cherax destructor* ADI (E). Note the increase in size that accompanies each successive molt in *H. americanus*. Pleopod buds (PB) are visible in stage I larvae and first appear as pleopods (Pl) in stage II larvae, but are not used for swimming until stage IV. *C. destructor* hatches with functional pleopods and the full complement of adult appendages. Note the dorsal spines of the pleurites in the larval stages of *H. americanus* and that these spines are totally absent in stage IV animals and ADI *C. destructor*. Scale bar = 5 mm.

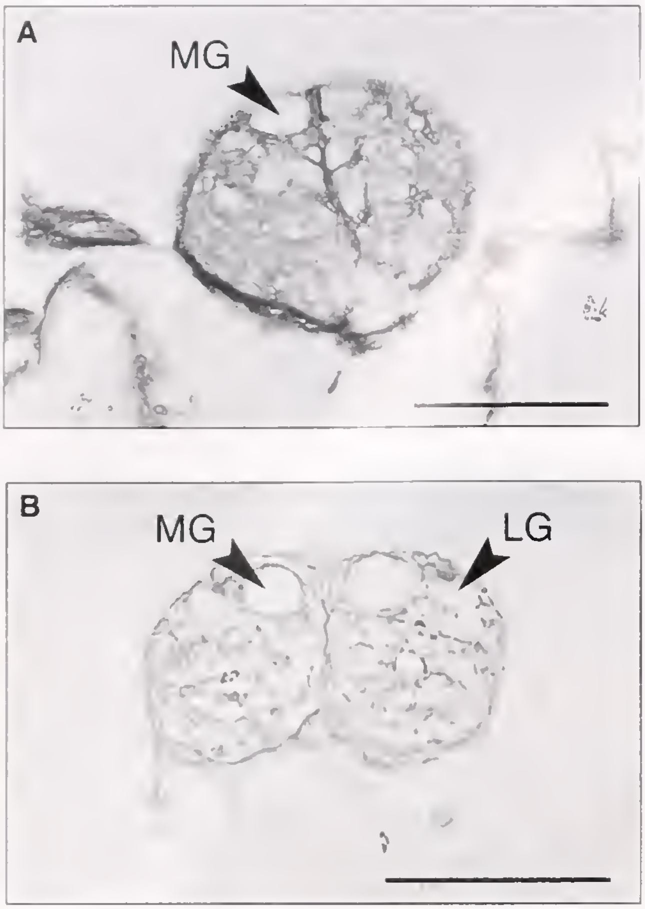

Figure 6. Sections (7 μm) of ventral nerve cords taken mid-abdomen, fixed in Bouin's fixative, and stained with Mallory's triple stain. Scale bar = 50 μm. (A) Sections taken from *Homarus americanus* larvae were the same irrespective of larval stage, so a representative stage II section is shown. Note the prominent medial giant (MG) fibers and the absence of lateral giant (LG) fibers. (B) Section of *Cherax destructor* ADI ventral nerve cord clearly showing the medial (MG) and lateral giant (LG) fibers.

any difference in the number of tailflicks over time to the three stimulus intensities used (Table 4B). ADI animals would typically respond with the same number of tailflicks on the 60th stimulus as on the first. This is reflected in the relatively low r^2 value (Fig. 8E).

Other observations

H. americanus larvae did not always respond to the water jet with tailflicks. Occasionally a different response was observed in which the abdomen was hyperextended (as in the hyperextension preceding a tailflick described above), the thorax was rolled dorsally, and the chelipeds and pereiopods thrust laterally. This position was often maintained for as long as [illegible] before a slow retraction of the abdomen, thorax, and lateral appendages. We termed this combination of hyperextension and lateral extension of the appendages "starburst" behavior. Starburst responses were not observed as often as tailflicks, but they occurred frequently enough to be of interest. Of the three possible responses (tailflick, starburst, or no response), starburst behavior occurred 13%, 21%, and 8% of the time for stage I, II, and III larvae respectively. Stage IV postlarvae and ADI *C. destructor* did not exhibit starburst behavior.

The LG tailflicks evoked by posterior stimulation of ADI *C. destructor* were often followed by a sequence of NonG tailflicks that carried the animal upward away from the bottom of the experimental tank. The animal would then sink slowly with its appendages extended. In larger holding aquaria, where objects such as PVC piping and rubble was present, the sinking trajectory appeared to be monitored by the animal to allow it to land on such objects. If the sinking trajectory needed adjustment to allow this to occur, the animal would initiate another tailflicking sequence (presumably NonG, although we have no way of knowing this) to bring it over the apparently desired landing site. When stimulated anteriorly, ADI animals produced MG flips that carried them in a flat trajectory backward and almost always occurred without further NonG flips.

Discussion

The tailflicking behavior of the larvae of *Homarus americanus* differs in a number of ways from that of juvenile and adult animals. Some of the differences revealed by our study are likely to reflect the different environments in which the animals live. One of the most interesting findings is that the larval stages do not exhibit giant fiber tailflick responses even though they have large medial giant fibers. This, coupled with the fact that the trajectory is not predicted by the location of the stimulus, suggests that tailflicking behavior in *H. americanus* larvae may advantage the animals in ways other than those normally associated with the behavior in adult animals. Our results suggest some possibilities. The hyperextension may be an important clue. The larvae remain in the water column and move slowly by beating the external rami, exopodites, of their biramous limbs (Ennis, 1995). The exopodites are paddle-like, with a fringe of setae (Herrick, 1909), and while this is an efficient arrangement for slow swimming (Laverack *et al.*, 1976; Macmillan *et al.*, 1976; Neil *et al.*, 1976), it is likely to

Table 4

Repeated measures ANOVA performed on Homarus americanus *and* Cherax destructor *habituation data*

Species	Interaction	Mean-square	*F*-ratio	*P* value
H. americanus	Stimulus × stage	40.39	1.53	0.217
H. americanus	Stimulus × intensity	120.38	4.57	0.015
C. destructor	Stimulus × intensity	0.70	1.155	0.333

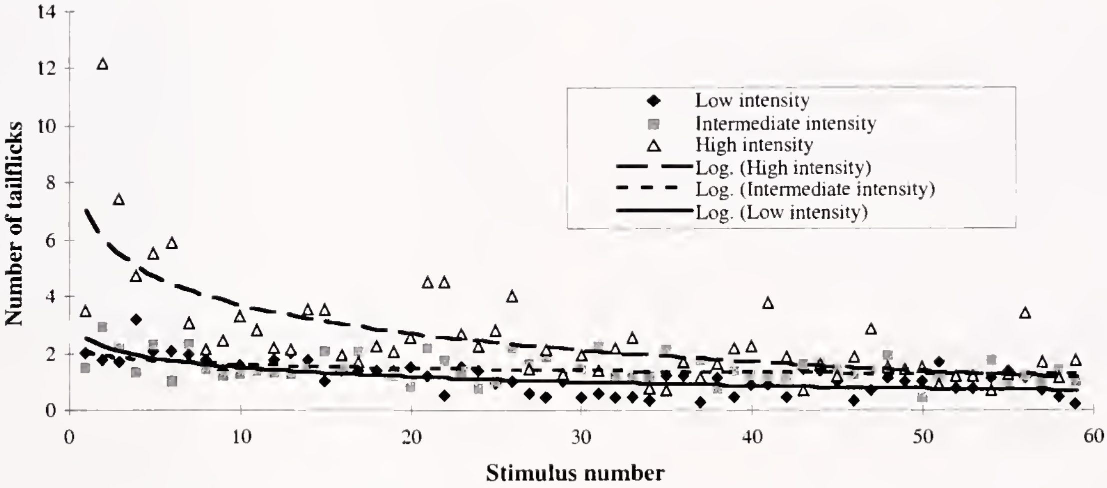

Figure 7. Mean number of tailflicks made by *Homarus americanus* in response to three stimulus intensities. The responses from stages I to IV were pooled for each stimulus intensity. A total of 21 animals (at least 5 from each stage) were stimulated at each intensity 20 times at 1-min intervals, and of these 11 (3 from stages I, II, and IV and 2 from stage III) were stimulated a further 40 times at 1-min intervals. A repeated measures ANOVA revealed that significantly more tailflicks are made in response to the high stimulus intensity for the first 20 min. Logarithmic curves were fitted by Excel 5.0.

increase viscous drag during tailflicking behavior. Drag is a significant issue in adult responses because animals reduce it by actively streamlining the legs during MG tailflicks (Cooke and Macmillan, 1985). The larval stages of *H. americanus* are unlikely to actively streamline the exopodites because the innervation and control of the limbs appears to be rudimentary (Hill and Govind, 1984; Macmillan, 1997). The hyperextension, a movement exhibited only by the larval stages, preceding the first tailflick may have evolved to overcome the drag created by the setae-laden exopodites, appendages specific to the larval stages; an initial tailflick of greater force may serve to passively streamline the exopodites and increase the displacement achieved by subsequent tailflicks. This hypothesis is supported by our finding that all of the larval stages travel significantly farther as a result of the second tailflick, whereas the first MG flick of stage IV animals, which lack exopodites, carries them significantly farther than the second flick. The comparison between ADI *C. destructor* and the larval stages also supports this hypothesis. ADI animals lack exopodites, have abdominal lengths similar to stage I larvae and significantly shorter than larval stages II and III, yet are able to travel farther (2.8–6.5 times) on the first tailflick. However, these comparisons of the tailflicking distance traveled by ADI *C. destructor,* stage IV *H. americanus,* and the larval stages must be made with the knowledge that these tailflick behaviors have different underlying neural mechanisms.

Because the hyperextended position is held for such a long time preceding flexion (127 ± 7 ms), therefore delaying displacement, the putative advantage it confers to streamlining the exopodites comes at a cost to a budget of total tailflicking time. Hydrodynamic factors are dominant features of the planktonic environment. Some feeding fish generate a bow wave that can carry material momentarily away from their bodies, the rate of water flow being dependent on the speed of approach (Lauder and Clark, 1984). Lobster larvae have been found in a number of fish and diving birds that would certainly produce a bow wave (Ennis, 1995). An initial sail-like hyperextension held by a larva for extended periods in response to an appropriate stimulus might increase the probability that the animal would be carried off in the bow wave of larger predators, thus conferring a selective advantage. Subsequent nondirectional NonG tailflicks could then help to keep the animal within any locally moving body of water, and would increase the handling time (in this case the time spent pursuing an individual larva) for visual predators.

In *H. americanus,* stage IV is considered to be the stage at which a benthic life is adopted. However, stage IV postlarvae are excellent swimmers and are found in the water column. The evidence concerning the proportion of time they spend in the water column as opposed to associated with the bottom is fragmentary (Ennis, 1995). One might have predicted that this transitional stage would exhibit some sort of transitional behavior; planktonic animals are faced with threats that can come from any direction in the surrounding sphere of water, whereas benthic ones deal largely with threats in the upper hemisphere, for which adult tailflicking is clearly appropriate. It is therefore interesting that stage IV has essentially adult escape behavior, albeit with different thresholds for activation (Lang *et al.,* 1977). ADI crayfish, in our holding tanks, spend more time on the bottom or on protruding objects than swimming. In this

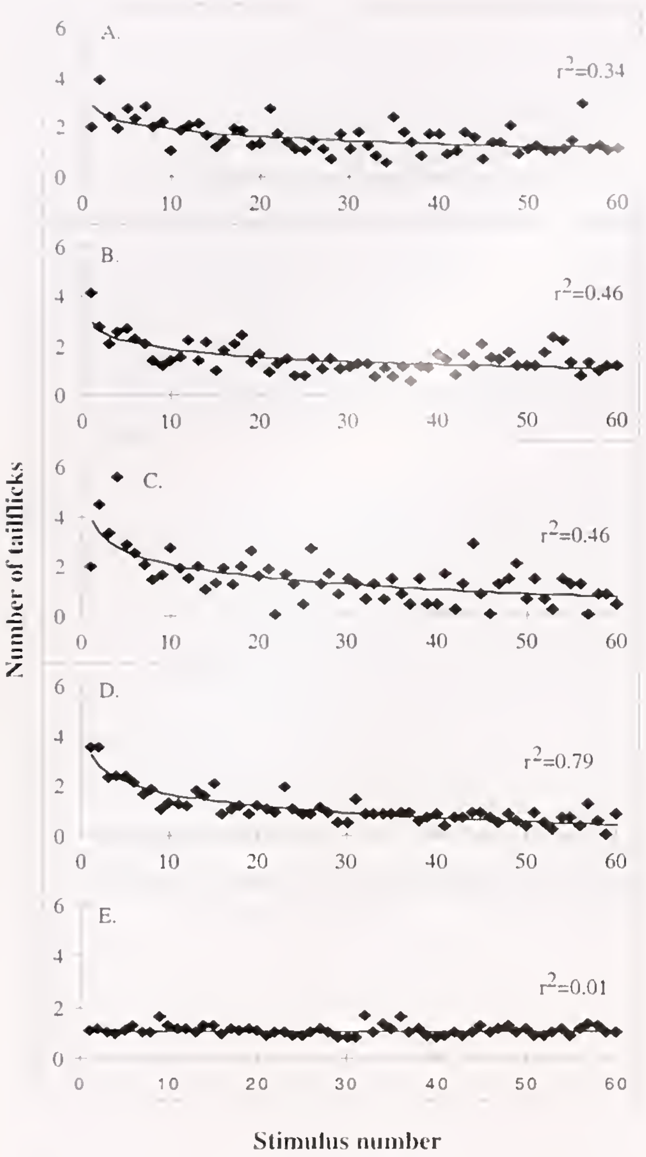

Figure 8. (A–D) Habituation of *Homarus americanus* stages I–IV to repeated stimulation at 1-min intervals. Three stimulus intensities were used and the results pooled for each developmental stage. Groups of six animals were stimulated 20 times at each stimulus intensity, and three animals from each group were stimulated a further 40 times. Although there is no significant difference between the four stages of *H. americanus*, the trend towards faster and more predictable habituation is clear through the increase in r^2 values with developmental stage. This trend suggests that the rate of habituation increases and becomes more predictable as animals grow. Fitted curves are logarithmic. (E) Habituation of *Cherax destructor* (ADI) to repeated stimulation at 1-min intervals. Three stimulus intensities were used and the results pooled. Groups of six animals were stimulated 20 times at each stimulus intensity, and three animals from each group were stimulated a further 40 times. The relatively low r^2 value indicates that there is no trend over time that differs significantly from the overall average number of tailflicks, *i.e.*, the mean number of tailflicks is as good a description of the data as the fitted logarithmic curve.

respect, our results suggest that both stage IV lobster postlarvae and ADI crayfish are more benthic than pelagic, but a more finely grained comparison with later stages might reveal subtle differences in these early developmental stages.

Our water jet stimulus did not always elicit a starburst response, but it did so with sufficient frequency that this response probably plays some part in the survival of the animals. Phillips and Olsen (1975) described a similar behavior in response to a touch stimulus by the pelagic puerulus larva of the Western rock lobster (*Panulirus longipes*) in which the animal "spreads its antennae to an angle of approximately 60° and the legs, abdomen and tailfan are also extended, while the animal remains motionless." Zoea larvae of the estuarine crab *Rhithropanopeus harrisii* also flare their antennal spines and flex their abdomens back over their carapace in response to a threatening stimulus (Morgan, 1987). Morgan showed, furthermore, that removal of the spines on zoea increases the probability that they will be eaten by small fish with a gape about the size of the larvae. We hypothesize that *H. americanus* larvae adopt the starburst posture as an antipredatory device, a theory supported by the observation that the numerous spines sculptured into the exoskeleton of the larval stages have been lost in stage IV animals, which do not exhibit the starburst behavior (Fig. 4).

These aspects of the tailflicking behavior of *H. americanus* larvae contrast sharply with those of stage IV lobsters and ADI crayfish. Both of these stages have essentially the same body form as their adult, although the proportions can be very different (Lang *et al.*, 1977) and, like the adult, they can execute a short-latency, directional response to threatening stimuli approaching anteriorly or posteriorly.

Our investigation into habituation is preliminary. From the extensive literature on habituation of tailflicking in crustaceans, we selected only a few aspects that one might expect to be different because of the differing ecology of the larvae and adults. Our data confirm earlier results (Lang *et al.*, 1977; Fricke, 1984, 1986) suggesting that habituation is an aspect of escape behavior in which one might expect to find subtle differences that have profound effects on the selective advantage to the animal. The larval and first postlarval stage of the lobster and the ADI of the crayfish will continue to tailflick to our threatening stimuli indefinitely. There are two possible explanations for this lack of habituation: there is no refuge in the plankton, and defensive behaviors are not likely to be effective against the types of predators that these animals face. The obvious conclusion from the results of the habituation experiment is that these animals cannot afford to habituate to this type of stimulus in the wild. Our results also predict that as later stages become equipped with larger chelipeds, the rate of habituation will gradually increase. This hypothesis is consistent with the work of Lang *et al.* (1977), who showed that smaller animals are more likely to employ escape behavior than larger animals, who are more likely to defend themselves.

The lack of GF tailflicks in the larval stages of *H. ameri-*

canus, despite the presence of large MG fibers, agrees with the work of Davis and Davis (1973), who recorded no giant fiber activity during rhythmic escape tailflicking induced by visual stimuli in semi-intact animals. Since the neuromusculature machinery for MG tailflicks is demonstrably present, a number of questions remain to be addressed. Are the MG fibers ever active in larval animals? At what stage do the LG fibers develop? What is the nature of the switch to GF tailflicks that occurs shortly after or during the molt from stage III larvae to stage IV postlarvae? These unresolved issues suggest that investigation of the development of the neural circuitry of this well-studied behavior is likely to be useful.

Our results provide a clear example of the way in which the different selective pressures operating on larval and adult forms within a species result in different behavioral outputs in response to similar sensory stimuli activating parallel neuromuscular systems. The differences between the species studied illustrate the way in which both the timing and the details of related behaviors can diverge markedly in related forms, again in response to a history of differing ecological and physiological conditions. We provide preliminary evidence for the neurobiological basis of some of the evolutionary changes, but this is an area that invites further investigation.

Acknowledgments

We gratefully acknowledge all manner of generous assistance from Dr. Rainer Voigt, without which the project would not have been possible. Our thanks also to Drs. Arthur Humes and Ken Forman for the loan of equipment, to Dr. C. K. Govind for advice on larval development, to Drs. E. A. Kravitz and T. J. Trott for helping us obtain lobster larvae, and to M. J. Keough for statistical advice. The larvae used in the project were supplied by the New England Aquarium Lobster Rearing Facility, Boston, Massachusetts, which is sponsored by NIH, NSF, and the Human Frontiers Project. We thank the staff there for their willing cooperation. The work was supported by a grant from the Australian Research Council to DLM at the Department of Zoology, University of Melbourne.

Literature Cited

Cooke, I. R. C. 1985. The neuronal mechanism underlying leg movements during crayfish escape. *J. Exp. Biol.* **118:** 367–377.

Cooke, I. R. C., and D. L. Macmillan. 1985. Further studies of crayfish escape behaviour. I. The role of the appendages and the stereotyped nature of non-giant escape swimming. *J. Exp. Biol.* **118:** 351–356.

Davey, N., and D. L. Macmillan. 1991. The role of the legs in the lateral giant fiber escape of the crayfish *Cherax destructor* (Crustacea: Decapoda: Astacura). *J. Exp. Zool.* **259:** 279–286.

Davis, W. J., and K. B. Davis. 1973. Ontogeny of a simple locomotor system: role of the periphery in the development of central nervous activity. *Am. Zool.* **13:** 409–425.

Edwards, D. H., W. J. Heitler, and F. B. Krasne. 1999. Fifty years of a command neuron: the neurobiology of escape behavior in the crayfish. *Trends Neurosci.* **22:** 153–161.

Ennis, G. P. 1995. Larval and postlarval ecology. Pp. 23–46 in *Biology of the Lobster* Homarus americanus. J. R. Factor, ed. Academic Press, San Diego.

Fricke, R. A. 1984. Development of habituation in the crayfish due to selective weakening of electrical synapses. *Brain Res.* **322:** 139–143.

Fricke, R. A. 1986. Structure function considerations in the development expression of crayfish behavioral plasticity. *Proc. IEEE Int. Conf. Systems, Man and Cybernetics,* **1:** 513–518.

Govind, C. K., and F. Lang. 1976. Growth of lobster giant axons: correlation between conduction velocity and axon diameter. *J. Comp. Neurol.* **170:** 421–434.

Haury, L. R., and H. Yamazaki. 1995. The dichotomy of scales in the perception and aggregation behavior of zooplankton. *J. Plankton Res.* **17:** 191–197.

Herrick, F. H. 1909. Natural history of the American lobster. *Bull. Bureau Fish.* (USA) **29:** 408.

Hill, R. H., and C. K. Govind. 1984. Larval innervation of the lobster claw closer muscle. *J. Exp. Zool.* **229:** 393–399.

Keough, M. J., and B. J. Downes. 1982. Recruitment of marine invertebrates: the role of active larval choices and early mortality. *Oecologia* **54:** 348–452.

Krasne, F. B., and K. S. Woodsmall. 1969. Waning of the escape response as a result of repeated stimulation. *Anim. Behav.* **17:** 416–424.

Lang, F., C. K. Govind, W. J. Costello, and S. I. Greene. 1977. Developmental neuroethology: changes in escape and defensive behavior during growth of the lobster. *Science* **197:** 682–684.

Lauder, G. V., and B. D. Clark. 1984. Water flow patterns during prey capture by teleost fishes. *J. Exp. Biol.* **113:** 143–150.

Laverack, M. S., D. L. Macmillan, and D. M. Neil. 1976. A comparison of beating parameters in larval and post-larval locomotor systems of the lobster *Homarus gammorus* (L.). *Philos. Trans. R. Soc. Lond.* **274:** 87–99.

Lenz, P., D. Hartline, J. Purcell, and D. L. Macmillan. 1996. *Zooplankton: Sensory Ecology and Physiology.* Harwood Scientific, Amsterdam. 590 pp.

Macmillan, D. L. 1997. Development of the motor system in the limbs of larval lobsters (*Homorus americanus*). *Biol. Bull.* **193:** 257–258.

Macmillan, D. L., D. M. Neil, and M. S. Laverack. 1976. A quantitative analysis of exopodite beating in the larvae of the lobster *Homarus gammarus* (L.). *Philos. Trans. R. Soc. Lond.* **274:** 69–85.

Mittenthal, J. E., and J. J. Wine. 1973. Connectivity patterns of crayfish giant interneurons: visualization of synaptic regions with cobalt dye. *Science* **179:** 182–184.

Morgan, S. G. 1987. Morphological and behavioural antipredatory adaptations of decapod zoeae. *Oecologia* **73:** 393–400.

Neil, D. M., D. L. Macmillan, R. M. Robertson, and M. S. Laverack. 1976. The structure and function of thoracic exopodites in the larvae of the lobster *Homarus gammarus* (L.). *Philos. Trans. R. Soc. Lond.* **274:** 53–68.

Newland, P. L., and D. M. Neil. 1990. The tail flip of the Norway Lobster, *Nephrops norvegicus.* Giant fibre activation in relation to swimming trajectories. *J. Comp. Physiol.* **166:** 517–527.

Phillips, B. F., and L. Olsen. 1975. Swimming behaviour of the puerulus larvae of the western rock lobster. *Aust. J. Mar. Freshwater Res.* **26:** 415–417.

Sandeman, R., and D. Sandeman. 1991. Stages in the development of the embryo of the fresh-water crayfish *Cherax destructor. Roux's Arch. Dev. Biol.* **200:** 27–37.

Schmitz, B. 1992. Directionality of antennal sweeps elicited by water jet stimulation of the tailfan in the crayfish *Procambarus clarkii. J. Comp. Physiol.* **171:** 617–627.

Shrameck, J. E. 1970. Crayfish swimming: alternating motor output and giant fiber activity. *Science* **169:** 698–700.

Umbach, J. A., and F. Lang. 1981. Synaptic interaction between the giant interneuron and the giant motorneuron in the hermit crab, *Pagurus pollicarus. Comp. Biochem. Physiol.* **68A:** 49–53.

Wine, J. J. 1984. The structural basis of an innate behavioural pattern. *J. Exp. Biol.* **112:** 283–319.

Wine, J. J., and F. B. Krasne. 1969. Independence of inhibition and habituation in the crayfish lateral giant fiber escape reflex. Pp. 237–238 in *Proceedings of the 77th Annual Convention,* American Psychological Association, Washington, DC.

Wine, J. J., and F. B. Krasne. 1982. The organization of escape behaviour in the crayfish. *J. Exp. Biol.* **56:** 1–18.

Wine, J. J., and F. B. Krasne. 1972. The cellular organization of crayfish escape behavior. Pp. 241–292 in *The Biology of Crustacea. Vol. 4. Neural Integration and Behavior.* D. C. Sandeman and H. L. Atwood, eds. Academic Press, New York.

Wine, J. J., F. B. Krasne, and L. Chen. 1975. Habituation and inhibition of the crayfish lateral giant fibre escape response. *J. Exp. Biol.* **62:** 771–782.

Reference: *Biol. Bull.* **198:** 319–331. (June 2000)

Catecholamines Modulate Metamorphosis in the Opisthobranch Gastropod *Phestilla sibogae*

ANTHONY PIRES,[1,*] ROGER P. CROLL[2], AND MICHAEL G. HADFIELD[3]

[1] *Department of Biology, Dickinson College, Carlisle, Pennsylvania 17013;* [2] *Department of Physiology & Biophysics, Dalhousie University, Halifax, Nova Scotia, Canada B3H 4H7; and* [3] *University of Hawaii, Pacific Biomedical Research Center, Kewalo Marine Laboratory, 41 Ahui St., Honolulu, Hawaii 96813*

Abstract. Larvae of the nudibranch *Phestilla sibogae* are induced to metamorphose by a factor from their adult prey, the coral *Porites compressa.* Levels of endogenous catecholamines increase 6 to 9 days after fertilization, when larvae become competent for metamorphosis. Six- to nine-day larvae, treated with the catecholamine precursor L-DOPA (0.01 m*M* for 0.5 h), were assayed for metamorphosis in response to coral inducer and for catecholamine content by high-performance liquid chromatography. L-DOPA treatment caused 20- to 50-fold increases in dopamine, with proportionally greater increases in younger larvae, so that L-DOPA-treated larvae of all ages contained similar levels of dopamine. A much smaller (about twofold) increase in norepinephrine occurred in all larvae. The treatment significantly potentiated the frequency of metamorphosis of 7- to 9-d larvae at low concentrations of inducer. In addition, L-DOPA treatment at 9 d increased aldehyde-induced fluorescence in cells that were also labeled in the controls, and revealed additional cells. However, all labeled cells were consistent with the locations of cells showing tyrosine-hydroxylase-like immunoreactivity. Catecholamines are likely to modulate metamorphosis in *P. sibogae,* but rising levels of catecholamines around the time of competence are insufficient alone to account for sensitivity to inducer in competent larvae.

Introduction

The larvae of many marine invertebrates settle and metamorphose in response to chemical signals in the environment. In some taxa, larvae become competent to respond to such chemical inducers only after an obligate planktonic phase (Pechenik, 1990; Hadfield and Strathmann, 1996). In gastropod molluscs, the minimum time to competence ranges from several days to several weeks and may or may not require feeding and growth, depending on the species. For example, the onset of competence occurs in a predictable, age-dependent fashion in the lecithotrophic larvae of the opisthobranch *Phestilla sibogae* (Miller and Hadfield, 1986), but is extremely variable in another opisthobranch, *Haminaea callidegenita* (Gibson, 1995). For planktotrophic larvae of the prosobranch genus *Crepidula,* the onset of competence is influenced by temperature, salinity, and nutritional history and is poorly predicted by size (Zimmerman and Pechenik, 1991; Pechenik *et al.,* 1996). Even after the onset of competence, responsiveness to an inducer can be affected by a larva's sensory history. Habituation to inducer has been studied in the gastropods *Phestilla sibogae* and *Haliotis rufescens* (Hadfield and Scheuer, 1985; Trapido-Rosenthal and Morse, 1986a, b). In the latter species, sensitization to an inducer by another external ligand has also been reported (Trapido-Rosenthal and Morse, 1985, 1986b), and both phenomenon have been related to regulation at the level of surface receptors for the inducer.

The structural and functional transformations that underlie the acquisition of competence and changes in responsiveness to inducers are not well understood. Competence may depend on the completion of neural networks that mediate between the initial chemosensory transduction of inducer and the behavioral and developmental events of metamorphosis. The modulation of such networks is an-

---

Received 6 August 1999; accepted 20 January 2000.

* To whom correspondence should be addressed.

Abbreviations: α-MMT, α-methyl-DL-*m*-tyrosine; CI, coral inducer; DA, dopamine; DHBA, dihydroxybenzylamine; DOPAC, dihydroxyphenylacetic acid; FaGlu, formaldehyde-glutaraldehyde; HPLC, high performance liquid chromatography; L-DOPA, L-3,4-dihydroxyphenylalanine; MBL-ASW, MBL artificial seawater; NE, norepinephrine; PBS, phosphate-buffered saline; TH-LIR, tyrosine-hydroxylase-like immunoreactive.

other possible cause of both age- and context-dependent shifts in responsiveness to inducers. Such networks are poorly characterized due to the difficulty of neurophysiological work in larvae (Arkett *et al.*, 1989; Barlow, 1990). In contrast, a wealth of information is available on the neural bases of many behaviors in adult gastropods, whose nervous systems are much more accessible. A common principle is that monoamine neurotransmitters and neurohormones often play critical roles in initiating and controlling behavior (Katz, 1995; Kabotyanski *et al.*, 1998). For example, dopamine is important in the control of several neural processes that are normally associated with a chemosensory stimulus: it has been shown to elicit feeding motor programs in several pulmonates (Quinlan *et al.*, 1997; Trimble and Barker, 1984; Wieland and Gelperin, 1983), modulate the activity of olfactory interneurons in *Limax maximus* (Gelperin *et al.*, 1993), and activate hunting behavior in the opisthobranch *Clione limacina* (Norekyan and Satterlie, 1993).

Given that gastropod veligers contain monoamines and other neuromodulatory transmitters (Kempf *et al.*, 1992, 1997; Pires *et al.*, 1997), it is reasonable to ask whether such compounds participate in the control of metamorphosis (Pires and Hadfield, 1991; Pires *et al.*, 1997; Couper and Leise, 1996; Froggett and Leise, 1999). We have used veligers of *P. sibogae*, which settle and metamorphose in response to an inducer derived from their adult prey, the coral *Porites compressa* (Hadfield, 1978; Hadfield and Pennington, 1990). The levels of catecholamines in these larvae increase several-fold within a period of 4–5 days after hatching, during which the larvae become competent for metamorphosis. α-methyl-DL-*m*-tyrosine (α-MMT), an inhibitor of the catecholamine-generative enzyme tyrosine hydroxylase (Uretsky *et al.*, 1975; Bernabe *et al.*, 1996), depletes catecholamines and inhibits induction of metamorphosis by coral inducer (Pires *et al.*, 1997). We now report that coral-induced metamorphosis is potentiated by exposure of competent larvae to L-DOPA, the synthetic precursor of catecholamines. This treatment substantially enhanced endogenous norepinephrine (NE) and especially dopamine (DA). L-DOPA treatment also restored catecholamine levels and ability to metamorphose in larvae that had been treated with α-MMT. Histochemical study of catecholamine-containing tissues suggested that enhancement of catecholamines was localized in populations of cells in locations consistent with those of cells exhibiting tyrosine hydroxylase-like immunoreactivity. Although these results support a role for catecholamines in the control of metamorphosis, experiments with younger larvae indicated that rising levels of catecholamines were not by themselves sufficient to account for the onset of competence.

Materials and Methods

Larval culture

Larvae were cultured as described by Miller and Hadfield (1986) with modifications given in Pires and Hadfield (1991). Larval ages are given as days postfertilization. All larvae were hatched at 5 d and held unfed in culture until needed. Veligers of *Phestilla sibogae* are facultative planktotrophs; under our culture conditions larvae begin to attain metamorphic competence at 7 d and by 10 d nearly all individuals are competent without having fed (Kempf and Hadfield, 1985; Miller and Hadfield, 1986).

Manipulation of catecholamine biosynthesis

Two sets of experiments were performed to test how manipulating catecholamine biosynthesis affected metamorphosis. In the first, content of endogenous catecholamines and frequency of metamorphosis were determined in 9-d larvae after treatment with α-MMT, L-DOPA (both from Sigma Chemical Co., St. Louis, MO), or both. (Endogenous catecholamines are depleted by α-MMT (Pires *et al.*, 1997), and preliminary experiments done for this study indicated that they are enhanced by L-DOPA at the concentrations used here.) Five replicates were performed on different culture batches on different dates. In each replicate, 1500–2000 larvae were taken from culture on day 8 and evenly divided among four treatments, all carried out in MBL artificial seawater (MBL-ASW; Cavanaugh, 1956) buffered to pH 8.2 with 10 mM Trizma: (1) 24 h in MBL-ASW alone; (2) 24 h in 1 mM α-MMT; (3) 21 h in MBL-ASW followed by 0.5 h in 10^{-5} M L-DOPA followed by 2 h in MBL-ASW; (4) 21 h in 1 mM α-MMT followed by 0.5 h in 10^{-5} M L-DOPA plus 1 mM α-MMT followed by 2 h in 1 mM α-MMT. L-DOPA was applied as a 0.5-h pulse followed by a MBL-ASW rinse because L-DOPA and other catechols oxidize rapidly in seawater and the oxidative products themselves affect metamorphosis (Pires and Hadfield, 1991). All treatments were carried out in 20-ml volume in 62-mm glass Stender dishes. At the end of the drug treatments, a sample of each group was homogenized for analysis of catecholamines by high-performance liquid chromatography (HPLC); the remainder was used to assay metamorphosis.

The second set of experiments tracked catecholamine content, frequency of metamorphosis, and onset of competence in larvae of increasing ages after modest or extreme enhancement of catecholamines by different doses of L-DOPA. Four replicate series were performed, beginning on different dates with different culture batches. In each replicate series about 1000 six-day-old larvae were pipetted from their culture into MBL-ASW, and then divided into three treatments, all in MBL-ASW: (1) 2–3 h in MBL-ASW alone; (2) 0.5 h in 5×10^{-7} M L-DOPA followed by 2 h in

MBL-ASW; (3) 0.5 h in 10^{-5} M L-DOPA followed by 2 h in MBL-ASW. A sample of each group was homogenized for analysis of catecholamines by HPLC; the remainder was used to assay metamorphosis. This experiment was repeated on days 7, 8, and 9 with larvae freshly drawn from the same culture in each replicate series. Nine-day-old larvae did not receive L-DOPA treatments; frequency of metamorphosis and catecholamine levels in these oldest larvae served for comparison with younger animals from the same batch that had been treated with L-DOPA on previous days.

Preparation of metamorphic inducer and assay of metamorphosis

Frequency of metamorphosis was assayed in response to preparations of the natural inducer. This "coral inducer" (CI) was made by incubating a few "fingers" of *Porites compressa* (about 50–75 g wet weight) in an 11.5-cm glass bowl filled with MBL-ASW. After 24 h the CI was filtered through coffee-filter paper, adjusted to 32 ppt salinity, and frozen in aliquots at −20°C. Aliquots to be used on a given day were thawed to room temperature and diluted with fresh MBL-ASW to make a graded dilution series of CI ranging up 0.5 times (0.5×) full strength (50% v/v CI in MBL-ASW). All experiments on a given culture batch of larvae used freshly thawed aliquots of the same CI. In each assay, 20–40 larvae were transferred to 37-mm glass Stender dishes containing 3 ml 0.05×, 0.1×, 0.2×, or 0.5× CI or MBL-ASW control. (For larvae that had been treated with α-MMT, the dilution series of CI used to assay metamorphosis also contained 1 mM α-MMT to maintain inhibition of catecholamine synthesis for the duration of the assay.) Assays were scored after 24 h. Individuals that had evacuated the larval shell were counted as having metamorphosed (Hadfield, 1978). Effects of CI concentration and of drug treatments on arcsine-transformed frequencies of metamorphosis were analyzed by ANOVA with Bonferroni adjustment for multiple comparisons (Zolman, 1993), using Data-Desk 6.1 statistical analysis software (Data Description, Ithaca, NY).

Extraction of catecholamines and analysis by HPLC

For each determination of catecholamine content, 150–250 larvae were counted and pipetted into a glass homogenization tube on ice. The tube was briefly centrifuged ($<150 \times g$), and excess water was drawn off to concentrate larvae in a volume of about 25 μl. Homogenization of larvae and extraction, separation, identification, and quantification of catecholamines by HPLC were modified from procedures described previously (Pires *et al.*, 1997). In summary, larvae were homogenized in a perchlorate buffer; supernatants of centrifuged homogenates were extracted over acid-washed alumina (Bioanalytical Systems) in 1.5 M Tris buffer (pH 8.6). Alumina was washed in deionized water and transferred to microcentrifuge filters, where excess water was spun off and catecholamines were eluted with 0.1 M perchloric acid. Efficiency of extraction of catecholamines, typically 60%–80%, was corrected with a dihydroxybenzylamine (DHBA) internal standard added to all larval homogenates. Catecholamines were separated on a Bioanalytical Systems MF-6213 analytical column (100 × 3.2 mm, 3 μm C-18 reversed phase packing). The aqueous portion of the mobile phase contained 100 mM monochloroacetic acid, 1.3 mM Na_2EDTA, and 1.3 mM sodium octyl sulfate. Mobile phase pH was adjusted between 3.0 and 3.3 with NaOH. The organic portion of the mobile phase was 2%–4% (v/v) acetonitrile. Flow rate was set at 1.0 ml/min. Catecholamines were detected with a Bioanalytical Systems LC-4C amperometric electrochemical detector with glassy carbon working electrode set at an oxidizing potential of 650 mV against a Ag/AgCl reference electrode. Detector output was low-pass filtered (1.0 Hz cutoff) and sent to a Hewlett-Packard 3395 integrator that printed chromatograms and calculated peak areas and retention times. Catecholamine contents were expressed as picomoles of free base per larva.

Histochemistry

At least 50 larvae were obtained from each group after scoring for frequency of metamorphosis in two replicates of the first set of experiments described above. In addition, several hundred 9-d larvae were taken directly from culture without drug treatment. All larvae were immobilized in a 1:1 mixture of MBL-ASW and 7.5% (w/v) $MgCl_2$ in water. These larvae were gathered into 1.5-ml microcentrifuge tubes and spun gently ($<150 \times g$ rpm) for 5–10 s and were then processed using the formaldehyde-glutaraldehyde (FaGlu) procedure modified from Furness *et al.* (1977) as follows: The MBL-ASW/$MgCl_2$ was replaced with FaGlu solution of 4% paraformaldehyde and 0.55% glutaraldehyde in phosphate-buffered saline (PBS: 50 mM $Na_2HPO_4 - 7H_2O$ and 140 mM NaCl, pH 7.4). After 18 h, the fixed larvae were decalcified in 10% EDTA for 10 min, washed briefly in PBS, and then dehydrated through an ascending ethanol series (70%, 80%, 90%, 95%, 100%, 100%; 2 min/step). The larvae were then cleared and mounted on glass slides with methyl salicylate. The slides were viewed through a Zeiss Axiophot microscope equipped for ultraviolet (UV) epifluorescence with a filter block containing 365-nm excitation and 420-nm longpass barrier filters and photographed using Kodak T-MAX 400 film. Negative controls were also prepared with no glutaraldehyde added to the fixative. Such control preparations exhibited none of the blue-green fluorescence reported in this study.

Immunocytochemistry

Several hundred 9-d larvae taken directly from culture without any drug treatment were also processed for immunocytochemistry using monoclonal antibodies raised against tyrosine hydroxylase (TH; IncStar #22941, Stillwater, MN) and procedures similar to those employed previously in gastropods (Hernádi *et al.*, 1993; Voronezhskaya *et al.*, 1999; Croll *et al.*, 1999).

Larvae were first immobilized with $MgCl_2$ as described above and then fixed in 100% methanol at −20°C. (Preliminary experiments had indicated that such methanol fixation yielded more intense labeling than using paraformaldehyde in another gastropod, *Lymnaea stagnalis*, in which catecholaminergic neurons have been well characterized [Croll and Chiasson, 1990; Elekes *et al.*, 1991; Voronezhskaya *et al.*, 1999; Croll *et al.*, 1999].) After 2–4 h, the fixed larvae were decalcified in 10% EDTA and then placed in a blocking solution of PBS with the addition of 2% bovine serum albumin and 1% Triton X-100. This and subsequent steps were performed at 4°C. After 12 h, larvae were transferred to the primary anti-TH antibody diluted 1:50 in the blocking solution for 48 h. After three 30-min washes, larvae were incubated overnight in a 1:50 dilution of fluorescein isothiocyanate-labeled polyclonal goat anti-mouse antibodies (Sigma #F5262). Following several more washes in PBS, larvae were placed on glass slides and mounted in 3:1 glycerol in 0.1 *M* Tris buffer (pH 8.5) with the addition of 2% *n*-propyl gallate (Giloh and Sedat, 1982).

Preparations were examined either on the Zeiss Axiophot microscope equipped with a filter block containing 450–490 nm excitation and 515–565 nm bandpass barrier filters or on a Zeiss Axiovert microscope equipped for confocal laser scanning (Zeiss model LSM 510; excitation 488 nm with 505–550 nm barrier filter). In the latter case, photographs were produced by superpositioning stacks of 20–40 images obtained through stepped sequences of focal planes at about 1.0-μm intervals.

Negative control experiments used identical procedures except that the primary antibody was omitted. No labeling was observed in these control preparations.

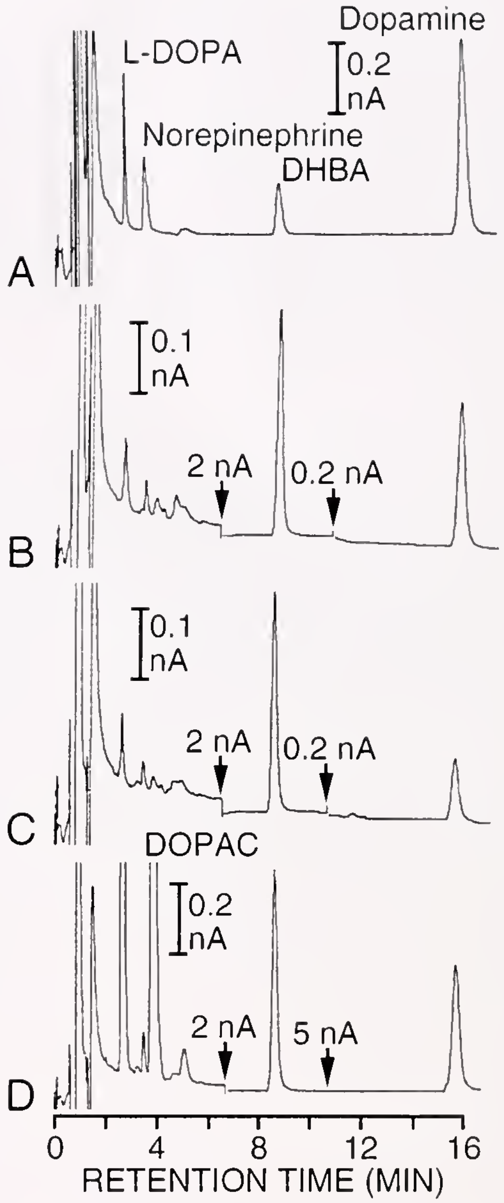

Figure 1. Chromatograms of catecholamine standards, and of alumina extracts of 9-d larvae of *Phestilla sibogae* from one replicate of an experiment in which catecholamine biosynthesis was manipulated. Standards (A) contained 0.32 pmol each of L-DOPA, norepinephrine, and dihydroxybenzylamine (DHBA), and 1.6 pmol of dopamine. (B) Extract of 210 larvae treated with MBL artificial seawater only; (C) extract of 210 larvae treated with 1 m*M* α-methyl-DL-*m*-tyrosine; (D) extract of 222 larvae treated with 10^{-5} *M* L-DOPA. Current scale of detector changes at points marked by vertical arrows.

Results

Depletion and enhancement of catecholamines in competent larvae

NE and DA were present in quantifiable amounts in larvae of all ages and all drug treatment groups used in this study. Figure 1 shows chromatograms of catecholamine standards and of alumina extracts of 9-d larvae that had been treated with MBL-ASW only, the tyrosine hydroxylase inhibitor α-MMT (1 m*M*), or the catecholamine precursor L-DOPA (10^{-5} *M*). Numbers of larvae and extraction efficiencies were very similar between treatments, so inspection of peaks roughly indicates relative amounts of catecholamines per larva. These chromatograms show the qualitative effects of catecholamine depletion by α-MMT and enhancement by L-DOPA, compared to larvae held in MBL-ASW. Enhancement of DA is especially evident in the chromatogram of L-DOPA-treated larvae (Fig. 1D). In addition, this chromatogram shows a prominent peak iden-

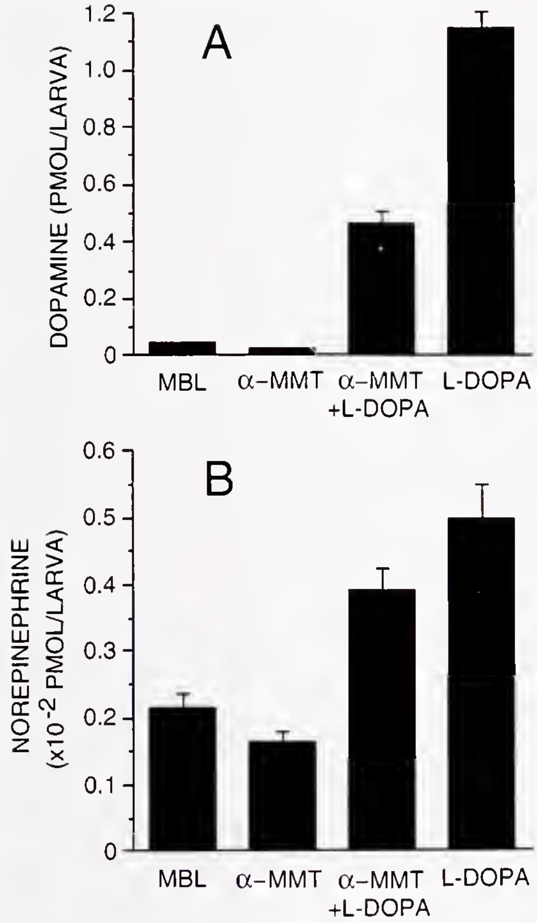

Figure 2. Content of dopamine (A) and norepinephrine (B) at 9 d postfertilization in larvae of *Phestilla sibogae* after treatment with 1 m*M* α-methyl-DL-*m*-tyrosine (α-MMT), 1 m*M* α-MMT plus 10^{-5} *M* L-DOPA, 10^{-5} *M* L-DOPA, or MBL artificial seawater control. Each column represents the mean (±1 SEM) of 5 replicate trials.

tified as the dopamine metabolite dihydroxyphenylacetic acid (DOPAC) on the basis of its co-elution with authentic DOPAC over a range of mobile phase pH and acetonitrile concentrations. Test extractions revealed that recovery of DOPAC was not accurately estimated by our DHBA internal standard, so we do not report quantitative values for DOPAC.

Treatment of 9-d larvae with a 0.5-h pulse of 10^{-5} *M* L-DOPA followed by a 2-h incubation in MBL-ASW resulted in an average 26-fold enhancement of endogenous DA (Fig. 2A), compared to larvae exposed to MBL-ASW alone. In contrast, DA was depleted to 49% of MBL-ASW control values in larvae that had been exposed to α-MMT (1 m*M* for 24 h). DA was elevated to 11 times the value of MBL-ASW controls in larvae that received a combined treatment of α-MMT and L-DOPA (1 m*M* α-MMT for 21 h, followed by an L-DOPA pulse as described above but in the continued presence of α-MMT). A similar pattern of depletion and enhancement of NE was observed following the above treatments (Fig. 2B), although the magnitude of these effects was much smaller than was observed for DA.

Analysis of variance revealed significant effects of culture batch ($P < 0.01$), CI concentration, drug treatment and (CI × drug) interaction (all $P < 0.0001$) on frequency of metamorphosis in 9-d larvae. No larva in any treatment metamorphosed in the absence of CI. Treatments with α-MMT and L-DOPA that modulated endogenous catecholamine levels had dramatic and opposite effects on the frequency of coral-induced metamorphosis (Fig. 3). Bonferroni *post-hoc* tests compared effects of individual drug treatments. Larvae that had been held 24 h in 1 m*M* α-MMT metamorphosed at much lower frequencies than control larvae held in MBL-ASW ($P < 0.0001$). Larvae that had received a 0.5-h pulse of 10^{-5} *M* L-DOPA, ending 2 h before exposure to CI, metamorphosed at significantly higher frequencies than did MBL-ASW controls when challenged with dilute preparations of CI ($P < 0.0001$). However, mean frequencies of metamorphosis were not significantly different in these two groups at the highest concentration of CI. Larvae that received a combined treatment of α-MMT and L-DOPA metamorphosed at frequencies that also were not significantly different than those of MBL-ASW controls.

Histochemistry

Nine-day larvae taken from two replicates of the experiment documented in Figures 2 and 3 were subjected to

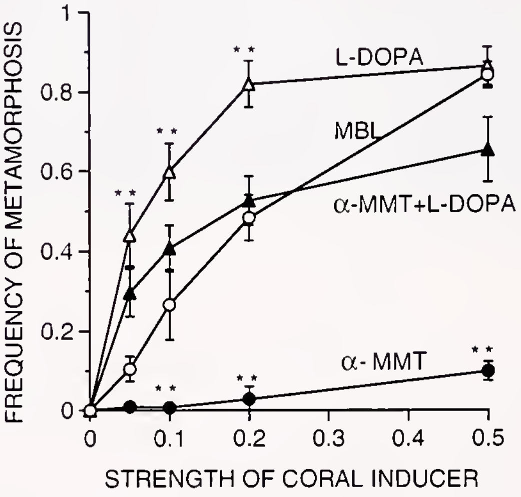

Figure 3. Frequency of metamorphosis of larvae of *Phestilla sibogae* after 24-h exposure to varying dilutions of coral inducer on day 9 postfertilization. Prior to inducer, larvae were subjected to the following treatments: 1 m*M* α-methyl-DL-*m*-tyrosine (α-MMT, filled circles), 1 m*M* α-MMT plus 10^{-5} *M* L-DOPA (filled triangles), 10^{-5} *M* L-DOPA (open triangles), or MBL artificial seawater control (open circles). Each point represents the mean (±1 SEM) of 5 replicate trials. Double asterisks indicate significant difference ($P < 0.01$) from MBL artificial seawater control at a given dilution of coral inducer.

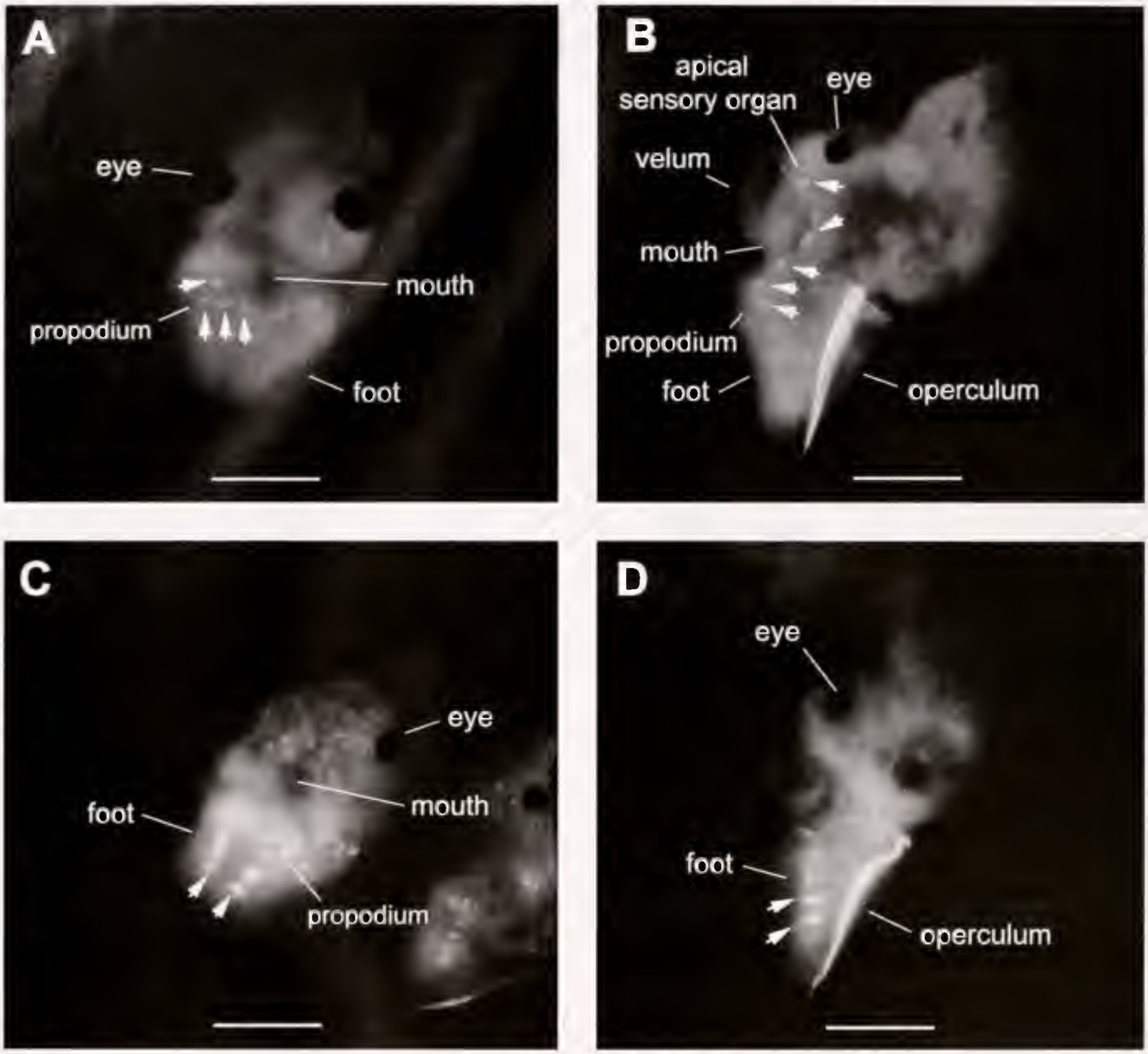

Figure 4. Aldehyde-induced histofluorescence. Frontal (A) and lateral (B) views of control larvae showing a few dimly fluorescent cells (arrowheads) in the region of the propodium, lateral to the mouth and near the apical sensory organ anterior to the eye. One or more cells were also sometimes observed near the base of the velum. No cells were generally found toward the distal tip of the foot to which the operculum is attached. Frontal (C) and lateral (D) views of larvae that were previously incubated in L-DOPA. Many more cells fluoresced brightly in such larvae. Most of these fluorescent cells were located in two rows running along the length of the foot (arrowheads in C) and in a patch on each side of the propodium. Several of these cells (arrowheads in D) appeared to be vase-shaped with slender processes projecting into the overlying epithelium. Calibration bars equal approximately 50 μm.

FaGlu histochemistry to visualize catecholamine-containing cells. The staining patterns in normal larvae without any prior drug treatment and those incubated in MBL-ASW or MBL-ASW plus α-MMT were all similar. Patches of 3 to 6 faint, blue-green fluorescent cells were reliably located in the propodial region of the foot of larvae from all of these groups (Fig. 4A). In addition, 2 to 4 fluorescent cells were located near the mouth, 1 to 2 cells were located more lateral to the mouth and near the base of the velum, and a final 2 to 4 fluorescent cells were located in regions anterior to the eyes (Fig. 4B).

The intensity of fluorescence and the numbers of fluorescent cells were markedly enhanced following treatment with L-DOPA alone or with L-DOPA plus α-MMT. In these

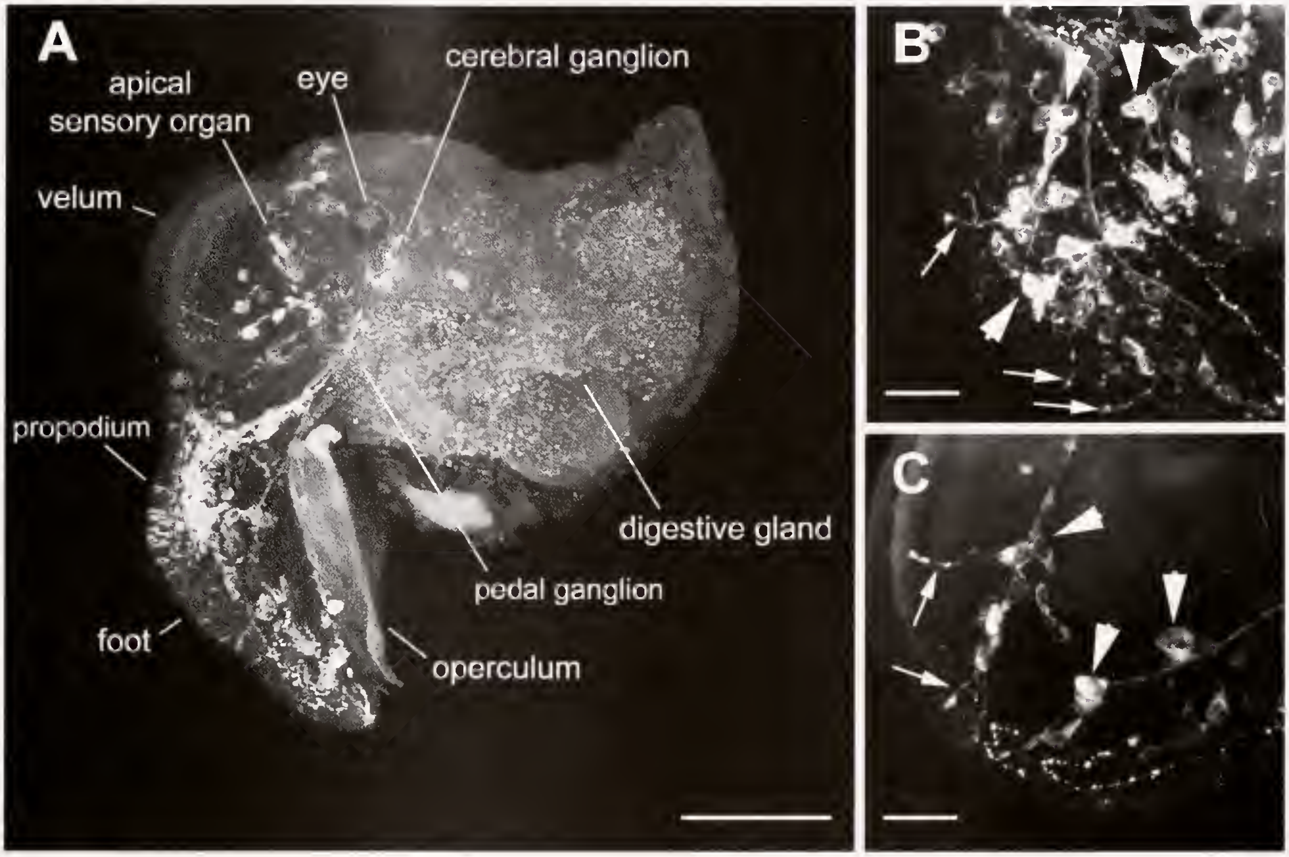

Figure 5. Tyrosine-hydroxylase-like immunoreactivity shown in projection patterns of normal larvae, reconstructed from multiple optic sections from a confocal microscope. (A) Lateral view of larva with velar lobes folded medially by mounting. A concentration of immunoreactive, subepithelial cells was labeled in the propodium. These cells appeared to send axons into the developing pedal ganglia. Large numbers of other cells were located along the length of the foot. Other cells were scattered near the mouth and velum, and in regions of the head near and dorsal to the apical sensory organ and eyes. (B) Magnified and more frontal view of somata (larger arrowheads) in propodium. Many of these cells possessed processes (slender arrows) that penetrated the overlying epithelium. (C) A smaller number of somata (arrowheads) with processes (slender arrows) are located near the distal tip of the foot. Calibration bar in A equals approximately 57 μm. Calibration bars in B and C equal approximate 12 μm.

larvae, the largest concentrations of fluorescent cells were again found in the propodial regions of the foot. Each of the bilateral patches contained 10 to 20 brightly fluorescent cells (Fig. 4C). In addition, several fluorescent cells were located in lateral bands along the length of the foot. At least some of these cells appeared to possess apical processes extending through the overlying epithelium (Fig. 4D).

Larvae treated with either L-DOPA or L-DOPA plus α-MMT also contained many brightly fluorescent cells in the head region. Several cells were routinely observed around the mouth, near the base of the velum (Fig. 4C), and anterior to the eyes. Thus the distribution of the cells in head regions was similar to that observed in normal larvae and in those incubated in MBL-ASW alone, or in MBL-ASW plus α-MMT. However, the cells observed in the head regions of larvae treated with L-DOPA or L-DOPA plus α-MMT appeared to be more intensely labeled and slightly more numerous.

Immunocytochemistry

Tyrosine-hydroxylase-like immunoreactive (TH-LIR) cells were labeled in 9-d larvae. The highest concentration of TH-LIR cells was located in bilateral patches in the propodium (Fig. 5A). Each patch contained about 40 to 50 cells (Fig. 5B). These cells appeared to be bipolar with one process penetrating the overlying epithelium and a long axon that projected to the region of the pedal ganglia. Similar cells were located at lesser densities on lateral edges along the length of the foot (Fig. 5C). Between 2 and 4 TH-LIR cells were located at each side near the mouth, and 2 to 4 additional cells were located more laterally near the

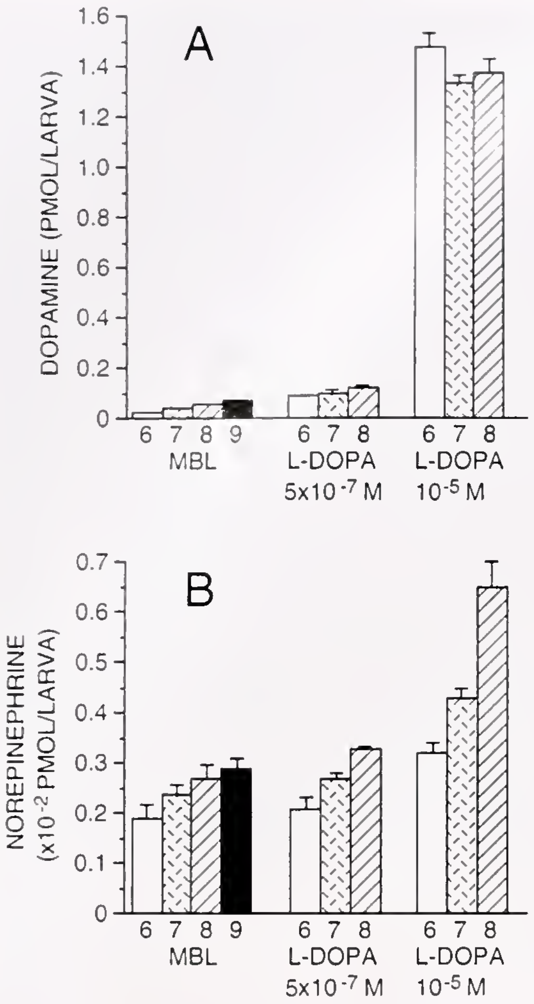

Figure 6. Content of dopamine (A) and norepinephrine (B) at 6, 7, 8, and 9 d postfertilization (numerals beneath horizontal axis) in larvae of *Phestilla sibogae*, following treatment with 5×10^{-7} *M* or 10^{-5} *M* L-DOPA, or MBL artificial seawater control. Each column represents the mean (± 1 SEM) of 5 replicate trials for 10^{-5} *M* L-DOPA and MBL, or 4 trials for 5×10^{-7} *M* L-DOPA.

base of the velum on each side. At least one of these latter cells appeared to project an axon into the velum. An additional 4 to 6 somata were located anterior to the eyes, in regions near and also more dorsal to the apical sensory organ. Although TH-LIR fibers were contained in pathways running through the pedal and cerebral ganglia, no TH-LIR somata were located in these ganglia.

Enhancement of catecholamines in precompetent larvae

Treatment of 6-, 7-, and 8-d larvae with pulses of L-DOPA enhanced levels of catecholamines in a dose-dependent manner (Fig. 6). A 0.5-h pulse of 5×10^{-7} *M* L-DOPA raised dopamine levels by two- to threefold above control larvae of the same age held in MBL-ASW. Following a pulse of 10^{-5} *M* L-DOPA, dopamine was elevated to 22–50 times control levels, with the greatest degree of enhancement seen in the youngest larvae. Norepinephrine levels were slightly elevated above control values after a pulse of 5×10^{-7} *M* L-DOPA, and were only 2–3 times higher than controls after a pulse of 10^{-5} *M* L-DOPA.

The effects of L-DOPA on metamorphosis were analyzed by ANOVA in 6-, 7-, and 8-d larvae (Fig. 7). Metamorphosis was rare in 6-d larvae; treatment effects of CI concentration were significant ($P < 0.005$), but effects of L-DOPA were not. Highly significant effects ($P \leq 0.0001$) of CI concentration and of 10^{-5} *M* but not 5×10^{-7} *M* L-DOPA were obtained in 7-d and 8-d larvae. Treatment of 7-d larvae with 10^{-5} *M* L-DOPA was followed by low frequencies of metamorphosis in response to all nonzero concentrations of CI; *post-hoc* comparisons revealed that these frequencies were significantly higher than in MBL-ASW control larvae at 0.1× CI and 0.2× CI ($P < 0.05$). At 8 d, larvae treated with 10^{-5} *M* L-DOPA metamorphosed at significantly higher frequencies than did control larvae upon exposure to 0.05× and 0.1× CI ($P < 0.01$). As was the case with 7-d larvae, responses to the highest concentration of CI (0.5×) did not differ significantly between 10^{-5} *M* L-DOPA-treated larvae and MBL-ASW controls. Only MBL-ASW control larvae were assayed for metamorphosis at 9 d. The response of these larvae to CI was similar to that of 9-d MBL-ASW control larvae in the first series of experiments.

Discussion

Pharmacological manipulations of catecholamine biosynthesis had profound effects on metamorphosis in response to CI in 9-d competent larvae of *Phestilla sibogae* (Fig. 3). Treatment of larvae with a 0.5-h pulse of 10^{-5} *M* L-DOPA enhanced contents of NE (more than twofold) and especially DA (26-fold), compared to control levels (Fig. 2). This treatment potentiated metamorphic responses to all but the highest concentration of CI, compared to MBL-ASW controls. At the highest concentration of CI, the mean frequencies of metamorphosis of control and L-DOPA-treated larvae were statistically indistinguishable (0.84 and 0.86, respectively) and may reflect metamorphosis of all larvae that were competent at that age (Miller and Hadfield, 1986). The catecholamine-depleting drug α-MMT inhibited metamorphosis over a range of CI concentrations, compared to controls treated only with MBL-ASW before exposure to CI (Pires *et al.*, 1997). In larvae that had been treated with 1 m*M* α-MMT for 24 h, DA was depleted to 48% of the control value measured in MBL-ASW-treated larvae, whereas NE was depleted only to 76% of the control value. It is likely that inhibition by α-MMT was due to depletion of catecholamines and not to an unknown toxic effect of α-MMT, because larvae treated with α-MMT and then pulsed with L-DOPA metamorphosed at high frequencies in

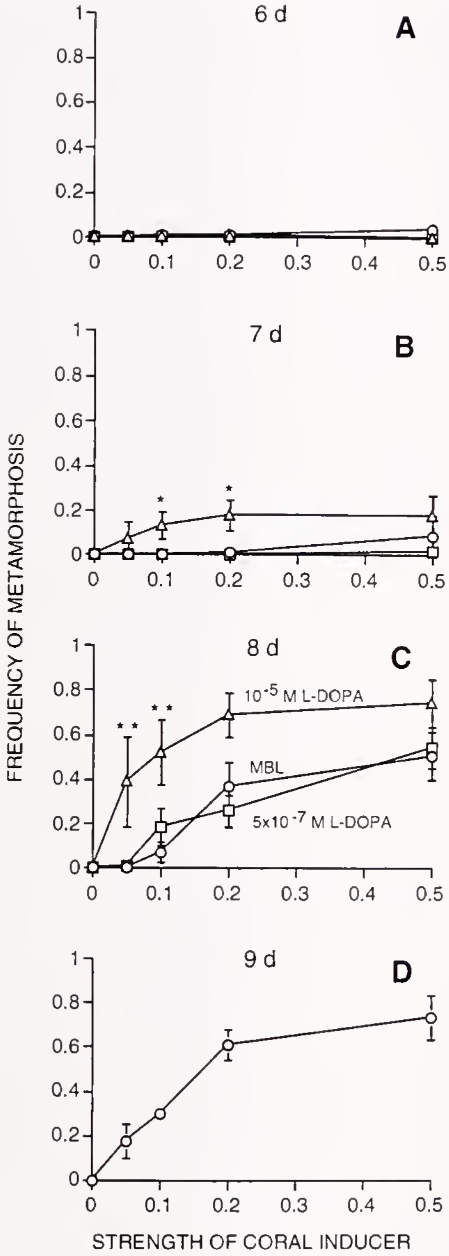

Figure 7. Frequency of metamorphosis of larvae of *Phestilla sibogae* after 24-h exposure to varying dilutions of coral inducer, following 0.5-h treatment with 5×10^{-7} *M* (squares) or 10^{-5} *M* (triangles) L-DOPA, or MBL-artificial seawater control (circles) on day 6 (A), 7 (B), 8 (C), or 9 (D, control only) postfertilization. Each point represents the mean (±1 SEM) of 5 replicate trials of 10^{-5} *M* L-DOPA and MBL, or 4 trials for 5×10^{-7} *M* L-DOPA. Asterisks indicate significant difference (*, $P < 0.05$; **, $P < 0.01$) from MBL artificial seawater control at a given dilution of coral inducer.

response to CI even in the continued presence of α-MMT. Larvae that received this combined treatment of L-DOPA and α-MMT had levels of DA and NE that were higher than those of MBL-ASW controls but lower than those measured in larvae treated with L-DOPA only. The mechanism by which α-MMT depletes endogenous DA, at least in mammalian nervous systems, involves both inhibition of tyrosine hydroxylase activity by α-MMT and displacement of stored DA by a decarboxylated metabolite of α-MMT (Uretsky *et al.*, 1975; Bernabe *et al.*, 1996). The latter mechanism may help explain why larvae treated with both α-MMT and L-DOPA contained less DA and NE than those treated with L-DOPA alone. Taken together, our manipulations of catecholamine biosynthesis with L-DOPA and α-MMT in competent larvae show that depletion of endogenous catecholamines is accompanied by inhibition of CI-induced metamorphosis, whereas enhancement of catecholamines is accompanied by potentiation of metamorphic responses to CI. Thus catecholamines appear to serve as endogenous modulators of metamorphosis in competent larvae of *P. sibogae*.

Catecholamine-containing cells in competent larvae were labeled by FaGlu histochemistry (Fig. 4) in order to map locations of these putative modulators of metamorphosis, and to test the anatomical specificity of catecholamine enhancement by L-DOPA. Intensity of labeling and numbers of labeled cells were dramatically enhanced by treatment of larvae with L-DOPA, without a concomitant increase in background fluorescence. Thus, the quantitative enhancement of catecholamine levels measured by HPLC in such larvae was localized in specific populations of cells. The locations of these cells were consistent with the locations of cells labeled with antibodies to tyrosine hydroxylase (Fig. 5). Immunocytochemistry combined with confocal microscopy, however, revealed larger numbers of cells than did FaGlu histochemistry. The former method presumably labeled a catecholamine-generative enzyme rather than catecholamines themselves, and yielded preparations with lower background fluorescence. Unfortunately, differences in fixative solutions for FaGlu and immunocytochemistry prevented double-labeling of cells in this study. Nonetheless, it remains likely that the cells labeled with FaGlu whose catecholamine contents were increased by L-DOPA treatment were cells that are capable of synthesizing catecholamines, but normally contain concentrations below the level of detection by histochemistry.

The location and morphology of TH-LIR cells hint at mechanisms by which catecholamines might modulate metamorphosis. Several of these cells are located near, and perhaps within, the apical sensory organ, which has been implicated as the chemosensory organ responsible for transduction of the CI stimulus (Kempf *et al.*, 1997; Hadfield *et al.*, 2000). Future studies must further examine the exact locations and morphologies of these cells, since they either may be chemosensory cells themselves or may modulate synaptic interactions between primary chemosensory neurons and postsynaptic cells in a signaling pathway. Dopamine is known to modulate the activity of procerebral olfactory interneurons in the pulmonate mollusc *Limax* *maximus* (Gelperin *et al.*, 1993) as well as several aspects of central olfactory processing in amphibians and mammals (Duchamp-Viret *et al.*, 1997; Doty *et al.*, 1998). One or two pairs of TH-LIR cells were located at the base of the velum, and at least one pair appeared to send an axon distally into the ipsilateral velar lobe. Dopamine inhibits ciliary beating in gill epithelium of the bivalve *Mytilus edulis* (Catapane *et al.*, 1978; Aiello *et al.*, 1986) and also inhibits velar ciliary beating in the larvae of this species (Beiras and Widdows, 1995a). Dopaminergic innervation of the velum of *P. sibogae* might possibly serve to inhibit ciliary beating as part of the settlement response to CI that precedes the initiation of metamorphosis (Hadfield, 1978). Many cells exhibiting TH-LIR and aldehyde-induced histofluorescence were present in the propodium of the foot. These cells possessed apical processes extending to the surface, a characteristic of sensory neurons; in immunocytochemical preparations some of these same cells were also seen to have axonal projections to the pedal ganglia. Similar cells have been labeled by TH-LIR in anterior regions of the foot in embryonic and postembryonic stages of the pulmonate *Lymnaea stagnalis*, and by aldehyde-induced histoflourescene in ventral anterior regions of the foot in pediveligers of the bivalves *Mytilus edulis* and *Placopecten magellanicus* (Croll *et al.*, 1997; Voronezhskaya *et al.*, 1999; Croll *et al.*, 1999). In *P. sibogae* the propodium becomes enlarged around the time of metamorphic competence, mostly due to the development of mucus-secreting glands (Bonar and Hadfield, 1974). Settlement in response to CI is accompanied by secretion of mucus from the foot, and normally there is extensive contact between the propodium and the substratum. Therefore, potentiation of a sensory or motor function of the foot associated with a settlement response to CI is a means by which catecholaminergic cells might promote the initiation of metamorphosis. Sensory neurons in the anterolateral propodial ganglia of veligers of the nudibranch *Onchidoris bilamellata* are depolarized by a soluble settlement cue that is derived from barnacle prey of adult *O. bilamellata* (Chia and Koss, 1989; Arkett *et al.*, 1989). Neither such cells nor such ganglia have been described in veligers of *P. sibogae*, but we cannot rule out the possibility that homologous cells in this species might have a role in chemosensory responses to CI.

Our final set of experiments investigated the relationship between levels of endogenous catecholamines and the onset of metamorphic competence in *P. sibogae*. Under our culture conditions, larvae normally begin to attain competence on day 7; most are competent on day 8, and nearly all are competent on day 10 (Miller and Hadfield, 1986). Previous work had indicated that larval contents of DA and NE increase severalfold during the period of 4 or 5 days between hatching and attainment of maximal competence (Pires *et al.*, 1997). In larvae of the bivalve *Crassostrea gigas*, there is a sharp increase in NE content that coincides with the onset of competence (Coon and Bonar, 1986); in that species, dopamine and norepinephrine have been further implicated in the control, respectively, of settlement and metamorphosis (Coon and Bonar, 1987; Bonar *et al.*, 1990; Beiras and Widdows, 1995b). These observations, together with the correlation of catecholamine enhancement and potentiation of metamorphosis in 9-d larvae in the present study, led us to ask whether the timing of competence in larvae of *P. sibogae* could be influenced by pharmacological enhancement of catecholamines. Larvae aged 6, 7, and 8 d were treated with either a low (5×10^{-7} *M*) or high (10^{-5} *M*) dose of L-DOPA, or with MBL-ASW, then assayed for catecholamine contents (Fig. 6) and for metamorphic response to CI (Fig. 7) as in the first set of experiments. The higher dose was the same as that used in the first set of experiments on 9-d competent larvae and also yielded dramatic increases in contents of catecholamines, especially DA, in younger larvae. Dopamine increased to a similar high level, 1.3–1.5 pmol/larva, in 6-, 7-, and 8-d larvae. These levels greatly exceed the range of values normally found in larvae and juveniles of *P. sibogae* (Pires *et al.*, 1997), and indicate that the ability to convert L-DOPA to DA and store it is already well developed by 6 d. The lower dose of L-DOPA brought about much more modest enhancements of DA and NE within their normal physiological ranges, in most cases close to levels typically found in older (9-d) competent larvae. Frequency of metamorphosis was always very low in 6-d larvae, never exceeding 0.1 even at the highest concentration of CI, and was not significantly affected by either dose of L-DOPA. In 7-d and 8-d larvae the higher dose but not the lower dose of L-DOPA significantly potentiated metamorphosis in response to CI, compared to controls treated with MBL-ASW.

The results of these final experiments clearly indicate that the increases in catecholamine levels that naturally occur around the time of competence, mimicked by exposure to the lower dose of L-DOPA, are not sufficient to confer competence. *Post-hoc* analysis of metamorphosis at each concentration of CI in 7-d and 8-d larvae revealed that the higher dose of L-DOPA significantly increased frequencies of metamorphosis at low concentrations of CI, but not at the highest concentration. After this L-DOPA treatment, the responses of larvae to CI saturated at frequencies of metamorphosis that were not significantly different from the responses of MBL-ASW control larvae to the highest concentration of CI. This suggests that potentiation of metamorphosis by L-DOPA operated mostly in larvae that had already become competent. However, we cannot exclude the possibility that the apparent differences between 10^{-5} *M* L-DOPA and MBL-ASW control treatments at the highest concentration of CI in Figure 7B and C reflect a small positive effect of catecholamine enhancement on the onset of competence.

How might catecholamines modulate metamorphosis in competent larvae of *P. sibogae* in nature? Both DA and NE are very weak inducers of metamorphosis when bath-applied in the absence of CI (Pires and Hadfield, 1991). Therefore it seems unlikely that either of these serves as the major neurotransmitter in a signaling pathway that directly mediates the induction of metamorphosis. The inhibition of coral-induced metamorphosis in larvae depleted of catecholamines by α-MMT (Fig. 3) suggests that catecholaminergic cells may modulate metamorphosis in the sense of gating or enabling (Harris-Warrick, 1988) a primary signaling pathway. This sort of modulatory function has been demonstrated in the serotonergic cerebral giant cells of the pulmonate *Lymnaea stagnalis*, which enable activation of a feeding motor program by other interneurons (Yeoman *et al.*, 1994). Pharmacological depletion of serotonin in this species lowers the proportion of animals that respond to a food stimulus, and increases the latency and diminishes the intensity of responses that do occur (Kemenes *et al.*, 1990). In similar fashion, depletion of catecholamines in modulatory neurons in larvae of *P. sibogae* may lower the proportion of animals that respond to CI.

Potentiation of coral-induced metamorphosis of L-DOPA was observed only after enhancement of catecholamine contents, especially DA, far beyond normal physiological values. Although we have demonstrated that these substances load into specific populations of cells, we remain ignorant of the extent of physiological release of catecholamines in these experiments and of the conditions that favor catecholamine release generally. Indeed, there is evidence in other systems that stored catecholamines are segregated into releasable and non-releasable pools (Kelly, 1993; Reimer *et al.*, 1998). Enhancement of release in L-DOPA-treated larvae would depend both on the presence of some of the elevated catecholamine contents in releasable cellular pools and on the level of activity in those cells. The enhancement of catecholamine release in our experiments may have been much more modest than the enhancement of total catecholamine contents, especially if we did not provide adequate stimuli to evoke activity in the appropriate cells. Under natural conditions, such catecholaminergic modulatory cells, carrying a normal complement of transmitter, might potentiate responses to CI by increasing their activity in the context of sensory cues or behaviors that precede or accompany natural settlement. The activity of serotonergic modulatory cerebral giant cells of adult molluscs has been shown by *in vivo* recording to be strikingly dependent on behavioral context—for example, whether the animal is quiescent, locomoting, or feeding, and whether or not a food stimulus is present (Weiss *et al.*, 1978; Yeoman *et al.*, 1994). Most assays of metamorphic responses to natural inducers in *P. sibogae* and other marine invertebrates have been performed with filtered extracts of inducers in laboratory glassware under static conditions. Intriguingly, responses to CI in larvae of *P. sibogae* are potentiated by mechanical agitation of the assay dishes (Pechenik *et al.*, 1995). More assays that better incorporate the sensory richness of a larva's experience leading up to natural metamorphosis might uncover behavioral contexts that allow modulation of responses to inducers.

Acknowledgments

This work was supported by Dickinson College, Natural Sciences and Engineering Research Council of Canada grant OPG 38863, and U.S. Office of Naval Research grant N00014-95-1-1015.

Literature Cited

Aiello, E., E. Hager, C. Akiwumi, and G. B. Stefano. 1986. An opioid mechanism modulates central and not peripheral dopaminergic control of ciliary activity in the marine mussel *Mytilus edulis*. *Cell. Mol. Neurobiol.* **6:** 17–30.

Arkett, S. A., F.-S. Chia, J. I. Goldberg, and R. Koss. 1989. Identified settlement receptor cells in a nudibranch veliger respond to a specific cue. *Biol. Bull.* **176:** 155–160.

Barlow, L. A. 1990. Electrophysiological and behavioral responses of larvae of the red abalone (*Haliotis rufescens*) to settlement-inducing substances. *Bull. Mar. Sci.* **46:** 537–554.

Beiras, R., and J. Widdows. 1995a. Effects of the neurotransmitters dopamine, serotonin and norepinephrine on the ciliary activity of mussel (*Mytilus edulis*) larvae. *Mar. Biol.* **122:** 597–603.

Beiras, R., and J. Widdows. 1995b. Induction of metamorphosis in larvae of the oyster *Crassostrea gigas* using neuroactive compounds. *Mar. Biol.* **123:** 327–334.

Bernabe, J., E. Proshlyakova, A. Sapronova, A. Trembleau, A. Calas, and M. Ugrumov. 1996. Pharmacological model of catecholamine depletion in the hypothalamus of fetal and neonatal rats and its application. *Cell. Mol. Neurobiol.* **16:** 617–624.

Bonar, D. B., and M. G. Hadfield. 1974. Metamorphosis of the marine gastropod *Phestilla sibogae* Bergh (Nudibranchia: Aeolidacea). I. Light and electron microscopic analysis of larval and metamorphic stages. *L. Exp. Mar. Biol. Ecol.* **16:** 227–255.

Bonar, D. B., S. L. Coon, M. Walch, R. M. Weiner, and W. Fitt. 1990. Control of oyster settlement and metamorphosis by endogenous and exogenous chemical cues. *Bull. Mar. Sci.* **46:** 484–498.

Catapane, E. J., G. B. Stefano, and E. Aiello. 1978. Pharmacological study of the reciprocal dual innervation of the lateral ciliated gill epithelium by the CNS of *Mytilus edulis* (Bivalvia). *J. Exp. Biol.* **74:** 101–113.

Cavanaugh, G. M. 1956. *Formulae and Methods VI of the Marine Biological Laboratory Chemical Room.* Marine Biological Laboratory, Woods Hole, Massachusetts.

Chia, F.-S., and R. Koss. 1989. The fine structure of the newly discovered propodial ganglia of the veliger larva of the nudibranch *Onchidoris bilamellata*. *Cell Tissue Res.* **256:** 17–26.

Coon, S. L., and D. B. Bonar. 1986. Norepinephrine and dopamine content of larvae and spat of the Pacific oyster, *Crassostrea gigas*. *Biol. Bull.* **171:** 632–639.

Coon, S. L., and D. B. Bonar. 1987. Pharmacological evidence that alpha-1 adrenoceptors mediate metamorphosis of the Pacific oyster *Crassostrea gigas*. *Neuroscience* **23:** 1169–1174.

Couper, J. M., and E. M. Leise. 1996. Serotonin injections induce metamorphosis in larvae of the gastropod mollusc *Ilyanassa obsoleta*. *Biol. Bull.* **191:** 178–186.

Croll, R. P., and B. J. Chiasson. 1990. Distribution of catecholamines and of immunoreactivity to substances like vertebrate enzymes for the synthesis of catecholamines within the central nervous system of the snail, *Lymnaea stagnalis*. *Brain Res.* **525:** 101–114.

Croll, R. P., D. L. Jackson, and E. E. Voronezhskaya. 1997. Catecholamine-containing cells in larval and postlarval bivalve molluscs. *Biol. Bull.* **193:** 116–124.

Croll, R. P., E. E. Voronezhskaya, L. Hiripi, and K. Elekes. 1999. Development of catecholaminergic neurons in the pond snail, *Lymnaea stagnalis:* II. Postembryonic development of central and peripheral neurons. *J. Comp. Neurol.* **404:** 297–309.

Doty, R. L., C. Li, R. Bagla, W. Huang, C. Pfeiffer, G. M. Brosvic, and J. M. Risser. 1998. SKF 38393 enhances odor detection performance. *Psychopharmacology* **136:** 75–82.

Duchamp-Viret, P., V. Coronas, J. C. Delaleu, E. Moyse, and A. Duchamp. 1997. Dopaminergic modulation of mitral cell activity in the frog olfactory bulb: a combined radioligand binding-electrophysiological study. *Neuroscience* **79:** 203–216.

Elekes, K., G. Kemenes, L. Hiripi, M. Geffard, and P. R. Benjamin. 1991. Dopamine-immunoreactive neurons in the central nervous system of the pond snail *Lymnaea stagnalis*. *J. Comp. Neurol.* **37:** 214–224.

Froggett, S. J., and E. M. Leise. 1991. Metamorphosis in the marine snail *Ilyanassa obsoleta*, yes or NO? *Biol. Bull.* **196:** 57–62.

Furness, J. B., M. Costa, and W. W. Blessing. 1977. Simultaneous fixation and production of catecholamine fluorescence in central nervous tissue by perfusion with aldehydes. *Histochem. J.* **9:** 745–750.

Gelperin, A., L. D. Rhines, J. Flores, and D. W. Tank. 1993. Coherent network oscillations by olfactory interneurons: modulation by endogenous amines. *J. Neurophysiol.* **69:** 1930–1939.

Gibson, G. 1995. Why be choosy? Temporal changes in larval sensitivity to several naturally-occurring metamorphic inducers in the opisthobranch *Haminaea callidegenita*. *J. Exp. Mar. Biol. Ecol.* **194:** 9–24.

Giloh, H., and J. W. Sedat. 1982. Fluorescence microscopy: reduced photobleaching of rhodamine and fluorescein protein conjugates by *n*-propyl gallate. *Science* **217:** 1252–1255.

Hadfield, M. G. 1978. Metamorphosis in marine molluscan larvae: an analysis of stimulus and response. Pp. 165–175 in *Settlement and Metamorphosis of Marine Invertebrate Larvae*, F.-S. Chia and M. Rice, eds. Elsevier/North-Holland, New York.

Hadfield, M. G., and J. T. Pennington. 1990. Nature of the metamorphic signal and its internal transduction in larvae of the nudibranch *Phestilla sibogae*. *Bull. Mar. Sci.* **46:** 455–464.

Hadfield, M. G., and D. Scheuer. 1985. Evidence for a soluble metamorphic inducer in *Phestilla sibogae:* ecological, chemical and biological data. *Bull. Mar. Sci.* **37:** 556–566.

Hadfield, M. G., and M. F. Strathmann. 1996. Variability, flexibility and plasticity in life histories of marine invertebrates. *Oceanol. Acta* **19:** 323–334.

Hadfield, M. G., E. A. Meleshkevitch, and D. Y. Boudko. 2000. The apical sensory organ of a gastropod veliger is a receptor for settlement cues. *Biol. Bull.* **198:** 67–76.

Harris-Warrick, R. M. 1988. Chemical modulation of central pattern generators. Pp. 285–331 in *Neural Control of Rhythmic Movements in Vertebrates*, A. H. Cohen, S. Rossignol, and S. Grillner, eds. Wiley, New York.

Hernadi, L., S. Juhos, and K. Elekes. 1993. Distribution of tyrosine-hydro[illegible] immunoreactive and dopamine-immunoreactive neurons in the [illegible] system of the snail, *Helix pomatia*. *Cell Tissue Res.* **274:** [illegible]

Kabotyanski, E. A., D. A. Baxter, and J. H. Byrne. 1998. Identification and characterization of a catecholaminergic neuron B65, which initiates and modifies [illegible] in the buccal ganglia of *Aplysia*. *J. Neurophysiol.* **79:** [illegible]

Katz, P. S. 1995. [illegible] and extrinsic neuromodulation of motor circuits. *Curr. Opin.* [illegible] **5:** 799–808.

Kelly, R. B. 1993. Storage and release of neurotransmitters. *Cell 72/Neuron* **10** **suppl.:** 43–53.

Kemenes, G., L. Hiripi, and P. R. Benjamin. 1990. Behavioural and biochemical changes in the feeding system of *Lymnaea* induced by the dopamine and serotonin neurotoxins 6-hydroxydopamine and 5,6-dihydroxytryptamine. *Philos. Trans. R. Soc. Lond. B Biol. Sci.* **329:** 243–255.

Kempf, S. C., and M. G. Hadfield. 1985. Planktotrophy by the lecithotrophic larvae of a nudibranch, *Phestilla sibogae* (Gastropoda). *Biol. Bull.* **169:** 119–130.

Kempf, S. C., G. Y. Chun, and M. G. Hadfield. 1992. An immunocytochemical search for potential neurotransmitters in larvae of *Phestilla sibogae* (Gastropoda, Opisthobranchia). *Comp. Biochem. Physiol.* **101C:** 299–305.

Kempf, S. C., L. R. Page, and A. Pires. 1997. Development of serotonin-like immunoreactivity in the embryos and larvae of nudibranch mollusks with emphasis on the structure and possible function of the apical sensory organ. *J. Comp. Neurol.* **386:** 507–528.

Miller, S. E., and M. G. Hadfield. 1986. Ontogeny of phototaxis and metamorphic competence in larvae of the nudibranch *Phestilla sibogae* Bergh (Gastropoda: Opisthobranchia). *J. Exp. Mar. Biol. Ecol.* **97:** 95–112.

Norekyan, T. P., and R. Satterlie. 1993. Neuronal analysis of hunting behavior of the pteropod mollusc *Clione limacina*. *Neurosci. Behav. Physiol.* **23:** 11–23.

Pechenik, J. A. 1990. Delayed metamorphosis by larvae of benthic marine invertebrates: Does it occur? Is there a price to pay? *Ophelia* **32:** 63–94.

Pechenik, J. A., M. G. Hadfield, and L. S. Eyster. 1995. Assessing whether larvae of the opisthobranch gastropod *Phestilla sibogae* Bergh become responsive to three chemical cues at the same age. *J. Exp. Mar. Biol. Ecol.* **191:** 1–17.

Pechenik, J. A., K. Hammer, and C. Weise. 1996. The effect of starvation on acquisition of competence and postmetamorphic performance in the marine prosobranch gastropod *Crepidula fornicata*. *J. Exp. Mar. Biol. Ecol.* **199:** 137–152.

Pires, A., and M. G. Hadfield. 1991. Oxidative breakdown products of catecholamines and hydrogen peroxide induce partial metamorphosis in the nudibranch *Phestilla sibogae* Bergh (Gastropoda: Opisthobranchia). *Biol. Bull.* **180:** 310–317.

Pires, A., S. L. Coon, and M. G. Hadfield. 1997. Catecholamines and dihydroxyphenylalanine in metamorphosing larvae of the nudibranch *Phestilla sibogae* Bergh. *J. Comp. Physiol. A* **181:** 187–194.

Quinlan, E. M., B. C. Arnett, and A. D. Murphy. 1997. Feeding stimulants activate an identified dopaminergic interneuron that induces the feeding motor program in *Helisoma*. *J. Neurophysiol.* **78:** 812–824.

Reimer, R. J., E. A. Fon, and R. H. Edwards. 1998. Vesicular neurotransmitter transport and the presynaptic regulation of quantal size. *Curr. Opin. Neurobiol.* **8:** 405–412.

Trapido-Rosenthal, H., and D. E. Morse. 1985. L-α, ω-diamino acids facilitate GABA induction of larval metamorphosis in a gastropod mollusc (*Haliotis rufescens*). *J. Comp. Physiol. B* **155:** 403–414.

Trapido-Rosenthal, H., and D. E. Morse. 1986a. Availability of chemosensory receptors is down-regulated by habituation of larvae to a morphogenetic signal. *Proc. Natl. Acad. Sci. USA* **83:** 7658–7662.

Trapido-Rosenthal, H., and D. E. Morse. 1986b. Regulation of receptor-mediated settlement and metamorphosis in larvae of a gastropod mollusc (*Haliotis rufescens*). *Bull. Mar. Sci.* **39:** 383–392.

Trimble, D. L., and D. L. Barker. 1984. Activation by dopamine of patterned motor output from the buccal ganglia of *Helisoma trivolvis*. *J. Neurobiol.* **15:** 37–48.

Uretsky, N. J., S. R. Snodgrass, and A. V. Lorenzo. 1975. Studies on the mechanism of depletion of striatal dopamine by α-methyl-*m*-tyrosine. *J. Pharmacol. Exp. Ther.* **195:** 465–479.

Voronezhskaya, E. E., L. Hiripi, K. Elekes, and R. P. Croll. 1999. Development of catecholaminergic neurons in the pond snail, *Lymnaea stagnalis:* I. Embryonic development of dopamine-containing neurons and dopamine-dependent behaviors. *J. Comp. Neurol.* **404:** 285–296.

Weiss, K. R., J. L. Cohen, and I. Kupfermann. 1978. Modulatory control of buccal musculature by a serotonergic neuron (metacerebral cell) in *Aplysia. J. Neurophysiol.* **41:** 181–203.

Wieland, S. J., and A. Gelperin. 1983. Dopamine elicits feeding motor program in *Limax maximus. J. Neurosci.* **3:** 1735–1745.

Yeoman, M. S., A. W. Pieneman, G. P. Ferguson, A. Ter Maat, and P. R. Benjamin. 1994. Modulatory role for the serotonergic cerebral giant cells in the feeding system of the snail, *Lymnaea.* I. Fine wire recording in the intact animal and pharmacology. *J. Neurophysiol.* **72:** 1357–1371.

Zimmerman, K. M., and J. A. Pechenik. 1991. How do temperature and salinity affect relative rates of growth, morphological differentiation, and time to metamorphic competence in larvae of the marine gastropod *Crepidula plana*? *Biol. Bull.* **180:** 372–386.

Zolman, J. F. 1993. *Biostatistics: Experimental Design and Statistical Inference.* Oxford University Press, New York.

Reference: *Biol. Bull.* **198:** 332–345. (June 2000)

Induction of Metamorphosis in the Sea Urchin *Holopneustes purpurascens* by a Metabolite Complex From the Algal Host *Delisea pulchra*

JANE E. WILLIAMSON*, ROCKY DE NYS, NARESH KUMAR[1], DAVID G. CARSON, AND PETER D. STEINBERG

School of Biological Science and Centre for Marine Biofouling & Bio-Innovation, and
[1]School of Chemistry, University of New South Wales, Sydney 2052, Australia

Abstract. Most benthic invertebrates have complex life cycles with planktonic larvae that return to the substratum to settle and metamorphose into a benthic stage. Although naturally produced chemical cues have long been thought to be important for the settlement or metamorphosis of invertebrate larvae, few ecologically relevant chemical cues have been clearly identified. The marine echinoid *Holopneustes purpurascens* has a complex life cycle, with a planktonic, nonfeeding dispersive larva that metamorphoses into a benthic stage that lives in the canopy of subtidal benthic algae such as the red alga *Delisea pulchra* and the kelp *Ecklonia radiata*. Recently recruited juveniles are found primarily on *D. pulchra*, and we hypothesized that this was in response to a chemical cue produced by this alga. Competent larvae metamorphosed in the presence of *D. pulchra*, or seawater surrounding this alga, but not in response to the presence of *E. radiata* or its extracts. A cue for metamorphosis was isolated and characterized from *D. pulchra* and found to be a water-soluble complex of the sugar floridoside and isethionic acid in a 1:1 molar ratio. The floridoside–isethionic acid complex also triggered settlement in *H. purpurascens;* however, this response was less specific than metamorphosis and was reversible. Larvae of *H. purpurascens* also metamorphosed in the presence of several other species of red, but not brown or green, algae from their habitat. Floridoside is found only in red algae, suggesting that the floridoside–isethionic acid complex may be acting as a cue for metamorphosis in other red algae as well as in *D. pulchra.*

Introduction

A fundamental problem in marine biology and ecology is understanding the demography of organisms with complex life histories in which planktonic and benthic stages occur in spatially distinct habitats (Pechenik, 1999). In particular, the question of how a planktonic larva that has dispersed through the water column since fertilization finds an appropriate benthic habitat for metamorphosis and the resumption of the benthic stage has been a central theme in the study of marine invertebrates for over 40 years (Thorson, 1950; Butman, 1987; Roughgarden *et al.*, 1988; Pawlik, 1992; McEdwards, 1995).

The current view of this issue is that successful recruitment of larvae back to the benthos is the result of a mixture of processes. Hydrodynamic processes are thought to dominate at larger scales, by controlling whether larvae are deposited at a suitable area when competent. Environmental cues are thought to become progressively more important at smaller spatial scales, such as finding a specific site or habitat within the area (Scheltema, 1986; Young and Chia, 1987; Butman *et al.*, 1988). These environmental cues may be physical, biological, or chemical (Svane and Young, 1989; Pawlik, 1992; McEdwards, 1995), but chemical cues in particular have received considerable attention in the literature. For many species, chemical cues associated with substrata appear to be of primary importance to competent larvae just prior to settling and metamorphosing (Burke, 1983; Pawlik and Hadfield, 1990; Pawlik, 1992).

Although there has been considerable screening of chemical compounds as potential cues that induce settlement and metamorphosis of marine invertebrates, few studies have definitively identified (characterized) chemical inducers for

Received 8 July 1999; accepted 4 April 2000.

* To whom correspondence should be addressed. E-mail: j.williamson@unsw.edu.au

these processes. Moreover, the ecological relevance of many inducers is not always clear. The majority of research in this area has focused on the effects of exogenous (to the target organism) metabolites, *e.g.* "artificial" inducers *sensu* Pawlik (1992). Examples include γ-aminobutyric acid (GABA) (Morse *et al.*, 1979), L-β-3,4-dihydroxyphenylalanine (L-DOPA) (Coon and Bonar, 1987), and epinephrine (Coon *et al.*, 1986), which have not been shown to occur naturally in the system being examined but are thought to act in a manner similar to those that do. The few studies that have identified putative naturally occurring inducers have either not characterized the compound or lacked data to support their ecological relevance (*e.g.*, Yvin *et al.*, 1985); that is, the presence of the inducer did not relate to the recruitment pattern of the organism (although see Tsukamato *et al.*, 1999).

The sea urchin *Holopneustes purpurascens* is an endemic Australian echinoid that lives in shallow subtidal waters. This urchin is atypical of echinoids because it inhabits the canopy of its two main host plants, *Delisea pulchra* and *Ecklonia radiata*, using the algae that it consumes as a habitat as well as a source of food (Steinberg, 1995). Thus, its distribution across habitats is tightly coupled with restrictions in diet breadth. Since both species of host algae are rich in secondary metabolites (Steinberg, 1989; van Altena and Steinberg, 1992; de Nys *et al.*, 1993), it was hypothesized that competent larvae may recruit to these hosts in response to a specific chemical settlement or metamorphosis cue.

In this study, we assess the response of competent larvae of *H. purpurascens* to potential chemical inducers from its host algae. Since such chemical cues can be either aggregative (released by conspecifics: Crisp, 1974; Burke, 1986) or associative (released by non-conspecifics such as host plants: Pawlik, 1992), we first determined whether *H. purpurascens* was settling or metamorphosing in response to cues associated with newly recruited conspecifics. The response of *H. purpurascens* larvae to algae (and their metabolites) associated with the urchin's habitat was then assessed. Where there was an indication of a potential positive inducer, this cue was isolated and identified through a series of bioassay-guided fractionations. Once the inducer had been isolated and identified, conditioned seawater was collected *in situ* and also tested to determine whether an inducer was present in the field. Finally, other algae in the habitat were tested for their ability to induce metamorphosis of larvae of *H. purpurascens*.

Materials and Methods

Study site and animal

This study was done in sublittoral habitats (3–5 m depth) at Bare Island (33° 59′ 38″ S, 151° 14′ 00″ E) at the north head of Botany Bay, Sydney, Australia. Bare Island is a mosaic of habitats typical of shallow subtidal areas in temperate southeastern Australia. Adult *Holopneustes purpurascens* (Temnopleuridae: Echinodermata) at this site are principally found on laminae of the kelp *Ecklonia radiata* (Laminariales: Phaeophyta) and in the fronds of the red foliose alga *Delisea pulchra* (Bonnemaisonales: Rhodophyta). Steinberg (1995) further describes some aspects of the ecology of *H. purpurascens* in these habitats.

Size distribution and abundance of Holopneustes purpurascens *on host plants*

Size distributions of *H. purpurascens* on individual plants of *D. pulchra* and *E. radiata* at Bare Island were assessed by measuring the maximum test diameter to the nearest millimeter of all *H. purpurascens* present *in situ* within an area of 10 m^2. Sampling was done during March (autumn) 1996 and repeated in September (spring) 1996; the data from both seasons were pooled. The size of urchins between the two host plants was compared with a two-tailed unpaired Student's *t* test.

The abundance of *H. purpurascens* on *D. pulchra* and *E. radiata* was also measured at Bare Island during March (autumn) 1996. Abundance was measured as the number of urchins per plant. The data was first tested for heterogeneity of variance using a Cochran's test (Winer, 1971) before analyzing differences in abundance between host plants with a one-factor analysis of variance (ANOVA).

Culture of larvae

All larval assays of *H. purpurascens* were done with larvae reared in the laboratory at the University of New South Wales, Australia. Larval cultures were established using gametes from several male and female urchins, obtained by intracoelomic injections with 3–5 ml (depending on their size) of 0.5 *M* KCl to induce spawning (Pennington, 1985; Levitan *et al.*, 1992). Viable eggs were fertilized immediately and washed twice (~15 min between adding sperm and washing) in sterile filtered seawater. This seawater had passed through a 0.2-μm filter, been autoclaved overnight, and had 36.5 mg l^{-1} streptomycin and 21.9 mg l^{-1} penicillin added to it. Fertilization success was determined as the percentage of eggs that had raised vitelline membranes. In all cases, at least 95% of the eggs were fertilized. Fertilized eggs were maintained in 2-l glass beakers at a maximum density of 100 eggs ml^{-1} until hatching, when this density was reduced to about 5 larvae ml^{-1}. Throughout their development, cultures were kept at 18°C in a 12-h light/12-h dark regime with a slow bubbling of filtered air. The seawater was changed every 24 h, and abnormal larvae (as determined by microscopy) were removed. Larvae reached competency (recognized by the presence of five well-developed tube feet) within 6 days, and those that had just developed competency were used in assays.

Initially, both settlement and metamorphosis were assessed. However, settlement for *H. purpurascens* is a reversible process in which the larvae cease swimming, cling to the substratum using their tube feet, and appraise the suitability of the substrate for metamorphosis. Metamorphosis in *H. purpurascens* is an irreversible developmental process in which the larvae change from bilateral to radial symmetry. Thus, metamorphosis is a clear transition from the planktonic stage to the benthic stage in the urchin's life history. Therefore, following initial experiments, assays focused on metamorphosis as an end point. In all experiments, percent metamorphosis was determined after a designated time interval (usually 24 h), and calculated as the number of larvae metamorphosed relative to the total number of replicate larvae for that treatment. Following experiments demonstrating that larval metamorphosis was not aggregative (below), all assays used one larva per replicate petri dish (40-mm diameter) in 5 ml of sterile filtered seawater (to maintain replicate dishes while minimizing the number of larvae needed).

Larval response to conspecifics

To determine whether settlement or metamorphosis of *H. purpurascens* was aggregative, larvae were exposed to treatments containing newly metamorphosed (7 days old) conspecifics in two densities and water that had been conditioned by adult conspecifics. Newly metamorphosed conspecifics were reared in the laboratory (see section above) and metamorphosed in bulk in the presence of pieces of *D. pulchra* 7 days prior to the start of the experiment. These individuals were then transferred to two 2-l glass beakers containing sterile filtered seawater, which was changed daily, and a continuous flow of filtered air. Metamorphosed individuals were identified on the day of the experiment by their change in shape, the presence of chromatophores, the start of spine development, and their active behavior. At the start of the experiment, one competent larva was added to treatments containing either one or five of these newly metamorphosed conspecifics in glass petri dishes with 5 ml of sterile filtered seawater.

Water conditioned by adult *H. purpurascens* was prepared by collecting 16 healthy mature urchins (20–45 mm diameter) from Bare Island and, in the laboratory, immersing each individual in 500 ml sterile filtered seawater for 3 h. Five millilitres of this conditioned seawater (containing no particulate matter) was then removed from each of the 500-ml replicates (16 in total) and added to a separate petri dish.

One competent larva was added to each replicate petri dish for each of the three treatments (the two densities of new recruits and adult conditioned water) and replicate controls of sterile filtered seawater. The controls (sterile filtered seawater) were included as a measure of settlement or metamorphosis in the absence of a cue. The percentage of larvae that had settled or metamorphosed after 24 h was analyzed using a chi-squared goodness-of-fit test, a sample statistic based on discrete frequencies (Sokal and Rohlf, 1995; pp. 695–696).

Larval response to extracts of Delisea pulchra *and* Ecklonia radiata

We investigated chemical cues from algae by examining whether larvae of *H. purpurascens* would preferentially settle or metamorphose in response to metabolites extracted from its host algae *D. pulchra* and *E. radiata*. Both water-soluble (polar) and lipid-soluble (nonpolar) extracts of the algae were investigated. To prepare extracts, each alga (~10 g wet weight) was collected from Bare Island and blotted dry, epiphytes and epifauna were removed, and the thallus was exhaustively extracted in methanol (MeOH). The extracts were filtered and reduced *in vacuo* at 50°C prior to partitioning between water (MilliQ) and dichloromethane (DCM). The concentrated polar extract of each alga was prepared by reducing the water-soluble fraction *in vacuo* to a volume of 10 ml. The nonpolar extract of each alga was prepared by reducing the DCM-soluble fraction to dryness *in vacuo*.

The polar extracts from *D. pulchra* were tested at final concentrations of 10 μl and 1 μl ml^{-1} in 5 ml of seawater, and the nonpolar extracts were tested at 1 μg ml^{-1} and 100 ng ml^{-1} in 5 ml of sterile filtered seawater (higher concentrations were not tested because they caused abnormal behavior in the larvae). The polar and nonpolar extracts of *E. radiata* were tested in 5 ml of sterile filtered seawater at the highest concentrations of 10 μl ml^{-1} and 1 μg ml^{-1} respectively. Solutions of crude nonpolar extract were made by dissolving the extract in dimethylsulfoxide (DMSO; 60 μl mg^{-1} of extract) and diluting to the above concentrations in sterile filtered seawater. The maximum concentration of DMSO in the extracts was 0.006%, and DMSO at this concentration was used as a control in the assays for the nonpolar extracts. MilliQ water (10 μl ml^{-1}) was included as a control for the assays with polar extracts, and sterile filtered seawater was used as a further control for both extracts. *D. pulchra* (15 mg per replicate) was included as a treatment to ensure that the larvae were competent to metamorphose (a "positive" control). One competent larva of *H. purpurascens* was added to each replicate petri dish (n = 10 dishes per treatment) and the percent settlement and metamorphosis of larvae was recorded over time. Data after 20 h were analyzed with chi-squared goodness-of-fit tests as before.

Isolation and identification of the settlement inducer from Delisea pulchra

To isolate and characterize the active inducer, *D. pulchra* (~1 kg wet weight) was collected from Bare Island, and the extract was prepared as above. The polar and nonpolar phases were separated, and the water fraction was retained and evaporated to dryness *in vacuo*. The dried, crude polar extract was redissolved in absolute ethanol (AR) and re-dried. This process was repeated twice. Analysis by ^{1}H and ^{13}C nuclear magnetic resonance (NMR) spectroscopy indicated that the resultant extract was predominantly composed of sugars. Fractionation of the extract by reversed-phase high-performance liquid chromatography (HPLC; Adsorbosil C18 @ 5 μm; 250 mm × 7.8 mm, Waters R410 RI detector) (100% MeOH, 2 ml min^{-1}) afforded two products: [1] and [2]. ^{1}H and ^{13}C NMR data and high field two-dimensional NMR studies (COSYDQF, HMBC and NOESY) (d_4 MeOH, Bruker DMX 500 NMR) were used to identify [1] and [2].

Larval response to isolated metabolites

The two products of the separation of the polar extract—[1] and [2]—were made up as stock solutions in MilliQ water, and aliquots were added to assay dishes to give final concentrations of 25 μM and 2.5 μM. MilliQ water (10 μl ml^{-1}) and sterile filtered seawater were used as controls. *D. pulchra* (15 mg per replicate) was included as a treatment as a measure of the competency of the larvae. One larva of *H. purpurascens* was added to each replicate petri dish (n = 12 dishes per treatment), and the percent metamorphosis of larvae was recorded over time. Metamorphosis after 5 h was analyzed with a chi-squared goodness-of-fit test as before.

Larval response to isolated and synthetic inducers

To confirm the activity of the floridoside-isethionic acid complex [1] as an inducer of metamorphosis, a synthetic floridoside–isethionic acid complex was prepared. Floridoside [α-D-galactopyranosyl-(1-2)-glycerol] was isolated following a modification of the method of Karsten *et al.* (1993). *D. pulchra* was collected from Bare Island and oven dried at 80°C. The dried tissue (179.4 g) was extracted with 1 l of 70% ethanol (v/v) overnight in a water bath at 70°C. The extract was reduced *in vacuo* and partitioned between water and ethyl acetate. The aqueous phase was reduced *in vacuo*, redissolved in absolute ethanol (AR), and subsequently taken to dryness. This residue was redissolved in MilliQ water (100 ml) and passed through a column of AG50WX2 (H$^+$ form) ion-exchange resin (Bio-Rad). Four fractions of 25 ml each were collected and analyzed by ^{1}H and ^{13}C NMR spectroscopy. Subsequently, the first two fractions were passed through a column of AG1X8 (OH$^-$ form) ion-exchange resins (Bio-Rad). The eluted fractions were combined and evaporated to dryness *in vacuo* to yield floridoside as colorless prisms. The ^{1}H and ^{13}C NMR data for floridoside agreed with the reported spectroscopic data (Karsten *et al.*, 1993). Isethionic acid was prepared by passing a solution of sodium isethionate (Aldrich) in MilliQ water through a column of AG50WX2 (H$^+$ form) ion-exchange resin. Purity was confirmed by comparison of ^{1}H and ^{13}C NMR data (Barrow *et al.*, 1993). Equimolar amounts of floridoside and isethionic acid were mixed in a reacti-vial and allowed to stand in a water bath overnight at 55°C prior to being used in the bioassay.

All compounds—[1], the synthetic floridoside–isethionic acid complex, floridoside [2], and isethionic acid—were made up in 10 mg ml^{-1} stock solutions in MilliQ water, and aliquots were added to treatment dishes to give a final concentration in the bioassay of 200 μM. MilliQ water and seawater controls were incorporated in the assay. *D. pulchra* (15 mg per replicate) was used as a positive measure of competency of the larvae. For the assay, one larva of *H. purpurascens* was added to each replicate petri dish (n = 10 dishes per treatment), and the percent metamorphosis of larvae was recorded over time. Data were analyzed with chi-squared goodness-of-fit tests as before.

Concentration-dependent response of larvae to the floridoside-isethionic acid complex

The response of competent larvae of *H. purpurascens* to a concentration gradient of [1] was tested to determine the minimum concentration for the induction of metamorphosis. [1] was tested at six concentrations: 125, 62.5, 25, 12.5, 2.5, and 1.25 μM. The complex [1] was made up in a 10 mg ml^{-1} stock solution in MilliQ water, and aliquots were added to treatment dishes with 0.45-μm filtered seawater to give the six concentrations in the assay. MilliQ water and seawater controls also were incorporated as treatments (*i.e.*, controls) in the assay. *D. pulchra* (15 mg per replicate) was again used as a positive measure of competency of the larvae. One larva of *H. purpurascens* was added to each replicate petri dish (n = 12 dishes per treatment), and the percent metamorphosis of larvae recorded over time. Metamorphosis after 6 h was analyzed with chi-squared goodness-of-fit tests as before.

Larval response to conditioned seawater collected in situ

Seawater samples were collected from Bare Island on a calm, sunny November afternoon to test for the *in situ* presence of a waterborne cue associated with *D. pulchra*. Plastic syringes were used to collect seawater from within 0.5 cm of fronds of *D. pulchra* and laminae of *E. radiata* but without touching the plants, and from the water column more than 2 m distant from any macroalgae. Samples (5 ml) were immediately transferred into glass vials and stored in the dark until the start of the experiment (~3 h later). Each sample was added to a separate petri dish (n = 10 dishes per treatment), along with one competent larva of *H. purpurascens*. Sterile filtered seawater controls were used in the assay as controls, and the percent metamorphosis of larvae was recorded over time.

Larval response to subtidal algae

Two replicate assays were done with *H. purpurascens* to determine whether larvae metamorphose in response to associative cues from other local species of algae, including a range of red algae. Ten species of subtidal algae, including the two common host plants of *H. purpurascens*, were collected from Bare Island on two occasions (November 1997 and February 1998), including six species of red algae: *Delisea pulchra*, *Laurencia rigida*, *Solieria robusta*, *Corallina officinalis*, *Amphiroa anceps*, *Pterocladiella capillacea;* two species of brown algae: *Ecklonia radiata*, *Sargassum linearifolium;* and two species of green algae: *Caulerpa filiformis* and *Ulva* sp. For each collection, the algae were brought back to the laboratory and 15 mg of the tip of each plant that was free of epiphytes and epifauna was removed and used in the assay. Each replicate (n = 12 dishes per treatment) consisted of the tip of one type of alga in 5 ml of sterilized filtered seawater in a glass petri dish. The response of larvae to sterile filtered seawater was used as a control. One competent larva of *H. purpurascens* was added to each replicate petri dish, and the percent metamorphosis of larvae was recorded after 24 h. For species of algae that induced metamorphosis, data comparing dates of collection were analyzed with a chi-squared goodness-of-fit test as before.

Results

Size distribution and abundance of Holopneustes purpurascens *on host plants*

The size distribution of *Holopneustes purpurascens* on its two main hosts differed significantly (Fig. 1). Of the 272 urchins found on *Delisea pulchra* and the 276 urchins on *Ecklonia radiata*, those inhabiting *D. pulchra* were significantly smaller than those found on *E. radiata* (unpaired t test, $t = 4.30$, $P < 0.001$). No urchins in the smallest size class (0–5 mm, reflecting new or recent recruits) were found on *E. radiata*, and small urchins in general (6–20 mm) were extremely rare on *E. radiata* (Fig. 1). Conversely, large urchins (>40 mm) were relatively scarce on *D. pulchra*, constituting only 5.1% of all observations made, compared to 73% of the total observations made on *E. radiata*. The abundance of *H. purpurascens* on *D. pulchra* and *E. radiata*, however, did not differ (one-factor ANOVA, $F_{1,38} = 2.023$, $P = 0.163$; untransformed data).

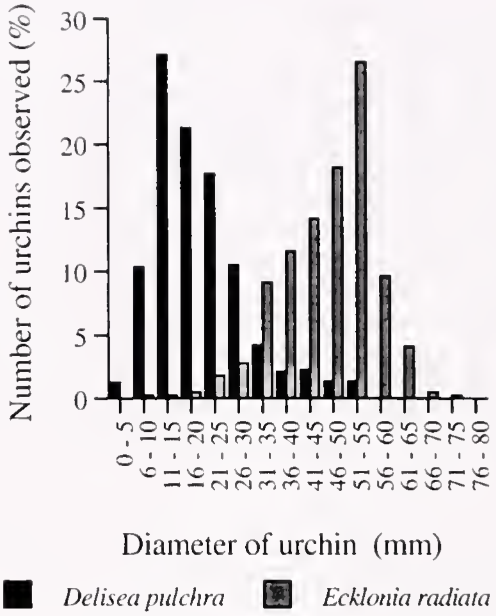

Figure 1. Size distributions of *Holopneustes purpurascens* on randomly selected plants of *Delisea pulchra* (number of urchins (n) = 272) and *Ecklonia radiata* (n = 276) at Bare Island, pooled over two seasons.

Larval response to conspecifics

No significant settlement or metamorphosis was observed after 24 h for competent larvae of *H. purpurascens* that were exposed to newly metamorphosed conspecifics or to water conditioned by adult conspecifics ($X^2 = 4.68$, 2 df, $P = 0.086$). No metamorphosis was observed in any of the treatments or controls, and of the 16 replicates, only one replicate larva had settled in the presence of one new recruit and two replicate larvae had settled in the presence of two new recruits. After 48 h, settlement was reduced to one individual in the presence of one new recruit. We concluded that settlement or metamorphosis in *H. purpurascens* was not aggregative, and subsequent assays were done with one larva per replicate petri dish.

Larval response to extracts of Delisea pulchra *and* Ecklonia radiata

There were significant differences in the response of larval *H. purpurascens* to the different extracts. All larvae that had been exposed to polar extracts from *D. pulchra* settled within the first 3 h of the experiment at both concentrations, whereas larvae exposed to pieces of *D. pulchra* settled after 7 h (Fig. 2A). These treatments had the highest final amount of settlement (Fig. 2A). Settlement of larvae exposed to nonpolar extracts from *D. pulchra* did occur, but this response was not constant over time and was significantly less than for polar treatments at the end of the assay ($X^2 = 21.95$, 3 df, $P < 0.001$). Although an initial settlement response occurred in the presence of pieces of *E.*

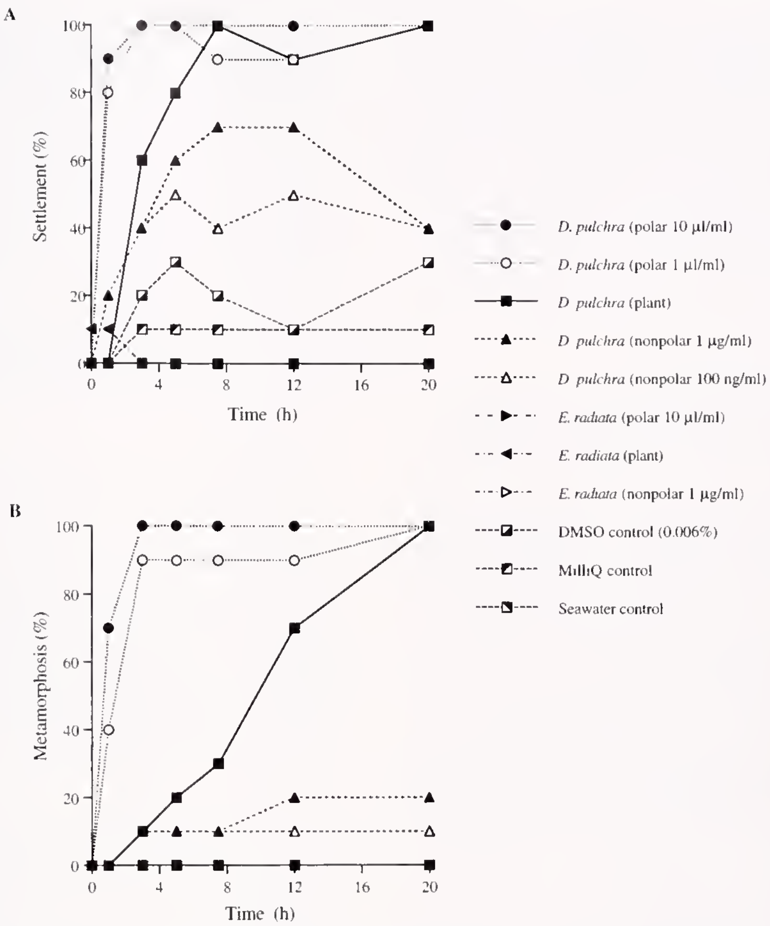

Figure 2. Percent (A) settlement and (B) metamorphosis over time of competent *Holopneustes purpurascens* (one larva per replicate; 10 replicates per treatment) when exposed to pieces of *Delisea pulchra* (15 mg per replicate) and its polar and nonpolar extract fractions. Controls of MilliQ water and sterile, filtered seawater were used.

radiata, no settlement occurred in response to its polar or nonpolar extracts. At the end of the assay, no significant difference in settlement was observed between larvae exposed to treatments containing *E. radiata*, and the MilliQ and seawater controls ($X^2 = 10.67$, 5 df, $P = 0.058$).

Larval *H. purpurascens* metamorphosed in response to extracts from *D. pulchra* but not those from *E. radiata* (Fig. 2B). After 20 h, all larvae of *H. purpurascens* had metamorphosed in the presence of pieces of *D. pulchra* and its polar extract, regardless of concentration (Fig. 2B). The polar extracts at both concentrations induced metamorphosis at a faster rate than did pieces of the alga. All larvae exposed to polar extracts from *D. pulchra* at 10 μl ml^{-1}, and the majority of larvae exposed to polar extracts from *D. pulchra* at 1 μl ml^{-1}, metamorphosed within 3 h (Fig. 2B). Nonpolar extracts from *D. pulchra* also induced a low percentage of metamorphosis; however, this rate was significantly lower than that for both polar extracts (20 h: $X^2 = 38.04$, 3 df, $P < 0.001$; Fig. 2B) and may have been due to small residual amounts of polar metabolites remaining in these nonpolar extracts. No metamorphosis occurred in the controls.

Isolation and identification of the settlement inducer from Delisea pulchra

The polar fraction of *D. pulchra* yielded two metabolites [1] and [2] (Fig. 3). The ^{1}H and ^{13}C NMR data for [1] corresponded to previously published data for floridoside [α-D-galactopyranosyl-(1-2)-glycerol] (Karsten *et al.*, 1993) and isethionic acid (Barrow *et al.*, 1993) in 1:1 integral ratios (Fig. 3). Spectroscopic data for [2] corresponded to floridoside [α-D-galactopyranosyl-(1-2)-glycerol] (Fig. 3). We were unable to further separate [1] using standard chromatographic techniques. High field two-dimensional NMR studies (COSYDQF, HMBC and NOESY) of [1] showed correlations between the proton and carbon signals identified as those for floridoside and isethionic acid respec-

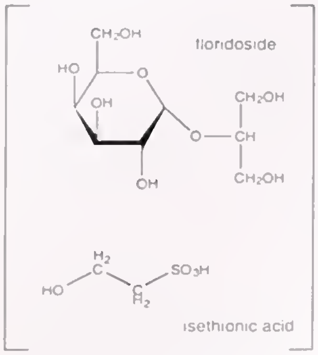

[1]

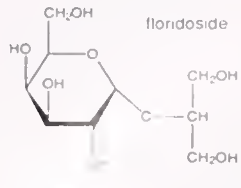

[2]

Figure 3. Structures of the floridoside and isethionic acid complex [1] and of floridoside [2].

tively within the spectra for [1]; however, there were no correlations between signals for the two compounds. Furthermore, floridoside and isethionic acid were separately spiked into [1] in d_4 MeOH, and the mixture was analyzed by ^{13}C NMR spectroscopy before and after spiking. Addition of floridoside and isethionic acid resulted in an increase in their respective signals in the ^{13}C NMR spectra of [1]. No additional signals were detected. This demonstrates the absence of any covalent bonding between the two species and is consistent with [1] being a complex of floridoside and isethionic acid (Fig. 3).

Larval response to isolated metabolites

Of the two metabolites [1] and [2], only the floridoside–isethionic acid complex [1] induced metamorphosis in larvae of *H. purpurascens* (Fig. 4). Therefore, we concluded that the active cue for metamorphosis of *H. purpurascens* was the floridoside–isethionic acid complex [1], as isolated from the polar extract of *D. pulchra* (Fig. 4). Floridoside [2] did not induce any metamorphosis of *H. purpurascens* after 15 h. The rate of metamorphosis of *H. purpurascens* in response to the floridoside–isethionic acid complex [1] was concentration dependent, with larvae exposed to 25 μM metamorphosing significantly faster than those exposed to 2.5 μM (5 h: $X^2 = 21.02$, 1 df, $P < 0.001$; Fig. 4). The higher concentration of 25 μM of [1] induced more rapid metamorphosis than did pieces of *D. pulchra* (Fig. 4). No metamorphosis was observed in either of the controls.

Larval response to isolated and synthetic inducers

The activity of the floridoside–isethionic acid complex was confirmed in assays comparing the natural and synthetic inducer. Larvae of *H. purpurascens* metamorphosed in a similar manner in the presence of both natural and synthetic complexes of the floridoside-isethionic acid complex (Fig. 5). After 24 h, substantially more metamorphosis occurred in treatments of pieces of *D. pulchra*, the pure complex [1] as isolated from the crude polar extract (200 μM), or synthetic floridoside–isethionic acid (200 μM) than in other treatments ($X^2 = 57.15$, 6 df, $P < 0.001$; Fig. 5). The synthetic floridoside–isethionic acid complex mimicked the percentage of metamorphosis of the natural floridoside–isethionic acid product [1] (Fig. 5). No metamorphosis was observed in treatments containing floridoside or isethionic acid, or in the controls. There was no significant change in the percentage of *H. purpurascens* that had meta-

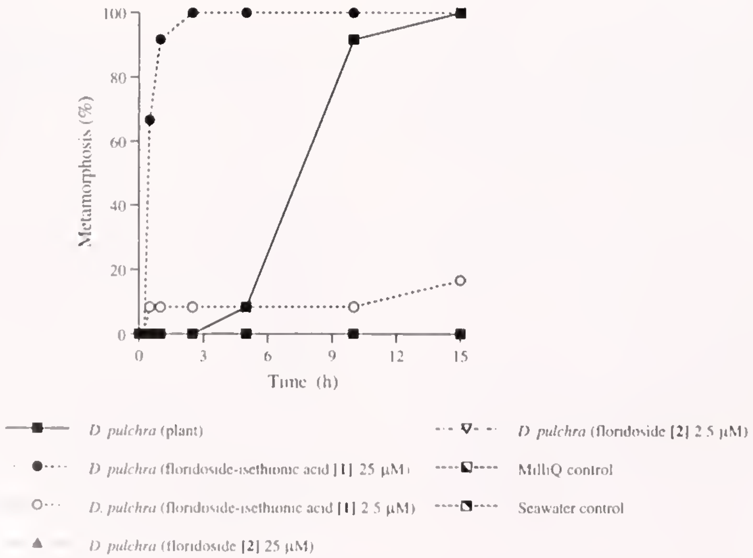

Figure 4. Percent metamorphosis over time of competent larvae of *Holopneustes purpurascens* (one larva [illegible] 12 replicates per treatment) when exposed to pieces of *Delisea pulchra* (15 mg per replicate) and the [illegible] fractions. Controls of MilliQ water and sterile, filtered seawater were used.

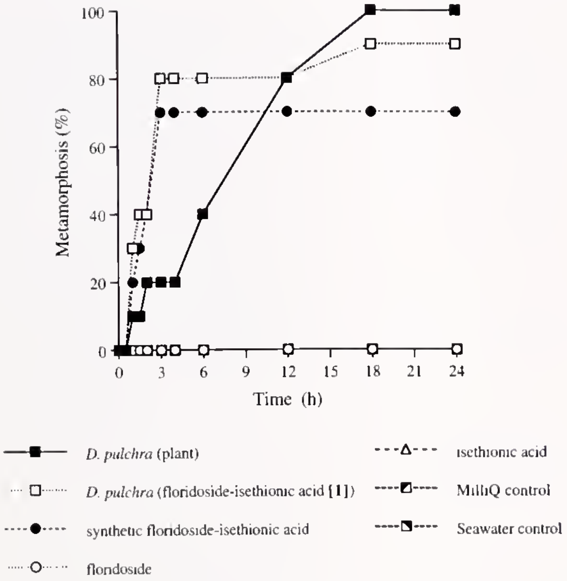

Figure 5. Percent metamorphosis over time of competent larvae of *Holopneustes purpurascens* (one larva per replicate; 10 replicates per treatment) when exposed to pieces of *Delisea pulchra* (15 mg per replicate), or 200 μM of either [1] as isolated from the crude polar extract of *D. pulchra*, the synthetic floridoside-isethionic acid complex in a 1:1 molar ratio, floridoside, or isethionic acid. Controls of MilliQ water and sterile, filtered seawater were used.

morphosed from 24 to 36 h, at which point the assay was stopped ($X^2 > 0.05$, 2 df, $P = 0.978$).

Concentration-dependent response of larvae to the floridoside-isethionic acid complex

The larvae of *H. purpurascens* metamorphosed at a concentration-dependent rate when exposed to different levels of the floridoside–isethionic acid complex [1] (Fig. 6). Larvae metamorphosed at a faster rate at higher concentrations of [1], with all concentrations from 125 μM to 25 μM inducing metamorphosis of larvae at the same rate. These concentrations also induced metamorphosis more rapidly than did pieces of *D. pulchra* (6 h: $X^2 = 24.88$, 3 d.f., $P < 0.001$). Concentrations of 12.5 μM and 2.5 μM also induced metamorphosis, albeit significantly more slowly than higher concentrations (6 h: $X^2 = 36.39$, 4 df, $P < 0.001$), and no metamorphosis occurred at a concentration of 1.25 μM, or in controls (Fig. 6).

Larval response to conditioned seawater collected in situ

Seawater surrounding *D. pulchra* induced 100% metamorphosis of larvae at a rate comparable to that of the floridoside-isethionic acid complex in earlier assays (compare Fig. 5 to Fig. 7). Seawater surrounding *E. radiata*, or water sampled away (>2 m) from any benthic algae, did not induce metamorphosis (Fig. 7).

Larval response to subtidal algae

As well as responding to *D. pulchra*, larvae of *H. purpurascens* were induced to metamorphose within 24 h in the presence of four other species of red algae (*Laurencia rigida, Solieria robusta, Corallina officinalis*, and *Amphiroa anceps*) in varying degrees (Fig. 8). *D. pulchra* induced the greatest response, with all larvae exposed to this alga metamorphosing (Fig. 8). Most of the larvae exposed to *L. rigida* also metamorphosed after 24 h. Larval response to the three other red algae was lower and more varied, and no metamorphosis occurred in the presence of any of the brown or green algae tested (Fig. 8). This pattern in the proportion of metamorphosis for algal species was consistent between the two times analyzed ($X^2 = 5.86$, 1 df, $P = 0.209$).

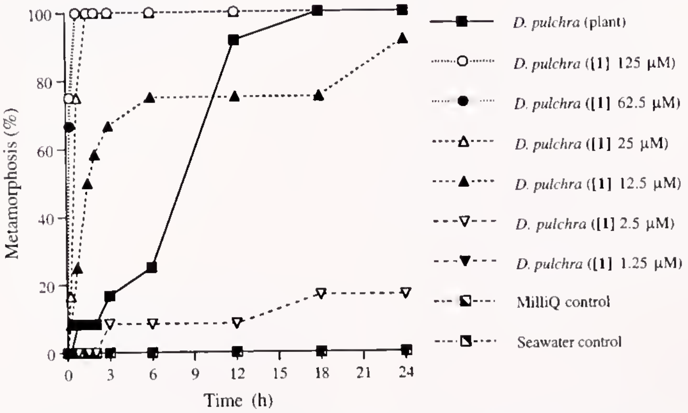

Figure 6. Percent metamorphosis over time of competent larvae of *Holopneustes purpurascens* (one larva per replicate; 12 replicates per treatment) when exposed to pieces of *Delisea pulchra* (15 mg per replicate) and different concentrations of the floridoside-isethionic acid complex. Controls of MilliQ water and sterile, filtered seawater were used.

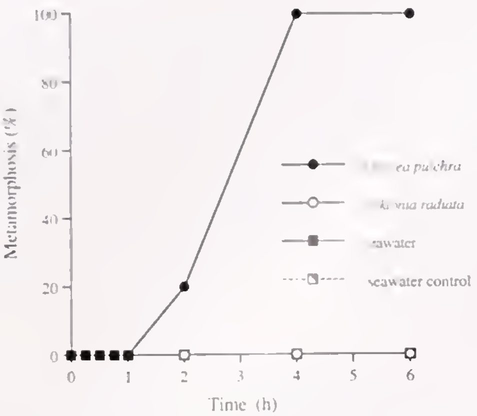

Figure 7. Percent metamorphosis over time of competent larvae of *Holopneustes purpurascens* (one larva per replicate; 10 replicates per treatment) when exposed to seawater surrounding plants of *Delisea pulchra* and *Ecklonia radiata*, and from seawater distant (>2 m) from any macroalgae. Sterile filtered seawater was used as a control.

Discussion

Environmental cues—physical, biological, or chemical—have long been thought to play an important role in the settlement and metamorphosis of marine invertebrate larvae (Svane and Young, 1989; Pawlik, 1992; McEdwards, 1995), and chemical cues in particular have received considerable attention in the last 20 years. Such chemical cues may be waterborne, associated with the surfaces of substrata, or derived from conspecifics (Pawlik, 1992), and there is now a substantial list of metabolites known to have strong effects on the settlement or metamorphosis of invertebrate larvae (reviewed in Pawlik, 1992; Slattery, 1997).

Few if any of these metabolites, however, have been characterized, quantified *in situ*, and shown to affect settlement or metamorphosis of larvae in a way that is consistent with the demography of the target organisms in the field. Many studies in this area have focused on what Pawlik (1992) termed "artificial" inducers; that is, the metabolites have not been shown to be present (either at all, or in active levels) in the environment of the settling organism, but rather are thought to mimic the action of naturally occurring inducers. Examples include the neurotransmitters γ-aminobutyric acid (GABA) (Morse *et al.*, 1979), L-β-3,4-dihydroxyphenylalanine (L-DOPA) (Coon and Bonar, 1987), and epinephrine (Coon *et al.*, 1986). Such compounds, many of which are widely distributed throughout the animal phyla, may play important internal roles as mediators of settlement and metamorphosis (see review in Coll *et al.*, 1989). Other studies have identified naturally occurring inducers of [illegible] are produced in the environment exogenously to the [illegible] but they have either failed to characterize (and [illegible] quantify) the relevant compound or have been unable to [illegible] the production or presence of the cue to the recruitment pattern of the organism (*e.g.*, Yvin *et al.*, 1985; Boettcher and Targett, 1996). Despite considerable ongoing work in this area (*e.g.*, Morse and Morse, 1984; Hadfield and Scheuer, 1985; Burke, 1986; Pawlik, 1986, 1988; Cochard *et al.*, 1989; Jensen and Morse, 1990; Morse, 1992; Davis and Stoner, 1994; Zimmer-Faust and Tamburri, 1994; Walters *et al.*, 1996; Zimmer-Faust *et al.*, 1997; Daume *et al.*, 1999; Tsukamoto *et al.*, 1999), to our knowledge there is no known chemical cue for larval settlement or metamorphosis that (a) can be clearly related to the pattern of settlement and recruitment of the target organism in the field, (b) is structurally characterized, and (c) is known to be present *in situ* at active concentrations.

We have demonstrated that the floridoside–isethionic acid complex fulfills many of the criteria necessary for an ecologically relevant cue for larval metamorphosis. The echinoid *Holopneustes purpurascens* was found almost exclusively on two host plants at our study site, *Delisea pulchra* and *Ecklonia radiata*. Although the abundance of urchins inhabiting the two hosts did not differ, the size of urchins on *D. pulchra* was significantly smaller than those on *E. radiata*, and in particular the smallest urchins (0–5 mm, reflecting new or recent recruits) were found exclusively on *D. pulchra*. Settlement or metamorphosis of larvae of *H. purpurascens* was not gregarious, unlike that of a

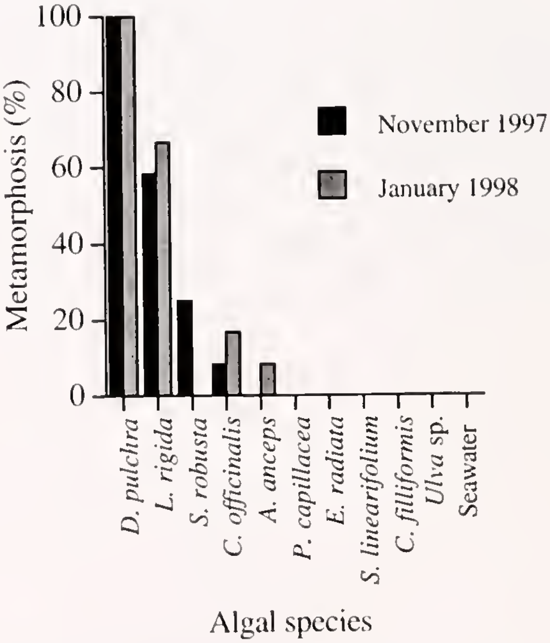

Figure 8. Percent metamorphosis of competent larvae of *Holopneustes purpurascens* (one larva per replicate; 12 replicates per treatment) after 24 h when exposed to subtidal algae (15 mg per replicate) from Bare Island on two occasions. Treatments included six species of red algae: *Delisea pulchra*, *Laurencia rigida*, *Solieria robusta*, *Corallina officinalis*, *Amphiroa anceps*, *Pterocladiella capillacea*; two species of brown algae: *Ecklonia radiata* and *Sargassum linearifolium*; and two species of green algae: *Caulerpa filiformis* and *Ulva* sp. The response of larvae to sterile filtered seawater was used as a control.

number of other echinoderms (Highsmith, 1982; Young and Chia, 1982; Pearce and Scheibling, 1990) and other invertebrates (Burke, 1986). Rather, these larvae metamorphosed in the presence of *D. pulchra,* the host on which new or recent recruits were found in the field. They showed no response to the alternative host, *E. radiata,* or its extracts. The larvae did not need to touch *D. pulchra* to metamorphose, indicating that the cue was water soluble.

Through bioassay-guided fractionation, the cue for metamorphosis was demonstrated to be a noncovalently-bound complex of the sugar floridoside and isethionic acid. The unusual (complexed) nature of the cue was confirmed by NMR spectroscopy, and by showing that the two components separately had no effect on metamorphosis. Larvae responded to the floridoside–isethionic acid complex in a dose-dependent manner, at concentrations similar to those of active levels of previously described inducers. Their response to synthetically prepared floridoside–isethionic acid complex was similar to their response to the naturally extracted cue.

As with all previous studies of larval inducers, we have not yet shown that the floridoside–isethionic acid complex is present *in situ* at levels that induce metamorphosis of *H. purpurascens.* We are currently developing quantitative methods in our laboratory, as well as methods for experimentally deploying the cue in the field (analogous to the "larval flypaper" of Morse and Morse, 1986). However, also consistent with the hypothesis that the floridoside–isethionic acid complex is an *in situ* cue, larvae metamorphosed in the presence of water collected close to *D. pulchra,* but not in the presence of water collected adjacent to *E. radiata* or away (>2 m) from any macroalgae. Larvae also metamorphosed in the presence of other red, but not green or brown, algae. Although other cues may be present in these algae, this is further support for the induction of metamorphosis by the floridoside–isethionic acid complex, as floridoside is found widely in red algae (Karsten *et al.,* 1993), but not in brown or green algae. These other red algae are less common than *D. pulchra* in our study habitats, and *H. purpurascens* is rarely found on these other species. One explanation for this pattern is that the greater abundance of *D. pulchra* may simply result in higher local concentrations of a shared cue (such as the floridoside–isethionic acid complex) in water near beds of *D. pulchra* than in water surrounding other local species of red algae. Concentrations of the metabolites may also vary among the different species, as is well known for both primary (*e.g.,* floridoside; Karsten *et al.,* 1999) and secondary (Hay, 1996) algal metabolites.

The response of *H. purpurascens* to red, but not green, algae is consistent with numerous previous studies indicating that sea urchins often settle or metamorphose preferentially in response to red algae, particularly corallines. For example, the sea urchins *Pseudocentrotus depressus* and *Anthocidaris crassispina* preferentially metamorphose in response to the coralline alga *Corallina pilulifera* (Kitamura *et al.,* 1993, 1994). Similarly, species of *Strongylocentrotus* preferentially metamorphose in response to turfing and crustose red algae such as *C. officinalis, Lithothamnion glaciale, Phymatolithon laevigatum,* and *P. rugulosum* (Hart and Scheibling, 1988; Pearce and Schiebling, 1991), and to a partially purified extract of coralline algae (Rowley, 1989). One interesting difference between the responses of *H. purpurascens* and other urchins cited above is that *H. purpurascens* did not respond most strongly to coralline algae. The four other species of red algae tested, including the corallines *C. officinalis* and *Amphiroa anceps,* also all induced metamorphosis but to a lesser degree than *Delisea pulchra.*

Red algae are also thought to be the primary stimuli for induction of settlement or metamorphosis among other invertebrates, including the coral *Agaricia humilis* (Morse, 1992), the abalone *Haliotis rufescens* (Morse *et al.,* 1979) and *H. laevigata* (Daume *et al.,* 1999), the queen conch *Strombus gigas* (Davis and Stoner, 1994; Boettcher and Targett, 1996), the sea hare *Aplysia californica* (Nadeau *et al.,* 1989), and the scallop *Pecten maximus* (Cochard *et al.,* 1989).

Although settlement in response to red algae is common, the cues responsible for these responses are largely unknown. Only one previous study has identified a naturally produced inducer from red algae, jacaranone, isolated from aqueous extracts of the red alga *Delesseria sanguinea* (Yvin *et al.,* 1985). However, although jacaronone stimulated metamorphosis of the bivalve scallop *Pecten maximus,* cooccurrence of the alga and the scallop was not reported, and subsequent reports indicated that these scallops lacked "substrate-specific recruitment" (Cochard *et al.,*1989). Perhaps the best known example of red algal cues is that of Morse and co-workers, who showed that larvae of the abalone *Haliotis rufescens* settled and metamorphosed preferentially onto red crustose algae such as *Lithothamnion* sp., *Lithophyllum* sp., and *Hildenbrandia* sp. (Morse *et al.,* 1979). Larvae of *H. rufescens* were also induced to settle and initiate metamorphosis in response to GABA. Morse and Morse (1984) subsequently found a mimetic peptide of GABA within the surface of the crustose red algae, which they concluded was likely to be the active cue for settlement and metamorphosis of *H. rufescens.* However, the mimetic peptide has not to date been characterized (research on the role of GABA and its mimetics in induction of larval settlement is reviewed by Slattery, 1997).

A recurring theme in the literature (see reviews by Pawlik, 1992; Slattery, 1997) on induction of larval settlement is whether cues are primarily nonpolar substances that are adsorbed to or incorporated within substrata, requiring larvae to physically contact a surface before encountering the cue (*e.g.,* Pawlik and Faulkner, 1986; Morse *et al.,* 1994; Clare and Matsumura, 2000), or whether they are polar metabolites that are detected in the water column, such as the cue or cues for *H. purpurascens*. Although both surface adsorbed (nonpolar) and water-soluble cues may be important for some larvae (Clare and Matsumura, 2000), a number of studies have highlighted the importance of waterborne, low-molecular-weight, water-soluble cues for settlement or metamorphosis of a taxonomically diverse array of invertebrates. These include the upside-down jellyfish *Cassiopea xamachana* (Fleck and Fitt, 1999), the tube worm *Hydroides elegans* (Walters *et al.*, 1996), the red abalone *Haliotis rufescens* (Morse *et al.*, 1984; Barlow, 1990), the queen conch *Strombus gigas* (Boettcher and Targett, 1996), the nudibranch *Phestilla sibogae* (Hadfield and Scheuer, 1985), the oyster *Crassostrea virginica* (Turner *et al.*, 1994; Zimmer-Faust and Tamburri, 1994; Browne *et al.*, 1998), and the Pacific sand dollar *Dendraster excentricus* (Burke, 1984). This pattern contrasts with the suggestion that naturally produced deterrents of settlement ("natural antifoulants") are likely to be nonpolar and thus able to adsorb to the surface of the producing organism (Schmitt *et al.*, 1995; Jennings and Steinberg, 1997; Steinberg *et al.*, 1998; Dworjanyn *et al.*, 1999).

One of the major arguments against the effectiveness of waterborne cues for induction of settlement is that *in situ* hydrodynamics will weaken the effect of the cue to the point where it ceases to be an effective signal. This can happen both by currents or turbulence inhibiting weakly swimming larvae from reaching an appropriate habitat once the cue has been detected (Chia *et al.*, 1984; Butman, 1986), or by the surrounding seawater simply diluting the cue to a level below larval detection. This assumed dilution and rapid dispersion of water-soluble chemicals in flowing seawater has resulted in such substances being traditionally dismissed as potential cues (Butman, 1989). Indirect support for this argument also comes from data showing that for some invertebrates, larval delivery to sites is similar to what would be expected for the delivery of inert particles with similar characteristics (*e.g.*, Eckman, 1983; Mullineaux and Butman, 1991; but see Eckman and Duggins, 1998).

In contrast to the "dilution" or "weakly swimming" hypotheses, several studies suggest that water-soluble cues can function as *in situ* inducers of settlement or metamorphosis. We have shown that larvae of *Holopneustes purpurascens* metamorphosed in response to seawater surrounding *Delisea pulchra* collected *in situ*, indicating that larvae of this urchin do detect and respond to *in situ* concentrations of a water-soluble inducer. Tamburri *et al.* (1996) showed that larvae of the oyster *Crassostrea virginica*, known to be weak swimmers, consistently detected and responded to waterborne chemical cues in raceway flumes at flow speeds and shear velocities typical of estuarine flows. In both of these studies, response of the larvae to the presence of a cue was very rapid. *C. virginica* responded within 5 s of initial exposure to the waterborne cue (Tamburri *et al.*, 1996). As with the floridoside–isethionic acid complex, larvae of *H. purpurascens* in still-water assays rapidly changed their position in the water column, moving to the bottom of petri dishes within 5 min of exposure to the cue (Williamson, pers. obs.). Within 15 min of exposure, the majority of larvae had settled and begun to metamorphose, suggesting that these larvae were able to rapidly respond both behaviorally and developmentally within a short time of detecting the cue. A rapid response to a cue, either behaviorally or developmentally (through metamorphosis), would obviously facilitate the ability of larvae to respond effectively to waterborne cues from particular sources in their habitats.

As well as a rapid response time, several other parameters should affect the utility of water-soluble metabolites as cues for settlement or metamorphosis. Decho *et al.* (1998) have argued that basic (alkaline) peptides should be common as signal molecules in marine systems because of their ability to resist biodegradation by marine bacteria (as well as because of the general importance of small peptides as chemical signals for animal sensory systems). An additional likely criterion for an effective water-soluble cue is that it be produced in large amounts, so that the cue is maintained at an effective concentration near the surface from which it emanates. Both oyster beds (Tamburri *et al.*, 1992; Zimmer-Faust *et al.*, 1997) and the algal system described here would appear to meet this criterion. Although the oysters are perhaps an extreme example, many other invertebrates on either soft or hard substrata also occur in high-density, nearly monocultural aggregations (*e.g.*, Woodin, 1976). Such assemblages are likely places to look for realistic waterborne settlement or metamorphosis cues.

In particular, many shallow, hard-substratum communities are dominated by dense assemblages composed of one or a few species of benthic algae that provide habitat, and often food, for a diverse array of invertebrates. Benthic algae are well known to "leak" metabolites, particularly carbohydrates, from their thalli (Lobban and Harrison, 1994). Such macroalgal sugars are often produced in high concentrations (*e.g.*, Karsten *et al.*, 1993, for floridoside), are exuded from the thallus (Moebus and Johnson, 1974), and are in a number of cases unique to a particular algal group. For example, floridoside and isethionic acid are widespread (if not ubiquitous) among red algae, but are also unique to this algal group (Barrow *et al.*, 1993, 1995; Clayton and King, 1996). Similarly, mannitol and its derivatives are widespread within the brown algae, but do not occur in other seaweeds (Clayton and King, 1996). Algal sugars or sugar derivatives would thus seem to generally meet at least two important criteria for an effective water-soluble cue: (i) the potential to reach high concentrations *in situ*, and (ii) some degree of source (substratum) specificity. There are now several studies demonstrating or implicating algal sugars as larval settlement cues (Bahamondes-Rojas and Dherbomez, 1990; Boettcher and Targett, 1996).

Conclusion

We have shown that larvae of the echinoid *Holopneustes purpurascens* metamorphose in response to a chemical cue—composed of a complex of the red algal sugar floridoside and isethionic acid—from one of its two main host plants, the red alga *Delisea pulchra.* The presence of the cue in *D. pulchra,* but not the alternative host *Ecklonia radiata,* is consistent with the demography of *H. purpurascens,* in which the most recently recruited individuals are found only on *D. pulchra.* We are currently developing methods for the quantification of the floridoside–isethionic acid complex in the field, and for the controlled, experimental release of the cue *in situ* to fully test the hypothesis that the floridoside–isethionic acid complex is an ecologically relevant cue for the induction of metamorphosis of *H. purpurascens.* Such experiments would also enable us to test more generally the relative importance of hydrodynamics *versus* chemical cues for settlement and metamorphosis of larvae of *H. purpurascens,* and to understand the differential response of larvae to different species of red algae. Finally, in contrast to some previous suggestions, we suggest that water-soluble metabolites, such as algal sugars or their derivatives, may be generally important as cues for marine invertebrate settlement.

Acknowledgments

This research was supported by an Australian Postgraduate Award to JEW, an ARC Research Fellowship to RdN, and an ARC Large Grant (A19530672) to PDS. We thank J. R. Pawlik, A. G. B. Poore, L. Barlow, and an anonymous reviewer for comments on the manuscript, and P. Selvakumaraswamy for help with larval culturing.

Literature Cited

Bahamondes-Rojas, I., and M. Dherbomez. 1990. Purification partielle de substances glycoconjuguées capables d'induire la métamorphose des larves compétentes d'*Eubranchus doriae* (Trinchèse, 1879), mollusque nudibranche. *J. Exp. Mar. Biol. Ecol.* **144:** 17–27.

Barlow, L. A. 1990. Electrophysiological and behavioral responses of larvae of the red abalone (*Haliotis rufescens*) to settlement-inducing substances. *Bull. Mar. Sci.* **46:** 537–554.

Barrow, K., U. Karsten, and R. J. King. 1993. Isethionic acid from the marine red alga *Ceramium flaccidum. Phytochemistry* **34:** 1429–1430.

Barrow, K., U. Karsten, R. J. King, and J. A. West. 1995. Floridoside in the genus *Laurencia* (Rhodomelaceae: Ceramiales)—a chemosystematic study. *Phycologia* **34:** 279–283.

Boettcher, A. A., and N. M. Targett. 1996. Induction of metamorphosis in queen conch, *Strombus gigas* Linnaeus, larvae by cues associated with red algae from their nursery grounds. *J. Exp. Mar. Biol. Ecol.* **196:** 29–52.

Browne, K. A., M. N. Tamburri, and R. K. Zimmer-Faust. 1998. Modeling quantitative structure-activity relationships between animal behavior and environmental signal molecules. *J. Exp. Biol.* **201:** 245–258.

Burke, R. D. 1983. The induction of metamorphosis of marine invertebrate larvae: stimulus and response. *Can. J. Zool.* **61:** 1701–1719.

Burke, R. D. 1984. Pheromonal control of metamorphosis in the Pacific sand dollar, *Dendraster excentricus. Science* **225:** 442–443.

Burke, R. D. 1986. Pheromones and the gregarious settlement of marine invertebrate larvae. *Bull. Mar. Sci.* **39:** 323–331.

Butman, C. A. 1986. Larval settlement of soft-sediment invertebrates: some predictions based on analysis of near-bottom velocity profiles. Pp. 487–513 in *Marine Interfaces Ecohydrodynamics*, J. C. J. Nihoul, ed. Elsevier Science, New York.

Butman, C. A. 1987. Larval settlement of soft-sediment invertebrates: the spatial scales of pattern explained by active habitat selection and the emerging role of hydrodynamical processes. *Oceanogr. Mar. Biol. Annu. Rev.* **25:** 113–165.

Butman, C. A. 1989. Sediment trap experiments on the importance of hydrodynamical processes in distributing settling invertebrate larvae in near-bottom waters. *J. Exp. Mar. Biol. Ecol.* **134:** 37–88.

Butman, C. A., J. P. Grassle, and C. M. Webb. 1988. Substrate choices made by marine larvae settling in still water and in a flume flow. *Nature* **333:** 771–773.

Chia, F. S., J. Buckland-Nicks, and C. M. Young. 1984. Locomotion of marine invertebrate larvae: a review. *Can. J. Zool.* **62:** 1205–1222.

Clare, A. S., and K. Matsumura. 2000. Nature and perception of barnacle settlement pheromones. *Biofouling* **15:** 57–71.

Clayton, M. N., and R. J. King. 1996. *Marine Botany: An Australasian Perspective.* Longman Cheshire, Melbourne, Australia.

Cochard, J. C., L. Chevolot, J. C. Yvin, and A. M. Chevolot-Magueur. 1989. Induction de la metamorphose de la coquille Saint Jacques *Pecten maximus* L. par des derives de la tyrosine extraits de l'algue *Delesseria sanguinea* Lamoroux ou synthetiques. *Haliotis* **19:** 129–154.

Coll, J., B. Bowden, M. Porifirio, A. Heaton, G. Konig, R. de Nys, R. Willis, P. Sammarco, and M. Clayton. 1989. Chemically mediated interactions between marine organisms. *Chem. Scr.* **29:** 383–388.

Coon, S. L., and D. B. Bonar. 1987. The role of DOPA and dopamine in oyster settlement behavior. *Am. Zool.* **27:** 128A.

Coon, S. L., D. B. Bonar, and R. M. Weiner. 1986. Chemical production of clutchless oyster spat using epinephrine and norepinephrine. *Aquaculture* **58:** 255–262.

Crisp, D. J. 1974. Factors influencing the settlement of marine invertebrate larvae. Pp. 177–265 in *Chemoreception in Marine Organisms,* P. T. Grant and A. M. Mackie, eds. Academic Press, New York.

Daume, S., S. Brand-Gardner, and W. J. Woelkerling. 1999. Settlement of abalone larvae (*Haliotis laevigata* Donovan) in response to non-geniculate coralline red algae (Corallinales, Rhodophyta). *J. Exp. Mar. Biol. Ecol.* **234:** 125–143.

Davis, M., and A. W. Stoner. 1994. Trophic cues induce metamorphosis of queen conch larvae (*Strombus gigas* Linnaeus). *J. Exp. Mar. Biol. Ecol.* **180:** 83–102.

Decho, A. W., K. A. Browne, and R. K. Zimmer-Faust. 1998. Chemical cues: Why basic peptides are signal molecules in marine environments. *Limnol. Oceanogr.* **43:** 1410–1417.

de Nys, R., A. D. Wright, G. M. Konig, and O. Sticher. 1993. New halogenated furanones from the marine alga *Delisea pulchra* (cf. *fimbriata*). *Tetrahedron* **39:** 11213–11220.

Dworjanyn, S. A., R. de Nys, and P. D. Steinberg. 1999. Localisation and surface quantification of secondary metabolites in the red alga *Delisea pulchra. Mar. Biol.* **133:** 727–736.

Eckman, J. E. 1983. Hydrodynamic processes affecting benthic recruitment. *Limnol. Oceanogr.* **28:** 241–257.

Eckman, J. E., and D. O. Duggins. 1998. Larval settlement in turbulent pipe flows. *J. Mar. Res.* **56:** 1285–1312.

Fleck, J., and W. K. Fitt. 1999. Degrading mangrove leaves of *Rhizophora mangle* Linne provide a natural cue for settlement and metamorphosis of the upside down jellyfish *Cassiopea xamachana* Bigelow. *J. Exp. Mar. Biol. Ecol.* **234:** 83–94.

Hadfield, M. G., and D. Scheuer. 1985. Evidence for a soluble metamorphic inducer in *Phestilla*: ecological, chemical and biological data. *Bull. Mar. Sci.* **37:** 556–566.

Hart, M. W., and R. E. Scheibling. 1988. Heat waves, baby booms, and the destruction of kelp beds by sea urchins. *Mar. Biol.* **99:** 167–176.

Hay, M. E. 1996. Marine chemical ecology: what's known and what's next? *J. Exp. Mar. Biol. Ecol.* **200:** 103–134.

Highsmith, R. C. 1982. Induced settlement and metamorphosis of sand dollar (*Dendraster excentricus*) larvae in predator-free sites: adult sand dollar beds. *Ecology* **63:** 329–337.

Jennings, J. G., and P. D. Steinberg. 1997. Phlorotannins *versus* other factors affecting epiphyte abundance on the kelp *Ecklonia radiata*. *Oecologia* **109:** 461–473.

Jensen, R. A., and D. E. Morse. 1990. Chemically induced metamorphosis of polychaete larvae in both the laboratory and ocean environment. *J. Chem. Ecol.* **16:** 911–930.

Karsten, U., K. D. Barrow, and R. J. King. 1993. Floridoside, 1-isofloridoside, and d-isofloridoside in the red alga *Porphyra columbina*. *Plant Physiol.* **103:** 485–491.

Karsten, U., J. A. West, G. C. Zucarello, O. Nixdorf, K. D. Barrow, and R. J. King. 1999. Low molecular weight carbohydrate patterns in the Bangiophyceae (Rhodophyta). *J. Phycol.* **35:** 967–976.

Kitamura, H., S. Kitahara, and H. B. Koh. 1994. Induction of larval settlement and metamorphosis in the sea urchins *Pseudocentrotus depressus* and *Anthocidaris crassispina* by fatty acids. *Fish. Sci.* **60:** 311–313.

Levitan, D. R., M. A. Sewell, and F. S. Chia. 1992. How distribution and abundance influence fertilization success in the sea urchin *Strongylocentrotus purpuratus*. *Ecology* **73:** 248–254.

Lobban, C. S., and P. J. Harrison. 1994. *Seaweed Ecology and Physiology*. Cambridge University Press, Melbourne, Australia.

McEdwards, L. D. 1995. *Ecology of Marine Invertebrate Larvae*. CRC Press, Boca Raton, FL.

Moebus, K., and K. M. Johnson. 1974. Exudation of dissolved organic carbon by brown algae. *Mar. Biol.* **26:** 117–125.

Morse, A. N. C. 1992. Role of algae in the recruitment of marine invertebrate larvae. Pp. 385–403 in *Plant-Animal Interactions in the Marine Benthos. Systematics Association Special*, Vol. 46, D. M. John, S. J. Hawkins, and J. H. Price, eds. Clarendon Press, Oxford.

Morse, A. N. C., and D. E. Morse. 1984. Recruitment and metamorphosis of *Haliotis* larvae induced by molecules uniquely available at the surfaces of crustose red algae. *J. Exp. Mar. Biol. Ecol.* **75:** 191–215.

Morse, A. N. C., and D. E. Morse. 1986. Flypapers for coral and other planktonic larvae. *Bioscience* **46:** 254–262.

Morse, D. E., N. Hooker, H. Duncan, and L. Jensen. 1979. γ-aminobutyric acid, a neurotransmitter, induces planktonic abalone larvae to settle and begin metamorphosis. *Science* **204:** 407–410.

Morse, A. N. C., C. A. Froyd, and D. E. Morse. 1984. Molecules from cyanobacteria and red algae that induce settlement and metamorphosis in the mollusc *Haliotis rufescens*. *Mar. Biol.* **81:** 293–298.

Morse, D. E., A. N. C. Morse, P. T. Raimondi, and N. Hooker. 1994. Morphogen-based chemical flypaper for *Agaricia humilis* coral larvae. *Biol. Bull.* **186:** 172–181.

Mullineaux, L. S., and C. A. Butman. 1991. Initial contact, exploration and attachment of barnacle cyprids settling in flow. *Mar. Biol.* **100:** 93–103.

Nadeau, L., J. A. Paige, A. Starczak, T. Capo, J. Lafler, and J. P. Bidwell. 1989. Metamorphic competence in *Aplysia californica* Cooper. *J. Exp. Mar. Biol. Ecol.* **131:** 171–193.

Pawlik, J. R. 1986. [illegible] induction of larval settlement and metamorphosis in the reef-building tube worm *Phragmatopoma californica* (Sabellariidae: Polychaeta). *Mar. Biol.* **91:** 59–68.

Pawlik, J. R. 1988. Larval settlement and metamorphosis of sabellariid polychaetes, with special reference to *Phragmatopoma lapidosa*, a reef-building species, and *Sabellaria floridensis*, a non-gregarious species. *Bull. Mar. Sci.* **43:** 41–60.

Pawlik, J. R. 1992. Chemical ecology of the settlement of benthic marine invertebrates. *Oceanogr. Mar. Biol. Annu. Rev.* **30:** 273–335.

Pawlik, J. R., and D. J. Faulkner. 1986. Specific free fatty acids induce larval settlement and metamorphosis of the reef-building tube worm *Phragmatopoma californica* Fewkes. *J. Exp. Mar. Biol. Ecol.* **102:** 301–310.

Pawlik, J. R., and M. G. Hadfield. 1990. A symposium on chemical factors that influence the settlement and metamorphosis of marine invertebrate larvae: introduction and perspective. *Bull. Mar. Sci.* **46:** 450–454.

Pearce, C. M., and R. E. Scheibling. 1990. Induction of settlement and metamorphosis in the sand dollar *Echinarachnius parma*: evidence for an adult associated factor. *Mar. Biol.* **107:** 363–369.

Pearce, C. M., and R. E. Scheibling. 1991. Effect of macroalgae, microbial films, and conspecifics on the induction of metamorphosis of the green sea urchin *Strongylocentrotus droebachiensis* (Müller). *J. Exp. Mar. Biol. Ecol.* **147:** 147–162.

Pechenik, J. A. 1999. On the advantages and disadvantages of larval stages in benthic marine invertebrate life cycles. *Mar. Ecol. Prog. Ser.* **177:** 269–297.

Pennington, J. T. 1985. The ecology of fertilization of echinoid eggs: the consequences of sperm dilution, adult aggregation and synchronous spawning. *Biol. Bull.* **169:** 417–430.

Roughgarden, J., S. Gaines, and H. Possingham. 1988. Recruitment dynamics in complex life cycles. *Science* **341:** 1460–1466.

Rowley, R. J. 1989. Settlement and recruitment of sea urchins (*Strongylocentrotus* spp.) in a sea-urchin barren ground and a kelp bed: are populations regulated by settlement or post-settlement processes? *Mar. Biol.* **100:** 485–494.

Scheltema, R. S. 1986. On dispersal and planktonic larvae of benthic invertebrates: an eclectic overview and summary of problems. *Bull. Mar. Sci.* **39:** 290–322.

Schmitt, T. M., M. E. Hay, and N. Lindquist. 1995. Constraints on chemically mediated coevolution: multiple functions for seaweed secondary metabolites. *Ecology* **76:** 107–123.

Slattery, M. 1997. Chemical cues in marine invertebrate larval settlement. Pp. 135–157 in *Marine Woodboring and Fouling Organisms of the Indian Ocean: A Review*, R. Naghabushanum and J. E. Thompson, eds. Oxford and IBH Publishing, New Delhi.

Sokal, R. R., and F. J. Rohlf. 1995. *Biometry*, 3rd ed. W. H. Freeman, New York.

Steinberg, P. D. 1989. Biogeographical variation in brown algal polyphenolics and other secondary metabolites: comparison between temperate Australasia and North America. *Oecologia* **78:** 373–382.

Steinberg, P. D. 1995. Interaction between the canopy dwelling echinoid *Holopneustes purpurescens* and its host kelp *Ecklonia radiata*. *Mar. Ecol. Prog. Ser.* **127:** 169–181.

Steinberg, P. D., R. de Nys, and S. Kjelleberg. 1998. Chemical inhibition of epibiota by Australian seaweeds. *Biofouling* **12:** 227–244.

Svane, I., and C. M. Young. 1989. The ecology and behaviour of ascidian larvae. *Oceanogr. Mar. Biol. Annu. Rev.* **27:** 45–90.

Tamburri, M. N., R. K. Zimmer-Faust, and M. L. Tamplin. 1992. Natural sources and properties of chemical inducers mediating settlement of oyster larvae: a re-examination. *Biol. Bull.* **183:** 327–338.

Tamburri, M. N., C. M. Finelli, D. S. Wethey, and R. K. Zimmer-Faust. 1996. Chemical induction of larval settlement behavior in flow. *Biol. Bull.* **191:** 367–373.

Thorson, G. 1950. Reproductive and larval ecology of marine bottom invertebrates. *Biol. Rev.* **25:** 1–45.

Tsukamoto, S., H. Kato, H. Hirotat, and N. Fusetani. 1999. Lumichrome. A larval metamorphosis-inducing substance in the ascidian *Halocynthia roretzi*. *Eur. J. Biochem.* **264:** 785–789.

Turner, E. J., R. K. Zimmer-Faust, M. A. Palmer, M. Luckenbach, and N. D. Pentcheff. 1994. Settlement of oyster (*Crassostrea virginica*) larvae: effects of water flow and a water-soluble chemical cue. *Limnol. Oceanogr.* **39:** 1579–1593.

van Altena, I. A., and P. D. Steinberg. 1992. Are differences in the responses between North American and Australasian marine herbivores to phlorotannins due to differences in phlorotannin structure? *Biochem. Syst. Ecol.* **20:** 493–499.

Walters, L. J., M. G. Hadfield, and C. M. Smith. 1996. Waterborne chemical compounds in tropical macroalgae: positive and negative cues for larval settlement. *Mar. Biol.* **126:** 383–393.

Winer, B. J. 1971. *Statistical Principles in Experimental Design.* McGraw-Hill, New York.

Woodin, S. A. 1976. Adult-larval interactions in dense infaunal assemblages: patterns of abundance. *J. Mar. Res.* **34:** 25–41.

Young, C. M., and F. S. Chia. 1982. Factors controlling spatial distribution of the sea cucumber *Psolus chitonoides:* settling and post-settling behavior. *Mar. Biol.* **69:** 195–205.

Young, C. M., and F. S. Chia. 1987. Abundance and distribution of pelagic larvae as influenced by predation, behavior, and hydrographic factors. Pp. 385–463 in *Reproduction of Marine Invertebrates.* Vol. 9, A. G. Giese and J. S. Pearse, eds. Blackwell, Palo Alto, CA.

Yvin, J. C., L. Chevolot, A. M. Chevolot-Magueur, and J. C. Cochard. 1985. First isolation of jacaranone from an alga, *Delesseria sanguinea.* A metamorphosis inducer of *Pecten* larvae. *J. Nat. Prod.* **48:** 814–816.

Zimmer-Faust, R. K., and M. N. Tamburri. 1994. Chemical identity and ecological implications of a waterborne, larval settlement cue. *Limnol. Oceanogr.* **39:** 1075–1087.

Zimmer-Faust, R. K., M. N. Tamburri, and A. W. Decho. 1997. Chemosensory ecology of oyster larvae: benthic-pelagic coupling. Pp. 37–50 in *Zooplankton: Sensory Ecology and Physiology,* D. K. Hartline, J. E. Purcell, and D. L. MacMillan, eds. Gordon and Breach, New York.

Reference: *Biol. Bull.* 198: 346–356. (June 2000)

Energetics of Larval Swimming and Metamorphosis in Four Species of *Bugula* (Bryozoa)

DEAN E. WENDT*

Department of Organismic and Evolutionary Biology, Harvard University,
Cambridge, Massachusetts 02138

Abstract. The amount of energy available to larvae during swimming, location of a suitable recruitment site, and metamorphosis influences the length of time they can spend in the plankton. Energetic parameters such as swimming speed, oxygen consumption during swimming and metamorphosis, and elemental carbon and nitrogen content were measured for larvae of four species of bryozoans, *Bugula neritina, B. simplex, B. stolonifera,* and *B. turrita.* The larvae of these species are aplanktotrophic with a short free-swimming phase ranging from less than one hour to a maximum of about 36 hours. There is about a fivefold difference in larval volume among the four species, which scales linearly with elemental carbon content and, presumably, with the amount of endogenous reserves available for swimming and metamorphosis. Mean larval swimming speeds (in centimeters per second) were similar among species. Specific metabolic rate and larval size were inversely related. For larvae of a given species, respiration rates remained similar for swimming and metamorphosis; however, because metamorphosis lasts about twice as long as a maximal larval swimming phase, it was more energetically demanding. Larger larvae expended more energy to complete metamorphosis than did smaller larvae, but in terms of the percentage of larval energy reserves consumed, swimming and metamorphosis were more "expensive" for smaller larvae. A comparison of the energy expended during larval swimming calculated on the basis of oxygen consumption and on the basis of elemental carbon decrease suggests that larvae of *Bugula* spp. may not use significant amounts of dissolved organic material (DOM) to supplement their endogenous energy reserves.

Introduction

The larval life of many marine invertebrates is characterized by three distinct phases. The first, a swimming phase, is both a means of dispersal and, in planktotrophic larvae, a time to sequester the energy needed for larval development and metamorphosis. The two subsequent phases—settlement and metamorphosis—can be temporally distinct, as in some echinoderm larvae (*e.g.,* Strathmann, 1974), or tightly coupled, as in bryozoan larvae (*e.g.,* Ryland, 1974). That the duration of the larval swimming phase can have detrimental effects on the latter two phases of the life cycle has been demonstrated for several species in at least three phyla, including bryozoans (Nielson, 1981; Woollacott *et al.,* 1989; Orellana and Cancino, 1991; Hunter and Fusetani, 1996; Wendt, 1996), barnacles (Pechenik *et al.,* 1993), and polychaetes (Qian *et al.,* 1990; Pechenik and Cerulli, 1991). In fact, an increased larval swimming phase can have long-term costs to adult growth and reproduction in bryozoans (Wendt, 1998). Effects associated with increased swimming duration are common, but not universal. For example, Highsmith and Emlet (1986) found no significant correlation between "delay time" and juvenile growth rate in the sand dollar *Echinarachnius parma,* which has planktotrophic larvae. For aplanktotrophic larvae, depletion of energetic reserves during larval swimming has been suggested to be responsible, at least in part, for the observed costs to later phases of the life cycle (Lucas *et al.,* 1979; Jaeckle, 1994; Pechenik, 1990; Pechenik and Fried, 1995; Wendt, 1996; Jarrett and Pechenik, 1997; Pechenik *et al.,* 1998).

Energy needed to sustain the three phases of larval existence is provided by a maternal source, by larval feeding while in the plankton (with relatively little maternal input), by uptake and utilization of dissolved organic materials (DOM), or by some combination of these sources (for a recent review of the developmental modes of marine inver-

Received 2 November 1999; accepted 31 January 2000.

* Current address: University of North Carolina at Greensboro. E-mail: dewendt@uncg.edu

tebrate larvae, see Levin and Bridges, [1995]). Regardless of the source, larval energy reserves must be sufficient to allow for dispersal (swimming phase), location of a suitable recruitment site (settlement phase), and transformation from larva to adult (metamorphic phase). The energy available for these processes *in part* influences the length of the dispersal and settlement phases (Crisp, 1974; Lucas, 1979; Pechenik, 1980, 1990; Richmond, 1987, 1988; Jaeckle, 1994; Shilling and Manahan, 1994; Zaslow and Benayahu, 1996; Hoegh-Guldberg and Emlet, 1997; Wilson and Harrison, 1998).

Metabolic costs are generally believed to be inversely related to animal size. For example, the theoretical cost of motility for small (<1 mm), ciliated animals and protozoans is inversely related to size and positively related to swimming speed (Crawford, 1992). That is, for a given swimming speed, the theoretical cost of transport is greater for smaller organisms. Additionally, body size and mass-specific basal metabolic rate are known to have an inverse relationship (Zeuthen, 1947, 1953). Based on these relationships, and assuming energy content is proportional to larval size, smaller larvae will have less energy to meet higher metabolic and locomotory costs. This situation raises some interesting questions about the energetics of swimming and metamorphosis as it is related to larval size. Does it in fact cost smaller larvae more to swim and metamorphose? If it does: Do smaller larvae swim slower to offset the increased energetic cost? Does the cost of metamorphosis decrease proportionately to offset the increased cost of swimming? Are the effects of increased swimming duration incurred sooner in smaller larvae?

The four bryozoans used in this study, *Bugula neritina, B. simplex, B. stolonifera,* and *B. turrita,* are ideal for energetic studies for several reasons: (1) Larvae are liberated synchronously and often in large quantities from adult colonies; thus, the larvae in a batch released at the same time are similar in age. (2) The larval swimming phase is short—ranging from minutes to tens of hours—and the length of the swimming phase can be readily prolonged using bright illumination and curtailed using elevated concentrations of exogenous KCl. (3) The size range of larvae among species is large, larvae are similar morphologically, and the adult colonies occupy similar ecological niches in that they are all common members of fouling communities. (4) Larval development, physiology, and anatomy are similar among the species. Embryonic stages of *Bugula* spp. are brooded on the adult colony in specialized structures called ovicells (Woollacott and Zimmer, 1972). The larvae are aplanktotrophic (nonfeeding), receiving nutrients translocationally *via* a placenta-like organ during embryogenesis (Woollacott and Zimmer, 1975). The larvae lack a digestive tract and have no coelomic and blastocoelic cavities (Woollacott and Zimmer, 1978). Most individuals are positively phototactic on release, becoming photonegative after the first several hours of larval swimming (Pires and Woollacott, 1997; Wendt and Woollacott, 1999). Metamorphosis begins with the eversion of the internal sac, which attaches the larva to the substratum. The first part of metamorphosis involves a rapid and cataclysmic reorganization of larval tissues, followed by differentiation of these tissues into adult structures (Woollacott and Zimmer, 1971, 1978; Reed and Woollacott, 1982, 1983). Thus, these species provide an elegant system in which to examine the relationship between larval size and the energetic costs of swimming and metamorphosis.

The present study was undertaken to compare the relative proportion of larval energy reserves used during swimming and metamorphosis, and to examine the relationship between larval size and several energetic parameters such as larval energy content and the energetic costs during swimming and metamorphosis. The following measurements were made: (1) larval size and swimming speeds for each of the four species; (2) oxygen consumption, and hence larval energy expenditure, during swimming and metamorphosis for each of the four species; and, (3) the amounts of carbon and nitrogen in newly released larvae compared to amounts in those swimming for 24 h, an additional estimation of energy expenditure during swimming.

Materials and Methods

Collection and maintenance of adults

Sexually mature colonies of *Bugula neritina* were collected from floating docks on the Indian River in Fort Pierce, Florida, during March 1997 and from Duke University Marine Laboratory in Beaufort, North Carolina, during May 1998. Colonies of *B. simplex, B. stolonifera,* and *B. turrita* were collected from floating docks on Eel Pond in Woods Hole, Massachusetts, during July and August, 1996 and 1997. Colonies collected in Florida were maintained at the Smithsonian Marine Station at Link Port (Fort Pierce) in plastic boxes that were continuously supplied with seawater. North Carolina and Woods Hole colonies were maintained at Harvard University in plastic aquaria. Colonies remained in the dark and received no supplemental food.

Larval release and swimming

Larvae for each experiment were obtained from several colonies to foster genetically heterogeneous populations. Parent colonies used for experiments were kept in the laboratory less than 5 days. Colonies were removed from the dark, placed in glass bowls with 1.0 l of seawater, and then exposed to fluorescent light. Larvae appeared within 10 min of illumination, and release was complete by 1 h. As most larvae of *Bugula spp.* are positively phototactic on release, they aggregated at the illuminated side of dishes, a behavior that facilitated collection. Both colonies and larvae appeared healthy throughout the 5-day experimental period. In fact, colonies continued to release larvae for several days afterward.

In experiments that required increased duration of larval swimming, larvae were transferred to an autoclaved 1.5-l glass finger bowl containing about 1.0 l of 0.2-μm filtered seawater. Larvae were prevented from initiating metamorphosis by continuous exposure to bright, fluorescent illumination accompanied by stirring (Wendt, 1996). The bowl was placed on an acrylic plastic table to reduce UV exposure and illuminated from below by three 20 W, 36-inch, full-spectrum Vite-lite lamps. Pieces of aluminum foil were arranged around the finger bowl to maintain constant levels of illumination from all directions. Illumination intensities ranged from 130 to 170 μE m^{-2} s^{-1}. A fan was used to blow air between the lights and the table, which served to maintain ambient room temperature (*ca.* 20°C) during larval swimming.

Carbon and nitrogen analysis

For each replicate sample, several hundred larvae were washed three times in autoclaved, 0.2-μm filtered seawater. Seawater was filtered before autoclaving and again immediately before larval washings to remove any particulate organic material. After washing, batches of about 100 larvae were transferred to an Eppendorf tube and centrifuged for 10 min to "pellet" the larvae. This process did not disrupt larval tissues, and the larvae swam normally when the pellet was resuspended. The larval pellet was then transferred to tin capsules in about 100 μl of seawater. The samples were dried overnight at 60°C and stored in a desiccator. Blank samples were prepared for each condition by transferring similar volumes of filtered seawater without larvae. The content of particulate organic nitrogen and carbon in samples was analyzed on a Europa Scientific Ltd. (Crewe, Lancashire, UK) model 20/20 mass spectrometer equipped with an automated Dumas combustion sample preparation system (model ANCA nt) in a continuous flow configuration (according to the method of McCarthy *et al.*, [1999]). The system was calibrated with a peptone standard (Sigma Chemical). Amounts of carbon and nitrogen per larva were calculated by dividing the total amount in the sample by the number of larvae. All samples were blank corrected.

Oxygen consumption of larvae and metamorphosing individuals

The metabolic rate of individuals was measured as the rate of oxygen consumption at 20° ± 0.5°C. Oxygen consumption rates were measured in a Strathkelvin model # RC 300 respiration chamber that was connected to a recirculating water bath. A Strathkelvin model # 1302 polarographic oxygen electrode served as the roof of chamber, which was connected to a Strathkelvin model # 781 oxygen meter. For experiments in Fort Pierce, Florida, the analog output from the oxygen meter was converted to a digital signal and transferred to a computer using an analog/digital converter and the Datacan IV computer software package (Sable Systems, Inc.). For the experiments in Cambridge, Massachusetts, the meter was connected to an analog chart recorder. The voltage output for the sensor was calibrated for a zero value using an oxygen-free solution of 0.01 *M* of disodium tetraborate and crystalline sodium sulfite. The voltage output at saturation was calibrated using seawater that was continuously bubbled for 30 min prior to the calibration. Saturation levels of oxygen for each experiment were calculated using the barometric pressure, vapor pressure, and standard values of oxygen solubility for water of a specific salinity and temperature (Weast and Astle, 1980). After each trial, the chamber and electrode membrane were swabbed with 70% ethanol and washed four times with 0.2-μm distilled water. The rate of oxygen consumption per individual was calculated as the slope of the regression line for the trial, divided by the number of individuals present, multiplied by 60 (*i.e.*, V O_2 consumed ind^{-1} h^{-1}). Using the ideal gas law, this value was converted to mol O_2 ind^{-1} h^{-1}. All rates were corrected for self-consumption of the electrode. The rates of oxygen consumption were converted to energy units using an oxyenthalpic equivalent of 468 KJ mol O_2^{-1}, which equals the average equivalent for protein (527 KJ mol O_2^{-1}), lipid (441 KJ mol O_2^{-1}), and carbohydrate (473 KJ mol O_2^{-1}) (Gnaiger, 1983).

Respiration rates were determined for larvae of *B. neritina*, *B. simplex*, *B. stolonifera*, and *B. turrita*. On release, about 20 larvae were transferred in 300 μl of 0.2-μm filtered seawater to the respiration chamber. After a 20-min acclimation, the chamber was sealed and the rate of oxygen depletion was followed for 30 min. The number of larvae was counted after each trial. Only larvae less than 4 h old were used.

Respiration rates during metamorphosis were determined for *B. neritina*, *B. simplex*, and *B. stolonifera*. Preliminary experiments demonstrated that *B. turrita* did not metamorphose normally under laboratory conditions, hence this species was not used. To determine oxygen consumption rates during metamorphosis, 30-min spot-measurements were taken on groups of 10–15 individuals during metamorphosis. The duration of metamorphosis was defined as the time from eversion of the larval metasomal sac to eversion of the lophophore of the ancestrular polypide. Larvae were placed in the tops of Beem capsules and exposed to 10 m*M* excess KCl in seawater to induce metamorphosis (Wendt and Woollacott, 1995). About 30 min after larvae initiated metamorphosis, the capsule tops were removed from the KCl solution and placed in finger bowls containing 200 ml of 0.2-μm filtered seawater. The finger bowls were covered and incubated at 20°C. To minimize bacterial and protozoan growth, 50 μg ml^{-1} of penicillin and streptomycin B were added to the seawater (Strathmann, 1987). Preliminary experiments showed that metamorphosis proceeded at typical rates in the presence of antibiotics and all metamorphs appeared anatomically normal. The use of Beem capsule tops ensured that individuals were never exposed to air during transfer from the culture dish to the respirometry chamber and that respiration measurements were made on the same group of individuals throughout metamorphosis. All measurements were made in 600 μl of 0.2-μm filtered seawater and individuals were acclimated for 10–15 minutes before the chamber was sealed. The first measurement was taken less than 1 h after the onset of metamorphosis and then at 12-h intervals until metamorphosis was completed by more than half the individuals in a given trial.

Initiation of metamorphosis as a function of swimming duration

Larvae of *B. stolonifera* and *B. turrita* were released and kept swimming as described above. Immediately after release and at 12-h intervals for 36 h, larvae were induced to metamorphose using 10 m*M* excess KCl in seawater. Three days (*ca.* 72 h) after initiation of metamorphosis, the number of individuals that completed metamorphosis was determined.

Larval swimming speeds and larval size

Swimming speeds and larval size were determined using a Motionscope high-speed video system (model HR500; Redlake Imaging Corporation) connected to a Zeiss photomicroscope III. Digital images were transferred to a videocassette recorder for later analysis. The monitor was calibrated with a stage micrometer, so that larval size and distance traveled could be measured directly. Larvae of *Bugula* spp. swim in a corkscrew path and thus have a vertical component in their horizontal trajectory. If a fixed bottom is used as a reference for distance traveled, the speed of the larva is underestimated because this method neglects the vertical distance covered in the spiral path. Use of high-speed video connected to a microscope allows very small portions of the animal's path to be isolated, thereby providing a more accurate estimate of swimming speed. To ensure the most accurate measurements, larval speeds were calculated only over distances where larvae remained in the same plane of focus (*i.e.*, functionally traveling in a horizontal manner). Therefore, total error in the vertical path was only 50 μm, which is equal to the depth of field for the Zeiss 6.3 neofluor objective. All experiments were conducted at room temperature (*ca.* 20°C) and at a constant level of illumination. Swimming speeds were measured in a circular chamber that was made by gluing a clear, acrylic cylinder onto a microscope slide. The chamber was open on top and had a diameter of 1.5 cm, a height of 0.5 cm, and a total volume of about 1 ml. Given the size of the larvae, it was calculated that the chamber was large enough to avoid any potential wall effects (Vogel, 1994), so long as swimming speeds were measured on larvae in the central portion of the chamber.

Statistical analysis

Between-species differences in swimming speeds and larval size were analyzed with a one-way factorial analysis of variance (ANOVA). Differences in oxygen consumption rates during metamorphosis were analyzed using a repeated measures ANOVA, since at 12-h intervals respiration rates were determined for the same group of individuals for each trial. A one-tailed Student's *t* test was used to identify significant differences in carbon and nitrogen of newly released larvae and those swimming for 24 h. All data are presented as means ± the standard error (SE) unless otherwise indicated. Data did not differ from a normal distribution, and there was no heteroscedasticity between treatments, as judged by an equality of variance test (*F* test).

Results

Oxygen consumption during larval swimming and metamorphosis

Average rates of larval oxygen consumption were 175 ± 25, 192 ± 38, 213 ± 46, 249 ± 49 pmol O_2 ind^{-1} h^{-1} for *Bugula stolonifera*, *B. simplex*, *B. turrita*, and *B. neritina*, respectively. Larval oxygen consumption rates were not significantly different between species (one-way ANOVA: df = 3, SS = 32849, MS = 10949, $F = 0.68$, $P = 0.57$). Oxygen consumption rates during metamorphosis were relatively constant for *B. neritina* and *B. simplex* (repeated measures ANOVA: df = 3, SS = 136030, MS = 45343, $F = 1.9$, $P = 0.14$ for *B. neritina;* df = 3, SS = 11752, MS = 3917, $F = 0.481$, $P = 0.70$ for *B. simplex*); whereas rates for *B. stolonifera* increased significantly during the last 12–24 h of metamorphosis (repeated measures ANOVA: df = 3, SS = 40352, MS = 13540, $F = 10.0$, $P = 0.003$) (Fig. 1).

Carbon and nitrogen utilization

For each species, elemental carbon content was significantly less in larvae that swam for 24 h than in newly released individuals (Table 1). Likewise, elemental nitrogen content was significantly less in larvae of *B. simplex* that swam for 24 h (Table 1). Larvae of *B. stolonifera* and *B. turrita* that swam for 24 h had significantly less elemental nitrogen compared to newly released larvae in three out of four trials (Table 1). For larvae of *B. neritina*, however, elemental nitrogen decreased significantly over 24 h in only one out of four trials. When all trials were combined for statistical analysis, elemental carbon was significantly less in batches of larvae swimming for 24 h; nitrogen content declined significantly for all species except *B. neritina*.

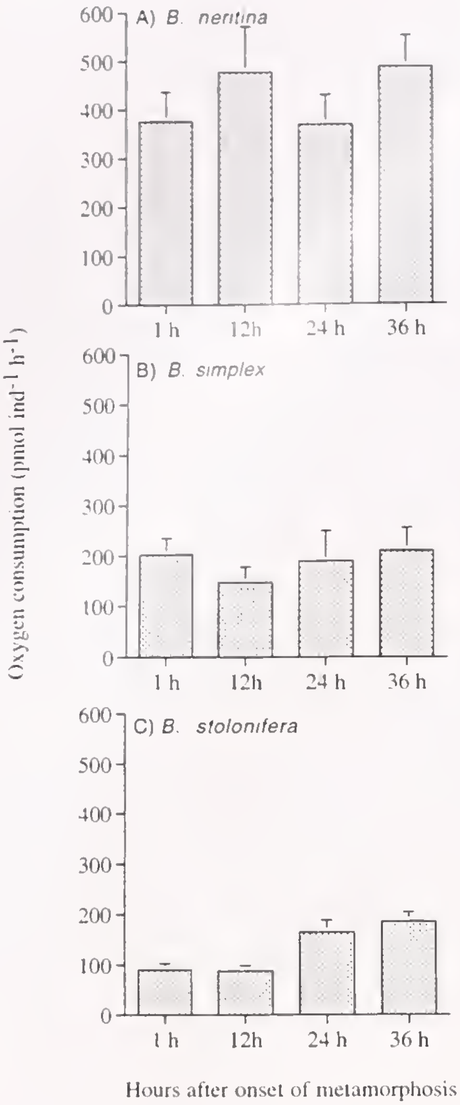

Figure 1. Rates of oxygen consumption (20°C) at 12-h intervals during metamorphosis for *Bugula neritina*, *B. simplex*, and *B. stolonifera*. Metamorphosis starts with eversion of the metasomal sac and concludes with eversion of the lophophore, the adult feeding structure. Metamorphosis was triggered using 10 m*M* excess KCl in seawater. Because replicate trials contained several metamorphosing individuals (*ca.* 10–20), oxygen measurements were made until more than 50% of the individuals in a replicate completed metamorphosis. *n* = 5 trials for each species. Bars = 1 standard error.

Mean protein content for newly released larvae (<1 h) was 0.25 ± 0.02, 0.47 ± 0.02, 0.67 ± 0.03, and 1.4 ± 0.05 μg larva^{-1} for *B. stolonifera*, *B. simplex*, *B. turrita*, and *B. neritina*, respectively (calculated based on an elemental nitrogen conversion factor of 5.8 [Gnaiger and Bitterlich, 1984]).

Completion of metamorphosis

The ability to complete metamorphosis as a function of larval swimming duration was followed for 36 h for *B. simplex* and *B. stolonifera*. For the other two species, only about 60% of the larvae completed metamorphosis after 12 h of larval swimming (Fig. 2). After 24 h of larval swimming, only 30% of larvae of *B. simplex* and only about 2% of larvae of *B. stolonifera* completed metamorphosis.

Larval size and parameters of larval swimming

Mean swimming speeds were similar for larvae of all species. Consequently, speed, measured as body lengths per second, was inversely related to body size (Table 2). *Bugula stolonifera*, the smallest larva (mean length = 160 ± 2 μm), swam at 0.49 ± 0.01 cm s^{-1}, traversing a distance equal to 31.0 ± 0.8 body lengths per second. In contrast, *B. neritina*, with the largest larvae (mean length = 271 ± 2 μm), swam at 0.46 ± 0.02 cm s^{-1}, covering a distance equivalent to 17.2 body lengths per second. *Bugula simplex* and *B. turrita*, of intermediate size, covered intermediate distances (Table 2). Mean Reynolds numbers for larvae of each species ranged from 0.75 ± 0.02 for the smallest larvae (*B. stolonifera*) to 1.20 ± 0.03 for the largest larvae (*B. neritina*) (Table 2).

Discussion

Relationship between energetic parameters and larval size

The amount of energy larvae possess determines, at least in part, the amount of time available for swimming and metamorphosis, and hence the ability to recruit to distant populations. On the basis of this relationship, one would predict that smaller larvae would lose the ability to successfully complete metamorphosis sooner than larger larvae. My data demonstrate this general relationship (Fig. 2).

Mean larval length and width varied by about 40% among the species of *Bugula* examined in this study (Table 2). This size difference translates into marked differences in larval volume and, therefore, in energy content (Table 1, Fig. 3). A similar relationship was found for echinoderms with lecithotrophic development (Jaeckle, 1995a). Carbon content spanned an order of magnitude between the smallest larva (*B. stolonifera*) and the largest larva (*B. neritina*) (Fig. 3, Table 1); and specific respiration rates declined exponentially with increasing carbon content (Fig. 4). Assuming that these larvae have finite energy reserves (ignoring the potential for DOM utilization [Jaeckle, 1994]), the specific respiration rates can be interpreted as a measure of how much energy is available for swimming and metamorphosis. Larvae of *B. neritina*, which are the largest, have the lowest respiration rates relative to their energy reserves, whereas larvae of *B. stolonifera*, which are the smallest, have the largest respiration rates relative to their energy reserves. The prediction is supported in that almost 50% of the individuals of *B. stolonifera* and *B. simplex* lose

Table 1

Comparison, for four species of Bugula, *of elemental carbon and nitrogen content in newly released (<1 h) larvae and in larvae that had been swimming for 24 h*

	Carbon (ng/larva)			Nitrogen (ng/larva)		
Species	1 h	24 h	Δ C	1 h	24 h	Δ N
B. stolonifera						
Trial 1 ($n = 3, 3$)	212 ± 21	120 ± 14	−92	47 ± 05	29 ± 03	−18
Trial 2 ($n = 3, 6$)	225 ± 08	181 ± 06	−44	52 ± 03	50 ± 01	−2*
Trial 3 ($n = 2, 1$)[1]	152 ± 12	106 ± —	−46	34 ± 03	24 ± —	−10
Trial 4 ($n = 4, 4$)	185 ± 05	126 ± 12	−60	44 ± 02	29 ± 03	−15
Mean of trials	194 ± 16	134 ± 16	−60 ± 10	44 ± 04	33 ± 06	−11 ± 04
B. simplex						
Trial 1 ($n = 4, 5$)	430 ± 24	358 ± 16	−72	82 ± 03	67 ± 03	−15
Trial 2 ($n = 4, 5$)	416 ± 34	345 ± 19	−71	85 ± 07	70 ± 04	−15
Trial 3 ($n = 2, 2$)	394 ± 05	282 ± 08	−112	77 ± 02	54 ± 01	−23
Mean of trials	413 ± 11	329 ± 23	−85 ± 14	81 ± 03	64 ± 05	−17 ± 03
B. turrita						
Trial 1 ($n = 4, 4$)	611 ± 25	503 ± 33	−108	122 ± 05	103 ± 06	−18
Trial 2 ($n = 4, 6$)	543 ± 09	484 ± 15	−59	108 ± 03	100 ± 03	−8*
Trial 3 ($n = 4, 4$)	527 ± 14	431 ± 25	−96	105 ± 03	87 ± 05	−18
Trial 4 ($n = 4, 4$)	626 ± 28	542 ± 10	−84	124 ± 06	111 ± 03	−13
Mean of trials	577 ± 24	490 ± 23	−87 ± 11	115 ± 5	100 ± 05	−14 ± 03
B. neritina						
Trial 1 ($n = 1, 5$)[1]	1334 ± —	1209 ± 32	−125	270 ± —	242 ± 07	−28
Trial 2 ($n = 4, 4$)	1340 ± 52	1207 ± 12	−133	238 ± 10	237 ± 04	−1*
Trial 3 ($n = 4, 4$)	1333 ± 54	1215 ± 34	−118	250 ± 07	237 ± 08	−14*
Trial 4 ($n = 4, 2$)	1245 ± 32	1129 ± 19	−116	238 ± 08	222 ± 15	−15*
Mean of trials	1313 ± 03	1190 ± 03	−123 ± 04	249 ± 08	234 ± 05	−15 ± 03*

Values are means plus or minus 1 standard error. Each replicate sample contained about 100 larvae; n represents the number of replicates for newly hatched larvae (1 h) and for larvae that had swum for 24 h (24 h). Carbon was significantly less in 24-h larvae in every trial ($P < 0.05$). For nitrogen, nonsignificant differences are marked with an asterisk (*).

[1] Statistical analysis was not possible due to lack of replicate samples in one treatment.

the ability to complete metamorphosis after a larval swimming period of 12 h; in contrast, almost all individuals of *B. neritina* are able to complete metamorphosis after 12 h of larval swimming (Fig. 2). After 24 h of larval swimming, almost no individuals of *B. stolonifera* completed metamorphosis, but 25% of *B. neritina* and *B. simplex* larvae were still competent to metamorphose. Thus, in larvae of *Bugula* spp., energetic reserves apparently control the length of the competent period to some extent, as has been suggested for larvae of barnacles (Lucas *et al.*, 1979; Jarret and Pechenik, 1997), corals (Richmond, 1987, 1988; Zaslow and Benayahu, 1996), bryozoans (Woollacott *et al.*, 1989; Jaeckle, 1994; Wendt, 1996), and trematodes (Pechenik and Fried, 1995). In contrast, some authors have reported that energetic reserves do not strongly control the length of the competent period (Orellana *et al.*, 1996; Wilson and Harrison, 1998). Thus, it appears that the amount of larval energy reserves in part controls the lengths of time larvae have to swim and metamorphose, but additional physiological factors may also be important for some species.

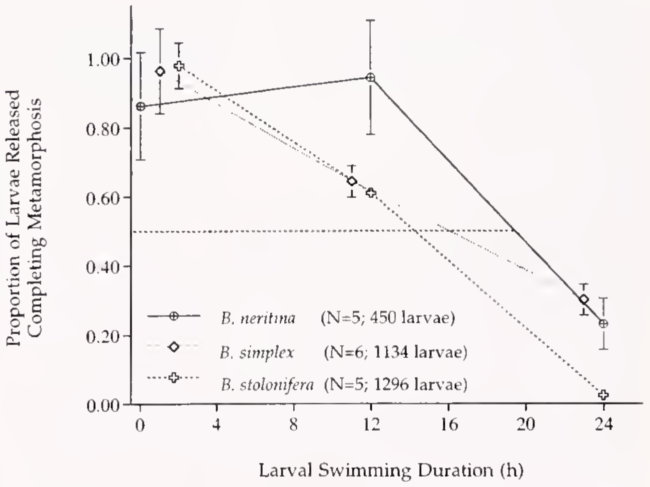

Figure 2. Loss of the ability to complete metamorphosis as a function of larval swimming duration for *Bugula stolonifera* and *B. simplex*. Larvae were released from parent colonies in bright illumination, which prevented them from metamorphosing. At 12-h intervals, samples of larvae were removed from the bright illumination and induced to metamorphose with 10 mM excess KCl in seawater. Data for *B. neritina* are from Wendt (1996). Bars = 95% confidence interval; n = number of experimental trials.

Table 2

Parameters used to calculate Reynolds numbers for larvae of Bugula *spp.*

Species	*n*	Length (µm)	Width (µm)	Velocity (cm s^{-1})	Body lengths s^{-1}	Reynolds Number[1]
B. stolonifera	40	160 ± 2	142 ± 2	0.49 ± 0.01	31.0 ± 0.8	0.75 ± 0.02
B. simplex	20	207 ± 9	201 ± 8	0.44 ± 0.01	24.5 ± 1.0	0.78 ± 0.03
B. turrita	20	202 ± 3	196 ± 2	0.34 ± 0.01	19.2 ± 0.5	0.76 ± 0.02
B. neritina	40	271 ± 2	231 ± 2	0.46 ± 0.02	17.2 ± 0.7	1.20 ± 0.03

All values are means plus or minus 1 standard error.

[1] Reynolds numbers were calculated individually for each larva on the basis of swimming speed and larval size, then averaged.

Metabolic cost of swimming and metamorphosis

Clear trends in the metabolic costs of swimming and metamorphosis emerged within and between species of *Bugula*. For the species tested, the process of metamorphosis demanded markedly more energy than did a larval swimming duration of maximal length (Fig. 5). For example, individuals of *B. neritina* expended almost 4 times more energy during metamorphosis than they did for 20 h of swimming, which was considered a maximum swimming duration (estimated from Fig. 2). Larvae of *B. stolonifera,* the smallest larva, consumed approximately twice as much energy during metamorphosis as during a maximal swimming period of 16 h (estimated from Fig. 2). The metabolic cost of larval swimming was similar for each species, whereas the cost of metamorphosis was significantly higher for species with larger larvae. Metamorphosing individuals of *B. neritina* used approximately 4 times more energy to complete metamorphosis than did those of *B. stolonifera.* However, when energy expenditure is normalized to endogenous energy reserves, smaller larvae actually expend more

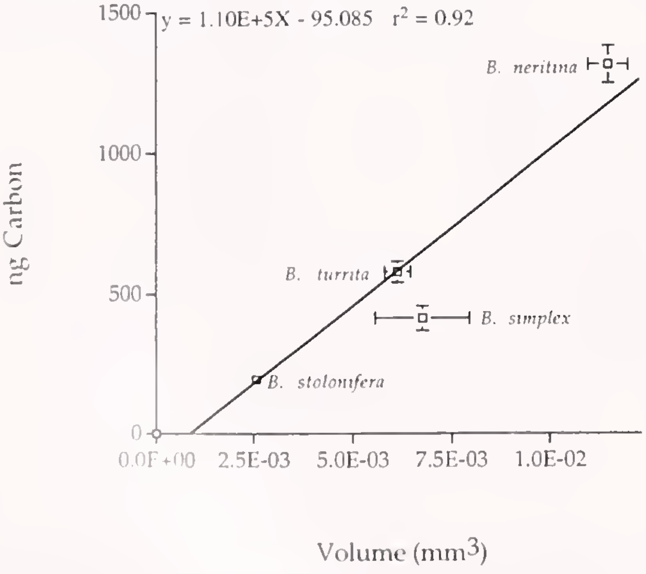

Figure 3. Amount of internal carbon as a function of larval volume for newly released larvae of *Bugula neritina, B. simplex, B. stolonifera,* and *B. turrita.* Volume was calculated using the formula for the volume of a cylinder ($\pi r^2 h$) based on the lengths (h) and widths (r = 0.5 width) from Table 2. Error bars = 1 standard deviation.

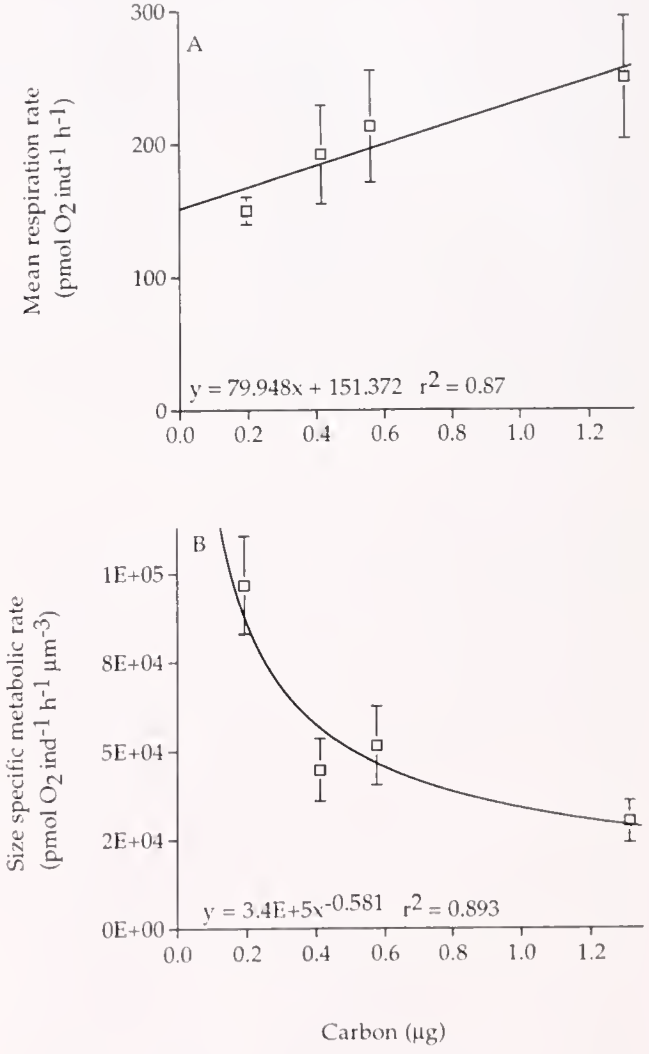

Figure 4. (A) Metabolic rate as a function of larval carbon content (µg C). (B) Specific metabolic rate (pmol O_2 ind^{-1} h^{-1} µm^{-3}) as a function of larval carbon content. Small larvae expended almost 4 times as much energy as a function of their endogenous energy reserves. Bars = 1 standard error.

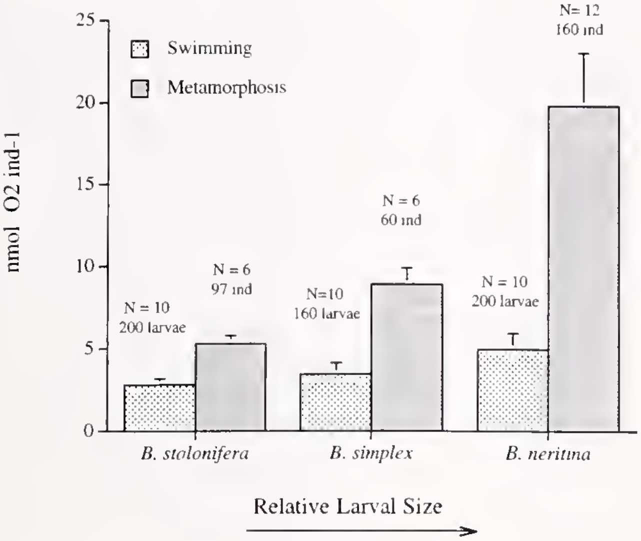

Figure 5. Metabolic cost of a maximum larval swimming phase compared with the overall metabolic cost of metamorphosis for larvae of *Bugula neritina, B. simplex,* and *B. stolonifera.* Total oxygen consumption for swimming and metamorphosis was calculated from rates in text and Fig. 2, respectively. Bars = 1 standard error; *n* = number of experimental trials.

energy. *Bugula stolonifera* expended about 52% of its initial energy reserves to complete metamorphosis and about 1.6% per h while swimming. In contrast, *B. neritina* used only 28% of its initial reserves during metamorphosis and about 0.36% per h during swimming. *Bugula simplex,* which has a larva of intermediate size, expended about 40% of its initial energy reserves during completion of metamorphosis and about 0.84% per h during swimming (Table 3). Thus, assuming similar distributions of inert and labile energetic reserves in larvae of these species, small individuals expend more energy, relative to their size, in swimming and in metamorphosis than do large individuals, which agrees with the general trend found across animal phyla (*e.g.,* Zeuthen, 1947, 1953; Pandian and Vernberg, 1987a, b, and several authors therein; Childress and Somero, 1990; Shilling and Manahan, 1994). This finding is in contrast to that reported for larvae of the echinoids *Heliocidaris erythrogramma* and *H. tuberculata,* where energetic output did not scale with larval size (Hoegh-Guldberg and Emlet, 1997).

Crawford's (1992) model demonstrated that the metabolic cost of swimming for small ciliated organisms increased with faster swimming speed and smaller size. Based on this relationship, it was predicted that small larvae would tend to swim slower to offset the increased metabolic cost. However, this was not the case for larvae of *Bugula spp.,* since the smallest larva, that of *B. stolonifera,* actually swam the fastest. Given that larval swimming requires only 0.3%–1.5% of larval energy stores per hour, it is not surprising that *B. stolonifera* did not swim slower, as predicted from Crawford's (1992) model.

Previous research on bryozoan larvae

Orellana *et al.* (1996), working with larvae of the bryozoan *Celleporella hyalina,* did not detect a significant decrease in the amounts of protein or lipid after a 24-h period of larval swimming. In contrast to those results, my data for larvae of *Bugula* spp. document that carbon and nitrogen content decreased significantly during 24 h of larval swimming in most trials (Table 1). The exception was nitrogen content in larvae of *B. neritina,* which decreased in only one of four trials (Table 1). That nitrogen did not decrease consistently in larvae of *B. neritina* can be readily explained, as it is likely that lipid and carbohydrate reserves are utilized first during larval swimming, and that proteins are metabolized only after those reserves are depleted

Table 3

Costs during a maximum larval swimming period and metamorphosis in three species of Bugula

	Calculated energy expenditure (mJ)				% of Endogenous reserves expended[4]		
Species	Swim (h^{-1})	Max swim[1]	Meta[2]	Energy content[3]	Swim (h^{-1})	Max swim	Meta
Bugula stolonifera	0.08 ± 0.01	1.3 ± 0.2	2.6 ± 0.2	5.0 ± 0.41	1.60	26	52
Bugula simplex	0.09 ± 0.02	1.7 ± 0.3	4.3 ± 0.5	10.7 ± 0.28	0.84	16	40
Bugula neritina	0.12 ± 0.02	2.4 ± 0.3	9.5 ± 1.5	33.7 ± 0.13	0.36	7	28

Values for swimming and metamorphosis were calculated based on the average oxyenthalpic equivalent of 468 kJ mol O_2^{-1} (Gnaiger, 1983). Metabolic rates are expressed as mJ ind^{-1}. Means ± 1 standard error.

[1] Oxygen consumption rates were integrated over a maximal swimming duration which was estimated as the amount of time after which 50% of larvae lose the ability to complete metamorphosis (16 h, 19 h, and 20 h for *B. stolonifera, B. simplex,* and *B. neritina,* respectively).

[2] Oxygen consumption values were integrated over the time it took 50% of the individuals in the experiment to complete metamorphosis (38 h, 48 h, and 48 h for *B. stolonifera, B. simplex,* and *B. neritina,* respectively).

[3] (mJ per larva) calculated from elemental carbon using the equation: kJ g $biomass^{-1}$ = 10.28 − 66.26*gC (Gnaiger, 1984). Multiplying both sides of the equation by "g biomass" gives mJ. Biomass was estimated using the factor 1 μg C = 2.5 μg biomass (McEdward and Carson, 1987).

[4] Calculated by dividing the average energy (mJ) used for swimming (or metamorphosis) by the total energy content of the larva.

(*e.g.*, Emerson, 1967; Stickle, 1971). Because larvae of *B. neritina* have the lowest average specific metabolic rate of the species in this study (Fig. 4), one would predict that these larvae would swim the longest before metabolizing protein. In fact, values for the average percentage decrease of larval nitrogen during 24 h of swimming were 25%, 20%, 12%, and 6% for larvae of *B. stolonifera*, *B. simplex*, *B. turrita*, and *B. neritina*, respectively (calculated from Table 1; larvae in order of increasing size).

Jaeckle (1994) determined respiration rates for larvae of *B. neritina* collected from the same field site as those used in this study. He reported a mean respiration rate of 306 ± 24.9 pmol O_2 ind^{-1} h^{-1} at 22°C, compared to 249 ± 45 pmol O_2 ind^{-1} h^{-1} measured in my study. The slightly higher rates reported by Jaeckle are expected, given that my experiments were carried out at 20°C, 2°C less than his experiments. He also measured larval energy content using the dichromate oxidation assay as described in Parsons *et al.* (1984) and modified by McEdward and Coulter (1987) for micro-samples. Jaeckle (1994) reports a total mean energy content of 15.24 ± 1.33 mJ larva^{-1} for larvae of *B. neritina*. This value is less than half as much as the 37.7 ± 0.14 mJ ind^{-1} measured here using elemental analysis. At present there is no way to resolve this discrepancy. However, given that oxygen demand during metamorphosis in my study was equivalent to an average of 9.5 ± 1.5 mJ, Jaeckle's estimate seems somewhat low in that metamorphosis alone would use 62% of a larva's internal energy reserves.

Sources of larval energetic reserves: realized contribution of dissolved organic material (DOM)

Energy used by larvae for swimming can potentially come from three sources: (1) endogenous reserves provided by the parent; (2) particulate organic matter consumed during feeding in the plankton; and (3) uptake and utilization of DOM. As larvae of *Bugula* spp. are anenteric and hence unable to ingest particulate food, their potential sources of energy are limited to parental ones and to DOM.

Recent work has demonstrated the uptake of DOM by larvae of several species of marine invertebrates (Manahan, 1989, 1990; Jaeckle and Manahan, 1989a, b; Welborn and Manahan, 1990; Ronnestad *et al.*, 1992; Hoegh-Guldberg, 1994; Jaeckle, 1994, 1995a, b; Shilling and Manahan, 1990). It is known that embryos of *B. neritina* receive nutrients translocationally *via* a placenta-like organ during embryogenesis (Woollacott and Zimmer, 1975) and that larvae of *B. neritina* could potentially transport palmitic acid at a rate sufficient to account for from 21% to 72% of their metabolic demand (Jaeckle, 1994). Given the limited energy reserves in larvae of *Bugula* spp. for swimming and metamorphosis, it would be beneficial for them to also utilize energy from DOM, particularly if the larvae are advected from a site suitable for metamorphosis. However, my data suggest that as much as 95%–100% of the measured respiration rate could be accounted for by the estimated decline in elemental carbon and nitrogen. For example, calculations based on mean oxygen consumption indicate that larvae of *B. neritina* used 2.9 mJ larva^{-1} during swimming for 24 h (assuming an oxyenthalpic equivalent of 468 KJ mol O_2^{-1}), whereas calculations based on elemental analysis indicate that they used 3.2 mJ larva^{-1}, a mean difference of −0.3 mJ larva^{-1} (see Table 3, footnote 3, for assumptions used in calculation), suggesting that all of the respired O_2 is the result of catabolism of endogenous carbon and nitrogen. Similar results are found for larvae of *B. simplex*, *B. stolonifera*, and *B. turrita*. These preliminary data suggest that larvae of *Bugula* spp. may not utilize significant amounts of DOM during their brief swimming phase. Clearly, more work is needed to determine the *realized* contribution of DOM to the nutrition of these and other larvae of marine invertebrates.

Acknowledgments

I thank Sherry Reed, Hugh Reichardt, and Dr. Mary E. Rice, all of the Smithsonian Marine Station at Fort Pierce, Fort Pierce, Florida, for their assistance in carrying out this research. Colleen Cavanaugh, Robert Woollacott (both of Harvard University), and Jan Pechenik (Tufts University) provided thoughtful discussions and comments which greatly improved the study. I extend my sincere gratitude to two anonymous reviewers whose suggestions also greatly improved the manuscript. Much appreciation goes to Edward Enos at the Marine Biological Laboratory and "Pinky" in Woods Hole, Massachusetts, for generously allowing us to collect animals from their respective facilities. I thank Wendy Lynn Wendt for editing the manuscript. Portions of this research were supported by a Smithsonian Fellowship and by a Grant-in-Aid of Research from Sigma Xi to Dean E. Wendt. This paper is contribution number 400 of the Smithsonian Marine Station, Fort Pierce, Florida.

Literature Cited

Childress, J. J., and G. N. Somero. 1990. Metabolic scaling: a new perspective based on scaling of glycolytic enzyme activities. *Am. Zool.* **30:** 161–173.

Crawford, D. W. 1992. Metabolic cost of motility in planktonic protists: theoretical considerations on size scaling and swimming speed. *Microb. Ecol.* **24:** 1–10.

Crisp, D. J. 1974. Energy relations of marine invertebrate larvae. *Thalassia Jugosl.* **10:** 103–120.

Emerson, D. N. 1967. Carbohydrate oriented metabolism of *Planorbis duplicatus* (Mollusca: Planorbidae) during starvation. *Comp. Biochem. Physiol.* **22:** 571–579.

Gnaiger, E. 1983. Calculation of energetic and biochemical equivalents of respiratory oxygen consumption. Pp. 337–345 in *Polarographic Oxygen Sensors: Aquatic and Physiological Applications*, E. Ganiger and H. Forstner, eds. Springer-Verlag, New York.

Gnaiger, E., and G. Bitterlich. 1984. Proximate biochemical composition and caloric content calculated from elemental CHN analysis: a stoichiometric concept. *Oecologica* **62:** 289–298.

Highsmith, R. C., and R. B. Emlet. 1986. Delayed metamorphosis: effect on growth and survival of juvenile sand dollars (Echinoidea: Clypeasteroida). *Bull. Mar. Sci.* **39:** 347–361.

Hoegh-Guldberg, O. 1994. Uptake of dissolved organic matter by larval stage of the crown-of-thorn starfish *Acanthaster planci. Mar. Biol.* **120:** 55–63.

Hoegh-Guldberg, O., and R. B. Emlet. 1997. Energy use during the development of a lecithotrophic and planktotrophic echinoid. *Biol. Bull.* **192:** 27–40.

Hunter, E., and N. Fusetani. 1996. Studies of the effects of larval swimming time on settlement, metamorphosis, and post-larval development of *Bugula neritina* (Cheilostomatida). Pp. 139–148 in *Bryozoa In Space and Time,* D. P. Gordon, A. M. Smith, and J. A. Grant-Mackie, eds. Colorographic International, Wellington, New Zealand.

Jaeckle, W. B. 1994. Rates of energy consumption and acquisition by lecithotrophic larvae of *Bugula neritina* (Bryozoa: Cheilstomata). *Mar. Biol.* **119:** 517–523.

Jaeckle, W. B. 1995a. Variation in the size, energy content, and biochemical composition of invertebrate eggs: correlates to the mode of larval development. Pp. 49–78 in *Ecology of Marine Invertebrate Larvae.* L. R. McEdward, ed. CRC Press, Boca Raton, FL.

Jaeckle, W. B. 1995b. Transport and metabolism of alanine and palmitic acid by field-collected larvae of *Tedania ignis* (Porifera, Demospongiae): estimated consequences of limited label translocation. *Biol. Bull.* **189:** 159–167.

Jaeckle, W. B., and D. T. Manahan. 1989a. Amino acid uptake and metabolism by larvae of the marine worm *Urechis caupo* (Echiura), a new species in axenic culture. *Biol. Bull.* **176:** 317–326.

Jaeckle, W. B., and D. T. Manahan. 1989b. Feeding by a "nonfeeding larva": uptake of dissolved amino acids from seawater by lecithotrophic larvae of the gastropod *Haliotis rufescens. Mar. Biol.* **103:** 87–89.

Jarret, J. N., and J. A. Pechenik. 1997. Temporal variation in cyprid quality and juvenile growth capacity for an intertidal barnacle. *Ecology* **78:** 1262–1265.

Levin, L. A., and T. S. Bridges. 1995. Pattern and diversity in reproduction and development. Pp. 1–48 in *Ecology of Marine Invertebrate Larvae.* L. R. McEdward, ed. CRC Press, Boca Raton, FL.

Lucas, M. I., G. Walker, D. L. Holland, and D. J. Crisp. 1979. An energy budget for the free-swimming and metamorphosing larva of *Balanus balanoides* (Crustacea: Cirripedia). *Mar. Biol.* **55:** 221–229.

Manahan, D. T. 1989. Amino acid fluxes to and from seawater in axenic veliger larvae of a bivalve (*Crassostrea gigas*). *Mar. Ecol. Prog. Ser.* **53:** 247–255.

Manahan, D. T. 1990. Adaptations by invertebrate larvae for nutrient acquisition from seawater. *Am. Zool.* **30:** 147–160.

McCarthy, J. J., C. Garside, and J. L. Nevins. 1999. Nitrogen dynamics during the Arabian Sea Northeast Monsoon. *Deep-Sea Res.* II **46:** 1623–1664.

McEdward, L. R., and S. F. Carson. 1987. Variation in organic content and its relationship with egg size in the starfish *Solaster stimpsoni. Mar. Ecol. Prog. Ser.* **37:** 159–169.

McEdward, L. R., and L. K. Coulter. 1987. Egg volume and energetic content are not correlated among sibling offspring of starfish: implications for life-history theory. *Evolution.* **41:** 914–917.

Nielsen, C. 1981. On morphology and reproduction of *Hippodiplosia insculpta* and *Fenestrulina malusii* (Bryozoa, Cheilostomata). *Ophelia* **20:** 91–125.

Orellana, M. C., and J. M. Cancino. 1991. The effects of delaying larval settlement on metamorphosis and early colonial growth in *Celleporella hyalina* (Bryozoa: Cheilostomata). Pp. 309–316 in *Bryozoa Living and Fossil,* F. P. Bigey, ed. *Bull. Soc. Sci. Nat. Ouest Fr.,* Mem. HS1. Saint-Herblain, Nantes, France.

Orellana, M. C., J. M. Cancino, and R. N. Hughes. 1996. Is settlement in lecithotrophic bryozoan larvae constrained by energy reserves? Pp. 221–226 in *Bryozoans in Space and Time,* D. P. Gordon, A. M. Smith, and J. A. Grant-Mackie, eds. NIWA (Nat. Inst. Water Atmospheric Res.), Wellington, NZ.

Pandian, T. J., and F. J. Vernberg, eds. 1987a. *Animal Energetics: Protozoa Through Insecta.* Vol 1. Academic Press, San Diego, CA.

Pandian, T. J., and F. J. Vernberg, eds. 1987b. *Animal Energetics: Bivalvia Through Reptillia.* Vol 2. Academic Press, San Diego, CA.

Parsons, T. R., Y. Maita, and C. M. Lalli. 1984. *A Manual of Chemical and Biological Methods for Seawater Analysis.* Pergamon Press, New York. Pp. 63–66.

Pechenik, J. A. 1980. Growth and energy balance during the larval lives of three prosobranch gastropods. *J. Exp. Mar. Biol. Ecol.* **44:** 1–28.

Pechenik, J. A. 1990. Delayed metamorphosis of benthic marine invertebrates: Does it occur? Is there a price to pay? *Ophelia* **32:** 63–94.

Pechenik, J. A., and T. R. Cerulli. 1991. Influence of delayed metamorphosis on survival, growth, and reproduction of the polychaete *Capitella* sp. I. *J. Exp. Mar. Biol. Ecol.* **151:** 17–27.

Pechenik, J. A., and B. Fried. 1995. Effect of temperature on survival and infectivity of *Echinostoma trivolvis* cercariae: a test of the energy limitation hypothesis. *Parasitology.* **111:** 373–378.

Pechenik, J. A., D. Rittschof, and A. R. Schmidt. 1993. Influence of delayed metamorphosis on survival and growth of juvenile barnacles *Balanus amphitrite. Mar. Biol.* **115:** 287–294.

Pechenik, J. A., D. E. Wendt, and J. N. Jarret. 1998. Metamorphosis is not a new beginning. *BioScience* **48:** 901–909.

Pires, A., and R. M. Woollacott. 1997. Serotonin and dopamine have opposite effects on phototaxis in larvae of the bryozoan *Bugula neritina. Biol. Bull.* **192:** 399–409.

Qian, P-Y., L. R. McEdward, and F-S. Chia. 1990. Effects of delayed settlement on survival, growth, and reproduction in the spionid polychaete, *Polydora ligni. Int. J. Invertebr. Reprod. Dev.* **18:** 147–152.

Reed, C. G., and R. M. Woollacott. 1982. Mechanisms of rapid morphogenetic movements in the metamorphosis of the bryozoan *Bugula neritina* (Cheilostomata, Cellularioidea). I Attachment to the substratum. *J. Morphol.* **172:** 335–348.

Reed, C. G., and R. M. Woollacott. 1983. Mechanisms of rapid morphogenetic movements in the metamorphosis of the bryozoan *Bugula neritina* (Cheilostomata, Cellularioidea). II The role of dynamic assemblages of microfilaments in the pallial epithelium. *J. Morphol.* **177:** 127–143.

Richmond, R. H. 1987. Energetics, competency, and long-distance dispersal of planula larvae of the coral *Pocillopora damicornis. Mar. Biol.* **93:** 527–533.

Richmond, R. H. 1988. Competency and dispersal potential of planula larvae of a spawning versus a brooding coral. *Proc. 6th Int. Coral Reef Symposium* **2:** 827–831.

Ronnestad, I., H. J. Fyhn, and K. Gravningen. 1992. The importance of free amino acids to the energy metabolism of eggs and larvae of turbot (*Scophthalmus maximus*). *Mar. Biol.* **114:** 517–525.

Ryland, J. S. 1974. Behaviour, settlement and metamorphosis of bryozoan larvae: a review. *Thalassia Jugosl.* **10:** 239–262.

Shilling, F. M., and D. T. Manahan. 1990. Energetics of early marine development for the sea urchins *Strongylocentrotus purpuratus* and *Lytechinus pictus* and the crustacean *Artemia* sp. *Mar. Biol.* **106:** 119–128.

Shilling, F. M., and D. T. Manahan. 1994. Energy metabolism and amino acid transport during early development of Antarctic and temperate echinoderms. *Biol. Bull.* **187:** 398–407.

Stickle, W. B. 1971. The metabolic effects of starving *Thais lamellosa* immediately after spawning. *Comp. Biochem. Physiol.* **40A:** 627–634.

Strathmann, M. F. 1987. *Reproduction and Development of Marine*

Invertebrates of the Northern Pacific Coast. University of Washington Press, Seattle, WA.

Strathmann, R. R. 1974. Introduction to function and adaptation in echinoderm larvae. *Thalassia Jugosl.* **10:** 321–339.

Vogel, S. 1994. *Life in Moving Fluids.* Princeton University Press, Princeton, NJ.

Weast, R. C., and M. J. Astle. 1980. *CRC Handbook of Chemistry and Physics,* 61st ed. CRC Press, Boca Raton, FL.

Welborn, J. R., and D. T. Manahan. 1990. Direct measurements of sugar uptake from seawater into molluscan larvae. *Mar. Ecol. Prog. Ser.* **65:** 233–239.

Wendt, D. E. 1996. Effect of larval swimming duration on success of metamorphosis and size of the ancestrular lophophore in *Bugula neritina* (Bryozoa). *Biol. Bull.* **191:** 224–233.

Wendt, D. E. 1998. Effect of larval swimming duration on growth and reproduction of *Bugula neritina* (Bryozoa) under field conditions. *Biol. Bull.* **195:** 126–135

Wendt, D. E., and R. M. Woollacott. 1995. Induction of larval settlement by KCl in three species of *Bugula* (Bryozoa). *Invertebr. Biol.* **114:** 345–351.

Wendt, D. E., and R. M. Woollacott. 1999. Ontogenies of larval phototaxis and metamorphic competence in *Bugula* spp. (Bryozoa). *Invertebr. Biol.* **118:** 75–84.

Wilson, J. R., and P. L. Harrison. 1998. Settlement-competency periods of larvae of three species of scleractinian corals. *Mar. Biol.* **131:** 339–345.

Woollacott, R. M., and R. L. Zimmer. 1971. Attachment and metamorphosis of the Cheilo-ctenostome bryozoan *Bugula neritina* (Linné). *J. Morphol.* **134:** 351–382.

Woollacott, R. M., and R. L. Zimmer. 1972. Origin and structure of the brood chamber in *Bugula neritina* (Bryozoa). *Mar. Biol.* **16:** 165–170.

Woollacott, R. M., and R. L. Zimmer. 1975. A simplified placenta-like system for the transport of extraembryonic nutrients during embryogenesis of *Bugula neritina. J. Morphol.* **147:** 355–377.

Woollacott, R. M., and R. L. Zimmer. 1978. Metamorphosis of cellularioid bryozoans. Pp. 49–63 in *Settlement and Metamorphosis of Marine Invertebrate Larvae.* F.-S. Chia and M. E. Rice, eds. Elsevier North-Holland, New York.

Woollacott, R. M., J. A. Pechenik, and K. M. Imbalzano. 1989. Effects of duration of larval swimming period on early colony development in *Bugula stolonifera* (Bryozoa: Cheilostomata). *Mar. Biol.* **102:** 57–63.

Zaslow, R. B-D., and Y. Benayahu. 1996. Longevity, competence and energetic content in planulae of the soft coral *Heteroxenia fuscescens. J. Exp. Mar. Biol. Ecol.* **206:** 55–68.

Zeuthen, E. 1947. Body size and metabolic rate in the animal kingdom with special regard to the marine microfauna. *C. R. Trav. Lab. Carlsberg. Ser. Chim.* **26:** 17–161.

Zeuthen, E. 1953. Oxygen uptake as related to body size in organisms. *Q. Rev. Biol.* **28:** 1–12.

Reference: *Biol. Bull.* **198:** 357–366. (June 2000)

The Calcium Dependence of Pigment Translocation in Freshwater Shrimp Red Ovarian Chromatophores

JOHN C. McNAMARA* AND MÁRCIA R. RIBEIRO

Departamento de Biologia, Faculdade de Filosofia, Ciências e Letras, Universidade de São Paulo, Ribeirão Preto, 14040-901 SP, Brazil

Abstract. The roles of calcium in cell signaling consequent to chromatophorotropin action and as an activator of mechanochemical transport proteins responsible for pigment granule translocation were investigated in the red ovarian chromatosomes of the freshwater shrimp *Macrobrachium olfersii*. Chromatosomes were perfused with known concentrations of free Ca^{++} (10^{-3} to 10^{-9} M) prepared in Mg^{++}-EGTA–buffered physiological saline after selectively permeabilizing with 25 μM calcium ionophore A23187 or with 10^{-8} M red pigment concentrating hormone (RPCH). The degree of pigment aggregation and the translocation velocity of the leading edges of the pigment mass were recorded in individual chromatosomes during aggregation induced by RPCH or A23187 and dispersion induced by low Ca^{++}. Aggregation is Ca^{++} dependent, showing a dual extracellular and intracellular requirement. After perfusion with reduced Ca^{++} (10^{-4} to 10^{-9} M), RPCH triggers partial aggregation (≈65%), although the maximum translocation velocities (≈16.5 μm/min) and velocity profiles are unaffected. After aggregation induced at or below 10^{-5} M Ca^{++}, spontaneous pigment dispersion ensues, suggesting a Ca^{++} requirement for RPCH coupling to its receptor, or a concentration-dependent, Ca^{++}-induced Ca^{++}-release mechanism. The Ca^{++}-channel blockers Mn^{++} (5 mM) and verapamil (50 μM) have no effect on RPCH-triggered aggregation. An intracellular Ca^{++} requirement for aggregation was demonstrated in chromatosomes in which the Ca^{++} gradient across the cell membrane was dissipated with A23187. At free $[Ca^{++}]$ above 10^{-3} M, aggregation is complete; at 10^{-4} M, aggregation is partial, followed by spontaneous dispersion; below 10^{-5} M Ca^{++}, pigments do not aggregate but disperse slightly. Aggregation velocities diminish from 11.6 ± 1.2 μm/min at 5.5 mM Ca^{++} to 7.4 ± 1.3 μm/min at 10^{-4} M Ca^{++}. Half-maximum aggregation occurs at 3.2×10^{-5} M Ca^{++} and half-maximum translocation velocity at 4.8×10^{-5} M Ca^{++}. Pigment redispersion after 5.5 mM Ca^{++}-A23187–induced aggregation is initiated by reducing extracellular Ca^{++}: slight dispersion begins at 10^{-7} M, complete dispersion being attained at 10^{-9} M Ca^{++}. Dispersion velocities increase from 0.6 ± 0.2 to 3.1 ± 0.5 μm/min. Half-maximum dispersion occurs at 7.6×10^{-9} M Ca^{++} and half-maximum translocation velocity at 2.9×10^{-9} M Ca^{++}. These data reveal an extracellular and an intracellular Ca^{++} requirement for RPCH action, and demonstrate that the centripetal or centrifugal direction of pigment movement, the translocation velocity, and the degree of pigment aggregation or dispersion attained are calcium-dependent properties of the granule translocation apparatus.

Introduction

Chromatic adaptation in the decapod Crustacea is brought about by the differential translocation of colored pigment granules contained within specialized, multicellular effectors known as chromatosomes (McNamara, 1981). The mechanisms responsible for the centripetal and centrifugal movement of the granules within the constituent chromatophores are regulated by small peptide hormones of neurosecretory origin, often specific and antagonistic for each pigment cell type, but generally termed pigment concentrating (PCH) and pigment dispersing (PDH) chromatophorotropins (Josefsson, 1983; Rao and Fingerman, 1983; Fingerman, 1985).

The signal transduction pathways and intracellular enzymatic cascades activated by these peptides are poorly known in the Crustacea, although they are fairly well established in vertebrate groups like the teleosts, amphibians,

---

Received 23 July 1999; accepted 17 February 2000.

* To whom correspondence should be addressed. E-mail: mcnamara@ffclrp.usp.br

and reptiles, which also exhibit color changes regulated by (neuro)endocrine and neural mechanisms (reviews in Novales, 1983; Nery and Castrucci, 1997; Tuma and Gelfand, 1999). Both intracellular free Ca^{++} concentrations and cyclic nucleotides have been implicated in the second messenger systems that respectively activate the pigment aggregating and dispersing mechanisms in the Crustacea (Fingerman, 1969; Rao and Fingerman, 1983; Nery *et al.*, 1997, 1998). However, it is difficult to establish generic regulatory mechanisms because the two principal groups studied, the brachyuran crabs and the caridean shrimps, differ considerably in their pigmentary responses to the same effector agents. To illustrate, chromatosome pigments spontaneously disperse in shrimp epidermal preparations *in vitro* (Fingerman *et al.*, 1975; Lambert and Fingerman, 1979; McNamara and Taylor, 1987; Tuma *et al.*, 1993), but they aggregate in crab preparations, in the absence of agonists (Lambert and Fingerman, 1976; Kulkarni and Fingerman, 1986). Intracellular Ca^{++}, increased by the calcium ionophore A23187 and calcium-containing salines, causes pigment aggregation in shrimps (Lambert and Fingerman, 1979; Britto *et al.*, 1990; McNamara and Ribeiro, 1999) but dispersion in crabs (Quackenbush, 1981). In shrimps, cyclic AMP disperses red chromatophore pigments (Fingerman, 1969; Nery *et al.*, 1998), but in crabs it is either without effect or also disperses chromatophore pigments (Quackenbush, 1981; Rao and Fingerman, 1983). However, cyclic GMP also disperses black and white but not red chromatophore pigments in crabs (Quackenbush, 1981) and has no effect on shrimp red chromatophores (Nery *et al.*, 1998). Clearly, unequivocal signal transduction pathways that modulate the molecular motors responsible for pigment aggregation and dispersion are yet to be established in the Crustacea as a whole.

Alterations in intracellular calcium concentrations appear to play a major role in the signaling transduction pathway or effector mechanism regulating the mechanochemical protein motors responsible for pigment translocation in caridean chromatophores. Red pigment concentrating hormone (RPCH) induces the aggregation of dispersed pigments, but its action is inhibited or impaired in Ca^{++}-free media (Lambert and Fingerman, 1979; McNamara and Taylor, 1987; Britto *et al.*, 1996) and in the presence of verapamil, an L-type Ca^{++} channel blocker (Britto *et al.*, 1996). In contrast, dispersion of A23187- or RPCH-aggregated pigments can be induced in [illegible]-free saline (Lambert and Fingerman, 1979; [illegible] and Ribeiro, 1999). However, unlike [illegible] chromatophores in which pigment aggregation [illegible] dependent (Luby-Phelps and Porter, 1982; [illegible] 1988; Kotz and McNiven, 1994), in crustaceans [illegible] the origin and role of Ca^{++} in pigment [illegible], and no estimates are available of changes in intracellular Ca^{++} concentration during pigment movements.

Using red ovarian chromatosomes from *Macrobrachium olfersii*, a freshwater caridean shrimp, the present study investigates the origin and calcium-dependent nature of pigment aggregation and dispersion induced by RPCH and A23187. The intracellular free $[Ca^{++}]$ associated with activation of the respective granule translocation mechanisms is also estimated with the aid of a Mg^{++}-EGTA buffer system.

Materials and Methods

Immature, female freshwater shrimp, *Macrobrachium olfersii*, presenting small, translucent ovaries, were collected from the Paúba River in São Paulo State, Brazil, and maintained under a natural photoperiod in about 100 l of river water (salinity $< 0.5‰$, temperature $\approx 23°C$) in 250-l tanks; they were fed celery, beetroot, carrot, and minced beef or chicken.

The ovarian chromatosome preparation employed has been described in detail previously (McNamara and Ribeiro, 1999). Briefly, after dissection, the red chromatosomes were gravity perfused (0.7 ml/min) in an acrylic microperfusion chamber (150 μl volume) and observed at 320× by reflected and transmitted light using a Wild M10 stereoscopic microscope coupled to a Sony DXC-151A CCD video camera and Trinitron monitor.

An ocular graticle was used to quantify the diameter of the pigment mass in chromatosomes of 220–240 μm diameter at 2-min intervals. The data were converted to percent maximum dispersion, and the translocation velocity (in micrometers per minute) of the leading edge of the pigment mass was calculated, for each interval, according to McNamara and Ribeiro (1999).

Perfusion salines were prepared based on ionic data from McNamara *et al.* (1990) for *M. olfersii*. The control saline contained (in millimoles): Na^{+} 177, K^{+} 5, Ca^{++} 5.5, and Mg^{++} 1 as chlorides (≈ 195).

Salines of specific low Ca^{++} concentration were prepared using a Mg^{++}-10 m*M* EGTA buffer system. For RPCH- and A23187-induced pigment aggregation, the respective $[Ca^{++}]$ and $[Mg^{++}]$ necessary to furnish final free Ca^{++} concentrations of 10^{-3} to 10^{-9} *M*, while holding free $[Mg^{++}]$ at 1.03 m*M*, were calculated using the MCalc computer program based on Fabiato (1988). For pigment dispersion in previously A23187-perfused preparations, the $[Ca^{++}]$ and $[Mg^{++}]$ given by Luby-Phelps and Porter (1982) were used to provide final free Ca^{++} concentrations of 10^{-7}, 10^{-8}, and 10^{-9} *M* at a final free $[Mg^{++}]$ of 1.3 m*M*. In the Ca^{++}-free saline (residual $[Ca^{++}] \approx 7 \times 10^{-11}$ *M*), Ca^{++} was substituted by 27.5 m*M* choline chloride, and 2 m*M* EDTA was added.

All salines contained 0.5% DMSO (dimethyl sulfoxide; Sigma, MO), 2.5 mM Na_2HCO_3, and 2 mM glucose (osmolality prior to DMSO, 354 ± 0.7 mOsm/kg H_2O) and were adjusted to pH 7.4. Calcium ionophore A23187 (free acid, Sigma, MO), dissolved in DMSO, was used at a final concentration of 25 μM. Red pigment concentrating hormone (Peninsula Laboratories Inc., CA), dissolved in distilled water or 10% DMSO, was used at a final concentration of either 10 or 30 nM. Verapamil hydrochloride and $MnCl_2$ (Sigma, MO) were dissolved in DMSO or distilled water and used at final concentrations of 50 μM (Hille, 1992) and 5 mM (Zhang *et al.*, 1997), respectively. All experiments were performed at room temperature (≈23°C). Under these conditions, the chromatosome preparation is functional for at least 3–4 h, and up to five successive cycles of aggregation and dispersion can be induced using A23187 and Ca^{++}-free saline, respectively.

Each experiment was repeated seven times, using measurements from a single chromatosome in each preparation. Since most data were not normally distributed, the treatment effect was evaluated using the Kruskal-Wallis one-way, nonparametric ANOVA, followed by Dunn's test to locate significantly different groups. Correlations between pigment translocation velocities and degree of aggregation or dispersion were evaluated employing Pearson's product moment correlation test (SigmaStat 2.03, SPSS Inc., CA). Concentration-effect curves and the 50% response values were obtained using the dose-response logistic curve-fitting function of SlideWrite 5.0 Plus (Advanced Graphics Software, Inc., CA). All tests were performed with a significance level of $P = 0.05$.

Results

Calcium dependence of pigment aggregation

Red pigment concentrating hormone. On perfusion with 10 nM RPCH in control (5.5 mM Ca^{++}) saline, the dispersed pigments aggregate rapidly and completely within 24 min (Fig. 1A1). Translocation velocity attains a customary peak of 17.0 ± 2.9 μm/min ($n = 11$) with a small right-hand shoulder, followed by a short plateau of 1.8 ± 0.3 μm/min, gradually declining thereafter (Fig. 1B1). RPCH washout induces immediate dispersion, reaching about 90% within about 40 min (Fig. 1A1). Dispersion velocity attains a maximum of 5.6 ± 2.5 μm/min (Fig. 1B1).

Perfusion with 10 nM RPCH and the various Mg^{++}-EGTA–buffered Ca^{++}-salines reveals a hormone effect notably dependent on extracellular Ca^{++}. In 10^{-3} M Ca^{++}, the degree of aggregation and the velocity profile (Fig. 1A2, 1B2) are similar to those in control saline (5.5 mM Ca^{++}, Fig. 1A1, 1B1). However, in salines containing reduced Ca^{++}, maximum aggregation varies from 90% (10^{-4} M, Fig. 1A3) to 63% (10^{-5} M, Fig. 1A4), 67% (10^{-6} M, Fig. 1A5) and 60% (10^{-9} M, Fig. 1A6), requiring about 13 min. However, the peak translocation velocities (≈16.5 μm/min) are unaffected by $[Ca^{++}]$ ($P = 0.97$), and the velocity profiles (Fig. 1B3–1B6) are virtually identical to that in 5.5 mM Ca^{++} (Fig. 1B1). Strikingly, at $[Ca^{++}] \leq 10^{-5}$ M, the aggregation effect is rapidly reversed and spontaneous pigment dispersion ensues, attaining 80%–100% of initial dispersion (Fig. 1A4–1A6) in the presence of RPCH. The mean dispersion velocity of about 5 μm/min is unaffected by $[Ca^{++}]$ ($P = 0.67$). Subsequent perfusion with 5.5 mM Ca^{++} induces full pigment aggregation (Fig. 1A4–1A6), and the translocation velocity profiles (Fig. 1B4–1B6) and peak velocities ($P = 0.99$) are the same as in preparations perfused directly with 5.5 mM Ca^{++} (Fig. 1B1).

Although the response to RPCH washout is immediate, dispersion is incomplete, reaching a maximum of about 50% (Fig. 1A2–1A6).

Calcium channel blockers. The time course and degree of pigment aggregation in response to 30 nM RPCH are unaffected by a 30-min preincubation with 5 mM Mn^{++} (Fig. 2A) or 50 μM verapamil (Fig. 3A). The velocity profiles are also typical (Figs. 2B and 3B, respectively, *cf.* Fig. 1B1) and the maximum velocities (≈20 μm/min) are similar ($P = 0.13$).

Calcium ionophore A23187. Perfusion with control (5.5 mM Ca^{++}) saline causes no net movement of the dispersed pigment mass (initial 10 min of Fig. 4A1–4), although 10-min perfusion with the EGTA-buffered salines containing either 10^{-3} (Fig. 4A2), 10^{-4} (Fig. 4A3), or 10^{-5} M Ca^{++} (Fig. 4A4) induces progressive pigment aggregation ($P < 0.001$) that attains a maximum of about 25% in 10^{-5} M Ca^{++} (Fig. 4A4). Translocation velocities are slow and range around a maximum of ≈2–4 μm/min (Fig. 4B2–4).

Perfusion with 25 μM A23187 while holding external Ca^{++} at the designated reduced levels leads to complete aggregation within 26 min with 5.5 mM Ca^{++} (Fig. 4A1) and virtually complete aggregation (90%) at 10^{-3} M (Fig. 4A2). Peak aggregation velocities (11.6 ± 1.2 μm/min, $n = 28$ [Fig. 4B1] and 9.0 ± 3.7 μm/min, $n = 7$ [Fig. 4B2] respectively) are similar ($P = 0.39$). However, with 10^{-4} M Ca^{++}, the initial aggregation response (7.4 ± 1.3 μm/min, $n = 7$ [Figs. 4A3, 4B3]) reverses after about 8 min, and slow, steady (≈1 μm/min) pigment *dispersion* ensues (Fig. 4A3, 4B3). With 10^{-5} M Ca^{++}, A23187 induces slight, slow (≈1.3 μm/min) pigment dispersion (Fig. 4A4, 4B4).

Further perfusion with 5.5 mM Ca^{++} produces complete, rapid pigment aggregation (Fig. 4A3, 4A4), regardless of the previous $[Ca^{++}]$ used. Velocity profiles and peak velocities (≈11 μm/min, Fig. 4B3, 4B4) do not differ ($P = 0.83$) from those in preparations perfused directly with 5.5 mM Ca^{++} (Fig. 4B1).

Removal of Ca^{++} (≈7 × 10^{-11} M Ca^{++}, 2 mM EDTA) and A23187 from the perfusate after previous buffering

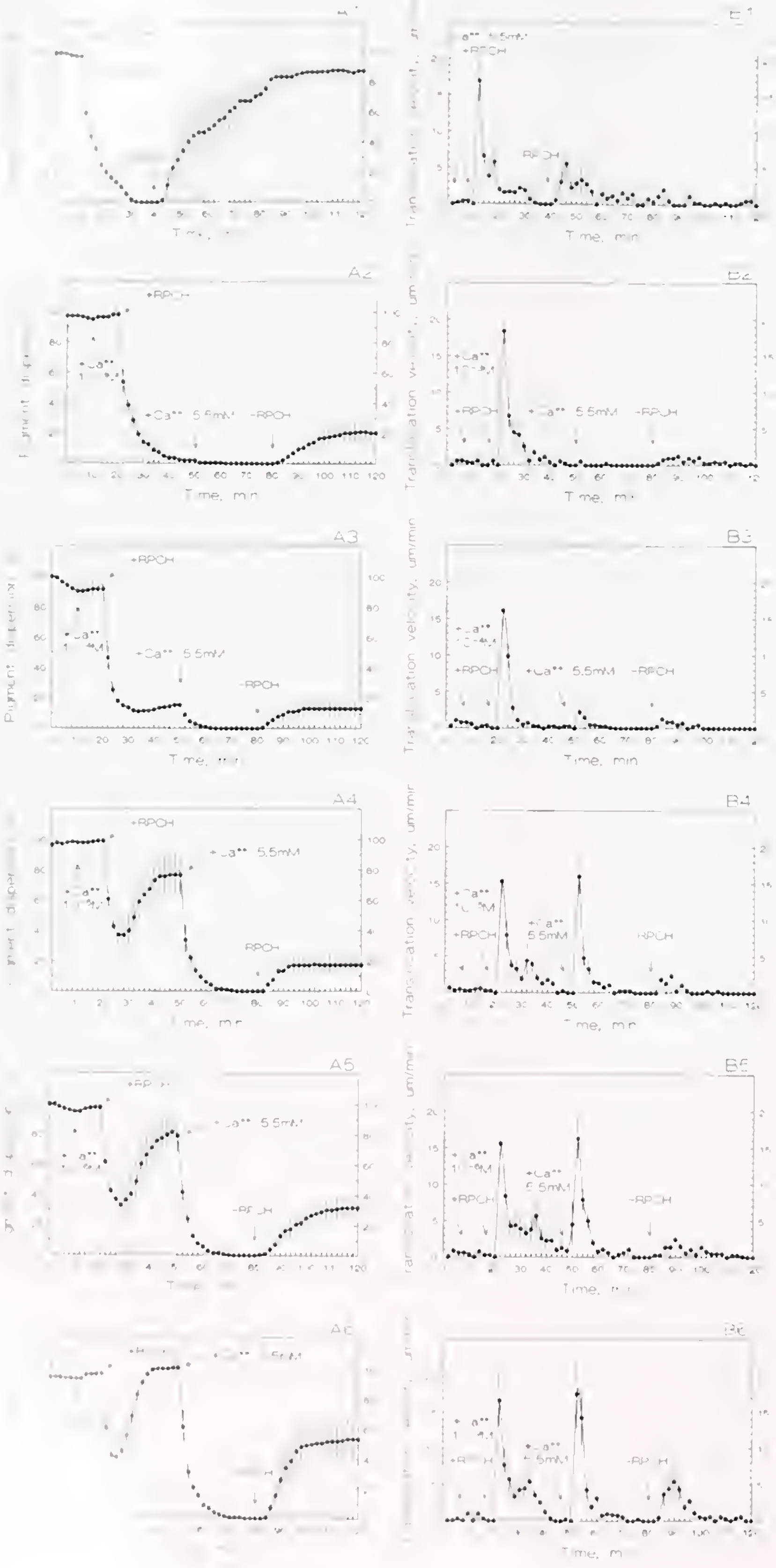
A1
A2
A3
A4
A5
A6
B1
B2
B3
B4
B5
B6
+RPCH
-RPCH
+Ca++ 10⁻⁴M
+Ca++ 5.5mM
Pigment dispersion
Translocation velocity, um/min
Time, min

with Mg^{++}-EGTA (Fig. 4A2–4) does not produce the customary full pigment dispersion seen with EDTA alone (*cf.* Fig. 4A1), possibly due to chelating interference by EGTA.

Dependence of pigment dispersion on reduced calcium

After complete pigment aggregation using 25 μM A23187 and saline containing 5.5 mM Ca^{++}, moderately rapid (maximum of 6.8 ± 1.7 μm/min [Fig. 5B1]), complete, pigment dispersion can be induced using a Ca^{++}-free saline (residual $Ca^{++} \approx 7 \times 10^{-11}$ M, 2 mM EDTA [minutes 90–130 of Fig. 5A1]); removal of the ionophore itself does not induce dispersion.

As the [Ca^{++}] in the Mg^{++}-EGTA–buffered perfusate is decreased from 10^{-7} (Fig. 5A2) to 10^{-8} (Fig. 5A3) and 10^{-9} M (Fig. 5A4), differential degrees of maximum pigment dispersion are induced, attaining about 80% in the latter. Maximum dispersion velocities increase (0.6 ± 0.3, 2.8 ± 2.1, and 4.7 ± 1.7 μm/min, respectively, [$P = 0.03$]) with decreasing [Ca^{++}] (Fig. 5B2–4). Further slight dispersion to about 90% can be induced using EDTA-buffered Ca^{++}-free saline (minutes 90–130 of Fig. 5A4).

Relationship between degree of aggregation or dispersion and translocation velocity

Both translocation velocity and the degree to which pigment aggregates respond in a positively correlated, concentration-dependent manner to *increasing* external free [Ca^{++}] between 10^{-5} M and 5.5 mM (Fig. 6); half-maximum translocation velocity (V_{50}) is reached at 4.8×10^{-5} M and half-maximum aggregation at 3.2×10^{-5} M external free Ca^{++}. The velocity and degree of pigment dispersion are also positively correlated and increase in a concentration-dependent manner to *decreasing* external free [Ca^{++}] between 10^{-7} and 10^{-11} M (Fig. 7), with V_{50} occurring at 2.9×10^{-9} M and half-maximum dispersion at 7.6×10^{-9} M external free Ca^{++}.

Discussion

The present data obtained with red pigment concentrating hormone (RPCH) and A23187 respectively reveal an extracellular and an intracellular calcium requirement for pigment aggregation in the red ovarian chromatophores of *Macrobrachium olfersii.*

RPCH requires extracellular Ca^{++} at $\geq 10^{-4}$ M to induce complete pigment aggregation. At lower concentrations (10^{-5} to 10^{-9} M Ca^{++}), aggregation is incomplete ($\approx$65%), although the maximum translocation velocities ($\approx$16.5 μm/min) and triphasic velocity profiles (McNamara and Ribeiro, 1999) are unaffected, except for minor suppression of the final low-velocity phase. This suggests that Ca^{++} is required for coupling between RPCH and its receptor, much as in neural nicotinic receptors (Ospina *et al.*, 1998; Booker *et al.*, 1998; Liu and Berg, 1999). Incomplete aggregation may result from diminished signal transduction consequent to a reduction in the affinity between RPCH and its receptor at low [Ca^{++}]. However, the intracellular signal generated is sufficient to transiently trigger the molecular motors responsible for aggregation at full capacity until the Ca^{++}-regulatory mechanisms restore intracellular free Ca^{++} to the resting concentration, leading to spontaneous dispersion.

Alternatively, an RPCH-activated, Ca^{++}-induced/Ca^{++}-release mechanism dependent on the Ca^{++} gradient across the cell membrane (Putney and Bird, 1993; Verkhratsky and Shmigol, 1996) may operate. The reduced Ca^{++} entering the chromatophore through RPCH-activated Ca^{++} channels would be insufficient to promote sustained opening of target smooth endoplasmic reticulum Ca^{++} channels, or to activate protein kinase C-dependent (Abrão *et al.*, 1991; Sugden and Rowe, 1992) or Ca^{++}-calmodulin-dependent effector pathways (Lee *et al.*, 1994; Verkhratsky and Shmigol, 1996; Mukhopadhyay *et al.*, 1997), also resulting in transient pigment aggregation. Since the Ca^{++}-channel blockers Mn^{++} and verapamil have no effect on the degree and velocity of pigment aggregation, these putative receptor-activated Ca^{++} channels seem not to be L-type channels (Britto *et al.*, 1996; Katz, 1996; Zhang *et al.*, 1997; Striessnig *et al.*, 1998). Although only a single maximum blocker dose was employed, and other Ca^{++} channel types may be present, this suggests that the Ca^{++} required to activate the granule transport motors may be intracellular rather than extracellular in origin.

When the limiting effect of low extracellular Ca^{++} is bypassed by dissipating the Ca^{++} gradient across the cell

Figure 1. Dependence of RPCH-induced pigment aggregation (A series) on extracellular free Ca^{++} (A1, 5.5 mM; A2, 10^{-3} M; A3, 10^{-4} M; A4, 10^{-5} M; A5, 10^{-6} M; A6, 10^{-9} M) in *Macrobrachium olfersii* red chromatosomes perfused sequentially with control (5.5 mM Ca^{++}) saline, respective Ca^{++}-10 mM EGTA–buffered saline, and Ca^{++}-EGTA–buffered saline + 10 nM RPCH. At and below 10^{-5} M Ca^{++} (A4–A6), aggregation is only partial and followed by spontaneous *dispersion.* Peak RPCH-induced aggregation velocities (B series) are unaffected by external [Ca^{++}] (B1, 5.5 mM; B2, 10^{-3} M; B3, 10^{-4} M; B4, 10^{-5} M; B5, 10^{-6} M; B6, 10^{-9} M). RPCH washout with control saline leads to complete pigment dispersion (A1). Data are the mean ± SEM ($n = 7$).

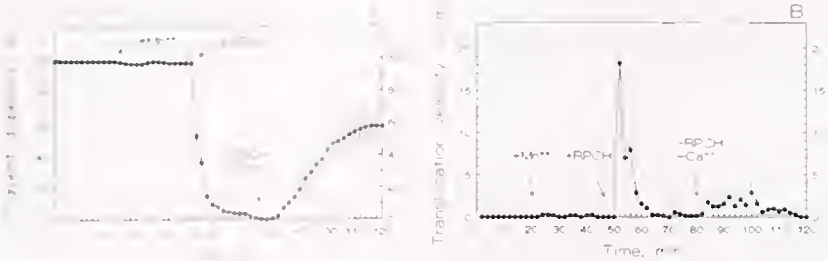

Figure 2. The calcium channel blocker Mn^{++} has no effect on 30 nM RPCH-induced pigment aggregation (A) in *Macrobrachium olfersii* red chromatosomes perfused with control (5.5 mM Ca^{++}) saline and 5 mM MnCl$_2$ for 30 min (*cf.*, Fig. 1A1). The peak aggregation velocity (B) is normal (*cf.*, Fig. 1B1), although dispersion during RPCH washout in Ca^{++}-free saline is incomplete (A). Data are the mean ± SEM (n = 7).

membrane with A23187, a second regulatory effect of Ca^{++} appears. Assuming rapid equilibration of cytosolic Ca^{++} with that in the extracellular medium (Lambert and Fingerman, 1978, 1979), both the degree of aggregation and the translocation velocity show Ca^{++}-dependence below about 10^{-3} M (Fig. 6). The transient aggregation followed by dispersion at 10^{-4} M Ca^{++} may result from decreased intracellular free [Ca^{++}] consequent to the action of smooth endoplasmic reticulum (Treiman *et al.*, 1998) and plasma membrane Ca^{++}-dependent ATPases (Carafoli, 1991). The mitochondrial electrogenic Ca^{++} uniporter and H^{+} (Na^{+})/Ca^{++} antiporter (Pozzan *et al.*, 1994), and plasma membrane Na^{+}/Ca^{++} antiporter (Missiaen *et al.*, 1991; Thastrup, 1990) may also act to reduce intracellular free [Ca^{++}]. At still lower concentrations ($\leq$10^{-5} to $\approx$10^{-11} M Ca^{++}), pigment dispersion ensues (Fig. 7). Thus, the direction of pigment movement, the translocation velocity of the edges of the pigment mass, and the degree of dispersion or aggregation appear to be calcium-dependent properties of the intracellular effector, the pigment translocation apparatus, or both.

Although the translocation mechanisms may depend on very different pathways of signal transduction and activation and on diverse mechanochemical motor proteins, the present data corroborate estimates of the threshold [Ca^{++}] necessary for pigment movements in teleost chromatophores; no such data are available for crustacean chromatophores. Pigment granules remain dispersed in cultured *Xiphophorus maculatus* erythrophores perfused with 10 μM A23187 and EGTA-buffered, 10^{-8} M free Ca^{++}; at 10^{-4} M Ca^{++}, erythrosome aggregation is almost complete (Oshima *et al.*, 1988). In isolated *Holocentrus ascensionis* erythrophores incubated in 10 μM A23187 and EGTA-buffered, external free Ca^{++} below 5 × 10^{-6} M, pigment granules are also dispersed; above 5 × 10^{-6} M Ca^{++}, reversible aggregation is induced (Luby-Phelps and Porter, 1982). Microinjection of 10 μM Ca^{++} also induces erythrosome aggregation (Kotz and McNiven, 1994). In cultured *H. ascencionis* erythrophores, stripped of their plasma membranes with Brij 58 detergent to reveal the cytoskeleton, pigment granules aggregate rapidly at 10^{-7} M free Ca^{++} in an EDTA-EGTA buffer system; with 10^{-8} M Ca^{++} the granules disperse (McNiven and Ward, 1988). Direct measurements using Fura-2 show that intracellular [Ca^{++}] in-

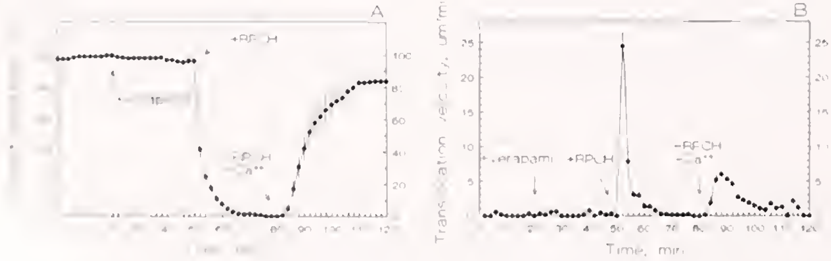

L type calcium channel blocker verapamil has no effect on 30 nM RPCH-induced pigment *robrachium olfersii* red chromatosomes perfused with control (5.5 mM Ca^{++}) saline and chloride for 30 min. Peak aggregation velocity (B) is normal (*cf.*, Fig. 1B1), and hout in Ca^{++}-free saline is nearly complete (A). Data are the mean ± SEM

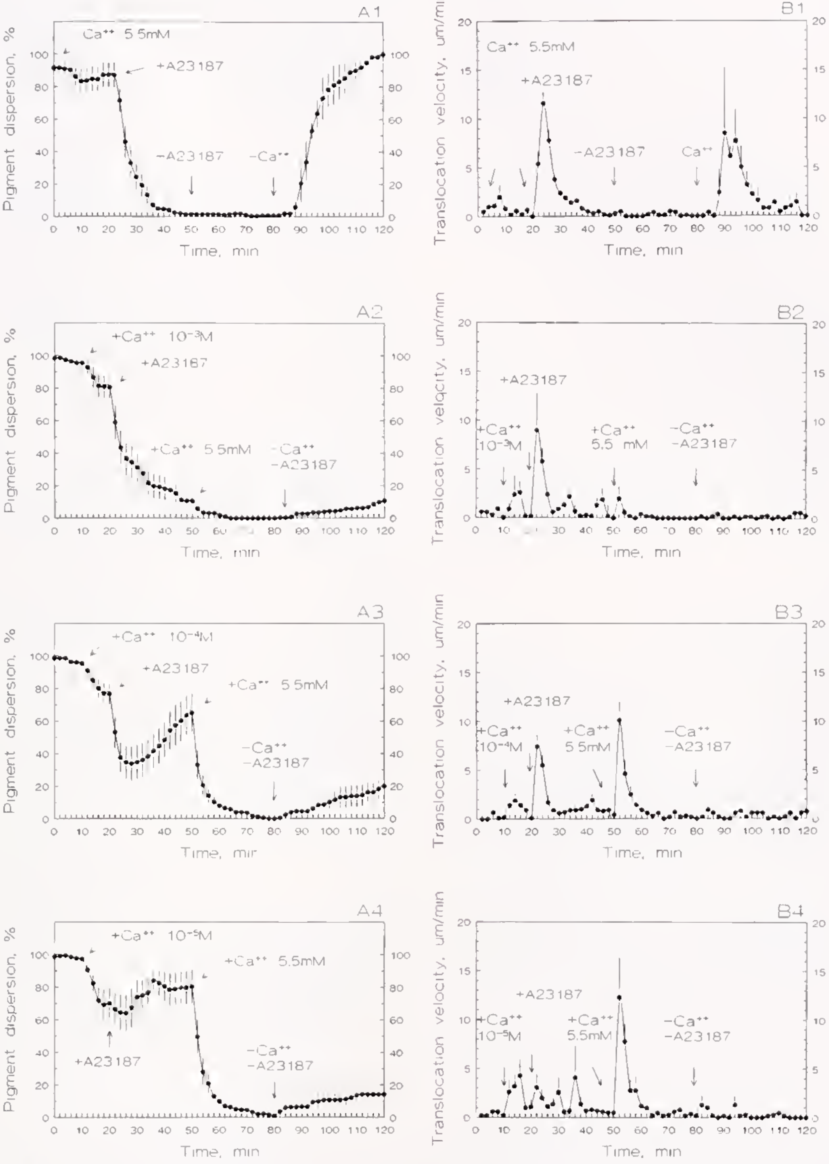

Figure 4. Dependence of ionophore-induced pigment aggregation (A series) on extracellular free Ca^{++} (A1, 5.5 m*M*; A2, 10^{-3} *M*; A3, 10^{-4} *M*; A4, 10^{-5} *M*) in *Macrobrachium olfersii* red chromatosomes perfused sequentially with control (5.5 m*M* Ca^{++}) saline, respective Ca^{++}-10 m*M* EGTA–buffered saline, and Ca^{++}-10 m*M* EGTA–buffered saline + 25 μ*M* A23187. At 10^{-4} *M* external free Ca^{++} (A3), pigment aggregation is only partial and followed by spontaneous *dispersion*. At 10^{-5} *M* Ca^{++}, pigment does not aggregate. The peak ionophore-induced aggregation velocities (B series) increase with *increasing* external [Ca^{++}] (B1, 5.5 m*M*; B2, 10^{-3} *M*; B3, 10^{-4} *M*; B4, 10^{-5} *M*). The slight aggregating effect in reduced [Ca^{++}] prior to A23187 perfusion may reflect DMSO-induced efflux of intracellular Ca^{++}. Data are the mean ± SEM (n = 7).

creases up to 100-fold or more, from about 30 n*M* in resting erythrophores to about 900 n*M* in epinephrine-stimulated *H. ascencionis* erythrophores (Kotz and McNiven, 1994). The present data, showing half-maximum aggregation at 3.2 × 10^{-5} *M* free Ca^{++} and half-maximum dispersion at 7.6 × 10^{-9} *M* free Ca^{++}, are consistent with these findings.

Although threshold intracellular Ca^{++} concentrations for chromatophore pigment aggregation and dispersion remain to be estimated in nearly all crustacean species, pigment translocation in caridean and brachyuran chromatophores is clearly affected by if not dependent on alterations in intracellular [Ca^{++}]. Lambert and Fingerman (1978) demon-

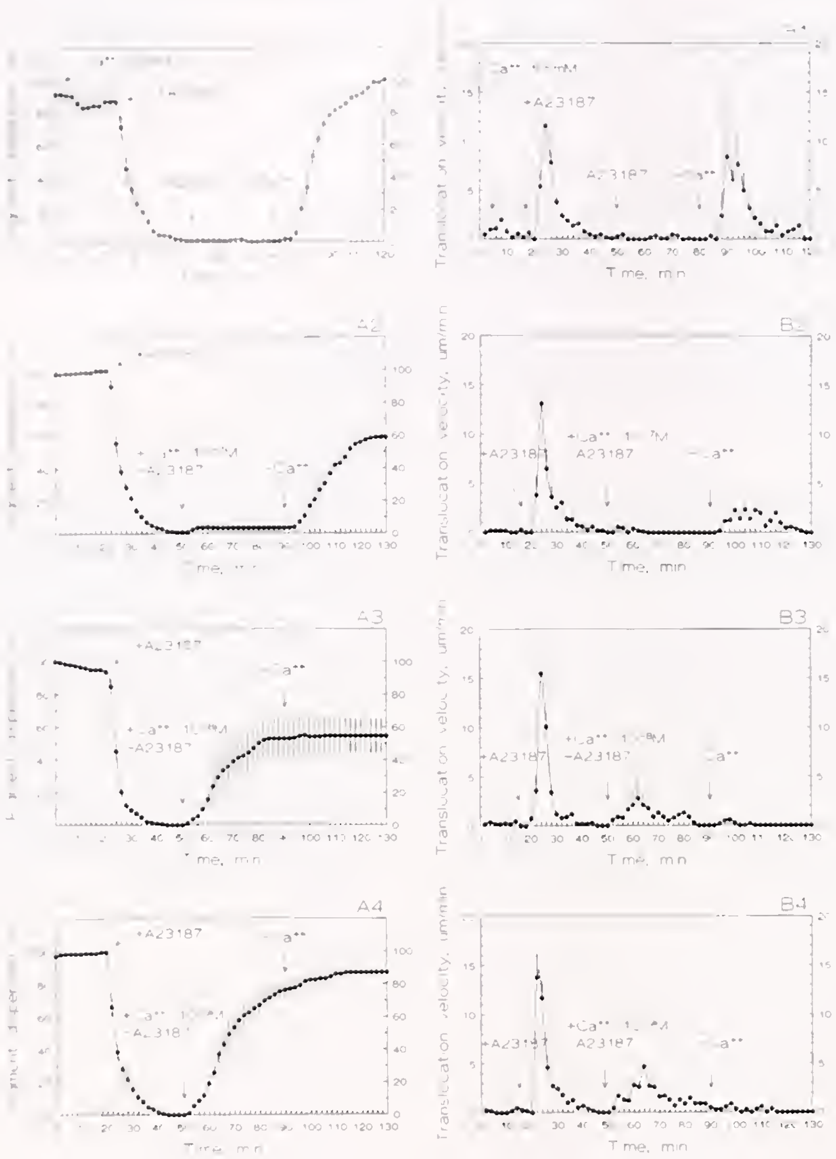

Figure 5. Dependence of pigment dispersion (A series) on *decreasing* external free Ca^{++} (A1, 5.5 mM; A2, 10^{-7} M, A3, 10^{-8} M, A4, 10^{-9} M) in *Macrobrachium olfersii* red chromatosomes perfused sequentially with control (5.5 mM Ca^{++}) saline, control saline + 25 μM A23187, respective Ca^{++}-10 mM EGTA-buffered saline, and Ca^{++}-free saline. Pigment disperses only at extracellular free [Ca^{++}] below 10^{-7} M (*cf.* A2 and A3). The peak dispersion velocities (B series) increase with *decreasing* external [Ca^{++}] (B1, 5.5 mM; B2, 10^{-7} M; B3, 10^{-8} M, B4, 10^{-9} M). Data are the mean ± SEM (n = 7).

strated A23187-induced (25 μM) aggregation in *Palaemon-* [illegible] ovarian chromatosomes perfused with Van [illegible] (11 mM Ca^{++}); subsequent perfusion [illegible] EDTA saline results in intermediate [illegible] Native pigment dispersing [illegible] duces granule dispersion in the [illegible] ntal chromatosomes of *Uca* [illegible] saline (12.7 mM Ca^{++}) [illegible] Quackenbush, 1981). Curiously, 10 and 25 μM A23187 not only inhibit the late phase (90–200 min) of PDH-induced pigment dispersion in *Uca pugilator* red chromatosomes, but also induce pigment aggregation (Quackenbush, 1981), much as in caridean chromatosomes. Complete aggregation in the polychromatic epidermal chromatosomes of *Palaemon affinis* is induced by an eyestalk extract delivered in physiological saline containing 10 mM Ca^{++}; in Ca^{++}-free saline, pigment aggregation is only partial (≈30%; McNamara and

Taylor, 1987). In the red integumental chromatosomes of *Macrobrachium potiuna* perfused with 6.5 m*M* Ca^{++}, A23187 (10^{-7} to 10^{-4} *M*) has a concentration-dependent aggregating effect, reversible by 10^{-8} *M* α-PDH (Britto *et al.*, 1990).

These various data demonstrate that pigment aggregation in the caridean shrimps and pigment dispersion in the brachyuran crabs can be brought about by changes in intracellular Ca^{++} concentrations. The effector pathways of such concentration changes, whether increased by signal transduction or after A23187, are poorly known. Based on rightward shifting of the PCH dose-response curve by inhibitors of intracellular effectors, Nery *et al.* (1997) have suggested that pigment aggregation in *M. potiuna* red integumental chromatosomes may involve an inositol-trisphosphate-like cascade coupled to protein phosphatase 1 activation. This latter effect may down-regulate effector protein phosphorylation *via* the cyclic AMP–protein kinase A signaling pathway (Nery and Castrucci, 1997), given that increased intracellular cyclic AMP also induces pigment dispersion in caridean shrimps (Fingerman, 1969; Lambert and Fingerman, 1978; Nery *et al.*, 1998). Clearly, possible convergence or cross-talk between the Ca^{++}-signaling and cyclic nucleotide-signaling pathways in crustacean pigment translocation mechanisms requires further investigation.

Acknowledgments

This study was financed by research grants to JCM (FAPESP 94/5981-7; CNPq 400517/95/7, 303282/84-3) and a postgraduate scholarship to MRR (FAPESP 94/4151-0).

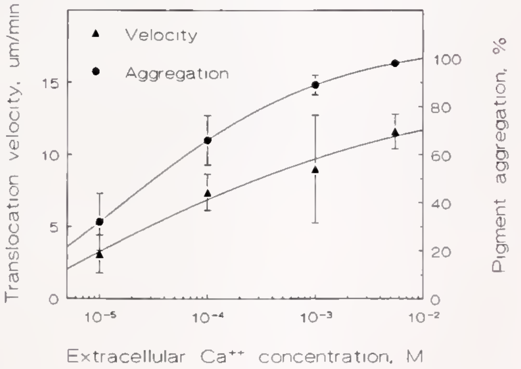

Figure 6. Mean (±SEM, $n \geq 7$) maximum pigment aggregation velocities ($R^2 = 0.98$) and degree of maximum aggregation increase as a concentration-effect function ($R^2 = 1.0$) of *increasing* extracellular free [Ca^{++}] and are positively correlated (Pearson correlation, $R = 0.98$, $P = 0.02$). Data from *Macrobrachium olfersii* red chromatosomes perfused with respective Ca^{++}-10 m*M* EGTA buffer and 25 μ*M* A23187.

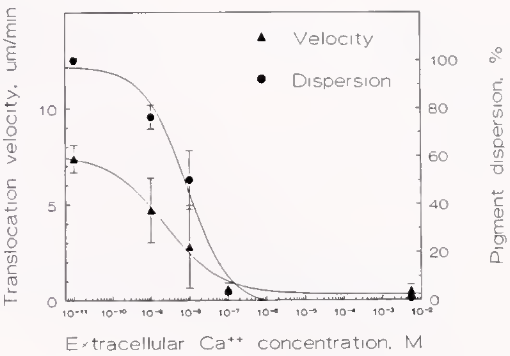

Figure 7. Mean (±SEM, $n \geq 7$) maximum pigment dispersion velocities ($R^2 = 0.99$) and degree of maximum dispersion ($R^2 = 0.98$) increase as a concentration-effect function of decreasing extracellular [Ca^{++}] and are positively correlated (Pearson correlation, $R = 0.98$, $P = 0.003$). Data from *Macrobrachium olfersii* red chromatosomes perfused with respective Ca^{++}-10 m*M* EGTA buffer after Ca^{++} loading with 25 μ*M* A23187 and 5.5 m*M* Ca^{++} for 30 min.

Literature Cited

Abrão, M. S., A. M. Castrucci, M. E. Hadley, and V. J. Hruby. 1991. Protein-kinase C mediates MCH signal transduction in teleost, *Synbranchus marmoratus*, melanocytes. *Pigm. Cell Res.* **4:** 66–70.

Booker, T. K., K. W. Smith, C. Dodrill, and A. C. Collins. 1998. Calcium modulation of activation and desensitization of nicotinic receptors from mouse brain. *J. Neurochem.* **71:** 1490–1500.

Britto, A. L., A. M. Castrucci, M. A. Visconti, and L. Josefsson. 1990. Quantitative *in vitro* assay for crustacean chromatophorotropins and other pigment cell agonists. *Pigm. Cell Res.* **3:** 28–32.

Britto, A. L., L. Josefsson, E. Scemes, M. A. Visconti, and A. M. Castrucci. 1996. Ionic requirements for PCH-induced pigment aggregation in the freshwater shrimp, *Macrobrachium potiuna*, erythrophores. *Comp. Biochem. Physiol.* **113A:** 351–359.

Carafoli, E. 1991. Calcium pump of the plasma membrane. *Physiol. Rev.* **71:** 129–153.

Fabiato, A. 1988. Computer programs for calculating total from specified free or free from specified total ionic concentrations in aqueous solutions containing multiple metals and ligands. *Methods Enzymol.* **157:** 378–417.

Fingerman, M. 1969. Cellular aspects of the control of physiological color changes in crustaceans. *Am. Zool.* **9:** 443–452.

Fingerman, M. 1985. The physiology and pharmacology of crustacean chromatophores. *Am. Zool.* **25:** 233–252.

Fingerman, M., S. W. Fingerman, and D. T. Lambert. 1975. Colchicine, cytochalasin B, and pigment movements in ovarian and integumentary erythrophores of the prawn, *Palaemonetes vulgaris*. *Biol. Bull.* **149:** 165–177.

Josefsson, L. 1983. Chemical properties and physiological actions of crustacean chromatophorotropins. *Am. Zool.* **23:** 507–515.

Katz, A. M. 1996. Calcium channel diversity in the cardiovascular system. *J. Am. Coll. Cardiol.* **28:** 522–529.

Kotz, K. J., and M. A. McNiven. 1994. Intracellular calcium and cAMP regulate directional pigment movements in teleost erythrophores. *J. Cell Biol.* **124:** 463–474.

Kulkarni, G. K., and M. Fingerman. 1986. Chromatophorotropic activity of extracts of the brain and nerve chord of the leech, *Macrobdella decora*, in the fiddler crab, *Uca pugilator*: an *in vivo* and *in vitro* study. *Comp. Biochem. Physiol.* **84C:** 369–372.

Lambert, D. T., and M. Fingerman. 1976. Evidence for a non-microtubular colchicine effect in pigment granule aggregation in melanophores of the fiddler crab, *Uca pugilator*. *Comp. Biochem. Physiol.* **53C:** 25–28.

Lambert, D. T., and M. Fingerman. 1978. Colchicine and cytochalasin B. A further characterization of their actions on crustacean chromatophores using the ionophore A23187 and thiol reagents. *Biol. Bull.* **155:** 563–575.

Lambert, D. T., and M. Fingerman. 1979. Evidence implicating calcium as the second messenger for red pigment-concentrating hormone in the prawn *Palaemonetes pugio*. *Physiol. Zool.* **52:** 497–508.

Lee, H. C., R. Aarhus, R. Graeff, M. E. Gurnack, and T. F. Walseth. 1994. Cyclic ADP ribose activation of the ryanodine receptor is mediated by calmodulin. *Nature* **370:** 307–309.

Liu, Q. S., and D. K. Berg. 1999. Extracellular calcium regulates responses of both alpha 3- and alpha 7-containing nicotinic receptors on chick ciliary ganglion neurons. *J. Neurophysiol.* **82:** 1124–1132.

Luby-Phelps, K., and K. R. Porter. 1982. The control of pigment migration in isolated erythrophores of *Holocentrus ascensionis* (Osbeck). II. The role of calcium. *Cell* **29:** 441–450.

McNamara, J. C. 1981. Morphological organization of crustacean pigmentary effectors. *Biol. Bull.* **161:** 270–280.

McNamara, J. C., and M. R. Ribeiro. 1999. Kinetic characterization of pigment migration and the role of the cytoskeleton in granule translocation in the red chromatophores of the shrimp *Macrobrachium olfersii* (Crustacea, Decapoda). *J. Exp. Zool.* **283:** 19–30.

McNamara, J. C., and H. H. Taylor. 1987. Ultrastructural modifications associated with pigment migration in palaemonid shrimp chromatophores (Decapoda, Palaemonidae). *Crustaceana* **53:** 113–133.

McNamara, J. C., L. C. Salomão, and E. A. Ribeiro. 1990. The effect of eyestalk ablation on haemolymph osmotic and ionic concentrations during acute salinity exposure in the freshwater shrimp *Macrobrachium olfersii* (Wiegmann) (Crustacea, Decapoda). *Hydrobiologia* **199:** 193–199.

McNiven, M. A., and J. B. Ward. 1988. Calcium regulation of pigment transport *in vitro*. *J. Cell Biol.* **106:** 111–125.

Missiaen, L., F. Wuytack, L. Raeymaekers, H. Smedt, G. Droogmans, I. Declerck, and R. Casteels. 1991. Ca^{2+} extrusion across plasma membrane and Ca^{2+} uptake by intracellular stores. *Pharmacol. Ther.* **50:** 191–232.

Mukhopadhyay, B., P. Roy, A. Chatterjee, and S. Bhattacharya. 1997. Intracellular events in response to GnRH causing gonadotropin release from pituitary cells of a channid fish, *Channa punctatus* (Bloch). *Comp. Biochem. Physiol.* **118C:** 129–136.

Nery, L. E., and A. M. Castrucci. 1997. Pigment cell signalling for physiological color change. *Comp. Biochem. Physiol.* **118A:** 1135–1144.

Nery, L. E., M. A. Silva, L. Josefsson, and A. M. Castrucci. 1997. Cellular signalling of PCH-induced pigment aggregation in the crustacean *Macrobrachium potiuna* erythrophores. *J. Comp. Physiol.* **167B:** 570–575.

Nery, L. E., M. A. Silva, and A. M. Castrucci. 1998. Role of cyclic nucleotides in pigment translocation within the freshwater shrimp, *Macrobrachium potiuna*, erythrophore. *J. Comp. Physiol.* **168B:** 624–630.

Novales, R. R. 1983. Cellular aspects of hormonally controlled pigment translocations within chromatophores of poikilothermic vertebrates. *Am. Zool.* **23:** 559–568.

Oshima, N., M. Suzuki, N. Yamaji, and R. Fujii. 1988. Pigment aggregation is triggered by an increase in free calcium ions within fish chromatophores. *Comp. Biochem. Physiol.* **91A:** 27–32.

Ospina, J. A., R. S. Broide, D. Acevedo, R. T. Robertson, and F. M. Leslie. 1998. Calcium regulation of agonist binding to alpha 7-type, nicotinic acetylcholine receptors in adult and fetal rat hippocampus. *J. Neurochem.* **70:** 1061–1068.

Pozzan, T., R. Rizzuto, P. Volpe, and J. Meldolesi. 1994. Molecular and cellular physiology of intracellular calcium stores. *Physiol. Rev.* **74:** 595–636.

Putney, J. W. Jr., and G. St. J. Bird. 1993. The inositol phosphate-calcium signaling system in nonexcitable cells. *Endocr. Rev.* **14:** 610–631.

Quackenbush, L. S. 1981. Studies on the mechanism of action of a pigment dispersing chromatophorotropin in the fiddler crab, *Uca pugilator*. *Comp. Biochem. Physiol.* **68A:** 597–604.

Rao, K. R., and M. Fingerman. 1983. Regulation of release and mode of action of crustacean chromatophorotropins. *Am. Zool.* **23:** 517–527.

Striessnig, J., M. Granber, J. Mitterdorfer, S. Hering, M. J. Sinnegger, and H. Grossmann. 1998. Structural basis of drug binding to L Ca^{2+} channels. *Trends Pharmacol. Sci.* **19:** 108–115.

Sugden, D., and S. J. Rowe. 1992. Protein kinase C activation antagonizes melatonin-induced pigment aggregation in *Xenopus laevis* melanophores. *J. Cell Biol.* **119:** 1515–1521.

Thastrup, O. 1990. Role of Ca^{2+}-ATPase in regulation of cellular Ca^{2+} signalling, as studied with the selective microsomal Ca^{2+}-ATPase inhibitor, thapsigargin. *Agents Actions* **29:** 8–15.

Treiman, M., C. Caspersen, and S. B. Christensen. 1998. A tool coming of age: thapsigargin as an inhibitor of sarcoplasmic reticulum Ca^{2+}-ATPases. *Trends Pharmacol. Sci.* **19:** 131–135.

Tuma, M. C., and V. I. Gelfand. 1999. Molecular mechanisms of pigment transport in melanophores. *Pigm. Cell Res.* **12:** 283–294.

Tuma, M. C., A. M. Castrucci, and L. Josefsson. 1993. Comparative activities of the chromatophorotropins RPCH, α-PDH, and β-PDH on three crustacean species. *Physiol. Zool.* **66:** 181–192.

Verkhratsky, A., and A. Shmigol. 1996. Calcium-induced calcium release in neurones. *Cell Calcium* **19:** 1–14.

Zhang, S., T. Sawanobori, Y. Hirano, and M. Hiraoka. 1997. Multiple modulations of action potential duration by different calcium channel blocking agents in guinea pig ventricular myocyte. *J. Cardiovasc. Pharmacol.* **30:** 489–496.

Reference: *Biol. Bull.* **198:** 367–378. (June 2000)

A Morphological Study of Nonrandom Senescence in a Colonial Urochordate

ROBERT J. LAUZON[1,*], BARUCH RINKEVICH[2], C. W. PATTON[3], AND IRVING L. WEISSMAN[4]

[1]*Department of Biological Sciences, Union College, Schenectady, New York 12308;* [2]*Israel Oceanography and Limnological Research, National Institute of Oceanography, Tel Shikmona, Haifa, Israel 31080;* [3]*Hopkins Marine Station of Stanford University, Pacific Grove, California 93950; and* [4]*Department of Pathology, Stanford University School of Medicine, Beckman Research Center, Stanford, California 94305*

Abstract. *Botryllus schlosseri* is a clonally modular ascidian, in which individuals (zooids) have a finite life span that is intimately associated with a weekly budding process called blastogenesis. Every blastogenic cycle concludes with a synchronized phase of regression called takeover, during which all zooids in a colony die, primarily by apoptosis, and are replaced by a new generation of asexually derived zooids. We have previously documented that, in addition to this cyclical death phase, entire colonies undergo senescence during which all asexually derived individuals in a colony, buds and zooids, die in concert. In addition, when a specific parent colony (genet) is experimentally separated into a number of clonal replicates (ramets), ramets frequently undergo senescence simultaneously, indicating that mortality can manifest itself in nonrandom fashion. Here, we document a morphological portrait of senescence in laboratory-maintained colonies from Monterey Bay, California, that exhibit nonrandom mortality. Nonrandom senescence proceeded according to a series of characteristic changes within the colony over a period of about one week. These changes included systemic constriction and congestion of the vasculature accompanied by massive accumulation of pigment cells in the zooid body wall (mantle), blood vessels, and ampullae; gradual shrinkage of individual zooids; loss of colonial architecture, and ultimately death. At the ultrastructural level, individual cells exhibited changes typical of ischemic cell death, culminating in necrotic cell lysis rather than apoptosis. Collectively, these observations indicate that senescence is accompanied by unique morphological changes that occur systemically, and which are distinct from those occurring during takeover. We discuss our findings in relation to current experimental models of aging and the possible role of a humoral factor in bringing about the onset of senescence.

Introduction

The colonial urochordate *Botryllus schlosseri* (Tunicata, Ascidiacea) is a ubiquitous, filter-feeding inhabitant of shallow waters and harbors worldwide, where it is found on a wide variety of hard substrates (Sabbadin, 1969). Each colony arises from a sexually produced, chordate larva that attaches itself to a substratum and undergoes metamorphosis. The resulting oozooid immediately begins to produce buds that originate as outgrowths from its lateral wall and are genetically identical to the parent. Within about one week between 16° and 20°C, the oozooid regresses and the first asexual generation of buds simultaneously reaches functional maturity (Sabbadin, 1969). This first generation of blastozooids produces its own buds, which in turn mature in about a week and subsequently die after giving rise to an additional set of zooids. Each such cycle, called blastogenesis, is entirely temperature-dependent and of shorter duration at higher temperatures (Milkman, 1967; Sabbadin, 1969; Rinkevich *et al.*, 1998). During the last stage of a typical blastogenic cycle (the takeover stage), all zooids in a colony regress over a 24- to 30-h period through the death of all visceral tissues, primarily by apoptosis (Lauzon *et al.*, 1992, 1993). Thus, the life history of a *B.*

---

[*] To whom correspondence should be addressed. E-mail: lauzonr@union.edu

schlosseri colony is characterized by a long series of such blastogenic cycles, which succeed one another periodically. In time, a colony can grow up to hundreds of genetically identical blastozooids, with all zooids and buds in the colony being developmentally synchronized (Milkman, 1967). Zooids are typically arranged in star-shaped groups called systems, which are embedded in a gelatinous tunic. Blood continuously flows throughout the systems, zooids, and buds, and into the peripheral endings of blood vessels called ampullae.

In addition to this weekly death process, individual colonies have finite life spans. Colonies grown under field conditions are characterized by short, sub-annual life spans (Berrill, 1950; Millar, 1952; Brunetti, 1974; Brunetti and Copello, 1978; Grosberg, 1988; Chadwick-Furman and Weissman, 1995a, b). For instance, in *B. schlosseri* colonies from Monterey Bay, maximum life span ranges from about 3 months for animals born in the spring to just over 8 months for those born in the fall (Chadwick-Furman and Weissman, 1995a). Senescence appears to be the primary cause of mortality in field-raised colonies, and involves a series of characteristic degenerative changes that culminate in the death of the entire colony (Brunetti, 1974; Chadwick-Furman and Weissman, 1995a). In contrast, laboratory-maintained colonies from Monterey Bay have been documented to exhibit life spans of more than 7 years (Rinkevich and Shapira, 1998), and counterparts from the Venetian Lagoon (Italy) were reported to have been kept alive for up to 3 years (Sabbadin, 1969). It is well documented that this species exhibits tremendous plasticity, and that life-history traits are subject to variation by changes in environmental conditions (Chadwick-Furman and Weissman, 1995a, b; Rinkevich *et al.*, 1998). For instance, colonies grown under field conditions attain large sizes, form compact structures, and reproduce rapidly, whereas laboratory-maintained colonies grow slowly, often fragment into subcolonies, and may not undergo sexual reproduction (Chadwick-Furman and Weissman, 1995b). Yet, it is precisely in the laboratory environment that this animal can best be manipulated and studied as a model system of invertebrate immunity (reviewed in Magor *et al.*, 1999), development (Milkman, 1967; Lauzon *et al.*, 1992; Rinkevich *et al.*, 1992; Lauzon *et al.*, 1993), cell and molecular biology (DeTomaso *et al.*, 1998), and evolutionary studies (Stoner *et al.*, 1999). We previously reported that laboratory colonies (genets) and the clonal replicates (ramets) derived from these genets underwent [illegible] changes at the end of their life span that [illegible] reproductive effort (Rinkevich *et al.*, [illegible]). [illegible] led to the death of previously separated [illegible] genet simultaneously within the same [illegible] nonrandom nature of this process stro[illegible] senescence could be mediated by a [illegible] [illegible]vich *et al.*, 1992). The findings repor[illegible] [illegible] our previous observations indicating that senescence is reproducibly associated with characteristic morphological changes that are conserved from colony to colony and appear identical to those reported in field colonies. Furthermore, since field studies have only described macroscopic changes occurring at the colony level (Brunetti, 1974; Chadwick-Furman and Weissman, 1995a), it has become imperative to document cellular and subcellular features occurring during nonrandom senescence, as a means of understanding its underlying mechanism. Here, we provide evidence that the histological and ultrastructural features of cell death during nonrandom senescence are distinct from those occurring during takeover and ultimately reflect systemic changes within the colonial vasculature.

Materials and Methods

Laboratory mariculture of Botryllus schlosseri

Animals were maintained between 16° and 17°C under laboratory conditions, as previously described (Boyd *et al.*, 1986; Rinkevich *et al.*, 1992). In our initial study on senescence and mortality in this species, we had observed that senescence in laboratory-maintained colonies could occur in either a random or a nonrandom fashion (Rinkevich *et al.*, 1992). To document the morphological changes that are consistently associated with senescence, we have focused solely on the latter type. For the animals reported in this study, individual colonies (genets) were separated with the use of a razor blade into several clonal replicates (ramets). Each ramet was attached to a slide, after which they were maintained separately or within the confines of the same tank. Our previous findings had indicated that, within the group of colonies exhibiting nonrandom senescence, the placement of ramets within the same or different tank did not affect the onset of senescence. That is, ramets derived from the same genet underwent simultaneous degenerative changes that led to their death, regardless of whether they were placed in the same tank or kept in separate tanks (Rinkevich *et al.*, 1992). Dates of subcloning, colony number, and numbers of ramets were recorded as previously described (Rinkevich *et al.*, 1992). Life span was recorded as number of blastogenic cycles until death. Observations of colonies and determination of zooid length were carried out with the use of a stereomicroscope (Stemi SV 6, Carl Zeiss, Germany) equipped with an ocular micrometer.

Transmission electron microscopy

Colonies undergoing nonrandom senescence were separated into individual systems (star-shaped groups of zooids) with a razor blade on the third day after the onset of systemic vasculature constriction and increased pigmentation of zooids. Day 3 was selected as representative of an early stage of senescence. The systems were processed for electron microscopy as previously described (Lauzon *et al.*, 1993). In brief, the systems were fixed in a solution of 1% glutaraldehyde, 1% acrolein (freshly distilled), and 80% artificial seawater (ASW) for 2 h at room temperature. Individual systems were washed several times in ASW for a total of 1 h and were then post-fixed in 1% osmium tetroxide for 1 h in ASW at room temperature. The specimens were subsequently dehydrated in a graded acetone series and embedded in Spurr's resin (Polysciences, Warrington, PA) according to the manufacturer's specifications. Ultrathin sections were cut with a diamond knife (EM Corp, Chestnut Hill, MA), placed onto Formvar-coated 300-mesh nickel grids, stained with 2% aqueous uranyl acetate and 1% lead citrate, and examined with a Phillips EM 201 transmission electron microscope.

Histology

Individual systems from senescent colonies (days 3 and 5) were isolated with the use of a razor blade and fixed in 1% paraformaldehyde-filtered seawater for 2 h at 4°C. Days 3 and 5 were selected as representative of early and middle senescence respectively. Specimens were subsequently dehydrated in a graded ethanol series, and embedded in JB-4 plastic (Polysciences, Warrington, PA) according to the manufacturer's specifications. Sections ranging between 2 and 3 μm in thickness were generated with a Histoknife (Diatome Inc., Switzerland) along the anteroposterior axis of zooids, as previously described (Lauzon *et al.*, 1992). Individual sections were stained with 0.01% toluidine blue-sodium bicarbonate, mounted with Permount (Fisher Scientific, Springfield, NJ), and observed under bright-field microscopy (Olympus BH-2 model, New York/New Jersey Scientific, Inc., Middlebush, NJ).

Results

Senescence is a heritable process in some Botryllus schlosseri *colonies*

In our previous study of senescence in *B. schlosseri* colonies maintained under laboratory mariculture, 17 of 41 genets were documented to exhibit nonrandom mortality (Rinkevich *et al.*, 1992). The life spans of some additional laboratory-born and raised colonies were determined by following animals until the entire colony manifested senescent features indicative of impending death. Eleven genets were selected on the basis of their ability to undergo nonrandom mortality. As illustrated in Figure 1, death was synchronous between all ramets in 7 of 11 colonies (Y8, 275jjr, 403d, 386i, 433z, 435h, 360c), occurring within the same blastogenic cycle. In 3 of the remaining 4 colonies (Y7, 248hsi and 433af), all ramets died simultaneously, with the exception of one ramet from each of the genets, which died either 4 (Y7) or 6 (248hsi and 433af) blastogenic cycles earlier. In colony 404b, two ramets died before the others—one 2 blastogenic cycles earlier and the other 24 cycles earlier (in this ramet, death was probably unrelated to senescence).

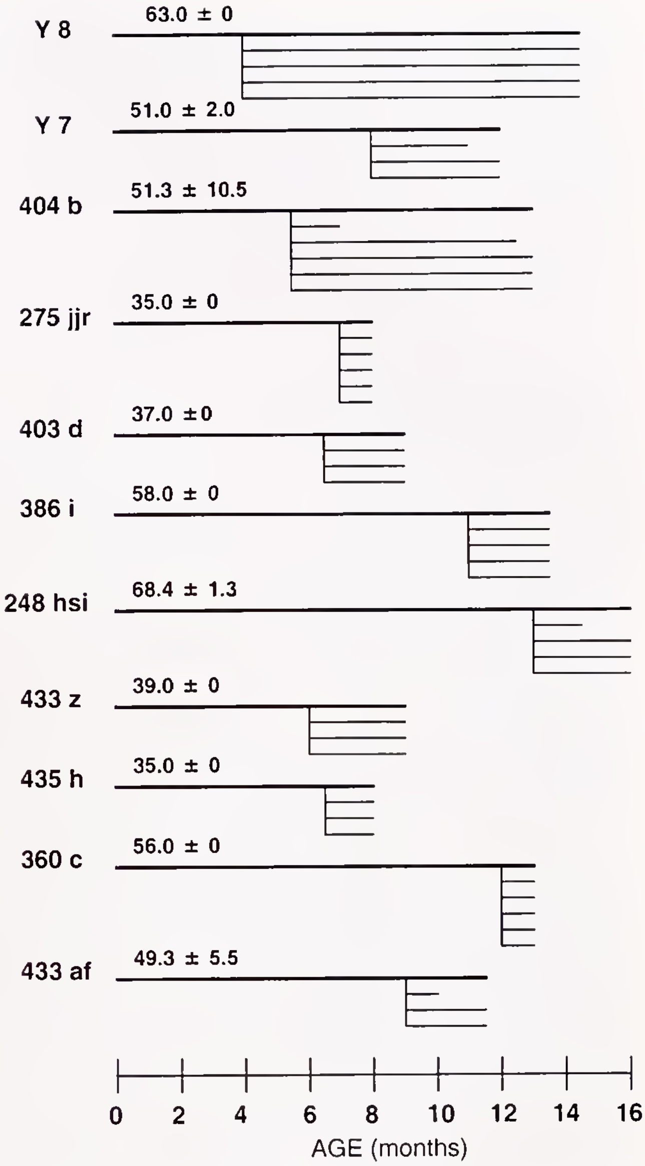

Figure 1. Lifespan of "parent" *Botryllus schlosseri* colonies and derived clonal replicates that express nonrandom mortality. The genet numbers are indicated on the left margin. The lifespan of the original parent part is indicated by a thick horizontal line, whereas lifespan from subcloned ramets derived from the original parent part is indicated by a thin line. When multiple ramets were subcloned on a given day, their lifespans are indicated by parallel horizontal lines originating from a common perpendicular line. The numbers above each thick line represents the mean number of blastogenic cycles until death ± standard deviation (SD) for each genet. Each blastogenic cycle lasts 7 days at 16°–17°C under laboratory conditions.

Stereomicroscopic observations of Botryllus schlosseri *colonies undergoing nonrandom senescence*

The findings in this report are based upon repeated observations, over several years, of characteristic changes that preceded death of individual colonies. Because the onset of senescence could not be accurately predicted within a given genet or ramet, colonies were observed daily for these characteristic changes. When observed under stereomicroscopy, ramets derived from the 11 genets displayed a series of regressive changes over a one-week period. These changes resulted in the near simultaneous death of a genet following a given number of blastogenic cycles.

The earliest recognizable features of nonrandom senescence involved the constriction of blood vessels throughout a colony, resulting in the accumulation of pigment cells within the zooid mantle, buds, blood vessels, and ampullae (Fig. 2). In nonsenescent colonies, ampullae serve as reservoirs for pigment cells during takeover, and thus accumulate within them only during this phase of the blastogenic cycle (Lauzon *et al.*, 1992). In senescent colonies, however, this morphological feature was consistently observed to occur independently of takeover. The ampullae also began to retract from the leading edge of the colony, perhaps as an indication of declining health (Fig. 2b). At this stage of senescence, zooids were still actively feeding, as assessed by the functional nature of both oral and excurrent siphons, but had begun to shrink in size relative to their nonsenescent counterparts. The average zooid length for randomly selected zooids from nonsenescent colonies during the asexual growth phase of the blastogenic cycle was 2.34 mm ± 0.29 ($n = 85$), compared to 1.69 mm ± 0.15 for early senescent zooids ($n = 105$; $P < 0.05$ by paired Student's t test). Blood flow slowed considerably between days 1 and 3, and as a result of heavy congestion of the vessel walls with pigment cells, blood circulation became progressively more sluggish between days 3 and 6 of nonrandom senescence. The first vessels to be affected were the marginal vessels near the periphery of the colony. Buds were also affected during this process: they gradually separated from the parent zooids (data not shown), eventually becoming developmentally arrested. By day 6 of nonrandom senescence the systems had become highly disorganized, with concomitant loss of the common excurrent siphon, and zooids had separated from one another (Fig. 2c). Zooids at this degenerative stage were further shrunken (1.01 mm ± 0.17, $n = 102$; P [illegible] by paired Student's t test), displayed a more [illegible] pattern, and were scattered individually [illegible] formed small groups of two to three [illegible] of individual zooids exhibited [illegible] signaling impending death. Between [illegible] nonrandom senescence the oral and excurrent [illegible] progressively more dilated (Fig. 2[illegible] [illegible] sensitivity to mechanical stimulus. By day 7, all zooids in the colony were dead, as assessed by lack of heartbeat and shutdown of the siphons (Fig. 2d). At day 9, the colony was in an advanced state of decay and zooids were no longer recognizable. Protozoa were observed swimming on the surface of the softened tunic, presumably contributing to the decay process (data not shown).

In some instances, the onset of senescence was also observed during the takeover phase of the blastogenic cycle. Takeover is characterized by the simultaneous regression of the previous generation of zooids and the increase in size and maturation of the new generation of pre-functional zooids. In nonsenescent colonies, takeover begins with the shutdown of the oral and excurrent siphons, followed by polarized zooid contraction; it is generally completed within 24 to 30 h between 16°–18°C (Lauzon *et al.*, 1992). At the conclusion of takeover, the zooid remnants appear as small vesicles, and a new blastogenic cycle begins with the opening of oral and excurrent siphons in the next generation of zooids (Lauzon *et al.*, 1992). In contrast to the process seen in nonsenescent colonies, zooids were never completely resorbed in colonies undergoing nonrandom senescence. In a representative colony at day 5 of the senescent process, the previous zooid generation was still visible 60 h after the onset of takeover, although considerable resorption had already taken place (Fig. 2e). At this stage, the next asexual generation of zooids had open oral and excurrent siphons but exhibited signs of fragmentation, in that they failed to form complete star-shaped systems. Instead, zooids were found individually or assembled into groups of two or three with a common excurrent siphon. In addition, the systemic vasculature had become sluggish, and pigment cells—which normally leave the ampullae at the conclusion of takeover—remained within them. At 110 h after takeover, the entire colony was dead, with resorption products still visible (Fig. 2f).

Histological observations of nonrandom senescence

Histological studies have previously been carried out on nonsenescent zooids during blastogenic growth (Lauzon *et al.*, 1992). In contrast to those nonsenescent zooids, individual zooids at day 3 of nonrandom senescence prominently displayed congested visceral tissues and vascular spaces (Fig. 3a). A large proportion of cells from visceral tissues also appeared swollen with a hollow appearance. These cells invariably took up very little stain (weakly basophilic) and were at times harboring pyknotic nuclei. In some cases, cells with large, open spaces suggestive of cell lysis were also found. At this stage of senescence, visceral tissues (Fig. 3a, b, for stomach, intestine, endostyle; pharyngeal slits and neural complex not shown) were still confined by an intact perivisceral epithelium, and thus few cells were free in the peribranchial cavity (Fig. 3b). In

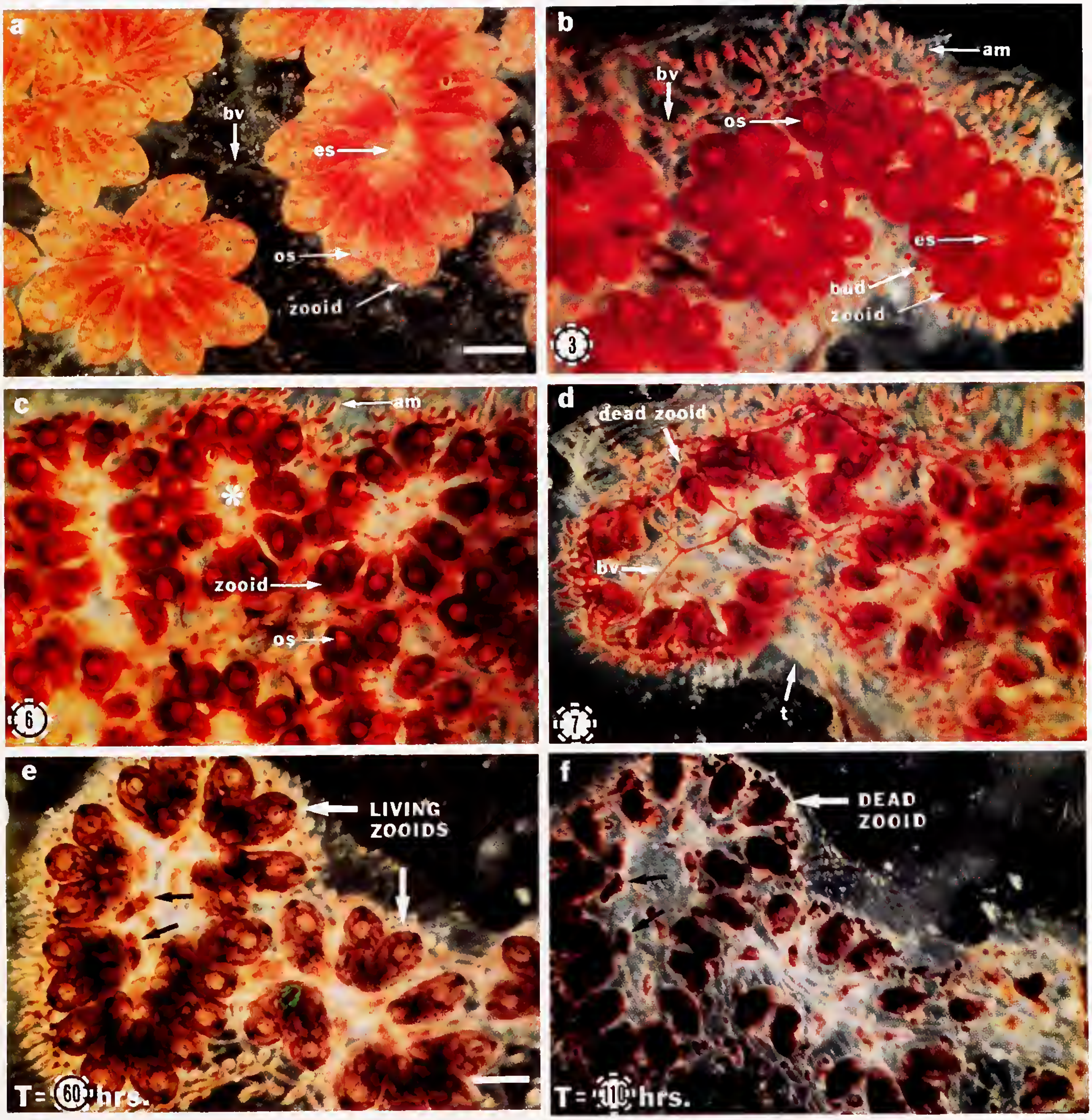

Figure 2. *Botryllus schlosseri* colonies at different stages of nonrandom senescence. (a) Appearance of star-shaped groups of zooids in a nonsenescent colony. (b) A representative colony 3 days following the onset of senescence. Note the dark pigmentation pattern within zooids and accumulation of pigment cells in blood vessels and ampullae. (c) At day 6 of nonrandom senescence, there is loss of colonial architecture. The zooids within individual systems have disconnected from one another following loss of the common excurrent siphon. Note that the siphons from individual zooids have greatly dilated. Systemic blood flow has almost shut down except for the central part of the colony. (d) The end stage of senescence (day 7) is characterized by complete stasis of the colonial vasculature and dead zooids with closed siphons. (e) A different colony at day 5 of nonrandom senescence, observed at 60 hours following the onset of takeover (bottom left corner). Note that the zooids of the previous asexual generation are still visible (black arrows).(f) The same colony observed at 110 hours following onset of takeover, depicting dead zooids with resorption products still visible (black arrows). Panels a–c and d represent dorsal and ventral views respectively of zooids from different portions of the same colony (orange color morph) undergoing nonrandom senescence. Panels e–f are dorsal views of the same part of a different colony (blue/brown color morph). The numbers at the bottom left portion of panels a–d represent the days following onset of nonrandom senescence. Abbreviations: am, ampulla; bv, blood vessels; es, excurrent siphon; os, oral siphon; t, tunic. Asterisks represent the region occupied by the common excurrent siphon. Scale bars equal 1 mm for panels a–d and e–f respectively.

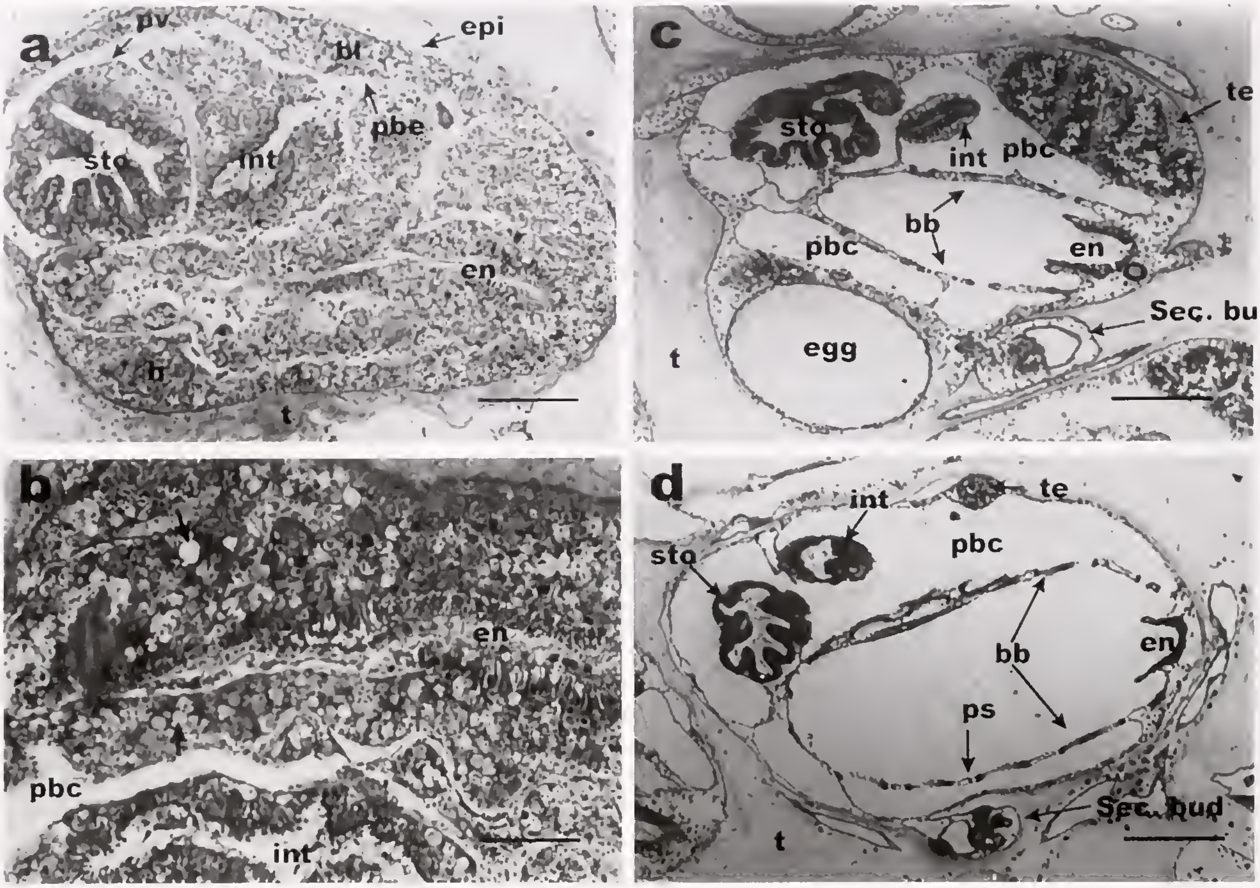

Figure 3. Histological observations of *Botryllus schlosseri* zooids and buds at day 3 of nonrandom senescence. (a) Ventral section of a senescent zooid. At this stage, zooids are congested and visceral organs have a spongy appearance, characterized by large empty spaces or swollen cells with weakly basophilic cytoplasm. (b) Higher magnification of the endostyle near the ventral sinus depicting the swollen cells that are weakly basophilic (large black arrows). Cells with multiple nuclei are widespread along the anteroposterior axis of the zooid, indicative of extensive phagocytosis of dying cells. (c) Primary and secondary buds of a day 3 senescent colony appear morphologically normal as compared with buds from a nonsenescent colony (d). Abbreviations: bb, branchial basket; bl, blood; en, endostyle; epi, epidermis; h, heart; int, intestine; pbc, peribranchial cavity; pbe, peribranchial epithelium; ps, pharyngeal slits; pv, perivisceral epithelium; sec. bud, secondary bud; sto, stomach; t, tunic; te, testes. Scale bars = 240 μm (a, c, d) and 120 μm (b).

contrast to the features associated with zooids at day 3 of senescence, primary and secondary buds were morphologically indistinguishable from buds of nonsenescent animals (Fig. 3c, d).

By day 5 of senescence, the squamous perivisceral and peribranchial epithelia and the epidermis of zooids was visibly swollen, thus exhibiting degenerative changes similar to those observed for other cells at day 3 (Fig. 4a). These changes presumably led to the release of individual cells or groups of cells from the viscera or blood into the peribranchial cavity (Fig. 4a). In contrast, filter-feeding zooids from nonsenescent animals retained intact squamous perivisceral and peribranchial epithelia (Fig. 4b). Throughout the progression of senescence, as blood vessels constricted and blood flow became sluggish, pigment cells and other blood cells accumulated within ampullae, thus conferring a congested appearance (Fig. 4c) not seen in nonsenescent colonies during blastogenic growth (Fig. 4d). In addition, phagocytic cells containing many ingested cells with pyknotic nuclei became more prevalent over the course of senescence (Fig. 4a, c). By day 5, the buds began to exhibit morphological degeneration similar to that seen in zooids two days earlier, and the colonies usually died at day 7, often loaded with trapped eggs and sperm (data not shown).

Ultrastructural observations of nonrandom senescence

The ultrastructure of senescent zooids revealed a number of features diagnostic of ischaemic cell death with cellular necrosis as an end-point; these supported the histological profile seen by light microscopy. At day 3, small groups of

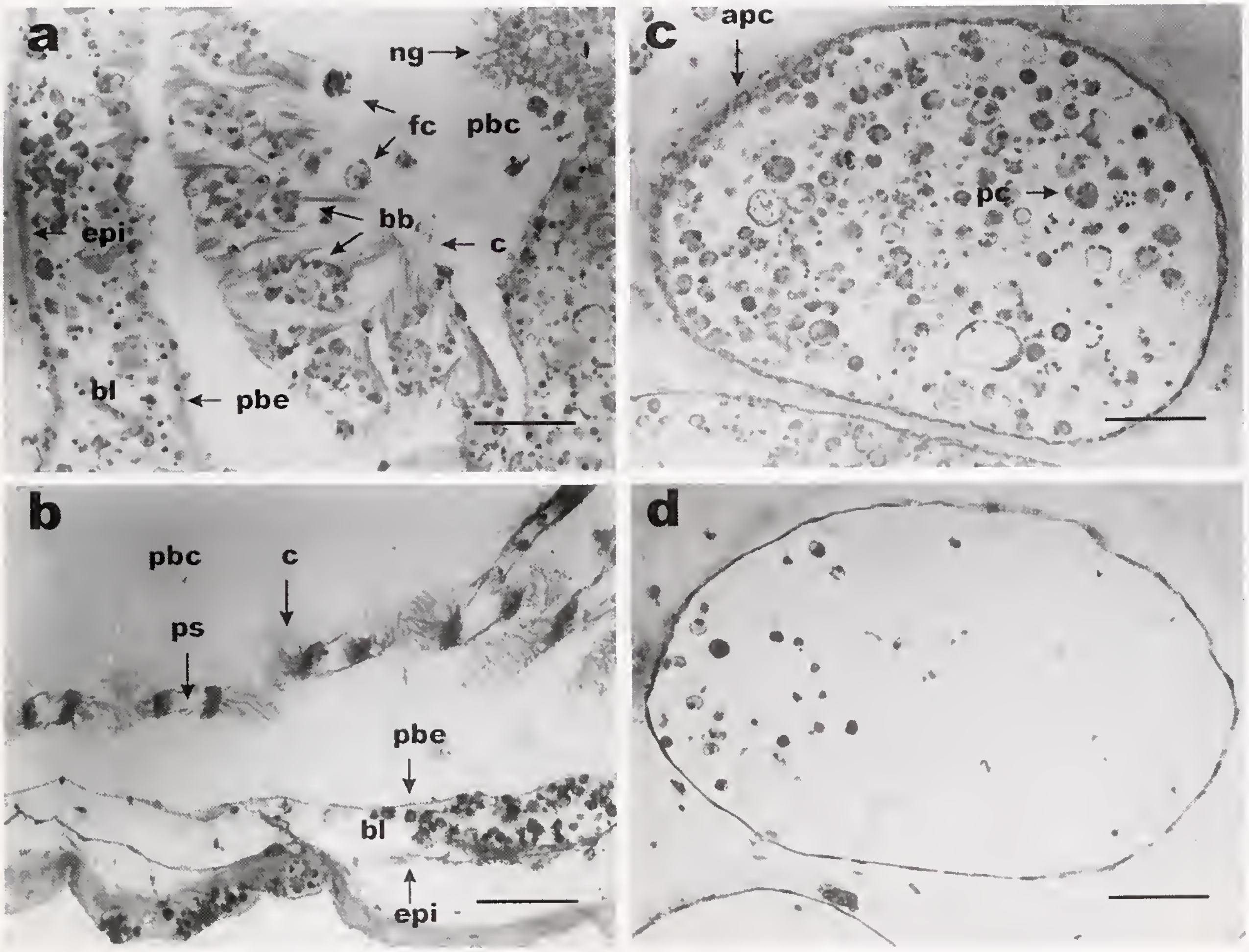

Figure 4. Histological observations of zooids at day 5 of nonrandom senescence. (a) Dorsal section of a day 5 senescent zooid near the neural complex, outlining the progressive disorganization of the pharyngeal slits within the branchial basket, and the shedding of individual cells or groups of cells into the peribranchial cavity. (b) Pharyngeal slits in a comparable dorsal section from a nonsenescent colony. Epithelia (peribranchial epithelium and epidermis) from nonsenescent zooids are squamous, whereas during senescence, the epithelium swells. (c) Cross-section through a peripheral ampulla from a senescent colony at day 5 of senescence. Note the congested appearance of blood cells within the ampulla as compared to an ampulla from a nonsenescent colony (d). Abbreviations: apc, ampullar pad cell; bb, branchial basket; bl, blood; c, cilia; epi, epidermis; fc, free cells in peribranchial cavity; ng, neural gland; pbc, peribranchial cavity; pbe, peribranchial epithelium; pc, phagocytic cell; ps, pharyngeal slits. Scale = 60 μm.

cells interspersed within visceral tissues began a sharp decrease in cytoplasmic density accompanied by pronounced distension of the endoplasmic reticulum (Fig. 5a, b: branchial basket; Fig. 5c, d: intestine). Within these cells, the inner and outer leaflets of the nuclear envelope separated, but the chromatin configuration remained nearly normal as compared with unaffected neighboring cells (Fig. 5a, d). The nuclear hallmarks of apoptosis, such as chromatin condensation and margination against the nuclear envelope, were not observed in the senescent tissues examined by electron microscopy (Fig. 5: branchial basket and intestine; Fig. 6: endostyle and stomach). Another change associated with the nonrandom senescent phenotype was a prominent Golgi apparatus, seen primarily in those cells in which cytoplasmic density was markedly reduced. In contrast, the plasma membrane remained intact at this time, and contacts with neighboring cells were maintained (Fig. 5a–d).

During the takeover phase of blastogenesis, visceral tissues from the zooid undergo apoptotic cell death, and mitochondrial architecture is generally preserved throughout this process (Lauzon *et al.*, 1993). However, examination of the mitochondria during nonrandom senescence revealed that they too underwent pronounced degenerative changes, appearing swollen, with their cristae both distended and disorganized (Fig. 5b–d). More importantly, these changes frequently preceded the loss of cytoplasmic density (Fig. 5a,

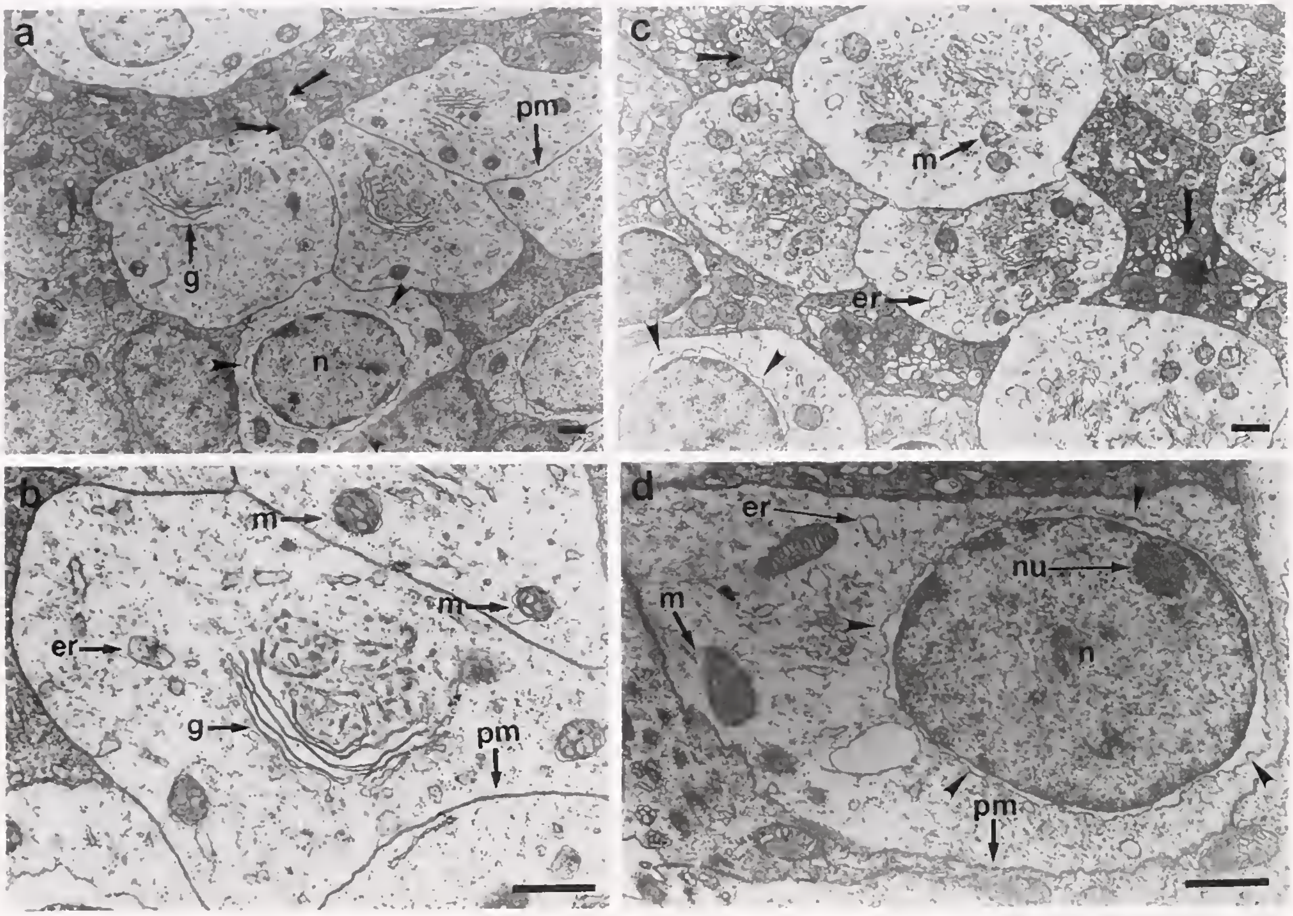

Figure 5. Ultrastructural analysis of visceral cell death at day 3 of nonrandom senescence. Cross-sections through the branchial basket (a, b) and intestine (c, d) at day 3 of nonrandom senescence. Ultrastructural features are diagnostic of ischemic cell death, and include the separation of the nuclear envelope (black arrowheads in a, c, and d), a pronounced decrease in cytoplasmic density (a–d), distension of the endoplasmic reticulum (b–d), swelling of mitochondria with concomitant distension and disorganization of cristae (b–d), and appearance of a prominent Golgi apparatus (a, b). Note that mitochondrial disruption is also observed in cells with normal cytoplasmic density (large black arrows in a, c). In contrast, the chromatin appears normal at this stage, and the plasma membrane remains intact (a–d). Abbreviations: er, endoplasmic reticulum; g, Golgi apparatus; m, mitochondria; n, nucleus; nu, nucleolus; pm, plasma membrane. Scale bars = 1 μm.

c). Interestingly, this degeneration did not occur simultaneously in all cells of a given visceral tissue (Fig. 5a) or other tissues (Fig. 6b, d). Other ultrastructural changes that were observed at day 3 of nonrandom senescence included accumulation of large intra-cytoplasmic lipid inclusions throughout cells of the viscera and blood (Fig. 6a), fusion of microvilli at the brush border of the digestive epithelium (Fig. 6b), and extensive phagocytosis of dying cells throughout the anteroposterior axis of the zooid (Fig. 6c). In addition, lysosomal activity was inferred to be an important component in cell death in some instances, as autophagosomes were frequently observed within cells of the endostyle near the ventral sinus, independently of the necrotic changes described above (Fig. 6d).

Discussion

We have previously documented the longevity of 41 independent, laboratory genets and observed that senescence in *Botryllus schlosseri* could manifest itself in either random or nonrandom fashion (Rinkevich *et al.*, 1992). During nonrandom senescence, specific parental colonies and their subcloned ramets died within a defined period of time, often within the same blastogenic cycle. Here, we have described a morphological profile of nonrandom senescence at the level of the genetic individual, the genet. Under laboratory conditions, specific colonies had finite life spans, and most of the ramets from a given genet exhibited in-concert, degenerative changes that signaled imminent death within about 7 days. The nonrandom senescent phe-

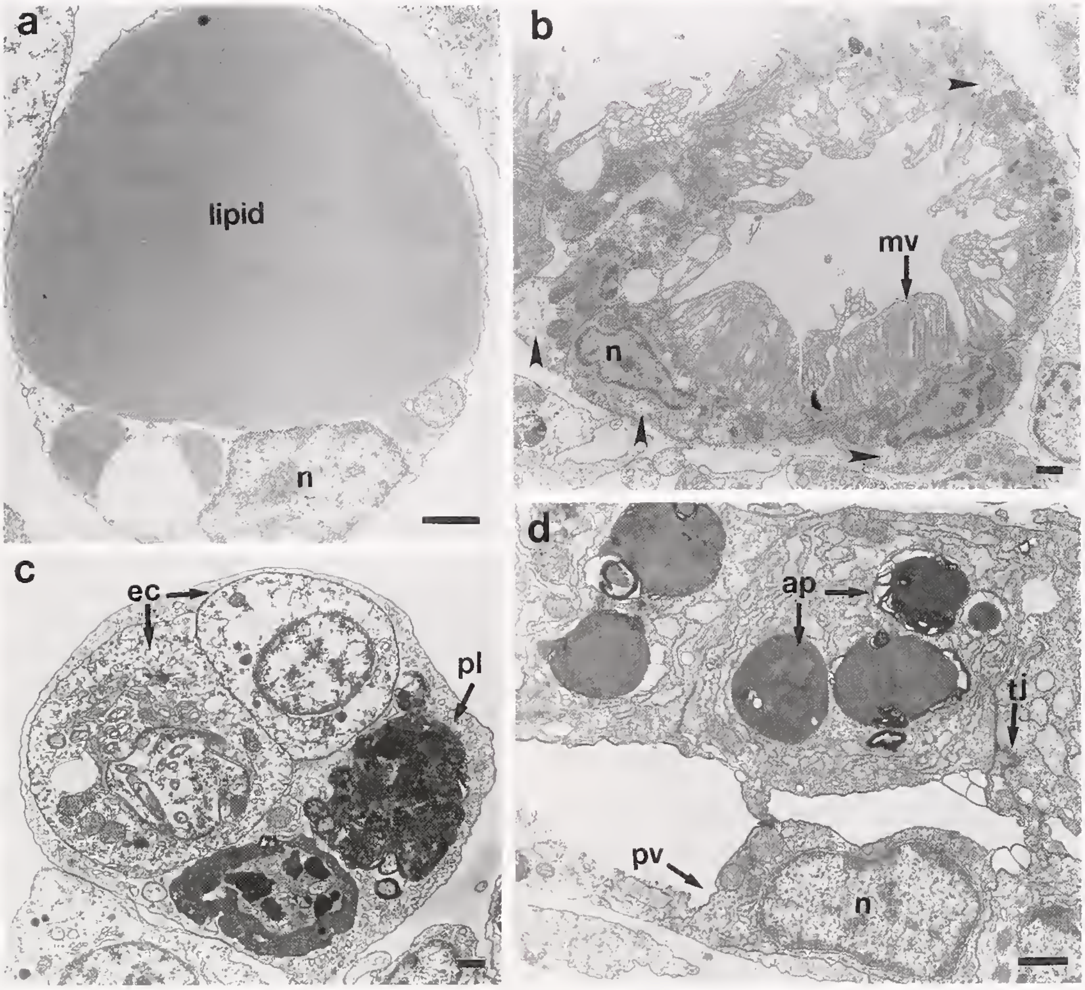

Figure 6. Further ultrastructural alterations in zooids at day 3 of nonrandom senescence. (a) Individual cell with prominent lipid inclusion found in blood space of zooid. Such cells are found randomly dispersed in blood and viscera throughout the dorsoventral plane of individual zooids. (b) Cross-section through the brush border of the gastric epithelium reveals fused microvilli. These cells do not yet display any disruption of the nuclear membrane, but some loss of cytoplasmic density can be observed (large black arrowheads). (c) Phagocyte found in the branchial basket with multiple phagolysosomes. (d) Longitudinal section of the endostyle, near the ventral sinus, reveals prominent membrane whorls indicative of autophagy. However, the tight junctions have remained intact. Abbreviations: ap, autophagic vacuoles; mv, microvilli; ec, engulfed cell; n, nucleus; pl, phagolysosome; pv, perivisceral epithelium; tj, tight junctions. Scale bars = 1 μm.

notype in this species was defined by characteristic morphological changes that were identical from colony to colony, and which began with the systemic constriction of the colonial vasculature, followed by cellular necrosis as an end-point. Macroscopic, senescence-associated changes similar to the ones reported here have been documented in field-grown *B. schlosseri* colonies (Brunetti, 1974; Chadwick-Furman, 1995a). For instance, Brunetti (1974) described a mortality process with rapid onset, in *B. schlosseri* colonies from the Venetian Lagoon (Italy). The features of this process included slowing of blood flow; storage of pigment cells within blood vessels, ampullae, and zooid body wall; inability of zooids to form complete systems; dilation of siphons; and separation of buds from the parent zooids. The concordance between our macroscopic observations of laboratory colonies and those resulting from field work are important because this species exhibits tremendous plasticity of life-history traits in response to environmental variation (Brunetti, 1974; Chadwick-Furman and Weissman, 1995b; Rinkevich *et al.*, 1998). Furthermore, our studies are the first to document in detail the morphology of senescence at the cellular and subcellular levels in this species.

In the clonally modular ascidian *B. schlosseri*, death processes can be investigated at three levels: the individual zooids, the ramets, and the genet. Studies on individual zooids (Milkman, 1967; Sabbadin, 1969; Lauzon *et al.*, 1992) have revealed the existence of a weekly, synchronized cycle of asexual development and regression, known as the blastogenic cycle, which concludes with massive visceral apoptosis (Lauzon *et al.*, 1993). On the other hand, senescence at the level of the ramet has not been extensively investigated. In contrast to nonrandom senescence, senescence at the ramet level can manifest itself at random, and thus may occur at any blastogenic cycle, independently of the genet (Rinkevich *et al.*, 1992). This process also exhibits a characteristic morphology; this includes synthesis of fewer than one bud or zooid per blastogenic cycle, constriction of blood vessels, accumulation of pigment cells within zooids and ampullae, dispersal of zooids within systems, degeneration of the tunic and loss of zooid resorption potential during takeover (Brunetti and Copello, 1978; Rinkevich *et al.*, 1998). These features resemble nonrandom senescence documented in *B. schlosseri* genets (Rinkevich *et al.*, 1992; this study). There are, however, two major differences between nonrandom and random senescence. First, nonrandom senescence is fast, being completed in 7 days from onset of morphological changes, as compared to the weeks and months of gradual deterioration that is typically associated with random senescence of ramets. Second, random senescence may be followed by rejuvenation. Degenerating ramets undergoing random senescence often do not die (Rinkevich *et al.*, 1998). Several weeks (sometimes more than 2 months) after the manifestation of senescent features, colonies may return to a fast growth rate characteristic of young colonies (Rinkevich *et al.*, 1998). Although senescence is regarded as an unavoidable part of the life histories of many organisms, it seems that some clonal organisms that produce genetically identical modules may escape aging at the level of the genet (Gardner and Mangel, 1997). According to this concept, ramets may senesce, but the further production of new ramets may enable the genet to escape senescence. Many colonial marine invertebrates have been documented to undergo periodic phases of degeneration and regeneration. These include bryozoans (Palumbi and Jackson, 1983) and clonal species of sponges, corals, hydrozoans, the related botryllid ascidian *Botrylloides leachi* and many other ascidians (Jackson, 1985; Rinkevich *et al.*, 1996). The mechanisms regulating such processes are unknown, and clearly deserve further attention.

Is nonrandom senescence genetically programmed?

The life span of an organism can best be conceptualized as the sum of harmful changes and compensatory mechanisms that either delay or limit such changes, thus promoting longevity (Johnson *et al.*, 1999). A number of mechanisms have been described as potentially affecting aging and senescence in eukaryotes. These include damage mediated by reactive oxygen species (oxidative stress), genomic instability, telomere shortening, cell death, genetically programmed life extension, and systemic control of aging (reviewed in Jazwinski, 1996; Sohal and Weindruch, 1996; Johnson *et al.*, 1999). The relevance of such processes in the regulation of life span in *Botryllus* is unknown. However, the universality of the nonrandom senescent phenotype in *B. schlosseri* genets argues for the existence of an underlying genetic program controlling the aging process. In some aspects, nonrandom senescence of *Botryllus* genets resembles other senescence and life-span phenomena seen in some aclonal invertebrates. It is well documented that the timing of expression of life-history stages is an important factor regulating aging and senescence in animals with complex life cycles (Miller and Hadfield, 1990). For instance, the expression of a genetic program associated with aging early in the larval life of a nudibranch mollusc (Miller and Hadfield, 1990) or prior to the subcloning of a *Botryllus* colony (Rinkevich *et al.*, 1992; this study) may already set the limit for the maximal longevity of a genet. The observation that ramets often die simultaneously within the same blastogenic cycle, months following their separation, further validates this hypothesis. Recent studies have further implicated genetic elements, and their often complex interactions, in the manifestation of senescence in mammals (Haan *et al.*, 1998) and invertebrates (Orr and Sohal, 1994; Gems, 1999; Taub *et al.*, 1999). One such study documented the life spans of individual mice originating from a recombinant inbred strain. Their findings indicated that, despite a homogeneous genetic background, life spans fell into two temporal groups, revealing a locus that causes variability in the rate at which members of a population die (Haan *et al.*, 1998). In the nematode *Caenorhabditis elegans*, at least 39 genes have been demonstrated to significantly affect worm life span (Murakami and Johnson, 1998; Gems, 1999; reviewed in Johnson *et al.*, 1999; Taub *et al.*, 1999).

The role of the vascular system in programmed mortalities

An intriguing observation reported here concerns the systemic nature of vasculature constriction and that this change appears to underlie all subsequent events within senescent colonies. These findings raise the possibility that in *B. schlosseri*, nonrandom senescence could be triggered by a humoral factor that initiates the vascular anomalies and that may be transferred throughout the colony *via* blood. Our previous findings in *B. schlosseri* chimeras (Rinkevich *et al.*, 1992) indicated that the onset of senescence occurred synchronously in both partners at the time of the earliest senescent partner. These observations were completely reproduced with vascular chimeras grown in the field, but not in the majority of laboratory cohorts (Chadwick-Furman and Weissman, 1995b). The reason for the discrepancy within laboratory chimeras is not immediately apparent, although the sample size in the study was small. These data tentatively suggest that senescence could be transmitted systemically through blood. Systemic control of the aging process has recently received experimental support in both nematodes (Apfeld and Kenyon, 1998) and mammals (Kuro-o *et al.,* 1997). According to this view, humoral factors coordinate the rate of aging in various tissues or organs (Johnson *et al.,* 1999). In mammals, a gene encoding a humoral factor termed *klotho* was recently implicated in the suppression of a wide variety of aging phenotypes (Kuro-o *et al.,* 1997). A defect in the expression of this gene in the mouse results in a phenotype that severely curtails life span, and leads to the development of aging-related pathologies. A more recent study in *C. elegans* using genetic mosaic animals for *daf-2,* a gene involved in a signal transduction pathway affecting resistance to oxidative stress and longevity, has shown that a small number of mutant cells in several sublineages were sufficient to confer enhanced longevity on the entire animal (Apfeld and Kenyon, 1998). A key finding in their study was that the ratio of mutant:wild-type *daf-2* was the most critical determinant affecting life span. These findings strongly suggest that *daf-2* may control the production of a humoral factor, and that the systemic levels of this factor determine the rate of aging in this species (Apfeld and Kenyon, 1998). The observation of a common, widespread vascular anomaly in the initial stages of nonrandom senescence in *Botryllus* lends credence to the hypothesis that aging and senescence are under systemic control. Further studies aimed at characterizing the nature and pattern of expression of this putative factor present in the vasculature of senescent colonies will be required to address this issue.

The vascular changes described herein may explain the underlying ultrastructural morphology observed. All of the visceral tissues examined revealed changes that were consistent with ischaemic cell death or oncosis, a term coined by Majno and Joris (1995). The characteristic ultrastructural changes associated with this mode of cell death, seen during nonrandom senescence in *B. schlosseri,* included cellular swelling, decrease in cytoplasmic density, organelle distension, and ultimately necrotic cell lysis, an end-point of this type of cell death (Abbott, 1983; Majno and Joris, 1995). This morphology differed from that observed during the takeover phase of the blastogenic cycle, in which apoptosis is the primary mode of cell death in the zooid viscera (Lauzon *et al.,* 1993). These subcellular features presumably corresponded to the enlarged, weakly basophilic cells seen in histological sections. On occasion, large empty spaces were also observed interspersed within the tissues of senescent zooids. These findings are interpreted as resulting from necrotic cell lysis, since no similar changes were observed in tissue sections from nonsenescent animals (Lauzon *et al.,* 1992; Rinkevich *et al.,* 1992). Since mitochondrial swelling appeared to either precede or accompany other ultrastructural changes, loss of mitochondrial function may underlie the subcellular morphology observed during nonrandom senescence. According to this scenario, a decrease in blood flow within a zooid, triggered by systemic blood vessel constriction, would limit the amount of oxygen delivered to visceral tissues. This state of ischaemia may in turn trigger a mitochondrial catastrophe, resulting in loss of ATP production. The subsequent failure of ionic pumps within the plasma membrane, a documented feature of ischaemic cell death (Majno and Joris, 1995), would in turn lead to an increase in cell permeability and ultimately to necrotic cell lysis as an end-point. Consequently, this model predicts that the subcellular changes observed during nonrandom senescence are secondary to the systemic changes occurring within the vasculature. However, the model does not provide a satisfactory explanation as to why zooids degenerate before buds do. Perhaps metabolic rate and oxygen consumption are substantially greater in filter-feeding zooids than in developing buds. Additional studies will be required to resolve this issue.

Cells with the characteristic ultrastructure of apoptosis were not directly observed during nonrandom senescence. However, some free or engulfed pyknotic cells were observed under bright-field microscopy; similarly, cells undergoing secondary necrotic lysis within phagocytes (phagolysosomes) were observed by electron microscopy. Secondary necrotic lysis is the fate of an apoptotic cell that has been engulfed by a phagocytic cell (Lauzon *et al.,* 1993). Consequently, the possibility that some apoptosis occurs prior to day 3 cannot be excluded, since electron microscopy samples were processed only at day 3 of the senescent phenotype. However, our findings are more consistent with the scenario that systemic changes, transmitted via blood, trigger ischaemic cell death with accompanying phagocytosis of dying cells. Furthermore, genetic data from other species do not support a role for apoptosis in aging and senescence. In *C. elegans,* the genetic programs underlying both processes do not overlap (reviewed in Johnson *et al.,* 1999).

We have previously shown that the vasculature also plays an important role in the clearance of dying tissues of the zooid viscera by macrophages during takeover. During this process, the hearts of regressing zooids continue pulsating until the zooids are almost completely resorbed, and thus blood flow in the dying zooid is uninterrupted throughout takeover (Lauzon *et al.,* 1992, 1993). The buds are also essential collaborators in this process, since their surgical removal in a colony markedly reduces the rate at which zooids become resorbed (Lauzon, unpubl. data). The vascular anomalies observed during nonrandom senescence could also explain why zooids are not completely resorbed during takeover. Since blood flow gradually slows down owing to the systemic constriction of all blood vessels, buds become developmentally arrested without a functional vasculature. Consequently, when a colony undergoing nonrandom senescence enters takeover, the parental generation of zooids cannot be completely resorbed because both vasculature and buds become incapacitated. In summary, the findings reported in this paper indicate that nonrandom senescence in *B. schlosseri* at the level of the genet exhibits a morphology and temporal sequence that is distinct from other death processes in this organism. Our observations may pave the way to understand how aging is regulated in this clonally-modular urochordate.

Acknowledgments

The authors are indebted to the staff of the Hopkins Marine Station where most of this work was conducted. In addition, we thank K. Ishizuka and K. Palmeri for their care in maintaining laboratory stocks of animals, and Lesley Dewing for photographic assistance. We also gratefully acknowledge Drs. Barbara Boyer, Stephen Horton, and Helena Birecka for discussions and critical review of this manuscript prior to submission. This study, which is part of the research done at the Minerva Center, was supported by a grant from the Israel Academy of Sciences to B. R., the Bi-National Science Foundation to B. R. and I. L. W., and a Union College faculty development grant to R. J. L.

Literature Cited

Abbott, L. A. 1983. Ultrastructure of cell death in Gamma- or X-irradiated imaginal wing discs of *Drosophila. Radiat. Res.* **96:** 611–627.

Apfeld, J., and C. Kenyon. 1998. Cell non-autonomy of *C. elegans daf-2* function in the regulation of diapause and life span. *Cell* **95:** 199–210.

Berrill, N. J. 1950. *The Tunicata.* Roy Society, London. 354 pp.

Boyd, H. C., S. K. Brown, J. A. Harp, and I. L. Weissman. 1986. Growth and sexual maturation of laboratory-cultured Monterey *Botryllus schlosseri. Biol. Bull.* **170:** 91–109.

Brunetti, R. 1974. Observations on the life cycle of *Botryllus schlosseri* (Pallas) (Ascidiacea) in the Venetian lagoon. *Boll. Zool.* **41:** 225–251.

Brunetti, R., and M. Copello. 1978. Growth and senescence in colonies of *Botryllus schlosseri* (Pallas) (Ascidiacea). *Boll. Zoll.* **45:** 352–356.

Chadwick-Furman, N. E., and I. L. Weissman. 1995a. Life histories and senescence of *Botryllus schlosseri* (Chordata, Ascidiacea) in Monterey Bay. *Biol. Bull.* **189:** 36–41.

Chadwick-Furman, N. E., and I. L. Weissman. 1995b. Life history plasticity in chimeras of the colonial ascidian *Botryllus schlosseri. Proc. R. Soc. London B* **262:** 157–162.

De Tomaso, A. W., Y. Saito, K. J. Ishizuka, K. J. Palmeri, and I. L. Weissman. 1998. Mapping the genome of a model protochordate. A low resolution genetic map encompassing the fusion/histocompatibility (Fu/HC) locus of *Botryllus schlosseri. Genetics* **149:** 277–287.

Gardner, S. N., and M. Mangel. 1997. When can a clonal organism escape senescence? *Am. Nat.* **150:** 462–490.

Gems, D. 1999. Nematode ageing: putting metabolic theories to the test. *Curr. Biol.* **9:** R614–R616.

Grosberg, R. K. 1988. Life history within a population of the colonial ascidian *Botryllus schlosseri.* I. The genetic and environmental control of seasonal variation. *Evolution* **42:** 900–920.

Haan, G. de, R. Gelman, A. Watson, E. Yunis, and G. V. Zant. 1998. A putative gene causes variability in life span among genotypically identical mice. *Nat. Genet.* **19:** 114–116.

Jackson, J. B. C. 1985. Distribution and ecology of clonal and aclonal benthic invertebrates. Pp. 297–355 in *Population Biology and Evolution of Clonal Organisms,* J. B. C. Jackson, L. W. Buss, and R. E. Cook, eds. Yale University Press, New Haven.

Jazwinski, S. M. 1996. Longevity, genes and aging. *Science* **273:** 54–58.

Johnson, F. B., D. A. Sinclair, and L. Guarente. 1999. Molecular biology of aging. *Cell* **96:** 291–302.

Kuro-o, M., Y. Matsumura, H. Aizawa, H. Kawaguchi, T. Suga, T. Utsugi, Y. Ohyama, M. Kurabayashi, T. Kaname, E. Kume, H. Iwazaki, L. Akihiro, T. Shiraki-Lida, S. Nishikawa, R. Nagai, and Y-i. Nabeshima. 1997. Mutation of the mouse *Klotho* gene leads to a syndrome resembling ageing. *Nature* **390:** 45–51.

Lauzon, R. J., K. J. Ishizuka, and I. L. Weissman. 1992. A cyclical, developmentally-regulated death phenomenon in a colonial urochordate. *Dev. Dyn.* **194:** 71–83.

Lauzon, R. J., C. W. Patton, and I. L. Weissman. 1993. A morphological and immunohistochemical study of programmed cell death in *Botryllus schlosseri* (Tunicata, Ascidiacea). *Cell Tissue Res.* **272:** 115–127.

Magor, B. G., A. De Tomaso, B. Rinkevich, and I. L. Weissman. 1999. Allorecognition in colonial tunicates: protection against predatory cell lineages. *Immunol. Rev.* **167:** 69–79.

Majno, G., and I. Joris. 1995. Apoptosis, oncosis and necrosis. An overview of cell death. *Am. J. Pathol.* **146:** 3–19.

Milkman, R. 1967. Genetic and developmental studies on *Botryllus schlosseri. Biol. Bull.* **132:** 229–243.

Millar, R. H. 1952. The annual growth and reproductive cycle in four ascidians. *J. Mar. Biol. Assoc. UK* **31:** 41–61.

Miller, S. E., and M. G. Hadfield. 1990. Developmental arrest during larval life and life-span extension in a marine mollusc. *Science* **248:** 356–358.

Murakami, S., and T. E. Johnson. 1998. Life extension and stress resistance in *Caenorhabditis elegans* by the *tkr-1* gene. *Curr. Biol.* **8:** 1091–1094.

Orr, W. C., and R. S. Sohal. 1994. Extension of life-span by overexpression of superoxide dismutase and catalase in *Drosophila melanogaster. Science* **263:** 1128–1130.

Palumbi, S. R., and J. B. C. Jackson. 1983. Aging in modular organisms: ecology of zooid senescence in *Stegmoporella* sp. (Bryozoa: Cheilostomata). *Biol. Bull.* **164:** 267–278.

Rinkevich, B., and M. Shapira. 1998. An improved diet for inland broodstock and the establishment of an inbred line from *Botryllus schlosseri,* a colonial sea squirt (Ascidiacea). *Aquat. Living Resour.* **11:** 163–171.

Rinkevich, B., R. J. Lauzon, B. W. Brown, and I. L. Weissman. 1992. Evidence for a programmed life span in a colonial protochordate. *Proc. Nat. Acad. Sci. U.S.A.* **89:** 3546–3550.

Rinkevich, B., Z. Schlemberg, and L. Fishelson. 1996. Survival budding processes in the colonial tunicate *Botrylloides* from the Mediterranean Sea: the role of totipotent blood cells. Pp. 1–9 in *Invertebrate Cell Culture: Looking Towards the Twenty-First Century,* K. Maramorosh and M. J. Loeb, eds. Society for In Vitro Biology, Largo, MD.

Rinkevich, B., B. Porat, and M. Goren. 1998. On the development and reproduction of *Botryllus schlosseri* (Tunicata) colonies from the eastern Mediterranean Sea: plasticity of life history traits. *Invertebr. Reprod. Dev.* **34:** 207–218.

Sabbadin, A. 1969. The compound ascidian *Botryllus schlosseri* in the field and in the laboratory. *Pubbl. Stn. Zool. Napoli* **37 suppl.:** 67–72.

Sohal, R. S., and R. Weindruch. 1996. Oxidative stress, caloric restriction, and aging. *Science* **273:** 59–63.

Stoner, D., B. Rinkevich, and I. L. Weissman. 1999. Heritable germ and somatic cell lineage competitions in chimeric colonial protochordates. *Proc. Natl. Acad. Sci. USA* **96:** 9148–9153.

Taub, J., J. F. Lau, C. Ma, J. H. Hahn, R. Hoque, J. Rothblatt, and M. Chalfie. 1999. A cytosolic catalase is needed to extend adult lifespan in *C. elegans daf-C* and *clk-1* mutants. *Nature* **399:** 162–166.

Reference: *Biol. Bull.* **198:** 379–386. (June 2000)

Vestigial Ophiopluteal Structures in the Lecithotrophic Larvae of *Ophionereis schayeri* (Ophiuroidea)

P. SELVAKUMARASWAMY* AND M. BYRNE

Department of Anatomy and Histology, F13; University of Sydney; N.S.W., 2006; Australia

Abstract. Evolution of echinoderm development from a feeding to a non-feeding mode can be examined by studying non-feeding larvae with structures that appear to be vestiges derived from a feeding ancestral state. The lecithotrophic larvae of the Australian brittle star *Ophionereis schayeri* possess such features, and the early development of this species was documented by light and scanning electron microscopy. The embryos undergo irregular cleavage, resulting in the formation of different sized blastomeres, with subsequent development through a wrinkled blastula stage. The lecithotrophic larva of *O. schayeri* possesses several vestigial ophiopluteal structures, including a continuous ciliated band, a larval gut, and a larval skeleton. The ciliated band is a reduced expression of the continuous ciliated band typical of ophioplutei. The larval gut is a transiently complete system, but an esophageal plug and rapid closure of the blastopore renders it nonfunctional. The larval skeleton, though reduced, consists of four rods corresponding to the body, posterolateral, anterolateral, and postoral rods characteristic of an ophiopluteus. Due to a heterochrony in larval skeletogenesis, the postoral rods develop early and simultaneously with the other rods. Compared with the larvae of other lecithotrophic ophiuroids, the larva of *O. schayeri* is one of the most reduced ophiopluteal forms reported to date.

Introduction

The diversity of developmental modes in marine invertebrates has intrigued investigators for many years (Wray, 1995). This diversity is presumed to be associated with life history evolution, but the direction of the evolutionary change, whether from planktotrophy to lecithotrophy or *vice versa*, has been a topic of debate. Phylogenetic analyses of larval morphological traits have been combined with molecular characters to produce a better understanding of the evolution of different life histories (Wray, 1996; Hart *et al.*, 1997; McHugh and Rouse, 1998). For echinoderms, planktotrophy is considered to be a plesiomorphic character. The loss of complex larval feeding structures in the evolution of non-feeding development involves major alterations in larval morphology, which are thought to be irreversible (Strathmann, 1974). Thus, the occurrence of ophiuroid and echinoid larvae with vestigial larval feeding structures (*e.g.*, pluteal arms, skeleton, ciliated band) indicates that they have evolved from an ancestral form that had a feeding larva. The transition from planktotrophy to lecithotrophy is predicted to be reversible, however, when maternal nutritional investment is altered due to selective pressures, without a resulting change in larval morphology (McEdward and Janies, 1997).

Planktotrophic development in ophiuroids occurs through an 8-armed ophiopluteus (Table 1). Lecithotrophic development in ophiuroids is associated with a range of larval forms—including planktonic ophioplutei with a reduced number of arms, vitellaria larvae, and benthic and brooded larval forms—that may or may not possess ophiopluteal features (Table 1). Thus far, eleven ophiuroid species are known to have lecithotrophic larvae with vestigial larval structures, seven with planktonic development, one with benthic development, and three with brooded development (Table 1). This list suggests that lecithotrophic species with developmental features intermediate between planktotrophy and lecithotrophy are uncommon. This may be due to evolutionary instability of intermediate larval forms (Vance, 1973) or may reflect inadequate sampling. Further examination of ophiuroids with lecithotrophic larvae and comparison of development in closely related species is needed to determine the processes and pathways underlying the loss of superfluous larval structures during the evolution of lecithotrophy.

Received 3 August 1998; accepted 25 February 2000.

* To whom correspondence should be addressed. E-mail: paulina@anatomy.usyd.edu.au.

Table 1

Developmental modes in the Ophiuroidea, with emphasis on lecithotrophic species that retain larval feeding structures

Developmental mode	Larval form	Species	Reference
Planktotrophic	8-arm ophiopluteus	>50 species	MacBride, 1907; Mortensen, 1921; Narasimhamurti, 1933; Olsen, 1942; Hendler, 1975; Mladenov, 1985; Yamashita, 1985; Hendler, 1991
Lecithotrophic (planktonic)	Reduced ophiopluteus		
	6 arms	*Amphiura filiformis*	Fell, 1945
	2 arms	*Ophiura affinis, Amphiura chiajei, Ophiothrix oerstedi*	Fell, 1945; Fenaux, 1963; Mladenov, 1979
	Armless	*Ophiopluteus claparedei*	Fell, 1945
	Vitellaria (with larval structures)	*Ophiolepis cincta, Ophionereis annulata*	Mortensen, 1938; *Hendler, 1982
	Vitellaria (no larval structures)	*Ophiura brevispina, Ophionereis squamulosa, Ophioderma longicauda, Ophiolepis elegans, Ophiolpocus japonicus*	Grave, 1900; *Mortensen, 1921; Fenaux, 1969; Stancyk, 1973; Komatsu and Shoshaku, 1993
Lecithotrophic (benthic)	(With larval structures)	*Amphioplus abditus*	Hendler, 1978
	(No larval structures)	Kirk's ophiuroid	Fell, 1941
Lecithotrophic (brooded)	(With larval structures)	*Amphipholis japonica, Amphipholis squamata, Ophiontus hexactis*	Murakami, 1940; Fell, 1946; Mortensen, 1921
	(No larval structures)	*Ophionereis olivacea, Ophionereis vivipara,* and >68 other species	*Byrne, 1991; Hendler, 1991; *Mortensen, 1933

* Previous studies on *Ophionereis* species.

The Australian ophiuroid *Ophionereis schayeri* develops through a lecithotrophic larva that retains a suite of larval feeding structures. It spawns 241 μm diameter, lipid-rich eggs and completes development in 6–7 days (Moloney and Byrne, 1994; Selvakumaraswamy and Byrne, 1995; Selvakumaraswamy and Byrne, 1998, 1999). The development of four other lecithotrophic *Ophionereis* species has been described, with two species possessing some pluteal features and the other two completely lacking them (Table 1). The selective pressures underlying the developmental diversity in ophiuroids are unknown, and the larval forms in these *Ophionereis* species are compared here to provide insights on how loss of larval structures may have occurred within this clade. In this study the early larvae of *O. schayeri* are described, with emphasis on the development of its vestigial ophiopluteal structures.

Materials and Methods

Ophionereis schayeri was collected from several sites in New South Wales during its summer spawning season, from January to April, in 1996 and 1997. Animals were induced to spawn by combined light and temperature shock. About 20 individuals were transferred repeatedly between seawater at 34°C and at ambient temperature (19°–23°C), then kept in the dark for half an hour. This was repeated every half hour for 2–3 h. For larval culture, fertilized eggs were rinsed three times in filtered seawater (1 μm), placed into 500-ml beakers at densities of 5 eggs/ml, and kept constantly stirred at ambient temperatures (19°–23°C). The seawater was changed every second day by aspiration through an 80-μm mesh.

The larval skeleton was visualized as follows. Embryos and larvae were fixed for 1 h in 2% paraformaldehyde buffered in 0.2-μm filtered seawater, and then stored in 70% ethanol. They were then made translucent by dehydration and clearing in a 1:1 solution of benzyl benzoate and benzyl alcohol, according to Amemiya and Emlet (1992). The cleared larvae were examined with cross polarized light. For scanning electron microscopy (SEM) and light microscopy (LM), embryos and larvae were fixed for 1 h in 2.5% gluteraldehyde, buffered in 0.2-μm filtered seawater, rinsed in 2.5% sodium hydrogen carbonate, postfixed for 1 h in 2% osmium tetroxide buffered in 2.5% sodium hydrogen carbonate, rinsed in distilled water, and dehydrated. Specimens for SEM were then critically point dried, coated with 20 nm of gold, and examined with a JEOL 35C scanning electron microscope set at 15 kv. Specimens for resin embedding and (LM) serial sectioning were further dehydrated, infiltrated,

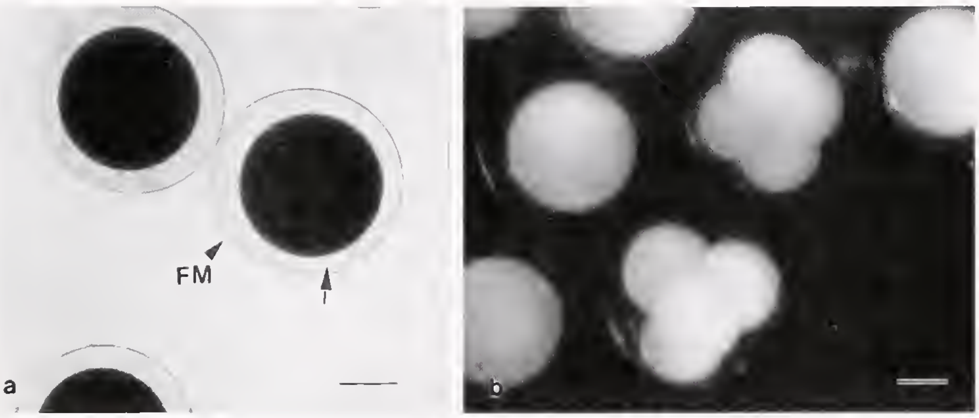

Figure 1. Fertilization and cleavage of *Ophionereis schayeri.* (a) Fertilized eggs have a raised fertilization membrane (FM) and large perivitelline space (arrow). (b) Fertilized eggs and four-cell embryos. Scale bars = 100 μm.

and embedded in Spurr's resin at 80°C for 20 h. Larvae were serial sectioned at 0.9 μm and stained with 1% toluidine blue in 0.5% ethanolamine.

Results

Early development

Fertilized eggs had a 50-μm-wide perivitelline space between the oolemma and the fertilization envelope (Fig. 1a, b). Although looked for, polar bodies were never observed, indicating that meiosis is completed during ovulation and spawning. Cleavage was initially equal and radial (Fig. 2a). After second cleavage, however, the division planes became offset, resulting in an irregular arrangement of the blastomeres (Fig. 2b). Beyond third cleavage, cell division became asynchronous, with some cells cleaving before others (Fig. 2b). The irregular arrangement of blastomeres remained evident to the blastula stage. About 12 h after fertilization, the embryos took on a slightly contorted shape as they developed into wrinkled blastulae. The wrinkles were shallow, forming slight indentations in the epithelium (Fig. 2c). The blastulae subsequently smoothed (Fig. 2d), the epithelium became uniformly ciliated, and the embryos started to rotate within the fertilization envelope. The blastulae hatched about 16 h after fertilization and swam with their anterior pole forward, in no particular direction or orientation. Gastrulation occurred about 21 h after fertilization by invagination of the vegetal plate (Fig. 2e). During gastrulation, the epithelial cells changed shape from cuboidal (Fig. 2d) to columnar (Fig. 2f). Round cells in the epithelium, which were situated towards the apical surface, may be recently divided cells (Fig. 2f). Lipid droplets in the eggs of *O. schayeri* were about 3 μm in diameter (Moloney and Byrne, 1994) and were conspicuous in the epithelial cells of gastrulae (Fig. 2f).

Formation of a reduced ophiopluteus

Larval gut. Twenty-five hours after fertilization the gastrulae elongated, and the blastopore started to close (Figs. 2g, 3c). An anterior ventral depression marking the position of the stomodeal invagination was also evident (Figs. 2g, 3a), but this opening was much smaller than the mouth of typical ophioplutei. Larvae sectioned at this stage had a digestive tract with an incomplete lumen; the esophagus was open to the exterior *via* the stomodeum, but its connection to the stomach was blocked by what appeared to be an esophageal plug (Fig. 3a, b). The larval gut was filled with mesenchyme cells, and opened posteriorly *via* the blastopore (Fig. 3c). Closure of the blastopore after 25 h, however, resulted in formation of a larval gut that was only transiently complete, and thus the larvae did not feed. Subsequently, the gut became a simple sac.

Ciliated band. After 36 h and further elongation, a distinct ventral ridge appeared near the posterior end of the larva, and the ciliated band subsequently formed along this structure (Fig. 2g). Formation of the ventral ridge transformed the late gastrula into an early larva that was bilaterally symmetrical through the anterior-posterior axis (Fig. 2g).

The larva (335 μm in length) developed a single continuous ciliated band about 42 h after fertilization (Fig. 2h, i). The ciliated band ran from the anterior to the posterior end of the larva, marking its ventral and dorsal halves (Fig. 2i). This was made clearly visible by red pigment cells that were associated with the ciliated band. The ciliated band also looped ventrally to run along the ventral ridge, forming a complete and continuous loop similar to that formed in the early stages of embryogenesis in other ophioplutei (Fig. 2h, i). Although the larvae had this continuous ciliated band, a characteristic of ophioplutei, pluteal arms were not formed (Fig. 2i).

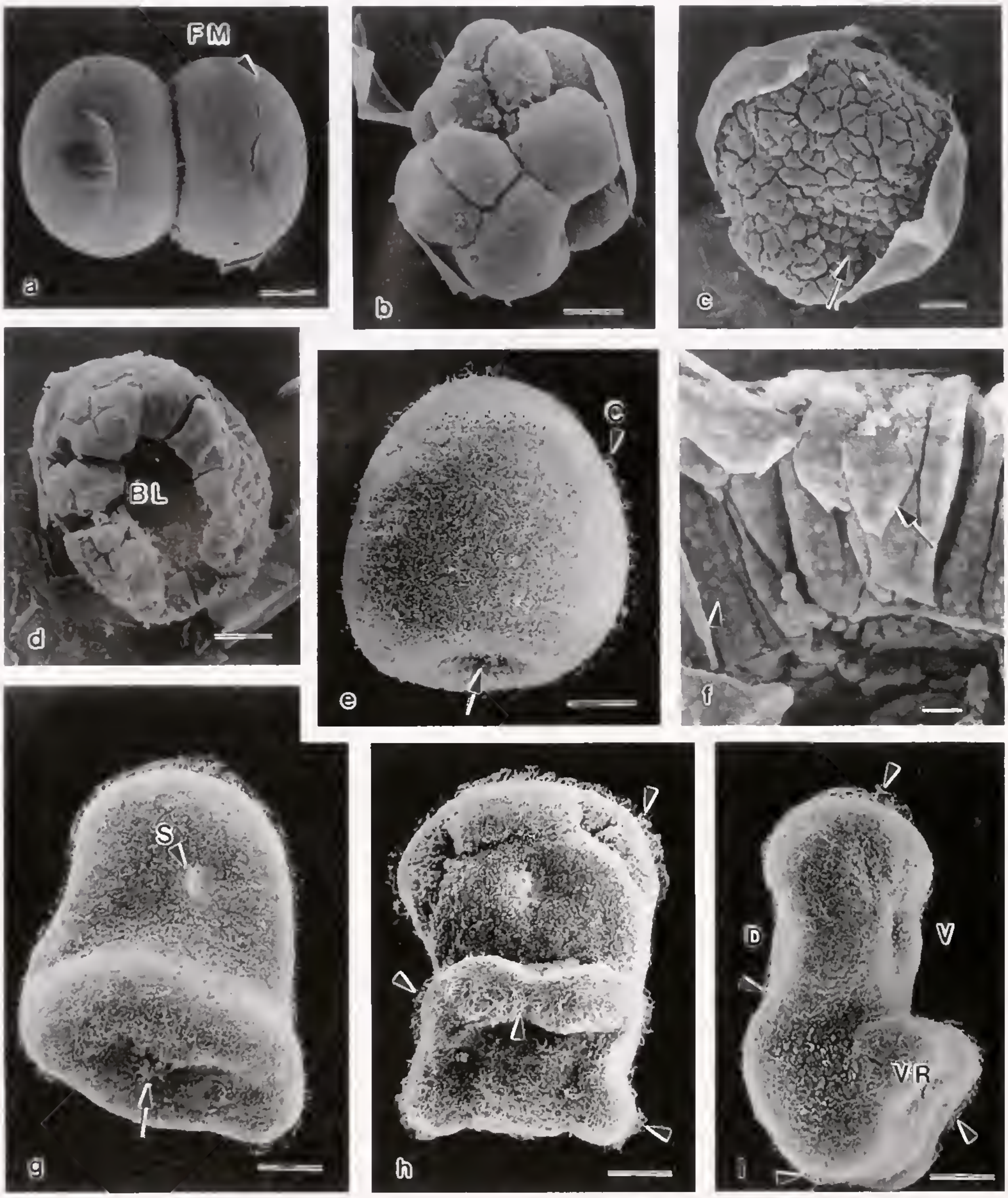

Figure 2. Scanning electron micrographs of the early events of development in *Ophionereis schayeri*. (a) Two-cell embryo. (b) Offset cleavage planes and asynchronous cleavage results in blastomeres of different sizes. (c) Wrinkled blastula with shallow wrinkled depressions (arrow). (d) Cracked open blastula with hollow blastocoel and ciliated epithelial cells. (e) Uniformly ciliated gastrula with vegetal blastopore (arrow). (f) Gastrula epithelium showing columnar cells with visible lipid droplets (arrowhead) and round cells (arrow). (g) Elongate gastrula with closed blastopore (arrow) and anterior stomodeal depression. (h) Early larva with a continuous ciliated band (arrowheads). (i) Side view of an early larva showing the prominent ventral ridge and the ciliated band (arrowheads) that bisects the larva into dorsal and ventral halves. Blastocoel, BL; cilia, C; dorsal, D; fertilization membrane, FM, stomodeal depression, S; ventral, V; ventral ridge, VR. Scale bars for a–e, g–i = 50 μm. Scale bar for f = 10 μm.

Larval skeleton. The bilateral larval skeleton first became evident in gastrulae as two birefringent spots on either side of the blastopore (Fig. 4a). As the gastrulae elongated, the skeleton quickly developed into a tetraradiate form (Fig. 4b). The rods reached their maximum length 42 h after fertilization, when the larvae had developed the ventral ridge and ciliated band. The rods of the tetraradiate larval skeleton formed simultaneously, and consisted of the posterior body rods ($\bar{x} = 52$ μm length, SE = 7 μm, range: 37–93 μm, $n = 7$), which anchored the three reduced larval arm rods. The posterolateral rods ($\bar{x} = 30$ μm, SE = 4 μm, range: 18–46 μm, $n = 7$) projected in the same plane as the

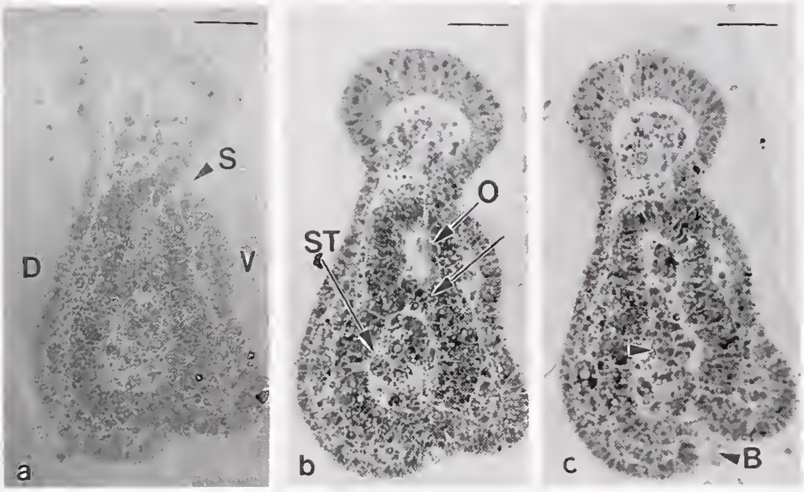

Figure 3. Serial semithin sections through a 28-h-old larva of *Ophionereis schayeri.* Sections are oriented with the animal, or anterior, end towards the top of the figure, and vegetal, or posterior, end towards the bottom. (a) The stomodeum opens on the ventral surface. (b) The larval digestive tract is bipartite, consisting of an esophagus that is separated from the stomach by what appears to be an esophageal sphincter (arrow). (c) The gut is transiently open posteriorly *via* the blastopore. The gut is filled with mesenchyme cells (arrowhead). Blastopore, B; dorsal, D; esophagus, O; stomodeum, S; stomach, ST; ventral, V. Scale bars = 50 μm.

body rods. The other two arm rods, the anterolateral and postoral rods, were approximately equal in length ($\bar{x}$ = 25 μm, SE = 3 μm, range: 12–36 μm, n = 9) (Fig. 4c). The posterodorsal rods of typical ophioplutei never developed in the larvae of *Ophionereis schayeri.* Subsequent development resulted in the skeletal rods all developing thorns simultaneously (Fig. 4d, e).

With onset of rudiment formation in the midventral region of the larva, 48–60 h after fertilization, the two body rods grew and met midway at the posterior end of the larva to form what appeared to be a continuous rod (Fig. 4d, f). The apparent joining of the two posterior body rods did not, however, seem to be accompanied by the presence of transverse or end rods, as in typical ophioplutei. Simultaneously, the adult skeleton appeared as six small birefringent spicules in the rudiment, corresponding to the central and five radial plates of the juvenile dorsal skeleton (Fig. 4d, e, f). The larval skeleton started to break up as the rudiment formed, and pieces of the larval rods migrated into the rudiment and could no longer be traced by polarized light (Fig. 4d). The adult skeletal spicules were very different from the larval skeleton. They had the multirayed shape typical of the early juvenile skeleton, and they occurred as plates rather than rods (Fig. 4e, f).

Discussion

The larva of *Ophionereis schayeri*, although non-feeding, appears to be in an intermediate stage of evolution, since it has features characteristic of both planktotrophic (ophiopluteal) and lecithotrophic development. Its ophiopluteal features include the vestigial larval skeleton, continuous ciliated band, and transiently complete larval gut. The nonpluteal features include a simple barrel-like shape and nonfunctional gut. The presence of vestigial larval structures in this lecithotrophic larva is evidence that the ancestral form had a feeding ophiopluteus. Ophiuroids with planktotrophic larvae typically have small (80–185 μm) eggs (Hendler, 1991; Sewell and Young, 1997). Acquisition of a larger egg in *O. schayeri* was probably a preadaptation for the evolution of non-feeding development, with subsequent loss of superfluous larval structures. This sequence of evolutionary changes is similar to the evolution of nonfeeding development in echinoids with large eggs, where loss of pluteal arms and acquisition of a simple larval shape also occurs (Olson *et al.*, 1993; Wray, 1996).

The ciliated band in *Ophionereis schayeri* larvae is a reduced expression of the continuous ciliated band typical of ophioplutei, similar to that seen in the brooded lecithotrophic larvae of *Ophionotus hexactis* (Mortensen, 1921). By contrast, its congener, *Ophionereis annulata,* has an early barrel-shaped larva that is uniformly ciliated, with no vestige of a ciliated band (Hendler, 1982). A continuous band is characteristic of feeding echinoderm larvae and is considered to reflect not only the functional requirements of feeding and swimming, but also selective pressures for a particular feeding clearance mechanism (Strathmann, 1974). Retention of a ciliated band by the non-feeding larvae of *O. schayeri* is similar to the reduction of the ciliated band in the non-feeding larvae of some echinoids (Olson *et al.*, 1993; Emlet, 1995). Like the larvae of *O. schayeri*, the brooded larvae of *O. hexactis* have a digestive tract consisting of a stomodeum, esophagus, and stomach.

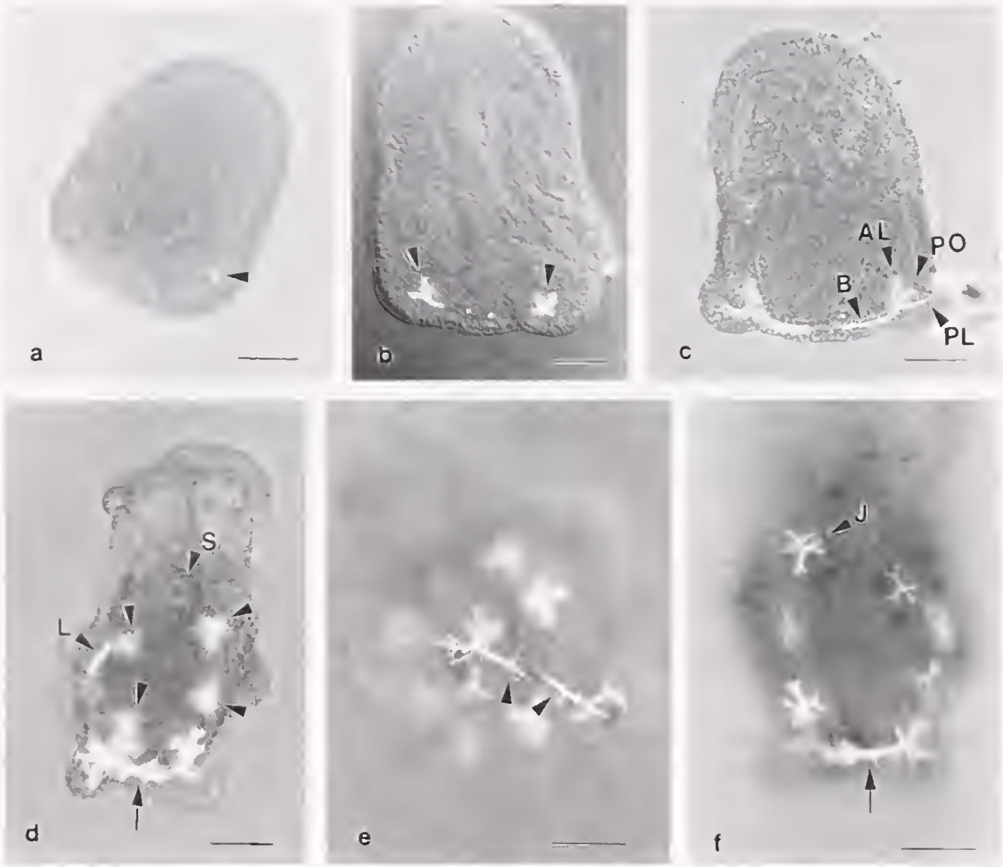

Figure 4. Cross-polarized light micrographs showing larval skeletogenesis in *Ophionereis schayeri.* (a) Gastrula with first appearance of a larval spicule (arrowhead); the other spicule is not in the plane of focus. (b) Early formation of the tetraradiate bilateral larval skeleton (arrowheads). (c) An early larva with tetraradiate skeleton consisting of anchoring posterior body rods and three arms rods—posterolaterals, anterolaterals, and postorals. (d) Rudiment formation and appearance of juvenile plates (4 unlabeled arrowheads). The two larval body rods meet midway at the posterior of the larva and seem to become continuous (arrow). The larval skeleton is thorny, starts to break up, and migrates into the rudiment. (e) Larva viewed from the posterior, showing bilateral thorny larval rods (arrowheads), with juvenile plates out of focus in the background. (f) Larva with larval skeleton still present and well-formed juvenile plates. A multirayed shape is typical of juvenile echinoderm plates. Anterolateral rods, AL; body rods, B; juvenile plates, J; larval skeleton, L; posterolateral rods, PL; postoral rods, PO; and stomodeal depression, S. Scale bars = 50 μm.

In contrast to *O. schayeri,* however, these larvae lack an anus (Mortensen, 1921). A transiently complete digestive tract, as seen in the larvae of *O. schayeri,* apparently has not been previously reported for other lecithotrophic echinoderm larvae.

The skeletal rods in *Ophionereis schayeri* larvae are considerably smaller than those of planktotrophic ophioplutei (Mortensen, 1921), and they do not support pluteal arms. Moreover, all four rods—body, posterolateral, anterolateral, and postoral—formed simultaneously, and developed their thorns simultaneously. This contrasts with typical ophioplutei, in which the body rod, posterolateral rod, and anterolateral rod develop prior to the postoral and posterodorsal rods (MacBride, 1907; Narasimhamurti, 1933; Olsen, 1942; Mladenov, 1985). In addition, the thorns on the rods of ophioplutei do not form at the same time (MacBride, 1907; Mortensen, 1921; Narasimhamurti, 1933; Olsen, 1942; Mladenov, 1985). Accelerated rod formation into a tetraradiate configuration shows that a heterochrony in skeletogenesis has occurred in the evolution of development in *O. schayeri.* A similar pattern of skeletogenesis is reported for the lecithotrophic larvae of *Amphiura chiajei* (Fenaux, 1963) and *Amphioplus abditus* (Hendler, 1978), and for the planktotrophic, 8-armed ophioplutei of *Amphipholis kochii,* which undergo rapid development (Yamashita, 1985). Accelerated skeletogenesis may be a mechanism to reduce the time to metamorphosis during the evolution of lecithotrophy. The skeleton is further reduced in the lecithotrophic larvae of *Ophiothrix oerstedi* and *Ophionereis annulata,* which form only three distinct skeletal rods (Mladenov, 1979; Hendler, 1982).

Posterodorsal arm rods, the last to be formed in typical ophioplutei, are not present in *Ophionereis schayeri* larvae, or in other ophiuroid larvae with a vestigial skeleton (Mortensen, 1921, 1933; Fell, 1945; Fenaux, 1963; Mladenov, 1979; Hendler, 1982). This suggests a potential sequence of morphogenetic change, with those functionally related larval structures (*e.g.*, pluteal arms, skeletal rods) that are formed late in planktotrophic development being the first to be lost in the evolution of lecithotrophic development. This kind of incremental loss, as depicted in Fell's (1945) diagrammatic series of ophiuroid larvae with a decreasing number of arms and shorter developmental times, is considered to be an important mechanism of evolutionary change (Anderson, 1987; Raff, 1996). The evolution of lecithotrophy in *O. schayeri* has involved reduction of several larval structures, including the skeletal rods, ciliated band, and gut, whose development is unlikely to be genetically linked. Reduction in these larval structures may have occurred independently in response to similar selective pressures.

The brooded larvae of *Ophionotus hexactis* are similar to the larvae of *Ophionereis schayeri* with respect to the form of the ciliated band, the presence of a partially developed digestive tract, and some skeletal rods (Mortensen, 1921). Similarly, the brooded larvae of *Amphipholis squamata* and *A. japonica* and the benthic embryos of *Amphioplus abditus* have a reduced larval skeleton (Murakami, 1940; Fell, 1946; Hendler, 1978). These findings show that phylogenetically diverse ophiuroids with a range of developmental modes have retained vestiges of an ancestral feeding state. Other species with lecithotrophic development, however, show no ophiopluteal features (Table 1). The evolution to lecithotrophy in ophiuroids has involved the reduction and loss of a suite of ophiopluteal structures, resulting in an increasingly simple larval form and accelerated development. Similarly, in echinoids, reducing the time to metamorphosis during the evolution of lecithotrophy involved complex developmental processes, resulting in a variety of morphological changes including loss of pluteal arms (Wray, 1996).

This study demonstrates that the internal events of development in what appear, externally, to be relatively simple lecithotrophic larvae warrant careful examination. Detection of the larval gut and skeleton in the larvae of *Ophionereis schayeri* provided important information on the extent of evolutionary change in development. A larval skeleton will be easily missed if it is dissolved by fixatives and storing buffers. Most important for ophiuroids, the discovery of larval rods in vitellariae demonstrated that this larval form evolved from an ophiopluteal ancestor (Mortensen, 1938; Hendler, 1982) and is not divergent, as previously thought (Fell, 1945). Similarly, the discovery of larval rods in the larvae of *Asthensoma ijimai* and *Heliocidaris erythrogramma* led to a reinterpretation of the extent of developmental change in these echinoids (Amemiya and Emlet, 1992; Emlet, 1995).

Within the genus *Ophionereis, O. schayeri* is the fifth species known to have lecithotrophic development (Table 1). Like *O. schayeri, O. squamulosa* and *O. annulata* have planktonic larvae (Mortensen, 1921; Hendler, 1982), whereas *O. vivipara* and *O. olivacea* have brooded larvae (Mortensen, 1933; Byrne, 1991). Only one species, *O. fasciata*, is known to have planktotrophic development (Selvakumaraswamy, unpubl. data), and thus most likely possesses the ancestral larval form for the genus. The relatively complete set of larval structures in the non-feeding larvae of *O. schayeri* (continuous ciliated band, tetraradiate skeleton, and transiently complete larval gut), indicates it may be the most recent member of the genus to have evolved lecithotrophy. Based on morphology, *O. annulata* might be expected to be next in this evolutionary progression, because it has retained only a triradiate skeleton. *O. squamulosa* would be expected next as it has a stomodeum and vestiges of the ciliated band. The extreme end of the morphological continuum would be illustrated by *O. olivacea* and *O. vivipara*, which completely lack larval structures. Non-feeding development thus appears to be common in this clade. A molecular approach is needed to determine whether the switch to lecithotrophy in *O. schayeri* was a single event or a multiple one as demonstrated for the sea star genus *Patiriella* (Hart *et al.*, 1997). The causes of selection for a particular mode of development in certain lineages are still relatively unknown, but they seem to be more prevalent in some echinoderm lineages than others (Pearse and Bosch, 1994; Byrne and Cerra, 1996).

Acknowledgments

This work was funded by an Australian Postgraduate Award. The authors thank Tony Romeo and Francis Chee for help with electron microscopy, Roland Smith and Clive Jeffery for help with photography, and all those who assisted in collection of specimens. The manuscript was greatly improved by comments from an anonymous reviewer.

Literature Cited

Amemiya, S., and R. B. Emlet. 1992. The development and larval form of an Echinothurioid echinoid, *Asthenosoma ijimai*, revisited. *Biol. Bull.* **182:** 15–30.

Anderson, D. T. 1987. Developmental pathways and evolutionary rates. Pp. 143–155 in *Rates of Evolution*, K. S. W. Campbell and M. F. Day, eds. Allen and Unwin, London.

Byrne, M. 1991. Reproduction, development and population biology of the Caribbean ophiuroid *Ophionereis olivacea*, a protandric hermaphrodite that broods its young. *Mar. Biol.* **111:** 387–399.

Byrne, M., and A. Cerra. 1996. Evolution of intragonadal development in the diminutive asterinid sea stars *Patiriella vivipara* and *P. parvivipara* with an overview of development in the Asterinidae. *Biol. Bull.* **191:** 17–26.

Emlet, R. B. 1995. Larval spicules, cilia and symmetry as remnants of indirect development in the direct developing sea urchin *Heliocidaris erythrogramma. Dev. Biol.* **167:** 405–415.

Fell, H. B. 1941. The direct development of a New Zealand ophiuroid. *Q. J. Microsc. Sci.* **82:** 377–441.

Fell, H. B. 1945. A revision of the current theory of echinoderm embryology. *Trans. R. Soc. NZ* **75:** 73–101.

Fell, H. B. 1946. The embryology of the viviparous ophiuroid *Amphipholis squamata* Delle Chiaje. *Trans. R. Soc. NZ* **75:** 419–464.

Fenaux, L. 1963. Note preliminaire sur le development larvaire de *Amphiura chiajei* (Forbes). *Vie Milieu* **14:** 91–96.

Fenaux, L. 1969. Le development larvaire chez *Opioderma longicauda* (Retzius). *Cah. Biol. Mar.* 59–62.

Grave, C. 1900. *Ophiura brevispina. Memoirs From the Biological Laboratory of the Johns Hopkins University* **4:** 83–100.

Hart, M. W., M. Byrne, and M. J. Smith. 1997. Molecular phylogenetic analysis of life-history evolution in asterinid starfish. *Evolution* **51:** 1848–1861.

Hendler, G. 1975. Adaptational significance of the patterns of ophiuroid development. *Am. Zool.* **15:** 691–715.

Hendler, G. 1978. Development of *Amphioplus abditus* (Verrill) (Echinodermata: Ophiuroidea). II Description and discussion of ophiuroid skeletal ontogeny and homologies. *Biol. Bull.* **154:** 79–95.

Hendler, G. 1982. An echinoderm vitellaria with a bilateral larval skeleton: evidence for the evolution of ophiuroid vitellariae from ophioplutei. *Biol. Bull.* **163:** 431–437.

Hendler, G. 1991. Echinodermata: Ophiuroidea. Pp. 356–479 in *Reproduction of Marine Invertebrates, Vol. VI Echinoderms and Lophophorates,* A. C. Giese, J. S. Pearse, and V. B. Pearse, eds. Boxwood Press, Pacific Grove, CA.

Komatsu, M., and T. Shosaku. 1993. Development of the brittle star *Ophioplocus japonicus* H. L. Clark. I. *Zool. Sci.* **10:** 295–306.

MacBride, E. W. 1907. The development of *Ophiothrix fragilis. Q. J. Microsc. Sci.* **51:** 557–606.

McEdward, L. R., and D. A. Janies. 1997. Relationships among development, ecology, and morphology in the evolution of echinoderm larvae and life cycles. *Biol. J. Linn. Soc.* **60:** 381–400.

McHugh, D., and G. W. Rouse. 1998. Life history evolution of marine invertebrates: new views from phylogenetic systematics. *Trends Ecol. Evol.* **13:** 182–186.

Mladenov, P. V. 1979. Unusual lecithotrophic development of the Caribbean brittle star *Ophiothrix oerstedi. Mar. Biol.* **55:** 55–62.

Mladenov, P. V. 1985. Development and metamorphosis of the brittle star *Ophiocoma pumila*: evolutionary and ecological implications. *Biol. Bull.* **168:** 285–295.

Moloney, P., and M. Byrne. 1994. Histology and ultrastructure of the ovary and oogenesis in the ophiuroid *Ophionereis schayeri.* Pp. 463–469 in *Echinoderms Through Time,* B. David, A. Guille, J. P. Feral, and M. Roux, eds. A. A. Balkema, Rotterdam.

Mortensen, T. H. 1921. *Studies of the Development and Larval Forms of Echinoderms.* G. E. C. Gad, Copenhagen.

Mortensen, T. H. 1933. Papers from Dr. Th. Mortensen's Pacific Expedition 1914–16. LXIII. Biological observations on ophiurids, with descriptions of two new genera and four new species. *Vidensk. Medd. Dan. Naturhist. Foren.* **93:** 171–194.

Mortensen, T. H. 1938. Contributions to the study of the development and larval forms of echinoderms IV. *K. Dan. Vidensk. Selsk. Skr. Naturvidenskabelige Og Mathematisk Afdeling.* **9. 7:** 1–59.

Murakami, S. 1940. On the development of the calcareous plates of an Ophiuran, *Amphioplus japonica* Matsumoto. *Jap. J. Zool.* **9:** 19–33.

Narasimhamurti, N. 1933. The development of *Ophiocoma nigra. Q. J. Microsc. Sci.* **76:** 63–88.

Olsen, H. 1942. Development of the brittle-star *Ophiopholis aculeata* (O. Fr. Muller) with a short note on the outer hyaline layer. *Bergens Museums Årbog. Naturvideskabelig række.* **6:** 1–107.

Olson, R. R., J. L. Cameron, and C. M. Young. 1993. Larval development (with observations on spawning) of the pencil urchin *Phyllacanthus imperialis*: a new intermediate larval form? *Biol. Bull.* **185:** 77–85.

Pearse, J. S., and I. Bosch. 1994. Brooding in the Antarctic: Ostergren had it nearly right. Pp. 111–120 in *Echinoderms Through Time,* B. David, A. Guille, J. P. Feral, and M. Roux, eds. A. A. Balkema, Rotterdam.

Raff, R. A. 1996. *The Shape of Life: Genes, Development, and the Evolution of Animal Form.* University of Chicago Press, Chicago.

Selvakumaraswamy, P., and M. Byrne. 1995. Reproductive cycle of two populations of *Ophionereis schayeri* (Ophiuroidea) in New South Wales. *Mar. Biol.* **124:** 85–97.

Selvakumaraswamy, P., and M. Byrne. 1998. A vitellaria with a reduced ophiopluteal skeleton. Pp. 420 in *Echinoderms: San Francisco,* R. Mooi and M. Telford, eds. A. A. Balkema, Rotterdam.

Selvakumaraswamy, P., and M. Byrne. 1999. Early events of coelomogenesis in a lecithotrophic ophiuroid larva. Pp. 227–228 in *Echinoderm Research 1998,* M. D. Carnevali and F. Bonasoro, eds. A. A. Balkema, Rotterdam.

Sewell, M. A., and C. M. Young. 1997. Are echinoderm egg size distributions bimodal? *Biol. Bull.* **193:** 297–305.

Stancyk, S. E. 1973. Development of *Ophiolepis elegans* (Echinodermata: Ophiuroidea) and its implications in the estuarine environment. *Mar. Biol.* **21:** 7–12.

Strathmann, R. R. 1974. Introduction to function and adaptation in echinoderm larvae. *Thalassia Jugosl.* **10:** 321–339.

Vance, R. R. 1973. On reproductive strategies in marine benthic invertebrates. *Am. Nat.* **107:** 339–352.

Wray, G. A. 1995. Evolution of larvae and developmental modes. Pp. 413–447 in *Ecology of Marine Invertebrate Larvae,* L. McEdward, ed. CRC Press, New York.

Wray, G. A. 1996. Parallel evolution of nonfeeding larvae in echinoids. *Syst. Biol.* **45:** 308–322.

Yamashita, M. 1985. Embryonic development of the brittle-star *Amphipholis kochii* in laboratory culture. *Biol. Bull.* **169:** 131–142.

Reference: *Biol. Bull.* **198:** 387–395. (June 2000)

Larval Development of the Tropical Deep-Sea Echinoid *Aspidodiadema jacobyi*: Phylogenetic Implications

CRAIG M. YOUNG* AND SOPHIE B. GEORGE†

Division of Marine Science, Harbor Branch Oceanographic Institution,
5600 U.S. Hwy. 1 N., Ft. Pierce, Florida 34946

Abstract. The complete larval development of an echinoid in the family Aspidodiadematidae is described for the first time from *in vitro* cultures of *Aspidodiadema jacobyi*, a bathyal species from the Bahamian Slope. Over a period of 5 months, embryos grew from small (98-μm) eggs to very large (3071-μm) and complex planktotrophic echinopluteus larvae. The fully developed larva has five pairs of red-pigmented arms (preoral, anterolateral, postoral, posterodorsal, and posterolateral); fenestrated triangular plates at the bases of fenestrated postoral and posterodorsal arms; a complex dorsal arch; posterodorsal vibratile lobes; a ring of cilia around the region of the preoral and anterolateral arms; and a long, unpaired posterior process containing a fenestrated rod. The presence of a posterior process and posterodorsal arms makes the larva of *Aspidodiadema jacobyi* much more similar to larvae of irregular urchins in the order Spatangoidea than to other families of the order Diadematoida, to which the family is normally assigned. This unexpected larval form lends support to a recommendation that the Aspidodiadematidae should be either elevated to ordinal status as a sister group of the order Diadematoida, or split off as a sister group of the other families within the order. In either case, if we accept the parsimonious hypothesis that the aboral process and posterodorsal arms were derived only once in the evolutionary history of euechinoids, then the larval data suggest that the Aspidodiadematidae may be very near the node where the irregular and regular euechinoids first diverged.

Introduction

Larval developmental mode has been inferred from egg size for a large number of echinoderm species from the deep sea, but only a few of these have been cultured into the early larval stages (Prouho, 1888; Mortensen, 1921; Young and Cameron, 1989; Young *et al.*, 1989), and no complete ontogenetic sequence of larval development has been published for any deep-sea invertebrate. One of the species whose early stages have been described (Young *et al.*, 1989) is *Aspidodiadema jacobyi*, a small-bodied sea urchin with long flexible spines that lives at bathyal depths in the tropical eastern Atlantic (Fig. 1). The early development of *A. jacobyi* is unusual in that its small eggs (94–100 μm) contain sufficient yolk reserves to support a prefeeding developmental period that extends well into the larval stage (Young *et al.*, 1989), a feature that might permit larvae to move long distances, either vertically or horizontally, before feeding becomes necessary. In this paper, we describe the complete larval development of *A. jacobyi*, document unexpected morphological traits in the late-stage larvae, and discuss how these unexpected traits could help justify a realignment of the currently accepted ordinal-level taxonomy of the Euechinoidea.

The echinoid family Aspidodiadematidae contains only two genera, *Aspidodiadema* and *Plesiodiadema*, all species of which are found at bathyal and abyssal depths (Hyman, 1955), many on island slopes in tropical seas. On the basis of adult characters, notably aulodont teeth and hollow spines, Mortensen (1927) placed the family in the order Diadematoida, suborder Aulodonta, in the company of the Echinothuriidae, the Pedinidae, and the Diadematidae. Recent authors (*e.g.*, Smith, 1984) have elevated the echinothuriids and pedinids to ordinal level, placing three fam-

---

Received 8 December 1999; accepted 1 February 2000.

* Author for correspondence. E-mail: youngc@hboi.edu

† Present address: Biology Department, Georgia Southern University, Statesboro, GA 30460.

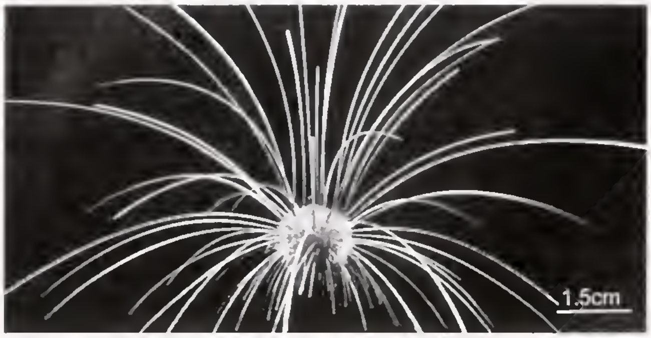

Figure 1. Adult *Aspidodiadema jacobyi* from the Bahamian Slope, showing long flexible spines. (Photo by L. F. Braithwaite).

ilies in the order Diadematoida: the Aspidodiadematidae, the Diadematidae, and the Lissodiadematidae. Larvae of the Lissodiadematidae remain unknown (Emlet, 1988a; Pearse and Cameron, 1991). Emlet (1988a) has argued on the basis of larval form that the Micropygidae, which have also been raised to ordinal status by Jensen (1981), should also be included as a family in the Diadematoida. Although it seems clear that the aspidodiadematids are closely related to the diadematoids, the relationships among orders and families near the base of the euechinoid tree remain obscure. This portion of the tree remains inadequately resolved because a thorough cladistic analysis of extant species has not been undertaken (R. Mooi, California Academy of Sciences, San Francisco, pers. comm.), and also because fossil material from the relevant time periods contains too few meaningful characters for construction of a robust tree (A. B. Smith, The Natural History Museum, London, pers. comm.). Fossil aspidodiadematids closely resembling modern urchins in the genus *Plesiodiadema* have been described from the upper Jurassic clays of England and France (Smith, 1995), indicating that the family differentiated more than 200 million years ago.

By analyzing the crystalline axes of echinoid apical plates (Raup, 1965), Emlet (1985, 1988a) was able to infer certain details of larval form for a number of rare species with unknown larvae. On the basis of this indirect evidence, he predicted that all members of the genera *Aspidodiadema* and *Plesiodiadema* should have larvae with both preoral and posterodorsal arms (Emlet, 1988a). This prediction is in stark contrast to the 2-arm larvae with widely spread arms (the "*Echinopluteus transversus*" of Mortensen, 1921) found in all members of the closely related families Diadematidae and Micropygidae. By assuming that the 2-arm larval form with widely spread arms is synapomorphic, Emlet (1988a) argues parsimoniously that the Aspidodiademidae must be a sister group to the Diadematoida, having branched off the major clade of regular euechinoids earlier than the diadematids or micropygids. Indeed, he recommends that the Aspidodiadematidae should be removed from the Diadematoids and elevated to the rank of order. In the present paper, we confirm Emlet's prediction concerning the presence of posterodorsal arms in the Aspidodiadematidae and document other larval characters supporting the idea that this family of urchins may have originated near the node where the regular and irregular urchins diverged.

Materials and Methods

Adult *Aspidodiadema jacobyi* were collected by suction using Johnson-Sea-Link submersibles between depths of 500 and 750 m at various sites in the Northern Bahamas (Young, 1992). They were transported to the surface in closed acrylic containers of seawater and transferred to 14°C incubators within minutes of arriving at the surface. Although we collected this species during the spring months of every year from 1985 through 1999, we were able to induce spawning only twice, once in 1987 (Young *et al.*, 1989) and once on 11 April 1994. Spawning was induced by intracoelomic injection of 0.55 *M* KCl. In the 1994 spawning, we injected 28 individuals; of these, 13 males and 2 females released gametes. Cultures were established by mixing the eggs of a single female with active sperm from 6 males in a small bowl of seawater. The other female was not used because she released very few oocytes, many of which appeared irregular. Zygotes were split among five 1-l jars of 0.45-μm filtered seawater, at an initial density of 800 embryos per liter. After larvae had developed complete guts, they were fed with a mixture of the algae *Isochrysis galbana, Thalassiosira weissflogii,* and *Dunaliella tertiolecta.* At the outset, we used an algal concentration of 1000–2000 cells/ml, but this was increased gradually as the larvae grew, up to a maximum of 5000 cells/ml, 49 days after fertilization and thereafter. These algal concentrations were chosen because similar concentrations promote optimal larval growth in some shallow-water echinoderm larvae (Fenaux *et al.*, 1985; George, 1990; George *et al.*, 1990). Larvae were reared in dark incubators except during water changes, when they were exposed briefly to the fluorescent overhead lights. To simulate temperature changes that bathyal larvae would encounter if they undertook ontogenetic vertical migration (Young *et al.*, 1996a), we increased the culture temperature from 14°C to 16°C 14 days after fertilization, reduced it to 14°C 66 days after fertilization, then finally to 13°C (the temperature near the bottom of the adult depth range) 77 days after fertilization. Initially, seawater was changed and the larvae were fed every 2 days. This interval was increased to 4 days beginning 28 days after fertilization.

Each time water was changed, we examined the larvae for the appearance of any new arms or other structures and measured the lengths of the postoral, somatic, posterodorsal, and posterolateral rods. Because there were 2-day or 4-day intervals between observations, the times for reported morphological changes (Table 1) should be regarded as only

Table 1

Developmental timetable for Aspidodiadema jacobyi, *showing the presence (x) and absence (—) of larval arms and other important structures on days when cultures were examined*

	Larval arms					Other structures					
Days after fertilization	Postoral	Anterolateral	Posterodorsal	Preoral	Posterolateral	Mouth	Posterior process	Ciliated ring	Posterodorsal lobes	Echinus rudiment	Podia
6	x	—	—	—	—	—	—	—	—	—	—
9	x	x	—	—	—	—	—	—	—	—	—
11	x	x	—	—	—	x	—	—	—	—	—
15	x	x	—	—	—	x	—	—	—	—	—
25	x	x	x	—	—	x	—	—	—	—	—
28	x	x	x	—	—	x	—	—	—	—	—
32	x	x	x	—	—	x	x	—	—	—	—
34	x	x	x	x	—	x	x	—	—	—	—
35	x	x	x	x	—	x	x	—	—	—	—
39	x	x	x	x	—	x	x	—	—	—	—
42	x	x	x	x	x	x	x	—	—	—	—
46	x	x	x	x	x	x	x	—	—	—	—
49	—	—	x	x	x	x	x	x	—	—	—
53	—	—	x	x	x	x	x	x	—	—	—
56	—	—	x	x	x	x	x	x	x	—	—
62	—	—	x	x	x	x	x	x	x	—	—
75	—	—	x	x	x	x	x	x	x	x	—
116	—	—	x	x	x	x	x	x	x	x	x
120	—	—	x	x	x	x	x	x	x	x	x

Larvae were reared at 14–16°C (see text for details). Because cultures were not examined every day, the times do not accurately represent the first occurrences of larval stages.

approximate markers for the initiation of larval stages. During the early larval stages, total larval length was defined as the linear measurement from the tip of the postoral rod to the point where the two somatic rods meet mid-sagittally on the posterior end of the larva. In the later stages, total larval length was defined as the linear measurement from the tip of the postoral rod to the posterior end of the unpaired aboral process. During the early stages, we generally made all measurements on at least 10 larvae. After the 46th day, when relatively few larvae remained in the cultures, we were concerned about stressing the remaining larvae, so we measured only the most advanced larva at each sampling period. Terminology used for larval arms and spicules is from Mortensen (1921).

Results

Larval growth and form

The early developmental stages of *Aspidodiadema jacobyi* have been described by Young *et al.* (1989), so the present study characterizes only the echinopluteus larval stages. The developmental timetable is summarized in Table 1 and linear growth is plotted in Figure 2. Mortality, size, and stage variability increased over time, but living larvae from all cultures generally appeared healthy, regardless of stage. Decreasing the temperature from 16°C to 13°C

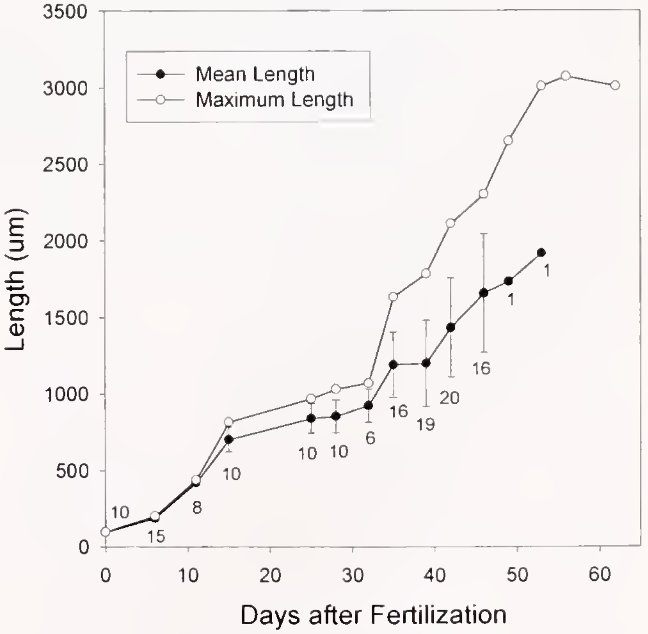

Figure 2. Mean and maximum observed body lengths of *Aspidodiadema jacobyi* larvae during the first 63 days after fertilization. Error bars are standard deviations. Sample size is reported directly below each mean value.

after the 77th day appeared to have a positive effect on larval development: larvae transferred to the lower temperature continued to increase in length and width, whereas larvae that remained at the higher temperature increased in length only. Throughout development, larvae swam with their anterior ends upwards, remaining near the surface during the early larval stages (2- to 6-arm stages) and near the bottom during later larval stages (8- and 10-arm stages).

The 2-arm stage began 6 days after fertilization with the appearance of postoral arms (Fig. 3A). Fenestrated arm rods were visible by cross-polarized light, but opacity of the gut region obscured skeletal details in the posterior end, as previously reported by Young *et al.* (1989). The postoral arms were widely spread, and red pigment spots were scattered throughout the larval arms. Nine days after fertilization, the anterolateral arms appeared, forming the 4-arm echinopluteus. The gut region became progressively less opaque during this period, and the digestive system could be clearly seen (Fig. 3B). Eleven days after fertilization, larvae had grown to more than twice the original length of the early embryos (Fig. 2). At this stage, the anterolateral arms were very small, but the mouth opened and the larvae began to feed. Fifteen days after fertilization, 4-arm larvae with well-developed postoral and anterolateral arms (Fig. 3C) were present in all cultures, and by the 25th day, these larvae were more than 700 μm in length (Fig. 2).

The posterodorsal arms characteristic of the 6-arm stage appeared 25 days after fertilization (Table 1, Fig. 3D) and were fully developed (Fig. 3E) by the 28th day. Some larvae remained in the 6-arm stage for up to 15 days, but small buds of preoral arms were apparent in some individuals as early as the 34th day (Fig. 3E). Red pigment spots initially present throughout the larval arms became increasingly concentrated at the tips after this stage. A gradual change in larval shape became apparent after the 28th day, and 4 days later an unpaired process supported by a fenestrated rod appeared at the posterior end of the larva (Fig. 3F). This posterior process continued to grow throughout the 6-arm stage and subsequent stages until it was as long as the rest of the larval body. At 16°C, the larvae remained in the 6-arm stage for about 10 days (Table 1).

By the 39th day, there was considerable variability among cultures in the relative proportions of individuals in different larval stages. Some culture jars contained only 6-arm larvae with posterior processes, whereas up to 60% of larvae in other cultures had attained an 8-arm stage. During the 8-arm stage and early 10-arm stage (Fig. 3G), the posterodorsal arms and the posterior process were similar in length, about one-third less than the length of the postoral arms. The base of the postoral arms broadened considerably at this stage and measured 122.4 μm in width.

Between the 39th and 42nd day, the buds of the posterolateral arms formed, thereby initiating the 10-arm stage (Fig. 3G). By the 42nd day these arms were fully developed in some individuals (Fig. 3H, I). Forty-six days after fertilization, however, as many as 80% of the larvae were still at the 8-arm stage. During the 10-arm stage, the posterodorsal and posterolateral arms continued to lengthen and widen, while the anterolateral and preoral arms were generally resorbed (Figs. 3H, I, 4A, D).

Forty-nine days after fertilization, two small ciliated lobes appeared in the basal region of the posterodorsal arms (Fig. 4A). By 53 days, these vibratile lobes had become very prominent, and it was apparent that they were not supported by skeletal elements (Fig. 4B). At 53 days, more than 50% of the larvae in all cultures were at the 10-arm stage, having posterolateral arms, posterodorsal vibratile lobes, and a posterior process. No additional arms developed after the 10-arm stage, though larvae continued to increase in size until the largest larva had attained a maximum length of 3071 μm 56 days after fertilization.

During the 10-arm stage, a ciliated ridge began to develop near each posterodorsal lobe. These two ridges ran in an anterior-posterior direction, parallel to the anterolateral rods on opposite sides of the larvae (Fig. 3H) and eventually joined to form a distinctive loop surrounding the region of the resorbing preoral and anterolateral arms (Fig. 4C). By the 75th day, the ciliated ridges were thick and heavily pigmented along their entire length (Fig. 4C) and were reflexed at the anterior end to form a loop that surrounded the region where the anterolateral and postoral arms had been (Fig. 4C). Also at this time, large brownish orange oil droplets were observed near the bases of the postoral, posterodorsal, and posterolateral arms.

Sixty-two days after fertilization, the posterior process of the largest larva attained its maximum length of 1224 μm; the posterolateral arm was now 459 μm in length. The posterodorsal lobes continued to elongate until they attained a maximum size of 237.5 μm, 127 days after fertilization. Larvae began to decrease in overall length after the 75th day, but the postoral arms began to widen near the bases, until on the 134th day they had attained a maximum basal diameter of 384 μm (Fig. 4D).

A few larvae survived in culture for up to 151 days, though none metamorphosed. An echinus rudiment appeared in a single larva before the 77th day. This larva was isolated and exposed to deep-sea sediments in an unsuccessful attempt to induce metamorphosis. Many more individuals developed echinus rudiments between the 77th and 134th days. In most animals, anatomical details of the rudiment were difficult to visualize because the rudiment was opaque and was partially obscured by an equally opaque gut region (Fig. 4D, E). Nevertheless, podia were observed in the rudiments of some animals beginning on the 116th day, and adult spines were observed between 120 and 127 days after fertilization. As in many other species (Mortensen, 1921), the arms of late-stage larvae became smaller as the rudiment grew.

Larval skeleton

The postoral, posterodorsal, and posterior rods were all fenestrated and thorny (Fig. 4F), whereas the anterolateral rods (Fig. 4F) and posterolateral rods (Figs. 3I, 4D) were simple, not fenestrated. The distal portions of the anterolateral and preoral rods were thorny and the proximal portions

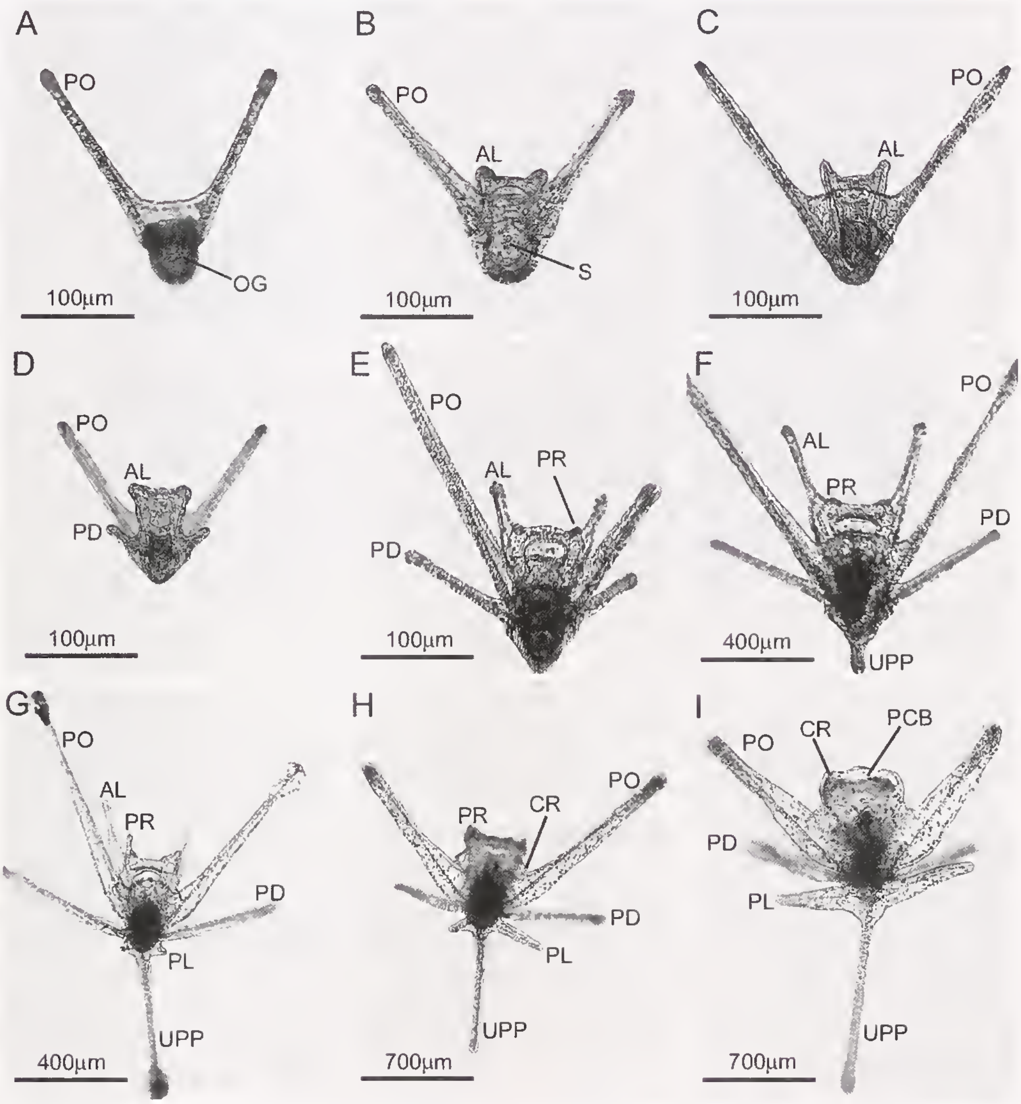

Figure 3. (A) Two-arm echinopluteus larva of *Aspidodiadema jacobyi* at 6 days, prior to the opening of the mouth, showing well-developed postoral arms (PO) and opaque gut region (OG). (B) Eleven-day-old larva in the early four-arm stage, viewed dorsally with newly formed anterolateral arms (AL). The stomach region (S) is becoming more visible. (C) Ventral view of a 15-day, 4-arm pluteus larva. Note that the anterolateral arms (AL) are supported by simple, unfenestrated rods. (D) Early 6-arm echinopluteus, 25 days old, viewed from the dorsal side with small posterodorsal arms (PD) developing. (E) Intermediate 6-arm echinopluteus stage viewed ventrally 28 days after fertilization, with well-developed posterodorsal arms (PD) and presumptive buds where the preoral arms (PR) will eventually develop. (F) Advanced 6-arm echinopluteus (ventral view), 32 days old, shortly after the first appearance of the unpaired posterior process (UPP). Preoral arms (PR) are still present only as tiny buds. (G) Ventral view of 39-day, early 10-arm larva showing well-developed unpaired posterior process (UPP) and preoral arms (PR). Posterolateral arms (PL) are just beginning to grow in this individual, but many in the same cultures were still at a late 8-arm stage. (H) Forty-two-day-old, 10-arm echinopluteus viewed ventrally just after the appearance of lateral ciliary ridges (CR). Posterolateral arms (PL) are growing asymmetrically and anterolateral arms have been resorbed. (I) Ten-arm larval stage (42 days old) after preoral and anterolateral arms have been resorbed. The posterior ciliary band (PCB) is visible as a dark region partially obscured by the transparent preoral lobe.

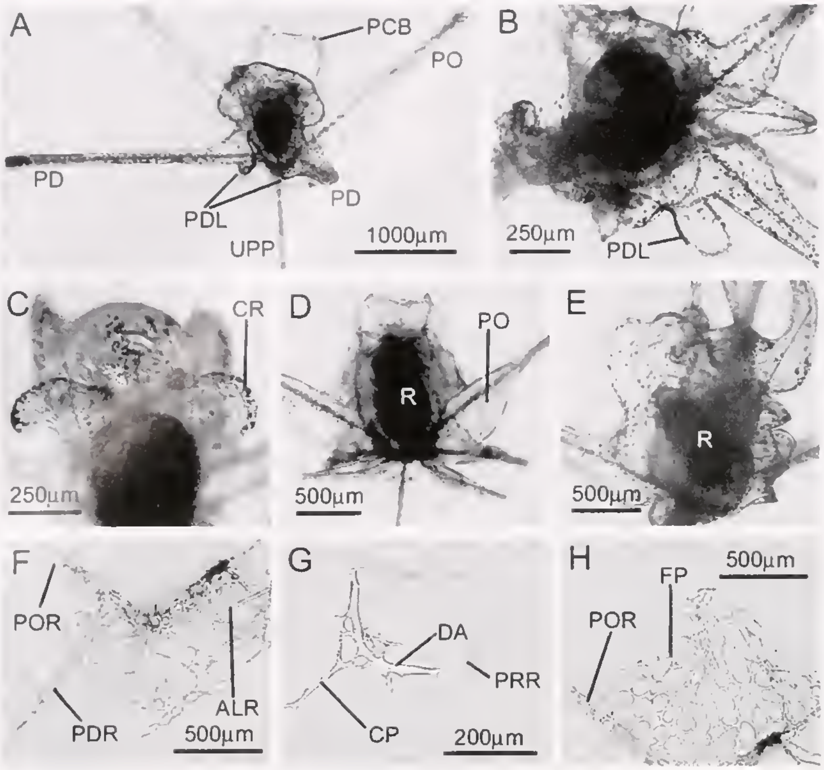

Figure 4. (A) Forty-nine-day-old echinopluteus larva of *Aspidodiadema jacobyi* in dorsal view. The posterodorsal lobes (PDL) have just appeared, and the posterior ciliary band is visible. PCB, posterior ciliary band; PO, postoral arm; PD, posterodorsal arm; UPP, unpaired posterior process. (B) Posterior view of a 53-day-old larva showing one of the large posterodorsal lobes (PDL). (C) Mid-anterior region of a 75-day-old echinopluteus, showing the lateral ciliated ridges (CR) now expanded into a large loop of cilia that surrounds the entire region of the resorbed pre-oral and anterolateral arms. (D) Ventral view of a 134-day-old larva with echinus rudiment (R) and very broad bases of the postoral arms (PO). (E) Echinopluteus larva 134 days old, showing echinus rudiment (R). (F) Posterior region of a late echinopluteus larva digested with sodium hypochlorite to reveal skeletal structures. Note that the postoral rods (POR) and posterodorsal rods (PDR) are fenestrated and tightly coupled with a basket-like sterom near their bases. The anterolateral rod (ALR) is simple. (G) Dorsal arch (DA) of an echinopluteus with preoral rods (PRR) originating on the two ends and a large central process (CP) in the middle. The central process is simple at the proximal end and fenestrated distally (barely visible at the far left-hand side of the micrograph). (H) Bases of the two postoral rods with their fenestrated plates of stereom (FP) fused together to create part of the posterior basket.

were smooth (Fig. 4G). The posterolateral rods were branched and extremely thorny. The dorsal arch was complex and slightly asymmetrical, having two large holes and one much smaller hole in the central region of the arch (Fig. 4G). A long central process, half of which was thorny and solid and the other half of which was thorny and fenestrated, projected from the base of the dorsal arch (Fig. 4G). Between the 42nd and 49th day after fertilization, the base of each postoral rod expanded into a dense network of stereom that eventually took the form of a highly fenestrated triangular plate (Fig. 4F). This plate fused with the corresponding plate at the base of the other postoral rod (Fig. 4F) to form a basket-like structure that filled the broad bases of the postoral arms (Fig. 4H, D). A slightly smaller fenestrated plate developed at the base of each posterodorsal rod (Fig. 4F). Together, the fenestrated plates originating from the postoral rods and the posterodorsal rods formed a truncated pyramidal structure. The posterolateral rod and the fenestrated thorny rod (Fig. 3H) of the posterior process developed from the posterior transverse rod, which was situated dorsally.

Discussion

Early stages of embryology and larval development have been reported for a number of bathyal and abyssal invertebrates (Prouho, 1888; Mortensen, 1921; Young and Cameron, 1989; Young and Tyler, 1993; Young *et al.*, 1996b, c), but the complete larval development has been described for only a single eurybathic echinoid, *Cidaris cidaris* (Prouho, 1888). Thus, the present work is not only the first complete description of larval development in the family Aspidodiadematidae, but also the only complete developmental sequence known for any exclusively deep-sea invertebrate.

For the first time, we also have a direct estimate of the length of the pelagic larval period for a deep-sea animal. On the basis of these laboratory rearings, we may conclude that, given adequate food, larvae are capable of dispersing for at least 5 months. In the Tongue of the Ocean, Bahamas, we have measured current speeds as high as 18 cm/s at the depths where *Aspidodiadema jacobyi* lives (Young *et al.*, 1993). The current speed in this region averages about 5 cm/s and flows mostly in a single direction (Young *et al.*, 1993). Using these flow values for a rough eulerian calculation of dispersal distance, a larva could drift about 4.3 km per day, or 645 km in 5 months. The real dispersal distance, of course, will be influenced by the local current regimes, topographical features, and settlement opportunities that the larva encounters during the course of its drift.

Young *et al.* (1996a) showed that larvae of *A. jacobyi* cannot tolerate the high temperatures found in the upper 200 m of the water column, suggesting that dispersal occurs below the permanent thermocline and that larvae must feed on items sinking out of the euphotic zone. In an earlier study (Young *et al.*, 1989), it was noted that the larvae of *A. jacobyi* have an unusually long prefeeding period, and that they can survive on maternal reserves for up to 2 months. It was hypothesized that this attribute may confer nutritional flexibility on these larvae, enabling them to disperse and survive in deep oligotrophic waters where food items are scarce and patchy (Young *et al.*, 1989). In the present study, we detected no additional morphological attributes that can be interpreted as special adaptations for deep-sea dispersal. Complex ciliation and long arms presumably keep these large larvae suspended in the water column, but similar complexity is found in late-stage larvae of many shallow-water echinoids (Mortensen, 1921; Emlet, 1988b; Pearse and Cameron, 1991). The large posterior process on the larva of *A. jacobyi* lowers the center of mass, presumably facilitating upright orientation (Pennington and Strathmann, 1990; Young, 1995), but this is a feature also found in shallow-water spatangoid larvae (Mortensen, 1921).

The developmental rate of *A. jacobyi* to the 2-arm stage (6 days) was similar to that reported by Young *et al.* (1989), but after the 2-arm stage, differences were observed between the two studies. The mouth opened 11 days after fertilization in the present study and between 18 and 21 days after fertilization in the study by Young *et al.* (1989). Fully developed 4-arm *A. jacobyi* larvae were observed in cultures 15 days after fertilization in the present study, but not until 24 days after fertilization by Young *et al.* (1989). Diet could explain differences in development after the onset of feeding, but not differences in the rate at which the mouth developed. The differences between these two studies could be attributed to genetics, egg quality (Emlet *et al.*, 1987; George *et al.*, 1990; George, 1996) or culture conditions.

Culture conditions might also explain why the preoral and anterolateral arms (and occasionally other arms: Fig. 4A) were resorbed in most individuals shortly after the onset of the 10-arm larval stage. On the other hand, many of these larvae survived for an additional 2 months or more and some developed rudiments, suggesting that they were not unhealthy. Resorption of some arms as others develop appears to be normal in certain species of echinoids (Mortensen, 1921; Pearse and Cameron, 1991).

Mortensen (1921, 1931) described the morphology of echinoderm larvae in minute detail with the expectation that larval characters would be keys to the unraveling of phylogenetic relationships within the phylum. Since that time, larval characters have been widely used for interpreting life-history evolution (reviewed by Havenhand, 1995; Wray, 1995), and for resolving phylogenetic issues at higher taxonomic levels (*e.g.*, Hadzi, 1963; Strathmann, 1988; Nielsen, 1995). However, recent analyses that combine genetic data with adult and larval character sets have shown that larval characters often evolved independently of adult body form (Smith and Littlewood, 1997) and that larval characters are more prone to homoplasy than adult characters (Smith *et al.*, 1995, 1996). Wray (1992) pointed out many similarities among larvae from groups as unrelated as ophiuroids and diadematoids, and as spatangoids and phymostomatoids. These commonalities are problematic for interpreting phylogeny; indeed, both Strathmann (1988) and Raff *et al.* (1988) have recognized that any phylogeny based on larval characters must accept a number of remarkable convergences. Despite the problems of interpreting larval characters from a phylogenetic standpoint, parsimony demands that we be very careful before concluding that an attribute has evolved independently in multiple clades.

The order Diadematoida is currently composed of three families: Diadematidae, Lissodiadematidae, and Aspidodiadematidae (Smith, 1984). The fully developed larva of *A. jacobyi* differs significantly from the known diadematid larvae in its extraordinary complexity. Whereas larvae of *A. jacobyi* have five pairs of larval arms and a posterior process, larvae in the family Diadematidae have only one pair of larval arms (the postorals) and no posterior process (Mortensen, 1921, 1931). Although the family Aspidodiadematidae is found exclusively in deep water and the other two families are restricted to shallow waters, the known larvae of diadematoids do share a number of common features. Like *Aspidodiadema*, all known larvae in the Family Diadematidae (*e.g.*, *Diadema antillarum*, *Astropyga pulvinata*, and *Diadema setosum;* Mortensen, 1921, 1931) have very long, thorny, and fenestrated postoral rods; a body skeleton in the shape of a 4-sided truncated pryramid; and a posterior transverse rod, which in some species takes the form of a fenestrated triangular plate during advanced stages. Most significantly, Mortensen (1921) reported that the larva of "*Echinopluteus transversus*" e and f (later shown to be *Diadema setosum*) has a very short, fenestrated, and unpaired ossicle immediately below the posterior transverse rod. He expressed the opinion (Mortensen, 1921, page 90) that although this structure bears a superficial resemblance to the posterior process of spatangoid larvae, the structures are not homologous. Whereas the spatangoid posterior process is an outgrowth of the posterior transverse rod, that of the diadematid larva is not connected to the rest of the skeleton.

Larvae of *Aspidodiadema jacobyi* have several features in common with larvae of the phymostomatoids *Arbacia lixula* (Fenaux, 1969) and *A. punctulata* (Garman and Colton, 1883). Like *A. jacobyi*, these species possess very long postoral and posterodorsal arms, swept-back posterolateral arms, a pair of vibratile lobes, and fenestrated triangles of stereom that form at the base of the postoral and posterodorsal rods before metamorphosis. The *Arbacia* species, like *A. jacobyi*, also develop parallel ciliated ridges that originate in the region of the posterodorsal arms and run parallel to the anterolateral rods along the midsection of the larva (Fenaux, 1969). However, these ridges terminate with the formation of the sixth pair of larval arms (anterodorsal arms) in the phymostomatoids, not with a ciliary ring around the base of the preoral and anterolateral arm region as in *A. jacobyi*.

Because of its posterolateral arms and unpaired posterior process, larvae of *A. jacobyi* bear a striking resemblance to the characteristic larval form of irregular urchins in the order Spatangoida (Mortensen, 1921; Rees, 1953). The fenestrated basket structure of *Aspidodiadema* larvae is also very similar to the basket that characterizes the Clypeasteroids, another major clade of irregular urchins (Pearse and Cameron, 1991). Larvae with posterior processes have been hitherto unknown outside the spatangoids, and all authors to date have considered this character to be absolutely diagnostic of this order (Mortensen, 1921; Pearse and Cameron, 1991). Other features shared by these two groups include long postoral and posterodorsal arms and well-developed anterolateral arms. However, spatangoid larvae have six pairs of arms, whereas Aspidodiadema larvae have only five. The loss of arms is easy to explain in the evolution of larval forms, but the independent acquisition of a structure as distinctive as a fenestrated, unpaired posterior process in two different clades seems improbable.

Emlet (1988a) used crystal orientations in the apical plates to predict that all larvae in the family Aspidodiadematidae should have at least two pairs of larval arms (postoral and posterodorsal arms) and less widely spread larval arms than the Diadematidae and Lissodiadematidae, both of which should have only widely spread postoral arms. On the basis of this prediction, Emlet (1988a) suggested that the family Aspidodiadematidae must be a sister group to the families Diadematidae, Lissodiadematidae, and Micropygidae, all of which have only a single pair of larval arms (Fig. 5). Our findings lend strong support to Emlet's recommendation. The larval form of *Aspidodiadema* is interpreted parsimoniously only if the Aspidodiadematidae are classified as a separate order outside the Diadematoida or as a sister group to the other families within the order. Indeed, the remarkable similarities between *A. jacobyi* larvae and those of the spatangoids and clypeasteroids suggest that the Aspidodiadematidae may be near the stem group that separated regular and irregular euechinoids.

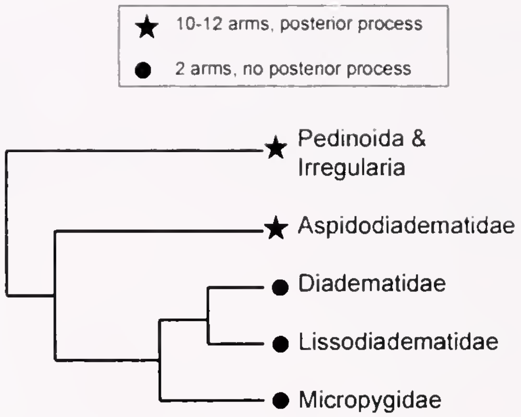

Figure 5. Phylogenetic tree suggested by and redrawn from Emlet (1988a). This tree organizes the Diadematida and related euechinoids in such a way as to preserve the important relationships of adult characters (Jensen, 1981) while requiring that the 2-arm echinopluteus evolve only once. The larval form of *Aspidodiadema* fits perfectly into this scheme, with no revisions required to satisfy the demands of parsimony.

Acknowledgments

We thank Mary Clark, who supplied us with algae; Paul Tyler, who assisted at sea and helped spawn the urchins; and Tracy Griffin, who assisted in the preparation of figures. Andrew Smith and Richard Mooi advised us in matters of phylogeny, though the opinions we express herein are entirely ours. This work was funded by the National Science Foundation (OCE-9116560 and OCE-9633784) and by a Harbor Branch postdoctoral fellowship to Sophie George. HBOI contribution number 1339.

Literature Cited

Emlet, R. B. 1985. Crystal axes in recent and fossil adult echinoids indicate trophic mode in larval development. *Science* **230:** 937–940.

Emlet, R. B. 1988a. Crystallographic axes of echinoid genital plates reflect larval form: some phylogenetic implications. Pp. 299–310 in *Echinoderm Phylogeny and Evolutionary Biology*, C. R. C. Paul and A. B. Smith, eds. Clarendon Press, Oxford.

Emlet, R. B. 1988b. Larval form and metamorphosis of a "primitive" sea urchin, *Eucidaris thouarsi* (Echinodermata: Echinoidea: Cidaroida), with implications for developmental and phylogenetic studies. *Biol. Bull.* **174:** 4–19.

Emlet, R. B., L. R. McEdward, and R. R. Strathmann. 1987. Echinoderm larval ecology viewed from the egg. Pp. 55–136 in *Echinoderm Studies* Vol. 2, M. Jangoux and J. M. Lawrence, eds. A. A. Balkema, Rotterdam.

Fenaux, L. 1969. Les echinopluteus de la Méditerranée. *Bull. Inst. Oceanogr. (Monaco)* **68:** 1–28.

Fenaux, L., C. Cellario, and M. Etienne. 1985. Variations in the ingestion rate of algal cells with morphological development of larvae of *Paracentrotus lividus* (Echinodermata: Echinoidea) *Mar. Ecol. Prog. Ser.* **24:** 161–165.

Garman, H., and B. Colton. 1883. Some notes on the development of *Arbacia punctulata* Lam. *Studies Biol. Lab. Johns Hopkins University* **2:** 247–255.

George, S. B. 1990. Population and seasonal differences in egg quality of *Arbacia lixula* (Echinodermata: Echinoidea) *Invertebr. Reprod. Dev.* **17:** 111–121.

George, S. B. 1996. Echinoderm egg and larval quality as a function of adult nutritional state. *Oceanol. Acta* **19:** 297–308.

George, S. B., C. Cellario, and L. Fenaux. 1990. Population differences in egg quality of *Arbacia lixula* (Echinodermata: Echinoidea): proximate composition of eggs and larval development. *J. Exp. Mar. Biol. Ecol.* **141:** 107–118.

Hadzi, J. 1963. *The Evolution of the Metazoa.* Pergamon Press, Oxford. 499 pp.

Havenhand, J. N. 1995. Evolutionary ecology of larval types. Pp. 79–122 in *Ecology of Marine Invertebrate Larvae,* L. McEdward, ed. CRC Press, Boca Raton, FL.

Hyman, L. H. 1955. *The Invertebrates: Echinodermata.* McGraw-Hill, New York. 763 pp.

Jensen, M. 1981. Morphology and classification of the Euechinoidea Bronn, 1860—a cladistic analysis. *Vidensk. Medd. Dan. Naturhist. Foren.* **143:** 7–99.

Mortensen, T. A. 1921. *Studies of the Development and Larval Forms of Echinoderms.* G. E. C. Gad, Copenhagen. 260 pp.

Mortensen, T. 1927. *Handbook of the Echinoderms of the British Isles.* Oxford University Press, London. 471 pp.

Mortensen, T. A. 1931. Contributions to the study of the development and larval forms of echinoderms. I-II. *K. Dan. Vidensk. Selsk., Skr. Naturvid. Math. Afd. 9,* **4:**(1) 1–65.

Nielsen, C. 1995. *Animal Evolution. Interrelationships of the Living Phyla.* Oxford University Press, Oxford. 467 pp.

Pearse, J. S., and R. A. Cameron. 1991. Echinodermata: Echinoidea. Pp. 513–662 in *Reproduction of Marine Invertebrates, Vol. 6,* A. C. Giese, J. S. Pearse, and V. B Pearse, eds. Boxwood Press, Pacific Grove, CA.

Pennington, J. T., and R. R. Strathmann. 1990. Consequences of the calcite skeletons of planktonic echinoderm larvae for orientation, swimming, and shape. *Biol. Bull.* **179:** 121–133.

Prouho, H. 1888. Recherches sur le *Dorocidaris papillata* et quelques autres échinides de la Méditerranée. *Arch. Zool. Exp. Gen.* (2) 213–380.

Raff, R. A., K. G. Field, M. T. Ghiselin, D. L. Lane, G. J. Olsen, N. R. Pace, A. L. Parks, B. A. Parr, and E. Raff. 1988. Molecular analysis of distant phylogenetic relationships in echinoderms. Pp. 30–41 in *Echinoderm Phylogeny and Evolutionary Biology,* C. R. C. Paul and A. B. Smith, eds. Clarendon Press, Oxford.

Raup, D. M. 1965. Crystal orientations in the echinoid apical system. *J. Paleontol.* **39:** 934–951.

Rees, C. B. 1953. The larvae of the Spatangidae. *J. Mar. Biol. Assoc. UK* **32:** 477–490.

Smith, A. B. 1984. *Echinoid Paleobiology.* George Allen and Unwin, London. 190 pp.

Smith, A. B. 1995. Echinoids from the Jurassic Oxford clay of England. *Palaeontology* **38:** 743–755.

Smith, A. B., and D. T. J. Littlewood. 1997. Molecular and morphological evolution during the post-Palaeozoic diversification of echinoids. Pp. 559–583 in *Molecular Evolution and Adaptive Radiation,* T. J. Givnish and K. J. Sytsma, eds. Cambridge University Press, Cambridge.

Smith, A. B., D. T. J. Littlewood, and G. A. Wray. 1995. Comparing patterns of evolution: larval and adult life history stages and ribosomal RNA of post-Palaeozoic echinoids. *Philos. Trans. R. Soc. Lond. B* **349:** 11–18.

Smith, A. B., D. T. J. Littlewood, and G. A. Wray. 1996. Comparative evolution of larval and adult life-history stages and small subunit ribosomal RNA amongst post-Palaeozoic echinoids. Pp. 234–254 in *New Uses for New Phylogenies,* P. H. Harvey, A. J. L. Brown, J. M. Smith, and S. Nee, eds. Oxford University Press, Oxford.

Strathmann, R. R. 1988. Larvae, phylogeny, and von Baer's law. Pp. 53–68 in *Echinoderm Phylogeny and Evolutionary Biology,* C. R. C. Paul and A. B. Smith, eds. Clarendon Press, Oxford.

Wray, G. 1992. The evolution of larval morphology during the post-Paleozoic radiation of echinoids. *Paleobiology* **18:** 258–287.

Wray, G. 1995. Evolution of larvae and developmental modes. Pp. 413–447 in *Ecology of Marine Invertebrate Larvae.* L. McEdward, ed. CRC Press, Boca Raton, FL.

Young, C. M. 1992. Episodic recruitment and cohort dominance in echinoid populations at bathyal depths. Pp. 239–246 in *Marine Eutrophication and Population Dynamics,* G. Colombo, I. Ferrari, V. U. Ceccherelli, and R. Rossi, eds. Olsen & Olsen, Fredensborg, Denmark.

Young, C. M. 1995. Behavior and locomotion during the dispersal phase of larval life. Pp. 249–277 in *Ecology of Marine Invertebrate Larvae,* L. McEdward, ed. CRC Press, Boca Raton, FL.

Young, C. M., and J. L. Cameron. 1989. Developmental rate as a function of depth in the bathyal echinoid *Linopneustes longispinus.* Pp. 225–231 in *Reproduction, Genetics and Distributions of Marine Organisms,* J. S. Ryland and P. A. Tyler, eds. Olsen & Olsen, Fredensborg, Denmark.

Young, C. M., and P. A. Tyler. 1993. Embryos of the deep-sea echinoid *Echinus affinus* require high pressure for fertilization. *Limnol. Oceanogr.* **38:** 178–181.

Young, C. M., J. L. Cameron, and K. J. Eckelbarger. 1989. Extended pre-feeding period in planktotrophic larvae of the bathyal echinoid *Aspidodiadema jacobyi. J. Mar. Biol. Assoc. UK* **69:** 695–702.

Young, C. M., P. A. Tyler, R. H. Emson, and J. D. Gage. 1993. Perception and selection of macrophyte detrital falls by the bathyal echinoid *Stylocidaris lineata. Deep-Sea Res.* **40:** 1475–1486.

Young, C. M., M. G. Devin, W. B. Jaeckle, S. U. K. Ekaratne, and S. B. George. 1996a. The potential for ontogenetic vertical migration by larvae of bathyal echinoderms. *Oceanol. Acta* **19:** 263–271.

Young, C. M., P. A. Tyler, and J. D. Gage. 1996b. Vertical distribution correlates with pressure tolerances of cleaving embryos in the deep-sea asteroid *Plutonaster bifrons. J. Mar. Biol. Assoc. UK* **76:** 749–757.

Young, C. M., E. Vazquez, A. Metaxas, and P. A. Tyler. 1996c. Embryology of vestimentiferan tube worms from deep-sea methane/sulfide seeps. *Nature* **314:** 514–516.

Reference: *Biol. Bull.* **198:** 396–403. (June 2000)

Genetic Diversity of Oceanic Island *Lasaea* (Mollusca: Bivalvia) Lineages Exceeds That of Continental Populations in the Northwestern Atlantic

JOONG-KI PARK AND DIARMAID Ó FOIGHIL*

Museum of Zoology and Department of Biology, University of Michigan, Ann Arbor, Michigan 48109-1079

Abstract. Direct-developing lineages of the intertidal marine bivalve *Lasaea* have colonized both upstream mainland (southeastern Florida) and downstream oceanic island (Bermuda) locations in the western North Atlantic. Replicate samples from these two regional populations, separated by about 1500 km of open ocean, were sequenced for a 655-nucleotide portion of the mitochondrial (mt) cytochrome oxidase subunit I gene. Twelve haplotypes (2 Floridian and 10 Bermudan) were obtained that differed by a maximum of four substitutions among pairwise comparisons. Phylogenetic analysis yielded a parsimony network within which the mainland lineages clustered in one of the terminal branches; a mirror image of *a priori* expectations based on regional surface-current polarity. It is difficult, however, to envisage a plausible countercurrent dispersal mechanism. This tree topology may stem from divergent demographic processes operating on these two evolutionarily recent regional populations. The starlike phylogenetic pattern of Bermudan lineages is consistent with a history of rapid population growth. The restricted genetic repertoire and relative ecological scarcity of Floridian lineages imply either a recent founder event by unstudied Caribbean source populations or else a history of pronounced bottlenecks in population size. Bermuda's impoverished Caribbean marine biota may allow western North Atlantic *Lasaea* lineages to escape severe competitive interactions impacting other parts of their geographic range.

Introduction

Oceanic islands have never been connected to continental landmasses and represent some of the most isolated environments on earth (Nunn, 1994). They receive their biotas solely through dispersal from geographically distant source populations and from subsequent *in situ* diversification (Paulay, 1994). Stretches of deep ocean surrounding such islands represent dispersal filters for benthic shallow-water marine taxa. The stringency of these filters varies according to physical parameters (*e.g.*, distance from potential source populations, current speed and polarity) and to taxon-specific life-history traits including presence of a prolonged pelagic larval ontogeny (Scheltema, 1992; Jaeckle, 1994; Palumbi *et al.*, 1997; Lessios *et al.*, 1998), rafting ability (Jokiel, 1990; Helmuth *et al.*, 1994; Ingólfsson, 1995; Ó Foighil *et al.*, 1999), and propensity for anthropogenic transfer (Carlton, 1989; Carlton and Geller, 1993; Carlton and Hodder, 1995). In general, classical oceanic island biotas exhibit a depauperate and disharmonic composition that may include relict taxa and endemic radiations (Paulay, 1994).

Bermuda is composed of a cluster of small western North Atlantic oceanic islands (32°18′N, 64°46′W) rising from a 65-km^2 carbonate platform and supported by a submerged volcanic peak (Nunn, 1994; Sterrer, 1998). It is situated within the warm Sargasso Sea section of the North Atlantic Gyre, about 1000 km east of the coast of North Carolina, and the main flow of the Gulf Stream System arcs well to the west and north of its position (Fig. 1). However, the Bermuda Platform is regularly approached by mesoscale anticyclonic eddies originating from the Gulf Stream System (Parker, 1971; Spitzer, 1989). It is generally assumed that Bermuda has remained stable throughout the Quater-

Received 15 September 1999; accepted 17 February 2000.

* To whom correspondence should be addressed. E-mail: diarmaid@umich.edu

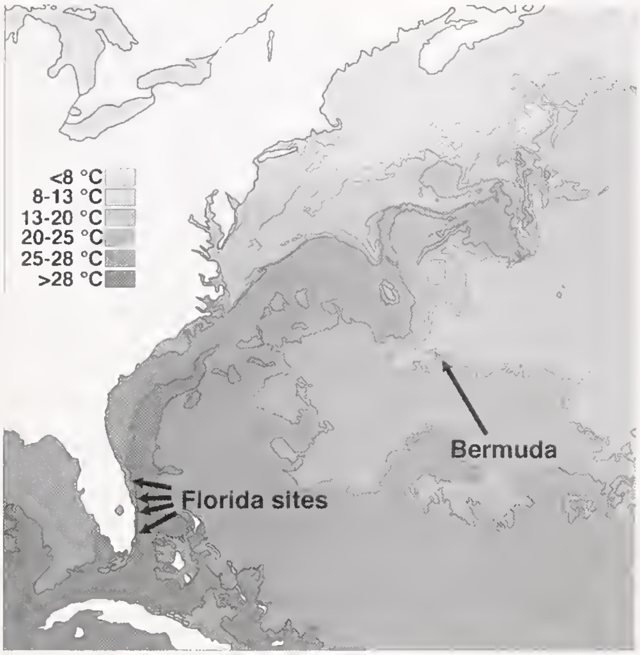

Figure 1. Location of the *Lasaea* sampling sites in the western North Atlantic, plotted onto a satellite image of sea-surface temperatures (modified from Thurman, 1997). The body of warm water flowing through the Florida Straits represents the Florida Current portion of the Gulf Stream System. Past Cape Hatteras, the Gulf Stream proper leaves the continental slope and develops a series of meanders that pinch off persistent mesoscale eddies. Cold eddies migrate southward and approach Bermuda.

nary (Nunn, 1994) and, although late Pleistocene (last 130,000 years) sea-level changes ranged up to 25 m, the island group was not submerged during this period (Harmon *et al.*, 1978, 1981).

The Bermudan shallow-water marine fauna encompasses a low level (2.4%) of endemic species and represents a moderately impoverished oceanic extension of the Caribbean fauna (Sterrer, 1986, 1998). Twenty-eight of a total of 49 common nearshore molluscs found throughout the Caribbean also occur on this oceanic island platform (Warmke and Abbott, 1961), and there is some evidence for a partial turnover of the Bermudan marine malacofauna on ecological timescales (Abbott and Jensen, 1967; Sterrer, 1986). The nearest source populations for Bermudan marine taxa of Caribbean origin are about 1500 km to the southwest, in southern Florida and the Bahamas. Based on net transport of drift bottles, this distance represents a minimum passage of 21–30 days for passive pelagic transport of larvae or rafted propagules (Jackson, 1986). Such a time frame does not pose a serious obstacle for species with long-lived pelagic larvae, but may approach the upper limit for many species with faster developing pelagic larval stages. The few data available on genetic distances of Bermudan marine invertebrates from Caribbean conspecifics are consistent with this view (Mitton *et al.*, 1989; Hateley and Sleeter, 1993). A number of Bermudan marine faunal constituents are known to have been introduced by human agency (Sterrer, 1986, 1998), a process that is independent of current polarity or geographic distance.

The genus *Lasaea* is composed of minute, crevice-dwelling, intertidal clams that have a near-cosmopolitan distribution on rocky shores; its North Atlantic lineages are exclusively composed of direct-developers (Ó Foighil, 1989). Molluscan systematists generally recognize one North Atlantic species, *Lasaea adansoni* (Gmelin) (=*L. rubra* Montagu; *L. bermudensis* Bush) (Sterrer, 1986). This systematic conclusion is based solely on shell characters and has not been corroborated by population genetic (Tyler-Walters and Crisp, 1989) and phylogenetic (Ó Foighil and Smith, 1995; Ó Foighil and Jozefowicz, 1999) studies. Ó Foighil and Jozefowicz (1999) constructed molecular phylogenetic trees for North Atlantic *Lasaea* lineages based on mitochondrial (mt) 16S gene variation in two continental putative source populations (Florida, the northern limit of distribution in North America; Iberia) and two oceanic island populations (Bermuda, Azores). No amphi-Atlantic genotypes were detected; Bermudan lineages co-clustered exclusively with Floridian congeners to form a western Atlantic clade and Azorean samples formed an exclusive clade with Iberian haplotypes. The western Atlantic lineages showed low levels of genetic diversity (a single Florida haplotype differed by one diagnostic nucleotide substitution from three Bermudan haplotypes), formed a shallow polytomy, and (remarkably) were sister to polyploid Australian clonal congeners in global phylogenetic trees (Ó Foighil and Jozefowicz, 1999).

Jackson (1986) attributed the presence of Caribbean species lacking an extended pelagic larval stage on Bermuda to colonization *via* rafting events from continental source populations. Based on present-day circulation patterns in the western North Atlantic, the hypothesis that Bermudan *Lasaea* populations were established by rafting events assumes that intermittent gene flow has occurred, over evolutionarily significant timeframes, from western continental margin source populations—for example, from south Florida. Island lineages are predicted to represent a subsample of mainland genetic diversity, and to contain endemic genotypes that cluster in the terminal tips of a western Atlantic clade. Ó Foighil and Jozefowicz's (1999) preliminary 16S data set had some features that were consistent with the rafting hypothesis: the three Bermudan haplotypes had close phylogenetic links to, but were genetically distinct from, the Floridian haplotype. However, these workers were unable to distinguish among ancestral and derived relationships among the four polytomous western Atlantic mt 16S genotypes, and it was unclear how representative the sole Floridian haplotype, sampled from a single population, was of mainland regional genetic diversity.

The aim of the present study was to perform a comprehensive cladistic analysis of Bermudan and Floridian *Lasaea* mitochondrial lineages to test their adherence to rafting hypothesis predictions. In addition to three Bermudan populations, four populations of *Lasaea* were sampled along 250 km of contiguous southeastern Floridian coastline. A total of 124 specimens of western Atlantic *Lasaea* were sequenced for a 655-nucleotide (nt) fragment of cytochrome oxidase 1, a protein-encoding mitochondrial gene that, for recently diverged lineages, typically accumulates substitutions at a faster rate than does 16S (Ó Foighil *et al.*, 1998). Twelve western Atlantic haplotypes were obtained and yielded a phylogenetic tree topology that was a mirror image of that predicted by the rafting hypothesis.

Materials and Methods

Specimens of *Lasaea* were sampled in April 1998 from four southeastern Florida locations (Sebastian Inlet State Park, Brevard County; Fort Pierce Inlet State Recreation Area, St. Lucie County; Phil Foster Park, West Palm Beach; and Bill Baggs Cape Florida State Recreation Area, Key Biscayne) spanning about 250 km of contiguous coastline (see Fig. 1). The bivalves were moderately abundant in the interstices of barnacle tests at three of the sites; however, intensive sampling at the Key Biscayne site yielded only four individuals. Additional collections were taken in May 1998 from intertidal algal tufts and barnacle test interstices at three Bermudan locations (Boaz Island, the main Island at North Shore Road, and St. George's Island at the Bermuda Biological Station for Research) spanning about 20 km of the archipelago's length. At each sampling location, clams were taken from a number of microsites on the shore and pooled prior to fixation in 95% ethanol; thus a representative sample of genetic diversity from the study population was obtained.

Extensive sampling of ostensibly suitable intertidal crevice habitats elsewhere in the Caribbean by the second author (Lower Florida Keys; Dry Tortugas; New Providence, Bahamas; Puerto Rico), and by A. Frias-Martins (Jamaica), yielded no further specimens of *Lasaea*. Attempts to amplify the target gene fragment from a single dried museum specimen sampled from Belize (USNM# 841332) and from a small number of preserved specimens sampled from Cabo Tres Puntas, Venezuela (R.C. Bullock, University of Rhode Island, pers. comm.) were also unsuccessful. In the absence of tractable Caribbean outgroup samples, we generated homologous cytochrome oxidase subunit I (CO I) sequences from Sydney samples of Australian direct-developing polyploid *Lasaea* lineages (Ó Foighil and Thiriot-Quiévreux, 1999) that are sister to the study populations in global phylogenetic trees (Ó Foighil and Jozefowicz, 1999; Taylor and Ó Foighil, 2000).

Twenty individuals from each of six study populations, and all four specimens from Key Biscayne, were genetically characterized by amplifying and directly sequencing a homologous 655-nt fragment of the mitochondrial CO I gene. DNA templates for thermal cycle amplification were individually extracted from entire adult *Lasaea* specimens using a QIAamp tissue kit (QIAGEN Inc.). The Folmer *et al.* (1994) CO I primer set (5′-GGTCAACAAATCATAAAGATATTGG-3′; 5′-TAAACTTCAGGGTGACCAAAAAATCA-3′) was used to amplify and to sequence the target gene fragment. A negative control (no template) was included in each run of 35 cycles of amplification (1 min 94°C denaturing, 30 s 45°C annealing, 1 min 72°C extension). Double-stranded products were isolated on 1% agarose gels, excised under long-wavelength UV light, and extracted using a GeneClean (Bio 101) NaI/glass powder kit. Both strands on the target fragments were cycle-sequenced using a Big Dye DNA sequencing kit (PE Applied Biosystems), and reaction products were electrophoresed on an ABI 377 automated DNA sequencer. Sequence alignments were initially performed by the CLUSTAL option of Sequence Navigator 1.0.1 (Kececioglu and Myers, 1994) and then optimized manually. Sequences were analyzed using an unweighted maximum parsimony approach (PAUP* 4.0b2a; Swofford, 1998), and root probabilities for individual haplotypes were estimated using the Castelloe and Templeton (1994) heuristic technique. Nucleotide mismatch distribution (Schneider *et al.*, 1999) and lineage-through-time (Nee *et al.*, 1996) analyses were respectively performed on the Bermudan lineages using Arlequin 2.0 (beta 2; Schneider *et al.*, 1999) and the Endemic-Epidemic Phylogenetic Process Analysis (Rambaut *et al.*, 1997).

Results

Alignment of the 655-nt CO I fragment sequences obtained from the 124 individuals of western Atlantic *Lasaea*

Table I

Alignment of the 10 variable sites in the 655 nucleotide fragment of CO I sequenced for 12 western North Atlantic Lasaea *COI genotypes (Genbank accession #s: AF152564, AF182733-AF182743)*

	1	2	2	2	2	3	3	4	4	5
	9	4	6	8	8	0	4	0	7	3
	5	5	4	4	7	5	4	7	9	9
FL1	C	C	C	A	A	A	A	A	**A**	A
FL2	C	C	C	A	A	A	A	A	**A**	G
BDA1	C	C	C	A	A	A	A	A	**G**	A
BDA2	C	C	C	A	G	A	A	A	**G**	A
BDA3	C	C	C	G	A	A	A	A	**G**	A
BDA4	C	T	C	A	A	A	A	A	**G**	A
BDA5	C	C	C	A	A	A	G	A	**G**	A
BDA6	T	C	C	A	A	A	A	A	**G**	A
BDA7	C	C	C	A	G	A	T	A	**G**	A
BDA8	C	C	C	A	A	A	A	G	**G**	A
BDA9	C	C	C	A	A	G	A	A	**G**	A
BDA10	C	C	T	G	A	A	A	A	**G**	A

Positions of the variable sites within the sequenced fragment are presented vertically above the nucleotide columns. The prefixes FL and BDA respectively indicate haplotypes found in Floridian and Bermudan populations, and these show one diagnostic difference (in bold).

Table 2

Relative distribution of the 12 western North Atlantic Lasaea *COI genotypes among the 7 sampling locations*

	FL1	FL2	BDA1	BDA2	BDA3	BDA4	BDA5	BDA6	BDA7	BDA8	BDA9	BDA10
FL, SI	20	—	—	—	—	—	—	—	—	—	—	—
FL, FP	20	—	—	—	—	—	—	—	—	—	—	—
FL, PB	19	1	—	—	—	—	—	—	—	—	—	—
FL, KB	4	—	—	—	—	—	—	—	—	—	—	—
BDA, BS	—	—	8	—	—	7	—	2	—	1	1	1
BDA, NS	—	—	4	7	9	—	—	—	—	—	—	—
BDA, BI	—	—	5	9	—	1	2	—	2	1	—	—
Totals	63	1	17	16	9	8	2	2	2	2	1	1

The prefixes FL and BDA respectively indicate haplotypes found in Floridian and Bermudan populations. SI: Sebastian Inlet; FP: Fort Pierce; PB: Palm Beach; KB: Key Biscayne; BS: Biological Station; NS: North Shore; BI: Boaz Island. Twenty individuals were sequenced from each sampling site except for Key Biscayne, where only four specimens were obtained.

revealed 10 variable sites and 12 haplotypes (Table 1). Of the 11 nucleotide substitutions (all synonymous) detected, 8 were third codon transitions, 2 were first codon transitions, and 1 was a third codon transversion. Genetic divergence levels among the haplotypes was very low, with a maximum of four substitutions (0.6%) among pairwise comparisons. Floridian and Bermudan haplotypes exhibited one diagnostic third codon transition—*i.e.*, no haplotype was shared among these two regional groupings. Table 2 shows the distribution pattern of the 12 haplotypes among the seven sampling sites. There was a striking discrepancy in the relative levels of haplotypic diversity and frequency in the Bermudan and Floridian samples. A total of 10 mt genotypes were contained in the combined oceanic island samples, none of which exceeded a frequency of 0.28. With the exception of a single individual from the Palm Beach population, the Floridian specimens were monomorphic for haplotype FL1.

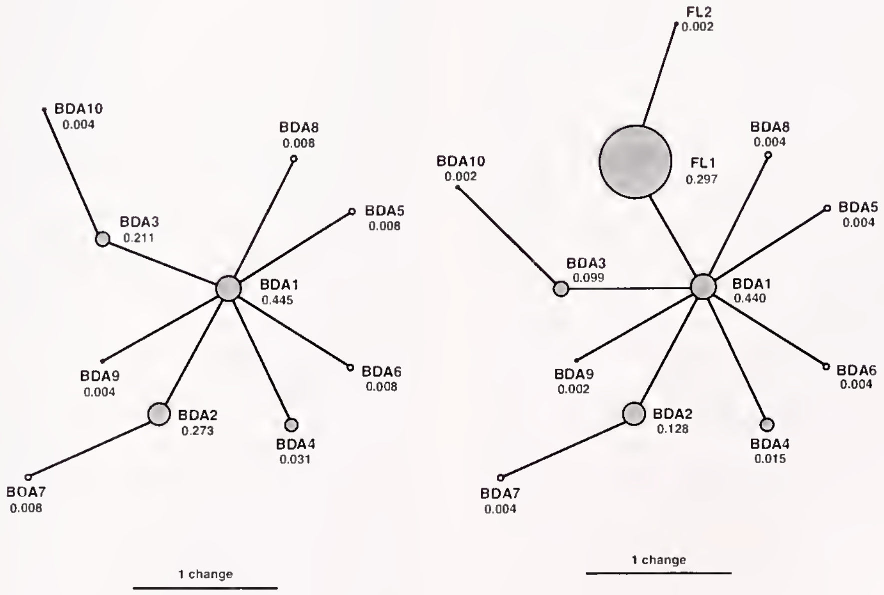

Figure 2. Unrooted phylograms of the 10 Bermudan (a) and 12 western Atlantic (b) *Lasaea* COI genotypes encountered in this study. Prefixes BDA and FL respectively identify Bermudan and Floridian lineages, and values underneath lineage titles indicate the relative outgroup weighting calculated for that haplotype. The diameter of the shaded spherical symbol associated with each haplotype is proportional to its relative frequency in the respective data sets (Table 2).

Figure 2a shows the single most parsimonious unrooted phylogram (9 steps; 2 parsimony-informative characters; CI = 1.0; RI = 1.0) obtained by exhaustive PAUP analysis of the 10 Bermudan haplotypes. This unrooted tree had a starlike topology in which there was a distinct lack of structure: 7 of the 10 haplotypes had only a single connection. A central topological position was occupied by BDA1, the most common Bermudan genotype, which was present in all three sampled sites and was one step away from 7 of the 9 other island CO I genotypes. Heuristic estimation of outgroup weighting (Castelloe and Templeton, 1994) for each of the Bermudan mt genotypes yielded a maximum value (0.445) for BDA1 (Fig. 2a), indicating that this is probably the oldest haplotype in the Bermudan dataset.

Phylogenetic analysis of the combined Floridian/Bermudan dataset (Fig. 2b) produced a single most parsimonious tree (11 steps; three parsimony-informative characters; CI = 1.0; RI = 1.0) that maintained a starlike topology and a central position for BDA1. Floridian haplotypes were peripherally positioned in a single branch of the tree topology. BDA1 was one step removed from eight western Atlantic haplotypes, including the predominant mainland lineage (FL1), and two steps away from the remaining three lineages. In contrast, FL1 was respectively, one, two and three steps removed from two, seven, and two western Atlantic lineages. Heuristic outgroup weighting of the haplotypes in the combined tree topology (Fig. 2b) identified BDA1 (0.440) as the oldest haplotype in the western North Atlantic dataset.

Caribbean outgroup populations were unavailable to root our western North Atlantic gene tree, so we generated homologous CO I sequence for an Australian direct-developing polyploid *Lasaea* lineage (GenBank# AF153064) that is sister to western Atlantic congeners in global phylogenetic trees (Ó Foighil and Jozefowicz, 1999; Taylor and Ó Foighil, 2000). The Australian haplotype differed by ≥4.4% from the western Atlantic lineages, and its utilization as an outgroup taxon produced a single most parsimonious tree (not shown; 39 steps, CI = 0.667, RI = 0.555) in which the ingroup topology (11 steps total length) was identical to that of Figure 2b and the outgroup taxon connected to BDA7, a peripheral Bermudan haplotype (Fig. 2b), by a relatively enormous branch length of 28 steps. The basal positioning of BDA7 resulted from it sharing a thymidine at position 344 with the outgroup, whereas other western Atlantic lineages had either an adenine or guanine residue (Table 1).

Discussion

The COI data set corroborates Ó Foighil and Jozefowicz's (1999) preliminary mt 16S characterization of Floridian and Bermudan *Lasaea* populations: they are genetically very similar, yet distinct, and genetic diversity levels are higher in the oceanic island samples. Surprisingly, the parsimony network generated was a mirror image of *a priori* source and founder topological expectations: continental populations contained a small number of endemic genotypes that positioned peripherally in the western North Atlantic *Lasaea* network (Fig. 2b). Rooting of this network is necessary to test dispersal hypotheses for these two regional populations; however, rooting is complicated by the unavailability of Caribbean outgroup genotypes.

Two rooting procedures were used: phylogenetic analyses utilizing an Australian sister lineage, and calculation of relative outgroup weights for individual haplotypes based on neutral coalescence expectations. BDA7, a relatively rare Bermudan haplotype, was identified as the root of the western North Atlantic clade when an Australian sister taxon was utilized as an outgroup. This result should be viewed with caution because of the 28:1 ratio of outgroup-to-ingroup branch lengths in the analysis and because of the peripheral positioning of BDA7 in unrooted analyses (Fig. 2b). Closely related species frequently fail to accurately root intraspecific trees if intraspecific differences are much less than interspecific differences (Templeton, 1992), and coalescence theory predicts that rare haplotypes occupying cladogram tips are likely to be recently derived lineages (Donnelly and Tavaré, 1986).

According to coalescence theory, the probability that a given haplotype is the oldest in a population is a function of its frequency and the centrality of its positioning in topological networks (Donnelly and Tavaré, 1986; Crandall and Templeton, 1993, 1996; Beckenbach, 1994). Castelloe and Templeton's (1994) heuristic method weights interior haplotypes more heavily than tip haplotypes and differentially weights interior haplotypes by their mutational connectedness and their proximity to high-multiplicity haplotypes. It unambiguously identified BDA1, the centrally positioned (Fig. 2a) and most common Bermudan haplotype (Table 2), as the most likely candidate for the oldest Bermudan mitochondrial genotype (outgroup weight = 0.445) in our sample. BDA7 is two steps away from the central topological position (Fig. 2a), received a much lower outgroup weighting (0.008), and cannot be accepted as the putative ancestral Bermudan lineage.

Haplotype BDA1 maintained its topological centrality and its high (0.44) outgroup weighting (Castelloe and Templeton, 1994) in combined analyses of Bermudan and Floridian lineages (Fig. 2b). Although the mainland haplotype, FL1, is by far the most common haplotype in the combined data set, its peripheral positioning in the phylogram and lack of connectedness to most of the other western North Atlantic haplotypes give it a relatively low outgroup weighting (0.297). Surprisingly, our analyses based on coalescence theory expectations indicate that the Bermudan lineage BDA1 is the oldest in our data set and represents the putative ancestral haplotype for both regional western North Atlantic populations.

Phylogenetic trees represent inferred historical relationships, and our CO I dataset, when rooted with BDA1, reveals a countercurrent topology of source (Bermuda) and founder (Florida) populations. Countercurrent gene-flow patterns have also been recently inferred for a variety of marine invertebrates (Palumbi *et al.*, 1997; Palumbi, 1997; Benzie, 1999; Lessios *et al.*, 1999; Ó Foighil and Jozefowicz, 1999) and may indicate that contemporary gene flow is insufficient in these cases to obscure genetic structuring produced under previous current regimes (Benzie, 1999). However, it is difficult to envisage a plausible countercurrent dispersal mechanism for the Floridian and Bermudan study populations. Although it has fluctuated in intensity, the Florida Current has apparently been a persistent feature of the North Atlantic Gyre (Keffer *et al.*, 1988; Lynch-Stieglitz *et al.*, 1999; Duplessy, 1999). In addition, unstudied Caribbean populations are much more plausible sources of Floridian lineages, and diagnostic genetic differences among island and mainland populations for two mitochondrial genes (COI and 16S [Ó Foighil and Jozefowicz, 1999]) rule out historical (anthropogenic) countercurrent gene flow.

It may be pertinent that the low values observed for genetic diversity are consistent with an evolutionarily recent origin for *both* regional *Lasaea* populations. The most detailed fossil-calibrated estimates of molluscan gene divergence are provided by Collins *et al.* (1996) for the marine snail *Nucella* (2%/myr/lineage for [predominantly synonymous] third codon transitional differences). The central mitochondrial genotype, BDA1, is a maximum of two nucleotide substitutions removed from all of the other members of the western Atlantic *Lasaea* clade. Although complicated by phylogenetic and other potential biases, application of the Collins *et al.* (1996) rate yields a crude maximum age estimate of 0.229 Ma for the entire western Atlantic clade and also for the Bermudan population. Intrapopulational allelic relationships are modulated by demographic history (Slatkin and Hudson, 1991; Nee *et al.*, 1996; Lavery *et al.*, 1996), and it is possible that the observed patterns of CO I gene variation stem from divergent demographic processes experienced by these two evolutionarily recent regional populations, rather than from a countercurrent pattern of gene flow.

Application of coalescence theory assumes that the study populations are at equilibrium. However, this assumption may not be met by our data set. Domination of the Floridian regional population by a single haplotype (FL1) is consistent with either a recent founder event from an unstudied source population, or else with a history of population size bottlenecking; a process that promotes stochastic elimination of novel and rare haplotypes. In contrast, the starlike allelic topology of the Bermuda samples is characteristic of a population founded by one ancestral type (presumably BDA1) that has experienced a phase of rapid growth, a process associated with lowered stochastic elimination of novel and rare lineages (Avise *et al.*, 1984; Slatkin and Hudson, 1991). Further support for this demographic interpretation of the Bermudan population was obtained when a lineages-through-time analysis (Nee *et al.*, 1996) (not shown) yielded profiles consistent with a historically growing population. However, nucleotide mismatch distribution analysis of the Bermudan population using Arlequin (Schneider *et al.*, 1999) failed to meet the sudden-expansion model (C. Cunningham, Duke University, pers. comm.), implying that the primary wave of growth for this oceanic island population may have occurred soon after the initial founding event. Differential historical rates of loss/gain of novel haplotypes in the two regional populations could act to displace ancestral haplotypes from central topological positions in the western Atlantic clade. For instance, if we were to assume that the mainland lineage FL1 represents the "true" ancestral haplotype in our western Atlantic data set, its noncentral position in the tree (Fig. 2b) might result from the repeated pruning of rare novel Floridian mt genotypes, one step removed from FL1, by sequential episodes of mainland population constrictions.

The demographic distinctions implicit in the mitochondrial genetic structure of Floridian and Bermudan *Lasaea* populations ultimately reflect environmental differences in the intertidal crevice habitat of this organism among the oceanic island and mainland locations. In Bermuda, *Lasaea* are easily sampled wherever such habitats exist (Ó Foighil, pers. observ.). In Florida, and in other Caribbean locations we investigated, *Lasaea* was respectively much more sporadic or nonexistent. This small clam seems to be a relatively rare component of the Caribbean rocky shore fauna. Indeed, apart from two lots from the Bahamas and a single individual from Belize, all museum records of western North Atlantic *Lasaea* examined in a previous survey (Ó Foighil, 1989) were from Bermuda and southern Florida.

Because of their reduced biotic diversity, oceanic islands may allow some taxa to escape competitive interactions that severely reduce survivorship in other parts of their geographic range (Paulay, 1994). Although we cannot rule out a contributing role for physical environmental factors, Bermuda may well represent such an ecological release for western Atlantic *Lasaea* lineages. If this interpretation is correct, future characterization of the genetic structure of Caribbean *Lasaea* populations, though likely to uncover novel haplotypes, is predicted to yield depauperate genetic profiles similar to that exhibited by our Floridian samples.

Acknowledgments

Our thanks to P. Mikkelsen, A. Frias-Martins, R. Bullock, and C. Simmons for facilitating our sampling efforts. The

Smithsonian Institution loaned us lot USNM# 841332, and D. Graf prepared Figure 1. C. Cunningham performed the mismatch distribution analysis using Arlequin and provided pointers on inferring demographic processes from gene trees. Early drafts were critically read by M. Frohlich and A. Merriwether, and we thank C. Cunningham and two anonymous reviewers for their input. Financial support was provided by a National Geographic Research Grant, and by NSF award OCE 9617689, to D. Ó Foighil.

Literature Cited

Abbott, R. T., and R. H. Jensen. 1967. Molluscan faunal changes around Bermuda. *Science* **155:** 687–688.

Avise, J. C., J. E. Neigel, and J. Arnold. 1984. Demographic influences on mitochondrial DNA lineages survivorship in animal populations. *J. Mol. Evol.* **20:** 99–105.

Beckenbach, A. T. 1994. Mitochondrial haplotype frequencies in oysters: neutral alternatives to selection models. Pp. 188–198 in *Non-neutral Evolution: Theories and Molecular Data*, B. Golding, ed. Chapman and Hall, New York.

Benzie, J. A. H. 1999. Genetic structure of coral reef organisms: ghosts of dispersal past. *Am. Zool.* **39:** 131–145.

Carlton, J. T. 1989. Man's role in changing the face of the ocean: biological invasions and implications for conservation of near-shore environments. *Conserv. Biol.* **3:** 265–273.

Carlton, J. T., and J. B. Geller. 1993. Ecological roulette: the global transport of non-indigenous marine organisms. *Science* **261:** 78–82.

Carlton, J. T., and J. Hodder. 1995. Biogeography and dispersal of coastal marine organisms: experimental studies on a replica of a 16th-century sailing vessel. *Mar. Biol.* **121:** 721–730.

Castelloe, J., and A. R. Templeton. 1994. Root probabilities for intraspecific gene trees under neutral coalescent theory. *Mol. Phylogenet. Evol.* **3:** 102–113.

Collins, T. M., K. Frazer, A. R. Palmer, G. J. Vermeij, and W. M. Brown. 1996. Evolutionary history of northern hemisphere *Nucella* (Gastropoda, Muricidae): molecular, morphological, ecological and paleontological evidence. *Evolution* **50:** 2287–2304.

Crandall, K. A., and A. R. Templeton. 1993. Empirical tests of some predictions from coalescent theory with applications to intraspecific phylogeny reconstruction. *Genetics* **134:** 959–969.

Crandall, K. A., and A. R. Templeton. 1996. Applications of intraspecific phylogenetics. Pp. 81–99 in *New Uses for New Phylogenies*, P. H. Harvey, A. J. Leigh Brown, J. Maynard Smith, and S. Need, eds. Oxford University Press, Oxford.

Donnelly, P., and S. Tavaré. 1986. The ages of alleles and a coalescent. *Adv. Appl. Probab.* **18:** 1–19.

Duplessy, J.-C. 1999. Climate and the Gulf Stream. *Nature* **402:** 593–595.

Folmer, O., M. Black, W. Hoeh, R. Lutz, and R. Vrijenhoek. 1994. DNA primers for amplification of mitochondrial cytochrome *c* oxidase subunit I from diverse metazoan invertebrates. *Mol. Mar. Biol. Biotechnol.* **3:** 294–299.

Harmon, R. S., H. P. Schwarcz, and D. C. Ford. 1978. Late Pleistocene sea level history of Bermuda. *Quat. Res.* **9:** 205–218.

Harmon, R. S., L. S. Land, R. M. Mitterer, P. Garrett, H. P. Schwarcz, and G. J. Larson. 1981. Bermuda sea level during the last interglacial. *Nature* **289:** 481–483.

Hateley, J. G., and T. D. Sleeter. 1993. A biochemical genetic investigation of spiny lobster (*Panulirus argus*) stock replenishment in Bermuda. *Bull. Mar. Sci.* **52:** 993–1006.

Helmuth, B., R. R. Veit, and R. Holberton. 1994. Long-distance dispersal of a subantarctic brooding bivalve (*Gaimardia trapesina*) by kelp-rafting. *Mar. Biol.* **120:** 421–426.

Ingólfsson, A. 1995. Floating clumps of seaweed around Iceland: natural microcosms and a means of dispersal for shore fauna. *Mar. Biol.* **122:** 13–21.

Jackson, J. B. C. 1986. Modes of dispersal of clonal benthic invertebrates: consequences for species' distributions and genetic structure of local populations. *Bull. Mar. Sci.* **39:** 588–606.

Jaeckle, W. B. 1994. Multiple modes of asexual reproduction by tropical and subtropical sea star larvae—an unusual adaptation for genet dispersal and survival. *Biol. Bull.* **186:** 62–71.

Jokiel, P. L. 1990. Transport of reef corals into the Great Barrier Reef. *Nature* **347:** 665–667.

Kececioglu, J., and E. Myers. 1994. Sequence Navigator, 1.0.1. Perkin Elmer Applied Biosystems, Inc., Foster City, CA.

Keffer, T., D. G. Martinson, and B. H. Corliss. 1988. The position of the Gulf Stream during Quaternary glaciations. *Science* **241:** 440–442.

Lavery, S., C. Moritz, and D. R. Fielder. 1996. Genetic patterns suggest exponential population growth in a declining species. *Mol. Biol. Evol.* **13:** 1106–1113.

Lessios, H. A., B. D. Kessing, and D. R. Robertson. 1998. Massive gene flow across the world's most potent marine biogeographic barrier. *Proc. R. Soc. Lond. B.* **267:** 583–588.

Lessios, H. A., B. D. Kessing, D. R. Robertson, and G. Paulay. 1999. Phylogeography of the pantropical sea urchin *Eucidaris* in relation to land barriers and ocean currents. *Evolution* **53:** 806–817.

Lynch-Stieglitz, J., W. B. Curry, and N. Slowey. 1999. Weaker Gulf Stream in the Florida Straits during the last glacial maximum. *Nature* **402:** 644–648.

Mitton, J. B., C. J. Berg, and K. S. Orr. 1989. Population structure, larval dispersal, and gene flow in the queen conch, *Strombus gigas*, of the Caribbean. *Biol. Bull.* **177:** 356–362.

Nee, S., E. C. Holmes, A. Rambaut, and P. H. Harvey. 1996. Inferring population history from molecular phylogenies. Pp. 66–80 in *New Uses for New Phylogenies*, P. H. Harvey, A. J. Leigh Brown, J. Maynard Smith, and S. Nee, eds. Oxford University Press, Oxford.

Nunn, P. D. 1994. *Oceanic Islands.* Blackwell, Oxford.

Ó Foighil, D. 1989. Planktotrophic larval development is associated with a restricted geographic range in *Lasaea*, a genus of brooding, hermaphroditic bivalves. *Mar. Biol.* **103:** 349–358.

Ó Foighil, D., and C. J. Jozefowicz. 1999. Amphi-Atlantic phylogeography of direct-developing lineages of *Lasaea*, a genus of brooding bivalves. *Mar. Biol.* **135:** 115–122.

Ó Foighil, D., and M. J. Smith. 1995. Evolution of asexuality in the cosmopolitan marine clam *Lasaea*. *Evolution* **49:** 140–150.

Ó Foighil, D., and C. Thiriot-Quiévreux. 1999. Sympatric Australian *Lasaea* species (Mollusca: Bivalvia) differ in their ploidy levels, reproductive modes and developmental modes. *Zool. J. Linn. Soc.* **127:** 477–494.

Ó Foighil, D., P. M. Gaffney, A. E. Wilbur, and T. J. Hilbish. 1998. Mitochondrial cytochrome oxidase I gene sequences support an Asian origin for the Portuguese oyster, *Crassostrea angulata*. *Mar. Biol.* **131:** 497–503.

Ó Foighil, D., B. A. Marshall, T. J. Hilbish, and M. A. Pino. 1999. Trans-Pacific range extension by rafting is inferred for the flat oyster *Ostrea chilensis*. *Biol. Bull.* **196:** 122–126.

Palumbi, S. R. 1997. Molecular biogeography of the Pacific. *Coral Reefs* **16:** S47–S52.

Palumbi, S. R., G. Grabowsky, T. Duda, L. Geyer, and N. Tachino. 1997. Speciation and population genetic structure in tropical Pacific sea urchins. *Evolution* **51:** 1506–1517.

Parker, C. E. 1971. Gulf Stream rings in the Sargasso Sea. *Deep-Sea Res.* **18:** 981–993.

Paulay, G. 1994. Biodiversity on oceanic islands—its origin and extinction. *Am. Zool.* **34:** 134–144.

Rambaut, A., P. H. Harvey, and S. Nee. 1997. End-Epi: an application for inferring phylogenetic and population dynamical processes from molecular sequences. *Comput. Appl. Biosci.* **13:** 303–306.

Scheltema, R. S. 1992. Passive dispersal of planktonic larvae and the biogeography of tropical sublittoral invertebrate species. Pp. 195–202 in *Marine Eutrophication and Population Dynamics.* Proceedings of the 25th EMBS. G. Colombo *et al.*, eds. Olsen and Olsen, Fredensborg, Denmark.

Schneider, S., D. Roessli, and L. Excoffier. 1999. *Arlequin ver. 2.0: a software for population genetic data analysis.* Genetics and Biometry Laboratory, University of Geneva, Switzerland.

Slatkin, M., and R. R. Hudson. 1991. Pairwise comparisons of mitochondrial DNA sequences in stable and exponentially growing populations. *Genetics* **129:** 555–562.

Spitzer, W. S. 1989. Rates of vertical mixing, gas exchange, and new production: estimates from seasonal gas cycles in the upper ocean near Bermuda. Ph.D. Thesis, Massachusetts Institute of Technology and Woods Hole Oceanographic Institution. Woods Hole Oceanographic Institution, Woods Hole, MA. WHOI-89-30, 122 pp.

Sterrer, W. 1986. *Marine Fauna and Flora of Bermuda.* Wiley and Sons, New York. 742 pp.

Sterrer, W. 1998. How many species are there in Bermuda? *Bull. Mar. Sci.* **62:** 809–840.

Swofford, D. L. 1998. PAUP*: Phylogenetic Analysis Using Parsimony (* and Other Methods), Version 4. Sinauer Associates, Sunderland, MA.

Taylor, D. J., and D. Ó Foighil. 2000. Transglobal comparisons of nuclear and mitochondrial genetic structure in a marine polyploid clam (*Lasaea*, Lasaeidae). *Heredity* **84:** 321–330.

Templeton, A. R. 1992. Human origins and the analysis of mitochondrial DNA sequences. *Science* **255:** 737.

Thurman, H. V. 1997. *Introductory Oceanography*, 8th ed. Prentice Hall, Upper Saddle River, NJ.

Tyler-Walters, H., and D. J. Crisp. 1989. The modes of reproduction in *Lasaea rubra* (Montagu) and *L. australis* (Lamarck): (Erycinidae; Bivalvia). Pp. 299–308 in *Proceedings of the 23rd European Marine Biological Symposium, Swansea.* J. S. Ryland and P. A. Tyler, eds. Olsen and Olsen, Fredensborg, Denmark.

Warmke, M., and R. T. Abbott. 1961. *Caribbean Seashells.* Livingston, Narberth, PA. 346 pp.

Reference: *Biol. Bull.* **198:** 404–414 (June 2000)

Cuttlebone Morphology Limits Habitat Depth in Eleven Species of *Sepia* (Cephalopoda: Sepiidae)

KRISTIN M. SHERRARD

Committee on Evolutionary Biology, University of Chicago, 1025 E. 57th St., Chicago, Illinois 60637

Abstract. The cuttlebone is a rigid buoyancy tank that imposes a depth limit on *Sepia*, the only living speciose cephalopod genus with a chambered shell. Sections of 59 cuttlebones from a geographically diverse sample of 11 species were examined using confocal microscopy. *Sepia* species that live at greater depths had thicker septa and less space between pillars than did shallow species. A plate theory analysis of cuttlebone strength based on these two measures predicted maximum capture depths accurately in most species. Thus cuttlebone morphology confers differing degrees of strength against implosion from hydrostatic pressure, which increases with increasing habitat depth. Greater strength may come at the cost of increased cuttlebone density, which impinges on the cuttlebone's buoyancy function.

Introduction

The chambered shells of cephalopods serve as buoyancy devices despite being made of heavy calcium carbonate. Unlike the swim bladders of fish, they are unpressurized, so they do not change significantly in volume or buoyancy as the animal changes depth (Denton and Gilpin-Brown, 1961a), and no adjustments to the buoyancy system are necessary during vertical movements (Denton, 1974; Ward, 1987). However, the shells must be strong enough to resist implosion from hydrostatic pressure, which increases with depth (Denton and Gilpin-Brown, 1961a, b; Ward and Boletzky, 1984). Thus the demands of buoyancy and strength conflict: if a chambered shell is too dense, buoyancy decreases; if it is too weak, the danger of fractures at the animal's normal habitat depths increases.

The functional morphology of chambered shells, or phragmocones, in living and fossil cephalopods has been the subject of much research (*e.g.*, Westermann, 1975; Ward, 1987; Hewitt and Westermann, 1986; Jacobs, 1990; Daniel *et al.*, 1997; for a review, see Jacobs, 1992). Shell strength is of interest in part because habitat depth is ultimately limited by resistance to implosion. Habitat depth has implications for the separation of populations, for speciation, and for evolution. The high diversity of one fossil group, the ammonoids, has fueled efforts to understand the functional morphology of their phragmocones.

There are two possible approaches to studying phragmocone strength against implosion. First, living cephalopods (or their fresh shells) can be subjected to increasing hydrostatic pressures until the shells break. This has been done for individuals and shells of *Nautilus* (Raup and Takahashi, 1966; Hewitt and Westermann, 1987; Ward, 1987), *Spirula* (Denton, 1971), and *Sepia* (Birchall and Thomas, 1983; Ward and Boletzky, 1984). It is problematic to use dried shells, however, because they are weaker than living shells to an uncertain degree (Jacobs, 1992). Although imploding fresh shells provides accurate data on strength against hydrostatic pressure, this method is impractical for rarely caught species and impossible to use for fossils.

Alternately, theoretical analyses may be used to estimate shell strength against implosion. This method allows inferences about the functional morphology and paleobiology of extinct animals, as well as of living shelled cephalopods, many of which are rarely observed in the wild. Theoretical approaches have been applied to fossil nautiloids (*e.g.*, Westermann, 1973) and ammonoids (Westermann, 1975; Hewitt and Westermann, 1986; Jacobs, 1990; Daniel *et al.*, 1997). A disadvantage of theoretical analyses is that it is difficult to test the accuracy of the estimates, which depend on a number of simplifying assumptions.

For example, breaking stress must be analyzed at the weakest part of the shell, but it is not always clear how to identify this region. Various studies of fossil cephalopods have assumed it to be the outer shell (Jacobs, 1990), the last

Received 3 November 1999; accepted 3 April 2000. E-mail: kmsherra@midway.uchicago.edu

septum (Westermann, 1973; Daniel *et al.*, 1997), or the siphuncle (as reviewed in Jacobs, 1992). If the shell fails catastrophically during implosion, as is the case for *Nautilus* (Ward *et al.*, 1980), empirical tests do not establish the site of initial failure. Thus relative strengths of different parts of the shell must sometimes be calculated theoretically without recourse to direct verification, even in a living animal.

Constructing a model of shell strength requires that structural geometry, loading conditions, and mode of failure be defined to form the basis for an appropriate model. Even when models are carefully chosen, they are simplifications of complex structures and circumstances. Some simplifications have little effect on strength estimates; others have larger or nonlinear effects that make it difficult to evaluate the reliability of the model's output. Thus it would be informative to evaluate the robustness of a theoretical model on a living cephalopod of known habitat depth to gauge how reliable such estimates are for fossil forms.

Habitat depth and morphology vary little among species of *Nautilus*, and the internally shelled squid *Spirula* is monospecific. Only one living genus, *Sepia*, presents a wide range of habitat depths and shell morphologies among its nearly 100 species (Adam and Rees, 1966). Its phragmocone, or cuttlebone (Fig. 1), is internal and has a complex microscopic morphology. A method for estimating habitat depth from cuttlebone morphology would improve our knowledge of little known species of *Sepia*, some of which have been described only on the basis of cuttlebones washed up on beaches.

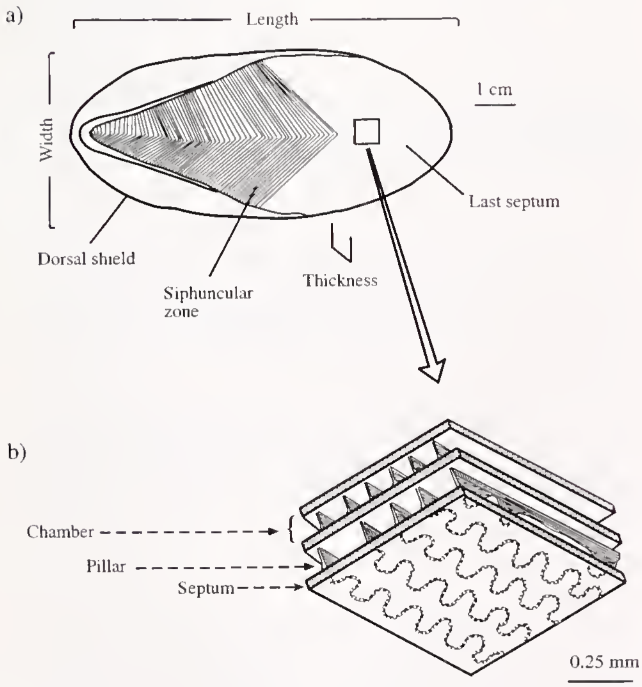

Figure 1. (a) Ventral view of the cuttlebone (anterior is to the right) of *Sepia papillata*. Chambers are emptied through the siphuncular zone, maintaining buoyancy. The last septum is the site of failure due to excessive hydrostatic pressure. (b) Microscopic structure of cuttlebone, showing chambers and the undulating, transverse pillars between the septa.

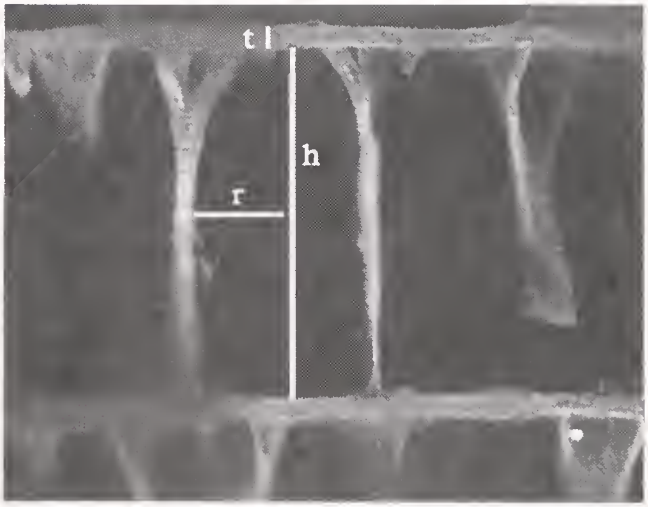

Figure 2. Confocal micrograph of *Sepia hieronis* cuttlebone. Measurements are septal thickness (t), pillar spacing (r), and chamber height (h).

Sepia is a genus of dibranchiate cephalopod that lives in coastal waters of Europe, Africa, Asia, and the South Pacific. It may be the only shelled cephalopod that alters its buoyancy on a daily basis; individuals of *S. officinalis* are heavy and rest on the bottom during the day, becoming more buoyant at night when they swim and hunt (Denton and Gilpin-Brown, 1961d). Extensive data from fisheries provide reliable estimates of maximum habitat depth in many species. Most species have a shallow habitat, not ranging deeper than 100 to 150 m. A dozen species have maximum capture records of 400 m and more (Adam and Rees, 1966; Roeleveld, 1972; Ward and Boletzky, 1984). There are very few species with intermediate maximum capture depths (200 to 300 m), though specimens of deeper dwelling species are often found at intermediate depths. This natural gap in maximum habitat depths permits the division of species into "shallow" and "deep" categories.

The cuttlebone appears to be a highly efficient structure, using a minimum of materials to achieve required strength. The siphuncular region is flat and open, rather than being a tube as in most chambered cephalopods, so it is not subject to explosion under hydrostatic pressure (Jacobs, 1992). The pillars buttress adjacent septa (see Fig. 1b, Fig. 2). It has been claimed that the pillars in cuttlebones are homologous to structures found on the siphuncle in *Spirula*, *Nautilus*, and fossil cephalopods (Bandel and Boletzky, 1979), but the cuttlebone's pillars are unique in having spread over the entire septal surface and in playing a major role in structural support of the septa. Though not homologous to ammonite sutures, which have been claimed to have a buttressing function (see Jacobs, 1992), pillars are similar to them in

Table 1

Comparison of estimated and actual maximum capture depths for Sepia *spp. used in this study*

		Estimated max depth*		
Species	Number of specimens	Species medians	Max specimen medians	Max capture depth (m)†
Deep				
S. australis	7	530 (460–611)	780 (708–840)	470 (a)
S. elegans	4	263 (204–301)	411 (310–479)	430 (b)
S. hieronis	6	332 (239–406)	855 (753–1087)	459 (a)
S. orbignyana	9	236 (209–248)	300 (212–335)	430 (b)
S. rex	7	216 (200–256)	377 (268–453)	400 (c)
Mean		306	545	438
Shallow				
S. apama	7	88 (80–104)	195 (106–263)	110 (c)
S. latimanus	4	61 (56–68)	99 (84–109)	100 (c)
S. mestus	4	42 (37–55)	73 (62–114)	160 (c)
S. officinalis	3	51 (44–65)	189 (64–227)	150 (c)
S. papillata	5	76 (68–84)	94 (62–142)	125 (a)
S. vercoi	3	109 (92–127)	130 (125–155)	100 (d)
Mean		67	130	124

* Estimated depths based on species medians and maximal specimen medians for r/t, assuming a safety factor of 1.33 (see text for details); 95% confidence intervals in parentheses.

† Maximum capture data from (a) Roeleveld, 1972, (b) Adam and Rees, 1966, (c) Ward and Boletsky, 1984, and (d) Nesis, 1987.

appearance (Figs. 1b, 2). In distributing hydrostatic pressure loads from the last septum to internal septa, pillars constitute a major innovation in cephalopod shell architecture.

The site of failure in an imploding cuttlebone has been shown empirically to be the last septum (Ward and Boletzky, 1984). The effect of hydrostatic pressure on the ventral surface of the septum is thus the proper subject in a theoretical strength analysis of cuttlebones.

Given the critical role of the septum for supporting loads and of the pillars for transmitting loads, microscopic morphology is likely to be significant in determining cuttlebone strength. Engineering plate models show that both a thicker septum and a smaller distance between pillars produce a stronger cuttlebone. Measurements of septal thickness and pillar spacing were together expected to distinguish the cuttlebones of deep and shallow species. Here, I compare cuttlebone morphologies of 11 species of *Sepia* from a variety of geographical locales and habitat depths (Table 1). Maximum depths of specimens and species predicted from theoretical models are compared with species' maximum capture depths reported in the literature to test the reliability and sensitivity of the models. The results have implications for the precision of theoretical strength models in inferring the habitat depth of extinct cephalopods.

Materials and Methods

The 59 dried cuttlebones used in this study (Table 2) were from two collections housed at the University of Washington (Burke Museum and P. Ward, Dept. of Geological Sciences). Specimens had been collected from beaches in Australia, South Africa, and the Mediterranean. Like most cephalopods, cuttlefish die after reproducing, and their cuttlebones subsequently wash up on beaches. Specimens used were within the size range of adults for each species, so it is reasonable to assume that they were from mature animals. Species chosen for the study are frequently caught by fishing and research vessels, so their maximum capture depths are likely to be adequately sampled.

Confocal microscopy

A razor blade was used to cut 5-mm-wide cross-sections from the midventral region, at right angles to the septal surface. This procedure sampled the most recently grown 10 to 20 chambers.

Images were direct-scanned at slow speed with 10×, 20×, and 40× lenses on a Bio-rad confocal microscope (MRC 600), using neutral density 1 and number 1 filters and a BHS filter block. The cuttlebone's chitinous component autofluoresces in the laser, and because this component coats all internal surfaces, it accurately represents their dimensions. Micrographs (see Fig. 2), with image scale bars, were stored digitally. Chamber height (h), septal thickness (t), and half-distance between adjacent pillars (r) were measured using NIH Image 1.61. Scale bars were used to check the accuracy and precision of the measuring technique.

Inter-pillar radius (r) was measured at the middle of pillars rather than at their tops, since in most specimens it

Table 2

Specimen identification numbers for Sepia *cuttlebones used in this study*

	Sepia australis	*S. elegans*	*S. hieronis*	*S. orbignyana*	*S. rex*	*S. apama*	*S. latimanus*	*S. mestus*	*S. officinalis*	*S. papillata*	*S. vercoi*
Burke Museum Collection											
	95961c	95959	95968a	95955	95958a	95909a		95970a		95951	
	95961f		95968b	95960.8	95958b	95909b		95970b		95952	
	95961o		95968c	95960	95958d	95907b		95970c		95953	
	95961q			95960.9	95958e	95954		95970d		95954	
	95906			95960b	95958f	95910				95925b	
	95912			95960c	95972						
	95915			95960e	95973						
				95960g							
Ward Collection											
		KS0002	S27	K57		K2002	S21		S9		K1100
		KS0003	97-01			K1001	S31		S11		K1101
		KS0004	97-02				S32		S15		K1102
							S33				

was difficult to see the location of pillars as they contacted the septum. Only regions in sharp focus were measured. An average of 19 chambers were measured in each specimen, for a total of 1093 chambers. Septal thickness, chamber height, and multiple examples of inter-pillar spacing were measured for each chamber. Measurements within a chamber formed the basis for analyses at the specimen, species, and depth-group levels.

Maximum capture data

Data on species' maximum habitat depths come from fisheries and research captures of *Sepia* (Adam and Rees, 1966; Roeleveld, 1972; Ward and Boletzky, 1984; Nesis, 1987). Individual variation may cause the typical maximum depth to be overestimated for a species. However, maximum capture depth proves adequate to divide species into two depth groups— "deep" and "shallow" (see Table 1). Species with a shallow maximum capture depth (less than 200 m) live on the continental shelves, whereas those that have been captured at depths of 350 m and more live on the outer continental slope and bathyal regions (Roeleveld, 1972; Nesis, 1987), indicating that the division into deep and shallow categories reflects a difference in natural histories.

Macroscopic measurements

In the only previous study of cuttlebone strength, Ward and Boletzky (1984) suggested that a high radius of septal curvature and a small, narrow cuttlebone were characteristic of a deep habitat. To test this interpretation, I measured cuttlebone length, width, and thickness to the nearest millimeter with digital calipers. Length, relative width (width/length), and relative thickness (thickness/width; a proxy for septal radius of curvature) of deep and shallow species were compared using Kolmogorov-Smirnov tests. The same specimens were used for confocal microscopy and macroscopic measurements, except in *S. australis, S. orbignyana,* and *S. papillata*, where different but size-comparable specimens were used.

Sampling and statistics

The data were not normally distributed and could not be normalized using logarithmic or other transformations; thus medians were used as the measure of central tendency. Bootstrap resampling (1000 replicates) was used to obtain 95% confidence intervals, using the program Resampling Statistics (Sells Software Service). Specimen confidence intervals for the *r/t* ratio were similarly computed, for use in depth predictions.

The Kolmogorov-Smirnov test and the Mann-Whitney test were applied using StatView 5.0 (Abacus Concepts) to determine whether deep and shallow groups were significantly different in the variables measured. Because there were unequal numbers of observations, a random subsample of measurements was taken, corresponding to the smallest number of measurements obtained in a species. To obtain equal numbers of samples in the deep and shallow groups, more measurements were used from each of the five deep species than from the six shallow species.

Because the predicted depths were based on ratios taken from non-normal distributions, the nonparametric Kendall rank correlation coefficient was used to relate predicted depths of specimens and species to maximum capture data. This test is a conservative estimate of the degree of correlation in the data.

Modeling

Two models, a plate theory model (Timoshenko, 1940) and a square grid model (Hewitt and Westermann, 1986), were applied to estimate maximum depth from measured values of septal thickness (t) and pillar spacing (r), under different sets of assumptions.

Plate theory model (Fig. 3A)

The plate theory model assumes a rigid, thin, circular plate with fixed edges (zero-displacement, zero-moment, positive shear). The plate is assumed to be uniformly loaded perpendicular to its surface, which is equivalent to hydrostatic loading provided the plate does not deform significantly. Under these conditions, the highest stress occurs at the plate edge, where deformation is least because of intersection with the pillar below. The maximum stress, or pressure P_{max} in newtons per square meter, that can be withstood by the structure is expressed as:

$$P_{max} = 4/3\ s\ (r/t)^2 \qquad (1)$$

where s = tensile material strength in N/m^2
r = plate radius in m
t = plate thickness in m

Because s is unknown for cuttlebone, a measured value for *Nautilus* septum under tensile stress was used (78 MN/m^2; Currey, 1980). This may be an overestimate of strength because *Nautilus* septa are nacreous aragonite whereas cuttlebone septa are prismatic aragonite (Bandel and Boletzky, 1979). However, the two reported prismatic values (for the bivalves *Pinna muricata* and *Atrina vexillum*) were 62 and 60 MN/m^2, respectively (Currey, 1980). Thus using the values for nacreous cephalopod septa should overestimate the depth of cuttlebone implosion only slightly, if at all.

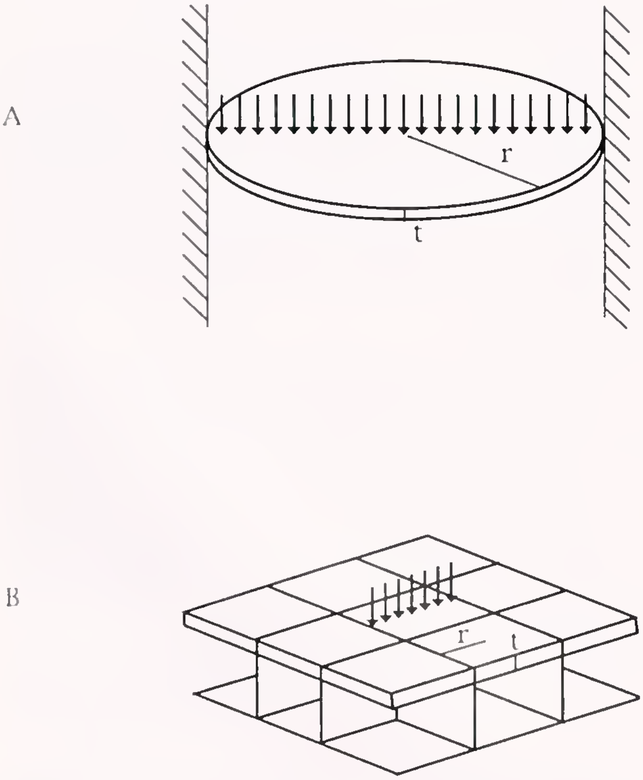

Figure 3. Illustration of the circular plate model (A) and square grid model (B), the latter after Hewitt and Westermann (1986).

Equation 1 can be rewritten to express P_{max} in terms of depth (each meter of depth underwater is equivalent to 1.015×10^4 N/m^2), using the value of 78 MN/m^2 for material strength.

$$\text{Meters depth}_{max} = 10246\ /\ (r/t)^2 \qquad (2)$$

Equation (2) was used to estimate maximum depth (*i.e.*, estimated implosion depth) using median values of r and t for each specimen and species.

Square grid model (Fig. 3B)

A model used by Hewitt and Westermann (1986, p. 58) to estimate the strength of ammonite septa is readily applicable to cuttlebones. Both the geometry of the model and the boundary conditions of support differ from the circular plate model. The square grid model assumes a flat square of shell simply supported on a rectangular suture grid: the flat square corresponds to the septum and the grid to the pillars. The plate is loaded uniformly. Because the plate's edges are not fixed, the maximum bending stress occurs in the center of the plate, and is given by:

$$b_{max} = 0.22\ P\ (2r/t)^2 \qquad (3)$$

where b_{max} = maximum bending stress in N/m^2
P = pressure in N/m^2
r = half-distance between grid members in m
t = plate thickness in m

This equation can be simplified, as for Equation (1), to express maximum implosion depth in meters underwater. The value of bending strength (b_{max}) given by Currey (1980) for *Nautilus* nacre is 193 MN/ m^2; the equation simplifies to:

$$\text{Meters depth}_{max} = 21900\ /\ (r/t)^2 \qquad (4)$$

An important difference between the square grid model and the circular plate model is that the former assumes simply supported edges, while the latter assumes the septum to be fused to the pillars. Values reported in Table 1 and Figure 5 are from the circular plate model, which more accurately represents cuttlebone morphology.

Safety margin

Implosion depth divided by maximum habitat depth gives the safety margin, an index of how close a structure comes to its ultimate strength limits during normal use. A safety margin can justifiably be applied to the cuttlebone because (1) it is static, in that it cannot be remodeled, and (2) the consequences of failure are sudden and usually fatal (Ward and Boletzky, 1984). Additionally, the stress on the cuttlebone is predictable, being simply a linear function of depth.

The concept of safety margins has been explored in living and extinct cephalopod shells (Denton, 1974; Ward *et al.*, 1980; Jacobs, 1992; Daniel *et al.*, 1997). Denton (1974) concludes that the safety margin is about 1.3 to 1.4 for the shells of living cephalopods. I assumed a safety factor of 1.33 for cuttlebones. Data reported as "predicted implosion depth" come directly from Equation 2; data reported as "predicted depth" are predicted implosion depths divided by 1.33.

Results

Microscopic measurements

Results of the Kolmogorov-Smirnov tests indicate that deep species had significantly thicker septa ($P < 0.0001$, $n = 276$, $\chi^2 = 99.8$), more closely spaced pillars ($P < 0.0001$, $n = 960$, $\chi^2 = 36.8$), and shorter chambers ($P < 0.0001$, $n = 252$, $\chi^2 = 10.7$) than did the shallow species, although there was some overlap. The ratio r/t (used in the plate theory analyses) was also significantly different between deep and shallow species ($P < 0.0001$, $n = 252$, $\chi^2 = 134.3$), as was septal density, t/h ($P < 0.0001$, $n = 252$, $\chi^2 = 77.8$). Mann-Whitney tests gave the same results, except for chamber height, which was not significantly different ($P > 0.2$, $U = 7254$). Table 3 presents species median values for these measurements with 95% confidence intervals.

Distributions of microscopic measurements were nearly all right-skewed, but differed qualitatively between deep and shallow species (Fig. 4). In shallow species, septal thickness (t) and septal density (t/h) measurements were smaller and had lower variance compared with deep species. In contrast, shallow species' chamber heights (h) and plate ratio (r/t) values had larger values and much larger variance. The plate ratio is minimized in deep species primarily by increased septal thickness (t), but deep species also showed a slight reduction in variance of pillar spacing (r).

Maximum depth calculations

Table 1 and Figure 5 show the estimated maximum depths of the 11 species and 59 specimens, along with actual maximum capture depths. For all species, maximum depths predicted by Equation (2) (divided by a safety factor of 1.33) were within an order of magnitude of known maximum capture depths, and the estimated values correlated significantly with the recorded data (Kendall rank correlation test, $P = 0.024$). In each species, the specimen with the

Table 3

Morphological measurements for Sepia *cuttlebones (species medians and bootstrapped 95% confidence intervals)*

Species	t (μm)	r (μm)	h (μm)	r/t	t/h %
Deep					
S. australis	5.5 ± 0.5	20.6 ± 0.9	144 ± 14	3.81 ± 0.28	3.8 ± 0.2
S. elegans	5.6 ± 1.23	34.2 ± 1.5	174 ± 14	5.41 ± 0.62	3.0 ± 0.2
S. hieronis	8.7 ± 0.6	42.2 ± 2.2	242 ± 17	4.81 ± 0.36	3.4 ± 0.3
S. orbignyana	7.4 ± 0.5	40.9 ± 1.9	246 ± 13	5.70 ± 0.27	3.0 ± 0.1
S. rex	5.1 ± 0.1	30.3 ± 1.6	138 ± 13	5.96 ± 0.43	3.7 ± 0.3
Mean*	6.88	34.2	192	5.43	3.85
Shallow					
S. apama	4.5 ± 0.4	40.3 ± 2.2	321 ± 13	9.33 ± 0.68	1.4 ± 0.1
S. latimanus	3.6 ± 0.3	38.0 ± 2.4	184 ± 29	11.23 ± 0.61	2.0 ± 0.4
S. mestus	2.7 ± 0.1	34.5 ± 2.9	91 ± 7	13.47 ± 1.53	3.0 ± 0.2
S. officinalis	4.2 ± 0.9	45.5 ± 12.3	259 ± 53	12.26 ± 1.24	1.5 ± 0.6
S. papillata	4.8 ± 0.2	43.1 ± 3.8	211 ± 17	10.09 ± 0.59	2.1 ± 0.3
S. vercoi	3.6 ± 0.2	30.8 ± 2.1	150 ± 32	8.41 ± 0.27	2.3 ± 0.3
Mean*	3.93	40.5	212	11.18	2.34
P values†	<0.0001	<0.0001	0.0094	<0.0001	<0.0001

Note that there is no overlap between deep and shallow species medians of septal thickness (t) and plate ratio (r/t), which are important factors in strength against implosion. Septal density (% t/h) shows almost no overlap, with deep species having higher values. Deep species also tend to have shorter chambers (h), although they overlap with shallow species. Medians for pillar spacing (r) are similar among species, but the shallow group has a strongly right-skewed distribution (see Fig. 3) at the level of chamber measurements, which leads to a significant difference from the deep species in this measurement as well.

* Means based on specimen measurements.

† *P* values from Kolmogorov-Smirnov tests of deep vs. shallow chamber measurements.

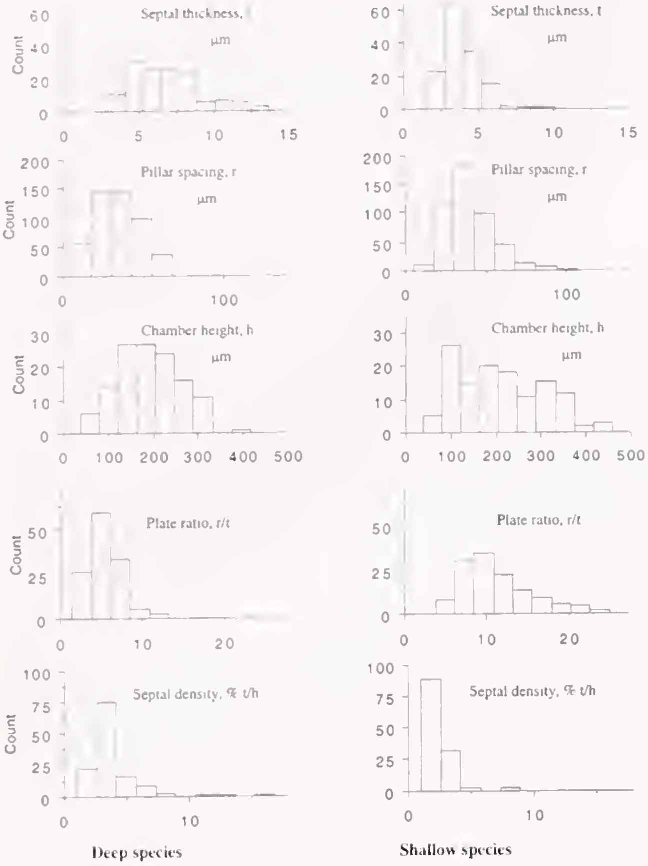

Figure 4. Histograms of deep and shallow groups for *t*, *r*, *h*, *r/t*, and % *t/h*. Compared to deep species, shallow species have thinner septa (*t*), a higher plate ratio (*r/t*), lower density of septal spacing (% *t/h*), and more right-skewed distributions for pillar spacing (*r*), chamber height (*h*), and plate ratio (*r/t*). Distributions for *r/t* differ more than those for *r* alone and *t* alone; this is because cuttlebone strength can be increased either by increasing *t* or by decreasing *r*, and deep species have used both strategies.

maximum predicted depth was also significantly correlated with the maximum capture depths for the species (P = 0.016).

For most species, variability in predicted depths among specimens was high (see Fig. 5). For example, predicted depths for specimens of *S. rex* ranged from 145 to 377 m, for *S. hieronis* from 130 to 855 m, and for *S. apama* from 68 to 195 m. However, no specimen of a shallow species had a predicted depth larger than 195 m, and within deep species, no specimen had a predicted depth shallower than 130 m. Deep species were more variable than shallow species, particularly the two with the deepest capture records (*S. australis* and *S. hieronis*).

Macroscopic measurements

Relative cuttlebone width (width/length) was greater in specimens of shallow species; the difference was significant at P = 0.0047 in a Kolmogorov-Smirnov test (n = 40 specimens). Relative thickness (thickness/width), an estimator of septal curvature, did not differ significantly ($P > 0.90$). Total length differed significantly among deep and shallow species ($P < 0.0001$), with deep specimens being uniformly small (45 to 102 mm) and shallow specimens either small or large (32 to 290 mm). Species averages and significance levels are summarized in Table 4.

When deep and shallow species were analyzed separately using the Kendall rank correlation test, neither specimen lengths nor relative widths were significantly correlated with r/t (length: for deep species, $P > 0.069$, $n = 18$, $Z = 1.82$; for shallow species, $P > 1.0$, $n = 18$, $Z = 1.0$; relative width: for deep species, $P = 0.45$, $n = 18$, $Z = -0.76$; for shallow species, $P > 1.0$, $n = 18$, $Z = 0.038$).

Discussion

The cuttlebones of deep and shallow species were readily distinguishable on the basis of microscopic measurements. In deep species, plate ratio (r/t) was consistently lower, and

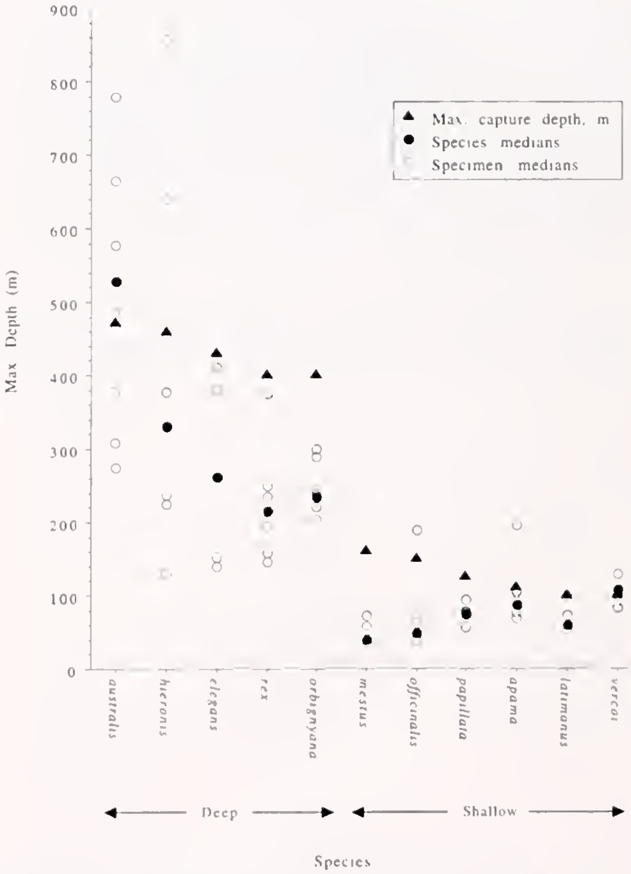

Figure 5. Estimated maximum capture depths of species and specimens (from *r/t* medians applied to Equation (2) and divided by a safety factor of 1.33), and species maximum capture depths (see Table 1). Deep species are more variable in estimated depths than are shallow species. In most species, maximal specimen estimates are close to maximum capture depths reported in the literature.

Table 4

Macroscopic cuttlebone measurements of Sepia *cuttlebones (species and depth category means from a total of 40 measured specimens)*

Species	Average length (mm)	Relative width (width/length)	Relative thickness (thickness/width)
Deep			
S. australis	50.6	0.32	0.24
S. elegans	53.1	0.27	0.31
S. hieronis	68.3	0.40	0.30
S. orbignyana	77.0	0.29	0.36
S. rex	86.8	0.34	0.27
Mean	69.6	0.32	0.30
Shallow			
S. apama	170.5	0.45	0.25
S. latimanus	254.5	0.33	0.38
S. mestus	80.4	0.44	0.18
S. officinalis	146.0	0.36	0.34
S. papillata	107.3	0.45	0.28
S. vercoi	32.0	0.25	0.36
Mean	158.5	0.41	0.28
P values*	<0.0001	0.0047	0.9000

Deep species were smaller than shallow species, and relatively narrower, although there was a good deal of overlap in the latter. Relative thickness (thickness/width), a proxy for septal radius of curvature, did not differ between deep and shallow species.

* *P* values from Kolmogorov-Smirnov tests of individual specimens.

septal thickness (t) and septal density (t/h) were consistently higher (see Table 3). Chamber height (h) was less characteristic of habitat depth, but tended to be lower in deep species. Note that septal thickness alone was not sufficient to account for strength differences: for example, *S. australis* had septa barely thicker than those found in several shallow species, yet lives at much greater depths.

Two of the measurements in combination, septal thickness and pillar spacing, were causally linked to cuttlebone strength on the basis of plate theory. Maximum predicted depths based on Equation (2) were, in most cases, well within the ranges reported for each species. Microscopic cuttlebone morphology was thus a reliable predictor of species' habitat depth in the 11 species studied.

Deep and shallow species were also distinct in the distribution of these measurements (see Fig. 4). Deep species had narrower distributions for plate ratio and chamber height, and shallow species had narrower distributions for septal thickness and septal density. This implies selective pressure for thinner septa and less dense cuttlebones in shallow species, and thicker septa and minimization of the plate ratio (r/t) in deep species.

Strength and depth estimates

Implosion depth, as opposed to maximum capture depth, is known within 50 m (Ward and Boletzky, 1984) for the three Mediterranean species: *S. officinalis* (200 m), *S. orbignyana* (550 m), and *S. elegans* (600 m). The largest predicted implosion depths (calculated directly from Equation 2) for specimens of these species were 252 m, 400 m, and 548 m, respectively; the 95% bootstrapped confidence intervals encompassed Ward and Boletzky's data.

In most species, estimated maximum depths were close to maximum capture depths (see Fig. 5). However, *S. mestus* and *S. orbignyana* had lower estimated implosion depths than their maximum capture depths would suggest. It may be that the maximum capture data for these species came from anomalous individuals. *S. hieronis* and *S. australis* present the opposite problem: estimates of strength in several specimens are much higher than capture records would imply. This may be because small changes in r/t lead to large changes in strength in the region of morphospace occupied by deep species (see Fig. 6). Given the problems of increased chamber flooding at greater depths in other cephalopods (Ward and Chamberlain, 1983), it would be surprising if these individuals actually lived as deep as their cuttlebone strength would allow. In any case, these discrepancies demonstrate the need for empirical data on intraspecific variation in capture depths and implosion depths.

Significance of within-species variation

Intraspecific variability in strength estimates was high, particularly in the deep species (Fig. 5). This may be largely due to the quadratic order of Equations (2) and (4) (Fig. 6), which means that for deep species slight changes in r/t cause large changes in strength.

The fact that the distribution of r/t was much narrower for deep species than shallow species (Fig. 4) suggests that selective pressure controls r/t in a region of morphospace where slight variations in r/t lead to large changes in strength. It may be that cuttlefish are depth-limited in an evolutionary sense not by an inability to grow stronger cuttlebones (for as Fig. 6 shows, very slight decreases in r/t lead to large increases in strength in deep species' morphospace), but by their inability to control variations in r/t tightly enough. The pillars of deep species tend to be aligned in long rows, which may reduce variation in r, whereas those of many shallow species are more random in orientation.

It is possible that cuttlebone growth is adaptively plastic with regard to strength. Chamber height is known to be influenced by aspects of the environment. Starvation causes cuttlefish to grow shorter chambers (Boletzky, 1974), and such cuttlebones are more resistant to implosion (Ward and Boletzky, 1984). Many species undertake seasonal depth migrations associated with growth and reproduction (*e.g., S. australis*, Roeleveld, 1972; *S. officinalis*, Boletzky, 1983). In *S. officinalis*, more closely spaced chambers are produced in the deeper winter habitat (Denton and Gilpin-Brown,

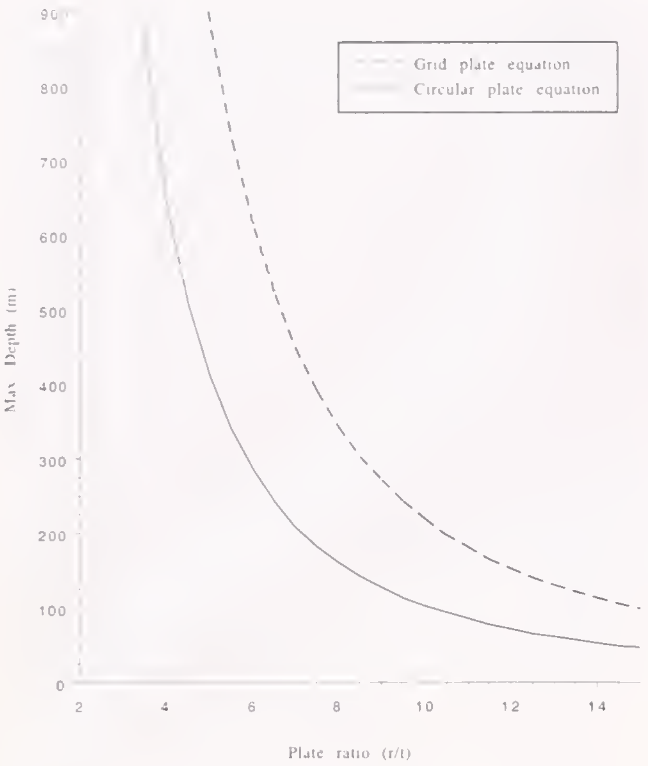

Figure 6. Comparison of predicted maximum depths based on *r/t* values for two models of cuttlebone strength (see Fig. 3). The curves could also be considered depth estimates based on different values of material strength. Predicted depths do not change greatly in the region of morphospace where shallow species are found ($r/t > 8$) but increase drastically in the morphospace of deep species ($r/t < 6$).

1961d, Hewitt and Stait, 1988). It is uncertain whether these changes are due to depth itself, or to slower growth associated with colder temperatures and reduced feeding, but it is likely to be a combination of both factors.

Other morphologies related to habitat depth

Cuttlebone strength imposes an absolute depth limit, but other aspects of cuttlefish functional morphology are likely to limit habitat depth as well. The cuttlebone faces an osmotic pumping limit: below about 240 m, the siphuncle probably cannot maintain an osmotic gradient to prevent cameral flooding. Reports by Denton and Gilpin-Brown (1961c) and Jacobs (1992) notwithstanding, this argument would appear to apply to *Sepia*, which has a very large siphuncular region. This limit can, however, be surpassed for short periods of time. Even the deep *Sepia* species seem to spend most of their time at the shallower part of their depth range (Roeleveld, 1972), perhaps due to the increasing difficulty of preventing flooding of the cuttlebone at greater depths.

Ward and Boletzky (1984) suggested that a short, narrow cuttlebone, a high radius of septal curvature, and a high density of septal spacing were key features associated with a deeper habitat. In the current study, shallow species had longer and relatively wider cuttlebones than deep species (Table 4). The ratio of cuttlebone thickness to width (a proxy for radius of septal curvature) did not differ significantly. Septal density was significantly higher among deep species. However, this metric combines two morphologies, septal thickness and chamber height, which influence strength in different ways. A thicker septum increases strength, whereas a taller chamber lessens it by affecting the pillars' buckling load.

Why might morphologies not directly related to strength, such as cuttlebone length and relative width, nevertheless correlate with maximum habitat depth? One possibility is that growth rate is limited by depth. Shell volume must increase at the same rate as body volume to maintain neutral buoyancy. In *Nautilus*, growth rate is limited by the rate at which chambers can be emptied, which is reduced at greater habitat depths (Ward and Chamberlain, 1983). Depth-based limitations to growth rate may account for the observations that deep species of *Sepia* generally have small cuttlebones, whereas shallow species in the genus can have either small or large ones (P. Ward, University of Washington, unpubl. data).

Limitations to modeling structural strength from morphology

Sources of error in strength estimates include (1) error in assignment of morphological parameters, (2) simplification of morphology, (3) error in material strength estimate, and (4) disregard for the effects of pillar strength. Nevertheless, the model is fairly robust to error in the range of *r/t* values observed in cuttlebones (Fig. 6). The fact that two models with different boundary conditions nevertheless give similar and biologically reasonable results also suggests that the estimates for r and t were adequate.

Median values of inter-pillar distance (r) and septal thickness (t) were used to characterize specimens and species, thus obscuring individual and intraspecific variability. Modeling the septum as a flat circular or square plate neglected the fact that regions of unsupported septum are irregular in shape. The septum thickens where it contacts the pillars, which should increase strength beyond the current estimates.

In both models the material strength term is uncertain. Although cuttlebones are composed of prismatic aragonite, a measured value for *Nautilus* nacre was used because it, too, functions in resisting implosion. The value reported for prismatic bivalve shell was only 20% lower (Currey, 1980), so it would not have greatly changed strength estimates. Cuttlebone material strength and implosion pressures were not measured directly because specimens were dry and of varying history. Microcracks and other damage occurs to an unknown degree, and bending and crushing tests do not provide reliable data under these conditions (Jacobs, 1992). The only fresh specimens readily available are aquacultured *S. officinalis*, and cuttlebones of captive-raised *Sepia* tend to grow abnormally (pers. obs.). Finally, because individual components of the cuttlebone are minute and cutting a sample would probably create microcracks, assessing material strength using a three-point bending test is impractical even with a fresh specimen.

The complex shapes of pillars make them intractable for theoretical analysis, but some qualitative points may be made. Pillar buckling becomes increasingly likely with greater chamber height. In shallow species (which tend to have taller chambers), the pillars are both thinner and more extensively folded than in the deeper species; the latter feature increases structural rigidity. In the current analysis, pillar strength is not addressed: I simply assumed that pillars and septa are equally strong. This is likely to be the case, since the cost incurred for including excess material in a buoyancy device is significant, and strength is limited by the weaker member in the structure.

Conclusion

The cuttlebone is an impressive feat of evolutionary design. Even cuttlebones of shallow species are strong enough to withstand 10 or more atmospheres of pressure. The deep species are caught between the Scylla and Charybdis of strength and buoyancy requirements, and hampered by the major consequences for strength of slight variations in plate ratio morphology. The cuttlebones of *S. australis* and *S. hieronis* may have become as strong as minor tinkering with morphology will permit. Even *Spirula* is limited to depths of 1200 to 1800 m, and its small size may be a result of depth-related limits to chamber emptying rate and hence growth rate. Ironically, only by eschewing the chambered shell altogether, as octopuses and squids have done, can cephalopods invade truly bathyal depths.

The success of the modeling approach at predicting maximum depths in these 11 species of *Sepia* bodes well for its use with extinct forms. Nevertheless, the degree of resolution such a model can achieve needs to be established. Does the variability in the specimen data correspond to variability in strength, or does it reflect the limitations of the modeling method? The current study demonstrates that theoretical strength models can distinguish shallow-water species from those that live several hundred meters deep.

The phragmocone of cephalopods is a buoyancy system that works best, in terms of both strength and emptying capability, in shallow water. This perception has been obscured by the fact that *Nautilus*, the best-known chambered cephalopod, lives at depths of 200 m and greater, essentially in a refugium. *Sepia* may well be a modern-day analog of ammonites in ecology and evolutionary pattern as well as in mode of buoyancy control.

Acknowledgments

I thank P. Ward for use of his cuttlebone collection and R. Collin, T. Daniel, A. Kohn, M. LaBarbera, R. Price, and P. Ward for discussion and comments on drafts of this work. I thank Friday Harbor Laboratories for use of confocal and scanning electron microscopes. This research was conducted in partial fulfillment of a Master of Science degree at the University of Washington, and was supported by a National Science Foundation pre-doctoral research fellowship and a grant from the Stephens Fund of the Department of Geological Sciences, University of Washington.

Literature Cited

Adam, W., and W. Rees. 1966. A review of the cephalopod family Sepiidae. *The John Murray Expedition, Scientific Reports*, **11**, 165 pp.

Bandel, K., and S. v. Boletzky. 1979. A comparative study of the structure, development, and morphological relationships of chambered cephalopod shells. *Veliger* **21**: 313-354.

Birchall, J. D., and N. L. Thomas. 1983. On the architecture and function of cuttlefish bone. *J. Mat. Sci.* **18**: 2081-2086.

Boletzky, S. v. 1974. Effets de la sous-nutrition prolongee sur le developpement de la coquille de *Sepia officinalis* L. (Mollusca: Cephalopoda). *Bull. Soc. Zool. Fr.* **99**: 667-673.

Boletzky, S. v. 1983. *Sepia officinalis*. Pp. 31-52 in *Cephalopod Life Cycles, Vol. I, Species Accounts*, P. R. Boyle, ed. Academic Press, London.

Currey, J. D. 1980. Mechanical properties of mollusk shell. Pp. 75-98 in *The Mechanical Properties of Biological Materials. Symp. Soc. Exp. Biol.* **34**.

Daniel, T., B. Helmuth, B. Saunders, and P. D. Ward. 1997. Septal complexity in ammonoid cephalopods increased mechanical risk and limited depth. *Paleobiology* **23**(4): 470-481.

Denton, E. J. 1971. Further observations on the buoyancy of *Spirula*. *J. Mar. Biol. Assoc. UK* **51**: 363-373.

Denton, E. J. 1974. On the buoyancy and lives of modern and fossil cephalopods. *Proc. R. Soc. Lond. B.* **185**: 273-299.

Denton, E. J., and J. B. Gilpin-Brown. 1961a. The buoyancy of the cuttlefish *Sepia officinalis*. *J. Mar. Biol. Assoc. UK* **41**: 319-342.

Denton, E. J., and J. B. Gilpin-Brown. 1961b. The osmotic mechanism of the cuttlebone. *J. Mar. Biol. Assoc. UK* **41**: 351-364.

Denton, E. J., and J. B. Gilpin-Brown. 1961c. The effect of light on the buoyancy of the cuttlefish. *J. Mar. Biol. Assoc. UK* **41**: 343-50.

Denton, E. J., and J. B. Gilpin-Brown. 1961d. The distribution of gas and liquid within the cuttlebone. *J. Mar. Biol. Assoc. UK* **41**: 365-381.

Hewitt, R. A., and B. Stait. 1988. Seasonal variation in septal spacing of *Sepia officinalis* and some Ordovician actinocerid nautiloids. *Lethaia* **21**: 383-394.

Hewitt, R. A., and G. E. G. Westermann. 1986. Function of complexly fluted septa in ammonoid shells I. Mechanical principles and functional models. *Neues Jahrb. Geol. Palaeontol.* **172**: 47-69.

Hewitt, R. A., and G. E. G. Westermann. 1987. *Nautilus* shell architecture. Pp. 435-461 in Nautilus: *the Biology and Paleobiology of a Living Fossil*, W. B. Saunders and N. H. Landman, eds. Pleoum Press, New York.

Jacobs, D. K. 1990. Sutural pattern and shell stress in *Baculites* with implications for other cephalopod shell morphologies. *Paleobiology* **16** (3): 336-348.

Jacobs, D. K. 1992. The support of hydrostatic load in cephalopod shells: adaptive and ontogenetic explanations of shell form and evolution from Hooke 1695 to the present. *Evol. Biol.* **26**: 287-349.

Nesis, K. N. 1987. *Cephalopods of the World.* T. H. F. Publications, Neptune City, NJ.

Raup, D. M., and T. Takahashi. 1966. Experiments on strength of cephalopod shells. *Geol. Soc. Am. Spec. Pap.* **101**: 172-173.

Roeleveld, M. A. 1972. A review of the Sepiidae (Cephalopoda) of Southern Africa. *Ann. S. Afr. Mus.* **59** (10): 313 pp.

Timoshenko, D. 1940. *Theory of Plates and Shells.* McGraw-Hill, New York.

Ward, P. 1987. *The Natural History of the Nautilus.* Allen and Unwin, Boston.

Ward, P., and S. v. Boletzky. 1984. Shell implosion depth and implosion morphologies in three species of *Sepia* (Cephalopoda) from the Mediterranean Sea. *J. Mar. Biol. Assoc. UK* **64**: 955-966.

Ward, P., and J. Chamberlain. 1983. Radiographic observation of chamber formation in *Nautilus pompilius*. *Nature* **304**: 57-59.

Ward, P., L. Greenwald, and F. Rougerie. 1980. Shell implosion depth for living *Nautilus macromphalus* and shell strength of extinct cephalopods. *Lethaia* **13**: 182.

Westermann, G. E. G. 1973. Strength of concave septa and depth limits of fossil cephalopods. *Lethaia* **6**: 383-403.

Westermann, G. E. G. 1975. Model for origin, function and fabrication of fluted cephalopod septa. *Palaeontol. Z.* **49**: 235-253.

INDEX

A

A dynamical model of communities and a new species-abundance distribution, 152
A morphological study of nonrandom senescence in a colonial urochordate, 367
Accessory boring organ, 272
Activated defenses, 225
Activity imaging, 1
Adhesive organ, 34
Advection, 168
Aging, 367
Algae, 254
Amino acid, 168
Anatomy, 121
Animal behavior, 203
Antarctic sponge, 29
Antennulary sensor, 213
Antic, Srdjan, see Michal Zochowski, 1
Apical sensory organ, 67
Aplacophora, 121
Apoptosis, 367
Arillo, Attilio, see Giorgio Bavestrello, 29
Ascidia, 22
Ascidian, 22, 26, 367
Aspidodiadema, 387
Attractant, 168

B

Bavestrello, Giorgio, Attilio Arillo, Barbara Calcinai, Riccardo Cattaneo-Vietti, Carlo Cerrano, Elda Gaino, Antonella Penna, and Michele Sarà, Parasitic diatoms inside Antarctic sponges, 29
Behavior, animal, 203
Benthoctopus, 94
Bentis, Christopher J., Les Kaufman, and Stjepko Golubic, Endolithic fungi in reef-building corals (Order: Scleractinia) are common, cosmopolitan, and potentially pathogenic, 254
Biomechanics, 88
Botryllus schlosseri, 367
Boudko, Dimitri Y., see Michael J. Hadfield, 67
Boundary layers, 188
Brain activity, 1
Bryozoan, 346
Buccinum undatum, 261
Buoyancy, 284
Butman, Cheryl Ann, see Richard K. Zimmer, 168
Byrne, M., see P. Selvakumaraswamy, 379

C

Calcinai, Barbara, see Giorgio Bavestrello, 29
Carson, David G., see Jane E. Williamson, 332
Cascadia Basin, 94
Castration, 261
Catecholamines, 319
Catecholamines modulate metamorphosis in the opisthobranch gastropod *Phestilla sibogae*, 319
Cattaneo-Vietti, Riccardo, see Giorgio Bavestrello, 29
Cellular growth of host and symbiont in a cnidarian-zooxanthellar symbiosis, 110
Cephalopod, 284, 404
Cerrano, Carlo, see Giorgio Bavestrello, 29
Chemical Communication in Ecology Symposium, 167
Chemical
  cue, 168
  defense, 168
  ecology, 168
  signaling, 225
Chemical signaling processes in the marine environment, 168
Chemoreception, 168
Chemosensory behavior, 188
Chemotaxis, 168
Cherax destructor, 307
Childress, James J., see Brad A. Seibel, 284
Citrate synthase, 284
Cladistics, 121
Clelland, Eric S., and A. S. M. Saleuddin, Vacuolar-type ATPase in the accessory boring organ of *Nucella lamellosa* (Gmelin) (Mollusca: Gastropoda): role in shell penetration, 272
Cnidarian, 110
Cohen, Lawrence C., see Michal Zochowski, 1
Compartmentation, 225
Competition, 22
Concepts in Imaging and Microscopy: Imaging membrane potential with voltage-sensitive dyes, 1
Cone, 254
Copepod, 213
Copulatory spicules, 121
Coral, 254
Crayfish, 307
Croll, Roger P., see Anthony Pires, 319
Cuttlebone morphology limits habitat depth in eleven species of *Sepia* (Cephalopoda: Sepiidae), 404
Cuttlefish, 404
Cuvierian tubule, 34

D

De Nys, Rocky, see Jane E. Williamson, 332
Deep-sea, 284
Delisea pulchra, 332
Deterrent, 168
Development
  echinoid, 387
  larval, 379
Dewdney, A. K., A dynamical model of communities and a new species-abundance distribution, 152
Diatom, 29
Diffusion, 188, 213
Dillaman, R. M., see C. S. Sikes, 50
Dimethyl sulfide, 245
Dinoflagellate, symbiotic, 110
Discrimination and phylogeny of solenogaster species through the morphology of hard parts (Mollusca, Aplacophora, Neomeniomorpha), 121

E

Echinodermata, 34, 88
Echinoid, 88, 332, 387
Ecological release, 396
Ecology, 22

Ecology and evolution, 152
Egg brooding by deep-sea octopuses in the North Pacific Ocean, 94
Egg care, 94
Elemental carbon and nitrogen, 346
Endolith, 254
Endolithic fungi in reef-building corals (Order: Scleractinia) are common, cosmopolitan, and potentially pathogenic, 254
Energetics, 346
Energetics of larval swimming and metamorphosis in four species of *Bugula* (Bryozoa), 346
Epidermal spicules, 121
Ereskovsky, Alexander V., Reproduction cycles and strategies of the cold-water sponges *Halisarca dujardini* (Demospongiae, Halisarcida), *Myxilla incrustans* and *Iophon piceus* (Demospongiae, Poecilosclerida) from the White Sea, 77
Escape behavior, 307
Evolution, 299, 379

F

Falk, Chun X., see Michal Zochowski, 1
Fast imaging, 1
Feeding, selective, 225
Fertilization, 22
Filamentous fungi associated with holothurians from the Sea of Japan, off the Primorye Coast of Russia, 101
Fitt, William K., Cellular growth of host and symbiont in a cnidarian-zooxanthellar symbiosis, 110
Flammang, Patrick, see Didier VandenSpiegel, 34
Fluid dynamics, 188
Flume, 168
Foraging, 245
Freshwater shrimp, 357
Functional morphology, 88, 404
Fungi, 101, 254
  marine facultative and obligatory, 101
  resistance of holothurian glycosides, 101

G

Gaino, Elda, see Giorgio Bavestrello, 29
Gastropoda, 272, 319
Genetic diversity of oceanic island *Lasaea* (Mollusca: Bivalvia) lineages exceeds that of continental populations in the northwestern Atlantic, 396
George, Sophie B., see Craig M. Young, 387
Germ-cell warfare in ascidians: sperm from one species can interfere with the fertilization of a second, 22
Giant
  fibers, 307
  squid, 284
GnRH neurons, 26
Golubic, Stjepko, see Christopher J. Bentis, 254
Graneledone, 94
Grehan, Anthony, see Janet R. Voight, 94

H

Habituation, 307
Hadfield, Michael G., see Anthony Pires, 319
Hadfield, Michael J., Ella A. Meleshkevitch, and Dmitri Y. Boudko, The apical sensory organ of a gastropod veliger is a receptor for settlement cues, 67
Himmelman, John H., see Françoise Tétreault, 261
Hochberg, Rick, and Marianne K. Litvaitis, Phylogeny of Gastrotricha: a morphology-based framework of gastrotrich relationships, 299
Holopneustes purpurascens, 332
Holothurian, 34, 101
Homarus americanus, 307
Hybridization, 22
Hydrodynamic, 168

I

Impact of a castrating trematode, *Neophasis* sp., on the common whelk, *Buccinum undatum*, in the northern Gulf of St. Lawrence, 261
Importance of chemical communication in ecology, 167
Inducer, 332
Induction of metamorphosis in the sea urchin *Holopneustes purpurascens* by a metabolite complex from the algal host *Delisea pulchra*, 332
Inertial force, 213
Interspecific, 22
Intracellular
  calcium, 357
  recording, 26

J

Jackson, D. J., and D. L. Macmillan, Tailflick escape behavior in larval and juvenile lobsters (*Homarus americanus*) and crayfish (*Cherax destructor*), 307
Jangoux, Michel, see Didier VandenSpiegel, 34
Johnson, Amy S., see Holly A. Leddy, 88
Johnston Atoll, 254

K

Kaufman, Les, see Christopher J. Bentis, 254
Kolmogorov scale, 213
Kumar, Naresh, see Jane E. Williamson, 332

L

Lam, Ying-Wan, see Michal Zochowski, 1
Lambert, Charles C., Germ-cell warfare in ascidians: sperm from one species can interfere with the fertilization of a second, 22
Larva, 168, 307, 319, 346
  deep-sea, 387
  settlement, 67
Larval development of the tropical deep-sea echinoid *Aspidodiadema jacobyi*: phylogenetic implications, 387
Lasaea, 396
Lauzon, Robert J., Baruch Rinkevich, C. W. Patton, and Irving L. Weissman, A morphological study of nonrandom senescence in a colonial urochordate, 367
Lecithotrophy, 379
Leddy, Holly A., and Amy S. Johnson, Walking *versus* breathing: mechanical differentiation of sea urchin podia corresponds to functional specialization, 88
Life in transition: balancing inertial and viscous forces by planktonic copepods, 213
Light, 26, 284
Light-limitation on predator-prey interactions: consequences for metabolism and locomotion of deep-sea cephalopods, 284
Light-sensitive voltage responses in the neurons of the cerebral ganglion of *Ciona savignyi* (Chordata: Ascidiacea), 26
Litvaitis Marianne K., see Rick Hochberg, 299
Lobster, 307
Locomotion, 284

M

Macmillan, D. L., see D. J. Jackson, 307
Macrobrachium, 357
Maintaining the line of defense: regeneration of Cuvierian tubules in the sea cucumber *Holothuria forskali* (Echinodermata, Holothuroidea), 34
Marine ecology, 168
McNamara, John C., and Márcia R. Ribeiro, The calcium dependence of pigment translocation in freshwater shrimp red ovarian chromatophores, 357
Measures, Lena, see Françoise Tétreault, 261
Mechanisms of animal navigation in odor plumes, 203
Mechanoreception, 213

Meleshkevitch, Ella A., see Michael J. Hadfield, 67
Metabolism, 284
Metamorphic induction, 67
Metamorphosis, 319, 332, 346
Microbial food web, 225
Migration, vertical, 284
Mingan Islands, 261
Mitochondria, 396
Mollusc, 121, 396
Mount, A. S., see C. S. Sikes, 50
Mycelial fungi, 101

N

Navigation, 168, 188, 203
Neophasis, 261
Neuron, 26
Nevitt, Gabrielle A., Olfactory foraging by Antarctic procellariiform seabirds: life at high Reynolds numbers, 245
Nucella, 272
Nucleation and growth of calcite on native *versus* pyrolyzed oyster shell folia, 50

O

Ó Foighil, Diarmaid, see Joong-Ki Park, 396
Oceanic island, 396
Octopine dehydrogenase, 284
Octopodidae, 94
Octopus predation, 94
Odor plume, 168, 188, 203
Oka, Yoshitaka, see Hidekazu Tsutsui, 26
Olfaction, 168, 188, 203, 245
Olfactory foraging by Antarctic procellariiform seabirds: life at high Reynolds numbers, 245
Ophiuroid, 379
Optical recording, 1
Orientation, 188, 203
Ostreobium, 254

P

Parasitic diatoms inside Antarctic sponges, 29
Parasitism, 29
Park, Joong-Ki, and Diarmaid Ó Foighil, Genetic diversity of oceanic island *Lasaea* (Mollusca: Bivalvia) lineages exceeds that of continental populations in the northwestern Atlantic, 396
Pathogen, 254
Patton, C. W., see Robert J. Lauzon, 367
Peclet number, 213
Penna, Antonella, see Giorgio Bavestrello, 29
Peptide, 168
Petrel, 245
Phallosia, 22
Pheromone, 168
Phragmocone, 404
Phylogeny
  echinoderm, 387
  gastrotrich, 299
Phylogeny of Gastrotricha: a morphology-based framework of gastrotrich relationships, 299
Phylogeography, 396
Pigment translocation, 357
Pires, Anthony, Roger P. Croll, and Michael G. Hadfield, Catecholamines modulate metamorphosis in the opisthobranch gastropod *Phestilla sibogae*, 319
Pivkin, Michael V., Filamentous fungi associated with holothurians from the Sea of Japan, off the Primorye Coast of Russia, 101
Plume, 188, 203
Podia, 88
Predation, 94, 168
Predator-prey, 284
Procellariiform seabirds, 245
Protists, 225

R

Radula, 121
Red alga, 332
Red chromatophores, 357
Red pigment concentrating hormone, 357
Regeneration, 34
Reproduction, 77
Reproduction cycles and strategies of the cold-water sponges *Halisarca dujardini* (Demospongiae, Halisarcida), *Myxilla incrustans* and *Iophon piceus* (Demospongiae, Poecilosclerida) from the White Sea, 77
Reproduction strategies, 77
Reynolds number, 188, 213
Ribeiro, Márcia R., see John C. McNamara, 357
Rinkevich, Baruch, see Robert J. Lauzon, 367

S

Saleuddin, A. S. M., see Eric S. Clelland, 272
Sará, Michele, see Giorgio Bavestrello, 29
Scaling, 284
Schander, Christoffer, see Amélie Scheltema, 121
Scheltema, Amélie H., and Christoffer Schander, Discrimination and phylogeny of solenogaster species through the morphology of hard parts (Mollusca, Aplacophora, Neomeniomorpha), 121
Sea cucumber, 34
Seibel, Brad A., Erik V. Thuesen, and James J. Childress, Light-limitation on predator-prey interactions: consequences for metabolism and locomotion of deep-sea cephalopods, 284
Selvakumaraswamy, P., and M. Byrne, Vestigial ophiopluteal structures in the lecithotrophic larvae of *Ophionereis schayeri* (Ophiuroidea), 379
Senescence, 367
Sensory ecology, 168
Settlement, 67, 168, 332
Sherrard, Kristin M., Cuttlebone morphology limits habitat depth in eleven species of *Sepia* (Cephalopoda: Sepiidae), 404
Signal, 168
  mechanisms, 225
  transduction, 357
Sikes, C. S., A. P. Wheeler, A. Wierzbicki, A. S. Mount, and R. M. Dillaman, Nucleation and growth of calcite on native *versus* pyrolyzed oyster shell folia, 50
Soluble cue, 332
Species diversity, 101
Sperm competition, 22
Spicules
  copulatory, 121
  epidermal, 121
Sponge, 29, 77
Steinberg, Peter D., see Jane E. Williamson, 332
Stimulus, 168
Symbiosis, 29, 110
Symbiotic dinoflagellate, 110

T

Tailflick, 307
Tailflick escape behavior in larval and juvenile lobsters *(Homarus americanus)* and crayfish *(Cherax destructor)*, 307
Tétreault, Françoise, John H. Himmelman, and Lena Measures, Impact of a castrating trematode, *Neophasis* sp., on the common whelk, *Buccinum undatum*, in the northern Gulf of St. Lawrence, 261
The apical sensory organ of a gastropod veliger is a receptor for settlement cues, 67
The calcium dependence of pigment translocation in freshwater shrimp red ovarian chromatophores, 357
The chemical defense ecology of marine unicellular plankton: constraints, mechanisms, and impacts, 225

The fluid dynamical context of chemosensory behavior, 188
Thuesen, Erik V., see Brad A. Seibel, 284
Trematode, 261
Triterpene glycosides, 101
Trophic interaction, 225
Tsutsui, Hidekazu, and Yoshitaka Oka, Light-sensitive voltage responses in the neurons of the cerebral ganglion of *Ciona savignyi* (Chordata: Ascidiacea), 26
Tube feet, 88
Tunicate, 22
Turbulence, 168, 188, 213

U

Urochordate, 367

V

V-ATPase, 272
Vacuolar-type ATPase , 272
Vacuolar-type ATPase in the accessory boring organ of *Nucella lamellosa* (Gmelin) (Mollusca: Gastropoda): role in shell penetration, 272
Vandenspiegel, Didier, Michel Jangoux, and Patrick Flammang, Maintaining the line of defense: regeneration of Cuvierian tubules in the sea cucumber *Holothuria forskali* (Echinodermata, Holothuroidea), 34
Veliger larva, 67, 319
Vertical migration, 284
Vestigial ophiopluteal structures in the lecithotrophic larvae of *Ophionereis schayeri* (Ophiuroidea), 379
Vickers, Neil J., Mechanisms of animal navigation in odor plumes, 203
Viscous forces, 213
Voight, Janet R., and Anthony Grehan, Egg brooding by deep-sea octopuses in the North Pacific Ocean, 94
Voltage response, 26
Voltage sensitive dyes, 1

W

Wachowiak, Matt, see Michal Zochowski, 1
Walking *versus* breathing: mechanical differentiation of sea urchin podia corresponds to functional specialization, 88
Weissburg, Marc J., The fluid dynamical context of chemosensory behavior, 188
Weissman, Irving L., see Robert J. Lauzon, 367
Wendt, Dean E., Energetics of larval swimming and metamorphosis in four species of *Bugula* (Bryozoa), 346
Wheeler, A. P., see C. S. Sikes, 50
Whelk, 261
Wierzbicki, A., see C. S. Sikes, 50
Williamson, Jane E., Rocky De Nys, Naresh Kumar, David G. Carson, and Peter D. Steinberg, Induction of metamorphosis in the sea urchin *Holopneustes purpurascens* by a metabolite complex from the algal host *Delisea pulchra*, 332
Wolfe, Gordon V., The chemical defense ecology of marine unicellular plankton: constraints, mechanisms, and impacts, 225

Y

Yen, Jeannette, Life in transition: balancing inertial and viscous forces by planktonic copepods, 213
Young, Craig M., and Sophie B. George, Larval development of the tropical deep-sea echinoid *Aspidodiadema jacobyi*: phylogenetic implications, 387

Z

Zecevic, Dejan, see Michal Zochowski, 1
Zimmer, Richard K., and Cheryl Ann Butman, Chemical signaling processes in the marine environment, 168
Zimmer, Richard K., Importance of chemical communication in ecology, 167
Zochowski, Michal, Matt Wachowiak, Chun X. Falk, Lawrence B. Cohen, Ying-Wan Lam, Srdjan Antic, and Dejan Zecevic, Concepts in Imaging and Microscopy: Imaging membrane potential with voltage-sensitive dyes, 1
Zooplankton, 284
Zooxanthellae, 110

Instructions for Submitting Digital Art

The Biological Bulletin will accept figures submitted in electronic form; however, digital art must conform to the following guidelines. Contact the editorial office for further information.

Format. Acceptable graphic formats are TIFF and EPS. Color submissions must be in EPS format, saved in CMKY mode.

Software. Preferred software is Adobe Illustrator or Adobe Photoshop for the Mac and Adobe Photoshop for Windows. Specific instructions for artwork created with varoius software programs are available on the Web at the Digital Art Information Site maintained by Cadmus Professional Communications at
http://cjs.cadmus.com/da/home.html

Resolution. The minimum requirements for resolution are 1200 DPI for line art and 300 for halftones.

Size. All digital artwork must be submitted at its acutal printed size so that no scaling is necessary.

Multipanel figures. Figures consisting of individual parts (*e.g.*, panels A, B, C) must be assembled into final format and submitted as one file.

Hard copy. Files must be accompanied by hard copy for use in case the electronic version is unusable.

Disk identification. Disks must be clearly labeled with the following information: author name and manuscript number; format (PC or Macintosh); name and version of software used.

Authors who create digital images are wholly responsible for the quality of their material, including color and halftone accuracy. *The Bulletin* will use authors' digital art as submitted, and will not alter the digital files in any way.

40 THE AMERICAN SOCIETY FOR CELL BIOLOGY

40TH ANNUAL MEETING

December 9-13, 2000

Moscone Convention Center, San Francisco

KEYNOTE SYMPOSIUM

The ASCB: 40 Years Leading the Revolution in Cell Biology

Saturday, Dec. 9, 6:00 p.m.

J. Michael Bishop, Michael S. Brown, Joseph L. Goldstein

The Mechanism of Protein Synthesis
Alan Hinnebusch, Harry F. Noller, Jr., Nahum Sonenberg

Novel Dimensions of Cell Motility
Marie-France Carlier, Thomas M. Roberts, H. Lee Sweeney

Chromosome Dynamics
Douglas E. Koshland, Victoria Lundblad, Daphne Preuss

Determination of Left-Right Asymmetry
Daniel Constam, Nobutaka Hirokawa, Elizabeth Robertson

Pathogen Recognition and Host Defense
Barbara Baker, Pamela Bjorkman, Ruslan M. Medzhitov

Cellular Organization at the Synapse
Mary Kennedy, Joshua R. Sanes, Morgan Sheng

Biological Clocks
Steve Kay, Ann Rougvie, Joseph S. Takahashi

Chemical Approaches to Biological Problems
Daniel E. Kahne, Jeff Kelly, Laura Kiessling

Plus six Minisymposia each afternoon, Award lectures, and workshops and sessions on careers, education, grantsmanship, public policy and issues of special interest to minorities and women

For more information, contact us at www.ascb.org/ascb, 301-530-7153 or ascbinfo@ascb.org

DIRECTOR

MARINE BIOLOGICAL LABORATORY
WOODS HOLE, MASSACHUSETTS

The Marine Biological Laboratory invites applications and nominations for the position of Director, who will serve as the chief operating officer and chief executive officer of the Corporation. Established in 1888, the MBL is a non-profit, independent institution devoted to research and education in the life sciences. It hosts more than 1200 students and scientists from around the world during the summer and has a year round staff of approximately 250. In consultation with the Board of Trustees, the Director is responsible for the scientific direction of the Laboratory, development and implementation of institutional policies, establishment of fund-raising priorities, general supervision of the Laboratory, and control of business of the Corporation. Candidates should have a strong record of scientific leadership, successful administrative experience and demonstrated ability to form consensus among people with different perspectives and to lead them in achieving policy objectives. Initial appointment will be made for a 5 year term. Please address expression of interest accompanied by resume to:

Dr. Sheldon J. Segal
Chair, Search Committee
Marine Biological Laboratory
Woods Hole, MA 02543
email: search@mbl.edu

Preference will be given to resumes received prior to July 1, 2000.

The MBL is an Affirmative Action/Equal Opportunity/Non-smoking Workplace.

583 74

The Ultimate Deconvolution Machine.

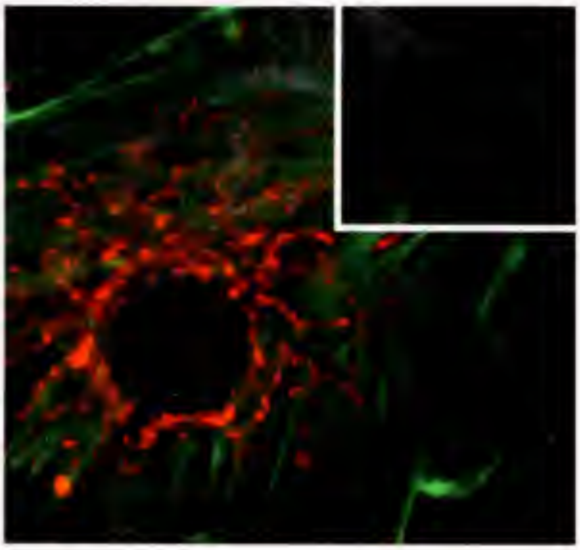

Original Widefield Image.

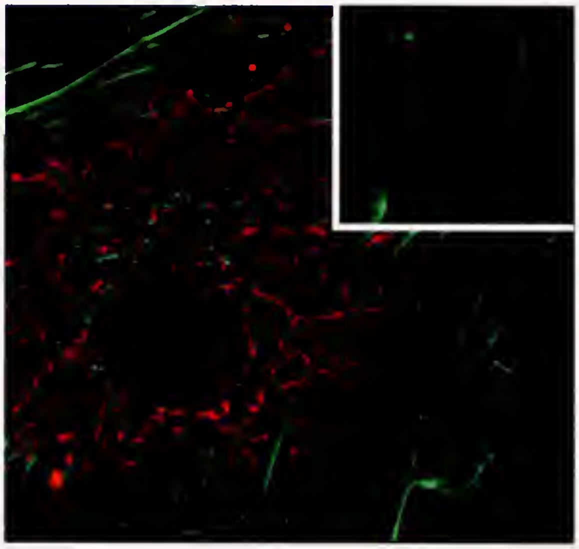

Iterative DCV (measured PSF):
Maximum Likelihood; 15 CG Iterations; Regularized.

When image quality is essential and capturing lost information is a must, Carl Zeiss 3D Deconvolution system is the answer.

Our fast, intuitive software allows reassignment of non-focal haze, noise and blur to provide image restoration to its brilliant best. Choose between theoretically calculated or measured PSF, iterative or non-iterative method, and the Zeiss 3D Deconvolution will do the rest.

Whether conventional widefield or confocal fluorescence imaging, your own 3D deconvolution system from Zeiss takes you to new heights of image fidelity.

Let us show you how!

For immediate demonstration, call **800-233-2343**.

Carl Zeiss, Inc.
Microscopy & Imaging Systems
One Zeiss Drive
Thornwood, NY 10594

800.233.2343
Fax 914.681.7446
micro@zeiss.com
www.zeiss.com/micro

ZEISS

MBL/WHOI LIBRARY
WH 1B36 R